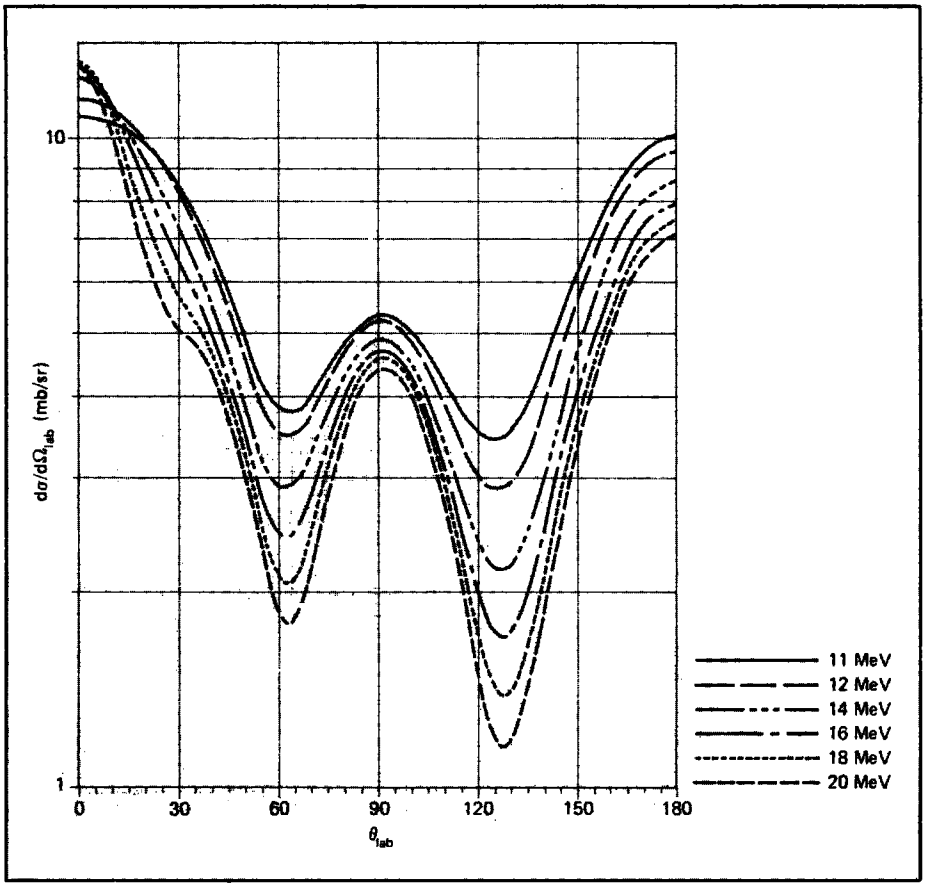

TECHNICAL REPORTS SERIES No. 273

Handbook on Nuclear Activation Data

INTERNATIONAL ATOMIC ENERGY AGENCY, VIENNA, 1987

HANDBOOK
ON NUCLEAR ACTIVATION DATA

The following States are Members of the International Atomic Energy Agency:

AFGHANISTAN
ALBANIA
ALGERIA
ARGENTINA
AUSTRALIA
AUSTRIA
BANGLADESH
BELGIUM
BOLIVIA
BRAZIL
BULGARIA
BURMA
BYELORUSSIAN SOVIET SOCIALIST REPUBLIC
CAMEROON
CANADA
CHILE
CHINA
COLOMBIA
COSTA RICA
COTE D'IVOIRE
CUBA
CYPRUS
CZECHOSLOVAKIA
DEMOCRATIC KAMPUCHEA
DEMOCRATIC PEOPLE'S REPUBLIC OF KOREA
DENMARK
DOMINICAN REPUBLIC
ECUADOR
EGYPT
EL SALVADOR
ETHIOPIA
FINLAND
FRANCE
GABON
GERMAN DEMOCRATIC REPUBLIC
GERMANY, FEDERAL REPUBLIC OF
GHANA
GREECE
GUATEMALA
HAITI
HOLY SEE
HUNGARY
ICELAND
INDIA
INDONESIA
IRAN, ISLAMIC REPUBLIC OF
IRAQ
IRELAND
ISRAEL
ITALY
JAMAICA
JAPAN
JORDAN
KENYA
KOREA, REPUBLIC OF
KUWAIT
LEBANON
LIBERIA
LIBYAN ARAB JAMAHIRIYA
LIECHTENSTEIN
LUXEMBOURG
MADAGASCAR
MALAYSIA
MALI
MAURITIUS
MEXICO
MONACO
MONGOLIA
MOROCCO
NAMIBIA
NETHERLANDS
NEW ZEALAND
NICARAGUA
NIGER
NIGERIA
NORWAY
PAKISTAN
PANAMA
PARAGUAY
PERU
PHILIPPINES
POLAND
PORTUGAL
QATAR
ROMANIA
SAUDI ARABIA
SENEGAL
SIERRA LEONE
SINGAPORE
SOUTH AFRICA
SPAIN
SRI LANKA
SUDAN
SWEDEN
SWITZERLAND
SYRIAN ARAB REPUBLIC
THAILAND
TUNISIA
TURKEY
UGANDA
UKRAINIAN SOVIET SOCIALIST REPUBLIC
UNION OF SOVIET SOCIALIST REPUBLICS
UNITED ARAB EMIRATES
UNITED KINGDOM OF GREAT BRITAIN AND NORTHERN IRELAND
UNITED REPUBLIC OF TANZANIA
UNITED STATES OF AMERICA
URUGUAY
VENEZUELA
VIET NAM
YUGOSLAVIA
ZAIRE
ZAMBIA
ZIMBABWE

The Agency's Statute was approved on 23 October 1956 by the Conference on the Statute of the IAEA held at United Nations Headquarters, New York; it entered into force on 29 July 1957. The Headquarters of the Agency are situated in Vienna. Its principal objective is "to accelerate and enlarge the contribution of atomic energy to peace, health and prosperity throughout the world".

Printed by the IAEA in Austria
April 1987

TECHNICAL REPORTS SERIES No. 273

HANDBOOK ON NUCLEAR ACTIVATION DATA

INTERNATIONAL ATOMIC ENERGY AGENCY
VIENNA, 1987

HANDBOOK ON NUCLEAR ACTIVATION DATA
IAEA, VIENNA, 1987
STI/DOC/10/273
ISBN 92-0-135087-2

FOREWORD

More than a decade has passed since the Handbook on Nuclear Activation Cross-Sections (Technical Reports Series No. 156) was issued. This publication was favourably received by scientists working in the fields of education and industrial applications, as well as in basic research, and there have been many requests since then for a more up to date version. In response to these requests, and with the endorsement of the International Nuclear Data Committee of the IAEA, this new Technical Report, Handbook on Nuclear Activation Data, is being issued for the particular benefit of the many scientists who use nuclear activation methods.

The preparation of such a handbook requires a number of compromises which may not be acceptable to everyone. The scope and treatment of each topic had to be limited in order to be concise and this limit may conflict with the wishes of readers interested in greater detail. However, the material in this Handbook is generally similar to that contained in the earlier version, though there are several important differences, besides the inclusion of more recent data. In Part 1-1, all necessary information on standard reference data has been assembled, something that was missing in the previous Handbook. Great efforts have been made to include as much recent information as possible. There is, however, one important omission. The ENDF/B-VI Standards File has not as yet been released and thus evaluated data from the ENDF/B-V Standards File have been quoted, together with up to date status reports. This part will almost certainly have to be revised when the ENDF/B-VI Standards File becomes available.

The contents of this Handbook are divided into four parts, i.e. standard reference data and neutron, charged particle and photonuclear activation data. The neutron source and gamma ray standards data in Part 1 and the californium spectrum averaged data in Part 2 have been added following requests by the users of the previous Handbook.

While every effort has been made to ensure consistency and uniformity of presentation between the different parts of this Handbook, there remain some inconsistencies concerning the standard reference values of some half-life, abundance and other data that are quoted. The reader is therefore requested to refer to Part 1-1 for appropriate citations.

The emphasis in this Handbook is on evaluated or recommended values rather than on an exhaustive presentation of all experimental results. This aim has been only partially achieved because in some cases it has not been possible to make a selection between parallel presentations of different results. A number of valuable suggestions for subjects to be included in this Handbook have been received and most of them have been adopted; it is hoped that those subjects not included, such as PIXE, can be considered in a separate publication.

It should be emphasized that many of the data contained in this Handbook have been assembled in special computer files in order to ease their updating and to facilitate their use in computations. These files are being updated continuously and can be obtained from the IAEA Nuclear Data Section upon request.

The Agency wishes to thank all of the contributors and also those who have critically reviewed the original manuscripts, especially H. Condé, A.B. Smith and A.D. Carlson for Part 1-2, and H. Vonach for Parts 2-2 and 2-3. The IAEA officer responsible for the planning, overall co-ordination between the authors and for the organization of this Handbook was K. Okamoto.

EDITORIAL NOTE

CONTENTS

PART 1. STANDARD REFERENCE DATA

Neutron Source Standards

PART 3. CHARGED PARTICLE ACTIVATION

PART 4. PHOTONUCLEAR ACTIVATION

Part 1
STANDARD REFERENCE DATA

1-1. NUCLEAR PROPERTIES*

J.K. TULI**
National Nuclear Data Center,
Brookhaven National Laboratory***,
Upton, New York,
United States of America

Abstract

NUCLEAR PROPERTIES.

The paper presents half-life, abundance and decay modes for all known nuclides and some of their isomeric states. The data are taken from the 1984 edition of the Evaluated Nuclear Structure Data File maintained by the National Nuclear Data Center at Brookhaven National Laboratory.

1. INTRODUCTION

Half-life, abundance and decay modes for all known nuclides and some of their isomeric states are presented in Table I. The nuclides for which none of these three properties are known have been omitted. The data given here are from the adopted properties of the various nuclides as given in the 30 Nov. 1984 edition of the Evaluated Nuclear Structure Data File (ENSDF), a computer file of evaluated experimental nuclear structure data maintained by the National Nuclear Data Center at Brookhaven National Laboratory, Upton, New York. The data in ENSDF are based on experimental results for A = 45 to 263 [1] and in Nuclear Physics for $A < 45$. For those nuclides for which either there is no data in ENSDF or more recent data are available, the half-lives and decay modes are taken from Ref. [2]. In some cases, the percentage decay modes are taken from material in Ref. [3]. Recent data, contained in Refs [4–16], have also been included. The isotopic abundances are those of Holden, Martin and Barnes [17]. Other references, experimental data and information on the data measurements can be found in the original evaluations contained in Ref. [1] and in Nuclear Physics.

---

* The nuclear properties given here are based upon the author's pocket-size handbook – Nuclear Wallet Cards (1985) – published and distributed free by the National Nuclear Data Center, Brookhaven National Laboratory, Upton, New York, 11973, USA. Other quantities contained in the Nuclear Wallet Cards and not presented here are spin, parity, mass excess and a number of appendices.

** This research was supported by the Office of Basic Energy Sciences, US Department of Energy.

*** Operated by Associated Universities, Inc., under contract with the US Department of Energy.

2. EXPLANATION OF SYMBOLS USED IN TABLE

2.1. Column 1. Isotope (Z, El, A)

Nuclides are listed in order of increasing atomic number (Z) and are subordered by increasing mass number (A). Included are all isotopic species, all isomers with half-life $\geqslant$1 s and other selected well known isomers. The nuclides for which neither the half-lives nor the decay modes are known have been omitted.

Isomeric states are denoted by the letter 'm' after the mass number and are given in order of increasing excitation energy. More than one entry for a nuclide, without the letter 'm' for any of them, indicates that their relative excitation energies are not known.

The symbols Rf (rutherfordium) and Ha (hahnium) have been used for elements with Z = 104 and 105, respectively. However, these have not been accepted internationally owing to conflicting claims of their discovery.

2.2. Column 2. $T_{1/2}$ or abundance

The half-life and the abundance are given followed by units (the % in the case of the abundance), followed by the uncertainty, in *italics*. The uncertainty given is in the last significant figures. For example, 8.1 s *10* means $T_{1/2}$ = 8.1 ± 1.0 s. For some very short-lived nuclei, level widths rather than half-lives are given. In these cases also the width is followed by the units (e.g. eV, keV or MeV), which are followed by the uncertainty, in *italics*, if known. Those half-life values for which there is no uncertainty given are taken from Ref. [2] and the uncertainty in most of these cases is $\leqslant$5 in the last figure given.

2.3. Column 3. Decay mode

Decay modes are given followed by the per cent branching, if known ('w' indicates a weak branch). The decay modes are given in decreasing strength from left to right. The percentage branching is omitted where there is no competing mode of decay.

The various modes of decay are:

$\beta-$	$\beta-$ decay;
ε	ε (electron capture) or $\varepsilon+\beta+$ or $\beta+$ decay;
IT	Isomeric transition (through γ or conversion-electron decay);
n, p, α, ...	Neutron, proton, alpha, ... decay;
SF	Spontaneous fission;

$2\beta-$, 3α, ...	Double $\beta-$ decay ($\beta-\beta-$), decay through emission of 3 α's, ...;
$\beta-n$, $\beta-p$, $\beta-\alpha$, ...	Delayed n, p, α, ..., emission following $\beta-$ decay;
εp, $\varepsilon \alpha$, εSF, ...	Delayed p, α, SF, ... decay following ε or $\beta+$ decay.

REFERENCES

[1] TULI, J.K., (Ed.), Nucl. Data Sheets **B7-46** (1972)-(1985).
[2] Chart of the Nuclides, 13th edn (WALKER, F.W., MILLER, D.G., FEINER, F., Eds), Knolls Power Laboratory, Schenectady, NY (1983).
[3] BROWNE, E., et al., Table of Isotopes, 7th edn (LEDERER, C.M., SHIRLEY, V.S. Eds), Wiley, New York (1978).
[4] ALBURGER, D.E., private communication on ^{180m}Ta, 1984.
[5] FREKERS, D., et al., Half-life of ^{44}Ti, Phys. Rev. C 28 (1983) 756.
[6] KUTSCHERA, W., et al., Half-life of ^{60}Fe, Nucl. Instrum. Methods **B5** (1984) 430.
[7] ROSE, H.J., JONES, G.A., A new kind of natural radioactivity, Nature (London) **307** (1984) 245. (^{223}Ra)
[8] LANGEVIN, M., et al., Observation of β-delayed triton emission, Phys. Lett. **146B** (1984) 176. (^{11}Li)
[9] Recent half-life measurements on ^{156}Pr, ^{163}Gd, ^{165}Tb, ^{168}Dy, carried out at the Idaho National Engineering Laboratory, as reported in the literature.
[10] LANGEVIN, M., et al., Nucl. Phys. **A414** (1984) 151. ($^{32-35}$Na, $^{29,31-34}$Mg)
[11] DETRAZ, C., et al., Phys. Rev. C **19** (1984) 164. (^{29}Mg, ^{31}Al)
[12] GUILLEMAUD-MUELLER, D., et al., Nucl. Phys. **A426** (1984) 37. (^{32}Al)
[13] MURPHY, M.Y., Phys. Rev. Lett. **49** (1982) 455. (^{32}Al)
[14] KAITA, R., et al., Nucl. Phys. **A344** (1980) 389. (^{32}Si)
[15] ELMORE, D., et al., Phys. Rev. Lett. **45** (1980) 589. (^{32}Si)
[16] VOSICKI, B., et al., Nucl. Instrum. Methods **186** (1981) 307. ($^{42-43}$Cl)
[17] HOLDEN, N.E., MARTIN, R.L., BARNES, I.L., Isotopic composition of the elements 1983, Pure Appl. Chem. **56** (1984) 675.

TABLE I. NUCLEAR PROPERTIES OF ALL KNOWN NUCLIDES AND SOME OF THEIR ISOMERIC STATES

Isotope Z	El	A	T1/2 or Abundance	Decay Mode
0	n	1	10.25 m *20*	β-
1	H	1	99.985% *1*	
		2	0.015% *1*	
		3	12.33 y *6*	β-
2	He	3	0.000138% *3*	
		4	99.999862% *3*	
		5	0.60 MeV *2*	n, α
		6	806.7 ms *15*	β-
		7	160 keV *30*	n
		8	119.0 ms *15*	β-, β-n 16%
		9		n
3	Li	5	≈1.5 MeV	p, α
		6	7.5% *2*	
		7	92.5% *2*	
		8	838 ms *6*	β-2α
		9	178.3 ms *4*	β-, β-n 49.5%, β-n2α
		10	1.2 MeV *3*	n
		11	8.7 ms *1*	β-, β-n 60.8%, β-t 0.01%
4	Be	6	92 keV *6*	p, α
		7	53.29 d *7*	ε
		8	6.8 eV *17*	2α
		9	100%	
		10	1.6×10^{6} y *2*	β-
		11	13.81 s *8*	β-, β-α 3.1%
		12	24.4 ms *30*	β-, β-n<1%
5	B	7	1.3 MeV *2*	p, α
		8	770 ms *3*	ε2α
		9	0.54 keV *21*	p2α
		10	19.9% *2*	
		11	80.1% *2*	
		12	20.20 ms *2*	β-, β-3α 1.58%
		13	17.36 ms *16*	β-, β-n 0.28%
		14	16.1 ms *12*	β-
		15		β-
6	C	8	230 keV *50*	α, p
		9	126.5 ms *9*	εp2α
		10	19.255 s *53*	ε
		11	20.385 m *20*	ε
		12	98.90% *3*	
		13	1.10% *3*	
		14	5730 y *40*	β-
		15	2.449 s *5*	β-
		16	0.747 s *8*	β-, β-n≥98.8%
7	N	11	0.74 MeV *10*	p
		12	11.000 ms *16*	ε, ε3α 3.44%
		13	9.965 m *4*	ε
		14	99.634% *9*	
		15	0.366% *9*	
		16	7.13 s *2*	β-, β-α 0.0012%
		17	4.173 s *4*	β-, β-n 95%
		18	624 ms *12*	β-
8	O	12	400 keV *250*	p
		13	8.90 ms *20*	ε
		14	70.606 s *18*	ε
		15	122.24 s *16*	ε
		16	99.762% *15*	
		17	0.038% *3*	
		18	0.200% *12*	
		19	26.91 s *8*	β-
		20	13.51 s *5*	β-
		21	3.4 s	β-
9	F	15	1.0 MeV *2*	p
		16	40 keV *20*	p
9	F	17	64.49 s *16*	ε
		18	109.77 m *5*	ε
		19	100.%	
		20	11.00 s *2*	β-
		21	4.32 s *3*	β-
		22	4.23 s *4*	β-
		23	2.23 s *14*	β-
10	Ne	16	≈50 keV	p
		17	109.0 ms *10*	ε, εp
		18	1.672 s *5*	ε
		19	17.22 s *2*	ε
		20	90.51% *9*	
		21	0.27% *2*	
		22	9.22% *9*	
		23	37.24 s *12*	β-
		24	3.38 m *2*	β-
		25	602 ms *8*	β-
11	Na	19	0.03 s ?	p
		20	446 ms *3*	ε, εα 21%
		21	22.48 s *3*	ε
		22	2.602 y *2*	ε
		23	100%	
		24	15.020 h *7*	β-
		24m	20.18 ms *10*	IT, β-≈0.003%
		25	59.6 s *7*	β-
		26	1.072 s *9*	β-
		27	302 ms *7*	β-, β-n 0.08%
		28	30.5 ms *4*	β-, β-n 0.58%
		29	42.9 ms *15*	β-, β-n 15.1%
		30	53 ms *3*	β-, β-n 33%
		31	16.9 ms *7*	β-, β-n 30%
		32	13.5 ms *15*	β-, β-n 39%
		33	8.0 ms *6*	β-, β-n 77%
		34	5.5 ms *10*	β-, β-n
		35	1.5 ms *5*	β-, β-n
12	Mg	20	0.1 s	ε, εp
		21	122 ms *3*	ε, εp 29.3%
		22	3.857 s *9*	ε
		23	11.317 s *11*	ε
		24	78.99% *3*	
		25	10.00% *1*	
		26	11.01% *2*	
		27	9.462 m *11*	β-
		28	20.90 h *3*	β-
		29	1.38 s *13*	β-
		30	0.33 s	β-
		31	0.23 s *3*	β-, β-n 1.7%
		32	120 ms *20*	β-, β-n 2.7%
		33	90 ms *20*	β-, β-n 17%
		34	20 ms *10*	β-, β-n
13	Al	22	70 ms	ε, εp
		23	0.47 s *3*	ε, εp
		24	2.066 s *10*	ε, εα 0.0067%
		24m	130 ms *4*	IT 93%, ε 7%, εα
		25	7.183 s *12*	ε
		26	7.2×10^{5} y *3*	ε
		26m	6.345 s *3*	ε
		27	100%	
		28	2.2406 m *5*	β-
		29	6.56 m *6*	β-
		30	3.60 s *6*	β-
		31	0.644 s *25*	β-
		32	35 ms *5*	
14	Si	24	0.10 s	ε, εp
		25	220 ms *3*	ε, εp
		26	2.210 s *21*	ε

Isotope Z El	A	T1/2 or Abundance	Decay Mode
14 Si	27	4.16 s *2*	ε
	28	92.23% *1*	
	29	4.67% *1*	
	30	3.10% *1*	
	31	2.62 h *1*	β-
	32	105 y *13*	β-
	33	6.11 s *21*	β-
	34	2.77 s *20*	β-
15 P	26	20 ms	ε, εp, ε2p?
	28	270.3 ms *5*	ε
	29	4.142 s *15*	ε
	30	2.498 m *4*	ε
	31	100%	
	32	14.26 d *4*	β-
	33	25.34 d *12*	β-
	34	12.43 s *8*	β-
	35	47.3 s *7*	β-
	36	5.9 s	β-
16 S	29	0.187 s *4*	ε, εp
	30	1.24 s *4*	ε
	31	2.584 s *18*	ε
	32	95.02% *9*	
	33	0.75% *1*	
	34	4.21% *8*	
	35	87.51 d *12*	β-
	36	0.02% *1*	
	37	5.05 m *2*	β-
	38	2.84 h *1*	β-
	39	11.5 s	β-
17 Cl	31	0.15 s	ε, εp
	32	298 ms *2*	ε, εp≈0.007%, εα≈0.01%
	33	2.511 s *3*	ε
	34	1.5262 s *25*	ε
	34m	32.23 m *14*	ε 53.1%, IT 46.9%
	35	75.77% *5*	
	36	3.01×10^5 y *2*	β- 98.1%, ε 1.9%
	37	24.23% *5*	
	38	37.24 m *5*	β-
	38m	715 ms *3*	IT
	39	55.6 m *2*	β-
	40	1.35 m *2*	β-
	41	34 s *3*	β-
	42	6.8 s *3*	
	43	3.3 s *2*	
18 Ar	32	0.1 s	ε, εp
	33	173 ms *2*	ε, εp 34%
	34	845 ms *3*	ε
	35	1.775 s *4*	ε
	36	0.337% *3*	
	37	35.04 d *4*	ε
	38	0.063% *1*	
	39	269 y *3*	β-
	40	99.600% *3*	
	41	1.827 h *7*	β-
	42	32.9 y *11*	β-
	43	5.37 m *6*	β-
	44	11.87 m *5*	β-
	45	21.48 s *15*	β-
	46	8 s *1*	β-
19 K	35	0.19 s	ε, εp
	36	342 ms *2*	ε, εp, εα
	37	1.226 s *7*	ε
	38	7.636 m *18*	ε
	38m	924.6 ms *15*	ε
	39	93.2581% *30*	

Isotope Z El	A	T1/2 or Abundance	Decay Mode
19 K	40	1.277×10^9 y *8*	β- 89.3%, ε 10.7%
		0.0117% *1*	
	41	6.7302% *30*	
	42	12.360 h *3*	β-
	43	22.3 h *1*	β-
	44	22.13 m *19*	β-
	45	17.3 m *6*	β-
	46	107 s *10*	β-
	47	17.5 s *3*	β-
	48	6.9 s *2*	β-
	49	1.3 s	β-, β-n
	50	472 ms *4*	β-, β-n 29%
	51	365 ms *5*	β-, β-n
	53	30 ms *5*	β-, β-n
20 Ca	36	0.1 s	ε, εp
	37	175 ms *3*	ε, εp
	38	447 ms *10*	ε
	39	859.6 ms *14*	ε
	40	96.941% *13*	
	41	1.03×10^5 y *4*	ε
	42	0.647% *3*	
	43	0.135% *3*	
	44	2.086% *5*	
	45	163.8 d *18*	β-
	46	0.004% *3*	
	47	4.535 d *4*	β-
	48	$\geq2\times10^{16}$ y	
		0.187% *3*	
	49	8.716 m *11*	β-
	50	13.9 s *6*	β-
	51	10 s	β-, β-n?
	53	90 ms *15*	β-
21 Sc	40	182.3 ms *7*	ε, εp
	41	596.3 ms *17*	ε
	42	681.3 ms *7*	ε
	42m	61.6 s *4*	ε
	43	3.891 h *12*	ε
	44	3.927 h *8*	ε
	44m	58.6 h *1*	IT 98.8%, ε 1.2%
	45	100%	
	45m	0.32 s *1*	IT
	46	83.83 d *2*	β-
	46m	18.70 s *5*	IT
	47	3.345 d *3*	β-
	48	43.7 h *1*	β-
	49	57.4 m	β-
	50	1.710 m *8*	β-
	50m	0.35 s *3*	IT 98.7%, β- 1.3%
	51	12.4 s *1*	β-
22 Ti	41	80 ms *2*	ε, εp
	42	199 ms *6*	ε
	43	513 ms *8*	ε
	44	54.2 y *21*	ε
	45	3.08 h *1*	ε
	46	8.0% *1*	
	47	7.3% *1*	
	48	73.8% *1*	
	49	5.5% *1*	
	50	5.4% *1*	
	51	5.76 m *1*	β-
	52	1.7 m *1*	β-
	53	32.7 s *9*	β-
23 V	44	90 ms *25*	ε, εα
	45	539 ms *18*	ε
	46	422.33 ms *20*	ε
	47	32.6 m *3*	ε

TABLE I (cont.)

Isotope Z	El	A	T1/2 or Abundance	Decay Mode
23	V	48	15.974 d *3*	ε
		49	330 d *15*	ε
		50	1.5×10^{17} y *+3-7*	ε>70%, β-<30%
			0.250% *2*	
		51	99.750% *2*	
		52	3.75 m *1*	β-
		53	1.61 m *4*	β-
		54	49.8 s *5*	β-
		55	6.54 s *15*	β-
24	Cr	45	50 ms *6*	ε, εp>25%
		46	0.26 s *6*	ε, εp
		47	508.0 ms *10*	ε
		48	21.56 h *3*	ε
		49	42.09 m *15*	ε
		50	4.345% *9*	
		51	27.704 d *4*	ε
		52	83.789% *12*	
		53	9.501% *11*	
		54	2.365% *5*	
		55	3.497 m *3*	β-
		56	5.94 m *10*	β-
		57	21 s	β-
25	Mn	49	0.38 s	ε
		50	283.0 ms *4*	ε
		50m	1.75 m *3*	ε
		51	46.2 m *1*	ε
		52	5.591 d *3*	ε
		52m	21.1 m *2*	ε 98.32%, IT 1.75%
		53	3.7×10^{6} y *4*	ε
		54	312.5 d *5*	ε
		55	100%	
		56	2.5785 h *6*	β-
		57	1.45 m	β-
		58	65.3 s *7*	β-
		58m	3.0 s *1*	β-
		59	4.6 s *1*	β-
		60	1.79 s *10*	β-
		62	0.9 s	β-
26	Fe	49	75 ms *10*	ε, εp
		51	0.25 s	ε
		52	8.275 h *8*	ε
		52m	46 s *2*	ε 80%, IT 20%
		53	8.51 m *2*	ε
		53m	2.58 m *6*	IT
		54	5.8% *1*	
		55	2.68 y	ε
		56	91.72% *30*	
		57	2.2% *1*	
		58	0.28% *1*	
		59	44.496 d *7*	β-
		60	1.49×10^{6} y *27*	β-
		61	5.98 m *6*	β-
		62	68 s *2*	β-
		63	4.9 s	β-
27	Co	53	262 ms *25*	ε
		53m	0.25 s	ε 98.5%, p≈1.5%
		54	193.23 ms *14*	ε
		54m	1.48 m *2*	ε
		55	17.53 h *3*	ε
		56	78.76 d *12*	ε
		57	270.9 d *6*	ε
		58	70.916 d *15*	ε
		58m	9.15 h *10*	IT
		59	100%	
		60	5.271 y *1*	β-
27	Co	60m	10.47 m *4*	IT 99.75%, β- 0.25%
		61	1.650 h *5*	β-
		62	1.50 m *4*	β-
		62m	13.91 m *5*	β-, IT<1%
		63	27.4 s *5*	β-
		64	0.30 s *3*	β-
28	Ni	53	45 ms *15*	ε, εp
		55	189 ms *5*	ε
		56	6.10 d *2*	ε
		57	36.08 h *9*	ε
		58	68.27% *1*	
		59	7.5×10^{4} y *13*	ε
		60	26.10% *1*	
		61	1.13% *1*	
		62	3.59% *1*	
		63	100.1 y *20*	β-
		64	0.91% *1*	
		65	2.520 h *2*	β-
		66	54.6 h *4*	β-
		67	21 s *1*	β-
		68		β-?
29	Cu	57	0.18 s ?	ε
		58	3.204 s *7*	ε
		59	81.5 s *5*	ε
		60	23.2 m *3*	ε
		61	3.408 h *10*	ε
		62	9.74 m *2*	ε
		63	69.17% *2*	
		64	12.701 h *2*	ε 62.9%, β- 37.1%
		65	30.83% *2*	
		66	5.10 m *2*	β-
		67	61.92 h *9*	β-
		68	31 s *1*	β-
		68m	3.75 m *5*	IT 86%, β- 14%
		69	3.0 m *1*	β-
		70	4.5 s *1*	β-
		70m	46 s *5*	β-
		71	20 s	β-
		72	6.6 s	β-
		73	3.9 s	β-
30	Zn	57	40 ms *10*	ε, εp
		58		ε
		59	183.7 ms *23*	ε, εp
		60	2.38 m *5*	ε
		61	89.1 s *2*	ε
		62	9.26 h *2*	ε
		63	38.1 m *3*	ε
		64	48.6% *3*	
		65	243.9 d *1*	ε
		66	27.9% *2*	
		67	4.1% *1*	
		68	18.8% *4*	
		69	55.6 m *16*	β-
		69m	13.76 h *2*	IT 99.97%, β- 0.03%
		70	0.6% *1*	
		71	2.45 m *10*	β-
		71m	3.94 h *5*	β-
		72	46.5 h *1*	β-
		73	23.5 s *10*	β-
		74	95 s *1*	β-
		75	10.2 s *3*	β-
		76	5.7 s *3*	β-
		77	1.4 s *3*	β-
		78	1.47 s *15*	β-
		79	2.63 s *9*	β-, β-n?

Isotope Z El	A	T1/2 or Abundance	Decay Mode
30 Zn	80		β-
31 Ga	62	116.12 ms *26*	ε
	63	32.4 s *5*	ε
	64	2.630 m *11*	ε
	65	15.2 m *2*	ε
	66	9.49 h *7*	ε
	67	3.261 d *1*	ε
	68	68.1 m *3*	ε
	69	60.1% *2*	
	70	21.15 m *5*	β- 99.59%, ε 0.41%
	71	39.9% *2*	
	72	14.10 h *1*	β-
	73	4.87 h *3*	β-
	74	8.1 m *1*	β-
	74m	9.5 s *10*	IT, β-?
	75	2.10 m *3*	β-
	76	32.6 s *6*	β-
	77	13.2 s *2*	β-
	78	5.09 s *5*	β-
	79	3.00 s *9*	β-, β-n 0.098%
	80	1.66 s *9*	β-, β-n 0.84%
	81	1.23 s *1*	β-, β-n 12%
	82	0.60 s	β-, β-n
	83	0.31 s	β-, β-n
32 Ge	61	40 ms *15*	ε, εp
	64	63.7 s *25*	ε
	65	30.9 s *7*	ε, εp 0.013%
	66	2.26 h *5*	ε
	67	18.7 m *5*	ε
	68	271 d	ε
	69	39.05 h *10*	ε
	70	20.5% *5*	
	71	11.8 d *4*	ε
	72	27.4% *6*	
	73	7.8% *2*	
	73m	0.499 s *11*	IT
	74	36.5% *7*	
	75	82.78 m *4*	β-
	75m	47.7 s *7*	IT 99.97%, β- 0.03%
	76	7.8% *2*	
	77	11.30 h *1*	β-
	77m	52.9 s *6*	β- 79%, IT 21%
	78	88 m *1*	β-
	79	19.1 s *3*	β-
	79m	39.0 s *10*	β- 96%, IT 4%
	80	29.5 s *4*	β-
	81	7.6 s	β-, β-
	82	4.6 s *4*	β-
	83	1.9 s *4*	β-
	84	1.2 s *3*	β-
33 As	66	95.8 ms *4*	ε
	67	42.5 s *12*	ε
	68	2.530 m *17*	ε
	69	15.2 m *2*	ε
	70	52.6 m *3*	ε
	71	62 h	ε
	72	26.0 h *1*	ε
	73	80.30 d *6*	ε
	74	17.78 d *3*	ε 65.8%, β- 34.2%
	75	100%	
	76	26.32 h *7*	β-
	77	38.83 h *5*	β-
	78	90.7 m *2*	β-
	79	9.01 m *15*	β-
	80	15.2 s *2*	β-

Isotope Z El	A	T1/2 or Abundance	Decay Mode
33 As	81	33 s *2*	β-
	82	19 s	β-
	82	14 s	β-
	83	13 s	β-, β-n
	84	5.5 s *3*	β-, β-n 0.1%
	84m	0.65 s	β-
	85	2.028 s *12*	β-, β-n 23%
	86	0.9 s *2*	β-, β-n≈4%
	87	0.75 s *6*	β-, β-n
34 Se	68	1.6 m	ε
	69	27.4 s *2*	ε, εp 0.07%
	70	41.1 m	ε
	71	4.74 m *5*	ε
	72	8.40 d *8*	ε
	73	7.15 h *8*	ε
	73m	39.8 m *13*	IT 73%, ε 27%
	74	0.9% *1*	
	75	119.770 d *10*	ε
	76	9.0% *2*	
	77	7.6% *2*	
	77m	17.45 s *10*	IT
	78	23.6% *6*	
	79	≤65000 y	β-
	79m	3.91 m *5*	IT
	80	49.7% *7*	
	81	18.5 m *1*	β-
	81m	57.25 m *9*	IT, β- 0.07%
	82	1.4×10^{20} y	2β-
		9.2% *5*	
	83	22.5 m *2*	β-
	83m	70.4 s *3*	β-
	84	3.2 m *2*	β-
	85	31.7 s *9*	β-
	86	15.3 s *9*	β-
	87	5.55 s *20*	β-, β-n 0.16%
	88	1.53 s *6*	β-, β-n 0.8%
	89	0.41 s *4*	β-, β-n 5%
	91	0.27 s *5*	β-, β-n≈21%
35 Br	70	80 ms	ε
	72	78.6 s *24*	ε
	73	3.4 m *3*	ε
	74	25.3 m *3*	ε
	74m	41.5 m *15*	ε
	75	97 m *2*	ε
	76	16.2 h *2*	ε
	76m	1.31 s *2*	IT 99.4%, ε 0.6%
	77	57.036 h *6*	ε
	77m	4.28 m *10*	IT
	78	6.46 m *4*	ε≥99.99%, β-≤0.01%
	79	50.69% *5*	
	79m	4.864 s *35*	IT
	80	17.68 m *2*	β- 91.7%, ε 8.3%
	80m	4.42 h *1*	IT
	81	49.31% *5*	
	82	35.30 h *3*	β-
	82m	6.13 m *8*	IT 97.6%, β- 2.4%
	83	2.39 h *2*	β-
	84	31.80 m *8*	β-
	84m	6.0 m *2*	β-
	85	2.90 m *6*	β-
	86	55.0 s *8*	β-
	87	55.69 s *13*	β-, β-n 2.3%
	88	16.3 s *3*	β-, β-n 6%
	89	4.53 s *10*	β-, β-n 13%
	90	1.71 s *14*	β-, β-n 23%
	91	0.541 s *5*	β-, β-n 9%

TABLE I (cont.)

Isotope Z	El	A	T1/2 or Abundance	Decay Mode
35	Br	92	0.365 s *7*	β-, β-n 21%
		94		β-, β-n >0%
36	Kr	71	0.1 s	ε
		72	17.2 s *3*	ε
		73	27.0 s *12*	ε, εp 0.68%
		74	11.50 m *11*	ε
		75	4.3 m *1*	ε
		76	14.8 h *1*	ε
		77	74.4 m *6*	ε
		78	0.35% *2*	
		79	35.04 h *10*	ε
		79m	50 s *3*	IT
		80	2.25% *2*	
		81	2.1×10^{5} y *2*	ε
		81m	13.3 s	IT
		82	11.6% *1*	
		83	11.5% *1*	
		83m	1.83 h 2	IT
		84	57.0% *3*	
		85	10.72 y *2*	β-
		85m	4.480 h *8*	β- 79%, IT 21%
		86	17.3% *2*	
		87	76.3 m 5	β-
		88	2.84 h *2*	β-
		89	3.07 m *9*	β-
		90	32.32 s *9*	β-
		91	8.57 s *5*	β-
		92	1.85 s *1*	β-, β-n 0.03%
		93	1.289 s *12*	β-, β-n 1.9%
		94	0.20 s *1*	β-, β-n 5.7%
		95	0.78 s *3*	β-, β-n
		97?	<0.1 s	β-
37	Rb	74	65 ms	ε
		75	17.2 s *8*	ε
		76	39.1 s *6*	ε
		77	3.70 m *15*	ε
		78	17.66 m *8*	ε
		78m	5.74 m *6*	ε 90%, IT 8%
		79	22.9 m *5*	ε
		80	34 s *4*	ε
		81	4.58 h *1*	ε
		81m	32 m	ε, IT
		82	1.25 m *3*	ε
		82m	6.2 h *5*	ε
		83	86.2 d *1*	ε
		84	32.87 d *11*	ε 96%, β- 4%
		84m	20.49 m *17*	IT
		85	72.165% *13*	
		86	18.66 d *2*	β-, ε 0.005%
		86m	1.017 m *3*	IT >99.7%, β- <0.3%
		87	4.80×10^{10} y *13*, 27.835% *13*	β-
		88	17.8 m *1*	β-
		89	15.2 m *1*	β-
		90	153 s *3*	β-
		90m	258 s *5*	β- 95.7%, IT 4.3%
		91	58.4 s *4*	β-
		92	4.50 s *2*	β-, β-n 0.012%
		93	5.85 s	β-, β-n 1.3%
		94	2.702 s *5*	β-, β-n 10.4%
		95	384 ms *6*	β-, β-n 9.1%
		96	0.199 s *3*	β-, β-n 13%
		97	171.8 ms *16*	β-, β-n 24.6%
		98	0.114 s *5*	β-, β-n 15.9%
		99	59 ms	β-, β-n
		100	50 ms	β-, β-n
37	Rb	102?	90 ms *20*	β-
38	Sr	77	9.0 s *10*	ε, εp <0.25%
		78	30.6? m *23*	ε
		79	2.25 m *10*	ε
		80	106.3 m *15*	ε
		81	22.2 m	ε
		82	25.6 d	ε
		83	32.4 h *2*	ε
		83m	4.95 s *12*	IT
		84	0.56% *1*	
		85	64.84 d *3*	ε
		85m	67.66 m 7	IT 87.3%, ε 12.7%
		86	9.86% *1*	
		87	7.00% *1*	
		87m	2.81 h *1*	IT 99.7%, ε 0.3%
		88	82.58% *1*	
		89	50.55 d *9*	β-
		90	28.6 y *3*	β-
		91	9.52 h *6*	β-
		92	2.71 h *1*	β-
		93	7.6 m *2*	β-
		94	75.1 s *7*	β-
		95	25.1 s *2*	β-
		96	1.06 s *4*	β-
		97	0.42 s *3*	β-, β-n 0.27%
		98	0.65 s *3*	β-, β-n 0.8%
		99	0.29 s	β-, β-n
		100	0.2 s	β-
		101	121 ms *6*	β-
		102	355 ms *50*	β-
39	Y	80	33.8 s *6*	ε
		81	72 s	ε
		82	9.5 s	ε
		83	7.06 m *8*	ε
		83	2.85 m *2*	ε
		84	40 m *1*	ε
		84m	4.6 s *2*	ε
		85	2.68 h *5*	ε
		85m	4.86 h *13*	ε
		86	14.74 h *2*	ε
		86m	48 m *1*	IT 99.31%, ε 0.7%
		87	80.3 h *3*	ε
		87m	12.9 h *4*	IT 98.43%, ε 1.57%
		88	106.64 d *8*	ε
		89	100%	
		89m	16.06 s *4*	IT
		90	64.1 h *1*	β-
		90m	3.19 h *1*	IT, β- 0.002%
		91	58.51 d *6*	β-
		91m	49.71 m *4*	IT
		92	3.54 h *1*	β-
		93	10.1 h *2*	β-
		93m	0.82 s	IT
		94	18.7 m *1*	β-
		95	10.3 m *2*	β-
		96	6.2 s *2*	β-
		96m	9.6 s *2*	β-
		96m	2.3 m *1*	β-
		97	3.5 s *2*	β-, β-n 0.06%
		97m	1.23 s *2*	β-
		98	0.64 s *3*	β-, β-n 0.3%
		98m	2.0 s *2*	β-
		99	1.5 s	β-, β-n 1%
		100	0.94 s	β-
		100m	0.5 s	β-
		101	0.50 s *5*	β-

Isotope Z El A	T1/2 or Abundance	Decay Mode
39 Y 102	0.27 s *7*	β-
40 Zr 81	11 m	ε
82	2.5 m	ε
83	44 s	ε
83	8 s	ε
84	28 m	ε
85	7.86 m *4*	ε
85m	10.9 s *3*	IT
86	16.5 h *1*	ε
87	1.73 h *8*	ε
87m	14.0 s *2*	IT
88	83.4 d *3*	ε
89	78.43 h *8*	ε
89m	4.18 m *1*	IT 93.76%, ε 6.24%
90	51.45% *2*	
90m	809.2 ms *20*	IT
91	11.22% *2*	
92	17.15% *1*	
93	1.53×10^{6} y *10*	β-
94	17.38% *2*	
95	64.02 d *4*	β-
96	$>3.56\times10^{17}$ y 2.80% *1*	
97	16.90 h *5*	β-
98	30.7 s *4*	β-
99	2.1 s	β-
100	7.1 s *4*	β-
101	2.1 s *3*	β-
102	2.9 s *2*	β-
104	1.2 s *1*	β-
41 Nb 84	12 s *3*	ε
86	1.45 m	ε
87	2.60 m *7*	ε
87m	3.82 m *9*	ε
88	14.3 m	ε
88m	7.8 m	ε
89	66 m *2*	ε
89	122 m *4*	ε
90	14.60 h *5*	ε
90m	18.8 s *1*	IT
91	7×10^{2} y	ε
91m	62 d	IT 95%, ε 5%
92	3.5×10^{7} y *3*	ε
92m	10.15 d *2*	ε
93	100%	
93m	13.6 y *3*	IT
94	2.03×10^{4} y *16*	β-
94m	6.26 m *1*	IT 99.5%, β- 0.5%
95	34.97 d *3*	β-
95m	3.61 d *3*	IT 94.4%, β- 5.6%
96	23.35 h *5*	β-
97	72.1 m *7*	β-
97m	60 s *8*	IT
98	2.86 s *6*	β-
98m	51.3 m *4*	β-
99	15.0 s	β-
99m	2.6 m *2*	β-, ITw
100	3.1 s *3*	β-
100	1.5 s *3*	β-
101	7.1 s *3*	β-
102	1.3 s *2*	β-
102	4.3 s *4*	β-
103	1.5 s *2*	β-
104	0.91 s *10*	β-
104	4.8 s *4*	β-
105	1.8 s *8*	β-

Isotope Z El A	T1/2 or Abundance	Decay Mode
41 Nb 106	1.1 s *1*	β-
42 Mo 87	14.6 s *15*	ε
88	8.2 m *5*	ε
89	2.2 m	ε
89m	0.19 s	IT
90	5.67 h *5*	ε
91	15.49 m *1*	ε
91m	65.2 s *8*	IT 50.1%, ε 49.9%
92	14.84% *4*	
93	3.5×10^{3} y *7*	ε
93m	6.85 h *7*	IT 99.88%, ε 0.12%
94	9.25% *2*	
95	15.92% *4*	
96	16.68% *4*	
97	9.55% *2*	
98	24.13% *6*	
99	66.0 h *2*	β-
100	9.63% *2*	
101	14.6 m *1*	β-
102	11.3 m *2*	β-
103	67.5 s *15*	β-
104	60 s *2*	β-
105	50 s	β-
105	30 s	β-
106	8.4 s *5*	β-
107	3.5 s *5*	β-
108	1.5 s *4*	β-
43 Tc 90	8.3 s	ε
90	49.2 s	ε
91	3.14 m *2*	ε
91m	3.3 m *1*	ε
92	4.4 m *3*	ε
93	2.75 h *5*	ε
93m	43.5 m *10*	IT 80%, ε 20%
94	4.88 h *2*	ε
94m	52 m *1*	ε, IT<0.1%
95	20.0 h *1*	ε
95m	61 d *2*	ε 96%, IT 4%
96	4.28 d *6*	ε
96m	51.5 m *10*	IT 98%, ε 2%
97	2.6×10^{6} y *4*	ε
97m	90.5 d *10*	IT
98	4.2×10^{6} y *3*	β-
99	2.13×10^{5} y *5*	β-
99m	6.02 h *3*	IT, β-w
100	15.8 s *1*	β-
101	14.2 m *1*	β-
102	5.28 s *15*	β-
102m	4.35 m *7*	β-≈98%, IT≈2%
103	54.2 s *8*	β-
104	18.3 m *3*	β-
105	7.7 m *2*	β-
106	36 s *1*	β-
107	21.2 s *2*	β-
108	5.17 s *7*	β-
109	1.4 s *4*	β-
110	0.83 s *4*	β-
44 Ru 92	3.65 m *5*	ε
93	60 s	ε
93m	10.8 s	ε 79%, IT 21%
94	51.8 m *6*	ε
95	1.64 h *1*	ε
96	5.52% *5*	
97	2.9 d *1*	ε
98	1.88% *5*	
99	12.7% *1*	

TABLE I (cont.)

Isotope Z El A	T1/2 or Abundance	Decay Mode
44 Ru 100	12.6% *1*	
101	17.0% *1*	
102	31.6% *2*	
103	39.26 d *2*	β-
104	18.7% *2*	
105	4.44 h *2*	β-
106	371.63 d *17*	β-
107	3.75 m *5*	β-
108	4.55 m *5*	β-
109	34.5 s *10*	β-
109?	12.9 s	β-, IT?
110	14.6 s *10*	β-
111	1.5 s	β-
112	4.65 s *14*	β-
113	2.69 s *10*	β-
45 Rh 94	70.6 s *6*	ε
94	25.8 s *2*	ε
95	5.02 m *10*	ε
95m	1.96 m *4*	IT 88%, ε 12%
96	9.6 m	ε
96m	1.51 m *2*	IT 60%, ε 40%
97	31.1 m *8*	ε
97m	44.3 m *8*	ε 95.1%, IT 4.9%
98	8.7 m *2*	ε
98m	3.5 m *3*	ε
99	16.1 d	ε
99m	4.7 h	ε
100	20.8 h *1*	ε
100m	4.7 m	IT 93%, ε 7%
101	3.3 y *3*	ε
101m	4.34 d *1*	ε 92.3%, IT 7.7%
102	≈2.9 y	ε
102m	207 d *3*	ε 75%, β- 20%, IT 5%
103	100%	
103m	56.12 m *1*	IT
104	42.3 s *4*	β- 99.55%, ε 0.45%
104m	4.34 m *5*	IT 99.87%, β- 0.13%
105	35.36 h *6*	β-
105m	45 s	IT
106	29.80 s *8*	β-
106m	130 m *2*	β-
107	21.7 m *4*	β-
108	6.0 m *3*	β-
108m	16.8 s *5*	β-
109	80 s *2*	β-
110	3.2 s *2*	β-
110	28.5 s *15*	β-
111	11 s *1*	β-
112	0.8 s *1*	β-
113?	0.91 s *8*	β-
114?	1.68 s *7*	β-
46 Pd 94	9.0 s *5*	ε
95m	13.3 s *3*	ε, εp 0.93%
96	2.0 m	ε
97	3.1 m *1*	ε
98	17.7 m *3*	ε
99	21.4 m	ε
100	3.63 d *9*	ε
101	8.47 h *6*	ε
102	1.020% *12*	
103	16.991 d *19*	ε
104	11.14% *8*	
105	22.33% *8*	
106	27.33% *5*	

Isotope Z El A	T1/2 or Abundance	Decay Mode
46 Pd 107	6.5×10^6 y *3*	β-
107m	21.3 s *5*	IT
108	26.46% *9*	
109	13.7 h *1*	β-
109m	4.69 m *1*	IT
110	11.72% *9*	
111	23.4 m *2*	β-
111m	5.5 h *1*	IT 73%, β- 27%
112	21.05 h *5*	β-
113	98 s	β-
113	89 s	β-
114	2.4 m *1*	β-
115	47 s	β-
116	12.7 s *4*	β-
117	5.0 s *6*	β-
118	3.1 s *3*	β-
47 Ag 96	5.1 s	ε, εp
97	21 s *3*	ε
98	44.5 s *12*	ε, εp>0%
99	2.07 m	ε
99m	11 s	IT
100	2.0 m	ε
100	2.3 m	ε
101	11.1 m *3*	ε
101m	3.10 s *10*	IT
102	12.9 m *3*	ε
102m	7.7 m *5*	ε 51%, IT 49%
103	65.7 m *7*	ε
103m	5.7 s *3*	IT
104	69.2 m *10*	ε
104m	33.5 m *20*	ε 67%, IT 33%
105	41.29 d *7*	ε
105m	7.23 m *16*	IT 98.12%, ε 1.88%
106	24.0 m *1*	ε ≥ 99%, β- ≤ 1%
106m	8.46 d *10*	ε
107	51.839% *5*	
107m	44.3 s *2*	IT
108	2.37 m *1*	β- 97.15%, ε 2.85%
108m	127 y *21*	ε 91.3%, IT 8.7%
109	48.161% *5*	
109m	39.6 s *2*	IT
110	24.6 s *2*	β- 99.7%, ε 0.3%
110m	249.76 d *4*	β- 98.64%, IT 1.36%
111	7.45 d *1*	β-
111m	64.8 s *8*	IT 99.3%, β- 0.7%
112	3.14 h *2*	β-
113	5.37 h *5*	β-
113m	68.7 s *50*	IT 80%, β- 20%
114	4.6 s *2*	β-
115	20.0 m *5*	β-
115	18.0 s *7*	β-
116	2.68 m *1*	β-
116m	10.4 s *8*	β- 98%, IT 2%
117	72.8 s *+20-7*	β-
117	5.34 s *5*	β-
118	4.0 s	β-
118m	2.8 s *3*	β- 59%, IT 41%
119	2.1 s *1*	β-
120	1.17 s *5*	β-
120m	0.32 s *4*	β- 63%, IT 37%
121	0.8 s *1*	β-
122	1.5 s *5*	β-, β-n
123	0.39 s *3*	β-, β-n
48 Cd 97	3 s	ε, εp

Isotope Z El A	T1/2 or Abundance	Decay Mode
48 Cd 98	≈8 s	ε, εp?
99	16 s	ε, εp
100	1.1 m *3*	ε
101	1.2 m *2*	ε
102	5.5 m *5*	ε
103	7.3 m *1*	ε
104	57.7 m *10*	ε
105	55.5 m *4*	ε
106	1.25% *3*	
107	6.50 h *2*	ε
108	0.89% *1*	
109	462.9 d *20*	ε
110	12.49% *9*	
111	12.80% *6*	
111m	48.6 m *3*	IT
112	24.13% *11*	
113	9.3×10^{15} y *19*	β-
	12.22% *6*	
113m	13.7 y	β- 99.86%, IT 0.14%
114	28.73% *21*	
115	53.46 h *10*	β-
115m	44.6 d *3*	β-
116	7.49% *9*	
117	2.49 h *4*	β-
117m	3.36 h *5*	β-
118	50.3 m *2*	β-
119	2.69 m *2*	β-
119m	2.20 m *2*	β-
120	50.80 s *21*	β-
121	13.5 s *3*	β-
121m	8 s	β-
122	5.5 s *1*	β-
124	0.9 s *2*	β-
126	0.506 s *15*	β-
128	0.94 s *5*	β-
49 In 100		ε, εp
102	23 s *4*	ε
103	65 s *7*	ε
104	1.7 m *2*	ε
105	4.9 m *3*	ε
105m	43 s	IT
106	6.2 m *1*	ε
106m	5.2 m *1*	ε
107	32.4 m *3*	ε
107m	50.4 s *6*	IT
108	39.6 m *7*	ε
108	58.0 m *12*	ε
109	4.2 h *1*	ε
109m	1.34 m *7*	IT
109m	0.21 s *1*	IT
110	69.1 m *5*	ε
110	4.9 h *1*	ε
111	2.83 d *1*	ε
111m	7.7 m *2*	IT
112	14.4 m *2*	ε 56%, β- 44%
112m	20.9 m *2*	IT
113	4.3% *2*	
113m	1.658 h *1*	IT
114	71.9 s *1*	β- 99.5%, ε 0.5%
114m	49.51 d *1*	IT 95.7%, ε 4.3%
115	4.41×10^{14} y *25*	β-
	95.7% *2*	
115m	4.486 h *4*	IT 95%, β- 5%
116	14.10 s *3*	β- > 99.94%, ε < 0.06%
116m	54.15 m *6*	β-

Isotope Z El A	T1/2 or Abundance	Decay Mode
49 In 116m	2.18 s *4*	IT
117	43.8 m *7*	β-
117m	116.5 m *7*	β- 52.9%, IT 47.1%
118	5.0 s *3*	β-
118m	4.45 m *5*	β-
118m	8.5 s *3*	IT 98.5%, β- 1.5%
119	2.4 m *1*	β-
119m	18.0 m *3*	β- 97.5%, IT 2.5%
120	44.4 s *10*	β-
120	3.08 s *8*	β-
121	23.1 s *6*	β-
121m	3.88 m *10*	β- 98.8%, IT 1.2%
122	10.0 s *5*	β-
122	1.5 s *3*	β-
123	5.98 s *6*	β-
123m	47.8 s *5*	β-
124	3.17 s *5*	β-
124m	2.4 s *4*	β-
125	2.33 s *4*	β-
125m	12.2 s *1*	β-
126	1.45 s *22*	β-
126m	1.5 s *2*	β-
127	1.15 s *5*	β-
127m	3.76 s *3*	β-, β-n
128	0.9 s *1*	β-, β-
129	0.59 s *2*	β-, β-n
129m	1.26 s *2*	β-, β-n
130	0.51 s	β-, β-n
130	0.53 s *5*	β-, β-n
131	0.27 s *2*	β-, β-n
132	0.22 s	β-, β-n
50 Sn 103	7 s *3*	ε, εp
104		ε
105	31 s	ε, εp
106	2.10 m *15*	ε
107	2.90 m *5*	ε
108	10.30 m *8*	ε
109	18.0 m *2*	ε
110	4.11 h *10*	ε
111	35.3 m *8*	ε
112	0.97% *1*	
113	115.09 d *4*	ε
113m	21.4 m *4*	IT 91.1%, ε 8.9%
114	0.65% *1*	
115	0.36% *1*	
116	14.53% *11*	
117	7.68% *7*	
117m	13.61 d *4*	IT
118	24.22% *11*	
119	8.58% *4*	
119m	293.0 d *13*	IT
120	32.59% *10*	
121	27.06 h *4*	β-
121m	55 y *5*	IT 77.6%, β- 22.4%
122	4.63% *3*	
123	129.2 d *4*	β-
123m	40.08 m *7*	β-
124	5.79% *5*	
125	9.64 d *3*	β-
125m	9.52 m *5*	β-
126	$\approx1.0\times10^{5}$ y	β-
127	2.10 h *4*	β-
127m	4.13 m *3*	β-
128	59.1 m *5*	β-
128m	6.5 s *5*	IT

TABLE I (cont.)

Isotope Z El A	T1/2 or Abundance	Decay Mode
50 Sn 129	2.16 m *4*	β-
129m	6.7 m *4*	β-, IT 0.0002%
130	3.72 m *11*	β-
130m	1.7 m *1*	β-
131	61 s *3*	β-
131m	39 s	β-
132	40 s *1*	β-
133	1.47 s	β-, β-n
134	1.04 s *2*	β-, β-n 17%
51 Sb 108	7.0 s *5*	ε, εp
109	17.0 s *7*	ε
110	23.0 s *4*	ε
111	75 s *1*	ε
112	51.4 s *10*	ε
113	6.67 m *7*	ε
114	3.49 m *3*	ε
115	32.1 m *3*	ε
116	15.8 m *8*	ε
116m	60.3 m *6*	ε
117	2.80 h *1*	ε
118	3.6 m	ε
118m	5.00 h *1*	ε
119	38.1 h *2*	ε
120	15.89 m *4*	ε
120	5.76 d *2*	ε
121	57.3% *9*	
122	2.70 d *1*	β- 97.62%, ε 2.38%
122m	4.2 m *2*	IT
123	42.7% *9*	
124	60.20 d *3*	β-
124m	93 s *5*	IT 75%, β- 25%
124m	20.2 m *2*	IT
125	2.73 y *3*	β-
126	12.4 d *1*	β-
126m	19.0 m *3*	β- 86%, IT 14%
126m	≈11 s	IT
127	3.85 d *5*	β-
128	9.01 h *3*	β-
128m	10.4 m *2*	β- 96.4%, IT 3.6%
129	4.40 h *1*	β-
129	17.7 m	β-
130	38.4 m	β-
130m	6.3 m *2*	β-
131	23 m *2*	β-
132	4.1 m	β-
132	3.07 m	β-
133	2.5 m	β-
134	0.85 s *10*	β-
134	10.43 s *14*	β-, β-n 0.1%
135	1.71 s	β-, β-n 20%
136	0.82 s *2*	β-, β-n 32%
52 Te 106	0.06 ms	α
107	3.6 ms *+6-4*	α 70%, ε 30%
108	2.1 s *1*	α 68%, ε 32%, εp
109	4.6 s *3*	ε 96%, εp, α 4%
110	18.6 s *8*	ε, α
111	19.3 s *4*	ε, εp, α
112	2.0 m *2*	ε
113	1.7 m *2*	ε
114	15.2 m *7*	ε
115	5.8 m *2*	ε
115m	6.7 m *4*	ε
116	2.49 h *4*	ε
117	62 m *2*	ε
118	6.00 d *2*	ε
119	16.05 h *5*	ε

Isotope Z El A	T1/2 or Abundance	Decay Mode
52 Te 119m	4.69 d *4*	ε
120	0.096% *2*	
121	16.78 d *35*	ε
121m	154 d *7*	IT 88.6%, ε 11.4%
122	2.60% *1*	
123	1.3×10^{13} y	ε
	0.908% *3*	
123m	119.7 d *1*	IT
124	4.816% *8*	
125	7.14% *1*	
125m	58 d *1*	IT
126	18.95% *1*	
127	9.35 h *7*	β-
127m	109 d *2*	IT 97.6%, β- 2.4%
128	$>8.\times10^{24}$ y	2β-
	31.69% *2*	
129	69.6 m *2*	β-
129m	33.6 d *1*	IT 64%, β- 36%
130	2.51×10^{21} y *27*	2β-
	33.80% *2*	
131	25.0 m *1*	β-
131m	30 h *2*	β- 77.8%, IT 22.2%
132	78.2 h *8*	β-
133	12.45 m *28*	β-
133m	55.4 m *4*	β- 83%, IT 17%
134	41.8 m *8*	β-
135	19.2 s	β-
136	18 s	β-, β-n 0.7%
137	3.5 s *5*	β-, β-n 2%
138	1.4 s *4*	β-, β-n 6%
53 I 110	0.65 s *2*	ε 83%, α 17%, εp, εα
111	7.5 s	ε 99.9%, α 0.1%
112	3.42 s *11*	ε, εp, εα, α
113	5.9 s *5*	ε, εα, α
114	2.1 s *2*	ε
115	28 s	ε
116	2.91 s *15*	ε
117	2.3 m *1*	ε
118	14.3 m	ε
118m	8.5 m *5*	ε, IT
119	19.1 m *4*	ε
120	81.0 m *6*	ε
120m	53 m *4*	ε
121	2.12 h *1*	ε
122	3.62 m *6*	ε
123	13.2 h *1*	ε
124	4.18 d *2*	ε
125	60.14 d *11*	ε
126	13.02 d *7*	ε 56.3%, β- 43.7%
127	100%	
128	24.99 m *2*	β- 93.1%, ε 6.9%
129	1.57×10^{7} y *4*	β-
130	12.36 h *1*	β-
130m	9.0 m *1*	IT 83%, β- 17%
131	8.04 d *1*	β-
132	2.30 h *3*	β-
132m	83.6 m *17*	IT 86%, β- 14%
133	20.8 h *1*	β-
133m	9 s	IT
134	52.6 m *4*	β-
134m	3.69 m *7*	IT 97.7%, β- 2.3%
135	6.61 h *1*	β-
136	84 s *1*	β-
136m	45 s *1*	β-
137	24.5 s *2*	β-, β-n 6.4%

Isotope Z El A	T1/2 or Abundance	Decay Mode
53 I 138	6.41 s *5*	β-, β-n 5%
139	2.30 s *5*	β-, β-n 10%
140	0.86 s *4*	β-, β-n 14%
141	0.43 s *2*	β-, β-n 21.2%
142	0.2 s	β-
54 Xe 110	0.2 s	ε, α
111	0.7 s	ε
111	0.9 s *2*	ε, α
112	2.8 s *2*	ε 99.16%, α 0.84%
113	2.8 s *2*	ε, εp, εα, α
114	10.0 s *4*	ε
115	18 s *4*	ε, εp 0.3%
116	56 s *2*	ε
117	61 s *2*	ε, εp 0.003%
118	4 m	ε
119	5.8 m *3*	ε
120	40 m *1*	ε
121	40.1 m *2*	ε
122	20.1 h *1*	ε
123	2.08 h *2*	ε
124	0.10% *1*	
125	16.9 h *2*	ε
125m	57 s *1*	IT
126	0.09% *1*	
127	36.4 d *1*	ε
127m	69.2 s *9*	IT
128	1.91% *3*	
129	26.4% *6*	
129m	8.89 d *2*	IT
130	4.1% *1*	
131	21.2% *4*	
131m	11.9 d *1*	IT
132	26.9% *5*	
133	5.245 d *6*	β-
133m	2.188 d *8*	IT
134	10.4% *2*	
134m	290 ms *17*	IT
135	9.09 h *1*	β-
135m	15.29 m *3*	IT, β- 0.004%
136	8.9% *1*	
137	3.818 m *13*	β-
138	14.08 m *8*	β-
139	39.68 s *14*	β-
140	13.60 s *10*	β-
141	1.73 s *1*	β-, β-n 0.044%
142	1.22 s *2*	β-, β-n 0.41%
143	0.30 s *3*	β-
143	0.96 s *2*	β-
144	1.15 s *20*	β-
145	0.9 s *3*	β-, β-n
55 Cs 114	0.57 s *2*	ε, εp 7%, εα 0.16%, α 0.02%
115	1.4 s *8*	ε, εp 0.3%
116	3.81 s *16*	ε, εp, εα
116	0.71 s *8*	ε, εp, εα
117	6.5 s	ε
118	16.4 s *12*	ε, εp 0.04%, εα 0.0024%
119	37.7 s *10*	ε, εα?
119	28 s *1*	
120	64 s	ε, εp, εα
120	60.2 s *15*	ε
121	136 s	ε
121m	121 s	IT, ε
122	4.5 m *2*	ε
122	21.0 s *7*	ε
123	5.87 m *5*	ε

Isotope Z El A	T1/2 or Abundance	Decay Mode
55 Cs 123m	1.60 s *15*	IT
124	30.8 s *5*	ε
124m	6.3 s *2*	IT
125	45 m *1*	ε
126	1.64 m *2*	ε
127	6.25 h *10*	ε
128	3.62 m *2*	ε
129	32.06 h *6*	ε
130	29.2 m	ε 98.4%, β- 1.6%
131	9.69 d *1*	ε
132	6.475 d *10*	ε 98%, β- 2%
133	100%	
134	2.062 y *5*	β-, ε 0.0003%
134m	2.91 h *1*	IT
135	3×10^6 y	β-
135m	53 m *2*	IT
136	13.16 d *3*	β-
136	19 s *2*	β-
137	30.17 y	β-
138	32.2 m *1*	β-
138m	2.90 m *10*	IT 81%, β- 19%
139	9.27 m *5*	β-
140	63.7 s *3*	β-
141	24.94 s *6*	β-, β-n 0.029%
142	1.8 s	β-, β-n 0.28%
143	1.78 s *1*	β-, β-n 1.7%
144	1.02 s *3*	β-, β-n 3%
144?	<1 s	β-
145	0.59 s *1*	β-, β-n 12%
146	0.343 s *7*	β-, β-n 14%
147	0.22 s *1*	β-, β-n
148	170 ms *7*	β-
56 Ba 117	1.9 s *2*	ε, εp
119	5.35 s *30*	ε, εp
120	32 s	ε
121	29.7 s *15*	ε, εp 0.02%
122	2.0 m	ε
123	2.7 m *4*	ε
124	11.9 m *10*	ε
125	3.5 m *4*	ε
125	8 m	ε
126	100 m *2*	ε
127	12.7 m *4*	ε
128	2.43 d *5*	ε
129	2.23 h *11*	ε
129m	2.17 h *4*	ε
130	0.106% *2*	
131	11.8 d *2*	ε
131m	14.6 m *2*	IT
132	0.101% *2*	
133	10.74 y *5*	ε
133m	38.9 h *1*	IT 99.99%, ε 0.01%
134	2.417% *27*	
135	6.592% *18*	
135m	28.7 h *2*	IT
136	7.854% *39*	
136m	0.306 s	IT
137	11.23% *4*	
137m	2.5513 m *7*	IT
138	71.70% *7*	
139	84.63 m *34*	β-
140	12.746 d *10*	β-
141	18.27 m *7*	β-
142	10.6 m *2*	β-
143	14.5 s *5*	β-
144	11.4 s *5*	β-

TABLE I (cont.)

Isotope Z El A	T1/2 or Abundance	Decay Mode
56 Ba 145	4.0 s	β-
146	2.20 s *3*	β-
147	0.72 s *7*	β-, β-n
148	0.607 s *25*	β-, β-n
57 La 123	17 s *3*	ε
124	29 s *3*	ε
125	76 s *6*	ε
126	1.0 m *3*	ε
127	3.8 m *5*	ε
127m	5.0 m ?	
128	5.0 m *3*	ε
129	11.6 m *2*	ε
129m	0.56 s *5*	IT
130	8.7 m *1*	ε
131	59 m *2*	ε
132	4.8 h *2*	ε
132m	24.3 m *5*	IT 76%, ε 24%
133	3.912 h *8*	ε
134	6.45 m *16*	ε
135	19.5 h	ε
136	9.87 m *3*	ε
137	6×10^{4} y *2*	ε
138	1.28×10^{11} y *12*	ε 66.7%, β- 33.3%
	0.09% *1*	
139	99.91% *1*	
140	40.272 h *7*	β-
141	3.92 h *3*	β-
142	91.1 m *5*	β-
143	14.23 m *14*	β-
144	40.9 s *4*	β-
145	24.8 s *20*	β-
146	6.27 s *10*	β-
146m	10.0 s *1*	β-
147	4.4 s *5*	β-, β-n
148	1.05 s *1*	β-
149	1.2 s *4*	β-
58 Ce 124	6 s *2*	ε
125	9 s	ε, εp
126	50 s *6*	ε
127	32 s *4*	ε
128	6 m	ε
129	3.5 m *5*	ε
130	25 m *2*	ε
131	10 m *1*	ε
131	5 m *1*	ε
132	3.5 h	ε
133	5.40 h *5*	ε
133	97 m	ε
134	75.9 h *9*	ε
135	17.6 h	ε
135m	20 s	IT
136	0.19% *1*	
137	9.0 h *3*	ε
137m	34.4 h *3*	IT 99.22%,
		ε 0.78%
138	0.25% *1*	
139	137.66 d *13*	ε
139m	56.4 s *5*	IT
140	88.48% *10*	
141	32.501 d *5*	β-
142	$>5\times10^{16}$ y	
	11.08% *10*	
143	33.0 h *2*	β-
144	284.4 d	β-
145	2.98 m *15*	β-
146	13.52 m *13*	β-
147	56.4 s *12*	β-

Isotope Z El A	T1/2 or Abundance	Decay Mode
58 Ce 148	56 s *1*	β-
149	5.2 s *3*	β-
150	4.0 s *6*	β-
151	1.02 s *6*	β-
59 Pr 121	1.4 s *8*	ε, εp
129	24 s *5*	ε
130	28 s	ε
132	1.6 m *3*	ε
133	6.5 m *3*	ε
134	17 m *2*	ε
134m	11 m	ε
135	25 m	ε
136	13.1 m *1*	ε
137	1.28 h *2*	ε
138	1.45 m *5*	ε
138m	2.1 h *1*	ε
139	4.41 h *4*	ε
140	3.39 m *1*	ε
141	100%	
142	19.12 h *4*	β- 99.98%,
		ε 0.02%
142m	14.6 m *5*	IT
143	13.58 d *3*	β-
144	17.28 m *5*	β-
144m	7.2 m *2*	IT 99.96%,
		β- 0.04%
145	5.98 h *2*	β-
146	24.15 m *18*	β-
147	13.6 m *5*	β-
148	2.27 m *4*	β-
148m	2.0 m *1*	β-
149	2.26 m *7*	β-
150	6.19 s *16*	β-
151	4.0 s *7*	β-
152	3.2 s	β-
60 Nd 129	5.9 s *6*	ε, εp
130	28 s	ε
132	1.8 m	ε
133	1.2 m	ε
134	8.5 m *15*	ε
135	12 m	ε
135m	≈5.5 m	ε
136	50.65 m *33*	ε
137	38.5 m *15*	ε
137m	1.60 s *15*	IT
138	5.04 h *9*	ε
139	29.7 m *5*	ε
139m	5.5 h *2*	ε 88%, IT 12%
140	3.37 d *2*	ε
141	2.49 h *3*	ε
141m	62.4 s *9*	IT 99.97%,
		ε 0.03%
142	27.13% *10*	
143	12.18% *5*	
144	2.1×10^{15} y *4*	α
	23.80% *10*	
145	$>6\times10^{16}$ y	α
	8.30% *5*	
146	17.19% *8*	
147	10.98 d *1*	β-
148	5.76% *3*	
149	1.725 h *7*	β-
150	$>1\times10^{18}$ y	2β-
	5.64% *3*	
151	12.44 m *7*	β-
152	11.4 m *2*	β-
154	40 s *10*	β-

Isotope Z El A	T1/2 or Abundance	Decay Mode
61 Pm 132	4 s	ε
133	12 s	ε
134	24 s *2*	ε
135	0.8 m	ε
136	107 s *6*	ε
137	2.4 m *1*	ε
138	3.24 m *5*	ε
139	4.15 m *5*	ε
140	9.2 s *2*	ε
140m	5.95 m *5*	ε
141	20.90 m *5*	ε
142	40.5 s *5*	ε
143	265 d *7*	ε
144	363 d *14*	ε
145	17.7 y *4*	ε, αw
146	5.53 y *5*	ε 66.1%, β- 33.9%
147	2.6234 y *2*	β-
148	5.370 d *9*	β-
148m	41.29 d *11*	β- 95.4%, IT 4.6%
149	53.08 h *5*	β-
150	2.68 h *2*	β-
151	28.40 h *4*	β-
152	4.1 m *1*	β-
152m	7.52 m *8*	β-
152m	15 m *1*	β-, IT
153	5.4 m *2*	β-
154	1.7 m *2*	β-
154	2.7 m *1*	β-
155	48 s *4*	β-
62 Sm 133	32.0 s	ε, εp
134	12 s *3*	ε
135	10 s	ε, εp
136	42 s	ε
137	44 s *8*	ε
138	3.0 m *3*	ε
139	2.57 m *10*	ε
139m	9.5 s *10*	IT 93.7%, ε 6.3%
140	14.82 m *10*	ε
141	10.2 m *2*	ε
141m	22.6 m *2*	ε 99.69%, IT 0.31%
142	72.49 m *5*	ε
143	8.83 m *1*	ε
143m	66 s *2*	IT 99.76%, ε 0.24%
144	3.1% *1*	
145	340 d *3*	ε
146	10.3×10^{7} y *5*	α
147	1.06×10^{11} y *2*	α
	15.0% *2*	
148	7×10^{15} y *3*	α
	11.3% *1*	
149	$>2\times10^{15}$ y	α?
	13.8% *1*	
150	7.4% *1*	
151	90 y *6*	β-
152	26.7% *2*	
153	46.7 h *1*	β-
154	22.7% *2*	
155	22.1 m *2*	β-
156	9.4 h *2*	β-
157	8.0 m *5*	β-
158	5.51 m *9*	β-
63 Eu 138	35 s *6*	ε
138	1.5 s *4*	ε
139	22 s *3*	ε
140	20 s *+15-1*	ε

Isotope Z El A	T1/2 or Abundance	Decay Mode
63 Eu 140	1.3 s *2*	ε
141	40.0 s *7*	ε
141m	3.3 s *3*	ε 67%, IT 33%
142	2.4 s *2*	ε
142m	1.22 m *2*	ε
143	2.63 m *5*	ε
144	10.2 s *1*	ε
145	5.93 d *4*	ε
146	4.59 d *3*	ε
147	24 d *1*	ε, αw
148	54.5 d *5*	ε, αw
149	93.1 d *4*	ε
150	12.62 h *10*	β- 89%, ε 11%
150	35.8 y *10*	ε
151	47.8% *5*	
152	13.33 y *4*	ε 72.08%, β- 27.92%
152m	9.32 h *1*	β- 72%, ε 28%
152m	96 m *1*	IT
153	52.2% *5*	
154	8.8 y *1*	β- 99.98%, ε 0.02%
154m	46.0 m *3*	IT
155	4.96 y *1*	β-
156	15.19 d *6*	β-
157	15.15 h *4*	β-
158	45.9 m *2*	β-
159	18.1 m *1*	β-
160	44 s *4*	β-
64 Gd 142	1.5 m *3*	ε
143	39 s *2*	ε
143m	1.83 m	ε, IT?
144	4.5 m *1*	ε
145	23.9 m *1*	ε
145m	85 s *3*	IT 95.3%, ε 4.7%
146	48.27 d *10*	ε
147	38.1 h *1*	ε
148	74.6 y *30*	α
149	9.4 d *3*	ε, αw
150	1.79×10^{6} y *8*	α
151	120 d *20*	ε, αw
152	1.08×10^{14} y *8*	α
	0.20% *1*	
153	241.6 d *2*	ε
154	2.18% *3*	
155	14.80% *5*	
156	20.47% *4*	
157	15.65% *3*	
158	24.84% *12*	
159	18.56 h *8*	β-
160	21.86% *4*	
161	3.66 m *5*	β-
162	8.4 m *2*	β-
163	68 s *3*	β-
65 Tb 144	5 s	ε
145	30 s	ε
146	8 s *4*	ε
146m	23 s *2*	ε
147	1.65 h *10*	ε
147	1.83 m *6*	ε
148	60 m *1*	ε
148m	2.20 m *5*	ε
149	4.13 h *2*	ε 82.8%, α 17.2%
149m	4.16 m *4*	ε, α 0.022%
150	3.27 h *10*	ε, α≤0.05%
150	5.8 m *2*	ε
151	17.6 h *1*	ε, α 0.01%

TABLE I (cont.)

Isotope Z El A	T1/2 or Abundance	Decay Mode
65 Tb 151m	50 s	IT
152	17.5 h *3*	ε
152m	4.3 m *2*	IT 78.9%, ε 21.1%
153	2.34 d *1*	ε
154	21.4 h *5*	ε
154m	9.0 h *5*	ε 78.2%, IT 21.8%
154m	22.6 h *6*	ε 98.2%, IT 1.8%
155	5.32 d *6*	ε
156	5.34 d *9*	ε
156m	5.0 h *1*	IT, ε, β-w
156m	24.4 h *10*	IT
157	150 y *30*	ε
158	150 y *30*	ε 82%, β- 18%
158m	10.5 s *2*	IT
159	100%	
160	72.3 d *2*	β-
161	6.90 d *2*	β-
162	7.76 m *10*	β-
163	19.5 m *3*	β-
164	3.0 m *1*	β-
165	2.11 m *10*	β-
66 Dy 145	18 s	ε
146	29 s *3*	ε
147	80 s	ε
147m	58 s	IT, ε, εp
148	3.1 m *1*	ε
149	4.23 m *18*	ε
150	7.17 m *2*	ε 64%, α 36%
151	16.9 m *5*	ε 94.4%, α 5.6%
152	2.38 h *2*	ε 99.9%, α 0.1%
153	6.4 h *1*	ε 99.99%, α 0.01%
154	3×10^{6} y	α
155	10.0 h *3*	ε
156	$>1.0\times10^{18}$ y 0.06% *1*	
157	8.1 h *1*	ε
158	0.10% *1*	
159	144.4 d *2*	ε
160	2.34% *5*	
161	18.9% *1*	
162	25.5% *2*	
163	24.9% *2*	
164	28.2% *2*	
165	2.334 h *6*	β-
165m	1.258 m *6*	IT 97.76%, β- 2.24%
166	81.6 h *1*	β-
167	6.2 m	β-
168	8.5 m *5*	β-
67 Ho 146	3.9 s *8*	ε
147	?	ε, εp
148	2.2 s *11*	ε
148m	9 s *1*	ε
149	21.4 s *18*	ε
150	72 s *10*	ε
150	24 s	ε
151	35.6 s *4*	ε 90%, α 10%
151	47 s *2*	ε 80%, α 20%
152	2.35 m *11*	ε 88%, α 12%
152	52.3 s *5*	ε 89.5%, α 10.5%
153	2.0 m *1*	ε 99.95%, α 0.05%
153m	9.3 m *5*	ε 99.82%, α 0.18%
154	11.8 m *5*	ε, α 0.017%
154	3.2 m *1*	ε, α<0.002%
155	48 m *1*	ε, α
156	2 m	ε
156m	55.6 m *6*	IT, ε

Isotope Z El A	T1/2 or Abundance	Decay Mode
67 Ho 156?	7.4 m	ε
157	12.6 m *2*	ε
158	11.3 m *4*	ε
158m	21.3 m *23*	ε
158m	27 m *2*	IT 65%, ε 35%
159	33 m *1*	ε
159m	8.30 s *8*	IT
160	25.6 m *3*	ε
160m	5.02 h *5*	IT 65%, ε 35%
160m	<2 m	?
161	2.48 h *5*	ε
161m	6.73 s *10*	IT
162	15 m *1*	ε
162m	67 m *1*	IT 63%, ε 37%
163	>10 y	ε
163m	1.09 s *3*	IT
164	29 m *1*	ε 58%, β- 42%
164m	37.5 m *+15-5*	IT
165	100%	
166	26.80 h *2*	β-
166m	1.20×10^{3} y *18*	β-
167	3.1 h *1*	β-
168	3.0 m *1*	β-
169	4.7 m *1*	β-
170	2.8 m	β-
170	43 s	β-
68 Er 147	2.5 s	ε, εp
148	4.5 s *4*	ε
149	9 s *2*	ε, εp
150	18.5 s *7*	ε
151	23 s *2*	ε
152	10.3 s	α 90%, ε 10%
153	37.1 s	α 53%, ε 47%
154	3.75 m *12*	ε, α 0.5%
155	5.3 m *3*	ε≤99.98%, α≥0.02%
156	20 m	ε
157	25 m *3*	ε
158	2.25 h *7*	ε
159	36 m	ε
160	28.59 h *9*	ε
161	3.21 h *3*	ε
162	0.14% *1*	
163	75.0 m *4*	ε
164	1.61% *1*	
165	10.36 h *4*	ε
166	33.6% *2*	
167	22.95% *13*	
167m	2.28 s *3*	IT
168	26.8% *2*	
169	9.40 d *2*	β-
170	14.9% *1*	
171	7.52 h *3*	β-
172	49.3 h *5*	β-
173	1.4 m *1*	β-
69 Tm 147	0.5 s	p
148	0.7 s *2*	ε
150	3.5 s *6*	ε
152	5 s	ε
153	1.59 s *8*	α≥95%, ε≤5%
154	8.3 s	ε, α
154	3.4 s	α, ε
155	25 s	α, ε
156	80 s *3*	ε, α
156	19 s *3*	α
157	3.5 m *2*	ε, αw
158	4.02 m *10*	ε

Isotope Z El A	T1/2 or Abundance	Decay Mode
69 Tm 159	9 m	ε
160	9.2 m *4*	ε
161	38 m *4*	ε
162	22.0 m *7*	ε
162m	24.3 s *17*	IT 90%, ε 10%
163	1.81 h *6*	ε
164	2.0 m *1*	ε
164m	5.1 m *1*	IT 80%, ε 20%
165	30.06 h *11*	ε
166	7.70 h *3*	ε
167	9.24 d *2*	ε
168	93.1 d *1*	ε, β-?
169	100%	
170	128.6 d *3*	β- 99.85%, ε 0.15%
171	1.92 y *1*	β-
172	63.6 h *2*	β-
173	8.24 h *8*	β-
174	5.4 m *1*	β-
175	15.2 m *5*	β-
176	1.9 m *1*	β-
70 Yb 153	4.0 s *5*	ε
154	0.42 s *2*	α
155	1.65 s *15*	α≈90%, ε
156	24 s *1*	ε, α 21%
157	38.6 s *10*	ε 99.5%, α 0.5%
158	1.38 m *14*	ε, α 0.003%
159	12 s	ε, α
160	4.8 m *2*	ε
161	4.2 m *2*	ε
162	18.87 m *19*	ε
163	11.05 m *25*	ε
164	75.8 m *17*	ε
165	9.9 m	ε
166	56.7 h *1*	ε
167	17.5 m *2*	ε
168	0.13% *1*	
169	32.022 d *8*	ε
169m	46 s *2*	IT
170	3.05% *5*	
171	14.3% *2*	
172	21.9% *3*	
173	16.12% *18*	
174	31.8% *4*	
175	4.19 d *1*	β-
176	12.7% *1*	
176m	11.4 s *5*	IT
177	1.9 h *1*	β-
177m	6.41 s *2*	IT
178	74 m *3*	β-
179	8 m	β-
71 Lu 151	0.09 s	p
154	1.0 s	ε
155	0.07 s *2*	α, ε
156	≈0.5 s	α, ε
156	0.23 s *3*	α
157	5.5 s *3*	ε 94%, α 6%
158	10.4 s *1*	ε>98.5%, α<1.5%
159	12 s	ε, α
160	35.5 s *8*	ε
161	72 s *6*	ε
162	1.37 m *2*	ε
162m	≈1.5 m	IT
162m	≈1.9 m	IT
163	4.1 m	ε
164	3.17 m	ε
164?	2 m	

Isotope Z El A	T1/2 or Abundance	Decay Mode
71 Lu 165	12 m *1*	ε
166	2.8 m	ε
166m	1.41 m *10*	ε 58%, IT 42%
166m	2.12 m *10*	ε>80%, IT<20%
167	51.5 m *10*	ε
168	5.5 m	ε
168m	6.7 m *4*	ε, IT?
169	34.06 h *5*	ε
169m	160 s *10*	IT
170	2.00 d *3*	ε
170m	0.67 s *10*	IT
171	8.24 d *3*	ε
171m	79 s *2*	IT
172	6.70 d *3*	ε
172m	3.7 m *5*	IT
173	1.37 y *1*	ε
174	3.31 y *5*	ε
174m	142 d *2*	IT 99.35%, ε 0.65%
175	97.41% *2*	
176	3.60×10^{10} y *16*	β- 2.59% *2*
176m	3.68 h *1*	β-
177	6.71 d *1*	β-
177m	160.9 d *3*	β- 79%, IT 21%
178	28.4 m *2*	β-
178m	23 m	β-
179	4.59 h *6*	β-
180	5.7 m *1*	β-
181	3.5 m *3*	β-
182	2.0 m	β-
183	58 s	β-
72 Hf 154	2 s	ε
155	0.9 s	ε
156	25 ms *4*	α
157	110 ms *6*	α 91%, ε 9%
158	2.9 s *2*	ε 54%, α 46%
159	5.6 s	ε, α
160	≈12 s	ε, α
161	17 s *2*	α
162	37.6 s *8*	ε
163	40 s	ε
164	2.8 m *2*	ε
166	6.77 m *30*	ε
167	2.05 m *5*	ε
168	25.95 m *2*	ε
169	3.24 m *4*	ε
170	16.01 h *13*	ε
171	12.1 h *4*	ε
172	1.87 y *3*	ε
173	23.6 h	ε
174	2.0×10^{15} y *4* 0.162% *2*	α
175	70 d *2*	ε
176	5.206% *4*	
177	18.606% *3*	
177m	1.08 s *6*	IT
177m	51.4 m *5*	IT
178	27.297% *3*	
178m	4.0 s *2*	IT
178m	31 y *1*	IT
179	13.629% *5*	
179m	18.68 s *6*	IT
179m	25.1 d	IT
180	35.100% *6*	
180m	5.5 h *1*	IT
181	42.39 d *6*	β-

TABLE I (cont.)

Isotope Z El A	T1/2 or Abundance	Decay Mode
72 Hf 182	9×10^{6} y *3*	β-
182m	61.5 m *15*	β- 54%, IT 46%
183	64 m *1*	β-
184	4.12 h *5*	β-
73 Ta 157	5.3 ms *18*	α
158	36.8 ms *16*	α 93%, ε 7%
159	0.6 s	α, ε
160	?	α
161	?	α
164	13.6 s *2*	ε, α 0.02%
166	32 s	ε
167	2.9 m *15*	ε
168	2.5 m *12*	ε
169	4.9 m *4*	ε
170	6.76 m *6*	ε
171	23.3 m *3*	ε
172	36.8 m *3*	ε
173	3.65 h *5*	ε
174	1.18 h *5*	ε
175	10.5 h *2*	ε
176	8.08 h *7*	ε
177	56.6 h *1*	ε
178	9.31 m *3*	ε
178	2.4 h	ε
179	664.9 d *42*	ε
180	8.1 h *1*	ε 87%, β- 13%
180m	$>1.2\times10^{15}$ y 0.012% *2*	ε, β-
181	99.988% *2*	
182	114.5 d	β-
182m	0.283 s	IT
182m	15.84 m *10*	IT
183	5.1 d *1*	β-
184	8.7 h *1*	β-
185	49 m *2*	β-
186	10.5 m *5*	β-
74 W 158	?	α
159	7 ms	α
160	41 ms *20*	α
161	410 ms *40*	α 82%, ε
162	1.39 s *4*	ε 54%, α 46%
163	2.8 s	ε, α≈50%
164	6.4 s *8*	ε 97.4%, α 2.6%
165	5.1 s *5*	ε, α 0.15%
166	16 s	α
170?	4 m *1*	ε
171?	9.0 m *15*	ε
172	6.7 m *10*	ε
173	16.5 m *5*	ε
174	29 m *1*	ε
175	34 m *1*	ε
176	2.5 h	ε
177	135 m *3*	ε
178	21.7 d *3*	ε
179	37.5 m *5*	ε
179m	6.4 m	IT 99.8%, ε 0.2%
180	$>1.1\times10^{15}$ y 0.13% *3*	
181	120.98 d *12*	ε
182	26.3% *2*	
183	14.3% *1*	
183m	5.15 s *3*	IT
184	$>3\times10^{17}$ y 30.67% *15*	
185	75.1 d *3*	β-
185m	1.67 m *3*	IT
186	28.6% *2*	

Isotope Z El A	T1/2 or Abundance	Decay Mode
74 W 187	23.9 h *1*	β-
188	69.4 d *5*	β-
189	11.5 m *3*	β-
190	30.0 m *15*	β-
75 Re 161	10 ms *+15-5*	α
162	100 ms *30*	α>3%
163	0.26 s	α, ε
164	0.88 s *24*	α 58%, ε 42%
165	2.4 s *6*	ε, α 13%
166	2.2 s	α
167	2.0 s	α
168	2.9 s	ε, α
169	short	α
170	8 s	ε
172	55 s	ε
172	15 s	ε
173?	2 m	α
174	2.3 m *1*	ε
175	4.6 m	ε
176	5.3 m	ε
177	14.0 m *10*	ε
178	13.2 m *2*	ε
179	19.7 m *5*	ε
180	2.43 m *6*	ε
181	19.9 h *7*	ε
182	12.7 h *2*	ε
182m	64.0 h *5*	ε
183	70.0 d *11*	ε
184	38.0 d *5*	ε
184m	165 d *5*	IT 74.7%, ε 25.3%
185	37.40% *2*	
186	90.64 h *9*	β- 93.5%, ε 6.5%
186m	2.0×10^{5} y	IT
187	5×10^{10} y *2* 62.60% *2*	β-
188	16.98 h *2*	β-
188m	18.6 m *1*	IT
189	24.3 h	β-
190	3.1 m *3*	β-
190m	3.2 h *2*	β- 54.5%, IT 45.5%
191	9.8 m *5*	β-
192	16 s *1*	β-
76 Os 163	?	α
164	41 ms *20*	α
165	65 ms *+70-30*	α
166	0.18 s	α, ε
167	0.7 s	α, ε
168	2.1 s *2*	α, ε
169	3.2 s *2*	ε 84%, α 16%
170	7.1 s *5*	ε, α
171	8.0 s *7*	ε 98.3%, α 1.7%
172	19 s *2*	ε, α≤0.3%
173	16 s *5*	ε 99.98%, α 0.02%
174	44 s *4*	ε 99.98%, α 0.02%
175	1.4 m *1*	ε
176	3.6 m	ε
177	2.8 m	ε
178	5.0 m *4*	ε
179	7 m	ε
180	22 m *3*	ε
181	2.7 m *1*	ε
181	105 m *3*	ε
182	21.5 h	ε
183	13.0 h *5*	ε
183m	9.9 h *3*	ε 89%, IT 11%

Isotope Z El A	T1/2 or Abundance	Decay Mode
76 Os 184	$>1\cdot10^{17}$ y	
	0.02% *1*	
185	93.6 d *5*	ε
186	$2.0\cdot10^{15}$ y *11*	α
	1.58% *10*	
187	1.6% *1*	
188	13.3% *2*	
189	16.1% *3*	
189m	5.8 h	IT
190	26.4% *4*	
190m	9.9 m *1*	IT
191	15.4 d *1*	β-
191m	13.10 h *5*	IT
192	41.0% *3*	
192m	6.1 s	IT
193	30.5 h *4*	β-
194	6.0 y *2*	β-
195	6.5 m	β-
196	34.9 m *2*	β-
77 Ir 166	>5 ms	α
167	>5 ms	α
168		α
169	0.4 s *1*	α
170	1.0 s	α
171	1.5 s *1*	α
172	2.1 s	α
173	3.0 s *1*	α
174	4 s *1*	α, ε
175	4.5 s *10*	α
176	8 s *1*	α
177	21 s *2*	α
178	12 s	ε
179	4 m	ε
180	1.5 m *1*	ε
181	4.92 m *13*	ε
182	15 m *1*	ε
183	57 m *4*	ε
184	3.02 h *6*	ε
185	14.0 h *9*	ε
186	15.8 h *3*	ε
186	1.75 h *15*	ε
187	10.5 h *3*	ε
188	41.5 h *5*	ε
189	13.2 d	ε
190	11.78 d *10*	ε
190m	1.2 h	IT
190m	3.2 h *2*	ε 94.4%, IT 5.6%
191	37.3% *5*	
191m	4.94 s *3*	IT
191m	5.5 s *7*	IT
192	73.831 d *8*	β- 95.4%, ε 4.6%
192m	1.45 m *5*	IT 99.98%, β- 0.02%
192m	241 y *9*	IT
193	62.7% *5*	
193m	10.60 d *11*	IT
194	19.15 h *3*	β-
194m	171 d *11*	β-
195	2.8 h	β-
195m	3.8 h *2*	β- 96%, IT 4%
196	52 s *2*	β-
196m	1.40 h *2*	β-
197	5.8 m *5*	β-
197m	8.9 m *3*	β-, IT
198	8 s *1*	β-
78 Pt 168	?	α
169	2.5 ms	α

Isotope Z El A	T1/2 or Abundance	Decay Mode
78 Pt 170	6 ms	α
171	25 ms *9*	α
172	0.10 s	α
173	0.34 s	α 84%, ε
174	0.90 s *1*	α 83%, ε 17%
175	2.52 s *8*	α 64%, ε
176	6.33 s *15*	ε 58%, α 42%
177	11 s *2*	ε 91%, α 9%
178	21.0 s *7*	ε, α
179	43 s	ε, α 0.27%
180	52 s *3*	ε, α 0.3%
181	51 s *5*	ε, α≈0.06%
182	2.6 m *1*	ε≈99.98%, α≈0.02%
183	6.6 m *9*	ε, α 0.0013%
183m	43 s	ε
184	17.3 m *2*	ε, α≈0.001%
185	70.9 m *24*	ε
185m	33.0 m *8*	ε
186	2.0 h *1*	ε, α≈0.0001%
187	2.35 h *3*	ε
188	10.2 d *3*	ε>99.99%, α<0.01%
189	10.89 h *1*	ε
190	$6\cdot10^{11}$ y *1*	α
	0.01% *1*	
191	2.9 d *1*	ε
192	0.79% *5*	
193	50 y *9*	ε
193m	4.33 d *3*	IT
194	32.9% *5*	
195	33.8% *5*	
195m	4.02 d *1*	IT
196	25.3% *5*	
197	18.3 h *3*	β-
197m	94.4 m *8*	IT 96.7%, β- 3.3%
198	7.2% *2*	
199	30.8 m *4*	β-
199m	13.6 s *4*	IT
200	12.5 h *3*	β-
201	2.5 m *1*	β-
79 Au 174	120 ms *20*	α
175	≈0.1 s	α
176	1.25 s *30*	α
177	1.3 s *4*	α
178	2.6 s *5*	α
179	7.5 s	α
180	8.1 s	ε
181	11.4 s *5*	ε 98.9%, α 1.1%
182	21 s *2*	ε≈99.96%, α≈0.04%
183	42 s	ε, α 0.3%
184	53.0 s *14*	ε 99.98%, α 0.02%
185	4.3 m *8*	ε≤99.9%, α≥0.093%
185m	6.8 m *3*	ε, IT
186	10.7 m *5*	ε
186	<2 m	ε
187	8.0 m *4*	ε, α?
188	8.84 m *6*	ε
189	28.7 m	ε
189m	4.59 m *1*	ε, IT>0%
190	42.8 m *10*	ε
191	3.18 h *8*	ε
191m	0.92 s *11*	IT
192	4.94 h *9*	ε
193	17.65 h *15*	ε

TABLE I (cont.)

Isotope Z El A	T1/2 or Abundance	Decay Mode
79 Au 193m	3.9 s *3*	IT≈99.97%, ε≈0.03%
194	39.5 h *5*	ε
195	186.1 d	ε
195m	30.5 s *2*	IT
196	6.183 d *10*	ε 92.5%, β- 7.5%
196m	8.1 s *2*	IT
196m	9.7 h *1*	IT
197	100%	
197m	7.8 s *1*	IT
198	2.696 d *2*	β-
198m	2.30 d *4*	IT
199	3.139 d *7*	β-
200	48.4 m *3*	β-
200m	18.7 h *5*	β- 82%, IT 18%
201	26 m *1*	β-
202	28 s *2*	β-
203	53 s *2*	β-
204	40 s *3*	β-
80 Hg 177	0.17 s	α, ε
178	0.47 s *14*	α≈84%, ε≈16%
179	1.09 s	α 53%, ε 47%, εpw
180	2.9 s *3*	ε, α
181	3.6 s *3*	ε>87%, α<13%, εpw, εαw
182	11.2 s *10*	ε 91%, α 9%
183	8.8 s *5*	ε 88%, α 12%, εpw
184	30.6 s *3*	ε 98.75%, α 1.25%
185	50 s *2*	ε≤95%, α≥5%
185m	20 s *2*	ε, IT, α
186	1.38 m *10*	ε, α 0.02%
187	2.4 m *3*	ε, α>0.0001%
187	1.9 m *3*	ε, α>0.0002%
188	3.25 m *15*	ε>99.99%, α<0.01%
189	7.6 m	ε
189	8.6 m	ε
190	20.0 m *5*	ε
191	49 m *10*	ε
191m	50.8 m *15*	ε
192	4.85 h *20*	ε
193	3.80 h *15*	ε
193m	11.8 h *2*	ε 92%, IT 8%
194	520 y	ε
195	9.5 h	ε
195m	40.0 h	IT 54.2%, ε 45.8%
196	0.14% *10*	
197	64.1 h *1*	ε
197m	23.8 h *1*	IT 93%, ε 7%
198	10.02% *7*	
199	16.84% *11*	
199m	42.6 m *2*	IT
200	23.13% *11*	
201	13.22% *11*	
202	29.80% *14*	
203	46.60 d *2*	β-
204	6.85% *5*	
205	5.2 m *1*	β-
206	8.15 m *10*	β-
207	2.9 m *2*	β-
81 Tl 184	11 s *1*	ε 98%, α 2%
185m	1.8 s *2*	IT, α
186	28 s	ε, αw
186m	4 s	IT
187	50 s	ε
187m	15.60 s *12*	IT, ε, α
188	71 s *10*	ε

Isotope Z El A	T1/2 or Abundance	Decay Mode
81 Tl 188m	71 s *1*	ε
189	2.3 m	ε
189m	1.4 m	ε
190	2.6 m *3*	ε
190	3.7 m *3*	ε
191m	5.22 m *16*	ε
192	9.6 m *4*	ε
192	10.8 m *2*	ε
193	21.6 m *8*	ε
193m	2.11 m *15*	IT 75%, ε 25%
194	33.0 m *5*	ε
194m	32.8 m *2*	ε
195	1.16 h *5*	ε
195m	3.6 s *4*	IT
196	1.84 h *3*	ε
196m	1.41 h *2*	ε 95.5%, IT 4.5%
197	2.84 h *4*	ε
197m	0.54 s *1*	IT
198	5.3 h *5*	ε
198m	1.87 h *3*	ε 54%, IT 46%
199	7.42 h *8*	ε
200	26.1 h *1*	ε
201	73.1 h *2*	ε
202	12.23 d *2*	ε
203	29.524% *9*	
204	3.78 y *2*	β- 97.45%, ε 2.55%
205	70.476% *9*	
206	4.20 m *2*	β-
206m	3.76 m *4*	IT
207	4.77 m *2*	β-
207m	1.33 s *11*	IT
208	3.053 m	β-
209	2.20 m *7*	β-
210	1.30 m *3*	β-, β-n 0.007%
82 Pb 183		α
184	0.6 s	α
185	4.1 s *3*	α
186	7.9 s *16*	ε, α≈2.4%
187	18.3 s *3*	ε 98%, α 2%
187	15.2 s *3*	α, ε
188	24.5 s *15*	ε 78%, α 22%
189	51 s	ε>99%, α≈0.4%
190	1.2 m *1*	ε 99.1%, α 0.9%
191	1.33 m *8*	ε 99.99%, α 0.01%
191m	2.2 m	ε
192	3.5 m *1*	ε 99.99%, α 0.01%
193	5.8 m *2*	ε
194	10 m	ε
195	15 m	ε
195m	15.8 m *2*	ε
196	37 m *3*	ε, α<0.0001%
197	8 m	ε
197m	43 m	ε 81%, IT 19%, α
198	2.4 h *1*	ε
199	90 m *10*	ε
199m	12.2 m *3*	IT 90%, ε
200	21.5 h *4*	ε
201	9.33 h	ε
201m	61 s *2*	IT
202	5.3×10^{4} y	ε
202m	3.53 h	IT 90.5%, ε 9.5%
203	51.88 h	ε
203m	0.48 s *2*	IT
203m	6.3 s *2*	IT
204	$\geq1.4\times10^{17}$ y 1.4% *1*	

Isotope Z El A	T1/2 or Abundance	Decay Mode
82 Pb 204m	66.9 m	IT
205	1.52×10^{7} y 7	ε
206	24.1% *1*	
207	22.1% *1*	
207m	0.796 s	IT
208	52.4% *1*	
209	3.253 h *14*	β-
210	22.3 y *2*	β-, αw
211	36.1 m *2*	β-
212	10.64 h *1*	β-
213	10.2 m *3*	β-
214	26.8 m	β-
83 Bi 188		α
189	≤1.5 s	α
190	5.4 s *5*	α≈90%, ε
191	13 s *1*	ε, α≈40%
191m	20 s *15*	ε, α
192	42 s *5*	ε 80%, α 20%
193	64 s *4*	α 60%, ε 40%
193m	3.5 s *2*	ε, α≈25%
194	105 s *15*	ε>99.8%, α<0.2%
195	170 s *20*	ε>99.8%, α<0.2%
195m	90 s *5*	ε, α 4%
196	4.6 m *5*	ε
197	?	ε
197m	9.5 m *10*	ε≈99.89%, α≈0.11%
198	11.85 m *18*	ε
198m	7.7 s *5*	IT
199	27 m *1*	ε
199m	24.70 m *5*	ε, α
200	36.4 m *5*	ε
200m	31 m *2*	ε
200m	0.40 s *5*	IT
201	108 m *3*	ε
201m	59.1 m *6*	ε, IT 10%, αw
202	1.72 h *5*	ε
203	11.76 h *5*	ε, αw
204	11.22 h *10*	ε
205	15.31 d *4*	ε
206	6.243 d *3*	ε
207	32.2 y *9*	ε
208	3.68×10^{5} y *4*	ε
209	100%	
210	5.013 d *5*	β-, α 0.0001%
210m	3.0×10^{6} y *1*	α
211	2.14 m *2*	α 99.72%, β- 0.28%
212	60.55 m *6*	β- 64.06%, α 35.94%, β-α 0.014%
212m	25 m	α≤93%, β-≥7%
212m	9 m	β-
213	45.59 m *6*	β- 97.84%, α 2.16%
214	19.9 m *4*	β- 99.98%, α 0.02%
215	7.4 m *6*	β-
84 Po 192	0.034 s *3*	α
193	450 ms *150*	α
193m	0.42 s	α
194	0.7 s	α
195	4.5 s *5*	α
195m	2.0 s *2*	α
196	5.5 s *5*	α, ε
197	56 s *3*	ε 56%, α 44%
197m	26 s *2*	α 84%, ε≤16%, IT?
198	1.76 m *3*	α 70%, ε 30%
199	5.2 m *1*	ε 88%, α 12%
199m	4.2 m *1*	ε 61%, α 39%
200	11.5 m *1*	ε 85%, α 15%
201	15.3 m *2*	ε 98.4%, α 1.6%
201m	8.9 m *2*	ε 57%, IT 40%, α≈3%
202	44.7 m *5*	ε 98%, α 2%
203	35 m	ε 99.89%, α 0.11%
203m	1.2 m *2*	IT 95.5%, ε 4.5%
204	3.53 h *2*	ε 99.34%, α 0.66%
205	1.66 h *2*	ε 99.96%, α 0.04%
206	8.8 d *1*	ε 94.55%, α 5.45%
207	5.80 h *2*	ε 99.98%, α 0.02%
207m	2.8 s *2*	IT
208	2.898 y *2*	α, ε 0.0018%
209	102 y *5*	α 99.74%, ε 0.26%
210	138.376 d *2*	α
211	0.516 s *3*	α
211m	25.2 s *6*	α
212	0.298 μs *3*	α
212m	45.1 s *6*	α
213	4.2 μs *8*	α
214	164.3 μs *18*	α
215	1.780 ms *4*	α, β- 0.0002%
216	0.15 s	α
217	<10 s	α>95%, β-<5%
218	3.11 m	α 99.98%, β- 0.02%
85 At 196	0.3 s *1*	α
197	0.4 s *1*	α≈96%, ε≈4%
198	4.9 s	α
198m	1.5 s *3*	α, IT?
199	7.0 s *1*	α 53%, ε 47%
200	43 s *2*	ε 65%, α 35%
200m	4.3 s *3*	α, IT?
201	89 s *3*	α 71%, ε 29%
202	181 s *3*	ε 88%, α 12%
202m	1.1 s	IT
203	7.37 m *20*	ε 69%, α 31%
204	9.2 m *2*	ε 95.6%, α 4.4%
205	26.2 m *5*	ε 90%, α 10%
206	29.4 m *3*	ε 99.04%, α 0.96%
207	1.80 h *4*	ε 91.3%, α 8.7%
208	1.63 h *3*	ε 99.45%, α 0.55%
209	5.41 h *5*	ε 95.9%, α 4.1%
210	8.1 h *4*	ε 99.82%, α 0.18%
211	7.214 h *7*	ε 58.3%, α 41.7%
212	0.314 s *2*	α
212m	0.119 s *3*	α
213	0.11 μs *2*	α
214	2 μs	α
215	0.10 ms *2*	α
216	0.30 ms *3*	α
217	32.3 ms *4*	α 99.99%, β- 0.01%
218	≈2 s	α 99.9%, β- 0.1%
219	0.9 m *1*	α 97%, β- 3%
86 Rn 199	0.5 s	α
199m	0.29 s	α
200	1.0 s *2*	α≈98%, ε≈2%
201	7.0 s *4*	α≈80%, ε≈20%
201m	3.8 s *4*	α, ε
202	9.85 s *20*	α≈85%, ε≈15%
203	45 s *3*	α 66%, ε 34%
203m	28 s *2*	α
204	1.24 m *3*	α 68%, ε 32%

TABLE I (cont.)

Isotope Z El A	T1/2 or Abundance	Decay Mode
86 Rn 205	2.83 m *7*	ε 77%, α 23%
206	5.67 m *17*	α 68%, ε 32%
207	9.3 m *2*	ε 77%, α 23%
208	24.35 m *14*	α 52%, ε 48%
209	28.5 m *10*	ε 83%, α 17%
210	2.4 h *1*	α 96%, ε 4%
211	14.6 h *2*	ε 74%, α 26%
212	24 m *2*	α
213	25.0 ms *2*	α
214	0.27 μs *2*	α
215	2.30 μs *10*	α
216	45 μs *5*	α
217	0.54 ms *5*	α
218	35 ms *5*	α
219	3.96 s *1*	α
220	55.6 s *1*	α
221	25 m *2*	β- 78%, α 22%
222	3.8235 d *3*	α
223	43 m *5*	β-
224	107 m *3*	β-
225	4.5 m *3*	β-
226	6.0 m *5*	β-
87 Fr 201	48 ms *15*	α
202	0.34 s *4*	α
203	0.55 s	α, ε?
204	2.1 s *2*	α≈80%, ε≈20%
205	3.85 s *10*	α, ε<1%
206	16.0 s *1*	α 85%, ε 15%
206m	0.7 s	IT, α
207	14.8 s *1*	α 95%, ε 5%
208	59.0 s *20*	α 77%, ε 23%
209	50.0 s *3*	α 89%, ε 11%
210	3.18 m *6*	α 60%, ε 40%
211	3.10 m *2*	α>70%, ε<30%
212	20.0 m *6*	ε 57%, α 43%
213	34.6 s *3*	α 99.45%, ε 0.55%
214	5.0 ms *2*	α
214m	3.35 ms *5*	α
215	0.12 μs	α
216	0.70 μs *2*	α
217	22 μs *5*	α
218	0.7 ms *6*	α
219	21 ms *1*	α
220	27.4 s *3*	α≈99.65%, β-≈0.35%
221	4.9 m *2*	α
222	14.4 m *4*	β-, α?
223	21.8 m *4*	β- 99.99%, α 0.01%
224	2.67 m *20*	β-
225	3.9 m *2*	β-
226	48 s *1*	β-
227	2.4 m *2*	β-
228	39 s *1*	β-
229	50 s *20*	β-
88 Ra 206	0.4 s *2*	α, ε?
207	1.3 s *2*	α, ε?
208	1.4 s *4*	α
209	4.6 s *2*	α
210	3.7 s *2*	α 96%, ε 4%
211	13 s *2*	α>93%, ε<7%
212	13.0 s *2*	α≈94%, ε≈6%
213	2.74 m *6*	α 80%, ε 20%
213m	2.1 ms *1*	IT 99%, α 1%
214	2.46 s *3*	α>99.9%, ε<0.1%
215	1.59 ms *9*	α
216	182 ns *10*	α

Isotope Z El A	T1/2 or Abundance	Decay Mode
88 Ra 217	1.6 μs *2*	α
218	14 μs *2*	α
219	10 ms *3*	α
220	23 ms *5*	α
221	29 s	α
222	38.0 s *5*	α
223	11.434 d *2*	α, ^{14}Cw
224	3.66 d *4*	α
225	14.8 d *2*	β-
226	1600 y *7*	α
227	42.2 m *5*	β-
228	5.75 y *3*	β-
229	4.0 m *2*	β-
230	93 m *2*	β-
89 Ac 209	0.10 s *5*	α
210	0.35 s *5*	α 96%, ε 4%
211	0.25 s *5*	α>99.8%, ε<0.2%
212	0.93 s *5*	α≈98%, ε≈2%
213	0.80 s *5*	α
214	8.2 s *2*	α≥89%, ε≤11%
215	0.17 s *1*	α 99.91%, ε 0.09%
216	≈0.33 ms	α, α
217	111 ns *7*	α
218	0.27 μs *4*	α
219	7 μs *2*	α
220	26.1 ms *5*	α
221	52 ms *2*	α
222	4.2 s *5*	α
222m	66 s *3*	α, IT?, ε?
223	2.2 m *1*	α 99%, ε 1%
224	2.9 h *2*	ε≈90%, α≈10%
225	10.0 d *1*	α
226	29 h	β- 82.8%, ε 17.2%, αw
227	21.773 y *3*	β- 98.62%, α 1.38%
228	6.13 h	β-
229	62.7 m *5*	β-
230	122 s *3*	β-
231	7.5 m *1*	β-
232	35 s *5*	β-
90 Th 212	30 ms	α
213	150 ms *25*	α
214	0.09 s	α
215	1.2 s *2*	α
216	0.028 s *2*	α
217	0.252 ms *7*	α
218	109 ns *13*	α
219	1.05 μs *3*	α
220	9.7 μs *6*	α
221	1.68 ms *6*	α
222	2.8 ms *3*	α
223	0.66 s *1*	α
224	1.04 s *5*	α
225	8.0 m *5*	α≈90%, ε≈10%
226	31 m	α
227	18.718 d *5*	α
228	1.9131 y *9*	α
229	7340 y *160*	α
230	$7.538 \cdot 10^4$ y *30*	α, SF?
231	25.52 h *1*	β-, αw
232	$1.405 \cdot 10^{10}$ y *6* 100%	α, SF?
233	22.3 m *1*	β-
234	24.10 d *3*	β-
235	6.9 m *2*	β-
236	37.1 m *15*	β-

Isotope Z El A	T1/2 or Abundance	Decay Mode
91 Pa 215	14 ms	α
216	0.20 s *4*	α
217	4.9 ms *6*	α
217m	1.6 ms	α
218	0.12 ms	α
221	6 μs	α
222	4.3 ms	α
223	6.5 ms *10*	α
224	0.95 s *15*	α
225	1.8 s *3*	α
226	1.8 m *2*	α 74%, ε 26%
227	38.3 m *3*	α≈85%, ε≈15%
228	22 h *1*	ε≈98%, α≈2%
229	1.4 d *4*	ε 99.75%, α 0.25%
230	17.4 d *5*	ε 91.6%, β- 8.4%, αw
231	3.276×10^4 y *11*	α, SF?
232	1.31 d *2*	β-, ε≈0.2%
233	27.0 d *1*	β-
234	6.70 h *5*	β-
234m	1.17 m *3*	β- 99.87%, IT 0.13%
235	24.1 m *2*	β-
236	9.1 m *2*	β-, SFw
237	8.7 m *2*	β-
238	2.3 m *1*	β-
92 U 222	1 μs	α
226	0.5 s *2*	α
227	1.1 m *3*	α
228	9.1 m *2*	α≥95%, ε≤5%
229	58 m *3*	ε≈80%, α≈20%
230	20.8 d	α
231	4.2 d *1*	ε, α 0.006%
232	68.9 y *4*	α, SFw
233	1.592×10^5 y *2*	α, SFw
234	2.45×10^5 y *2* 0.0055% *5*	α, SFw
235	703.8×10^6 y *5* 0.7200% *12*	α, SFw
235m	≈25 m	IT
236	2.3415×10^7 y *14*	α, SFw
237	6.75 d *1*	β-
238	4.468×10^9 y *3* 99.2745% *15*	α, SFw
239	23.50 m *5*	β-
240	14.1 h *1*	β-
242	16.8 m *5*	β-
93 Np 227?	60 s *5*	SF
229	4.0 m *2*	α>50%, ε<50%
230	4.6 m *3*	ε≤97%, α≥3%
231	48.8 m *2*	ε 98%, α 2%
232	14.7 m *3*	ε, α≈0.003%
233	36.2 m *1*	ε, α≤0.001%
234	4.4 d *1*	ε
235	396.2 d *12*	ε, α 0.0014%
236	115×10^3 y *12*	ε 91%, β- 8.9%, α
236m	22.5 h *4*	ε 52%, β- 48%
237	2.14×10^6 y *1*	α
238	2.117 d *2*	β-
239	2.355 d *4*	β-
240	61.9 m *2*	β-
240m	7.22 m *2*	β- 99.88%, IT 0.12%
241	13.9 m *2*	β-
242	2.2 m *2*	β-
242	5.5 m *1*	β-
94 Pu 232	34.1 m *7*	ε≈80%, α≈20%

Isotope Z El A	T1/2 or Abundance	Decay Mode
94 Pu 233	20.9 m *4*	ε 99.88%, α 0.12%
234	8.8 h *1*	ε 94%, α 6%
235	25.3 m *10*	ε, α 0.0027%
236	2.851 y *8*	α, SFw
237	45.3 d *2*	ε, α 0.005%
237m	0.18 s *2*	IT
238	87.74 y *4*	α, SFw
239	24119 y *26*	α, SF
240	6570 y *6*	α, SFw
241	14.35 y *10*	β-, α 0.0025%
242	3.763×10^5 y *12*	α, SFw
243	4.956 h *3*	β-
244	8.08×10^7 y *10*	α 99.88%, SF 0.12%
245	10.5 h *1*	β-
246	10.85 d *2*	β-
95 Am 232	55 s *7*	ε≈98%, α≈2%, εSF
234	2.6 m *2*	ε, α?
235	?	
237	73.0 m *10*	ε 99.97%, α 0.03%
238	98 m *2*	ε, α 0.0001%
239	11.9 h *1*	ε 99.99%, α 0.01%
240	50.9 h *2*	ε, αw
241	432.2 y *5*	α, SF
242	16.02 h *2*	β- 82.7%, ε 17.3%
242m	141 y *2*	IT 99.5%, α 0.5%, SFw
243	7380 y *40*	α, SFw
244	10.1 h *1*	β-
244m	≈26 m	β-, εw
245	2.05 h *1*	β-
246	39 m *3*	β-
246m	25.0 m *2*	β-
247	22 m *3*	β-
96 Cm 238	2.4 h *1*	ε≥90%, α≤10%
239	≈2.9 h	ε, α<0.1%
240	27 d	α>99.5%, ε<0.5%, SFw
241	32.8 d *2*	ε 99%, α 1%
242	162.8 d *2*	α, SFw
243	28.5 y *2*	α 99.76%, ε 0.24%
244	18.10 y *2*	α, SFw
245	8500 y *100*	α
246	4730 y *100*	α 99.97%, SF 0.03%
247	1.56×10^7 y *5*	α
248	3.40×10^5 y *3*	α 91.74%, SF 8.26%
249	64.15 m *3*	β-
250	≈7400 y	SF≈65%, α≈28%, β-≈7%
251	16.8 m *2*	β-
252	<2 d	β-
97 Bk 240	5 m *2*	ε, εSFw
242	7.0 m *13*	ε, α<1%, SF<0.03%
243	4.5 h *2*	ε 99.85%, α 0.15%
244	4.35 h *15*	ε, α 0.006%
245	4.94 d *3*	ε 99.88%, α 0.12%
246	1.80 d *2*	ε, α<0.2%
247	1380 y *250*	α
248	>9 y	α>70%, β-<30%, ε?
248m	23.7 h *2*	β- 70%, ε 30%
249	320 d *6*	β-, α 0.0015%, SFw
250	3.22 h *1*	β-

TABLE I (cont.)

Isotope Z El A	T1/2 or Abundance	Decay Mode
97 Bk 251	56 m *2*	β^-, $\alpha \approx 0.0001\%$
252	?	
98 Cf 239	39 s *+37-1*	α
240	1.06 m *15*	α
241	3.8 m *7*	$\varepsilon \approx 90\%$, $\alpha \approx 10\%$
242	3.49 m *12*	α, ε?
243	10.7 m *5*	$\varepsilon \approx 86\%$, $\alpha \approx 14\%$
244	19.4 m *6*	α, ε?
245	43.6 m *8*	$\varepsilon \approx 70\%$, $\alpha \approx 30\%$
246	35.7 h *5*	α, SF 0.0002%, $\varepsilon < 0.0001\%$
247	3.11 h *3*	ε 99.96%, α 0.03%
248	333.5 d *28*	α, SFw
249	350.6 y *21*	α, SFw
250	13.08 y *9*	α 99.92%, SF 0.08%
251	898 y *44*	α, SFw
252	2.638 y *10*	α 96.91%, SF 3.09%
253	17.81 d *8*	β^- 99.69%, α 0.31%
254	60.5 d *2*	SF 99.69%, α 0.31%
255	1.4 h *3*	β^-
256	12.3 m *12*	SF
99 Es 243	21 s *2*	$\varepsilon \leq 70\%$, $\alpha \geq 30\%$
244	37 s *4*	ε 96%, α 4%
245	1.33 m *15*	ε 60%, α 40%
246	7.7 m *5*	ε 90.1%, α 9.9%, εSF
247	4.7 m *3*	$\varepsilon \approx 93\%$, $\alpha \approx 7\%$
248	27 m *3*	ε, $\alpha \approx 0.25\%$
249	1.70 h *1*	ε 99.43%, α 0.57%
250	8.6 h *1*	$\varepsilon \geq 97\%$, $\alpha \leq 3\%$
250m	2.22 h *5*	$\varepsilon \geq 99\%$, $\alpha \leq 1\%$
251	33 h *1*	ε 99.5%, α 0.5%
252	471.7 d *19*	α 76%, ε 24%, $\beta^- \approx 0.01\%$
253	20.47 d *3*	α, SFw
254	275.5 d *5*	α
254m	39.3 h *2*	β^- 99.59%, α 0.33%, ε 0.08%
255	39.8 d *12*	β^- 92%, α 8%, SF
256	25 m	β^-
256m	≈7.6 h	β^-
257	?	
100 Fm 242	0.8 ms *2*	SF, α?
243	0.18 s *+8-4*	α
244	3.7 ms *4*	SF ≈ 99%, $\alpha \approx 1\%$
245	4.2 s *13*	α
246	1.1 s *2*	α 92%, SF 8%
247	35 s *4*	α 50%, ε 50%
247	9.2 s *23*	α
248	36 s *3*	α 99%, $\varepsilon \approx 1\%$, SF ≈ 0.05%
249	2.6 m *7*	$\varepsilon \approx 85\%$, $\alpha \approx 15\%$
250	30 m *3*	$\alpha > 90\%$, SF ≈ 0.0006%, $\varepsilon < 10\%$
250m	1.8 s	IT
251	5.30 h 8	ε 98.2%, α 1.8%
252	25.39 h *5*	α, SFw
253	3.00 d *12*	ε 88%, α 12%
254	3.240 h *2*	α 99.94%, SF 0.06%
255	20.07 h *7*	α, SFw
256	2.63 h *2*	SF 91.9%, α 8.1%

Isotope Z El A	T1/2 or Abundance	Decay Mode
100 Fm 257	100.5 d *2*	α 99.79%, SF 0.21%
258	380 μs *60*	SF
259	1.5 s *3*	SF
101 Md 247	3 s	α
248	7 s *3*	ε 80%, α 20%
249	24 s *4*	$\alpha \approx 70\%$, $\varepsilon \approx 30\%$
250	52 s *6*	ε 94%, α 6%
251	4.0 m *5*	$\varepsilon \geq 94\%$, $\alpha \leq 6\%$
252	2.3 m *8*	$\varepsilon > 50\%$, $\alpha < 50\%$
254	10 m *3*	ε
254	28 m *8*	ε
255	27 m *2*	ε 92%, α 8%
256	76 m *4*	ε 90.7%, α 9.3%
257	5.2 h *5*	ε 90%, α 10%
258	55 d *4*	α
258m	43 m *4*	ε
259	103 m	SF > 95%, $\alpha < 5\%$, ε?
102 No 250	0.25 ms *5*	SF, $\alpha \approx 0.1\%$
251	0.8 s *3*	α, $\varepsilon \approx 1\%$
252	2.30 s *22*	α 73.1%, SF 26.9%
253	1.7 m *3*	$\alpha \approx 80\%$, $\varepsilon \approx 20\%$, SF ≈ 0.001%
254	55 s *5*	$\alpha > 99\%$, $\varepsilon < 1\%$, SF < 0.06%
254m	0.28 s *4*	IT
255	3.1 m *2*	α 61.4%, ε 38.6%
256	3.3 s *2*	α 99.7%, SF ≈ 0.25%
257	25 s *2*	α
258	1.2 ms	SF
259	60 m *5*	α 78%, ε 22%, SF < 2%
260	?	SF
103 Lr 252	≈1 s	$\alpha \approx 90\%$, $\varepsilon \approx 10\%$, SF < 1%
253	1.4 s	α, SF < 2%, $\varepsilon \approx 1\%$
254	≈20 s	α, ε, SF < 0.1%
255	22 s *5*	$\alpha > 70\%$, $\varepsilon < 30\%$, SF < 1%
256	28 s *3*	$\alpha > 80\%$, $\varepsilon < 20\%$, SF < 0.03%
257	0.646 s *25*	$\alpha > 85\%$, $\varepsilon < 15\%$
258	4.3 s *5*	$\alpha > 95\%$, $\varepsilon < 5\%$
259	5.4 s *8*	$\alpha > 90\%$, SF < 10%, $\varepsilon < 0.5\%$
260	180 s *30*	α, ε?
104 Rf 253?	≈1.8 s	SF ≈ 50%, $\alpha \approx 50\%$
254?	0.5 ms *2*	SF, $\alpha \approx 0.3\%$
255?	≈2 s	$\alpha \approx 50\%$, SF ≈ 50%
256?	≈5 ms	SF
257	4.8 s *3*	$\alpha \approx 82\%$, $\varepsilon \approx 18\%$
258	11 ms *2*	SF ≈ 90%, $\alpha \approx 10\%$
259	3.1 s *7*	$\alpha \approx 93\%$, SF ≈ 6%, $\varepsilon \approx 0.3\%$
260?	20 ms	SF, $\alpha < 10\%$
261	65 s *10*	$\alpha > 80\%$, SF < 10%, $\varepsilon < 10\%$
262?	63 ms	SF
105 Ha 255?	1.5 s	SF
257	1 s	$\alpha \approx 80\%$, SF ≈ 20%, ε?
258	4 s	α, ε
259?	1.2 s	SF
260	1.52 s *13*	$\alpha \geq 90\%$, SF ≤ 9.6%

Isotope Z	El	A	T1/2 or Abundance	Decay Mode
105	Ha	260	1.52 s *13*	ε<2.5%
		261	1.8 s *4*	α>50%, SF<50%
		262	34 s *4*	SF 71%, α 27%, ε<5%
106		259?	7 ms *3*	SF≈70%, α≈30%
		263	0.8 s *2*	SF≈70%, α≈30%
107		261?	1.5 ms *5*	α≈80%, SF≈20%
		262	115 ms	α
		262m	4.7 ms	α
109		266?	5 ms	α

1-2. STANDARD MONITOR REACTIONS FOR NEUTRONS

Z. BÖDY*
Nuclear Data Section,
Division of Research and Laboratories,
International Atomic Energy Agency,
Vienna

Abstract

STANDARD MONITOR REACTIONS FOR NEUTRONS.

The most important cross-section standards are given, both in the form of graphs and numerical tabulations, from the Evaluated Neutron Data File/B-V (ENDF/B-V) evaluations. Remarks and comments are added on the status of these standards. Linear-linear interpolations should be used unless otherwise stated.

1. INTRODUCTION

Neutron cross-section measurements often require a determination of the neutron flux and this action can be the most difficult part of the experiment. The flux determination can be significantly simplified by the use of one of the cross-section standards, thus avoiding any complications associated with direct neutron flux determinations.

It is essential that these cross-section standards be well defined, accurately known, easy to use, easily referenceable and available without any difficulties. The IAEA International Nuclear Data Committee/(OECD) Nuclear Energy Agency Nuclear Data Committee (INDC/NEANDC) Nuclear Standards File provides just such a set of cross-section standards. There are about ten standards in the File, since in the case of a single standard, not all of the requirements can be fulfilled simultaneously at each energy point. Indeed, it is safe to say that there are as many compromises as there are standards. As a result, the user can choose which standard is the most acceptable. The choice will also be influenced by whether the user wants to measure a capture, a scattering or a fission cross-section, the ultimate decision being made in order to avoid experimental difficulties. With regard to activation standards, a further consideration in making a choice is that the half-life of the activity should be nearly the same as that of the activity for the irradiated sample. If the half-lives differ considerably, then temporal variations in the flux will not be properly taken into account by the standard monitor (see also Part 2-2).

---

*Present address: Institute of Experimental Physics, Kossuth University, Debrecen, Hungary.

The following subsections detail the Evaluated Neutron Data File/B-V (ENDF/B-V) evaluations for the standards already completed, together with the ENDF/B-V values for some recommended dosimetry standards. The latter are not included as standards in the INDC/NEANDC Nuclear Standards File, though they are very often used because of several advantages they possess (e.g. high specific activity). The ENDF/B-V values presented are accompanied by some comments and remarks on the status of the particular cross-section in question, made on the basis of information obtained at a recent meeting on neutron standard reference data[1] and from papers referred to in the Computer Index of Neutron Data (CINDA) master file up to April 1985. Version V of ENDF/B will hopefully be changed to version VI in the near future, the latter being the outcome of a simultaneous evaluation using a generalized least squares program, R-matrix evaluations and a procedure for combining the results of the evaluations. The simultaneous evaluation process will provide cross-sections for the ^{6}Li(n, t), ^{10}B(n, α_1), ^{10}B(n, α), ^{197}Au(n, γ), ^{235}U(n, f), ^{238}U(n, f), ^{238}U(n, γ) and ^{239}Pu(n, f) reactions, while evaluations of ^{3}He(n, p) and C(n, n) are being performed separately.

2. THE ^{1}H(n, n) ^{1}H CROSS-SECTION

The hydrogen elastic scattering cross-section is currently the most accurately known of all the standards. This cross-section can be determined from the total neutron cross-section, which is easily measured and with which it coincides, except at low energies, where neutron capture makes a significant contribution [1, 2]. A number of techniques have been employed in utilizing this cross-section. At low neutron energies (~1 keV to ~1 MeV), gas proportional counters have been used. Extrapolating the pulse height distribution of such a counter to zero energy and summing the events in the distribution yields a result which is directly proportional to the product of the flux and the hydrogen cross-section. The timing jitter of these (both methane- and hydrogen-filled) proportional counters limits their use in time of flight experiments in the MeV energy region. Proton recoil telescopes represent the other extreme, in that their response is directly proportional to the product of the flux and the cross-section for neutron–proton scattering into the appropriate solid angle of the detector. This can provide fast timing, but suffers from low efficiency. A new scintillation detector [3] reported recently provides moderate efficiency with fast timing and small corrections [1]. The ^{1}H(n, n) ^{1}H cross-section is considered to be a standard between 1 keV and 20 MeV [1].

---

[1] IAEA–OECD/NEANDC, Nuclear Standard Reference Data (Proc. Advisory Group Meeting Geel, Belgium, 1984), IAEA-TECDOC-335, IAEA, Vienna (1985).

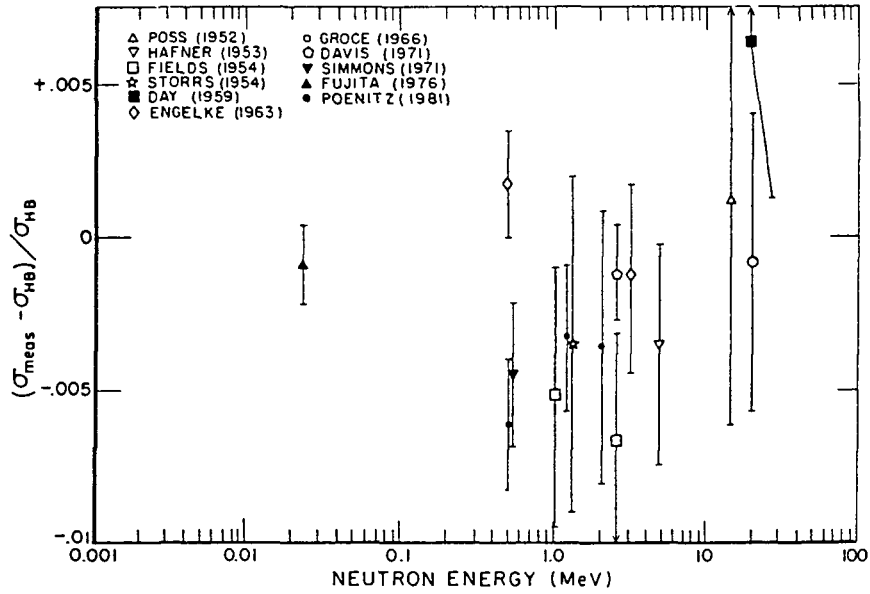

FIG. 1. Comparison between transmission measurements of the hydrogen total neutron cross-section and the Hopkins-Breit evaluation [1]. (Reference details for the individuals listed in this figure can be found in Ref. [1].)

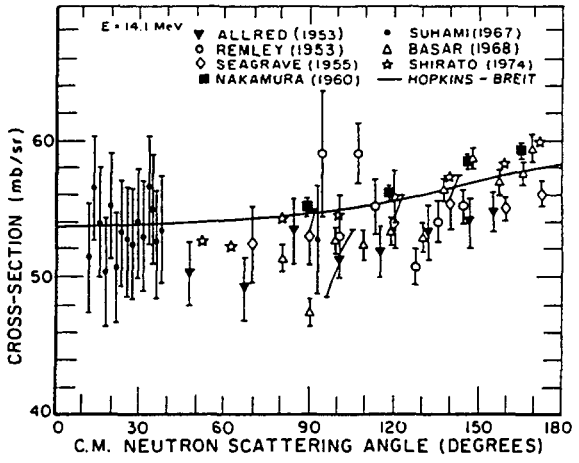

FIG. 2. Hopkins-Breit evaluation compared with differential cross-section measurements for n-p scattering [1]. (Reference details for the individuals listed in this figure can be found in Ref. [1].)

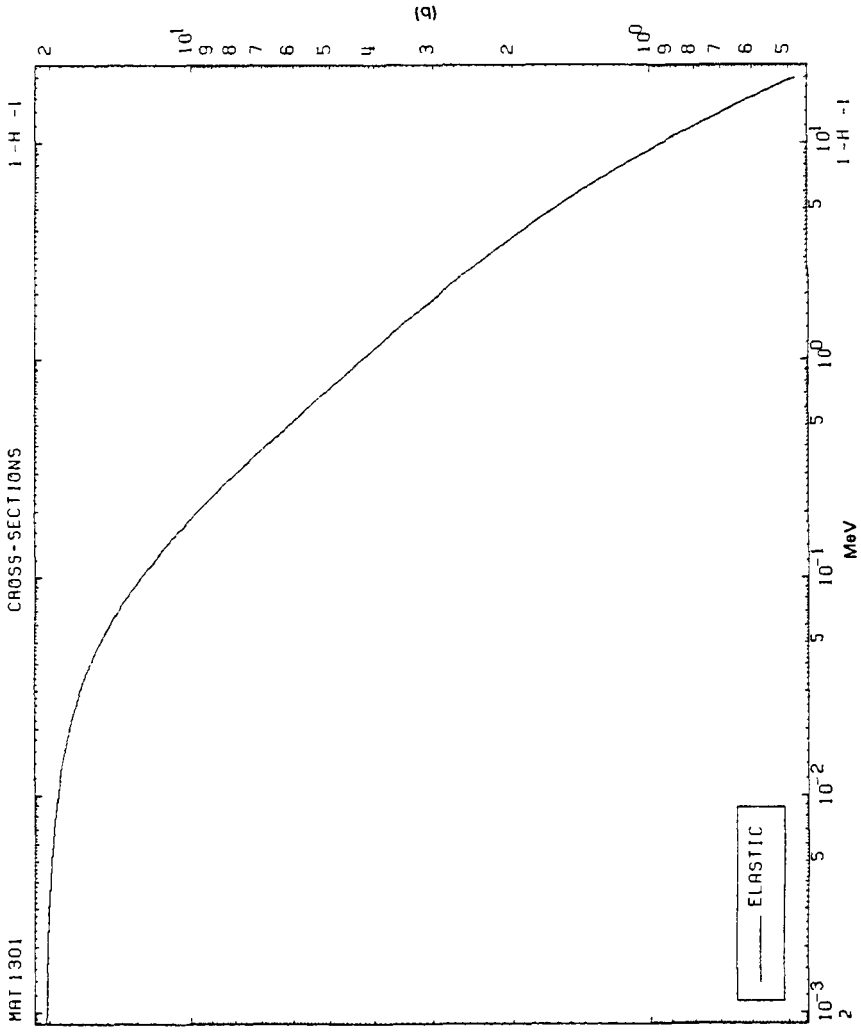
MAT 1301
CROSS-SECTIONS
1-H-1
(b)
ELASTIC
MeV
1-H-1

1-H - 1 ELASTIC MAT 1301

ENERGY (eV)	SIGMA (b)	ENERGY (eV)	SIGMA (b)	ENERGY (eV)	SIGMA (b)	ENERGY (eV)	SIGMA (b)
1.0000E-05	2.0449E 01	3.2000E 05	7.7340E 00	1.5000E 06	3.4290E 00	7.0000E 06	1.2690E 00
1.0000E 04	1.9213E 01	3.4000E 05	7.5010E 00	1.6000E 06	3.3090E 00	7.5000E 06	1.2010E 00
2.0000E 04	1.8126E 01	3.6000E 05	7.2840E 00	1.7000E 06	3.1980E 00	8.0000E 06	1.1390E 00
3.0000E 04	1.7172E 01	3.8000E 05	7.0830E 00	1.8000E 06	3.0970E 00	8.5000E 06	1.0830E 00
4.0000E 04	1.6327E 01	4.0000E 05	6.8970E 00	2.0000E 06	2.9150E 00	9.0000E 06	1.0320E 00
5.0000E 04	1.5575E 01	4.4000E 05	6.5650E 00	2.2000E 06	2.7590E 00	9.5000E 06	9.8590E-01
6.0000E 04	1.4900E 01	4.8000E 05	6.2750E 00	2.4000E 06	2.6220E 00	1.0000E 07	9.4320E-01
7.0000E 04	1.4291E 01	5.0000E 05	6.1430E 00	2.6000E 06	2.5010E 00	1.0500E 07	9.0350E-01
8.5000E 04	1.3481E 01	5.5000E 05	5.8450E 00	2.8000E 06	2.3920E 00	1.1000E 07	8.6650E-01
1.0000E 05	1.2774E 01	6.0000E 05	5.5840E 00	3.0000E 06	2.2930E 00	1.1500E 07	8.3230E-01
1.1000E 05	1.2351E 01	6.5000E 05	5.3540E 00	3.2000E 06	2.2030E 00	1.2000E 07	8.0050E-01
1.2000E 05	1.1964E 01	7.0000E 05	5.1480E 00	3.4000E 06	2.1200E 00	1.2500E 07	7.7100E-01
1.3000E 05	1.1607E 01	7.5000E 05	4.9640E 00	3.6000E 06	2.0430E 00	1.3000E 07	7.4330E-01
1.5000E 05	1.0965E 01	8.0000E 05	4.7970E 00	3.8000E 06	1.9730E 00	1.3500E 07	7.1730E-01
1.7000E 05	1.0398E 01	8.5000E 05	4.6450E 00	4.0000E 06	1.9070E 00	1.4500E 07	6.6980E-01
1.9000E 05	9.8980E 00	9.0000E 05	4.5060E 00	4.2000E 06	1.8450E 00	1.5500E 07	6.2740E-01
2.0000E 05	9.6710E 00	9.5000E 05	4.3780E 00	4.6000E 06	1.7340E 00	1.6500E 07	5.8930E-01
2.2000E 05	9.2580E 00	1.0000E 06	4.2610E 00	5.0000E 06	1.6350E 00	1.7500E 07	5.5490E-01
2.4000E 05	8.8920E 00	1.1000E 06	4.0510E 00	5.2000E 06	1.5890E 00	1.8500E 07	5.2380E-01
2.6000E 05	8.5620E 00	1.2000E 06	3.8680E 00	5.6000E 06	1.5060E 00	1.9500E 07	4.9550E-01
2.8000E 05	8.2620E 00	1.3000E 06	3.7060E 00	6.0000E 06	1.4300E 00	2.0000E 07	4.8230E-01
3.0000E 05	7.9870E 00	1.4000E 06	3.5610E 00	6.6000E 06	1.3290E 00		

FIG. 3. The H(n, n) cross-section (ENDF/B-V, Standards File).

TABLE I. UNCERTAINTY DATA FOR THE H(n, n) CROSS-SECTION

Energy range (eV)	Uncertainty (%)
1.0E+03 to 1.0E+05	0.5
1.0E+05 to 1.0E+06	0.7
1.0E+06 to 1.4E+07	0.9
1.4E+07 to 2.0E+07	1.0

Correlation matrix

+1.000			
+0.339	+1.000		
-0.110	+0.330	+1.000	
-0.040	-0.110	+0.335	+1.00

TABLE II. RELATIVE CENTRE OF MASS NEUTRON ANGULAR DISTRIBUTIONS

*(Legendre polynomial form: sum over A(I)*P(I), I = 0, 1, 2, 3, 4; A(0) = 1.0; linear-linear interpolation [10])*

E(keV)	A(1)	A(2)	A(3)	A(4)
1.0E 00	+0.0000E 00	+0.0000E 00	+0.0000E 00	+0.0000E 00
1.0E 02	-5.5958E-04	+1.4582E-07	+1.0491E-11	-6.2615E-12
2.0E 02	-1.0415E-03	+7.7858E-07	+2.4558E-14	-7.1725E-12
4.0E 02	-1.9165E-03	-8.2911E-06	+8.8759E-09	+9.1619E-10
6.0E 02	-2.7587E-03	+2.2326E-05	-1.5830E-07	+4.0976E-09
8.0E 02	-3.5996E-03	-2.0225E-05	-2.9604E-07	+1.3141E-08
1.0E 03	-4.3923E-03	-2.1837E-05	-9.5840E-07	+5.5044E-08
2.0E 03	-7.8534E-03	-1.4939E-04	-3.2478E-05	+1.3443E-06
4.0E 03	-1.3744E.02	-3.9492E-04	-1.8595E-04	+1.6038E-05
6.0E 03	-1.9007E-02	+3.5263E-04	-5.7961E-04	+4.5184E-05
8.0E 03	-2.3419E-02	+7.5344E-04	-1.1913E-03	+2.7082E-04
1.0E 04	-2.7817E-02	+3.9395E-03	-2.1302E-03	+4.2552E-04
1.2E 04	-3.2412E-02	+7.8464E-03	-3.3448E-03	+1.2151E-03
1.4E 04	-3.5926E-02	+1.2899E-02	-4.6372E-03	+1.9550E-03
1.6E 04	-3.8681E-02	+1.9119E-02	-6.0657E-03	+3.1383E-03
1.8E 04	-4.0592E-02	+2.6532E-02	-7.5378E-03	+4.6980E-03
2.0E 04	-4.1766E-02	+3.5148E-02	-8.9187E-03	+6.5867E-03

2.1. Status

Gammel [4] has analysed the available experimental data between 0 and 40 MeV and provided a formulation for the $^{1}H(n, n)^{1}H$ cross-section which has been used as a reference in many subsequent cross-section measurements [2]. Newer experimental data were taken into account in a phase shift analysis by Hopkins and Breit [5] and the resulting cross-sections were used in ENDF/B-II [6] and were retained in ENDF/B-III through V [7]. Neither the cross-sections nor the angular distributions have been changed since version II, except to add one more significant figure to the total cross-sections and to include correlated error data and different interpolation rules [7].

Analysis of the neutron–proton interaction by Lomon and Wilson [8] differs from the Hopkins–Breit (HB) analysis by only $\leqslant 0.3\%$ at low energies (< 5 MeV) and thus this difference is well within the uncertainty range of 0.5–1.0% stated in the error files of ENDF/B-V. Dilg [9] measured the $^{1}H(n, n)^{1}H$ cross-section at 135 eV and obtained a parameter set which results in cross-section values that are within $\leqslant 0.2\%$ of those of ENDF/B-V [2].

In Fig. 1, transmission measurements of the hydrogen total neutron cross-section, with reported uncertainties of less than 1%, are compared with the Hopkins–Breit evaluation. All experimental data in Fig. 1 agree with the respective ENDF/B-V values within their quoted errors.

Above about 1 MeV, where proton recoil telescopes are used, angular distribution determinations are required [1]. In Fig. 2, differential cross-section measurements for n-p scattering at 14.1 MeV are compared with the Hopkins–Breit evaluation [5]. However, this cross-section has not been measured well enough to determine the flux with 1% accuracy above approximately 10 MeV, nor can it be calculated with sufficient accuracy because of uncertainties in P-wave phase shifts [1, 10, 11]. High accuracy polarization measurements should provide a more sensitive method for establishing the phase shifts. Recently, analysing power measurements for n-p scattering have been performed by, for example, Tornow et al. [12]. Other similar measurements are mentioned in Refs [1] and [10]. These analysing power measurements were successfully reproduced in the R-matrix analysis of Dodder and Hale (see Ref. [1]), but the calculated total cross-sections were $\sim 0.3\%$ lower than those predicted by Hopkins and Breit [5]. The final version of this Dodder–Hale analysis was accepted in 1983 as the hydrogen standard for ENDF/B-VI [13]. Figure 3. and Tables I and II detail the H(n, n) cross-section.

3. THE $^{3}He(n, p)^{3}H$ CROSS-SECTION

The $^{3}He(n, p)^{3}H$ cross-section is often used as a standard in the neutron energy range from thermal to 50 keV. However, this cross-section is not accepted as a standard in the INDC/NEANDC Standards File because of the lack of a good

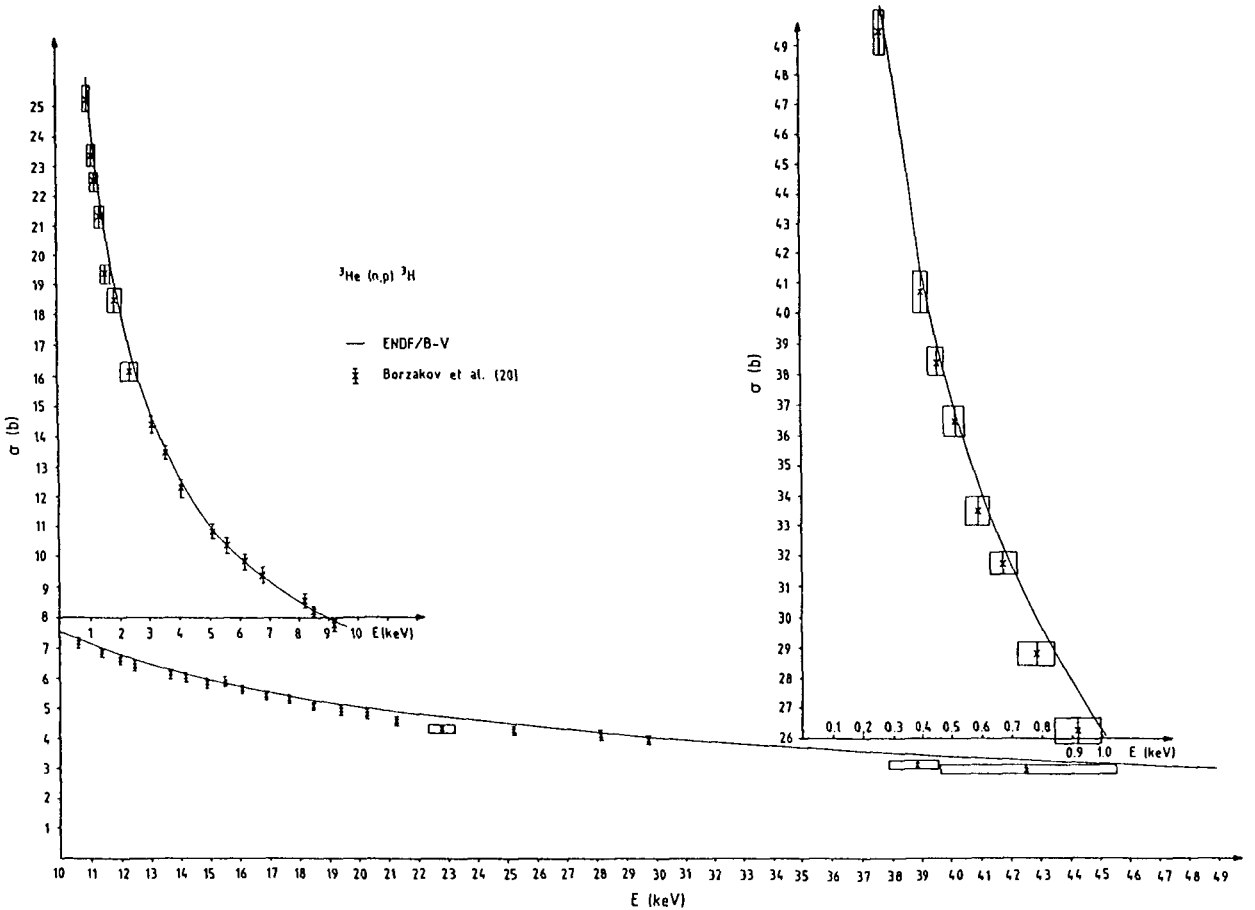

FIG. 4. The ^{3}He(n, p) cross-section: the ENDF/B-V and the Borzakov et al. measurements.

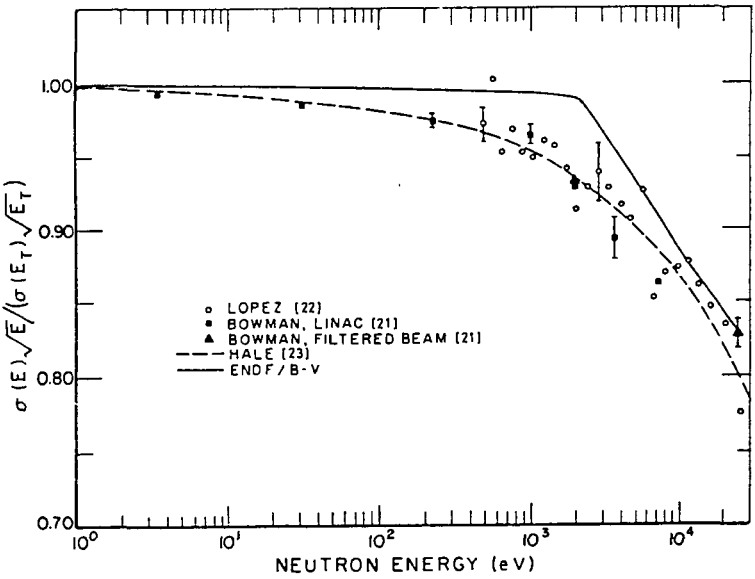

FIG. 5. Various measurements of the $^3He(n, p)$ cross-section [1].

detector. Development of a new detector at the US National Bureau of Standards was reported at the 1984 IAEA-OECD/NEANDC Advisory Group Meeting in Geel, Belgium. If this development is successful, the situation might change [11].

3.1. Status

The data contained in version V of the ENDF/B evaluation were originally produced in 1968 and were accepted by the US Cross Section Evaluation Working Group (CSEWG) Standard Subcommittee for version III in 1971, which in turn was carried over intact again to version V [14] through version IV [15].

The thermal cross-section of 5327 b was derived from precise (better than 1%) measurements by Als-Nielsen and Dietrich [16] of the total cross-section up to an energy of 11 eV. The $^3He(n, p)$ cross-section was assumed to follow 1/v up to 1.7 keV. Gibbons and Macklin [17, 18] determined the $^3He(n, p)$ cross-section from 5 keV and up. The ENDF/B evaluation was based on the results of the measurements detailed in Refs [16–18] (at least for the thermal to 50 keV energy range) and an error of 10% has been estimated for the recommended values [14, 15]. Carlson [1] mentions that the uncertainty varies from 0.2 to ~4% from the thermal to 50 keV region. Wasson [19] ascribed errors of 3–5% in the ENDF/B-V evaluation for the $E < 1$ MeV energy range, but these numbers have not been universally accepted as being of reliable enough precision [20].

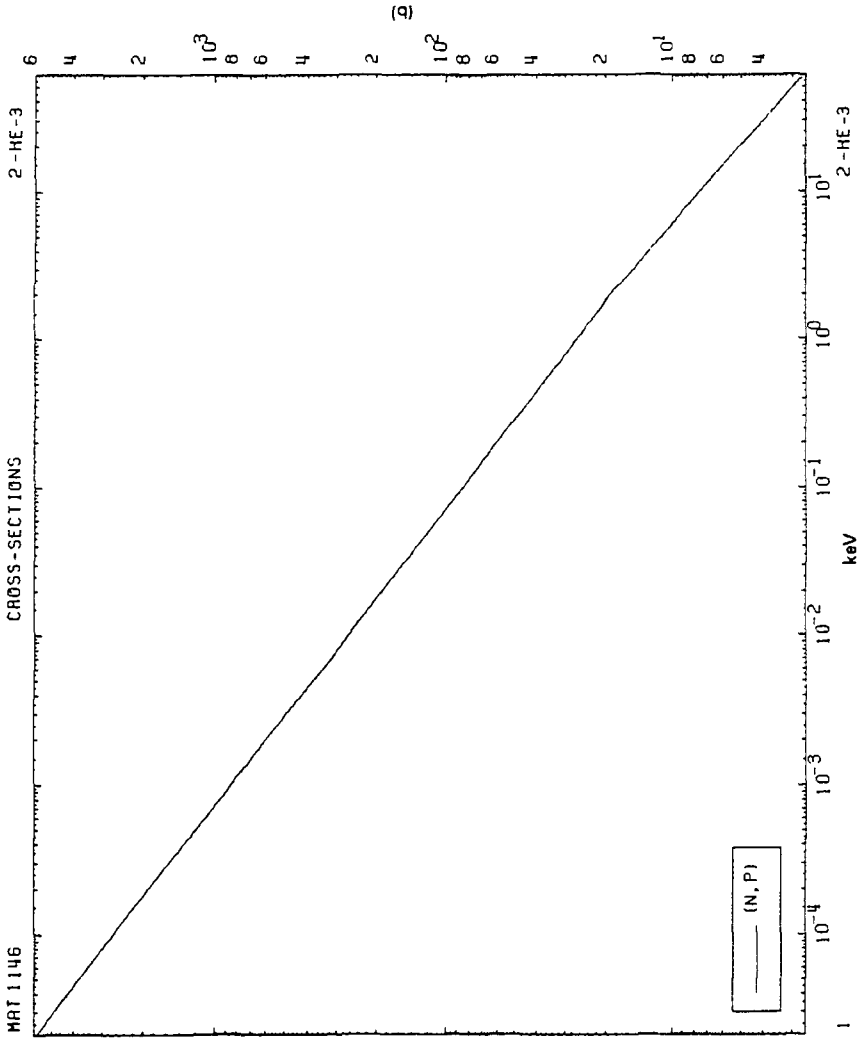
MAT 1146
CROSS-SECTIONS
2-HE-3
2-HE-3
(b)
keV
(N,P)

1 2-HE- 3 (N,P) MAT 1146

ENERGY (eV)	SIGMA (b)	ENERGY (eV)	SIGMA (b)	ENERGY (eV)	SIGMA (b)	ENERGY (eV)	SIGMA (b)
2.5300E-02	5.3270E 03	1.2355E 00	7.6135E 02	5.0834E 01	1.1856E 02	1.9554E 03	1.9026E 01
2.8076E-02	5.0566E 03	1.3363E 00	7.3206E 02	5.5146E 01	1.1383E 02	2.2403E 03	1.7692E 01
3.1123E-02	4.8025E 03	1.4436E 00	7.0432E 02	5.9519E 01	1.0956E 02	2.4472E 03	1.6804E 01
3.4455E-02	4.5643E 03	1.5576E 00	6.7804E 02	6.6186E 01	1.0389E 02	2.6807E 03	1.5936E 01
3.8103E-02	4.3402E 03	1.6786E 00	6.5313E 02	7.2807E 01	9.9055E 01	2.8525E 03	1.5369E 01
4.2082E-02	4.1297E 03	1.8069E 00	6.2951E 02	7.9464E 01	9.4813E 01	3.0733E 03	1.4716E 01
4.6429E-02	3.9315E 03	2.0133E 00	5.9634E 02	8.3830E 01	9.2309E 01	3.2721E 03	1.4195E 01
5.1160E-02	3.7453E 03	2.2382E 00	5.6556E 02	9.2673E 01	8.7792E 01	3.5089E 03	1.3647E 01
5.6315E-02	3.5696E 03	2.4815E 00	5.3711E 02	1.0117E 02	8.4021E 01	3.7928E 03	1.3061E 01
6.1913E-02	3.4043E 03	2.7453E 00	5.1063E 02	1.0925E 02	8.0854E 01	4.1225E 03	1.2461E 01
6.8000E-02	3.2483E 03	3.0293E 00	4.8610E 02	1.2032E 02	7.7040E 01	4.4438E 03	1.1945E 01
7.4595E-02	3.1013E 03	3.3358E 00	4.6321E 02	1.3046E 02	7.3987E 01	4.7910E 03	1.1449E 01
8.1751E-02	2.9623E 03	3.6641E 00	4.4196E 02	1.4274E 02	7.0729E 01	5.2675E 03	1.0849E 01
8.9487E-02	2.8313E 03	4.0169E 00	4.2209E 02	1.5720E 02	6.7397E 01	5.6916E 03	1.0383E 01
9.7862E-02	2.7074E 03	4.3932E 00	4.0360E 02	1.7145E 02	6.4532E 01	6.1840E 03	9.9050E 00
1.0690E-01	2.5904E 03	4.7958E 00	3.8628E 02	1.8700E 02	6.1790E 01	6.6634E 03	9.4940E 00
1.1666E-01	2.4796E 03	5.2234E 00	3.7012E 02	2.0686E 02	5.8689E 01	7.1810E 03	9.0994E 00
1.2717E-01	2.3748E 03	5.6790E 00	3.5495E 02	2.2955E 02	5.5655E 01	7.5568E 03	8.8400E 00
1.3850E-01	2.2755E 03	6.1611E 00	3.4077E 02	2.4643E 02	5.3676E 01	8.2625E 03	8.4038E 00
1.5067E-01	2.1816E 03	6.6728E 00	3.2744E 02	2.6833E 02	5.1394E 01	9.0593E 03	7.9764E 00
1.6377E-01	2.0925E 03	7.0295E 00	3.1902E 02	2.8000E 02	5.0290E 01	9.6461E 03	7.6976E 00
1.7782E-01	2.0081E 03	7.7885E 00	3.0307E 02	3.0987E 02	4.7807E 01	1.0401E 04	7.3758E 00
1.9291E-01	1.9279E 03	8.6018E 00	2.8837E 02	3.4402E 02	4.5375E 01	1.1361E 04	7.0113E 00
2.0905E-01	1.8519E 03	9.4706E 00	2.7482E 02	3.6943E 02	4.3788E 01	1.2415E 04	6.6605E 00
2.2636E-01	1.7797E 03	1.0396E 01	2.6230E 02	4.0242E 02	4.1957E 01	1.3604E 04	6.3171E 00
2.4485E-01	1.7111E 03	1.1378E 01	2.5071E 02	4.4192E 02	4.0039E 01	1.4480E 04	6.0932E 00
2.6463E-01	1.6459E 03	1.2419E 01	2.3997E 02	4.8308E 02	3.8296E 01	1.5605E 04	5.8350E 00
2.9319E-01	1.5636E 03	1.3517E 01	2.3001E 02	5.3144E 02	3.6513E 01	1.6611E 04	5.6287E 00
3.2432E-01	1.4866E 03	1.4673E 01	2.2076E 02	5.7908E 02	3.4979E 01	1.7798E 04	5.4112E 00
3.5819E-01	1.4146E 03	1.5888E 01	2.1214E 02	6.3100E 02	3.3510E 01	1.9219E 04	5.1789E 00
3.9498E-01	1.3470E 03	1.7161E 01	2.0412E 02	6.6838E 02	3.2556E 01	2.0868E 04	4.9410E 00
4.3489E-01	1.2837E 03	1.8491E 01	1.9664E 02	7.3921E 02	3.0953E 01	2.2472E 04	4.7363E 00
4.7811E-01	1.2243E 03	2.0586E 01	1.8636E 02	8.2012E 02	2.9381E 01	2.4821E 04	4.4739E 00
5.2485E-01	1.1685E 03	2.2816E 01	1.7701E 02	8.8031E 02	2.8356E 01	2.6613E 04	4.2969E 00
5.7531E-01	1.1160E 03	2.5155E 01	1.6857E 02	9.5840E 02	2.7173E 01	2.8760E 04	4.1081E 00
6.2973E-01	1.0667E 03	2.7621E 01	1.6087E 02	1.0448E 03	2.6030E 01	3.1254E 04	3.9150E 00
6.8832E-01	1.0202E 03	3.0184E 01	1.5388E 02	1.1281E 03	2.5063E 01	3.3683E 04	3.7490E 00
7.5131E-01	9.7650E 02	3.2863E 01	1.4747E 02	1.2247E 03	2.4066E 01	3.6300E 04	3.5900E 00
8.1895E-01	9.3528E 02	3.5623E 01	1.4164E 02	1.3517E 03	2.2921E 01	3.8192E 04	3.4864E 00
8.9148E-01	8.9640E 02	3.8487E 01	1.3627E 02	1.4938E 03	2.1803E 01	4.1742E 04	3.3121E 00
9.6915E-01	8.5971E 02	4.2483E 01	1.2970E 02	1.6324E 03	2.0846E 01	4.5750E 04	3.1416E 00
1.0522E 00	8.2506E 02	4.6606E 01	1.2382E 02	1.7951E 03	1.9868E 01	4.8701E 04	3.0304E 00
1.1409E 00	7.9232E 02						

FIG. 6. The $^3He(n, p)$ cross-section (ENDF/B-V, Standards File). No uncertainties have been included in the ENDF/B-V listing (see text for other, different estimations).

After the release of the ENDF/B-V evaluation Borzakov and co-workers [20] measured the $^{3}He(n, p)$ cross-section for the neutron energy range from 0.15 to 150 keV. Their experimental data are accurate to 2–3%. These new measurements generally support [13] the lower values obtained by Bowman et al. [21] and Lopez et al. [22]. The preliminary evaluation by Hale [23] is in good agreement with these measurements (see Figs 4 and 5). It is apparent that the ENDF/B-V evaluation is consistently higher at higher neutron energies compared with the more recent measurements. However, the new evaluation by Hale [23] appears to better describe the $^{3}He(n, p)$ cross-section [13]; Fig. 6 details the $^{3}He(n, p)$ cross-section.

4. THE $^{6}Li(n, t)^{4}He$ CROSS-SECTION

The $^{6}Li(n, t)^{4}He$ cross-section is a very important standard in monitoring neutron flux via detection of triton + α-particles by scintillation – glass, LiI (Eu), plastic foils – or by surface barrier detectors and ionization chambers [24]. Reviews of detectors using this cross-section as a standard can be found in Refs [25–27]. In addition, it should be noted that tritium and/or ^{4}He buildup can be a precise detection method [28], e.g. by using high sensitivity mass spectrometers [29–33]. The recommended energy range for use as a standard is thermal to 100 keV [24].

4.1. Status

The low energy neutron cross-sections of ^{6}Li – including the standard (n, t) cross-section – were obtained from a multichannel, multilevel, R-matrix analysis for ENDF/B-V [34]. In the analysis, the database included the Harwell total cross-section [35], the shapes of the n-^{6}Li elastic angular distributions and polarizations, $^{6}Li(n, t)$ angular distributions and (normalized) integrated cross-sections and further t-α elastic angular distributions [34].

Several new ^{6}Li total cross-section data sets have become available since the evaluation of ENDF/B-V [36], but they differ from the previous data sets only above 100 keV (at the region of the 240 keV resonance) and their influence on the (n, t) cross-sections in the R-matrix fit together with new scattering cross-section data. New absolute measurements on the $^{6}Li(n, t)$ cross-section were also made, as mentioned in Refs [36] and [37]. The data of Gayther [38], measured relative to $^{235}U(n, f)$ at energies between 3 and 800 keV, agree rather well with the ENDF/B-V results if the ENDF/B-V values are also used for $^{235}U(n, f)$. Renner et al. [39] measured the $^{6}Li(n, t)$ cross-section between 80 and 470 keV; their data are also consistent with ENDF/B-V, except possibly for a small normalization difference [37]. The only value that was not quite consistent was that measured by Engdahl et al. [40], which was obtained at 23 keV with a quoted

TABLE III. UNCERTAINTY LEVELS OF THE $^{6}Li(n, t)$ CROSS-SECTION DATA

Energy range (eV)	Uncertainty given by Hale (Ref. [37]) (%)	Deviations from JENDL-3 (Ref. [41]) (%)
Thermal to 2.000+2	0.4	0.5
2.000+2 to 2.000+3	0.5	0.7
2.000+3 to 1.000+4	0.5	1.0
1.000+4 to 3.000+4	1.0	1.4
3.000+4 to 1.000+5	2.0	1.7

uncertainty of 2.4%, 6% lower than the value of ENDF/B-V. Such a value is difficult to reconcile with the known resonances of the ^{7}Li compound nucleus [36].

In Table III, the uncertainties of the $^{6}Li(n, t)$ cross-section data are given, specifically the uncertainty given by Hale [37] as well as the percentage differences between ENDF/B-V and JENDL-3 [41] in different energy regions.

It should also be noted that even if the previous results of ENDF/B-VI [42] are taken as reference values, the outcome of a comparison with ENDF/B-V still does not contradict the conclusion that below 2 keV the uncertainty level of the latter is less than 1%, and between 2 and 100 keV it is at most 2% [19]. To sum up, the $^{6}Li(n, t)$ cross-section below 100 keV is known reasonably well, though the desired goal of 1% accuracy has not yet been achieved even at these lower neutron energies [1]. Figure 7 and Table IV detail the $^{6}Li(n, t)$ cross-section.

5. THE $^{10}B(n, \alpha)^{7}Li$, $^{10}B(n, \alpha_0)^{7}Li$ AND $^{10}B(n, \alpha_1)^{7}Li^*$ CROSS-SECTIONS

The $^{10}B(n, \alpha_1)^{7}Li^*$ and the $^{10}B(n, \alpha_0 + \alpha_1)^{7}Li = {}^{10}B(n, \alpha)^{7}Li$ cross-sections are often used for neutron flux determination via, respectively, the detection of the isotropic 478 keV γ-emission of $^{7}Li^*$ in boron slab detectors and via the detection of α-particles in ionization chambers with surface barrier detectors (or scintillators) [24]. A recent review of these detectors, using the above standards, has been made by Carlson [43]. The recommended energy range for use as a standard is thermal to 200 keV for both cross-sections [24].

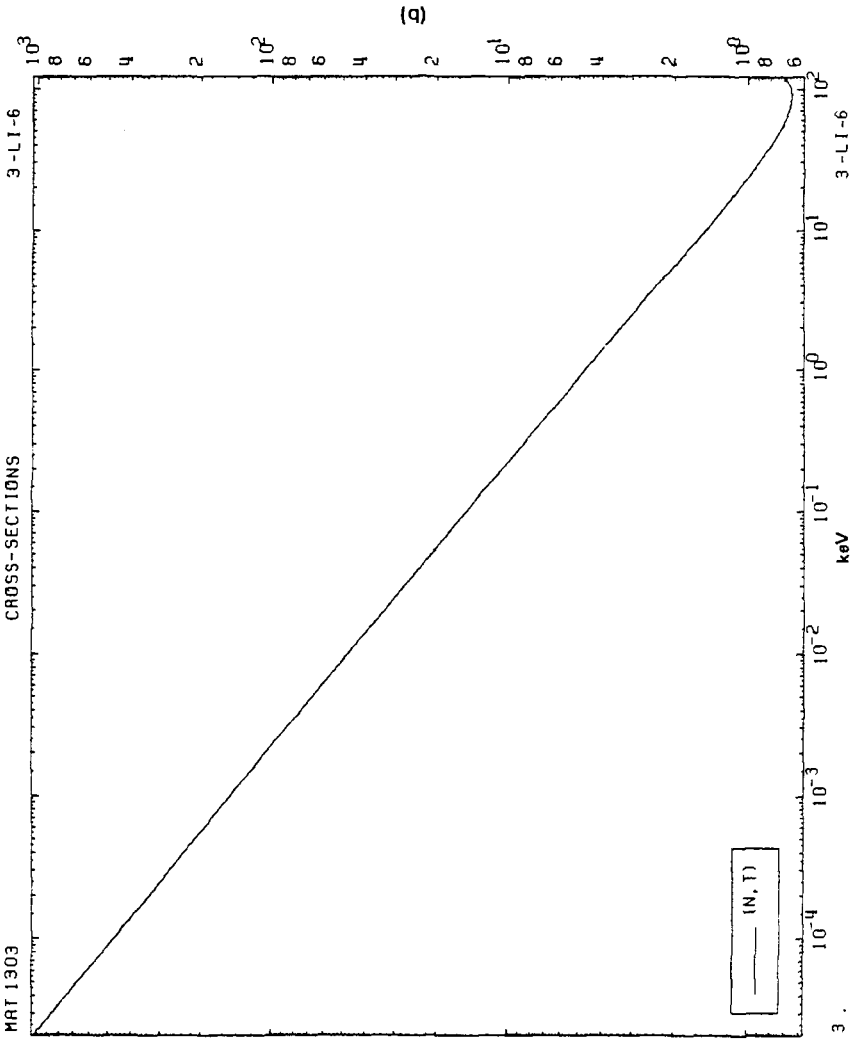
(b)
MAT 1303
CROSS-SECTIONS
3-LI-6
3-LI-6
keV
(N, T)
3.

1 3-LI- 6 (N,T) MAT 1303

ENERGY (eV)	SIGMA (b)	ENERGY (eV)	SIGMA (b)	ENERGY (eV)	SIGMA (b)	ENERGY (eV)	SIGMA (b)
2.6410E-02	9.1601E 02	1.1522E 00	1.3866E 02	5.1947E 01	2.0630E 01	2.0000E 03	3.3175E 00
2.8702E-02	8.7867E 02	1.2737E 00	1.3188E 02	5.6379E 01	1.9802E 01	2.1810E 03	3.1772E 00
3.1031E-02	8.4506E 02	1.4021E 00	1.2569E 02	6.2624E 01	1.8788E 01	2.4321E 03	3.0092E 00
3.4588E-02	8.0042E 02	1.5359E 00	1.2009E 02	6.6397E 01	1.8246E 01	2.6644E 03	2.8754E 00
3.8129E-02	7.6235E 02	1.6761E 00	1.1496E 02	7.3555E 01	1.7334E 01	2.9493E 03	2.7334E 00
4.1695E-02	7.2902E 02	1.8209E 00	1.1029E 02	8.1746E 01	1.6442E 01	3.2750E 03	2.5943E 00
4.4038E-02	7.0936E 02	1.9714E 00	1.0600E 02	8.7847E 01	1.5861E 01	3.5174E 03	2.5035E 00
4.8792E-02	6.7391E 02	2.1820E 00	1.0075E 02	9.5773E 01	1.5190E 01	3.8322E 03	2.3988E 00
5.3371E-02	6.4435E 02	2.3998E 00	9.6068E 01	1.0443E 02	1.4546E 01	4.1232E 03	2.3131E 00
5.7729E-02	6.1955E 02	2.6237E 00	9.1876E 01	1.1357E 02	1.3947E 01	4.4821E 03	2.2194E 00
6.3719E-02	5.8971E 02	2.8525E 00	8.8113E 01	1.2287E 02	1.3408E 01	4.9186E 03	2.1196E 00
6.9207E-02	5.6585E 02	3.0852E 00	8.4725E 01	1.3228E 02	1.2922E 01	5.4132E 03	2.0213E 00
7.5878E-02	5.4040E 02	3.4368E 00	8.0272E 01	1.4657E 02	1.2275E 01	6.0098E 03	1.9193E 00
8.3430E-02	5.1536E 02	3.7947E 00	7.6392E 01	1.6072E 02	1.1721E 01	6.5000E 03	1.8462E 00
9.2530E-02	4.8936E 02	4.1477E 00	7.3068E 01	1.7490E 02	1.1235E 01	7.1905E 03	1.7571E 00
1.0000E-01	4.7073E 02	4.5004E 00	7.0145E 01	1.9333E 02	1.0686E 01	7.8086E 03	1.6875E 00
1.1127E-01	4.4625E 02	4.9727E 00	6.6730E 01	2.1173E 02	1.0210E 01	8.5298E 03	1.6160E 00
1.2327E-01	4.2398E 02	5.4265E 00	6.3878E 01	2.2925E 02	9.8116E 00	9.2357E 03	1.5543E 00
1.3584E-01	4.0388E 02	5.8574E 00	6.1483E 01	2.5388E 02	9.3228E 00	1.0000E 04	1.4949E 00
1.4909E-01	3.8551E 02	6.4483E 00	5.8598E 01	2.6873E 02	9.0613E 00	1.1067E 04	1.4237E 00
1.6285E-01	3.6886E 02	6.9884E 00	5.6287E 01	2.9682E 02	8.6211E 00	1.2286E 04	1.3538E 00
1.7723E-01	3.5358E 02	7.6434E 00	5.3821E 01	3.2888E 02	8.1896E 00	1.3194E 04	1.3081E 00
1.9204E-01	3.3967E 02	8.4134E 00	5.1298E 01	3.5270E 02	7.9078E 00	1.4372E 04	1.2553E 00
2.0740E-01	3.2685E 02	9.1724E 00	4.9129E 01	3.8357E 02	7.5824E 00	1.5549E 04	1.2091E 00
2.2883E-01	3.1117E 02	1.0000E 01	4.7052E 01	4.2358E 02	7.2149E 00	1.7012E 04	1.1591E 00
2.5092E-01	2.9715E 02	1.1127E 01	4.4603E 01	4.4694E 02	7.0235E 00	1.8446E 04	1.1159E 00
2.7357E-01	2.8459E 02	1.2327E 01	4.2375E 01	4.9427E 02	6.6782E 00	2.0000E 04	1.0743E 00
2.9666E-01	2.7329E 02	1.3584E 01	4.0366E 01	5.3979E 02	6.3900E 00	2.2051E 04	1.0275E 00
3.2006E-01	2.6310E 02	1.4909E 01	3.8528E 01	5.8303E 02	6.1480E 00	2.3976E 04	9.8897E-01
3.5573E-01	2.4956E 02	1.6285E 01	3.6863E 01	6.4238E 02	5.8567E 00	2.6166E 04	9.5095E-01
3.9114E-01	2.3800E 02	1.7723E 01	3.5335E 01	6.9668E 02	5.6235E 00	2.8663E 04	9.1349E-01
4.2671E-01	2.2786E 02	1.9204E 01	3.3944E 01	7.6256E 02	5.3747E 00	3.0000E 04	8.9531E-01
4.7307E-01	2.1641E 02	2.0740E 01	3.2662E 01	8.1603E 02	5.1953E 00	3.5000E 04	8.3871E-01
5.1947E-01	2.0652E 02	2.2883E 01	3.1094E 01	9.0334E 02	4.9375E 00	4.0000E 04	7.9464E-01
5.6378E-01	1.9823E 02	2.5092E 01	2.9692E 01	1.0000E 03	4.6924E 00	4.5000E 04	7.5964E-01
6.2624E-01	1.8809E 02	2.7357E 01	2.8436E 01	1.0905E 03	4.4934E 00	5.0000E 04	7.3154E-01
6.6397E-01	1.8266E 02	2.9666E 01	2.7306E 01	1.1764E 03	4.3261E 00	6.0000E 04	6.9063E-01
7.3555E-01	1.7355E 02	3.2006E 01	2.6287E 01	1.2941E 03	4.1246E 00	7.0000E 04	6.6488E-01
8.1746E-01	1.6462E 02	3.5573E 01	2.4934E 01	1.4016E 03	3.9632E 00	8.0000E 04	6.5081E-01
8.7847E-01	1.5880E 02	3.9114E 01	2.3778E 01	1.5319E 03	3.7909E 00	9.0000E 04	6.4679E-01
9.5773E-01	1.5209E 02	4.2671E 01	2.2764E 01	1.6849E 03	3.6145E 00	1.0000E 05	6.5235E-01
1.0366E 00	1.4619E 02	4.7307E 01	2.1619E 01	1.8357E 03	3.4628E 00		

FIG. 7. The $^{6}Li(n, t)$ cross-section (ENDF/B-V, Standards File).

TABLE IV. UNCERTAINTY DATA FOR THE ^{6}Li(n, t) CROSS-SECTION [37]

Energy range (eV)	Uncertainty (%)
1.0E−05 to 2.0E 02	0.4
2.0E 02 to 2.0E 03	0.5
2.0E 03 to 1.0E 04	0.5
1.0E 04 to 3.0E 04	1.0
3.0E 04 to 1.0E 05	2.0

Correlation matrix

+1.00				
+0.99	+1.00			
+0.93	+0.96	+1.00		
+0.67	+0.72	+0.88	+1.00	
+0.30	+0.35	+0.58	+0.89	+1.00

5.1. Status

This ENDF/B-V [44] evaluation is the result of R-matrix analysis. The analysis considers simultaneously data from all the neutron interactions with ^{10}B, as well as measurements of the ^{4}He+^{7}Li system [1].

At present, the positions of these cross-sections are not very secure in the set of standards, though these ENDF/B-V values can be used for the time being. It is possible that they are too low [1, 45, 46, 42], and it is almost certain that the given uncertainties are too small. Wattecamps [47] has commented that these uncertainties are much smaller than the accuracies requested in WRENDA (World Request List for Nuclear Data) 81/82 and this is true also for WRENDA 83/84 [48]. Many users would like to see this cross-section have an accuracy of 1%.

In support of the above statements, it is appropriate to quote Poenitz:

"Consideration of the ^{6}Li + n and ^{10}B + n data bases shows that substantial progress has been made for the ^{6}Li(n, α) cross section but the ^{10}B(n, α) and ^{10}B(n, α_1) cross sections remain poorly defined. There are few absolute measurements of these cross sections and those available have large uncertainties and/or are followed by various shortcomings. It is therefore recommended that the ^{6}Li(n, α) cross-section should be used as a reference cross section below 100–150 keV until a reasonable data base for the ^{10}B + n interactions becomes available." [36].

Similarly, it was concluded at the 1984 IAEA-OECD/NEANDC Advisory Group Meeting in Geel that the $^{6}Li(n, t)$ and $^{10}B(n, \alpha)$ cross-sections both have to be studied over a far wider energy range than that recommended in order to understand the reaction mechanism and to make accurate theoretical calculations. The experimental database for $^{6}Li(n, t)$ has yielded results that are not very different from the ENDF/B-V data for $E_n < 1$ MeV, while the database for $^{10}B(n, \alpha)$ shows large disagreements between new and old measurements [11], especially for $^{10}B(n, \alpha_1)$.

It is hoped that the forthcoming ENDF/B-VI evaluation will improve the situation in the future [42]. Figure 8 details the $^{10}B(n, \alpha)$ cross-section, while Tables V and VI provide, respectively, the recommended reference data for the $^{10}B(n, \alpha_0)$ and $^{10}B(n, \alpha_1)$ cross-sections.

6. THE C(n, n)C CROSS-SECTION

The C(n, n)C cross-section is widely used primarily as a scattering standard, the relevant energy range being 1 keV to 1.8 MeV. While the presence of resonances hinders the use of this cross-section as a standard above 2 MeV, it is useful up to 4.8 MeV if care is taken to avoid prominent resonance structure. Since the capture cross-section is negligible above thermal energies and below 2 MeV, the elastic scattering cross-section is actually identical to the total cross-section. This standard is also very useful for verification of total cross-section measurements [49]. A slight uncertainty comes from the fact that the scattering cross-section of natural carbon is recommended as a standard, while R-matrix evaluations refer to the $^{12}C(n, n)^{12}C$ cross-section (discussed below).

Carbon has several advantages over hydrogen as a scattering standard, one being the fact that the angular distribution in the laboratory system for carbon changes more slowly with angle than it does for hydrogen. Also, there is reduced energy loss and more simplified multiple scattering corrections for carbon compared with hydrogen [1, 13]. In addition, it should be noted that the energy of the 2078 keV resonance is a valued energy-scale reference point [50].

6.1. Status

The ENDF/B-V evaluation is taken from the R-matrix fits of Fu and Perey [51]. Concurrent with this work, Holt, Smith and Whalen have reported new neutron total and scattering measurements, together with an R-matrix interpretation [52]. The latter work is consistent with that of Ref. [51] and supports the ENDF/B-V evaluation to accuracies of $< 1\%$ [50]. Recent precision neutron total cross-section measurements by Poenitz and Whalen [2, 50] (shown in Fig. 9) verify the ENDF/B-V file to fractional per cent accuracies [50]. The new evaluation for JENDL-3 [53] differs from that of ENDF/B-V by a negligible amount only below 5 MeV.

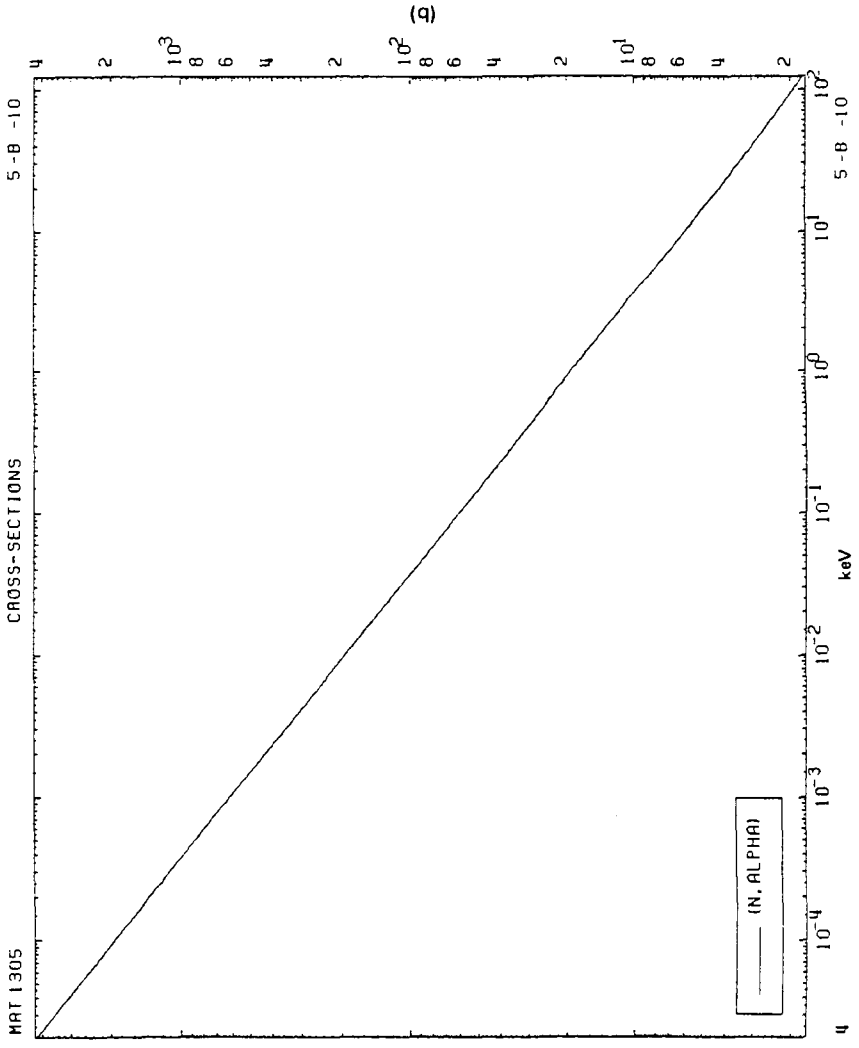
(q)
MAT 1305
CROSS-SECTIONS
5-B -10
5-B -10
keV
(N,ALPHA)

1 5-B - 10 (N,ALPHA) MAT 1305

ENERGY (eV)	SIGMA (b)	ENERGY (eV)	SIGMA (b)	ENERGY (eV)	SIGMA (b)	ENERGY (eV)	SIGMA (b)
2.4030E-02	3.9367E 03	1.4021E 00	5.1498E 02	7.6434E 01	6.9414E 01	4.2671E 03	9.0612E 00
2.6410E-02	3.7551E 03	1.5359E 00	4.9202E 02	8.4134E 01	6.6150E 01	4.5004E 03	8.8190E 00
2.8702E-02	3.6020E 03	1.6761E 00	4.7097E 02	9.1724E 01	6.3344E 01	4.9727E 03	8.3822E 00
3.1031E-02	3.4642E 03	1.8209E 00	4.5183E 02	1.0000E 02	6.0657E 01	5.4265E 03	8.0178E 00
3.4588E-02	3.2812E 03	1.9714E 00	4.3422E 02	1.1127E 02	5.7472E 01	5.8574E 03	7.7119E 00
3.8129E-02	3.1251E 03	2.1820E 00	4.1271E 02	1.2327E 02	5.4576E 01	6.4483E 03	7.3438E 00
4.1695E-02	2.9885E 03	2.3998E 00	3.9351E 02	1.3584E 02	5.1965E 01	6.9884E 03	7.0491E 00
4.4038E-02	2.9079E 03	2.6237E 00	3.7633E 02	1.4909E 02	4.9579E 01	7.6434E 03	6.7349E 00
4.8792E-02	2.7626E 03	2.8525E 00	3.6090E 02	1.6285E 02	4.7417E 01	8.1746E 03	6.5085E 00
5.3371E-02	2.6414E 03	3.0852E 00	3.4701E 02	1.7723E 02	4.5434E 01	9.0413E 03	6.1831E 00
5.7729E-02	2.5397E 03	3.4368E 00	3.2876E 02	1.9204E 02	4.3629E 01	1.0000E 04	5.8739E 00
6.3719E-02	2.4174E 03	3.7947E 00	3.1285E 02	2.0740E 02	4.1967E 01	1.0905E 04	5.6232E 00
6.9207E-02	2.3195E 03	4.1477E 00	2.9923E 02	2.2883E 02	3.9934E 01	1.1764E 04	5.4126E 00
7.5878E-02	2.2152E 03	4.5004E 00	2.8725E 02	2.5092E 02	3.8118E 01	1.2941E 04	5.1589E 00
8.3430E-02	2.1126E 03	4.9727E 00	2.7325E 02	2.7357E 02	3.6491E 01	1.4016E 04	4.9557E 00
9.2530E-02	2.0060E 03	5.4265E 00	2.6156E 02	2.9666E 02	3.5028E 01	1.5319E 04	4.7388E 00
1.0000E-01	1.9296E 03	5.8574E 00	2.5175E 02	3.2006E 02	3.3710E 01	1.6849E 04	4.5170E 00
1.1127E-01	1.8292E 03	6.4483E 00	2.3992E 02	3.5573E 02	3.1959E 01	1.8357E 04	4.3262E 00
1.2327E-01	1.7379E 03	6.9884E 00	2.3045E 02	3.9114E 02	3.0464E 01	2.0000E 04	4.1435E 00
1.3584E-01	1.6555E 03	7.6434E 00	2.2035E 02	4.2671E 02	2.9154E 01	2.2134E 04	3.9412E 00
1.4909E-01	1.5802E 03	8.4134E 00	2.1001E 02	4.5004E 02	2.8380E 01	2.4573E 04	3.7429E 00
1.6285E-01	1.5119E 03	9.1724E 00	2.0112E 02	4.9727E 02	2.6986E 01	2.6388E 04	3.6134E 00
1.7723E-01	1.4493E 03	1.0000E 01	1.9261E 02	5.4265E 02	2.5822E 01	2.8744E 04	3.4640E 00
1.9204E-01	1.3922E 03	1.1127E 01	1.8256E 02	5.8574E 02	2.4844E 01	3.1098E 04	3.3330E 00
2.0740E-01	1.3397E 03	1.2327E 01	1.7342E 02	6.4483E 02	2.3667E 01	3.4024E 04	3.1910E 00
2.2883E-01	1.2754E 03	1.3584E 01	1.6517E 02	6.9885E 02	2.2725E 01	3.6891E 04	3.0684E 00
2.5092E-01	1.2179E 03	1.4909E 01	1.5763E 02	7.6434E 02	2.1720E 01	4.0000E 04	2.9505E 00
2.7357E-01	1.1664E 03	1.6285E 01	1.5080E 02	8.4134E 02	2.0693E 01	4.4102E 04	2.8167E 00
2.9666E-01	1.1201E 03	1.7723E 01	1.4453E 02	9.1724E 02	1.9809E 01	4.7951E 04	2.7068E 00
3.2006E-01	1.0783E 03	1.9204E 01	1.3883E 02	1.0000E 03	1.8964E 01	5.2332E 04	2.5975E 00
3.5573E-01	1.0228E 03	2.0740E 01	1.3357E 02	1.1127E 03	1.7960E 01	5.7327E 04	2.4890E 00
3.9114E-01	9.7541E 02	2.2883E 01	1.2714E 02	1.2327E 03	1.7048E 01	6.2357E 04	2.3936E 00
4.2671E-01	9.3385E 02	2.5092E 01	1.2139E 02	1.3584E 03	1.6226E 01	6.7354E 04	2.3100E 00
4.7307E-01	8.8690E 02	2.7357E 01	1.1624E 02	1.4909E 03	1.5475E 01	7.4833E 04	2.2012E 00
5.1947E-01	8.4635E 02	2.9666E 01	1.1161E 02	1.6285E 03	1.4795E 01	8.2391E 04	2.1068E 00
5.6378E-01	8.1239E 02	3.2006E 01	1.0744E 02	1.7723E 03	1.4172E 01	9.0000E 04	2.0243E 00
6.2624E-01	7.7080E 02	3.5573E 01	1.0189E 02	1.9204E 03	1.3604E 01	1.0000E 05	1.9304E 00
6.6397E-01	7.4857E 02	3.9114E 01	9.7151E 01	2.0740E 03	1.3082E 01	1.0954E 05	1.8528E 00
7.3555E-01	7.1120E 02	4.2671E 01	9.2999E 01	2.2883E 03	1.2443E 01	1.2000E 05	1.7783E 00
8.1746E-01	6.7462E 02	4.5004E 01	9.0548E 01	2.5092E 03	1.1873E 01	1.3471E 05	1.6871E 00
8.7847E-01	6.5076E 02	4.9727E 01	8.6125E 01	2.7357E 03	1.1362E 01	1.4967E 05	1.6066E 00
9.5773E-01	6.2324E 02	5.4265E 01	8.2432E 01	2.9666E 03	1.0903E 01	1.6971E 05	1.5123E 00
1.0366E 00	5.9903E 02	5.8574E 01	7.9331E 01	3.2006E 03	1.0490E 01	1.9480E 05	1.4075E 00
1.1522E 00	5.6816E 02	6.4483E 01	7.5596E 01	3.5573E 03	9.9404E 00	2.6000E 05	1.1568E 00
1.2737E 00	5.4036E 02	6.9884E 01	7.2605E 01	3.9114E 03	9.4718E 00		

FIG. 8. The $^{10}B(n, \alpha)$ cross-section (ENDF/B-V, Standards File).

TABLE V. RECOMMENDED REFERENCE DATA FOR THE $^{10}B(n, \alpha_0)$ CROSS-SECTION

(numerical values are from ENDF/B-V, MAT-1305; applicable energy range: thermal to 200 keV; log-log interpolation [47])

Cross-section values

E (keV)	XSEC (b)	E (keV)	XSEC (b)	E (keV)	XSEC (b)
1.00E-08	1.2287E 04	1.00E-05	3.8853E 02	2.53E-05	2.4425E 02
1.00E-04	1.2285E 02	1.00E-03	3.8830E 01	1.00E-02	1.2263E 01
1.00E-01	3.8622E 00	1.00E 00	1.2092E 00	1.00E 01	3.8004E-01
2.00E 01	2.7184E-01	3.00E 01	2.2520E-01	4.00E 01	1.9802E-01
5.00E 01	1.7988E-01	6.00E 01	1.6680E-01	7.00E 01	1.5690E-01
8.00E 01	1.4919E-01	9.00E 01	1.4307E-01	1.00E 02	1.3819E-01
1.20E 02	1.3121E-01	1.40E 02	1.2707E-01	1.60E 02	1.2506E-01
1.80E 02	1.2458E-01	2.00E 02	1.2495E-01		

Uncertainties

ENERGY RANGE (keV)	UNCERTAINTY (PER CENT)
1.0E-08 TO 4.0E 01	2.2
4.0E 01 TO 1.0E 02	2.0
1.0E 02 TO 1.8E 02	1.2
1.8E 02 TO 2.0E 02	1.6

CORRELATION MATRIX

+1.000			
+0.924	+1.000		
+0.055	+0.323	+1.000	
+0.316	+0.302	+0.627	+1.000

TABLE VI. RECOMMENDED REFERENCE DATA FOR THE $^{10}B(n, \alpha_1)$ CROSS-SECTION

(numerical values are from ENDF/B-V, MAT-1305; applicable energy range: thermal to 200 keV; log-log interpolation [47])

Cross-section values

E (keV)	XSEC (b)	E (keV)	XSEC (b)	E (keV)	XSEC (b)
1.00E-08	1.8071E 05	1.00E-05	5.7142E 03	2.53E-05	3.5923E 03
1.00E-04	1.8067E 03	1.00E-03	5.7109E 02	1.00E-02	1.8035E 02
1.00E-01	5.6795E 01	1.00E 00	1.7754E 01	1.00E 01	5.4939E 00
2.00E 01	3.8717E 00	3.00E 01	3.1664E 00	4.00E 01	2.7524E 00
5.00E 01	2.4736E 00	6.00E 01	2.2697E 00	7.00E 01	2.1124E 00
8.00E 01	1.9859E 00	9.00E 01	1.8812E 00	1.00E 02	1.7922E 00
1.20E 02	1.6471E 00	1.40E 02	1.5307E 00	1.60E 02	1.4320E 00
1.80E 02	1.3442E 00	2.00E 02	1.2626E 00		

Uncertainties

ENERGY RANGE (keV)	UNCERTAINTY (PER CENT)
1.0E-08 TO 4.0E 01	0.3
4.0E 01 TO 1.0E 02	0.7
1.0E 02 TO 1.8E 02	0.8
1.8E 02 TO 2.0E 02	1.2

CORRELATION MATRIX

+1.000			
+0.981	+1.000		
+0.861	+0.928	+1.000	
+0.729	+0.810	+0.921	+1.000

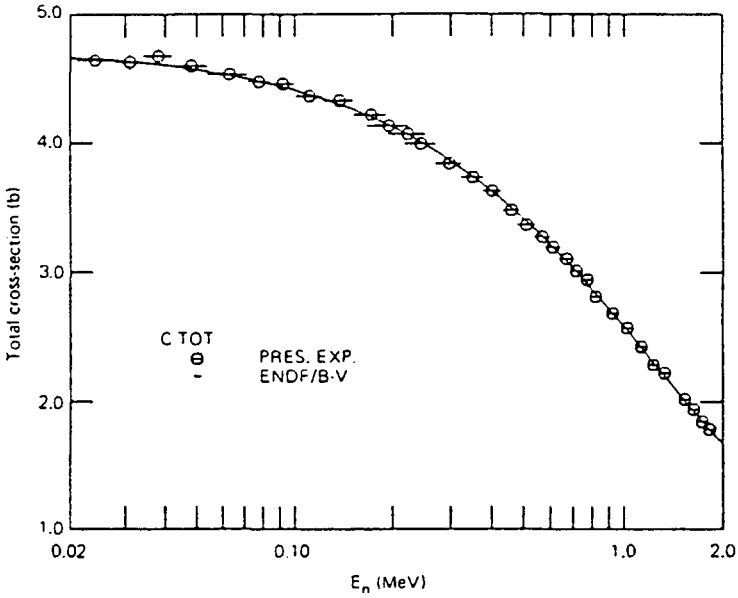

FIG. 9. Comparison of the neutron total cross-sections of natural carbon, as measured by Poenitz and Whalen, with the corresponding values given in the ENDF/B-V file [50].

It should be noted that all data considered in Ref. [51] are for natural carbon (containing 1.11% ^{13}C), while the analysis is for ^{12}C. There are two resonances in ^{13}C below 2 MeV and each resonance will still contribute about 0.2% to the natural carbon cross-sections. Therefore, the energy ranges from 0.13 to 0.18 MeV and from 1.72 to 1.78 MeV are not recommended as standards until sufficiently detailed investigations are carried out for these resonances [51]. In the upcoming ENDF/B-VI evaluation for natural carbon, the contribution to the elemental cross-section from the ^{13}C resonances at 153 keV and 1.75 MeV will be included in the R-matrix analysis [1]. Figure 10 and Tables VII and VIII detail the C(n, n) cross-section.

7. THE $^{27}Al(n, \alpha)^{24}Na$ CROSS-SECTION

This activation cross-section is a Category-I dosimetry reference and is widely employed as a standard in dosimetry and activation measurements [54]. The ENDF/B-V evaluation is recommended for the energy region from ~ 11 to 20 MeV.

7.1. Status

This ENDF/B-V evaluation was made by Hale, Stewart and Young [55]. The evaluation agrees with that of Tagesen and Vonach [54, 56] within the given errors. Except for the low threshold region at 8–9 MeV, the accuracy of the Tagesen–Vonach evaluation was claimed to be better than 5%. In particular, an accuracy of about 0.5% was estimated for the 13.5–14.8 MeV region [57]. Evain et al. have used the results of the Tagesen–Vonach evaluations [58] as well as the evaluations of Winkler and Ryves [59] and Ryves [60].

Recently, a new evaluation was performed by Kornilov et al. [61], the recommended data of which are plotted in Fig. 11, while the assigned errors can be found in Table IX. In the figure, the cited evaluations were plotted together with the results of those measurements which were not included in the evaluations (to renormalize the results of Garlea, ENDF/B-V values were used for the $^{235}U(n, f)$ cross-section). It can also be seen from this figure that ENDF/B-V agrees well (within 5%) with the experiments and evaluations cited, except in the neighbourhood of the threshold. However, in the 14 MeV region, ENDF/B-V might possibly be higher by approximately 1–2% than the majority of the experimental values. In the table, the lower and upper limits of uncertainty mean the ± uncertainties 'at least' and 'at most', respectively.

In Fig. 12, the ratios of the ENDF/B-V (dashed-dotted line) and Tagesen–Vonach (dashed line) evaluations are contrasted with the evaluation of Kornilov et al. It should be noted, however, that there is an apparent presence of structure in the evaluation by Kornilov et al. from 6 to 8.5 MeV which must be taken into account in the use of this cross-section. It was recommended at the 1984 IAEA–OECD/NEANDC Advisory Group Meeting in Geel that the reasons for the differences in the Vonach and Kornilov evaluations should be fully investigated [11]. Figure 13 and Table X illustrate and detail the $^{27}Al(n, \alpha)$ cross-section.

8. THE $^{56}Fe(n, p)^{56}Mn$ CROSS-SECTION

The cross-section standard $^{56}Fe(n, p)^{56}Mn$ is frequently used to measure fast-neutron fluence rates, especially around 14 MeV. The $^{27}Al(n, \alpha)$ or the $^{56}Fe(n, p)$ cross-sections are clearly the references for the majority of measurements where a monitor-foil or mixed-powder technique is employed and the measured quantity is, in fact, a ratio of cross-sections. However, it should be noted that the $^{56}Fe(n, p)$ cross-section was not accepted as a standard at the 1984 IAEA–OECD/NEANDC meeting in Geel because the standard cross-section of the $^{27}Al(n, \alpha)$ reaction is available in the energy region of interest. Nevertheless, the activation of natural Fe may be used as a reference, taking advantage of the higher specific activity. For this purpose, an evaluation was strongly recommended [11]. The present version of the ENDF/B-V evaluation is recommended for the energy region from ~ 11 to 20 MeV.

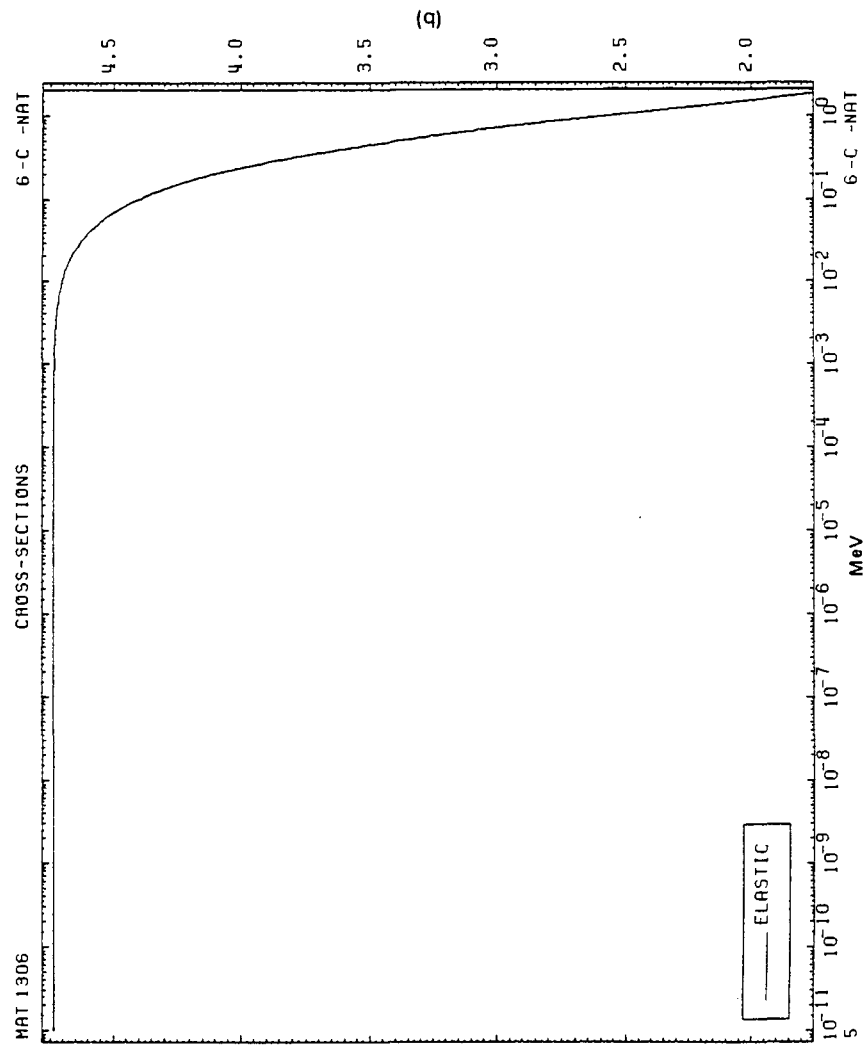
MAT 1306
CROSS-SECTIONS
6-C -NAT
(q)
4.5
4.0
3.5
3.0
2.5
2.0
ELASTIC
MeV
6-C -NAT

1 6-C - 0 ELASTIC MAT 1306

ENERGY (eV)	SIGMA (b)	ENERGY (eV)	SIGMA (b)	ENERGY (eV)	SIGMA (b)	ENERGY (eV)	SIGMA (b)
1.0000E-05	4.7392E 00	4.0000E 05	3.6182E 00	8.5000E 05	2.7888E 00	1.3500E 06	2.1739E 00
2.0000E 04	4.6653E 00	5.0000E 05	3.4033E 00	9.7500E 05	2.6108E 00	1.4750E 06	2.0552E 00
1.0000E 05	4.4084E 00	6.0000E 05	3.2076E 00	1.1000E 06	2.4503E 00	1.6250E 06	1.9277E 00
2.0000E 05	4.1172E 00	7.2500E 05	2.9868E 00	1.2250E 06	2.3052E 00	1.7750E 06	1.8155E 00
3.0000E 05	3.8551E 00						

FIG. 10. The C(n, n) cross-section (ENDF/B-V, Standards File).

TABLE VII. UNCERTAINTY DATA FOR THE C(n, n)C CROSS-SECTION [50]

ENERGY RANGE (keV)			UNCERTAINTY (PER CENT)
1	TO	250	0.46
250	TO	500	0.46
500	TO	600	0.53
600	TO	700	0.53
700	TO	750	0.53
750	TO	800	0.53
800	TO	900	0.53
900	TO	1000	0.53
1000	TO	1100	0.53
1100	TO	1200	0.53
1200	TO	1280	0.53
1280	TO	1300	0.53
1300	TO	1400	0.53
1400	TO	1500	0.53
1500	TO	1600	0.60
1600	TO	1700	0.60
1700	TO	1750	0.60
1750	TO	1800	0.60

CORRELATION MATRIX (PER CENT)

100																
38	100															
33	33	100														
33	33	71	100													
33	33	71	71	100												
33	33	29	29	57	100											
33	33	29	29	29	71	100										
33	33	29	29	29	71	71	100									
33	33	29	29	29	29	29	29	100								
33	33	29	29	29	29	29	29	71	100							
33	33	29	29	29	29	29	29	29	29	57	100					
33	33	29	29	29	29	29	29	29	29	29	71	100				
33	33	29	29	29	29	29	29	29	29	29	71	71	100			
29	29	25	25	25	25	25	25	25	25	25	25	25	25	100		
29	29	25	25	25	25	25	25	25	25	25	25	25	25	77	100	
29	29	25	25	25	25	25	25	25	25	25	25	25	25	77	77	100
29	29	25	25	25	25	25	25	25	25	25	25	25	25	22	22	67	100

TABLE VIII. RELATIVE CENTRE OF MASS NEUTRON ANGULAR DISTRIBUTIONS [50]

*(Legendre polynomial form: sum over A(I)*P(I), I = 0, 1, 2, 3, 4, 5; A(0) = 1.0)*

E (keV)	A(1)	A(2)	A(3)	A(4)	A(5)
.1000E 01	.4203E-03				
.5000E 01	.2095E-02				
.1000E 02	.4173E-02				
.5000E 02	.2018E-01	.3749E-03			
.1000E 03	.3876E-01	.1397E-02			
.2000E 03	.7164E-01	.4868E-02			
.3000E 03	.9948E-01	.9585E-02	.4437E-03		
.4000E 03	.1230E-00	.1498E-01	.8995E-03		
.5000E 03	.1426E-00	.2065E-01	.1569E-02		
.6000E 03	.1588E-00	.2636E-01	.2444E-02		
.7000E 03	.1718E-00	.3196E-01	.3498E-02	-.5140E-03	
.8000E 03	.1819E-00	.3742E=01	.4679E-02	-.9234E-03	
.9000E 03	.1892E-00	.4275E-01	.5912E-02	-.1549E-02	
.1000E 04	.1939E-00	.4807E-01	.7091E-02	-.2463E-02	
.1100E 04	.1961E-00	.5355E-01	.8092E-02	-.3750E-02	
.1200E 04	.1957E-00	.5945E-01	.8736E-02	-.5510E-02	
.1300E 04	.1927E-00	.6605E-01	.8792E-02	-.7850E-02	
.1400E 04	.1869E-00	.7385E-01	.7973E-02	-.1088E-01	.6801E-03
.1500E 04	.1784E-00	.8340E-01	.5893E-02	-.1471E-01	.9821E-03
.1600E 04	.1666E-00	.9530E-01	.1978E-02	-.1939E-01	.1388E-02
.1700E 04	.1511E-00	.1104E-00	-.4672E-02	-.2478E-01	.1923E-02
.1800E 04	.1311E-00	.1295E-00	-.1583E-01	-.3022E-01	.2604E-02
.1850E 04	.1187E-00	.1407E-00	-.2433E-01	-.3225E-01	.2998E-02
.1900E 04	.1038E-00	.1531E-00	-.3641E-01	-.3267E-01	.3410E-02
.1925E 04	.9486E-01	.1596E-00	-.4474E-01	-.3155E-01	.3610E-02
.1950E 04	.8445E-01	.1665E-00	-.5565E-01	-.2866E-01	.3789E-02
.1960E 04	.7965E-01	.1693E-00	-.6109E-01	-.2670E-01	.3850E-02
.1970E 04	.7437E-01	.1723E-00	-.6738E-01	-.2408E-01	.3900E-02
.1980E 04	.6846E-01	.1754E-00	-.7476E-01	-.2053E-01	.3934E-02
.1990E 04	.6171E-01	.1788E-00	-.8365E-01	-.1571E-01	.3947E-02
.2000E 04	.5385E-01	.1827E-00	-.9457E-01	-.9072E-02	.3927E-02

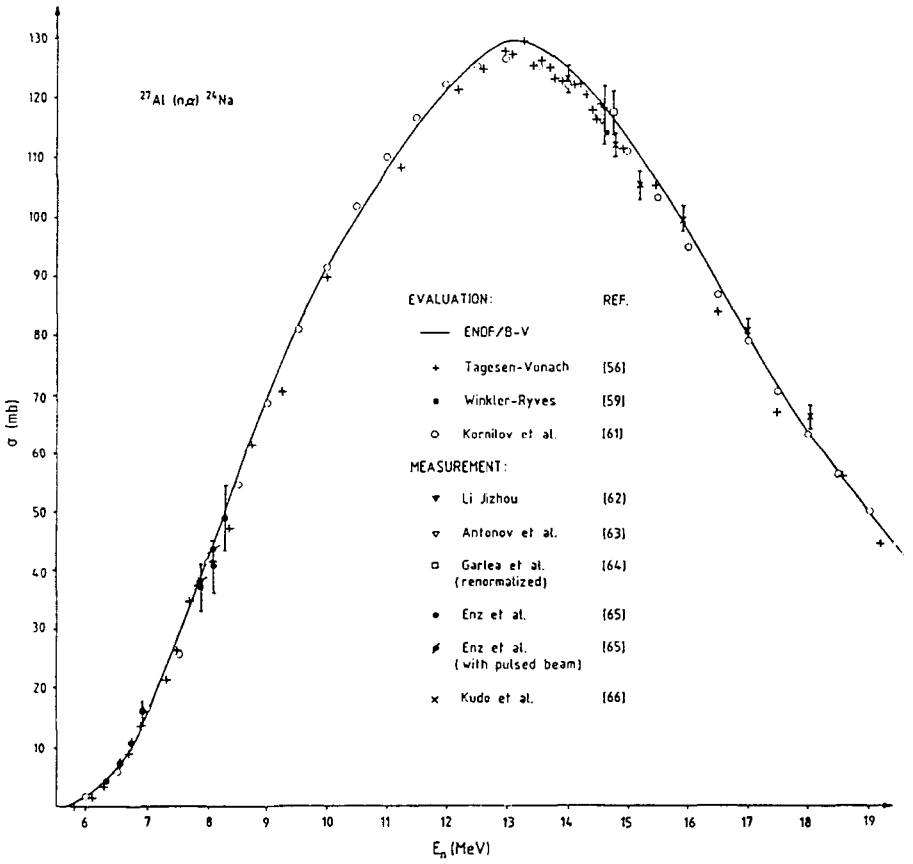

FIG. 11. Different measurements and evaluations for the $^{27}Al(n, \alpha)$ cross-section.

TABLE IX. UPPER AND LOWER UNCERTAINTY LIMITS FOR THE ^{27}Al(n, α) REACTION CROSS-SECTION [61]

Energy region (MeV)	Lower limit of uncertainty (%)	Upper limit of uncertainty (%)
5.5–6.0	15	15
6.0–8.5	5	5
8.5–11	0.8	3.8
11–13.5	0.7	5.8
13.5–15.5	0.6	2.5
15.5–17.5	0.9	4.1
17.5–20.0	1.4	7.6

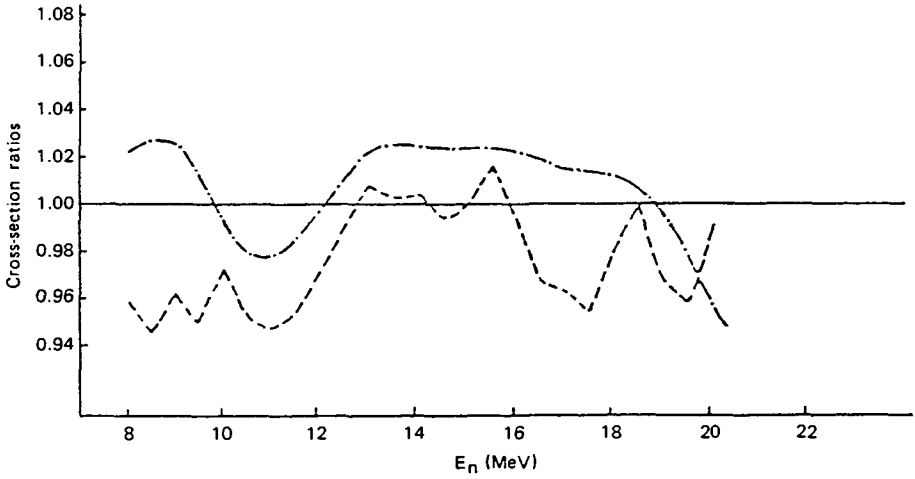

FIG. 12. Cross-section ratios of the ENDF/B-V (dashed-dotted line) and Tagesen-Vonach (dashed line) evaluations compared with the evaluation of Kornilov [61].

8.1 Status

This ENDF/B-V evaluation was carried out by Fu [67] based on work by Dudey and Kennerley [68], Smith and Meadows [69] and on other experimental data that were current at that time.

In Fig.14, the ENDF/B-IV and ENDF/B-V values are plotted as curves and are supplemented by more recent experimental data which have errors of less than 5% (these data were not included in ENDF/B-V). For the 14 MeV (and upper) energy region, the new data are, in general, above the ENDF/B-V curve (they are higher by about 4% on average). Particularly interesting are the values of Fu et al. [70], who carried out a simultaneous evaluation of the $^{32}S(n, p)$, $^{56}Fe(n, p)$ and $^{65}Cu(n, 2n)$ cross-sections, the input evaluations being those they had previously submitted for the ENDF/B-V Dosimetry File (Table XI).

Concern has been expressed that ENDF/B-V data are too low in the lower energy region. Raics et al., for example, have measured cross-sections of the $^{56}Fe(n, p)$ and other reactions relative to the $^{238}U(n, f)$ reaction in the 6.5–10.5 MeV region and calculated normalized χ^2 values for different data sets. Based on these calculations, they concluded that at an acceptance level of 97.5%, two of the data sets they examined could not be used for the $^{238}U(n, f)$ reaction, nor could ENDF/B-V be used for the $^{56}Fe(n, p)$ reaction in the 6.5–10.5 MeV energy region. It was their belief that ENDF/B-IV was the most acceptable and consistent data set for the $^{56}Fe(n, p)$ and $^{238}U(n, f)$ reactions [75].

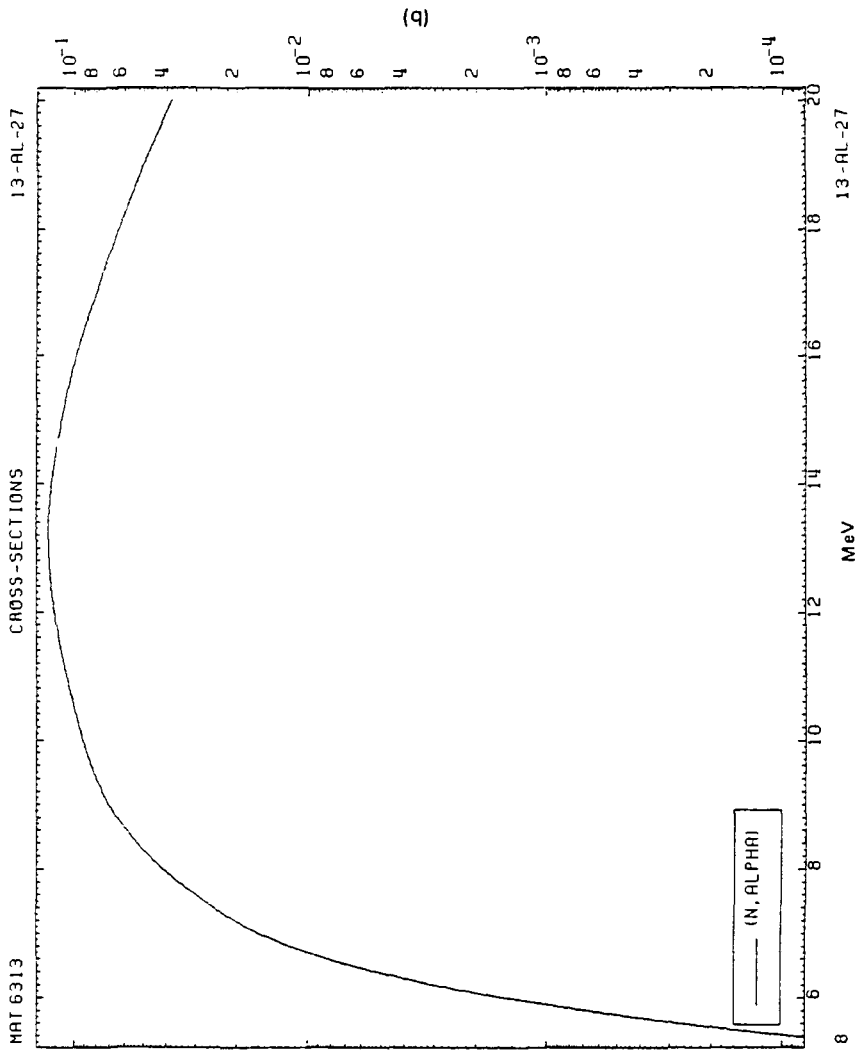
MAT 6313
CROSS-SECTIONS
13-AL-27
(b)
10^{-1}
8
6
4
2
10^{-2}
8
6
4
2
10^{-3}
8
6
4
2
10^{-4}
8
6
8
10
12
14
16
18
20
MeV
13-AL-27
(N,ALPHA)

1 13-AL- 27 (N,ALPHA) MAT 6313

ENERGY (eV)	SIGMA (b)	ENERGY (eV)	SIGMA (b)	ENERGY (eV)	SIGMA (b)	ENERGY (eV)	SIGMA (b)
5.4125E 06	9.6749E-05	5.7677E 06	5.7751E-04	6.8000E 06	1.1800E-02	1.1000E 07	1.0750E-01
5.4282E 06	1.0567E-04	5.7839E 06	6.2065E-04	6.9000E 06	1.3700E-02	1.1500E 07	1.1493E-01
5.4414E 06	1.1376E-04	5.8180E 06	7.1863E-04	7.0000E 06	1.5900E-02	1.2000E 07	1.2120E-01
5.4560E 06	1.2350E-04	5.8330E 06	7.6490E-04	7.2000E 06	2.0100E-02	1.2500E 07	1.2604E-01
5.4711E 06	1.3442E-04	5.8498E 06	8.1994E-04	7.4000E 06	2.5000E-02	1.3000E 07	1.2880E-01
5.4876E 06	1.4744E-04	5.8677E 06	8.8332E-04	7.6000E 06	3.0000E-02	1.3500E 07	1.2794E-01
5.5180E 06	1.7341E-04	5.8892E 06	9.6587E-04	7.8000E 06	3.5600E-02	1.4000E 07	1.2470E-01
5.5330E 06	1.8743E-04	5.9125E 06	1.0603E-03	8.0000E 06	4.1300E-02	1.4500E 07	1.1936E-01
5.5498E 06	2.0438E-04	5.9344E 06	1.1544E-03	8.2000E 06	4.7100E-02	1.5000E 07	1.1290E-01
5.5670E 06	2.2347E-04	5.9569E 06	1.2603E-03	8.4000E 06	5.3300E-02	1.5500E 07	1.0521E-01
5.5788E 06	2.3750E-04	5.9723E 06	1.3379E-03	8.6000E 06	5.9200E-02	1.6000E 07	9.7000E-02
5.5929E 06	2.5549E-04	5.9908E 06	1.4375E-03	8.8000E 06	6.4900E-02	1.6500E 07	8.8406E-02
5.6180E 06	2.8872E-04	6.0000E 06	1.4900E-03	9.0000E 06	7.0200E-02	1.7000E 07	7.9400E-02
5.6330E 06	3.1019E-04	6.1000E 06	2.1400E-03	9.2000E 06	7.5100E-02	1.7500E 07	7.1187E-02
5.6498E 06	3.3599E-04	6.2000E 06	2.9900E-03	9.4000E 06	7.9700E-02	1.8000E 07	6.3700E-02
5.6670E 06	3.6485E-04	6.3000E 06	4.0000E-03	9.6000E 06	8.3800E-02	1.8500E 07	5.6537E-02
5.6859E 06	3.9916E-04	6.4000E 06	5.1400E-03	9.8000E 06	8.7700E-02	1.9000E 07	4.9800E-02
5.7180E 06	4.6263E-04	6.5000E 06	6.5400E-03	1.0000E 07	9.1200E-02	1.9500E 07	4.3437E-02
5.7330E 06	4.9472E-04	6.7000E 06	9.8700E-03	1.0500E 07	9.9612E-02	2.0000E 07	3.8000E-02
5.7498E 06	5.3309E-04						

FIG. 13. The $^{27}Al(n, \alpha)$ cross-section (ENDF/B-V, Mod. 2, Dosimetry Library).

TABLE X. UNCERTAINTY DATA FOR THE $^{27}Al(n, \alpha)$ CROSS-SECTION

Energy range (eV)	Uncertainty (%)
5.4E+6 to 5.9E+6	30
5.9E+6 to 8.0E+6	25
8.0E+6 to 9.0E+6	23
9.0E+6 to 1.0E+7	22
1.0E+7 to 1.1E+7	21
1.1E+7 to 2.0E+7	5

TABLE XI. INPUT-OUTPUT DATA SETS FOR THE $^{56}Fe(n, p)$ REACTION [70]

	Input data set		Output data set	
E (MeV)	XS (mb)	STD (%)	XS (mb)	STD (%)
10	69.3	4.0	71.0	3.4
13	112.0	2.5	114.3	1.9
16	81.8	2.0	85.0	1.1

Lu Hanlin et al. [76] have concluded that between 5 and 8 MeV, the Chinese evaluation is about the same as ENDF/B-IV. Between 8 and 12 MeV, their curve is situated roughly at the half-way point between ENDF/B-IV and the evaluation of Simons and McElroy [77], the difference between the lowest curve (see Ref. [68]) and the highest curve [77] being about 7%. For the 12 to 20 MeV energy region, the evaluation of Lu Hanlin et al. is higher than that of ENDF/B-IV, indirectly implying that their curve is also higher than the ENDF/B-V curve. Evain et al. [58] also appear to believe that ENDF/B-V is too low, since they use an ENDF/B-V shape, but normalize it to the (higher) Ryves value.

As a result of the above criticisms concerning ENDF/B-V, it is recommended that only values higher than 11 MeV be used in this file. Furthermore, it is suspected that uncertainties somewhat higher than the presented ones would be more reliable. Figure 15 and Table XII detail the $^{56}Fe(n, p)$ cross-section.

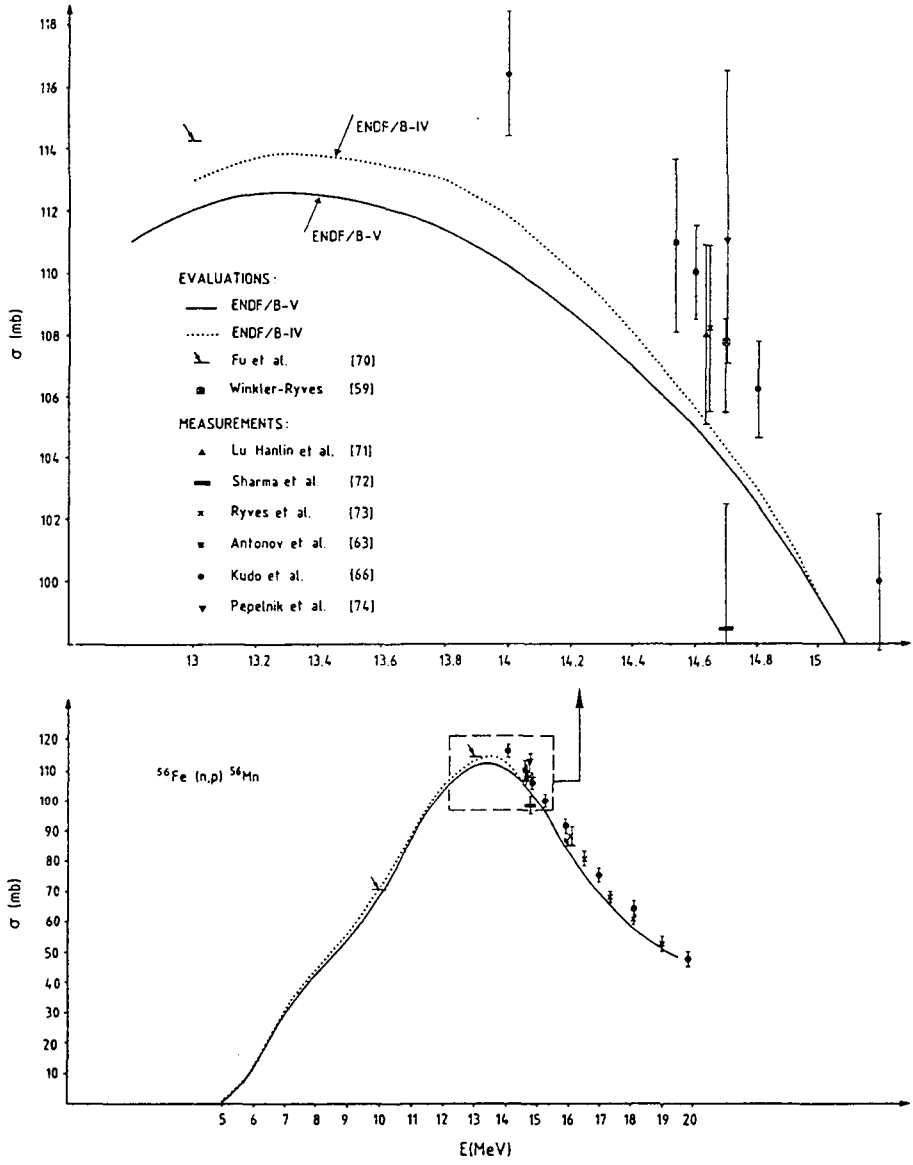

FIG. 14. ENDF/B-IV and ENDF/B-V curves compared with other recent evaluations and measurements.

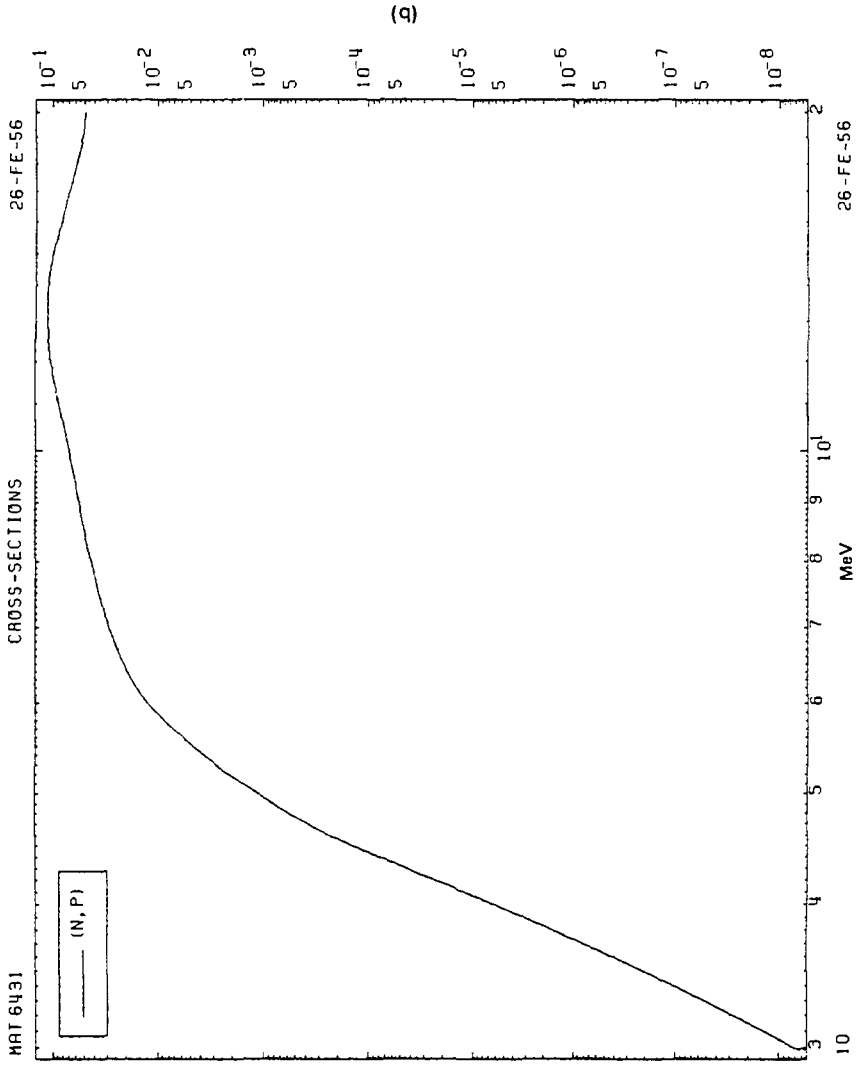
(b)
MAT 6431
CROSS-SECTIONS
26-FE-56
(N,P)
MeV
26-FE-56

1 26-FE- 56 (N,P) MAT 6431

ENERGY (eV)	SIGMA (b)	ENERGY (eV)	SIGMA (b)	ENERGY (eV)	SIGMA (b)	ENERGY (eV)	SIGMA (b)
3.0000E 06	7.0000E-09	3.6351E 06	5.1047E-07	4.2500E 06	3.2000E-05	5.2166E 06	2.2401E-03
3.0117E 06	7.5750E-09	3.6465E 06	5.5133E-07	4.2578E 06	3.3510E-05	5.2389E 06	2.4102E-03
3.0233E 06	8.1904E-09	3.6576E 06	5.9404E-07	4.2729E 06	3.6643E-05	5.2500E 06	2.5000E-03
3.0347E 06	8.8469E-09	3.6683E 06	6.3856E-07	4.2871E 06	3.9845E-05	5.2813E 06	2.7053E-03
3.0460E 06	9.5483E-09	3.6786E 06	6.8486E-07	4.3004E 06	4.3101E-05	5.3086E 06	2.8986E-03
3.0571E 06	1.0295E-08	3.6887E 06	7.3292E-07	4.3129E 06	4.6394E-05	5.3430E 06	3.1616E-03
3.0682E 06	1.1092E-08	3.6984E 06	7.8269E-07	4.3246E 06	4.9709E-05	5.3718E 06	3.4000E-03
3.0790E 06	1.1938E-08	3.7078E 06	8.3413E-07	4.3356E 06	5.3033E-05	5.4038E 06	3.6867E-03
3.0898E 06	1.2840E-08	3.7215E 06	9.1451E-07	4.3507E 06	5.7976E-05	5.4369E 06	4.0076E-03
3.1005E 06	1.3796E-08	3.7344E 06	9.9790E-07	4.3645E 06	6.2915E-05	5.4730E 06	4.3897E-03
3.1110E 06	1.4813E-08	3.7468E 06	1.0849E-06	4.3770E 06	6.7708E-05	5.5000E 06	4.7000E-03
3.1214E 06	1.5890E-08	3.7585E 06	1.1745E-06	4.3884E 06	7.2427E-05	5.5313E 06	5.0231E-03
3.1317E 06	1.7032E-08	3.7698E 06	1.2673E-06	4.4023E 06	7.8646E-05	5.5706E 06	5.4612E-03
3.1418E 06	1.8241E-08	3.7805E 06	1.3621E-06	4.4145E 06	8.4525E-05	5.6035E 06	5.8571E-03
3.1519E 06	1.9521E-08	3.7907E 06	1.4596E-06	4.4302E 06	9.2717E-05	5.6401E 06	6.3319E-03
3.1651E 06	2.1341E-08	3.8038E 06	1.5944E-06	4.4427E 06	9.9843E-05	5.6793E 06	6.8834E-03
3.1781E 06	2.3307E-08	3.8160E 06	1.7321E-06	4.4532E 06	1.0623E-04	5.7147E 06	7.4207E-03
3.1909E 06	2.5419E-08	3.8275E 06	1.8720E-06	4.4649E 06	1.1382E-04	5.7500E 06	8.0000E-03
3.2036E 06	2.7684E-08	3.8383E 06	2.0133E-06	4.4775E 06	1.2255E-04	5.7949E 06	8.6680E-03
3.2160E 06	3.0111E-08	3.8484E 06	2.1555E-06	4.4925E 06	1.3392E-04	5.8325E 06	9.2697E-03
3.2283E 06	3.2708E-08	3.8579E 06	2.2980E-06	4.5180E 06	1.5424E-04	5.8744E 06	9.9891E-03
3.2403E 06	3.5483E-08	3.8709E 06	2.5096E-06	4.5330E 06	1.6726E-04	5.9193E 06	1.0822E-02
3.2522E 06	3.8445E-08	3.8829E 06	2.7209E-06	4.5487E 06	1.8203E-04	5.9596E 06	1.1631E-02
3.2639E 06	4.1601E-08	3.8937E 06	2.9258E-06	4.5615E 06	1.9506E-04	6.0000E 06	1.2500E-02
3.2754E 06	4.4962E-08	3.9035E 06	3.1273E-06	4.5753E 06	2.1005E-04	6.2000E 06	1.5900E-02
3.2867E 06	4.8535E-08	3.9156E 06	3.3927E-06	4.5918E 06	2.2957E-04	6.4000E 06	1.9200E-02
3.2979E 06	5.2329E-08	3.9261E 06	3.6433E-06	4.6000E 06	2.4000E-04	6.8000E 06	2.5600E-02
3.3088E 06	5.6353E-08	3.9397E 06	3.9922E-06	4.6184E 06	2.5962E-04	7.0000E 06	2.8700E-02
3.3196E 06	6.0617E-08	3.9472E 06	4.2008E-06	4.6352E 06	2.7904E-04	7.5000E 06	3.6100E-02
3.3303E 06	6.5129E-08	3.9604E 06	4.5923E-06	4.6558E 06	3.0476E-04	8.0000E 06	4.2700E-02
3.3407E 06	6.9899E-08	3.9740E 06	5.0344E-06	4.6738E 06	3.2921E-04	8.5000E 06	4.8900E-02
3.3510E 06	7.4934E-08	3.9833E 06	5.3600E-06	4.6896E 06	3.5220E-04	9.0000E 06	5.5000E-02
3.3612E 06	8.0246E-08	3.9944E 06	5.7786E-06	4.7094E 06	3.8342E-04	9.5000E 06	6.1400E-02
3.3712E 06	8.5842E-08	4.0078E 06	6.3222E-06	4.7260E 06	4.1166E-04	1.0000E 07	6.9300E-02
3.3810E 06	9.1732E-08	4.0190E 06	6.8161E-06	4.7445E 06	4.4557E-04	1.0500E 07	7.7500E-02
3.3906E 06	9.7924E-08	4.0298E 06	7.3258E-06	4.7584E 06	4.7283E-04	1.1000E 07	8.7000E-02
3.4002E 06	1.0443E-07	4.0367E 06	7.6712E-06	4.7792E 06	5.1686E-04	1.1500E 07	9.5600E-02
3.4095E 06	1.1125E-07	4.0500E 06	8.3875E-06	4.8000E 06	5.6500E-04	1.2200E 07	1.0600E-01
3.4233E 06	1.2212E-07	4.0625E 06	9.1196E-06	4.8250E 06	6.1407E-04	1.2600E 07	1.1000E-01
3.4368E 06	1.3373E-07	4.0742E 06	9.8639E-06	4.8469E 06	6.6049E-04	1.3000E 07	1.1200E-01
3.4500E 06	1.4616E-07	4.0852E 06	1.0617E-05	4.8744E 06	7.2388E-04	1.3400E 07	1.1250E-01
3.4628E 06	1.5939E-07	4.0955E 06	1.1375E-05	4.8974E 06	7.8160E-04	1.3800E 07	1.1140E-01
3.4753E 06	1.7349E-07	4.1052E 06	1.2134E-05	4.9231E 06	8.5131E-04	1.4200E 07	1.0880E-01
3.4876E 06	1.8844E-07	4.1185E 06	1.3264E-05	4.9495E 06	9.2971E-04	1.4600E 07	1.0500E-01
3.4995E 06	2.0431E-07	4.1307E 06	1.4393E-05	4.9675E 06	9.8727E-04	1.5000E 07	9.9400E-02
3.5112E 06	2.2107E-07	4.1416E 06	1.5488E-05	4.9892E 06	1.0611E-03	1.5500E 07	9.0700E-02
3.5226E 06	2.3880E-07	4.1517E 06	1.6566E-05	5.0156E 06	1.1579E-03	1.6000E 07	8.1800E-02
3.5338E 06	2.5744E-07	4.1640E 06	1.7987E-05	5.0371E 06	1.2427E-03	1.6500E 07	7.6200E-02
3.5447E 06	2.7711E-07	4.1747E 06	1.9330E-05	5.0569E 06	1.3259E-03	1.7000E 07	6.9200E-02
3.5553E 06	2.9770E-07	4.1885E 06	2.1202E-05	5.0810E 06	1.4353E-03	1.7500E 07	6.3500E-02
3.5657E 06	3.1935E-07	4.1996E 06	2.2830E-05	5.1021E 06	1.5384E-03	1.8000E 07	5.8900E-02
3.5758E 06	3.4196E-07	4.2088E 06	2.4287E-05	5.1293E 06	1.6816E-03	1.8500E 07	5.4700E-02
3.5857E 06	3.6564E-07	4.2191E 06	2.6021E-05	5.1443E 06	1.7671E-03	1.9000E 07	5.1300E-02
3.5987E 06	3.9905E-07	4.2301E 08	2.8016E-05	5.1708E 06	1.9272E-03	1.9500E 07	4.9200E-02
3.6112E 06	4.3433E-07	4.2434E 06	3.0613E-05	5.1980E 06	2.1075E-03	2.0000E 07	4.8800E-02
3.6234E 06	4.7147E-07						

FIG. 15. The $^{56}Fe(n, p)$ cross-section (ENDF/B-V, Mod. 2, Dosimetry Library).

TABLE XII. UNCERTAINTY DATA FOR THE $^{56}Fe(n, p)$ CROSS-SECTION

Energy range (eV)	Uncertainty (%)
3.0E+6 to 5.0E+6	10
5.0E+6 to 5.8E+6	8
5.8E+6 to 6.4E+6	6
6.4E+6 to 8.5E+6	5
8.5E+6 to 1.1E+7	4
1.1E+7 to 1.2E+7	3
1.2E+7 to 1.6E+7	2
1.6E+7 to 2.0E+7	3

9. THE $^{197}Au(n, \gamma)^{198}Au$ CROSS-SECTION

Gold has excellent properties as a capture standard. Sample preparation is particularly easy, since the material is monoisotopic, easy to fabricate and the product nucleus has a simple decay scheme. The standard is applied with two different methods, activation and prompt gamma ray detection [1, 78]. The activation method for gold is well understood; ^{198}Au has a well known decay scheme which makes it very attractive for beta-gamma coincident counting with its inherent self-calibration [28]. The recommended energy range is from 0.2 to 3.5 MeV [78].

9.1. Status

The ENDF/B-V evaluation was carried out in conjunction with the Standards and Normalization Subcommittee of CSEWG and its Au Task Force [79].

According to one report on the status of the ENDF/B-V evaluations using experimental data published before January 1982: "There seems to be a general consensus that the most recent measurements have cross section values lower than the ENDF/B-V points for $E_n > 1$ MeV. Moreover, Macklin's work suggests that this trend continues also at lower energies" [78]. The latter statement is supported by Carlson et al. in their preliminary approach to ENDF/B-VI [42]. Blinov et al. consider ENDF/B-V to be too high for energies greater than 2 MeV [80]. Tolstikov considers ENDF/B-V "slightly overestimated" for the same energy region [81].

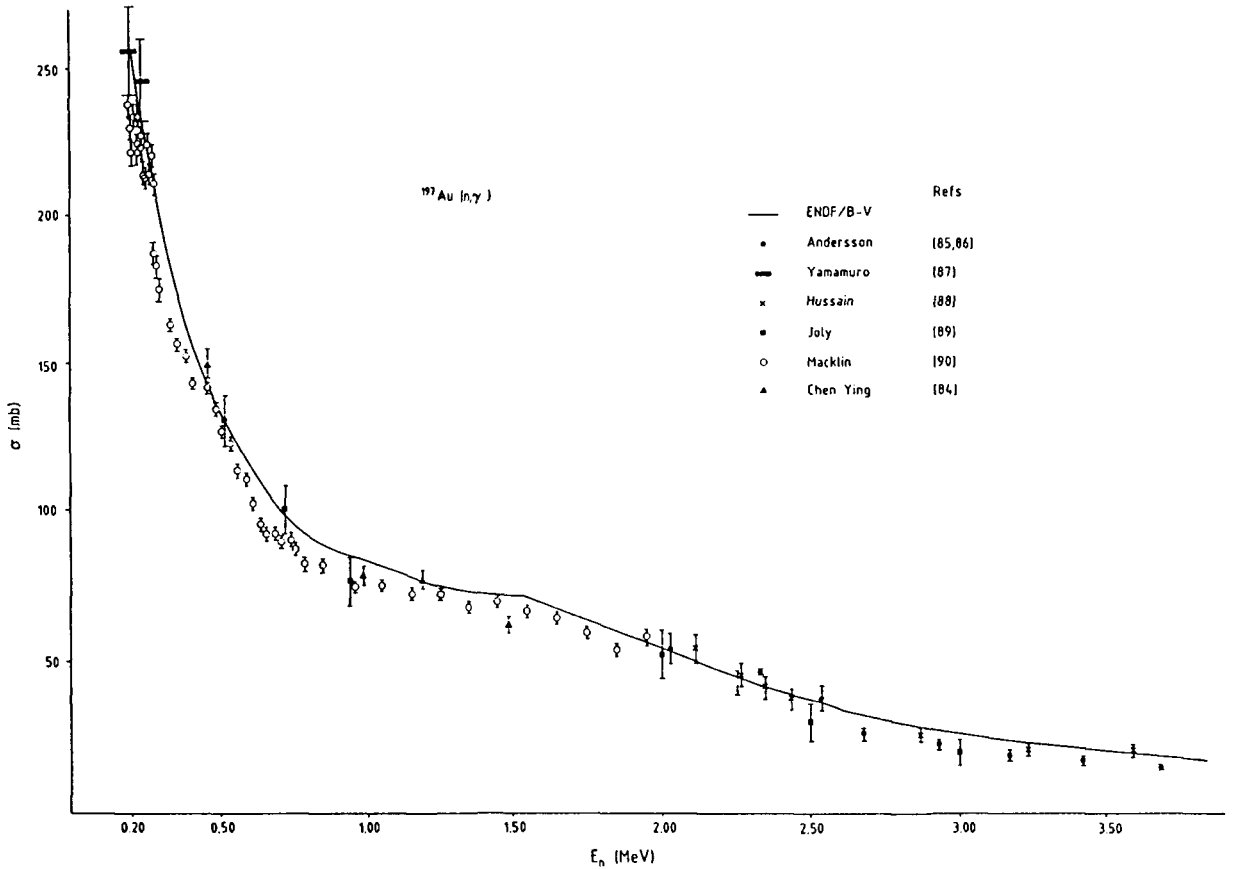

FIG. 16. Plots of ENDF/B-V versus recent data of other evaluations and measurements.

MAT 1379
CROSS-SECTIONS
79-AU-197
(N, GAMMA)
MeV
79-AU-197
(b)

1 79-AU-197 (N,GAMMA) MAT 1379

ENERGY (eV)	SIGMA (b)	ENERGY (eV)	SIGMA (b)	ENERGY (eV)	SIGMA (b)	ENERGY (eV)	SIGMA (b)
1.9900E 05	2.4420E-01	3.4000E 05	1.8600E-01	7.0000E 05	1.0100E-01	1.7000E 06	6.5000E-02
2.0000E 05	2.5750E-01	3.6000E 05	1.7500E-01	7.5000E 05	9.5200E-02	1.8000E 06	6.1500E-02
2.2000E 05	2.4500E-01	3.9000E 05	1.6300E-01	8.0000E 05	9.0800E-02	2.0000E 06	5.4000E-02
2.3000E 05	2.4000E-01	4.1000E 05	1.5600E-01	8.5000E 05	8.7200E-02	2.2000E 06	4.6000E-02
2.4000E 05	2.3400E-01	4.2000E 05	1.5280E-01	9.0000E 05	8.5500E-02	2.4000E 06	4.0000E-02
2.7000E 05	2.1900E-01	4.4000E 05	1.4700E-01	1.0000E 06	8.3000E-02	2.5000E 06	3.7500E-02
2.8000E 05	2.1480E-01	4.8000E 05	1.3800E-01	1.1000E 06	7.9200E-02	2.6000E 06	3.4200E-02
2.9000E 05	2.1000E-01	4.9000E 05	1.3600E-01	1.2000E 06	7.6000E-02	2.7000E 06	3.2000E-02
3.0000E 05	2.0650E-01	5.0000E 05	1.3460E-01	1.3000E 06	7.3500E-02	2.8000E 06	2.9500E-02
3.1000E 05	2.0100E-01	5.2000E 05	1.3000E-01	1.4000E 06	7.2000E-02	2.9000E 06	2.7500E-02
3.2000E 05	1.9500E-01	5.4000E 05	1.2600E-01	1.5000E 06	7.1500E-02	3.0000E 06	2.6000E-02
3.3000E 05	1.9100E-01	6.5000E 05	1.0800E-01	1.5500E 06	7.1000E-02	3.5000E 06	2.0500E-02

FIG. 17. The $^{197}Au(n, \gamma)$ cross-section (ENDF/B-V, Standards File).

TABLE XIII. UNCERTAINTY DATA FOR THE $^{197}Au(n, \gamma)$ CROSS-SECTION [78]

Energy range (eV)	Uncertainty (%)
2.0E 02 to 5.0E 02	6.1
5.0E 02 to 6.0E 02	4.1
6.0E 02 to 1.0E 03	4.1
1.0E 03 to 2.5E 03	20.0
2.5E 03 to 3.5E 03	20.0

Correlation matrix

+1.000				
+0.040	+1.000			
+0.040	+0.060	+1.000		
+0.000	+0.000	+0.190	+1.000	
+0.000	+0.000	+0.000	+0.960	+1.000

For the energy region below 1.15 MeV, Davletshin et al. published recently re-evaluated experimental data [82]. The original data of the same authors were different from ENDF/B-V by 16% maximally [78]. However, the former data have now been corrected for neutron scattering and they fit well to ENDF/B-V.

An evaluation by Chen Ying et al. yielded results above ENDF/B-V for energies $E_n < 2$ MeV (by 7% maximally) and very slightly below that for energies from 2.5 to 3.5 MeV [83, 84]. According to Carlson et al., who have published preliminary results for ENDF/B-VI, the new evaluation "is very similar to that of ENDF/B-V. There are changes of 5–6% in the energy range from 200 to 270 keV compared to ENDF/B-V as a result of the inclusion of data... which show structure due to competition with inelastic scattering" (page 81 of Ref. [42]).

The most recent data are plotted with the ENDF/B-V curve in Fig. 16. The agreement can be considered to be good for the energy region from 1.95 to 2.55 MeV, but otherwise ENDF/B-V is a little higher than the experiments. Andersson et al. present a slightly corrected version of the data set presented in Ref. [85], though the differences between the two data sets remain within the given errors in every case [86]. According to the results of Hussain and Hunt, the discrepancy is not as high as previously suspected for the $E_n > 2.5$ MeV region [88]. In general, it is desirable to have more (activation-type) measurements available for analysis.

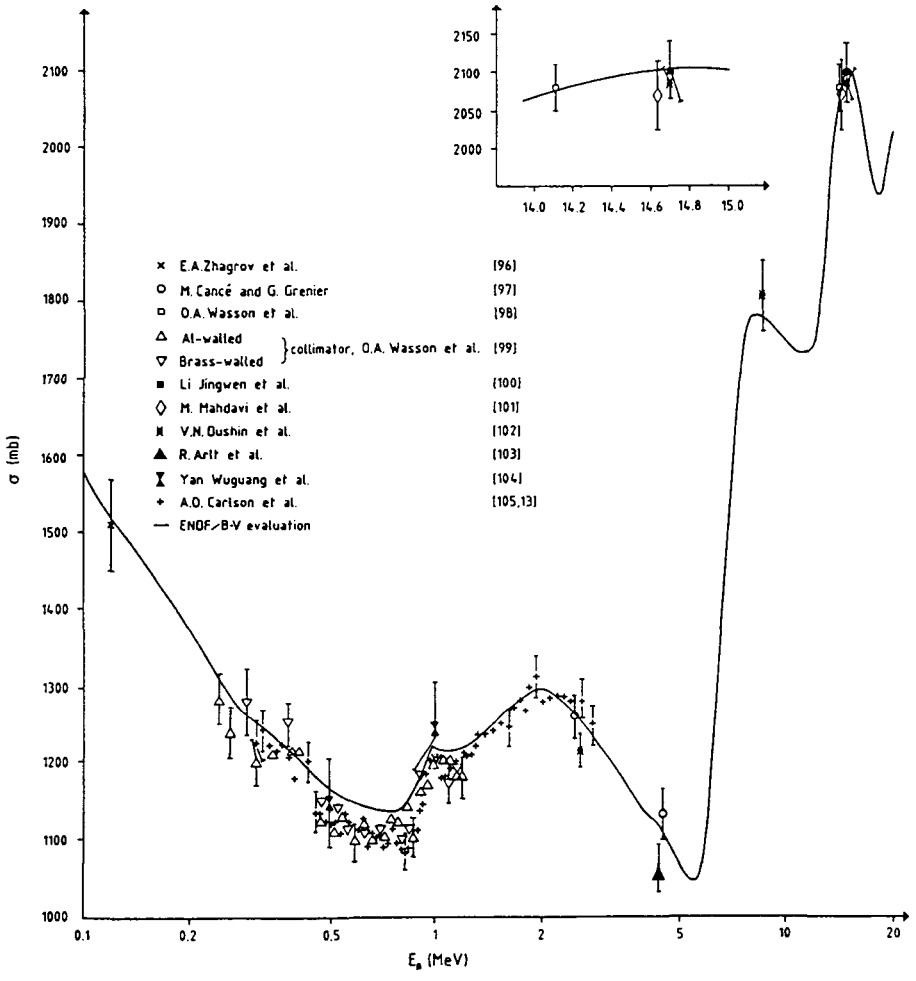

FIG. 18. Post-1980 measurements of the $^{235}U(n, f)$ cross-section plotted alongside the ENDF/B-V evaluation.

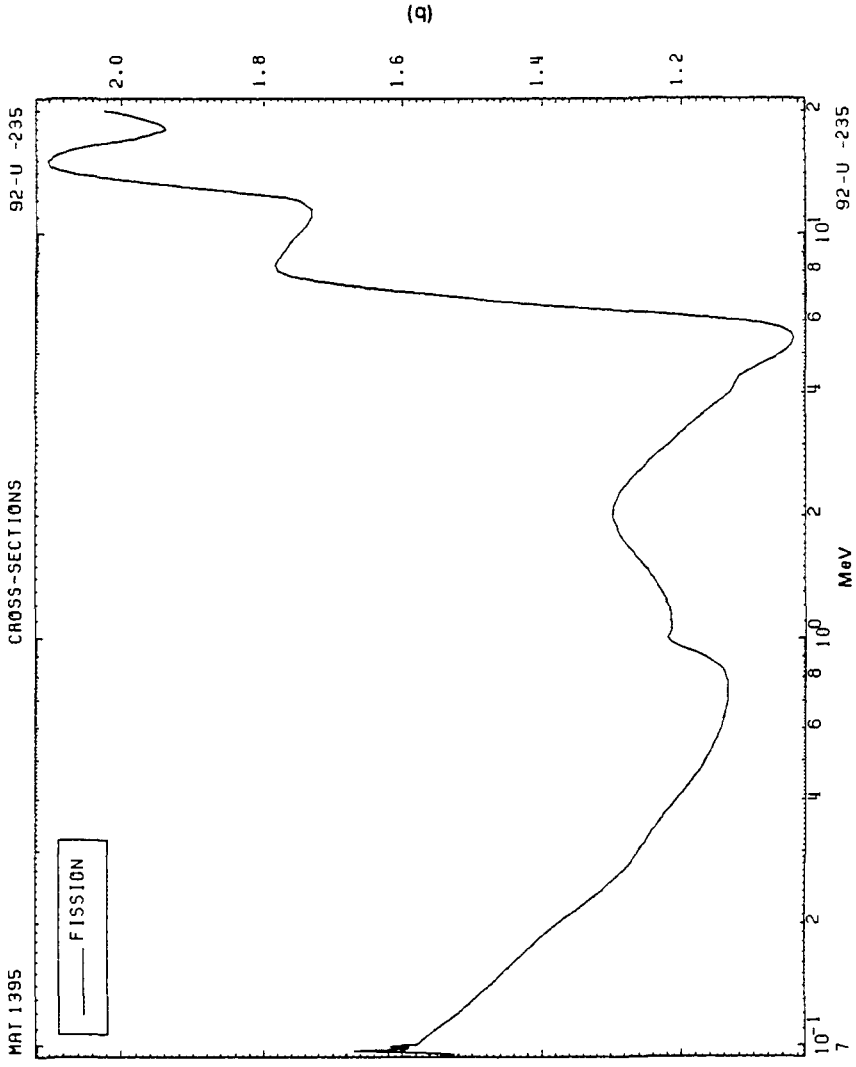
(b)
2.0
1.8
1.6
1.4
1.2
92-U -235
CROSS-SECTIONS
MAT 1395
FISSION
MeV
92-U -235

1 92-U -235 FISSION MAT 1395

ENERGY (eV)	SIGMA (b)	ENERGY (eV)	SIGMA (b)	ENERGY (eV)	SIGMA (b)	ENERGY (eV)	SIGMA (b)
9.9300E 04	1.6172E 00	9.6000E 05	1.2070E 00	5.3000E 06	1.0480E 00	1.0500E 07	1.7380E 00
9.9900E 04	1.5992E 00	9.8000E 05	1.2170E 00	5.5000E 06	1.0470E 00	1.1000E 07	1.7320E 00
1.0000E 05	1.5810E 00	1.0000E 06	1.2200E 00	5.6400E 06	1.0510E 00	1.1500E 07	1.7320E 00
1.2000E 05	1.5200E 00	1.0500E 06	1.2150E 00	5.7000E 06	1.0550E 00	1.2000E 07	1.7480E 00
1.4000E 05	1.4760E 00	1.1500E 06	1.2160E 00	5.8000E 06	1.0660E 00	1.2200E 07	1.7710E 00
1.6000E 05	1.4400E 00	1.2500E 06	1.2230E 00	5.9000E 06	1.0830E 00	1.3000E 07	1.9150E 00
2.0000E 05	1.3770E 00	1.4000E 06	1.2390E 00	6.0000E 06	1.1120E 00	1.3500E 07	1.9980E 00
2.2000E 05	1.3430E 00	1.7000E 06	1.2780E 00	6.2000E 06	1.2070E 00	1.4000E 07	2.0680E 00
2.4000E 05	1.3140E 00	1.8000E 06	1.2880E 00	6.4000E 06	1.3060E 00	1.4500E 07	2.0990E 00
2.6000E 05	1.2910E 00	2.0000E 06	1.2980E 00	6.5000E 06	1.3640E 00	1.5000E 07	2.1030E 00
2.8000E 05	1.2720E 00	2.1000E 06	1.2970E 00	6.7000E 06	1.4560E 00	1.5500E 07	2.0930E 00
4.2500E 05	1.1960E 00	2.3000E 06	1.2860E 00	7.0000E 06	1.5530E 00	1.6000E 07	2.0680E 00
4.7500E 05	1.1740E 00	2.8000E 06	1.2400E 00	7.2500E 06	1.6500E 00	1.6500E 07	2.0360E 00
5.4000E 05	1.1570E 00	3.0000E 06	1.2190E 00	7.5000E 06	1.7190E 00	1.7000E 07	1.9860E 00
6.0000E 05	1.1450E 00	3.8000E 06	1.1480E 00	7.7500E 06	1.7630E 00	1.7500E 07	1.9600E 00
7.0000E 05	1.1370E 00	4.0000E 06	1.1320E 00	8.0000E 06	1.7820E 00	1.8000E 07	1.9390E 00
7.8000E 05	1.1370E 00	4.4000E 06	1.1200E 00	8.2500E 06	1.7840E 00	1.8500E 07	1.9450E 00
8.3000E 05	1.1420E 00	5.0000E 06	1.0640E 00	8.5000E 06	1.7820E 00	1.9500E 07	1.9900E 00
8.5000E 05	1.1470E 00	5.2000E 06	1.0520E 00	9.5000E 06	1.7620E 00	2.0000E 07	2.0240E 00
9.0000E 05	1.1680E 00						

FIG. 19. The $^{235}U(n, f)$ fission cross-section (ENDF/B-V, Standards File).

TABLE XIV. UNCERTAINTY DATA FOR THE ^{235}U FISSION CROSS-SECTION [110]

ENERGY RANGE	UNCERTAINTY (PER CENT)
100 keV TO 150 keV	4.0
150 keV TO 200 keV	3.0
200 keV TO 400 keV	3.0
400 keV TO 1 MeV	3.5
1 MeV TO 2 MeV	2.5
2 MeV TO 4 MeV	3.0
4 MeV TO 10 MeV	3.5
10 MeV TO 15 MeV	4.0
15 MeV TO 20 MeV	6.0

CORRELATION MATRIX

+1.00								
+0.60	+1.00							
+0.25	+0.60	+1.00						
+0.35	+0.50	+0.60	+1.00					
+0.07	+0.10	+0.15	+0.30	+1.00				
+0.05	+0.10	+0.15	+0.25	+0.40	+1.00			
+0.00	+0.00	+0.00	+0.05	+0.30	+0.40	+1.00		
+0.00	+0.00	+0.00	+0.00	+0.05	+0.25	+0.45	+1.00	
+0.00	+0.00	+0.00	+0.00	+0.03	+0.20	+0.40	+0.80	+1.00

Another matter of interest is what uncertainties could be ascribed to ENDF/B-V. Originally, in 1982, values of 6.1% for 0.2 to 0.5 MeV, 4.1% for 0.5 to 1.0 MeV and 20.0% for 1.0 to 3.5 MeV were given [79]. Since then, Ryves, in a very detailed investigation using data published before 1983, has proposed the following uncertainties for ENDF/B-V: 8% below 2 MeV and 4% for 2 to 3.5 MeV [91]. It should be mentioned that at the 1984 IAEA–OECD/NEANDC Advisory Group Meeting in Geel, the usefulness of the gold capture standard above 1 MeV was questioned because of the small cross-section and because of background problems [11].

Finally, it should be noted that recently a deformed optical model and Hauser–Feshbach calculation, together with gamma-ray strength function formulations have been found to describe well the $n+^{197}Au$ cross-sections for E_n = 0.01–20 MeV, as well as neutron emission spectra from 14 MeV neutron reactions [92]. Figure 17 and Table XIII detail the $^{197}Au(n, \gamma)$ cross-section.

10. THE $^{235}U(n, f)$ CROSS-SECTION

The $^{235}U(n, f)$ cross-section is considered to be a standard at thermal and in the energy region from 0.1 to 20 MeV. Detectors which have been employed to implement this cross-section are basically of two types. Either the very energetic fission fragments or fission neutrons are counted. Fission fragment detection is performed with gaseous ionization chambers, scintillation chambers, solid state detectors and track-etch film techniques. Fission neutron detection is usually accomplished by using large, high efficiency neutron detectors [1].

10.1. Status

The ENDF/B-V file was derived from the evaluation by Poenitz [93] using pre-1978 data. Below 1 MeV the ENDF/B-IV, ENDF/B-V and the Sowerby et al. [94] evaluations agree reasonably well, the largest differences being less than 2%. From 1 to 1.5 MeV, the ENDF/B-V evaluation is lower than ENDF/B-IV, though the Sowerby et al. evaluation is even lower than ENDF/B-V. Above 13 MeV, ENDF/B-V is significantly lower than both the ENDF/B-IV and the Sowerby et al. evaluations, according to Carlson [1]. Otherwise, ENDF/B-V, JENDL-2, ENDL-82 and KEDAK-4 all agree with each other within 4% over the relevant MeV region [95].

The results of measurements reported since 1980 are plotted in Fig. 18 along with the ENDF/B-V evaluation. It is apparent that below about 2 MeV, the majority of the data lie below the ENDF/B-V values. (Sowerby and Patrick arrived at the same conclusion earlier using nearly the same data [106].) Above this energy the results are in reasonable agreement with ENDF/B-V (see also Ref. [107]).

According to a preliminary evaluation of ENDF/B-VI, it is approximately the same above 4 MeV, ~ 1–2% lower from 1–4 MeV and ~ 2% lower from 0.1–1 MeV compared with ENDF/B-V. An indication of the reduction in the evaluated cross-section is given by the calculated average $^{235}U(n, f)$ cross-section in a ^{252}Cf spontaneous fission neutron spectrum. This quantity is ~ 1.5% lower for the new evaluation as compared with ENDF/B-V [42]. Specifically, the value of $\langle\sigma\rangle$, that is the ^{252}Cf spectrum averaged neutron cross-section of $^{235}U(n, f)$, is 1210 ± 14 mb (recommended value), while this cross-section is 1236 mb (see Part 2–4) if calculated using ENDF/B-V for ^{235}U (n, f). The $\langle\sigma\rangle$ value calculated using ENDF/B-VI is smaller. Therefore, one can say, on the basis of the experimental values of $\langle\sigma\rangle$, that version VI of ENDF/B is preferable, or that a reduction of the ENDF/B-V values is justified in some average sense. However, it is a general feeling that the uncertainties contained in the ENDF/B-V file [93] are more or less correct, except for data at around 14 MeV where the cross-section is known to be $\leqslant 1\%$ [1, 106, 108, 109, 80]. Figure 19 and Table XIV detail the ^{235}U (n, f) cross-section.

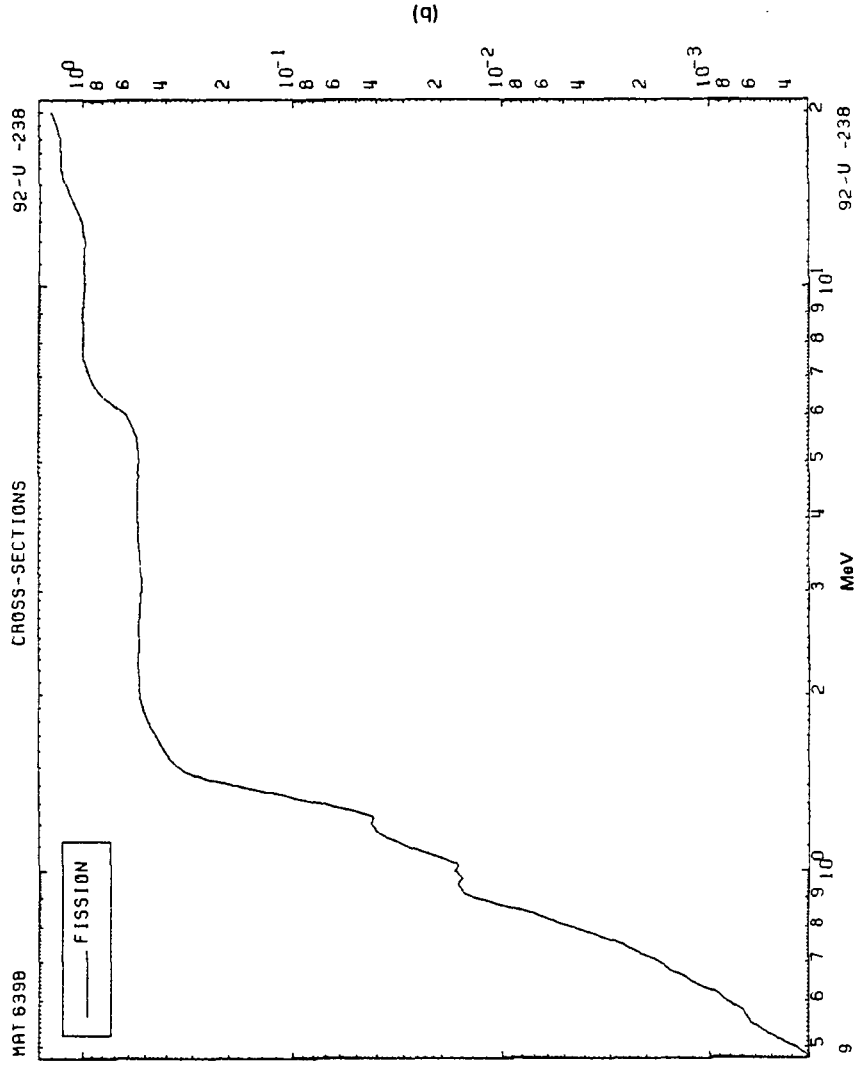
(q)
MAT 6398
CROSS-SECTIONS
92-U -238
FISSION
MeV
92-U -238

1 92-U -238 FISSION MAT 6398

ENERGY (eV)	SIGMA (b)	ENERGY (eV)	SIGMA (b)	ENERGY (eV)	SIGMA (b)	ENERGY (eV)	SIGMA (b)
5.0000E 05	3.7850E-04	1.0000E 06	1.7120E-02	1.5000E 06	3.4670E-01	6.4000E 06	7.7360E-01
5.5000E 05	6.3300E-04	1.0200E 06	1.6650E-02	1.5500E 06	3.8020E-01	6.5000E 06	8.0910E-01
5.8000E 05	6.9460E-04	1.0300E 06	1.7020E-02	1.6000E 06	4.0630E-01	6.6000E 06	8.3980E-01
5.9000E 05	7.6300E-04	1.0500E 06	1.9550E-02	1.8000E 06	4.8910E-01	6.8000E 06	8.9350E-01
6.0000E 05	8.2710E-04	1.0800E 06	2.4800E-02	1.9000E 06	5.1890E-01	7.0000E 06	9.2180E-01
6.2000E 05	9.3280E-04	1.1000E 06	2.8850E-02	2.0000E 06	5.3370E-01	7.5000E 06	9.8710E-01
6.4000E 05	1.1340E-03	1.1300E 06	3.3890E-02	2.1000E 06	5.3880E-01	9.0000E 06	9.9840E-01
6.5000E 05	1.2460E-03	1.1400E 06	3.5640E-02	2.2000E 06	5.4170E-01	1.0000E 07	9.8200E-01
6.6000E 05	1.3010E-03	1.1500E 06	3.7630E-02	2.5020E 06	5.3895E-01	1.1000E 07	9.8670E-01
6.8000E 05	1.5830E-03	1.1700E 06	4.0470E-02	2.8000E 06	5.3120E-01	1.1500E 07	9.8730E-01
7.0000E 05	1.7260E-03	1.2000E 06	4.2320E-02	3.0000E 06	5.2260E-01	1.2000E 07	9.8480E-01
7.5000E 05	2.5880E-03	1.2300E 06	4.1580E-02	3.1000E 06	5.2280E-01	1.3000E 07	1.0200E 00
7.8000E 05	3.5980E-03	1.2400E 06	4.2970E-02	3.5000E 06	5.3270E-01	1.3500E 07	1.0670E 00
8.0000E 05	4.4950E-03	1.2500E 06	4.5810E-02	3.7000E 06	5.4390E-01	1.4500E 07	1.1720E 00
8.5000E 05	7.2080E-03	1.2800E 06	5.9160E-02	4.2000E 06	5.4780E-01	1.5000E 07	1.2160E 00
8.8000E 05	1.0830E-02	1.3000E 06	7.0590E-02	4.5000E 06	5.4920E-01	1.6000E 07	1.2720E 00
9.0000E 05	1.3700E-02	1.3500E 06	1.1250E-01	5.0000E 06	5.3340E-01	1.7000E 07	1.2740E 00
9.2000E 05	1.5580E-02	1.4000E 06	1.8890E-01	5.5000E 06	5.4740E-01	1.8000E 07	1.2880E 00
9.5000E 05	1.6630E-02	1.4500E 06	2.8380E-01	6.0000E 06	6.1260E-01	1.9000E 07	1.3360E 00
9.7000E 05	1.5910E-02	1.4800E 06	3.2990E-01	6.2000E 06	6.8640E-01	2.0000E 07	1.4180E 00

FIG. 20. The $^{238}U(n, f)$ fission cross-section (ENDF/B-V, Mod. 2, Dosimetry Library).

TABLE XV. UNCERTAINTY DATA FOR THE ^{238}U FISSION CROSS-SECTION [111]

Energy (MeV)	Uncertainty (%)
0.3	8.9
0.4	10.0
0.5	12.0
0.6	11.3
0.7	11.0
0.8	8.3
0.9	7.7
1.0	7.9
1.2	6.1
1.4	7.4
1.6	1.3
2.0	1.3
2.5	2.9
3.0	2.4
4.0	2.3
5.0	2.6
6.0	3.9
8.0	3.2
10.0	2.9
12.0	3.7
14.0	4.3
20.0	8.4

11. THE ^{238}U (n, f) CROSS-SECTION

This cross-section is a useful reference standard in fast-neutron flux determinations, relative fission cross-section measurements and dosimetry applications. The threshold nature of the process makes it reasonably free of thermal background problems [111]. Detectors which have been employed to implement this cross-section are basically of two types. Either the very energetic fission

fragments or fission neutrons are counted. Fission fragment detection is performed with gaseous ionization chambers, scintillation chambers, solid state detectors and track-etch film techniques. Fission neutron detection is usually accomplished by using large, high efficiency neutron detectors [24, 1]. Originally, these cross-sections were recommended as standards between threshold and 20 MeV [24], but nowadays for energies below 2 MeV they are not recommended.

11.1. Status

The ENDF/B-V evaluation was carried out at the Argonne National Laboratory by a task force [112]. Most of the experimental information was available in the form of fission cross-section ratios relative to the ^{235}U fission cross-section, while a smaller fraction came from measurements employing absolute flux determinations. The two sources of information were separately evaluated in order to obtain the cross-sections from the ratio and absolute measured values; the two results were combined to obtain the final $^{238}U(n, f)$ cross-section values [111].

A comparison of ENDF/B-V with other files (such as JENDL-2, KEDAK-4, ENDL-82 and UKNDL-1981) has been done by Kanda and Uenohara, who concluded that the differences between the data sets were below ±6% when UKNDL-1981 was included, and below ±4% when it was excluded between 2 and 15 MeV [95]. The differences below 2 MeV were found to be very great (20% or more). It is worthwhile taking note here of Smith's conclusion concerning the applicability of the $^{238}U(n, f)$ cross-section, that it is not useful as a standard below 2 MeV [28].

Kanda made an extensive comparison with new experimental data reported since 1977. He concluded that it was not necessary to revise the earlier conclusions. In the region from threshold to 10 MeV, the recommended cross-sections were as accurate as a few per cent, while above 10 MeV, the difference between the experimental data was as large as 10% of the values [113]. It should be mentioned that there are some new measurements currently in progress that will considerably improve the situation at higher energies [28]. Finally, $^{238}U(n, f)$ values will be forthcoming from the standards evaluation process for ENDF/B-VI, as described in the Introduction. Figure 20 and Table XV detail the $^{238}U(n, f)$ cross-section.

ACKNOWLEDGEMENTS

The assistance of A.D. Carlson, H. Condé, A.B. Smith, K. Okamoto and D.E. Cullen in the preparation of this chapter is acknowledged.

REFERENCES

[1] CARLSON, A.D., Prog. Nucl. Energy **13** (1984) 79.
[2] POENITZ, W.P., WHALEN, J.F., Nucl. Phys. **A383** (1982) 224.
[3] DIAS, M.D., et al., in Nuclear Data for Science and Technology (Proc. Int. Conf. Antwerp, 1982) (BÖCKHOFF, K.H., Ed.), Reidel, Dordrecht (1983) 875.
[4] GAMMEL, J.L., in Fast Neutron Physics (MARION, J.B., FOWLER, J.L., Eds), Wiley-Interscience, New York (1963).
[5] HOPKINS, J.C., BREIT, G., Nucl. Data **A9** (1971) 137.
[6] STEWART, L., et al., Los Alamos Scientific Lab., NM, Rep. LA-4574 (1971).
[7] STEWART, L., LABAUVE, R.J., YOUNG, P.G., in Brookhaven National Lab., Upton, NY, Rep. BNL-NCS-51619 (1982) 3.
[8] LOMON, E., WILSON, R., Phys. Rev. C **9** (1974) 1329.
[9] DILG, W., Phys. Rev. C **11** (1975) 103.
[10] UTTLEY, C.A., "The H(n, n) cross section", Nuclear Data Standards for Nuclear Measurements, Technical Reports Series No. 227, IAEA, Vienna (1983) 3.
[11] CONDÉ, H., private communication to K. Okamoto, 1985.
[12] TORNOW, W., et al., Nucl. Phys. **A340** (1980) 34.
[13] CARLSON, A.D., private communication to K. Okamoto, 1985.
[14] STEWART, L., in Brookhaven National Lab., Upton, NY, Rep. BNL-NCS-51619 (1982) 19.
[15] HALE, G.M., STEWART, L., YOUNG, P.G., Los Alamos Scientific Lab., NM, Rep. LA-6518-MS (1976).
[16] ALS-NIELSEN, J., DIETRICH, O., Phys. Rev. **133B** (1964) 925.
[17] GIBBONS, J.H., MACKLIN, R.L., Phys. Rev. **114** (1959) 571.
[18] MACKLIN, R.L., GIBBONS, J.H., in Study of Nuclear Structures with Neutrons (Proc. Int. Conf. Antwerp, 1965), North-Holland, Amsterdam (1966) 498.
[19] WASSON, O.A., in Nuclear Cross Sections for Technology (Proc. Int. Conf. Knoxville, TN, 1979), US National Bureau of Standards Special Publication 594–GA1, US Government Printing Office, Washington, DC (1980) 720.
[20] BORZAKOV, S.B., et al., Yad. Fiz. **35** (1982) 532; Sov. J. Nucl. Phys. (Engl. Transl.) **35** 3 (1982) 307.
[21] BOWMAN, C.D., et al., in Nuclear Cross Sections for Technology (Proc. Int. Conf. Knoxville, TN, 1979), US National Bureau of Standards Special Publication 594–AC6, US Government Printing Office, Washington, DC (1980) 97.
[22] LOPEZ, W.M., et al., Gulf General Atomic Co., San Diego, Rep. GA-8835 (1968) 59.
[23] HALE, G.M., Brookhaven National Lab., Upton, NY, Rep. BNL-NCS-51363, Vol. 2 (1981) 509.
[24] DERUYTTER, A. J., "Requirements for nuclear standard reference data from the users' point of view", Nuclear Standard Reference Data, IAEA-TECDOC-335, IAEA, Vienna (1985) 65.
[25] LAMAZE, G.P., in Neutron Standards and Applications (Proc. Int. Symp. Gaithersburg, MD, 1977), US National Bureau of Standards Special Publication 493, US Government Printing Office, Washington, DC (1977) 37.
[26] WESTON, L.W., ibid., p. 43.
[27] HARVEY, J.A., HILL, N.W., Nucl. Instrum. Methods **162** (1979) 507.
[28] SMITH, A.B., private communication to K. Okamoto, 1983, 1985.
[29] FARRAR, H., IV, et al., Nucl. Technol. **25** (1975) 305.
[30] FARRAR, H., IV, et al., Brookhaven National Lab., Upton, NY, Rep. BNL-NCS-50681 (1977) 175.

[31] KNEFF, D.W., et al., Brookhaven National Lab., Upton, NY, Rep. BNL-NCS-51245 (1980) 289.
[32] WU, C.H., WOELFLE, R., QAIM, S.M., Nucl. Phys. **A329** (1979) 63.
[33] WU, C.H., WOELFLE, R., QAIM, S.M., Nucl. Phys. **A410** (1983) 421.
[34] HALE, G.M., STEWART, L., YOUNG, P.G., in Brookhaven National Lab., Upton, NY, Rep. BNL-NCS-51619 (1982) 25.
[35] DIMENT, K.M., UTTLEY, C.A., UKAEA Atomic Energy Research Establishment, Harwell, Rep. AERE-PR/NP 15,16 (1969).
[36] POENITZ, W.P., "The data for the neutron interactions with ^{6}Li and ^{10}B", Nuclear Standard Reference Data, IAEA-TECDOC-335, IAEA, Vienna (1985) 112.
[37] HALE, G.M., "The ^{6}Li(n, t)^{4}He cross section", Nuclear Data Standards for Nuclear Measurements, Technical Reports Series No. 227, IAEA, Vienna (1983) 11.
[38] GAYTHER, D.B., UKAEA Atomic Energy Research Establishment, Harwell, Rep. AERE-R-8856 (1977).
[39] RENNER, C., et al., Bull. Am. Phys. Soc. **23** (1978) 526.
[40] ENGDAHL, F.C., et al., Nucl. Sci. Eng. **78** (1981) 44.
[41] SHIBATA, K., Japan Atomic Energy Research Institute, Tokyo, Rep. JAERI-M-84-198 (1984).
[42] CARLSON, A.D., et al., "The neutron cross-section standards evaluations for ENDF/B-VI", Nuclear Standard Reference Data, IAEA-TECDOC-335, IAEA, Vienna (1985) 77.
[43] CARLSON, A.D., in Neutron Standards and Applications (Proc. Int. Symp. Gaithersburg, MD, 1977), US National Bureau of Standards Special Publication 493, US Government Printing Office, Washington, DC (1977) 85.
[44] HALE, G.M., STEWART, L., YOUNG, P.G., in Brookhaven National Lab., Upton, NY, Rep. BNL-NCS-51619 (1982) 31.
[45] YOUNG, P.G., The ^{10}B(n, α)^{7}Li Reaction, Los Alamos National Lab., NM, Rep. LA-UR-84-2083 (1984).
[46] QI, Huiquan, et al., in IAEA/International Nuclear Data Committee, Vienna, Rep. INDC(CPR)-001/L (1985) 14.
[47] WATTECAMPS, E., "The ^{10}B(n, α) cross section", Nuclear Data Standards for Nuclear Measurements, Technical Reports Series No. 227, IAEA, Vienna (1983) 19.
[48] WRENDA 83/84 (PIKSAIKIN, V., Ed.), IAEA/International Nuclear Data Committee, Vienna, Rep. INDC(SEC)-88/URSF (1983).
[49] SMITH, A.B., et al., in Nuclear Data for Science and Technology (Proc. Int. Conf. Antwerp, 1982) (BÖCKHOFF, K.H., Ed.), Reidel, Dordrecht (1983) 39.
[50] SMITH, A.B., "The C(n, n) cross section", Nuclear Data Standards for Nuclear Measurements, Technical Reports Series No. 227, IAEA, Vienna (1983) 25.
[51] FU, C.Y., PEREY, F.G., in Brookhaven National Laboratory, Upton, NY, Rep. BNL-NCS-51619 (1982) 35.
[52] HOLT, R., SMITH, A., WHALEN, J., Argonne National Lab., IL, Rep. ANL/NDM-43 (1978).
[53] SHIBATA, K., Japan Atomic Energy Research Institute, Tokyo, Rep. JAERI-M-83-221 (1983).
[54] VONACH, H., "The ^{27}Al(n, α) cross section", Nuclear Data Standards for Nuclear Measurements, Technical Reports Series No. 227, IAEA, Vienna (1983) 59.
[55] HALE, G.M., STEWART, L., YOUNG, P.G., Los Alamos Scientific Lab., NM, Rep. LA-8036-PR (1979) 13.
[56] TAGESEN, S., VONACH, H., Physics Data 13-1, Fachinformationszentrum, Karlsruhe (1981).

[57] CONDÉ, H., "INDC/NEANDC standards file, status report", Nuclear Standard Reference Data, IAEA-TECDOC-335, IAEA, Vienna (1985) 84.
[58] EVAIN, B.P., SMITH, D.L., LUCCHESE, P., Argonne National Lab., IL, Rep. ANL/NDM-89 (1985).
[59] WINKLER, G., RYVES, T.B., Ann. Nucl. Energy **10** (1983) 601.
[60] RYVES, T.B., "A simultaneous evaluation of some important cross-sections at 14.70 MeV, Nuclear Standard Reference Data, IAEA-TECDOC-335, IAEA, Vienna (1985)
[61] KORNILOV, N.V., et al., "Evaluation of the ^{27}Al(n, α) reaction cross-section in energy range 5.5 MeV-20 MeV", Nuclear Standard Reference Data, IAEA-TECDOC-335, IAEA, Vienna (1985) 135.
[62] LI, Jizhou, in IAEA/International Nuclear Data Committee, Vienna, Rep. INDC(CPR)-001/L (1985).
[63] ANTONOV, A., et al., Bulg. J. Phys. **10** (1983) 601.
[64] GARLEA, I., et al., IAEA/International Nuclear Data Committee, Vienna, Rep. INDC(ROM)-15/GI (1983).
[65] ENZ, W., et al., OECD/NEA Nuclear Data Committee, Paris, Rep. NEANDC-(E)-242-U (1983), Vol. 5, p. 57.
[66] KUDO, K., et al., "Cross-section measurements of ^{56}Fe (n, p)^{56}Mn and ^{27}Al(n, α)^{24}Na between 14.0 and 19.9 MeV", Nuclear Standard Reference Data, IAEA-TECDOC-335, IAEA, Vienna (1985) 449.
[67] FU, C.Y., ORNL, Oak Ridge National Lab., TN, ENDF/B-V Dosimetry File (1978) Mat. 6431.
[68] DUDEY, N.D., KENNERLEY, R., in Brookhaven National Lab., Upton, NY, Rep. BNL-NCS-50446 (1975) 80.
[69] SMITH, D.L., MEADOWS, J.W., Nucl. Sci. Eng. **58** (1975) 314.
[70] FU, C.Y., et al., in Nuclear Cross Sections for Technology (Proc. Int. Conf. Knoxville, TN, 1979), US National Bureau of Standards Special Publication 594-AB7, US Government Printing Office, Washington, DC (1980) 63.
[71] LU, Hanlin, et al., At. Energy Sci. Technol. 2 (1975) 113.
[72] SHARMA, D., et al., in Nuclear Physics and Solid State Physics (Proc. Int. Symp. Bombay, 1978), Vol. 2, Department of Atomic Energy, Bombay (1979) 349.
[73] RYVES, T.B., et al., Metrologia **14** (1978) 127.
[74] PEPELNIK, R., et al., OECD/NEA Nuclear Data Committee, Paris, Rep. NEANDC-(E)-252U (1984) 30.
[75] RAICS, P., et al., in Neutron Physics (Proc. 5th All-Union Conf. Kiev, 1980), Vol. 1, TsNII atominform, Moscow (1980) 242.
[76] LU, Hanlin, Chin. J. Phys. 3 (1981) 289.
[77] SIMONS, R.L., McELROY, W.N., Battelle Pacific Northwest Labs., Richland, WA, Rep. BNWL-1312 (1970).
[78] CORVI, F., "The ^{197}Au(n, γ) cross section", Nuclear Data Standards for Nuclear Measurements, Technical Reports Series No. 227, IAEA, Vienna (1983) 33.
[79] MUGHABGHAB, S.F., in Brookhaven National Lab., Upton, NY, Rep. BNL-NCS-51619 (1982) 47.
[80] BLINOV, M.V., et al., "IAEA standards file: some comments and recommendations", Nuclear Standard Reference Data, IAEA-TECDOC-335, IAEA, Vienna (1985) 89.
[81] TOLSTIKOV, V.A., "Comments to the evaluation of fast neutron radiation capture by ^{197}Au given in the book of standard nuclear data", Nuclear Standard Reference Data, IAEA-TECDOC-335, IAEA, Vienna (1985) 147.
[82] DAVLETSHIN, A.N., et al., in Nuclear Physics (Proc. 6th All-Union Conf. Kiev, 1983), Neutronnaya Fiz. 3 (1984) 211 (in Russian).

[83] CHEN, Ying, et al., in Nuclear Data for Science and Technology (Proc. Int. Conf. Antwerp, 1982) (BÖCKHOFF, K.H., Ed.), Reidel, Dordrecht (1983) 462.
[84] CHEN, Ying, et al., Chin. J. Phys. 3 (1981) 52.
[85] ANDERSSON, P., ZORRO, R., BERGQVIST, I., "Neutron-capture cross-section measurements for ^{197}Au and ^{115}In in the energy region 2.0–7.7 MeV using the activation technique", Nuclear Standard Reference Data, IAEA-TECDOC-335, IAEA, Vienna (1985) 143.
[86] ANDERSSON, P., et al., Nucl. Phys. **A443** (1985) 404.
[87] YAMAMURO, N., et al., J. Nucl. Sci. Technol. **20** 10 (1983) 797.
[88] HUSSAIN, H.A., HUNT, S.E., Int. J. Appl. Radiat. Isot. **34** (1983) 731.
[89] JOLY, S., et al., Nucl. Sci. Eng. **70** (1979) 53.
[90] MACKLIN, R.L., Nucl. Sci. Eng. **79** (1981) 265.
[91] RYVES, T.B., Argonne National Lab., IL, Rep. ANL-83-4 (1983).
[92] YOUNG, P.G., ARTHUR, E.D., in Capture Gamma-Ray Spectroscopy and Related Topics (Proc. Int. Symp. Knoxville, TN, 1984) (RAMAN, S., Ed.), AIP Conf. Proc. No. 125, American Institute of Physics, New York (1985) 530.
[93] POENITZ, W.P., in Brookhaven National Lab., Upton, NY, Rep. BNL-NCS-51619 (1982) 59.
[94] SOWERBY, M.G., et al., Ann. Nucl. Sci. Eng. **1** (1974) 409.
[95] KANDA, Y., UENOHARA, Y., "Fission ratios involving ^{238}U, ^{237}Np, ^{239}Pu and ^{235}U fission cross-sections", Nuclear Standard Reference Data, IAEA-TECDOC-335, IAEA, Vienna (1985) 200.
[96] ZHAGROV, E.A., et al., in Neutron Physics (Proc. 5th All-Union Conf. Kiev, 1980), Vol. 3, TsNII atominform, Moscow (1980) 45.
[97] CANCÉ, M., GRENIER, G., CEA Centre d'Études de Bruyères-le-Châtel, France, Rep. CEA-N-2194 (1981).
[98] WASSON, O.A., et al., Nucl. Sci. Eng. **80** (1982) 282.
[99] WASSON, O.A., et al., Nucl. Sci. Eng. **81** (1982) 196.
[100] LI, Jingwen, et al., in Nuclear Data for Science and Technology (Proc. Int. Conf. Antwerp, (1982) (BÖCKHOFF, K.H., Ed.), Reidel, Dordrecht (1983) 55.
[101] MAHDAVI, M., et al., ibid., p. 58.
[102] DUSHIN, V.M., et al., At. Ehnerg. **55** (1983) 218.
[103] ARLT, R., et al., "Absolute measurement of the ^{235}U fission cross-section at 4.45 MeV neutron energy using the time-correlated associated particle method (TCAPM)", Nuclear Standard Reference Data, IAEA-TECDOC-335, IAEA, Vienna (1985) 174.
[104] YAN, Wuguang, et al., At. Energy Sci. Technol. **2** (1975) 133.
[105] CARLSON, A.D., et al., "Absolute measurements of the ^{235}U(n, f) cross-section for neutron energies from 0.3 to 3 MeV", Nuclear Standard Reference Data, IAEA-TECDOC-335, IAEA, Vienna (1985) 162.
[106] SOWERBY, M.G., PATRICK, B.H., "Review of recent measurements of the U-235 fission cross-section and fission fragment angular distribution between 0.1 and 20 MeV", Nuclear Standard Reference Data, IAEA-TECDOC-335, IAEA, Vienna (1985) 151.
[107] DIAS, M.S., CARLSON, A.D., JOHNSON, R.G., WASSON, O.A., "Application of the dual thin scintillator neutron flux monitor in a ^{235}U(n, f) cross-section measurement", Nuclear Standard Reference Data, IAEA-TECDOC-335, IAEA, Vienna (1985) 467.
[108] YUAN, Hanrong, IAEA/International Nuclear Data Committee, Vienna, Rep. INDC(CPR)-001/L (1985).
[109] YUAN, Hanrong, "AEP measurements of ^{235}U(n, f) and ^{238}U(n, f) cross-section", Nuclear Standard Reference Data, IAEA-TECDOC-335, IAEA, Vienna (1985) 167.

[110] YANKOV, G.B., "The ^{235}U fission cross section", Nuclear Data Standards for Nuclear Measurements, Technical Reports Series No. 227, IAEA, Vienna (1983) 39.
[111] SMITH, A.B., "The ^{238}U fission cross section", Nuclear Data Standards for Nuclear Measurements, Technical Reports Series No. 227, IAEA, Vienna (1983) 53.
[112] POENITZ, W.P., et al., Argonne National Lab., IL, Rep. ANL/NDM-32 (1977).
[113] KANDA, Y., "The ^{238}U fission cross-section, threshold to 20 MeV", Nuclear Standard Reference Data, IAEA-TECDOC-335, IAEA, Vienna (1985) 191.

Neutron Source Standards

1-3. PRODUCTION OF MONOENERGETIC NEUTRONS BETWEEN 0.1 AND 23 MeV

Neutron energies and cross-sections

M. DROSG
Institute for Experimental Physics,
University of Vienna,
Vienna, Austria

O. SCHWERER
Nuclear Data Section,
Division of Research and Laboratories,
International Atomic Energy Agency,
Vienna

Abstract

PRODUCTION OF MONOENERGETIC NEUTRONS BETWEEN 0.1 AND 23 MeV: NEUTRON ENERGIES AND CROSS-SECTIONS.

The angular dependences of neutron energies and cross-sections are given in the form of graphs for neutron production by the $^{1}H(t, n)^{3}He$, $^{1}H(^{7}Li, n)^{7}Be$, $^{2}H(d, n)^{3}He$, $^{2}H(t, n)^{4}He$, $^{3}H(p, n)^{3}He$, $^{3}H(d, n)^{4}He$ and $^{7}Li(p, n)^{7}Be$ reactions. In addition, tables with Legendre coefficients are given which allow the accurate calculation of cross-sections at arbitrary angles and energies utilizing a short computer code. The same code also calculates, relativistically, neutron energies and the conversion of angles and cross-sections from the centre of mass to the laboratory system. A discussion of the individual source properties and an intercomparison of the various sources are presented to assist in selecting the optimum neutron source for a given experimental situation.

1. INTRODUCTION

Fast monoenergetic neutrons can be produced by two-body nuclear reactions induced by projectiles from an accelerator. The target nuclei of the reaction isotope are situated in the active region of the target assembly. The target structure, which contains or supports the active part of the target and usually stops the unused portion of the beam, may affect the beam characteristics (divergence, energy profile) and may contribute neutrons of undesired energy (background). For these reasons, not only must intrinsic source properties, such as intensity (absolute value and angular dependence), energy (definition, resolution and angular dependence) and background (contamination by secondary neutrons), be discussed, but also the technical realizations of neutron sources.

Not considered here are (p, n) reactions in medium weight nuclei which produce monoenergetic neutrons down to a few keV, e.g. $^{45}Sc(p, n)^{45}Ti$, $^{51}V(p, n)^{51}Cr$ and $^{57}Fe(p, n)^{57}Co$. The properties of these reactions have been collected elsewhere [1–3]. The reactions that are discussed here are those involving the hydrogen isotopes, as well as the p-^{7}Li reaction and its inverse. The data on the former reactions are based mostly on previous work [4–8] and, for low energies, on the compilation of Liskien and Paulsen [9]. The data on the latter reactions are derived solely from a compilation by Liskien and Paulsen [10].

A number of graphs provide first information on neutron laboratory production cross-sections and energies. The ready availability of computers nowadays makes a presentation in tabular form unnecessary. The short Fortran IV program given in the appendix permits the accurate calculation of these quantities at any angle and for any energy within the range covered by the tables of the Legendre coefficients that are included here. Upon request, an even more sophisticated program, which includes the Legendre coefficients needed, can be obtained from the Nuclear Data Section (Division of Research and Laboratories) of the IAEA. This latter program was written in Fortran for ready use on PDP-11 computers of the Digital Equipment Corporation.

2. SELECTION OF THE APPROPRIATE SOURCE

The suitability of a neutron source for a given experimental problem can only be discussed in general terms because of the large variety of different experimental set-ups. The following discussion should help in selecting the most suitable type of source. However, it may not be the one routinely used at any particular installation. If that is the case, then the benefits of switching to a better source must be weighed against the effort involved. This discussion is kept at a more general level than is actually required for standard neutron activation work. Therefore, for specific applications, some of the following considerations may be disregarded.

It is obvious that the optimum source yields a result that is within the desired degree of precision in a minimum amount of time and effort. Whereas the effort depends strongly on the individual experimental set-up (such as ion sources, the accelerator, the detecting system, etc.) and, therefore, must be ignored here, the time element is strongly correlated to the type of neutron source (its intensity and the background situation). Of course, these two properties also depend on the specific experimental situation (e.g. maximum beam current, target structure, layout of the experimental area and type of sample). These influences, however, cannot be dealt with in a general way and, therefore, must be considered individually. A more detailed discussion, especially of the monochromaticity of the neutron beam, can be found elsewhere [3].

2.1. Neutron source intensity

Source intensities should be compared for equal neutron energy spreads in the sample at equal beam currents. (In practice, one would allow for the difference in maximum beam currents delivered by the machine or allowed by the maximum heat dissipation in the target.)

The neutron energy resolution depends on the effective energy spread of the charged particle beam in the active volume of the target (accelerator and target properties) and on the geometric neutron energy spread (caused by the opening angle of the sample and increased by angular straggling of the charged particles in the target and any intrinsic divergence of the charged particle beam). Using a gas target, the main contributors to the full width at half maximum (FWHM) of the energy spread for measurements at 0° are the energy straggling in the entrance foil and the energy loss in the active volume. (According to Klein et al. [11], these two contributions must be added cubically rather than quadratically.)

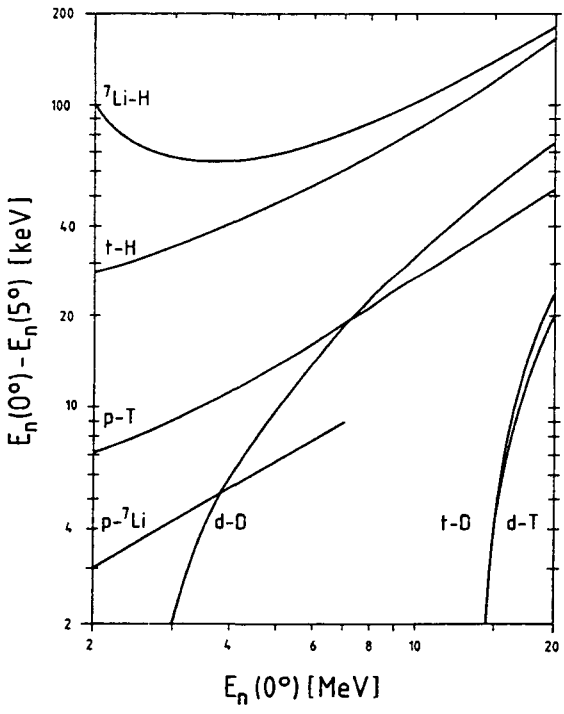

FIG. 1. Energy dependence of the maximum geometric neutron energy spread at 0° caused by a 5° opening angle of the sample for projectiles with no energy spread. The curves for t-H, p-T and p-^{7}Li can be approximated by a constant relative energy spread of 1, 0.3 and 0.15%, respectively.

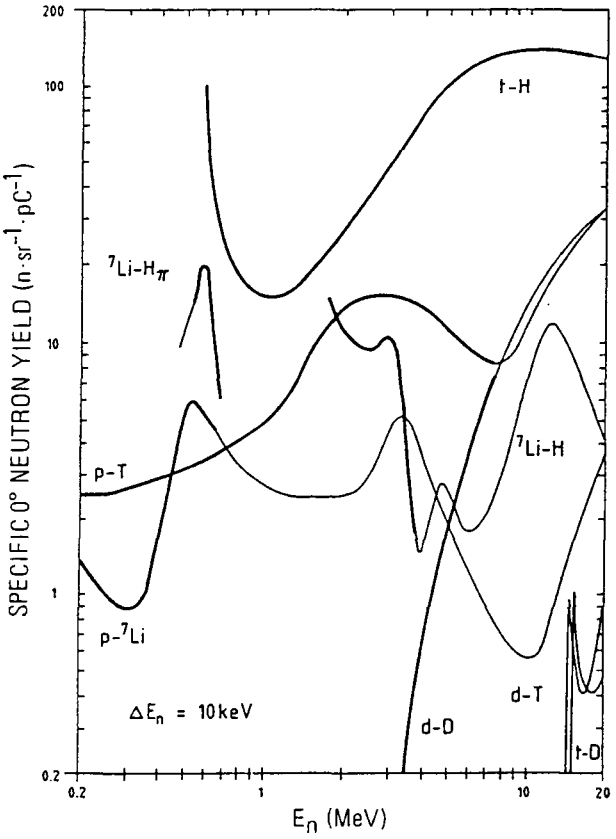

FIG. 2. Energy dependence of the specific 0° neutron yield. Except for d-T and t-D, the thick curves indicate the monoenergetic range of the reaction in question. The index π denotes the second neutron group at 0° (180° in the centre of mass system).

The finite opening angle of the sample not only further broadens the energy spread, but also results in a shift of the neutron energy to its mean by weighting the neutron energies with their intensities (the angular dependences of laboratory cross-sections and of the effective solid angles). (However, there is strong angle dependence: near 90° this shift will vanish.) Figure 1 gives the difference in neutron energy at 0° and 5° for the reactions considered here. This difference is the minimum energy spread that can be achieved for an opening angle of the sample of 5°. The curves for t-H, p-T and p-^{7}Li are quite linear, corresponding to an energy independent relative energy spread of 1, 0.3 and 0.15%, respectively. There is no simple relation to combine the FWHM geometric energy spread (for neutrons generated in the centre of the target) with the FWHM energy spread at

0° (from the energy loss of the projectile in the target) because the energy dependence of the kinematics must not be neglected. It appears that the *absolute* (additive) contribution from the finite opening angle to the FWHM of the total energy spread is minimum if the two spreads discussed before are about equal. Also, for thicker targets the geometric contribution remains small. The beam straggling [11] in the foil hardly affects the FWHM of the energy spread or the mean neutron energy, but it changes the profile of the energy distribution by producing a low energy tail.

From all these contributions to the energy resolution, the target thickness must (and can easily) be included in a general yield comparison. To first order, both the yield and the energy spread (caused by the energy loss of the charged particle beam) are proportional to the target thickness. For the reactions considered here, Fig. 2 presents the specific neutron yield at 0° as a function of the neutron energy, with a target thickness corresponding to a neutron energy spread of 10 keV (assuming singly charged incoming particles). Neutron production at 0° is usually preferred because the neutrons are unpolarized and, in general, all properties (anisotropies, the energy spread, the signal to background ratio, etc.) are optimum at this angle. For a larger acceptable neutron energy spread (at higher energies a spread of the order 0.1 MeV is more common), the yield increases in proportion to the spread. If the active region of the target consists not only of the reaction isotope, then the yield is decreased because of the additional energy loss by the other nuclei, e.g. by a factor of 10 when Ti hydrides are used for the hydrogen isotopes [3]. Nevertheless, such solid hydrogen targets can give a better overall performance when high energy resolution at lower neutron energies is necessary because the entrance foil of an equivalent gas target would give too much straggling.

The following general features can be seen from Fig. 2. The t-H reaction (^{1}H(t, n)^{3}He) has the highest specific yield, followed by the p-T reaction (^{3}H(p, n)^{3}He). Above 8 MeV, the d-D reaction (^{2}H(d, n)^{3}He) has a marginally higher yield (less than 20% higher) than the p-T reaction, while below 0.75 MeV, the p-^{7}Li reaction (^{7}Li(p, n)^{7}Be) has a higher yield than p-T. Finally, the yield of the d-T reaction (^{3}H(d, n)^{4}He), even at the resonance, is less (by more than a factor of 100) than that of the t-H reaction, while the t-D reaction (^{2}H(t, n)^{4}He) has a higher specific yield than the d-T reaction between 15.07 and 17.02 MeV. Only below about 1.7 MeV is the yield of the ^{7}Li-H reaction (^{1}H(^{7}Li, n)^{7}Be) outstanding. However, even in the 'monoenergetic' range, the second line (corresponding to 180° in the centre of mass (c.m.) system) is negligible neither in energy nor in intensity. Near 0.6 MeV, the specific neutron yield from this second line is three times that of p-^{7}Li. In special cases, where a higher energy background line is acceptable, it is possible to take advantage of this high yield.

The closeness of the d-D and the p-T curves above 8 MeV suggests the need for a more detailed comparison in this energy range. This was done in Table I under the assumption of identical gas targets (entrance foils of 5.3 mg/cm^2 molybdenum) for total energy spreads of 0.1 MeV neutron energy (which includes contributions

TABLE I. YIELD COMPARISON FOR THE SAME TOTAL NEUTRON ENERGY SPREAD (FWHM = 100 keV) AND SAME POWER (0.2 W) IN A 5.3 mg/cm^2 MOLYBDENUM ENTRANCE FOIL OF A GAS TARGET
(All energies in MeV)

	Projectile data					Neutron data				
	E_m[a]	ΔE_f[b]	ΔE_{gas}	ΔE_{geo}[c]	I_{max}[d] (μA)	ΔE_{str}[e]	ΔE_{gas}	ΔE_{geo}	Specific yield[f]	Flux[g]
8 MeV neutrons										
p-T	8.957	0.136	0.040	0.012	1.47	0.051	0.080	0.024	8.36	1.0
d-D	5.115	0.307	0.043	0.013	0.65	0.040	0.083	0.026	7.66	0.4
10 MeV neutrons										
p-T	10.941	0.118	0.040	0.015	1.70	0.052	0.079	0.030	10.9	1.5
d-D	7.134	0.252	0.043	0.017	0.79	0.043	0.082	0.032	12.5	0.8

[a] Energy of accelerated projectile.
[b] Energy loss in entrance foil.
[c] Correction of beam energy to give the correct mean neutron energy with an opening angle of $\pm 5^\circ$.
[d] Maximum current for a power of 0.2 W dissipated in the entrance foil.
[e] FWHM of energy smearing due to energy straggling.
[f] In units of $n \cdot sr^{-1} \cdot pC^{-1}$ for an energy loss in the gas resulting in a 10 keV energy spread.
[g] In units of $10^8\ n \cdot sr^{-1} \cdot s^{-1}$.

from energy and angular straggling in the entrance foil [11], energy loss of the projectiles in the gas and a typical opening angle of the sample of $\pm 5°$) and for the same dissipated power of 0.2 W in the entrance foil. Under these conditions, the yield from p-T is about a factor of two higher than that of d-D. In time of flight experiments, the p-T reaction is even more advantageous because of the better time resolution.

2.2. Neutron background and target structure

In general, in neutron activation work, the signal to background ratio cannot be increased by improving the energy resolution of the set-up. The background cannot simply be determined by integration over its energy distribution. The neutron flux within each energy bin must be weighted with its effectiveness. Since the energy dependence of the activation cross-section differs from case to case, only the intensity of the integrated background can be considered here and not its effectiveness.

The intensity of the neutron background in an actual experiment depends on a mixture of physical properties and technical possibilities. The latter cannot be dealt with in much detail because they are strongly dependent on the individual set-up. Thus, only general guide-lines will be given.

The physical properties of a source relevant to the background intensity are:

(1) The intrinsic background from the source reaction (breakup neutrons or neutrons from excited target nuclei or neutrons from a second line at forward angles when the velocity of the centre of mass is larger than that of the neutron in the c.m. system).
(2) The angular dependence of the energy and intensity of the primary neutrons.

The signal to background ratio from the first property is independent of the experiment. In the monoenergetic range indicated by the heavy lines in Fig. 2, there is no such background. When it shows up the intrinsic background cannot be subtracted experimentally by a background run. However, a correction can be calculated from known differential cross-sections of the background reaction.

The room background (scattering from air and any objects in the experimental area and its environment) is affected by the anisotropy of the intensity and of the energy of the neutron emission. For experiments at 0°, strong anisotropies of both properties give maximum signal to background ratios. However, for a simultaneous measurement at several angles, a small anisotropy of the differential laboratory cross-section will be better.

In Fig. 3, the anisotropy of the differential cross-section is expressed by the ratio of the 0° value over the angle integrated value. Three main classes of cross-section anisotropies can be discerned:

(a) (Nearly) isotropic: d-T near threshold
(b) Strong forward peaking: d-D for higher energies
(c) Containment of neutrons in a forward cone: t-H, ^{7}Li-H.

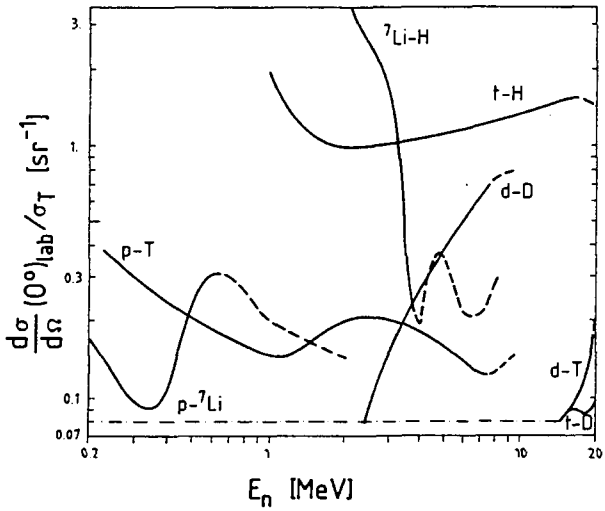

FIG. 3. Energy dependence of the forward peaking of the differential laboratory cross-sections. Inside the monoenergetic range of each reaction the curves are full. Isotropic neutron production gives a value of 0.08.

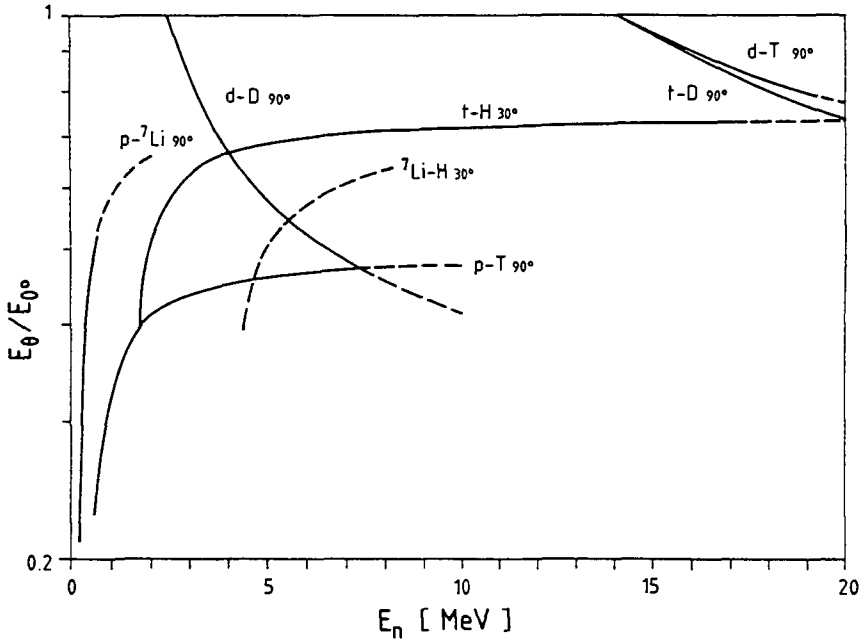

FIG. 4. Energy dependence of the forward peaking of the neutron energy distribution. The neutron energy at 90° is compared with that at 0°, except for 'contained' neutrons, where 30° is compared with 0°. Inside the monoenergetic range the curves are full.

The last class depends on the confinement of the neutrons into a forward cone when the velocity of the centre of mass is larger than the c.m. velocity of the neutron. This confinement gives minimum room background and simplifies shielding. However, at each angle inside the cone there will be two neutron groups with different energies.

For negative Q-value reactions which are of interest here, the half-angle Θ of the cone for projectiles of energy E_{in} can be derived from the equation

$$\sin^2\Theta = \frac{M_2 M_4}{M_1 M_3}\left(1 - \frac{E_{th}}{E_{in}}\right) \qquad (1)$$

The masses M_i are those of the projectile, the target, the neutron and of the residual nucleus, respectively, while E_{th} is the threshold energy of the reaction in question. The cone opens with increasing energy E_{in} and the energy of the transition from the double-valued to the single-valued region can be obtained by setting Eq. (1) equal to 1.

For the t-H and the ^{7}Li-H reactions mentioned above, the mass factor in Eq. (1) is close to 1 so that in both cases Θ is given approximately by

$$\Theta = \arcsin\left[\left(1 - \frac{E_{th}}{E_{in}}\right)^{1/2}\right] \qquad (2)$$

This approximation agrees, to better than 0.1°, with the relativistic results for all incoming energies that are considered here.

In Fig. 4, the decrease of the neutron energy with the laboratory angle is presented by the ratio of the energy at 90° (or, for contained neutrons, at 30°) over the energy at 0°. A strong decrease with angle (as in the p-T case), i.e. a strong 'anisotropy' of the energy, reduces the effectiveness of room background, especially in reactions (or detectors) which are insensitive to lower energy neutrons.

The structural background stems from the interaction of the incoming charged particle beam with matter other than the actual target isotope. Usually contributions from the machine (beam line) and the target structure (including the beam stop) will be noticed. This background should be minimized by using high Z materials (such as gold, tantalum and platinum) in the case of deuteron beams and (isotopically pure) materials with sufficiently high (p, n) thresholds for proton beams. In the case of deuteron beams, carbon, stemming from hydrocarbonates in the vacuum system and deposited on the target, is often a source of background neutrons. Therefore, either cold traps must remove the hydrocarbonates from the vacuum or hydrocarbonates must be avoided, e.g. by using mercury diffusion pumps.

The structural background can be subtracted experimentally, at least to a first order, by substituting the neutron production target with a dummy of the same construction, but without the actual target isotope. For thick targets there

will be a noticeable over-correction due to the absence of the energy loss in the target isotope.

2.2.1. Gas targets [12, 13]

For gaseous targets the evacuated gas cell can serve as the dummy for the background run. In favourable cases, such as the p-T reaction, a dummy gas with a sufficiently high neutron production threshold (in our example, H_2) can be used to make up for the energy loss by the target isotope.

The entrance foil of a gas target which separates the gas from the vacuum of the beam line must be of a material with the following, in some respects contradictory, properties:

(1) Good mechanical strength to withstand a pressure difference of several atmospheres.[1]
(2) Good thermal conductivity to avoid an excessive local temperature at the beam spot.
(3) Small neutron production cross-sections to minimize the intensity of background neutrons.
(4) A low atomic number and/or a small areal density to minimize energy loss and straggling of the incoming beam.

Commonly used materials are Havar[2], nickel, molybdenum, tantalum and tungsten in thicknesses of several μm [3].

A practical very low background cell for the p-T reaction would have a ^{58}Ni entrance foil and a ^{28}Si beam stop [14]. However, when nickel is heated (e.g. locally by an intense beam), it becomes slightly permeable for the hydrogen isotopes, resulting in small losses of tritium into the vacuum system. No leakage is observed when a molybdenum foil is used as the entrance window. The high gamma flux associated with such a low neutron background cell should not matter in activation work. A more detailed comparison of monoenergetic neutron sources with respect to the background can be found in Refs [14] and [15].

The advantages of gas targets are:

(a) Convenient determination of the areal density of the target isotope by pressure and temperature measurements, *continuously* during the experiment;
(b) Even areal thickness of the target isotope;
(c) Convenient background subtraction after emptying the cell (or replacing the target isotope with a suitable dummy gas, if available);
(d) Easy adjustment of the areal thickness of the target isotope by pressure adjustment.

---

[1] 1 standard atmosphere (atm) = 1.013 25 × 10^5 Pa (pascal).
[2] Hamilton Watch Company, Lancaster, PA, USA. Havar is a complex alloy of Co, Fe, Cr and Ni.

The disadvantages are:

(i) The entrance foil gives an energy loss and adds to the effective neutron energy spread because of angular and energy straggling, thus causing problems with very thin targets;
(ii) The entrance foil adds to the neutron background;
(iii) A longer target because of the smaller density of the target isotope, giving a less favourable geometry (and worse time resolutions which can be important in time of flight experiments);
(iv) The effective target thickness depends on the beam current (beam heating).

The beam heating not only affects the actual neutron flux, but also the effective neutron energy. The safest way to correct for the beam heating effect is to determine it experimentally by monitoring the dependence of the flux on the beam current under otherwise constant experimental conditions. For a straightforward calculation of the beam heating effect, the mean gas temperature in the target cell and in the dead volume of the filling system, as well as the ratio of cell volume to dead volume, must be known.

3. PARAMETRIZATION OF THE DIFFERENTIAL CROSS-SECTIONS

As has been pointed out earlier (Ref. [4]), the uncertainties in the effective projectile energy and in the actual 0° position are sometimes much more serious than those of the differential cross-sections themselves. Figure 5 gives the energy dependence of the relative change in the 0° cross-section for a 1% change in the projectile energy. This effect is very serious for the p-^{7}Li reaction (up to 30%) and even more so for the ^{7}Li-H reaction (with a maximum of 50% at 16 MeV). The latter reaction is not shown because its structure would not be resolved in the figure.

Figure 6 shows the maximum percentage change of the differential cross-sections for a 0.1° offset of the 0° direction. The curve for t-D coincides with the p-T curve above 7 MeV and falls rapidly below that energy. The other two inverse reactions (with their contained neutron emission) are omitted for obvious reasons.

These uncertainties not only affect the reference data, but they *must* also be considered in the experiment in which these data are needed. Therefore, the effective beam energy and/or the actual 0° position must be determined carefully if their uncertainties contribute too much to the total error. The uncertainty in the 0° position can be cancelled to a first order by performing the experiment both to the left and to the right of the incident beam.

The data presented here are not a collection of all of the experimental results, but rather their presentation in consistent sets of Legendre coefficients. These coefficients were taken from the latest available evaluations. Their accuracies are

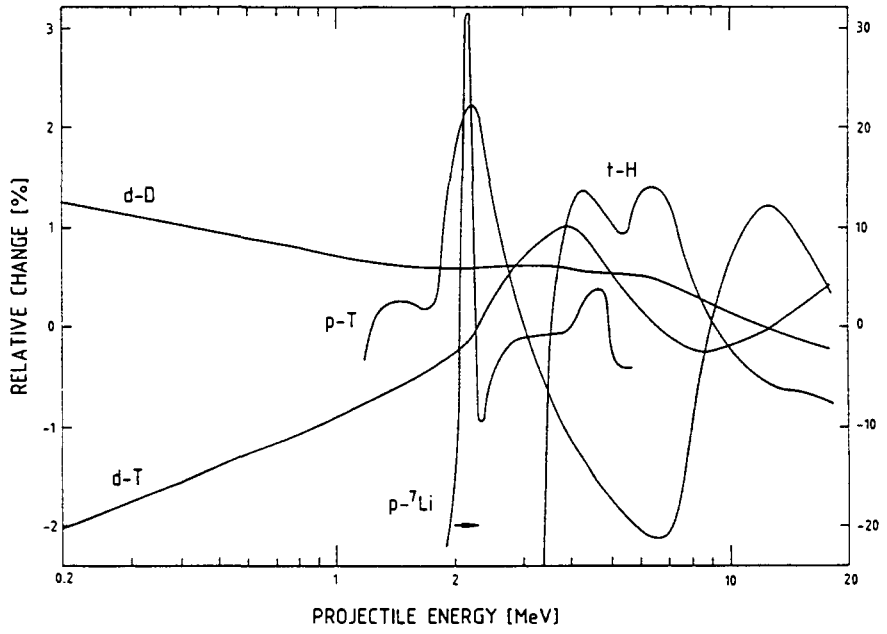

FIG. 5. Percentage change in the 0° cross-section for a 1% change in the projectile energy (use the right-hand scale for the p-^{7}Li reaction).

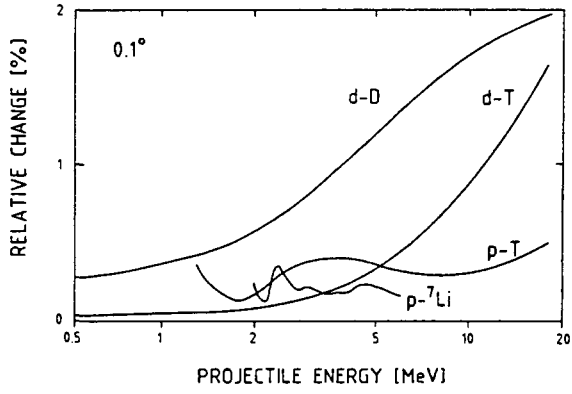

FIG. 6. Maximum percentage change in the differential cross-sections at a given projectile energy when the 0° position is offset by 0.1°.

discussed later for each reaction. The presentation follows that of Liskien and Paulsen [9]. The absolute differential c.m. cross-section at an angle Θ is given by

$$\frac{d\sigma(\Theta)}{d\Omega} = \frac{d\sigma(0^\circ)}{d\Omega} \sum A_i P_i(\Theta) \qquad (3)$$

where P_i are the Legendre polynomials and A_i the *reduced* Legendre coefficients.

The reaction kinematics data (thresholds and neutron energies) were calculated relativistically using nuclear masses derived from atomic mass tables [16]. The graphs within each section are meant to provide a convenient overview of the energy and angular dependences of the neutron energies and the laboratory cross-sections. Accurate calculations can be performed using the tables containing the Legendre coefficients and the short, interactive, self-explanatory computer code given in the appendix of this paper. A more sophisticated program, which interpolates non-linearly and includes the Legendre coefficients, can be obtained from the Nuclear Data Section (Division of Research and Laboratories) of the IAEA.

3.1. Interaction of protons with tritons

Table II gives the reduced c.m. Legendre coefficients for the $^3H(p, n)^3He$ reaction. These coefficients are taken from Ref. [4] for incoming energies, E_{in}, of 13 MeV and higher. At lower energies a new evaluation was performed [8] which included angular distributions of the $^1H(t, n)^3He$ reaction for energies E_{in} between 1.99 and 6.40 MeV and other new p-T data [17].

The scale error of the evaluated data increases from about ±1.5% between 10 and 16 MeV to about 4% at energies of 3 MeV and lower. The shape error of the angular distributions is close to ±2% between 3 and 14 MeV; it increases to ±3% at 16 and at 2.5 MeV and becomes even higher below 1.3 MeV. The uncertainty in the 0° position is typically ±0.1°, with a maximum of ±0.6° near 3 MeV. The energy uncertainty is approximately ± 0.02 MeV and decreases with decreasing energy.

Since there are not enough independent data with adequate agreement available on both sides of the resonance at 3.1 MeV, the error estimate given here might be optimistic in this energy range. Other original papers on which this evaluation is based are listed in Refs [4, 5, 9].

3.1.1. $^3H(p, n)^3He$

Above 0.7 MeV this reaction has the highest yield, if the $^1H(t, n)^3He$ reaction is disregarded. Below $E_n = 0.7$ MeV, $^7Li(p, n)^7Be$ is the better choice, not only because of the higher specific yield between 0.45 and 0.7 MeV, but also because of the ease in producing thin targets with good energy resolution. In addition, the relative kinematic energy spread at 0° (owing to the finite opening angle

TABLE II. THE $^3H(p, n)^3He$ REACTION

(Proton energy: E_{in}; c.m. differential cross-section at 0°: S_0; reduced Legendre coefficients: A_i; c.m. differential cross-section at 180°: S_π; integrated cross-section: S_t)

E_{in} (MeV)	S_0 (mb/sr)	A_0	A_1	A_2	A_3	A_4	A_5	A_6	A_7	A_8	A_9	S_π (mb/sr)	S_t (mb)
1.20	14.9	1.072	-0.150	0.078								19.4	201.
1.30	17.55	1.1070	-0.2460	0.1389								26.2	244.2
1.40	19.55	1.1365	-0.3550	0.2185								33.4	279.2
1.50	21.22	1.1688	-0.4593	0.2947	-0.0042							40.9	311.7
1.60	22.56	1.1985	-0.5455	0.3615	-0.0145							47.8	339.7
1.70	23.67	1.2229	-0.6252	0.4265	-0.0263	0.0022						54.5	363.7
1.80	24.60	1.2396	-0.6918	0.4868	-0.0376	0.0046	-0.0017					60.6	383.2
1.90	25.94	1.2281	-0.7285	0.5460	-0.0481	0.0068	-0.0043					66.5	400.4
2.00	28.39	1.1789	-0.7280	0.6023	-0.0556	0.0086	-0.0062					73.2	420.6
2.10	31.69	1.1149	-0.7035	0.6470	-0.0613	0.0098	-0.0069					80.6	444.0
2.20	35.38	1.0515	-0.6725	0.6817	-0.0650	0.0107	-0.0074	0.0008				88.1	467.6
2.30	39.50	0.9860	-0.6365	0.7129	-0.0680	0.0114	-0.0075	0.0017				95.7	489.3
2.40	43.60	0.9300	-0.6032	0.7370	-0.0704	0.0119	-0.0076	0.0022				103.0	509.5
2.50	47.03	0.8877	-0.5812	0.7603	-0.0745	0.0125	-0.0076	0.0028				109.4	524.6
2.60	50.15	0.8495	-0.5597	0.7796	-0.0779	0.0131	-0.0076	0.0032				114.9	535.3
2.70	52.28	0.8254	-0.5469	0.7948	-0.0828	0.0137	-0.0077	0.0035				118.9	542.3
2.80	53.86	0.8067	-0.5348	0.8060	-0.0885	0.0145	-0.0078	0.0038				121.9	546.0
2.90	54.93	0.7920	-0.5250	0.8160	-0.0949	0.0157	-0.0079	0.0042				123.9	546.7
3.00	55.72	0.7806	-0.5195	0.8269	-0.1015	0.0170	-0.0079	0.0045				125.8	546.5

3.20	56.23	0.7624	-0.5138	0.8515	-0.1168	0.0198	-0.0084	0.0053				128.1	538.7
3.40	55.55	0.7551	-0.5175	0.8767	-0.1355	0.0240	-0.0090	0.0062				129.1	527.1
3.60	53.84	0.7556	-0.5281	0.9042	-0.1584	0.0295	-0.0098	0.0070				128.8	511.2
3.80	51.48	0.7618	-0.5418	0.9336	-0.1868	0.0359	-0.0108	0.0080				127.6	492.8
4.00	48.96	0.7709	-0.5571	0.9633	-0.2178	0.0435	-0.0119	0.0090				126.0	474.4
4.50	42.37	0.8123	-0.5998	1.0241	-0.3024	0.0691	-0.0153	0.0120				120.1	432.6
5.00	36.36	0.8616	-0.6520	1.0866	-0.3958	0.1047	-0.0197	0.0155	-0.0009			114.1	393.7
5.50	30.88	0.9170	-0.7163	1.1700	-0.5122	0.1499	-0.0256	0.0196	-0.0024			108.5	355.8
6.00	26.27	0.9750	-0.7761	1.2513	-0.6454	0.2078	-0.0329	0.0246	-0.0043			102.9	321.8
6.50	22.28	1.0404	-0.8454	1.3330	-0.7903	0.2809	-0.0423	0.0305	-0.0066			97.3	291.3
7.00	19.06	1.1117	-0.9068	1.3914	-0.9372	0.3673	-0.0550	0.0373	-0.0089			91.8	266.3
7.50	16.77	1.1745	-0.9374	1.4040	-1.0607	0.4580	-0.0706	0.0440	-0.0117			86.6	247.5
8.00	15.30	1.2045	-0.9294	1.3542	-1.1202	0.5423	-0.0871	0.0500	-0.0144			81.1	231.6
8.50	14.54	1.1931	-0.8758	1.2566	-1.1144	0.6035	-0.1017	0.0547	-0.0160			75.8	218.0
9.00	14.29	1.1555	-0.7892	1.1221	-1.0631	0.6473	-0.1135	0.0571	-0.0162			70.9	207.5
9.50	14.53	1.0955	-0.6851	0.9790	-0.9722	0.6587	-0.1200	0.0581	-0.0141			66.6	200.1
10.00	14.91	1.0338	-0.5834	0.8480	-0.8807	0.6559	-0.1213	0.0584	-0.0108			62.5	193.7
11.00	16.15	0.8780	-0.4057	0.6399	-0.6787	0.6245	-0.1090	0.0557	-0.0046			54.8	178.2
12.00	17.85	0.7328	-0.2624	0.4940	-0.4948	0.5708	-0.0956	0.0548	0.0005			48.3	164.4
13.00	19.73	0.6131	-0.1527	0.4052	-0.3520	0.5084	-0.0809	0.0526	0.0049	0.0014		42.6	152.0
14.00	21.50	0.5219	-0.0684	0.3437	-0.2478	0.4571	-0.0677	0.0510	0.0081	0.0039	-0.0018	37.7	141.0
15.00	23.02	0.4530	-0.0036	0.3023	-0.1725	0.4117	-0.0543	0.0504	0.0108	0.0069	-0.0047	33.3	131.0
16.00	24.38	0.3983	0.0445	0.2761	-0.1151	0.3710	-0.0423	0.0505	0.0133	0.0095	-0.0058	29.5	122.0

TABLE III. Q-VALUES, THRESHOLDS AND NEUTRON ENERGIES AT $0°_{lab}$ FOR p-T
(All energies in MeV)

Exit channel	n + ^{3}He		n + p + d	2n + 2p
E_{in}	$E_n(0°_{c.m.})$	$E_n(180°_{c.m.})$	E_{nmax1}	E_{nmax2}
1.019	0.064	0.064		
1.147	0.288	0.000		
8.354	7.585	–	0.525	
11.328	10.560	–	4.561	0.712
Q	−0.764		−6.257	−8.482

of the sample) is about twice that of p-^{7}Li, namely, 0.3% for a half-angle of 5° (see Fig. 1). For a 1% change in the proton energy the 0° cross-section changes by more than 1% between 1.9 and 2.6 MeV, between 3.8 and 8.1 MeV and near 12.5 MeV (see Fig. 5).

Table III summarizes the relevant reaction data, Figs 7–13 illustrate the angular dependence of the neutron energies and differential cross-sections. Above a proton energy of 8.354 MeV ($E_n(0°) = 7.585$ MeV), a continuum of breakup neutrons will be present with a maximum energy (E_{nmax}) which is typically 6 MeV less than that of the primary neutrons. Above 11.328 MeV, another source of breakup neutrons will contribute to the continuum. However, the intensity of the continuum is much less severe than in the d-D case, so that experiments even at 14.4 MeV neutron energy [18] are feasible (with an intensity 25 times higher than that of the d-T resonance neutrons). As was discussed earlier the structural neutron background can be reduced by using materials with high (p, n) thresholds. Measurements of the breakup cross-section are collected in Ref. [5], while a recent measurement [19] also includes breakup spectra.

3.1.2. $^1H(t,n)^3He$

This reaction has the highest yield (for $E_n \gtrsim 1.7$ MeV) among all known monoenergetic reactions. Between 5.6 and 11.4 MeV, the yield is at least ten times larger than for the competing p-T reaction. Up to 17.64 MeV, the reaction is intrinsically monoenergetic.

In addition, the background situation is very good, because neutrons are only emitted into a forward cone with a half-angle Θ according to Eq. (2).

Text cont. on p. 111.

THE $^{3}H(p,n)^{3}He$ REACTION

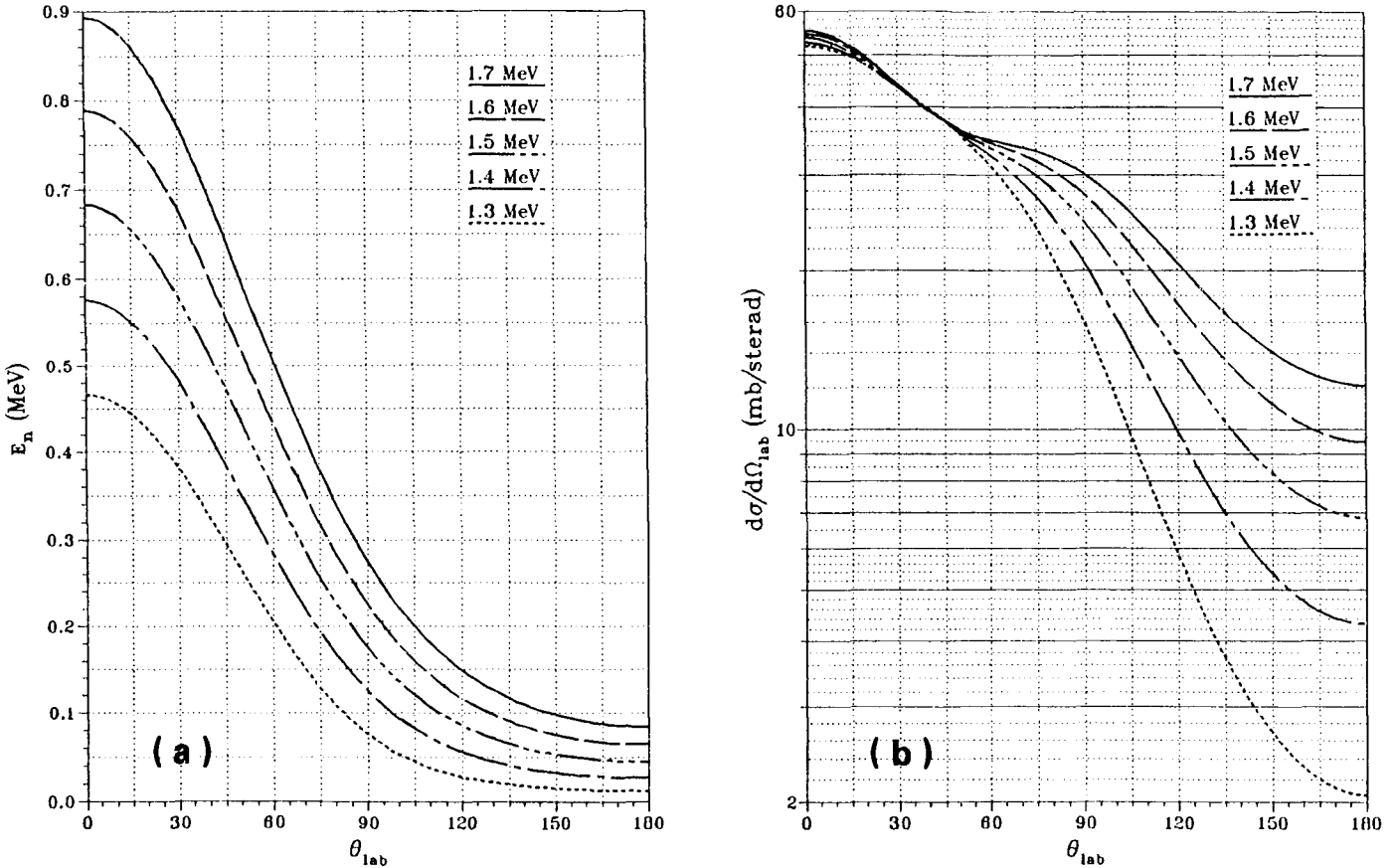

FIG. 7. (a) Neutron energy values and (b) differential cross-sections for the $^3H(p, n)^3He$ reaction: 1.3–1.7 MeV.

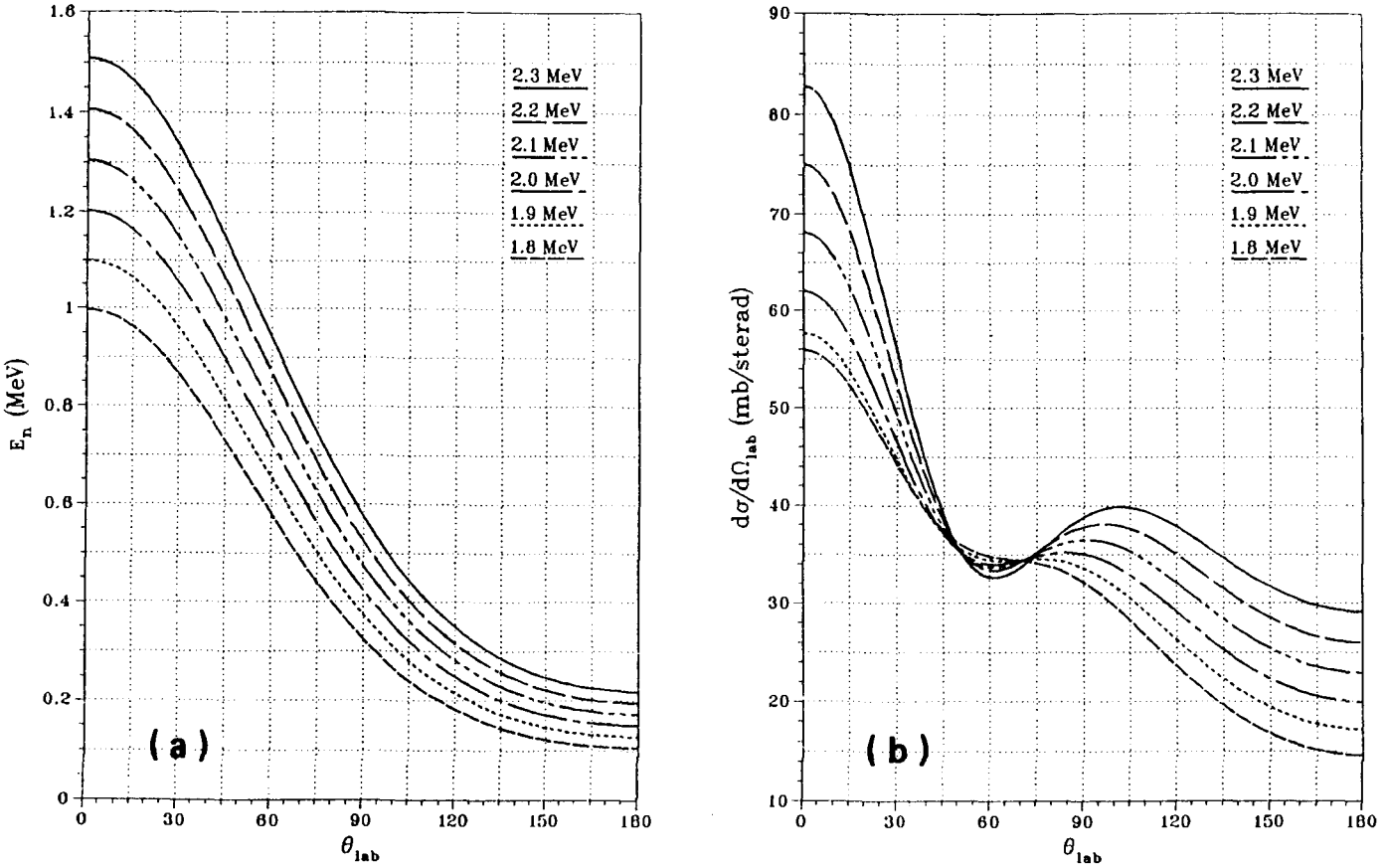

FIG. 8. (a) Neutron energy values and (b) differential cross-sections for the $^3H(p, n)^3He$ reaction: 1.8–2.3 MeV.

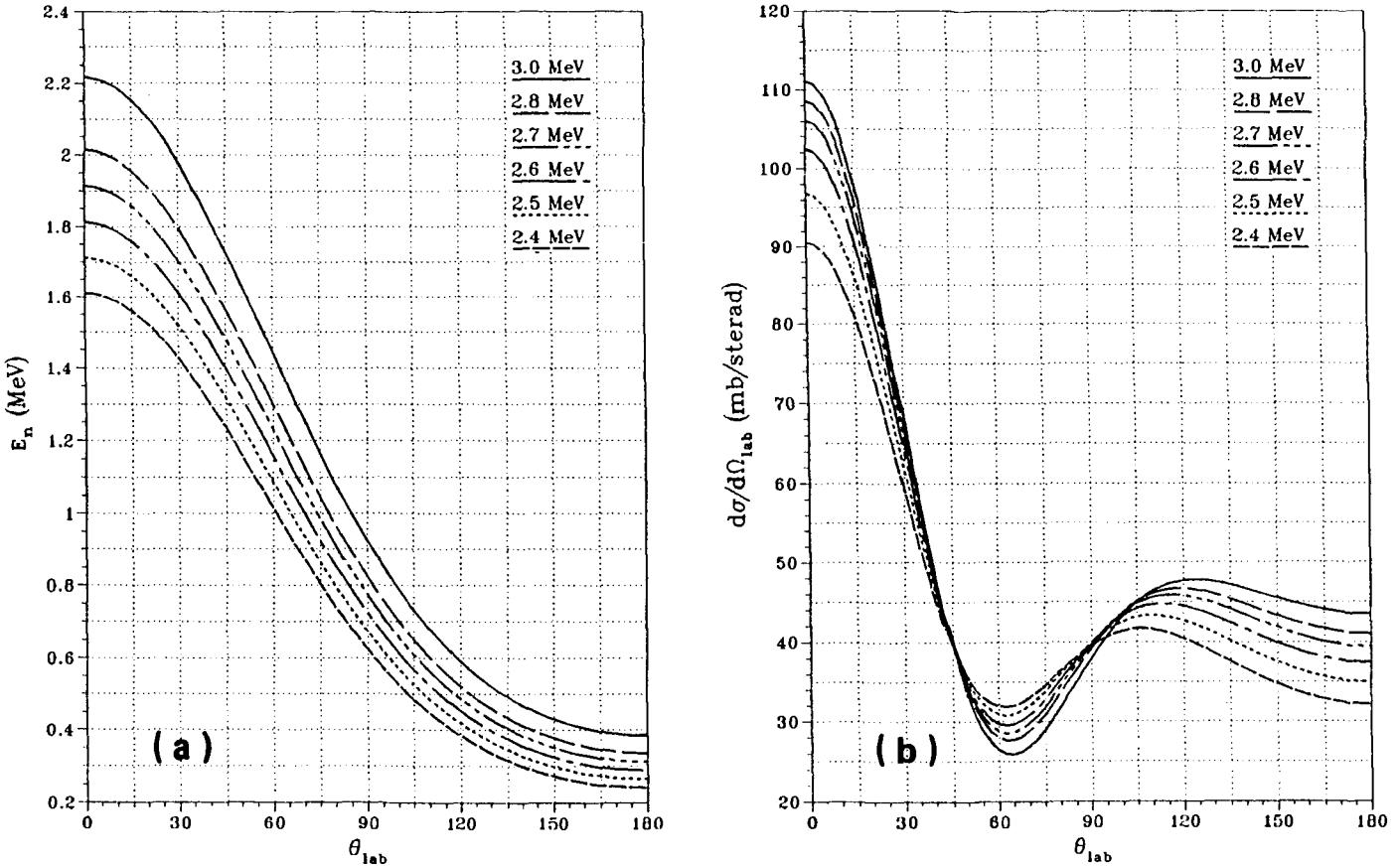

FIG. 9. (a) Neutron energy values and (b) differential cross-sections for the $^3H(p, n)^3He$ reaction: 2.4–3.0 MeV.

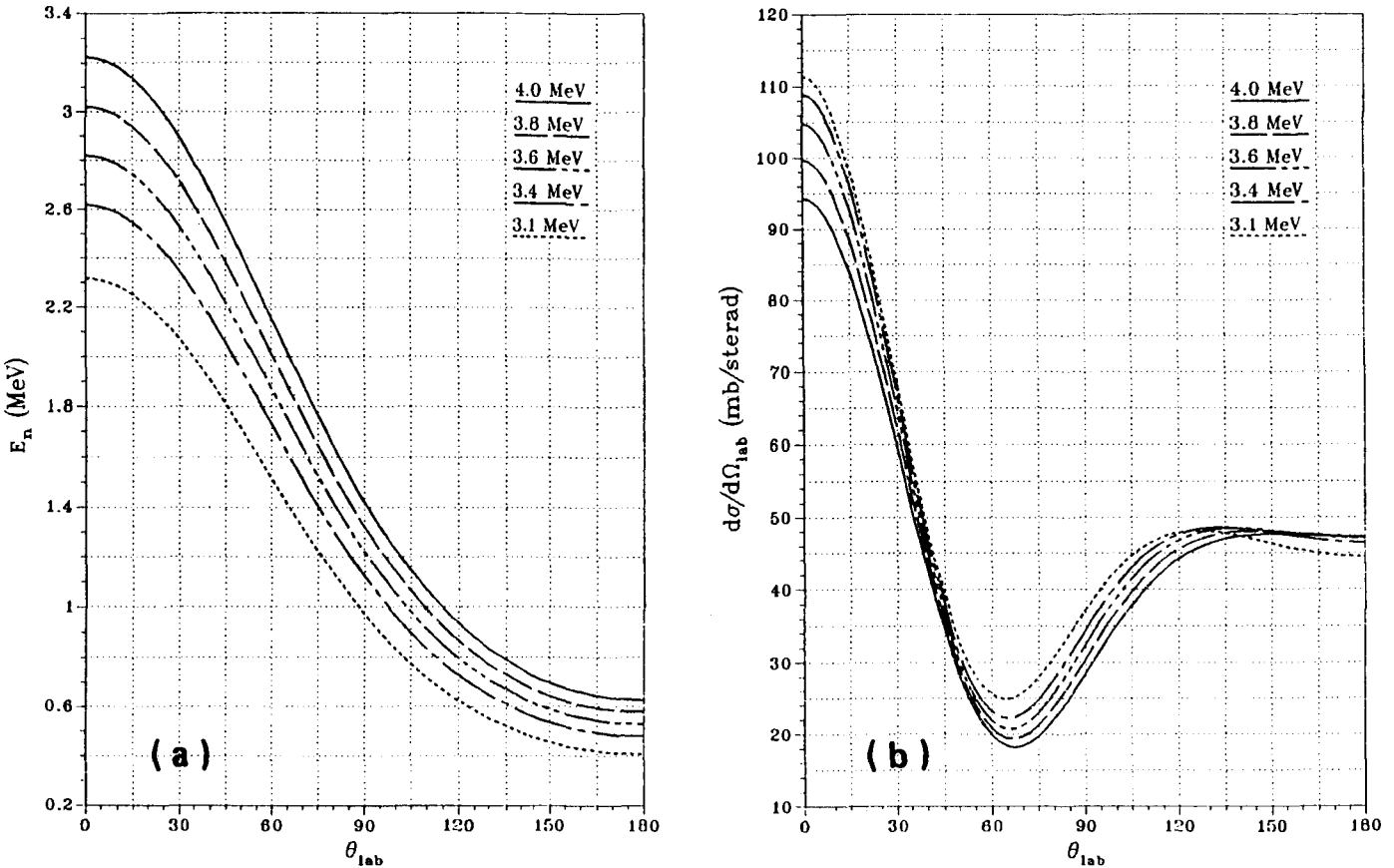

FIG. 10. (a) Neutron energy values and (b) differential cross-sections for the $^3H(p, n)^3He$ reaction: 3.1–4.0 MeV.

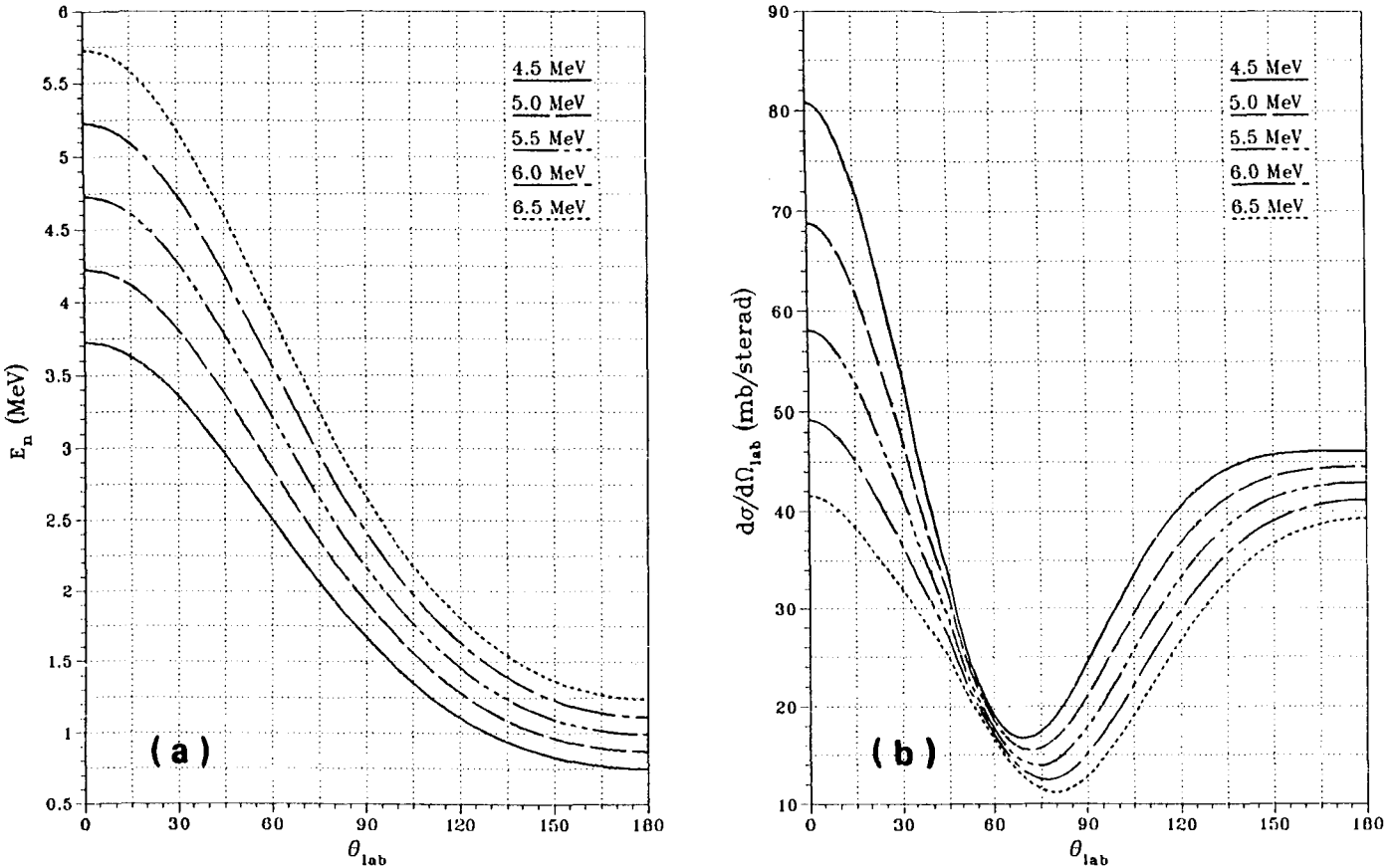

FIG. 11. (a) Neutron energy values and (b) differential cross-sections for the $^3H(p, n)^3He$ reaction: 4.5–6.5 MeV.

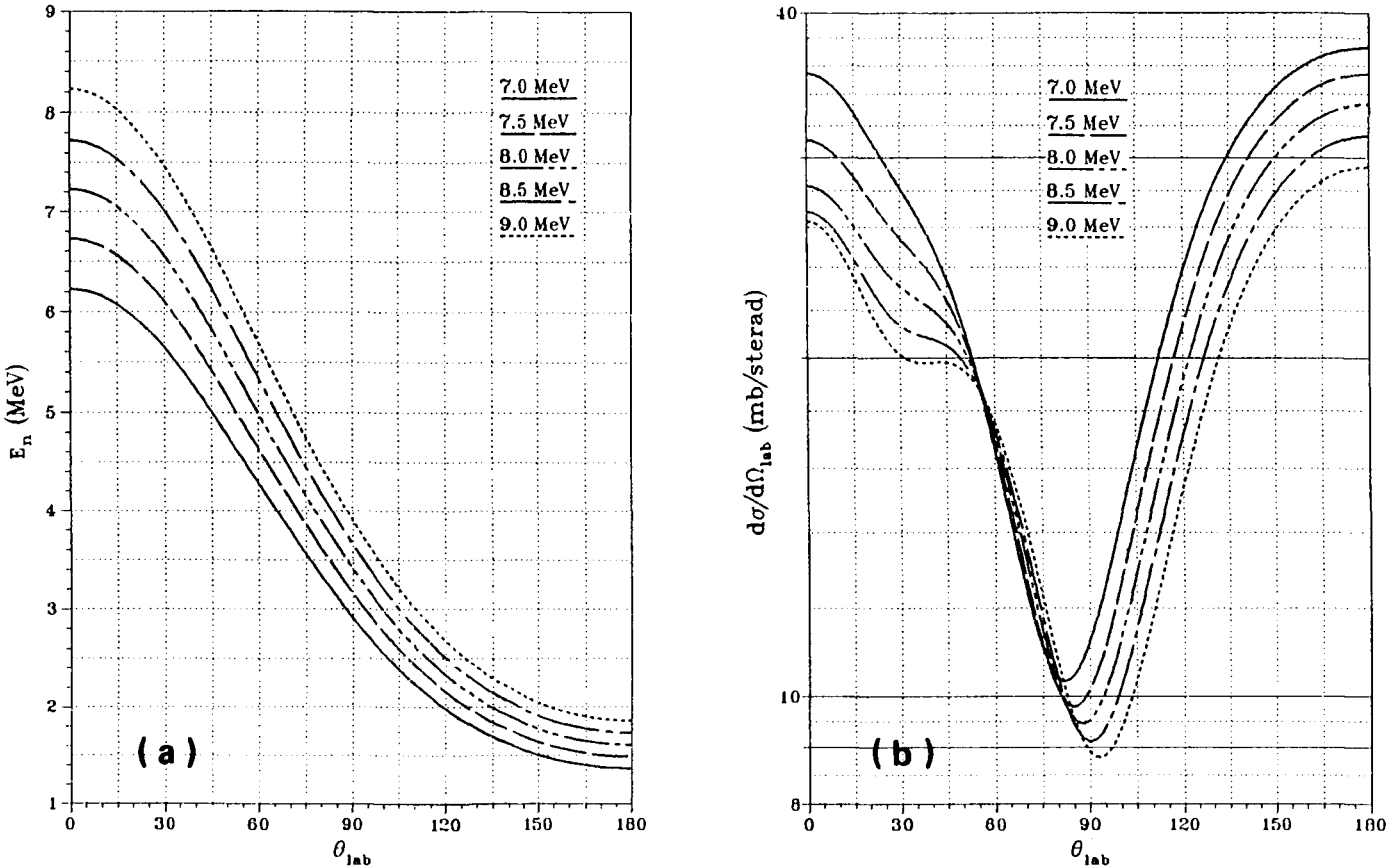

FIG. 12. (a) Neutron energy values and (b) differential cross-sections for the $^3H(p, n)^3He$ reaction: 7.0–9.0 MeV.

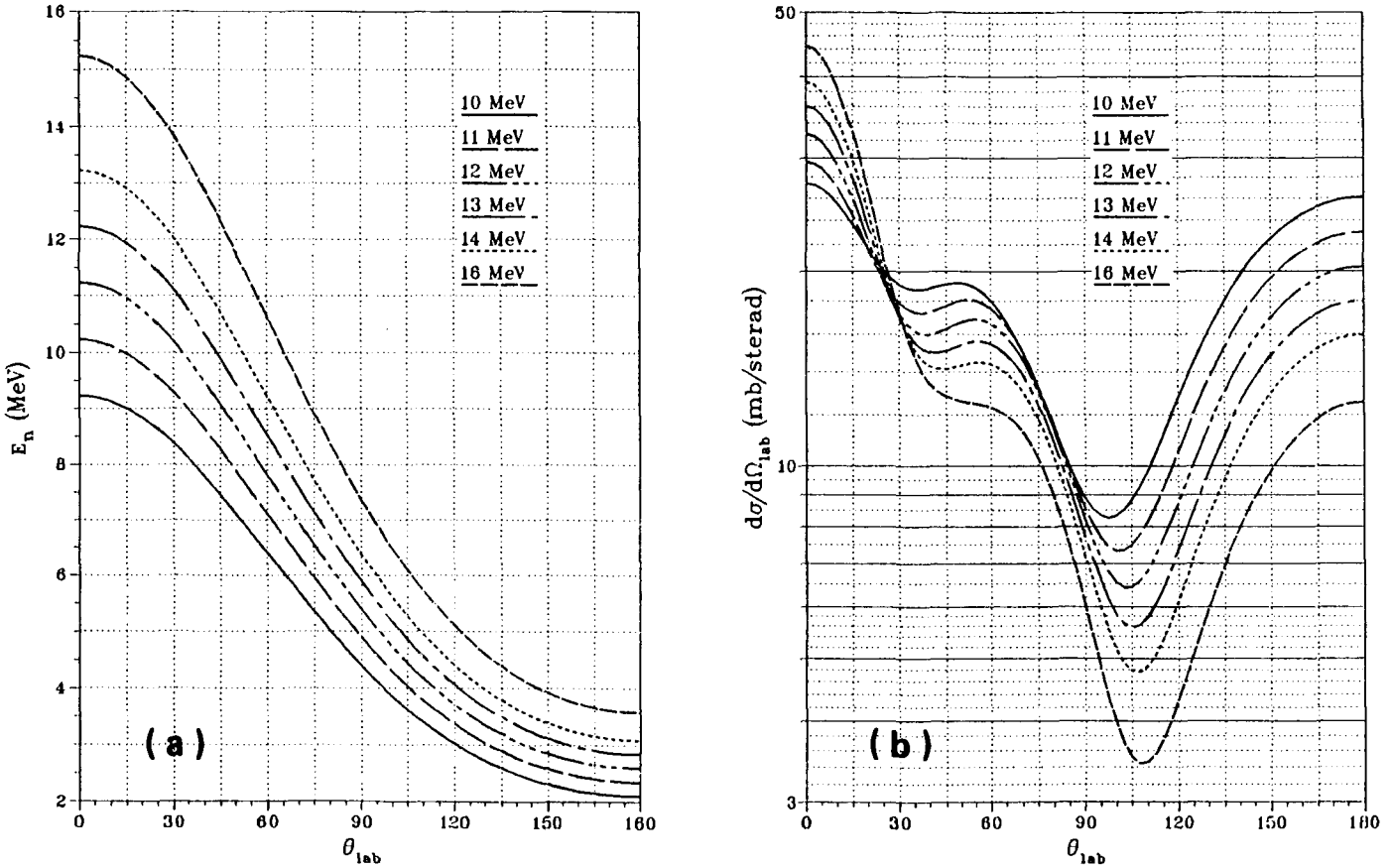

FIG. 13. (a) Neutron energy values and (b) differential cross-sections for the $^3H(p, n)^3He$ reaction: 10–16 MeV.

THE $^{1}H(t,n)^{3}He$ REACTION

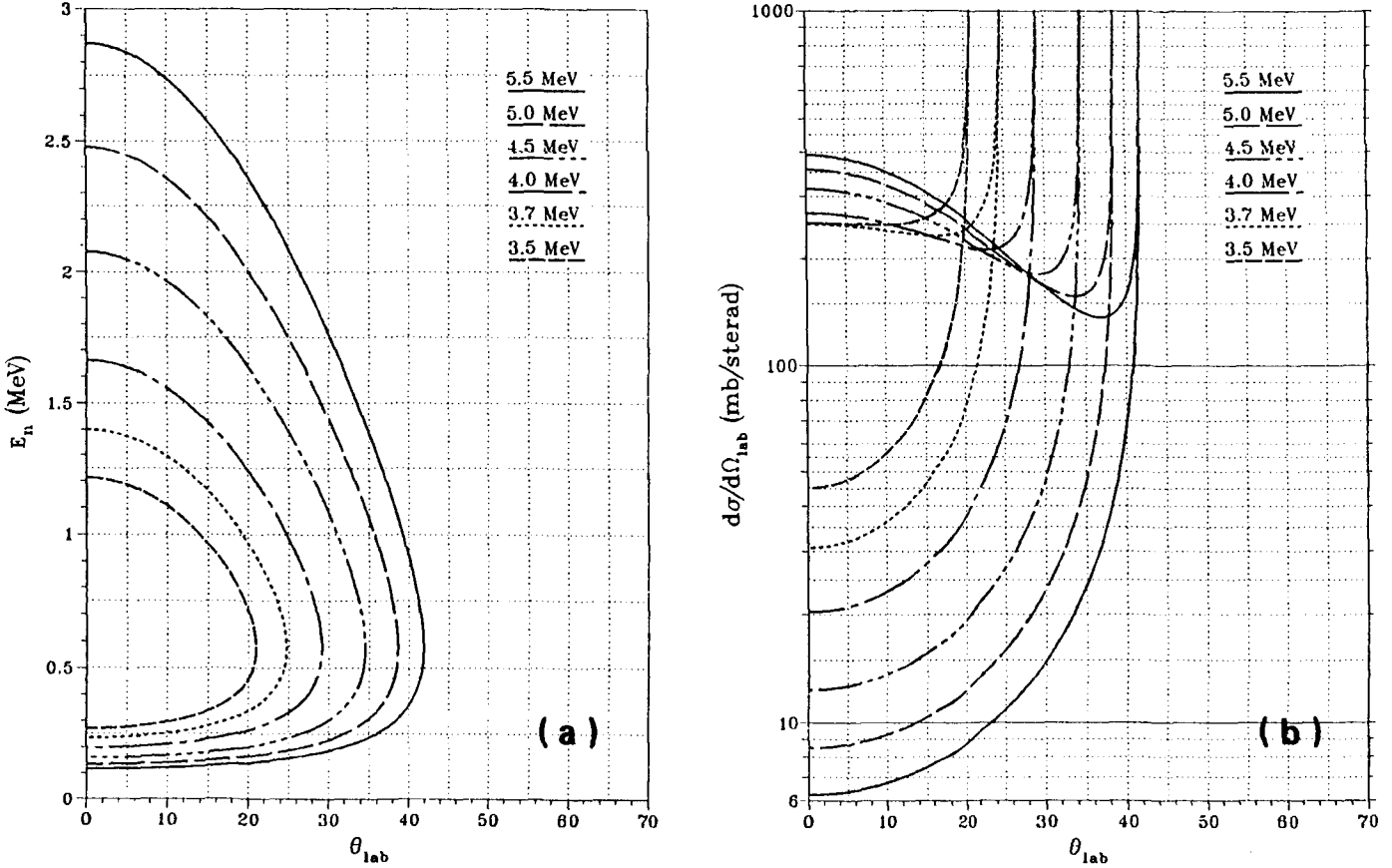

FIG. 14. (a) Neutron energy values and (b) differential cross-sections for the $^1H(t, n)^3He$ reaction: 3.5–5.5 MeV.

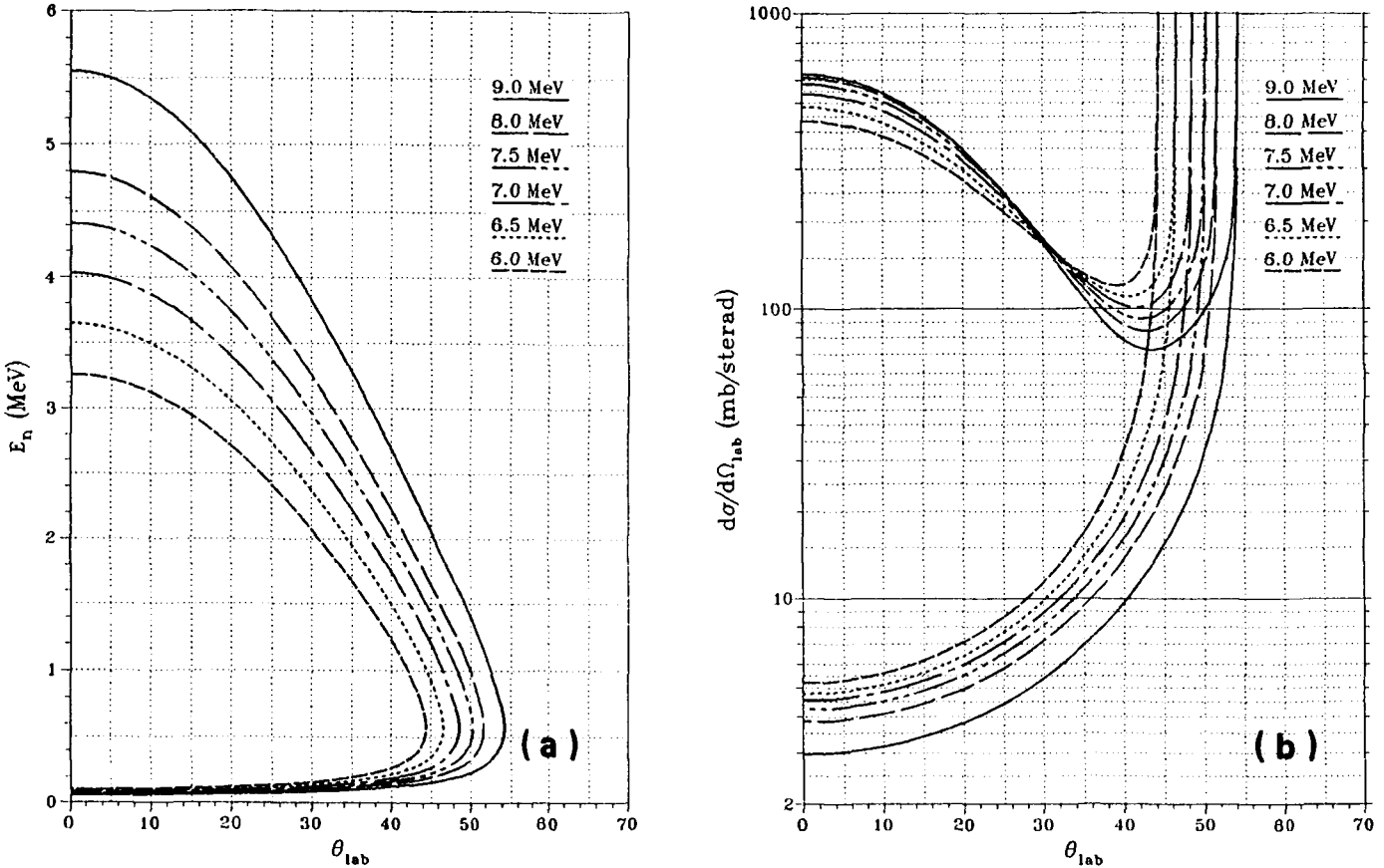

FIG. 15. (a) Neutron energy values and (b) differential cross-sections for the $^1H(t, n)^3He$ reaction: 6.0–9.0 MeV.

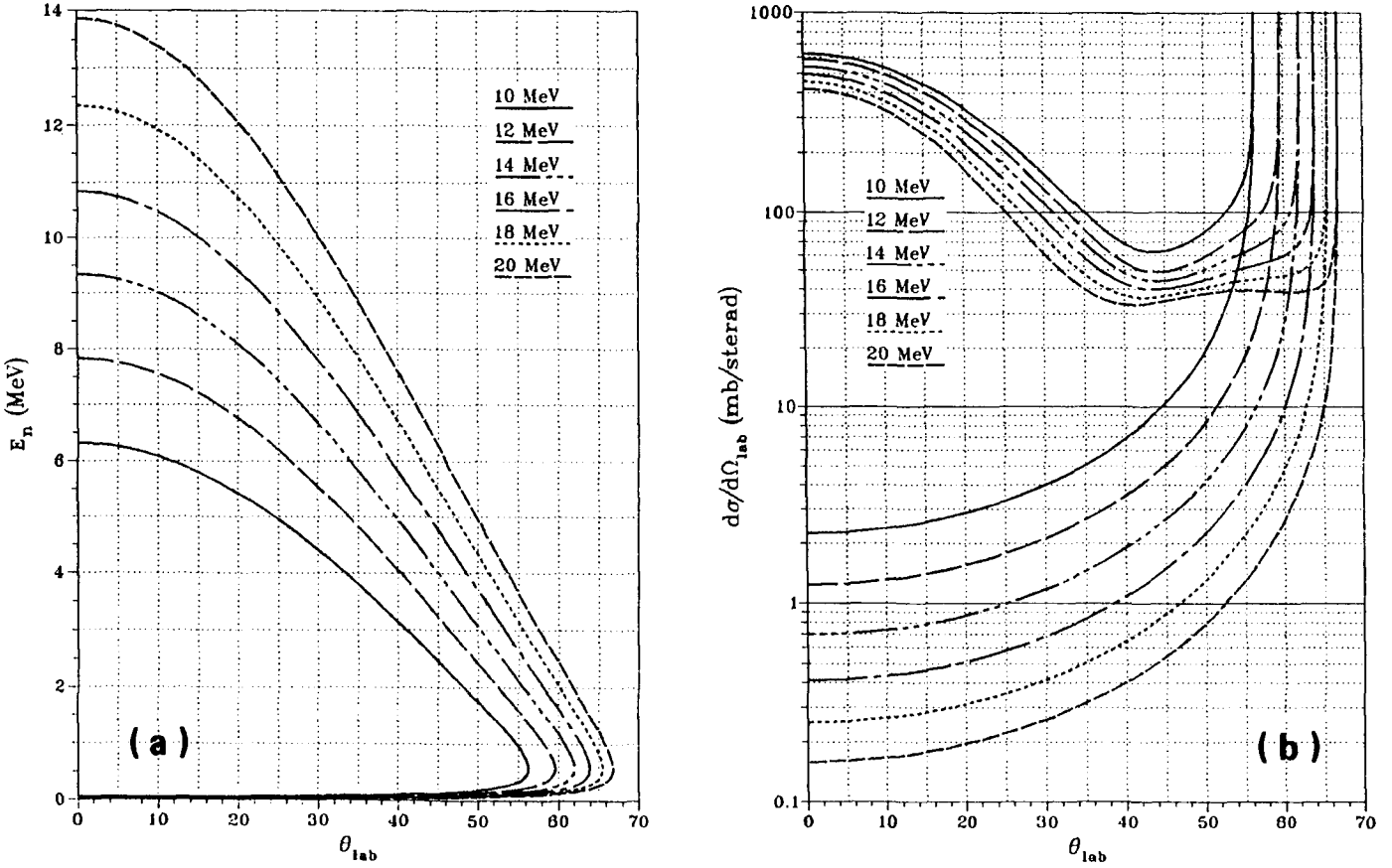

FIG. 16. (a) Neutron energy values and (b) differential cross-sections for the $^1H(t, n)^3He$ reaction: 10-20 MeV.

TABLE IV. Q-VALUES, THRESHOLDS AND NEUTRON ENERGIES AT $0°_{lab}$ FOR t-H

(All energies in MeV)

Exit channel	$n + {}^3He$		$n + p + d$	$2n + 2p$
E_{in}	$E_n(0°_{c.m.})$	$E_n(180°_{c.m.})$	E_{nmax1}	E_{nmax2}
3.051	0.573	0.573		
25.011	17.640	0.019	4.694	
33.913	24.347	0.014	14.569	6.362
Q	−0.764		−6.257	−8.482

As shown in Figs 14–16, the second neutron group at 0° (corresponding to emission at 180° in the c.m. system) becomes very low both in energy and intensity with increasing triton energy so that it may be neglected in many cases (see also Table IV). The main disadvantage is the radioactivity of the triton beam, and the need for a rather high beam energy. The latter has limited up to now the routine use of this source to neutron energies below 13 MeV. In addition, the high triton energy gives a rather high structural background.

The kinematic energy spread is approximately three times as large as in the p-T case, e.g. at a half-angle of 5° for the aperture of the sample, the relative energy resolution for neutrons between 2 and 20 MeV is close to 1% (see Fig. 1). Table IV gives the relevant kinematic data and Table II the relevant reduced c.m. Legendre coefficients for the differential cross-sections. However, the E_{in} values in the latter table must be multiplied by 2.9937 and Θ must be changed to $180° - \Theta$ in order for those data to be valid for the t-H case.

3.2. Interaction of deuterons with deuterons

3.2.1. $^2H(d, n)^3He$

The data in Table V are from Liskien and Paulsen [9] for incoming energies $\leqslant 3$ MeV and from Ref. [4]. The anisotropy at low energies, as given by Liskien and Paulsen [9], agrees with recent accurate measurements [20], resolving the discrepancy suspected near 0.2 MeV [5]. By including these new data the scale of the cross-sections below 0.4 MeV can be improved as compared with the original evaluation [9]. These new data have shape errors of 1% and scale errors of 1.5%.

TABLE V. THE $^{2}H(d, n)^{3}He$ REACTION

(Deuteron energy: E_{in}; c.m. differential cross-section at 0°: S_0; reduced Legendre coefficients: A_i; integrated cross-section: S_t)

E_{in} (MeV)	S_0 (mb/sr)	A_0	A_2	A_4	A_6	A_8	A_{10}	A_{12}	A_{14}	A_{16}	S_t (mb)
0.02	0.027	0.819	0.181								0.28
0.03	0.119	0.785	0.215								1.17
0.04	0.282	0.758	0.241	0.001							2.69
0.05	0.50	0.737	0.261	0.002							4.63
0.06	0.76	0.719	0.279	0.002							6.85
0.07	1.04	0.705	0.292	0.003							9.19
0.08	1.34	0.692	0.304	0.004							11.65
0.09	1.65	0.681	0.314	0.005							14.1
0.10	1.95	0.671	0.323	0.006							16.5
0.15	3.39	0.633	0.356	0.011							27.0
0.20	4.68	0.605	0.379	0.016							35.6
0.25	5.91	0.583	0.395	0.022							43.3
0.30	7.10	0.564	0.408	0.028							50.3
0.35	8.25	0.547	0.418	0.035							56.7
0.40	9.4	0.532	0.426	0.042							63.0
0.45	10.4	0.518	0.433	0.049							67.7
0.50	11.4	0.506	0.437	0.057							72.5
0.55	12.4	0.494	0.440	0.066							77.0
0.60	13.4	0.483	0.443	0.074							81.3
0.65	14.3	0.474	0.444	0.082							85.2
0.70	15.1	0.465	0.445	0.090							88.2
0.75	15.8	0.456	0.446	0.098							90.5
0.80	16.5	0.447	0.445	0.108							92.7
0.85	17.2	0.439	0.444	0.117							94.9
0.90	17.8	0.432	0.443	0.125							96.9
0.95	18.4	0.425	0.441	0.134							98.3
1.00	19.0	0.418	0.439	0.142	0.001						99.8
1.10	20.0	0.405	0.434	0.158	0.003						101.8
1.20	21.0	0.393	0.428	0.174	0.005						103.7
1.30	21.9	0.381	0.422	0.189	0.008						104.9

1.40	22.7	0.370	0.416	0.203	0.011						105.5
1.50	23.4	0.360	0.410	0.216	0.014						105.9
1.60	24.0	0.351	0.404	0.228	0.017						105.9
1.70	24.6	0.342	0.398	0.240	0.020						105.8
1.80	25.2	0.334	0.392	0.251	0.023						105.7
1.90	25.8	0.326	0.387	0.260	0.027						105.5
2.00	26.4	0.318	0.382	0.270	0.030						105.3
2.10	26.9	0.311	0.377	0.279	0.033						105.2
2.20	27.5	0.304	0.372	0.287	0.037						105.0
2.30	28.0	0.298	0.367	0.294	0.041						104.8
2.40	28.4	0.293	0.362	0.301	0.044						104.5
2.50	28.9	0.287	0.357	0.308	0.048						104.3
2.60	29.3	0.282	0.353	0.314	0.051						104.0
2.70	29.8	0.277	0.349	0.320	0.054						103.8
2.80	30.3	0.272	0.345	0.326	0.057						103.5
2.90	30.7	0.268	0.341	0.331	0.060						103.2
3.00	31.2	0.262	0.337	0.337	0.064						102.8
3.50	33.4	0.241	0.321	0.358	0.080						101.2
4.00	35.5	0.2233	0.3060	0.3697	0.0950	0.0060					99.6
4.50	37.1	0.2103	0.2930	0.3763	0.1090	0.0114					98.0
5.00	38.6	0.1990	0.2819	0.3792	0.1224	0.0175					96.5
5.50	40.0	0.1892	0.2721	0.3796	0.1347	0.0232	0.0012				95.0
5.80	40.8	0.1837	0.2656	0.3783	0.1417	0.0266	0.0038	0.0003			94.1
6.00	41.3	0.1804	0.2615	0.3775	0.1460	0.0287	0.0051	0.0008			93.5
6.20	41.8	0.1769	0.2584	0.3757	0.1505	0.0311	0.0062	0.0011	0.0001		92.9
7.00	43.5	0.1659	0.2465	0.3690	0.1664	0.0400	0.0093	0.0020	0.0009		90.6
8.00	45.0	0.1552	0.2364	0.3589	0.1836	0.0496	0.0118	0.0027	0.0018		87.8
9.00	45.9	0.1477	0.2284	0.3489	0.1977	0.0568	0.0142	0.0036	0.0027		85.0
10.00	46.1	0.1425	0.2226	0.3382	0.2093	0.0629	0.0165	0.0040	0.0036		82.4
11.00	46.0	0.1383	0.2177	0.3275	0.2196	0.0684	0.0189	0.0052	0.0044		79.8
12.00	45.7	0.1348	0.2136	0.3167	0.2287	0.0738	0.0213	0.0060	0.0051		77.4
12.31	45.6	0.1340	0.2122	0.3133	0.2312	0.0753	0.0220	0.0063	0.0053	0.0004	76.6
13.00	45.3	0.1316	0.2098	0.3057	0.2362	0.0792	0.0236	0.0068	0.0058	0.0013	75.0
14.00	44.7	0.1290	0.2070	0.2948	0.2423	0.0843	0.0261	0.0077	0.0064	0.0024	72.6
15.00	44.1	0.1266	0.2045	0.2842	0.2481	0.0893	0.0285	0.0085	0.0068	0.0035	70.3

TABLE VI. Q-VALUES, THRESHOLDS AND NEUTRON ENERGIES AT $0°_{lab}$ FOR d-D
(All energies in MeV)

Exit channel	$n + {}^3He$	$n + p + d$	$2n + 2p$
E_{in}	$E_n(0°_{c.m.})$	E_{nmax1}	E_{nmax2}
0.000	2.449		
4.451	7.706	0.557	
8.904	11.986	5.512	1.114
Q	+3.269	−2.225	−4.449

Liskien and Paulsen give an absolute deviation of the reduced Legendre coefficients of 0.01 (resulting in worst-case shape uncertainties between ±2.8% at 0.4 MeV and ±7.1% at 3 MeV), a 4% relative deviation of the 0° cross-section and a 5% relative deviation of the integrated cross-section.

The scale uncertainty between 5 and 12 MeV is approximately ±1%, while the shape uncertainty between 5 and 10 MeV is close to ±1%, increasing to about ±4% at 17 MeV. The 0° position has an error of ±0.1° and the incoming energy has a typical uncertainty of ±0.02 MeV which decreases with decreasing energy. Relevant papers are listed in Refs [4, 5 and 9].

The monoenergetic range extends from 2.45 to 7.71 MeV neutron energy at 0°. At energies that are not too low, the yield is strongly forward peaked (see Fig. 3), which gives a reduced in-scattered background. On the other hand, this strong angle dependence even in the neighbourhood of 0° makes it necessary to integrate the differential cross-sections over the opening angle whenever this angle is larger than 1°–2°. Not to do so may result in systematic errors of a few per cent.

Above 4.45 MeV deuteron energy, the deuteron breakup gives a neutron continuum with an energy gap at 0° between its maximum and the primary neutrons of, typically, 7 MeV. The intensity of this intrinsic background increases rapidly with energy, severely limiting the usefulness of the d-D source outside of its monoenergetic range.

Often there is no choice other than to use the d-D reaction for monoenergetic neutron production, despite its lower yield in primary neutrons (see Fig. 2 and Table I) and higher yield in background neutrons [14] when compared with the p-T reaction.

Text cont. on p. 121.

THE $^{2}H(d,n)^{3}He$ REACTION

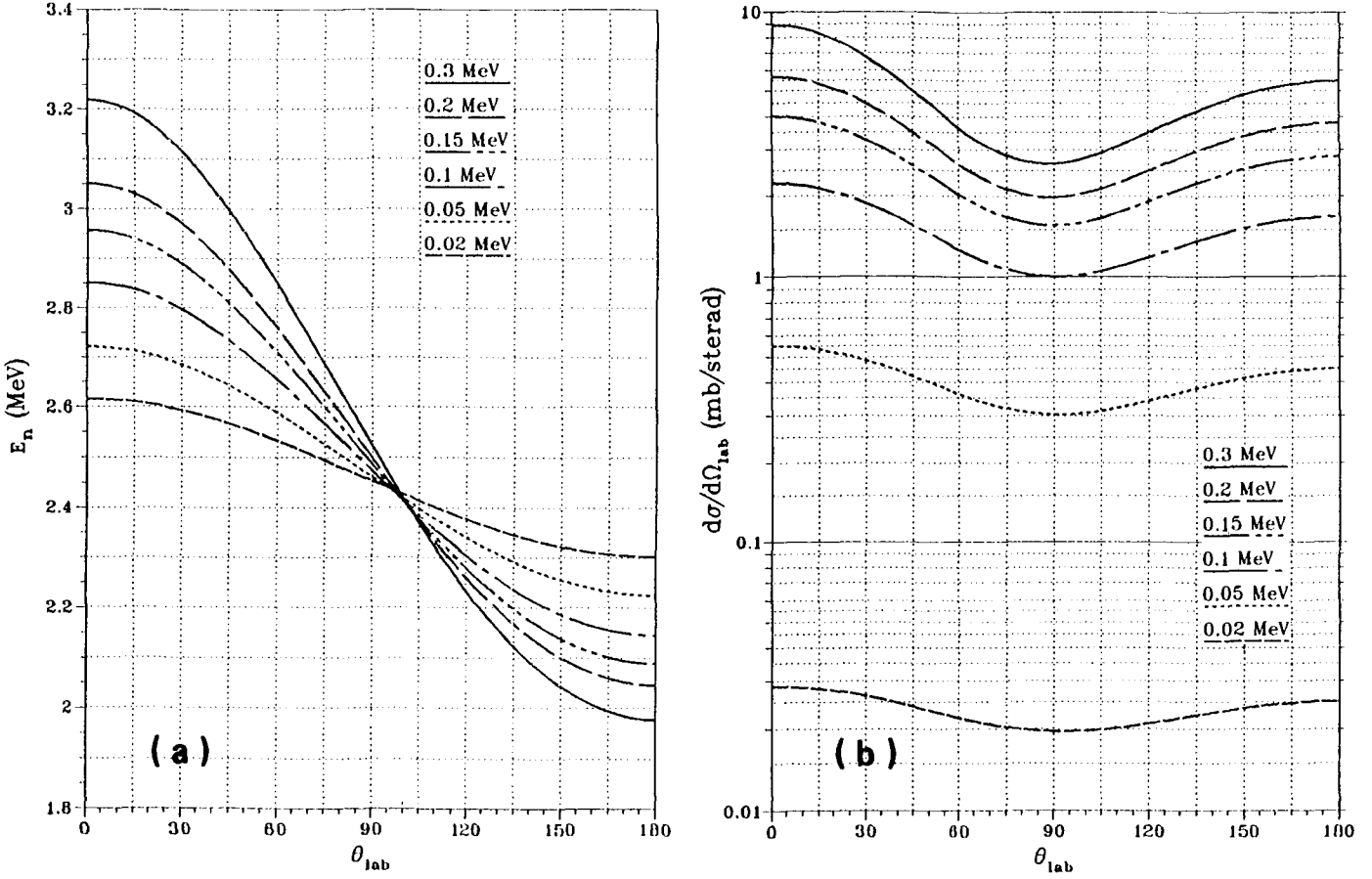

FIG. 17. (a) Neutron energy values and (b) differential cross-sections for the $^2H(d, n)^3He$ reaction: 0.02-0.3 MeV.

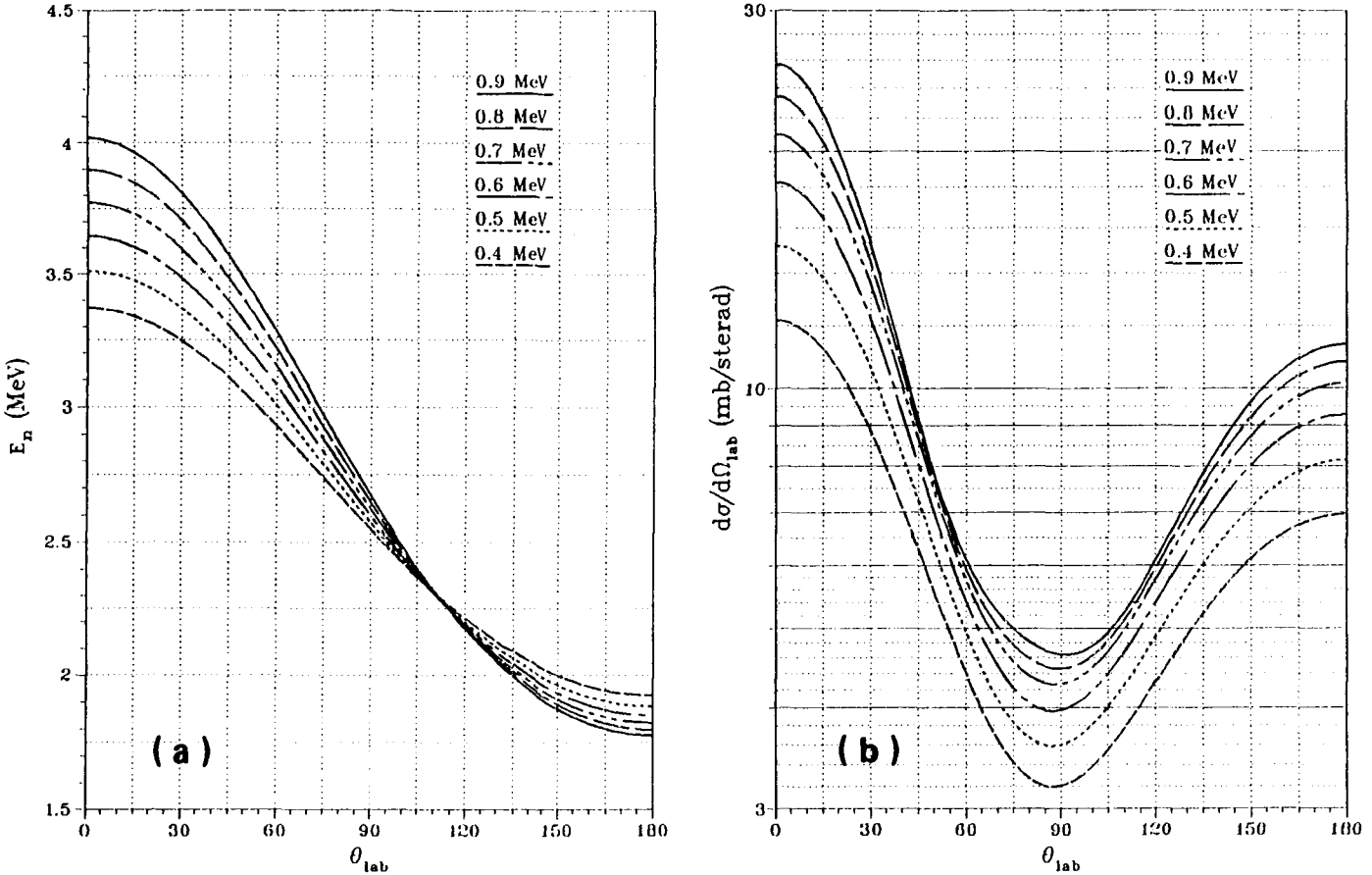

FIG. 18. (a) Neutron energy values and (b) differential cross-sections for the $^2H(d, n)^3He$ reaction: 0.4–0.9 MeV.

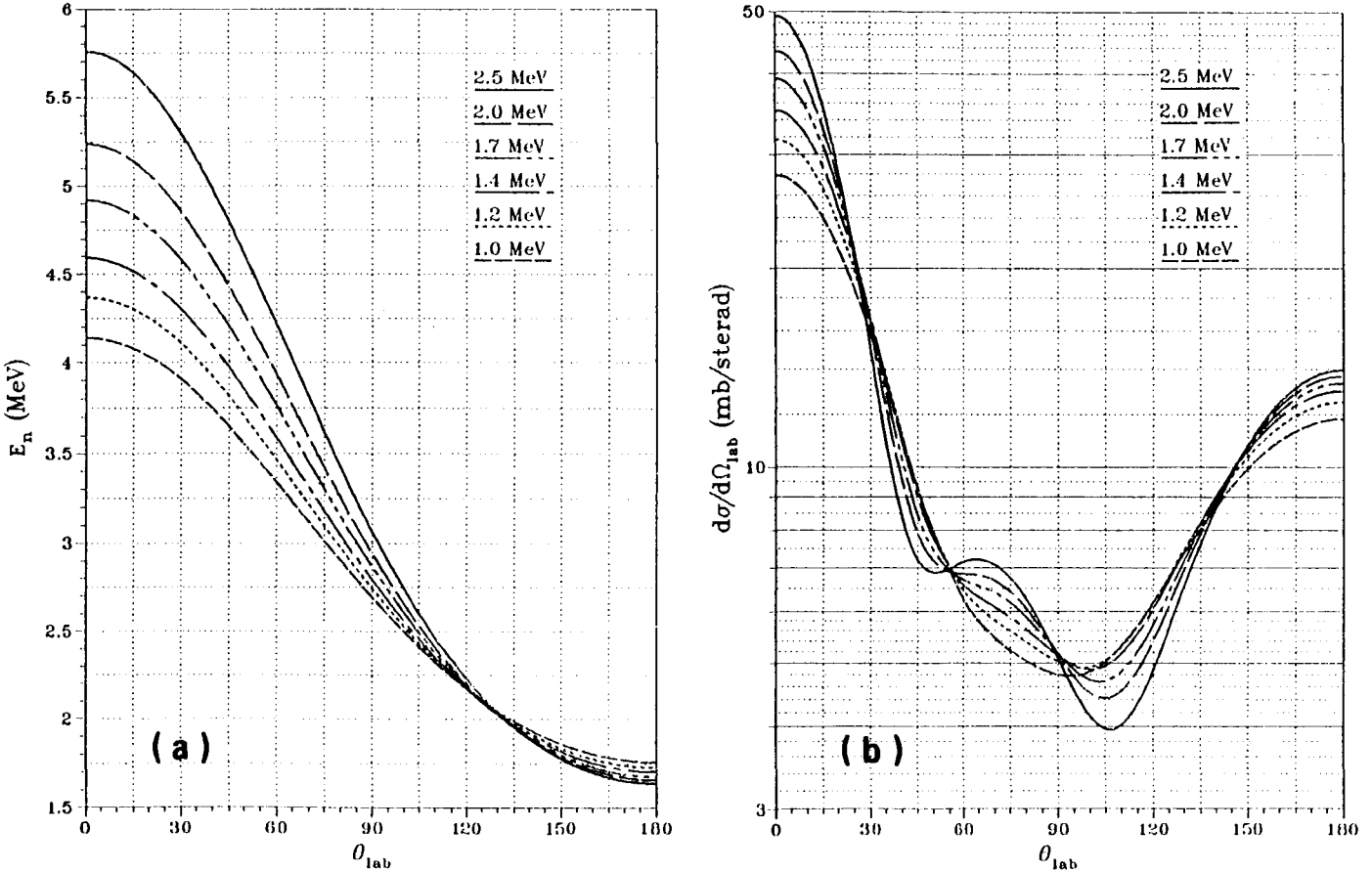

FIG. 19. (a) Neutron energy values and (b) differential cross-sections for the $^2H(d, n)^3He$ reaction: 1.0–2.5 MeV.

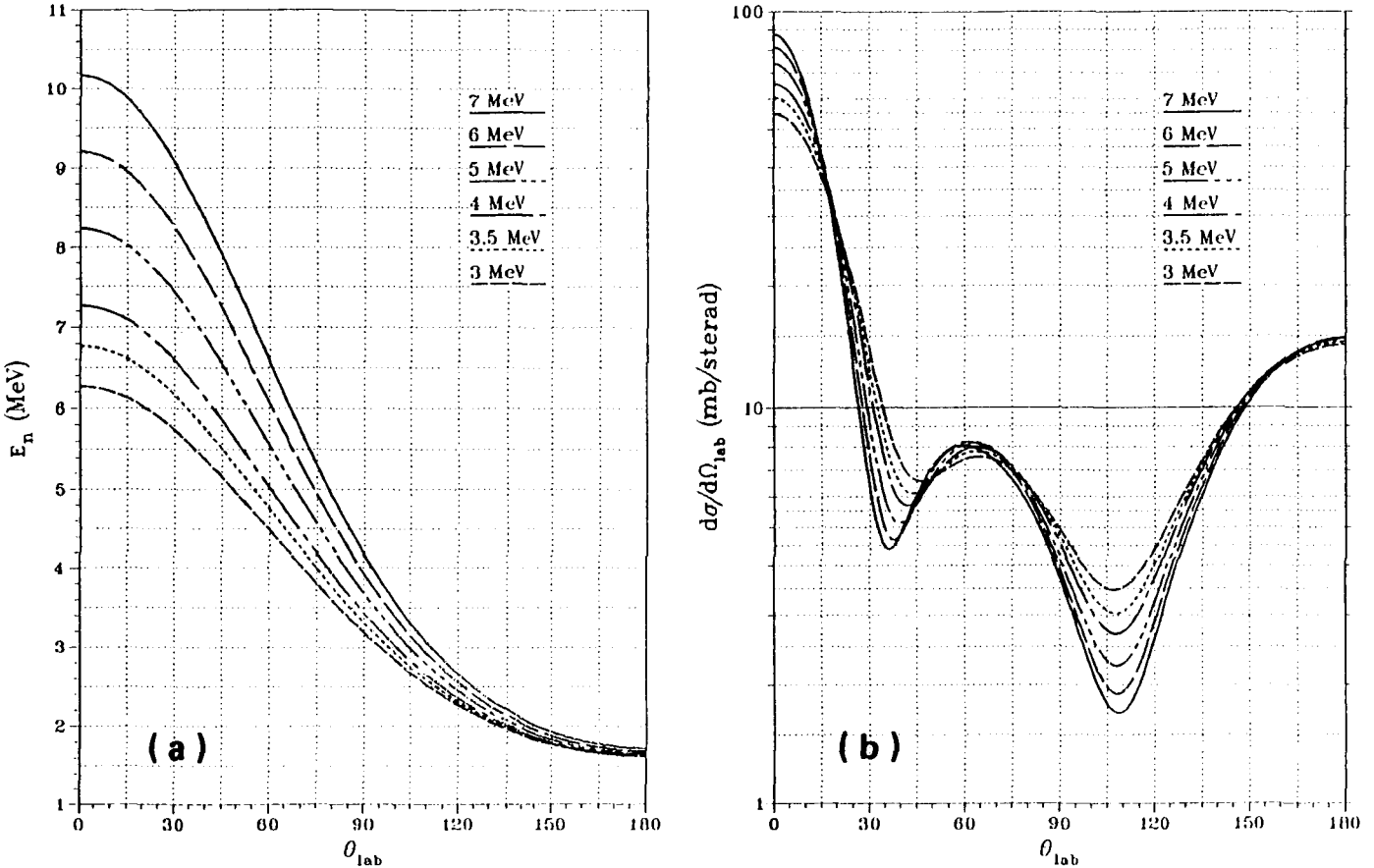

FIG. 20. (a) Neutron energy values and (b) differential cross-sections for the $^2H(d, n)^3He$ reaction: 3–7 MeV.

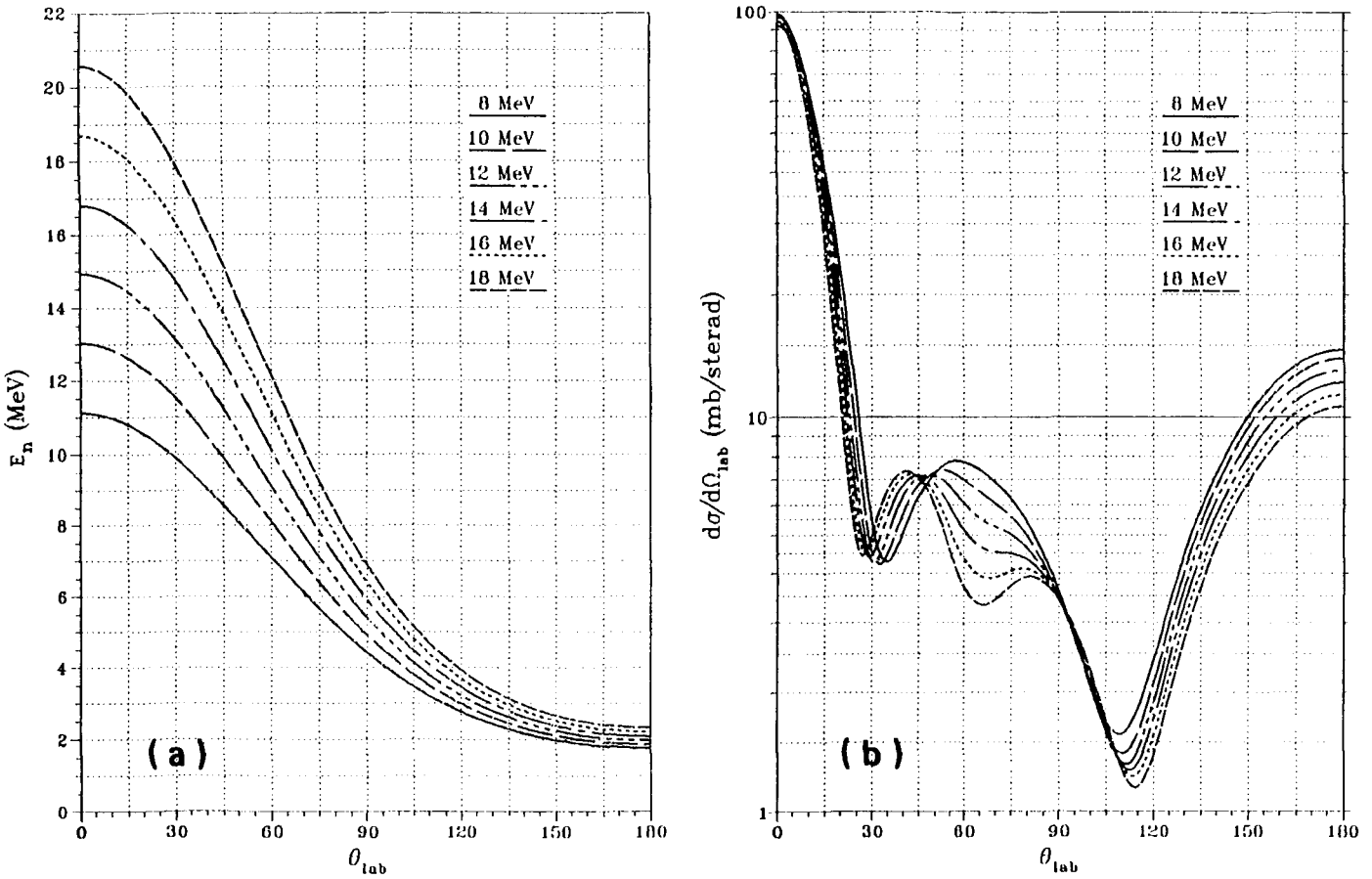

FIG. 21. (a) Neutron energy values and (b) differential cross-sections for the $^2H(d, n)^3He$ reaction: 8–18 MeV.

Data contaminated by d-D breakup neutrons have been corrected by one of these two procedures:

(1) An experimental subtraction of the background contribution is done by using ^{3}He as a dummy gas, which is reported to give a similar breakup spectrum [21].
(2) The effect of the background neutrons is subtracted by a calculation [22] using measured double-differential breakup cross-sections ($d^2\sigma/dEd\Omega$). Breakup cross-sections and sources of the original data are listed in Refs [4, 5, 14, 22, 23].

Other disadvantages of the d-D reaction (as compared with the p-T reaction) are a lower projectile energy, which gives a bigger energy loss (and therefore stronger heating) in the entrance foil; larger straggling and a worse time resolution (only important in time of flight applications); and the self-target buildup in the beam stop which gives additional low energy background neutrons (noticeable after long use of the same target) when the deuteron energy is increased. Owing to the rather high yield of the d-D reaction, this latter effect is not so pronounced as in the d-T case. In addition, the differential cross-sections of the d-D reaction have a much stronger angle dependence (see Fig. 6). Above 4 MeV deuteron energy, a change in the 0° direction by 0.1° results in a maximum cross-section change of more than 1%. Table VI summarizes the relevant reaction data and Figs 17-21 illustrate the angular dependence of the neutron energies and of the differential cross-sections.

3.3. Interaction of deuterons with tritons

The data in Table VII were derived from Ref. [24] (<0.4 MeV), from Ref. [9] (≤2.9 MeV), from Ref. [6] (≤9.5 MeV) and from Ref. [4]. Below 0.4 MeV the typical total error is less than 1.5%. For the 0.4 to 2.9 MeV range, Ref. [9] gives an absolute deviation of 0.01 for the reduced Legendre coefficients (resulting in *worst case* shape uncertainties between ±1.4% at 0.4 MeV and ±6.5% at 2.9 MeV), 3–4% relative deviation of the 0° cross-section and a 7% relative deviation of the integrated cross-section. The scale error of the two evaluations in the higher energy range is generally 1.5%, except near 4 MeV, where it increases to 2%. The shape error is estimated to be ±3% at 3 MeV, decreasing to ±2% between 5 and 10 MeV and then increasing again (±2.5% at 13 MeV, ±5% at 16.5 MeV).

The 0° position has an error of ±0.1° and the incoming energy a typical uncertainty of ±0.02 Me V, decreasing with decreasing energy. Sources for the relevant data are listed in Refs [4, 5 and 9]. As pointed out [6], there is an indication that the scale at higher energies is too high by (1.5 ± 0.8)%.

3.3.1. $^3H(d, n)^4He$

This reaction is best known for its resonance at 107 keV [3], culminating in a peak cross-section of about 5 b. Owing to the high Q-value (+17.59 MeV), low

TABLE VII. THE $^3H(d, n)^4He$ REACTION

(Deuteron energy: E_{in}; c.m. differential cross-section at 0°: S_0; reduced Legendre coefficients: A_i; c.m. differential cross-section at 180°: S_π; integrated cross-section: S_t; the coefficients are multiplied by 1000 to save space)

E_{in} (MeV)	S_0 (mb/sr)	A_0	A_1	A_2	A_3	A_4	A_5	A_6	A_7	A_8	A_9	A_{10}	A_{11}	A_{12}	A_{13}	A_{14}	A_{15}	S_π (mb/sr)	S_t (mb)
0.02	4.6	1000.																4.6	58.2
0.03	21.7	1000.																21.7	273.
0.04	55.5	1000.																55.5	697.
0.05	106.6	1000.																106.6	1339.
0.06	172.4	1000.																172.4	2166.
0.07	245.8	1000.																245.8	3089.
0.08	313.9	1000.																313.9	3945.
0.09	366.5	1000.																366.5	4608.
0.10	393.6	1000.																393.6	4947.
0.12	384.1	1000.																384.1	4827.
0.15	306.6	1000.																306.6	3853.
0.17	254.6	1000.																254.6	3200.
0.20	196.6	1000.																196.6	2470.
0.25	132.1	1000.																132.1	1660.
0.30	97.5	1000.																97.5	1225.
0.35	77.1	1000.																77.1	969.
0.40	63.5	999.	4.	-3.														63.0	797.
0.45	53.0	998.	13.	-11.														51.6	665.
0.50	45.5	997.	21.	-18.														43.6	570.
0.55	39.4	995.	30.	-25.														37.0	493.
0.60	35.5	993.	38.	-31.														32.8	443.
0.65	31.9	989.	46.	-35.														29.0	396.
0.70	29.4	986.	53.	-39.														26.3	364.
0.75	27.0	983.	60.	-43.														23.8	334.
0.80	25.0	978.	67.	-45.														21.7	307.
0.90	22.0	968.	77.	-45.														18.6	268.
1.00	19.8	957.	87.	-44.														16.4	239.
1.10	17.9	946.	94.	-40.														14.5	213.
1.20	16.7	931.	100.	-32.		1.												13.4	195.
1.30	15.8	915.	105.	-23.		3.												12.5	182.

1.40	15.0	898.	110.	-13.		4.		1.										11.7	169.
1.50	14.3	878.	113.	2.		5.		2.										11.0	158.
1.60	13.8	858.	116.	16.		7.	1.	2.										10.6	149.
1.70	13.3	835.	120.	29.	1.	8.	4.	3.										10.0	140.
1.80	12.9	814.	122.	42.	2.	9.	7.	4.										9.5	132.
1.90	12.6	793.	124.	54.	4.	11.	10.	4.										9.1	126.
2.00	12.3	771.	127.	67.	5.	12.	13.	5.										8.7	119.
2.10	12.1	749.	129.	80.	7.	13.	16.	6.										8.4	114.
2.20	11.9	730.	130.	91.	9.	14.	19.	7.										8.14	109.0
2.30	11.8	707.	132.	104.	12.	16.	22.	7.										7.88	105.0
2.40	11.8	688.	132.	115.	15.	17.	25.	8.										7.74	102.0
2.50	11.8	666.	133.	127.	19.	18.	28.	9.										7.55	98.6
2.60	11.9	646.	133.	137.	23.	20.	31.	10.										7.45	96.5
2.70	12.0	627.	132.	148.	27.	21.	34.	11.										7.37	94.7
2.80	12.1	608.	131.	159.	31.	22.	37.	12.										7.28	92.1
2.90	12.2	589.	130.	169.	34.	24.	40.	14.										7.22	90.1
3.00	12.60	571.0	129.0	181.5	37.9	23.5	42.0	15.1										7.34	90.4
3.50	14.09	485.8	123.7	229.1	53.5	29.9	56.3	21.7										7.51	86.0
4.00	15.86	419.5	121.0	258.9	64.3	35.9	70.5	28.4		0.8	0.7							7.72	83.6
4.50	17.56	375.4	120.0	267.9	71.4	41.6	84.6	35.0		2.8	1.3							7.77	82.4
5.00	18.56	348.2	119.4	261.1	74.2	47.6	98.9	42.4	1.8	4.4	2.0							7.58	81.2
5.50	19.24	328.4	118.2	243.9	71.6	55.8	114.9	50.5	8.3	5.8	2.6							7.10	79.4
6.00	19.58	311.0	116.7	221.9	65.0	69.9	131.6	59.2	14.4	7.0	3.3							6.62	76.5
6.50	19.61	293.8	113.1	196.6	55.3	90.6	147.2	70.7	20.0	8.5	3.9	0.3						6.30	72.4
7.00	19.40	280.0	100.9	181.8	43.0	109.3	161.9	82.8	24.6	10.2	4.6	0.6	0.3					6.40	68.3
7.50	19.10	271.0	84.8	176.2	29.0	119.7	175.8	94.7	29.5	12.2	5.2	1.1	0.6	0.2				6.67	64.9
7.90	18.80	264.9	75.7	172.6	17.8	125.8	183.5	103.8	33.2	14.0	5.5	1.6	0.8	0.8				6.89	62.4
8.40	18.30	258.8	69.1	168.0	4.6	131.4	188.3	115.2	36.8	16.7	6.1	2.3	1.1	1.6				7.11	59.5
9.10	17.80	249.0	64.5	161.9	-7.7	133.2	191.7	132.1	40.0	21.0	6.7	3.4	1.5	2.7				7.23	55.6
9.50	17.50	243.9	63.2	158.5	-13.5	132.3	192.1	141.7	41.5	24.1	7.1	4.1	1.7	3.3				7.29	53.8
10.00	17.30	237.3	62.2	154.3	-20.2	129.9	192.9	153.6	43.1	27.3	7.6	5.1	2.0	4.2	0.7			7.32	51.6
11.00	16.90	226.7	61.4	145.9	-30.5	123.1	192.3	177.6	46.0	31.8	8.6	7.5	2.4	5.8	1.4			7.38	48.1
12.00	16.70	215.2	62.3	137.9	-35.6	114.7	189.8	197.4	49.2	36.1	9.7	9.5	2.7	7.1	2.4	1.6		7.31	45.1
13.00	16.50	204.5	64.0	130.7	-36.0	105.6	186.4	212.5	52.4	40.4	10.9	11.2	3.0	8.0	3.0	3.4		7.15	42.5
13.36	16.50	200.9	65.0	127.9	-35.3	102.2	185.1	217.0	53.4	42.0	11.3	11.7	3.0	8.2	3.2	4.3	0.1	7.07	41.7
14.00	16.50	194.8	67.1	123.3	-33.2	95.5	182.4	224.7	55.7	45.2	12.0	12.6	3.2	8.5	3.4	4.3	0.5	6.89	40.4
15.00	16.60	185.1	71.0	116.9	-27.3	85.1	177.7	234.0	59.2	50.8	13.5	14.3	3.3	8.5	2.8	3.6	1.5	6.57	38.5
16.00	16.70	175.1	75.0	110.4	-18.0	74.8	174.0	239.3	62.6	57.0	15.1	16.5	3.4	7.9	0.5	3.2	3.2	6.15	36.7

energy accelerators can be used to produce '14 MeV' neutrons (which is what is done in many installations). Comprehensive overviews of such 14 MeV neutron generators are available (e.g. Refs [25, 26]).

Although there are no secondary neutrons up to 20.46 MeV, the room background even at lower energies is comparatively high because of the rather small anisotropies of the cross-sections and neutron energies. In addition, the specific yield, even at the resonance, is very low (see Fig. 2). Thus there are cases where p-T is a better choice than d-T for experiments with 14 MeV neutrons (e.g. Ref. [18]).

After prolonged use of a target, the deuterium self-buildup in the beam stop can become an undesired source of low energy background neutrons, especially after an increase in the deuteron energy. Since secondary neutrons (with a maximum energy that is about 20 MeV less than the primary neutron energy) affect measurements above 20.5 MeV only, there was up to now little need for breakup data. The few measurements available are listed in Ref. [5].

Figure 22 compares the specific yields of various sources using gas targets for neutron production near 14 MeV. The advantage of using 90° rather than 0° for the d-T (and the t-D) source is obvious. At this angle the energies of the emitted neutrons are quite independent of the beam energy. However, in an actual experiment the neutrons intercepted by the sample will be from a finite angular range around 90° (depending on the opening angle of the sample and the angular straggling of the beam). Thus the actual specific yield will be lower (even more so with solid tritium targets owing to much increased angular straggling). The reaction data are collected in Table VIII, the angular dependence of the neutron energies and of the differential cross-sections are illustrated in Figs 23–30.

3.3.2. $^{2}H(t, n)^{4}He$

Exchanging the projectile with the target nuclei of the d-T reaction increases the upper limit for monoenergetic neutron production from 20.5 to 23.0 MeV. The maximum neutron yield at 0° then occurs for 15.2 instead of 14.8 MeV neutrons, so that the specific yield is higher (up to 80%) between 15.07 and 17.02 MeV. Owing to the smaller *relative* energy loss of the projectile, the total neutron yield is 1.5 times higher for the same c.m. conditions, which results in the higher 90° yield curve in Fig. 22.

No data on the breakup cross-sections have been published. Table IX summarizes the reaction data. The maximum energy of the breakup continuum is about 22 MeV less than the primary neutron energy. The primary c.m. cross-sections can be calculated by using the Legendre coefficients from Table VII, multiplying E_{in} by 1.4976 and changing Θ to $180° - \Theta$. Figures 31–34 illustrate the angular dependence of the neutron energies and of the differential cross-sections.

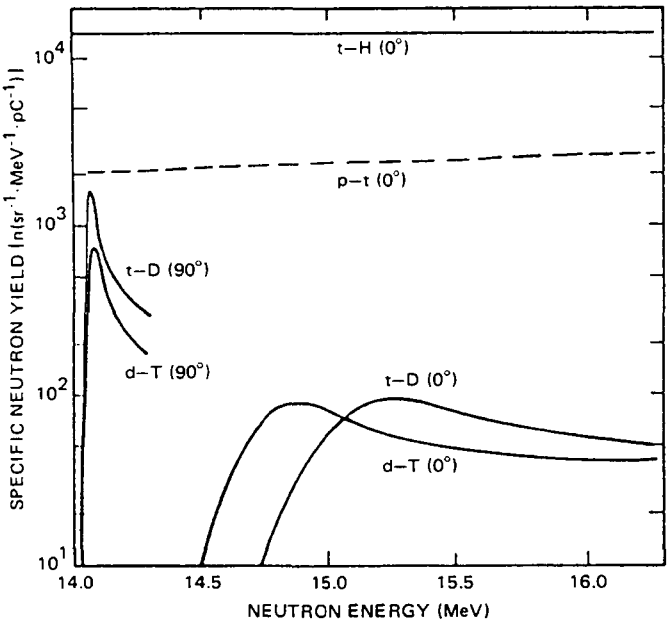

FIG. 22. Specific neutron yields from monoenergetic neutron sources near 14 MeV employing gas targets.

TABLE VIII. Q-VALUES, THRESHOLDS AND NEUTRON ENERGIES AT $0°_{lab}$ FOR d-T
(All energies in MeV)

Exit channel	n + ^{4}He	n + p + t	2n + ^{3}He	n + d + d	2n + p + d	3n + 2p
E_{in}	$E_n(0°_{c.m.})$	E_{nmax1}	E_{nmax2}	E_{nmax3}	E_{nmax4}	E_{nmax5}
0.000	14.028					
3.711	20.461	0.298				
4.985	21.964	2.000	0.400			
10.443	27.891	7.356	6.416	0.838		
14.159	31.717	10.918	10.006	5.763	1.136	
17.876	35.465	14.472	13.573	9.521	6.414	1.435
Q	17.589	−2.225	−2.988	−6.257	−8.482	−10.707

TABLE IX. Q-VALUES, THRESHOLDS AND NEUTRON ENERGIES AT $0°_{lab}$ FOR t-D
(All energies in MeV)

Exit channel	n + ^{4}He	n + p + t	2n + ^{3}He	n + d + d	2n + p + d	3n + 2p
E_{in}	$E_n(0°_{c.m.})$	E_{nmax1}	E_{nmax2}	E_{nmax3}	E_{nmax4}	E_{nmax5}
0.000	14.028					
5.558	23.006	0.668				
7.466	25.032	2.990	0.897			
15.639	32.946	10.038	8.934	1.879		
21.204	38.023	14.713	13.650	8.592	2.547	
26.771	42.985	19.375	18.331	13.559	9.789	3.214
Q	17.589	−2.225	−2.988	−6.257	−8.482	−10.707

3.4. Interaction of protons with ^{7}Li

Reduced c.m. Legendre coefficients are given in Tables X and XI for the ^{7}Li(p, n_0)^{7}Be and the ^{7}Li(p, n_1)^{7}Be* reactions, respectively (^{7}Be* is in the 0.43 MeV excited state). The coefficients used in these tables are taken from Liskien and Paulsen [10]. For the ground state reaction they give an absolute deviation of the reduced Legendre coefficients of 0.03 at proton energies above 2.2 MeV (resulting in *minimum* worst case shape uncertainties of ±5.9%) and 5% for the relative deviation of the 0° cross-sections. For the reaction leading to the 0.43 MeV excited state, the absolute deviation of the Legendre coefficients for proton energies above 3.2 MeV is 0.1 (resulting in *minimum* worst case shape uncertainties of ±33%), while the uncertainty in the cross-section ratio at 0° is 9%.

The quality of the evaluated coefficients in the light of more recent data has been discussed [2, 3]. Recent data for the ^{1}H(^{7}Li, n)^{7}Be reaction [27] show surprisingly large deviations of the 180° excitation function from the evaluated data near 2.0 and 2.5 MeV proton energy which could be caused by discrepant projectile energies [7]. From this and other evidence, it can be estimated that the accuracy of the cross-sections calculated from the coefficients will be of the order of 10% over most of the energy range. Experimental papers on the p-^{7}Li interaction are listed in Refs [2] and [10].

Text cont. on p. 138.

TABLE X. THE $^{7}Li(p, n)^{7}Be$ REACTION

(Proton energy: E_{in}; c.m. differential cross-section at 0°: S_0; reduced Legendre coefficients: A_i; c.m. differential cross-section at 180°: S_π; integrated cross-section: S_t)

E_{in} (MeV)	S_0 (mb/sr)	A_0	A_1	A_2	A_3	S_π (mb/sr)	S_t (mb)
1.95	19.0	1.125	-0.125			23.75	269.
2.00	15.0	1.425	-0.430	0.005		27.90	269.
2.05	12.1	1.805	-0.825	0.020		32.06	275.
2.10	13.1	1.810	-0.845	0.035		35.24	298.
2.15	22.6	1.380	-0.435	0.055		42.26	392.
2.20	46.7	0.815	0.110	0.075		36.43	478.
2.25	79.2	0.585	0.330	0.085		26.93	582.
2.30	83.4	0.475	0.430	0.095		11.68	498.
2.35	71.4	0.460	0.440	0.100		8.57	413.
2.40	61.2	0.445	0.445	0.110		6.73	342.
2.45	53.0	0.465	0.420	0.115		8.48	310.
2.50	47.4	0.490	0.400	0.110		9.48	292.
2.60	40.5	0.545	0.350	0.105		12.15	277.
2.70	36.0	0.585	0.320	0.095		12.96	265.
2.80	34.2	0.590	0.330	0.080		11.63	253.
2.90	33.0	0.580	0.350	0.070		9.90	241.
3.00	32.0	0.575	0.365	0.060		8.64	232.
3.10	31.2	0.580	0.360	0.060		8.74	227.
3.20	30.5	0.585	0.355	0.060		8.84	223.
3.30	29.9	0.590	0.345	0.065		9.27	222.
3.40	29.3	0.600	0.330	0.070		9.96	221.
3.50	28.7	0.620	0.305	0.075		11.19	224.
3.60	28.2	0.640	0.295	0.080	-0.015	12.41	227.
3.70	27.8	0.660	0.285	0.095	-0.040	14.18	231.
3.80	27.4	0.685	0.275	0.105	-0.065	15.89	236.
3.90	27.0	0.710	0.250	0.125	-0.085	18.09	241.
4.00	26.7	0.730	0.225	0.145	-0.100	20.03	245.
4.10	27.1	0.740	0.210	0.175	-0.125	22.49	252.
4.20	28.2	0.740	0.200	0.210	-0.150	25.38	262.
4.30	30.0	0.720	0.190	0.260	-0.170	28.80	271.
4.40	32.2	0.705	0.180	0.295	-0.180	32.20	285.
4.50	34.6	0.685	0.165	0.320	-0.170	34.95	298.
4.60	37.5	0.660	0.155	0.340	-0.155	37.50	311.
4.70	41.1	0.630	0.140	0.355	-0.125	39.87	325.
4.80	44.8	0.605	0.130	0.360	-0.095	41.66	341.
4.90	48.1	0.590	0.115	0.365	-0.070	43.77	357.
5.00	50.0	0.590	0.090	0.365	-0.045	45.50	371.
5.10	48.6	0.600	0.065	0.365	-0.030	45.20	366.
5.20	45.6	0.615	0.035	0.365	-0.015	43.78	352.
5.30	42.4	0.635	0.005	0.360		41.98	338.
5.40	39.6	0.655	-0.025	0.355	0.015	40.39	326.
5.50	36.6	0.675	-0.050	0.345	0.030	38.06	310.
5.60	33.9	0.695	-0.085	0.340	0.050	36.27	296.
5.70	31.6	0.710	-0.110	0.335	0.065	34.44	282.
5.80	29.0	0.725	-0.135	0.330	0.080	32.19	264.
5.90	26.7	0.745	-0.160	0.325	0.090	30.44	250.
6.00	24.4	0.760	-0.180	0.320	0.100	28.30	233.
6.10	22.6	0.775	-0.205	0.315	0.115	26.67	220.
6.20	21.0	0.785	-0.220	0.310	0.125	24.99	207.
6.30	19.5	0.800	-0.240	0.305	0.135	23.60	196.
6.40	18.2	0.810	-0.255	0.305	0.140	22.39	185.
6.50	16.9	0.820	-0.265	0.300	0.145	20.96	174.
6.60	15.6	0.830	-0.275	0.295	0.150	19.50	163.
6.70	14.6	0.840	-0.285	0.290	0.155	18.40	154.
6.80	13.7	0.850	-0.295	0.285	0.160	17.40	146.
6.90	12.9	0.850	-0.300	0.285	0.165	16.38	138.
7.00	12.2	0.855	-0.305	0.280	0.170	15.49	131.

TABLE XI. THE $^{7}Li(p, n)^{7}Be^{*}$ REACTION

(Proton energy: E_{in}; c.m. differential cross-section at 0°: S_0; reduced Legendre coefficients: A_i; c.m. differential cross-section at 180°: S_π; integrated cross-section: S_t)

E_{in} (MeV)	S_0 (mb/sr)	A_0	A_1	A_2	A_3	S_π (mb/sr)	S_t (mb)
2.5	0.65	1.010	0.000	-0.005	-0.005	0.66	8.0
2.6	1.10	1.095	-0.025	-0.020	-0.050	1.26	15.0
2.7	1.45	1.275	-0.080	-0.050	-0.145	2.10	23.0
2.8	1.75	1.540	-0.220	-0.115	-0.205	3.24	33.5
2.9	2.05	1.755	-0.310	-0.220	-0.225	4.24	45.0
3.0	2.25	1.885	-0.355	-0.315	-0.215	4.82	53.0
3.1	2.40	1.905	-0.400	-0.355	-0.150	5.04	58.0
3.2	2.60	1.865	-0.415	-0.345	-0.105	5.30	61.0
3.3	2.75	1.780	-0.440	-0.275	-0.065	5.53	61.0
3.4	2.85	1.700	-0.470	-0.210	-0.020	5.64	60.5
3.5	2.95	1.585	-0.490	-0.115	0.020	5.72	58.5
3.6	3.00	1.485	-0.515	-0.020	0.050	5.79	55.5
3.7	3.05	1.390	-0.535	0.125	0.020	6.19	53.5
3.8	3.05	1.335	-0.550	0.240	-0.025	6.56	51.5
3.9	3.05	1.300	-0.570	0.340	-0.070	6.95	50.0
4.0	3.05	1.280	-0.585	0.420	-0.115	7.32	49.0
4.1	3.00	1.280	-0.600	0.475	-0.155	7.53	48.0
4.2	2.90	1.285	-0.610	0.520	-0.195	7.57	47.0
4.3	2.85	1.290	-0.615	0.555	-0.230	7.67	46.0
4.4	2.80	1.290	-0.620	0.590	-0.260	7.73	45.0
4.5	2.75	1.290	-0.620	0.615	-0.285	7.73	44.5
4.6	2.70	1.290	-0.615	0.630	-0.305	7.67	43.5
4.7	2.65	1.285	-0.610	0.645	-0.320	7.58	43.0
4.8	2.60	1.275	-0.600	0.655	-0.330	7.44	42.0
4.9	2.60	1.265	-0.585	0.660	-0.340	7.41	41.0
5.0	2.65	1.230	-0.550	0.660	-0.340	7.37	40.5
5.1	2.70	1.180	-0.500	0.655	-0.335	7.21	40.0
5.2	2.80	1.110	-0.420	0.640	-0.330	7.00	39.0
5.3	3.10	0.970	-0.280	0.620	-0.310	6.76	38.0
5.4	3.55	0.840	-0.140	0.580	-0.280	6.53	37.5
5.5	4.00	0.745	-0.045	0.550	-0.250	6.36	37.5
5.6	4.55	0.665	0.010	0.525	-0.200	6.28	38.0
5.7	5.10	0.600	0.050	0.500	-0.150	6.12	38.5
5.8	5.60	0.560	0.080	0.470	-0.110	5.94	39.5
5.9	6.15	0.525	0.105	0.445	-0.075	5.78	40.5
6.0	6.50	0.515	0.130	0.400	-0.045	5.40	42.0
6.1	6.95	0.520	0.145	0.360	-0.025	5.28	45.5
6.2	7.25	0.525	0.155	0.325	-0.005	5.07	48.0
6.3	7.40	0.535	0.165	0.290	0.010	4.81	49.5
6.4	7.20	0.545	0.170	0.260	0.025	4.39	49.5
6.5	6.75	0.560	0.175	0.230	0.035	3.91	47.5
6.6	6.25	0.580	0.180	0.200	0.040	3.50	45.5
6.7	5.80	0.600	0.185	0.170	0.045	3.13	43.5
6.8	5.30	0.630	0.190	0.135	0.045	2.81	41.5
6.9	4.75	0.655	0.195	0.105	0.045	2.47	39.0
7.0	4.25	0.675	0.200	0.080	0.045	2.17	36.0

THE $^{3}H(d,n)^{4}He$ REACTION

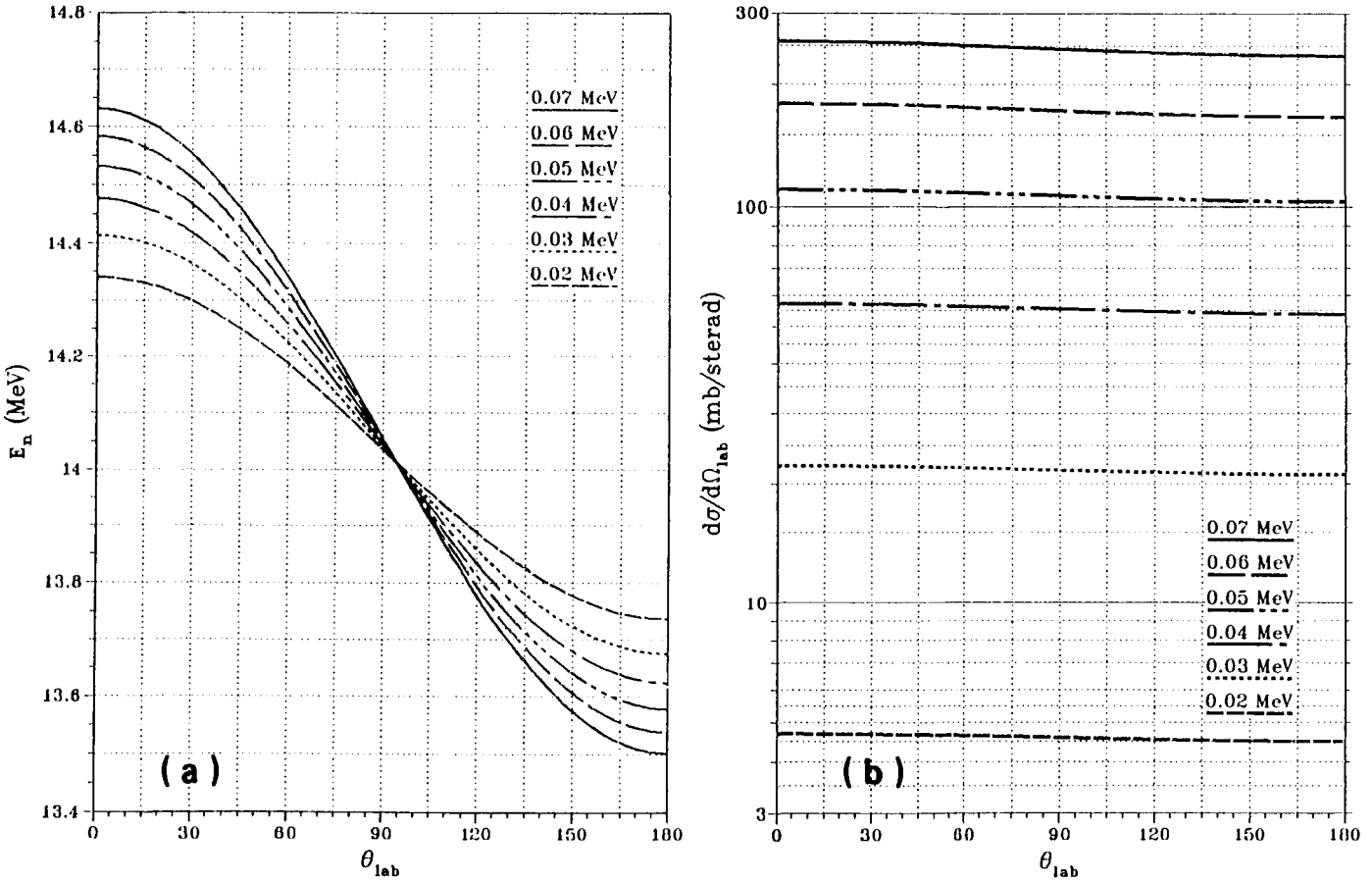

FIG. 23. (a) Neutron energy values and (b) differential cross-sections for the $^3H(d, n)^4He$ reaction: 0.02–0.07 MeV.

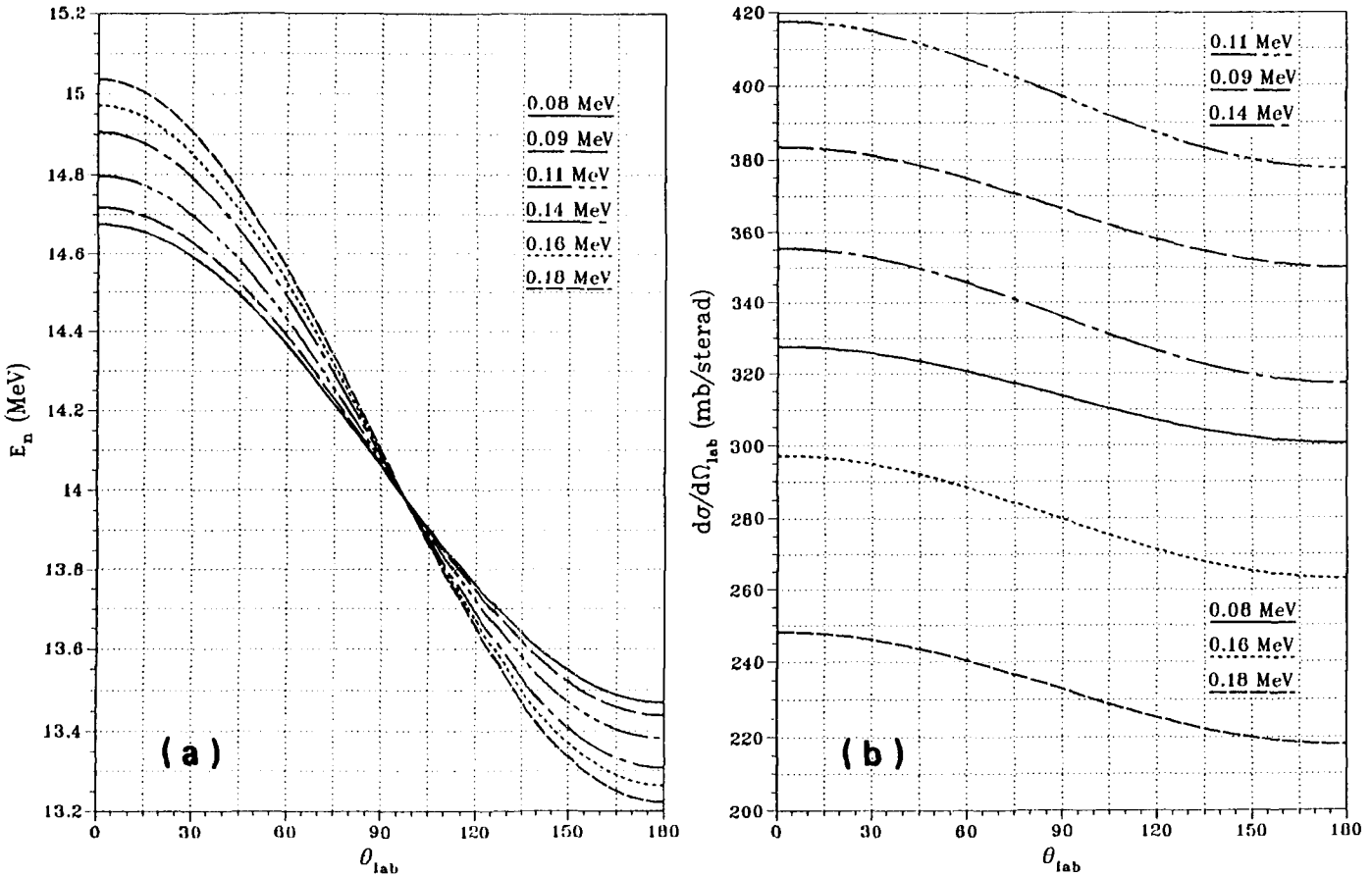

FIG. 24. (a) Neutron energy values and (b) differential cross-sections for the $^3H(d, n)^4He$ reaction: 0.08–0.18 MeV.

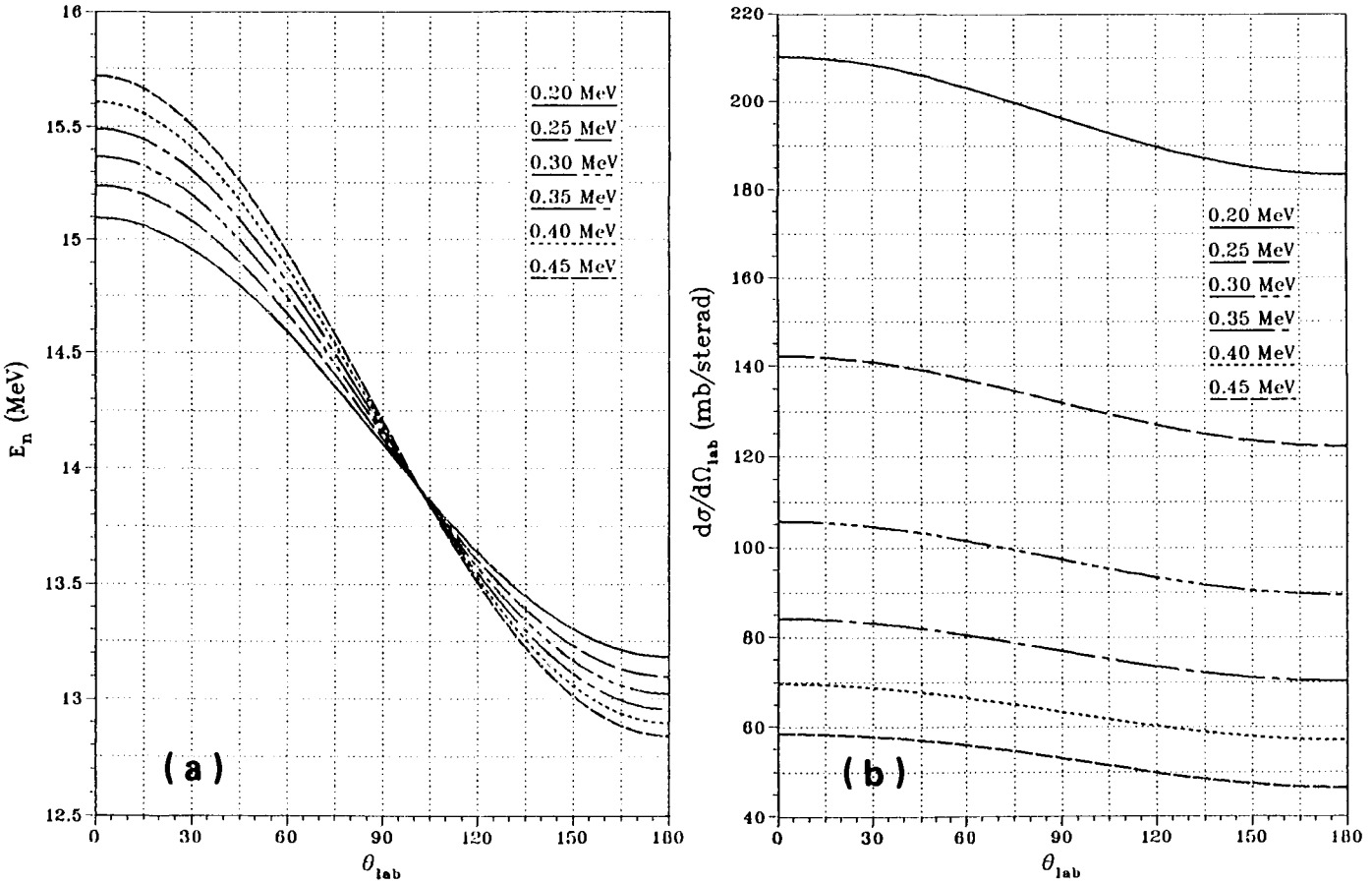

FIG. 25. (a) Neutron energy values and (b) differential cross-sections for the $^3H(d, n)^4He$ reaction: 0.20-0.45 MeV.

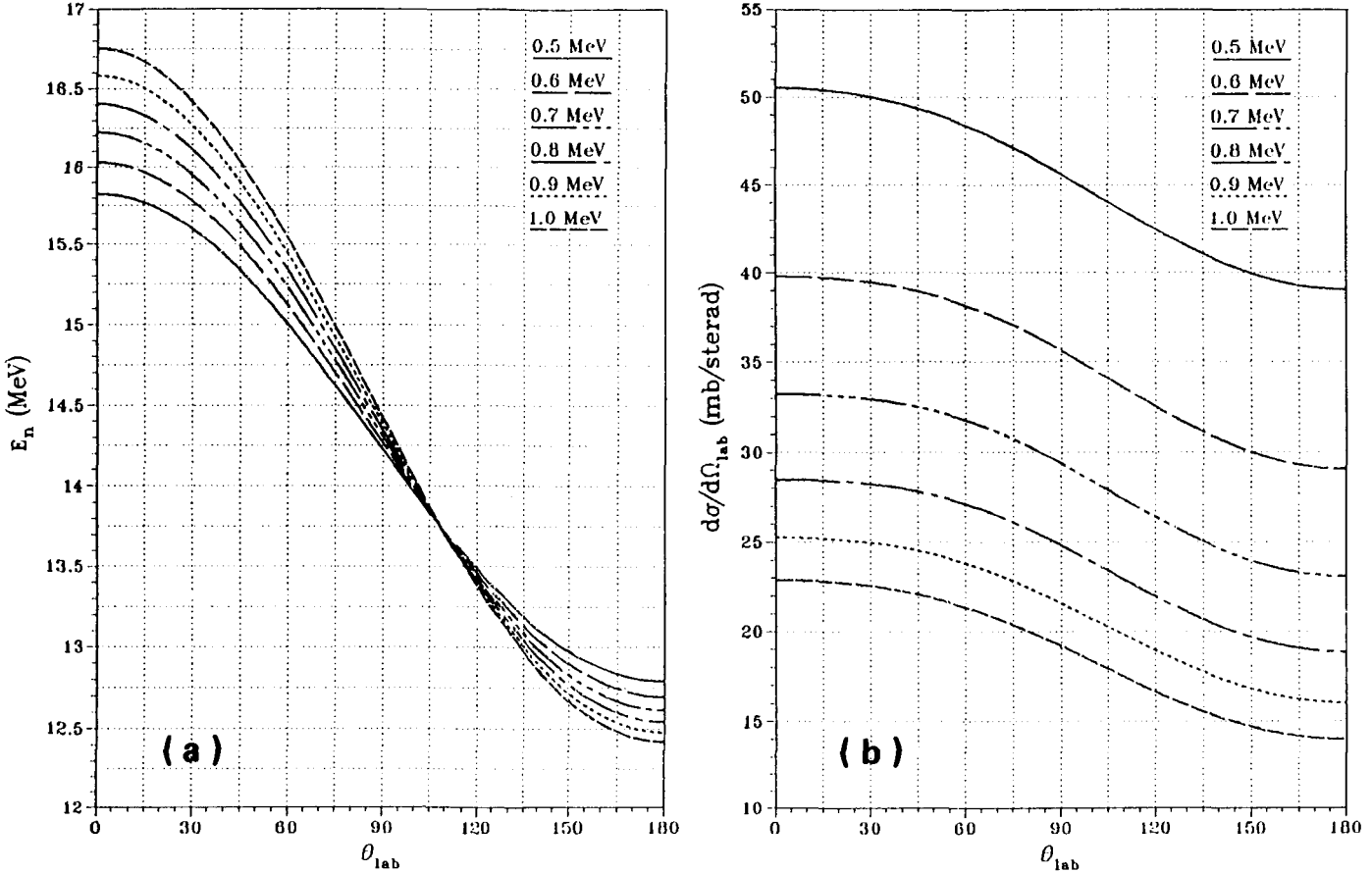

FIG. 26. (a) Neutron energy values and (b) differential cross-sections for the $^3H(d, n)^4He$ reaction: 0.5–1.0 MeV.

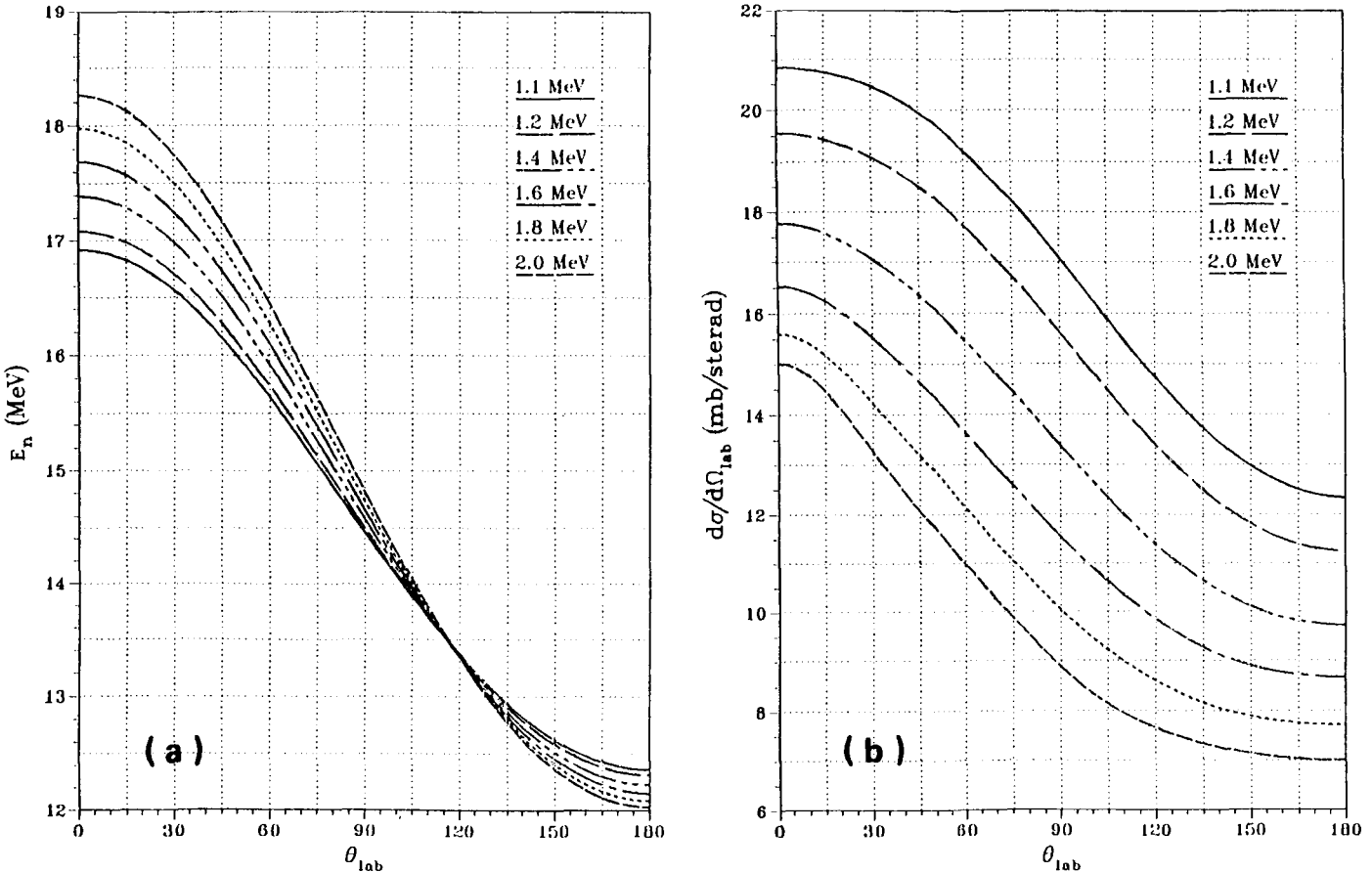

FIG. 27. (a) Neutron energy values and (b) differential cross-sections for the $^3H(d, n)^4He$ reaction: 1.1–2.0 MeV.

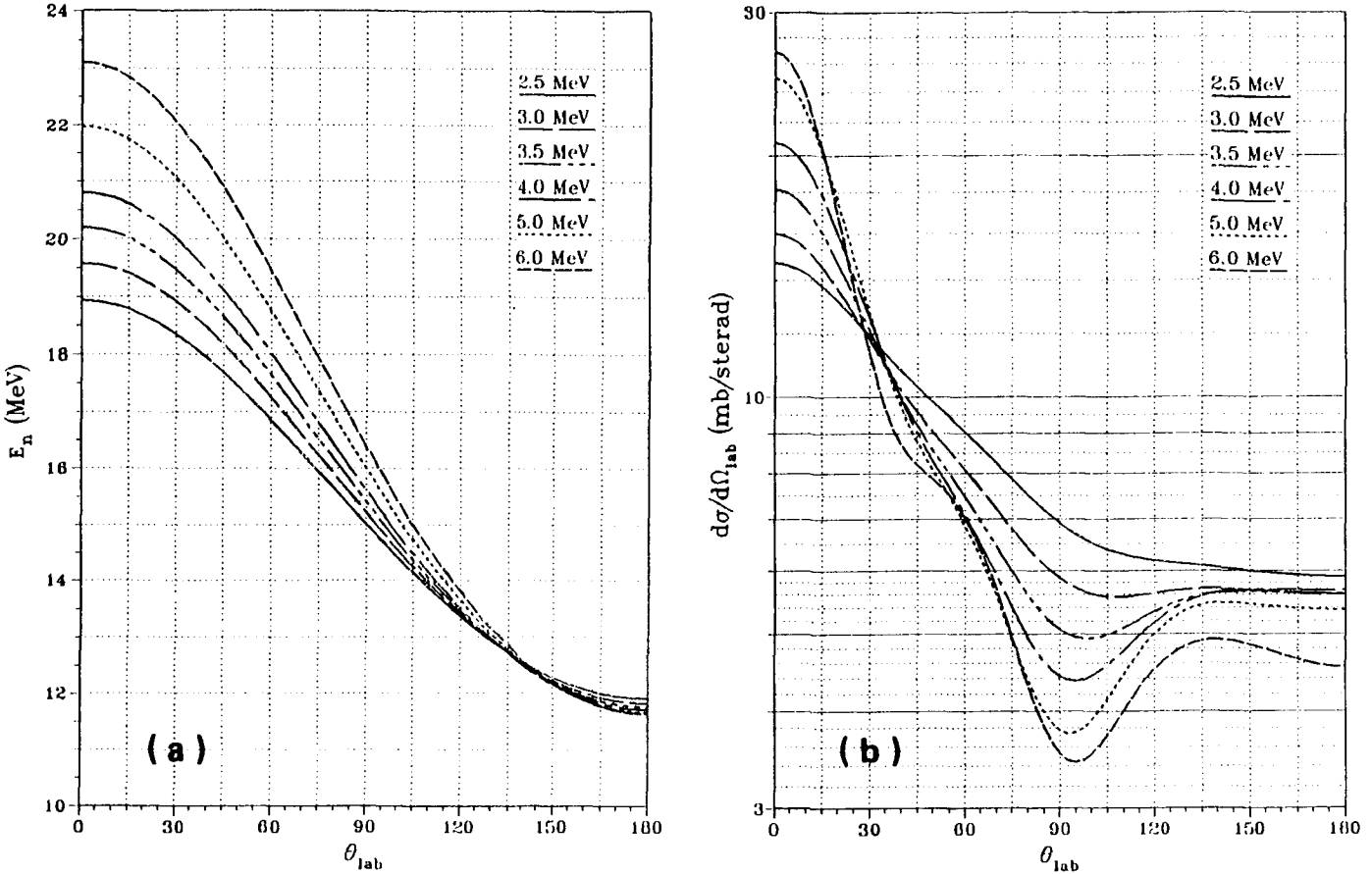

FIG. 28. (a) Neutron energy values and (b) differential cross-sections for the $^3H(d, n)^4He$ reaction: 2.5-6.0 MeV.

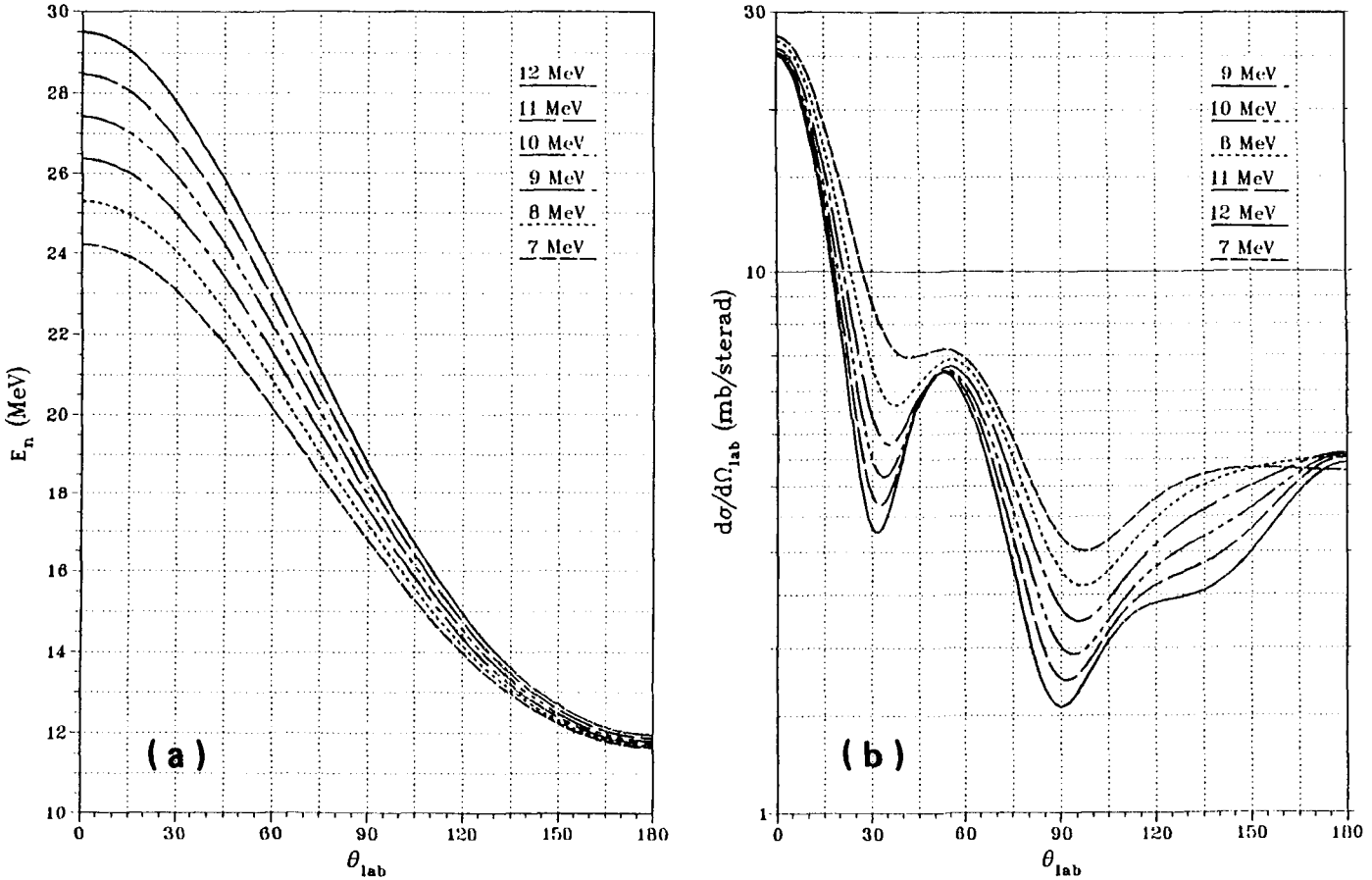

FIG. 29. (a) Neutron energy values and (b) differential cross-sections for the $^3H(d, n)^4He$ reaction: 7–12 MeV.

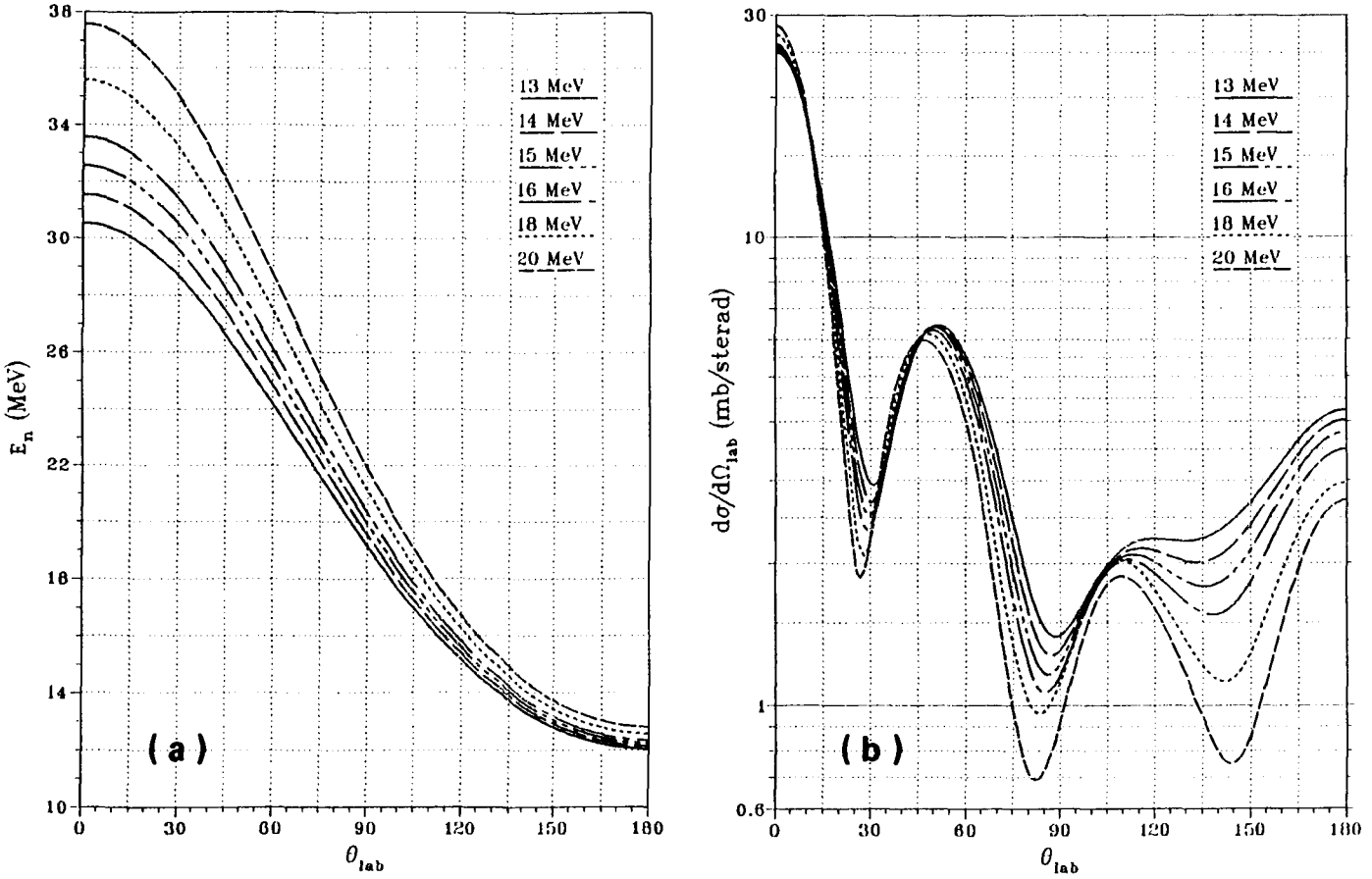

FIG. 30. (a) Neutron energy values and (b) differential cross-sections for the $^3H(d, n)^4He$ reaction: 13–20 MeV.

*3.4.1. $^{7}Li(p, n_0)^{7}Be$ and $^{7}Li(p, n_1)^{7}Be$**

Table XII gives the relevant reaction data and Figs 35–40 illustrate the angular dependence of the neutron energies and of the differential cross-sections. Although above $E_p = 2.37$ MeV ($E_n(0°) = 0.65$ MeV) a second neutron line (from the 0.43 MeV excitation of ^{7}Be) is present (actually, up to 2.42 MeV there is even a third line), its intensity is less than 10%, so it can be tolerated in some applications. The onset of breakup neutrons at 3.69 MeV ($E_n(0°) = 2.01$ MeV) further limits the use of this reaction as a 'monoenergetic' source to neutron energies below 4 MeV. As in the case of d-D breakup, calculated corrections using double-differential cross-sections can be applied [28].

From Fig. V it can be seen that the energy dependence of the 0° cross-section is very strong for proton energies below 2.5 MeV (0.8 MeV neutron energy). In this region the energy dependence is generally larger than 5% for a 1% change in beam energy. Therefore, a careful determination of the effective beam energy will often be necessary when using this reaction.

Single line spectra below $E_n = 121$ keV can be obtained at angles $>0°$. However, in such cases the background from the neutrons at smaller angles (with higher energy) is troublesome.

The advantages of the p-^{7}Li source are:

(1) Small kinematic energy spread (see Fig. 1). For an opening angle of the sample of ±5°, the relative energy resolution caused by the kinematic spread is close to 0.15% of the neutron energy over the range of interest.
(2) Between 0.4 and 0.7 MeV neutron energy, the yield is higher than for the competing p-T reaction. An additional advantage over the p-T reaction is the higher projectile energy, which gives, e.g. better time resolution in time of flight experiments.
(3) The production of targets for high resolution work is comparatively simple. Usually they consist of lithium metal evaporated on a tantalum [23, 28, 29], silver or tungsten backing. Even natural lithium, which contains 7.5% ^{6}Li, can be used (the (p, n) threshold of ^{6}Li at 5.92 MeV is outside the useful range of the p-^{7}Li reaction). Although the handling of the compound LiF, which is also used as a target material, is easier, metallic Li is better because its specific neutron yield is three times as large.

*3.4.2. $^{1}H(^{7}Li, n_0)^{7}Be$ and $^{1}H(^{7}Li, n_1)^{7}Be$**

If the incoming energy E_{in} in Tables X and XI is multiplied by a factor of 6.9637 and the c.m. angle Θ is changed to $180° - \Theta$, those tables can also be used to calculate the cross-sections for the ^{7}Li-H reactions.

Table XIII summarizes the relevant reaction data. The special feature of this source is the containment of the neutrons in a forward cone with a half-angle

Text cont. on p. 158.

THE $^{2}H(t,n)^{4}He$ REACTION

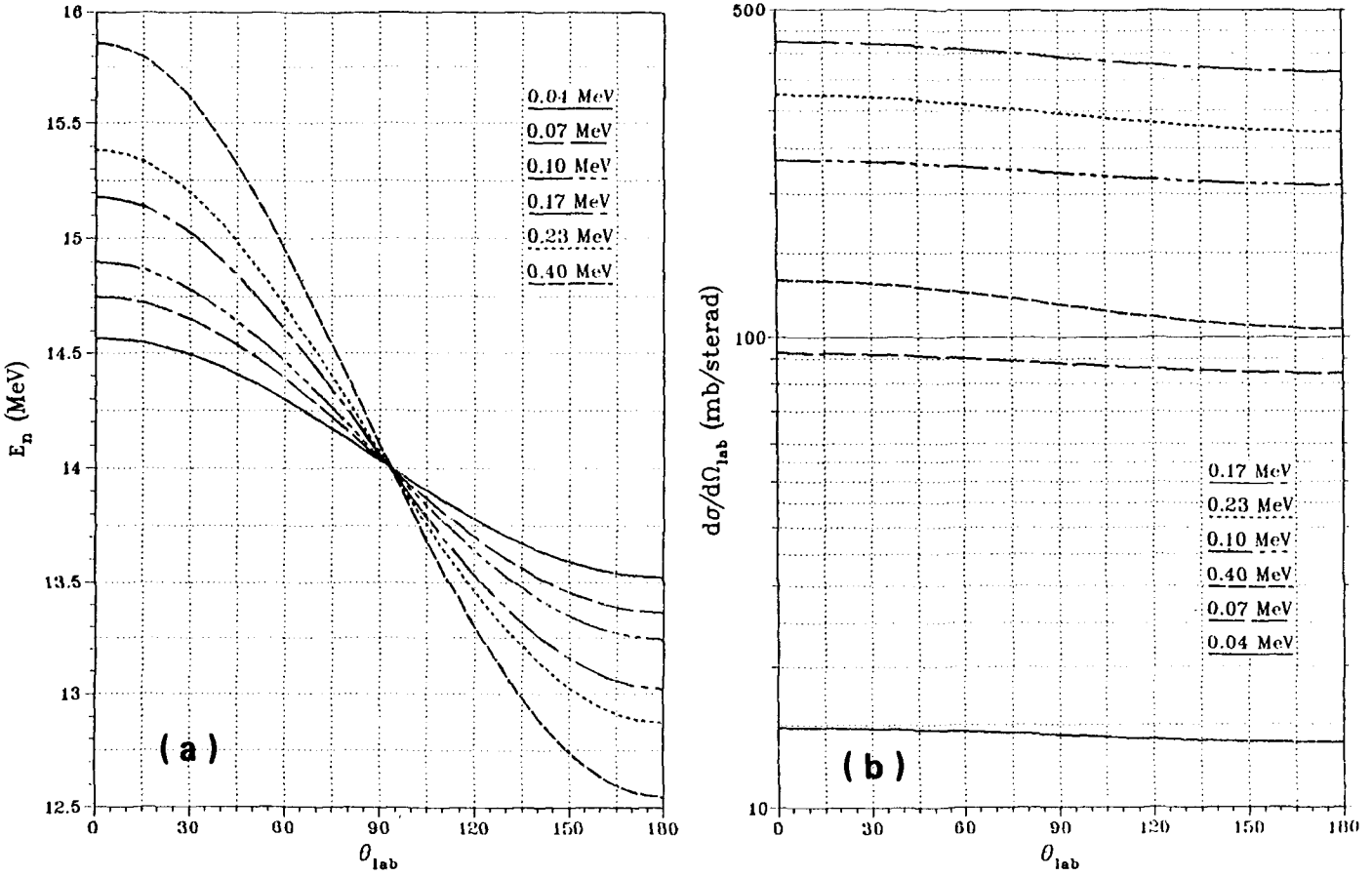

FIG. 31. (a) Neutron energy values and (b) differential cross-sections for the $^2H(t, n)^4He$ reaction: 0.04-0.40 MeV.

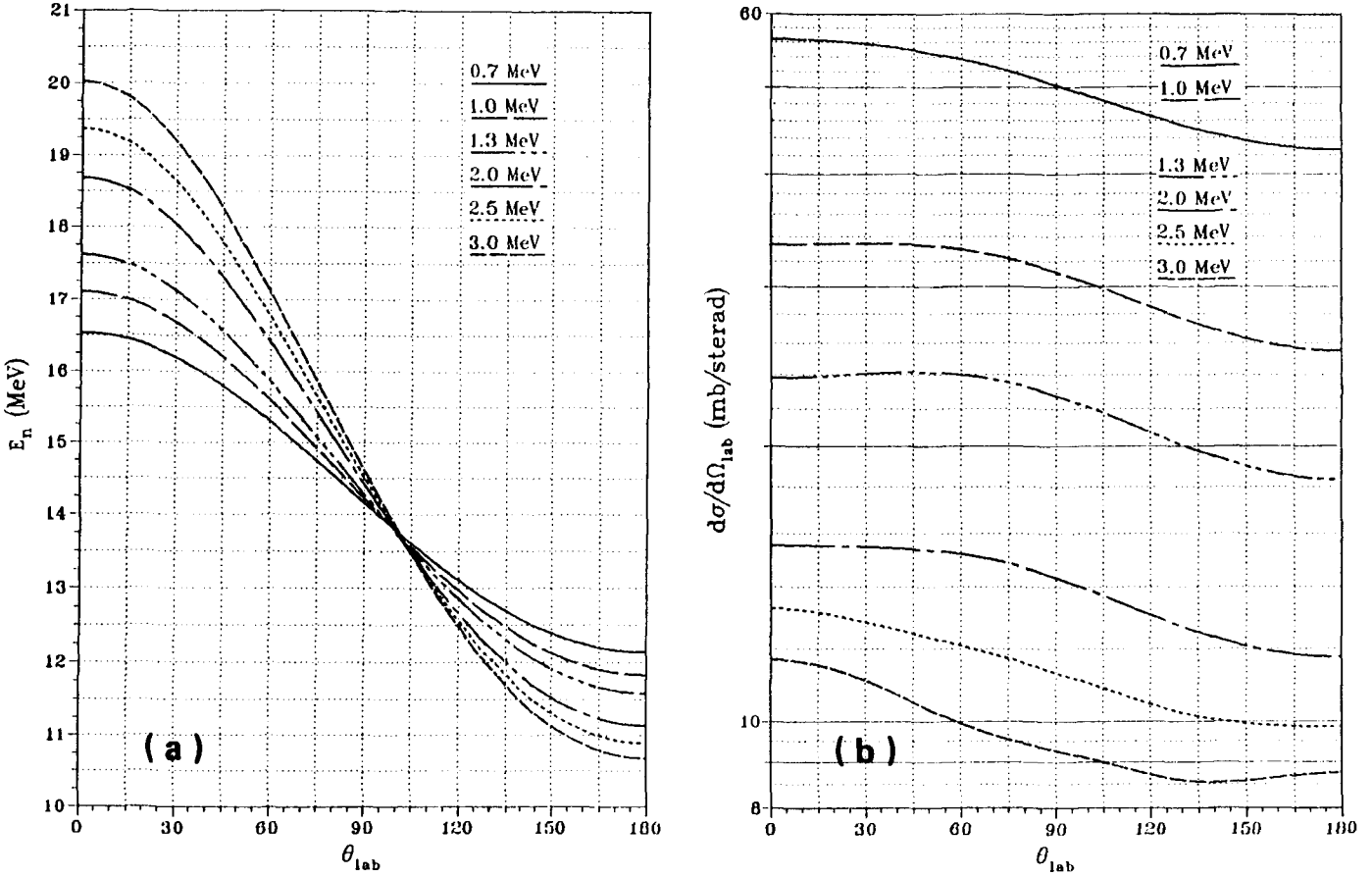

FIG. 32. (a) Neutron energy values and (b) differential cross-sections for the $^2H(t, n)^4He$ reaction: 0.7–3.0 MeV.

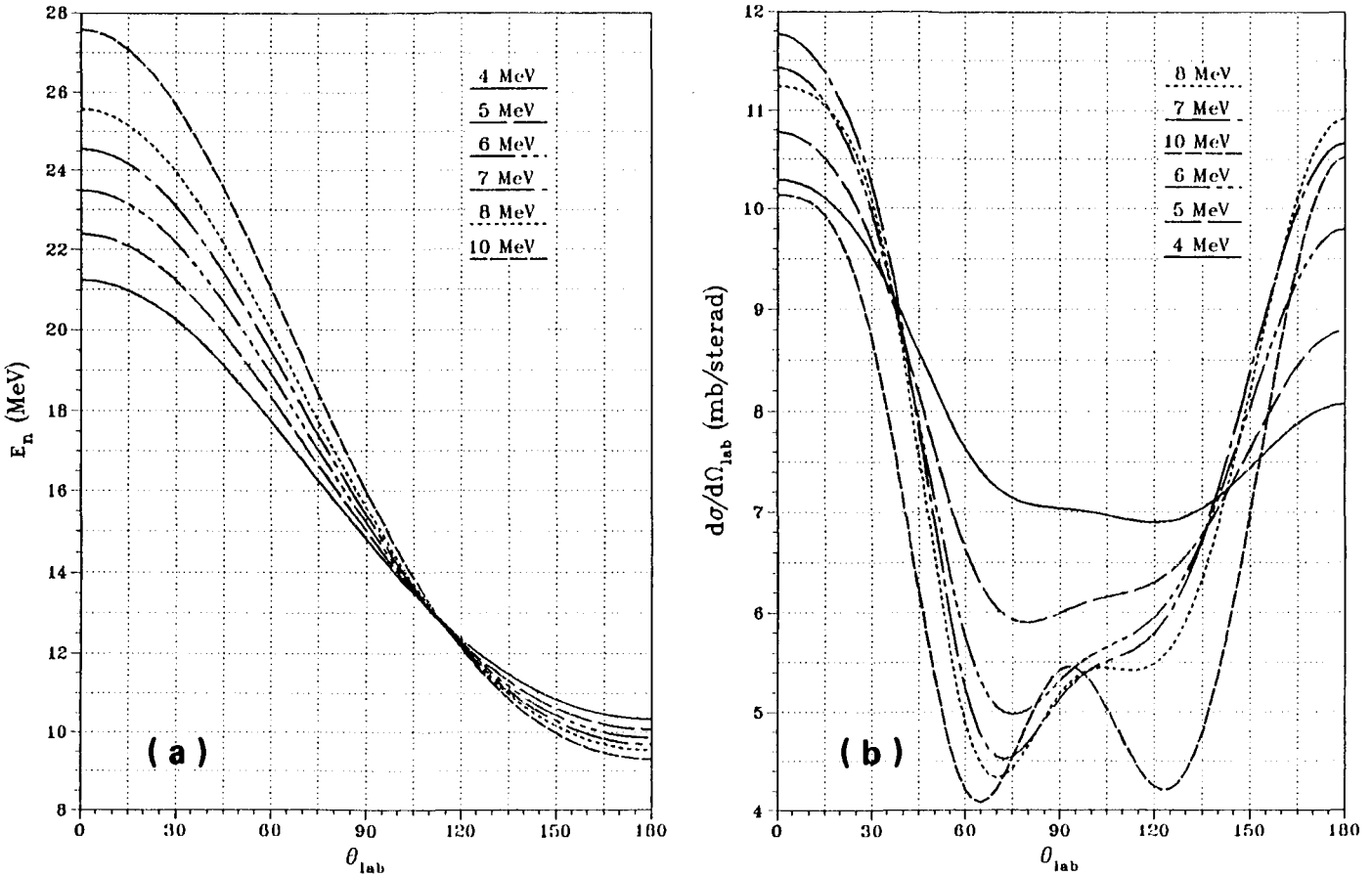

FIG. 33. (a) Neutron energy values and (b) differential cross-sections for the $^2H(t, n)^4He$ reaction: 4-10 MeV.

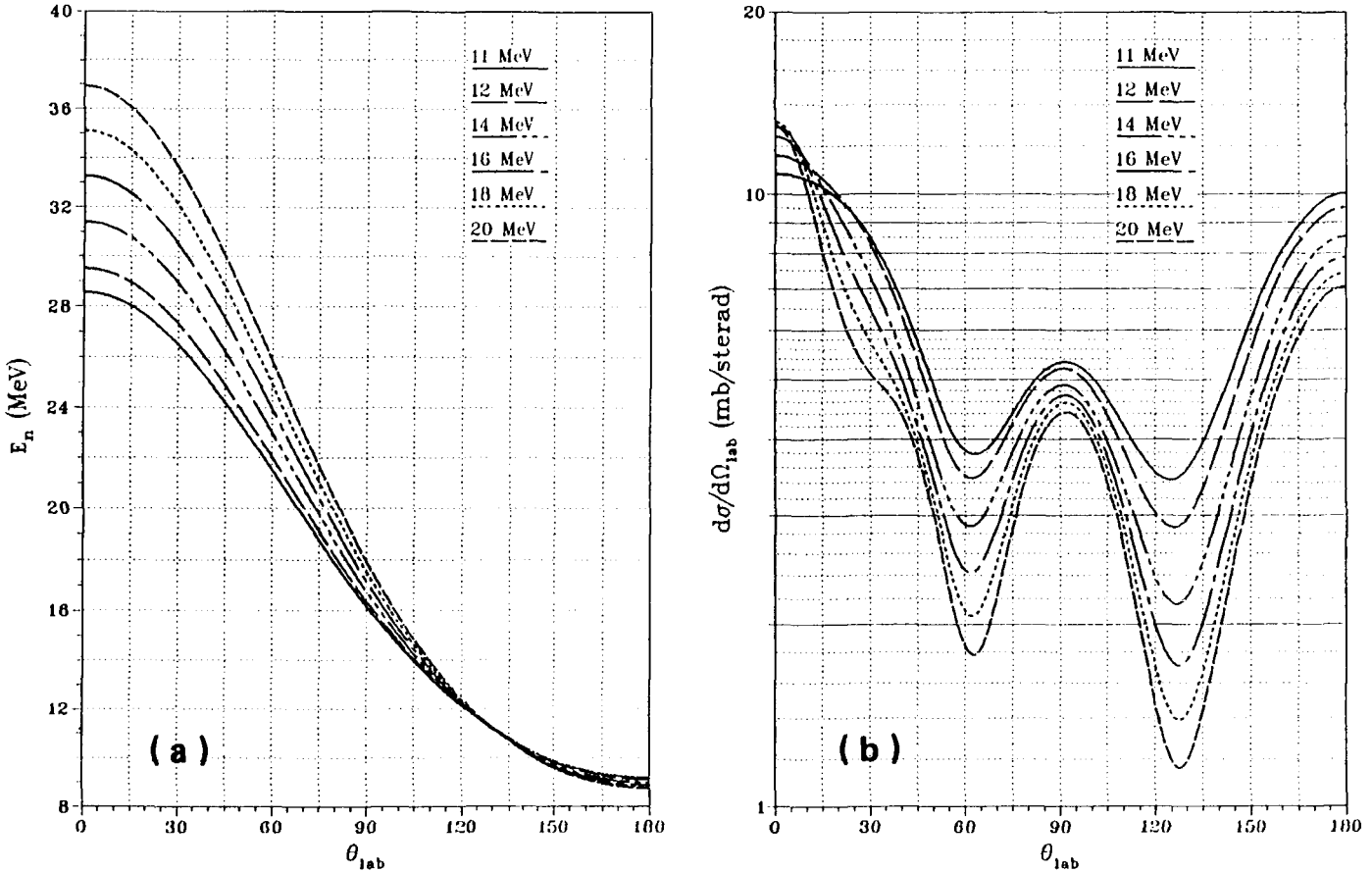

FIG. 34. (a) Neutron energy values and (b) differential cross-sections for the $^2H(t, n)^4He$ reaction: 11–20 MeV.

TABLE XII. Q-VALUES, THRESHOLDS AND NEUTRON ENERGIES AT $0°_{lab}$ FOR p-^{7}Li
(All energies in MeV)

Exit channel	n + ^{7}Be		n + ^{7}Be* (0.43)		n + ^{3}He + α	n + ^{7}Be** (4.57)	
E_{in}	$E_{n0}(0°_{c.m.})$	$E_{n0}(180°_{c.m.})$	$E_{n1}(0°_{c.m.})$	$E_{n1}(180°_{c.m.})$	E_{nmax}	$E_{n2}(0°_{c.m.})$	$E_{n2}(180°_{c.m.})$
1.881	0.030	0.030					
1.920	0.121	0.000					
2.372	0.650	–	0.037	0.037			
2.422	0.703	–	0.153	0.000			
3.695	2.015	–	1.556	–	0.058		
7.110	5.450	–	5.010	–	3.805	0.112	0.112
7.260	5.600	–	5.161	–	3.958	0.460	0.000
Q	−1.644		−2.073		−3.230	−6.214	

THE $^{7}Li(p,n)^{7}Be$ REACTION

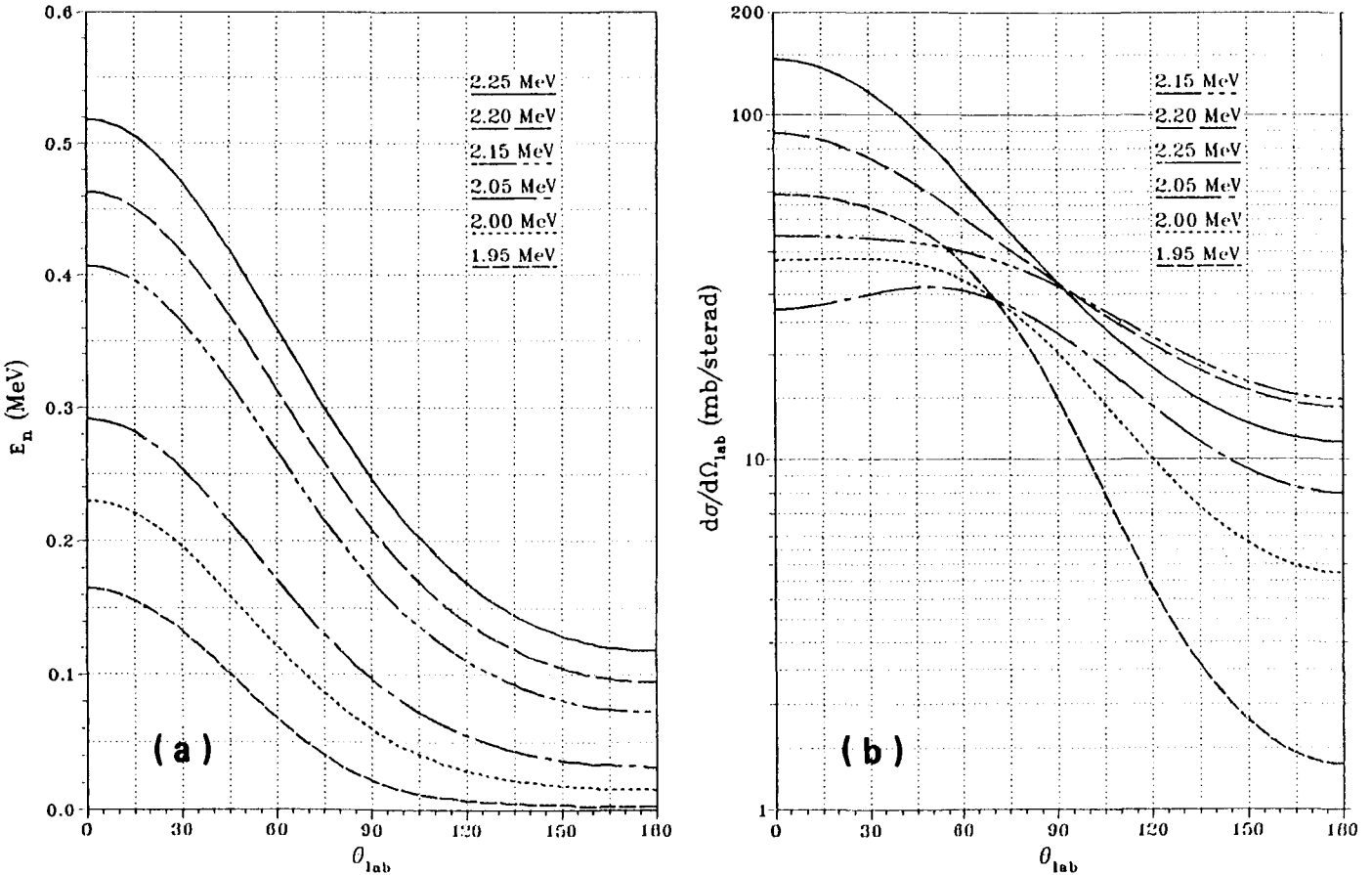

FIG. 35. (a) Neutron energy values and (b) differential cross-sections for the $^7Li(p, n)^7Be$ reaction: 1.95–2.25 MeV.

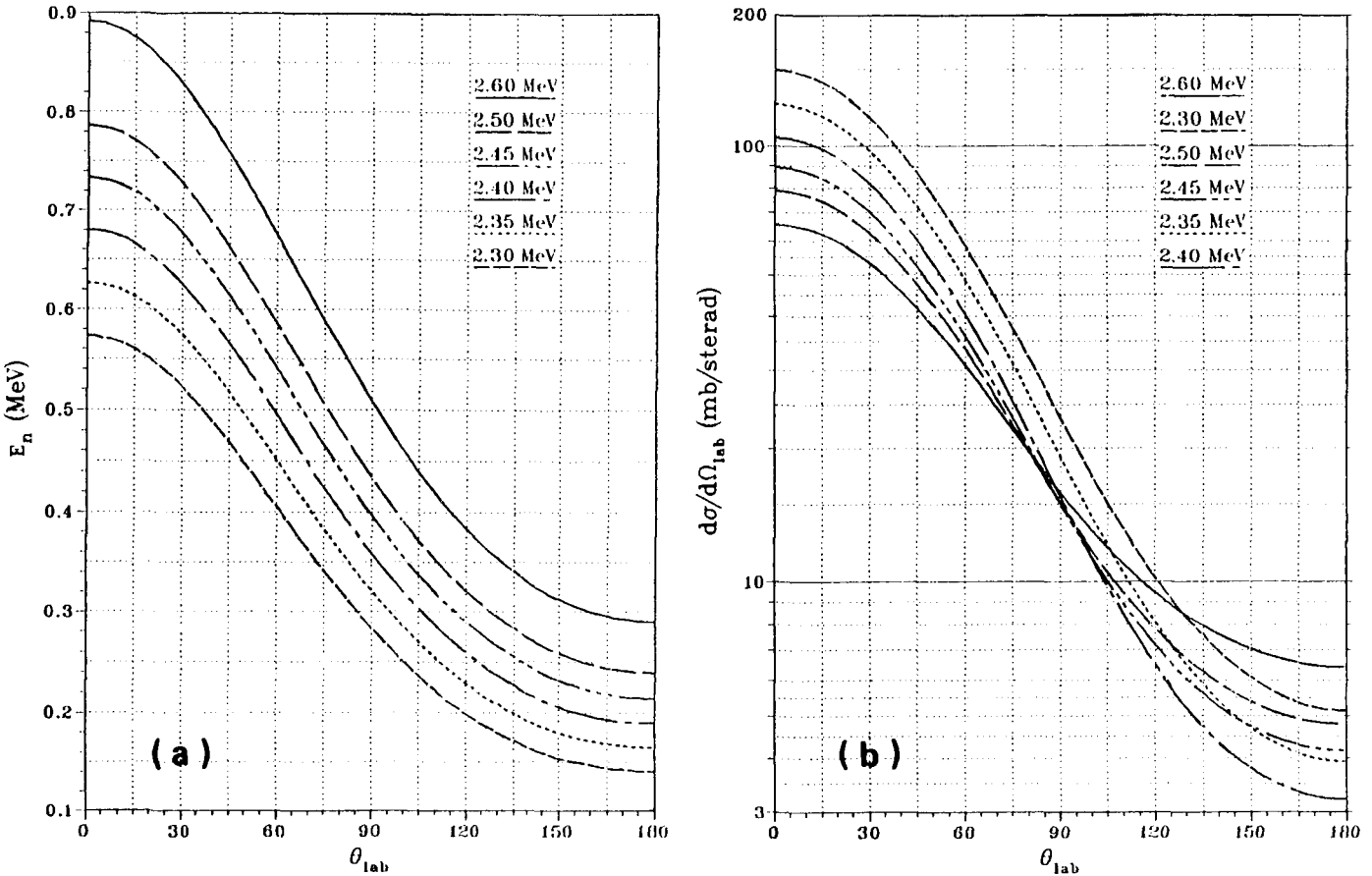

FIG. 36. (a) Neutron energy values and (b) differential cross-sections for the $^7Li(p, n)^7Be$ reaction: 2.30–2.60 MeV.

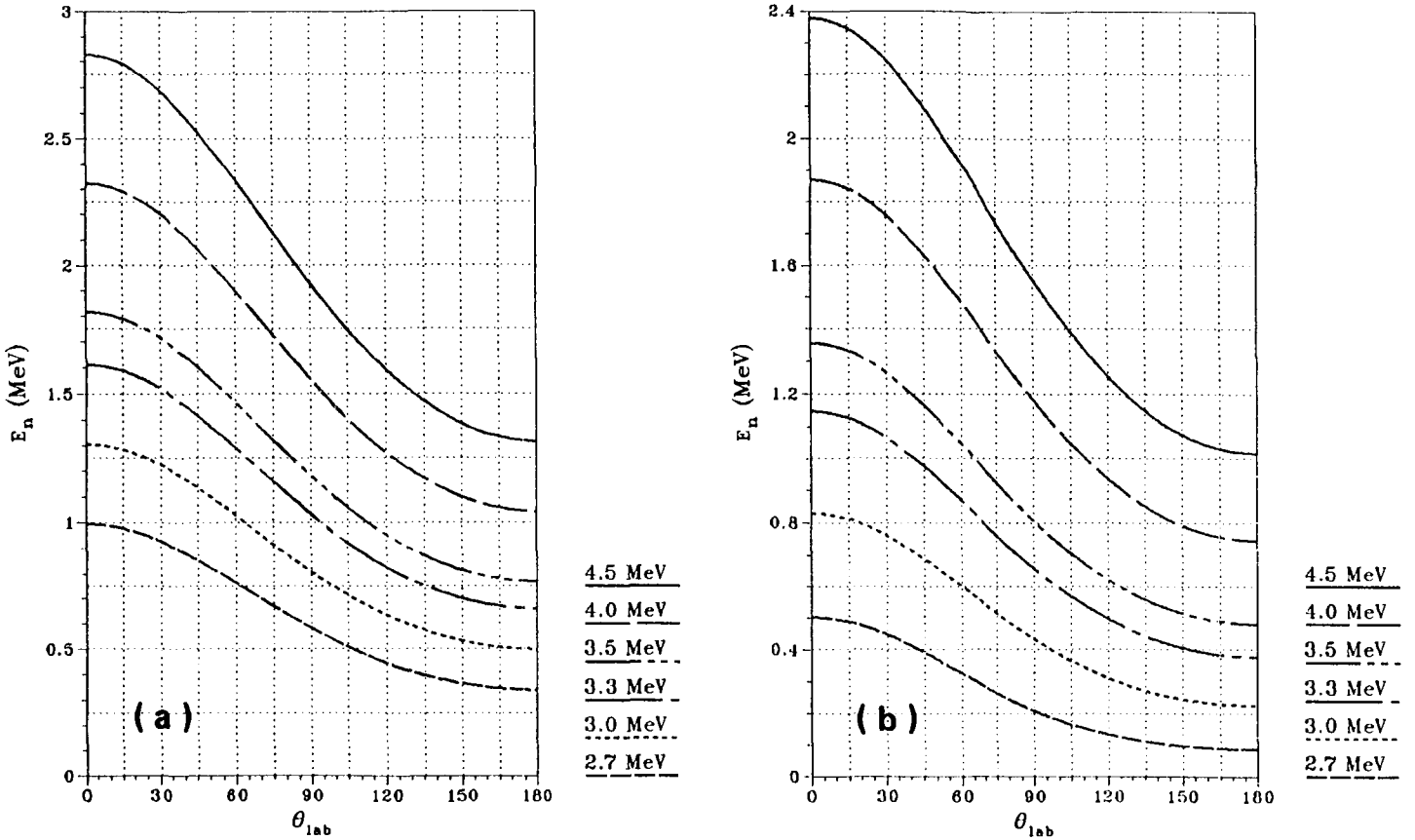

FIG. 37. Neutron energy values for the (a) $^7Li(p, n)^7Be$ and (b) $^7Li(p, n)^7Be^*$ reactions: 2.7–4.5 MeV.

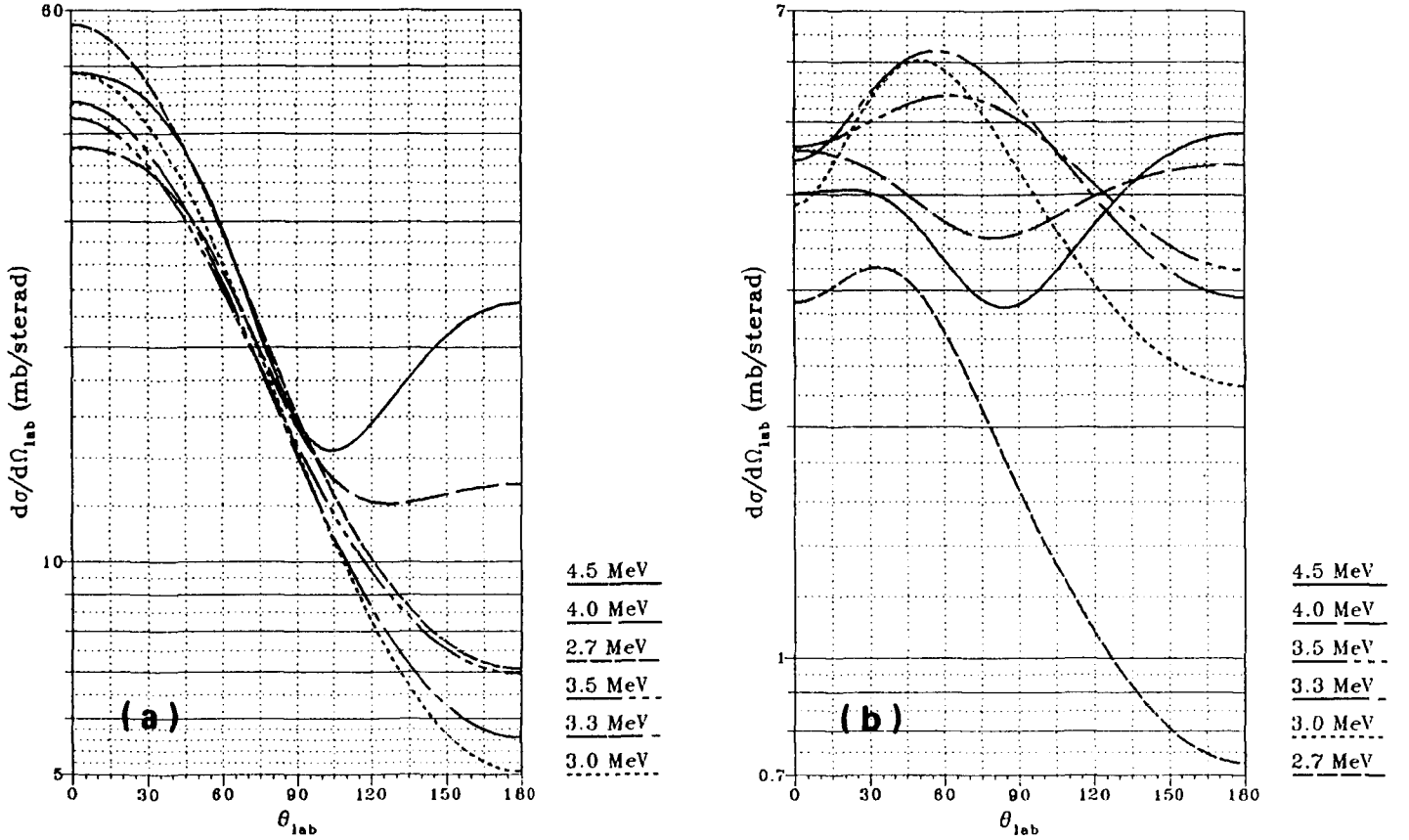

FIG. 38. Differential cross-sections of the (a) $^{7}Li(p, n)^{7}Be$ and (b) $^{7}Li(p, n)^{7}Be^{*}$ reactions: 2.7–4.5 MeV.

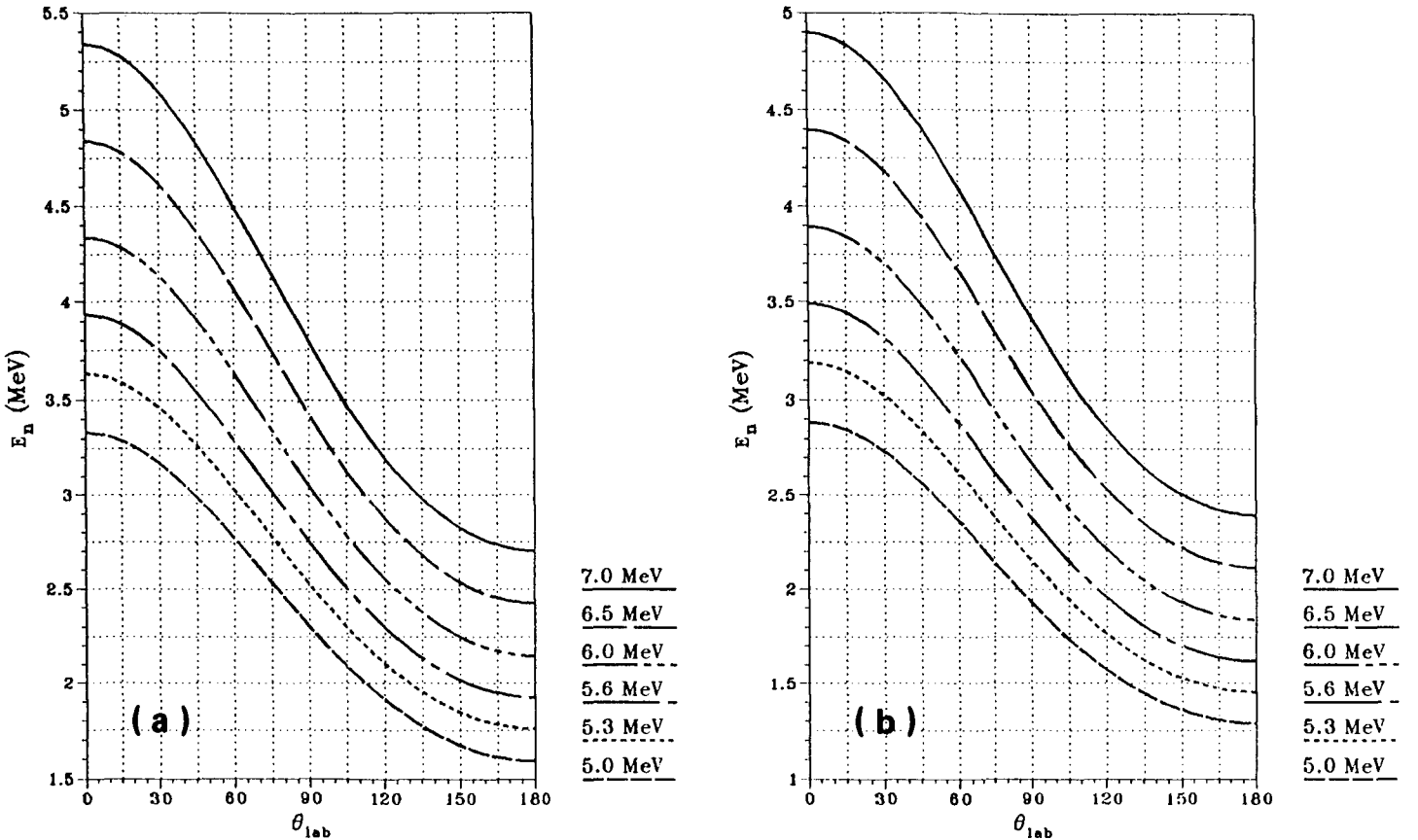

FIG. 39. Neutron energy values for the (a) $^7Li(p, n)^7Be$ and (b) $^7Li(p, n)^7Be^*$ reactions: 5.0–7.0 MeV.

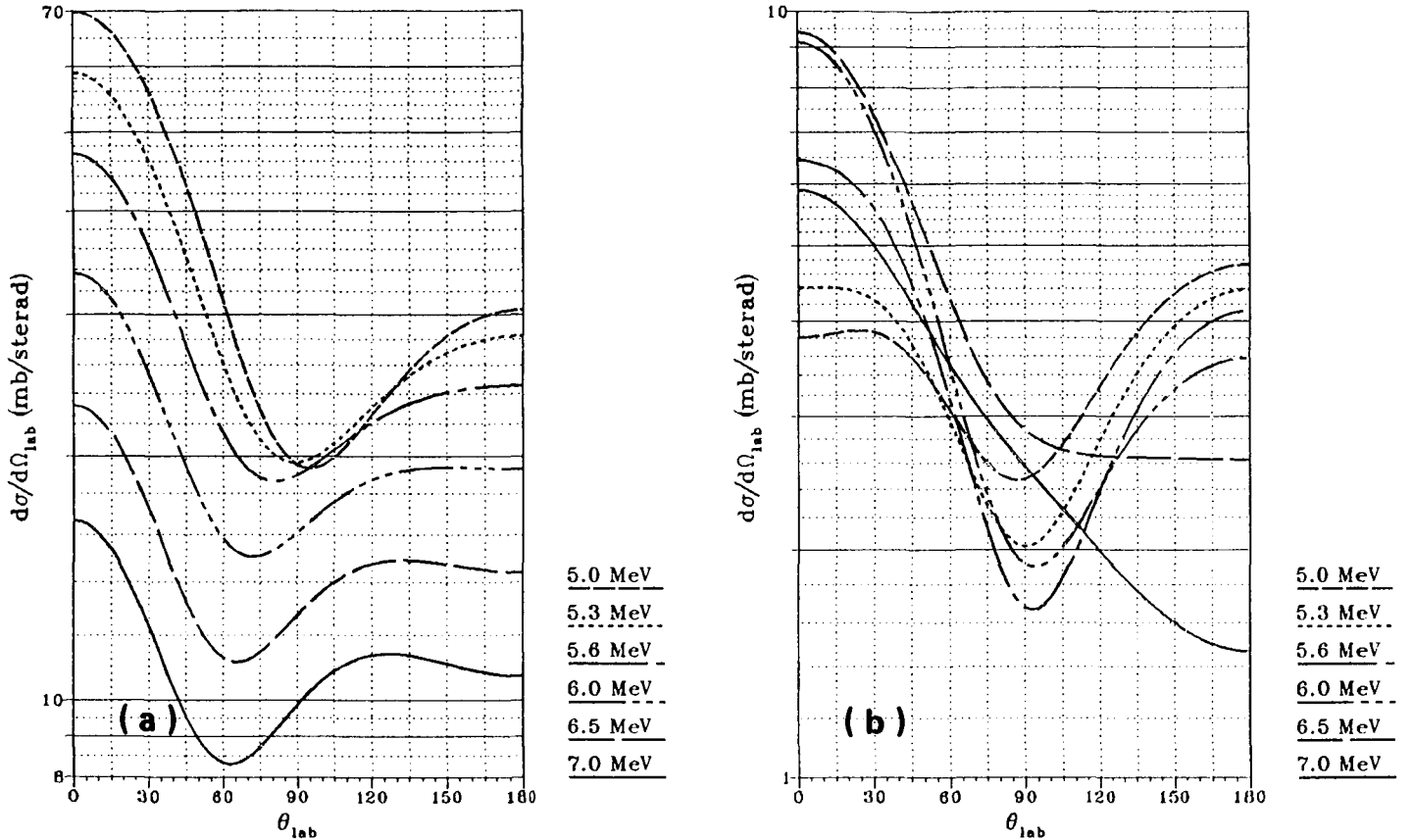

FIG. 40. Differential cross-sections of the (a) $^{7}Li(p, n)^{7}Be$ and (b) $^{7}Li(p, n)^{7}Be^{*}$ reactions: 5.0–7.0 MeV.

TABLE XIII. Q-VALUES , THRESHOLDS AND NEUTRON ENERGIES AT $0°_{lab}$ FOR ^{7}Li-H
(All energies in MeV)

Exit channel	n + ^{7}Be		n + ^{7}Be* (0.43)		n + ^{3}He + α	n + ^{7}Be** (4.57)
E_{in}	$E_{n0}(0°_{c.m.})$	$E_{n0}(180°_{c.m.})$	$E_{n1}(0°_{c.m.})$	$E_{n1}(180°_{c.m.})$	E_{nmax}	$E_{n2}(0°)$
13.095	1.439	1.439				
16.514	3.843	0.540	1.815	1.815		
25.732	8.184	0.254	7.229	0.457	2.828	
49.509	18.803	0.111	17.975	0.184	15.612	5.439
Q	−1.644		−2.073		−3.230	−6.214

THE $^{1}H(^{7}Li,n)^{7}Be$ REACTION

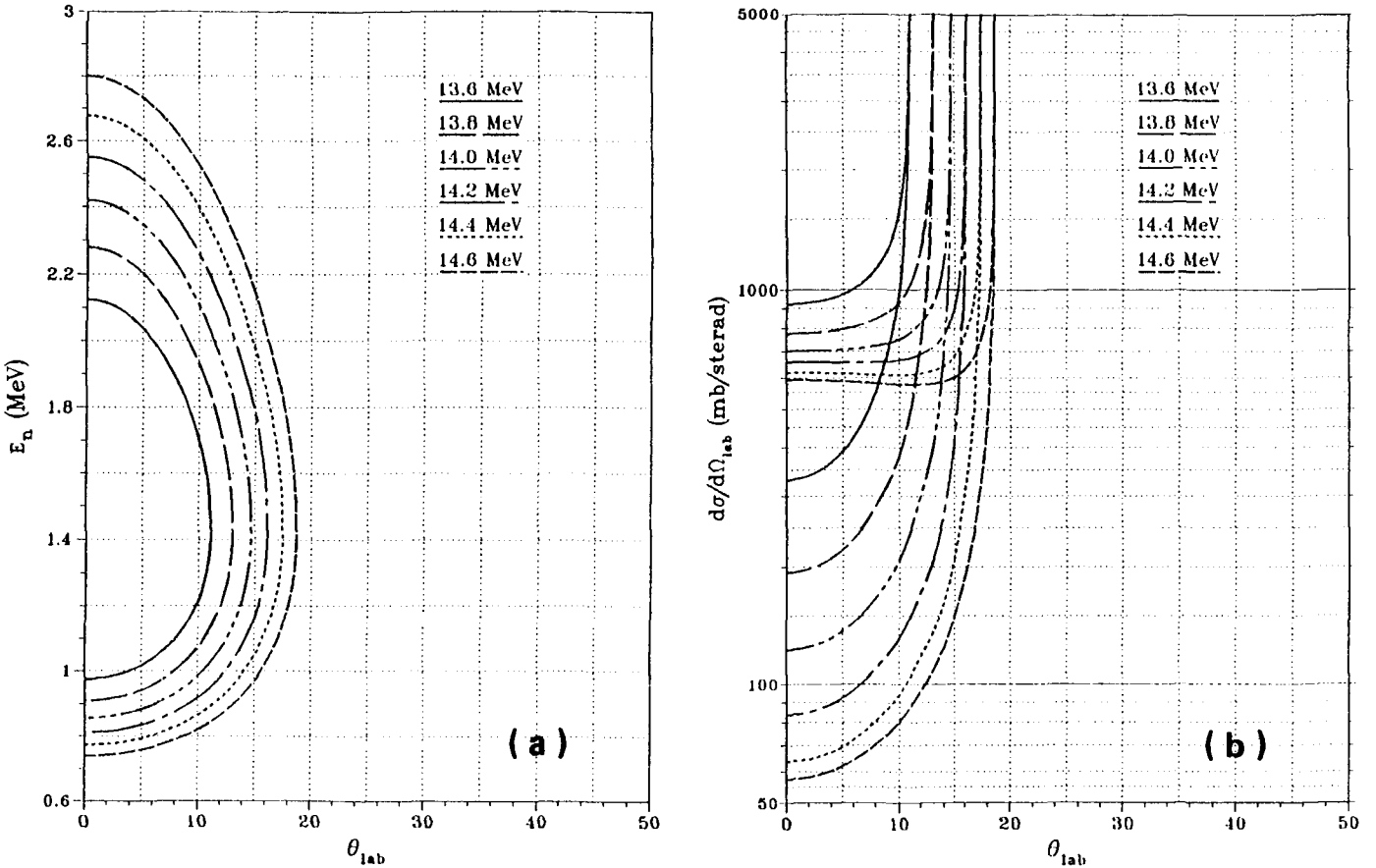

FIG. 41. (a) Neutron energy values and (b) differential cross-sections for the $^1H(^7Li, n)^7Be$ reaction: 13.6–14.6 MeV.

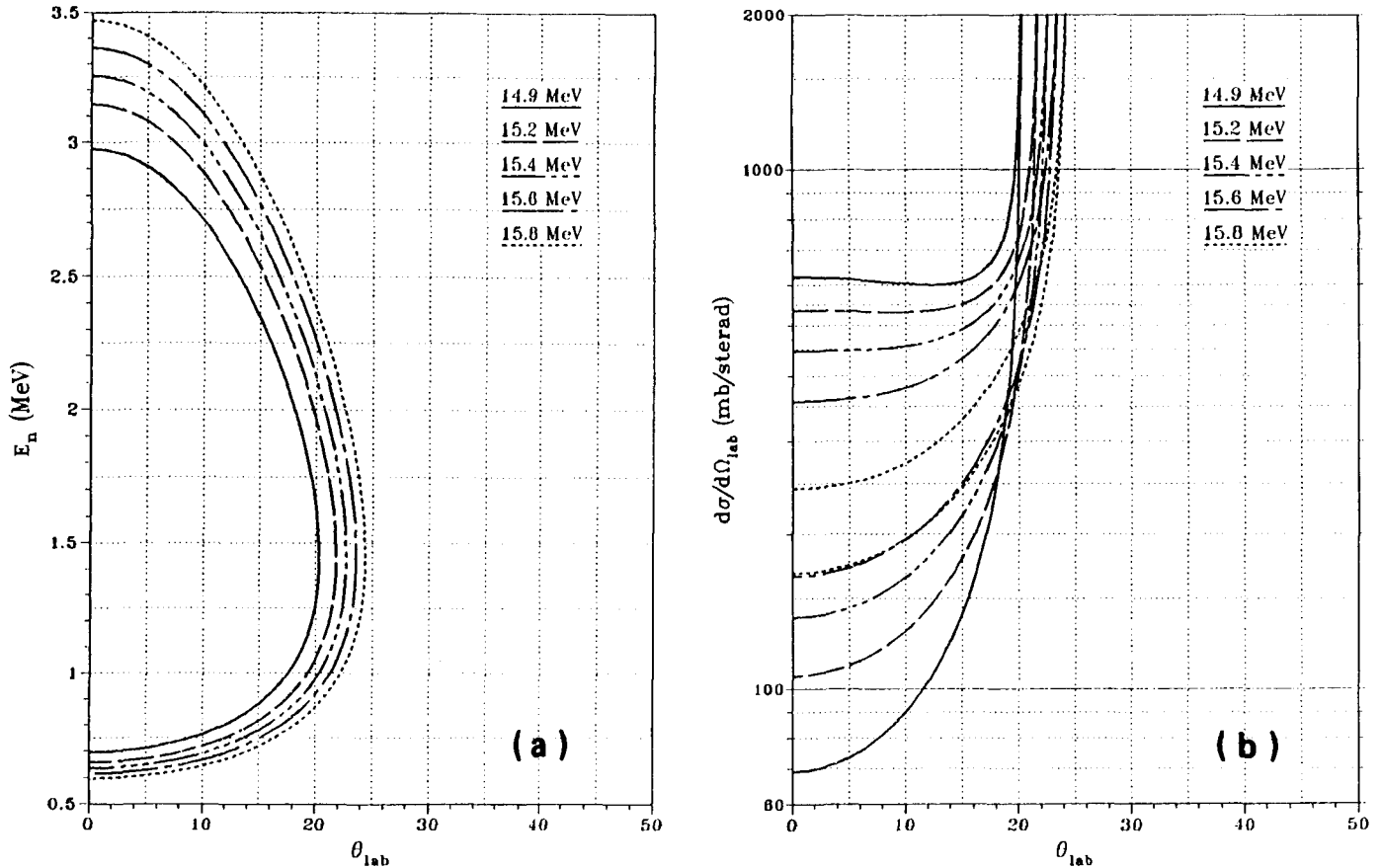

FIG. 42. (a) Neutron energy values and (b) differential cross-sections for the $^1H(^7Li, n)^7Be$ reaction: 14.9–15.8 MeV.

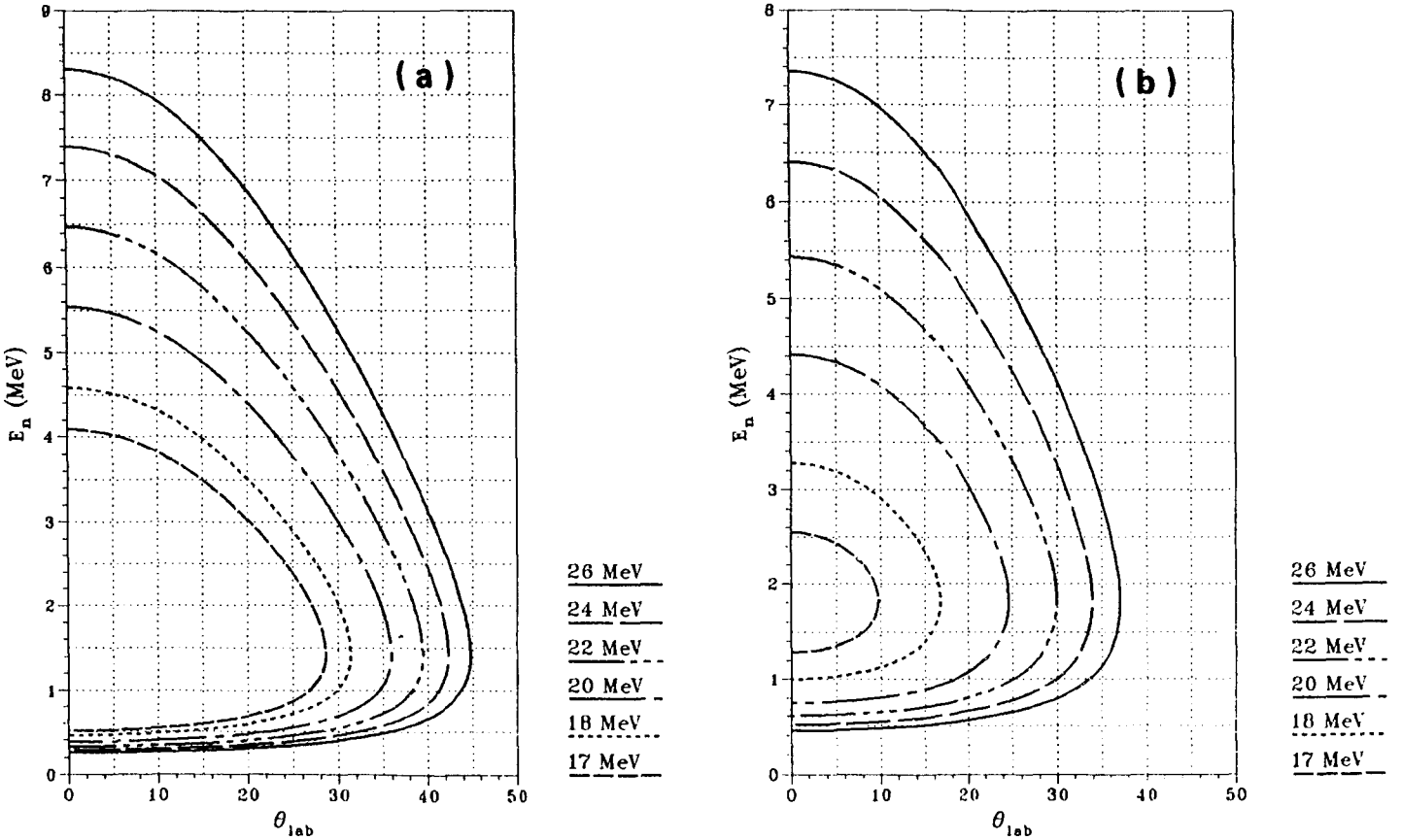

FIG. 43. Neutron energy values for the (a) $^1H(^7Li, n)^7Be$ and (b) $^1H(^7Li, n)^7Be^*$ reactions: 17–26 MeV.

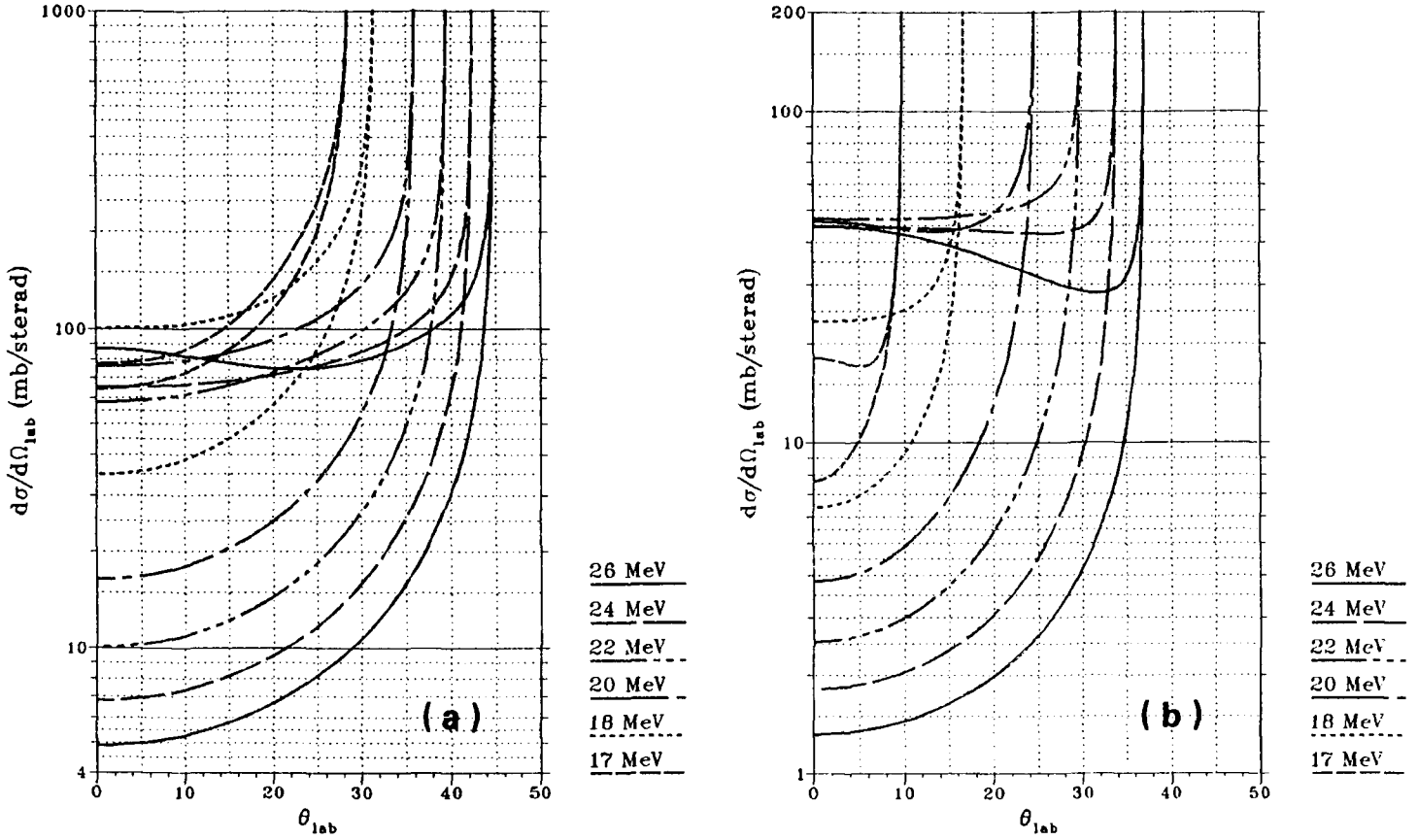

FIG. 44. Differential cross-sections of the (a) $^{1}H(^{7}Li, n)^{7}Be$ and (b) $^{1}H(^{7}Li, n)^{7}Be^{*}$ reactions: 17–26 MeV.

according to formula(2). However, the second neutron group at 0° (corresponding to 180° in c.m.) is in most cases not negligible (neither in energy nor in intensity) [30]. Nevertheless, the high yield below $E_n = 1.7$ MeV and near 0.6 MeV (from the 180° group), together with the strong forward peaking, makes it a useful source for special applications at lower neutron energies. Using double- or triple-charged ^{7}Li ions, the necessary incident energy can easily be obtained even with moderate accelerators. However, the effective beam energy must be determined very carefully because the cross-section changes rapidly with energy (at 16 MeV, a 1% change of the projectile energy changes the 0° cross-section by more than 50%) Figures 41–44 illustrate the angular dependence of the neutron energies and of the differential cross-sections.

Appendix

An interactive Fortran IV program is reproduced here for calculating neutron laboratory and c.m. angles, as well as differential cross-sections and laboratory neutron energies. Calculation of these quantities is possible at any angle and any energy within the ranges covered by the Legendre coefficients given in Tables II, V, VII, X and XI. S_0 and A_i are required as inputs from those tables.

```
      DOUBLE PRECISION WA,WB,WC,WD,OUTRE,MASS
      DIMENSION MASS(8),OUTRE(5),REAIN(10)
      DATA MASS/938.2796434D0,1875.6280461D0,2808.9437446D0,2808.4141347
     1D0,3727.4094091D0,6534.6662515D0,6533.8864536D0,6534.2372515D0/
      DATA REAIN/4H  1H,4H  2H,4H  3H,4H  P,4H  D,4H  T,4H 7LI,
     21H ,1H ,4H(7LI/NLEG/0/WC/939.5730306D0/NIT/1/DIFF/0./FC/.5/IKI/0/
      DATA OUTRE/8H,N ) 3HE,8H,N ) 4HE,8H,N )7BE*,1H ,8H,N ) 7BE/IC/0./
  100 WRITE(5,1)
    1 FORMAT(15X,' MONOENERGETIC NEUTRON PRODUCTION'/)
      WRITE(5,2)
    2 FORMAT(' LABEL REACTION BY MASS NUMBERS OF PROJECTILE AND TARGET')
      READ(5,3)MNP,MNT
    3 FORMAT(2I3)
      MNSUM=MNP+MNT
      IF (MNSUM .GT. 8) GO TO 100
      IF (MNP .GT. MNT) NLEG=1
      IF (MNSUM .NE. 8) GO TO 20
      WRITE(5,4)
    4 FORMAT(' IF BE-7 IS EXCITED, INPUT 1')
      READ(5,3)IEXC
      IF (IEXC .EQ. 1) MNSUM=6
    6 FORMAT(' LAB CROSS SECTIONS ARE DOUBLE VALUED. ACCESS TO LOW',
     3' ENERGY GROUP'/' VIA CM ANGLES')
   20 WA=MASS(MNP)
      WB=MASS(MNT)
      WD=MASS(MNSUM)
      IF (DABS(WA+WB-WC-WD) .GT. 20.D0) GO TO 100
      WRITE(5,7) REAIN(MNT),REAIN(MNP+3),OUTRE(MNSUM-3)
    7 FORMAT(10X,' NEUTRONS FROM THE REACTION',2A4,A8/)
      WRITE(1,7) REAIN(MNT),REAIN(MNP+3),OUTRE(MNSUM-3)
      IF ((WA+WB-WC-WD) .GT. 0.D0) GOTO 23
      IF (MNP .GT. MNT) WRITE(5,6)
```

```
23 WRITE(5,8)
 8 FORMAT(' PROJECTILE ENERGY OR NEGATIVE NEUTRON ENERGY AT 0 DEG',
  1' IN MEV')
   READ(5,9)YA
 9 FORMAT(F10.5)
   IF (MNT .NE. MNP) MNT=1
   IF (YA .GT. 0.) GO TO 21
   TYA=-YA
   YA=TYA-SNGL(WA+WB-WC-WD)
22 YA=ABS(YA+FC*DIFF)
   CALL RELKIN(YA,WA,WB,WC,WD,NIT,TC,MNT,NLEG,IKI)
   DIFF=TYA-TC
   IF (ABS(DIFF) .LT. 0.0002) GO TO 21
   FC=FC-0.01
   IF (FC .LT. 0.05) FC=0.05
   GO TO 22
21 NIT=0
   CALL RELKIN(YA,WA,WB,WC,WD,NIT,TC,MNT,NLEG,IKI)
   IF (IKI .EQ. 1) WRITE(1,6)
   STOP
   END
   SUBROUTINE RELKIN(YA,WA,WB,WC,WD,NIT,TC,MNT,NLEG,IKI)
   DOUBLE PRECISION PA,EA,RAD,ZC,THC,WA,WB,WC,WD,XXXC,WS,EC
   DOUBLE PRECISION YC,XCCMIA,XXC,GAMACM,BETACM,BETCCM,ECCM,PCCM,PC
   DIMENSION TABANG(181)
   DATA RAD/1.745329252D-2/ROUTE/1./TABANG(1)/0./
   EA=DBLE(YA)
   PA=DSQRT(EA**2+2.*EA*WA)
   EA=DSQRT(PA**2+WA**2)
   BETACM=PA/(EA+WB)
   GAMACM=1./DSQRT(1.-BETACM**2)
   WS=(EA+WB)/GAMACM
   IF ((WS-WD-WC) .LT. 0.) GO TO 56
   NANG=1
   IF (NIT .EQ. 1) GO TO 31
27 WRITE(5,90)
90 FORMAT(' NUMBER OF ANGLES, NEGATIVE IF C.M.')
   READ(5,66)NANG
   IF (NANG .GT. 0) ROUTE=0.
   NANG=IABS(NANG)
   IF (NANG .GT. 181) GO TO 27
   IF (NANG .LT. 1) NANG=1
   WRITE(5,91)
91 FORMAT(' ANGLES,ONE BY ONE. 1 NEGATIVE VALUE FOR CST.ANG.SPACING')
   READ(5,61)DANG
   DO 34 J=1,NANG
   IF (J .EQ. 1) GO TO 34
   IF (DANG .GE. 0.) GOTO 30
   TABANG(J)=TABANG(J-1)-DANG
   GO TO 34
30 READ(5,61)TABANG(J)
34 IF (TABANG(J) .GT. 180.) TABANG(J)=360.-TABANG(J)
   IF (DANG. GE. 0.) TABANG(1)=DANG
   WRITE(1,88) YA
   WRITE(1,84)
   EN=YA
   IF (NLEG .EQ. 1) EN=EN*WB/WA
31 ROUSA=ROUTE
   ECCM=(WS**2+WC**2-WD**2)/(2.*WS)
   PCCM=DSQRT(ECCM**2-WC**2)
   BETCCM=PCCM/ECCM
   LINES=5
   DO 53 IA=1,NANG
   THC=RAD*TABANG(IA)
   FACT=0.48
```

```
39 XCCMIA=DCOS(THC)
   YC=DSIN(THC)
   XXC=GAMACM*(XCCMIA+BETACM/BETCCM)
   IF (XXC .NE. 0.D0) GOTO 40
   ANGC=90.
   GOTO 41
40 XXXC=YC/XXC
   ANGC=SNGL(DATAN(XXXC)/RAD)
   IF (XXC .LT. 0.D0) ANGC=ANGC+180.
41 IF (ROUTE .GT. 0.) GOTO 42
   DTHAN=ANGC-TABANG(IA)
   IF (ABS(DTHAN) .LE. 0.001) GO TO 42
   FACT=FACT-0.01
   IF (FACT .LT. 0.1) FACT=0.1
   THC=THC*(1. -(DTHAN/ANGC)*FACT)
   IF (THC .LT. 3.14159265D0) GOTO 39
   IF (FACT .EQ. 0.1) THC=0.035898D-5+3.141592654D0
   IF (FACT .EQ. 0.1) ROUTE=1.
   GOTO 39
42 PC=PCCM*DSQRT(YC**2+XXC**2)
   EC=DSQRT(PC**2+WC**2)
   TC=SNGL(EC-WC)
   IF (NIT .EQ. 1) GO TO 57
   ZC=1.-XXC*PCCM*EC*BETACM/PC**2
   SOLC=SNGL(GAMACM*PCCM/PC*ZC)
   LINES=LINES+1
   IF (LINES-50) 50,47,47
47 LINES=0
   WRITE(1,88) YA
50 ANGCCM=SNGL(THC/RAD)
   ACM=ANGCCM
   IF (NLEG .EQ. 1) ACM=180.-ACM
   CALL LCAL(ACM,EN,WQCM,MNT,IA)
   SOLC=ABS(WQCM/SOLC)
   WRITE(1,85) ANGC,SOLC,TC,ANGCCM,WQCM
   ROUTE=ROUSA
   IF (ROUTE .GT. 0.) GO TO 53
   IF (ANGCCM .GT. 180.) IKI=1
   IF (IKI .EQ. 1) GO TO 57
53 CONTINUE
   GOTO 57
56 IF (NIT. NE. 1) WRITE(1,74)
   IF (NIT. NE. 1) WRITE(5,74)
57 RETURN
61 FORMAT(10F6.2)
66 FORMAT(I4)
74 FORMAT(1H0,15HBELOW THRESHOLD)
84 FORMAT(/1H ,7X,'LABORATORY SYSTEM',10X,'CENTER-OF-MASS',
  1/1H ,4X,'ANGLE',5X,'CROSS',4X,'ENERGY',5X,'ANGLE',
  3   5X,'CROSS', /1H ,13X,'SECTION',23X,'SECTION')
85 FORMAT(1H ,F10.2,2F10.3,F10.2,F10.3)
88 FORMAT ('0INCIDENT LAB ENERGY',F9.3)
   END
    SUBROUTINE LCAL(ANGCCM,ENIN,WQCM,MNT,IA)
    DIMENSION P(64)
    DATA P/64*0./N/0/IP/0/
    IF (IA .NE. 1) GOTO 12
    WRITE(5,48) ENIN
48  FORMAT(' USE ',F6.3,' MEV IN LEGENDRE TABLE')
10  SUM=0.
    WRITE(5,50)
    READ(5,3) P(32+N)
    WRITE(5,49)
49  FORMAT(' HIGHEST ORDER OF LEGENDRE COEFFICIENTS')
    READ(5,2)IP1
 2  FORMAT(I3)
    IP1=IP1+1
```

```
50  FORMAT(' PROJECTILE ENERGY FROM TABLE IN MEV')
    WRITE(5,99)
99  FORMAT(' SIGMA-0'  )
    READ(5,3)SKF
    WRITE(5,5)
 5  FORMAT(' INPUT OF (REDUCED) PARAMETERS, ONE BY ONE')
    IF (MNT .NE. 2) MNT=1
    IF (MNT .EQ. 2) WRITE(5,4)
 4  FORMAT(' SYMMETRIC IN C.M., INPUT OF EVEN PARAMETERS ONLY')
    DO 11 I=1,IP1,MNT
    READ(5,3) P(I+N)
    P(I+N)=SKF*P(I+N)
11  SUM=SUM+P(I+N)
    IF (ABS(SUM/SKF - 1.) .GT. 0.002) WRITE(5,51)
51  FORMAT(' CAUTION: CHECK LEGENDRE COEFFICIENTS')
 3  FORMAT(F10.5)
    IF (IP1 .GT. IP) IP=IP1
    IF (ABS(ENIN-P(32)) .LT. 0.005) GO TO 12
    IF (N .EQ. 32) GOTO 13
    N=32
    WRITE(5,6)
 6  FORMAT(  ' ADDITIONAL LEGENDRE DATA SET FOR INTERPOLATION'/)
    GO TO 10
13  FACT=(ENIN-P(32))/(P(64)-P(32))
    DO 1 I=1,IP
 1  P(I)=P(I)+FACT*(P(I+32)-P(I))
12  WQCM=0.
    XA=1.
    XM=COS(ANGCCM*3.141593/180.)
    T=XM+XM
    DO 87 J=1,IP,MNT
    XJE=J+1
    XJ=XJE-1.
    XLEG=XA
    XE=(XJ/XJE)*(T*XM*((XJ+XJE)/(XJ+XJ))-XA)
    XA=XM
    XM=XE
87  WQCM=WQCM+P(J)*XLEG
    RETURN
    END
```

ACKNOWLEDGEMENTS

Thanks are due to our colleagues, D.E. Cullen of the Nuclear Data Section, IAEA, and G. Winkler of the Institut für Radiumforschung und Kernphysik, Vienna, for helpful discussions and criticisms, to J.J. Smith of the IAEA Computer Section for his help in implementing the graphics software and to H. Wurz for her efforts with the manuscript.

REFERENCES

[1] Fast Neutron Physics (MARION, J.B., FOWLER, J.L., Eds), Interscience, New York (1960).

[2] DROSG, M., "Properties of monoenergetic neutron sources from proton reactions with nuclei other than tritons", Neutron Source Properties (Proc. Consultants Meeting Debrecen, Hungary, 1980) (OKAMOTO, K., Ed.), IAEA/International Nuclear Data Committee, Vienna, Rep. INDC (NDS)-114/GT (1980) 241–264.

[3] UTTLEY, C.A., "Sources of monoenergetic neutrons", Neutron Sources for Basic Physics and Applications (CIERJACKS, S., Ed.), Pergamon Press, Oxford (1983) 19.

[4] DROSG, M., Nucl. Sci. Eng. 67 (1978) 190.
[5] DROSG, M., "Production of fast monoenergetic neutrons by charged particle reactions among the hydrogen isotopes. Source properties, experimental techniques and limitations of the data", Neutron Source Properties (Proc. Consultants Meeting, Debrecen, Hungary, 1980) (OKAMOTO, K., Ed.), IAEA/International Nuclear Data Committee, Vienna Rep. INDC (NDS)-114/GT (1980) 201–240.
[6] DROSG, M., Z. Phys. **A300** (1981) 315.
[7] DROSG, M., "Production of fast neutrons with targets of the hydrogen isotopes. Source properties and evaluation status of the cross-sections", Neutron Source Properties (Proc. Advisory Group Meeting Leningrad, 1986) (OKAMOTO, K., Ed.), IAEA-TECDOC-410, IAEA, Vienna (1987).
[8] DROSG, M., HAOUAT, G., STOEFFEL, W., DRAKE, D.M., Los Alamos National Lab., NM, Rep. LA-10444-MS (1985).
Germany, 1984.
[9] LISKIEN, H., PAULSEN, A., Nucl. Data Tables **11** (1973) 569.
[10] LISKIEN, H., PAULSEN, A., At. Data Nucl. Data Tables **15** (1975) 57.
[11] KLEIN, H., BREDA, H.J., SIEBERT, B.R.L., Nucl. Instrum. Methods Phys. Res. **193** (1982) 635.
[12] MARTIN, J.T., SMITH, R.K., Los Alamos Scientific Lab., NM, Rep. LA-6237-MS (1976).
[13] MITTAG, S., PILZ, W., SCHMIDT, D., SEELIGER, D., STREIL, T., Kernenergie 22 (1979) 237.
[14] DROSG, M., AUCHAMPAUGH, G.F., Nucl. Instrum. Methods **140** (1977) 515.
[15] DROSG, M., AUCHAMPAUGH, G.F., GURULE, F., Los Alamos Scientific Laboratory, NM, Rep. LA-6459-MS (1976).
[16] WAPSTRA, A.H., BOS, K., At. Data Nucl. Data Tables **19** (1977) 177.
[17] DROSG, M., VESELY, F., HAOUAT, G., DRAKE, D.M., Verh. Dtsch. Phys. Ges. **19** (1984) 922.
[18] DROSG, M., et al., Phys. Rev. C **9** (1974) 179.
[19] THAMBIDURAI, P., BEYERLE, A.G., GOULD, C.R., Nucl. Instrum. Methods Phys. Res. **196** (1982) 415.
[20] JARMIE, N., BROWN, R.E., Nucl. Instrum. Methods Phys. Res. **B10/11** (1985) 405.
[21] GRABMAYR, P., RAPAPORT, J., FINLAY, R.W., KULKARNI, V., GRIMES, S.M., in Nuclear Cross Sections for Technology (Proc. Int. Conf. Knoxville, TN, 1979), US National Bureau of Standards Special Publication 594, US Government Printing Office, Washington, DC (1980) 542.
[22] SMITH, D.L., MEADOWS, J.W., Argonne National Lab., IL, Rep. ANL/NDM-9 (1974).
[23] MEADOWS, J.W., SMITH, D.L., Argonne National Lab., IL, Rep. ANL/NDM-53 (1980).
[24] JARMIE, N., BROWN, R.E., HARDEKOPF, R.A., Phys. Rev. C **29** (1984) 2031.
[25] CSIKAI, J., "Production of 14 MeV neutrons by low voltage accelerators", Neutron Source Properties (Proc. Consultants Meeting Debrecen, Hungary, 1980) (OKAMOTO, K., Ed.), IAEA/International Nuclear Data Committee, Vienna, Rep. INDC (NDS)-114/GT (1980) 265–291.
[26] BARSCHALL, H.H., "14 MeV D-T sources", Neutron Sources for Basic Physics and Applications (CIERJACKS, S., Ed.), Pergamon Press, Oxford (1983) 57.
[27] DAVE, J.H., GOULD, C.R., WENDER, S.A., SHAFROTH, S.M., Nucl. Instrum. Methods Phys. Res. **200** (1982) 285.
[28] MEADOWS, J.W., SMITH, D.L., Argonne National Lab., IL, Rep. ANL-7938 (1972).
[29] MEADOWS, J.W., Argonne National Lab., IL, Rep. ANL/NDM-25 (1977).
[30] DROSG, M., Los Alamos Scientific Lab., NM, Rep. LA-8842-MS (1981).

Neutron Source Standards

1–4. THE NEUTRON SPECTRUM OF SPONTANEOUS FISSION OF CALIFORNIUM-252

W. MANNHART
Physikalisch-Technische Bundesanstalt,
Braunschweig,
Federal Republic of Germany

Abstract

THE NEUTRON SPECTRUM OF SPONTANEOUS FISSION OF CALIFORNIUM-252.

The spectral distribution of the ^{252}Cf neutron spectrum, together with a complete covariance uncertainty matrix, has been evaluated on the basis of least squares principles. The least squares adjustment was based on experimental data on spectrum averaged neutron cross-sections. The result can be regarded as one of the first steps towards future evaluations and further experiments. This result is compared with recent data from time of flight experiments and with the data of nuclear evaporation theory models.

1. INTRODUCTION

The ^{252}Cf neutron field is one of the few which can be realized with only minor perturbations of the neutron spectrum. This fact, and its similarity to the technically important neutron field of neutron-induced fission in ^{235}U, is the reason for the importance of the ^{252}Cf field in reactor dosimetry and for surveillance purposes. Its usefulness also extends to other applications, such as the calibration of neutron detectors. The result has been a recommendation to treat the ^{252}Cf neutron spectrum as a standard [1]. However, the shape of this spectrum has yet to be unambiguously defined, since the data from spectrum measurements are contradictory even if some convergence of the results has been recently observed. While the situation has been reviewed periodically, and recommendations have been made regarding the shape of the neutron spectrum [2, 3], an improvement in the situation has only been detected since 1982 [4]. Recent experiments, using more refined techniques, have given increasingly precise results and have diminished the divergence of the data.

In this context, it was considered of interest to use these data for a new evaluation of the ^{252}Cf neutron spectrum [3]. There has also been great demand for a covariance matrix of the spectrum in order to allow correct propagation of the spectrum uncertainties to the integral parameters determined in reactor

dosimetry [5]. As discussed in this chapter, there is at present only a very limited quantity of data that meets the requirements for use in an evaluation of the neutron spectrum with a complete covariance matrix. It is planned to expand this evaluation in future work and to include other experiments as soon as the covariances of these data are available. However, this work does not represent all of the information available on the ^{252}Cf neutron spectrum; it should be regarded instead as the first version of future evaluations.

2. STATUS OF DATA FOR THE NEUTRON SPECTRUM

A complete review of the experiments up to 1979 is given in Ref. [2]. Over the last five years, much additional effort has been concentrated on carrying out new experiments [6–15] aimed at resolving discrepancies in the data of the spectrum, found mainly at low (<1 MeV) and at high (>6 MeV) neutron energies. The data available now cover the neutron energy range between 1 keV and 28 MeV. Most of the recent experiments have been of a preliminary nature, i.e. the final analyses have not been completed owing to corrections that require additional investigation. For these, and all other experiments, detailed uncertainty analyses, indispensable in an updated evaluation, are outstanding. It is known from experience that a reanalysis of older experiments aimed at obtaining sufficient details of the uncertainty components is a hopeless task; this makes reanalysis of recent experiments all the more necessary, while memory of the experimental details is still fresh.

In addition to high resolution time of flight experiments, there is another group of experiments which must be regarded as 'broad' resolution experiments. These experiments, of spectrum averaged cross-section measurements of threshold and non-threshold neutron reactions, cover various energy ranges in the ^{252}Cf neutron spectrum between the limits of a few keV and about 18 MeV. The data can be determined with a high level of precision, with relative uncertainties of 2–3%. A review of all available data is given in Part 2–4. Furthermore, analyses of the uncertainties resulting from experiments carried out since 1979, as well as the covariances generated, are given in Ref. [16]. Based on this information, data from the various experiments have been combined by least squares techniques (see Part 2–4). This means that the results of spectrum averaged neutron cross-section measurements are at present the only data set with a complete covariance matrix containing the full uncertainty information required for evaluations based on the least squares principle.

It should also be mentioned that some progress has recently been made in theoretical calculations of the ^{252}Cf neutron spectrum [14, 17–19]. Based on nuclear evaporation theories, results have been obtained which are in good agreement with the experimental data. However, sometimes physical parameters of the theories which are not sufficiently well known must be adjusted by using experimental results.

3. EVALUATION OF THE NEUTRON SPECTRUM BY LEAST SQUARES METHODS

The aim of an evaluation must be to obtain results which are based as far as possible on objective facts and to avoid subjectivity. This requires consistent attention to all data uncertainties involved in the evaluation process. The only method which meets this requirement is a generalized least squares method. The urgent need of reactor technology to specify results with appropriate uncertainties [20] has led to the use of such methods. A variety of computer codes for these purposes have recently become available, e.g. STAY'SL [21, 22], FERRET [23] and others. All of these evaluation methods are based on the least squares principle and combine prior information and experimental data, with full regard to their uncertainties, with the objective of obtaining results with a maximum likelihood.

The application of this method to the present problem of evaluating the ^{252}Cf neutron spectrum has already been described in detail [24]. Only a few essential points of the procedure are repeated here, the main emphasis being on the data used in this evaluation.

3.1. Principles of the least squares adjustment

Experimental reaction rates a_i^0 of various neutron detectors i, measured in the ^{252}Cf neutron field, are compared with calculations a_i based on energy dependent cross-sections and the ^{252}Cf neutron spectrum. Minimization of the χ^2 gives a minimum value of

$$\chi^2_{min} = \sum_i \sum_j (a_i^0 - a_i) w_{ij} (a_j^0 - a_j) \qquad (1)$$

The elements w_{ij} are the components of the weight matrix of the problem explained below. In the present case, the experimental reaction rates are normalized by the neutron flux density, i.e. they are spectrum averaged neutron cross-sections:

$$a_i^0 \equiv \langle \sigma \rangle_i^{exp} \qquad (2)$$

The corresponding calculated quantities are

$$a_i \equiv \langle \sigma \rangle_i^{calc} = \int_0^\infty \sigma^i(E) \chi(E) dE \qquad (3)$$

The integral of Eq. (3) contains the energy dependent cross-section of the neutron reaction i and the normalized spectral flux density distribution of ^{252}Cf, with

$$\int_0^\infty \chi(E)dE = 1 \tag{4}$$

Both of these quantities are parameters of the problem and can be formally written as a parameter vector P with an absolute covariance matrix $\underline{N}_P$, i.e.

$$P = \begin{pmatrix} \chi \\ \Sigma \end{pmatrix} \quad \text{and} \quad \underline{N}_P = \begin{pmatrix} \underline{N}_\chi & 0 \\ 0 & \underline{N}_\Sigma \end{pmatrix} \tag{5}$$

χ being the vector of the spectral distribution and Σ the vector of the full set of energy dependent cross-sections involved in the problem.

The evaluation results in a new vector P′ and a corresponding matrix $\underline{N}'_P$, which fulfils the minimum condition of Eq. (1). P is often called the problem's 'prior information'. P′ is then the most likely adjusted value with regard to the prior information and $\underline{N}'_P$ is the resulting uncertainty covariance matrix with reduced uncertainties as a result of taking into account the experimental information in Eq. (2). From Eq. (5), it is clear that the spectral distribution, as well as the energy dependent cross-section data, were adjusted, i.e. the zero correlation of $\underline{N}_P$ in Eq. (5) vanishes for $\underline{N}'_P$. The result of the adjusted neutron spectrum χ' and its covariance matrix $\underline{N}'_\chi$ is derived from P′ and $\underline{N}'_P$. The weight matrix of Eq. (1) contains the uncertainties of the experimental data of Eq. (2), as well as the uncertainties of the calculated data of Eq. (3). The matrix is thus an inverse:

$$\left(\underline{N}_{A^0} + \underline{N}_A\right)^{-1} \tag{6}$$

$\underline{N}_A$ contains the covariance matrices $\underline{N}_\chi$ and $\underline{N}_\Sigma$ transformed to the calculated values (see Eqs (7) and (10) of Ref. [24]).

3.2. Data on spectrum averaged neutron cross-sections

These data, based on various experiments, have been pre-processed (see Part 2–4). In all, the data from 25 different neutron reactions were used. The reactions and the numerical values of the spectrum averaged cross-sections are listed in columns 1 and 2 of Table I. The covariance matrix is shown in the form of relative standard deviations in column 3 of the table and a correlation

TABLE I. SPECTRUM AVERAGED DATA USED IN THE LEAST SQUARES EVALUATION

Reaction	$\langle\sigma\rangle^{exp}$ (b)	Relative standard deviation[a] (%)	$\langle\sigma\rangle^{calc}$ (b)	Exp/calc	χ^2_{part}
F-19(n,2n)	1.628E-5	3.33	1.628E-5	1.000	0.00
Mg-24(n,p)	2.005E-3	2.39	2.160E-3	0.928	2.62
Al-27(n,p)	4.892E-3	2.16	5.140E-3	0.952	0.61
Al-27(n,α)	1.021E-3	1.42	1.013E-3	1.008	0.10
Ti-46(n,p)	1.420E-2	1.68	1.347E-2	1.054	0.16
Ti-48(n,p)	4.275E-4	1.81	4.096E-4	1.044	0.17
Mn-55(n,2n)	4.079E-4	2.26	4.462E-4	0.914	0.47
Fe-54(n,p)	8.729E-4	1.29	8.823E-2	0.989	0.17
Fe-56(n,p)	1.471E-3	1.73	1.415E-3	1.039	0.66
Ni-58(n,p)	1.176E-1	1.25	1.138E-1	1.034	0.19
Ni-58(n,2n)	8.965E-6	3.32	8.471E-6	1.058	0.72
Co-59(n,α)	2.221E-4	1.78	2.164E-4	1.027	0.32
Co-59(n,2n)	4.058E-4	2.49	4.107E-4	0.988	0.02
Cu-63(n,γ)	1.055E-2	3.08	9.772E-3	1.080	0.37
Cu-63(n,α)	6.897E-4	1.88	6.767E-4	1.019	0.08
Cu-63(n,2n)	1.866E-4	3.82	1.982E-4	0.941	2.96
Zn-64(n,p)	4.047E-2	1.85	3.922E-2	1.032	0.13
Zr-90(n,2n)	2.211E-4	2.78	2.058E-4	1.075	3.73
In-115(n,γ)	1.261E-1	2.19	1.222E-1	1.032	0.47
In-115(n,n')	1.981E-1	1.31	1.819E-1	1.089	0.52
Au-197(n,γ)	7.711E-2	1.54	7.720E-2	0.999	0.00
U-235(n,f)	1.210E+0	1.19	1.238E+0	0.978	1.89
Np-237(n,f)	1.356E+0	1.65	1.353E+0	1.003	0.00
U-238(n,f)	3.234E-1	1.72	3.134E-1	1.032	2.89
Pu-239(n,f)	1.811E+0	1.37	1.792E+0	1.010	0.05

[a] Correlation matrix in Table II.

matrix is given in Table II. The data are least squares averages (see Part 2–4) of diverse experiments and it can be seen from Table I that for 15 reactions the relative uncertainties are smaller than 2%.

3.3. Prior information on the neutron spectrum

Slightly modified data of a United States National Bureau of Standards (NBS) evaluation of the ^{252}Cf neutron spectrum were used as the source of prior

TABLE II. CORRELATION MATRIX OF THE EXPERIMENTAL SPECTRUM AVERAGED NEUTRON CROSS-SECTIONS

	Correlation matrix (x 100)																							
F-19(n,2n)	100																							
Mg-24(n,p)	15	100																						
Al-27(n,p)	8	27	100																					
Al-27(n,α)	26	54	44	100																				
Ti-46(n,p)	23	33	33	57	100																			
Ti-48(n,p)	21	30	33	50	64	100																		
Mn-55(n,2n)	43	23	25	40	34	30	100																	
Fe-54(n,p)	31	39	40	65	55	50	46	100																
Fe-56(n,p)	21	35	34	57	46	42	32	56	100															
Ni-58(n,p)	36	43	44	73	63	56	53	85	59	100														
Ni-58(n,2n)	28	15	13	26	22	20	40	30	21	35	100													
Co-59(n,α)	36	28	39	49	42	37	58	56	39	66	34	100												
Co-59(n,2n)	39	20	22	36	31	28	60	42	29	49	36	50	100											
Cu-63(n,γ)	17	18	49	29	23	23	21	28	23	30	11	23	19	100										
Cu-63(n,α)	24	25	29	42	35	32	36	50	34	57	29	50	32	16	100									
Cu-63(n,2n)	24	14	43	23	18	18	30	22	18	24	17	25	28	36	15	100								
Zn-64(n,p)	19	32	33	55	44	39	29	50	43	54	19	37	27	22	31	18	100							
Zr-90(n,2n)	35	19	19	32	27	25	50	37	26	43	38	41	45	16	30	25	24	100						
In-115(n,γ)	16	25	31	41	33	33	23	39	34	43	16	29	21	22	26	17	31	19	100					
In-115(n,n')	26	40	54	64	52	55	38	63	53	69	26	46	34	39	44	31	48	31	53	100				
Au-197(n,γ)	23	35	44	59	48	45	33	56	47	61	22	41	30	31	38	25	45	27	54	75	100			
U-235(n,f)	13	17	19	27	23	22	19	35	23	35	13	24	17	13	23	11	21	16	19	32	27	100		
Np-237(n,f)	9	12	14	20	16	16	14	25	17	25	9	17	13	10	17	8	15	11	13	23	19	67	100	
U-238(n,f)	8	10	12	17	14	13	12	22	14	22	8	15	11	8	15	7	13	10	12	20	17	78	67	100
Pu-239(n,f)	11	14	16	23	19	18	16	30	20	30	11	20	15	11	20	9	18	13	16	28	23	79	66	67	100

information [25]. The NBS evaluation covered spectrum measurements up to 1974 and parametrized the spectral distribution by a Maxwellian of kT = 1.42 MeV [26]. The deviations of the data from the Maxwellian were taken into account by five energy dependent, segment correction functions fitted to the data. The result was:

$$\chi(E) = 0.6672\sqrt{E}\exp(-E/1.42)f(E) \qquad (E \text{ in MeV}) \qquad (7)$$

The correction functions f(E) were linear below 6 MeV and exponential above this. The NBS evaluation showed some structure below 0.8 MeV, which is not confirmed by recent spectrum measurements. The data of Lajtai et al. between 25 keV and 1.2 MeV show no deviations from a Maxwellian with kT = 1.42 MeV [15]. This is also confirmed by the data of Blinov et al. taken between 1 keV and 1 MeV [8]. The recent data of Batenkov et al. show that between 10 keV and 5-6 MeV, no essential deviations from the Maxwellian can be identified [14]. Above 6 MeV, the NBS evaluation states a deficit of neutrons compared with the Maxwellian. This fact has been confirmed by spectrum averaged cross-section measurements of high threshold reactions [27] and also, recently, by direct spectrum measurements [13]. However, other data exist which contradict these measurements [6].

Taking all these facts as a basis, it was decided to represent the spectral distribution by a pure Maxwellian between 0 and 6 MeV and omit the segments of the NBS evaluation in this energy range, but include the segment of the NBS evaluation above 6 MeV. After renormalization, the following form was obtained:

$$\chi(E) = 0.6680\sqrt{E}\exp(-E/1.42)g(E) \qquad (8)$$

with

$$g(E) = \begin{cases} 1 & \text{for } 0 \leqslant E \leqslant 6 \text{ MeV} \\ \exp[-0.03(E-6)] & \text{for } 6 \leqslant E \leqslant 20 \text{ MeV} \end{cases} \qquad (9)$$

Equation (8) assumes that up to 6 MeV, a Maxwellian of kT = 1.42 MeV with a scaling factor of 1.002 is valid and that the spectrum above 6 MeV is described by another Maxwellian of kT = 1.362 MeV with a scaling factor of 1.126. It is well known that the Maxwellian is only a rough approach to describe the fission spectrum in the laboratory system. On the other hand, it is adequate and convenient for the present purposes.

In all, 30 group averages of Eq. (8) were formed and used in the evaluation. The energy bins were 0.5 MeV between 0 and 10 MeV and 1 MeV between 10 and 20 MeV. With these averages $\overline{\chi}$, Eq. (4) must be rewritten as

$$\sum_{i=1}^{30} \overline{\chi_i} = 1 \qquad (10)$$

TABLE III. RELATIVE STANDARD DEVIATIONS FROM THE NBS EVALUATION AS DETERMINED FROM THE SCATTER OF THE EXPERIMENTAL DATA

Energy range (MeV)	Relative standard deviations (%)
0 - 0.25	13.0
0.25 - 0.8	1.1
0.8 - 1.5	1.8
1.5 - 2.3	1.0
2.3 - 3.7	2.0
3.7 - 6.0	2.1
6.0 - 8.0	2.1
8.0 - 12.0	8.5
12.0 - 20.0	15.0[a]

[a] This value is based on an estimate by the author.

The NBS evaluation gave relative standard deviations (1σ level) in various energy ranges. These are given in Table III. The data contained in this table were used in the generation of the covariance matrix of the neutron spectrum. The relative uncertainties of the data in the table are very similar to those obtained by attributing a 2% uncertainty to the kT = 1.42 MeV of a Maxwellian [28]. However, taking into account the Maxwellian shape of Eq. (8) would result in full correlations between all of the data in Table III in the case of a non-normalized spectrum, or full correlations and anticorrelations for a normalized spectrum. These rigid conclusions hamper any adjustment procedure in obtaining sufficiently detailed results, as they indicate a pure shape adjustment (by a scale factor) of the spectrum over the whole energy range in the non-normalized case (for a normalized spectrum the shape adjustment factor runs in opposite directions below and above the average energy of the Maxwellian). The implicit inclusion of the Maxwellian shape in the covariance matrix was therefore avoided.

After the generation of a union group structure [24] containing the energy delimiters of the data in Table III, as well as those of the groups of Eq. (10), all diagonal elements of the union group matrix were filled with the corresponding uncertainties of the data in Table III, which meant that these uncertainties were regarded as belonging to a non-normalized spectrum. All data between one of

the energy ranges in Table III were assumed to be equally correlated by 75%. No correlations between the different energy ranges were used. A correlation coefficient of 1.00 for one of the energy ranges in Table III would mean that the whole range would be adjusted by the same factor, whereas a correlation coefficient of 0.50 would surely underestimate the Maxwellian-type structure in the range. A correlation coefficient of 0.75 was therefore chosen. This procedure is a compromise which takes account of the lack of detailed information. It avoids fixing the adjustment procedure on a Maxwellian shape, but it takes into account the fact that the data of a segment of the NBS evaluation must at least be correlated owing to the fitting functions.

The union group matrix was then collapsed to the final group structure of the evaluation. Up to this point, it was not taken into account that the neutron spectrum can be normalized according to Eqs (4) and (10). However, this was now done by a transformation of the matrix from the non-normalized to the normalized case, as shown in Eqs (17) and (18) of Ref. [24]. The adjustment of the neutron spectrum in a certain energy group can now be compensated for in other groups with a full conservation of the normalization. This is automatically taken into account owing to the special structure of the *absolute* covariance matrix of the normalized spectral distribution, with the sum over each row and over each column of the matrix being equal to zero.

3.4. Energy dependent cross-section data

Most of the cross-sections of the reactions listed in Table I were taken from the Evaluated Neutron Data File/B-V (ENDF/B-V). For the ^{24}Mg(n,p), ^{64}Zn(n,p), ^{90}Zr(n,2n) and ^{63}Cu(n,2n) reactions, the data are taken from Ref. [29], while Ref. [30] is the source for ^{19}F(n,2n). The ENDF/B-V data on the ^{27}Al(n,α), ^{63}Cu(n,α) and ^{58}Ni(n,2n) reactions have been replaced with more recent data. For ^{27}Al(n,α), the data are from Ref. [31], for ^{63}Cu(n,α) from Ref. [32] and for ^{58}Ni(n,2n) from Refs [33] and [34].

The original point-wise data on the energy dependent cross-sections are transformed to group cross-sections according to the structure of Eq. (10). The data are then weighted with the spectral distributions of Eqs (8) and (9), resulting in an exact identity of the integral of Eq. (3) with the sum over the group constants of the cross-sections $\bar{\sigma}$ and of the spectral distribution $\bar{\chi}$, with

$$\int_0^\infty \sigma^i(E)\chi(E)dE \equiv \sum_{j=1}^{30} \bar{\sigma}_j^i \bar{\chi}_j \qquad (11)$$

Thus the usual problem of the group sums forming the integral only in a first approximation is avoided. The covariance matrices of the energy dependent

cross-sections have been taken from the literature (i.e. from ENDF/B-V and from references already mentioned). These matrices, showing their own group structures, have been transformed to the group structure of the present problem according to the rules given in detail in Refs [24] and [35].

For the neutron reactions considered here, the ENDF/B-V covariance file shows a cross-correlation only between the ^{235}U(n,f) and ^{239}Pu(n,f) reactions. For all other reactions, no cross correlations were stated. It is well known that this is far removed from experimental reality (see, for example, Refs [36–38]). However, owing to the lack of data, the covariance matrix of the whole set of energy dependent cross-sections generated here shows no such cross correlations. Consequently, the ^{235}U(n,f) to ^{239}Pu(n,f) correlations have been neglected as a result of the consistency between the other reactions, i.e. the present covariance matrix contains only correlations between data belonging to the same reaction.

4. RESULTS OF THE EVALUATION OF THE SPECTRAL DISTRIBUTION

Before the least squares adjustment was performed, the minimum value of χ^2 in Eq. (1) was calculated. This quantity is a measure of the consistency of the experimental data (Section 3.2) with the prior information on the spectral distribution and on the energy dependent cross-section data used. This consistency test takes the uncertainties of all these data fully into account. An evaluation can only be justified when this consistency test is positive.

With the present data a minimum χ^2 of 19.3 was obtained, which should be considered at 25 degrees of freedom. The result indicates that an adequate consistency was given. The calculated spectrum averaged cross-sections of Eq. (1) are shown in column 4 of Table I. In addition, the ratio of the experiment to the calculation that was formed is given in column 5 of that table. In the last column of the table, the partial components χ^2_{part} of the minimum χ^2 belonging to the various reactions are given. These values were obtained by performing only the second summation in Eq. (1). The data should not be mistaken for individual χ^2 calculated without regard to the other reactions. The data of χ^2_{part} are of some use in identifying problems between the experiment and the calculation. Values exceeding unity indicate the probability of such problems. Here, this is true of the ^{24}Mg(n,p), ^{63}Cu(n,2n), ^{90}Zr(n,2n), ^{235}U(n,f) and ^{238}U(n,f) reactions. Within their uncertainties the experiment and the calculation disagree. These inconsistencies are not new and were already quoted for ^{235}U and ^{238}U in Ref. [5] and for ^{24}Mg, ^{63}Cu and ^{90}Zr in Fig. 5 of Ref. [39]. In all cases the inconsistency is not large enough to justify a rejection of the data. From the last two columns of Table I it can also be seen that an exp/calc value strongly deviating from unity does not automatically result in a large contribution to the χ^2.

The inputs and outputs of the evaluation are listed in Table IV. The energy delimiters of the group structure are listed in the first two columns of this table.

TABLE IV. INPUTS AND OUTPUTS OF THE EVALUATION OF THE SPECTRAL DISTRIBUTION

E_L (MeV)	E_U (MeV)	$\bar{x}_{in}$	Relative standard deviation (%)	$\bar{x}_{out}$	Relative standard deviation[a] (%)
0.0	0.5	1.280E-1	4.51	1.253E-1	3.79
0.5	1.0	1.689E-1	1.03	1.691E-1	1.01
1.0	1.5	1.545E-1	1.65	1.544E-1	1.63
1.5	2.0	1.288E-1	1.21	1.294E-1	1.16
2.0	2.5	1.029E-1	1.05	1.034E-1	0.95
2.5	3.0	8.003E-2	1.86	8.056E-2	1.75
3.0	3.5	6.121E-2	1.87	6.160E-2	1.76
3.5	4.0	4.625E-2	1.40	4.650E-2	1.25
4.0	4.5	3.464E-2	2.09	3.480E-2	1.95
4.5	5.0	2.575E-2	2.09	2.587E-2	1.96
5.0	5.5	1.904E-2	2.10	1.913E-2	1.96
5.5	6.0	1.402E-2	2.10	1.408E-2	1.97
6.0	6.5	1.020E-2	2.24	1.025E-2	2.15
6.5	7.0	7.347E-3	2.25	7.376E-3	2.15
7.0	7.5	5.275E-3	2.25	5.296E-3	2.15
7.5	8.0	3.778E-3	2.25	3.793E-3	2.15
8.0	8.5	2.701E-3	8.49	2.675E-3	5.32
8.5	9.0	1.927E-3	8.49	1.912E-3	5.37
9.0	9.5	1.372E-3	8.49	1.363E-3	5.46
9.5	10.0	9.761E-4	8.49	9.695E-4	5.53
10.0	11.0	1.185E-3	8.49	1.177E-3	5.39
11.0	12.0	5.954E-4	8.49	5.863E-4	5.60
12.0	13.0	2.979E-4	15.02	2.839E-4	7.40
13.0	14.0	1.486E-4	15.02	1.502E-4	6.39
14.0	15.0	7.392E-5	15.02	7.663E-5	6.48
15.0	16.0	3.668E-5	15.02	3.790E-5	7.07
16.0	17.0	1.816E-5	15.02	1.860E-5	7.64
17.0	18.0	8.978E-6	15.02	9.150E-6	7.97
18.0	19.0	4.430E-6	15.02	4.503E-6	8.15
19.0	20.0	2.183E-6	15.02	2.215E-6	8.24

[a] Correlation matrix given in Table V.

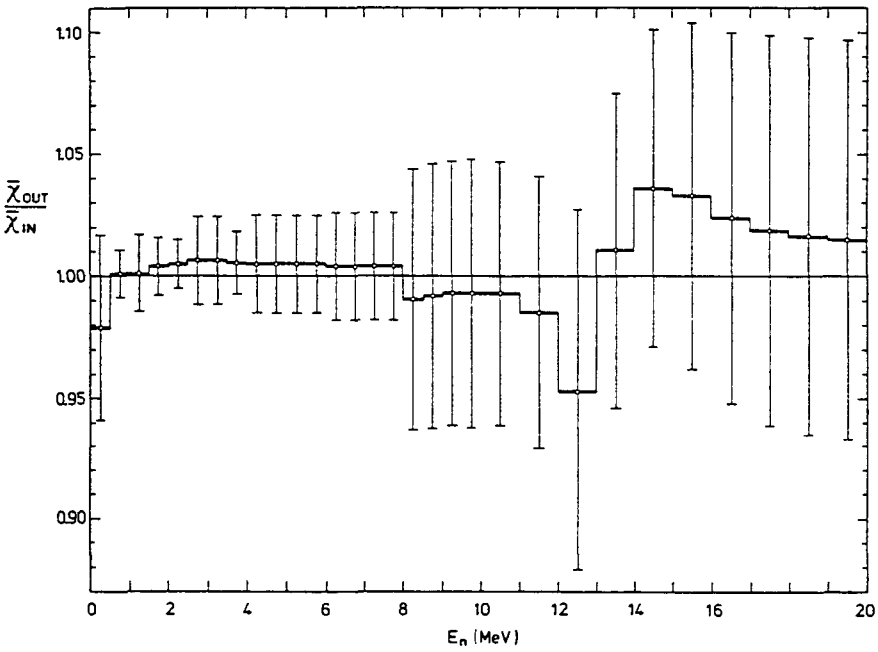

FIG. 1. Ratio of the output to the input for the evaluation of the spectral distribution of ^{252}Cf.

The averages of the spectral distributions of Eqs (8) and (9), and their uncertainties, are listed in columns 3 and 4. The relative standard deviations shown in column 4 are those obtained after the collapse of the group and after the normalization of the input covariance matrix. This explains the deviations between 0 and 4 MeV compared with the data in Table III. The adjusted spectral distribution and its uncertainty are given in the last two columns of Table IV. It can be seen that an essential uncertainty reduction was obtained for the spectrum data above 8 MeV.

The ratio of the output of the evaluation relative to the input is shown in Fig. 1. The error bars quoted correspond to the uncertainties of the output data. The figure shows that within the uncertainties the adjusted spectral distribution is fully consistent with the prior information. Between 0.5 and 8 MeV the maximum deviation from Eq. (8) is 0.6%. However, too high a value should not be placed on the remaining structures, especially at high neutron energies. Obviously, a part of this structure is due to the missing cross correlations between the various energy dependent cross-section data sets. It should also be mentioned that not more than 0.93% of the total spectrum intensity is above 8 MeV and only 0.06% is above 12 MeV of neutron energy.

The absolute covariance matrix of the input spectrum $\underline{N}_\chi$ takes into account the normalization of χ. As shown in Ref. [24], this results automatically in an

output covariance matrix $\underline{N}'_\chi$ which also fulfils the normalization condition. The correlation matrix of the adjusted spectral distribution shown in Table V therefore gives correlations as well as anticorrelations. The data in this table show that the ranges of maximum intensity of the spectral distribution are only weakly correlated with the low intensity ranges at high neutron energies. Between 4 and 8 MeV the correlation pattern is only slightly modified owing to the experimental data, whereas below 4 MeV and above 8 MeV the experimental data essentially change the structure of the correlations as compared with the prior information.

Finally, it should be mentioned that the reconstruction of the *absolute* covariance matrix of the spectral distribution from the data given in Tables IV and V can (owing to rounding errors) result in a matrix which does not fully take into account the normalization. This can be circumvented by applying Eq. (17) in Ref. [24] to the matrix. With this procedure the matrix remains unchanged if it already corresponds to the normalized spectrum; otherwise the normalization will be regenerated.

5. COMPARISON WITH OTHER EXPERIMENTAL AND THEORETICAL DATA

The aim of this work was to obtain a result with a complete uncertainty description. As mentioned earlier, this resulted in a strong limitation of the database available. To get an impression of the adequacy of the present data, some of the latest experimental and theoretical data are compared in Figs 2–4.

The approximation of the ^{252}Cf neutron spectrum of Eqs (8) and (9) is compared with the results of two nuclear evaporation models. In the model calculations of Madland and Nix [40] and Madland et al. [41], a remaining free parameter, the level density parameter, has been adjusted with regard to the experimental data of Poenitz and Tamura [10]. This adjustment has been made in the neutron energy range between 0.225 and 9.8 MeV, the energy range covered by the experiment. The other theoretical description, by Märten and Seeliger [42, 43] using a complex cascade evaporation model (CEM), takes into account that the emission of neutrons is not isotropic in the centre of mass system of the fission fragments due to the fragment spin. A 10% anisotropy is involved in the calculation. In contrast to the Madland and Nix model, the CEM model has no free parameter. Both models differ substantially below 0.5 MeV and above 10 MeV neutron energy.

The experimental data used in the comparison are taken from Lajtai et al. between 25 keV and 1.2 MeV [15], Blinov et al. between 42 keV and 11.4 MeV [44] and Märten et al. between 8.9 and 19.8 MeV [45]. The data are plotted in Figs 2–4 in the form of ratios, relative to a Maxwellian with kT = 1.42 MeV.

The experimental as well as the theoretical data show a clear deviation from the Maxwellian, with kT = 1.42 MeV above about 6 MeV neutron energy. This

TABLE V. CORRELATION MATRIX OF THE EVALUATED SPECTRAL DISTRIBUTION $\overline{\chi}_{out}$

Energy range (MeV)	Correlation matrix (×100)
0.0 - 0.5	100
0.5 - 1.0	-57 100
1.0 - 1.5	-48 44 100
1.5 - 2.0	-44 19 -3 100
2.0 - 2.5	-53 6 -15 57 100
2.5 - 3.0	-29 -17 -20 -11 40 100
3.0 - 3.5	-29 -16 -19 -10 41 68 100
3.5 - 4.0	-36 -10 -19 -4 18 27 27 100
4.0 - 4.5	-20 -3 -9 1 -11 -19 -18 53 100
4.5 - 5.0	-20 -2 -9 1 -10 -18 -18 54 72 100
5.0 - 5.5	-20 -2 -9 2 -9 -18 -17 54 72 72 100
5.5 - 6.0	-20 -2 -9 2 -9 -17 -17 54 72 72 72 100
6.0 - 6.5	-18 13 1 15 10 -4 -4 -2 -1 -0 -0 -0 100
6.5 - 7.0	-18 13 1 16 10 -4 -3 -2 -0 -0 -0 -0 76 100
7.0 - 7.5	-18 13 1 16 11 -4 -3 -1 -0 -0 0 0 76 76 100
7.5 - 8.0	-18 13 1 16 11 -4 -3 -1 -0 0 0 0 76 76 76 100
8.0 - 8.5	7 -6 -3 -6 -6 -2 -2 -4 -3 -3 -4 -4 -20 -20 -21 -21 100
8.5 - 9.0	6 -6 -3 -6 -6 -2 -2 -4 -3 -3 -3 -3 -19 -20 -20 -20 36 100
9.0 - 9.5	6 -5 -3 -5 -5 -1 -1 -4 -3 -3 -3 -3 -18 -19 -19 -19 37 37 100
9.5 - 10	6 -5 -3 -5 -5 -1 -1 -3 -3 -3 -3 -3 -18 -18 -19 -19 38 38 39 100
10 - 11	6 -5 -3 -5 -5 -1 -1 -3 -3 -3 -3 -3 -19 -19 -19 -20 36 37 38 39 100
11 - 12	6 -5 -3 -5 -5 -1 -1 -3 -3 -3 -3 -3 -17 -18 -18 -18 38 39 40 41 39 100
12 - 13	1 -1 -1 -0 -1 -0 -0 0 1 1 1 1 1 1 1 1 -5 -5 -5 -5 -5 -8 100
13 - 14	1 -1 -1 -0 -1 -1 -1 0 1 1 1 1 1 1 1 1 2 2 2 2 2 -0 -17 100
14 - 15	1 -1 -1 -0 -1 -1 -0 0 1 1 1 1 1 1 1 1 4 4 4 3 4 3 -6 -26 100
15 - 16	0 -1 -1 -0 -0 -0 -0 0 1 1 1 1 1 1 1 1 3 3 3 3 3 2 3 -15 -14 100
16 - 17	0 -0 -1 -0 -0 -0 -0 0 1 1 1 1 1 1 1 1 2 2 2 2 2 1 7 -6 -5 2 100
17 - 18	0 -0 -1 0 -0 -0 -0 0 1 1 1 1 1 1 1 1 2 2 2 2 2 1 10 -2 -0 6 12 100
18 - 19	0 -0 -1 0 -0 -0 -0 0 1 1 1 1 1 1 1 1 2 1 1 1 1 0 12 0 2 9 14 17 100
19 - 20	0 -0 -1 0 -0 -0 -0 0 1 1 1 1 1 1 1 1 1 1 1 1 1 0 12 2 4 10 15 17 19 100

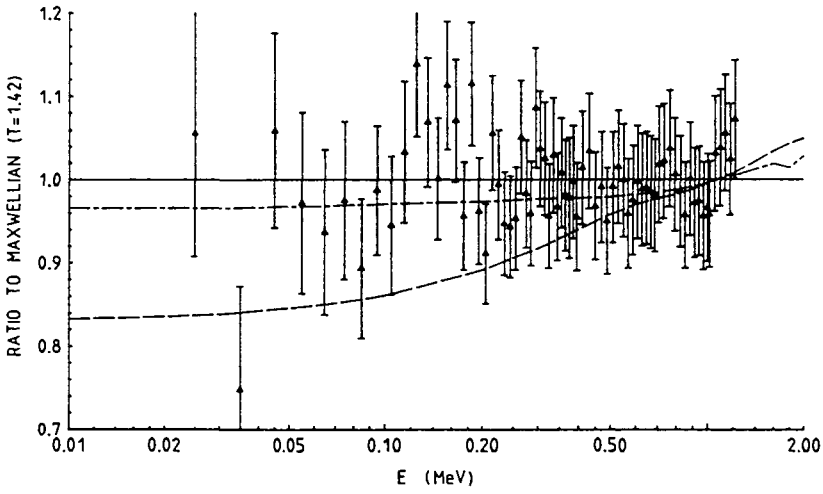

FIG. 2. Various representations of the ^{252}Cf neutron spectrum relative to a reference Maxwellian, with $kT = 1.42$ MeV. The solid curve denotes the spectrum of Eqs (8) and (9). The dashed curve represents the theoretical calculations of Madland and Nix [40] *and Madland et al.* [41]. *The dot-dashed curve represents the calculations of Märten and Seeliger* [42, 43], *with $\beta = 0.1$. The experimental data (triangles) are from Lajtai et al.* [15].

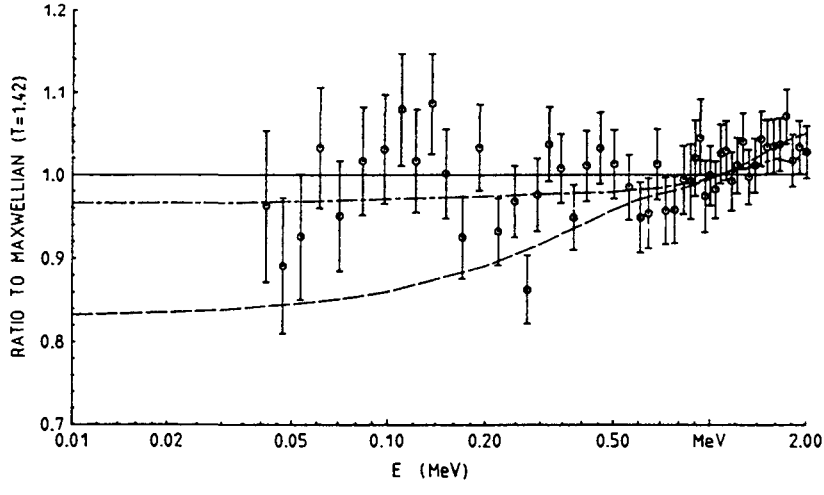

FIG. 3. Same details as for Fig. 2. The experimental data (circles) are from Blinov et al. [44].

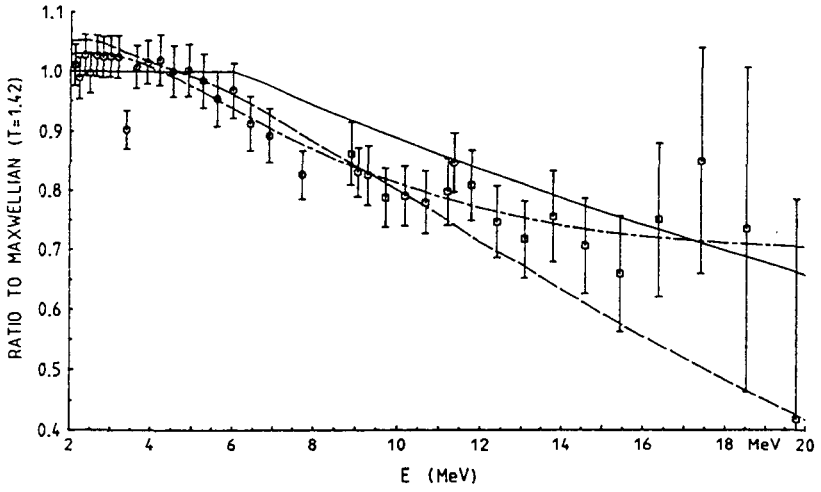

FIG. 4. Same details as for Fig. 2, except that the neutron energy range is from 2 to 20 MeV. The experimental data above 2 MeV are from Blinov et al. [44] *(circles) and from Märten et al.* [45] *(squares).*

effect seems to be best described by the theory of Märten and Seeliger [42, 43] (dot-dashed curve). The formula for Eqs (8) and (9) (solid curve) underestimates the effect, whereas the theoretical data of Madland and Nix and Madland et al. (dashed curve) show an overestimation. Between 1 MeV and 4 MeV, the experimental data show a slight enhancement relative to the reference Maxwellian. This effect is well described by both evaporation theories. Below 1 MeV neutron energy, the experimental data strongly support the reference Maxwellian of kT = 1.42 MeV. Below 0.5 MeV, the data of both evaporation theories diverge. The theoretical data of Märten and Seeliger are compatible with the experimental data available. The same is not true of the theory of Madland and Nix and Madland et al. This is easily understandable, since the latters' theory has been optimized between 0.2 and 10 MeV owing to the adjustment of their data to the data of Poenitz and Tamura [10]. The logical consequence is that their theory must have some deficiencies outside of the range of adjustment, i.e. their data are restricted in validity below 0.2 MeV and above 10 MeV.

The data of both evaporation theories are listed numerically in Tables VI and VII. They are given between 1 keV and 20 MeV. For both theoretical calculations no original uncertainty information is available. Thus, the plots of Figs 2–4 must be used to obtain some rough estimates of the accuracy of these calculations.

TABLE VI. NUMERICAL DATA FROM THE THEORY OF MADLAND et al. ON THE ^{252}Cf NEUTRON SPECTRUM [40, 41]

(Data from Los Alamos National Laboratory; applicable energy range: 1 keV to 20 MeV; interpolation: ln (N(E)), linear in E)

E (MEV)	N(E) (1/MEV)	E (MEV)	N(E) (1/MEV)	E (MEV)	N(E) (1/MEV)
1.00E-3	1.750E-2	1.10E-3	1.835E-2	1.20E-3	1.917E-2
1.30E-3	1.995E-2	1.40E-3	2.070E-2	1.50E-3	2.143E-2
1.60E-3	2.213E-2	1.70E-3	2.281E-2	1.80E-3	2.347E-2
1.90E-3	2.411E-2	2.00E-3	2.474E-2	2.10E-3	2.535E-2
2.20E-3	2.595E-2	2.30E-3	2.653E-2	2.40E-3	2.710E-2
2.50E-3	2.766E-2	2.60E-3	2.820E-2	2.70E-3	2.874E-2
2.80E-3	2.927E-2	2.90E-3	2.978E-2	3.00E-3	3.029E-2
3.10E-3	3.079E-2	3.20E-3	3.128E-2	3.30E-3	3.177E-2
3.40E-3	3.224E-2	3.50E-3	3.271E-2	3.60E-3	3.318E-2
3.70E-3	3.363E-2	3.80E-3	3.408E-2	3.90E-3	3.453E-2
4.00E-3	3.497E-2	4.10E-3	3.540E-2	4.20E-3	3.583E-2
4.30E-3	3.625E-2	4.40E-3	3.667E-2	4.50E-3	3.708E-2
4.60E-3	3.749E-2	4.70E-3	3.789E-2	4.80E-3	3.829E-2
4.90E-3	3.869E-2	5.00E-3	3.908E-2	5.10E-3	3.947E-2
5.20E-3	3.985E-2	5.30E-3	4.023E-2	5.40E-3	4.061E-2
5.50E-3	4.098E-2	5.60E-3	4.135E-2	5.70E-3	4.172E-2
5.80E-3	4.208E-2	5.90E-3	4.244E-2	6.00E-3	4.280E-2
6.10E-3	4.315E-2	6.20E-3	4.350E-2	6.30E-3	4.385E-2
6.40E-3	4.419E-2	6.50E-3	4.454E-2	6.60E-3	4.488E-2
6.70E-3	4.521E-2	6.80E-3	4.555E-2	6.90E-3	4.588E-2
7.00E-3	4.621E-2	7.10E-3	4.654E-2	7.20E-3	4.686E-2
7.30E-3	4.718E-2	7.40E-3	4.750E-2	7.50E-3	4.782E-2
7.60E-3	4.814E-2	7.70E-3	4.845E-2	7.80E-3	4.877E-2
7.90E-3	4.908E-2	8.00E-3	4.938E-2	8.10E-3	4.969E-2
8.20E-3	4.999E-2	8.30E-3	5.030E-2	8.40E-3	5.060E-2
8.50E-3	5.090E-2	8.60E-3	5.119E-2	8.70E-3	5.149E-2
8.80E-3	5.178E-2	8.90E-3	5.207E-2	9.00E-3	5.236E-2
9.10E-3	5.265E-2	9.20E-3	5.294E-2	9.30E-3	5.322E-2
9.40E-3	5.351E-2	9.50E-3	5.379E-2	9.60E-3	5.407E-2
9.70E-3	5.435E-2	9.80E-3	5.463E-2	9.90E-3	5.490E-2
1.00E-2	5.518E-2	1.10E-2	5.785E-2	1.20E-2	6.040E-2
1.30E-2	6.285E-2	1.40E-2	6.520E-2	1.50E-2	6.747E-2
1.60E-2	6.966E-2	1.70E-2	7.178E-2	1.80E-2	7.383E-2
1.90E-2	7.583E-2	2.00E-2	7.777E-2	2.10E-2	7.967E-2
2.20E-2	8.152E-2	2.30E-2	8.332E-2	2.40E-2	8.509E-2
2.50E-2	8.681E-2	2.60E-2	8.850E-2	2.70E-2	9.016E-2
2.80E-2	9.178E-2	2.90E-2	9.337E-2	3.00E-2	9.494E-2
3.10E-2	9.648E-2	3.20E-2	9.799E-2	3.30E-2	9.947E-2
3.40E-2	1.009E-1	3.50E-2	1.024E-1	3.60E-2	1.038E-1
3.70E-2	1.052E-1	3.80E-2	1.066E-1	3.90E-2	1.079E-1
4.00E-2	1.093E-1	4.10E-2	1.106E-1	4.20E-2	1.119E-1
4.30E-2	1.132E-1	4.40E-2	1.144E-1	4.50E-2	1.157E-1
4.60E-2	1.169E-1	4.70E-2	1.182E-1	4.80E-2	1.194E-1
4.90E-2	1.206E-1	5.00E-2	1.217E-1	5.10E-2	1.229E-1
5.20E-2	1.241E-1	5.30E-2	1.252E-1	5.40E-2	1.264E-1
5.50E-2	1.275E-1	5.60E-2	1.286E-1	5.70E-2	1.297E-1
5.80E-2	1.308E-1	5.90E-2	1.319E-1	6.00E-2	1.329E-1

TABLE VI (cont.)

E (MEV)	N(E) (1/MEV)	E (MEV)	N(E) (1/MEV)	E (MEV)	N(E) (1/MEV)
6.10E-2	1.340E-1	6.20E-2	1.350E-1	6.30E-2	1.361E-1
6.40E-2	1.371E-1	6.50E-2	1.381E-1	6.60E-2	1.391E-1
6.70E-2	1.401E-1	6.80E-2	1.411E-1	6.90E-2	1.421E-1
7.00E-2	1.431E-1	7.10E-2	1.441E-1	7.20E-2	1.450E-1
7.30E-2	1.460E-1	7.40E-2	1.469E-1	7.50E-2	1.479E-1
7.60E-2	1.488E-1	7.70E-2	1.497E-1	7.80E-2	1.506E-1
7.90E-2	1.515E-1	8.00E-2	1.524E-1	8.10E-2	1.533E-1
8.20E-2	1.542E-1	8.30E-2	1.551E-1	8.40E-2	1.560E-1
8.50E-2	1.569E-1	8.60E-2	1.577E-1	8.70E-2	1.586E-1
8.80E-2	1.594E-1	8.90E-2	1.603E-1	9.00E-2	1.611E-1
9.10E-2	1.620E-1	9.20E-2	1.628E-1	9.30E-2	1.636E-1
9.40E-2	1.644E-1	9.50E-2	1.653E-1	9.60E-2	1.661E-1
9.70E-2	1.669E-1	9.80E-2	1.677E-1	9.90E-2	1.685E-1
1.00E-1	1.692E-1	1.10E-1	1.769E-1	1.20E-1	1.841E-1
1.30E-1	1.909E-1	1.40E-1	1.974E-1	1.50E-1	2.036E-1
1.60E-1	2.095E-1	1.70E-1	2.151E-1	1.80E-1	2.205E-1
1.90E-1	2.257E-1	2.00E-1	2.307E-1	2.10E-1	2.354E-1
2.20E-1	2.400E-1	2.30E-1	2.444E-1	2.40E-1	2.487E-1
2.50E-1	2.528E-1	2.60E-1	2.567E-1	2.70E-1	2.605E-1
2.80E-1	2.642E-1	2.90E-1	2.677E-1	3.00E-1	2.711E-1
3.10E-1	2.744E-1	3.20E-1	2.776E-1	3.30E-1	2.807E-1
3.40E-1	2.836E-1	3.50E-1	2.864E-1	3.60E-1	2.892E-1
3.70E-1	2.918E-1	3.80E-1	2.943E-1	3.90E-1	2.967E-1
4.00E-1	2.991E-1	4.10E-1	3.013E-1	4.20E-1	3.035E-1
4.30E-1	3.056E-1	4.40E-1	3.076E-1	4.50E-1	3.095E-1
4.60E-1	3.113E-1	4.70E-1	3.131E-1	4.80E-1	3.147E-1
4.90E-1	3.163E-1	5.00E-1	3.178E-1	5.10E-1	3.192E-1
5.20E-1	3.204E-1	5.30E-1	3.217E-1	5.40E-1	3.228E-1
5.50E-1	3.239E-1	5.60E-1	3.249E-1	5.70E-1	3.259E-1
5.80E-1	3.268E-1	5.90E-1	3.276E-1	6.00E-1	3.284E-1
6.10E-1	3.291E-1	6.20E-1	3.297E-1	6.30E-1	3.303E-1
6.40E-1	3.308E-1	6.50E-1	3.312E-1	6.60E-1	3.316E-1
6.70E-1	3.320E-1	6.80E-1	3.323E-1	6.90E-1	3.326E-1
7.00E-1	3.328E-1	7.10E-1	3.330E-1	7.20E-1	3.332E-1
7.30E-1	3.334E-1	7.40E-1	3.335E-1	7.50E-1	3.336E-1
7.60E-1	3.336E-1	7.70E-1	3.336E-1	7.80E-1	3.336E-1
7.90E-1	3.336E-1	8.00E-1	3.335E-1	8.10E-1	3.334E-1
8.20E-1	3.333E-1	8.30E-1	3.332E-1	8.40E-1	3.330E-1
8.50E-1	3.329E-1	8.60E-1	3.327E-1	8.70E-1	3.324E-1
8.80E-1	3.322E-1	8.90E-1	3.319E-1	9.00E-1	3.317E-1
9.10E-1	3.314E-1	9.20E-1	3.311E-1	9.30E-1	3.307E-1
9.40E-1	3.304E-1	9.50E-1	3.300E-1	9.60E-1	3.296E-1
9.70E-1	3.292E-1	9.80E-1	3.288E-1	9.90E-1	3.283E-1
1.00E+0	3.279E-1	1.10E+0	3.225E-1	1.20E+0	3.160E-1
1.30E+0	3.087E-1	1.40E+0	3.006E-1	1.50E+0	2.919E-1
1.60E+0	2.827E-1	1.70E+0	2.729E-1	1.80E+0	2.628E-1
1.90E+0	2.525E-1	2.00E+0	2.421E-1	2.10E+0	2.315E-1
2.20E+0	2.211E-1	2.30E+0	2.107E-1	2.40E+0	2.005E-1
2.50E+0	1.906E-1	2.60E+0	1.809E-1	2.70E+0	1.715E-1
2.80E+0	1.625E-1	2.90E+0	1.538E-1	3.00E+0	1.454E-1
3.10E+0	1.374E-1	3.20E+0	1.298E-1	3.30E+0	1.225E-1
3.40E+0	1.156E-1	3.50E+0	1.090E-1	3.60E+0	1.028E-1

TABLE VI (cont.)

E (MEV)	N(E) (1/MEV)	E (MEV)	N(E) (1/MEV)	E (MEV)	N(E) (1/MEV)
3.70E+0	9.689E-2	3.80E+0	9.128E-2	3.90E+0	8.597E-2
4.00E+0	8.094E-2	4.10E+0	7.619E-2	4.20E+0	7.169E-2
4.30E+0	6.745E-2	4.40E+0	6.344E-2	4.50E+0	5.965E-2
4.60E+0	5.607E-2	4.70E+0	5.269E-2	4.80E+0	4.951E-2
4.90E+0	4.650E-2	5.00E+0	4.367E-2	5.10E+0	4.099E-2
5.20E+0	3.847E-2	5.30E+0	3.610E-2	5.40E+0	3.386E-2
5.50E+0	3.176E-2	5.60E+0	2.977E-2	5.70E+0	2.791E-2
5.80E+0	2.615E-2	5.90E+0	2.450E-2	6.00E+0	2.295E-2
6.10E+0	2.149E-2	6.20E+0	2.011E-2	6.30E+0	1.883E-2
6.40E+0	1.762E-2	6.50E+0	1.648E-2	6.60E+0	1.542E-2
6.70E+0	1.442E-2	6.80E+0	1.348E-2	6.90E+0	1.260E-2
7.00E+0	1.178E-2	7.10E+0	1.101E-2	7.20E+0	1.029E-2
7.30E+0	9.610E-3	7.40E+0	8.977E-3	7.50E+0	8.385E-3
7.60E+0	7.831E-3	7.70E+0	7.313E-3	7.80E+0	6.828E-3
7.90E+0	6.375E-3	8.00E+0	5.952E-3	8.10E+0	5.556E-3
8.20E+0	5.185E-3	8.30E+0	4.839E-3	8.40E+0	4.516E-3
8.50E+0	4.214E-3	8.60E+0	3.932E-3	8.70E+0	3.669E-3
8.80E+0	3.422E-3	8.90E+0	3.192E-3	9.00E+0	2.978E-3
9.10E+0	2.777E-3	9.20E+0	2.590E-3	9.30E+0	2.415E-3
9.40E+0	2.252E-3	9.50E+0	2.100E-3	9.60E+0	1.958E-3
9.70E+0	1.825E-3	9.80E+0	1.701E-3	9.90E+0	1.585E-3
1.00E+1	1.477E-3	1.10E+1	7.265E-4	1.20E+1	3.543E-4
1.30E+1	1.716E-4	1.40E+1	8.266E-5	1.50E+1	3.963E-5
1.60E+1	1.893E-5	1.70E+1	9.006E-6	1.80E+1	4.271E-6
1.90E+1	2.019E-6	2.00E+1	9.522E-7		

TABLE VII. NUMERICAL DATA FROM THE THEORY OF MÄRTEN AND SEELIGER ON THE ^{252}Cf NEUTRON SPECTRUM [42, 43]

(Data from the Technical University of Dresden, German Democratic Republic; applicable energy range: 1 keV to 20 MeV; interpolation: ln (N(E)), linear in E)

E (MEV)	N(E) (1/MEV)	E (MEV)	N(E) (1/MEV)	E (MEV)	N(E) (1/MEV)
1.00E-3	2.032E-2	1.50E-3	2.489E-2	2.00E-3	2.873E-2
2.50E-3	3.211E-2	3.00E-3	3.516E-2	3.50E-3	3.797E-2
4.00E-3	4.058E-2	4.50E-3	4.303E-2	5.00E-3	4.534E-2
6.00E-3	4.964E-2	7.00E-3	5.358E-2	8.00E-3	5.725E-2
9.00E-3	6.068E-2	1.00E-2	6.393E-2	1.10E-2	6.700E-2
1.20E-2	6.994E-2	1.30E-2	7.275E-2	1.40E-2	7.545E-2
1.50E-2	7.805E-2	1.60E-2	8.056E-2	1.80E-2	8.533E-2
2.00E-2	8.984E-2	2.20E-2	9.410E-2	2.40E-2	9.816E-2
2.60E-2	1.020E-1	2.80E-2	1.058E-1	3.00E-2	1.093E-1
3.30E-2	1.144E-1	3.70E-2	1.209E-1	4.00E-2	1.254E-1
4.30E-2	1.298E-1	4.70E-2	1.354E-1	5.00E-2	1.393E-1

TABLE VII (cont.)

E (MEV)	N(E) (1/MEV)	E (MEV)	N(E) (1/MEV)	E (MEV)	N(E) (1/MEV)
5.30E-2	1.432E-1	5.70E-2	1.481E-1	6.00E-2	1.516E-1
6.50E-2	1.573E-1	7.00E-2	1.627E-1	7.50E-2	1.679E-1
8.00E-2	1.728E-1	8.50E-2	1.776E-1	9.00E-2	1.822E-1
9.50E-2	1.865E-1	1.00E-1	1.908E-1	1.10E-1	1.987E-1
1.20E-1	2.062E-1	1.30E-1	2.132E-1	1.40E-1	2.198E-1
1.50E-1	2.260E-1	1.60E-1	2.318E-1	1.80E-1	2.426E-1
2.00E-1	2.523E-1	2.20E-1	2.611E-1	2.40E-1	2.691E-1
2.60E-1	2.763E-1	2.80E-1	2.828E-1	3.00E-1	2.888E-1
3.30E-1	2.967E-1	3.70E-1	3.056E-1	4.00E-1	3.112E-1
4.30E-1	3.161E-1	4.70E-1	3.215E-1	5.00E-1	3.248E-1
5.30E-1	3.276E-1	5.70E-1	3.306E-1	6.00E-1	3.323E-1
6.50E-1	3.344E-1	7.00E-1	3.355E-1	7.50E-1	3.358E-1
8.00E-1	3.353E-1	8.50E-1	3.343E-1	9.00E-1	3.327E-1
9.50E-1	3.304E-1	1.00E+0	3.282E-1	1.10E+0	3.222E-1
1.20E+0	3.149E-1	1.30E+0	3.068E-1	1.40E+0	2.978E-1
1.50E+0	2.883E-1	1.60E+0	2.784E-1	1.80E+0	2.554E-1
2.00E+0	2.370E-1	2.20E+0	2.164E-1	2.40E+0	1.966E-1
2.60E+0	1.777E-1	2.80E+0	1.600E-1	3.00E+0	1.436E-1
3.30E+0	1.213E-1	3.70E+0	9.612E-2	4.00E+0	8.025E-2
4.30E+0	6.676E-2	4.70E+0	5.199E-2	5.00E+0	4.295E-2
5.30E+0	3.541E-2	5.70E+0	2.729E-2	6.00E+0	2.241E-2
6.50E+0	1.609E-2	7.00E+0	1.151E-2	7.50E+0	8.224E-3
8.00E+0	5.864E-3	8.50E+0	4.171E-3	9.00E+0	2.967E-3
9.50E+0	2.110E-3	1.00E+1	1.498E-3	1.10E+1	7.553E-4
1.20E+1	3.806E-4	1.30E+1	1.918E-4	1.40E+1	9.667E-5
1.50E+1	4.875E-5	1.60E+1	2.461E-5	1.80E+1	6.286E-6
2.00E+1	1.606E-6				

6. CONCLUSIONS

The results of the present evaluation were used to derive a complete covariance uncertainty matrix based on integral spectrum data (spectrum averaged cross-sections measurements) and also implicitly taking into account some recent direct spectrum measurements (in the prior information). However, these results must be updated, and data from direct measurements in particular should be explicitly included in the evaluation as soon as their covariances are available. These data can easily be combined with the present results. Thus, further steps in the evaluation are necessary in the future in order to obtain an optimum result for the spectral distribution of ^{252}Cf.

REFERENCES

[1] INTERNATIONAL ATOMIC ENERGY AGENCY, Neutron Cross Sections for Reactor Dosimetry (Proc. Consultants Meeting Vienna, 1976), IAEA-TECDOC-208, IAEA, Vienna (1978) 1.

[2] BLINOV, M.V., "Neutron energy spectra of spontaneous fission sources", Neutron Source Properties (Proc. Consultants Meeting Debrecen, Hungary, 1980) (OKAMOTO, K., Ed.), IAEA/International Nuclear Data Committee, Vienna, Rep. INDC(NDS)-114/GT (1980) 79.

[3] The Cf-252 Fission Neutron Spectrum (Proc. Consultants Meeting Smolenice, Czechoslovakia, 1983) (LEMMEL, H.D., CULLEN, D.E., Eds), IAEA/International Nuclear Data Committee, Vienna, Rep. INDC(NDS)-146 (1983).

[4] Nuclear Data for Science and Technology (Proc. Int. Conf. Antwerp, 1982) (BÖCKHOFF, K.H., Ed.), Reidel, Dordrecht (1983).

[5] WAGSCHAL, J.J., MAERKER, R.E., BROADHEAD, B.L., ibid., p. 436.

[6] BOLDEMAN, J.W., CULLEY, D., CAWLEY, R.W., Trans. Am. Nucl. Soc. **32** (1979) 733.

[7] BENSCH, F., JASICEK, H., "The fast neutron emission spectrum of ^{252}Cf", Neutron Source Properties (Proc. Consultants Meeting Debrecen, Hungary, 1980) (OKAMOTO, K., Ed.), IAEA/International Nuclear Data Committee, Vienna, Rep. INDC(NDS)-114/GT (1980) 302.

[8] BLINOV, M.V., VITENKO, V.A., YUREVICH, V.I., in Interaction of Fast Neutrons with Nuclei (Proc. Int. Symp. Gaussig, German Democratic Republic, 1979), Zentralinstitut für Kernforschung, Rossendorf bei Dresden, Rep. ZfK-410 (1980) 104.

[9] MON, Jiangshen, et al., Chin. J. Nucl. Phys. **3** (1981) 163.

[10] POENITZ, W.P., TAMURA, T., in Nuclear Data for Science and Technology (Proc. Int. Conf. Antwerp, 1982) (BÖCKHOFF, K.H., Ed.), Reidel, Dordrecht (1983) 465.

[11] BLINOV, M.V., BOYKOV, G.S., VITENKO, V.A., ibid., p. 479.

[12] BÖTTGER, R., KLEIN, H., CHALUPKA, A., STROHMAIER, B., ibid., p. 484.

[13] MÄRTEN, H., SEELIGER, D., STOBINSKI, B., ibid., p. 488.

[14] BATENKOV, O.I., BLINOV, M.V., BOYKOV, G.S., VITENKO, V.N., RUBCHENYA, V.A., "Experimental and theoretical investigation of the energy distribution of californium-52 spontaneous fission neutrons", The Cf-252 Fission Neutron Spectrum (Proc. Consultants Meeting Smolenice, Czechoslovakia, 1983) (LEMMEL, H.D., CULLEN, D.E., Eds), IAEA/International Nuclear Data Committee, Vienna, Rep. INDC(NDS)-146 (1983) 161.

[15] LAJTAI, A., et al., "An absolute measurement of ^{252}Cf prompt fission neutron spectrum at low energy range", ibid., p. 177.

[16] MANNHART, W., PEREY, F.G., in Reactor Dosimetry (Proc. 3rd ASTM-EURATOM Symp. Ispra, Italy, 1979) (RÖTTGER, H., Ed.), Vol. 2, Commission of the European Communities, Brussels, Rep. EUR-6813 (1980) 1016.

[17] MADLAND, D.G., NIX, J.R., in Nuclear Data for Science and Technology (Proc. Int. Conf. Antwerp, 1982) (BÖCKHOFF, K.H., Ed.), Reidel, Dordrecht (1983) 473.

[18] MADLAND, D.G., NIX, J.R., Nucl. Sci. Eng. **81** (1982) 213.

[19] MÄRTEN, H., NEUMANN, D., SEELIGER, D., "Theoretical analysis of the Cf-252 fission neutron spectrum", The Cf-252 Fission Neutron Spectrum (Proc. Consultants Meeting Smolenice, Czechoslovakia, 1983) (LEMMEL, H.D., CULLEN, D.E., Eds), IAEA/International Nuclear Data Committee, Vienna, Rep. INDC(NDC)-146 (1983) 199.

[20] PEELLE, R.W., Adv. Nucl. Sci. Technol. **14** (1982) 11.

[21] PEREY, F.G., Oak Ridge National Lab., TN, Rep. ORNL/TM-6062 (1977).

[22] PEREY, F.G., Oak Ridge National Lab., TN, Rep. ORNL/TM-6267 (1978).

[23] SCHMITTROTH, F., Hanford Engineering Development Lab., Richland, WA, Rep. HEDL/TME 79-40 (1979).
[24] MANNHART, W., "Approaches for the generation of a covariance matrix for the Cf-252 fission neutron spectrum", The Cf-252 Fission-Neutron Spectrum (Proc. Consultants Meeting Smolenice, Czechoslovakia, 1983) (LEMMEL, H.D., CULLEN, D.E., Eds), IAEA/International Nuclear Data Committee, Vienna, Rep. INDC(NDS)-146 (1983) 229.
[25] HEATON, H.T., II, GILLIAM, D.M., SPIEGEL, V., EISENHAUER, C., GRUNDL, J.A., in Fast Neutron Fission Cross Sections of U-233, U-238, Pu-239 (Proc. NEANDC/NEACRP Specialists Meeting Argonne, IL, 1976) (POENITZ, W.P., SMITH, A.B., Eds), Argonne National Lab., IL, Rep. ANL-76-90 (1976) 333.
[26] GRUNDL, J.A., EISENHAUER, C., in Nuclear Cross Sections and Technology (Proc. Int. Conf. Washington, DC, 1975), US National Bureau of Standards Special Publication 425, US Government Printing Office, Washington, DC (1975) 250.
[27] MANNHART, W., in Nuclear Data for Science and Technology (Proc. Int. Conf. Antwerp, 1982) (BÖCKHOFF, K.H., Ed.), Reidel, Dordrecht (1983) 429.
[28] MAERKER, R.E., WAGSCHAL, J.J., BROADHEAD, B.L., Electric Power Research Institute, Palo Alto, CA, Rep. EPRI-NP-2188 (1981).
[29] TAGESEN, S., VONACH, H., STROHMAIER, B., Phys. Data **13-1** (1979).
[30] STROHMAIER, B., TAGESEN, S., VONACH, H., Phys. Data **13-2** (1980).
[31] TAGESEN, S., VONACH, H., Phys. Data **13-3** (1981).
[32] WINKLER, G., SMITH, D.L., MEADOWS, J.W., Nucl. Sci. Eng. 76 (1980) 30.
[33] WINKLER, G., PAVLIK, A., VONACH, H., PAULSEN, A., LISKIEN, H., in Nuclear Data for Science and Technology (Proc. Int. Conf. Antwerp, 1982) (BÖCKHOFF, K.H., Ed.), Reidel, Dordrecht (1983) 400.
[34] PAVLIK, A., WINKLER, G., Evaluation of the ^{58}Ni(n, 2n)^{57}Ni Cross Sections, IAEA/International Nuclear Data Committee, Vienna, Rep. INDC(AUS)-9/L (1983).
[35] MUIR, D.W., MacFARLANE, R.E., BOICOURT, R. M., in Reactor Dosimetry (Proc. 4th ASTM-EURATOM Symp. Gaithersburg, MD, 1982), Vol. 2, US Nuclear Regulatory Commission, Washington, DC, Rep. NUREG/CP-0029 (1982) 655.
[36] MANNHART, W., "Status and further needs of cross section covariance files", Nuclear Data for Radiation Damage Assessment and Related Safety Aspects (Proc. Advisory Group Meeting Vienna, 1981), IAEA-TECDOC-263, IAEA, Vienna (1982) 47.
[37] FU, C.Y., HETRICK, D.M., PEREY, F.G., in Nuclear Cross Sections for Technology (Proc. Int. Conf. Knoxville, TN, 1979), US National Bureau of Standards Special Publication 594, US Government Printing Office, Washington, DC (1980) 63.
[38] FU, C.Y., HETRICK, D.M., in Reactor Dosimetry (Proc. 4th ASTM-EURATOM Symp. Gaithersburg, MD, 1982), Vol. 2, US Nuclear Regulatory Commission, Washington, DC, Rep. NUREG/CP-0029 (1982) 877.
[39] MANNHART, W., "Information on the Cf-252 fission-neutron spectrum deduced from integral experiments", The Cf-252 Fission-Neutron Spectrum (Proc. Consultants Meeting Smolenice, Czechoslovakia, 1983) (LEMMEL, H.D., CULLEN, D.E., Eds), IAEA/International Nuclear Data Committee, Vienna, Rep. INDC(NDS)-146 (1983) 213.
[40] MADLAND, D.G., NIX, J.R., Brookhaven National Lab., Upton, NY, Rep. BNL-51778 (1983) 423.
[41] MADLAND, D.G., LaBAUVE, R.J., NIX, J.R., "Differential and integral comparisons of three representations of the prompt neutron spectrum for the spontaneous fission of ^{252}Cf", Nuclear Standard Reference Data (Proc. IAEA-OECD/NEANDC Advisory Group Meeting Geel, Belgium, 1984), IAEA-TECDOC-335, IAEA, Vienna (1985) 267.
[42] MÄRTEN, H., SEELIGER, D., "Measurement and theoretical calculation of the ^{252}Cf spontaneous-fission neutron spectrum", ibid., p.255.

[43] SEELIGER, D., personal communication, 1985.
[44] BLINOV, M.V., BOYKOV, G.S., VITENKO, V.A., "Experimental study of an energy distribution shape of spontaneous fission neutrons of californium-252", Neutron Physics (Proc. 6th All-Union Conf. Kiev, 1983), IAEA/International Nuclear Data Committee, Vienna, Rep. INDC(CCP)-238/L (1984).
[45] MÄRTEN, H., RICHTER, D., SEELIGER, D., "Analysis of experimental data on the high-energy end of the ^{252}Cf spontaneous-fission neutron spectrum", IAEA/International Nuclear Data Committee, Vienna, Rep. INDC(GDR)-28L (1984).

1-5. DECAY DATA FOR RADIONUCLIDES USED AS CALIBRATION STANDARDS

A. LORENZ
Nuclear Data Section,
Division of Research and Laboratories,
International Atomic Energy Agency,
Vienna

Abstract

DECAY DATA FOR RADIONUCLIDES USED AS CALIBRATION STANDARDS.
A tabulation of the most current evaluated values of gamma ray energies and emission probabilities, used as calibration standards in nuclear data measurements, is given.

1. INTRODUCTION

The most current evaluated values of gamma ray energies and emission probabilities of radionuclides used as calibration standards in nuclear data measurements are presented in Table I. The tabulated data have been selected from the most recent available evaluations on the basis of their use by individual groups performing decay data measurements. This compilation was reviewed by members of the IAEA/International Nuclear Data Committee (INDC) Standards Subcommittee and the IAEA Co-ordinated Research Programme for the Measurement and Evaluation of Transactinium Isotope Nuclear Decay Data. It is also derived from the 1982 edition of the INDC-OECD/Nuclear Energy Agency Nuclear Data Committee (NEANDC) Nuclear Standards File, published as an IAEA technical report [1]. The reader is referred to the first chapter of this Handbook for the corresponding half-lives.

2. SELECTION OF STANDARDS INCLUDED IN THE FILE

The radionuclides chosen to be included in this review were selected on the basis of their inclusion in the following compilations:

(1) The INDC/NEANDC Nuclear Standards File [2].
(2) The list of standards for gamma ray energy calibration recommended by the International Union of Pure and Applied Physics (IUPAP) [3].

(3) The report by the Atomic Energy of Canada Ltd (AECL) Radioisotope Standardization Group to the Spectrometry Working Group of the International Committee for Radionuclide Metrology (ICRM) [4].
(4) The list of radionuclides used as standards by groups performing transactinium isotope decay measurements.

3. SELECTION OF RECOMMENDED GAMMA RAY ENERGIES AND INTENSITIES

Following the recommendation of the INDC Standards Subcommittee, all gamma ray energy standards recommended by the IUPAP Commission on Atomic Masses and Fundamental Constants [3] were adopted for those radionuclides included in this file. Beyond this initial criterion, the recommended values of E and P were selected from the following sources of evaluated data:

(1) Emission probabilities of selected gamma rays for radionuclides used as detector calibration standards [5].
(2) Evaluations of gamma ray energies and emission probabilities performed specifically for Ge(Li) spectrometer calibration (see Refs [6–9]).
(3) The Laboratoire de métrologie des rayonnements ionisants (LMRI) tables of radionuclides [10–15].
(4) The evaluation of gamma ray intensities [16].
(5) Nuclear spectroscopy standards listed in the publication Table of Isotopes [17].
(6) The report of the AECL Radioisotope Standardization Group [4].
(7) The journal Nuclear Data Sheets.
(8) The Table of Isotopes (used primarily in those cases where the isotope has not been evaluated since 1976 [17].

4. KEY TO THE COMMENTS COLUMN IN THE TABLE

The numbers and letters in the comments column should be read individually.

1 – Gamma ray lines of radionuclides included in the list of standards for gamma ray energy calibration recommended by the IUPAP [3].
2 – Radionuclides used as standards by groups performing transactinium isotope decay measurements.
3 – Radionuclides included in the list of gamma ray standards submitted to the α-, β- and γ-ray Spectrometry Working Group of the ICRM [4].
4 – Radionuclides included as gamma ray standards in the 1982 INDC/NEANDC Nuclear Standards File [1].
P – Radionuclides considered in Ref. [5] as primary references.
S – Radionuclides considered in Ref. [5] as secondary references.

Text cont. on p. 195.

TABLE I. PHOTON ENERGIES AND EMISSION PROBABILITIES FOR RADIONUCLIDES USED AS STANDARDS

NUCLIDE	DECAY MODE	ENERGY (keV) LEVEL DATA	ENERGY (keV) UNCERTAINTY	ENERGY (keV) PER CENT	ENERGY (keV) REFERENCE	EMISSION PROBABILITY DATA	EMISSION PROBABILITY UNCERTAINTY	EMISSION PROBABILITY PER CENT	EMISSION PROBABILITY REFERENCE	COMMENTS
4-BE- 7		(477.605	+- 0.003)	0.001	[14]	(0.1045	+- 0.0004)	0.383	[5]	13S
11-NA- 22		(1274.542	+- 0.007)	0.001	[3]	(0.99935	+- 0.00020)	0.020	[5]	1234P
11-NA- 24		(1368.633	+- 0.006)	0.000	[3]	(0.99994	+- 0.00002)	0.002	[5]	1234P
11-NA- 24		(2754.030	+- 0.014)	0.001	[3]	(0.99878	+- 0.00008)	0.008	[5]	1234P
19-K - 42		(1524.665	+- 0.020)	0.001	[12]	(0.179	+- 0.005)	2.793	[12]	3
21-SC- 46		(889.277	+- 0.003)	0.000	[3]	(0.99984	+- 0.00001)	0.001	[5]	134P
21-SC- 46		(1120.545	+- 0.004)	0.000	[3]	(0.99987	+- 0.00001)	0.001	[5]	134P
24-CR- 51		(320.0842	+- 0.0009)	0.000	[3]	(0.0985	+- 0.0009)	0.914	[5]	1234P
25-MN- 54		(834.843	+- 0.006)	0.001	[3]	(0.99975	+- 0.00001)	0.001	[5]	1234P
25-MN- 56		(846.754	+- 0.020)	0.002	[18]	(0.9887	+- 0.0003)	0.030	[5]	3S
25-MN- 56		(1810.72	+- 0.04)	0.002	[18]	(0.272	+- 0.008)	2.941	[5]	3S
25-MN- 56		(2113.05	+- 0.04)	0.002	[18]	(0.143	+- 0.004)	2.797	[5]	3S
25-MN- 56		(2522.88	+- 0.06)	0.002	[18]	(0.0100	+- 0.0003)	3.000	[18]	3
25-MN- 56		(2657.45	+- 0.05)	0.002	[18]	(0.0066	+- 0.0002)	3.030	[18]	3
25-MN- 56		(2959.77	+- 0.06)	0.002	[18]	(0.0031	+- 0.0001)	3.226	[18]	3
25-MN- 56		(3369.60	+- 0.07)	0.002	[18]	(0.0017	+- 0.0001)	5.882	[18]	3
26-FE- 59		(142.652	+- 0.002)	0.001	[6]	(0.0102	+- 0.0004)	3.922	[19]	1
26-FE- 59		(192.349	+- 0.005)	0.003	[6]	(0.0308	+- 0.0010)	3.247	[19]	1
26-FE- 59		(334.99	+- 0.05)	0.015	[10]	(0.0027	+- 0.0001)	3.704	[19]	1
26-FE- 59		(382.5	+- 0.2)	0.052	[10]	(0.00018	+- 0.00003)	16.667	[19]	1
26-FE- 59		(1099.251	+- 0.004)	0.000	[6]	(0.565	+- 0.015)	2.655	[19]	1
26-FE- 59		(1291.596	+- 0.007)	0.001	[6]	(0.432	+- 0.011)	2.546	[19]	1
26-FE- 59		(1481.7	+- 0.1)	0.007	[10]	(0.00059	+- 0.00006)	10.169	[19]	1
27-CO- 56		(846.764	+- 0.006)	0.001	[3]	(0.99925	+- 0.00006)	0.006	[5]	1S
27-CO- 56		(1037.844	+- 0.004)	0.000	[3]	(0.1411	+- 0.0005)	0.354	[5]	1S
27-CO- 56		(1175.099	+- 0.008)	0.001	[3]	(0.0227	+- 0.0002)	0.881	[12]	1
27-CO- 56		(1238.287	+- 0.006)	0.000	[3]	(0.663	+- 0.005)	0.754	[5]	1S
27-CO- 56		(1360.206	+- 0.006)	0.000	[3]	(0.0426	+- 0.0002)	0.469	[5]	1S
27-CO- 56		(1771.350	+- 0.015)	0.001	[3]	(0.1548	+- 0.0004)	0.258	[5]	1S
27-CO- 56		(1810.722	+- 0.017)	0.001	[3]					
27-CO- 56		(1963.714	+- 0.012)	0.001	[3]					
27-CO- 56		(2015.179	+- 0.011)	0.001	[3]	(0.0303	+- 0.0004)	1.320	[12]	1
27-CO- 56		(2034.759	+- 0.011)	0.001	[3]	(0.0776	+- 0.0004)	0.515	[5]	1S
27-CO- 56		(2112.921	+- 0.010)	0.000	[3]					
27-CO- 56		(2113.117	+- 0.012)	0.001	[3]					
27-CO- 56		(2598.460	+- 0.010)	0.000	[3]	(0.1696	+- 0.0004)	0.236	[5]	1S
27-CO- 56		(3009.596	+- 0.017)	0.001	[3]					
27-CO- 56		(3201.954	+- 0.014)	0.000	[3]	(0.0318	+- 0.0008)	2.516	[12]	1
27-CO- 56		(3253.417	+- 0.014)	0.000	[3]	(0.0770	+- 0.0012)	1.558	[5]	1S
27-CO- 56		(3272.998	+- 0.014)	0.000	[3]	(0.018	+- 0.001)	5.556	[12]	1
27-CO- 56		(3451.154	+- 0.013)	0.000	[3]	(0.0093	+- 0.0003)	3.226	[12]	1
27-CO- 56		(3548.18	+- 0.12)	0.003	[12]	(0.0019	+- 0.0001)	5.263	[12]	1
27-CO- 57		14.41			[5]	(0.093	+- 0.002)	2.151	[6]	P

TABLE I (cont.)

NUCLIDE	DECAY MODE	ENERGY (keV) LEVEL DATA	UNCERTAINTY	PER CENT	REFERENCE	EMISSION PROBABILITY DATA	UNCERTAINTY	PER CENT	REFERENCE	COMMENTS
27-CO- 57		(122.06135	+- 0.00030)	0.000	[3]	(0.8563	+- 0.0015)	0.175	[5]	124P
27-CO- 57		(136.4743	+- 0.0005)	0.000	[3]	(0.1062	+- 0.0010)	0.942	[5]	124P
27-CO- 58		(810.775	+- 0.009)	0.001	[14]	(0.9944	+- 0.0002)	0.020	[5]	4P
27-CO- 58		(863.959	+- 0.009)	0.001	[14]	(0.0069	+- 0.0002)	2.899	[14]	4
27-CO- 58		(1674.730	+- 0.009)	0.001	[14]	(0.00519	+- 0.00004)	0.771	[14]	4
27-CO- 60		(1173.238	+- 0.004)	0.000	[3]	(0.9989	+- 0.0002)	0.020	[5]	1234P
27-CO- 60		(1332.502	+- 0.005)	0.000	[3]	(0.99983	+- 0.00001)	0.001	[5]	1234P
28-NI- 65		1482.			[4]	(0.235	+- 0.004)	1.702	[4]	3
29-CU- 64		(1345.77	+- 0.06)	0.004	[20]	(0.0077	+- 0.0006)	7.792	[20]	3
30-ZN- 65		(1115.546	+- 0.004)	0.000	[3]	(0.5065	+- 0.0020)	0.395	[5]	124P
34-SE- 75		(24.38	+- 0.03)	0.123	[14]	(0.0030	+- 0.0006)	20.000	[14]	3
34-SE- 75		(66.060	+- 0.0007)	0.001	[14]	(0.0113	+- 0.0002)	1.770	[14]	3
34-SE- 75		(80.92	+- 0.02)	0.025	[14]	(0.00008	+- 0.00002)	25.000	[14]	3
34-SE- 75		(96.734	+- 0.002)	0.002	[14]	(0.0349	+- 0.0007)	2.006	[14]	3
34-SE- 75		(121.119	+- 0.003)	0.002	[14]	(0.176	+- 0.002)	1.136	[14]	3
34-SE- 75		(136.002	+- 0.003)	0.002	[14]	(0.596	+- 0.005)	0.839	[14]	3
34-SE- 75		(198.596	+- 0.006)	0.003	[14]	(0.0151	+- 0.0002)	1.325	[14]	3
34-SE- 75		(264.656	+- 0.004)	0.002	[14]	(0.596	+- 0.003)	0.503	[14]	3
34-SE- 75		(279.538	+- 0.003)	0.001	[14]	(0.253	+- 0.003)	1.186	[14]	3
34-SE- 75		(303.924	+- 0.003)	0.001	[14]	(0.0134	+- 0.0002)	1.493	[14]	3
34-SE- 75		(400.657	+- 0.002)	0.000	[14]	(0.1160	+- 0.0015)	1.293	[14]	3
34-SE- 75		(419.0	+- 0.2)	0.048	[14]	(0.00012	+- 0.00002)	16.667	[14]	3
34-SE- 75		(469.1	+- 0.2)	0.043	[14]	(0.000032	+- 0.000006)	18.750	[14]	3
34-SE- 75		(572.5	+- 0.2)	0.035	[14]	(0.00038	+- 0.00002)	5.263	[14]	3
34-SE- 75		(617.6	+- 0.2)	0.032	[14]	(0.000045	+- 0.000002)	4.444	[14]	3
34-SE- 75		(821.7	+- 0.2)	0.024	[14]	(0.000013	+- 0.000002)	15.385	[14]	3
35-BR- 82		(92.184	+- 0.007)	0.008	[14]	(0.0072	+- 0.0003)	4.167	[14]	3
35-BR- 82		(137.23	+- 0.04)	0.029	[14]	(0.0012	+- 0.0005)	41.667	[14]	3
35-BR- 82		(221.48	+- 0.03)	0.014	[14]	(0.0227	+- 0.0005)	2.203	[14]	3
35-BR- 82		(273.47	+- 0.03)	0.011	[14]	(0.0081	+- 0.0003)	3.704	[14]	3
35-BR- 82		(554.348	+- 0.003)	0.001	[14]	(0.706	+- 0.003)	0.425	[14]	3
35-BR- 82		(606.33	+- 0.02)	0.003	[14]	(0.0125	+- 0.0007)	5.600	[14]	3
35-BR- 82		(619.106	+- 0.004)	0.001	[14]	(0.433	+- 0.003)	0.693	[14]	3
35-BR- 82		(698.374	+- 0.005)	0.001	[14]	(0.284	+- 0.004)	1.408	[14]	3
35-BR- 82		(776.517	+- 0.003)	0.000	[14]	(0.834	+- 0.002)	0.240	[14]	3
35-BR- 82		(827.828	+- 0.006)	0.001	[14]	(0.241	+- 0.003)	1.245	[14]	3
35-BR- 82		(951.95	+- 0.04)	0.004	[14]	(0.0038	+- 0.0002)	5.263	[14]	3
35-BR- 82		(1007.54	+- 0.03)	0.003	[14]	(0.0127	+- 0.0006)	4.724	[14]	3
35-BR- 82		(1044.002	+- 0.007)	0.001	[14]	(0.275	+- 0.006)	2.182	[14]	3
35-BR- 82		(1081.3	+- 0.1)	0.009	[14]	(0.0063	+- 0.0004)	6.349	[14]	3
35-BR- 82		(1317.476	+- 0.006)	0.000	[14]	(0.27	+- 0.008)	2.963	[14]	3
35-BR- 82		1426.				(0.0011	+- 0.0005)	45.455	[14]	3
35-BR- 82		(1474.884	+- 0.006)	0.000	[14]	(0.164	+- 0.002)	1.220	[14]	3
35-BR- 82		(1650.339	+- 0.008)	0.000	[14]	(0.0075	+- 0.0002)	2.667	[14]	3
35-BR- 82		(1779.58	+- 0.05)	0.003	[14]	(0.00116	+- 0.00003)	2.586	[14]	3

NUCLIDE	DECAY MODE	ENERGY (keV) LEVEL DATA	UNCERTAINTY	PER CENT	REFERENCE	EMISSION PROBABILITY DATA	UNCERTAINTY	PER CENT	REFERENCE	COMMENTS
36-KR- 85		(514.009	+- 0.012)	0.002	[14]	(0.00437	+- 0.00011)	2.517	[14]	3
38-SR- 85		(514.009	+- 0.012)	0.002	[14]	(0.988	+- 0.005)	0.506	[5]	234P
39-Y - 88		(898.042	+- 0.004)	0.000	[3]	(0.942	+- 0.004)	0.425	[5]	124P
39-Y - 88		(1836.063	+- 0.013)	0.001	[3]	(0.9930	+- 0.0005)	0.050	[5]	124P
39-Y - 88		(2734.087	+- 0.087)	0.003	[17]	(0.0072	+- 0.0007)	9.722	[14]	124
40-ZR- 95		(204.12	+- 0.02)	0.010	[11]	(0.0003	+- 0.0001)	33.333	[11]	13
40-ZR- 95		(235.69	+- 0.02)	0.008	[11]	(0.0029	+- 0.0005)	17.241	[11]	13
40-ZR- 95		(561.66	+- 0.02)	0.004	[11]	(0.00010	+- 0.00004)	40.000	[11]	13
40-ZR- 95		(724.199	+- 0.005)	0.001	[3]	(0.4415	+- 0.0020)	0.453	[5]	13S
40-ZR- 95		(756.729	+- 0.012)	0.002	[6]	(0.5450	+- 0.0025)	0.459	[5]	13S
41-NB- 94		(702.645	+- 0.006)	0.001	[3]	(0.9982	+- 0.0001)	0.010	[5]	12P
41-NB- 94		(871.119	+- 0.004)	0.000	[3]	(0.9989	+- 0.0001)	0.010	[5]	12P
41-NB- 95		(765.807	+- 0.006)	0.001	[7]	(0.9980	+- 0.0002)	0.020	[5]	4P
43-TC- 99M1		(140.511	+- 0.001)	0.001	[14]	(0.890	+- 0.002)	0.225	[5]	3S
47-AG-108M1		(433.936	+- 0.004)	0.001	[3]	(0.905	+- 0.007)	0.773	[16]	1
47-AG-108M1		(614.281	+- 0.004)	0.001	[3]	(0.910	+- 0.007)	0.769	[16]	1
47-AG-108M1		(722.929	+- 0.004)	0.001	[3]	(0.907	+- 0.008)	0.882	[16]	1
47-AG-110M1		(446.811	+- 0.003)	0.001	[14]	(0.0372	+- 0.0003)	0.806	[5]	1S
47-AG-110M1		(620.360	+- 0.003)	0.000	[14]	(0.0279	+- 0.0002)	0.717	[14]	1
47-AG-110M1		(657.7622	+- 0.0020)	0.000	[6]	(0.9440	+- 0.0010)	0.106	[5]	1S
47-AG-110M1		(677.623	+- 0.002)	0.000	[6]	(0.1040	+- 0.0008)	0.769	[5]	1S
47-AG-110M1		(687.015	+- 0.003)	0.000	[14]	(0.0644	+- 0.0003)	0.466	[5]	1S
47-AG-110M1		(706.682	+- 0.003)	0.000	[14]	(0.1660	+- 0.0010)	0.602	[5]	1S
47-AG-110M1		(744.277	+- 0.003)	0.000	[14]	(0.0470	+- 0.0004)	0.851	[5]	1S
47-AG-110M1		(763.944	+- 0.003)	0.000	[14]	(0.2239	+- 0.0008)	0.357	[5]	1S
47-AG-110M1		(818.031	+- 0.004)	0.000	[14]	(0.0732	+- 0.0004)	0.546	[5]	1S
47-AG-110M1		(884.685	+- 0.003)	0.000	[14]	(0.727	+- 0.003)	0.413	[5]	1S
47-AG-110M1		(937.493	+- 0.004)	0.000	[14]	(0.3431	+- 0.0012)	0.350	[5]	1S
47-AG-110M1		(1384.300	+- 0.004)	0.000	[14]	(0.2425	+- 0.0008)	0.330	[5]	1S
47-AG-110M1		(1475.788	+- 0.006)	0.000	[14]	(0.0399	+- 0.0002)	0.501	[5]	1S
47-AG-110M1		(1505.040	+- 0.005)	0.000	[14]	(0.1304	+- 0.0004)	0.307	[5]	1S
47-AG-110M1		(1562.302	+- 0.005)	0.000	[14]	(0.0118	+- 0.0001)	0.847	[14]	1
48-CD-109		(88.0341	+- 0.0011)	0.001	[6]	(0.0368	+- 0.0005)	1.359	[5]	24P
49-IN-111		(171.28	+- 0.03)	0.018	[21]	(0.902	+- 0.003)	0.333	[5]	4S
49-IN-111		(245.35	+- 0.04)	0.016	[21]	(0.940	+- 0.002)	0.213	[5]	4S
49-IN-111		(537.	+- 1.)	0.186	[21]	0.87			[14]	4
49-IN-113M1		(391.702	+- 0.004)	0.001	[14]	(0.649	+- 0.002)	0.308	[5]	3P
49-IN-115M1		336.23			[5]	(0.459	+- 0.002)	0.436	[5]	3P
50-SN-113		(255.115	+- 0.015)	0.006	[6]	(0.0182	+- 0.0008)	4.396	[22]	234

TABLE I (cont.)

NUCLIDE	DECAY MODE	ENERGY (keV) LEVEL DATA	UNCERTAINTY	PER CENT	REFERENCE	EMISSION PROBABILITY DATA	UNCERTAINTY	PER CENT	REFERENCE	COMMENTS
51-SB-124		(602.730	+- 0.003)	0.000	[3]	(0.9800	+- 0.0010)	0.102	[5]	1S
51-SB-124		(645.855	+- 0.002)	0.000	[3]	(0.0730	+- 0.0010)	1.370	[5]	1S
51-SB-124		(709.320	+- 0.013)	0.002	[17]	(0.0135	+- 0.0002)	1.481	[23]	1
51-SB-124		(713.781	+- 0.005)	0.001	[3]	(0.0227	+- 0.0003)	1.322	[23]	1
51-SB-124		(722.786	+- 0.004)	0.001	[3]	(0.1130	+- 0.0020)	1.770	[5]	1S
51-SB-124		(790.712	+- 0.006)	0.001	[3]	(0.0074	+- 0.0001)	1.351	[23]	1
51-SB-124		(968.201	+- 0.004)	0.000	[3]	(0.0189	+- 0.0002)	1.058	[23]	1
51-SB-124		(1045.131	+- 0.003)	0.000	[3]	(0.0184	+- 0.0004)	2.174	[23]	1
51-SB-124		(1325.512	+- 0.005)	0.000	[3]	(0.0163	+- 0.0004)	2.454	[23]	1
51-SB-124		(1355.175	+- 0.022)	0.002	[23]	(0.0104	+- 0.0004)	3.846	[23]	1
51-SB-124		(1368.164	+- 0.006)	0.000	[3]	(0.0262	+- 0.0005)	1.908	[23]	1
51-SB-124		(1436.563	+- 0.006)	0.000	[3]	(0.0123	+- 0.0005)	4.065	[23]	1
51-SB-124		(1690.980	+- 0.004)	0.000	[3]	(0.485	+- 0.003)	0.619	[5]	1S
51-SB-124		(2090.942	+- 0.007)	0.000	[3]	(0.0566	+- 0.0009)	1.590	[5]	1S
53-I -125		(35.4919	+- 0.0005)	0.001	[14]	(0.0660	+- 0.0010)	1.515	[5]	4P
54-XE-133		(79.623	+- 0.010)	0.013	[14]	(0.0027	+- 0.0003)	11.111	[14]	3
54-XE-133		(80.997	+- 0.003)	0.004	[6]	(0.380	+- 0.007)	1.842	[14]	3
54-XE-133		(160.613	+- 0.008)	0.005	[14]	(0.00066	+- 0.00005)	7.576	[14]	3
54-XE-133		(223.234	+- 0.012)	0.005	[14]	(0.0000012	+- 0.0000002)	16.667	[14]	3
54-XE-133		(302.853	+- 0.001)	0.000	[14]	(0.000048	+- 0.000003)	6.250	[14]	3
54-XE-133		(383.851	+- 0.003)	0.001	[14]	(0.000024	+- 0.000002)	8.333	[14]	3
55-CS-131		(355.	+- 6.)	1.690	[14]	1.0			[14]	
55-CS-134		(475.34	+- 0.02)	0.004	[14]	(0.0150	+- 0.0002)	1.333	[14]	3
55-CS-134		(563.23	+- 0.02)	0.004	[14]	(0.0838	+- 0.0003)	0.358	[14]	3
55-CS-134		(569.32	+- 0.02)	0.004	[14]	(0.1539	+- 0.0005)	0.325	[14]	3
55-CS-134		(604.69	+- 0.02)	0.003	[14]	(0.9763	+- 0.0004)	0.041	[5]	3P
55-CS-134		(795.84	+- 0.01)	0.001	[14]	(0.8552	+- 0.0004)	0.047	[5]	3P
55-CS-134		(801.93	+- 0.02)	0.002	[14]	(0.0870	+- 0.0002)	0.230	[14]	3
55-CS-134		(1038.555	+- 0.020)	0.002	[14]	(0.00991	+- 0.00004)	0.404	[14]	3
55-CS-134		(1167.92	+- 0.02)	0.002	[14]	(0.01792	+- 0.00008)	0.446	[14]	3
55-CS-134		(1365.16	+- 0.02)	0.001	[14]	(0.03015	+- 0.00013)	0.431	[14]	3
55-CS-134M1		(11.28	+- 0.02)	0.177	[14]	(0.0094	+- 0.0009)	9.574	[14]	
55-CS-134M1		(127.42	+- 0.06)	0.047	[14]	(0.126	+- 0.004)	3.175	[14]	
55-CS-134M1		(138.70	+- 0.03)	0.022	[14]	(0.00004	+- 0.00001)	25.000	[14]	
55-CS-137		32.1			[17]	(0.0557	+- 0.0016)	2.873	[14]	
55-CS-137		36.4			[17]	(0.0107	+- 0.0004)	3.738	[14]	
55-CS-137		37.3			[17]	(0.0025	+- 0.0001)	4.000	[14]	
55-CS-137		(661.660	+- 0.003)	0.000	[14]	(0.852	+- 0.001)	0.117	[5]	1234P
56-BA-133		(53.161	+- 0.001)	0.002	[8]	(0.0219	+- 0.0003)	1.370	[5]	23S
56-BA-133		(79.623	+- 0.010)	0.013	[12]	(0.0262	+- 0.0007)	2.672	[5]	S
56-BA-133		(80.997	+- 0.003)	0.004	[17]	(0.341	+- 0.005)	1.466	[5]	23S
56-BA-133		(160.613	+- 0.008)	0.005	[12]	(0.0062	+- 0.0002)	3.226	[12]	23
56-BA-133		(223.234	+- 0.012)	0.005	[12]	(0.00447	+- 0.00020)	4.474	[12]	23
56-BA-133		(276.398	+- 0.002)	0.001	[8]	(0.0716	+- 0.0004)	0.559	[5]	23S
56-BA-133		(302.853	+- 0.001)	0.000	[8]	(0.1831	+- 0.0007)	0.382	[5]	23S
56-BA-133		(356.017	+- 0.002)	0.001	[8]	(0.6200	+- 0.0014)	0.226	[5]	23S

NUCLIDE	DECAY MODE	LEVEL ENERGY (keV) DATA	UNCERTAINTY	PER CENT	REFERENCE	EMISSION PROBABILITY DATA	UNCERTAINTY	PER CENT	REFERENCE	COMMENTS
56-BA-133		(383.851	+- 0.003)	0.001	[8]	(0.0892	+- 0.0005)	0.561	[5]	23S
56-BA-137M1		(661.660	+- 0.003)	0.000	[14]	(0.9007	+- 0.0004)	0.044	[14]	
58-CE-139		(165.857	+- 0.006)	0.004	[14]	(0.799	+- 0.001)	0.125	[5]	234P
58-CE-141		(145.4442	+- 0.0014)	0.001	[6]	(0.486	+- 0.004)	0.823	[5]	234P
58-CE-144		(33.622	+- 0.010)	0.030	[14]	(0.0029	+- 0.0002)	6.897	[14]	14
58-CE-144		(40.89	+- 0.05)	0.122	[14]	(0.0039	+- 0.0006)	15.385	[14]	14
58-CE-144		(53.432	+- 0.010)	0.019	[14]	(0.00095	+- 0.00005)	5.263	[14]	14
58-CE-144		(59.03	+- 0.03)	0.051	[14]	(0.000012	+- 0.000002)	16.667	[14]	14
58-CE-144		(80.106	+- 0.005)	0.006	[14]	(0.0112	+- 0.0013)	11.607	[14]	14
58-CE-144		(99.963	+- 0.020)	0.020	[14]	(0.00039	+- 0.00003)	7.692	[14]	14
58-CE-144		(133.544	+- 0.005)	0.004	[14]	(0.110	+- 0.002)	1.818	[14]	14
63-EU-152		(121.7824	+- 0.0004)	0.000	[3]	(0.2840	+- 0.0023)	0.810	[5]	1234S
63-EU-152		(244.6989	+- 0.0010)	0.000	[3]	(0.0751	+- 0.0007)	0.932	[5]	1234S
63-EU-152		(344.2811	+- 0.0019)	0.001	[3]	(0.2658	+- 0.0019)	0.715	[5]	1234S
63-EU-152		(411.115	+- 0.005)	0.001	[17]	(0.0223	+- 0.0002)	0.897	[5]	1234S
63-EU-152		(443.976	+- 0.005)	0.001	[17]	(0.0312	+- 0.0003)	0.962	[5]	1234S
63-EU-152		(778.903	+- 0.006)	0.001	[17]	(0.1296	+- 0.0007)	0.540	[5]	1234S
63-EU-152		(964.131	+- 0.009)	0.001	[17]	(0.1462	+- 0.0006)	0.410	[5]	1234S
63-EU-152		(1085.914	+- 0.013)	0.001	[17]	(0.1014	+- 0.0006)	0.592	[5]	1234S
63-EU-152		(1112.116	+- 0.017)	0.002	[17]	(0.1354	+- 0.0006)	0.443	[5]	1234S
63-EU-152		(1408.011	+- 0.014)	0.001	[17]	(0.2085	+- 0.0008)	0.384	[5]	1234S
64-GD-153		(69.6734	+- 0.0020)	0.003	[3]	(0.0232	+- 0.0015)	6.466	[25]	1
64-GD-153		(83.367	+- 0.003)	0.004	[24]	(0.00193	+- 0.00022)	11.399	[25]	1
64-GD-153		(97.4316	+- 0.0030)	0.003	[3]	(0.276	+- 0.015)	5.435	[25]	1
64-GD-153		(103.1807	+- 0.0030)	0.003	[3]	(0.196	+- 0.011)	5.612	[25]	1
69-TM-170		(84.25510	+- 0.00030)	0.000	[3]	(0.0326	+- 0.0016)	4.908	[27]	1
70-YB-169		(63.1208	+- 0.0002)	0.000	[26]	(0.43695	+- 0.01500)	3.433	[26]	3
70-YB-169		(93.6151	+- 0.0004)	0.000	[26]	(0.02656	+- 0.00087)	3.276	[26]	3
70-YB-169		(109.7802	+- 0.0003)	0.000	[26]	(0.17345	+- 0.00506)	2.917	[26]	3
70-YB-169		(118.1901	+- 0.0010)	0.001	[26]	(0.01878	+- 0.00053)	2.822	[26]	3
70-YB-169		(130.5239	+- 0.0004)	0.000	[26]	(0.11098	+- 0.00490)	4.415	[26]	3
70-YB-169		(177.2144	+- 0.0005)	0.000	[26]	(0.21429	+- 0.00602)	2.809	[26]	3
70-YB-169		(197.9581	+- 0.0006)	0.000	[26]	(0.349	+- 0.008)	2.292	[26]	3
70-YB-169		(261.0788	+- 0.0007)	0.000	[26]	(0.01895	+- 0.00050)	2.639	[26]	3
70-YB-169		(307.7382	+- 0.0008)	0.000	[26]	(0.10784	+- 0.00160)	1.484	[26]	3
73-TA-182		(31.7378	+- 0.004)	0.013	[17]	(0.00892	+- 0.00021)	2.354	[9]	12
73-TA-182		(42.7154	+- 0.006)	0.014	[17]	(0.00266	+- 0.00008)	3.008	[9]	12
73-TA-182		57.98			[9]	(0.2802	+- 0.0052)	1.856	[9]	
73-TA-182		(65.72247	+- 0.00014)	0.000	[17]					12
73-TA-182		(67.75001	+- 0.00020)	0.000	[3]	(0.571	+- 0.013)	2.277	[9]	12
73-TA-182		(84.6808	+- 0.0003)	0.000	[3]	(0.0263	+- 0.0010)	3.802	[9]	12
73-TA-182		(100.10653	+- 0.00030)	0.000	[3]	(0.1423	+- 0.0025)	1.757	[5]	12S
73-TA-182		(113.6723	+- 0.0004)	0.000	[3]	(0.0187	+- 0.0006)	3.209	[9]	12
73-TA-182		(116.4186	+- 0.0007)	0.001	[3]	(0.00445	+- 0.00015)	3.371	[9]	12

TABLE I (cont.)

NUCLIDE	DECAY MODE	ENERGY (keV) LEVEL DATA	UNCERTAINTY	PER CENT	REFERENCE	EMISSION PROBABILITY DATA	UNCERTAINTY	PER CENT	REFERENCE	COMMENTS
73-TA-182		(152.4308	+- 0.0005)	0.000	[3]	(0.0702	+- 0.0008)	1.140	[5]	12S
73-TA-182		(156.3874	+- 0.0005)	0.000	[3]	(0.0263	+- 0.0005)	1.901	[9]	12
73-TA-182		(179.3948	+- 0.0005)	0.000	[3]	(0.0309	+- 0.0004)	1.294	[9]	12
73-TA-182		(198.3530	+- 0.0006)	0.000	[3]	(0.0144	+- 0.0002)	1.389	[9]	12
73-TA-182		(222.1099	+- 0.0006)	0.000	[3]	(0.0757	+- 0.0008)	1.057	[5]	12S
73-TA-182		(229.3220	+- 0.0009)	0.000	[3]	(0.0364	+- 0.0005)	1.374	[9]	12
73-TA-182		(264.0755	+- 0.0008)	0.000	[3]	(0.0362	+- 0.0006)	1.657	[9]	12
73-TA-182		(1121.301	+- 0.005)	0.000	[3]	(0.3530	+- 0.0020)	0.567	[6]	12S
73-TA-182		(1189.050	+- 0.005)	0.000	[3]	(0.1642	+- 0.0010)	0.609	[5]	12S
73-TA-182		(1221.408	+- 0.005)	0.000	[3]	(0.2720	+- 0.0022)	0.809	[5]	12S
73-TA-182		(1231.016	+- 0.005)	0.000	[3]	(0.1157	+- 0.0008)	0.691	[5]	12S
73-TA-182		(1257.418	+- 0.005)	0.000	[3]	(0.0150	+- 0.0002)	1.333	[9]	12
73-TA-182		(1289.156	+- 0.005)	0.000	[3]	(0.0136	+- 0.0002)	1.471	[9]	12
77-IR-192		(136.3434	+- 0.0005)	0.000	[3]	(0.0018	+- 0.0001)	5.556	[13]	1
77-IR-192		(205.7955	+- 0.0005)	0.000	[3]	(0.0331	+- 0.0006)	1.813	[13]	1
77-IR-192		(295.95821	+- 0.0008)	0.000	[3]	(0.287	+- 0.001)	0.348	[5]	1S
77-IR-192		(308.45685	+- 0.0008)	0.000	[3]	(0.298	+- 0.001)	0.336	[5]	1S
77-IR-192		(316.50800	+- 0.0008)	0.000	[3]	(0.830	+- 0.003)	0.361	[5]	1S
77-IR-192		(468.0715	+- 0.0012)	0.000	[12]	(0.477	+- 0.002)	0.419	[5]	1S
77-IR-192		(484.5779	+- 0.0013)	0.000	[3]	(0.0316	+- 0.0003)	0.949	[12]	1
77-IR-192		(588.5851	+- 0.0016)	0.000	[3]	(0.0449	+- 0.0002)	0.445	[5]	1S
77-IR-192		(604.41455	+- 0.0016)	0.000	[3]	(0.0811	+- 0.0004)	0.493	[5]	1S
77-IR-192		(612.46569	+- 0.0016)	0.000	[3]	(0.0528	+- 0.0003)	0.568	[5]	1S
77-IR-192		(884.5423	+- 0.0020)	0.000	[3]	(0.0029	+- 0.0001)	3.448	[12]	1
79-AU-198		(411.8044	+- 0.0011)	0.000	[3]	(0.9556	+- 0.0007)	0.073	[6]	1234P
79-AU-198		(675.8875	+- 0.0019)	0.000	[3]	(0.0082	+- 0.0003)	3.659	[14]	1234
79-AU-198		(1087.6905	+- 0.0029)	0.000	[6]	(0.00167	+- 0.00009)	5.389	[14]	1234
80-HG-203		(70.8319	+- 0.0008)	0.001	[14]	(0.038	+- 0.001)	2.632	[14]	
80-HG-203		(72.8715	+- 0.0009)	0.001	[14]	(0.064	+- 0.002)	3.125	[14]	
80-HG-203		82.4			[14]	(0.022	+- 0.001)	4.545	[14]	
80-HG-203		85.2			[14]	(0.0063	+- 0.0003)	4.762	[14]	
80-HG-203		(279.1967	+- 0.0012)	0.000	[6]	(0.8150	+- 0.0008)	0.098	[5]	1234P
83-BI-207		(569.702	+- 0.002)	0.000	[3]	(0.979	+- 0.001)	0.102	[5]	1S
83-BI-207		(1063.662	+- 0.004)	0.000	[3]	(0.741	+- 0.003)	0.405	[5]	1S
83-BI-207		(1770.237	+- 0.010)	0.001	[3]	(0.0687	+- 0.0004)	0.582	[5]	1S
90-TH-228		(84.371	+- 0.003)	0.004	[17]	(0.01248	+- 0.00029)	2.324	[15]	
90-TH-228		(131.610	+- 0.004)	0.003	[17]	(0.00128	+- 0.00015)	11.719	[15]	1
90-TH-228		(166.407	+- 0.004)	0.002	[17]	(0.00107	+- 0.00002)	1.869	[15]	1
95-AM-241		(26.345	+- 0.001)	0.004	[17]	(0.0241	+- 0.0005)	2.075	[5]	24P
95-AM-241		(33.195	+- 0.011)	0.033	[17]	(0.00103	+- 0.00011)	10.680	[17]	24
95-AM-241		(43.423	+- 0.020)	0.046	[17]	(0.00057	+- 0.00018)	31.579	[17]	24
95-AM-241		(59.537	+- 0.001)	0.002	[17]	(0.359	+- 0.003)	0.836	[5]	24P

REFERENCES

[1] INTERNATIONAL ATOMIC ENERGY AGENCY, Nuclear Data Standards for Nuclear Measurements, Technical Reports Series No. 227, IAEA, Vienna (1983).

[2] INDC/NEANDC Nuclear Standards File, 1978, IAEA/International Nuclear Data Committee, Vienna, Rep. INDC–30/L+Sp (1980).

[3] HELMER, R.G., VAN ASSHE, P.H.M., VAN DER LEUN, C., Recommended standards for gamma-ray energy calibration, At. Data Nucl. Data Tables **24** (1979) 39-48.

[4] RUTLEDGE, A.R., SMITH, L.V., MERRITT, J.S., Decay Data for Radionuclides Used for the Calibration of X- and γ- Ray Spectrometers, Atomic Energy of Canada Ltd, Chalk River Nuclear Labs, Chalk River, Ontario, Rep. AECL-6692 (1980).

[5] VANINBROUKX, R., "Emission probabilities of selected gamma rays for radionuclides used as detector-calibration standards", Nuclear Standard Reference Data (Proc. IAEA - OECD/NEANDC Advisory Group Meeting Geel, Belgium, 1984), IAEA-TECDOC-335, IAEA, Vienna (1985) 403–412.

[6] HELMER, R.G., GREENWOOD, R.C., GEHRKE, R.J., Nucl. Instrum. Methods **155** (1978) 189.

[7] GREENWOOD, R.C., HELMER, R.G., GEHRKE, R.J., Nucl. Instrum. Methods **159** (1979) 465.

[8] HELMER, R.G., CAFFREY, A.J., GEHRKE, R.J., GREENWOOD, R.C., Nucl. Instrum. Methods **188** (1981) 671.

[9] SCHOETZIG, U., DEBERTIN, K., WALZ, K.F., Nucl. Instrum. Methods **169** (1980) 43.

[10] Table of Radionuclides (LAGOUTINE, F., Evaluator), CEA Centre d'études nucléaires de Saclay, Laboratoire de métrologie des rayonnements ionisants, Gif-sur-Yvette (1979).

[11] Table of Radionuclides (LAGOUTINE, F., Evaluator), CEA Centre d'études nucléaires de Saclay, Laboratoire de métrologie des rayonnements ionisants, Gif-sur-Yvette (1977).

[12] Table of Radionuclides (COURSOL, N., LAGOUSTINE, F., Evaluators), CEA Centre d'études nucléaires de Saclay, Laboratoire de métrologie des rayonnements ionisants, Gif-sur-Yvette (1980).

[13] COURSOL, N., Private communication, CEA Centre d'études nucléaires de Saclay, Laboratoire de métrologie des rayonnements ionisants, Gif-sur-Yvette, 1981.

[14] COURSOL, N., Private communication, CEA Centre d'études nucléaires de Saclay, Laboratoire de métrologie des rayonnements ionisants, Gif-sur-Yvette, 1982.

[15] COURSOL, N., Private communication, CEA Centre d'études nucléaires de Saclay, Laboratoire de métrologie des rayonnements ionisants, Gif-sur-Yvette, 1984.

[16] YOSHIZAWA, Y., *et al.*, Evaluation of Gamma-ray Intensities, Japan Atomic Energy Research Institute, Tokyo, Rep. JAERI-M-8811 (1980).

[17] Table of Isotopes, 7th edn (LEDERER, C.M., SHIRLEY, V.S., Eds), Wiley, New York (1978).

[18] AUBLE, R.L., Mass chain evaluation A=56, Nucl. Data Sheets **20** 3 (1977) 253.

[19] ANDERSSON, P., EKSTROEM, L.P., LYTTKENS, J., Mass chain evaluation A=59, Nucl. Data Sheets **39** 4 (1983) 641.

[20] HALBERT, M.L., Mass chain evaluation A=64, Nucl. Data Sheets **28** 2 (1979) 179.

[21] HARMATZ, B., Mass chain evaluation A=111, Nucl. Data Sheets **27** 3 (1979) 453.

[22] LYTTKENS, J., et al., Mass chain evaluation A=113, Nucl. Data Sheets **33** 1 (1981) 1.

[23] TAMURA, T., MIYANO, K., OHAYA, H., Mass chain evaluation A=124, Nucl. Data Sheets **41** (1984) 413.

[24] Handbook of Radioactivity Measurement Procedures (MARTIN, M.J., Ed.), National Council on Radiation Protection and Measurements, Washington, DC, Rep. 58 (1978), Appendix.

[25] LEE, M.A., Mass chain evaluation A=153, Nucl. Data Sheets **37** (1982) 487.
[26] SHIRLEY, V., Mass chain evaluation A=169, Nucl. Data Sheets **36** 4 (1982) 443.
[27] SCHMORAK, M.R., Mass chain evaluation A=170, Nucl. Data Sheets **15** 3 (1975) 371.

Part 2
NEUTRON ACTIVATION

2-1. THERMAL NEUTRON CROSS-SECTIONS AND INFINITE DILUTION RESONANCE INTEGRALS

E. GRYNTAKIS, D.E. CULLEN, G. MUNDY
Nuclear Data Section,
Division of Research and Laboratories,
International Atomic Energy Agency,
Vienna

Abstract

THERMAL NEUTRON CROSS-SECTIONS AND INFINITE DILUTION RESONANCE INTEGRALS.

The compilation comprises recommended values for thermal neutron cross-sections and resonance integrals (including the 1/v contribution) of nuclides (hydrogen to fermium) for neutron capture and fission reactions. The main gamma rays of neutron capture, their absolute intensities and, for the non-1/v nuclide, the $g(T_n = 20°C)$ Westcott factors are also given.

1. INTRODUCTION

The table of resonance integrals presented in this chapter is based on the compilations of Gryntakis and Kim [1], which include all experimental, calculated and recommended values of resonance integrals available in the literature up to August 1981. Using the resonance integrals from this compilation, together with some new results (published up to January 1985), the recommended values of resonance integrals for nuclides from hydrogen to fermium have been evaluated here. The given values are in most cases the mean values of the existing experimental results, while the given error is the standard deviation of these results. In some cases, because of the large disagreement between the few existing results, the recommended value was selected based on a single measurement. Whenever possible the isotopic thermal neutron cross-sections and resonance integrals were renormalized in order to be in agreement with the corresponding values of the natural element. For most of the thermal cross-sections, the recommended values are those given in Ref. [6]. Most of the values of the $g(T_n = 20°C)$ Westcott factors are taken from Ref. [307], in which the $g(T_n)$ functions for about 50 (n,γ) and (n,f) reactions of non-1/v nuclides were calculated for the temperature range 0 to 2000°C.

Some radioanalytical laboratories have recently introduced in activation analysis the concept of the effective resonance energy, first proposed by Ryves (see Ref. [1] in the Annex) for the correction of the epithermal flux to an ideal

1/E flux. A paper by F. De Corte, giving explanations on the calculations of the effective resonance energies, is included here as an annex.

All of the resonance integrals given in Table II are from the cadmium cut-off energy (E_c = 0.5 eV) to infinity and include the 1/v contribution. The user should not confuse these with the excess resonance integrals (the 1/v contributions excluded) or with the resonance integrals from μkT energy. The theoretical and physical meanings of the different resonance integrals, and the methods for their determination, are explained in Ref. [1] and for convenience have been reproduced below.

2. DEFINITION OF A RESONANCE INTEGRAL

The microscopic cross-section averaged over a pure 1/E flux is the resonance integral:

$$I = \int_{E_1}^{E_2} \sigma(E)dE/E \quad \text{(for the 1/E spectrum)} \tag{1}$$

where E_1 and E_2 are the lower and the upper limits of the 1/E flux, respectively.

When the $\sigma(E)$ function for a specific nuclide reaction is known, the resonance integral can be easily calculated using Eq. (1). Theoretically, the $\sigma(E)$ function can be determined from the following Breit-Wigner formula [413], or by similar formulas:

$$\sigma(E) = \frac{\lambda^2}{4\pi} g \sqrt{E_r/E} \frac{\Gamma_n \Gamma_\gamma}{(E_r - E)^2 + (\Gamma/2)^2} \tag{2}$$

where λ is the de Broglie wavelength, g is a statistical factor, E_r is the resonance energy and Γ_n, Γ_γ and Γ are the neutron, radiative and total widths, respectively.

In the usual manner of determining the resonance integral experimentally, the target nuclide is irradiated in a reactor spectrum which can be assumed to be the sum of two components, a Maxwellian distribution corresponding to T(°K) and a 1/E epithermal flux with lower limit μkT, where k is the Boltzmann constant and μ varies with the type of reactor. For D_2O reactors, μ is about 5 and for some graphite reactors about 3, so that at T = 293.6°K, μkT will in these cases be equal to about 0.126 and 0.076 eV, respectively. The two spectra are continuous and overlap each other at a neutron energy of about 0.5 eV. When a nuclide is irradiated in this spectrum, the activation result of the resonance integral must be corrected by subtracting the contribution of the Maxwellian component and thus the expression becomes

$$I_1' = \int_{\mu kT}^{\infty} [\sigma(E) - g(T)\sigma_0 \sqrt{E_0/E}]\, dE/E \tag{3}$$

where g(T) is a parameter depending on the neutron temperature (see Section 3) and $E_0 = 0.0253$ eV.

The usual experimental method of separating the thermal cross-section due to the Maxwellian spectrum and the resonance integral due to the 1/E spectrum is to irradiate a nuclide under a Cd filter which absorbs neutrons below the effective Cd cut-off energy (E_c). Calculations of this cut-off energy for various shapes and thicknesses of the Cd filter have been made by several authors [207, 292, 379]. In these calculations, it is observed that a small cylindrical Cd filter of 1 mm thickness has a cut-off energy of about 0.55 eV. Under this condition, the resonance integral is divided into two parts: one between μkT and E_c and the other from E_c to ∞, so that Eq. (3) becomes

$$I_1' = \int_{\mu kT}^{E_c} [\sigma(E) - g(T)\sigma_0 \sqrt{E_0/E}]\, dE/E$$

$$+ \int_{E_c}^{\infty} [\sigma(E) - g(T)\sigma_0 \sqrt{E_0/E}]\, dE/E$$

$$= [\Delta I - \Delta I(1/v)] + [I - I(1/v)] = \Delta I' + I' \tag{4}$$

where I' is the epicadmium resonance integral (excluding the 1/v part) and $\Delta I'$ is the part (shielded by a Cd filter) which depends on the neutron temperature and is negligibly small for nuclides obeying the 1/v law in the thermal energy region. However, for those nuclides where a resonance peak lies near the cut-off energy, such as ^{113}Cd, ^{151}Eu, ^{176}Lu, ^{182}Ta, ^{191}Ir, ^{231}Pa, ^{239}Pu, etc., the value of $\Delta I'$ becomes very large and cannot be neglected. When the resonance peak appears near the cut-off energy ($E_r \cong E_c$), $\Delta I'$ can be calculated from the expression [368]:

$$\Delta I'/I' = (\Gamma/\pi E_r)[(2/\sqrt{E_r})(\sqrt{E_c} - \sqrt{\mu kT})$$

$$- (g-1)\sqrt{E_r}(1/\sqrt{\mu kT} - 1/\sqrt{E_c})] \tag{5}$$

where Γ and E_r are the resonance width and the resonance energy, respectively. Since $\Delta I'$ is a temperature-dependent term, its evaluation must follow the temperature of the neutron spectrum.

TABLE I. RESONANCE INTEGRALS

Symbol	Meaning	Limits	Remarks
I'	Epicadmium excess resonance integral	E_c to ∞	Cd filter method: Eq. (4)
$I(1/v)$	1/v part of resonance integral	E_c to ∞	Eq. (6)
I	Epicadmium resonance integral including the 1/v part	E_c to ∞	$I = I' + I(1/v)$
I_1'	Excess resonance integral	μkT to ∞	Method without Cd filter (Eq. (4))
$\Delta I'$	Excess resonance integral below E_c energy	μkT to E_c	$\Delta I' = I_1' - I'$

The data from available literature on the epicadmium resonance integral represent either the value of I' or I, which then includes the 1/v part $[I(1/v)]$. This 1/v tailing can be easily calculated if the cut-off energy is known:

$$I(1/v) = I - I' = \int_{E_c}^{\infty} g(T)\sigma_0 \sqrt{E_0/E}\, dE/E \cong 2g(T)\sigma_0 \sqrt{E_0/E_c} \qquad (6)$$

The meanings of the several resonance integrals are summarized in Table I.

3. EXPERIMENTAL MEASUREMENT WITH A Cd FILTER

3.1. The Westcott method

According to Westcott (Ref. [292]), the reaction rate per target atom is given by

$$R = \phi_0 \hat{\sigma}(T) = nv_0 \sigma_0 [g(T) + r\sqrt{T/T_0} s_0] \qquad (7)$$

where

$\phi_0 = nv_0$ is the neutron flux defined as the total neutron density times the 2200 m/s velocity;

$\hat{\sigma}(T)$ is the effective cross-section:

σ_0 is the thermal cross-section for 2200 m/s neutrons;

g(T) is the parameter which represents the departure of the cross-section from the 1/v law in the thermal region (g(T) = 1 if the nuclide obeys the 1/v law in this energy region) and which can be calculated from the expression:

$$g(T) = (1/\sigma_0 v_0) \int_0^\infty [(4/\sqrt{\pi})(v^3/v_T^3) \exp(-v^2/v_T^2)]\sigma(v)dv \qquad (8)$$

or

$$g(T) = \frac{2}{\sqrt{\pi}\sqrt{E_0}\sigma_0} \int_0^\infty \sqrt{E}\,\sigma(E)\sqrt{E/E_T}\exp(-E/E_T)dE/E_T \qquad (8a)$$

where $E_T = E_0 T/T_0$, $E_0 = 0.0253$ eV and $T_0 = 293.6°K$.

The g(T) functions for about 50 non-1/v reactions of the (n,γ), (n,f) and (n, abs) types have been calculated in the temperature range from 0 to 2000°C in Ref. [307]. The $r\sqrt{T/T_0}$ is the epithermal index which denotes the strength of the epithermal flux. It is zero for a pure thermal flux and can be determined with the knowledge of the Cd ratio (CR) of a monitor nuclide:

$$r\sqrt{T/T_0} = g(T)/[(CR-1)s_0 + 4\,g(T)CR\sqrt{E_0/\pi E_c}] \qquad (9)$$

s_0 is the parameter which represents the ratio of the resonance integral and thermal cross-section such that

$$s_0 = \frac{2}{\sqrt{\pi}\sigma_0} \int_{\mu kT}^\infty [\sigma(E) - g(T)\sigma_0\sqrt{E_0/E}]dE/E = (2/\sqrt{\pi})(I_1'/\sigma_0) \qquad (10)$$

The epicadmium resonance integral (I′) can be determined by measuring the CR of the nuclide of interest at the irradiation position, where the epithermal index is already known:

$$(2/\sqrt{\pi})(I'/\sigma_0) = [1/CR-1)][g(T)/r\sqrt{T/T_0} - 4\,g(T)\,CR\sqrt{E_0/\pi E_c}] \qquad (11)$$

The epithermal index can be determined either using Eq. (9) or from the irradiation without Cd cover of two different monitor nuclides, one sensitive to thermal activation and the other sensitive to epithermal activation [179, 382]:

$$r\sqrt{T/T_0} = [g_1(T)\sigma_{01} - g_2(T)\sigma_{02}R_{1/2}]/(s_{02}\sigma_{02}R_{1/2} - s_{01}\sigma_{01}) \quad (12)$$

where $R_{1/2} = \hat{\sigma}_1/\hat{\sigma}_2$, which may easily be determined by the activity ratio of monitors 1 and 2.

3.2. The common method

This method, theoretically less rigorous, but commonly used (see Refs [207] and [146]),defines the reaction rate by

$$R = \phi_{th}\sigma_{th} + \phi_{epi}I \quad (13)$$

where

σ_{th}, I are the subcadmium and epicadmium cross-sections, respectively;
ϕ_{th} is the neutron flux defined as the thermal neutron density times the 2200 m/s neutron velocity;
ϕ_{epi} is the epithermal flux per unit ln(E).

From the knowledge of the Cd ratio of a monitor nuclide the ratio of the epicadmium flux can be determined as

$$\frac{\phi_{epi}}{\phi_{th}} = \frac{\sigma_{th}}{I(CR-1)} \quad (14)$$

From Eqs (7) and (13) it follows that

$$\sigma_{th} = g(T)\sigma_0 + \frac{\phi_{epi}}{\phi_{th}}(1 - 2\sqrt{E_0 - E_c})g(T)\sigma_0 \quad (15)$$

or

$$\sigma_{th} = g(T)\sigma_0 + \frac{\phi_{epi}}{\phi_{th}}[\Delta I' - I(1/v)] \quad (15a)$$

The quantity $[\Delta I' - I(1/v)]$ results in a positive or negative value depending on whether a nuclide follows the 1/v law or not. When the activation is performed in a reactor neutron spectrum with low epithermal flux ($\phi_{epi} \ll \phi_{th}$), $\sigma_{th} \cong g(T)\sigma_0$. The epicadmium resonance integral, including the 1/v tailing, can then be determined with the knowledge of the Cd ratios for the nuclide of interest (x) and the monitor (s):

$$I_x = I_s[(CR-1)_s\sigma_{thx}]/[(CR-1)_x\sigma_{ths}] \quad (16)$$

Many authors often assume that $\sigma_{th} = \sigma_0$ in order to calculate the epicadmium resonance integral (I). However, such an assumption is not completely justified, unless the nuclide obeys the 1/v law and the activation is undertaken in a well thermalized neutron spectrum ($\phi_{epi} \ll \phi_{th}$). For obvious reasons, it is clear that the epicadmium resonance integral thus determined should not be considered as a constant physical parameter [379]. The quantity of the 1/v tailing included in the epicadmium resonance integral varies with respect to the Cd cut-off energy (E_c), which is a function of the thickness of Cd, its shape, neutron energy and angle of incidence and also of the neutron temperature (see Eq. (6)).

4. EXPERIMENTAL MEASUREMENT WITHOUT A Cd FILTER

When the evaluation of the resonance integral is very sensitive to the Cd cut-off energy (E_c) due to the presence of low energy resonances which contribute significantly to the total resonance integral, the use of a Cd filter does not lead to an appropriate differentiation of the thermal cross-section and resonance integral. On the contrary, the measured value of the resonance integral is sharply reduced by the absorption of neutrons near the Cd cut-off energy. The solution to this problem relies on the special method which differentiates the neutron spectrum without the use of a Cd filter, but with knowledge of the relationship between the two different neutron spectra [179].

Looking at Eq. (7), one notices that the effective cross-section varies as a function of g(T) and epithermal index ($r\sqrt{T/T_0}$), which are temperature-dependent quantities. When irradiation is performed in two different neutron spectra having different neutron temperatures and epithermal components, the constant value s_0 can be determined from the knowledge of the ratio between effective cross-sections, provided that g(T) and the epithermal indices are known for the two spectra:

$$s_0 = (2\sqrt{\pi})(I_1'/\sigma_0) = [R_{1/2}\,g_2(T) - g_1(T)]/[(r\sqrt{T/T_0})_1 - R_{1/2}\,(r\sqrt{T/T_0})_2] \qquad (17)$$

where $R_{1/2}$ is equal to $\hat{\sigma}_1/\hat{\sigma}_2$ from two different irradiation positions.

With Eq. (17) it is possible to determine directly the I_1' value, which otherwise can only be evaluated through tedious and approximate corrections for neutron attenuation, absorption and perturbation by the Cd filter used.

Explanation of the columns in Table II is given on p. 248.

TABLE II. RECOMMENDED VALUES FOR THERMAL NEUTRON CROSS-SECTIONS AND RESONANCE INTEGRALS OF NUCLIDES FOR NEUTRON CAPTURE AND FISSION REACTIONS

TARGET NUCLIDE		A+1 NUCLIDE		TYPE OF REACTION	THERMAL CROSS-SECTIONS (b) AND $g(T)$ FACTOR	RESONANCE INTEGRALS (b)	RESONANCE INTEGRALS: REFERENCES	MAIN GAMMA RAYS FOR A+1 NUCLIDE ENERGY (keV) (ABSOLUTE INTENSITY: %)
Z-SYMBOL-A	ABUNDANCE (%) OR HALF-LIFE	HALF-LIFE	ISOMER STATE IT (%)					
1-H -NAT	-	-	-	ACT	0.3326+-0.0007	0.1489		
1	99.985	-		ACT	0.3326+-0.0007	0.1489	409	
2	0.015	12.346Y		ACT	(0.519+-0.007)E-3	6.298E-4	409	
3	*12.346Y			ACT	<0.006E-3			
2-HE-NAT	-	-	-	ACT	(0.040+-0.010)E-9			
				ABS	0.0069+-0.0001	0.0031+-0.0001		
3	1.3E-4	-		ACT	(0.031+-0.009)E-3			
				N,P	5333+-7	2401+-10	6 409	
4	99.99987			ACT	0.0			
3-LI-NAT	-	-	-	ACT	0.0448+-0.0030			
				ABS	70.5+-0.3	32	11	
6	7.5	-		ACT	0.0385+-0.0030			
				N,A	940+-4	425.5	409	
7	92.5	844MS		ACT	0.0454+-0.0030	0.01756	409	
4-BE- 7	*53.40D			N,P	48000+-9000	21940	409	
				N,A	<0.1			
9	100	1.6E+6Y		ACT	0.0076+-0.0008	0.0040+-0.0004	6 409	
10	*1.6E+6Y	13.8S		ACT	<0.001			
5-B -NAT	-	-	-	ACT	0.10+-0.09			
				ABS	767+-4	344.4+-2.2	6 13	
10	20	-		ACT	0.5+-0.2			
				ABS	3837+-9	1722+-10	6 409	
11	80	0.0203S		ACT	0.0055+-0.0033	0.0757	409	4439 (3)
6-C -NAT	-	-	-	ACT	(3.50+-0.07)E-3	(1.55+-0.05)E-3		

TARGET NUCLIDE		A+1 NUCLIDE		TYPE OF REACTION	THERMAL CROSS-SECTIONS (b) AND g(T) FACTOR	RESONANCE INTEGRALS (b)	RESONANCE INTEGRALS: REFERENCES	MAIN GAMMA RAYS FOR A+1 NUCLIDE ENERGY (keV) (ABSOLUTE INTENSITY: %)
Z-SYMBOL-A	ABUNDANCE (%) OR HALF-LIFE	HALF-LIFE	ISOMER STATE IT (%)					
12	98.89	-		ACT	(3.53+-0.07)E-3	(1.57+-0.05)E-3	6 409	
13	1.11	5736Y		ACT	(1.37+-0.04)E-3	0.0017+-0.0002	6	
14	*5736Y	2.46S		ACT	<0.001E-3			5298 (68)
7-N -NAT	-	-	-	ACT	0.0747+-0.0073	0.034	6	
				ABS	1.90+-0.03	4.8+-2.4	6 13	
14	99.64	-		ACT	0.0750+-0.0075	0.034	6	
				N.P	1.83+-0.03			
15	0.36	7.14S		ACT	(0.024+-0.008)E-3	0.00011	6	6129 7117 (69) (5)
8-O -NAT	-	-	-	ACT	(0.19+-0.02)E-3	0.00036		
16	99.756			ACT	(0.190+-0.019)E-3	0.00036	6 409	
17	0.039	-		ACT	(0.538+-0.065)E-3	0.00039	6	
				N.A	0.235+-0.010			
18	0.205	27.1S		ACT	(0.16+-0.01)E-3	(0.87+-0.04)E-3	6 311	110 197 1356 1444 1550 (3) (90) (50) (3) (2)
9-F - 19	100	11.0S		ACT	0.0096+-0.0005	0.039+-0.003	6 13 312 409	1634 (100)
10-NE-NAT	-	-	-	ACT	0.039+-0.007	0.0188		
20	90.5	-		ACT	0.037+-0.004	0.0175	6	
21	0.27	-		ACT	0.666+-0.110	0.296	6	
22	9.23	38S		ACT	0.0455+-0.0060	0.023	6	440 (33)
11-NA- 22	*2.60Y	-		ACT	29000+-1000	(170+-30)E+3	6 316 396	
23	100	0.02S	M IT=100	ACT	0.40+-0.03			
		15.03H	G	ACT	0.13+-0.03			1369 2754 (100)(100)
			M+G	ACT	0.530+-0.007	0.320+-0.015	6 10 11 23 47 124 128 144 152 154 312 314 315 398 399 409	
12-MG-NAT	-	-	-	ACT	0.063+-0.005	0.038+-0.004	6 11 14 41 409	

TABLE II (cont.)

TARGET NUCLIDE		A+1 NUCLIDE		TYPE OF REACTION	THERMAL CROSS-SECTIONS (b) AND g(T) FACTOR	RESONANCE INTEGRALS (b)	RESONANCE INTEGRALS: REFERENCES	MAIN GAMMA RAYS FOR A+1 NUCLIDE ENERGY (keV) (ABSOLUTE INTENSITY: %)
Z-SYMBOL-A	ABUNDANCE (%) OR HALF-LIFE	HALF-LIFE	ISOMER STATE IT (%)					
24	78.99	-		ACT	0.051+-0.005	0.032+-0.004	6	
25	10.00	-		ACT	0.190+-0.030	0.098+-0.015	6	
26	11.01	9.46M		ACT	0.035+-0.002	0.027+-0.002	6 23 312 339 398 399 432	844 1014 (72) (28)
27	*9.46M	21.1H		ACT	0.07+-0.02			31 401 941 1342 1373 (66) (37) (38) (53) (5)
13-AL- 27	100	2.246M		ACT	0.232+-0.003	0.175+-0.005	6 10 11 14 22 23 41 312 339 398 399 409	1779 (100)
14-SI-NAT	-	-	-	ACT	0.171+-0.006	0.127+-0.018	11 409	
28	92.2	-		ACT	0.177+-0.005	0.110+-0.015	6	
29	4.7	-		ACT	0.101+-0.014	0.077+-0.015	6	
30	3.1	2.62H		ACT	0.107+-0.002	0.66+-0.060	6 312 432	
31	*2.62H	280Y		ACT	0.18+-0.04			
15-P - 31	100	14.3D		ACT	0.172+-0.006	0.085+-0.010	6 10 11 409 432	
16-S -NAT	-	-	-	ACT	0.52+-0.01	0.10	11	
				ABS	0.53+-0.01			
				N,A	0.008+-0.004			
				N,P	(0.015+-0.008)E-3			
32	95.0	-		ACT	0.53+-0.04	0.08	6 409	
				N,A	0.007+-0.004			
33	0.75	-		ACT	0.35+-0.04	0.097	6 394	
				N,A	0.190+-0.080			
				N,P	0.002+-0.001			
34	4.2	-		ACT	0.240+-0.010	0.534+-0.023	6 317	
36	0.015	5.1M		ACT	0.15+-0.03	0.17+-0.04	6	3102 (90)
17-CL-NAT	-	-	-	ACT	33.1+-0.3	14.0+-1.0	6 11 13 318 409	
				ABS	33.5+-0.3			

TARGET NUCLIDE		A+1 NUCLIDE		TYPE OF REACTION	THERMAL CROSS-SECTIONS (b) AND g(T) FACTOR	RESONANCE INTEGRALS (b)	RESONANCE INTEGRALS: REFERENCES	MAIN GAMMA RAYS FOR A+1 NUCLIDE ENERGY (keV) (ABSOLUTE INTENSITY: %)
Z-SYMBOL-A	ABUNDANCE (%) OR HALF-LIFE	HALF-LIFE	ISOMER STATE IT (%)					
				N,P	0.37+-0.02			
35	75.77	3.0E+5Y		ACT	43.6+-0.4	18+-2	6 317	
				N,P	0.489+-0.014			
				N,A	(0.08+-0.04)E-3			
36	*3.0E+5Y	-		ACT	<10			
37	24.23	1S	M IT=100	ACT	0.047+-0.010			
		37.18M	G	ACT	0.376+-0.011			1642 2168 (32) (44)
			M+G	ACT	0.423+-0.007	0.30+-0.06	6 21 23 312 399	
18-AR-NAT	-	-	-	ACT	0.675+-0.009	0.43+-0.03	6 409	
36	0.34	34.8D		ACT	5.2+-0.5	2.5+-0.5	6	
				N,A	0.0055+-0.0005			
37	*34.8D	-		N,A	1970+-330			
		-		N,P	69+-14			
38	0.07	269Y		ACT	0.8+-0.2	0.4+-0.1	6	
39	*269Y	-		ACT	600+-300			
40	99.59	1.83H		ACT	0.660+-0.010	0.42+-0.03	6 319	1294 (99)
41	*1.83H	33Y		ACT	0.5+-0.1			
19-K -NAT	-	-	-	ACT	2.1+-0.1	1.1+-0.1	6	
39	93.3	-	1.3E+9Y	ACT	2.1+-0.2	1.1+-0.1	6	1461 (100)
				N,A	0.0043+-0.0005			
40	0.012 *1.3E+9Y			ACT	30+-8	13+-4	6	
				N,P	4.4+-0.3	2.0+-0.2	6	
				N,A	0.39+-0.03			
41	6.70	12.36H		ACT	1.46+-0.03	1.40+-0.10	6 23 58 65 312 320 399 432	1525 (18)
20-CA-NAT	-	-	-	ACT	0.43+-0.02	0.23+-0.02	6 11 409	

TABLE II (cont.)

TARGET NUCLIDE		A+1 NUCLIDE		TYPE OF REACTION	THERMAL CROSS-SECTIONS (b) AND g(T) FACTOR	RESONANCE INTEGRALS (b)	RESONANCE INTEGRALS: REFERENCES	MAIN GAMMA RAYS FOR A+1 NUCLIDE ENERGY (keV) (ABSOLUTE INTENSITY: %)
Z-SYMBOL-A	ABUNDANCE (%) OR HALF-LIFE	HALF-LIFE	ISOMER STATE IT (%)					
40	96.94	1.3E+5Y		ACT	0.41+-0.02	0.22+-0.02	6	
				N,A	0.0025+-0.0011			
41	*1.3E+5Y	-		ACT	4			
42	0.65	-		ACT	0.680+-0.070	0.39+-0.04	6	
43	0.14	-		ACT	6.2+-0.6	3.93+-0.15	6	
44	2.08	165D		ACT	0.88+-0.05	0.56+-0.01	6 102	
45	*165D	-		ACT	15			
46	0.003	4.54D		ACT	0.74+-0.07	0.32+-0.12	6 47	489 808 1297 (7) (7) (75)
48	0.19	8.72M		ACT	1.09+-0.14	0.90+-0.10	6 312 432	3084 4072 (92) (7)
21-SC- 45	100	18.7S	M IT=100	ACT	9.8+-1.1	5.4+-0.6	6	
		84.0D	G	ACT	17.4+-1.1	6.1+-0.8		889 1121 (100)(100)
			M+G	ACT	27.2+-0.2	11.5+-0.5	2 6 10 11 47 48 154 312 399	
46	*84.0D	3.42D		ACT	8.0+-1.0			159 (68)
22-TI-NAT	-	-	-	ACT	6.09+-0.13	3.1+-0.2	6 11 13 409	
46	8.0	-		ACT	0.59+-0.18	0.30+-0.09	6	
47	7.5	-		ACT	1.7+-0.2	1.5+-0.2	6	
48	73.7	-		ACT	7.84+-0.25	3.9+-0.2	6	
49	5.54	-		ACT	2.2+-0.3	1.2+-0.2	6	
50	5.3	5.8M		ACT	0.179+-0.003	0.120+-0.015	2 6 23 312 398 399	320 609 929 (93) (1) (7)
23-V -NAT	-	-	-	ACT	5.07+-0.11	2.7+-0.1	6 13 14	
50	0.25	-		ACT	60+-40	43+-15	6	
51	99.75	3.75M		ACT	4.93+-0.06	2.6+-0.1	2 6 10 11 23 312 320 323 324 334 365 398 399 403 405 409	1434 (100)
24-CR-NAT	-	-	-	ACT	3.07+-0.08	1.5+-0.1	6 11 13 324 325 409	

TARGET NUCLIDE		A+1 NUCLIDE		TYPE OF REACTION	THERMAL CROSS-SECTIONS (b) AND g(T) FACTOR	RESONANCE INTEGRALS (b)	RESONANCE INTEGRALS: REFERENCES	MAIN GAMMA RAYS FOR A+1 NUCLIDE ENERGY (keV) (ABSOLUTE INTENSITY: %)
Z-SYMBOL-A	ABUNDANCE (%) OR HALF-LIFE	HALF-LIFE	ISOMER STATE IT (%)					
50	4.35	27.7D		ACT	15.9+-0.2	8.1+-0.5	2 6 46 58 312 324 325 398 399	320 (10)
52	83.79	-		ACT	0.76+-0.06	0.33+-0.04	6 324 325	
53	9.50	-		ACT	18.2+-1.5	9.5+-1.0	6 324 325	
54	2.36	3.60M		ACT	0.36+-0.04	0.08+-0.03	6 324 325	
25-MN- 53	*3.7E+6Y	312.5D		ACT	70+-10	30.5+-5.0	6	835 (100)
54	*312.5D	-		ACT	38	17	6	
55	100	2.58H		ACT	13.3+-0.2	13.8+-0.4	2 6 10 11 13 14 22 41 45 60 122 125 128 152 266 309 312 314 320 322 326 327 328 329 330 331 332 333	847 1811 2113 (99) (27) (14)
26-FE-NAT	-	-	-	ACT	2.56+-0.03	1.4+-0.2	6 11 13 14 41 45 336 409	
54	5.8	2.7Y		ACT	2.25+-0.18	1.2+-0.2	6	
56	91.7	-		ACT	2.59+-0.14	1.4+-0.2	6	
57	2.19	-		ACT	2.48+-0.30	1.6+-0.2	6	
58	0.31	44.6D		ACT	1.28+-0.05	1.4+-0.1	2 6 47 48 58 154 156 312 398	192 1099 1292 (3) (56) (44)
27-CO- 58M	*8.94H	-		ACT	140000+-10000	540000+-200000	275 341 342	
G	*70.78D	-		ACT	1880+-120	6890	6 9	
59	100	10.5M	M IT=99.7	ACT	18.80+-1.50	39.7+-4.3	339	826 1333 (3)(100)
		5.272Y	G	ACT	18.65+-1.70	31.4+-4.8	339	1173 1333 (100)(100)
			M+G	ACT	37.45+-0.45	71.1+-1.8	2 6 11 13 45 47 96 125 129 146 154 166 312 314 328 329 337 338 339 340 377 403 409	
60M	*10.5M	99.0M		ACT	58.+-8	230+-50	6 344	67 909 (86) (3)
G	*5.272Y			ACT	2.0+-0.2	4.1+-1.0	6 344 444	
28-NI-NAT	-	-	-	ACT	4.49+-0.16	2.8+-0.3	6 11 13 14 17 41 45 117 409	

TABLE II (cont.)

TARGET NUCLIDE		A+1 NUCLIDE		TYPE OF REACTION	THERMAL CROSS-SECTIONS (b) AND g(T) FACTOR	RESONANCE INTEGRALS (b)	RESONANCE INTEGRALS: REFERENCES	MAIN GAMMA RAYS FOR A+1 NUCLIDE ENERGY (keV) (ABSOLUTE INTENSITY: %)
Z-SYMBOL-A	ABUNDANCE (%) OR HALF-LIFE	HALF-LIFE	ISOMER STATE IT (%)					
58	67.76	7.5E+4Y		ACT	4.6+-0.3	2.8+-0.3	6 409	
				N,A	<0.00003			
59	*7.5E+4Y	-		ACT	77.7+-4.1	140+-28	6 395	
				ABS	92+-4			
				N,P	2.0+-0.5			
				N,A	12.3+-0.6			
60	26.42	-		ACT	2.9+-0.2	2.10+-0.21	6 324	
61	1.16	-		ACT	2.5+-0.8	1.5+-0.4	6	
				N,A	<0.00003			
62	3.71	100Y		ACT	14.5+-0.3	8.1+-0.4	6 102	
63	*100Y	-		ACT	24.4+-3.0			
64	0.95	2.52H		ACT	1.58+-0.04	1.19+-0.06	6 23 312 339 399 432	366 1116 1482 (5) (15) (23)
65	*2.52H	54.6H		ACT	22.4+-2.0		6 430	
29-CU-NAT	-	-	-	ACT	3.78+-0.02	4.13+-0.08	6 10 11 12 13 14 41 45 117 409	
63	69.1	12.7H		ACT	4.50+-0.02	4.94+-0.10	6 11 23 123 124 128 145 154 312 313 314 321 400	511 1346 (37) (0.5)
65	30.9	5.10M		ACT	2.17+-0.03	2.32+-0.08	6 11 23 124 145 312 313 314	1039 (8)
66	*5.10M	61.9H		ACT	135+-10			91 93 185 (7) (16) (49)
30-ZN-NAT	-	-	-	ACT	1.11+-0.02	2.8+-0.2	6 11 13 14 41	
64	48.9	265D		ACT	0.76+-0.02	1.40+-0.05	6 47 109 146 156 312 345 399	1116 (51)
65	*265D	-		N,A	250+-150			
66	27.8	-		ACT	0.85+-0.20	1.77	6	
				N,A	<0.00002			
67	4.1	-		ACT	6.8+-0.8	25.2	6	
68	18.6	13.9H	M IT=99	ACT	0.072+-0.004	0.24+-0.03	47 58 119 146 156 312 399 432	574 (100)

TARGET NUCLIDE		A+1 NUCLIDE		TYPE OF REACTION	THERMAL CROSS-SECTIONS (b) AND g(T) FACTOR	RESONANCE INTEGRALS (b)	RESONANCE INTEGRALS: REFERENCES	MAIN GAMMA RAYS FOR A+1 NUCLIDE ENERGY (keV) (ABSOLUTE INTENSITY: %)
Z-SYMBOL-A	ABUNDANCE (%) OR HALF-LIFE	HALF-LIFE	ISOMER STATE IT (%)					
		56M	G	ACT	1.0+-0.1	3.36+-0.3		
			M+G	ACT	1.072+-0.100	3.6+-0.3	6 109	
70	0.62	3.9H	M IT=0	ACT	0.0087+-0.0005			386 487 512 596 620 (93) (62) (28) (28) (57)
		2.4M	G	ACT	0.083+-0.005			122 390 512 910 1120 (3) (4) (32) (8) (2)
			M+G	ACT	0.092+-0.005	0.86+-0.06	6	
72	*46.5H	23.5S		ACT	0.059	0.07	26	
31-GA-NAT	-	-	-	ACT	2.9+-0.1	21.7+-1.5	6 13 409	
69	60	21.1M		ACT	1.68+-0.07	15.5+-1.5	6 10 11 57 312	175 1039 (0.2) (0.5)
71	40	36MS	M IT=100	ACT	0.15+-0.05			
		14.1H	G	ACT	4.56+-0.23			630 834 894 2202 2508 (25) (96) (10) (26) (13)
			M+G	ACT	4.71+-0.23	31.1+-2.9	6 10 11 57 312 399	
72	*14.1H	4.8H		ACT	4.25	25.7	26	297 326 739 768 1065 (80) (11) (4) (1) (1)
32-GE-NAT	-	-	-	ACT	2.3+-0.2	6.0+-1.0	6 13	
70	20.7	20MS	M IT=100	ACT	0.28+-0.07			
		11.2D	G	ACT	3.15+-0.16			
			M+G	ACT	3.43+-0.2	1.50	6	
72	27.5	0.53S	M IT=100 G					
			M+G	ACT	0.98+-0.09	0.76	6 19 24 26 32	
73	7.7	-		ACT	15.+-2.	63.7	6 24 26 32	
74	36.4	48S	M IT=99	ACT	0.17+-0.03	0.41+-0.07	6	140 (34)
		83M	G	ACT	0.34+-0.08	0.59+-0.2		199 265 (1) (11)
			M+G	ACT	0.51+-0.08	1.0+-0.2	6 24 26 32 92 312	
76	7.7	54S	M IT=19.8	ACT	0.10+-0.01	1.2+-0.2	6 25 92	215 (26)
		11.3H	G	ACT	0.06+-0.01	0.8+-0.2	20 25 29	211 216 264 416 558 (29) (27) (51) (21) (15)
			M+G	ACT	0.16+-0.02	2.0+-0.4	6 24 26 32 92 312	

TABLE II (cont.)

TARGET NUCLIDE Z-SYMBOL-A	ABUNDANCE (%) OR HALF-LIFE	A+1 NUCLIDE HALF-LIFE	ISOMER STATE IT (%)	TYPE OF REACTION	THERMAL CROSS-SECTIONS (b) AND g(T) FACTOR	RESONANCE INTEGRALS (b)	RESONANCE INTEGRALS: REFERENCES	MAIN GAMMA RAYS FOR A+1 NUCLIDE ENERGY (keV) (ABSOLUTE INTENSITY: %)
77M	*54S							
G	*11.3H							
M+G		88M		ACT	1.48	7.01	26	277 294 (96) (4)
33-AS- 75	100	26.4H		ACT	4.48+-0.11	61+-4	6 10 11 18 19 24 26 53 57 125 128 312 376 399 432	559 657 1213 1216 1229 (45) (6) (2) (4) (1)
76	*26.4H	38.8H		ACT	60.8	216.1	26	239 (2)
77	*38.8H	1.5H		ACT	12.69	68.25	26	614 695 828 1240 1309 (54) (17) (9) (6) (12)
34-SE-NAT	-	-	-	ACT	11.7+-0.2	12.6	6 13	
74	0.9	120.0D		ACT	51.8+-1.2	514+-65	2 6 20 312 345	121 136 265 280 401 (17) (59) (59) (25) (12)
76	9.0	17.5S	M IT=100	ACT	22+-1	17+-2	6	
			G	ACT	63+-7	23.3		
			M+G	ACT	85+-7	40.3	6 24 26 32	
77	7.5	-		ACT	42+-4	32+-3	6 19 24 25 26	
78	23.5	3.9M	M IT=100	ACT	0.38+-0.2	3.7+-0.6	6 32 369	
		6.5E+4Y	G	ACT	0.05+-0.1	1.06+-0.80		
			M+G	ACT	0.43+-0.2	4.76+-0.60	6 19 20 24 25 26 27	
79M	*3.9M	-						
G	*6.5E+4Y	-		ACT		16.0	32	
M+G		-		ACT	3.28	36+-26	26 27	
80	50.0	57.3M	M IT=99	ACT	0.08+-0.01	0.42+-0.11	6 312	260 276 (96) (100)
		18M	G	ACT	0.53+-0.04	1.28+-0.32		
			M+G	ACT	0.610+-0.045	1.70+-0.30	6 19 20 24 25 26 27	
82	9.1	69S	M IT=0	ACT	0.039+-0.003			357 674 988 1030 2051 (17) (15) (15) (21) (11)
		22.4M	G	ACT	0.0052+-0.0004			225 357 510 718 799 (32) (69) (44) (16) (16)
			M+G	ACT	0.044+-0.003	0.08+-0.04	6 24 25 27	
35-BR-NAT	-	-	-	ACT	6.9+-0.2	91+-6	6 13 40	

TARGET NUCLIDE		A+1 NUCLIDE		TYPE OF REACTION	THERMAL CROSS-SECTIONS (b) AND g(T) FACTOR	RESONANCE INTEGRALS (b)	RESONANCE INTEGRALS: REFERENCES	MAIN GAMMA RAYS FOR A+1 NUCLIDE ENERGY (keV) (ABSOLUTE INTENSITY: %)
Z-SYMBOL-A	ABUNDANCE (%) OR HALF-LIFE	HALF-LIFE	ISOMER STATE IT (%)					
76	*16.2H	57H	-	N,P	224+-42			
79	50.69	4.42H	M IT=100	ACT	2.4+-0.6	35.7+-4.0	6 23	37 (36)
		18M	M IT=100 G	ACT	8.6+-0.4	95.7+-10	6 23	616 (7) 666 (13)
			M+G	ACT	11.0+-0.7	131+-11	6 10 11 18 24 432	
81	49.31	6.1M	M	ACT	2.43+-0.4	41.3	347	698 (1) 776 (8)
		35.34H	IT=97.6 G	ACT	0.26	8.9	347	554 (71) 619 (43) 698 (28) 776 (84) 1317 (27)
			M+G	ACT	2.7+-0.2	50.2+-5.9	6 18 19 20 23 24 25 26 27 28 38 312 347 399 432	
82M	*6.1M							
G	*35.34H							
M+G		2.40H		ACT	18.09	90.46	26	529 (1)
36-KR-NAT	-	-	-	ACT	24.5+-3.5	49+-4	6	
78	0.35	50S	M IT=100	ACT	0.17+-0.02			
		34.9H	G	ACT	6.03+-0.90			261 (13) 300 (2) 306 (3) 398 (9) 606 (8)
			M+G	ACT	6.2+-0.9	20+-1	6 420	
80	2.25	13.3S	M IT=100	ACT	4.55+-0.65			
		2.1E+5Y	G	ACT	6.95+-0.82			
			M+G	ACT	11.5+-0.5	56+-7	6 24 348 420	
82	11.6	1.83H	M IT=100	ACT	14.0+-2.5			
			G	ACT	16+-10			
			M+G	ACT	30+-10	190+-20	6 19 24 25 26	
83	11.5	-		ACT	180+-30	210+-30	6 19 24 25 26 27 28 34 38 384 424	
84	57.0	4.48H	M IT=21.2	ACT	0.090+-0.013	2.4	25	151 (95)
		10.76Y	G	ACT	0.042+-0.004	0.8	25	
			M+G	ACT	0.110+-0.015	3.2+-0.5	6 19 24 26 27 28 38	
85	*10.76Y	-		ACT	1.66+-0.2	1.8+-1.0	6 24 26 27 28 390	

TABLE II (cont.)

TARGET NUCLIDE		A+1 NUCLIDE		TYPE OF REACTION	THERMAL CROSS-SECTIONS (b) AND g(T) FACTOR	RESONANCE INTEGRALS (b)	RESONANCE INTEGRALS: REFERENCES	MAIN GAMMA RAYS FOR A+1 NUCLIDE ENERGY (keV) (ABSOLUTE INTENSITY: %)
Z-SYMBOL-A	ABUNDANCE (%) OR HALF-LIFE	HALF-LIFE	ISOMER STATE IT (%)					
86	17.3	76.3M		ACT	0.003+-0.002	0.1+-0.04	6 24 26 27 28	403 845 2012 2555 2558 (50) (7) (3) (9) (4)
87	*76.3M	2.80H		ACT	<12600	<270	27	196 835 1530 2196 2392 (26) (13) (11) (13) (35)
37-RB-NAT	-	-	-	ACT	0.35+-0.01	4.6+-0.4	6 13 40 109	
84	*32.9D	-		N,P	12+-2			
85	72.17	1.02M	M IT=100	ACT	0.053+-0.005	1.74+-0.10	312	
		18.7D	G	ACT	0.427+-0.011	3.76+-0.50		1077 (9)
			M+G	ACT	0.48+-0.01	5.50+-0.50	2 6 19 24 25 26 27 28 47 48 312 345	
86M	*1.02M							
G	*18.7D							
M+G		47E+9Y	M					
		-	G					
			M+G	ACT	4.92	33+-10	24 26	
87	27.83	17.8M		ACT	0.120+-0.030	2.2+-0.3	6 19 24 25 26 27 28 312	898 1836 2678 (14) (21) (2)
88	*17.8M	15.4M		ACT	1.0+-0.3			658 1032 1248 2196 2570 (10) (58) (43) (13) (10)
38-SR-NAT	-	-	-	ABS	1.28+-0.06	10.0+-2.6	6 11 13 17	
84	0.56	67.7M	M IT=87	ACT	0.60+-0.06	4.59+-0.15	6 92 312	151 (95)
		64.9D	G	ACT	0.35+-0.07	6.6+-1.1		514 (98)
			G+0.87M	ACT	0.87+-0.07	10.6+-1.1	6 47 312	
			M+G	ACT	0.95+-0.07	11.2+-1.1		
86	9.9	2.81H	M IT=99.7	ACT	0.84+-0.06	4.79+-0.24	6 26 312	388 (83)
		-	G	ACT	0.20+-0.03	0.38		
			G+M	ACT	1.04+-0.07	5.17	24 25	
87	7.0	-		ACT	16+-3	120+-15	6 19 24 25	
88	82.6	50.5D		ACT	0.058+-0.004	0.06+-0.01	6 24 25 26 27 28	
89	*50.5D	28.5Y		ACT	0.42+-0.04	0.56+-0.22	24 26 27	

TARGET NUCLIDE		A+1 NUCLIDE		TYPE OF REACTION	THERMAL CROSS-SECTIONS (b) AND g(T) FACTOR	RESONANCE INTEGRALS (b)	RESONANCE INTEGRALS: REFERENCES	MAIN GAMMA RAYS FOR A+1 NUCLIDE ENERGY (keV) (ABSOLUTE INTENSITY: %)
Z-SYMBOL-A	ABUNDANCE (%) OR HALF-LIFE	HALF-LIFE	ISOMER STATE IT (%)					
90	*28.5Y	9.5H		ACT	0.9+-0.5	0.47+-0.07	24 26 27 28	556 653 750 926 1024 (56) (8) (24) (4) (33)
91	*9.5H	2.71H		ACT	0.148	0.62	26	242 431 953 1142 1384 (3) (3) (4) (3) (90)
39-Y - 89	100	3.19H	M IT=99	ACT	0.001+-0.0002			
		64.1H	G	ACT	1.279+-0.020			
			M+G	ACT	1.28+-0.02	0.85+-0.15	6 10 11 19 24 25 26 27 28 40 57 312	
90	*64.1H	49.7M	M IT=100			1.6		
		58.5D	G	ACT		1.4	32	
			M+G	ACT	<6.5	3.0+-1.5	24 26	
91G	*58.5D	3.54H		ACT	1.4+-0.3	1.6+-0.5	24 26 27 32	448 561 844 934 1405 (2) (2) (1) (14) (5)
93	*10.1H	19M		ACT	0.078	0.99	26	550 751 918 1139 1669 (6) (3) (73) (7) (3)
40-ZR-NAT	-	-	-	ACT	0.185+-0.003	1.18+-0.16	6 10 11 13 41 45 365 409 418 431	
90	51.4			ACT	0.011+-0.005	0.21+-0.09	6 19 24 25 26 27 32 365	
91	11.2			ACT	1.24+-0.25	6.8+-1.3	6 19 24 25 26 27 28 349 357 365	
92	17.1	1.5E+6Y		ACT	0.220+-0.060	0.63+-0.11	6 19 24 25 26 27 28	
93	*1.5E+6Y			ACT	2.6+-1.4	20+-10	6 19 24 25 26 27 28	
94	17.5	64D		ACT	0.0499+-0.0024	0.30+-0.07	2 6 19 24 25 26 27 28 38 92 312 350 365 393	724 757 (45) (55)
95	*64.0D	-		ACT	0.49	6.5+-1.4	24 26 34 384	
96	2.8	16.8H		ACT	0.0229+-0.0010	5.6+-0.9	2 6 19 24 25 26 27 28 38 92 350 393	355 508 1021 1148 1750 (2) (5) (1) (3) (1)
97	*16.8H	30.7S		ACT	0.202	1.55	26	
41-NB- 93	100	6.2M	M IT=99.5					871 (100)
		2.0E+4Y	G					703 871 (100)(100)
			M+G	ACT	1.15+-0.05	8.2+-1.5	6 10 11 14 17 18 24 34 41 57 312 352 353 354 398 409 432	

TABLE II (cont.)

TARGET NUCLIDE		A+1 NUCLIDE		TYPE OF REACTION	THERMAL CROSS-SECTIONS (b) AND g(T) FACTOR	RESONANCE INTEGRALS (b)	RESONANCE INTEGRALS: REFERENCES	MAIN GAMMA RAYS FOR A+1 NUCLIDE ENERGY (keV) (ABSOLUTE INTENSITY: %)
Z-SYMBOL-A	ABUNDANCE (%) OR HALF-LIFE	HALF-LIFE	ISOMER STATE IT (%)					
94	*2.0E+4Y	86.6H	M IT=97.5	ACT	0.6+-0.1			
		35.15D	G	ACT	14.9+-1.0			766 (100)
			M+G	ACT	20+-1.0	120+-10	24 352 353	
95	*35.15D	23.4H		ACT	<7	24+-2	24 26 34 384	460 (29) 569 (56) 778 (97) 850 (21) 1091 (49)
42-MO-NAT	-	-	-	ACT	2.55+-0.05	25+-1	6 11 13 14 17 40 41 45 115 117 120 355 409	
92	14.8	6.9H	M IT=99.8					
		3.5E+3Y	G					
			M+G	ACT	0.019	0.81	6	
94	9.1	-		ACT	0.015	0.86	6 24	
95	15.9	-		ACT	14.0+-0.5	108+-4	6 14 15 19 24 25 26 27 28 34 40 384	
96	16.7	-		ACT	0.5+-0.2	24+-4	6 19 24 25 26 27	
97	9.5	-		ACT	2.1+-0.5	15+-1	6 15 19 24 25 26 27 28 34 384	
98	24.4	66.0H		ACT	0.130+-0.006	7.3+-1.8	6 18 19 24 25 26 27 28 34 38 47 58 117 119 124 147 148 312 314 356 400 432 440	41 (1) 140 (5) 181 (6) 739 (12) 778 (4)
99	*66.0H	-		ACT	1.733	26+-2	24 26 34	
100	9.6	14.6M		ACT	0.199+-0.003	4.2+-0.5	6 18 19 24 25 26 27 28 34 40 109 117 124 312 358 400 432	192 (19) 506 (12) 591 (16) 696 (7) 1012 (13)
43-TC- 98	*4.2E+6Y	6.0H	M IT=99	ACT	0.93+-0.2			
		2.1E+5Y	G	ACT	1.67+-1.3			
			M+G	ACT	2.6+-1.3			
99M	*6.0H			ACT	1.62	26.7	26	
G	*2.1E+5Y	15.8S		ACT	20+-1	230+-50	6 15 26 27 28 40 424	540 (7) 591 (6)
44-RU-NAT	-	-	-	ACT	2.57+-0.21	40+-4	6 53	

TARGET NUCLIDE		A+1 NUCLIDE		TYPE OF REACTION	THERMAL CROSS-SECTIONS (b) AND g(T) FACTOR	RESONANCE INTEGRALS (b)	RESONANCE INTEGRALS: REFERENCES	MAIN GAMMA RAYS FOR A+1 NUCLIDE ENERGY (keV) (ABSOLUTE INTENSITY: %)
Z-SYMBOL-A	ABUNDANCE (%) OR HALF-LIFE	HALF-LIFE	ISOMER STATE IT (%)					
96	5.5	2.9D		ACT	0.29+-0.02	5.8+-1.2	6 312 359	216 325 (86) (10)
98	1.9			ACT	<8.0			
99	12.7			ACT	7.1+-1.0	166+-20	6 24 359	
100	12.6			ACT	5.0+-0.6	11.0+-0.7	6 24 25 26 27 359	
101	17.1			ACT	3.4+-0.9	88+-17	6 15 24 25 26 27 28 34 359 384	
102	31.6	39.35D		ACT	1.21+-0.07	4.6+-0.9	6 24 25 26 27 28 34 90 109 312 359 384	497 610 (89) (6)
103	*39.35D	-		ACT	7.71	60+-20	24 26 34 384	
104	18.6	4.44H		ACT	0.32+-0.02	5.2+-0.5	6 24 26 27 28 34 312 360 384	130 316 469 676 724 (6) (11) (17) (15) (47)
105	*4.44H	368D		ACT	0.39+-0.06	6.4+-1.4	24 26 27 34 384	
106	*368D	3.8M		ACT	0.146+-0.045	1.8+-0.4	6 24 25 26 27 28 34 38 361 372 384	194 374 463 579 848 (11) (4) (4) (3) (6)
45-RH-103	100	4.4M	M IT=99.8	ACT	10+-1	83+-6	6 147 148 312 362	357 741 759 768 1237 (13) (10) (11) (77) (49)
		42S	G	ACT	135+-2	993+-63		358 556 (4) (2)
			M+G	ACT	145+-2	1076+-63	6 10 11 15 19 24 25 26 27 28 40 55 96 147 148 362 384 389	
104M	*4.4M	45S	M IT=100					
		35.5H	G					306 319 (5) (19)
			M+G	ACT	800+-100			
G	*42S	45S	M IT=100		39.53	360	27	
		35.5H	G		0.47	4.6	25	306 319 (5) (19)
			M+G	ACT	40+-30	364.6		
105G	*35.5H	2.2H	M IT=0	ACT	5000+-1000			451 512 616 717 1047 (25) (87) (21) (29) (31)
		30S	G	ACT	11000+-3000			512 622 1050 (21) (10) (2)
			M+G	ACT	16000+-3160	16500+-2500	6 24 25 26 27 34 38 360 364 384 410	
46-PD-NAT	-	-	-	ACT	6.9+-0.4	83+-7	6 11 40 53	

TABLE II (cont.)

TARGET NUCLIDE		A+1 NUCLIDE		TYPE OF REACTION	THERMAL CROSS-SECTIONS (b) AND g(T) FACTOR	RESONANCE INTEGRALS (b)	RESONANCE INTEGRALS: REFERENCES	MAIN GAMMA RAYS FOR A+1 NUCLIDE ENERGY (keV) (ABSOLUTE INTENSITY: %)
Z-SYMBOL-A	ABUNDANCE (%) OR HALF-LIFE	HALF-LIFE	ISOMER STATE IT (%)					
102	1.0	17.0D		ACT	3.4+-0.3	10+-2	6	
104	11	-		ACT	0.6+-0.3	16+-2	6 19 24 26 27	
105	22.2	-		ACT	20+-3	83+-9	6 19 24 25 26 27 28 34 384	
106	27.3	21.3S	M IT=100	ACT	0.013+-0.002			
		6.5E+6Y	G	ACT	0.292+-0.029			
			M+G	ACT	0.305+-0.029	5.90+-0.53	6 19 24 25 26 27 28 34 360 384	
107M	*21.3S	-						
G	*6.5E+6Y	-		ACT	1.8+-0.2	77+-7	6 24 26 27 28 34 384	
108	26.7	4.69M	M IT=100	ACT	0.183+-0.033	2.26+-0.04	312 432	
		13.4GH	G	ACT	8.3+-0.5	224.74+-25.00	432	
			M+G	ACT	8.483+-0.501	227+-25	6 19 24 25 26 27 28 312	
109M	*4.69M	-						
G	*13.4GH	-		ACT	5.24	60.6	26 34	
110	11.8	5.5H	M IT=71	ACT	0.037+-0.006	0.6+-0.2	6 312	70 (31) 391 (20) 575 (12) 633 (13) 694 (7)
		22M	G	ACT	0.190+-0.030	4.50+-0.63		
			M+G	ACT	0.227+-0.031	5.1+-0.6	24 25 26 27 28 312	
112	*20.1H	1.6M		ACT	0.29	10+-5	25 26	
47-AG-NAT	-	-	-	ACT	63.3+-0.4 G(T)=1.0034	748+-20	6 11 13 14 40 45 96 111 340 363	
107	51.83	127Y	M IT=8.5	ACT	0.33+-0.08	1.26+-0.19	6 425	434 (99) 614 (98) 723 (99)
		2.41M	G	ACT	37.27+-1.20	93.74+-6.00		434 (17) 619 (9) 633 (2)
			M+G	ACT	37.6+-1.2	95+-6	6 10 11 24 27 34 57 145 312 409	
109	48.17	250.4D	M IT=1.5	ACT	4.7+-0.2 G(T)=1.0048	72.8+-5.0	25 46 312 351 367 368 407 425 426 427	658 (96) 764 (23) 885 (74) 937 (35) 1384 (25)
		24.6S	G	ACT	86.3+-3.0	1377.2+-55.0	312	658 (5)
			M+G	ACT	91.0+-1.0	1450+-55	6 10 11 14 15 19 24 25 26 27 28 34 38 40	

TARGET NUCLIDE		A+1 NUCLIDE		TYPE OF REACTION	THERMAL CROSS-SECTIONS (b) AND g(T) FACTOR	RESONANCE INTEGRALS (b)	RESONANCE INTEGRALS: REFERENCES	MAIN GAMMA RAYS FOR A+1 NUCLIDE ENERGY (keV) (ABSOLUTE INTENSITY: %)
Z-SYMBOL-A	ABUNDANCE (%) OR HALF-LIFE	HALF-LIFE	ISOMER STATE IT (%)					
							343 409	
110	*250.4D	1.2M	M IT=99.7 G					171 245 507 620 753 (17) (71) (6) (17) (6)
		7.5D						245 342 (1) (7)
			M+G	ACT	82+-11	41.3	25	
111M	*1.2M							
G	*7.5D	3.12H		ACT	3+-2	105+-20	6 25 38 408	607 617 695 1388 1614 (3) (43) (3) (5) (3)
48-CD-NAT	-	-	-	ACT	2520+-50	69.6+-5.7	3 6 409	
106	1.2	6.5H		ACT	1	4	6	93 (5)
108	0.9	453D		ACT	1.1	11	6 24	88 (4)
109	*453D			ACT	700+-100			
				N.A	0.05			
110	12.4	49M	M IT=100 G	ACT	0.14+-0.05 10.9	2.5+-1	6 29 398	
			M+G	ACT	11+-1	40.5+-7.5	6 19 24 26 27 398	
111	12.8	-		ACT	24+-3	53+-7	6 19 24 25 26 27 28	
112	24.0	14.6Y	M IT=0.1 G					
		9.0E+15						
			M+G	ACT	2.2+-0.5	13.5+-1.9	6 19 24 26 27 28	
113	12.3	-		ACT	20600+-400 G(T)=1.3266	388+-45	19 24 26 27 28 34 384	
114	28.8	44.8D	M IT=0 G	ACT	0.036+-0.007	3.1+-1.5	25 398	934 (2)
		53.38H		ACT	0.30+-0.02	19.9+-2.5		261 336 492 528 (2) (46) (8) (27)
			G+M	ACT	0.336+-0.021	23+-2	6 19 24 25 26 27 28 29 346	
115M	*44.8D	-		ACT	31.2	195.9	24 26	
G	*53.38H	-		ACT	5.43	79.9	26	
116	7.6	3.31H	M IT=0 G	ACT	0.025+-0.010	0.422+-0.248	398	564 1029 1066 1433 1997 (15) (12) (23) (13) (26)
		2.42H		ACT	0.050+-0.080	0.928+-0.514		273 344 434 1303 1577 (28) (18) (10) (18) (11)

TABLE II (cont.)

TARGET NUCLIDE		A+1 NUCLIDE		TYPE OF REACTION	THERMAL CROSS-SECTIONS (b) AND g(T) FACTOR	RESONANCE INTEGRALS (b)	RESONANCE INTEGRALS: REFERENCES	MAIN GAMMA RAYS FOR A+1 NUCLIDE ENERGY (keV) (ABSOLUTE INTENSITY: %)
Z-SYMBOL-A	ABUNDANCE (%) OR HALF-LIFE	HALF-LIFE	ISOMER STATE IT (%)					
			G+M	ACT	0.075+-0.081	1.35+-0.45	6 24 26 27 32	
49-IN-NAT	-	-	-	ACT	193.8+-1.5	3133+-75	6 13 14 40 45 96	
113	4.3	42MS	M2 IT=100	ACT	3.1+-0.7			
		49.5D	M1	ACT	5.0+-1.0			558 725 (102)(101)
			M1+M2 IT=96.7	ACT	8.1+-0.8	220+-15	6 109 312 371	
		71.9S	G	ACT	3.9+-0.4	90+-33		558 (13)
			G+M1+M2	ACT	12.0+-1.1	310+-30	6 10 11 24	
115	95.7	2.2S	M2 IT=100	ACT	81+-8			
		54M	M1	ACT	81.3+-8.0			417 819 1097 1294 2112 (29) (11) (56) (84) (16)
			M1+M2 IT=0	ACT	162.3+-0.7	2605+-115	11 23 25 124 125 133 165 312 326 373 374	
		14S	G	ACT	40+-2	655+-30	124 374	1294 (1)
			G+M1+M2	ACT	202.3+-2.0 G(T)=1.0175	3260+-150	6 10 15 19 24 26 27 28 40 41 60 123 124 125 129 152 266 330 366 374 375	
50-SN-NAT	-	-	-	ACT	0.626+-0.009	6.4+-0.5	6 11 13 14 41 409	
112	1.0	20M	M IT=91	ACT	0.30+-0.04			
		115D	G	ACT	0.71+-0.10			255 392 (2) (64)
			G+0.91M	ACT	0.98+-0.10	34+-4	6 312 398 423 429	
			G+M	ACT	1.01+-0.11	35+-4		
114	0.66	-		ACT	0.115+-0.030	5.1+-1.5	6	
115	0.35	-		ACT	30+-7	27+-5	6 24 26	
116	14.4	14.0D	M IT=100	ACT	0.006+-0.002	0.49+-0.10	6 58 312	
		-	G	ACT	0.134+-0.030	13.21+-2.50		
			M+G	ACT	0.140+-0.030	13.7+-2.5	6 19 24 25 26	
117	7.6	-		ACT	2.3+-0.5	15.7+-2.1	6 19 24 25 26 27	
118	24.1	245D	M IT=100	ACT	0.010+-0.006	1.26	25	
		-	G	ACT	0.21+-0.05	5.04	25	

TARGET NUCLIDE		A+1 NUCLIDE		TYPE OF REACTION	THERMAL CROSS-SECTIONS (b) AND g(T) FACTOR	RESONANCE INTEGRALS (b)	RESONANCE INTEGRALS: REFERENCES	MAIN GAMMA RAYS FOR A+1 NUCLIDE ENERGY (keV) (ABSOLUTE INTENSITY: %)
Z-SYMBOL-A	ABUNDANCE (%) OR HALF-LIFE	HALF-LIFE	ISOMER STATE IT (%)					
			M+G	ACT	0.22+-0.05	6.3+-1.5	6 19 24 26 27	
119	8.6	-		ACT	2.2+-0.5	4.2+-0.9	6 19 24 25 26 27	
120	32.8	55Y	M IT=0	ACT	0.001+-0.001			37 (8)
		27.0H	G	ACT	0.140+-0.030	1.25+-0.3	6 19 24 25 26 27	
			M+G	ACT	0.141+-0.030			
121M	*55Y	-						
G	*27.0H	-						
M+G		-		ACT	5.77	26.29	26	
122	4.7	40.1M	M IT=0	ACT	0.001+-0.001			160 (86)
		129.2D	G	ACT	0.180+-0.020	0.84+-0.10	6 24 25 26 27 32 312 398 429	
			M+G	ACT	0.181+-0.020			
123M	*40.1M	-						
G	*129.2D	-						
M+G		-		ACT	0.033	2.53	24 26	
124	5.8	9.5M	M IT=0	ACT	0.130+-0.005	8.5+-0.8	25 92 312 400 404	332 (100)
		9.64D	G	ACT	0.004+-0.002	0.032	25	822 (4) 916 (4) 1067 (9) 1089 (4) 2002 (2)
			M+G	ACT	0.134+-0.006	8.532+-0.800	6 24 26 27 398	
125M	*9.5M							22 (1) 23 (7) 64 (10) 87 (9) 88 (37)
G	*9.64D							
M+G		(1E+5Y)		ACT	0.55	14.26	24 26	
126	*(1E+5Y)	4.4M	M IT=0					491 (90) 1348 (5) 1564 (4)
		2.1H	G					806 (8) 823 (11) 859 (8) 1096 (19) 1114 (38)
			M+G	ACT	0.297	0.195	24 26 32 38	
51-SB-NAT	-	-	-	ACT	5.1+-0.1	170+-20	6 12 13	
121	57.3	4.2M	M IT=100	ACT	0.06+-0.01	13+-1	6	
		2.7D	G	ACT	5.84+-0.20	189+-15		564 (72) 693 (4) 1141 (31)
			M+G	ACT	5.9+-0.2	202+-15	6 10 11 18 19 23 24	

TABLE II (cont.)

TARGET NUCLIDE		A+1 NUCLIDE		TYPE OF REACTION	THERMAL CROSS-SECTIONS (b) AND g(T) FACTOR	RESONANCE INTEGRALS (b)	RESONANCE INTEGRALS: REFERENCES	MAIN GAMMA RAYS FOR A+1 NUCLIDE ENERGY (keV) (ABSOLUTE INTENSITY: %)
Z-SYMBOL-A	ABUNDANCE (%) OR HALF-LIFE	HALF-LIFE	ISOMER STATE IT (%)					
							25 26 27 38 47 60 92 312 399 432	
122M	*4.2M	-						
G	*2.7D	-						
M+G		-		ACT	21.5	159.0	26	
123	42.7	20M	M2 IT=100	ACT	0.019+-0.010			
		1.6M	M1 IT=80	ACT	0.037+-0.010			498 603 646 1101 (99)(100)(100) (2)
		60.3D	G	ACT	4.1+-0.1			603 646 723 1691 2091 (98) (7) (11) (49) (6)
			G+0.8M1 +0.8M2	ACT	4.145+-0.101	128+-10	2 6 10 11 18 23 25 38 46 48 60 109 312 432	
			G+M1+M2	ACT	4.156+-0.101		6 19 24 26 27	
124	*60.3D	2.77Y		ACT	17.4+-2.8	22.83	9 24 26	176 428 463 601 636 (7) (29) (10) (18) (11)
125	*2.77Y	19.0M	M IT=14	ACT		0.62	32	414 620 666 695 1035 (100) (2)(100) (96) (2)
		12.4D	G	ACT		19.38		415 666 695 697 720 (84)(100)(100) (29) (54)
			M+G	ACT	0.97	20	24 26 27	
126M	*19.0M							
G	*12.4D							
M+G		3.85D		ACT	5.81	64.5	24 26	252 412 473 686 784 (8) (4) (25) (35) (15)
127	*3.85D	10.4M	M IT=3.6					314 594 743 754 788 (95) (3)(100)(100) (7)
		9.0H	G					314 526 636 743 754 (61) (45) (36)(100)(100)
			M+G	ACT	0.92	14.7	26	
128M	*10.4M							
G	*9.0H							
M+G		4.32H		ACT	1.14	15.9	26	545 684 813 915 1030 (18) (12) (43) (20) (13)
52-TE-NAT	-	-	-	ACT	4.7+-0.1	54+-4	6 11 13 14	
120	0.09	154D	M IT=90.2	ACT	0.34+-0.06			37 1102 (8) (22)
		16.8D	G	ACT	2.0+-0.3			470 508 573 (1) (18) (80)

TARGET NUCLIDE		A+1 NUCLIDE		TYPE OF REACTION	THERMAL CROSS-SECTIONS (b) AND g(T) FACTOR	RESONANCE INTEGRALS (b)	RESONANCE INTEGRALS: REFERENCES	MAIN GAMMA RAYS FOR A+1 NUCLIDE ENERGY (keV) (ABSOLUTE INTENSITY: %)
Z-SYMBOL-A	ABUNDANCE (%) OR HALF-LIFE	HALF-LIFE	ISOMER STATE IT (%)					
			M+G	ACT	2.34+-0.31			
122	2.4	119.7D	M IT=100	ACT	1.1+-0.5			
		12E+12Y	G	ACT	2.3+-0.7			
			M+G	ACT	3.4+-0.5	64+-12	6 19 24 25 26	
123M	*119.7D	-		ACT	42.89	273.1	26	
G	0.87 *12E+12Y	-		ACT	418+-30	5547+-113	6 19 24 25 26	
124	4.6	58D	M IT=100	ACT	0.040+-0.025			
			G	ACT	6.76+-1.31			
			M+G	ACT	6.8+-1.3	5.9+-1.5	6 19 24 26	
125M	*58D	-		ACT	11.09	78.85	26	
G	7.0			ACT	1.55+-0.16	19+-3	6 19 24 25 26	
126	18.7	109D	M IT=97.6	ACT	0.135+-0.023	1.04	25	58 (21)
		9.35H	G	ACT	0.90+-0.15	8.56		
			M+G	ACT	1.035+-0.15	9.6+-1.6	6 19 24 25 26 27 28 29	
127M	*109D	-		ACT	3380+-510	1140+-170	6 24 26	
G	*9.35H	-		ACT	2.76	48.2	26	
128	31.8	33.6D	M IT=63.4	ACT	0.015+-0.001	0.0774+-0.0050	6 370	696 730 (9) (2)
		69.6M	G	ACT	0.1997+-0.0080	1.54+-0.11	6 25 370	
			M+G	ACT	0.2147+-0.0081	1.62+-0.11	6 19 24 26 27 28 29 391	
129M	*33.6D	-		ACT	1.11	20.51	24 26	
G	*69.6M	-		ACT	0.37	7.41	26	
130	34.5	30H	M IT=18	ACT	0.02+-0.01	0.0485	25	774 794 852 1125 1207 (50) (18) (27) (15) (13)
		25.0M	G	ACT	0.27+-0.06	0.446	25	150 452 493 602 1147 (69) (18) (5) (4) (5)
			M+G	ACT	0.29+-0.06	0.49+-0.05	6 20 24 26 27 28 29 32 391	
131M	*30H	78H		ACT	0.11	0.16	26	50 112 116 228 (14) (2) (2) (88)

TABLE II (cont.)

TARGET NUCLIDE		A+1 NUCLIDE		TYPE OF REACTION	THERMAL CROSS-SECTIONS (b) AND g(T) FACTOR	RESONANCE INTEGRALS (b)	RESONANCE INTEGRALS: REFERENCES	MAIN GAMMA RAYS FOR A+1 NUCLIDE ENERGY (keV) (ABSOLUTE INTENSITY: %)
Z-SYMBOL-A	ABUNDANCE (%) OR HALF-LIFE	HALF-LIFE	ISOMER STATE IT (%)					
G	*25.0M			ACT	0.04	0.05	26	
132	*78H	55.4M	M IT=17					262 647 864 913 915 (14) (34) (29) (100) (19)
		12.5M	G	ACT		0.06	24 26	312 408 720 787 1333 (71) (30) (7) (6) (10)
53-I -125	*60.2D	12.8D		ACT	894+-90	13730+-2000	6 8	389 491 666 754 880 (78) (7) (59) (7) (2)
126	*12.8D	-		ACT	5960	40600	6 9	
127	100	24.99M		ACT	6.2+-0.2	148+-5	6 10 11 12 13 14 15 16 17 18 19 20 21 22 23 24 25 26 27 28 29 40 400 432	443 527 743 (17) (2) (2)
129	*1.6E+7Y	9.0M	M IT=83	ACT	18+-2			536 586 1122 1614 (100) (7) (1) (3)
		12.4H	G	ACT	9+-1			418 536 669 739 1157 (34) (99) (96) (82) (11)
			M+G	ACT	27.0+-2.2	37+-5	6 15 16 19 24 25 26 27 28 30 31 40	
130	*12.4H	8.05D		ACT	18+-3	178	24 26 32	80 284 364 637 723 (3) (6) (81) (7) (2)
131	*8.05D	83.6M	M					175 600 614 668 773 (63) (100) (18) (100) (99)
		2.3H	G					523 630 668 773 955 (16) (14) (99) (76) (18)
			M+G	ACT	0.7	8.5+-1.2	24 25 26 27 33 34 38 384	
133M	*9S	3.5M						234 847 884 (68) (99) (99)
G	*20.3H	52.0M						595 622 847 884 1073 (11) (11) (95) (65) (15)
M+G				ACT	0.003	0.005	26	
135	*6.68H	45.0S	M					197 370 381 750 1313 (78) (17) (100) (6) (100)
		84.0S	G					1313 1321 2290 2415 2634 (67) (25) (11) (7) (7)
			M+G	ACT	0.022	0.023	24 26 34 384	
54-XE-NAT	-	-	-	ACT	23.9+-1.2	262+-45	6	
124	0.096	55.0S	M IT=100	ACT	28+-5	600+-100	6	
		16.8H	G	ACT	137+-21	2545+-650		55 188 243 454 846 (6) (55) (29) (4) (1)
			M+G	ACT	165+-20	3145+-645	6 35 36	
125	*16.8H	-		N,A	<0.03			

TARGET NUCLIDE		A+1 NUCLIDE		TYPE OF REACTION	THERMAL CROSS-SECTIONS (b) AND g(T) FACTOR	RESONANCE INTEGRALS (b)	RESONANCE INTEGRALS: REFERENCES	MAIN GAMMA RAYS FOR A+1 NUCLIDE ENERGY (keV) (ABSOLUTE INTENSITY: %)
Z-SYMBOL-A	ABUNDANCE (%) OR HALF-LIFE	HALF-LIFE	ISOMER STATE IT (%)					
126	0.090	75.0S	M IT=100	ACT	0.45+-0.13	8+-2	6	
		36.41D	G	ACT	3.05+-0.81	42+-15		58 145 172 203 375 (1) (4) (26) (68) (17)
			M+G	ACT	3.5+-0.8	50+-15	6 37	
127	*36.41D	-		N,A	<0.01			
128	1.919	8.9D	M IT=100	ACT	0.48+-0.10	20+-10	6 25	
		-	G	ACT	6.02+-1.5	85+-22	25	
			M+G	ACT	6.5+-1.5	105+-20	6 24 26 32	
129	26.44	-		ACT	21+-5	252+-17	19	
130	4.08	11.8D	M IT=100	ACT	0.45+-0.10	1.17	25	164 (2)
		-	G	ACT	6+-1	13.72	25	
			M+G	ACT	6.45+-1	14.89	6 24 26 32	
131	21.18	-		ACT	85+-10	890+-120	15	
132	26.89	2.26D	M IT=100	ACT	0.050+-0.010	0.9+-0.2	6 25 35	233 (10)
		5.27D	G	ACT	0.400+-0.061	3.7+-0.6	25	81 (37)
			M+G	ACT	0.450+-0.060	4.6+-0.6	6 24 26 27 28	
133	*5.27D	-		ACT	190+-90	356.3	24 26 27 32 34 384	
134	10.4	15.6M	M IT=99	ACT	0.003+-0.001	0.1	25	787 1133 1358 (100) (5) (5)
		9.14H	G	ACT	0.262+-0.020	0.29	25	250 608 (90) (3)
			M+G	ACT	0.265+-0.020	0.30	6 24 26 27 28 35 39	
135	*9.14H	-		ACT	(2.65+-0.11)E+6	7475+-275	6 19 24 26 27 32 34	
136	8.87	3.9M		ACT	0.26+-0.02	0.74+-0.21	6 24 26 27 28	456 (30)
55-CS-133	100	2.89H	M IT=100	ACT	2.5+-0.2	30+-6	23 29 432	
		2.05Y	G	ACT	26.5+-1.5	407+-24	14 19 25 29 34 47 432	569 605 796 802 847 (15) (98) (85) (9) (100)
			M+G	ACT	29.0+-1.5	422+-23	2 6 13 15 24 26 27 28 38 40 41 42 43 45 46 47 48 50 411 412	
134	*2.05Y	2.3E+6Y		ACT	140+-12	54.2	6 24 26 27 32	

TABLE II (cont.)

TARGET NUCLIDE		A+1 NUCLIDE		TYPE OF REACTION	THERMAL CROSS-SECTIONS (b) AND g(T) FACTOR	RESONANCE INTEGRALS (b)	RESONANCE INTEGRALS: REFERENCES	MAIN GAMMA RAYS FOR A+1 NUCLIDE ENERGY (keV) (ABSOLUTE INTENSITY: %)
Z-SYMBOL-A	ABUNDANCE (%) OR HALF-LIFE	HALF-LIFE	ISOMER STATE IT (%)					
135	*2.3E+6Y	13.7D		ACT	8.7+-0.5	66+-8	6 24 25 26 27 28 30 34 49 384	177 341 818 1048 1235 (14) (49) (100) (80) (20)
136	*13.7D	30.0Y		ACT	1.3	44+-15	6 24 26	
137	*30.0Y	2.9M	M					112 192 324 463 1436 (8) (81) (6) (98) (100)
		32.2M	G					463 547 1010 1436 2218 (31) (11) (30) (76) (15)
			M+G	ACT	0.110+-0.033	0.43+-0.15	24 26 27 28 34	
56-BA-NAT	-	-	-	ACT	1.2+-0.1	9+-2	6 11 13 17	
130	0.101	14.5M	M IT=100	ACT	2.5+-0.3			
		11.6D	G	ACT	8.8+-0.9			124 216 249 373 496 (29) (20) (3) (13) (44)
			M+G	ACT	11.3+-1.0	235+-25	2 6 29 47 48	
132	0.097	39H	M IT=99	ACT	0.5	3.3+-0.5	6 29	
		10.5Y	G	ACT	6.5+-0.8			81 276 303 356 384 (33) (7) (18) (62) (9)
			M+G	ACT	7.0+-0.8			
134	2.42	29H	M IT=100	ACT	0.158+-0.024	24+-4	6 29 32	268 (16)
		-	G	ACT	1.84+-1.6	13+-11		
			M+G	ACT	2.0+-1.6	37+-10	6 24 25 26	
135	6.59	0.32S	M IT=100	ACT	0.0139+-0.0007	0.465+-0.070		
		-	G	ACT	5.78+-0.90	109.5+-17.0		
			M+G	ACT	5.8+-0.9	110+-17	6 24 25	
136	7.81	2.6M	M IT=100	ACT	0.010+-0.001	0.75+-0.04	29	662 (90)
		-	G	ACT	0.39+-0.40	0.85+-0.30		
			M+G	ACT	0.4+-0.4	1.6+-0.3	6 19 24 25 26 27	
137	11.32	-		ACT	5.1+-0.4	4.8+-0.6	6 19 24 25 26 27 32	
138	71.66	83.3M		ACT	0.360+-0.036	0.32+-0.07	6 20 24 25 26 27 28 29 400 409	166 (22)
139	*83.3M	12.79D		ACT	6.2+-1.6			30 163 305 424 537 (11) (6) (4) (3) (24)
140	*12.79D	18M		ACT	1.6+-0.3	13.2+-0.8	6 24 25 26 27 29 32 38 51	190 277 304 344 648 (46) (23) (25) (14) (6)

TARGET NUCLIDE		A+1 NUCLIDE		TYPE OF REACTION	THERMAL CROSS-SECTIONS (b) AND g(T) FACTOR	RESONANCE INTEGRALS (b)	RESONANCE INTEGRALS: REFERENCES	MAIN GAMMA RAYS FOR A+1 NUCLIDE ENERGY (keV) (ABSOLUTE INTENSITY: %)
Z-SYMBOL-A	ABUNDANCE (%) OR HALF-LIFE	HALF-LIFE	ISOMER STATE IT (%)					
57-LA-NAT	-	-	-	ACT	8.97+-0.05	12.7+-0.8	11 12 52 53 54 55	
138	0.089	-		ACT	57.2+-5.7	548+-96	6 388 428	
139	99.911	40.22H		ACT	8.93+-0.04	12.2+-0.8	2 6 15 19 24 25 26 27 28 29 34 40 47 48 56 57 58 59 60 383 384 388 399	329 (21) 487 (46) 816 (24) 925 (7) 1596 (95)
140	*40.22H	3.87H		ACT	2.7+-0.3	69+-3	24 25 26 27 38 56 388	1355 (3)
58-CE-NAT	-	-	-	ACT	0.63+-0.04	0.67+-0.05	6 13	
136	0.193	34.4H	M IT=99.2	ACT	0.95+-0.25			169 (27) 762 (15) 825 (34) 835 (8) 1005 (2)
		9.0H	G	ACT	6.3+-1.5			447 (1)
			M+G	ACT	7.25+-1.52	58+-12	6 388	
138	0.25	55.0S	M IT=100	ACT	0.015+-0.005			
		137.2D	G	ACT	1.1+-0.3			166 (80)
			M+G	ACT	1.115+-0.300			
139	*137.2D	-		ACT	500			
140	88.48	32.5D		ACT	0.57+-0.04	0.48+-0.04	2 6 20 24 25 26 27 28 29 47 48 61 62 388	145 (48)
141	*32.5D	-		ACT	29+-3	23.7+-4.5	6 24 26 27 34 384	
142	11.07	33H		ACT	0.95+-0.05	1.14+-0.04	6 20 24 25 26 27 28 29 62 388	57 (12) 293 (42) 351 (3) 665 (5) 722 (5)
143	*33H	284D		ACT	6.0+-0.7	40	24 26 27 32	80 (1) 134 (11)
144	*284D	3.0M		ACT	1.0+-0.1	2.6+-0.2	6 24 25 26 27 39 63 388	63 (15) 284 (9) 440 (6) 724 (59) 1148 (9)
59-PR-141	100	14.6M	M	ACT	3.9+-0.3			
		19.2H	G	ACT	7.6+-0.3			642 (12) 1576 (4)
			M+G	ACT	11.5+-0.3	17.8+-3.5	6 10 11 12 15 19 24 25 26 27 28 29 34 40 47 52 384 388 412	
142	*19.2H	13.59D		ACT	20+-3	144	24 26 32	
143	*13.59D	17.27M		ACT	90+-10	185+-15	6 24 25 26 27 34 38 64 384 388	696 (1)

TABLE II (cont.)

TARGET NUCLIDE		A+1 NUCLIDE		TYPE OF REACTION	THERMAL CROSS-SECTIONS (b) AND g(T) FACTOR	RESONANCE INTEGRALS (b)	RESONANCE INTEGRALS: REFERENCES	MAIN GAMMA RAYS FOR A+1 NUCLIDE ENERGY (keV) (ABSOLUTE INTENSITY: %)
Z-SYMBOL-A	ABUNDANCE (%) OR HALF-LIFE	HALF-LIFE	ISOMER STATE IT (%)					
145	*5.98H	24.0M		ACT	18.44	445.1	26	
60-ND-NAT	-	-	-	ACT	50.5+-2.0	43.5+-5.5	6 12 55	
142	27.13	-		ACT	18.7+-0.7	8.5+-1.0	6 24 25 26 32 388 417	
143	12.20	-		ACT	325+-10	136+-35	6 14 15 19 24 25 26 27 28 34 40 384 388	
144	23.87	-		ACT	3.6+-0.3	5+-1	6 24 25 26 27 28 38 388	
145	8.29	-		ACT	42+-2	255+-40	6 14 15 19 24 25 26 27 28 34 40 384 388 424 436	
146	17.18	11.06D		ACT	1.4+-0.1	2.7+-0.4	6 24 25 26 27 28 29 47 62 65 66 388	91 (28) 319 (2) 440 (1) 531 (13)
147	*11.06D	-		ACT	440+-150	540+-150	24 26 34 384 437	
148	5.72	1.8H		ACT	2.5+-0.2	14.0+-1.5	6 24 25 26 27 28 29 59 62 65 66 67 388	114 (19) 211 (27) 270 (11) 424 (9) 541 (8)
150	5.60	12M		ACT	1.2+-0.2	14.5+-2.0	6 24 25 26 27 28 29 59 62 65 66 388	117 (47) 139 (8) 175 (8) 256 (17) 1181 (15)
61-PM-146	*5.53Y	2.62Y		ACT	8400+-1680			
147	*2.62Y	41.3D	M IT=4.65	ACT	85+-5	1045+-265	6 25 34 69 70 388 414	550 (98) 630 (93) 726 (34) 915 (20) 1014 (21)
		5.37D	G	ACT	96+-2	1320+-85	6 25 38 69 70 71 388 414 417	550 (23) 611 (1) 915 (13) 1465 (22)
			M+G	ACT	181+-7	2230+-70	6 15 19 24 26 27 28 34 40 69 70 72 73 384 388 435	
148M	*41.3D	53.1H		ACT	22000+-2500	3600+-2400	6 24 26 27 34 69 384 388	286 (3)
G	*5.37D			ACT	2000+-1000	43500+-4500	24 26 27 34 69 384	
149	*53.1H	2.68H		ACT	1400+-300	825+-50	24 26 27 34 384	334 (69) 832 (12) 876 (7) 1166 (16) 1325 (18)
151	*28.4H	15M	M2					
		7.5M	M1					122 (45) 245 (78) 340 (31) 1097 (29) 1437 (23)
		4.2M	G					122 (16) 696 (1) 841 (2) 961 (2) 963 (2)
			M2+M1+G	ACT	173	1400+-400	24 26 34 384	

TARGET NUCLIDE		A+1 NUCLIDE		TYPE OF REACTION	THERMAL CROSS-SECTIONS (b) AND g(T) FACTOR	RESONANCE INTEGRALS (b)	RESONANCE INTEGRALS: REFERENCES	MAIN GAMMA RAYS FOR A+1 NUCLIDE ENERGY (keV) (ABSOLUTE INTENSITY: %)
Z-SYMBOL-A	ABUNDANCE (%) OR HALF-LIFE	HALF-LIFE	ISOMER STATE IT (%)					
62-SM-NAT	-	-	-	ACT	5800+-100	1430+-120	6 13	
144	3.16	340D		ACT	0.7			61 (12)
147	15.07	-		ACT	64+-5	650+-50	6 14 24 25 26 27 28 34 38 40 75 384 387 388 424	
148	11.27	-		ACT	2.7+-0.6	27+-14	6 24 26 27 28 34 38 74 75 384 388	
149	13.82	-		ACT	41000+-2000 G(T)=1.5860	3700+-400	6 19 24 26 27 28 34 76 411	
150	7.47	93Y		ACT	102+-5	280+-30	6 19 24 25 26 27 28 34 74 76 77 384 387 388 418	
151	*93Y	-		ACT	15000+-1800	3100+-500	6 16 19 24 25 26 27 28 34 38 135 384 388 411	
152	26.63	46.8H		ACT	206+-6	2960+-150	10 11 14 15 18 19 24 26 27 28 29 34 40 41 47 79 80 81 82 384 388 412 432	70 103 (5) (28)
153	*46.8H	-		ACT	334.5	3700+-2000	24 26 34 384	
154	22.53	23.5M		ACT	5.5+-1.1	29+-7	6 24 26 27 28 29 82 83 388	104 141 246 (75) (2) (4)
156	*9.4H	8.0M		ACT	17.16	331.9	26	
63-EU-NAT	-	-	-	ACT	4600+-100 G(T)=0.9069	4346+-170	6 53 55 84 85 409	
151	47.77	96M	M2 IT=100	ACT	4.2+-2.0			
		9.3H	M1 IT=0	ACT	3211+-82 G(T)=0.8936	1823+-146	10 14 29 58 59 84 85 86 87 88 392	122 344 842 963 1389 (26) (3) (52) (43) (3)
		12.7Y	G IT=0	ACT	5935+-73 G(T)=0.9022	3552+-264	48 59 84 85 392	122 344 779 964 1408 (39) (95) (46) (20) (29)
			G+M1+M2	ACT	9146+-109 G(T)=0.8992	5367+-263	6 18 24 27 29 34 53 59 82 83 84 85 392 432	
152		-		ACT	2313			
153	52.23	8.5Y		ACT	603+-23 G(T)=1.0290	3414+-197	6 11 14 15 19 24 25 26 27 28 29 34 40 53 82 83 84 85 392 424	123 185 723 1005 1274 (40) (20) (20) (18) (35)
154	*8.5Y	4.65Y		ACT	1500+-400	1500+-450	6 24 26 27 32 34 384 442	45 60 87 105 (1) (1) (31) (21)

TABLE II (cont.)

TARGET NUCLIDE		A+1 NUCLIDE		TYPE OF REACTION	THERMAL CROSS-SECTIONS (b) AND g(T) FACTOR	RESONANCE INTEGRALS (b)	RESONANCE INTEGRALS: REFERENCES	MAIN GAMMA RAYS FOR A+1 NUCLIDE ENERGY (keV) (ABSOLUTE INTENSITY: %)
Z-SYMBOL-A	ABUNDANCE (%) OR HALF-LIFE	HALF-LIFE	ISOMER STATE IT (%)					
155	*4.65Y	15.4D		ACT	4040+-125	1680+-300	6 24 26 27 28 34 78 89 384 442	89 812 1153 1231 1242 (9) (10) (7) (9) (7)
156	*15.4D	15.1H		ACT	480	1660+-340	24 26 28 34 384	
157	*15.1H	46M		ACT	190	1350+-380	24 26 34 384	79 898 944 977 1108 (11) (10) (25) (14) (4)
64-GD-NAT	-	-	-	ACT	49000+-1000	420+-15	6 13 78 89 409	
152	0.20	242D		ACT	1100+-100	3000+-300	6 47 89 392	70 97 103 (2) (28) (20)
154	2.15	-		ACT	85+-12	280+-60	6 24 25 75 83 89 90 392	
155	14.7	-		ACT	61000+-500 G(T)=0.8387	1570+-40	6 24 26 27 28 34 78 89 384	
156	20.47	-		ACT	1.5+-1.2	100+-20	6 24 25 26 27 28 75 78 89 90 392	
157	15.68	-		ACT	254000+-2000 G(T)=0.8561	850+-100	6 19 24 26 27 28 34 78 89 384	
158	24.9	18.0H		ACT	2.5+-0.5	80+-15	6 24 25 26 27 28 29 47 59 78 83 89 392	58 364 (2) (11)
159	*18.0H	-		ACT	16.3	186.7	26	
160	21.9	3.7M		ACT	0.77+-0.02	7+-1	6 24 25 26 32 78 83 89 392	56 102 283 315 361 (5) (16) (7) (24) (65)
65-TB-159	100	72.1D		ACT	23.2+-0.5	400+-25	2 6 18 19 24 25 26 28 29 47 48 62 91 92 145 392 432	87 299 879 966 1178 (13) (27) (29) (25) (15)
160	*72.1D	6.9D		ACT	525+-100	1135	24 26 32	26 49 57 75 (21) (15) (2) (10)
161	*6.9D	7.48M		ACT	96.6	655.9	26	185 260 808 882 888 (16) (79) (45) (12) (39)
66-DY-NAT	-	-	-	ACT	1000+-40	1520+-80	6 93 94 95 96	
156	0.0524	8.1H		ACT	33+-3	960+-80	6 97	182 326 (2) (95)
158	0.0902	144D		ACT	43+-6	120+-20	6 97	58 (2)
160	2.294	-		ACT	95+-10	1240+-140	5 6 12 13 95 424	
161	18.88	-		ACT	510+-30	1300+-100	6 19 24 25 26 75 95 392 424	

TARGET NUCLIDE		A+1 NUCLIDE		TYPE OF REACTION	THERMAL CROSS-SECTIONS (b) AND g(T) FACTOR	RESONANCE INTEGRALS (b)	RESONANCE INTEGRALS: REFERENCES	MAIN GAMMA RAYS FOR A+1 NUCLIDE ENERGY (keV) (ABSOLUTE INTENSITY: %)
Z-SYMBOL-A	ABUNDANCE (%) OR HALF-LIFE	HALF-LIFE	ISOMER STATE IT (%)					
162	25.53	-		ACT	245+-40	2500+-250	6 19 24 25 26 75 95 392 424	
163	24.97	-		ACT	305+-25	1700+-200	6 19 24 25 26 75 95 392 424	
164	28.18	1.15M	M IT=97.7	ACT	1700+-250			
		2.35H	G	ACT	1000+-150			
			M+G	ACT	2700+-75	650+-100	6 19 24 26 29 34 59 86 95 97 98 145 381 392 424	
165	*2.35H	81.5H		ACT	3900+-300	22000+-3000	6 97	82 (13)
67-HO-165	100	1200Y	M IT=0	ACT	3.5+-0.5	55+-25		81 (13) 184 (75) 280 (30) 712 (60) 810 (64)
		27.2H	G	ACT	61.2+-1.1	660+-35	18 25 29 32 47 59 142 145 432	81 (6)
			M+G	ACT	64.7+-1.2	715+-55	6 19 24 26 55 392 409	
68-ER-NAT	-	-	-	ACT	162+-8	745+-25	3 6 91	
162	0.136	75.1M		ACT	19+-2	480+-30	6 99 392	
164	1.56	10.34H		ACT	13+-2	120+-10	6 99 392	
166	33.41	2.35S	M IT=100	ACT	15+-2			
		-	G	ACT	20+-2			
			M+G	ACT	35+-4	125+-15	6 24 75 83 101 392	
167	22.94	-		ACT	670+-30	3000+-150	6 24 83 101 136 392	
168	27.07	9.6D		ACT	1.95+-0.05	35+-5	6 83 99 101 136 392	
170	14.88	7.52H		ACT	5.7+-0.2	24+-4	6 18 29 59 83 99 136 392 432	112 (21) 117 (2) 124 (9) 296 (30) 308 (66)
171	*7.52H	49.5H		ACT	280+-30			
69-TM-169	100	0.004MS	M IT=100	ACT	8+-1			
		130D	G	ACT	95+-2			79 (3) 84 (3)
			M+G	ACT	103+-3	1710+-70	6 19 29 47 91 97 102 136 392	

TABLE II (cont.)

TARGET NUCLIDE		A+1 NUCLIDE		TYPE OF REACTION	THERMAL CROSS-SECTIONS (b) AND g(T) FACTOR	RESONANCE INTEGRALS (b)	RESONANCE INTEGRALS: REFERENCES	MAIN GAMMA RAYS FOR A+1 NUCLIDE ENERGY (keV) (ABSOLUTE INTENSITY: %)
Z-SYMBOL-A	ABUNDANCE (%) OR HALF-LIFE	HALF-LIFE	ISOMER STATE IT (%)					
170	*130D	1.92Y		ACT	92+-4	460+-50	6 136	
171	*1.92Y	63.6H		ACT	4.5+-0.2	118+-6	6 136	
70-YB-NAT	-	-	-	ACT	36.6+-2.0	195+-15	6 91 103	
168	0.140	46S	M IT=100					
		31.8D	G					63 110 177 198 308 (44) (17) (21) (35) (11)
			M+G	ACT	3470+-100	30500+-2500	6 29 47 83 92 97 102 103 392	
170	3.03			ACT	10+-1	270+-60	75 83 103 392	
171	14.31	-		ACT	50+-4	380+-45	6 75 83 101 103 392	
172	21.82	-		ACT	1.3+-0.8	25.2+-1.6	6 75 83 101 103 392	
173	16.13	-		ACT	19+-2	450+-55	6 75 103 392	
174	31.84	67MS	M IT=100	ACT	46+-4			
		4.2D	G	ACT	19+-6			114 283 396 (2) (3) (6)
			M+G	ACT	65+-5	34.5+-4.5	6 29 47 83 97 101 102 103 392	
176	12.73	6.5S	M IT=100					
		1.9H	G					122 139 150 1080 1241 (3) (1) (20) (5) (3)
			M+G	ACT	2.4+-0.2	8.1+-1.6	6 29 59 83 97 103 392	
71-LU-NAT	-	-	-	ACT	77+-3 G(T)=1.4968	732+-63	6 12 53	
175	97.40	3.69H	M IT=0	ACT	15.10+-1.24	523+-57	29 59 86 339	88 (9)
		3.3E10Y	G	ACT	7+-1	202+-30		88 202 307 (13) (84) (93)
			M+G	ACT	22.1+-1.6	725+-65	6 53 83 88 392 433	
176	2.60	0.160MS	M1	ACT	315+-60			
	*3.3E10Y							
		155D	M2 IT=22	ACT	2.1+-0.7	3.8+-1.0	339	113 208 228 379 419 (28) (79) (48) (36) (26)
		6.74D	G	ACT	1778+-75			113 208 (6) (11)
			M1+M2+G	ACT	2100+-50 G(T)=1.6914	1017+-45	6 29 53 86 88 98 433	

TARGET NUCLIDE		A+1 NUCLIDE		TYPE OF REACTION	THERMAL CROSS-SECTIONS (b) AND g(T) FACTOR	RESONANCE INTEGRALS (b)	RESONANCE INTEGRALS: REFERENCES	MAIN GAMMA RAYS FOR A+1 NUCLIDE ENERGY (keV) (ABSOLUTE INTENSITY: %)
Z-SYMBOL-A	ABUNDANCE (%) OR HALF-LIFE	HALF-LIFE	ISOMER STATE IT (%)					
72-HF-NAT	-	-	-	ACT	102+-2	2020+-65	6 10 11 12 13 14 41 45 94 104 105 106 107 108 142	
174	0.163	70D		ACT	390+-55	288+-24	6 29 108	
176	5.21	-		ACT	38+-6	428+-55	6 94 104 105 106 108	
177	18.56	4.3S	M IT=100	ACT	1.1+-0.1			
		-	G	ACT	363+9			
			M+G	ACT	365+-20	7478+-244	6 94 104 105 106 108	
178	27.1	25.1D	M2 IT=100					
		18.6S	M1 IT=100	ACT	53+-6			
		-	G	ACT	33+-8			
			M+G	ACT	86+-7	1914+-95	6 94 104 105 106 108	
179	13.75	5.5H	M IT=100	ACT	0.34+-0.03	4.75+-0.16	29	
		-	G	ACT	44.66	563+-55		
			M+G	ACT	45+-5	568+-55	6 94 104 105 106 108	
180	35.22	42.5D		ACT	12.6+-0.7	33.6+-3.2	2 6 10 11 29 47 48 94 104 105 106 108 109	133 136 137 346 482 (43) (6) (2) (14) (86)
181	*42.5D	61.5M	M					114 340 603 800 943 (12) (11) (10) (18) (37)
		9E+6Y	G					114 156 270 (3) (7) (80)
			M+G	ACT	40+-30			
73-TA-NAT	-	-	-	ACT	21.6+-0.7	717+-25	3 13 14 41 53 110 111 138 142	
180	0.0123	-		ACT	700+-200	600+-200	6	
181	99.9877	16.5M	M IT=100	ACT	0.012+-0.003	0.415+-0.110	29 339 398 432	
		115.1D	G	ACT	21.5+-0.6	717+-25	180 432	68 100 1121 1189 1221 (41) (14) (35) (16) (27)
			M+G	ACT	21.5+-0.6	717+-25	6 10 11 18 29 47 48 112 113 114 139 144 180 409	
182	*115.1D	5.0D		ACT	8530+-450	977+-58	2 6 110 114 180	108 161 244 246 354 (11) (12) (9) (27) (11)
74-W -NAT	-	-	-	ACT	18.5+-0.5 G(T)=1.6880	352+-23	3 6 12 13 14 93 115 116 117 118 120 409	

TABLE II (cont.)

TARGET NUCLIDE		A+1 NUCLIDE		TYPE OF REACTION	THERMAL CROSS-SECTIONS (b) AND g(T) FACTOR	RESONANCE INTEGRALS (b)	RESONANCE INTEGRALS: REFERENCES	MAIN GAMMA RAYS FOR A+1 NUCLIDE ENERGY (keV) (ABSOLUTE INTENSITY: %)
Z-SYMBOL-A	ABUNDANCE (%) OR HALF-LIFE	HALF-LIFE	ISOMER STATE IT (%)					
180	0.135	121D		ACT	3.5	200	6	
182	26.4	-		ACT	20.7+-0.5	591+-45	6 83 118	
183	14.4	-		ACT	10.2+-0.3	367+-38	6 83 118	
184	30.6	1.62M	M IT=100	ACT	0.002+-0.001			
		75D	G	ACT	1.8+-0.2			
			M+G	ACT	1.8+-0.2	13.4+-2.5	6 29 83 93 116 118 121 140	
186	28.4	23.9H		ACT	37.0+-1.5	490+-15	6 10 11 18 29 58 83 86 93 116 118 121 122 123 124 125 126 127 128 129 143 400 432	72 (11) 134 (9) 480 (21) 618 (6) 686 (26)
187	*23.9H	69.4D		ACT	64+-10	2670+-550	6 126	
75-RE-NAT	-	-	-	ABS	88.7+-3.8	828+-36	6 130 141 416	
185	37.07	88.9H		ACT	112+-3	1718+-45	6 10 11 29 131 132 133 134 137 141 409	
187	62.93	18.7M	M IT=100	ACT	73+-4	8.8+-0.8	29	
		16.7H	G	ACT	1.6+-0.3	296.2+-10.0		155 (15) 478 (1) 633 (1)
			M+G	ACT	75+-4	305+-10	6 10 11 29 132 137 141 409	
76-OS-NAT	-	-	-	ACT	15.3+-0.7	172+-35	13 53	
184	0.018	93.6D		ACT	3005+-122	1354+-52	29 146	592 (1) 646 (81) 717 (4) 875 (7) 881 (5)
186	1.59			ACT	0.001			
187	1.64	-		ACT	336+-17	890+-100	6	
188	13.3	5.7H	M IT=100					
		-	G					
			M+G	ACT	4.3+-1.0	135+-35	6	
189	16.1	10M	M IT=100	ACT	0.26+-0.03	0.013+-0.001	29	
		-	G	ACT	22.74+-4.00	750+-50		
			M+G	ACT	23+-4	750+-50	6	

TARGET NUCLIDE		A+1 NUCLIDE		TYPE OF REACTION	THERMAL CROSS-SECTIONS (b) AND g(T) FACTOR	RESONANCE INTEGRALS (b)	RESONANCE INTEGRALS: REFERENCES	MAIN GAMMA RAYS FOR A+1 NUCLIDE ENERGY (keV) (ABSOLUTE INTENSITY: %)
Z-SYMBOL-A	ABUNDANCE (%) OR HALF-LIFE	HALF-LIFE	ISOMER STATE IT (%)					
190	26.4	15H	M IT=100	ACT	13.20+-0.31	26.5+-2.5	29 146	
		15D	G	ACT	3.9+-0.8	31.7+-2.5	29	129 (26)
			M+G	ACT	17.1+-0.9	58.2+-3.7	6	
192	41.0	31.5H		ACT	1.97+-0.11	5.4+-1.3	6 29 146	73 (3) 139 (4) 322 (1) 387 (1) 460 (4)
193	*31.5H	6.0Y		ACT	1540			43 (2)
77-IR-NAT	-	-	-	ACT	426+-4 G(T)=1.0320	2606+-120	6 13 53	
191	38.5	241Y	M2 IT=100	ACT	0.32+-0.17			
		1.4M	M1 IT=99	ACT	300+-30	1060+-150	147 148	
		74.2D	G	ACT	624+-20	3535+-250	29 86	206 (70) 308 (31) 316 (87) 468 (50) 485 (67)
			M+G	ACT	924+-53 G(T)=1.0326	4595+-290	6 10 11 46 147 148	
192	*74.2D	-		ACT	1100+-400			
193	61.5	171D	M IT=0	ACT	5.8+-2.0			328 (93) 483 (97) 562 (70) 600 (62) 688 (59)
		19H	G	ACT	110+-15			294 (3) 328 (13) 645 (1)
			M+G	ACT	112.5+-7.5 G(T)=1.0218	1362+-33	6 10 11 29 86	
78-PT-NAT	-	-	-	ACT	10.0+-0.2	128+-15	6 11 14 41 142 409	
190	0.0127	3.0D		ACT	150+-150			82 (5) 172 (4) 360 (6) 409 (8) 539 (14)
192	0.78	4.4D	M IT=100	ACT	2.2+-0.8			
		(50)Y	G					
			M+G	ACT	<14	83+-10	6	
194	32.9	4.1D	M IT=100	ACT	0.090+-0.013			
		-	G	ACT	1.11			
			M+G	ACT	1.2+-0.9	4+-2	6	
195	33.8	-		ACT	27+-2	355+-50	6	
196	25.2	1.5H	M IT=96.7	ACT	0.050+-0.10			130 (3) 202 (1) 279 (71)
		18H	G					77 (17) 191 (4)
			M+G	ACT	0.74+-0.08	8.3+-2.0	6 29 57	

TABLE II (cont.)

TARGET NUCLIDE		A+1 NUCLIDE		TYPE OF REACTION	THERMAL CROSS-SECTIONS (b) AND g(T) FACTOR	RESONANCE INTEGRALS (b)	RESONANCE INTEGRALS: REFERENCES	MAIN GAMMA RAYS FOR A+1 NUCLIDE ENERGY (keV) (ABSOLUTE INTENSITY: %)
Z-SYMBOL-A	ABUNDANCE (%) OR HALF-LIFE	HALF-LIFE	ISOMER STATE IT (%)					
198	7.19	14S	M IT=100	ACT	0.027+-0.003			
		31M	G	ACT	3.673			77 (2) 186 (3) 317 (5) 494 (6) 543 (15)
			M+G	ACT	3.7+-0.2	55.6+-2.5	6 18 29 57 119 123 432	
199	*31M	11.5H		ACT	1.5+-1.0			60 (2) 76 (13) 136 (3) 227 (2) 244 (3)
79-AU-197	100	2.7D		ACT	98.8+-0.3 G(T)=1.0038	1551+-13	2 3 6 86 88 123 129 149 150 151 153 154 409 446	412 (95) 676 (1)
198	*2.70	3.15D		ACT	26736+-850	-(41240+-4190)	417	158 (37) 208 (8)
80-HG-NAT	-	-	-	ACT	375+-5	73+-10	6 11 12 13	
196	0.146	24H	M IT=93.5	ACT	120+-13	58.9+-2.4	6 29 155	130 (3) 202 (1) 279 (71)
		65H	G	ACT	3080+-200	413+-15	6 29 155	77 (18)
			M+G	ACT	3200+-200	471.9+-15.2	155	
198	10.02	43M	M IT=100	ACT	0.018+-0.004	1.8+-0.3	29	
		-	G	ACT	1.882+-0.200	68.2+-30.0		
			M+G	ACT	1.9+-0.2	70+-30	6	
199	16.84	-		ACT	2000+-1000	153+-30	6	
200	23.73	-		ACT	<60			
201	13.22	-		ACT	<60			
202	29.80	46.9D		ACT	4.9+-0.1	4.43+-0.25	6 29 46 155 156	279 (81)
204	6.85	5.5M		ACT	0.43+-0.10	0.80+-0.04	29	204 (2)
81-TL-NAT	-	-	-	ACT	3.4+-0.5	12.3+-2.5	6 96 157	
203	29.50	3.78Y		ACT	11.0+-0.5	40+-2	6 10 11 102 157	
204	<3.78Y	-		ACT	21.6+-2.0	86+-17	6	
205	70.50	4.19M		ACT	0.10+-0.03	0.7+-0.2	6 10 11	
82-PB-NAT	-	-	-	ACT	0.170+-0.002	0.16+-0.05	6 11 14 409	
204	1.40	1.4E+7Y		ACT	0.661+-0.070	1.7+-0.5	6	

TARGET NUCLIDE		A+1 NUCLIDE		TYPE OF REACTION	THERMAL CROSS-SECTIONS (b) AND g(T) FACTOR	RESONANCE INTEGRALS (b)	RESONANCE INTEGRALS: REFERENCES	MAIN GAMMA RAYS FOR A+1 NUCLIDE ENERGY (keV) (ABSOLUTE INTENSITY: %)
Z-SYMBOL-A	ABUNDANCE (%) OR HALF-LIFE	HALF-LIFE	ISOMER STATE IT (%)					
206	25.1	-		ACT	0.0305+-0.008	0.2+-0.1	6	
207	21.7	-		ACT	0.709+-0.010	0.4+-0.2	6	
208	52.3	3.3H		ACT	0.487+-0.030			
83-BI-209	100	3.5E+6Y	M IT=0	ACT	0.019+-0.002			266 305 650 (50) (28) (4)
		5.01D	G	ACT	0.014+-0.003			
			M+G	ACT	0.033+-0.004	0.20+-0.06	6 11 14 41	
210	*5.01D	2.16M		ACT	0.054+-0.005	0.20+-0.02	158	351 (13)
84-PO-210	*138.4D	25.0S	M IT=0	ACT	<0.0005			
		0.52S	G	ACT	<0.030			
85-AT-211	*7.21H	122MS						63 (8)
86-RN-220	*55.6S	25.0M		ACT	<0.2			150 186 217 254 265 (6) (26) (3) (10) (5)
222	*3.8D	43.0M		ACT	0.72+-0.07			
87-FR-223	*22.0M	2.7M						
88-RA-223	*11.43D	3.64D		ACT	130+-20			241 (4)
224	*3.64D	14.8D		ACT	12.0+-0.5			40 (29)
226	*1600Y	41.2M		ACT	11.5+-1.5 G(T)=1.0708	222+-15	6	27 277 284 300 303 (17) (3) (3) (5) (5)
228	*5.75Y	4.0M		ACT	36+-5			
89-AC-227	*21.77Y	6.13H		ACT	762+-29	1017+-103	159 160	209 338 911 965 969 (5) (12) (29) (5) (17)
90-TH-227	*18.72D	1.913Y		FISS	200+-20			
228	*1.913Y	7340Y		FISS	<0.3			
				ACT	123+-15	>1013	6	31 86 137 194 211 (4) (3) (2) (5) (3)
229	*7340Y	8E+4Y		FISS	30.5+-3.0 G(T)=1.0494	350+-80	6 177 415	
				ACT	54+-6	1000+-175	6	

TABLE II (cont.)

TARGET NUCLIDE		A+1 NUCLIDE		TYPE OF REACTION	THERMAL CROSS-SECTIONS (b) AND g(T) FACTOR	RESONANCE INTEGRALS (b)	RESONANCE INTEGRALS: REFERENCES	MAIN GAMMA RAYS FOR A+1 NUCLIDE ENERGY (keV) (ABSOLUTE INTENSITY: %)
Z-SYMBOL-A	ABUNDANCE (%) OR HALF-LIFE	HALF-LIFE	ISOMER STATE IT (%)					
				ABS	84.5+-6.7	1350+-190		
230	*8E+4Y	25.6H		FISS	<0.0012			
				ACT	23.2+-0.6	990+-40	6 161 162 163 178 415 448	26 (15) 84 (6)
231	*25.6H	-		FISS	26.68	156.2	409	
				ACT	160.1	837.6	409	
				ABS	186.78	993.8	409	
232	100	22.12M		FISS	(39+-4)E-6	0.0746+-0.0016	164 409	
				ACT	7.40+-0.08	82.3+-2.4	6 11 22 29 38 47 48 165 166 167 168 169 170 171 207 239 409 415	29 (2) 86 (3) 459 (1)
				ABS	7.40+-0.08	82.4+-2.4	3 13 14 22 45 172 173 174 176 235 302 409	
233	*22.12M	24.1D		FISS	15+-2	84	409	
				ACT	1500+-100	408+-75	6 207 409	63 (4) 92 (3) 93 (3)
				ABS	1515	492+-75	409	
234	*24.1D	6.9M		FISS	<0.01			
				ACT	1.8+-0.5			
91-PA-230	*17.4D	32500Y		FISS	1500+-200			
231	*32500Y	1.31D		FISS	0.006+-0.001 G(T)=1.0670	0.049+-0.013	180	
				ACT	219+-6 G(T)=1.0378	1040+-40	3 6 180 181 182 183 448	150 (11) 454 (9) 819 (7) 894 (20) 969 (42)
232	*1.31D	27.0D		FISS	700+-100			
				ACT	464+-95	289+-67	180	87 (2) 300 (6) 312 (36) 340 (4) 416 (2)
				ABS	1164+-135			
233	*27.0D	1.17M	M IT=0.13	ACT	21+-3	425+-33	30 175 184 415	
		6.67H	G	ACT	20+-3	440+-48	175 184	131 (20) 569 (14) 883 (12) 926 (11) 946 (12)
			M+G	FISS	<0.1			
				ACT	41+-3 G(T)=1.0579	865+-35	6 38 175 184 186 207 385 415	

TARGET NUCLIDE		A+1 NUCLIDE		TYPE OF REACTION	THERMAL CROSS-SECTIONS (b) AND g(T) FACTOR	RESONANCE INTEGRALS (b)	RESONANCE INTEGRALS: REFERENCES	MAIN GAMMA RAYS FOR A+1 NUCLIDE ENERGY (keV) (ABSOLUTE INTENSITY: %)
Z-SYMBOL-A	ABUNDANCE (%) OR HALF-LIFE	HALF-LIFE	ISOMER STATE IT (%)					
234M	*1.17M	23.7M		FISS	<5000			
G	*6.67H			FISS	<500			
92-U -NAT	-	-	-	FISS	4.19+-0.01			
				ACT	3.35+-0.02			
				ABS	7.54+-0.02			
230	*20.8D	4.3D		FISS	25+-10			
231	*4.3D	72Y		FISS	400+-300			
232	*72Y	162000Y		FISS	74+-3 G(T)=0.9739	348+-35	3 6 180 415	
				ACT	73.1+-1.5 G(T)=0.9932	280+-15	3 6 182 188 415	
				ABS	147.1+-3.4 G(T)=0.9836	628+-38	3 415	
233	*162E+3Y	247000Y		FISS	522.6+-2.8 G(T)=0.9963	783.4+-7.8	3 6 38 169 180 185 187 189 190 191 192 193 194 195 196 197 199 200 201 202 203 204 206 207 260 409 415	
				ACT	47.7+-2.0 G(T)=1.0152	138.1+-4.6	3 6 38 190 192 193 195 196 197 200 203 204 207 409 415	
				ABS	578.8+-2.0 G(T)=0.9977	921.5+-9.1	3 38 192 193 195 196 197 200 203 204 207 409 415	
234	0.005 *2.4E+5Y	7.1E+8Y		FISS	<0.65	5.96	226 228 409	
				ACT	100.2+-1.5	678+-38	3 6 38 207 227 228 409 415	109 144 163 186 205 (1) (10) (5) (54) (5)
				ABS	101+-2 G(T)=1.001	684+-38	228 409	
235	0.720 *7.1E+8Y	239E+5Y		FISS	582.2+-1.3 G(T)=0.9757	276.3+-2.8	3 6 29 38 88 124 154 191 193 196 197 203 205 206 207 208 209 210 211 212 213 214 215 216 217 218 219 220	
				ACT	93.6+-1.5 G(T)=1.0052	141.8+-4.2	3 6 11 38 193 196 197 203 207 209 210 212 214 216 218 221 222 223 225 287 381 409 415	
				ABS	680.8+-1.3 G(T)=0.9801	418.1+-5.1	3 38 193 196 197 203 207 209 210 211 212 214 218 224 225 287 381 409 415	

TABLE II (cont.)

TARGET NUCLIDE		A+1 NUCLIDE		TYPE OF REACTION	THERMAL CROSS-SECTIONS (b) AND g(T) FACTOR	RESONANCE INTEGRALS (b)	RESONANCE INTEGRALS: REFERENCES	MAIN GAMMA RAYS FOR A+1 NUCLIDE ENERGY (keV) (ABSOLUTE INTENSITY: %)
Z-SYMBOL-A	ABUNDANCE (%) OR HALF-LIFE	HALF-LIFE	ISOMER STATE IT (%)					
236	*239E+5Y	6.75D		FISS	0.0	2	225 226 228 409	
				ACT	5.2+-0.3	358+-8	207 227 228 409 415 448	26 (2) 60 (33) 65 (1) 165 (2) 208 (22)
				ABS	5.2+-0.3 G(T)=1.007	360+-8	3 6 15 30 38 113 217 225 228 229 230 231 232 233 234 236 409	
237	*6.75D	451E+7Y		FISS	2.	95.60	226 409	
				ACT	411+-100	373.3	6 409	
				ABS	413+-100	468.9	225 409	
238	99.275 *451E+7Y	23.5M		FISS	<0.0005	0.0013+-0.0002	397 409	
				ACT	2.70+-0.02 G(T)=1.009	276.3+-2.7	3 6 11 14 29 38 47 124 168 207 217 218 219 237 238 239 240 241 242 287 409 415 419	44 (4) 75 (50)
				ABS	2.70+-0.02	276.3+-2.7		
239	*23.5M	14.1H		FISS	14+-3	264.2	409	
				ACT	22+-5	156.6	409	44 (2)
				ABS	36+-6	420.8	409	
240	*14.1			FISS	0.0	1.62	409	
				ACT	1.524	176.2	409	
				ABS	1.524	177.82	409	
93-NP-234	*4.4D	396D		FISS	900+-300			
235	*396D	22.5H	M	ACT	1600+-200			642 (2)
		129E+4Y	IT=0 G	ACT	184+-4			100 (6) 104 (8) 160 (30)
			M+G	ACT	1784			
236G	*129E+4Y	214E+4Y		FISS	2500+-150			
237	*214E+4Y	2.12D		FISS	0.019+-0.003 G(T)=1.0015	6.5+-1.2	38 154 409	
				ACT	169+-3 G(T)=1.0072	821.5+-58.0	41 228 409 415 448	924 (3) 984 (24) 1026 (8) 1029 (17)
				ABS	169+-3 G(T)=1.0072	828+-58	6 14 38 53 113 225 243 409	

TARGET NUCLIDE		A+1 NUCLIDE		TYPE OF REACTION	THERMAL CROSS-SECTIONS (b) AND g(T) FACTOR	RESONANCE INTEGRALS (b)	RESONANCE INTEGRALS: REFERENCES	MAIN GAMMA RAYS FOR A+1 NUCLIDE ENERGY (keV) (ABSOLUTE INTENSITY: %)
Z-SYMBOL-A	ABUNDANCE (%) OR HALF-LIFE	HALF-LIFE	ISOMER STATE IT (%)					
238	*2.12D	2.35D		FISS	2200+-200	1454+-150	6 38 225 243 244	
				ACT	43	29	38 225 226 243	106 (23) 210 (3) 228 (11) 278 (14) 316 (2)
				ABS	2243+-200	1483	3 38 225 243	
239	*2.35D	7.5M	M IT=.113	ACT	31+-6			263 (1) 303 (1) 555 (22) 597 (12) 818 (1)
		65M	G	ACT	14+-14			448 (18) 566 (29) 601 (22) 896 (14) 974 (23)
			M+G	FISS	<1			
				ACT	45+-15			
94-PU-236	*2.85Y	45.6D		FISS	165+-20	960	226	
				ACT	33	197	226	229 (8) 280 (22) 299 (16) 313 (6) 321 (13)
				ABS	195	1157		
237	*45.6D	87.8Y		FISS	2400+-300			
238	*87.8Y	24390Y		FISS	16.5+-0.5	24.2+-2.7	6 30 38 225 228 243 245 246 247 409 415	
				ACT	547+-20	154+-9	6 38 225 228 243 245 246 247 248 409 415	
				ABS	564+-20	178.2+-9.4	6 38 225 228 243 245 246 247 249 250 409 415	
239	*24390Y	6450Y		FISS	744.4+-1.7 G(T)=1.0489	312.2+-8.2	3 6 38 88 154 191 193 197 199 202 203 206 207 208 213 216 217 218 243 246 251 252 253 254 255 257 258 259	
				ACT	268.8+-3.0 G(T)=1.1686	191+-16	3 6 38 88 203 207 216 217 218 243 246 251 252 254 261 287 409 415	
				ABS	1013.2+-3.5 G(T)=1.0812	503.2+-18.0	3 38 88 203 207 216 217 218 243 246 251 252 254 287 409 415	
240	*6450Y	15Y		FISS	0.030+-0.045	5	262 409 415	
				ACT	289.5+-1.4	8460+-305	3 6 14 38 41 207 228 243 261 263 264 265 266 267 268 269 287 304 409 415	104 (4) 149 (8)
				ABS	289.53+-1.41	8465+-305	409 415	

TABLE II (cont.)

TARGET NUCLIDE		A+1 NUCLIDE		TYPE OF REACTION	THERMAL CROSS-SECTIONS (b) AND g(T) FACTOR	RESONANCE INTEGRALS (b)	RESONANCE INTEGRALS: REFERENCES	MAIN GAMMA RAYS FOR A+1 NUCLIDE ENERGY (keV) (ABSOLUTE INTENSITY: %)
Z-SYMBOL-A	ABUNDANCE (%) OR HALF-LIFE	HALF-LIFE	ISOMER STATE IT (%)					
241	*15Y	387E+3Y		FISS	1009+-8 G(T)=1.0421	558+-18	3 6 38 191 197 202 203 207 208 228 243 246 268 270 409 415	
				ACT	368+-10 G(T)=1.0314	161+-13	3 6 38 203 207 228 243 246 268 409 415	
				ABS	1377+-10 G(T)=1.0388	719+-22	3 38 203 207 228 243 246 268 271 409 415	
242	*387E+3Y	4.96H		FISS	<0.2	5	6 272 273 409 415	
				ACT	18.5+-0.4	1131+-57	6 207 228 248 275 409 415	84 (23)
				ABS	18.7+-0.4	1136+-57	3 243 245 268 272 273 274 276 277 278 306 409	
243	*4.96H	8.3E+7Y		FISS	180	518	273 409	
				ACT	87.4	267	273 409	
				ABS	267.4	785	273 409	
244	*8.3E+7Y	10.5H		ACT	1.7+-0.1	39+-6	6 279	308 (5) 327 (25) 377 (3) 492 (3) 560 (5)
245	*10.5H	10.85D		ACT	150+-30	220+-40	6	28 (4) 44 (25) 180 (10) 224 (23)
95-AM-241	*433Y	13.0S	M2	ACT	(10+-5)E-5			
		152Y	M1 IT=9	ACT	83.8+-2.6	208+-18	6 243 279 281 282	49 (41) 67 (5) 87 (8) 110 (5) 163 (5)
		16.02H	G	ACT	748+-20	1330+-117	6 243 279 281 282 421 434	
			M+G	FISS	3.15+-0.10 G(T)=1.0287	21.5+-1.7	6 228 281 301 409 415 434	
				ACT	832+-20 G(T)=1.0020	1538+-118	228 281 283 409 415	
				ABS	836.15 G(T)=1.0021	1559.5+-118.0	228 278 281 409 415	
242 M1	*152Y	7370Y		FISS	6600+-300	2260+-200	6 243 246 284 286 301 409 415	
				ACT	1400+-860	1100+-500	243 246 409	44 (5) 75 (60)
				ABS	8000+-800	3360+-540	6 243 246 279 409	
G	*16.02H			FISS	2900+-100	300	281 415	
243	*7370Y	26M	M IT=0	ACT	75.2+-1.8	2089+-11		
		10.1H	G	ACT	4.1+-0.2	111+-10	6 113 422	99 (5) 154 (18) 746 (66) 900 (27)
			M+G	FISS	0.20+-0.11	13+-2.5	228 272 273 301 409 415 434	

TARGET NUCLIDE		A+1 NUCLIDE		TYPE OF REACTION	THERMAL CROSS-SECTIONS (b) AND g(T) FACTOR	RESONANCE INTEGRALS (b)	RESONANCE INTEGRALS: REFERENCES	MAIN GAMMA RAYS FOR A+1 NUCLIDE ENERGY (keV) (ABSOLUTE INTENSITY: %)
Z-SYMBOL-A	ABUNDANCE (%) OR HALF-LIFE	HALF-LIFE	ISOMER STATE IT (%)					
				ACT	79.3+-1.8	2200+-15	6 228 243 248 272 273 274 281 306 409 415 422 434	
				ABS	79.5+-1.8 G(T)=0.9182	2213+-15	113 228 247 273 276 285 409 415	
244M	*26M	2.07H		FISS	1600+-300			
G	*10.1H			FISS	2300+-300			
96-CM-242	*163D	20Y		FISS	5	33	226 243 409	
				ACT	16+-5	156+-35	6 226 243 279 409	210 228 278 (3) (11) (14)
				ABS	21+-5	189+-35	243 409 438	
243	*28Y	17.9Y		FISS	672+-60	1527+-142	6 243 288 289 402 409 439	
				ACT	138+-10	214+-17	243 402 409	
				ABS	810+-61	1741+-143	6 243 290 409	
244	*17.9Y	8.5E+3Y		FISS	1.2+-0.1	13.4+-1.5	6 228 243 245 246 247 272 273 276 278 289 294 301 409 415	
				ACT	13.9+-1.0	632.6+-32.0	6 228 243 245 246 247 272 273 276 278 279 289 409 415 441	133 174 (5) (5)
				ABS	15.1	646+-32	228 243 245 246 247 273 276 278 289 290 306 409 415 438	
245	*8.5E+3Y	4760Y		FISS	2020+-40	805+-80	6 243 272 273 276 278 289 293 294 301 409 415	
				ACT	345+-20	101+-8	6 243 272 273 276 278 289 291 409 415 441	
				ABS	2365+-45	906+-80	243 273 276 278 279 289 290 409 415 441	
246	*4760Y	154E+5Y		FISS	0.17+-0.10	11.3+-1.2	6 243 272 273 278 294 301 409 415	
				ACT	1.3+-0.3	121.3+-7.5	6 243 272 273 279 289 291 296 409 415 441	278 287 346 402 (3) (2) (1) (72)
				ABS	1.47+-0.32	132.6+-7.6	243 273 276 278 306 409 415 438	
247	*154E+5Y	3.5E+5Y		FISS	80+-7	754+-60	6 243 272 273 278 289 293 294 301 409 415	

TABLE II (cont.)

TARGET NUCLIDE		A+1 NUCLIDE		TYPE OF REACTION	THERMAL CROSS-SECTIONS (b) AND $g(T)$ FACTOR	RESONANCE INTEGRALS (b)	RESONANCE INTEGRALS: REFERENCES	MAIN GAMMA RAYS FOR A+1 NUCLIDE ENERGY (keV) (ABSOLUTE INTENSITY: %)
Z-SYMBOL-A	ABUNDANCE (%) OR HALF-LIFE	HALF-LIFE	ISOMER STATE IT (%)					
				ACT	60+-15	650+-250	6 243 272 273 278 289 409 415 441	
				ABS	140+-17	1404+-257	243 273 278 289 409 415	
248	*3.5E+5Y	64M		FISS	0.34+-0.07	13.1+-1.5	6 272 273 278 294 301 409 415	
				ACT	4+-1	275+-75	6 243 272 273 289 295 296 409 415 441	634 (1)
				ABS	4.34+-1.00	288.1+-75.0	273 278 409 415 438	
249	*64M	11300Y		ACT	1.6+-0.8			
97-BK-249	*311D	3.22H		FISS	3	5	272 273 409 415	
				ACT	1300+-3	1170+-80	243 272 273 409 434	890 (2) 929 (1) 989 (45) 1029 (5) 1032 (36)
				ABS	1303+-300	1175+-80	6 273 276 278 409	
250	*3.22H	57M		FISS	960+-150			
98-CF-249	*350.6Y	13.1Y		FISS	1676+-51	2157+-70	6 243 273 278 293 294 298 301 409 434	
				ACT	492+-28	743+-65	6 243 273 278 386 409 434	
				ABS	2168+-58	2900+-96	243 273 278 409	
250	*13.1Y	900Y		FISS	350	85	272 273 409 415	
				ACT	2030+-200	11600+-500	243 272 273 386 409 415 441	177 (18) 227 (6) 285 (1)
				ABS	2380+-200	11685+-500	6 273 276 278 409 415	
251	*900Y	2.63Y		FISS	4300+-300	5400+-1500	6 243 272 273 276 278 409 415	
				ACT	2850+-150	1600+-30	6 243 272 273 276 278 386 409 415	
				ABS	7150+-350	7000+-1500	243 273 276 278 409 415	
252	*2.63Y	17.8D		FISS	32+-4	110+-30	6 243 272 273 278 297 409 415	
				ACT	20.4+-1.5	43.5+-3.0	6 243 272 273 278 305 409 415	
				ABS	52.4+-4.3	153.5+-30.1	243 273 276 278 299 303 409 415	

TARGET NUCLIDE		A+1 NUCLIDE		TYPE OF REACTION	THERMAL CROSS-SECTIONS (b) AND g(T) FACTOR	RESONANCE INTEGRALS (b)	RESONANCE INTEGRALS: REFERENCES	MAIN GAMMA RAYS FOR A+1 NUCLIDE ENERGY (keV) (ABSOLUTE INTENSITY: %)
Z-SYMBOL-A	ABUNDANCE (%) OR HALF-LIFE	HALF-LIFE	ISOMER STATE IT (%)					
253	*17.8D	60.5D		FISS	1300+-240	2117	272 273 278 415	
				ACT	17.6+-1.8	13	272 273 278	
				ABS	1317.6+-240.0	2130	273 278	
254	*60.5D			FISS	2	28	272	
				ACT	88+-30	1650	272	
				ABS	90+-30	1678	278	
99-ES-253	*20.47D	39.3H	M IT=0	ACT	155+-20	3009+-168	6 256	71 177 212 649 694 (13) (17) (29) (29) (25)
		276D	G	ACT	3	4299+-218	6 256	63 (2)
			M+G	FISS	0.0	0.0	273	
				ACT	158+-20	7308+-275	256	
254M	*39.3H	39D		FISS	1840+-80	1000	256	
				ACT	1.3			
				ABS	1841.3			
G	*276D			FISS	2830+-130	2200+-90	6 300	
				ACT	40			
				ABS	2870+-130			
255	*39D			ACT	43+-10			
100-FM-254	*3.24H	20.1H		ACT	76			81 (1)
255	*20.1H	2.63H		FISS	3400+-170			
				ACT	26+-3			
				ABS	3426+-170			
256	*2.63H	100.5D		ACT	45			62 179 241 (1) (9) (10)
257	*100.5D	0.38MS		FISS	2950+-160			
				ACT	3150			
				ABS	6100+-600	5000	401	

5. EXPLANATION OF THE COLUMNS IN TABLE II

Column 1 – Atomic number, symbol and mass number of the target nuclides. M signifies a metastable state and G the ground state.

Column 2 – Per cent abundance of natural nuclides. Data with an asterisk represent the half-lives of radioactive nuclides.

Column 3 – Half-lives of A + 1 nuclides.

Column 4 – Metastable state (M), ground state (G) and per cent internal transition (IT) of the upper to the next lower state, taken in most cases from Ref. [310].

Column 5 – Type of thermal cross-section and resonance integral.

Column 6 – Thermal cross-sections at 2200 m/s neutron velocity ($E_0 = 0.0253$ eV). For the non-1/v nuclides, the $g(T_n = 20°C)$ Westcott factor is also given.

Column 7 – Resonance integrals I (from $E_c = 0.5$ eV), including the 1/v contribution.

Column 8 – References for the resonance integrals.

Column 9 – Main gamma rays and their absolute intensities, taken in most cases from the Evaluated Nuclear Structure Data File library [447] and from the Table of Isotopes [310].

ACKNOWLEDGEMENTS

The authors are grateful to H. Lemmel and K. Okamoto of the Nuclear Data Section of the IAEA for their assistance and co-operation in the preparation of this compilation.

REFERENCES

1. E.M.GRYNTAKIS,J.I.KIM,J.RADIOANAL.CHEM.,76(1983)341.
2. A.AHMAD,ANN.NUCL.ENERGY,10(1983)41.
3. M.K.DRAKE,NUCLEONICS,24(1966)NO.8,108.
4. H.ALBINSON,IAEA,TECHNICAL REPORTS SERIES NO.156,VIENNA,1974 P.15.
5. P.RIBON,J.KREPS,73 BOLOGNA,REVIEW PAPER NO.10(1973) OR IAEA-169, FISSION PRODUCT NUCLEAR DATA,1(1974)235.
6. NEUTRON CROSS SECTIONS,BNL-325,3RD ED.,VOL.1, 1973,AND VOL.1PART A,1981.
7. CINDA 79,IAEA,VIENNA,1979.
8. M.BRESESTI,A.M.BRESESTI DEL TURCO,H.NEUMANN,E.ORVINI,J.INORG.NUCL. CHEM.,26(1964)1625.
9. M.F.ELGART,THESIS,CITY UNIV.OF NEW YORK,1971,UNIV.MICROFILMS ORDER NO.72-988,DA/B32,3245,1971.
10. S.P.HARRIS,C.O.MUEHLHAUSE,G.E.THOMAS,PHYS.REV.,79(1950)11.
11. R.L.MACKLIN,H.S.POMERANCE,PROC.CONF.PEACEFUL USES OF ATOMIC ENERGY, GENEVA,5(1956)96.
12. P.E.SPIVAK,B.G.EROZOLIMSKY,V.I.LAVERENCHIK,PROC.CONF.PEACEFUL USES OF ATOMIC ENERGY,GENEVA,5(1956)91.
13. V.B.KLIMENTOV,V.M.GRIAZEV,J.NUCL.ENERGY,9(1959)20,TRANSL. FROM AT. ENERG. (USSR)3(1957)507.
14. R.B.TATTERSALL,H.ROSE,S.K.PATTENDEN,D.JOWITT,J.NUCL.ENERGY,12(1960)32

15. E.A.NEPHEW,REP.ORNL-2869,REACTORS-POWER TID-4500(15TH ED.),1960.
16. N.J.PATTENDEN,NUCL.SCI.ENG.,17(1963)371.
17. YU.A.PROKHOROV,INDSWG-64,1964,P.75.
18. OFFICE OF ATOMIC ENERGY FOR PEACE,BANGKOK, CERTAIN ACCOUNTS ON THE UTILIZATION OF THE THAI RESEARCH REACTOR,BANGKOK CONF.REP. THAI-AEC-10,1967.
19. M.A.PALMUCCI,COMITATO NATIONALE ENERGIA NUCLEARE,RT/FI(67)4,ROMA,1967
20. M.D.RICABARRA,R.TURJANSKI,G.H.RICABARRA,C.B.BIGHAM,CAN J.PHYS.,46 (1968)2473.
21. D.BRUNE,RADIOCHIM.ACTA,12(1969)119.
22. L.BREITENHUBER,H.HEIMER,M.PINTER,ATOMKERNENERGIE,15(1970)83 (SEE ALSO EANDC(OR)-68,1968,P.10).
23. T.B.RYVES,J.NUCL.ENERGY,24(1970)35.
24. R.E.SCHENTER, PRIVATE COMMUNICATIONS TO NEA/DATA BANK, CALCULATIONS FROM ENDF/B-IV LIBRARY,HANFORD ENG. DEVELOPMENT LABORATORY, RICHLAND,WASH.USA,1975.
25. W.H.WALKER,AECL-3037,PART I,1972.
26. E.CLAYTON,AUSTRALIAN AEC,REP.AAEC/TM619(1972).
27. H.H.SAKATA,S.NAGAYAMA,JAP.ATOMIC ENERGY RESEARCH,TOKAI,UNPUBLISHED (SEE REF.5).
28. G.LAUTENBACH,REP.RCN-191,1973.
29. R.VAN DER LINDEN,F. DE CORTE,J.HOSTE,J.RADIOANAL.CHEM.,20(1974)695 (SEE ALSO 73PARIS,IAEA,2(1973)241.
30. T.A.EASTWOOD,A.P.BAERG,C.B.BIGHAM,F.BORWN,M.J.CABELL,W.E.GRUMMITT, J.C.ROY,L.P.ROY,R.P.SCHUMAN,2ND PROC.CONF.PEACEFUL USES OF ATOMIC ENERGY,IAEA,GENEVA,16(1958)54.
31. J.C.ROY,D.WUSCHE,CAN.J.CHEM.,36(1958)1424.
32. T.R.ENGLAND,WAPD-TM-333,1965.
33. J.HALPERIN,R.E.DURSCHEL,ORNL-3488,1963,P.15.
34. A.L.POPE,AEEW-M-1266,1974(SEE ALSO AEEW-M-1234,1973 AND AEEW-M-1191, 1973).
35. T.A.EASTWOOD,F.BROWN,EANDC(CAN),16(1963)6.
36. M.BRESESTI,F.CAPPELANI,A.M.DEL TURCO,E.ORVINI,J.INORG.NUCL.CHEM.,26 (1964)9.
37. M.BRESESTI,F.CAPPELANI,A.M.DEL TURCO,H.NEUMANN,E.ORVINI,J.INORG.NUCL. CHEM.,27(1965)1175.
38. O.J.EDER,M.LAMMER,NUCLEAR DATA IN SCIENCE AND TECHNOLOGY,IAEA,73PARIS 1,1973,P.233.
39. E.S.STIPPEL,ORNL-TR-1365,1965.
40. J.D.GARRISON,B.W.ROOS,NUCL.SCI.ENG.,12(1962)115.
41. H.ROSE,W.A.COOPER,R.B.TATTERSALL,2ND PROC.CONF.PEACEFUL USES OF ATOMIC ENERGY,IAEA,GENEVA,1(1958)16.
42. A.P.BAERG,R.M.BARTHOLOMEW,CAN.J.CHEM.,38(1960)2528.
43. F.BROWN,P.J.CAMPION,B.H.OLIVER,J.NUCL.ENERGY,13A(1961)141.
44. R.VIDAL,E.CARDOSO-MARTINHO,CEA-R-2840,1965 (SEE ALSO CEA-R-2486. 1964 AND REF.45).
45. J.C.CARRE,R.VIDAL,NUCLEAR DATA FOR REACTORS,IAEA,66PARIS,1(1966)479 (SEE ALSO REF.44,68).
46. G.H.E.SIMS,D.G.JUHNKE,J.INORG.NUCL.CHEM.,30(1968)349.
47. E.STEINNES,J.INORG.NUCL.CHEM.,34(1972)2699.
48. A.ALIAN,H.-J.BORN,J.I.KIM,J.RADIONAL.CHEM.,15(1973)535.
49. A.P.BAERG,F.BROWN,M.LOUNSBURY,CAN.J.PHYS.,36(1958)863.
50. H.M.EILAND,F.B.FEHR,E.C.HANSEN,J.L.MEWHERTER,KAPL-2000-11,III-30,1960
51. J.HALPERIN,J.S.ELDRIDGE,H.A.O'BRIEN,JR.,R.E.DRUSCHEL,ORNL-4164,1,1967
52. V.A.KONKS,YU.P.POPOV,F.L.SHAPIRO,J.EXPERIM.THEORET.PHYS.,46(1964)80.
53. J.W.ROGERS,J.J.SCOVILLE,TRANS.AM.NUCL.SOC.,10(1967)259(SEE ALSO REF. 55).
54. H.SHWE,R.E.COTE,W.V.PRESTWICH,PHYS.REV.,159(1967)1050.
55. J.J.SCOVILLE,J.W.ROGERS,IN-1195,1968 (SEE ALSO REF.53).
56. H.A.O'BRIEN,JR.,J.S.ELDRIDGE,R.E.DRUSCHEL,J.HALPERIN,J.INORG.NUCL. CHEM.,29(1967)584.
57. T.B.RYVES,J.NUCL.ENERGY,25(1971)129(SEE ALSO REF.304).
58. F.DE CORTE,A.SPEECKE,J.HOSTE,J.RADIOANAL.CHEM.,9(1971)9.
59. E.STEINNES,J.INORG.NUCL.CHEM.,37(1975)1591.
60. E.ORVINI,G.GAGGERO,L.LESCA,A.M.BRESESTI,M.BRESESTI,J.INORG.NUCL. CHEM.,30(1968)1353.
61. P.M.LANTZ,C.R.BALDOCK,L.E.IDON,NUCL.SCI.ENG.,20(1964)302(SEE ALSO TRANS.AM.NUCL.SOC.,6(1963)44).
62. J.ALSTAD,T.JAHNSEN,A.C.PAPPAS,J.INORG.NUCL.CHEM.,29(1967)2155(SEE ALSO INDC(NOR)-1/G,1972,P.1).
63. P.M.LANTZ,NUCL.SCI .ENG.,13(1962)289.
64. J.C.ROY,L.P.ROY,CAN.J.PHYS.,37(1959)907.
65. J.I.KIM,E.M.GRYNTAKIS,RADIOCHIM.ACTA,17(1972)191.
66. M.D.RICABARRA,R.TURJANSKI,G.H.RICABARRA,CAN.J.PHYS.,51(1973)1454.
67. C.P.RUITZ,J.P.PETERSON,JR.,B.F.RIDER,TRANS.AM.NUCL.SOC.,7(1964)270.
68. R.VIDAL,EANDC(E)-57,1965,P.170(SEE ALSO EANDC(E)-57,1965,P.171 AND REF.45).
69. R.P.SCHUMAN,J.R.BERRETH,NUCL.SCI.ENG.,12(1962)519.
70. N.C.FENNER,R.S.LARGE,J.INORG.NUCL.CHEM.,29(1967)2147(SEE ALSO EANDC(UK)-75-5,1966).
71. M.J.CABELL,J.INORG.NUCL.CHEM.,32(1970)3433.
72. J.E.CODDING,JR.,R.L.TROMP,F.B.SIMPSON,NUCL.SCI.ENG.,43(1971)58.

73. G.J.KIROUAC,H.M.EILAND,C.A.CONRAD,R.E.SLOVACEK,K.W.SEEMAN,NUCL.SIC. ENG.,52(1973)310.
74. H.M.EILAND,S.WEINSTEIN,K.W.SEEMAN,NEUTRON CROSS SECTION AND TECHNO., PROC.OF THE 3RD CONF.(CONF-710301)OF UNIV.OF TENESSEE,KNOXVILLE,1971, P.673.
75. R.DOBROZEMSKY,F.PICHLMAYER,F.P.VIEHBOECK,INTERN.J.MASS SPECTROM.ION PHYS.,6(1971)435(SEE ALSO REF.100).
76. K.L.AITKIN,F.W.CORNISH,J.INORG.NUCL.CHEM.,17(1961)6.
77. J.HALPERIN,R.E.DRUSCHEL,C.R.BALDOCK,TRANS.AM.NUCL.SOC.,5(1962)376.
78. S.F.MUGHABGHAB,R.E.CHRIEN,PHYS.REV.,180(1969)1131.
79. W.H.WALKER,R.E.GREEN,CAN.J.PHYS.,39(1961)1184.
80. R.E.CHRIEN,CAN.J.PHYS.,39(1961)1193.
81. M.S.CABELL,J.INORG.NUCL.CHEM.,24(1962)749.
82. F.J.RAHN,C.HO,TRANS.AM.NUCL.SOC.,12(1969)749.
83. F.J.RAHN,H.S.CAMARDA,G.HACKEN,W.W.HAVENS,JR.,H.I.LIOU,J.RAINWATER, M.SLAGOWITZ,S.WYNCHANK,NUCL.SCI.ENG.,49(1972)219.
84. G.H.E.SIMS,O.G.JUHNKE,J.INORG.NUCL.CHEM.,29(1967)2671.
85. J.I.KIM,E.M.GRYNTAKIS,H.-J.BORN,RADIOCHIM.ACTA,22(1975)20.
86. P.P.DAMLE,A.FABRY,H.VAN DEN BROECK,BLG-421,CEN-SCK,MOL(1967).
87. F.V.ORESTANO,F.PISTELLA,NUCL.SCI.ENG.,37(1969)478.
88. A.GIBELLO,F.V.ORESTANO,F.PISTELLA,E.SANTANDREA,NUCL.SCI.ENG.,40 (1970)51.
89. S.J.FRIESENHAHN,M.P.FRICKE,D.G.COSTELLO,W.M.LOPEZ,D.CARLSON,NUCL. PHYS.,A146(1970)337.
90. P.M.LANTZ,C.R.BALDOCK,L.E.IDOM,ORNL-3832,1965,P.7.
91. J.J.SCOVILLE,J.W.ROGERS,TRANS.AM.NUCL.SOC.,8(1965)290.
92. G.H.RICABARRA,R.TURJANSKI,M.D.RICABARRA,CN-26/1,1970(THE SAME AS 70 HELS,2(1970)589).
93. J.J.SCOVILLE,D.W.KNIGHT,E.FAST,TRANS.AM.NUCL.SOC.,5(1962)377.
94. J.J.SCOVILLE,E.FAST,D.W.KNIGHT,NUCL.SCI.ENG.,18(1964)400.
95. J.J.SCOVILLE,E.FAST,J.W.ROGERS,NUCL.SCI.ENG.,25(1966)12.
96. G.HUETTEL,KERNENERGIE,14(1971)73.
97. J.ALSTAD,A.C.PAPPAS,T.SYVERSEN,INDC(NOR)-1/G,1972,P.2.
98. W.L.ZIJP,NUCLEAR DATA IN SCIENCE AND TECHN.,IAEA,VIENNA,2(1973)271.
99. O.GLOMSET,A.C.PAPPAS,INDC(NOR)-1/G,1972,P.3.
100. R.DOBROZEMSKY,F.PICHLMAYER,F.P.VIEHBOECK,SGAE-PH-104,1971(SEE ALSO REF.75 AND ALSO EANDC(OR)-68,1968,P.11).
101. H.LIOU,F.RAHN,C.HO,J.RAINWATER,W.W.HAVENS,JR.,TRANS AM.NUCL.SOC.,13 (1970)300.
102. G.H.E.SIMS,D.G.JUHNKE,J.INORG.NUCL.CHEM.,32(1970)2839.
103. S.F.MUGHABGHAB,R.E.CHRIEN,PHYS.REV.,174(1968)1400.
104. J.W.ROGERS,J.J.SCOVILLE,NUCL.SCI.ENG.,33(1968)350.
105. J.T.REYNOLDS,C.R.LUBITZ,I.ITKIN,D.R.HARRIS,KAPL-3327(ENDF-112),1967.
106. R.H.FULMER,L.J.ESCH,F.FEINER,T.F.RUANE,WASH 68 E20,1968.
107. M.DEMMELER,R.HECKER,H.IONAS,K.KLEINSCHNITTGER,D.V.S.RAMAKRISHNA, ATOMWIRTSCHAFT,16(1971)532.
108. H.JONAS,R.HECHER,W.GIESSER,ATOMKERNENERGIE,25(1975)271.
109. M.D.RICABARRA,R.TURJANSKI,G.H.RICABARRA,CAN.J.PHYS.,47(1969)2031.
110. G.E.STOKES,R.P.SCHUMAN,O.D.SIMPSON,NUCL.SCI.ENG.,33(1968)16(SEE ALSO TRANS.AM.NUCL.SOC.,6(1963)41).
111. S.LATEK,J.TOPA,NUKLEONIKA,13(1968)881.
112. L.LESAGE,R.SHER,REACTOR PHYSICS IN THE RESONANCE AND THERMAL REGIONS, PROC.ANSMATH.TOP.MEET.SAN DIEGO,CALIF.,2(1966)175.
113. R.P.SCHUMAN,J.R.BERRETH,IN-1296,1969.
114. E.H.OTTEWITTE,J.M.OTTER,P.F.ROSE,C.L.DUNFORD,AI-AEC-12990,1971.
115. ARGONNE NATIONAL LAB.,ANL-6580,1962,P.32.
116. E.FAST,J.J.SCOVILLE,IDO-16781,1962,P.2.
117. S.P.KAPCHIGASHEV,YU.P.POPOV,AT.ENERG.(USSR),15(1963)120.
118. G.JOANOU,C.STEVENS,GA-5885,1964.
119. P.W.DE LANGE,C.B.BIGHAM,NUCL.APPL.,4(1968)190.
120. H.HEIMEL,M.HEINDLER,ATOMKERNENERGIE,20(1972)135.
121. C.R.PIERCE,D.F.SHOOK,NUCL.SCI.ENG.,31(1968)431.
122. C.M.JACKS,DP-608,1961.
123. J.W.CONNOLLY,A.ROSE,T.WALL,AAEC/TM 191,1963.
124. N.P.BAUMANN,DP-817,1963.
125. M.BRESESTI,A.M.BRESESTI-DEL TURCO,A.ROTA,AERE-R-4500,PART III,1964, P.221.
126. J.H.GILLETTE,ORNL-4013,1965,P.5.
127. L.BELLER,D.LATHAM,J.OTTER,NORTH AMERICAN ARIATION,INC.,NAA-SR-12500, 1967.
128. G.BORCHARDT,JUL-503-RX,1967.
129. T.WALL,AAEC/TM466,1968.
130. R.A.KARAM,T.F.PARKINSON,66WASH,1966,P.171.
131. R.SHER,L.LESAGE,T.J.CONNOLLY,H.L.BORWN,TRANS.AM.NUCL.SOC.,9(1966)248.
132. D.F.SHOOK,C.R.PIERCE,TRANS.AM.NUCL.SOC.,10(1967)261.
133. H.L.BROWN,JR.,T.J.CONNOLLY,W.K.FOELL,TRANS.AM.NUCL.SOC.,5(1962)375.
134. H.L.BROWN,DISSERTATION ABSTRACTS SECTION B,27(1966)1244.
135. G.J.KIROUAC,H.M.EILAND,PHYS.REV.C,11(1975)895.
136. J.H.GILLETTE,ORNL-4155,1967.
137. S.J.FRIESENHAHN,D.A.GIBBS,E.HADDAO,F.FROEHNER,W.M.LOPEZ,J.NUCL. ENERGY,22(1968)191.
138. C.R.PIERCE,D.F.SHOOK,D.BOGART,NASA-TN5628,1970.

139. V.MARKOVIC,A.KOCIC,BULL.BORIS KINDRIC INST.NUCL.SCI.NUCL.ENG., 22(1971)1.
140. R.E.COTE BULL.AM PHYS.SOC.,6(1961)417.
141. C.R.PIERCE,NASA/D-4938,1968.
142. R.SHER,PERSONAL COMMUNICATION CITED IN NEA/DATA BANK INTERNAL FILE(SEE ALSO "KEY TO NOTES" NO.16).
143. P.P.DAMLE,A.FABRY,R.JACQUEMIN,EANDC(E)-76,1967,P.107.
144. G.WOLF,NUKLEONIK,2(1960)255.
145. T.B.RYVES,K.J.ZIEBA,J.PHYS.A,7(1974)2318.
146. J.I.KIM,F.ADAMS,RADIOCHIM.ACTA,9(1968)61.
147. W.KOEHLER,E.SCHNEIDER,NUKLEONIK,12(1969)197(SEE ALSO REF.148).
148. E.SCHNEIDER,EANDC(E)89,1968,P.43.
149. K.JIRLOW,E.JOHANSSON,J.NUCL.ENERGY,PART A,11(1960)101.
150. R.A.BENNETT,NUCLEAR PHYSICS RESEARCH QUARTERLY REP.,HW-63576, 1960,P.26.
151. M.BROSE,DISSERTATION TECHNISCHE HOCHSCHULE KARLSRUHE,1960(SEE ALSO NUKLEONIK,6(1964)134).
152. G.BEN-DAVID,B.HUEBSCHMANN,J.NUCL.ENERGY,PARTS A/B,16(1962)291.
153. E.JOHANSSON,DISS.CHALMERS TEKN.HOGSKOLA,GOTEBORG,1966.
154. R.L.SIMONS,W.N.MC ELROY,BNWL-1312(UC-34)1970.
155. J.I.KIM,F.ADAMS,RADIOCHIM.ACTA,8(1967)165.
156. D.BRUNE,K.JIRLOW,J.NUCL.ENERGY,17(1963)350.
157. V.A.KONKS,F.L.SHAPIRO,SOV.PHYS.,JETP,20(1965)531.
158. J.HALPERIN,J.H.OLIVER,ORNL-3320,1962,P.2.
159. M.J.CABELL,CAN.J.CHEM.,37(1959)1094.
160. M.MONSECOUR,P.DE REGGE,J.INORG.NUCL.CHEM.,37(1975)1841.
161. R.W.ATTREE,M.J.CABELL,R.L.CUSHING,J.J.PIERONI,CAN.J.PHYS.,40(1962)194
162. R.E.COTE,H.DIAMOND,J.E.GINDLER,H.L.A.SHWE,PHYS.REV.,176(1968)1421.
163. S.M.KALEBIN,P.N.PALEJ,P.N.IVANOV,Z.K.KARALOVA,G.M.KUKAVADZE, Z.I.PYZHOVA,G.V.RUKOLAJNE,68DUBNA,ACC-61/18,1968,P.18(SEE ALSO ATOM-NAYA ENERGIYA,26(1969)507 AND SOVIET ATOMIC ENERGY,26(1969)588).
164. J.R.DEEN,E.LINN DRAPER,JR.,J.J.CHRDMIK,TRANS.AM.NUCL.SOC.,16(1973)316
165. G.G.MYASISCHEVA,M.P.ANIKINA,L.L.GOLD'DIN,B.V.ERSHLER,AT.ENERG.(USSR). 2(1957)22(TRANSL.IN SOVIET ATOMIC ENERGY,5(1957)230).
166. F.J.JOHSTON,J.HALPERIN,R.W.STOUGHTON,H.NUCL.ENERGY,11(1960)95.
167. L.I.TIREN,J.M.JENKINS,UK AEE REPORT AEEW-R,1962,P.163.
168. J.B.SAMSON,GA-3069,1962.
169. J.HARDY,NUCL.SCI.ENG.,22(1965)121.
170. M.BROSE,NUCL.SCI.ENG.,19(1964)244.
171. N.M.STEEN,WAPD-TM-971,1970.
172. W.K.FOELL,T.J.CONNOLLY,NUCL.SCI.ENG.,21(1965)406.
173. M.ASGHAR,C.M.CHAFFEY,M.C.MOXON,N.J.PATTENDEN,E.R.RAE,C.A.UTTLEY,NUCL. PHYS.76(1966)196.
174. M.R.BHAT,R.E.CHRIEN,PHYS.REV.,155(1967)1362.
175. R.R.SMITH,T.O.PASSEL,S.D.REEDER,N.P.ALLEY,R.L.HEATH,IDO-16226,1955.
176. H.DERRIEN,NEANDC(E)163U,1975,P.73.
177. YU.YA.KONAKHOVICH,M.I.PEVZNER,AT.ENERG.(USSR),8(1960)47(TRANSL.IN SOVIET ATOMIC ENERGY,8(1961)39).
178. M.J.CABELL,CAN.J.PHYS.,36(1958)989.
179. E.M.GRYNTAKIS,J.I.KIM,J.INORG.NUCL.CHEM.,36(1974)1447 (SEE ALSO REF. 180).
180. E.M.GRYNTAKIS,THESIS,TECHNICAL UNIVERSITY OF MUNICH,DM-6909,1976 (SEE ALSO REF. 179).
181. F.B.SIMPSON,W.H.BURGOS,J.E.EVANS,H.W.KIRBY,NUCL.SCI.ENG.,12(1962)243.
182. M.K.DRAKE,P.F.NICHOLS,GA-7462,1967.
183. B.M.ALEKSANDROV,M.A.BAK,A.S.KRIVOKHATSKII,E.A.SHLYAMIN,SOVIET ATOMIC ENERGY,32(1972)203.
184. T.A.EASTWOOD,R.W.WERNER,CAN.J.PHYS.,38(1960)751.
185. J.HALPERIN,R.E.DRUSCHEL,R.W.STOUGHTON,A.E.CAMERON,R.L.WALKER, ORNL-3320,1962,P.2.
186. J.C.CONNOR,R.T.BAYARD,D.MAC DONALD,S.B.GUNST,NUCL.SCI.ENG.,29(1967) 408.
187. F.B.SIMPSON,J.W.CODDING,JR.,NUCL.SCI.ENG.,28(1967)133.
188. J.HALPERIN,C.R.BALDOCK,J.H.OLIVER,NUCL.SCI.ENG.,21(1965)257(SEE ALSO REF.275).
189. M.S.MOORE,L.G.MILLER,O.D.SIMPSON,PHYS.REV.,118(1960)714.
190. J.HALPERIN,F.J.JOHNSTON,R.W.STOUGHTON,J.H.OLIVER,E.L.BLEVINS, R.E.DRUSCHEL,A.L.HARKNESS,B.A.SWARZ,NUCL.SCI.ENG.,16(1963)245.
191. C.B.BIGHAM,AECL-1910,1964 (SEE ALSO CRRP-1183,1964).
192. L.J.ESCH,F.FEINER,TRANS.AM.NUCL.SOC.,7(1964)272.
193. F.FEINER,L.J.ESCH,66 SAN DIEGO,2(1966)299.
194. T.YASUNO,NUCL.SCI.TECHN.,2(1965)532.
195. N.L.SNIDOW,ADVANCED PRODUCTS ENG.DEPART.,BAW-393-5,1966.
196. D.E.CONWAY,S.B.GUNST,NUCL.SCI.ENG.,29(1967)1.
197. H.H.HENNIES,66PARIS II,IAEA,1967,P.333.
198. M.J.CABELL,66 PARIS II,IAEA,1967,P.3.
199. J.HARDY,JR.,NUCL.SCI.ENG.,27(1967)135.
200. L.W.WESTON,R.GWIN,G.DE SAUSSURE,R.R.FULLWOOD,R.W.HOCKENBURY,NUCL.SCI. ENG.,34(1968)1(SEE ALSO TRANS.AM.NUCL.SOC.,10(1967)220).
201. M.G.CAO,E.MIGNECO,J.P.THEOBALD,M.MERLA,J.NUCL.ENERGY,24(1970)111(SEE ALSO NUCL.DATA FOR REACTORS,VOL.I,IAEA-CN-26/19,1970,P.419.).
202. M.A.BAK,K.A.PETRZHAK,YU.G.PETROV,YU.F.ROMANOV,E.A.SHLYAMIN,AT.ENERG. (USSR),28(1970)359(TRANSL.IN SOVIET ATOMIC ENERGY,28(1970)460).

203. H.M.EILAND,L.S.ESCH,F.FEINER,J.L.MEWHERTER,NUCL.SCI.ENG.,44(1971)180.
204. A.OKAZAKI,M.LOUNSBURY,R.W.DURHAM,CHALK RIVER REP.,AECL-2148,1964.
205. E.CLAYTON,AECD-4167,1955.
206. C.G.CAMPBELL,R.G.FREEMANTLE,M.J.POOLE,PROC.2ND INTERN.CONF.PEACEFUL USES ATOMIC ENERGY,GENEVA,16(1958)233.
207. R.W.STOUGHTON,J.HALPERIN,NUCL.SCI.ENG.,6(1959)100.
208. J.HARDY,JR.,D.KLEIN,G.G.SMITH,NUCL.SCI.ENG.,9(1961)341.
209. G.H.HANNA,W.H.WALKER,EANDC(CAN)-20,1963.
210. K.PARKER,AWRE-O-82/63,1963.
211. G.JOANOU,GA-5944,1964.
212. R.G.FREEMANTLE,REP.AEEW-M-502,1965.
213. HELLSTRAND,NUCKLEONIK,8(1966)1(SEE ALSO AKTIEBOLAGET ATOMENERGI REPORTS,AE-181,1965).
214. G.DE SAUSSURE,L.W.WESTON,R.GWIN,R.W.INGLE,J.H.TODD,NUCLEAR DATA FOR REACTORS,(PROC.CONF.PARIS,1966),IAEA,2(1966)233.
215. A.J.DERUYTTER,C.WAGEMANS,68WASH,1(1968)475.
216. UY.V.RYABOV,SO DON-SIK,N.CHIKOV,N.YANEVA,AT.ENERG.(USSR),24(1968)351 (TRANSL.IN SOVIET ATOMIC ENERGY,24(1968)435).
217. E.M.PAGE,K.L.MAHNA,NEUTRON CROSS SECTIONS AND TECHNOLOGY,PROC.OF THE 3RD CONF.(CONF-710301) OF UNIV.OF TENNESSEE,KNOXVILLE,1971,P.469.
218. J.GADO,CENTRAL RESEARCH INSTITUT FOR PHYSICS,BUDAPEST,REP.KFKI-74-45, 1974.
219. G.K.UNDERHILL,DISSERTATION ABSTRACTS SECTION B,34(1974)6026.
220. C.WAGEMANS,A.J.DERUYTTER,PERSONNAL COMMUNICATION CITED IN NEA DB FILE (SEE "KEY TO NOTES",NR.16).1976.
221. R.W.JONES,EAN(CAN)13/4,1962.
222. I.H.CROCKER,EAN(CAN)17/4,1963.
223. R.W.DURHAM,G.C.HANNA,M.LOUNSBURY,C.B.BIGHAM,R.G.HART,R.W.JONES, 66PARIS II,IAEA,1967,P.17.
224. I.V.GORDEEV,V.Y.PUPKO,PROC.2ND INTERN.CONF.PEACEFUL USES OF ATOMIC ENERGY,IAEA,GENEVA,16(1958)141.
225. E.J.HENNELLY,W.R.CORNMAN,N.P.BAUMANN,68WASH-1271,1968.
226. B.HINKELMANN,2ND INTERN.CONF.ON NUCLEAR DATA,HELSINKI,CN-26/15,1970.
227. V.E.PILCHER,D.J.HUGHES,J.A.HARVEY,BULL AM.PHYS.SOC.,1(1956)187.
228. S.PEARLSTEIN,CONFERENCE ON NEUTRON CROSS SECTION TECHNOLOGY, CONF-660303,BOOK 1,P.251,WASHINGTON 22-24 MARCH 1966.
229. J.HARVEY,R.SCHWARTZ,PROGRESS IN NUCL ENERGY,PHYS.AND MATH.,VOL.2 (PERGAMON PRESS,LONDON,1958)P.51.
230. M.J.CABELL,T.A.EASTWOOD,P.J.CAMPION,J.NUCL.ENERGY,7(1958)81.
231. J.HALPERIN,J.H.OLIVER,PROC.2ND INTERN.CONF.PEACEFUL USES ATOMIC ENERGY,IAEA GENEVA,16(1958)64.
232. J.R.BERRETH,R.P.SCHUMAN,WASH-1041,1962,P.37.
233. A.OKAZAKI,M.LOUNSBURY,R.W.DURHAM,I.H.CROCKER,AECL-1965,1964.
234. N.P.BAUMANN,J.D.HALFORD,D.J.PELLARIN,NUCL.SCI.ENG.,32(1968)265.
235. B.R.SEHGAL,TRANS.AM.NUCL.SOC.,6(1963)41.
236. A.D.CARLSON,S.J.FRIESENHAHN,W.M.LOPEZ,M.P.FRICKE,NUCL.PHYS.A,141 (1970)577.
237. H.L.ANDERSON,PHYS.REV.,80(1950)499.
238. J.A.HARVEY,D.J.HUGHES,R.S.CARTER,V.E.PILCHER,PHYS.REV.,99(1955)10.
239. R.L.MACKLIN,H.S.POMERANCE,J.NUCL.ENERGY,2(1956)243.
240. L.M.BOLLINGER,R.E.COTE,D.A.DAHLBERG,G.E.THOMAS,PHYS.REV.,105(1957)661
241. J.HARDY,JR.,G.G.SMITH,D.KLEIN,NUCL SCI.ENG.,14(1962)358.
242. J.W.WEBSTER,ORNL-TM-1448,1966.
243. S.H.EBERLE,H.J.BLEYL,H.BRAUN,A.V.BAECKMANN,L.KOCH,REPORT KFK-1453 (EUR-4726D),1972,P.1(SEE ALSO REF.280).
244. J.D.SPENCER,N.P.BAUMANN,TRANS.AM.NUCL.SOC.12(1969)284.
245. C.L.DUNFORD,H.ALTER,NAA-SR-12271,1967.
246. H.IHLE,H.MICHAEL,A.NEUBERT,A.J.F.BLAIR,P.DAMLE,M.V.BODNARESCU,J. INORG.NUCL.CHEM.,34(1972)2427.
247. L.P.ABAGYAN,A.G.DOVOJENKO,S.N.ZAKHAROVA,V.F.KAPUSTINA,M.N.NIKOLAEV, D.V.PETROVA,PROC.2ND SOVIET CONF.,73KIEV,1(1973)246.
248. J.P.BUTLER,M.LOUNSBURY,J.S.MERRIT,CAN.J.PHYS.,35(1957)147.
249. F.B.SIMPSON,R.P.SCHUMAN,TRANS.AM.NUCL.SOC.,6(1963)43.
250. T.E.YOUNG,F.B.SIMPSON,J.R.BERRETH,M.S.COOPS,NUCL.SCI.ENG.,30(1967)355
251. L.M.BOLLINGER,R.E.COTE,G.E.THOMAS,PROC 2ND INTERN.CONF.PEACEFUL USES ATOMIC ENERGY(PROC.CONF.GENEVA,1958),15(1958)127.
252. P.J.PERSIANI,J.J.KAGANOVE,A.E.MC ARTY,TID-18590,1963.
253. M.J.CABELL,M.WILKINS,J.INORG.NUCL.CHEM.,27(1965)2481.
254. J.J.SCHMIDT,KFK-120,1966.
255. L.G.PONCELET,ARGONNE CODE CENTER ABSTRACT 249,WCAP-6073,1966.
256. R.M.HARBOUR,K.W.MAC MURDO,J.INORG.NUCL.CHEM.,35(1973)1821.
257. T.YASUNO,NUCL.SCI.TECHN.,4(1967)43.
258. G.C.HANNA,C.H.WESTCOTT,H.D.LEMMEL,B.R.LEONARD,JR.,J.S.STORY, P.M.ATTREE,IAEA,ATOMIC,ENERGY REV.,7(1969)3.
259. A.PRINCE,68WASH,2(1968)951(SEE ALSO REF.272).
260. J.I.KIM,R.BECK,E.M.GRYNTAKIS,R.ZAGHLOUL,NUCLEAR INSTRUMENTS AND METHODS,165(1979)565.
261. F.W.CORNISH,M.LOUNSBURY,CRC-633,1956.
262. M.W.DYOS,NUCL.SCI.ENG.,34(1968)181.
263. B.G.EROZOLYMSKY,I.E.KUTIKOV,Y.P.DOBRYNIN,M.I.PEVZNER,L.S.DANELYAN, S.S.MOSKALEV,J.NUCL.ENERGY,4(1957)86.
264. P.A.KRUPCHINSKY,J.NUCL.ENERGY,6(1957)155.
265. B.R.LEONARD,JR.,E.J.SEPPI,W.J.FRIESEN,NUCL.SCI.ENG.,5(1959)32.

266. W.H.WALKER,C.H.WESTCOTT,T.K.ALEXANDER,CAN.J.PHYS.,38(1960)57.
267. W.H.NICHOLS,NUCL.SCI.ENG.,17(1963)144(SEE ALSO TRANS.AM.NUCL.SOC.,5 (1962)374).
268. M.K.DRAKE,GA-6576,1965.
269. J.L.COOK,A.L.WALL,AAEC/TM362,1966.
270. C.WAGEMANS,A.J.DERUYTTER,NUCL.SCI.ENG.,60(1976)44(SEE ALSO 75WASH,GB 17,1975).
271. D.S.CRAIG,C.H.WESTCOTT,CAN.J.PHYS.,42(1964)2384.
272. A.PRINCE,TRANS.AM.NUCL.SOC.,10(1967)228(SEE ALSO REF.259).
273. R.W.BENJAMIN,V.D.VANDERVELDE,T.C.GORELL,F.J.MC CROSSON,75WASH,1975, P.224.
274. R.E.COTE,L.M.BOLLINGER,R.F.BARNES,H.DIAMOND,PROC.2ND INTERN.CONF. PEACEFUL USES ATOMIC ENERGY,IAEA,GENEVA,16(1958)77.
275. J.HALPERIN,J.H.OLIVER,ORNL-2679,1964,P.13.
276. R.L.FOLGER,J.A.SMITH,L.C.BROWN,R.F.OVERMAN,H.P.HOLCOMB,68WASH,2(1968) 1279.
277. T.E.YOUNG,S.D.REEDER,NUCL.SCI.ENG.,40(1970)389.
278. B.C.RUSCHE,TRANS.AM.NUCL.SOC.,14(1971)344.
279. R.P.SCHUMAN,WASH-1136,1969,PAGES 51,53 AND 53(SEE ALSO REF.113, REF.288 AND IN-1317,1969).
280. S.H.EBERLE,KFK-1544,1972,P.62(SEE ALSO REF.243).
281. M.A.BAK,A.S.KRIVOKHATSKII,K.A.PETRZHAK,YU.G.PETROV,YU.F.ROMANOV, E.A.SHLYAMIN,AT.ENERG.(USSR),23(1967)316(TRANSL.IN SOVIET ATOMIC ENERGY,23(1967)1059).
282. R.M.HARBOUR,K.W.MAC MURDO,F.J.MC CROSSON,NUCL.SCI.ENG.,50(1973)364.
283. J.J.SCOVILLE,E.FAST,WASH-1053,1964,P.78.
284. S.T.PERKINS,G.F.AUCHAMPAUGH,R.W.HOFF,C.D.BOWMAN,NUCL.SCI.ENG.,32 (1968)131.
285. O.D.SIMPSON,F.B.SIMPSON,J.A.HARVEY,G.G.SLAUGHTER,R.W.BENJAMIN, C.E.AHLFELD,NUCL.SCI.ENG.,55(1974)273.
286. C.D.BOWMAN,G.F.AUCHAMPAUGH,S.C.FULTS,R.W.HOFF,PHYS.REV.,166(1968)1219
287. R.C.KIIKALA,W.L.PURCELL,J.R.WORDEN,66WASH,1(1966)75.
288. R.P.SCHUMAN,WASH-1124,1968,P.72(SEE ALSO REF.113,279).
289. M.C.THOMPSON,M.L.HYOER,R.J.REULAND,J.INORG.NUCL.CHEM.,33(1971)1553.
290. J.R.BERRETH,F.B.SIMPSON,B.C.RUSCHE,NUCL.SCI.ENG.,49(1972)145.
291. J.HALPERIN,R.E.RUSCHE,R.E.EBY,ORNL-4437,1969,P.20.
292. C.H.WESTCOTT,W.H.WALKER,TK.ALEXANDER,2ND INT.CONF.PEACEFUL USES OF ATOMIC ENERGY,IAEA,GENEVA,16(1958)70.
293. J.HALPERIN,J.H.OLIVER,R.W.STROUGHTON,ORNL-4581,1970,P.37.
294. R.W.BENJAMIN,K.M.MAC MURDO,J.D.SPENCER,NUCL.SCI.ENG.,47(1972)203(SEE ALSO 3RD CONF.NEUTRON CROSS SECTION AND TECHN.,KNOXVILLE,TENNESSEE CONF-710301,2(1971)843).
295. CHETHAM-STRODE,ORNL-3832,1965,P.1.
296. R.W.BENJAMIN,C.E.AHLFELD,BULL.AM.PHYS.SOC.,19(1974)599.
297. J.HALPERIN,J.H.OLIVER,R.W.STOUGHTON,ORNL-4706,1971.
298. C.E.BEMIS,JR.,J.W.T.DABBS,G.D.JAMES,N.W.HILL,M.S.MOORE,A.N.ELLIS, ORNL-4976,1974,P.36.
299. M.S.MOORE,J.H.MC NALLY,R.D.BAYBARZ,PHYS.REV.C,4(1971)273.
300. K.W.MAC MURDO,R.M.HARBOUR,J.INORG.NUCL.CHEM.,34(1972)449.
301. K.D.ZHURAVLEV,N.I.KROSKIN,A.P.UJETVJERIKOV,AT.ENERG.(USSR),39(1975) 285.
302. O.GRENECHE,NEANOC(E)163U,1975,P.43.
303. B.GORDON,E.V.WEINSTOCK,WASH-1093,1968,P.28.
304. P.E.SPIVAK ET AL.,PROC.OF INTERN.CONF.ON PEACEFUL USES OF ATOMIC ENERGY,GENEVA,5(1956)172.
305. J.HALPERIN,C.E.BEMIS,R.E.DRUSCHEL,J.R.STOKELY,NUCL.SCI.ENG.,37(1969) 228.
306. J.A.SMITH,C.J.BANICK,R.L.FOLGER,H.P.H.P.HOLCOMB,I.B.RITCHER,68WASH,2 (1968)1285.
307. E.M.GRYNTAKIS,J.I.KIM,RADIOCHIMICA ACTA,22(1975)128.
308. IAEA,TECHNICAL REPORTS SERIES NO.107,VIENNA,1970.
309. N.P.BAUMANN, WASH-1046, P.49,1964.
310. C.M.LEDERER,V.S.SHIRLEY,TABLE OF ISOTOPES,SEVEN EDITION 1978, (ALSO 6TH ED.1967), WILEY-INTERSCIENCE PUBL.,NEW YORK.
311. W.BLASER,A.WYTTENBACH,P.BAERTSCHI,J.INORG.NUCL.CHEM.,33(1971)1221.
312. R.VAN DER LINDEN,F.DE CORTE,P.VAN DEN WINKEL,J.HOSTER,J.RADIONAL. CHEM.,11(1972)133.
313. R.A.BENNETT,NUCLEAR PHYSICS RESEARCH QUATERLY REP.,HW 68389(1961)50.
314. R.DAHLBERG,K.JIRLOU,E.JOHANSSON,J.NUCL.ENERGY,14(1961)53.
315. T.E.STEPHENSON,BNL961(T-401),1965.
316. G.H.SIMS,J.INORG.NUCL.CHEM.,29(1967)593.
317. G.H.E.SIMS,D.G.JUHNKE,J.INORG.NUCL.CHEM.,31(1969)3721.
318. N.T.KASHUKEEV,YU.P.POPOV,F.L.SHAPIRO,J.NUCL.ENERGY,PART.A/B, 14(1961)76.
319. R.L.D.FRENCH,B.BRADLEY,NUCL.PHYS.,65(1965)225.
320. W.KOHLER,H.SCHMELZ,NUKLEONIK,9(1967)270.
321. L.L.ANDERSON,HEALTH PHYS.,10(1964)315.
322. R.G.BARDES,R.K.LANGE,J.B.SAMPSON,L.J.TODT,REPORT GA 3069,1962.
323. K.W.GEIGER,L.VAN DER ZWAN,NUKEONIK,10(1967)277.
324. R.G.STIEGLITZ,R.W.HOCKENBURG,R.C.BLOCK,NUCL.PHYS.,A163(1971)592.
325. S.P.KAPCHIGASHEV,YU.P.POPOV,AT.ENERG.(USSR),16(1964)256.
326. W.E.LAMB,PHYS.REV.,55(1939)190.
327. T.B.RYVES,J.B.HUNT,I.W.GOODIER,J.NUCL.ENERGY,22(1968)465.

328. J.J.SCOVILLE ET AL.,WASH-1041,1962,P.37.
329. J.R.BERRETH,R.P.SCHUMAN,REPORT IDO-16827,1962,P.18.
330. F.FEINER,REP.KAPL 2000-16,1961.
331. E.J.AXTON,J.NUCL.ENERGY,17(1963)125.
332. R.C.BARRALL,W.N.MCELROY,IAEA,PROC.SYMP.VIENNA,1965,P.251.
333. P.LOUWRIER,A.ATEN,JR.,J.NUCL.ENERGY,PARTS A/B,19(1965)267.
334. R.O.BARDES,J.BROWN,M.DRAKE,J.SAMPSON,TRANS.AM.NUCL.SOC.,4(1961)276.
335. T.NANJYO,J.NUCL.SCI.TECHN.,7(1970)126.
336. O.O.MOXON,AERE-PR/NP14,1968,P.12.
337. F.FEINER,L.J.ESCH,REP.KAPL2000-12,1960.
338. T.A.EASTWOOD,R.D.WERNER,CAN.J.PHYS.,41(1963)1263.
339. E.M.GRYNTAKIS,J.I.KIM,J.RADIOANAL.CHEMISTRY,46(1978)159.
340. LESAGE,R.SHER,PROC.ANS NAT.TOP.MEET.SAN DIEGO,CALIF.,1966,P.4.
341. C.H.HOGG,L.D.WEBER,E.C.YATES,IDO-16744,1962.
342. I.A.KONDUROV,A.I.EGOROV,M.KAMINKEV,E.M.KOROTKIN,A.M.NIKITIN,AT.ENERG. (USSR),24(1968)533.
343. J.S.STORY,REP.AEEW-M122,1961.
344. C.H.HOGG,L.D.WEBER,IN-1024,1966.
345. G.H.SIMS,D.G.JUHNKE,J.INORG.NUCL.CHEM.,29(1967)2853.
346. S.PEARLSTEIN,R.F.MILLIGAN,NUCL.SCI.ENG.,26(1966)281.
347. J.F.EMERY,J.INORG.NUCL.CHEM.,27(1965)903.
348. J.G.BRADLEY,W.H.JOHNSON,NUCL.SCI.ENG.,47(1972)151.
349. W.SKOLNIK,N.C.FRANCIS,TRANS.AM.NUCL.SOC.,2(1959)121.
350. R.H.FULMER,D.P.STRIKOS,T.F.RUANE,NUCL.SCI.ENG.,46(1971)314.
351. R.NILSSON,NUCLEAR PHYSICS,29(1962)66.
352. R.P.SCHUMAN,IDO-16760,1961,P.13.
353. R.E.DRUSCHEL,J.HALPERIN,ORNL-4306,1968,P.2.
354. E.HELLSTRAND,G.LUNDGREN,NUKLEONIK,4(1962)323.
355. H.SHWE,R.E.COTE,PHYS.REV.,179(1969)1148.
356. M.J.CABELL,J.INORG.NUCL.CHEM.,21(1961)1.
357. H.F.FEINER,TRANS.AM.NUCL.SOC.,2(1959)121.
358. M.J.CABELL,J.NUCL.ENERGY,PARTA,12(1960)172.
359. J.HALPERIN ET AL.,ORNL-3832,1965,P.4.
360. P.M.LANTZ,ORNL-3679,1964,P.10.
361. R.D.WERNER,T.A.EASTWOOD,NUCL.SCI.ENG.,21(1965)20.
362. W.H.WALKER,L.A.COPLEY,CAN.J.PHYS.,44(1966)1985.
363. V.MARKOVIC,A.KONIC,BULLETIN BORIS KIDRIC INST.NUCL.SCI.,NUCL.ENG., 18(1967)11.
364. J.HALPERIN ET AL.,ORNL-3994,1966,P.2.
365. S.P.KAPCHIGASHEV,AT.ENERG.(USSR),19(1965)294.
366. J.J.SCOVILLE,E.FAST,T.F.PARKINSON,REACTOR PHYS.CONST.CENTER NEWS LETTER NO.10,1965.
367. F.LUX,W.KOHLER,PROGRESS REPORT IN NUCLEAR DATA RESEARCH IN THE EURATOM COMMUNITY,1964,EANDC(E)57"V",1965,P.28.
368. A.M.BRESESTI,M.BRESESTI,H.NEUMANN,J.INORG,NUCL.CHEM.,29(1967)2477.
369. H.H.KRAMER,W.H.WALL,NUCL.SCI.ENG.,22(1965)373
370. V.MAXIA,E.ORVINI,M.A.ROLLIER,NUCL.SCI.ENG.,35(1969)88.
371. F.DE CORTE,A.SPEECKE,J.HOSTE,J.RADIOANAL.CHEM.,3(1969)205.
372. J.HALPERIN,R.E.DRUSCHEL,ORNL-3679,1964,P.15.
373. D.A.KLOPP,W.F.ZAGOTTA,TRANS.AM.NUCL.SOC.,5(1962)337.
374. K.H.BECKURTS,M.BROSE,M.KNOCHE,G.GRUGER,W.PONITZ,H.SCHMIDT,NUCL.SCI. ENG.,17(1963)329.
375. C.N.KLEBER,NUCLEONICS,20(1962)162.
376. E.K.SOKOLOWSKI,R.BLADH,REP.AE-351,1969.
377. A.P.JAIN,R.E.CHRIEN,J.A.MOORE,H.PALERSKY,NUCL.SCI.ENG.,17(1963)319.
378. I.E.DAYTON,W.G.PETTUS,NUCLEONICS,15(1957)86.
379. T.A.EASTWOOD,E.MATYAS,D.J.HNATOWICH,CAN.J.PHYS.,41(1963)1519.
380. H.D.LEMMEL,C.H.WESTCOTT,J.NUCL.ENERGY,21(1967)417.
381. L.J.ESCH,F.FEINER, TRANS.AM.NUCL.SOC., 7(1964)78.
382. R.G.HART,G.B.BIGHAM,F.C.MILLER,AECL-1503,1962.
383. R.E.COTE ET AL.,PHYS.REV.,159(1967)1050.
384. BNL/NNDC,PRIVATE COMMUNICATION TO NEA/DATA BANK, USA,1971.
385. J.C.CONNOR, WAPD-TM-837,1970.
386. J.HALPERIN,C.E.BEMIS,JR.,R.E.DRUSCHEL,R.E.EBY,ORNL-4706,1971,P.47.
387. H.M.EILAND,S.WEINSTEN,K.W.SEEMAN,NUC.SCI.ENG.,54(1974)286(SEE ALSO REF.74).
388. A.F.FEDOROVA,J.I.PISANKO,G.M.NOVOSYELOV,REPORT KIYAI-76-6,1976, INSTITUTE JADERNYKH ISSLEDOVANIJ,KIEV/USSR.
389. M.FRICKE,A.CARLSON,GULF-RI-A-10739,197.
390. C.E.BEMIS,JR,R.E.DRUSCHEL,J.HALPERIN,J.R.WALTON,NUC.SCI.ENG., 47(1972)371.
391. W.BROWNE,B.L.BERMAN,PHYS.REV./C,8(1973)24 (SEE ALSO UCRL-74840,1973).
392. A.F.FEDOROVA,J.I.PISANKO,G.M.NOVOSYELOV,REPORT KIYAI-76-7,1976. INSTITUTE JADERNYKH ISSLEDOVANIJ,KIEV/USSR.
393. D.C.SANTRY,R.D.WERNER,CAN.J.PHYSICS,51(1973)2441.
394. G.F.AUCHAMPAUGH,J.HALPERIN,P.L.MACLIN,W.M.HOWARD,PHYS.REV./C, 12(1975)1126.
395. G.J.KIROUAC,H.M.EILAND,75WASH,2(1975)776.
396. M.F.ELGART,H.F.FINSTON,R.RUNDBERG,E.T.WILLIAMS,NUC.SCI.ENG., 58(1975)291 (SEE ALSO 75WASH,2(1975)792).
397. R.E.SLOVACEK,D.S.CRAMER,E.B.BEAN,R.W.HOCKENBURY,J.R.VALENTINE, R.C.BLOCK,NUC.SCI.ENG.,62(1977)455 (SEE ALSO BULL.AM.PHYS.SOC., 20(1975)581).

398. L.SAGE,A.K.FURR,TRANS.AMER.NUCL.SOC.,23(1976)501.
399. G.GLEASON,RADIOCHEMICAL AND RADIOANAL.LETTERS,23(1975)317.
400. W.GLEASON,PRIVATE COMMUNICATION TO NEA/DATA BANK,ORL,USA,1977.
401. C.E.BEMIS,JR,R.E.DRUSCHEL,J.HALPERIN,R.D.BAYBARZ,ORNL-4581,1970,P.43.
402. C.E.BEMIS,JR,J.H.OLIVER,R.EBY,J.HALPERIN,NUCL.SCI.ENG.,63(1977)413.
403. J.B.GARG,J.RAINWATER,W.W.HAVENS,JR,NUCL.SCI.ENG.,65(1978)76 (SEE ALSO CR-1860,1964) .
404. G.GLEASON,RADIOCHEMICAL AND RADIOANAL.LETTERS,26(1976)39.
405. R.R.WINTERS,R.L.MACKLIN,J.HALPERIN,PHYS.REV.C,18(1978)2092.
406. R.SHER,68WASH,1(1968)253.
407. S.A.REYNONS,W.T.MULLINS,ORNL-4466,1970,P.74.
408. R.E.DRUSCHEL,J.HALPERIN,ORNL-3994,1966,P.6.
409. ENDL : TABULAR AND GRAPHICAL PRESANTATION OF 175 NEUTRON-GROUP CONSTANTS DERIVED FROM THE LLL EVALUATED-NUCLEAR DATA LIBRARY, E.E.PLECHATY,D.E.CULLEN,R.J.HOWERTON,J.R.KIMLINGER, REPORT UCRL-50400,VOL.16,REV.2, 1978.
410. P.LANTZ,C.BALDOCK,R.STOUGHTON,L.IDOM,ORNL-3994,1966,P.2.
411. D.BIDINOSTI,H.FICKEL,R.TOMLINSON,58GENEVA,15(1958)459.
412. E.FEHR,E.HANSEN,KAPL-2000-12,I,1960,P.33 (SEE ALSO KAPL-2000, 1,1960,P.30).
413. G.BREIT,E.WIGNER,J.PHYSICAL REVIEW 49(1936)519.
414. R.W.STOUGTON,J.HALPERIN,R.E.DRUSCHEL,F.J.JOHNSTON,P.M.LANTZ, J.H.OLIVER,G.W.PARKER,60VIENNA,1960,P.239.
415. BIPAL : A DATA LIBRARY FOR COMPUTING THE BURNUP OF FISSIONABLE ISOTOPES AND PRODUCTS OF THEIR DECAY, E.KRAZOVCOVA,J.HEP,V. VALENTA,REPORT ZJE-227(1978),NUCL.POWER CONSTRUCTION DIVISION, INFORMATION CENTRE,PIZEN,CZECHOSLOVAKIA.
416. R.A.KARAM,T.F.PARKINSON,M.F.PANCZYK,AD-402668,FLA,USA,1963.
417. M.J.CABELL,M.WILKINS,AERE-R-6384,1970.
418. W.SKOLNIK,N.C.FRANCIS,TRANS .AMER.NUCL.SOC.,2(1959)135.
419. N.P.BAUMANN,D.J.PELLARIN,TRANS.AMER.NUCL.SOC.,(1964)27.
420. H.T.MAGUIRE JR,H.M.FISHER,R.C.BLOCK,INT.CONF. ON NEUTRON PHYSICS AND NUCLEAR DATA FOR REACTORS AND OTHER APPLIED PURPOSES, AERE HARWELL, 25-29 SEPT.1978,PAGE 472.
421. R.A.DEAL,R.P.SCHUMAN,WASH-1053,1964,P.76.
422. R.P.SCHUMAN,IN-1126,MTR,USA,1967,P.19.
423. W.LYON,H.ROSS,ORNL-4196,1967,P.66.
424. M.LUCAS,R.HAGEMANN,R.NAUDET,C.RENSON,C.CHEVALIER, MEETING ON THE TECHN. COMMITTEE ON NATURAL FISSION REACTORS, PARIS 19-21 DEC.1977, 1(1979)431.
425. T.B.RYVES, NUCLEAR SCIENCE AND ENGINEERING, 72(1979)357.
426. J.OLSEN, RISO-M-1516,1972.
427. J.K.AALDIJK,H.M.M.KORSTJENS,W.L.ZIJP,RCN-176,1972.
428. H.MICHAEL,A.NEUBERT,R.WAGNER,A.J.BLAIR,NEANDC(E)-172U,176,P.43
429. W.MAENHAUT,F.ADAMS,J.HOSTE, J.RADIOANAL.CHEMISTRY,16(1973)39.
430. T.SEKINE,H.BABA, J.INORG.NUCL.CHEMISTRY,40(1978)1977.
431. A.KOCIC,V.MARKOVIC,BULL.INST.BORIS KIDRIC,VOL.18,NUC.ENG.,19(1968)13.
432. V.HAYODOM,W.BOONKONG,S.MAHAPANYAWONG,C.CHAIMONKON,BANGKOK,THAILAND, THAI-AEC-23 PROGRESS REPORT,1969.
433. E.ABUL-ELA,I.HAMOUDA,AREAEE-165,CAIRO,UAR,1973.
434. V.D.GAVRILOV,V.A.GONCHAROV,V.V.IVANENKO,V.P.SMIRNOV,V.N.KUSTOV, 75KIEV,6(1975)71.
435. V.A.ANUFRIEV,T.S.BELANOVA,YU.S.ZAMJATNIN,A.G.KOLESOV,S.N.NIKOLSKIJ, V.A.PORUCHIKOV,S.M.KALEBIN,V.S.ARTAMONOV,R.N.IVANOV,76LOWELL, 2(1976),1252.
436. V.A.ANUFRIEV,A.G.KOLESOV,S.I.,BABICH,V.A.SAFONOV,PROCEEDING OF THE INTERN. CONF. ON NUCLEAR CROSS SECTIONS FOR TECHNOLOGY, KNOXVILLE 22-26 OCT. 1979, PAGE 877.
437. V.A.ANUFRIEV,S.I.BABICH,V.N.NEFEDOV,V.A.PORUCHIKDV,V.S.ARTOMONOV, R.N.IVANOF,S.M.KALEBIN, PROCEEDING OF THE INTERN. CONF. ON NUCLEAR CROSS SECTIONS FOR TECHNOLOGY, KNOXVILLE 22-26 OCT. 1979, PAGE 907.
438. S.I.BABICH,N.G.KOCHERYGIN,A.G.KOLESOV,V.A.PORUCHIKOV,V.A.SAFONOV, V.N.NEFEDOV,V.S.ATTOMONOV,T.S.BELANOVA,R.N.IVANOV,S.M.KALEBIN, PROCEEDING OF THE INTERN. CONF. ON NUCLEAR CROSS SECTIONS FOR TECHNOLOGY, KNOXVILLE 22-26 OCT. 1979, PAGE 908.
439. K.D.ZHURAVLEV,N.I.KROSHKIN, SOVIET ATOMIC ENERGY 47(1979)565.
440. M.KUROSAWA,K.SHIMIZU,J.ATOMIC ENERGY SOC.JAPAN,21(1979)505.
441. V.D.GAVRILOV,V.A.GONCHAROV,ATOMNAYA ENERGIYA(USSR),44(1978)246. (SEE ALSO REPORT JADERNO-FIZICHESKIE ISSLEDOVANIJA,YFI-25(1979)49).
442. V.A.ANUFRIJEV,A.G.KOLESOV,V.N.NEFJODOV,R.N.IVANOV,S.I.BABICH, A.P.CHETVERIKOV,V.A.PORUCHIKOV,V.A.SAFONOV,V.S.ARTAMONOV,S.M. KALEBIN,ATOMNAYA ENERGIYA(USSR),46(1979)158 (SEE ALSO REPORT JADERNYE KOSTANTY,OBNINSK(USSR),YK-1,32,1979,P.24).
443. V.A.ANUFRIJEV,A.G.KOLESOV,S.N.NIKOL'SKIJ,V.A.SAFONOV,ATOMNAYA ENERGIYA(USSR),47(1979)269.
444. V.A.ANUFRIJEV,S.I.BABICH,A.G.KOLESOV,V.N.NEFJODOV,V.S.ARTAMONOV, R.N.IVANOV,S.M.KALEBIN,REPORT JADERNYE KONSTANTY,OBNINSK(USSR), YK-1,32,1979,P.19.
445. U.N.SINGH,R.C.BLOCK,Y.NAKAGOME, NUCL.SCIENCE ENGINEERING,67(1980)54.
446. N.E.HOLDEN,REPORT BNL-NCS-51388,1981.

447. "EVALUATED NUCLEAR STRUCTURE DATA FILE" (ENSDF) EDITED AND MAINTAINED BY THE U.S NATIONAL NUCLEAR DATA CENTRE, BROOKHAVEN NATIONAL LABORATORY, ON BEHALF OF THE INTERNATIONAL NETWORK FOR NUCLEAR STRUCTURE DATA EVALUATION (JUNE 1984).
448. L.N.JUROVA, A.A.POLJAKOV, V.P.RUKHLO, JU.E.TITARENKO, S.F.KOMIN, O.V.SHVEDOV, B.F.MJASOEDOV, A.V.DAVYDOV, S.S.TRAVNIKOV, REPORT JADERNYE KONSTANTY, OBNINSK (USSR), ISSUE 1(55) (1984) P.3.

Annex

EFFECTIVE RESONANCE ENERGY VALUES

F. De Corte
Rijksuniversiteit Gent, Gent, Belgium

Many significant discrepancies in resonance integral data can be explained by the fact that the epithermal neutron flux distribution is not proportional to $1/E$, but rather to $1/E^{1+\alpha}$, where α is a positive or negative constant close to zero which can be determined for the irradiation facility used. The corresponding correction to the infinite dilute resonance integral requires a tabulation of 'effective resonance energy' values, which is given here.

The concept of the effective resonance energy (E_r) – first developed by Ryves [1] and later introduced in the field of (n,γ) activation analysis by Moens et al. [2] and Jovanovic et al. [3] – is associated strictly with the assumption of a $1/E^{1+\alpha}$ epithermal neutron flux distribution, where α is considered to be independent of neutron energy. For nuclides which obey the $\sigma(v) \sim 1/v$ law up to 1–2 eV, it can be shown that it is possible to calculate, with acceptable accuracy, an α-independent E_r value (in eV) [2, 3]:

$$\ln \bar{E}_r = \frac{1}{\sum_i w_i} \sum_i w_i \ln E_{r,i}$$

with

$$w_i = \frac{g_i \Gamma_{n,i} \Gamma_{\gamma,i}}{\Gamma_i} / E_{r,i}^2$$

Here $E_{r,i}$ is the energy of the ith resonance (in eV);
g_i is the statistical weight factor;
$\Gamma_{n,i}$ is the neutron width;
$\Gamma_{\gamma,i}$ is the radiative width;
Γ_i is the total width of resonance.

$\bar{E}_r$ thus calculated is a useful parameter for the description of the epicadmium reaction rate in a $1/E^{1+\alpha}$ epithermal neutron flux distribution:

$$R_e = \phi_e \int_{E_{Cd}}^{\infty} \frac{\sigma(E)\,dE}{E^{1+\alpha}}\ 1\ eV^{\alpha} \qquad (E \text{ in eV})$$

$$= \phi_e I_0(\alpha)$$

with ϕ_e equal to the conventional epithermal flux

$$I_0(\alpha) = \left(\frac{I_0 - 0.429\,\sigma_0}{(\bar{E}_r)^{\alpha}} + \frac{0.429\,\sigma_0}{(2\alpha+1)(0.55)^{\alpha}} \right) 1\ eV^{\alpha}$$

where σ_0 is the 2200 m/s (n,γ) activation cross-section and I_0 is the usually tabulated (n,γ) activation resonance integral integrated from the effective Cd cut-off energy (= 0.55 eV), and with the 1/v tail included, valid for an ideal 1/E epithermal neutron flux distribution

$$\left(I_0 = \int_{E_{Cd}}^{\infty} \frac{\sigma(E)\,dE}{E} \right)$$

In the analysis outlined above, $\bar{E}_r$ is an indispensable parameter in the conversion of experimentally determined $I_0(\alpha)$ values to I_0 (which can be tabulated) and the conversion of tabulated I_0 values to practically useful $I_0(\alpha)$ values. Thus, I_0 tabulations should be accompanied by $\bar{E}_r$ values. It should be noted that simple methods have been described for experimental α determination that are suitable in ordinary radioanalytical laboratories [4, 5]. Finally, the above-mentioned assumptions and approximations were shown to yield fairly satisfactory results in the practice of (n,γ) activation analysis [5–7].

Table A–I lists calculated $\bar{E}_r$ values for the (n,γ) reaction on 128 target isotopes which are of interest in (n,γ) activation analysis [8]. Calculation is based mainly on resonance parameter data from Brookhaven National Laboratory, Upton, New York [10, 11].

TABLE A-I. CALCULATED $\bar{E}_r$ VALUES FOR THE (n, γ) REACTION ON 128 TARGET ISOTOPES

Target isotope	$\bar{E}_r$ (eV)	Target isotope	$\bar{E}_r$ (eV)
^{18}O	1 140 000 ± 80 000	^{80}Se	2940 ± 410
^{19}F	44 700 ± 2200	^{82}Se	8540 ± [b]
^{23}Na	3380 ± 370	^{79}Br	69.3 ± 6.2
^{26}Mg	257 000 ± 33 000	^{81}Br	152 ± 14
^{27}Al	11 800 ± 700	^{85}Rb	839 ± 50
^{30}Si	2280 ± 10	^{87}Rb	364 ± 11
^{31}P	38 500 ± 6900	^{84}Sr	469 ± 33
^{36}S	[a]	^{86}Sr	795 ± 16
^{37}Cl	13 700 ± 1900	^{89}Y	4300 ± 340
^{40}Ar	31 000 ± 5600	^{94}Zr	6260 ± 250
^{41}K	2960 ± 210	^{96}Zr	338 ± 7
^{46}Ca	[a]	^{93}Nb	574 ± 46
^{48}Ca	1 330 000 ± [b]	^{98}Mo	241 ± 48
^{45}Sc	5130 ± 870	^{100}Mo	672 ± 94
^{50}Ti	63 200 ± 2500	^{96}Ru	776 ± 124[c]
^{51}V	7230 ± 290	^{102}Ru	181 ± 7
^{50}Cr	7530 ± 830	^{104}Ru	495 ± 50
^{55}Mn	468 ± 51	^{103}Rh	1.45 ± 0.01
^{58}Fe	637 ± 153	^{106}Pd	282 ± 6
^{59}Co	136 ± 7	^{108}Pd	39.7 ± 2.0
^{64}Ni	14 200 ± 1700	^{110}Pd	950 ± 86
^{63}Cu	1040 ± 50	^{107}Ag	38.5 ± 1.9
^{65}Cu	766 ± 130	^{109}Ag	6.08 ± 0.06
^{64}Zn	2560 ± 260	^{108}Cd	243 ± 24
^{68}Zn	590 ± 60	^{110}Cd	125 ± 16
^{69}Ga	201 ± 16	^{114}Cd	207 ± 39
^{71}Ga	154 ± 18	^{116}Cd	726 ± 87
^{74}Ge	3540 ± 280	^{113}In	6.41 ± 0.96
^{76}Ge	583 ± 23	^{115}In	1.56 ± 0.03
^{75}As	106 ± 36	^{112}Sn	1.07 ± 3
^{74}Se	29.4 ± 1.2	^{116}Sn	128 ± 4
^{76}Se	577 ± 46	^{122}Sn	424 ± 59
^{78}Se	501 ± 35	^{124}Sn	74.2 ± 5.2

Target isotope	$\bar{E}_r$ (eV)	Target isotope	$\bar{E}_r$ (eV)
^{121}Sb	13.1 ± 0.5	^{169}Tm	4.80 ± 0.10
^{123}Sb	28.2 ± 1.7	^{168}Yb	0.61 ± 0.01
^{120}Te	[a]	^{174}Yb	602 ± 48
^{122}Te	92.3 ± 3.7	^{176}Yb	412 ± 21
^{124}Te	1210 ± 100	^{175}Lu	16.1 ± 0.8
^{126}Te	285 ± 20	^{174}Hf	29.6 ± 2.1
^{128}Te	738 ± 52	^{177}Hf	2.08 ± [b]
^{130}Te	2950 ± 210	^{178}Hf	8.01 ± 0.16
^{127}I	57.6 ± 2.3	^{179}Hf	16.2 ± 1.9
^{133}Cs	9.27 ± 1.02	^{180}Hf	115 ± 7
^{130}Ba	69.9 ± 3.5	^{181}Ta	10.4 ± 0.6
^{132}Ba	143 ± [b]	^{182}W	9.20 ± 0.55
^{134}Ba	115 ± 6	^{186}W	20.5 ± 0.2
^{136}Ba	545 ± 38	^{185}Re	3.40 ± 0.14
^{138}Ba	15 700 ± 500	^{187}Re	41.1 ± 1.6
^{139}La	76.0 ± 3.0	^{189}Os	12.3 ± 0.4
^{138}Ce	[a]	^{190}Os	114 ± 2
^{140}Ce	7200 ± 1300	^{192}Os	89.7 ± 3.6
^{142}Ce	1540 ± 1850	^{193}Ir	2.21 ± 0.20
^{141}Pr	296 ± 12	^{190}Pt	27.6 ± 0.6
^{146}Nd	874 ± 52	^{196}Pt	291 ± 44
^{148}Nd	236 ± 14	^{198}Pt	106 ± 3
^{150}Nd	173 ± 21	^{197}Au	5.65 ± 0.40
^{152}Sm	8.53 ± 0.09	^{196}Hg	93.5 ± 0.1
^{154}Sm	142 ± 10	^{198}Hg	39.3 ± 2.8
^{153}Eu	5.80 ± 0.23	^{202}Hg	1960 ± 160
^{158}Gd	48.2 ± 3.9	^{204}Hg	[a]
^{160}Gd	480 ± 34	^{203}Tl	276 ± 28
^{159}Tb	18.1 ± 0.9	^{205}Tl	2960 ± 360
^{164}Dy	224 ± 11	^{206}Pb	10 500 ± 1200
^{165}Ho	12.3 ± 0.4	^{208}Pb	145 000 ± 4000
^{166}Er	59.3 ± 4.2	^{209}Bi	1210 ± 60
^{170}Er	129 ± 3	^{232}Th	54.4 ± 0.5
		^{238}U	16.9 ± 0.2

[a] No resonance data available.
[b] No error assignment possible.
[c] Experimental value (see Ref. [9]).

REFERENCES TO THE ANNEX

[1] RYVES, T.B., Metrologia 5 (1969) 119.
[2] MOENS, L., DE CORTE, F., SIMONITS, A., DE WISPELAERE, A., HOSTE, J., J. Radioanal. Chem. 52 (1979) 379.
[3] JOVANOVIC, S., DE CORTE, F., MOENS, L., SIMONITS, A., HOSTE, J., J. Radioanal. Nucl. Chem. Articles 82/2 (1984) 379.
[4] DE CORTE, F., et al., J. Radioanal. Chem. 62 (1981) 209.
[5] DE CORTE, F., JOVANOVIC, S., SIMONITS, A., MOENS, L., HOSTE, J., in Use and Developments of Low and Medium Flux Research Reactors (Proc. Int. Symp. Cambridge, MA, 1983), Supplement to Atomkernenerg. Kerntech. 44 (1984) 641.
[6] DE CORTE, F., et al., J. Radioanal. Chem. 72 (1982) 275.
[7] MOENS, L., et al., J. Radioanal. Nucl. Chem. Articles 82/2 (1984) 385.
[8] JOVANOVIC, S., Ph. D. thesis, Rijksuniversiteit Gent, 1984.
[9] SIMONITS, A., JOVANOVIC, S., DE CORTE, F., MOENS, L., HOSTE, J., J. Radioanal. Nucl. Chem. Articles 82/1 (1984) 169.
[10] MUGHABGHAB, S.F., DIVADEENAM, M., HOLDEN, N.E., Neutron Cross Sections: Neutron Resonance Parameters and Thermal Cross Sections. Part A:Z = 1-60, Vol. 1, Academic Press, New York (1981).
[11] MUGHABGHAB, S.F., Neutron Cross Sections: Neutron Resonance Parameters and Thermal Cross Sections. Part B:Z = 61-100, Vol. 1, Academic Press, New York (1984).

2-2. DATA FOR 14 MeV NEUTRON ACTIVATION ANALYSIS

Z. BÖDY, J. CSIKAI
Institute of Experimental Physics,
Kossuth University,
Debrecen, Hungary

Abstract

DATA FOR 14 MeV NEUTRON ACTIVATION ANALYSIS.

Suggested reactions for analysis are presented, together with their characteristic data, for almost all natural elements. In addition, 337 recommended cross-sections at 14.5 MeV are also given for the (n, 2n), (n, p) and (n, α) reactions.

1. INTRODUCTION

One can advantageously use low-voltage neutron generators [1] as fast (and occasionally thermal) neutron sources in neutron activation analysis. The energy of neutrons produced in the $^{3}H(d,n)^{4}He$ reaction depends on E_d, the bombarding deuteron energy, and on the emission angle. The neutron energy and the relative yield, as functions of the angle at E_d = 175 keV (commonly used with low-voltage accelerators) are given in Table I for thick targets. The effective cross-section values for the $^{27}Al(n,\alpha)$ standard reaction are also given there.

TABLE I. NEUTRON ENERGY AND RELATIVE YIELD VERSUS THE ANGLE AT E_d = 175 keV FOR A THICK TARGET[a]

Angle	Average neutron energy (MeV)	Relative intensity	σ_{eff} (mb) for Al-27(n, α)
0	14.774(0.17)	1.049	112.3
30	14.678(0.15)	1.043	113.1
60	14.417(0.12)	1.025	116.0
90	14.069(0.08)	1.000	121.9
120	13.730(0.10)	0.976	124.0
150	13.487(0.12)	0.958	125.1
180	13.400(0.13)	0.951	127.2

[a] The cross-sections are taken from Refs [2,3].

Although comparison with a standard is preferred for absolute measurements in neutron activation analysis, knowledge of nuclear data – and of cross-sections, in particular – is important in order to choose the most favourable reaction or to estimate the expected activity and the role of interfering reactions. Taking into account nuclear data only, the most effective identifying reaction is given for each element in Table II.

2. THE ACTIVATION PROCESS

Let N be the number of radioactive nuclei, σ the cross-section of the reaction, Φ the neutron flux, n the number of target nuclei and λ the decay constant of the radionuclides formed. The following differential equation can then be described:

$$\frac{dN(t)}{dt} = \Phi(t)\sigma n - \lambda N(t) \tag{1}$$

where the first term on the right-hand side gives the increase in N because of the activation process, while the second term gives the decrease owing to decay.

The general solution of this first-order linear inhomogeneous differential equation is

$$N(t) = e^{-\lambda t}\left[C + \sigma n \int \Phi(t) e^{+\lambda t} dt\right] \tag{2}$$

where C is a constant of integration. Restricting the solution to a constant flux $\Phi = \Phi_0$ and assuming the initial condition $N = 0$ for $t = 0$ yields

$$N(t) = \frac{\Phi_0 \sigma n}{\lambda}(1 - e^{-\lambda t}) \tag{3}$$

from which the activity at time t (i.e. the number of decays per unit time) will be

$$A(t) = \lambda N(t) = \Phi_0 \sigma n(1 - e^{-\lambda t}) \tag{4}$$

The specific activity, i.e. the activity per unit target mass (m) – in disintegrations per second per gram ((dis/s)/g) – will then be given as

$$\frac{A(t)}{m} = 6.02 \times 10^{-6} \frac{\sigma a \Phi_0}{M}(1 - e^{-\lambda t}) \tag{5}$$

where σ is given in mb, the atomic weight of element M is in grams and the target isotopic abundance a is in per cent.[1] This specific activity has been calculated for different reactions assuming a flux of $\Phi_0 = 10^9$ neutrons $\cdot$ cm$^{-2} \cdot$ s^{-1}, as well as irradiation times of t = 10 min and t = 1 h, respectively (columns 9 and 10 of Table II. The saturation values are also given in column 11 under the heading '$t = \infty$'). It should be noted here that this neutron flux value is a realistic one for fast neutrons if they are produced by a neutron generator of average intensity, while for thermal neutrons (produced by the same generator) this value is too high, the overestimation being about two orders of magnitude.

Another consideration also has relevance if the final nucleus has more than a single final state and if the ground state activity is used for analysis. In such a case, instead of Eq. (1), as many differential equations would have to be solved simultaneously as the number of the final states. For example, for two states we have

$$\frac{dN_m}{dt} = \Phi\sigma_m n - \lambda_m N_m \tag{6a}$$

and

$$\frac{dN_g}{dt} = \Phi\sigma_g n - \lambda_g N_g + \beta\lambda_m N_m \tag{6b}$$

where m and g indicate metastable and ground state quantities, respectively, and β is the ratio of the internal transition (IT) events (leading from the metastable to the ground state) to all decay events of the metastable state. All other quantities are the same as before.

Assuming again a constant flux $\Phi = \Phi_0$ and initial condition $N_m = N_g = 0$ for t = 0, the solution of Eq. (6) will be

$$N_m(t) = \frac{\Phi_0\sigma_m n\ 1(-e^{-\lambda_m t})}{\lambda_m} \tag{7a}$$

and

$$N_g(t) = \Phi_0 n\left[\frac{\beta\sigma_m + \sigma_g}{\lambda_g}(1 - e^{-\lambda_g t}) + \frac{\beta\sigma_m}{\lambda_g - \lambda_m}(e^{-\lambda_g t} - e^{-\lambda_m t})\right] \tag{7b}$$

[1] 1 disintegration per second $\equiv 1.00 \times 10^0$ Bq (becquerel).

Explanations of Tables II–V are given on pp. 300 and 301.

TABLE II. RECOMMENDED REACTIONS FOR ACTIVATION ANALYSIS WITH SMALL NEUTRON GENERATORS

Atomic No./ Element	Atomic weight of element	Target isotopic abundance (%)	Reaction	Cross-section (mb)	Half-life	Gamma energy (keV)
5-B	10.811	80.2	B-11(n,p)Be-11	3.3(0.6)	13.81(8) s	2124.8(7)
7-N	14.0067	99.63	N-14(n,2n)N-13	7.1(0.6)	9.963(9) min	Annihilation
8-O	15.9994	99.76	O-16(n,p)N-16	35(4)	7.13(4) s	2741.2(5) 6129.2(1)
9-F	18.9984	100	F-19(n,2n)F-18	55(4)	109.72(6) min	Annihilation
			F-19(n,p)O-19	19(2)	26.76(8) s	197.1(1) 1356.8(1)
10-Ne	20.183	90.51	Ne-20(n,p)F-20	92	10.996(20) s	1633.7(1)
11-Na	22.9898	100	Na-23(n,α)F-20	150(15)	10.996(20) s	1633.7(1)
			Na-23(n,p)Ne-23	35(4)	37.6(1) s	439.9(2)
12-Mg	24.312	78.99	Mg-24(n,p)Na-24	181(8)	14.959(7) h	1368.5(1) 2754.9(1)
13-Al	26.9815	100	Al-27(n,p)Mg-27	75(4)	9.462(12) min	843.7(1) 1014.43(1)
			Al-27(n,α)Na-24	116(0.7)[a]	14.959(7) h	1368.5(1) 2754.9(1)
14-Si	28.086	92.23	Si-28(n,p)Al-28	226(30)	2.2405(3) min	1779.0(1)
15-P	30.9738	100	P-31(n,α)Al-28	118(15)	2.2405(3) min	1779.0(1)
16-S	32.064	4.21	S-34(n,α)Si-31	138(35)	2.62(1) h	1266.1(1)

Atomic No./ Element	Gammas per decay (%)	(dis/s)/g (t = 10 min)	(dis/s)/g (t = 1 h)	(dis/s)/g (t = ∞)	Interfering reactions
5-B	33.0	1.47×10^5	1.47×10^5	1.47×10^5	
7-N	200.	1.52×10^5	2.99×10^5	3.04×10^5	
8-O	0.76 68.8	1.31×10^6	1.31×10^6	1.31×10^6	N-15(n,γ); F-19(n,α); O-17(n,d)
9-F	194.	1.07×10^5	5.50×10^5	1.74×10^6	
	95.9 50.4	6.02×10^5	6.02×10^5	6.02×10^5	O-18(n,γ)
10-Ne	100.	2.48×10^6	2.48×10^6	2.48×10^6	F-19(n,γ); Na-23(n,α); Ne-21(n,d)
11-Na	100.	3.93×10^6	3.93×10^6	3.93×10^6	F-19(n,γ); Ne-20(n,p); Ne-21(n,d)
	33.0	9.17×10^5	9.17×10^5	9.17×10^5	Ne-22(n,γ)
12-Mg	100. 99.9	2.72×10^4	1.60×10^5	3.54×10^6	Na-23(n,γ); Al-27(n,α); Mg-25(n,d)
13-Al	71.8 28.2	8.69×10^5	1.65×10^6	1.67×10^6	Mg-26(n,γ); Si-30(n,α)
	100. 99.9	1.99×10^4	1.17×10^5	2.59×10^6	Na-23(n,γ); Mg-24(n,p); Mg-25(n,d)
14-Si	100.	4.27×10^6	4.47×10^6	4.47×10^6	Al-27(n,γ); P-31(n,α); Si-29(n,d)
15-P	100.	2.19×10^6	2.29×10^6	2.29×10^6	Al-27(n,γ); Si-28(n,p); Si-29(n,d)
16-S	0.07	4.71×10^3	2.54×10^4	1.09×10^5	Si-30(n,γ); P-31(n,p)

TABLE II (cont.)

Atomic No./ Element	Atomic weight of element	Target isotopic abundance (%)	Reaction	Cross-section (mb)	Half-life	Gamma energy (keV)
17-Cl	35.453	24.23	Cl-37(n,p)S-37	28(3)	4.99(2) min	3103.3(2)
18-Ar	39.948	99.60	Ar-40(n,p)Cl-40	16(2)	1.32(2) min	1460.8(1) 2840.2(3)
			Ar-40(n,α)S-37	10.0(1.5)	4.99(2) min	3103.3(2)
19-K	39.102	6.73	K-41(n,p)Ar-41	51(8)	1.827(7) h	1293.7(1)
			K-41(n,α)Cl-38	33.5(2)	37.24(5) min	1642.4(1) 2167.6(1)
20-Ca	40.08	2.09	Ca-44(n,p)K-44	39(4)	22.15(2) min	1157.0(1) 2150.8(1)
21-Sc	44.956	100	Sc-45(n,2n)Sc-44g	188(14)	3.927(8) h	1157.0(1)
22-Ti	47.90	73.7	Ti-48(n,p)Sc-48	66(6)	43.67(9) h	983.5(1) 1312.1(1)
23-V	50.942	99.75	V-51(n,p)Ti-51	33(3)	5.752(7) min	320.1(1)
24-Cr	51.996	83.79	Cr-52(n,p)V-52	102(20)	3.760(8) min	1434.1(1)
25-Mn	54.9380	100	Mn-55(n,α)V-52	32(5)	3.760(8) min	1434.1(1)
			Mn-55(n,γ)Mn-56	13 300(200)	2.5785(6) h	846.8(1) 1810.7(1)
26-Fe	55.847	91.8	Fe-56(n,p)Mn-56	98(7)	2.5785(6) h	846.8(1) 1810.7(1)

Atomic No./ Element	Gammas per decay (%)	(dis/s)/g (t = 10 min)	(dis/s)/g (t = 1 h)	(dis/s)/g (t = ∞)	Interfering reactions
17-Cl	94.1	8.65×10^4	1.15×10^5	1.15×10^5	S-36(n,γ); Ar-40(n,α)
18-Ar	77.5 29.9	2.39×10^5	2.40×10^5	2.40×10^5	
	94.1	1.13×10^5	1.50×10^5	1.50×10^5	S-36(n,γ); Cl-37(n,p)
19-K	99.1	3.24×10^3	1.67×10^4	5.30×10^4	Ar-40(n,γ); Ca-44(n,α)
	31.6 42.4	5.90×10^3	2.34×10^4	3.47×10^4	Cl-37(n,γ); Ar-38(n,p)
20-Ca	58.2 22.8	3.30×10^3	1.04×10^4	1.22×10^4	
21-Sc	99.9	7.30×10^4	4.08×10^5	2.51×10^6	
22-Ti	100. 100.	1.62×10^3	9.63×10^3	6.12×10^5	V-51(n,α); Ti-49(n,d)
23-V	93.0	2.73×10^5	3.89×10^5	3.89×10^5	Ti-50(n,γ); Cr-54(n,α)
24-Cr	100.	8.34×10^5	9.89×10^5	9.89×10^5	V-51 (n,γ); Mn-55(n,α); Cr-53(n,d)
25-Mn	100.	2.95×10^5	3.51×10^5	3.51×10^5	V-51(n,γ); Cr-52(n,p); Cr-53(n,d)
	98.9 27.2	6.39×10^6	3.44×10^7	1.46×10^8	Fe-56(n,p); Co-59(n,α); Fe-57(n,d)
26-Fe	98.9 27.2	4.25×10^4	2.29×10^5	9.71×10^5	Mn-55(n,γ); Co-59(n,α); Fe-57(n,d)

TABLE II (cont.)

Atomic No./ Element	Atomic weight of element	Target isotopic abundance (%)	Reaction	Cross-section (mb)	Half-life	Gamma energy (keV)
27-Co	58.9332	100	Co-59(n,γ)Co-60m	18 800(1500)	10.47(2) min	58.6(1)
			Co-59(n,α)Mn-56	29(2)	2.5785(6) h	846.8(1) 1810.7(1)
			Co-59(n,2n)Co-58m+g	720(50)	70.78(10) d	810.8(1)
28-Ni	58.71	26.1	Ni-60(n,p)Co-60m	95(10)	10.47(2) min	58.6(1)
		68.3	Ni-58(n,2n)Ni-57	30(3)	36.16(11) h	1377.6(1)
29-Cu	63.54	69.2	Cu-63(n,2n)Cu-62	551(11)	9.74(2) min	Annihilation
		30.8	Cu-65(n,p)Ni-65	25(5)	2.520(2) h	1481.8(1)
			Cu-65(n,2n)Cu-64	931.8(13.1)[b]	12.701(2) h	Annihilation 1345.8(1)
30-Zn	65.37	48.6	Zn-64(n,2n)Zn-63	178(27)	38.1(1) min	669.6(1)
31-Ga	69.73	60.1	Ga-69(n,2n)Ga-68	945(50)	68.1(2) min	1077.4(1)
32-Ge	72.59	7.8	Ge-76(n,2n)Ge-75m+g	1148(120)	82.80(4) min	264.6(1)
33-As	74.9216	100	As-75(n,2n)As-74	1061(100)	17.78(5) d	595.8(1)
			As-75(n,p)Ge-75m+g	19.2(2.0)	82.80(4) min	264.6(1)
34-Se	78.96	9.0	Se-82(n,2n)Se-81m	1008(120)	57.28(5) min	103.1(1)
35-Br	79.909	50.69	Br-79(n,2n)Br-79m	974(50)	6.46(4) min	613.7(1)
36-Kr	83.80	17.3	Kr-86(n,2n)Kr-85m	350(35)	4.480(8) h	151.2(1)

Atomic No./ Element	Gammas per decay (%)	(dis/s)/g (t = 10 min)	(dis/s)/g (t = 1 h)	(dis/s)/g (t = ∞)	Interfering reactions
27-Co	2.02	9.31×10^{7}	1.89×10^{8}	1.92×10^{8}	Ni-60(n,p); Cu-63(n,α); Ni-61(n,d)
	98.9 27.2	1.30×10^{4}	6.99×10^{4}	2.96×10^{5}	Mn-55(n,γ); Fe-56(n,p); Fe-57(n,d)
	99.4	5.00×10^{2}	3.00×10^{3}	7.35×10^{6}	Ni-58(n,p)
28-Ni	2.02	1.23×10^{5}	2.50×10^{5}	2.54×10^{5}	Co-59(n,γ); Cu-63(n,α); Ni-61(n,d)
	77.9	6.69×10^{2}	3.98×10^{3}	2.09×10^{5}	
29-Cu	196.	1.84×10^{6}	3.57×10^{6}	3.62×10^{6}	
	23.5	3.27×10^{3}	1.76×10^{4}	7.30×10^{4}	Ni-64(n,γ); Zn-68(n,α)
	35.8 0.48	2.46×10^{4}	1.44×10^{5}	2.72×10^{6}	Cu-63(n,γ); Zn-64(n,p)
30-Zn	8.40	1.32×10^{5}	5.30×10^{5}	7.97×10^{5}	
31-Ga	2.93	4.75×10^{5}	2.24×10^{6}	4.91×10^{6}	
32-Ge	11.3	5.94×10^{4}	2.91×10^{5}	7.38×10^{5}	Ge-74(n,γ); As-75(n,p); Se-78(n,α)
33-As	60.3	2.33×10^{3}	1.39×10^{4}	8.53×10^{6}	Se-74(n,p)
	11.3	1.24×10^{4}	6.09×10^{4}	1.54×10^{5}	Ge-74(n,γ); Ge-76(n,2n); Se-78(n,α)
34-Se	9.79	7.89×10^{4}	3.57×10^{5}	6.92×10^{5}	Se-80(n,γ); Br-81(n,p); Kr-84(n,α)
35-Br	13.6	2.45×10^{6}	3.72×10^{6}	3.72×10^{6}	Kr-78(n,p)
36-Kr	75.0	1.11×10^{4}	6.24×10^{4}	4.35×10^{5}	Kr-84(n,γ); Rb-85(n,p); Sr-88(n,α)

TABLE II (cont.)

Atomic No./ Element	Atomic weight of element	Target isotopic abundance (%)	Reaction	Cross-section (mb)	Half-life	Gamma energy (keV)
37-Rb	85.47	72.17	Rb-85(n,2n)Rb-84m	505(34)	20.5(2) min	215.6(1) 248.0(1) 463.6(1)
38-Sr	87.62	9.8	Sr-86(n,2n)Sr-85m	247(22)	67.66(7) min	231.9(1)
39-Y	88.905	100	Y-89(n,2n)Y-88	966(100)	106.61(2) d	898.0(1) 1836.0(1)
			Y-89(n,n'γ)Y-89m	438(44)	16.06(4) s	909.2(1)
40-Zr	91.22	51.5	Zr-90(n,2n)Zr-89m	86(8)	4.180(1) min	587.8(1)
41-Nb	92.906	100	Nb-93(n,2n)Nb-92m	482(35)	10.150(2) d	934.5(1)
42-Mo	95.94	9.6	Mo-100(n,2n)Mo-99	1420(150)	66.02(1) h	181.1(1) 739.4(1)
44-Ru	101.07	5.5	Ru-96(n,2n)Ru-95	700(100)	1.65(2) h	336.4(1)
45-Rh	102.905	100	Rh-103(n,n'γ)Rh-103m	216(26)	56.12(1) min	20.1X 39.7(1)
			Rh-103(n,γ)Rh-104m	$10(1) \times 10^3$	4.34(7) min	51.4(1) 97.1(1)
46-Pd	106.4	11.8	Pd-110(n,2n)Pd-109m	510(35)	4.69(1) min	188.9(1)
47-Ag	107.870	51.83	Ag-107(n,2n)Ag-106g	870(100)	24.0(1) min	511.9(1) 621.9(1)

Atomic No./ Element	Gammas per decay (%)	(dis/s)/g (t = 10 min)	(dis/s)/g (t = 1 h)	(dis/s)/g (t = ∞)	Interfering reactions
37-Rb	26.4 59.0 35.4	7.36×10^5	2.23×10^6	2.57×10^6	Sr-84(n,p)
38-Sr	84.4	1.62×10^4	7.64×10^4	1.66×10^5	Sr-84(n,γ)
39-Y	94.0 99.4	2.95×10^2	1.77×10^3	6.54×10^6	
	99.1	2.97×10^6	2.97×10^6	2.97×10^6	Zr-90(n,d)
40-Zr	89.5	2.37×10^5	2.92×10^5	2.92×10^5	Mo-92(n,α)
41-Nb	99.1	1.49×10^3	8.88×10^3	3.12×10^6	Mo-92(n,p)
42-Mo	6.08 12.1	1.50×10^3	8.94×10^3	8.56×10^5	Mo-98(n,γ); Ru-102(n,α)
44-Ru	70.8	1.55×10^4	7.87×10^4	2.29×10^5	
45-Rh	6.37 0.0684	1.47×10^5	6.62×10^5	1.26×10^6	Pd-104(n,d)
	48.2 3.00	4.68×10^7	5.86×10^7	5.86×10^7	Pd-104(n,p); Ag-107(n,α); Pd-105(n,d)
46-Pd	55.7	2.63×10^5	3.41×10^5	3.41×10^5	Pd-108(n,γ); Ag-109(n,p); Cd-112(n,α)
47-Ag	16.8 0.312	6.32×10^5	2.07×10^6	2.52×10^6	Cd-106(n,p)

TABLE II (cont.)

Atomic No./ Element	Atomic weight of element	Target isotopic abundance (%)	Reaction	Cross-section (mb)	Half-life	Gamma energy (keV)
47-Ag			Ag-107(n,2n)Ag-106m	600(80)	8.46(10) d	451.0(1)
		48.17	Ag-109(n,2n)Ag-108g	840(150)	2.37(1) min	633.0(1)
48-Cd	112.40	24.1	Cd-112(n,2n)Cd-111m	725(50)[c]	48.6(3) min	150.8(1) 245.4(1)
49-In	114.82	95.7	In-115(n,γ)In-116m	162 300(700)	54.12(5) min	416.9(1) 1097.3(2) 1293.5(1)
			In-115(n,n'γ)In-115m	63(6)	4.486(4) h	336.2(1)
50-Sn	118.69	5.64	Sn-124(n,2n)Sn-123m	547(23)	40.08(7) min	160.3(1)
		1.01	Sn-112(n,2n)Sn-111	1180(120)	35.3(8) min	762.0(1) 1153.0(1)
51-Sb	121.75	57.3	Sb-121(n,2n)Sb-120g[d]	1080(90)	15.89(4)[e] min	1171.2(3)
		42.7	Sb-123(n,2n)Sb-122m	731(73)	4.21(2) min	61.4(1) 76.1(1)
52-Te	127.60	34.5	Te-130(n,2n)Te-129g	570(30)	69.6(5) min	459.6(1)
53-I	126.9044	100	I-127(n,γ)I-128	6200(200)	24.99(2) min	442.9(1)
			I-127(n,2n)I-126	1550(100)	13.02(7) d	388.6(1) 666.3(1)
54-Xe	131.30	8.9	Xe-136(n,2n)Xe-135m	750(50)	15.6(1) min	526.6(1)

Atomic No./ Element	Gammas per decay (%)	(dis/s)/g (t = 10 min)	(dis/s)/g (t = 1 h)	(dis/s)/g (t = ∞)	Interfering reactions
47-Ag	28.4	9.87×10^2	5.91×10^3	1.74×10^6	Cd-106(n,p)
	1.75	2.14×10^6	2.26×10^6	2.26×10^6	Ag-107(n,γ); Cd-108(n,p)
48-Cd	30.3 94.0	1.24×10^5	5.78×10^5	9.36×10^5	Cd-110(n,γ); Sn-114(n,α)
49-In	29.2 56.2 84.4	9.79×10^7	4.37×10^8	8.14×10^8	Sn-116(n,p); Sn-117(n,d)
	45.8	8.02×10^3	4.51×10^4	3.16×10^5	Sn-115(n,p); Sn-116(n,d)
50-Sn	85.6	2.49×10^4	1.01×10^5	1.57×10^5	Sn-122(n,γ); Sb-123(n,p); Te-126(n,α)
	1.40 2.51	1.08×10^4	4.19×10^4	6.05×10^4	
51-Sb	1.69	1.08×10^6	2.84×10^6	3.03×10^6	Te-120(n,p)
	57.5 19.6	1.25×10^6	1.54×10^6	1.54×10^6	Sb-121(n,γ); Te-122(n,p); Te-123(n,d)
52-Te	7.14	8.80×10^4	4.18×10^5	9.28×10^5	Te-128(n,γ); Xe-132(n,α)
53-I	16.0	7.12×10^6	2.39×10^7	2.94×10^7	Xe-128(n,p); Xe-129(n,d)
	32.2 31.3	2.72×10^3	1.63×10^4	7.36×10^6	Xe-126(n,p)
54-Xe	80.5	1.10×10^5	2.85×10^5	3.06×10^5	Xe-134(n,γ); Ba-138(n,α)

TABLE II (cont.)

Atomic No./ Element	Atomic weight of element	Target isotopic abundance (%)	Reaction	Cross-section (mb)	Half-life	Gamma energy (keV)
55-Cs	132.905	100	Cs-133(n,2n)Cs-132	1603(100)	6.974(14) d	667.5(1)
56-Ba	137.34	71.7	Ba-138(n,2n)Ba-137m	1020(70)	2.5513(7) min	661.6(1)
57-La	138.91	99.911	La-139(n,γ)La-140	8930(40)	40.27(5) h	328.8(1) 487.0(1)
58-Ce	140.12	88.5	Ce-140(n,2n)Ce-139m	963(120)	56.44(48) s	754.2(1)
		0.19	Ce-136(n,2n)Ce-135m+g	1600(140)	17.76(31) h	265.6(1) 300.1(1)
59-Pr	140.907	100	Pr-141(n,2n)Pr-140	1660(120)	3.39(1) min	Annihilation 306.9(2) 1596.5(1)
60-Nd	144.24	5.6	Nd-150(n,2n)Nd-149	1906(160)	1.73(1) h	114.3(1) 211.3(1)
62-Sm	150.35	3.1	Sm-144(n,2n)Sm-143m	652(38)	66(2) s	754.0(2)
63-Eu	151.96	47.9	Eu-153(n,2n)Eu-152m	72(6)	96(1) min	89.8(1)
64-Gd	157.25	21.8	Gd-160(n,2n)Gd-159	1960(180)	18.56(8) h	363.6(1)
65-Tb	158.924	100	Tb-159(n,2n)Tb-158m	450(65)	10.5(2) s	50.3X 51.7X 110. (1)
66-Dy	162.50	0.10	Dy-158(n,2n)Dy-157	1950(170)	8.1(1) h	326.2(2)

Atomic No./ Element	Gammas per decay (%)	(dis/s)/g (t = 10 min)	(dis/s)/g (t = 1 h)	(dis/s)/g (t = ∞)	Interfering reactions
55-Cs	97.4	5.40×10^3	3.23×10^4	7.26×10^6	Ba-132(n,p)
56-Ba	89.9	2.99×10^6	3.20×10^6	3.20×10^6	Ba-136(n,γ); Ce-140(n,α); La-138(n,d)
57-La	20.7 45.9	1.11×10^5	6.60×10^5	3.87×10^7	Ce-140(n,p)
58-Ce	92.4	3.66×10^6	3.66×10^6	3.66×10^6	Ce-138(n,γ); Nd-142(n,α)
	42.4 22.9	8.47×10^1	5.00×10^2	1.31×10^4	
59-Pr	98 0.19 0.50	6.18×10^6	7.09×10^6	7.09×10^6	
60-Nd	19.0 25.9	2.88×10^4	1.47×10^5	4.45×10^5	Nd-148(n,γ); Sn-152(n,α)
62-Sm	89.9	8.10×10^4	8.11×10^4	8.11×10^4	
63-Eu	69.9	9.52×10^3	4.81×10^4	1.37×10^5	Eu-151(n,γ)
64-Gd	10.8	1.02×10^4	6.00×10^4	1.64×10^6	Gd-158(n,γ); Tb-159(n,p); Dy-162(n,α)
65-Tb	7.70 2.20 0.881	1.71×10^6	1.71×10^6	1.71×10^6	Dy-158(n,p)
66-Dy	93.2	1.02×10^2	5.93×10^2	7.23×10^3	Dy-156(n,γ)

TABLE II (cont.)

Atomic No./ Element	Atomic weight of element	Target isotopic abundance (%)	Reaction	Cross-section (mb)	Half-life	Gamma energy (keV)
66-Dy		28.1	Dy-164(n,γ)Dy-165m	1.7(0.25) X 10^6	1.257(6) min	108.2(1)
67-Ho	164.930	100	Ho-165(n,2n)Ho-164m	1211(180)	37.3(5) min	56.6(1) 99.0(1)
68-Er	167.26	1.56	Er-164(n,2n)Er-163	1820(270)	75.1(4) min	53.8X 436.1(1) 1113.5(3)
69-Tm	168.934	100	Tm-169(n,2n)Tm-168	1971(152)	93.1(1) d	198.2(1) 815.9(1)
70-Yb	173.04	12.6	Yb-176(n,2n)Yb-175	2150(230)	4.19(1) d	282.5(1) 396.3(1)
71-Lu	174.97	97.39	Lu-175(n,2n)Lu-174m	627(52)	142(2) d	63.0X 67.1(1)
			Lu-175(n,γ)Lu-176m	15 100(1240)	3.684(6) h	88.3(1)
72-Hf	178.49	0.16	Hf-174(n,2n)Hf-173	1886(145)	24.0(5) h	123.7(1) 297.0(1)
		5.2	Hf-176(n,2n)Hf-175	2076(150)	70(2) d	343.4(1)
73-Ta	180.948	99.9877	Ta-181(n,2n)Ta-180m	1258(50)	8.11(2) h	63.2X 93.3(1)
74-W	183.85	0.13	W-180(n,2n)W-179m	490(50)	6.7(3) min	222.0(1)

Atomic No./ Element	Gammas per decay (%)	(dis/s)/g (t = 10 min)	(dis/s)/g (t = 1 h)	(dis/s)/g (t = ∞)	Interfering reactions
66-Dy	3.01	1.77×10^{9}	1.77×10^{9}	1.77×10^{9}	Ho-165(n,p); Er-168(n,α)
67-Ho	6.67 0.14	7.50×10^{5}	2.97×10^{6}	4.42×10^{6}	Er-164(n,p)
68-Er	12.5 0.028 0.049	9.01×10^{3}	4.35×10^{4}	1.02×10^{5}	Er-162(n,γ)
69-Tm	50.0 46.3	3.64×10^{2}	2.18×10^{3}	7.03×10^{6}	Yb-168(n,p)
70-Yb	3.08 6.55	1.08×10^{3}	6.48×10^{3}	9.43×10^{5}	Lu-176(n,p); Hf-178(n,α)
71-Lu	3.10 7.44	7.12×10^{1}	4.27×10^{2}	2.10×10^{6}	
	8.86	1.56×10^{6}	8.66×10^{6}	5.04×10^{7}	Hf-176(n,p); Hf-177(n,d)
72-Hf	82.7 33.8	4.85×10^{1}	2.90×10^{2}	1.02×10^{4}	
	86.6	2.50×10^{1}	1.50×10^{2}	3.64×10^{5}	Hf-174(n,γ)
73-Ta	11.6 4.28	5.91×10^{4}	3.43×10^{5}	4.18×10^{6}	W-180(n,p)
74-W	8.59	1.35×10^{3}	2.08×10^{3}	2.09×10^{3}	

TABLE II (cont.)

Atomic No./ Element	Atomic weight of element	Target isotopic abundance (%)	Reaction	Cross-section (mb)	Half-life	Gamma energy (keV)
74-W		28.6	W-186(n,2n)W-185m	642(60)	1.67(8) min	131.5(1) 173.7(1)
75-Re	186.2	62.60	Re-187(n,2n)Re-186g	1720(160)	90.64(9) h	63.0X 137.2(1)
76-Os	190.2	41.0	Os-192(n,2n)Os-191m	1067(318)	13.10(5) h	63.0X 71.3X 74.4(1)
77-Ir	192.2	37.3	Ir-191(n,2n)Ir-190m	220(26)	3.25(20) h	186.7(1)D[f] 361.1(1)D 502.6(1)D 616.1(2)D
78-Pt	195.09	7.2	Pt-198(n,2n)Pt-197m	910(60)	94.4(8) min	346.5(2)
79-Au	196.967	100	Au-197(n,n'γ)Au-197m	280(64)	7.86(4) s	279.0(1)
			Au-197(n,2n)Au-196m	150(20)	9.7(1) h	147.8(1) 188.3(1)
			Au-197(n,2n)Au-196m+g	2160(35)[g]	6.183(10) d	333.0(1) 355.7(1)
80-Hg	200.59	23.1	Hg-200(n,2n)Hg-199m	789(120)[h]	42.6(2) min	158.4(1) 374.1(1)
81-Tl	204.37	29.5	Tl-203(n,2n)Tl-202	2065(150)	12.23(2) d	439.6(1)

Atomic No./ Element	Gammas per decay (%)	(dis/s)/g (t = 10 min)	(dis/s)/g (t = 1 h)	(dis/s)/g (t = ∞)	Interfering reactions
74-W	4.34 3.30	5.92×10^5	6.01×10^5	6.01×10^5	W-184(n,γ); Re-185(n,p); Os-188(n,α)
75-Re	1.92 9.20	4.44×10^3	2.65×10^4	3.48×10^6	Re-185(n,γ); Os-186(n,p); Os-187(n,d)
76-Os	4.14 1.43 0.074	1.22×10^4	7.14×10^4	1.39×10^6	Os-190(n,γ); Ir-191(n,p); Pt-194(n,α)
77-Ir	69.9 95.2 97.8 98.5	8.98×10^3	4.94×10^4	2.57×10^5	Pt-190(n,p)
78-Pt	11.2	1.43×10^4	7.21×10^4	2.02×10^5	Pt-196(n,γ); Au-197(n,p); Hg-200(n,α)
79-Au	70.9	8.56×10^5	8.56×10^5	8.56×10^5	Hg-198(n,d)
	42.5 37.4	5.43×10^3	3.17×10^4	4.59×10^5	Hg-196(n,p)
	22.9 86.9	5.14×10^3	3.08×10^4	6.60×10^6	Hg-196(n,p)
80-Hg	52.5 13.8	8.22×10^4	3.41×10^5	5.47×10^5	
81-Tl	91.4	7.06×10^2	4.23×10^3	1.80×10^6	

TABLE II (cont.)

Atomic No./ Element	Atomic weight of element	Target isotopic abundance (%)	Reaction	Cross-section (mb)	Half-life	Gamma energy (keV)
82-Pb	207.19	1.42	Pb-204(n,n'γ)Pb-204m	51(10)	66.9(1) min	374.7(1) 899.2(1) 911.7(2)
90-Th	232.038	100	Th-232(n,2n)Th-231	1259(50)	25.52(1) h	84.2(1) 163.1(1)
92-U	238.03	99.275	U-238(n,2n)U-237	745(30)	6.752(2) d	101.1X 208.0(1)

Atomic No./ Element	Gammas per decay (%)	(dis/s)/g (t = 10 min)	(dis/s)/g (t = 1 h)	(dis/s)/g (t = ∞)	Interfering reactions
82-Pb	94.2 99.2 91.1	2.07×10^2	9.75×10^2	2.11×10^3	
90-Th	6.60 0.16	1.48×10^4	8.76×10^4	3.27×10^6	
92-U	23.8 21.7	1.33×10^3	7.99×10^3	1.87×10^6	

[a] This cross-section is taken from Refs [2,3].
[b] This cross-section is taken from Ref. [12].
[c] This cross-section contains a contribution from the Cd-111 (n, n'γ) reaction.
[d] No transition has been observed between the two states; this may also be the m state.
[e] Must be separated by the half-life taken from Sb-120m.
[f] Gammas from the 9.9(1) min daughter (Os-190m). Intensities are those observed in transient equilibrium.
[g] The cross-section at 14.70 MeV is taken from Ref. [13] (it is the same as that at 14.5 MeV, within error).
[h] This cross-section contains a contribution from the Hg-199 (n, n'γ) reaction of a cross-section less than 80 mb.

TABLE III. RECOMMENDED (n, 2n) CROSS-SECTIONS

Target nucleus	Final nucleus	σ (mb) (Ref. [5])	σ (mb) (Ref. [4])	Product half-life	Internal transition to ground state (%)
F-19	F-18	55(4)	49(2)[a]	109.72(0.06) min	
P-31	P-30	10.5(1.)	12.5(4.)[a]	2.498(0.004) min	
S-36	S-35	–	20	87.51(0.12) d	
Ca-48	Ca-47	920(180)	1000(100)	4.5401(0.003) d	
Sc-45	Sc-44g	188(14)	–	3.927(0.008) h	98.61
Sc-45	Sc-44m	149(12)	116(23)[a]	2.442(0.004) d	
Ti-46	Ti-45	38(4)	39.4(4)[a]	3.08(0.01) h	
Cr-50	Cr-49	26(3)	20(4)[a]	41.9(0.3) min	
Cr-52	Cr-51	304(20)	357(30)[a]	27.703(0.004) d	
Mn-55	Mn-54	890(60)	809(35)[a]	312.2(0.1) d	
Co-59	Co-58m+g	720(50)	788(230)[a]	70.78(0.10) d	~100
Co-59	Co-58m	402(41)	473(140)[a]	9.15(0.10) h	
Ni-58	Ni-57	35(3)	30(3)[a]	35.99(0.12) h	
Cu-63	Cu-62	593(36)	550(11)[a]	9.74(0.02) min	
Cu-65	Cu-64	926(60)	968(30)[a]	12.701(0.002) h	
Zn-64	Zn-63	200(23)	178(27)[a]	38.1(0.3) min	
Zn-66	Zn-65	605(55)	690(70)[a]	244.0(0.2) d	
Zn-70	Zn-69m	754(96)	–	13.76(0.02) h	
Ga-69	Ga-68	1007(63)	945(50)[a]	68.1(0.3) min	
Ga-71	Ga-70	1085(280)	1146(70)[a]	21.10(0.07) min	
Ge-70	Ge-69	588(75)	605(40)[a]	39.05(0.10) h	

Target nucleus	Final nucleus	σ (mb) (Ref. [5])	σ (mb) (Ref. [4])	Product half-life	Internal transition to ground state (%)
Ge-72	Ge-71	–	1022(300)[a]	11.8(0.4) d	
Ge-76	Ge-75m+g	1151(137)	1148(120)[a]	82.78(0.04) min	99+
Ge-76	Ge-75m	790(80)	730(100)	47.7(0.7) s	
As-75	As-74	970(80)	1061(100)[a]	17.79(0.05) d	
Se-74	Se-73m	197(50)	35	39.8(1.3) min	
Se-76	Se-75	944(66)	879(90)[a]	119.78(0.01) d	
Se-78	Se-77m	<738	800	17.45(0.10) s	
Se-80	Se-79m	680(100)	90	3.91(0.05) min	
Se-82	Se-81m	1008(120)	900	57.28(0.05) min	
Br-79	Br-78	1070(120)	974(50)[a]	6.46(0.04) min	
Br-81	Br-80g	437(30)	–	17.68(0.02) min	~100
Br-81	Br-80*m*	737(74)	665(50)[a]	4.42(0.01) h	
Kr-78	Kr-77	721(50)	245(20)	74.4(0.6) min	
Kr-80	Kr-79m+g	810(60)	810(60)	35.04(0.10) h	~100
Kr-80	Kr-79m	415(50)	415	50. (3.) s	
Kr-82	Kr-81m	160(15)	–	13. (1.) s	
Kr-86	Kr-85m	350(35)	350	4.480(0.008) h	
Rb-85	Rb-84m+g	1093(105)	1123(100)[a]	32.87(0.11) d	~100
Rb-85	Rb-84m	505(34)	350	20.49(0.17) min	
Rb-87	Rb-86m+g	1550(150)	1195(180)[a]	18.82(0.02) d	~100

TABLE III (cont.)

Target nucleus	Final nucleus	σ (mb) (Ref. [5])	σ (mb) (Ref. [4])	Product half-life	Internal transition to ground state (%)
Rb-87	Rb-86m	584(40)	580	1.020(0.002) min	
Sr-84	Sr-83m+g	–	1054(100)[a]	32.4(0.2) h	~100[b]
Sr-86	Sr-85m	247(22)	340	67.66(0.07) min	
Sr-88	Sr-87m	246(22)	318(45)[a]	2.81(0.01) h	
Y-89	Y-88	907(68)	966(100)[a]	106.6(0.2) d	
Zr-90	Zr-89m+g	768(78)	764(38)[a]	78.43(0.08) h	94
Zr-90	Zr-89m	80(6)	86(8)	4.18(0.01) min	
Zr-96	Zr-95	1529(141)	1400(100)	63.98(0.06) d	
Nb-93	Nb-92m	512(46)	482(35)[a]	10.15(0.02) d	
Mo-92	Mo-91m+g	219(19)	192(20)[a]	15.49(0.01) min	50
Mo-92	Mo-91m	17(3)	14.5	65.2(0.8) s	
Mo-94	Mo-93m	3(1)	560	6.95(0.05) h	
Mo-100	Mo-99	1390(60)	1420(150)	66.02(0.01) h	
Ru-96	Ru-95	569(30)	700(100)	1.65(0.02) h	
Ru-98	Ru-97	790(94)	1050(100)	2.88(0.04) d	
Ru-104	Ru-103	1230(146)	1440(100)	39.35(0.05) d	
Rh-103	Rh-102m	522(45)	–	207. (3.) d	
Pd-102	Pd-101	637(45)	650(60)	8.47(0.06) h	
Pd-108	Pd-107m	448(32)	500	21.3(0.5) s	
Pd-110	Pd-109m+g	1884(136)	1500(150)	13.427(0.014) h	~100
Pd-110	Pd-109m	510(35)	500	4.69(0.01) min	

Target nucleus	Final nucleus	σ (mb) (Ref. [5])	σ (mb) (Ref. [4])	Product half-life	Internal transition to ground state (%)
Ag-107	Ag-106g	870(100)	937(280)[a]	24.0(0.1) min	~0
Ag-107	Ag-106m	600(80)	400	8.46(0.10) d	
Ag-109	Ag-108g	840(150)	–	2.37(0.01) min	9[c]
Cd-108	Cd-107	915(85)	–	6.50(0.02) h	
Cd-112	Cd-111m	725(50)	675	48.6(0.03) min	
Cd-116	Cd-115g	830(80)	–	53.46(0.10) h	~0
Cd-116	Cd-115m	790(80)	820	44.6(0.3) d	
In-113	In-112m	1317(200)	790	20.9(0.2) min	
In-115	In-114g	269(20)	–	71.9(0.1) s	96.7
In-115	In-114m	1515(100)	1223(120)[a]	49.51(0.01) d	
Sn-112	Sn-111	1275(100)	1180(120)[a]	35.3(0.8) min	
Sn-114	Sn-113m+g	1239(130)	1300(200)	115.10(0.17) d	91
Sn-114	Sn-113m	–	1050	21.4(0.4) min	
Sn-118	Sn-117m	966(100)	1200	14.0(0.3) d	
Sn-120	Sn-119m	1444(210)	–	293.0(1.3) d	
Sn-122	Sn-121g	875(135)	–	27.06(0.04) h	~0
Sn-124	Sn-123g	900(180)	–	129.2(0.4) d	~0
Sn-124	Sn-123m	547(23)	–	40.08(0.07) min	
Sb-121	Sb-120g	1080(90)	–	15.89(0.04) min	~0
Sb-121	Sb-120m	427(20)	610	5.76(0.02) d	
Sb-123	Sb-122m+g	1542(80)	1420(140)[a]	2.681(0.003) d	~100

TABLE III (cont.)

Target nucleus	Final nucleus	σ (mb) (Ref. [5])	σ (mb) (Ref. [4])	Product half-life	Internal transition to ground state (%)
Sb-123	Sb-122m	731(73)	1000	4.21(0.02) min	
Te-120	Te-119g	685(80)	–	16.05(0.05) h	~0
Te-120	Te-119m	535(85)	–	4.68(0.05) d	
Te-122	Te-121g	725(40)	–	16.78(0.35) d	90
Te-122	Te-121m	890(100)	700	154. (7.) d	
Te-124	Te-123m	980(100)	–	119.7(0.1) d	
Te-128	Te-127g	780(60)	–	9.35(0.07) h	97.6
Te-128	Te-127m	940(100)	900	109. (2.) d	
Te-130	Te-129g	570(30)	–	69.5(0.5) min	63
Te-130	Te-129m	885(45)	1000	33.52(0.12) d	
I-127	I-126	1649(80)	1550(100)[a]	13.02(0.07) d	
Xe-124	Xe-123	997(80)	1200(100)	2.08(0.02) h	
Xe-126	Xe-125m+g	1480(130)	1400(100)	17.3(0.4) h	~100
Xe-126	Xe-125m	410(125)	700	57. (1.) s	
Xe-128	Xe-127m+g	1446(140)	1550(150)	36.4(0.1) d	~100
Xe-128	Xe-127m	317(25)	840	69.2(0.9) s	
Xe-130	Xe-129m	1435(130)	–	8.89(0.02) d	
Xe-132	Xe-131m	775(65)	770	11.770(0.012) d	
Xe-134	Xe-133m	665(80)	665	2.19(0.03) d	
Xe-136	Xe-135m+g	–	1750(100)	9.104(0.020) h	99+
Xe-136	Xe-135m	750(50)	750	15.65(0.10) min	

Target nucleus	Final nucleus	σ (mb) (Ref. [5])	σ (mb) (Ref. [4])	Product half-life	Internal transition to ground state (%)
Cs-133	Cs-132	1620(150)	1603(100)[a]	6.474(0.014) d	
Ba-132	Ba-131	1576(100)	1600(100)	12.0(0.1) d	
Ba-134	Ba-133m	783(56)	940	38.9(0.1) h	
Ba-136	Ba-135m	<1150	700	28.7(0.2) h	
Ba-138	Ba-137m	1020(70)	1250	2.554(0.002) min	
Ce-136	Ce-135m+g	1604(148)	1600(140)	17.76(0.31) h	~100[d]
Ce-138	Ce-137m	974(88)	970(90)	34.4(0.4) h	
Ce-140	Ce-139m+g	1810(85)	1750(70)[a]	137.65(0.03) d	~100
Ce-140	Ce-139m	900(120)	963(120)[a]	56.44(0.48) s	
Ce-142	Ce-141	1774(140)	1760(70)[a]	32.50(0.01) d	
Pr-141	Pr-140	1710(120)	1660(120)[a]	3.39(0.01) min	
Nd-142	Nd-141m+g	1692(120)	1701(120)[a]	2.50(0.08) h	99.97
Nd-142	Nd-141m	591(45)	600(50)	61.5(2.0) s	
Nd-148	Nd-147	1950(150)	1710(500)[a]	10.98(0.01) d	
Nd-150	Nd-149	1906(160)	1690(500)[a]	1.73(0.01) h	
Sm-144	Sm-143m+g	1678(185)	1488(450)[a]	8.83(0.01) min	99.8
Sm-144	Sm-143m	652(38)	–	65. (3.) s	
Sm-154	Sm-153	1882(130)	1870(550)[a]	46.8(0.1) h	
Eu-151	Eu-150m	467(43)	–	12.55(0.05) h	
Eu-153	Eu-152m_1	–	500(100)	9.32(0.01) h	0.0[e]
Eu-153	Eu-152m_2	72(6)	70	96. (1.) min	

TABLE III (cont.)

Target nucleus	Final nucleus	σ (mb) (Ref. [5])	σ (mb) (Ref. [4])	Product half-life	Internal transition to ground state (%)
Gd-152	Gd-151	1867(233)	1800(200)	120. (20.) d	
Gd-154	Gd-153	1995(280)	1900(150)	241.6(0.2) d	
Gd-160	Gd-159	1975(185)	1960(180)	18.56(0.08) h	
Tb-159	Tb-158m	451(65)	450(65)	10.5(0.2) s	
Dy-156	Dy-155	1852(143)	1850(150)	10.0(0.3) h	
Dy-158	Dy-157	1990(167)	1950(170)	8.06(0.08) h	
Dy-160	Dy-159	2020(218)	2000(200)	144.4(0.2) d	
Ho-165	Ho-164m	1211(180)	1050(300)[a]	37.5(1.0) min	
Er-162	Er-161	1927(130)	1900(130)	3.24(0.04) h	
Er-164	Er-163	1824(270)	1820(270)	75.0(0.4) min	
Er-166	Er-165	1954(147)	1960(150)	10.34(0.05) h	
Er-168	Er-167m	690(110)	1000	2.28(0.03) s	
Er-170	Er-169	1900(135)	1930(130)	9.40(0.02) d	
Tm-169	Tm-168	1971(152)	2070(600)[a]	93.1(0.1) d	
Yb-168	Yb-167	1913(217)	1920(150)	17.7(0.2) min	
Yb-170	Yb-169	1985(151)	1940(150)	32.022(0.008) d	
Yb-176	Yb-175	2166(230)	2150(230)	4.19(0.01) d	
Lu-175	Lu-174m	627(52)	558(170)[a]	142. (2.) d	
Hf-174	Hf-173	1886(145)	1900(150)	24.0(0.5) h	
Hf-176	Hf-175	2076(150)	2050(150)	70. (2.) d	
Hf-179	Hf-178m	–	900	4.3(0.1) s	

Target nucleus	Final nucleus	σ (mb) (Ref. [5])	σ (mb) (Ref. [4])	Product half-life	Internal transition to ground state (%)
Hf-180	Hf-179m	–	600	18.67(0.04) s	
Ta-181	Ta-180m	1150(100)	1258(50)[a]	8.00(0.05) h	
W-180	W-179m+g	1866(176)	2100(600)[a]	37.5(0.5) min	99.69
W-180	W-179m	490(45)	490(50)	6.4(0.1) min	
W-182	W-181	2162(140)	2020(600)[a]	120.95(0.02) d	
W-184	W-183m	790(90)	1600	5.4(0.1) s	
W-186	W-185m+g	2272(250)	1840(550)[a]	75.1(0.3) d	~100
W-186	W-185m	642(60)	600(60)	1.67(0.03) min	
Re-185	Re-184g	1430(220)	1500(450)[a]	38.0(0.5) d	75
Re-185	Re-184m	260(100)	300(90)[a]	169. (8.) d	
Re-187	Re-186g	1720(160)	1700(200)	90.64(0.09) h	~100[f]
Os-184	Os-183m	488(39)	–	9.9(0.3) h	
Os-186	Os-185	2000(120)	–	93.6(0.5) d	
Os-192	Os-191m+g	1993(200)	2120(150)	15.4(0.1) d	~100
Os-192	Os-191m	1067(318)	–	13.10(0.05) h	
Ir-191	Ir-190g	1716(125)	–	11.78(0.10) d	5[g]
Ir-191	Ir-190m	220(26)	370	3.2(0.2) h	
Ir-193	Ir-192	2062(121)	2048(150)[a]	74.1(0.2) d	
Pt-192	Pt-191	2026(168)	2030(100)	2.9(0.1) d	
Pt-196	Pt-195m	460(55)	460	4.020(0.009) d	
Pt-198	Pt-197m+g	–	2300(200)	18.3(0.3) h	97

TABLE III (cont.)

Target nucleus	Final nucleus	σ (mb) (Ref. [5])	σ (mb) (Ref. [4])	Product half-life	Internal transition to ground state (%)
Pt-198	Pt-197m	910(60)	1200	94.4(0.8) min	
Au-197	Au-196m+g	–	2100(150)[a]	6.183(0.010) d	~100
Au-197	Au-196m	150(20)	133(40)[a]	9.7(0.1) h	
Hg-196	Hg-195m	1617(160)	–	40.0(0.5) h	
Hg-198	Hg-197m	910(85)	–	23.8(0.1) h	
Hg-200	Hg-199m	789(120)	–	42.6(0.2) min	
Hg-204	Hg-203	2030(140)	1924(550)[a]	46.585(0.008) d	
Tl-203	Tl-202	1950(200)	2065(150)[a]	12.23(0.02) d	
Pb-204	Pb-203m+g	–	2103(200)[a]	52.02(0.05) h	~100
Pb-204	Pb-203m	860(180)	1200	6.09(0.10) s	
Th-232	Th-231	1320(130)	1259(50)[a]	25.52(0.03) h	
U-238	U-237	703(50)	745(30)[a]	6.75(0.01) d	

[a] This is a value of the respective excitation function at 14.5 MeV.
[b] The half-life of Sr-83m is 4.95(0.15) s.
[c] The half-life of Ag-108m is 127. (21.) years.
[d] The half-life of Ce-135m is 20. (2.) s.
[e] Internal transition to the m_1 state.
[f] The half-life of Re-186m is 2×10^5 years.
[g] The 3.2 h half-life state decays partially to the ground state across an intermediate state with a 1.2 h half-life.

TABLE IV. RECOMMENDED (n, p) CROSS-SECTIONS

Target nucleus	Final nucleus	σ (mb) (Ref. [5])	σ (mb) (Ref. [4])	Product half-life	Internal transition to ground state (%)
N-15	C-15	38(3)	16(4)	2.449(0.004) s	
O-16	N-16	35(4)	40(3)[a]	7.13(0.02) s	
O-17	N-17	5.5(2.)	35	4.173(0.004) s	
F-19	O-19	19(2)	20(2)[a]	26.76(0.08) s	
Ne-20	F-20	–	92	10.996(0.020) s	
Na-23	Ne-23	35(4)	44(13)[a]	37.24(0.12) s	
Mg-24	Na-24	181(8)	188(8)[a]	15.020(0.007) h	
Mg-25	Na-25	56(6)	45(13)[a]	59.6(0.7) s	
Mg-26	Na-26	39(11)	25(5)	1.072(0.009) s	
Al-27	Mg-27	75(4)	74(22)[a]	9.462(0.011) min	
Si-28	Al-28	226(30)	256(20)[a]	2.2406(0.0005) min	
Si-29	Al-29	129(15)	115(15)	6.56(0.06) min	
Si-30	Al-30	95(20)	–	3.60(0.06) s	
P-31	Si-31	97(15)	88(4)[a]	2.622(0.005) h	
S-32	P-32	254(25)	230(70)[a]	14.26(0.04) d	
S-33	P-33	134(22)	190(57)[a]	25.34(0.12) d	
S-34	P-34	78(8)	73(10)[a]	12.43(0.08) s	
S-36	P-36	–	50	3. s	
Cl-35	S-35	125(15)	110(10)	87.51(0.12) d	
Cl-37	S-37	28(3)	20(5)	5.05(0.02) min	

TABLE IV (cont.)

Target nucleus	Final nucleus	σ (mb) (Ref. [5])	σ (mb) (Ref. [4])	Product half-life	Internal transition to ground state (%)
Ar-38	Cl-38	75(1.5)	100(20)	37.24(0.05) min	
Ar-40	Cl-40	16(2)	18	1.32(0.2) min	
K-41	Ar-41	51(8)	43(5)[a]	1.827(0.007) h	
Ca-42	K-42	178(12)	153(20)[a]	12.360(0.003) h	
Ca-43	K-43	101(13)	100(10)	22.3(0.1) h	
Ca-44	K-44	46(5)	39(4)[a]	22.13(0.19) min	
Ca-46	K-46	–	52(15)[a]	107. (10.) s	
Sc-45	Ca-45	57(6)	58(6)[a]	165.1(0.7) d	
Ti-46	Sc-46m+g	–	242(30)[a]	83.83(0.02) d	~100
Ti-46	Sc-46m	48(8)	–	18.72(0.06) s	
Ti-47	Sc-47	116(15)	107(15)[a]	3.422(0.004) d	
Ti-48	Sc-48	53(6)	66(6)[a]	43.67(0.09) h	
Ti-49	Sc-49	23(5)	29.5(5.)[a]	57.00(0.18) min	
Ti-50	Sc-50	12(2)	16.5(3.)[a]	1.71(0.01) min	
V-51	Ti-51	33(3)	31.5(3)[a]	5.80(0.03) min	
Cr-52	V-52	80(6)	102(20)[a]	3.746(0.007) min	
Cr-53	V-53	48(7)	43(5)	1.60(0.05) min	
Cr-54	V-54	18(3)	16(3)	43. (3.) s	
Mn-55	Cr-55	57(7)	44(13)[a]	3.52(0.03) min	
Fe-54	Mn-54	332(30)	365(30)[a]	312.2(0.1) d	
Fe-56	Mn-56	98(7)	106(30)[a]	2.5785(0.0006) h	

Target nucleus	Final nucleus	σ (mb) (Ref. [5])	σ (mb) (Ref. [4])	Product half-life	Internal transition to ground state (%)
Fe-57	Mn-57	55(4)	56(16)[a]	1.54(0.05) min	
Fe-58	Mn-58	7(1.5)	17(5)	65.3(0.7) s	
Co-59	Fe-59	73(10)	60(10)[a]	45.54(0.05) d	
Ni-58	Co-58m+g	375(22)	378(110)[a]	70.78(0.10) d	~100
Ni-58	Co-58m	190(18)	147(44)[a]	9.15(0.10) h	
Ni-60	Co-60m	95(10)	59(18)[a]	10.47(0.04) min	
Ni-61	Co-61	95(10)	85(25)[a]	1.650(0.005) h	
Ni-62	Co-62g	–	22(7)[a]	1.50(0.04) min	~0
Ni-62	Co-62m	21(2.5)	22(7)[a]	13.91(0.05) min	
Cu-65	Ni-65	27(5)	25(5)[a]	2.520(0.001) h	
Zn-64	Cu-64	160(12)	164(10)[a]	12.701(0.002) h	
Zn-66	Cu-66	72(8)	68(13)[a]	5.10(0.02) min	
Zn-67	Cu-67	38(6)	45(5)	62.01(0.14) h	
Zn-68	Cu-68m	16.5(2.5)	–	3.75(0.05) min	
Ga-69	Zn-69g	38(5)	34(3)	55.6(1.6) min	99+
Ga-69	Zn-69m	26(2)	25(2)[a]	13.76(0.02) h	
Ga-71	Zn-71g	8(1)	12(4)	2.45(0.10) min	~0
Ga-71	Zn-71m	12.5(1.5)	11(1)	3.94(0.05) h	
Ge-70	Ga-70	73(8)	77(23)[a]	21.10(0.07) min	
Ge-72	Ga-72	31(3)	41(12)[a]	14.10(0.2) h	
Ge-73	Ga-73	27(4)	22(7)[a]	4.87(0.03) h	

TABLE IV (cont.)

Target nucleus	Final nucleus	σ (mb) (Ref. [5])	σ (mb) (Ref. [4])	Product half-life	Internal transition to ground state (%)
Ge-74	Ga-74	11(2)	12(4)[a]	8.25(0.05) min	
As-75	Ge-75m+g	29(2.5)	19.2(2)[a]	82.78(0.04) min	99+
As-75	Ge-75m	16(1.5)	18	47.7(0.7) s	
Se-74	As-74	134(13)	147(30)[a]	17.79(0.05) d	
Se-76	As-76	75(6)	55(5)	26.37(0.07) h	
Se-77	As-77	35(5)	35(5)	38.83(0.05) h	
Se-78	As-78	17(2)	18(4)	90.7(0.2) min	
Se-80	As-80	16(4)	–	15.2(0.2) s	
Br-79	Se-79m	10(3)	10	3.91(0.05) min	
Br-81	Se-81m	15(2)	15(2)	57.28(0.05) min	
Kr-80	Br-80m	55(9)	–	4.42(0.01) h	
Kr-82	Br-82	23(4)	23(4)	35.30(0.03) h	
Kr-83	Br-83	14(3)	–	2.39(0.03) h	
Rb-87	Kr-87	12(1.3)	10(2)	76.31(0.62) min	
Sr-84	Rb-84m+g	96(8)	96(8)	32.87(0.11) d	~100
Sr-84	Rb-84m	47(7)	47(7)	20.49(0.17) min	
Sr-86	Rb-86m+g	44(4)	44.5(4)[a]	18.82(0.02) d	~100[b]
Sr-88	Rb-88	13.5(1.5)	15(2)[a]	17.78(0.11) min	
Y-89	Sr-89	28(6)	24.6(3)[a]	50.55(0.09) d	
Zr-90	Y-90m+g	–	45(3)[a]	64.06(0.11) h	99+[c]
Zr-91	Y-91m+g	29(4)	32.5(3)[a]	58.51(0.06) d	~100

Target nucleus	Final nucleus	σ (mb) (Ref. [5])	σ (mb) (Ref. [4])	Product half-life	Internal transition to ground state (%)
Zr-91	Y-91m	14.2(1.2)	14(2)	49.71(0.04) min	
Zr-92	Y-92	19.5(2.5)	18.5(5.5)[a]	3.54(0.01) h	
Zr-94	Y-94	11(1)	9.6(2.8)[a]	18.7(0.1) min	
Mo-92	Nb-92m	60(5)	64(19)[a]	10.15(0.02) d	
Mo-95	Nb-95m+g	31(4)	38(11)[a]	35.05(0.10) d	97.5
Mo-95	Nb-95m	–	24	86.6(0.8) h	
Mo-96	Nb-96	19(2)	20.3(6)[a]	23.35(0.05) h	
Mo-97	Nb-97m+g	14(1.8)	12.5(3.7)[a]	72.1(0.7) min	~100[d]
Mo-98	Nb-98g	–	11(4)	2.86(0.06) s	~0[e]
Ru-96	Tc-96m+g	170(30)	150(20)	4.28(0.07) d	98
Ru-96	Tc-96m	–	62	51.5(1.0) min	
Ru-99	Tc-99m	<16	15	6.007(0.002) h	
Ru-100	Tc-100	15(6)	–	15.8(0.1) s	
Ru-101	Tc-101	–	36(4)	14.2(0.1) min	
Rh-103	Ru-103	17(3)	16(1)	39.35(0.05) d	
Pd-104	Rh-104m	31(6)	–	4.41(0.02) min	
Pd-105	Rh-105m+g	31(3)	38(8)	35.36(0.06) h	~100
Pd-105	Rh-105m	23(8)	–	45. s	
Pd-106	Rh-106g	16(4)	–	29.80(0.08) s	~0[f]
Ag-107	Pd-107m	15(2)	15	21.3(0.5) s	
Ag-109	Pd-109m+g	10(3)	14(2.1)[a]	13.427(0.014) h	~100[g]

TABLE IV (cont.)

Target nucleus	Final nucleus	σ (mb) (Ref. [5])	σ (mb) (Ref. [4])	Product half-life	Internal transition to ground state (%)
Cd-106	Ag-106g	76(24)	–	24.0(0.1) min	~0
Cd-106	Ag-106m	54(20)	76	8.46(0.10) d	
Cd-110	Ag-110g	23(4)	27(5)	24.42(0.14) s	1.5
Cd-110	Ag-110m	–	20	249.8(0.1) d	
Cd-111	Ag-111m+g	19(2)	22(5)[a]	7.45(0.01) d	99.7[h]
Cd-112	Ag-112	12(2)	16(2)	3.14(0.02) h	
In-115	Cd-115g	18(4)	15(5)	53.46(0.10) h	~0[i]
Sn-116	In-116m	11(1.3)	11	54.15(0.06) min	
Sn-117	In-117g	10(1.2)	–	43.8(0.7) min	47[j]
Te-122	Sb-122m+g	10.5(1.5)	12(2)	2.681(0.003) d	~100[k]
Xe-128	I-128	27(4)	–	24.99(0.02) min	
Nd-142	Pr-142m+g	13(2)	14(2)	19.2(0.1) h	~100[l]
Nd-143	Pr-143	11(2)	12(2)	13.59(0.04) d	
Sm-144	Pm-144	19(4)	–	363. (14.) d	
Ho-165	Dy-165m+g	–	40(12)[a]	2.334(0.006) h	97.76[m]

[a] This is a value of the respective excitation function at 14.5 MeV.
[b] The half-life of Rb-86m is 1.020(0.002) min.
[c] The half-life of Y-90m is 3.19(0.01) h.
[d] The half-life of Nb-97m is 60. (8.) s.
[e] The half-life of Nb-98m is 51.3(0.3) min.
[f] The half-life of Rh-106m is 130. (2.) min.
[g] The half-life of Pd-109m is 4.69(0.01) min.
[h] The half-life of Ag-111m is 64.8(0.8) s.
[i] The half-life of Cd-115m is 44.6(0.3) d.
[j] The half-life of In-117m is 1.93(0.02) h and $\sigma(n,p)$ leading to this isomeric state is approximately 6.5 mb.
[k] The half-life of Sb-122m is 4.21(0.02) min.
[l] The half-life of Pr-142m is 14.6(0.5) min.
[m] The half-life of Dy-165m is 1.257(0.006) min.

TABLE V. RECOMMENDED (n, α) CROSS-SECTIONS

Target nucleus	Final nucleus	σ (mb) (Ref. [5])	σ (mb) (Ref. [4])	Product half-life	Internal transition to ground state (%)
F-19	N-16	15(5)	33(7)[a]	7.13(0.02) s	
Na-23	F-20	150(30)	150(15)[a]	10.996(0.020) s	
Mg-26	Ne-23	77(8)	75(22)[a]	37.24(0.12) s	
Al-27	Na-24	121(6)	119(36)[a]	15.020(0.007) h	
Si-30	Mg-27	70(10)	89(27)[a]	9.462(0.011) min	
P-31	Al-28	118(15)	110(10)[a]	2.2406(0.0005) min	
S-34	Si-31	138(35)	134(67)[a]	2.622(0.005) h	
S-36	Si-33	–	15	6.18(0.18) s	
Cl-35	P-32	117(15)	117(10)[a]	14.26(0.04) d	
Cl-37	P-34	36(10)	45(13)[a]	12.43(0.08) s	
Ar-40	S-37	10.0(1.5)	11.3(2.0)[a]	5.05(0.02) min	
K-41	Cl-38m+g	39(8)	33.5(2)[a]	37.24(0.05) min	~100[b]
Ca-40	Ar-37	138(20)	115(35)[a]	35.04(0.04) d	
Ca-44	Ar-41	35(6)	36(5)[a]	1.827(0.007) h	
Ca-46	Ar-43	–	21(6)[a]	5.37(0.06) min	
Sc-45	K-42	56(6)	55(5)[a]	12.360(0.003) h	
Ti-48	Ca-45	31(3)	40(12)[a]	165.1(0.7) d	
V-51	Sc-48	16(1)	16(2)[a]	43.67(0.09) h	
Cr-54	Ti-51	14(1.2)	12.4(3.7)[a]	5.80(0.03) min	
Mn-55	V-52	32(5)	29(9)[a]	3.746(0.007) min	
Fe-54	Cr-51	100(10)	119(20)[a]	27.703(0.004) d	

Target nucleus	Final nucleus	σ (mb) (Ref. [5])	σ (mb) (Ref. [4])	Product half-life	Internal transition to ground state (%)
Fe-58	Cr-55	21(2)	21(6)[a]	3.52(0.03) min	
Co-59	Mn-56	30(2)	29(2)[a]	2.5785(0.0006) h	
Ni-62	Fe-59	20(3)	21(3)[a]	45.54(0.05) d	
Cu-63	Co-60m	23(3)	21(6)[a]	10.47(0.04) min	
Cu-65	Co-62m	16(4)	7.2(2.1)[a]	13.91(0.05) min	
Zn-68	Ni-65	9(1)	11.6(2.3)[a]	2.520(0.001) h	
Ga-69	Cu-66	34(4)	18(2)	5.10(0.02) min	
Ga-71	Cu-68	–	60(4)	31. (1.) s	
Ge-76	Zn-73	–	14(4)[a]	23.5(1.0) s	
As-75	Ga-72	10(1)	11.6(1)[a]	14.10(0.2) h	
Br-79	As-76	16(2)	12.0(1.8)[a]	26.37(0.07) h	
Sr-88	Kr-85m	75(30)	–	4.480(0.008) h	
Mo-92	Zr-89m+g	22(3)	25(3)	78.43(0.08) h	94[c]
Rh-103	Tc-100	11(2)	11(2)	15.8(0.1) s	
Ag-107	Rh-104m	–	11.3(3.4)[a]	4.41(0.02) min	
Cd-106	Pd-103	–	100(40)	16.96(0.02) d	
Nd-144	Ce-141	10(1)	–	32.50(0.01) d	

[a] This is a value of the respective excitation function at 14.5 MeV.
[b] The half-life of Cl-38m is 0.715(0.003) s.
[c] The half-life of Zr-89m is 4.18(0.01) min.

Now, while the result for N_m (Eq. (7a)) is just the same as that for N (Eq. (3)), N_g is a rather complicated function of the parameters and of time. However, there are limiting cases where N_g is proportional either to $(\sigma_m + \sigma_g)$ or to σ_g. Asymptotically, N_g will always be proportional to $(\beta\sigma_m + \sigma_g)$, but one can only use this fact to advantage if either $\lambda_m \gg \lambda_g$ or $\lambda_g \gg \lambda_m$. In the former case, if it is also true that $\beta \approx 1$ (IT $\approx$ 100%), one can use the $(\sigma_m + \sigma_g)$ 'total' cross-section in calculating ground state activity. Now, of course, a cooling time of $t_C \gg T^m_{1/2}$ has to be chosen in order to obtain exponential decay. On the other hand, if $\lambda_g \gg \lambda_m$ and, in addition, the inequality $\sigma_m\beta\lambda_m t \ll \sigma_g$ also holds, then one can use σ_g for the same purpose. A short cooling time ($t_C \ll T^m_{1/2}$) is appropriate. In Tables III–V the $(\sigma_m + \sigma_g)$ or the σ_g values are presented according to whether the final nucleus is denoted either by $X - A_{m+g}$ or $X - A_g$, respectively, where A is the mass number and X is the symbol of the element. If neither of the inequalities between λ_m and λ_g hold, then no cross-section (involving the ground state) is given, unless $\beta \approx 0$ (that is, unless the two states are totally separated from each other).

However, it has to be noted that the use of ground state activity (if a metastable state is also present) should be carried out with care or, preferably, be avoided whenever a proper substitution is possible.

3. EXPLANATION OF THE NUCLEAR DATA IN TABLE II

Details on the origins of the data in Table II, as well as on the errors, are summarized as follows. The (n, 2n), (n, p) and (n, α) cross-sections are either from Refs [4] or [5]. The (n, n'γ) cross-sections are from Ref. [5] in every case, while the thermal (n, γ) cross-sections are from Ref. [7].

The cross-sections, except (n, γ), are determined nominally at a neutron energy of 14.5 MeV. Data for isotopic abundances were taken from Ref. [8], half-life data from Ref. [9] and gamma energies and intensities from Ref. [10]. Errors in the last digit(s) of the half-life values are placed within parentheses, as are the energy errors: the uncertainty is in the last digit of the energy value (0.1 keV is the minimum error by definition). The energy errors may be replaced by the symbol X for an X-ray of known intensity which is associated with the decay of the nuclide.

The 'Gammas per decay' column denotes the number of photons emitted in 100 decays of the nuclide. Here the number of digits given is a measure of the accuracy of the value, i.e. a three-digit figure (e.g. 90.1 or 9.23) signifies an uncertainty of <10%, while a two-digit figure (90 or 9.2) signifies an uncertainty of between 10 and 20%. A one-digit figure (9., 0.9, 0.09) signifies a level of 20% or greater uncertainty. Further information (e.g. for IT values) can be found in Tables III–V.

4. EXPLANATION OF THE CROSS-SECTION TABLES

The (n, 2n), (n, p) and (n, α) cross-sections are given in Tables III, IV and V, respectively. They are the recommended values of Bychkov et al. ([4] or [6]), as well as of Qaim [5]. The cross-sections are assigned nominally to 14.5 MeV. However, this energy value (which is not the best one from the point of view of the measuring technique) is of use only in some of the cases, i.e. where a great deal of independent experimental data are available or an excitation function has been measured (marked by superscript 'a' in column 4 of Tables III–V). In some cases, measurements at 14.1 or 14.8 MeV are also included.

The tables present cross-section values (based on experimental data) only in cases where the following two conditions are both fulfilled:

(1) The half-life of the product nucleus is within the one second and the one year interval.
(2) The cross-section (according to at least one of the references) is greater than 10 mb.

The half-lives in these tables are very recent and are taken from Ref. [11]. The values of the internal transitions (leading to the ground state) are taken from Ref. [9]. The 'Product half-life' column presents the ground state value whenever the final nucleus is either $X-A_{m+g}$ or $X-A_g$.

TABLE VI. SOME VERY PRECISE CROSS-SECTIONS AT 14.7 MeV FROM A SIMULTANEOUS EVALUATION

(The proton scattering cross-section of hydrogen is also included because it is a frequently used standard. The data were taken from Refs [12,13].)

Reaction	Cross-section (mb)	Uncertainty (%)
Al-27(n, α)Na-24	113.7	0.6
Fe-56(n, p)Mn-56	107.8	0.6
Cu-63(n, 2n)Cu-62	537	1.2
Cu-65(n, 2n)Cu-64	962	1.2
Au-197(n, 2n)Au-196m+g	2160	1.6
Nb-93(n, 2n)Nb-92m	451	1.6
S-32(n, p)P-32	215	1.5
H-1(n, n)H-1	650	1.4

TABLE VII. ISOTOPIC AND ELEMENTAL CROSS-SECTIONS AT 14.7 MeV FROM A RECENT EVALUATION [14]

Reaction	Isotopic cross-sections[a] (mb)	Elemental cross-sections (mb)	Standard deviation (%)
Al-27(n, p)Mg-27	70.5	Same	2.0
Si(n, X)Al-28	257.3	237.3	2.5
Ti(n, X)Sc-46	294.8	24.18	2.3
Ti(n, X)Sc-47	223.1	16.51	17.2
Ti(n, X)Sc-48	60.6	44.67	2.4
V-51(n, p)Ti-51	31.87	31.79	4.4
V-51(n, α)Sc-48	15.89	15.85	2.4
Cr(n, X)V-52	72.49	60.74	4.4
Mn-55(n, α)V-52	31.21	Same	4.2
Mn-55(n, 2n)Mn-54	816.7	Same	2.6
Fe(n, X)Mn-54	284.4	16.50	2.0
Fe-54(n, α)Cr-51	87.9	5.096	2.7
Co-59(n, p)Fe-59	56.60	Same	16.2
Co-59(n, α)Mn-56	30.17	Same	1.4
Co-59(n, 2n)Co-58	747.7	Same	2.4
Cu-65(n, p)Ni-65	20.46	6.303	7.0
Zn(n, X)Cu-64	165.4	80.4	2.6
Zn-64(n, 2n)Zn-63	162.2	78.8	2.4

[a] Calculated by assuming that the yield is attributed to that single isotope which is responsible for the dominant portion of the yield.

Finally, it should be mentioned that it is not too essential whether data from Refs [4] or [5] are used. The difference between these two sets of data is greater than their summed errors in about 8% of all cases, while this number is reduced to 1.4% if only those data are included which were taken from excitation functions (Refs [4, 6]). Therefore, a preference for the value of Bychkov et al. is suggested if this value is taken from an excitation function (although the errors seem to be slightly overestimated here in some cases).

The results of a simultaneous evaluation of some important cross-sections at 14.7 MeV are presented in Table VI. These are very precise values and are used frequently as standards [12, 13]. In Table VII, some cross-sections – also measured at 14.7 MeV – are given from a recent evaluation, including elemental cross-sections [14].

ACKNOWLEDGEMENTS

The authors are very much indebted to H. Vonach for his useful remarks.

REFERENCES

[1] CSIKAI, J., At. Energy Rev. **11** 3 (1973) 415.
[2] TAGESEN, S., VONACH, H., Physics Data, Vol. 13-1, Fachinformationszentrum, Karlsruhe (1981).
[3] VONACH, H., "The $^{27}Al(n,\alpha)$ cross-section", Nuclear Data Standards for Nuclear Measurements, Technical Reports Series No. 227, IAEA, Vienna (1983) 59.
[4] BYCHKOV, V.M., MANOKHIN, V.N., PASHCHENKO, A.B., PLYASKIN, V.I., Cross sections for neutron induced threshold reactions, Energoizdat, Moscow (1982) (in Russian).[2]
[5] QAIM, S.M., "14 MeV neutron activation cross sections", Handbook of Spectroscopy, Vol. 3, CRC Press, Boca Raton, FL (1981) 141.
[6] MANOKHIN, V.N., PASHCHENKO, A.B., PLYASKIN, V.I., BYCHKOV, V.M., PRONYAEV, V.G., Chapter 2-3, this Handbook.
[7] GRYNTAKIS, E.M., MUNDY, G., CULLEN, D.E., Part 2-1, this Handbook.
[8] YOSHIZAWA, Y., HARIGUCHI, T., YAMADA, M., Chart of the Nuclides, Tokai, Ibaraki (1980).
[9] Table of Isotopes, 7th edn (LEDERER, C.M., SHIRLEY, V.S., Eds) Wiley, New York (1978).
[10] REUS, U., WESTMEIER, W., At. Data Nucl. Data Tables **29** 2 (1983) 205.
[11] LORENZ, A., Nuclear Data Section, IAEA, private communication, 1984.
[12] WINKLER, G., RYVES, T.B., Ann. Nucl. Energy **10** (1983) 601.
[13] RYVES, T.B., "A simultaneous evaluation of some important cross-sections at 14.70 MeV", Nuclear Standard Reference Data (Proc. IAEA-OECD/NEANDC Advisory Group Meeting Geel, Belgium, 1984), IAEA-TECDOC-335, IAEA, Vienna (1985) 431.
[14] EVAIN, B.P., SMITH, D.L., LUCCHESE, P., Argonne National Lab., IL, Rep. ANL/NDM-89 (1985).

[2] If an excitation function is presented in Ref. [6], then this value is accepted instead of a value from Ref. [4], even in the case when the new error is greater than the old one.

2-3. ACTIVATION CROSS-SECTIONS INDUCED BY FAST NEUTRONS

V.N. MANOKHIN, A.B. PASHCHENKO,
V.I. PLYASKIN
Institute of Physics
and Power Engineering,
Obninsk,
Union of Soviet Socialist Republics

V.M. BYCHKOV*
Department of Safeguards,
International Atomic Energy Agency,
Vienna

V.G. PRONYAEV*
Nuclear Data Section,
Division of Research and Laboratories,
International Atomic Energy Agency,
Vienna

Abstract

ACTIVATION CROSS-SECTIONS INDUCED BY FAST NEUTRONS.

Evaluated cross-sections for the most important activation reactions induced by fast neutrons have been compiled on the basis of internationally available evaluated data libraries. The computer file includes evaluated neutron cross-section data for 206 (n, 2n), (n, p) and (n, α) reactions in the energy range from threshold to 20 MeV, leading to well specified radioactivities. The data are presented in the form of graphical plots and tables. An estimate of the accuracy of the evaluated data is also given in the tables wherever possible. The file can be obtained on magnetic tape in the ENDF-V computer format upon request from the Nuclear Data Section of the IAEA.

1. INTRODUCTION

The present compilation of fast neutron induced activation reaction cross-sections, covering energies from threshold to 20 MeV, is based on evaluated data taken from different evaluated data libraries and individual evaluations. The majority of these evaluations were prepared by using available experimental data

---

* Present address: Institute of Physics and Power Engineering, Obninsk, Union of Soviet Socialist Republics.

for selecting the parameters needed in theoretical computations and for normalizing the results of such computations. Theoretical calculations were also used for the interpolation and extrapolation of experimental cross-section data.

The significant progress achieved over the last ten years in the theoretical description of these activation reactions must be emphasized, especially since the previous edition of this Handbook [1] included only a compilation of experimental data. The reasons for this progress are (1) development of statistical and pre-equilibrium decay models [2–4] and (2) a better understanding of nuclear level density problems [5].

2. PROCEDURE FOR FILE PREPARATION

The following libraries and individual files of evaluated neutron cross-section data were used for the selection of the activation cross-sections: the BOSPOR Library [6], the Activation File of the Evaluated Nuclear Data Library [7], the Evaluated Neutron Data File (ENDF/B-V) Activation File [8], the International Reactor Dosimetry File (IRDF-82) [9] and individual evaluations carried out under various IAEA research contracts [10, 11]. All of the evaluated data curves were compared with experimental data that have been reported over the last four years. Only those cross-sections not in contradiction with the latest experimental data were retained in the present activation data file. In cases of several conflicting evaluations, that evaluation was chosen which best corresponded to the experimental data. A few evaluated curves were renormalized in accordance with the results of the latest precision measurements.

The file of selected reactions contains 206 evaluated cross-section curves of the (n, 2n), (n, p) and (n, α) reactions which lead to radioactive products and may be used in many practical applications of neutron activation analysis. Some competing activation reactions, usually with low cross-section values, are given for completeness.

3. PRESENTATION OF THE DATA

A graphical form was chosen for the presentation of the data. The computer codes Linear and Evalplot [12] were used for plotting the figures. To provide more information, and to make it possible to use this Handbook for simple estimates, tables of numerical values of the cross-sections, in neutron energy steps of about 1 MeV, were added to the figures. Whenever possible, an estimate of the accuracy of the evaluated curves is also given in the tables. If the accuracy of an evaluation is not given, it is supposed, in most cases, that the accuracy is ± 30% or lower.

The computer file of the cross-sections (plus the covariance matrices of the uncertainties in a few instances) for all compiled activation reactions in the ENDF/B-V format is available from the Nuclear Data Section of the IAEA and may be obtained upon request either on magnetic tape or in the form of listings. This file contains more detailed information about the energy dependence of the cross-sections (a 100 keV energy mesh is normal) and some additional bibliographic information.

An attempt has been made to specify clearly the activity created by a given reaction. In the case of the formation of an isomeric state, the term 'Isomeric state' is given in the figure. In the case of a cross-section for the independent formation of ground state activity of the residual nucleus (without population through internal transitions from an isomeric state) the term 'Ground state' is used. No label on a figure means that the radioactive residual nucleus has no isomeric state. If it does have an isomeric state, then the sum of m + g is given only if it is equal to the cumulative cross-section of formation of ground state activity. This will only be the case if the half-life of the isomeric state is much smaller than the half-life of the ground state, the branching ratio for the internal transition from the isomeric state is close to 1 and the cooling time for measurement of this activity is chosen which is much larger than the half-life of the isomeric state. Cumulative cross-sections of formation of ground state activity for activation analysis purposes should therefore be used with great care.

4. RELATIONSHIPS WITH OTHER SECTIONS OF THIS HANDBOOK

Owing to limitations of space, it is not possible in this section to give more detailed information on the decay properties of residual nuclei. It is assumed that this information can be taken from other chapters of this Handbook, or from other publications [13].

Regarding the degree of consistency with data presented in Part 2-2, it should be emphasized that the 14 MeV values from both sets agreed within the limits of the estimated errors.

ACKNOWLEDGEMENTS

The authors are greatly indebted to the staff of the Nuclear Data Section, IAEA, for their help in the preparation of this chapter.

REFERENCES

[1] INTERNATIONAL ATOMIC ENERGY AGENCY, Handbook on Nuclear Activation Cross-Sections, Technical Reports Series No. 156, IAEA, Vienna (1974).

[2] INTERNATIONAL ATOMIC ENERGY AGENCY, Nuclear Theory for Applications (Proc. Course Trieste, 1978), IAEA-SMR-43, IAEA, Vienna (1980).

[3] INTERNATIONAL ATOMIC ENERGY AGENCY, Nuclear Theory for Applications–1980 (Proc. Interregional Advanced Training Course Trieste, 1980), IAEA-SMR-68/1, IAEA, Vienna (1981).

[4] INTERNATIONAL ATOMIC ENERGY AGENCY, Nuclear Theory for Applications–1982 (Proc. Course Trieste, 1982) IAEA-SMR-93, IAEA, Vienna (1984).

[5] Basic and Applied Problems of Nuclear Level Densities (Proc. IAEA Advisory Group, Mtg. Upton, NY, 1983) (BHAT, M.R., Ed.), Rep. BNL-NCS-51694, Brookhaven National Lab., Upton, NY (1983).

[6] BYCHKOV, V.M., MANOKHIN, V.N., PASHCHENKO, A.B., PLYASKIN, V.I., Cross Sections for the (n, p), (n, α) and (n, 2n) Threshold Reactions, Rep. INDC(CCP) - 146/LJ (1980);
BYCHKOV, V.M., ZOLOTAREV, K.I., PASHCHENKO, A.B., PLYASKIN, V.I., Establishment of the BOSPOR-80 Machine Library of Evaluated Threshold Reaction Cross-Sections and its Testing by Means of Integral Experiments, Rep. INDC(CCP) – 183/L (1982), Nuclear Data Committee, IAEA, Vienna. (English translations from Yad. Konstanty **1** 32 (1979) 27; **2** 33 (1979) 51; **4** 35 (1979) 21; 3 42 (1981) 60.)

[7] The LLNL Neutron Activation Cross-Section Library of 1982, documented in Rep. UCRL-50400, Vol. 18, 17 October 1978, Lawrence Livermore National Laboratory, Livermore, CA (1978).

[8] The ENDF/B-V Neutron Activation Cross Section Files, documented in Rep. BNL-NCS-50496, Brookhaven National Laboratory, Upton, NY (1979).

[9] CULLEN, D.E., KOCHEROV, N., McLAUGHLIN, P.K., The International Reactor Dosimetry File (IRDF-82) in Energy Dependent Form, Internal Rep. IAEA-NDS-48, IAEA, Vienna, 1982.

[10] ADAMSKI, L., HERMAN, M., MARCINKOWSKI, A., Evaluation of the cross-sections for the ^{28}Si(n, p)^{28}Al and the ^{181}Ta(n, 2n)^{180}Ta reactions, Final Report, IAEA Research Contract No. 2741/RB, 1983.

[11] IVASCU, M., AVRIGENAU, M., AVRIGENAU, V., Nuclear Model Calculations of (n, p) and (n, n′p) Reactions on Molybdenum Isotopes, NP-28-1983, Final Report, IAEA Research Contract No. 2983/RB, 1983.

[12] CULLEN, D.E., Program LINEAR (Version 78-1): Linearize Data in the Evaluated Nuclear Data File/Version B (ENDF/B) Format, Rep. UCRL-50400, Vol. 17, Part A, Rev. 1, 1978; Program EVALPLOT (Version 79-1): Plot Data in the Evaluated Nuclear Data File/ Version B (ENDF/B) Format, Rep. UCRL-50400, Vol. 17, Part E, 1979, University of California, Berkeley.

[13] Table of Isotopes, 7th edn (LEDERER, C.M., SHIRLEY, V.S., Eds) Wiley, New York (1978).

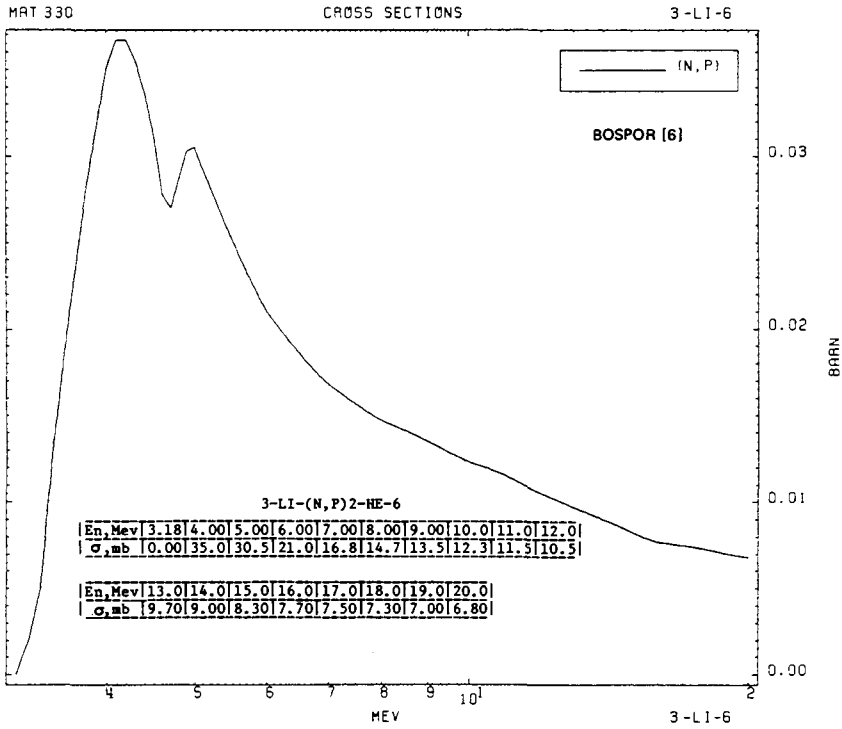
MAT 330
CROSS SECTIONS
3-LI-6
(N,P)
BOSPOR [6]
0.03
0.02
0.01
0.00
BARN
3-LI-(N,P)2-HE-6
En,Mev | 3.18 | 4.00 | 5.00 | 6.00 | 7.00 | 8.00 | 9.00 | 10.0 | 11.0 | 12.0
σ,mb | 0.00 | 35.0 | 30.5 | 21.0 | 16.8 | 14.7 | 13.5 | 12.3 | 11.5 | 10.5
En,Mev | 13.0 | 14.0 | 15.0 | 16.0 | 17.0 | 18.0 | 19.0 | 20.0
σ,mb | 9.70 | 9.00 | 8.30 | 7.70 | 7.50 | 7.30 | 7.00 | 6.80
4 5 6 7 8 9 10^1 2
MEV
3-LI-6

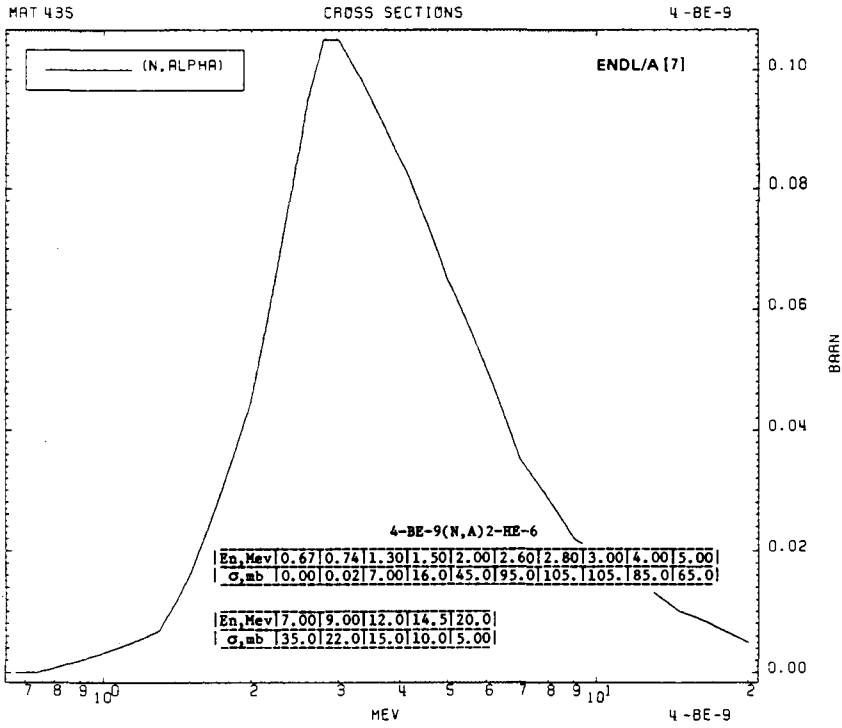
MAT 435
CROSS SECTIONS
4-BE-9
(N,ALPHA)
ENDL/A [7]
0.10
0.08
0.06
0.04
0.02
0.00
BARN
4-BE-9(N,A)2-HE-6
En,Mev | 0.67 | 0.74 | 1.30 | 1.50 | 2.00 | 2.60 | 2.80 | 3.00 | 4.00 | 5.00
σ,mb | 0.00 | 0.02 | 7.00 | 16.0 | 45.0 | 95.0 | 105. | 105. | 85.0 | 65.0
En,Mev | 7.00 | 9.00 | 12.0 | 14.5 | 20.0
σ,mb | 35.0 | 22.0 | 15.0 | 10.0 | 5.00
7 8 9 10^0 2 3 4 5 6 7 8 9 10^1 2
MEV
4-BE-9

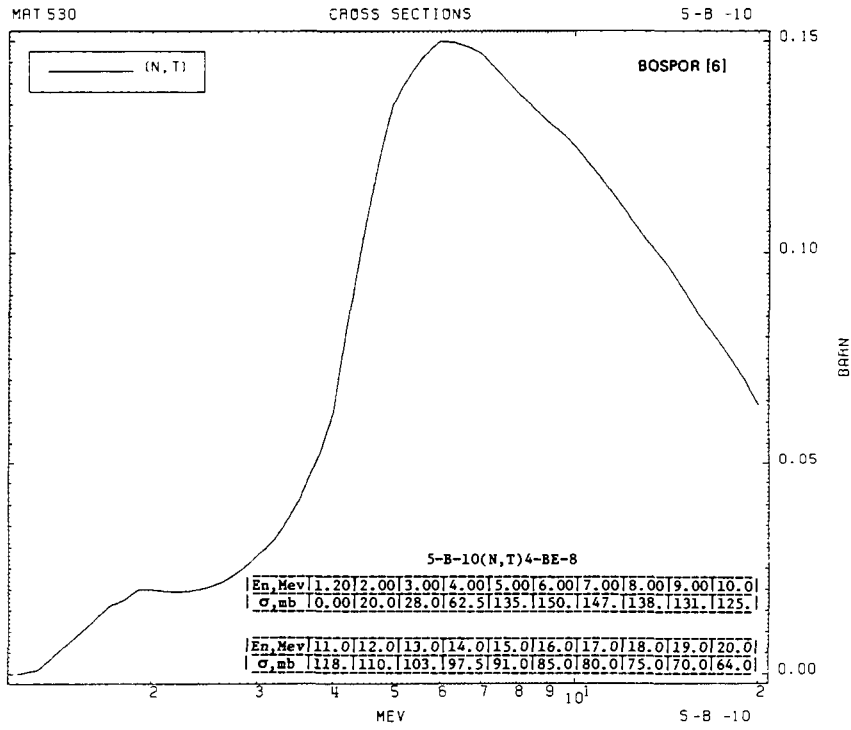
MAT 530
CROSS SECTIONS
5-B -10
(N, T)
BOSPOR [6]
0.15
0.10
0.05
0.00
BARN
5-B-10(N,T)4-BE-8
En,Mev | 1.20 | 2.00 | 3.00 | 4.00 | 5.00 | 6.00 | 7.00 | 8.00 | 9.00 | 10.0
σ,mb | 0.00 | 20.0 | 28.0 | 62.5 | 135. | 150. | 147. | 138. | 131. | 125.
En,Mev | 11.0 | 12.0 | 13.0 | 14.0 | 15.0 | 16.0 | 17.0 | 18.0 | 19.0 | 20.0
σ,mb | 118. | 110. | 103. | 97.5 | 91.0 | 85.0 | 80.0 | 75.0 | 70.0 | 64.0
2 3 4 5 6 7 8 9 10^1 2
MEV
5-B -10

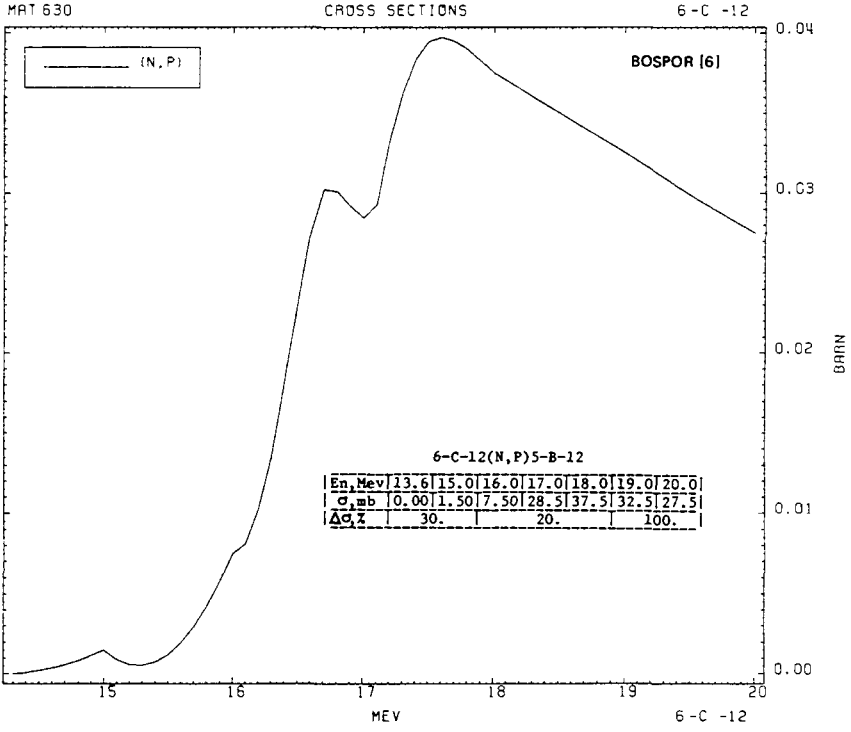
MAT 630
CROSS SECTIONS
6-C -12
(N, P)
BOSPOR [6]
0.04
0.03
0.02
0.01
0.00
BARN
6-C-12(N,P)5-B-12
En,Mev | 13.6 | 15.0 | 16.0 | 17.0 | 18.0 | 19.0 | 20.0
σ,mb | 0.00 | 1.50 | 7.50 | 28.5 | 37.5 | 32.5 | 27.5
Δσ,% | 30. | 20. | 100.
15 16 17 18 19 20
MEV
6-C -12

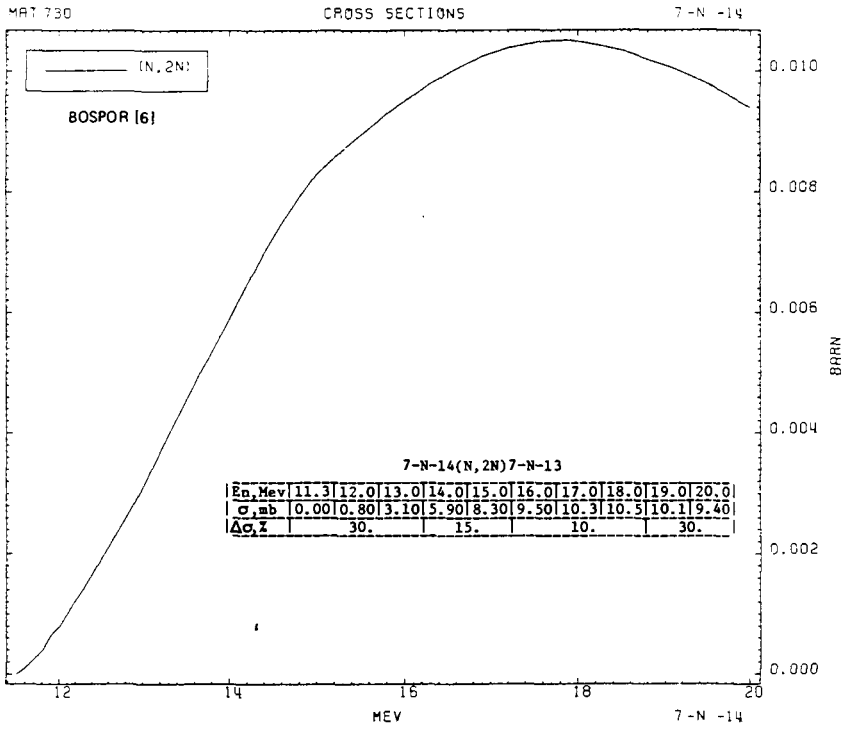
MAT 730
CROSS SECTIONS
7-N -14
(N,2N)
BOSPOR [6]
0.010
0.008
0.006
0.004
0.002
0.000
BARN
7-N-14(N,2N)7-N-13
En,Mev | 11.3 | 12.0 | 13.0 | 14.0 | 15.0 | 16.0 | 17.0 | 18.0 | 19.0 | 20.0
σ,mb | 0.00 | 0.80 | 3.10 | 5.90 | 8.30 | 9.50 | 10.3 | 10.5 | 10.1 | 9.40
Δσ,% | 30. | 15. | 10. | 30.
12
14
16
18
20
MEV
7-N -14

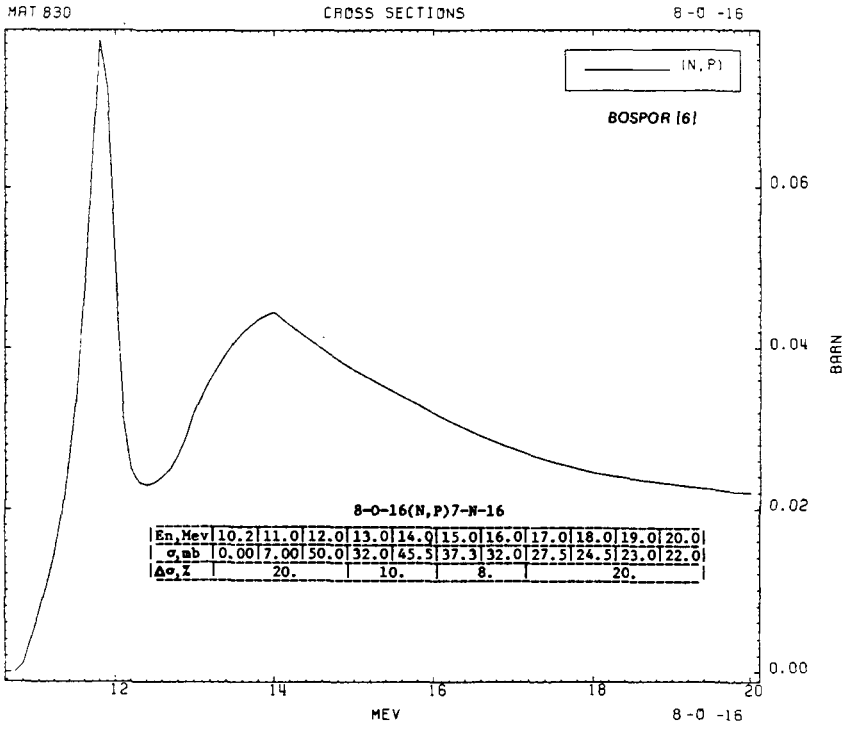
MAT 830
CROSS SECTIONS
8-O -16
(N,P)
BOSPOR [6]
0.06
0.04
0.02
0.00
BARN
8-O-16(N,P)7-N-16
En,Mev | 10.2 | 11.0 | 12.0 | 13.0 | 14.0 | 15.0 | 16.0 | 17.0 | 18.0 | 19.0 | 20.0
σ,mb | 0.00 | 7.00 | 50.0 | 32.0 | 45.5 | 37.3 | 32.0 | 27.5 | 24.5 | 23.0 | 22.0
Δσ,% | 20. | 10. | 8. | 20.
12
14
16
18
20
MEV
8-O -16

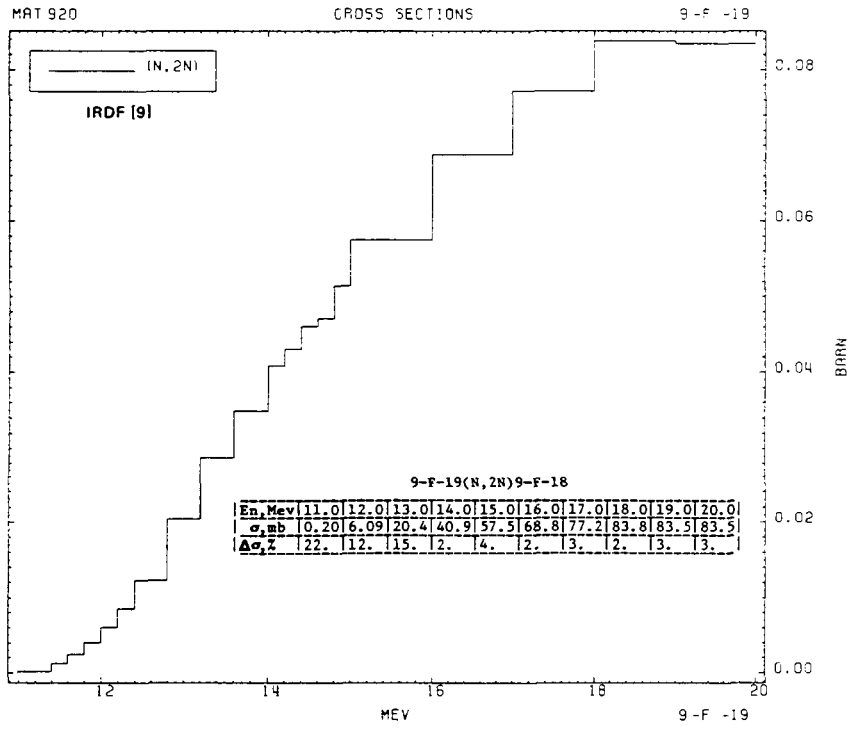
MAT 920
CROSS SECTIONS
9-F -19
(N,2N)
IRDF [9]
9-F-19(N,2N)9-F-18
En,Mev 11.0 12.0 13.0 14.0 15.0 16.0 17.0 18.0 19.0 20.0
σ,mb 0.20 6.09 20.4 40.9 57.5 68.8 77.2 83.8 83.5 83.5
Δσ,% 22. 12. 15. 2. 4. 2. 3. 2. 3. 3.
0.08
0.06
0.04
0.02
0.00
BARN
12
14
16
18
20
MEV
9-F -19

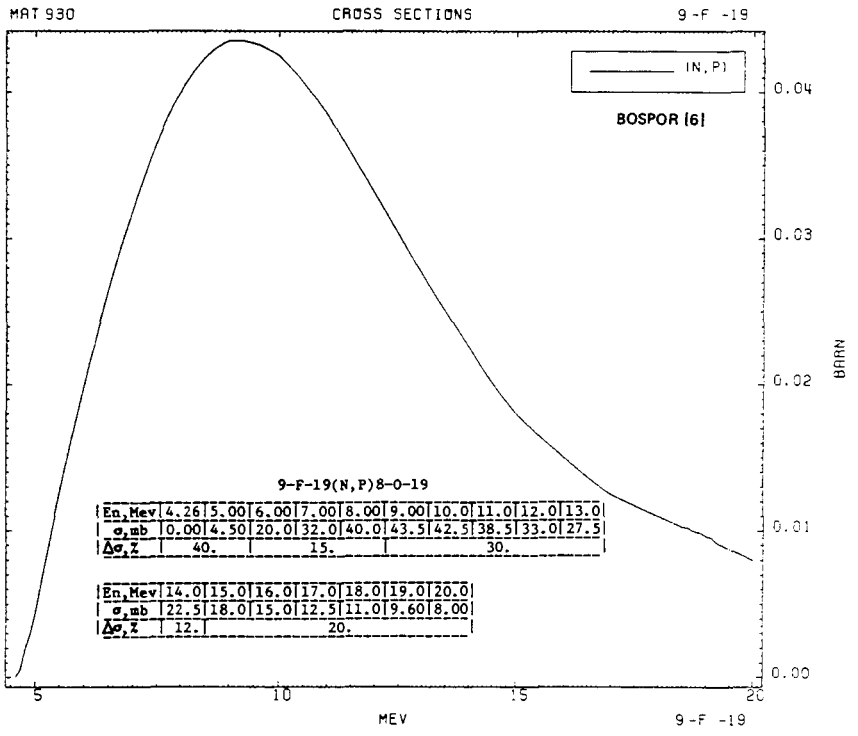
MAT 930
CROSS SECTIONS
9-F -19
(N,P)
BOSPOR [6]
9-F-19(N,P)8-O-19
En,Mev 4.26 5.00 6.00 7.00 8.00 9.00 10.0 11.0 12.0 13.0
σ,mb 0.00 4.50 20.0 32.0 40.0 43.5 42.5 38.5 33.0 27.5
Δσ,% 40. 15. 30.
En,Mev 14.0 15.0 16.0 17.0 18.0 19.0 20.0
σ,mb 22.5 18.0 15.0 12.5 11.0 9.60 8.00
Δσ,% 12. 20.
0.04
0.03
0.02
0.01
0.00
BARN
5
10
15
20
MEV
9-F -19

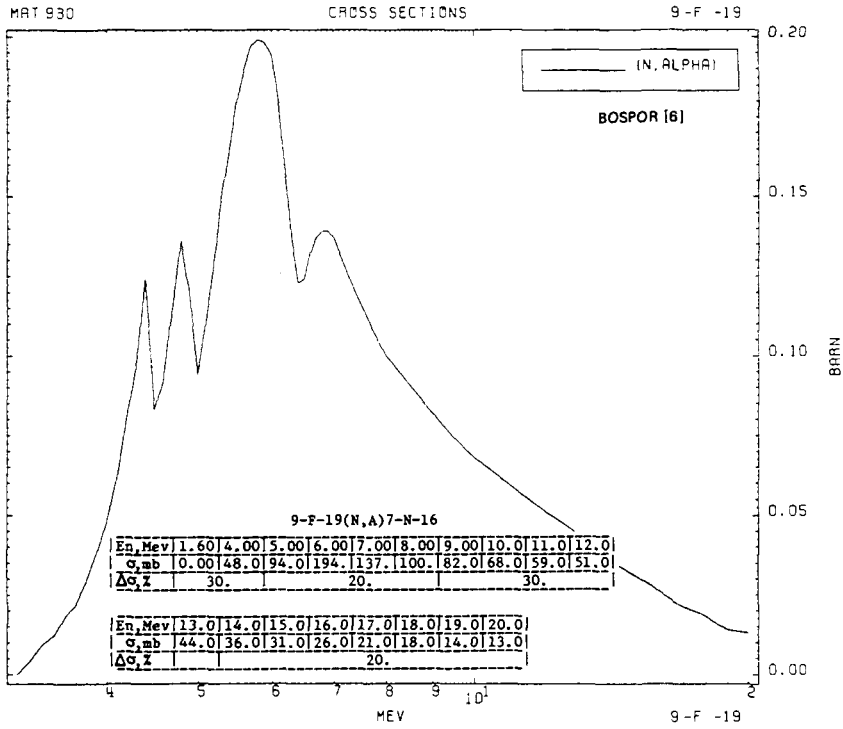
MAT 930
CROSS SECTIONS
9-F -19
(N,ALPHA)
BOSPOR [6]
9-F-19(N,A)7-N-16
En,Mev | 1.60 | 4.00 | 5.00 | 6.00 | 7.00 | 8.00 | 9.00 | 10.0 | 11.0 | 12.0
σ,mb | 0.00 | 48.0 | 94.0 | 194. | 137. | 100. | 82.0 | 68.0 | 59.0 | 51.0
Δσ,% | 30. | 20. | 30.
En,Mev | 13.0 | 14.0 | 15.0 | 16.0 | 17.0 | 18.0 | 19.0 | 20.0
σ,mb | 44.0 | 36.0 | 31.0 | 26.0 | 21.0 | 18.0 | 14.0 | 13.0
Δσ,% | 20.
0.20
0.15
0.10
0.05
0.00
BARN
4
5
6
7
8
9
10¹
2
MEV
9-F -19

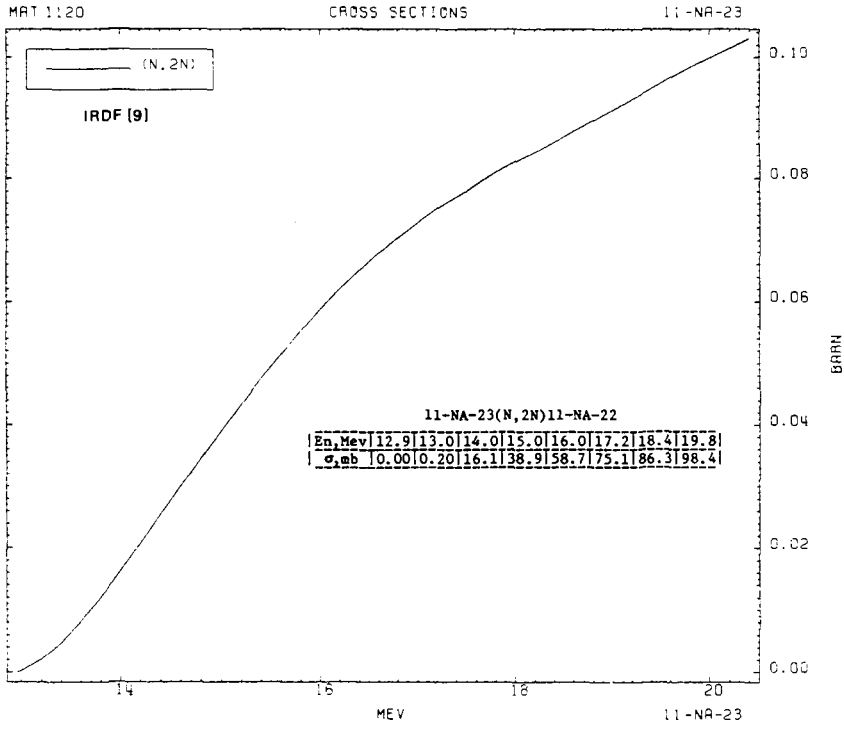
MAT 1120
CROSS SECTIONS
11-NA-23
(N,2N)
IRDF [9]
11-NA-23(N,2N)11-NA-22
En,Mev | 12.9 | 13.0 | 14.0 | 15.0 | 16.0 | 17.2 | 18.4 | 19.8
σ,mb | 0.00 | 0.20 | 16.1 | 38.9 | 58.7 | 75.1 | 86.3 | 98.4
0.10
0.08
0.06
0.04
0.02
0.00
BARN
14
16
18
20
MEV
11-NA-23

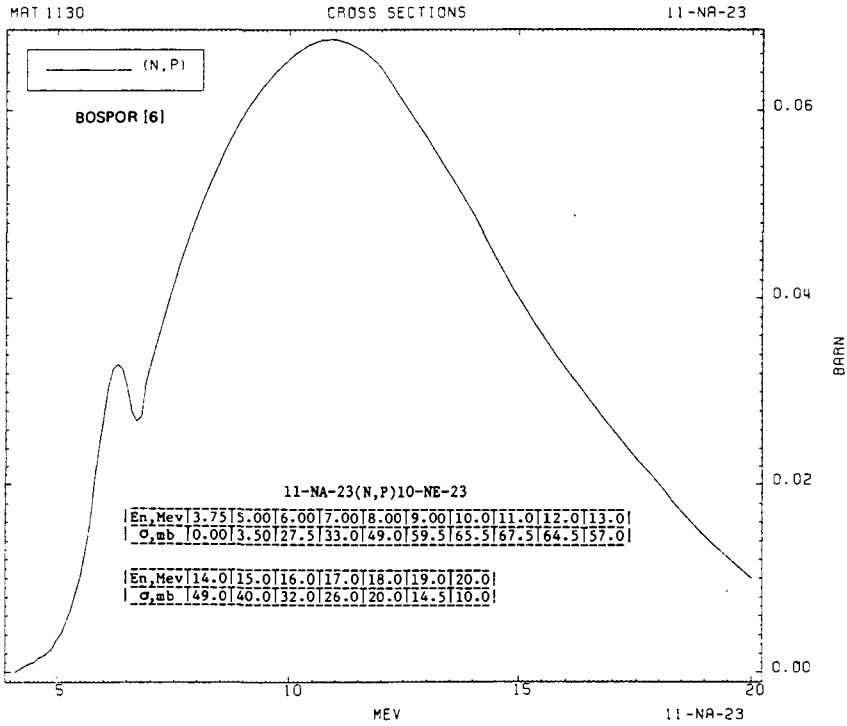
MAT 1130
CROSS SECTIONS
11-NA-23
(N,P)
BOSPOR [6]
11-NA-23(N,P)10-NE-23
En,Mev | 3.75 | 5.00 | 6.00 | 7.00 | 8.00 | 9.00 | 10.0 | 11.0 | 12.0 | 13.0
σ,mb | 0.00 | 3.50 | 27.5 | 33.0 | 49.0 | 59.5 | 65.5 | 67.5 | 64.5 | 57.0
En,Mev | 14.0 | 15.0 | 16.0 | 17.0 | 18.0 | 19.0 | 20.0
σ,mb | 49.0 | 40.0 | 32.0 | 26.0 | 20.0 | 14.5 | 10.0
0.06
0.04
0.02
0.00
BARN
5
10
15
20
MEV
11-NA-23

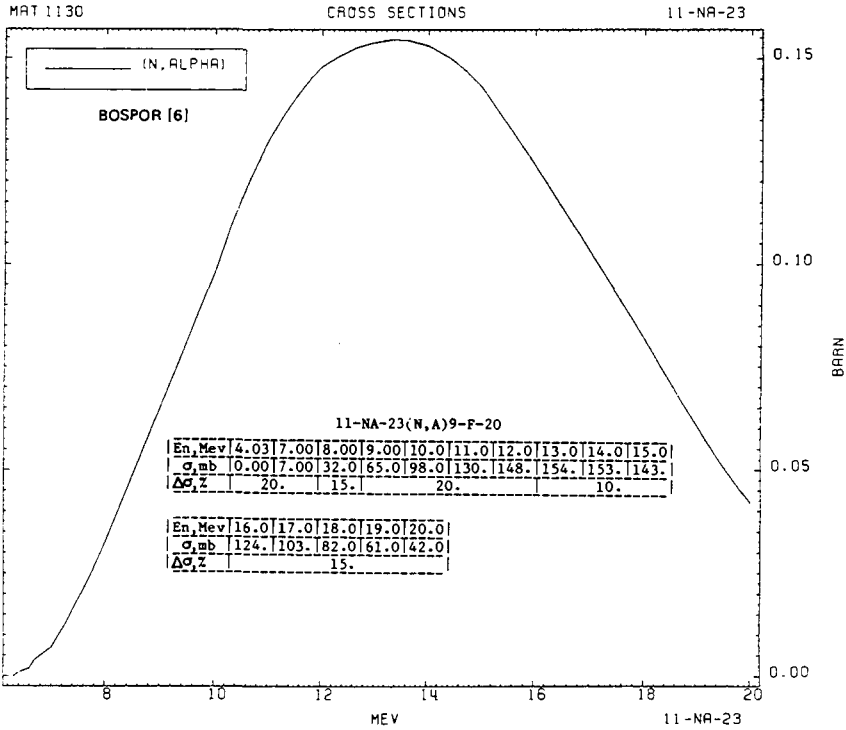
MAT 1130
CROSS SECTIONS
11-NA-23
(N,ALPHA)
BOSPOR [6]
11-NA-23(N,A)9-F-20
En,Mev | 4.03 | 7.00 | 8.00 | 9.00 | 10.0 | 11.0 | 12.0 | 13.0 | 14.0 | 15.0
σ,mb | 0.00 | 7.00 | 32.0 | 65.0 | 98.0 | 130. | 148. | 154. | 153. | 143.
Δσ,% | 20. | 15. | 20. | 10.
En,Mev | 16.0 | 17.0 | 18.0 | 19.0 | 20.0
σ,mb | 124. | 103. | 82.0 | 61.0 | 42.0
Δσ,% | 15.
0.15
0.10
0.05
0.00
BARN
8
10
12
14
16
18
20
MEV
11-NA-23

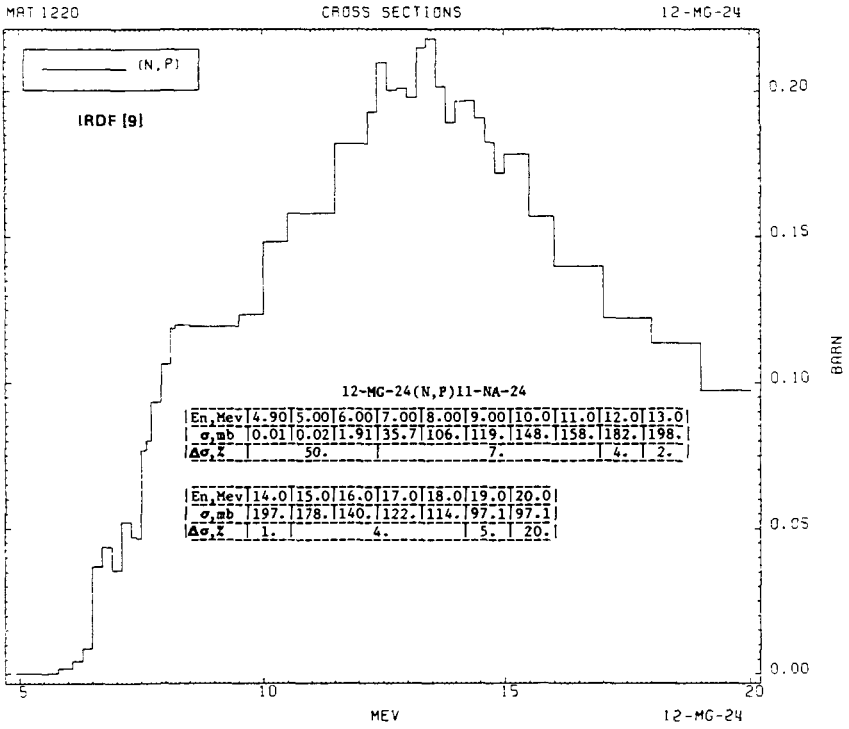
MAT 1220
CROSS SECTIONS
12-MG-24
(N,P)
IRDF [9]
12-MG-24(N,P)11-NA-24
En,Mev | 4.90 | 5.00 | 6.00 | 7.00 | 8.00 | 9.00 | 10.0 | 11.0 | 12.0 | 13.0
σ,mb | 0.01 | 0.02 | 1.91 | 35.7 | 106. | 119. | 148. | 158. | 182. | 198.
Δσ,% | 50. | 7. | 4. | 2.
En,Mev | 14.0 | 15.0 | 16.0 | 17.0 | 18.0 | 19.0 | 20.0
σ,mb | 197. | 178. | 140. | 122. | 114. | 97.1 | 97.1
Δσ,% | 1. | 4. | 5. | 20.
0.20
0.15
0.10
0.05
0.00
BARN
5
10
15
20
MEV
12-MG-24

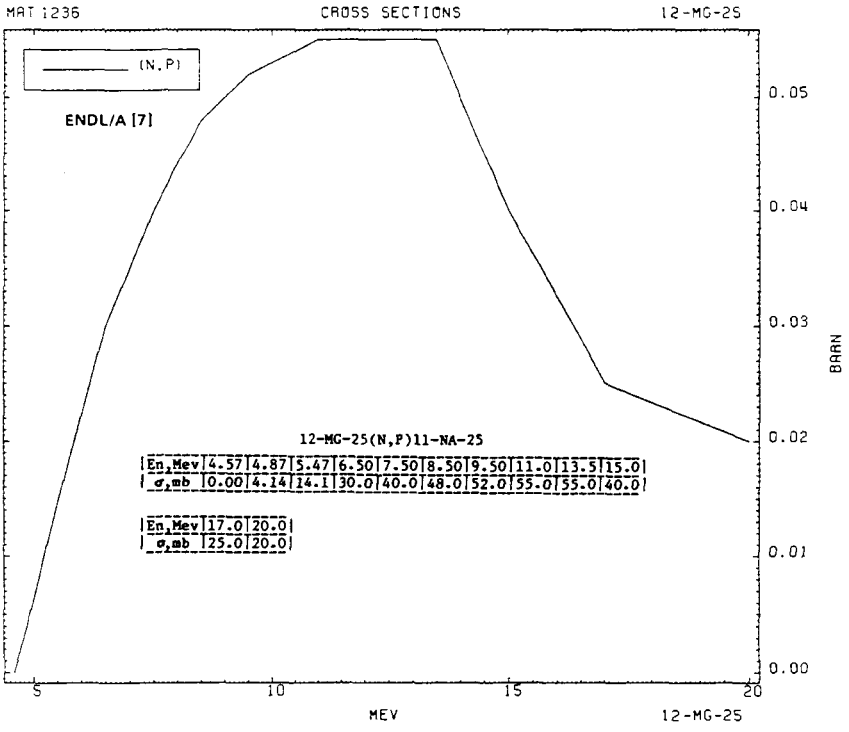
MAT 1236
CROSS SECTIONS
12-MG-25
(N,P)
ENDL/A [7]
12-MG-25(N,P)11-NA-25
En,Mev | 4.57 | 4.87 | 5.47 | 6.50 | 7.50 | 8.50 | 9.50 | 11.0 | 13.5 | 15.0
σ,mb | 0.00 | 4.14 | 14.1 | 30.0 | 40.0 | 48.0 | 52.0 | 55.0 | 55.0 | 40.0
En,Mev | 17.0 | 20.0
σ,mb | 25.0 | 20.0
0.05
0.04
0.03
0.02
0.01
0.00
BARN
5
10
15
20
MEV
12-MG-25

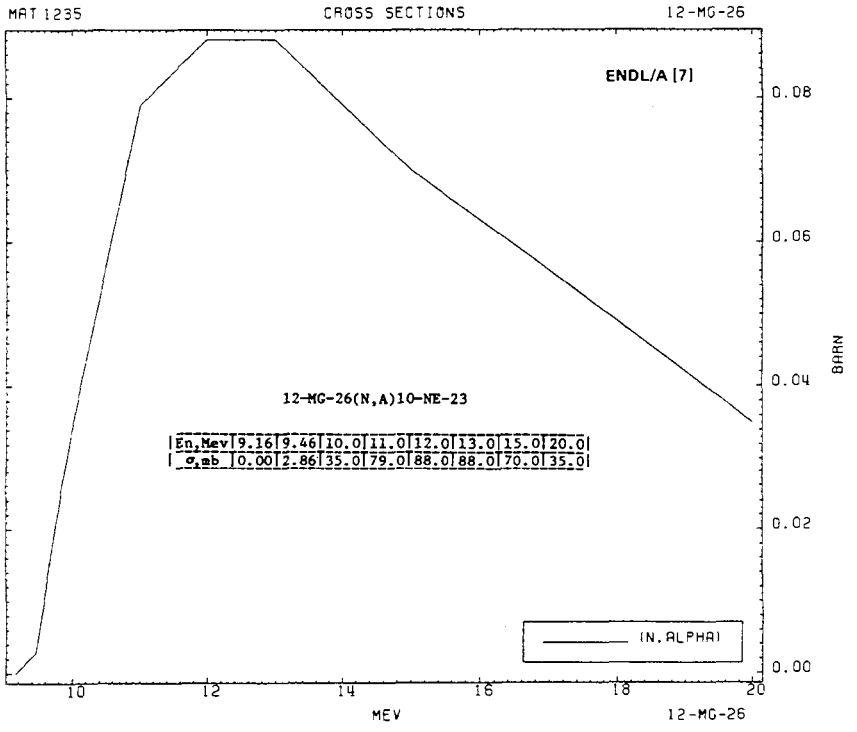
MAT 1235
CROSS SECTIONS
12-MG-26
ENDL/A [7]
12-MG-26(N,A)10-NE-23
En,Mev 9.16 9.46 10.0 11.0 12.0 13.0 15.0 20.0
σ,mb 0.00 2.86 35.0 79.0 88.0 88.0 70.0 35.0
(N,ALPHA)
BARN
MEV
12-MG-26

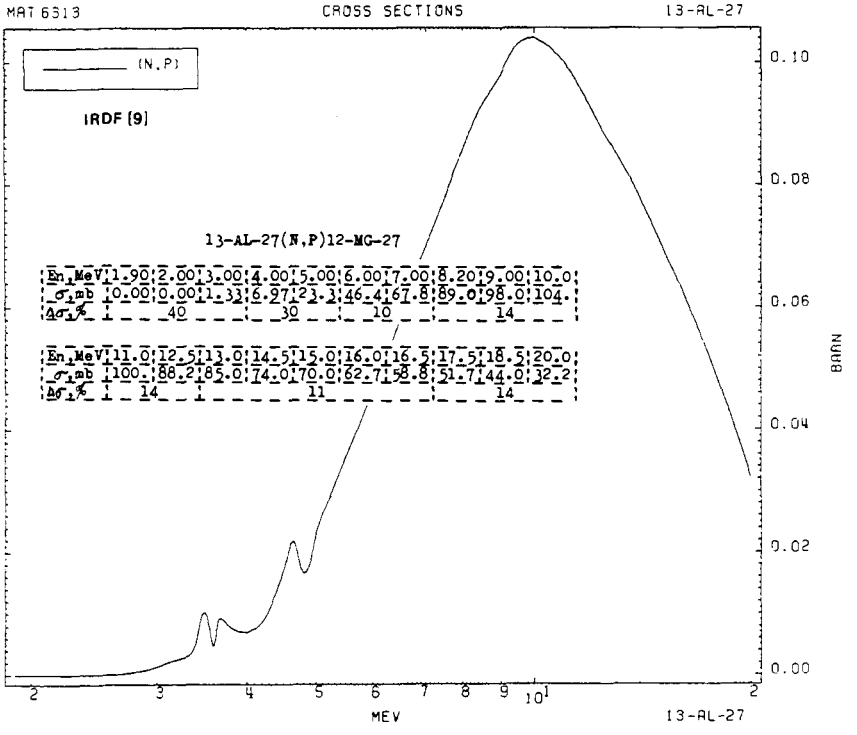
MAT 6313
CROSS SECTIONS
13-AL-27
(N,P)
IRDF [9]
13-AL-27(N,P)12-MG-27
En,MeV 1.90 2.00 3.00 4.00 5.00 6.00 7.00 8.20 9.00 10.0
σ,mb 0.00 0.00 1.31 6.97 23.1 46.4 67.8 89.0 98.0 104.
Δσ/σ % 40 30 10 14
En,MeV 11.0 12.5 13.0 14.5 15.0 16.0 16.5 17.5 18.5 20.0
σ,mb 100. 88.2 85.0 74.0 70.0 62.7 58.8 51.7 44.0 32.2
Δσ/σ % 14 1 11 14
BARN
MEV
13-AL-27

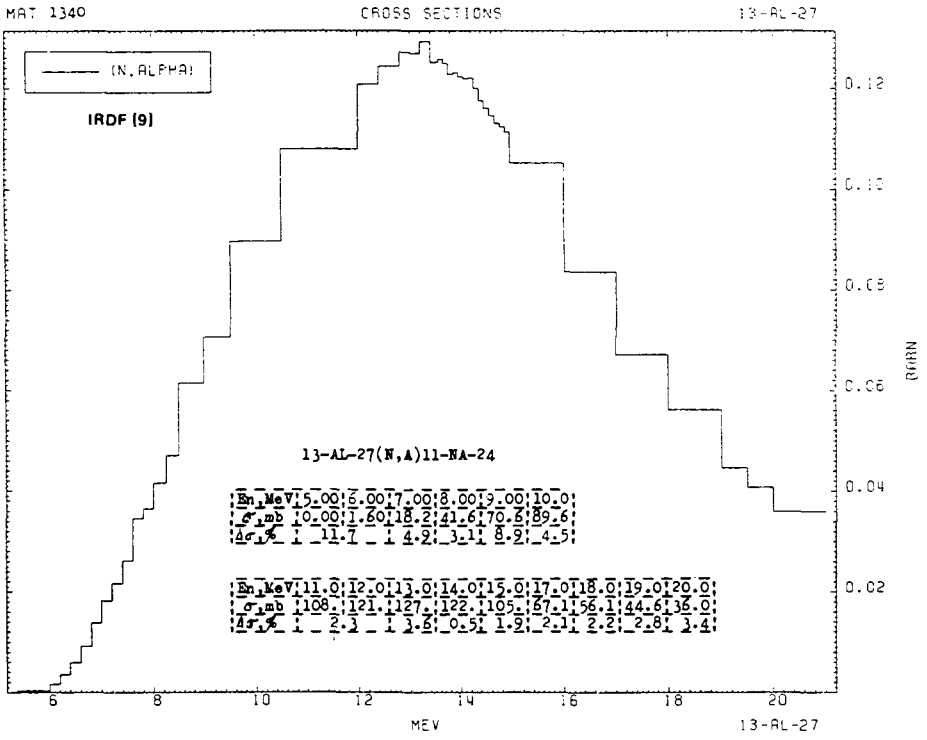
MAT 1340
CROSS SECTIONS
13-AL-27
(N,ALPHA)
IRDF [9]
13-AL-27(N,A)11-NA-24
En,MeV 5.00 6.00 7.00 8.00 9.00 10.0
σ,mb 1.00 1.60 18.2 41.6 70.6 89.6
Δσ,% 1 11. 1 4.2 3.1 8.9 4.5
En,MeV 11.0 12.0 13.0 14.0 15.0 17.0 18.0 19.0 20.0
σ,mb 108. 121. 127. 122. 105. 87.1 56.1 44.6 36.0
Δσ,% 1 2.3 1 3.6 0.5 1.9 2.1 2.2 2.8 3.4
BARN
MEV
13-AL-27

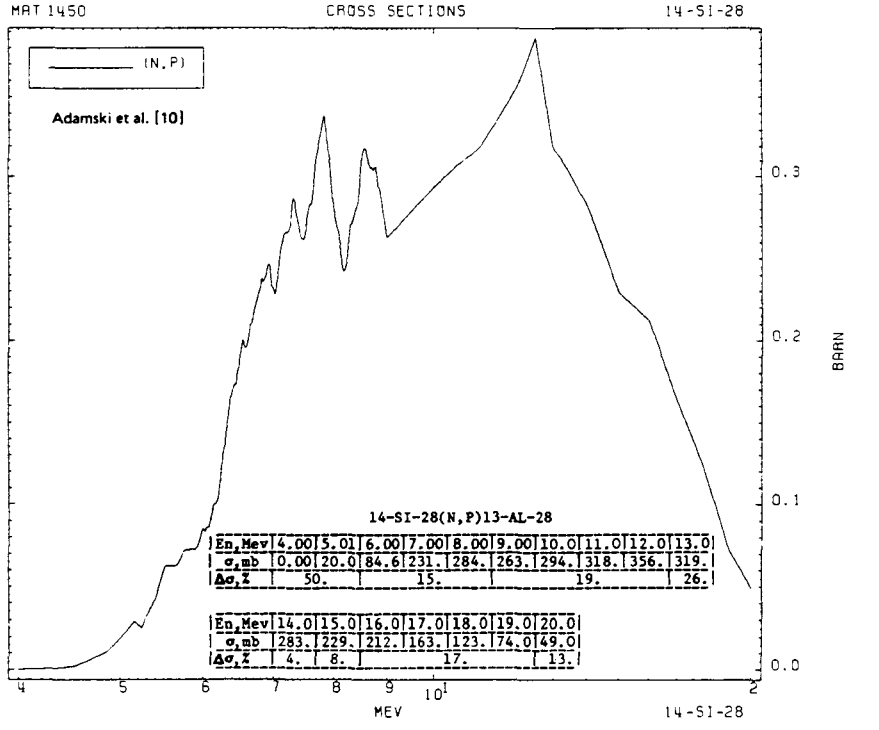
MAT 1450
CROSS SECTIONS
14-SI-28
(N,P)
Adamski et al. [10]
14-SI-28(N,P)13-AL-28
En,Mev 4.00 5.00 6.00 7.00 8.00 9.00 10.0 11.0 12.0 13.0
σ,mb 0.00 20.0 84.6 231. 284. 263. 294. 318. 356. 319.
Δσ,% 50. 15. 19. 26.
En,Mev 14.0 15.0 16.0 17.0 18.0 19.0 20.0
σ,mb 283. 229. 212. 163. 123. 74.0 49.0
Δσ,% 4. 8. 17. 13.
BARN
MEV
14-SI-28

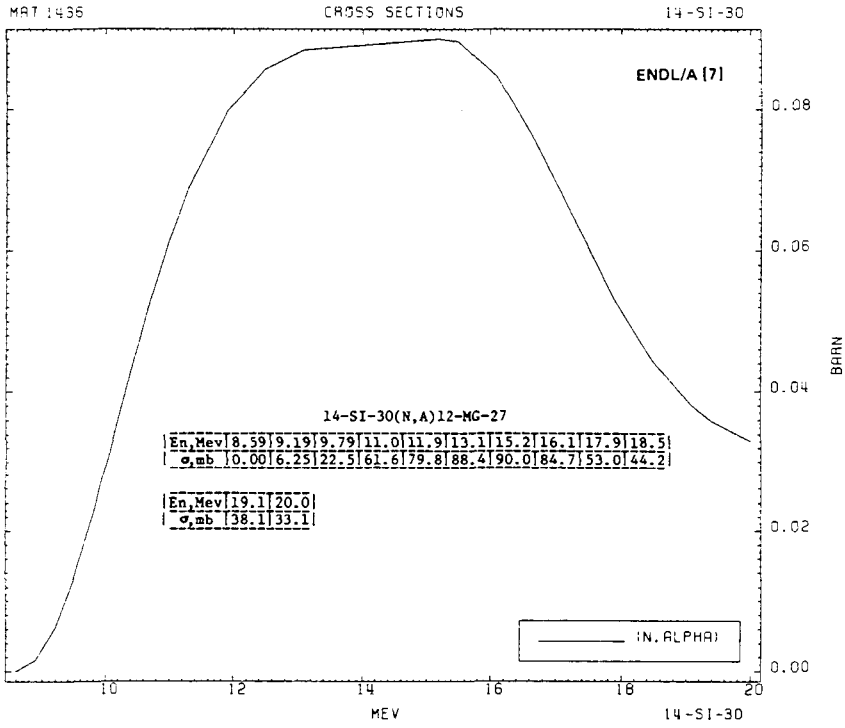
MAT 1436
CROSS SECTIONS
14-SI-30
ENDL/A [7]
0.08
0.06
0.04
0.02
0.00
BARN
14-SI-30(N,A)12-MG-27
En,Mev 8.59 9.19 9.79 11.0 11.9 13.1 15.2 16.1 17.9 18.5
σ,mb 10.00 6.25 22.5 61.6 79.8 88.4 90.0 84.7 53.0 44.2
En,Mev 19.1 20.0
σ,mb 38.1 33.1
(N,ALPHA)
10
12
14
16
18
20
MEV
14-SI-30

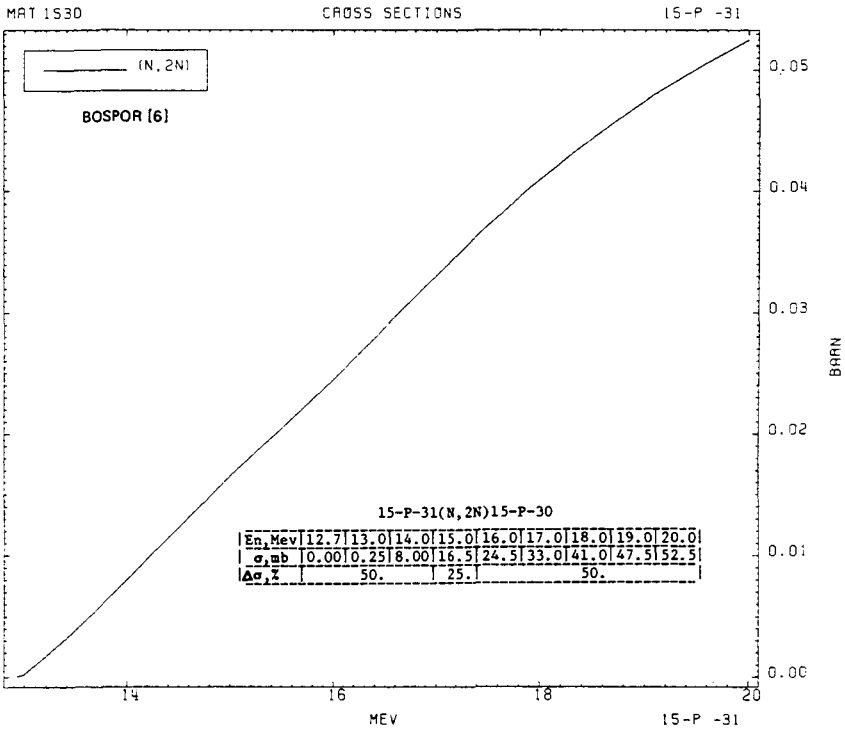
MAT 1530
CROSS SECTIONS
15-P -31
(N,2N)
BOSPOR [6]
0.05
0.04
0.03
0.02
0.01
0.00
BARN
15-P-31(N,2N)15-P-30
En,Mev 12.7 13.0 14.0 15.0 16.0 17.0 18.0 19.0 20.0
σ,mb 0.00 0.25 8.00 16.5 24.5 33.0 41.0 47.5 52.5
Δσ,% 50. 25. 50.
14
16
18
20
MEV
15-P -31

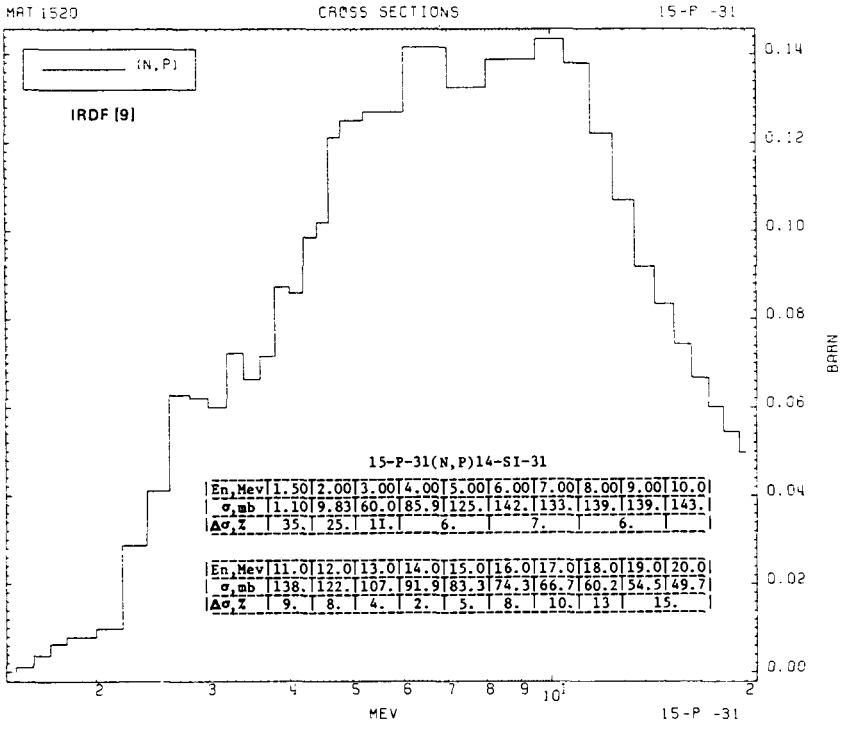
MAT 1520
CROSS SECTIONS
15-P -31
(N,P)
IRDF [9]
15-P-31(N,P)14-SI-31
En,Mev | 1.50 | 2.00 | 3.00 | 4.00 | 5.00 | 6.00 | 7.00 | 8.00 | 9.00 | 10.0
σ,mb | 1.10 | 9.83 | 60.0 | 85.9 | 125. | 142. | 133. | 139. | 139. | 143.
Δσ,% | 35. | 25. | 11. | 6. | 7. | 6.
En,Mev | 11.0 | 12.0 | 13.0 | 14.0 | 15.0 | 16.0 | 17.0 | 18.0 | 19.0 | 20.0
σ,mb | 138. | 122. | 107. | 91.9 | 83.3 | 74.3 | 66.7 | 60.2 | 54.5 | 49.7
Δσ,% | 9. | 8. | 4. | 2. | 5. | 8. | 10. | 13. | 15.
0.14
0.12
0.10
0.08
0.06
0.04
0.02
0.00
BARN
2
3
4
5
6
7
8
9
10
2
MEV
15-P -31

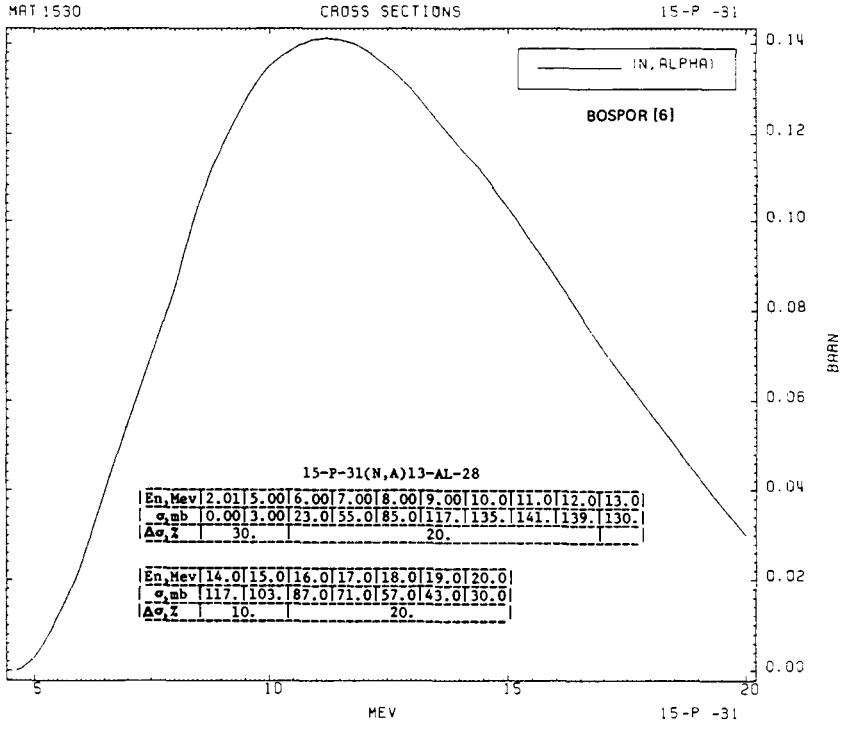
MAT 1530
CROSS SECTIONS
15-P -31
(N,ALPHA)
BOSPOR [6]
15-P-31(N,A)13-AL-28
En,Mev | 2.01 | 5.00 | 6.00 | 7.00 | 8.00 | 9.00 | 10.0 | 11.0 | 12.0 | 13.0
σ,mb | 0.00 | 3.00 | 23.0 | 55.0 | 85.0 | 117. | 135. | 141. | 139. | 130.
Δσ,% | 30. | 20.
En,Mev | 14.0 | 15.0 | 16.0 | 17.0 | 18.0 | 19.0 | 20.0
σ,mb | 117. | 103. | 87.0 | 71.0 | 57.0 | 43.0 | 30.0
Δσ,% | 10. | 20.
0.14
0.12
0.10
0.08
0.06
0.04
0.02
0.00
BARN
5
10
15
20
MEV
15-P -31

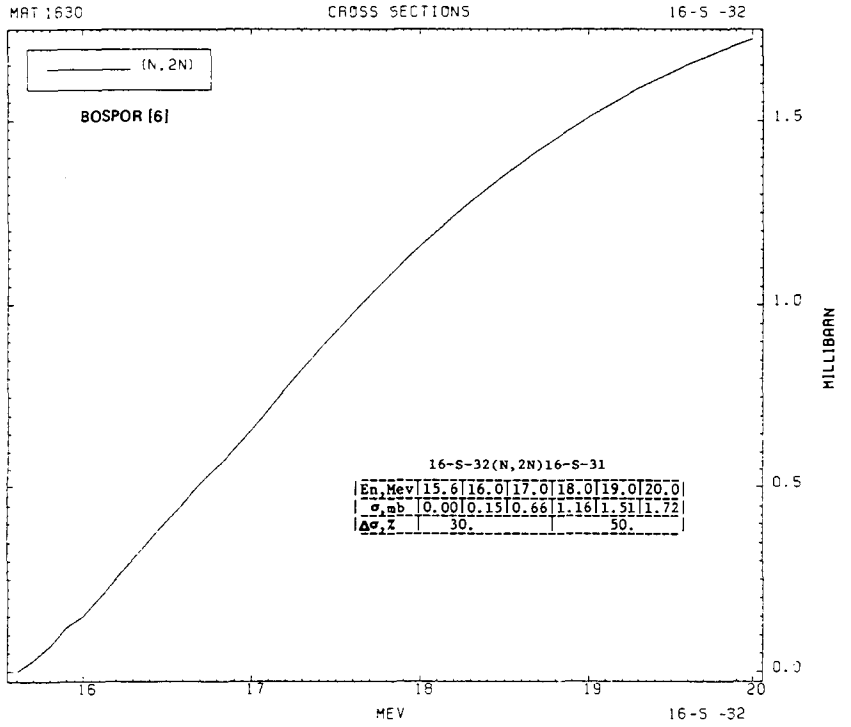
MAT 1630
CROSS SECTIONS
16-S -32
(N,2N)
BOSPOR [6]
16-S-32(N,2N)16-S-31
En,Mev | 15.6 | 16.0 | 17.0 | 18.0 | 19.0 | 20.0
σ,mb | 0.00 | 0.15 | 0.66 | 1.16 | 1.51 | 1.72
Δσ,% | 30. | 50.
MILLIBARN
MEV
16-S -32

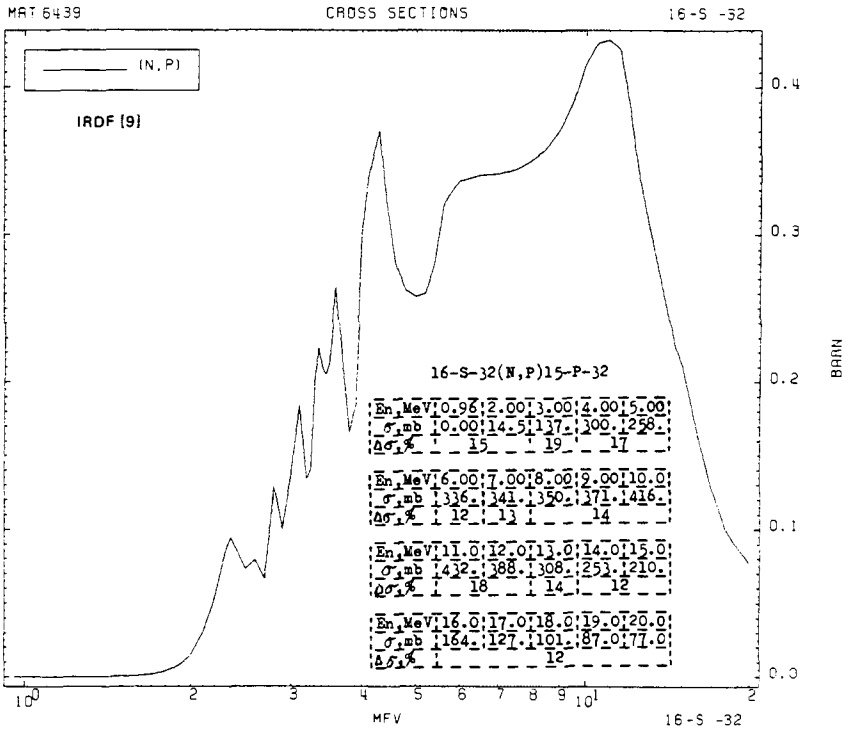
MAT 6439
CROSS SECTIONS
16-S -32
(N,P)
IRDF [9]
16-S-32(N,P)15-P-32
En,MeV | 0.96 | 2.00 | 3.00 | 4.00 | 5.00
σ,mb | 0.00 | 14.5 | 137. | 300. | 258.
Δσ,% | 15 | 19 | 17
En,MeV | 6.00 | 7.00 | 8.00 | 9.00 | 10.0
σ,mb | 336. | 341. | 350. | 371. | 416.
Δσ,% | 12 | 13 | 14
En,MeV | 11.0 | 12.0 | 13.0 | 14.0 | 15.0
σ,mb | 432. | 388. | 308. | 251. | 210.
Δσ,% | 18 | 14 | 12
En,MeV | 16.0 | 17.0 | 18.0 | 19.0 | 20.0
σ,mb | 164. | 127. | 101. | 87.0 | 77.0
Δσ,% | 12
BARN
MEV
16-S -32

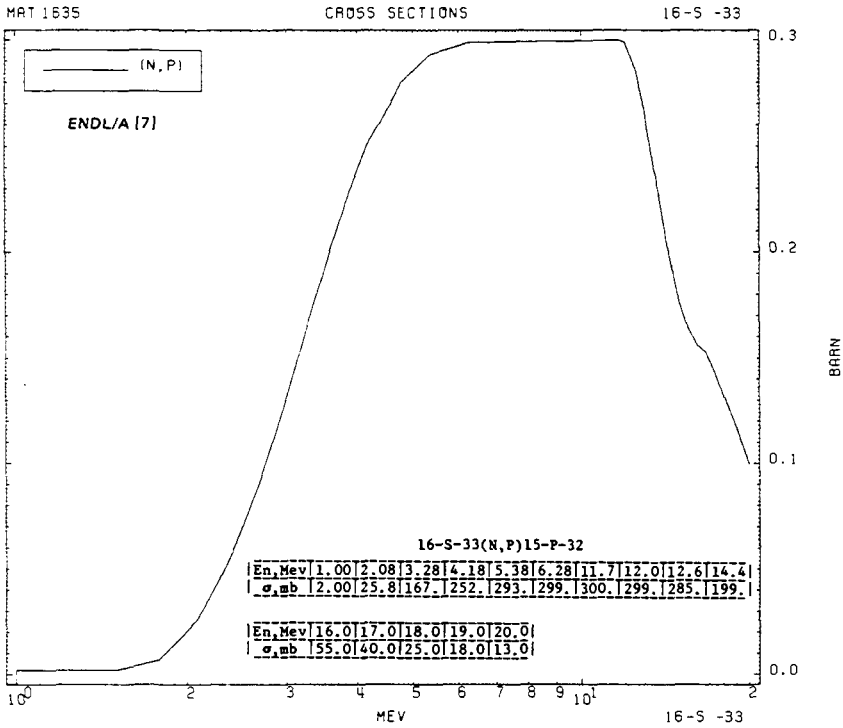
MAT 1635
CROSS SECTIONS
16-S -33
(N,P)
ENDL/A [7]
16-S-33(N,P)15-P-32
En,Mev 1.00 2.08 3.28 4.18 5.38 6.28 11.7 12.0 12.6 14.4
σ,mb 2.00 25.8 167. 252. 293. 299. 300. 299. 285. 199.
En,Mev 16.0 17.0 18.0 19.0 20.0
σ,mb 55.0 40.0 25.0 18.0 13.0
0.3
0.2
0.1
0.0
BARN
MEV
16-S -33

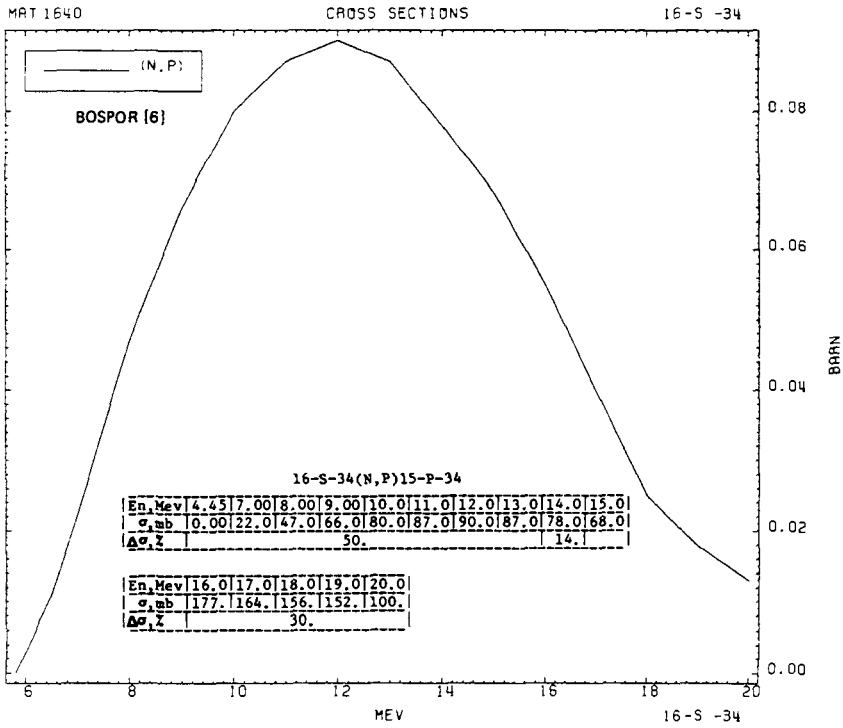
MAT 1640
CROSS SECTIONS
16-S -34
(N,P)
BOSPOR [6]
16-S-34(N,P)15-P-34
En,Mev 4.45 7.00 8.00 9.00 10.0 11.0 12.0 13.0 14.0 15.0
σ,mb 0.00 22.0 47.0 66.0 80.0 87.0 90.0 87.0 78.0 68.0
Δσ,% 50. 14.
En,Mev 16.0 17.0 18.0 19.0 20.0
σ,mb 177. 164. 156. 152. 100.
Δσ,% 30.
0.08
0.06
0.04
0.02
0.00
BARN
MEV
16-S -34

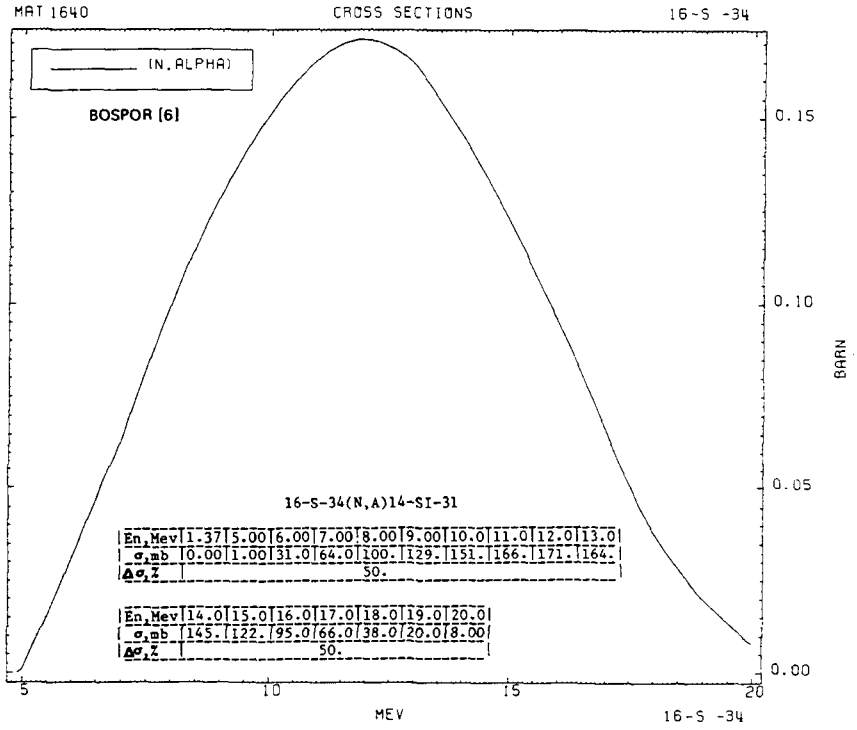
MAT 1640
CROSS SECTIONS
16-S -34
(N,ALPHA)
BOSPOR [6]
16-S-34(N,A)14-SI-31
En,Mev | 1.37 | 5.00 | 6.00 | 7.00 | 8.00 | 9.00 | 10.0 | 11.0 | 12.0 | 13.0
σ,mb | 0.00 | 1.00 | 31.0 | 64.0 | 100. | 129. | 151. | 166. | 171. | 164.
Δσ,% | 50.
En,Mev | 14.0 | 15.0 | 16.0 | 17.0 | 18.0 | 19.0 | 20.0
σ,mb | 145. | 122. | 95.0 | 66.0 | 38.0 | 20.0 | 8.00
Δσ,% | 50.
0.15
0.10
0.05
0.00
BARN
5
10
15
20
MEV
16-S -34

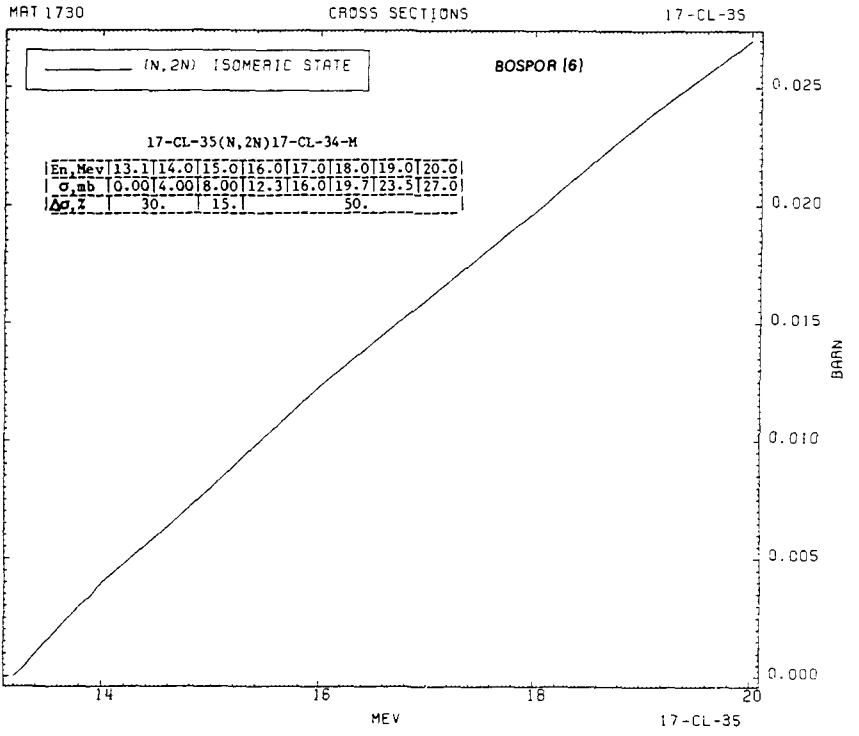
MAT 1730
CROSS SECTIONS
17-CL-35
(N,2N) ISOMERIC STATE
BOSPOR [6]
17-CL-35(N,2N)17-CL-34-M
En,Mev | 13.1 | 14.0 | 15.0 | 16.0 | 17.0 | 18.0 | 19.0 | 20.0
σ,mb | 0.00 | 4.00 | 8.00 | 12.3 | 16.0 | 19.7 | 23.5 | 27.0
Δσ,% | 30. | 15. | 50.
0.025
0.020
0.015
0.010
0.005
0.000
BARN
14
16
18
20
MEV
17-CL-35

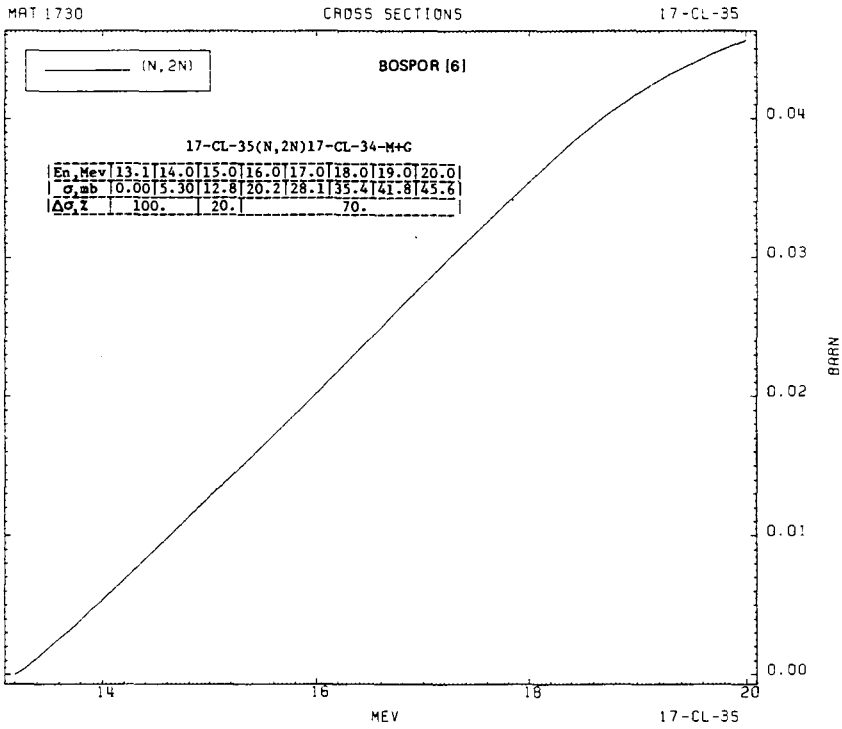
MAT 1730
CROSS SECTIONS
17-CL-35
(N,2N)
BOSPOR [6]
17-CL-35(N,2N)17-CL-34-M+G
En,Mev | 13.1 | 14.0 | 15.0 | 16.0 | 17.0 | 18.0 | 19.0 | 20.0
σ,mb | 0.00 | 5.30 | 12.8 | 20.2 | 28.1 | 35.4 | 41.8 | 45.6
Δσ,% | 100. | 20. | 70.
0.04
0.03
0.02
0.01
0.00
BARN
14
16
18
20
MEV
17-CL-35

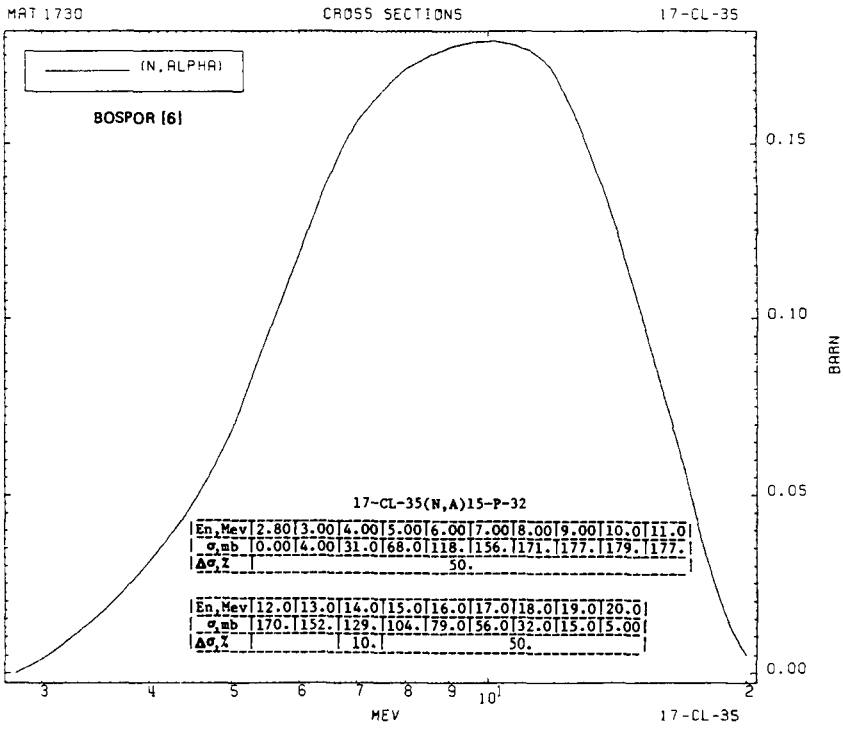
MAT 1730
CROSS SECTIONS
17-CL-35
(N,ALPHA)
BOSPOR [6]
17-CL-35(N,A)15-P-32
En,Mev | 2.80 | 3.00 | 4.00 | 5.00 | 6.00 | 7.00 | 8.00 | 9.00 | 10.0 | 11.0
σ,mb | 0.00 | 4.00 | 31.0 | 68.0 | 118. | 156. | 171. | 177. | 179. | 177.
Δσ,% | 50.
En,Mev | 12.0 | 13.0 | 14.0 | 15.0 | 16.0 | 17.0 | 18.0 | 19.0 | 20.0
σ,mb | 170. | 152. | 129. | 104. | 79.0 | 56.0 | 32.0 | 15.0 | 5.00
Δσ,% | 10. | 50.
0.15
0.10
0.05
0.00
BARN
3
4
5
6
7
8
9
10
2
MEV
17-CL-35

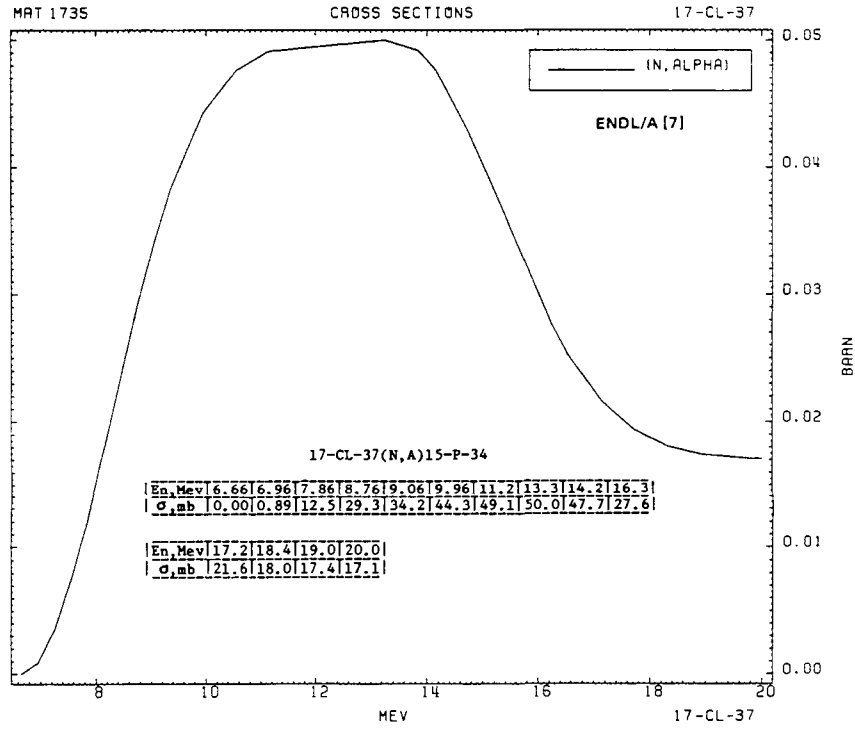
MAT 1735
CROSS SECTIONS
17-CL-37
(N,ALPHA)
ENDL/A [7]
17-CL-37(N,A)15-P-34
En,Mev | 6.66 | 6.96 | 7.86 | 8.76 | 9.06 | 9.96 | 11.2 | 13.3 | 14.2 | 16.3
σ,mb | 0.00 | 0.89 | 12.5 | 29.3 | 34.2 | 44.3 | 49.1 | 50.0 | 47.7 | 27.6
En,Mev | 17.2 | 18.4 | 19.0 | 20.0
σ,mb | 21.6 | 18.0 | 17.4 | 17.1
0.05
0.04
0.03
0.02
0.01
0.00
BARN
8
10
12
14
16
18
20
MEV
17-CL-37

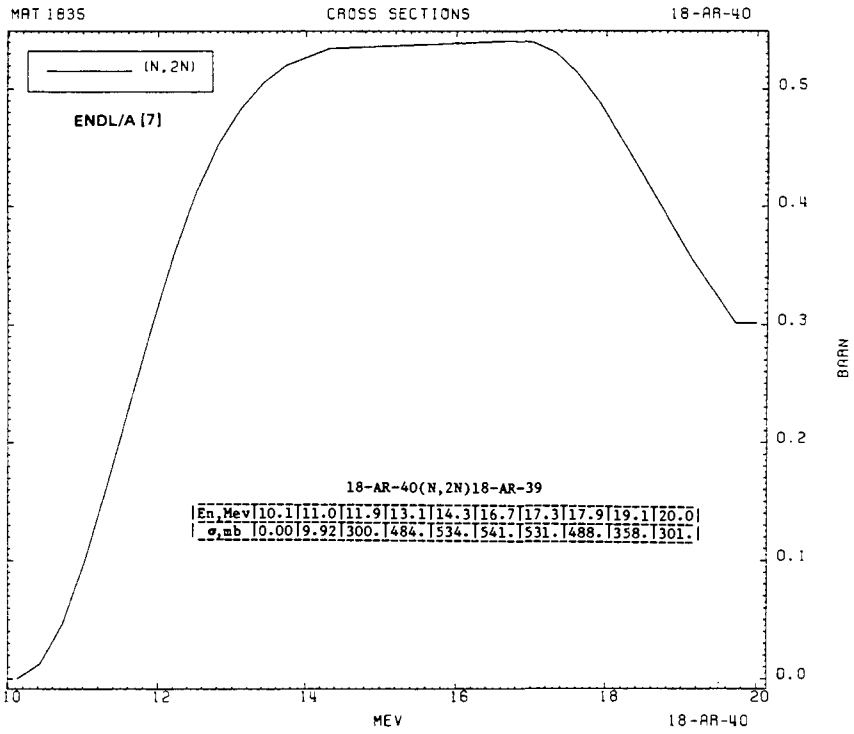
MAT 1835
CROSS SECTIONS
18-AR-40
(N,2N)
ENDL/A [7]
18-AR-40(N,2N)18-AR-39
En,Mev | 10.1 | 11.0 | 11.9 | 13.1 | 14.3 | 16.7 | 17.3 | 17.9 | 19.1 | 20.0
σ,mb | 0.00 | 9.92 | 300. | 484. | 534. | 541. | 531. | 488. | 358. | 301.
0.5
0.4
0.3
0.2
0.1
0.0
BARN
10
12
14
16
18
20
MEV
18-AR-40

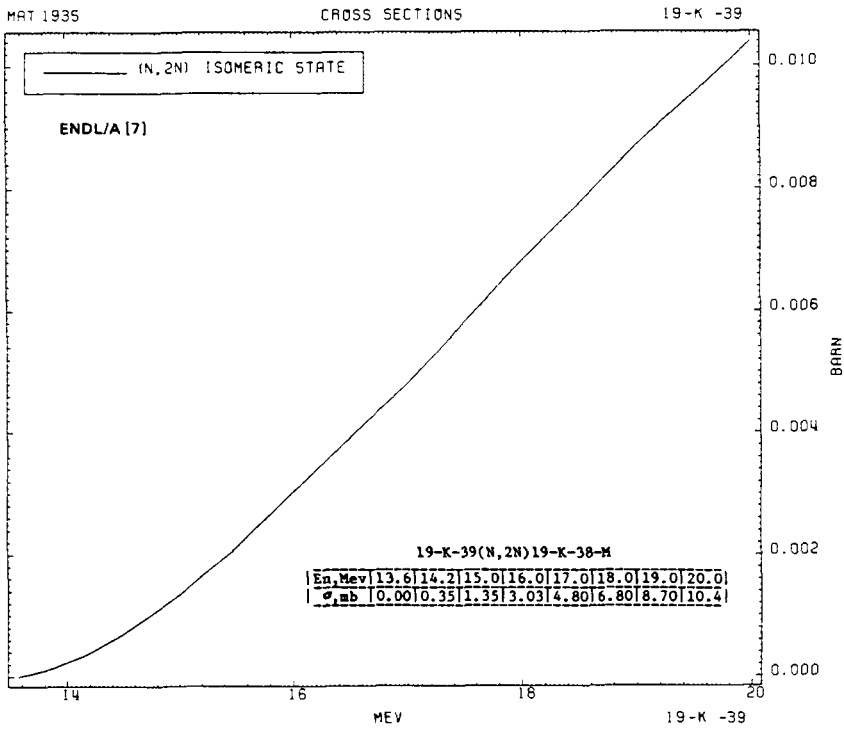
MAT 1935
CROSS SECTIONS
19-K -39
(N,2N) ISOMERIC STATE
ENDL/A [7]
19-K-39(N,2N)19-K-38-M
En,Mev | 13.6 | 14.2 | 15.0 | 16.0 | 17.0 | 18.0 | 19.0 | 20.0
σ,mb | 0.00 | 0.35 | 1.35 | 3.03 | 4.80 | 6.80 | 8.70 | 10.4
0.010
0.008
0.006
0.004
0.002
0.000
BARN
14
16
18
20
MEV
19-K -39

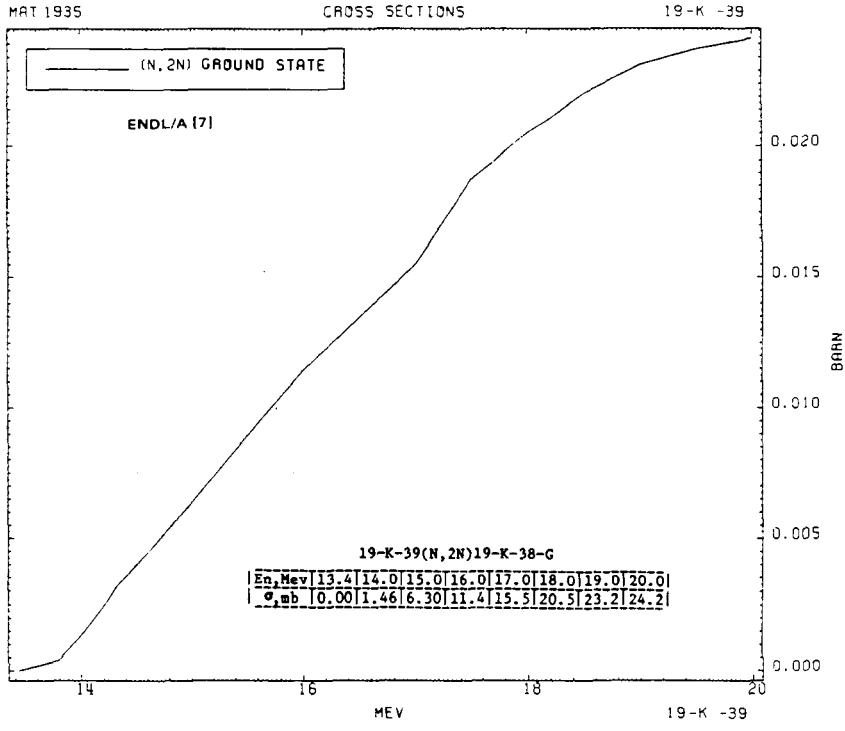
MAT 1935
CROSS SECTIONS
19-K -39
(N,2N) GROUND STATE
ENDL/A [7]
19-K-39(N,2N)19-K-38-G
En,Mev | 13.4 | 14.0 | 15.0 | 16.0 | 17.0 | 18.0 | 19.0 | 20.0
σ,mb | 0.00 | 1.46 | 6.30 | 11.4 | 15.5 | 20.5 | 23.2 | 24.2
0.020
0.015
0.010
0.005
0.000
BARN
14
16
18
20
MEV
19-K -39

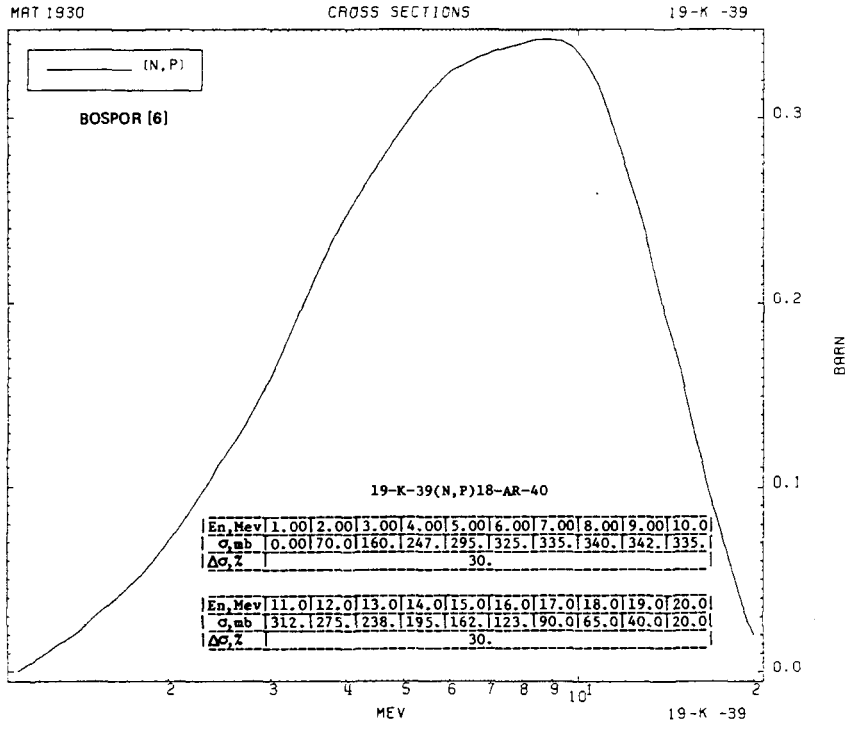
MAT 1930
CROSS SECTIONS
19-K -39
(N,P)
BOSPOR [6]
19-K-39(N,P)18-AR-40
En,Mev | 1.00 | 2.00 | 3.00 | 4.00 | 5.00 | 6.00 | 7.00 | 8.00 | 9.00 | 10.0
σ,mb | 0.00 | 70.0 | 160. | 247. | 295. | 325. | 335. | 340. | 342. | 335.
Δσ,% | 30.
En,Mev | 11.0 | 12.0 | 13.0 | 14.0 | 15.0 | 16.0 | 17.0 | 18.0 | 19.0 | 20.0
σ,mb | 312. | 275. | 238. | 195. | 162. | 123. | 90.0 | 65.0 | 40.0 | 20.0
Δσ,% | 30.
0.3
0.2
0.1
0.0
BARN
2 3 4 5 6 7 8 9 10^1 2
MEV
19-K -39

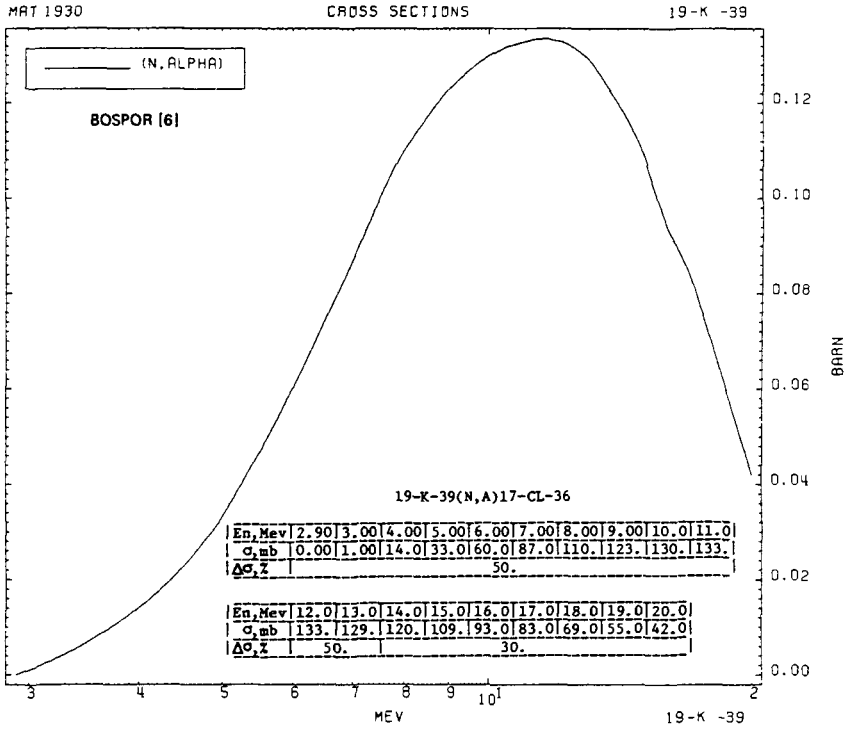
MAT 1930
CROSS SECTIONS
19-K -39
(N,ALPHA)
BOSPOR [6]
19-K-39(N,A)17-CL-36
En,Mev | 2.90 | 3.00 | 4.00 | 5.00 | 6.00 | 7.00 | 8.00 | 9.00 | 10.0 | 11.0
σ,mb | 0.00 | 1.00 | 14.0 | 33.0 | 60.0 | 87.0 | 110. | 123. | 130. | 133.
Δσ,% | 50.
En,Mev | 12.0 | 13.0 | 14.0 | 15.0 | 16.0 | 17.0 | 18.0 | 19.0 | 20.0
σ,mb | 133. | 129. | 120. | 109. | 93.0 | 83.0 | 69.0 | 55.0 | 42.0
Δσ,% | 50. | 30.
0.12
0.10
0.08
0.06
0.04
0.02
0.00
BARN
3 4 5 6 7 8 9 10^1 2
MEV
19-K -39

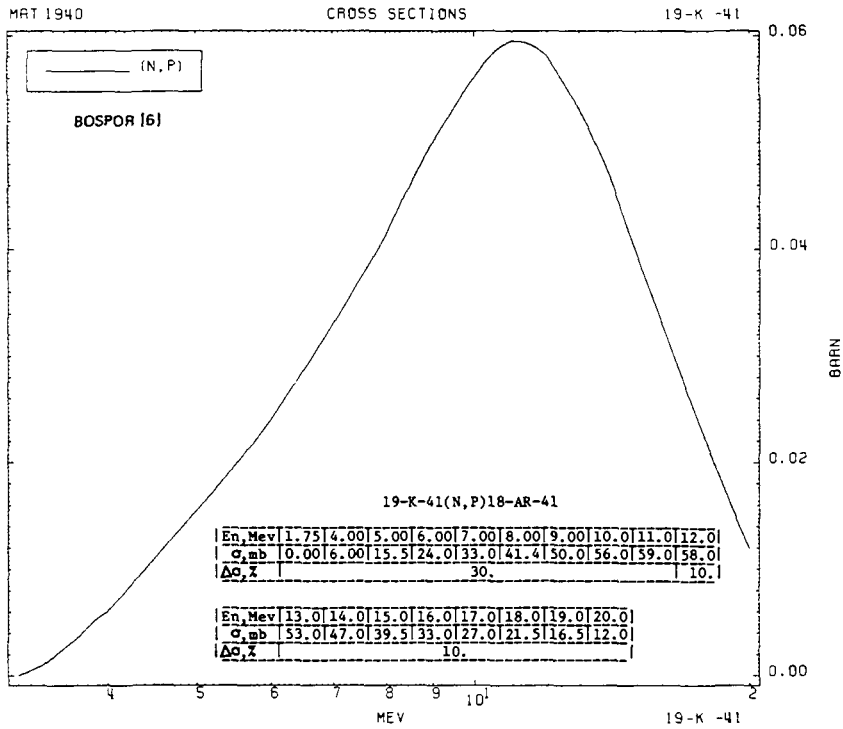
MAT 1940
CROSS SECTIONS
19-K -41
(N,P)
BOSPOR [6]
0.06
0.04
0.02
0.00
BARN
19-K-41(N,P)18-AR-41
En,Mev | 1.75 | 4.00 | 5.00 | 6.00 | 7.00 | 8.00 | 9.00 | 10.0 | 11.0 | 12.0
σ,mb | 0.00 | 6.00 | 15.5 | 24.0 | 33.0 | 41.4 | 50.0 | 56.0 | 59.0 | 58.0
Δσ,% | 30. | 10.
En,Mev | 13.0 | 14.0 | 15.0 | 16.0 | 17.0 | 18.0 | 19.0 | 20.0
σ,mb | 53.0 | 47.0 | 39.5 | 33.0 | 27.0 | 21.5 | 16.5 | 12.0
Δσ,% | 10.
4 5 6 7 8 9 10 2
MEV
19-K -41

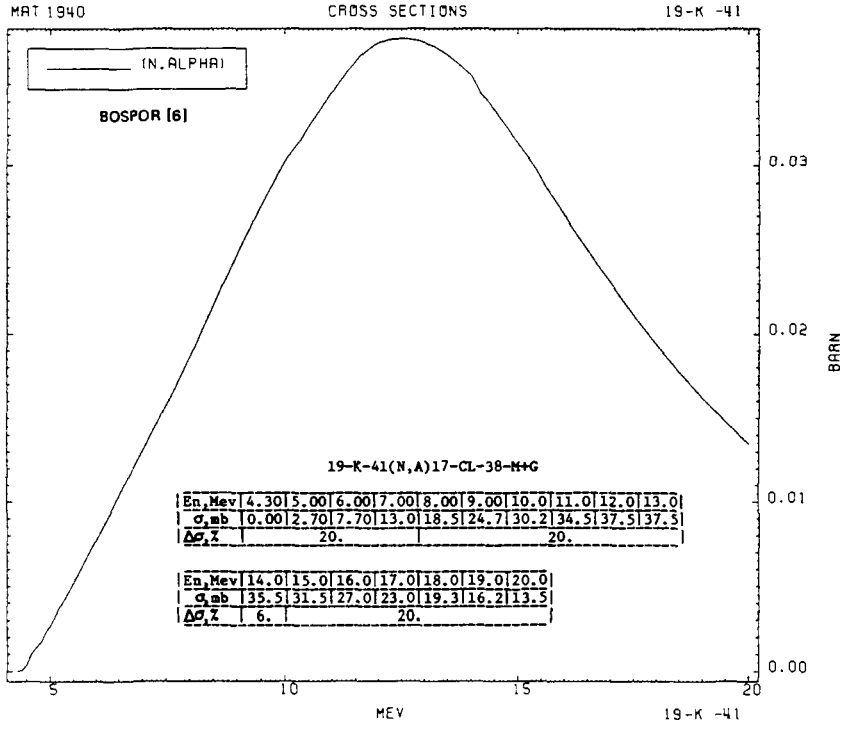
MAT 1940
CROSS SECTIONS
19-K -41
(N,ALPHA)
BOSPOR [6]
0.03
0.02
0.01
0.00
BARN
19-K-41(N,A)17-CL-38-M+G
En,Mev | 4.30 | 5.00 | 6.00 | 7.00 | 8.00 | 9.00 | 10.0 | 11.0 | 12.0 | 13.0
σ,mb | 0.00 | 2.70 | 7.70 | 13.0 | 18.5 | 24.7 | 30.2 | 34.5 | 37.5 | 37.5
Δσ,% | 20. | 20.
En,Mev | 14.0 | 15.0 | 16.0 | 17.0 | 18.0 | 19.0 | 20.0
σ,mb | 35.5 | 31.5 | 27.0 | 23.0 | 19.3 | 16.2 | 13.5
Δσ,% | 6. | 20.
5 10 15 20
MEV
19-K -41

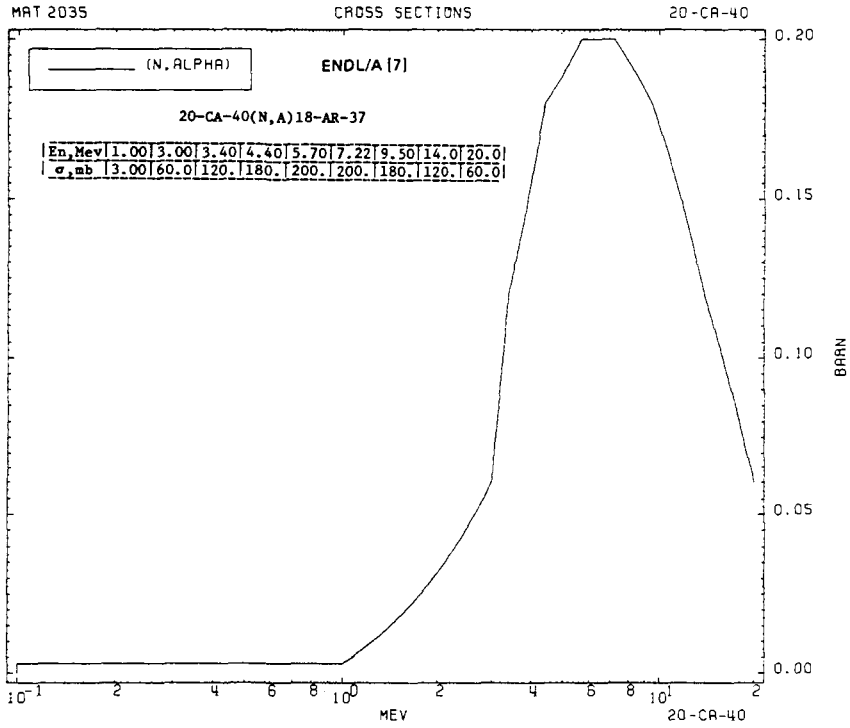
MAT 2035
CROSS SECTIONS
20-CA-40
(N,ALPHA)
ENDL/A [7]
20-CA-40(N,A)18-AR-37
En,Mev 1.00 3.00 3.40 4.40 5.70 7.22 9.50 14.0 20.0
σ,mb 3.00 60.0 120. 180. 200. 200. 180. 120. 60.0
0.20
0.15
0.10
0.05
0.00
BARN
MEV
20-CA-40

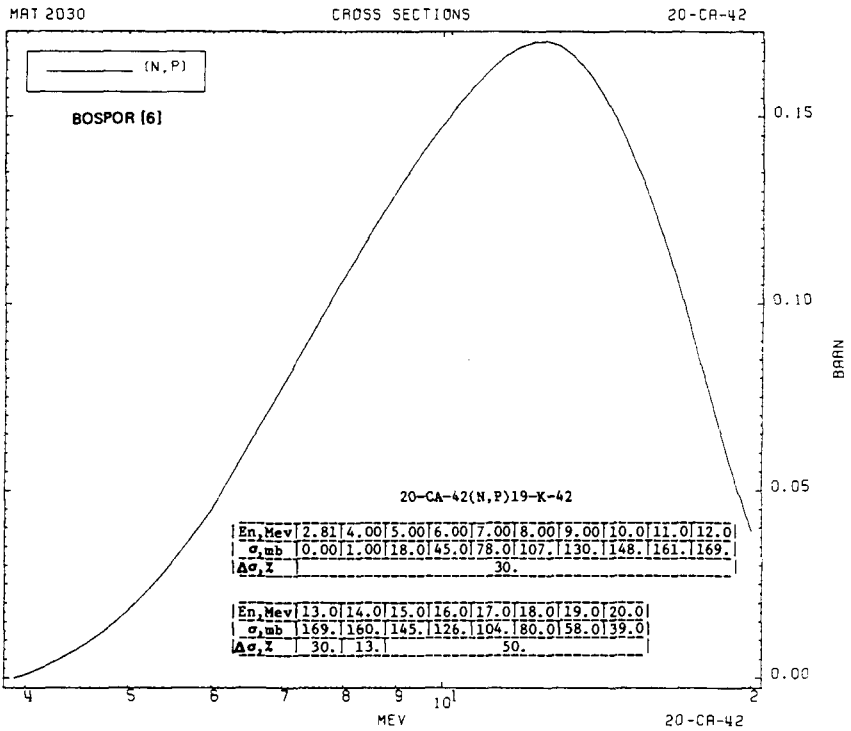
MAT 2030
CROSS SECTIONS
20-CA-42
(N,P)
BOSPOR [6]
20-CA-42(N,P)19-K-42
En,Mev 2.81 4.00 5.00 6.00 7.00 8.00 9.00 10.0 11.0 12.0
σ,mb 0.00 1.00 18.0 45.0 78.0 107. 130. 148. 161. 169.
Δσ,% 30.
En,Mev 13.0 14.0 15.0 16.0 17.0 18.0 19.0 20.0
σ,mb 169. 160. 145. 126. 104. 80.0 58.0 39.0
Δσ,% 30. 13. 50.
0.15
0.10
0.05
0.00
BARN
MEV
20-CA-42

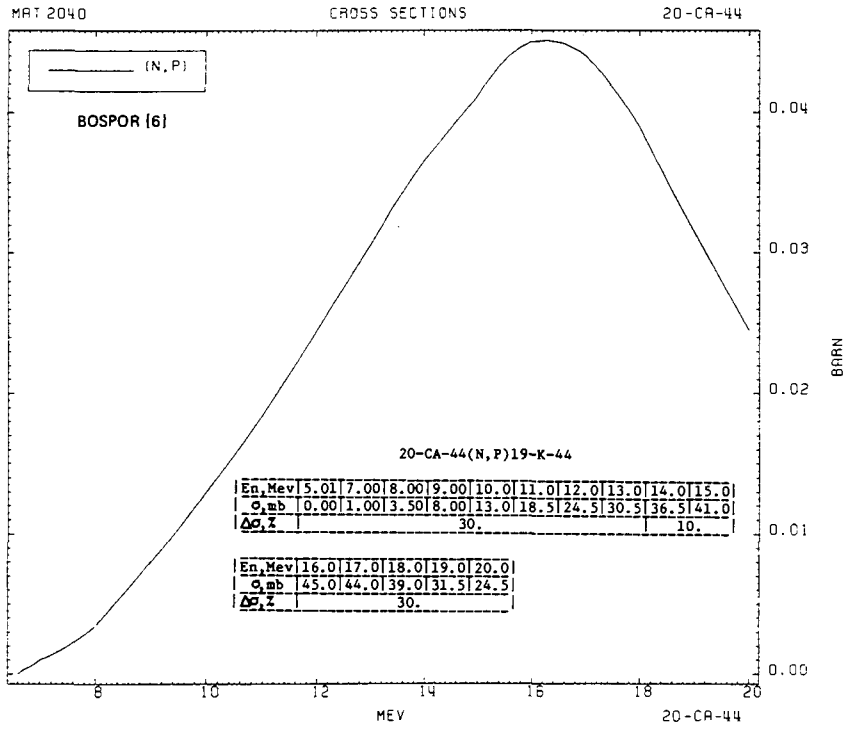

20-CA-44(N,P)19-K-44

En,Mev	5.01	7.00	8.00	9.00	10.0	11.0	12.0	13.0	14.0	15.0
σ,mb	0.00	1.00	3.50	8.00	13.0	18.5	24.5	30.5	36.5	41.0
Δσ,%	30.								10.	

En,Mev	16.0	17.0	18.0	19.0	20.0
σ,mb	45.0	44.0	39.0	31.5	24.5
Δσ,%	30.				

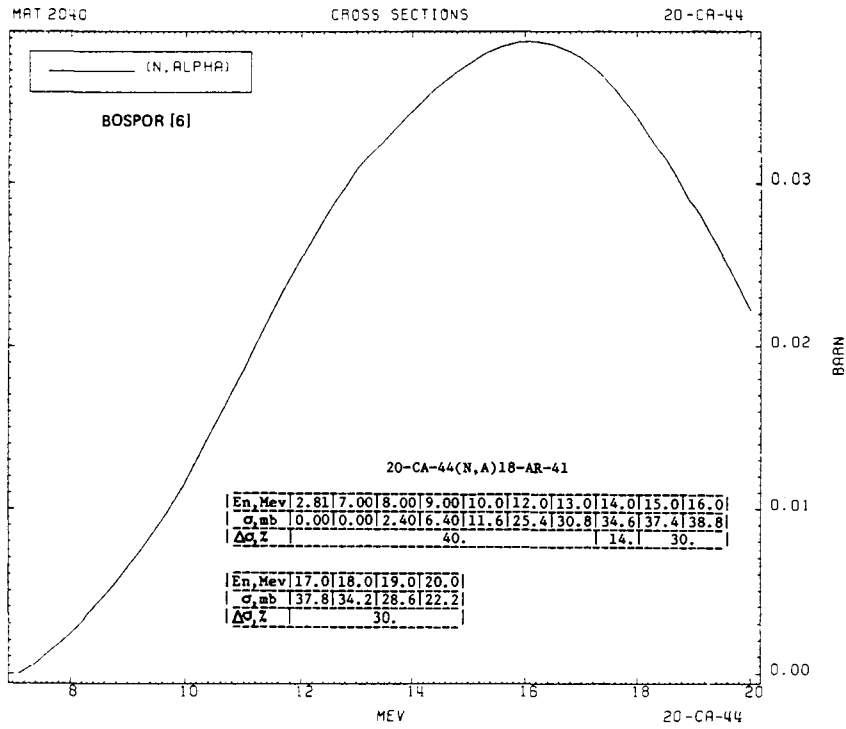

20-CA-44(N,A)18-AR-41

En,Mev	2.81	7.00	8.00	9.00	10.0	12.0	13.0	14.0	15.0	16.0
σ,mb	0.00	0.00	2.40	6.40	11.6	25.4	30.8	34.6	37.4	38.8
Δσ,%	40.							14.	30.	

En,Mev	17.0	18.0	19.0	20.0
σ,mb	37.8	34.2	28.6	22.2
Δσ,%	30.			

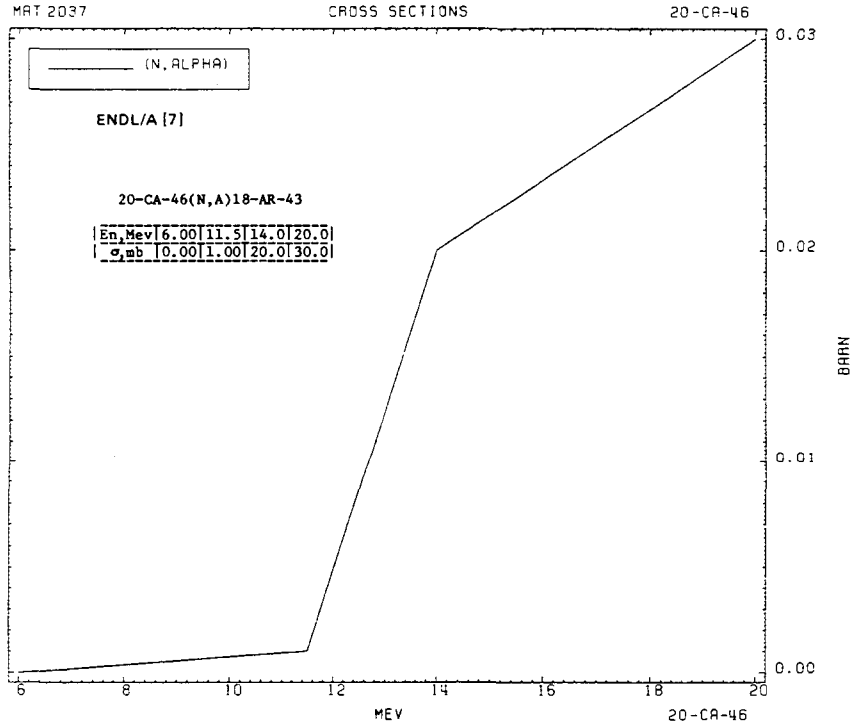
MAT 2037
CROSS SECTIONS
20-CA-46
(N, ALPHA)
ENDL/A [7]
20-CA-46(N,A)18-AR-43
En,Mev 6.00 11.5 14.0 20.0
σ,mb 0.00 1.00 20.0 30.0
0.03
0.02
0.01
0.00
BARN
6
8
10
12
14
16
18
20
MEV
20-CA-46

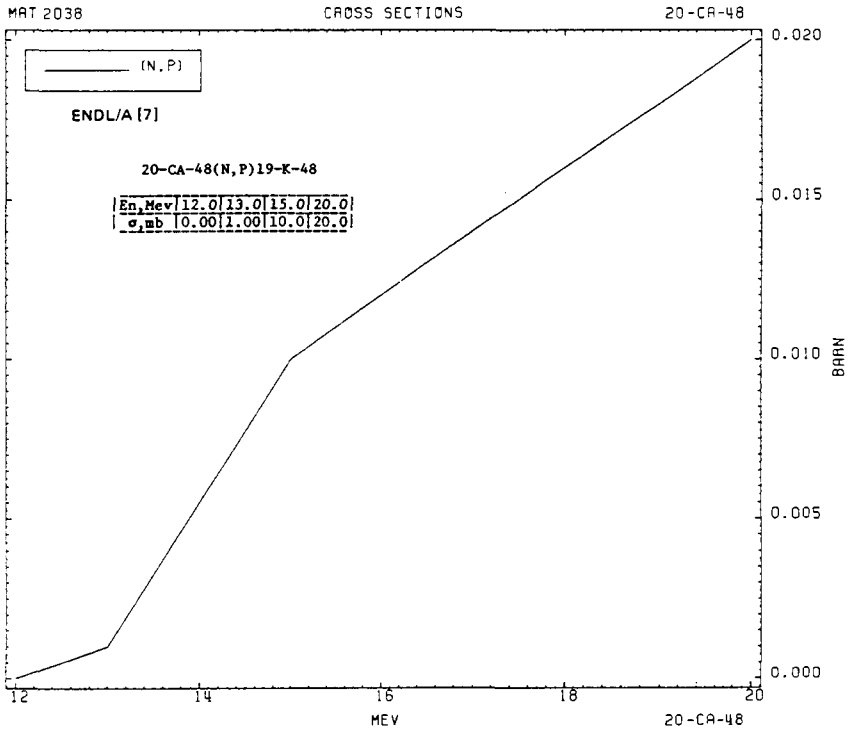
MAT 2038
CROSS SECTIONS
20-CA-48
(N, P)
ENDL/A [7]
20-CA-48(N,P)19-K-48
En,Mev 12.0 13.0 15.0 20.0
σ,mb 0.00 1.00 10.0 20.0
0.020
0.015
0.010
0.005
0.000
BARN
12
14
16
18
20
MEV
20-CA-48

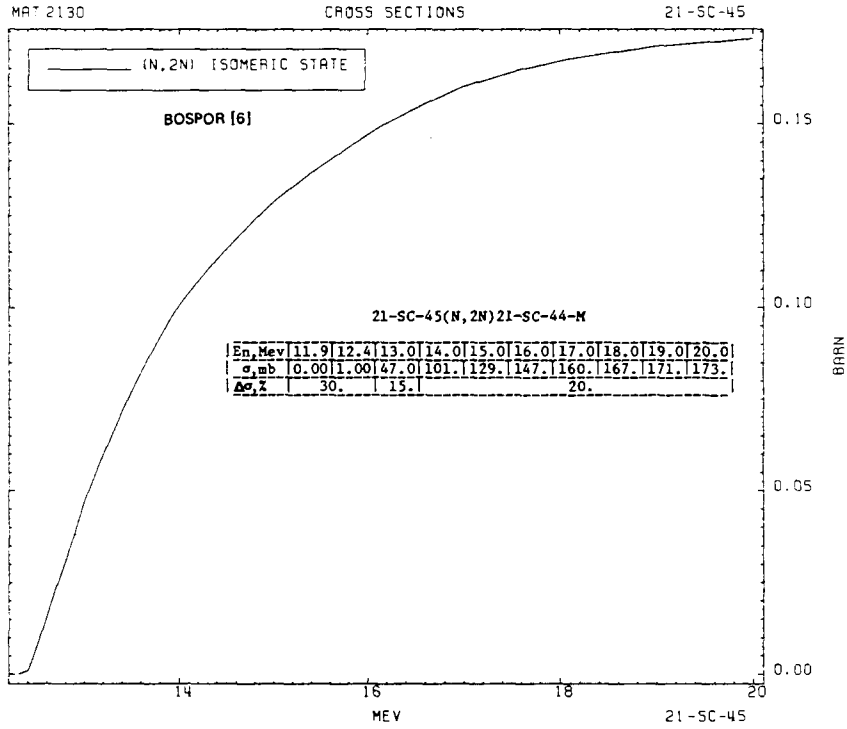
MAT 2130
CROSS SECTIONS
21-SC-45
(N,2N) ISOMERIC STATE
BOSPOR [6]
21-SC-45(N,2N)21-SC-44-M
En,Mev | 11.9 | 12.4 | 13.0 | 14.0 | 15.0 | 16.0 | 17.0 | 18.0 | 19.0 | 20.0
σ,mb | 0.00 | 1.00 | 47.0 | 101. | 129. | 147. | 160. | 167. | 171. | 173.
Δσ,% | 30. | 15. | 20.
0.15
0.10
0.05
0.00
BARN
14
16
18
20
MEV
21-SC-45

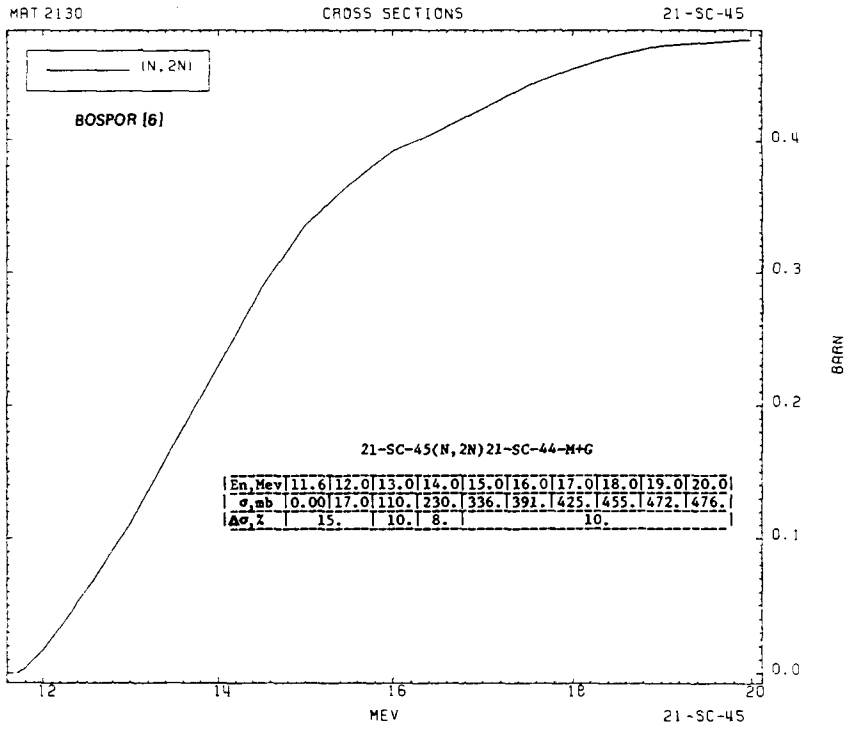
MAT 2130
CROSS SECTIONS
21-SC-45
(N,2N)
BOSPOR [6]
21-SC-45(N,2N)21-SC-44-M+G
En,Mev | 11.6 | 12.0 | 13.0 | 14.0 | 15.0 | 16.0 | 17.0 | 18.0 | 19.0 | 20.0
σ,mb | 0.00 | 17.0 | 110. | 230. | 336. | 391. | 425. | 455. | 472. | 476.
Δσ,% | 15. | 10. | 8. | 10.
0.4
0.3
0.2
0.1
0.0
BARN
12
14
16
18
20
MEV
21-SC-45

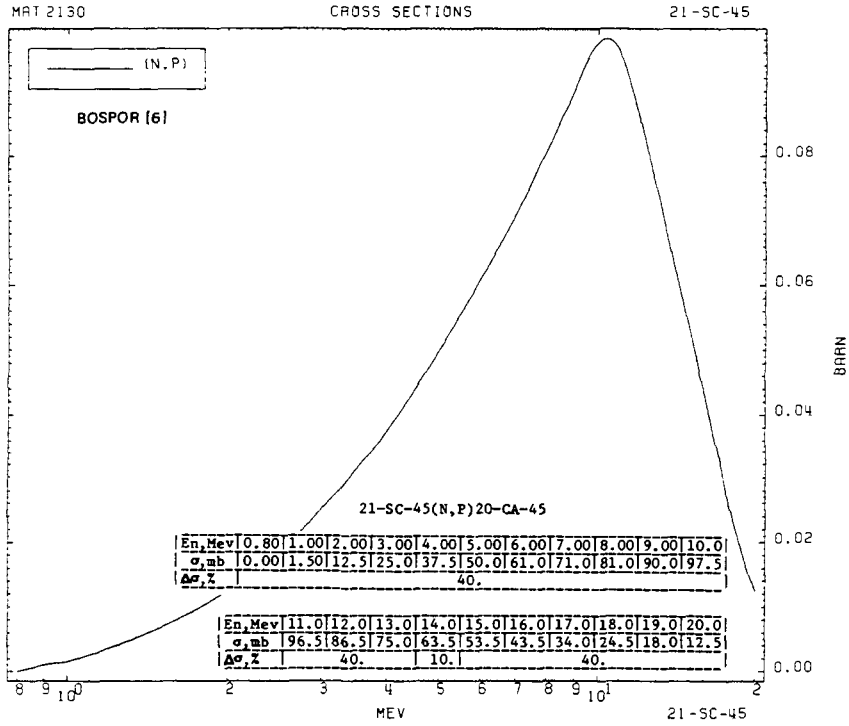
MAT 2130
CROSS SECTIONS
21-SC-45
(N,P)
BOSPOR [6]
21-SC-45(N,P)20-CA-45
En,Mev | 0.80 | 1.00 | 2.00 | 3.00 | 4.00 | 5.00 | 6.00 | 7.00 | 8.00 | 9.00 | 10.0
σ,mb | 0.00 | 1.50 | 12.5 | 25.0 | 37.5 | 50.0 | 61.0 | 71.0 | 81.0 | 90.0 | 97.5
Δσ,% | 40.
En,Mev | 11.0 | 12.0 | 13.0 | 14.0 | 15.0 | 16.0 | 17.0 | 18.0 | 19.0 | 20.0
σ,mb | 96.5 | 86.5 | 75.0 | 63.5 | 53.5 | 43.5 | 34.0 | 24.5 | 18.0 | 12.5
Δσ,% | 40. | 10. | 40.
0.08
0.06
0.04
0.02
0.00
BARN
MEV
21-SC-45

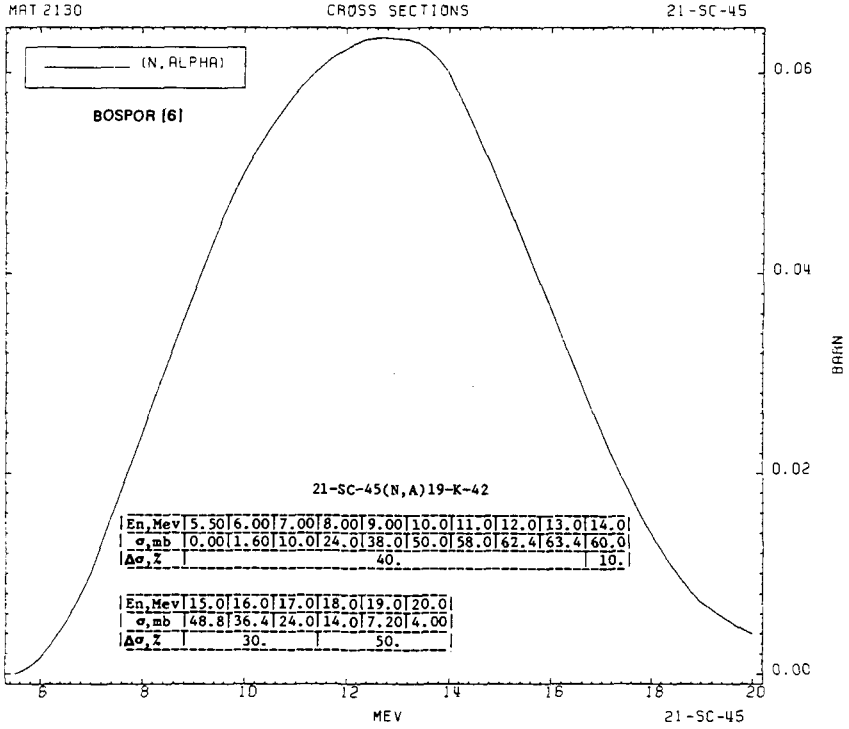
MAT 2130
CROSS SECTIONS
21-SC-45
(N,ALPHA)
BOSPOR [6]
21-SC-45(N,A)19-K-42
En,Mev | 5.50 | 6.00 | 7.00 | 8.00 | 9.00 | 10.0 | 11.0 | 12.0 | 13.0 | 14.0
σ,mb | 0.00 | 1.60 | 10.0 | 24.0 | 38.0 | 50.0 | 58.0 | 62.4 | 63.4 | 60.0
Δσ,% | 40. | 10.
En,Mev | 15.0 | 16.0 | 17.0 | 18.0 | 19.0 | 20.0
σ,mb | 48.8 | 36.4 | 24.0 | 14.0 | 7.20 | 4.00
Δσ,% | 30. | 50.
0.06
0.04
0.02
0.00
BARN
MEV
21-SC-45

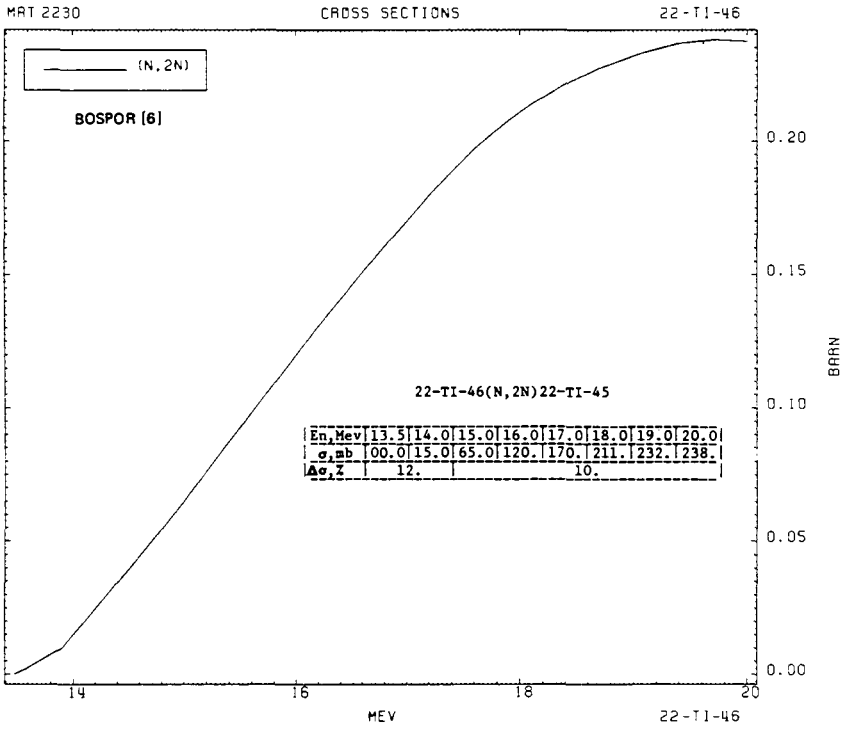
MAT 2230
CROSS SECTIONS
22-TI-46
(N,2N)
BOSPOR [6]
22-TI-46(N,2N)22-TI-45
En,Mev | 13.5 | 14.0 | 15.0 | 16.0 | 17.0 | 18.0 | 19.0 | 20.0
σ,mb | 00.0 | 15.0 | 65.0 | 120. | 170. | 211. | 232. | 238.
Δσ,% | 12. | 10.
0.20
0.15
0.10
0.05
0.00
BARN
14
16
18
20
MEV
22-TI-46

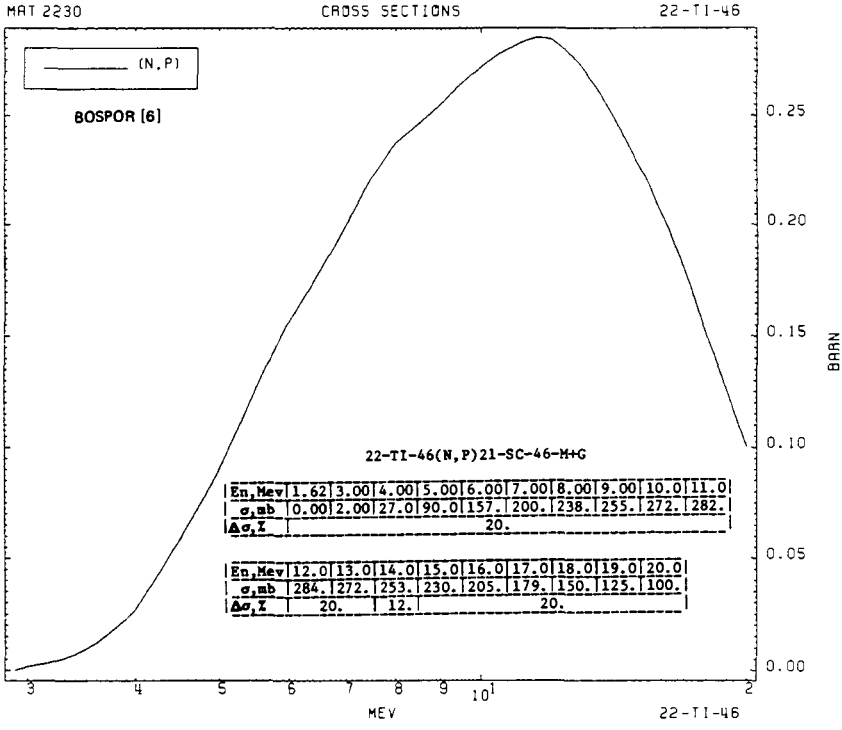
MAT 2230
CROSS SECTIONS
22-TI-46
(N,P)
BOSPOR [6]
22-TI-46(N,P)21-SC-46-M+G
En,Mev | 1.62 | 3.00 | 4.00 | 5.00 | 6.00 | 7.00 | 8.00 | 9.00 | 10.0 | 11.0
σ,mb | 0.00 | 2.00 | 27.0 | 90.0 | 157. | 200. | 238. | 255. | 272. | 282.
Δσ,% | 20.
En,Mev | 12.0 | 13.0 | 14.0 | 15.0 | 16.0 | 17.0 | 18.0 | 19.0 | 20.0
σ,mb | 284. | 272. | 253. | 230. | 205. | 179. | 150. | 125. | 100.
Δσ,% | 20. | 12. | 20.
0.25
0.20
0.15
0.10
0.05
0.00
BARN
3
4
5
6
7
8
9
10¹
2
MEV
22-TI-46

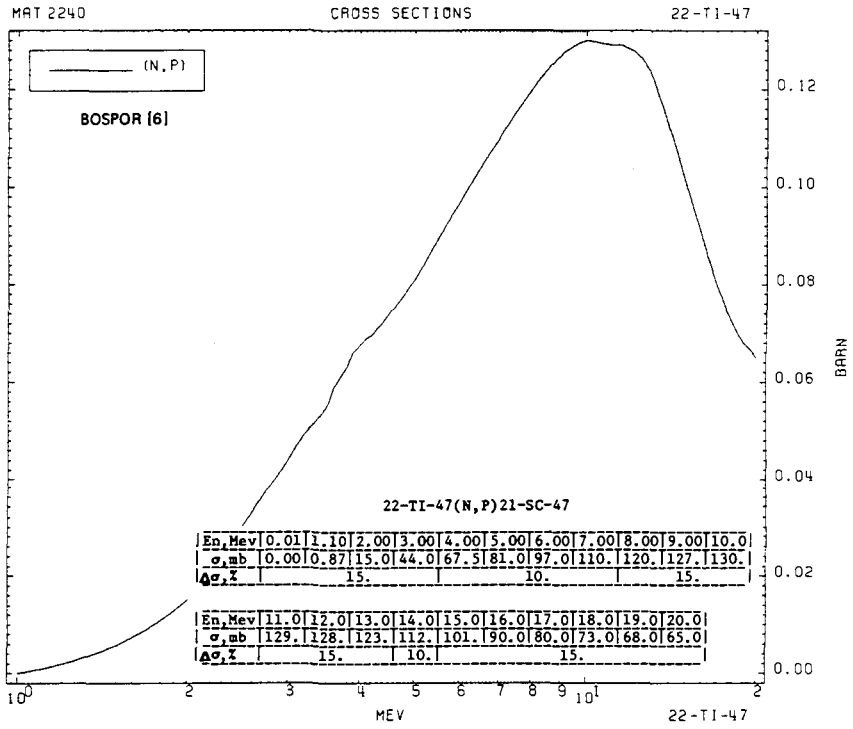
MAT 2240
CROSS SECTIONS
22-TI-47
(N,P)
BOSPOR [6]
22-TI-47(N,P)21-SC-47
En,Mev | 0.01 | 1.10 | 2.00 | 3.00 | 4.00 | 5.00 | 6.00 | 7.00 | 8.00 | 9.00 | 10.0
σ,mb | 0.00 | 0.87 | 15.0 | 44.0 | 67.5 | 81.0 | 97.0 | 110. | 120. | 127. | 130.
Δσ,% | 15. | 10. | 15.
En,Mev | 11.0 | 12.0 | 13.0 | 14.0 | 15.0 | 16.0 | 17.0 | 18.0 | 19.0 | 20.0
σ,mb | 129. | 128. | 123. | 112. | 101. | 90.0 | 80.0 | 73.0 | 68.0 | 65.0
Δσ,% | 15. | 10. | 15.
0.12
0.10
0.08
0.06
0.04
0.02
0.00
BARN
10^0
2
3
4
5
6
7
8
9
10^1
2
MEV
22-TI-47

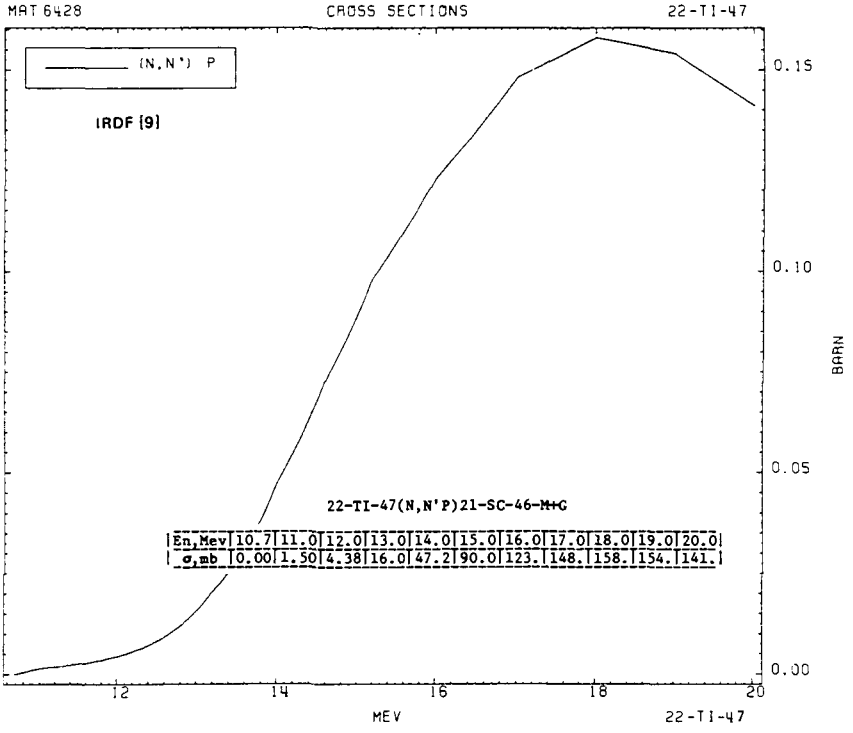
MAT 6428
CROSS SECTIONS
22-TI-47
(N,N') P
IRDF [9]
22-TI-47(N,N'P)21-SC-46-M+G
En,Mev | 10.7 | 11.0 | 12.0 | 13.0 | 14.0 | 15.0 | 16.0 | 17.0 | 18.0 | 19.0 | 20.0
σ,mb | 0.00 | 1.50 | 4.38 | 16.0 | 47.2 | 90.0 | 123. | 148. | 158. | 154. | 141.
0.15
0.10
0.05
0.00
BARN
12
14
16
18
20
MEV
22-TI-47

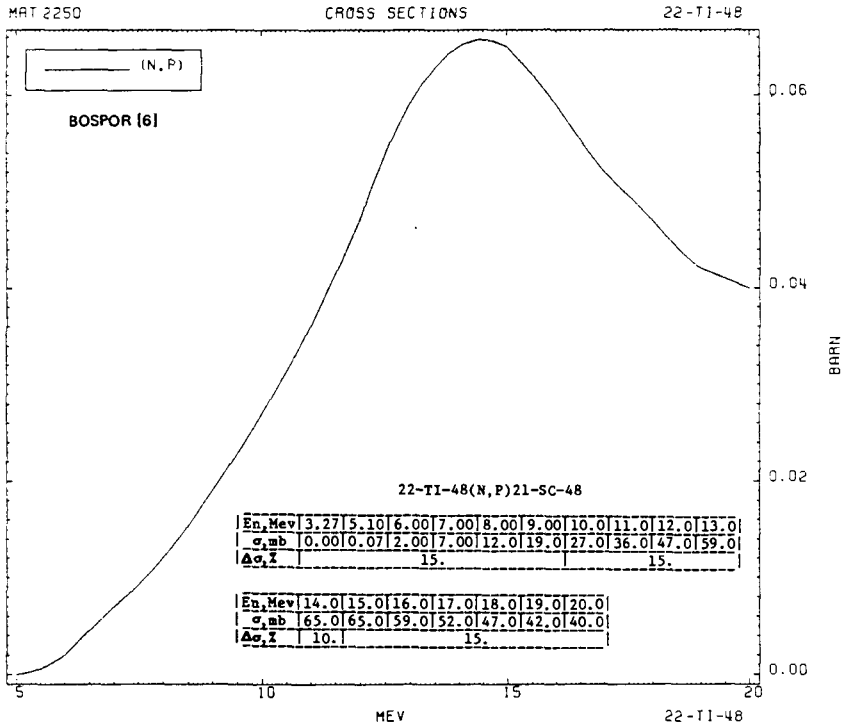
MAT 2250
CROSS SECTIONS
22-TI-48
(N,P)
BOSPOR [6]
22-TI-48(N,P)21-SC-48
En,Mev | 3.27 | 5.10 | 6.00 | 7.00 | 8.00 | 9.00 | 10.0 | 11.0 | 12.0 | 13.0
σ,mb | 0.00 | 0.07 | 2.00 | 7.00 | 12.0 | 19.0 | 27.0 | 36.0 | 47.0 | 59.0
Δσ,% | 15. | 15.
En,Mev | 14.0 | 15.0 | 16.0 | 17.0 | 18.0 | 19.0 | 20.0
σ,mb | 65.0 | 65.0 | 59.0 | 52.0 | 47.0 | 42.0 | 40.0
Δσ,% | 10. | 15.
0.06
0.04
0.02
0.00
BARN
5
10
15
20
MEV
22-TI-48

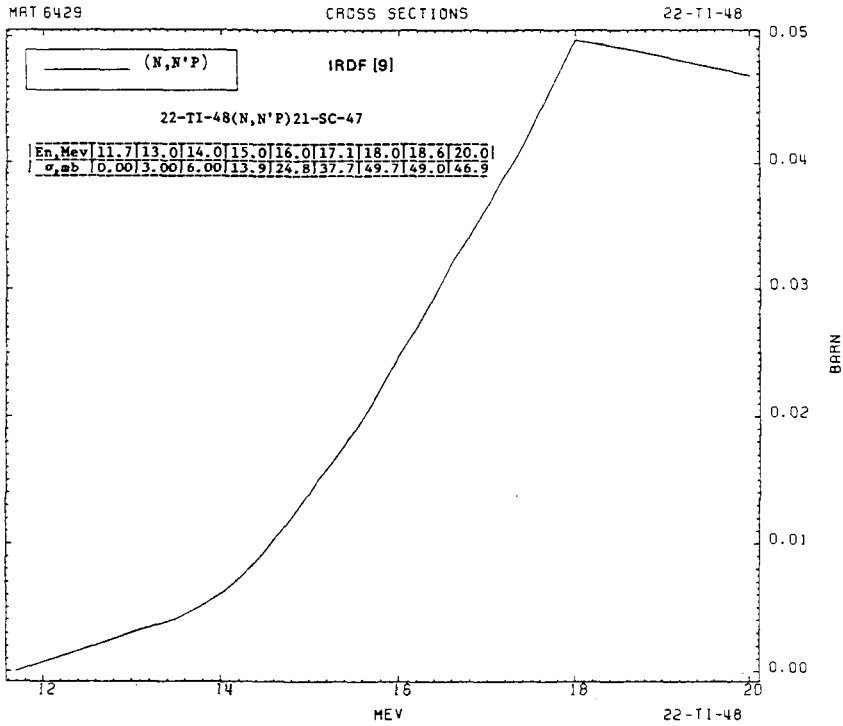
MAT 6429
CROSS SECTIONS
22-TI-48
(N,N'P)
IRDF [9]
22-TI-48(N,N'P)21-SC-47
En,Mev | 11.7 | 13.0 | 14.0 | 15.0 | 16.0 | 17.1 | 18.0 | 18.6 | 20.0
σ,mb | 0.00 | 3.00 | 6.00 | 13.9 | 24.8 | 37.7 | 49.7 | 49.0 | 46.9
0.05
0.04
0.03
0.02
0.01
0.00
BARN
12
14
16
18
20
MEV
22-TI-48

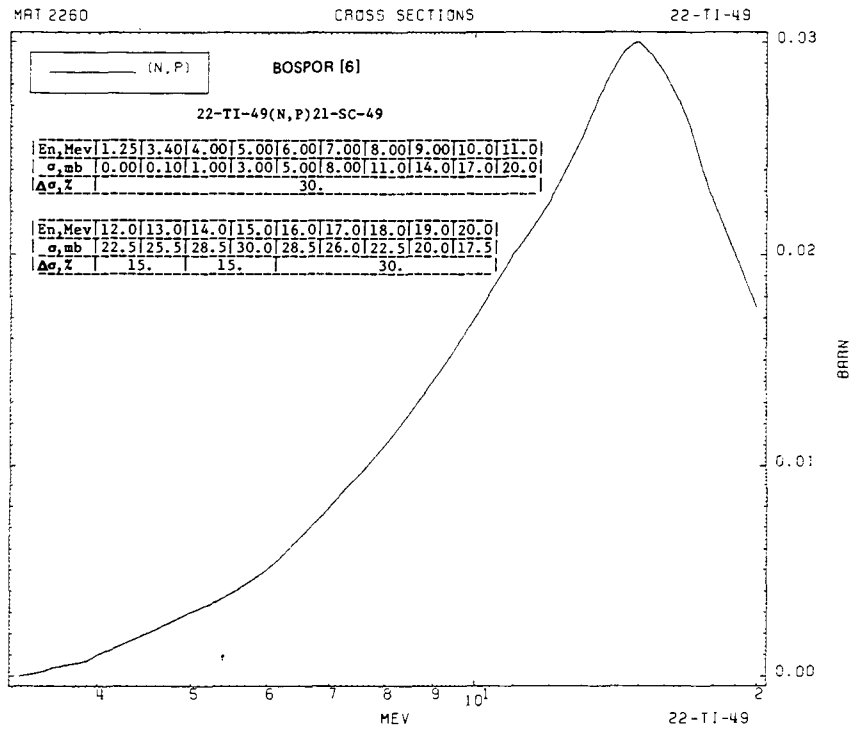
MAT 2260
CROSS SECTIONS
22-TI-49
(N,P)
BOSPOR [6]
22-TI-49(N,P)21-SC-49
En,Mev | 1.25 | 3.40 | 4.00 | 5.00 | 6.00 | 7.00 | 8.00 | 9.00 | 10.0 | 11.0
σ,mb | 0.00 | 0.10 | 1.00 | 3.00 | 5.00 | 8.00 | 11.0 | 14.0 | 17.0 | 20.0
Δσ,% | 30.
En,Mev | 12.0 | 13.0 | 14.0 | 15.0 | 16.0 | 17.0 | 18.0 | 19.0 | 20.0
σ,mb | 22.5 | 25.5 | 28.5 | 30.0 | 28.5 | 26.0 | 22.5 | 20.0 | 17.5
Δσ,% | 15. | 15. | 30.
0.03
0.02
0.01
0.00
BARN
4
5
6
7
8
9
10¹
2
MEV
22-TI-49

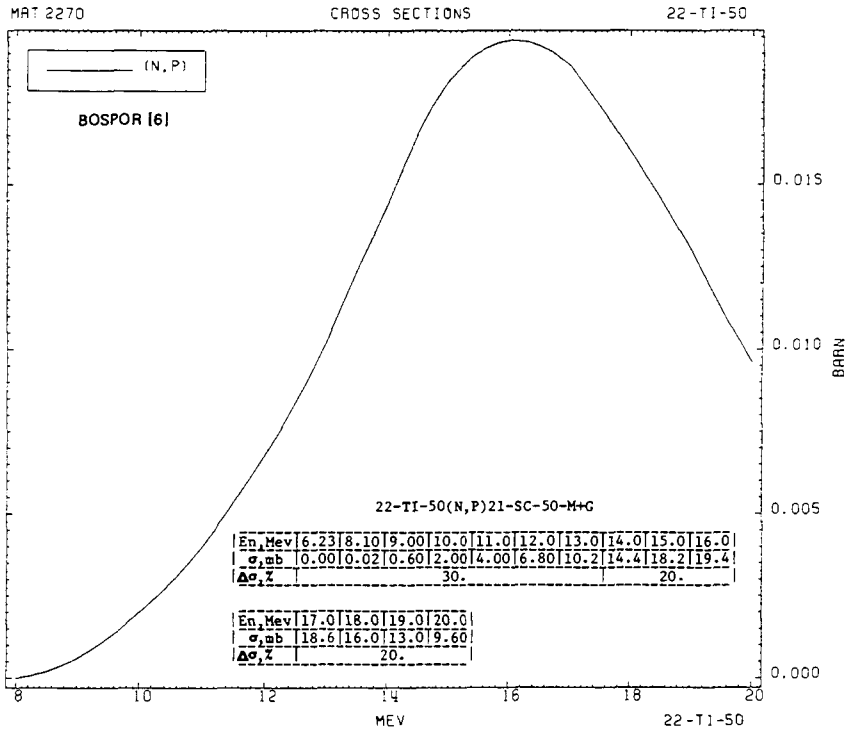
MAT 2270
CROSS SECTIONS
22-TI-50
(N,P)
BOSPOR [6]
22-TI-50(N,P)21-SC-50-M+G
En,Mev | 6.23 | 8.10 | 9.00 | 10.0 | 11.0 | 12.0 | 13.0 | 14.0 | 15.0 | 16.0
σ,mb | 0.00 | 0.02 | 0.60 | 2.00 | 4.00 | 6.80 | 10.2 | 14.4 | 18.2 | 19.4
Δσ,% | 30. | 20.
En,Mev | 17.0 | 18.0 | 19.0 | 20.0
σ,mb | 18.6 | 16.0 | 13.0 | 9.60
Δσ,% | 20.
0.015
0.010
0.005
0.000
BARN
8
10
12
14
16
18
20
MEV
22-TI-50

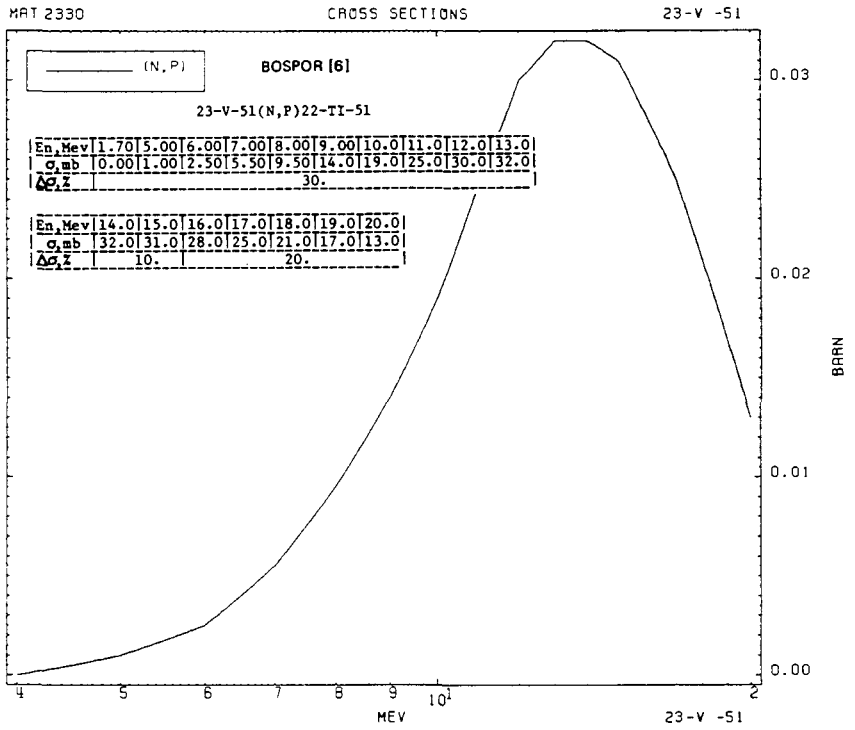
MAT 2330
CROSS SECTIONS
23-V -51
(N,P)
BOSPOR [6]
23-V-51(N,P)22-TI-51
En,Mev | 1.70 | 5.00 | 6.00 | 7.00 | 8.00 | 9.00 | 10.0 | 11.0 | 12.0 | 13.0
σ,mb | 0.00 | 1.00 | 2.50 | 5.50 | 9.50 | 14.0 | 19.0 | 25.0 | 30.0 | 32.0
Δσ,Z | 30.
En,Mev | 14.0 | 15.0 | 16.0 | 17.0 | 18.0 | 19.0 | 20.0
σ,mb | 32.0 | 31.0 | 28.0 | 25.0 | 21.0 | 17.0 | 13.0
Δσ,Z | 10. | 20.
0.03
0.02
0.01
0.00
BARN
4
5
6
7
8
9
10¹
2
MEV
23-V -51

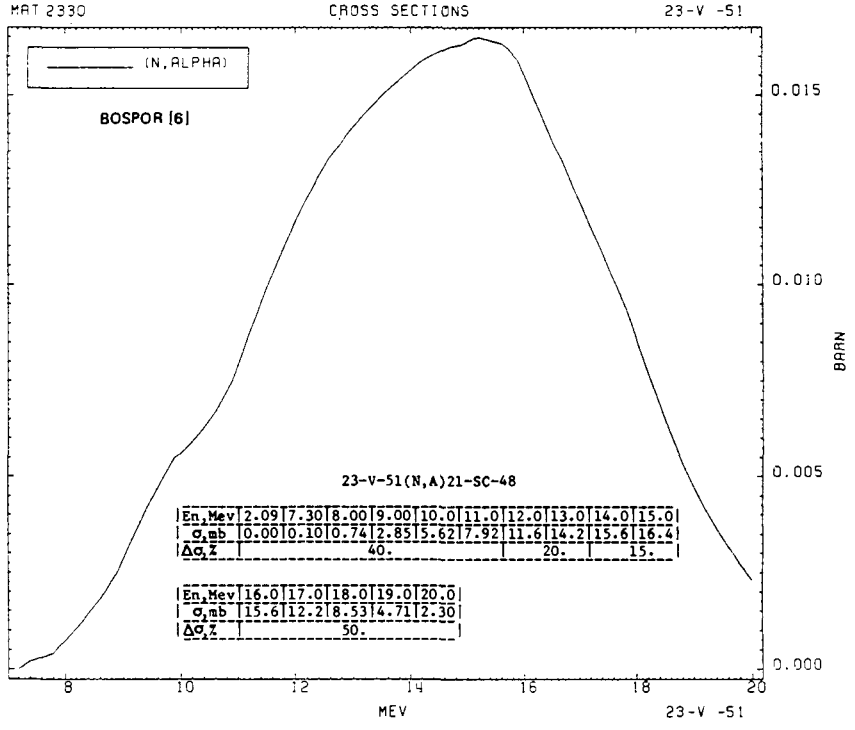
MAT 2330
CROSS SECTIONS
23-V -51
(N,ALPHA)
BOSPOR [6]
23-V-51(N,A)21-SC-48
En,Mev | 2.09 | 7.30 | 8.00 | 9.00 | 10.0 | 11.0 | 12.0 | 13.0 | 14.0 | 15.0
σ,mb | 0.00 | 0.10 | 0.74 | 2.85 | 5.62 | 7.92 | 11.6 | 14.2 | 15.6 | 16.4
Δσ,Z | 40. | 20. | 15.
En,Mev | 16.0 | 17.0 | 18.0 | 19.0 | 20.0
σ,mb | 15.6 | 12.2 | 8.53 | 4.71 | 2.30
Δσ,Z | 50.
0.015
0.010
0.005
0.000
BARN
8
10
12
14
16
18
20
MEV
23-V -51

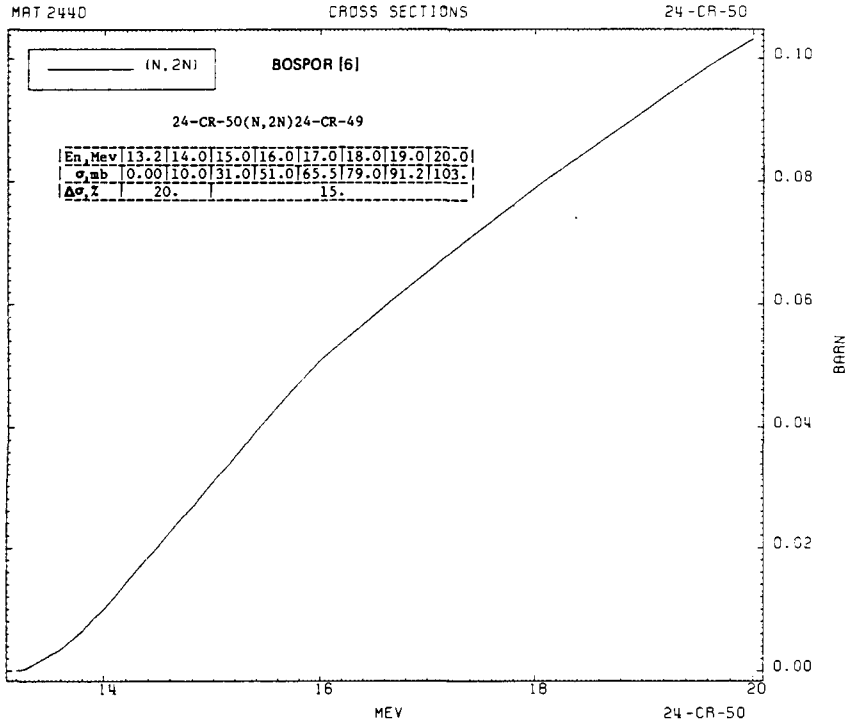
MAT 2440
CROSS SECTIONS
24-CR-50
(N,2N)
BOSPOR [6]
24-CR-50(N,2N)24-CR-49
En,Mev | 13.2 | 14.0 | 15.0 | 16.0 | 17.0 | 18.0 | 19.0 | 20.0
σ,mb | 0.00 | 10.0 | 31.0 | 51.0 | 65.5 | 79.0 | 91.2 | 103.
Δσ,% | 20. | 15.
0.10
0.08
0.06
0.04
0.02
0.00
BARN
14
16
18
20
MEV
24-CR-50

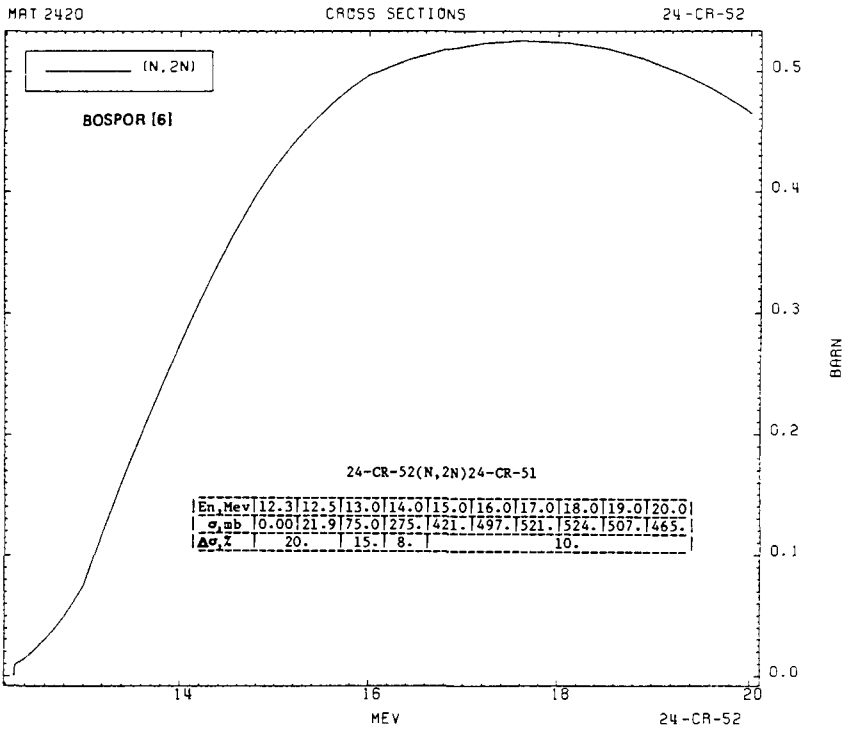
MAT 2420
CROSS SECTIONS
24-CR-52
(N,2N)
BOSPOR [6]
24-CR-52(N,2N)24-CR-51
En,Mev | 12.3 | 12.5 | 13.0 | 14.0 | 15.0 | 16.0 | 17.0 | 18.0 | 19.0 | 20.0
σ,mb | 0.00 | 21.9 | 75.0 | 275. | 421. | 497. | 521. | 524. | 507. | 465.
Δσ,% | 20. | 15. | 8. | 10.
0.5
0.4
0.3
0.2
0.1
0.0
BARN
14
16
18
20
MEV
24-CR-52

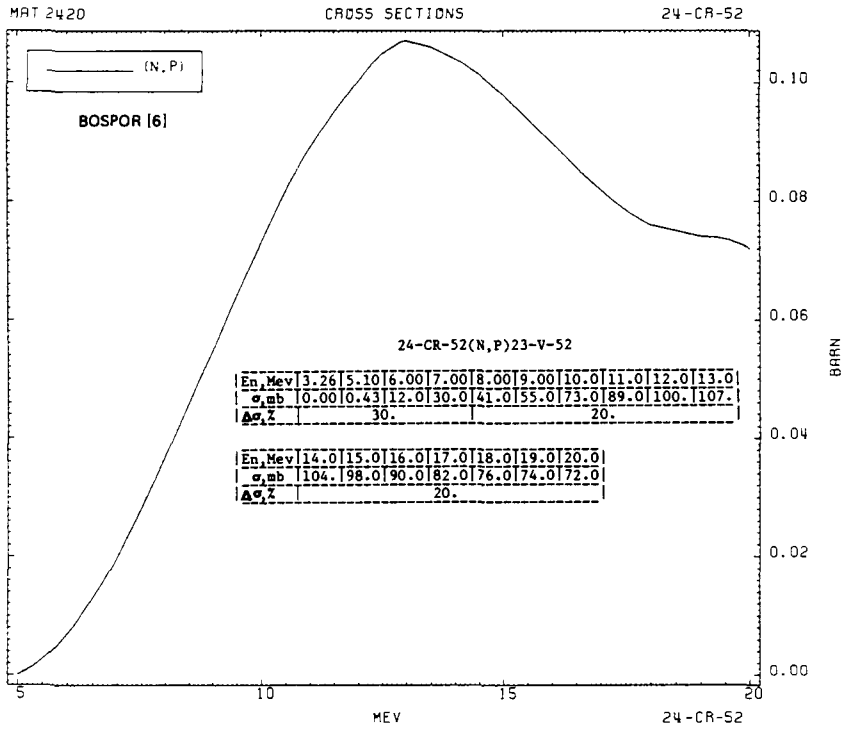
MAT 2420
CROSS SECTIONS
24-CR-52
(N,P)
BOSPOR [6]
24-CR-52(N,P)23-V-52
En,Mev | 3.26 | 5.10 | 6.00 | 7.00 | 8.00 | 9.00 | 10.0 | 11.0 | 12.0 | 13.0
σ,mb | 0.00 | 0.43 | 12.0 | 30.0 | 41.0 | 55.0 | 73.0 | 89.0 | 100. | 107.
Δσ,% | 30. | 20.
En,Mev | 14.0 | 15.0 | 16.0 | 17.0 | 18.0 | 19.0 | 20.0
σ,mb | 104. | 98.0 | 90.0 | 82.0 | 76.0 | 74.0 | 72.0
Δσ,% | 20.
0.10
0.08
0.06
0.04
0.02
0.00
BARN
5
10
15
20
MEV
24-CR-52

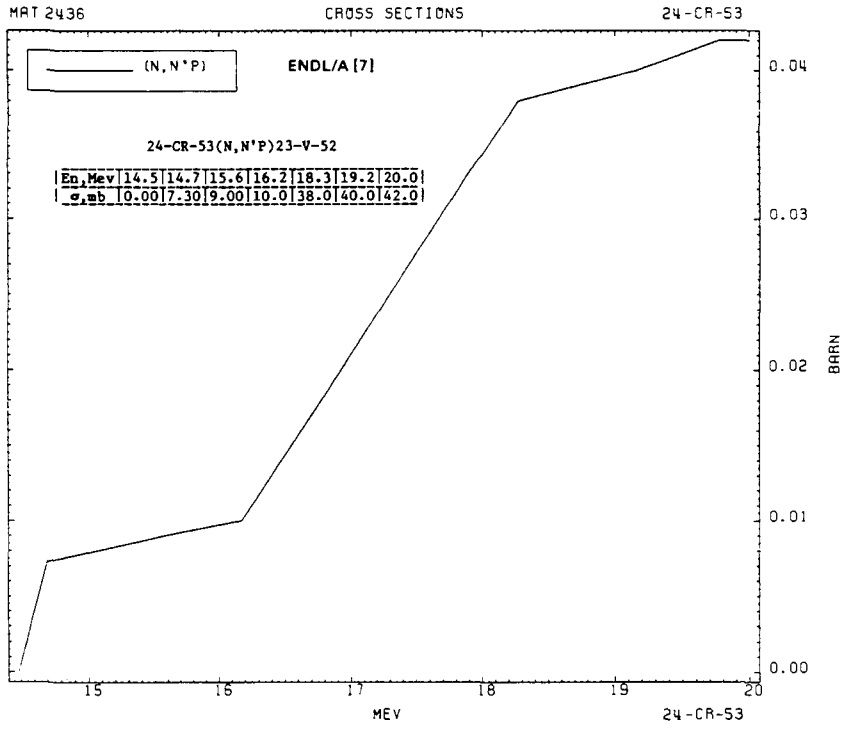
MAT 2436
CROSS SECTIONS
24-CR-53
(N,N'P)
ENDL/A [7]
24-CR-53(N,N'P)23-V-52
En,Mev | 14.5 | 14.7 | 15.6 | 16.2 | 18.3 | 19.2 | 20.0
σ,mb | 0.00 | 7.30 | 9.00 | 10.0 | 38.0 | 40.0 | 42.0
0.04
0.03
0.02
0.01
0.00
BARN
15
16
17
18
19
20
MEV
24-CR-53

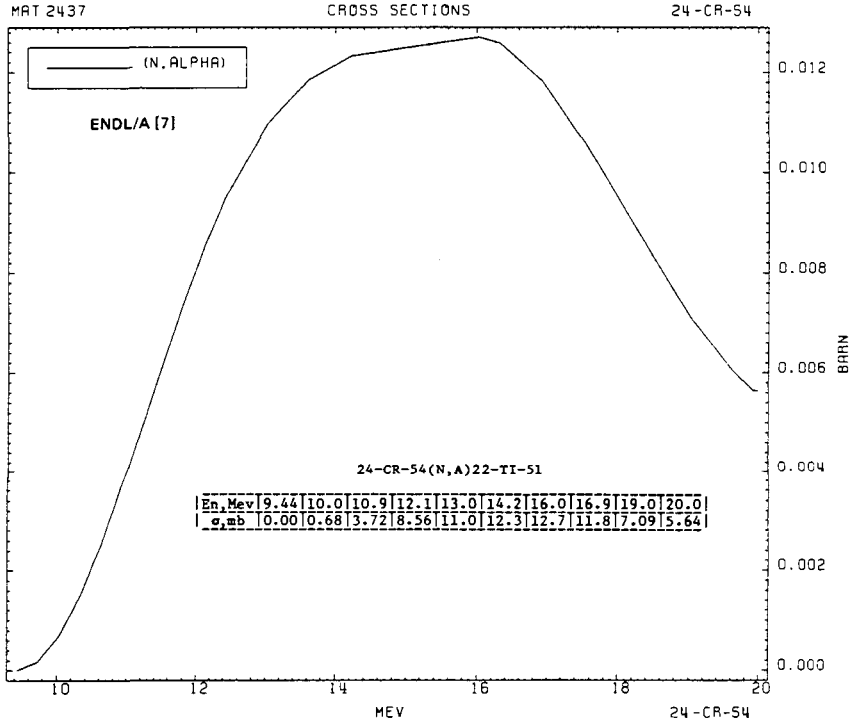
MAT 2437
CROSS SECTIONS
24-CR-54
(N,ALPHA)
ENDL/A [7]
24-CR-54(N,A)22-TI-51
En,Mev | 9.44 | 10.0 | 10.9 | 12.1 | 13.0 | 14.2 | 16.0 | 16.9 | 19.0 | 20.0
σ,mb | 0.00 | 0.68 | 3.72 | 8.56 | 11.0 | 12.3 | 12.7 | 11.8 | 7.09 | 5.64
0.012
0.010
0.008
0.006
0.004
0.002
0.000
BARN
10
12
14
16
18
20
MEV
24-CR-54

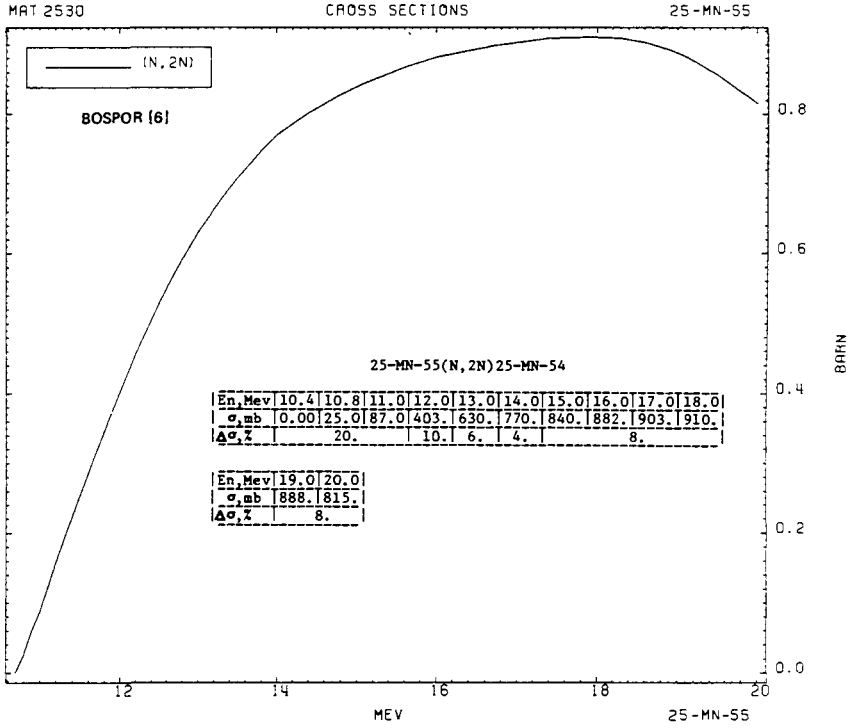
MAT 2530
CROSS SECTIONS
25-MN-55
(N,2N)
BOSPOR [6]
25-MN-55(N,2N)25-MN-54
En,Mev | 10.4 | 10.8 | 11.0 | 12.0 | 13.0 | 14.0 | 15.0 | 16.0 | 17.0 | 18.0
σ,mb | 0.00 | 25.0 | 87.0 | 403. | 630. | 770. | 840. | 882. | 903. | 910.
Δσ,% | 20. | 10. | 6. | 4. | 8.
En,Mev | 19.0 | 20.0
σ,mb | 888. | 815.
Δσ,% | 8.
0.8
0.6
0.4
0.2
0.0
BARN
12
14
16
18
20
MEV
25-MN-55

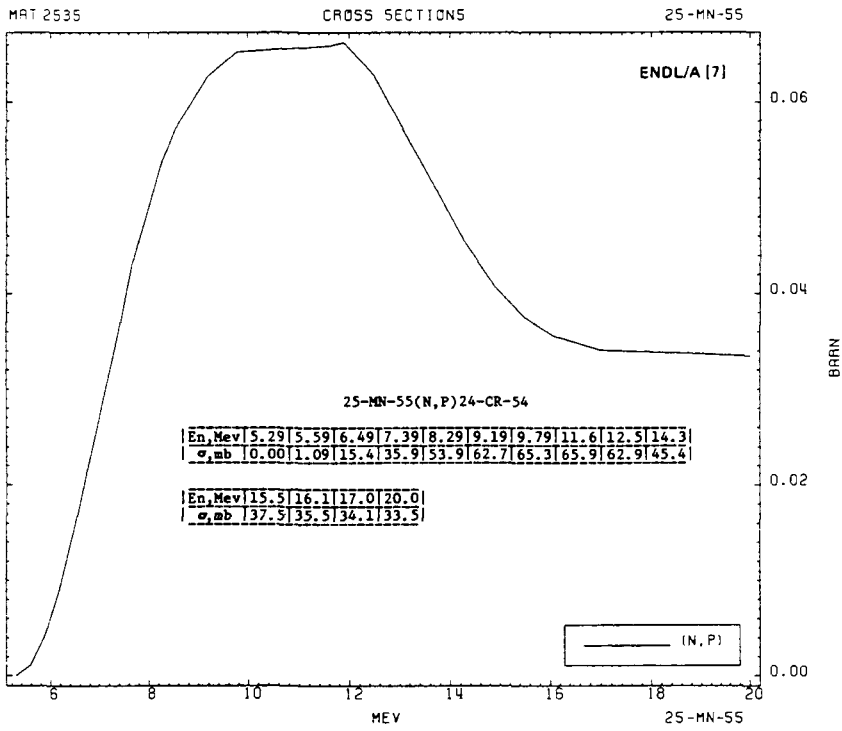
MAT 2535
CROSS SECTIONS
25-MN-55
ENDL/A [7]
0.06
0.04
0.02
0.00
BARN
25-MN-55(N,P)24-CR-54
En,Mev 5.29 5.59 6.49 7.39 8.29 9.19 9.79 11.6 12.5 14.3
σ,mb 0.00 1.09 15.4 35.9 53.9 62.7 65.3 65.9 62.9 45.4
En,Mev 15.5 16.1 17.0 20.0
σ,mb 37.5 35.5 34.1 33.5
(N,P)
6 8 10 12 14 16 18 20
MEV
25-MN-55

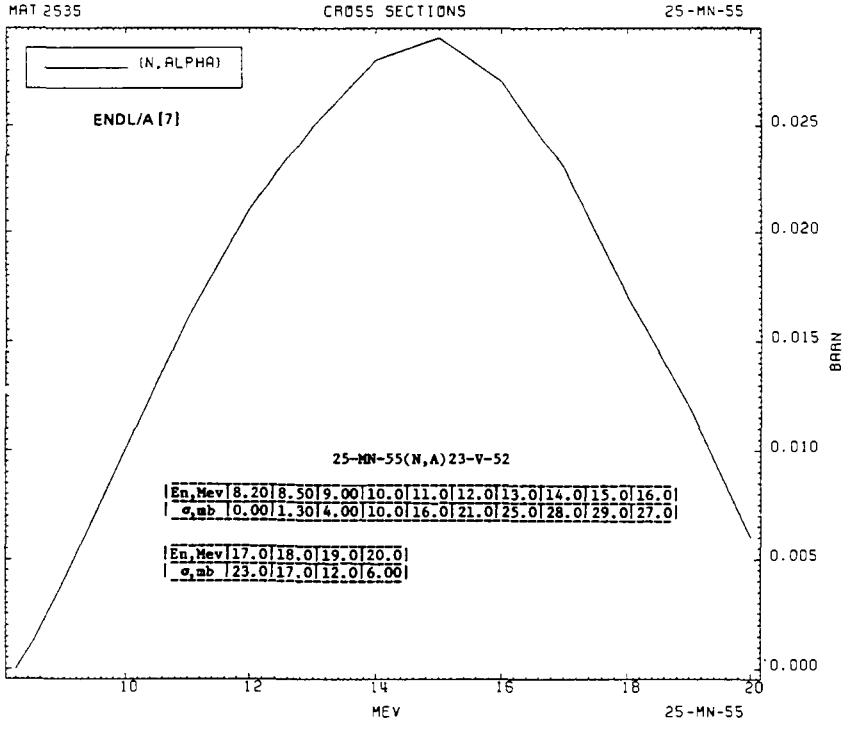
MAT 2535
CROSS SECTIONS
25-MN-55
(N,ALPHA)
ENDL/A [7]
0.025
0.020
0.015
0.010
0.005
0.000
BARN
25-MN-55(N,A)23-V-52
En,Mev 8.20 8.50 9.00 10.0 11.0 12.0 13.0 14.0 15.0 16.0
σ,mb 0.00 1.30 4.00 10.0 16.0 21.0 25.0 28.0 29.0 27.0
En,Mev 17.0 18.0 19.0 20.0
σ,mb 23.0 17.0 12.0 6.00
10 12 14 16 18 20
MEV
25-MN-55

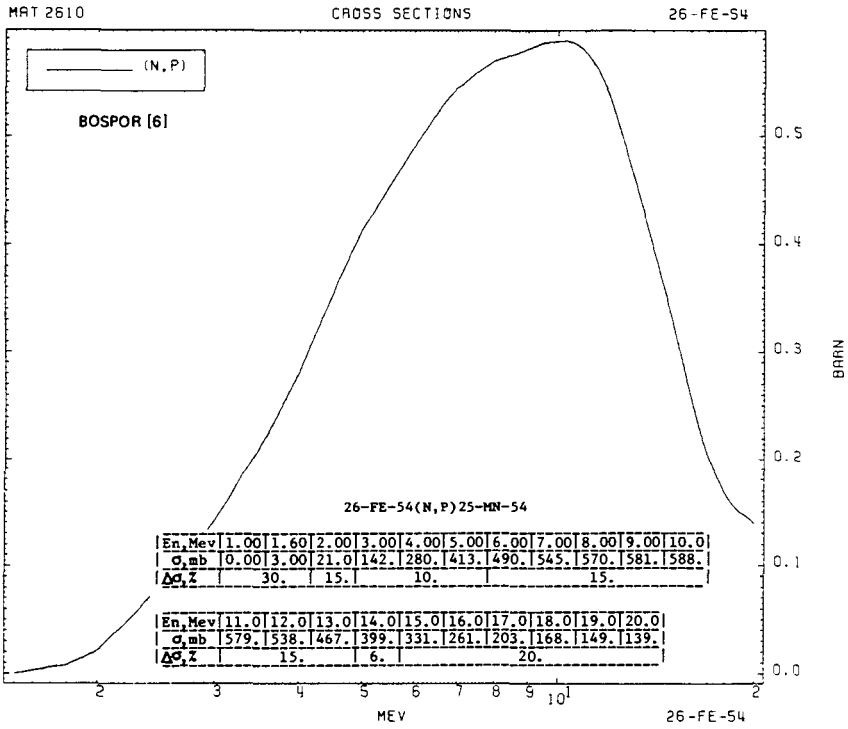
MAT 2610
CROSS SECTIONS
26-FE-54
(N,P)
BOSPOR [6]
26-FE-54(N,P)25-MN-54
En,Mev | 1.00 | 1.60 | 2.00 | 3.00 | 4.00 | 5.00 | 6.00 | 7.00 | 8.00 | 9.00 | 10.0
σ,mb | 0.00 | 3.00 | 21.0 | 142. | 280. | 413. | 490. | 545. | 570. | 581. | 588.
Δσ,% | 30. | 15. | 10. | 15.
En,Mev | 11.0 | 12.0 | 13.0 | 14.0 | 15.0 | 16.0 | 17.0 | 18.0 | 19.0 | 20.0
σ,mb | 579. | 538. | 467. | 399. | 331. | 261. | 203. | 168. | 149. | 139.
Δσ,% | 15. | 6. | 20.
0.5
0.4
0.3
0.2
0.1
0.0
BARN
2 3 4 5 6 7 8 9 10^1 2
MEV
26-FE-54

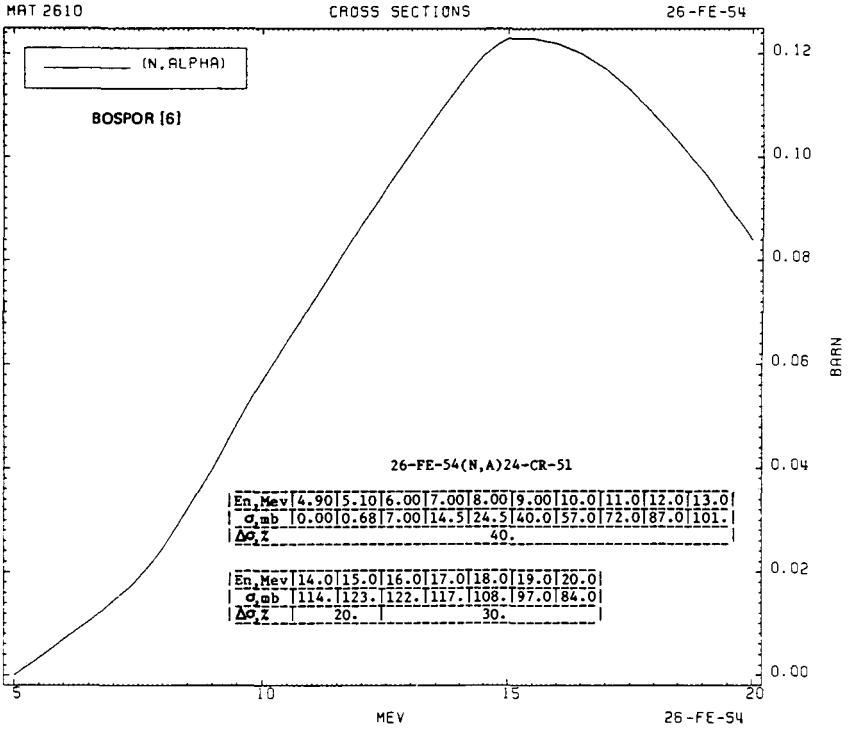
MAT 2610
CROSS SECTIONS
26-FE-54
(N,ALPHA)
BOSPOR [6]
26-FE-54(N,A)24-CR-51
En,Mev | 4.90 | 5.10 | 6.00 | 7.00 | 8.00 | 9.00 | 10.0 | 11.0 | 12.0 | 13.0
σ,mb | 0.00 | 0.68 | 7.00 | 14.5 | 24.5 | 40.0 | 57.0 | 72.0 | 87.0 | 101.
Δσ,% | 40.
En,Mev | 14.0 | 15.0 | 16.0 | 17.0 | 18.0 | 19.0 | 20.0
σ,mb | 114. | 123. | 122. | 117. | 108. | 97.0 | 84.0
Δσ,% | 20. | 30.
0.12
0.10
0.08
0.06
0.04
0.02
0.00
BARN
5 10 15 20
MEV
26-FE-54

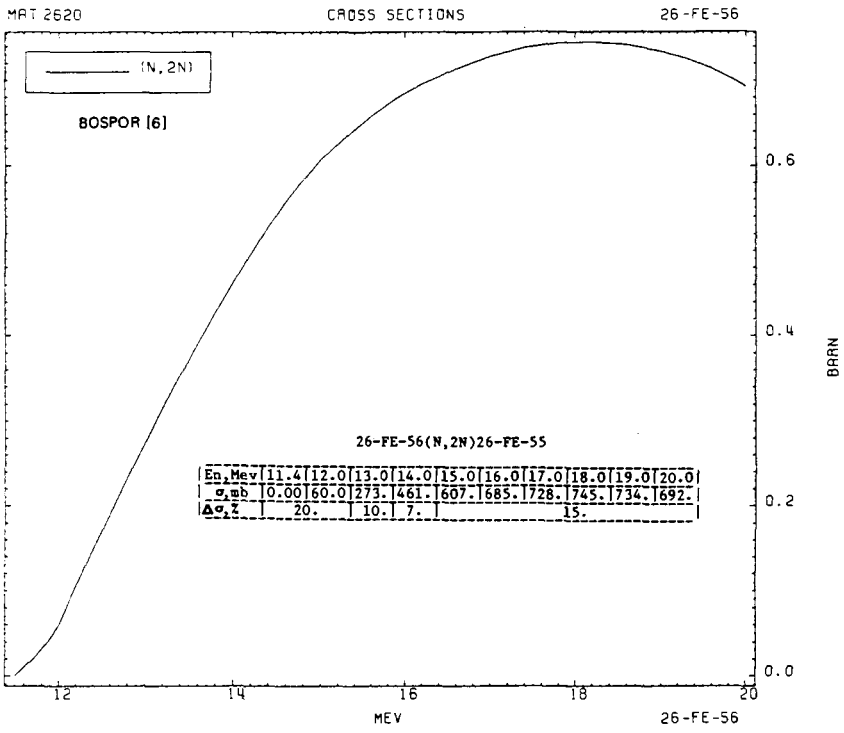
MAT 2620
CROSS SECTIONS
26-FE-56
(N,2N)
BOSPOR [6]
26-FE-56(N,2N)26-FE-55
En,Mev | 11.4 | 12.0 | 13.0 | 14.0 | 15.0 | 16.0 | 17.0 | 18.0 | 19.0 | 20.0
σ,mb | 0.00 | 60.0 | 273. | 461. | 607. | 685. | 728. | 745. | 734. | 692.
Δσ,% | 20. | 10. | 7. | 15.
0.6
0.4
0.2
0.0
BARN
12
14
16
18
20
MEV
26-FE-56

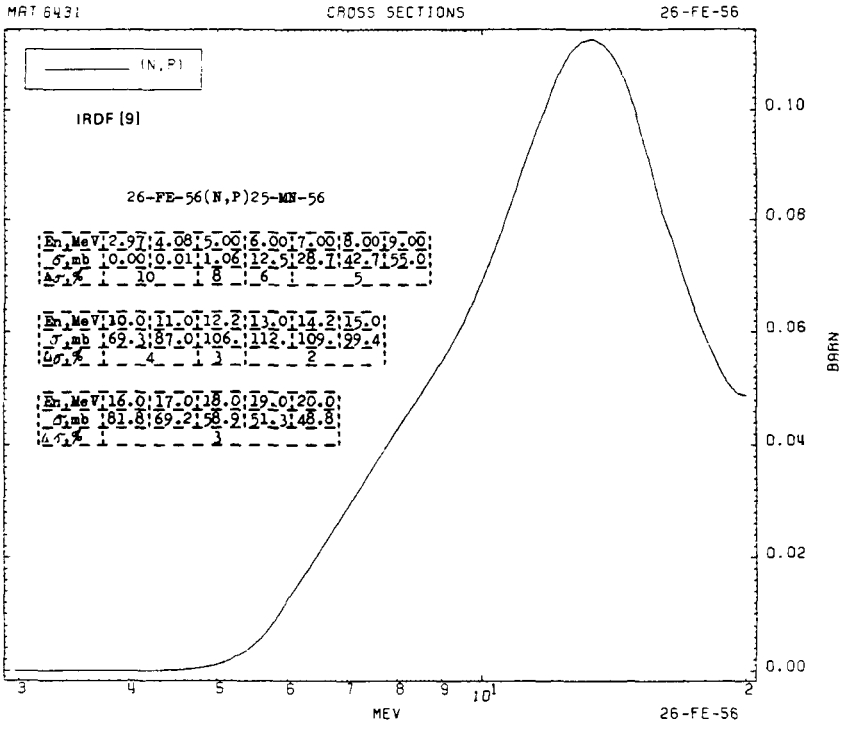
MAT 6431
CROSS SECTIONS
26-FE-56
(N,P)
IRDF [9]
26-FE-56(N,P)25-MN-56
En,MeV | 2.97 | 4.08 | 5.00 | 6.00 | 7.00 | 8.00 | 9.00
σ,mb | 0.00 | 0.01 | 1.06 | 12.5 | 28.7 | 42.7 | 55.0
Δσ,% | 1 | 10 | 1 | 8 | 6 | 1 | 5
En,MeV | 10.0 | 11.0 | 12.2 | 13.0 | 14.2 | 15.0
σ,mb | 69.3 | 87.0 | 106. | 112. | 109. | 99.4
Δσ,% | 1 | 4 | 1 | 3 | 2
En,MeV | 16.0 | 17.0 | 18.0 | 19.0 | 20.0
σ,mb | 81.8 | 69.2 | 58.9 | 51.3 | 48.8
Δσ,% | 1 | 3
0.10
0.08
0.06
0.04
0.02
0.00
BARN
3
4
5
6
7
8
9
10¹
2
MEV
26-FE-56

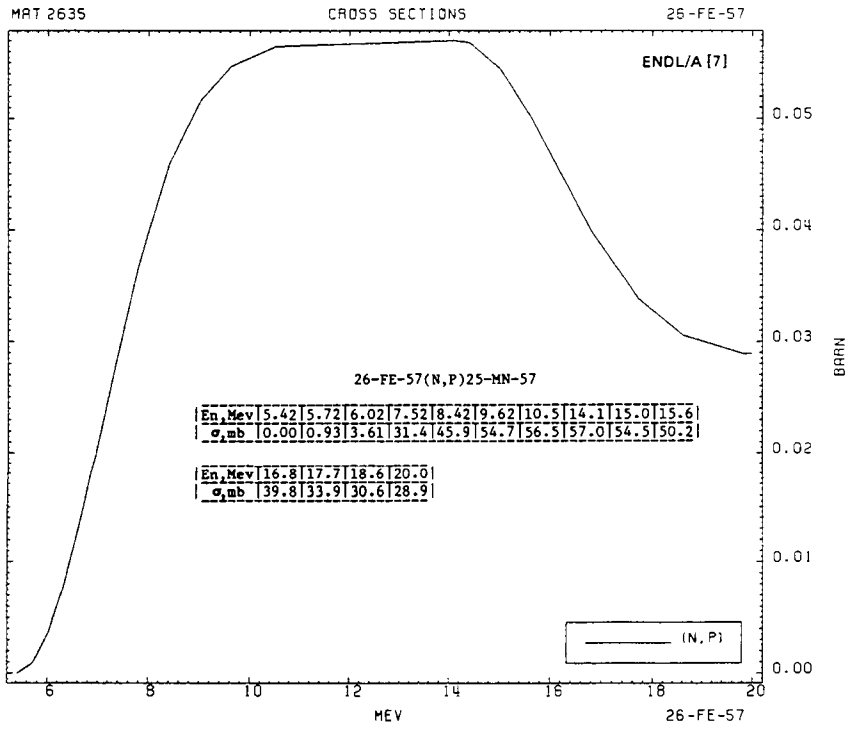
MAT 2635
CROSS SECTIONS
26-FE-57
ENDL/A [7]
26-FE-57(N,P)25-MN-57
En,Mev | 5.42 | 5.72 | 6.02 | 7.52 | 8.42 | 9.62 | 10.5 | 14.1 | 15.0 | 15.6
σ,mb | 0.00 | 0.93 | 3.61 | 31.4 | 45.9 | 54.7 | 56.5 | 57.0 | 54.5 | 50.2
En,Mev | 16.8 | 17.7 | 18.6 | 20.0
σ,mb | 39.8 | 33.9 | 30.6 | 28.9
(N,P)
BARN
MEV
26-FE-57

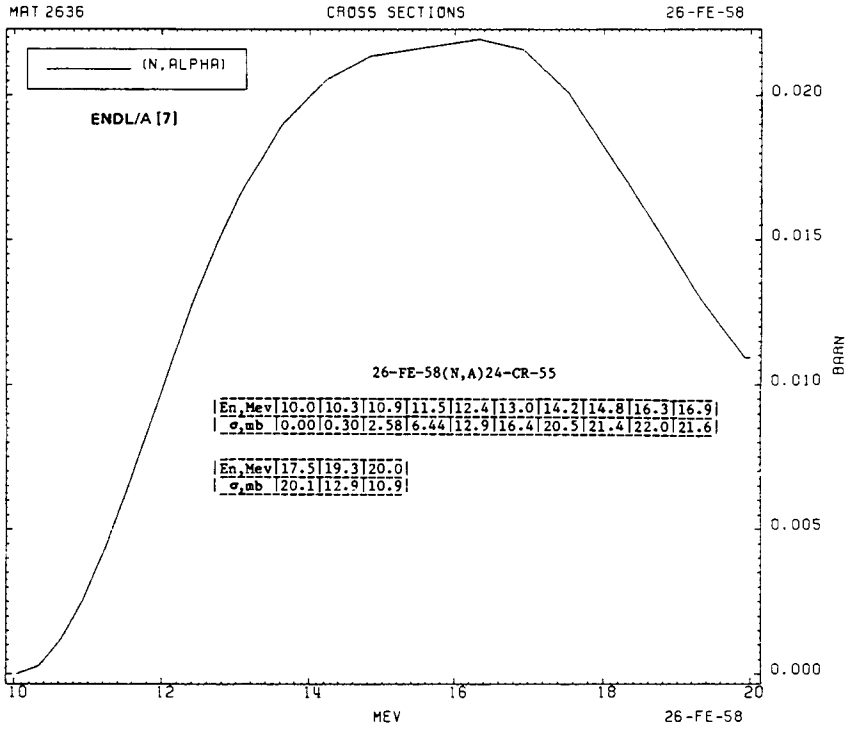
MAT 2636
CROSS SECTIONS
26-FE-58
(N,ALPHA)
ENDL/A [7]
26-FE-58(N,A)24-CR-55
En,Mev | 10.0 | 10.3 | 10.9 | 11.5 | 12.4 | 13.0 | 14.2 | 14.8 | 16.3 | 16.9
σ,mb | 0.00 | 0.30 | 2.58 | 6.44 | 12.9 | 16.4 | 20.5 | 21.4 | 22.0 | 21.6
En,Mev | 17.5 | 19.3 | 20.0
σ,mb | 20.1 | 12.9 | 10.9
BARN
MEV
26-FE-58

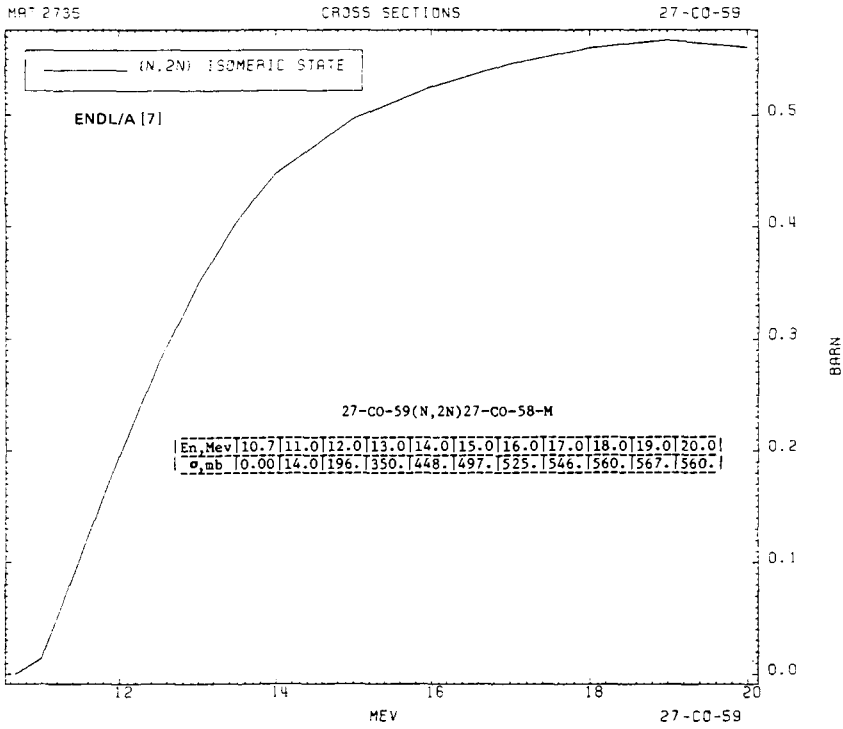
MAT 2735
CROSS SECTIONS
27-CO-59
(N,2N) ISOMERIC STATE
ENDL/A [7]
27-CO-59(N,2N)27-CO-58-M
En,Mev 10.7 11.0 12.0 13.0 14.0 15.0 16.0 17.0 18.0 19.0 20.0
σ,mb 0.00 14.0 196. 350. 448. 497. 525. 546. 560. 567. 560.
0.5
0.4
0.3
0.2
0.1
0.0
BARN
12
14
16
18
20
MEV
27-CO-59

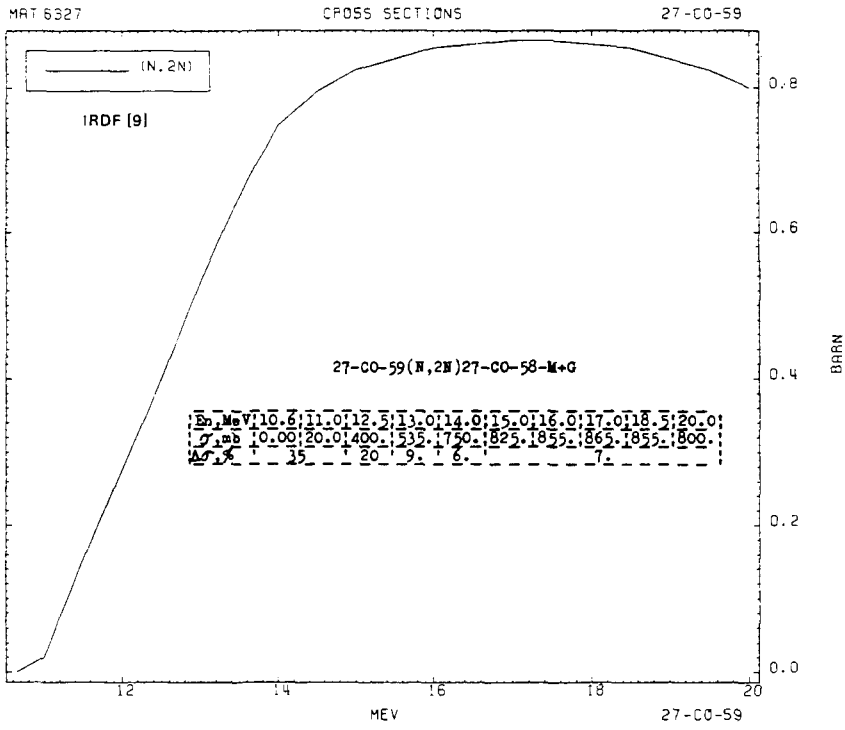
MAT 6327
CROSS SECTIONS
27-CO-59
(N,2N)
IRDF [9]
27-CO-59(N,2N)27-CO-58-M+G
En,MeV 10.6 11.0 12.5 13.0 14.0 15.0 16.0 17.0 18.5 20.0
σ,mb 0.00 20.0 400. 535. 750. 825. 855. 865. 855. 800.
Δσ,% + 35 + 20 9. 6. 7.
0.8
0.6
0.4
0.2
0.0
BARN
12
14
16
18
20
MEV
27-CO-59

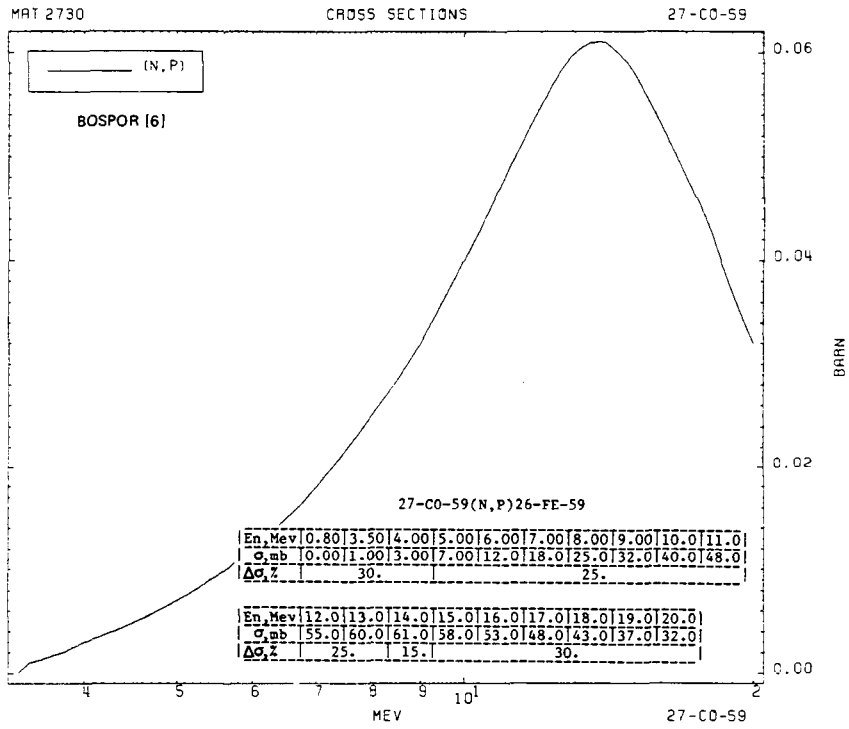
MAT 2730
CROSS SECTIONS
27-CO-59
(N,P)
BOSPOR [6]
27-CO-59(N,P)26-FE-59
En,Mev | 0.80 | 3.50 | 4.00 | 5.00 | 6.00 | 7.00 | 8.00 | 9.00 | 10.0 | 11.0
σ,mb | 0.00 | 1.00 | 3.00 | 7.00 | 12.0 | 18.0 | 25.0 | 32.0 | 40.0 | 48.0
Δσ,% | 30. | 25.
En,Mev | 12.0 | 13.0 | 14.0 | 15.0 | 16.0 | 17.0 | 18.0 | 19.0 | 20.0
σ,mb | 55.0 | 60.0 | 61.0 | 58.0 | 53.0 | 48.0 | 43.0 | 37.0 | 32.0
Δσ,% | 25. | 15. | 30.
0.06
0.04
0.02
0.00
BARN
4
5
6
7
8
9
10
2
MEV
27-CO-59

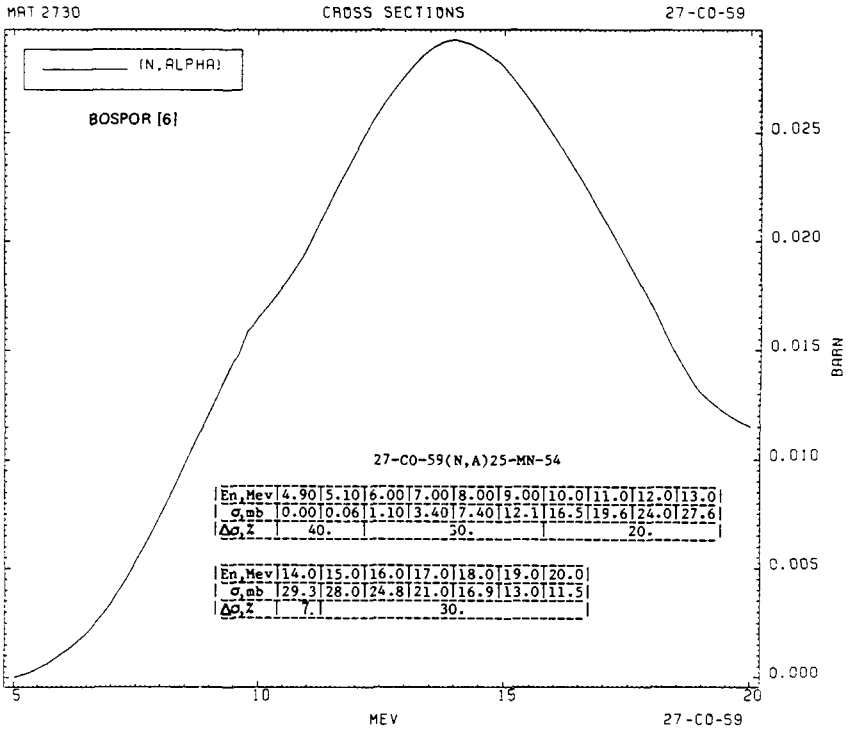
MAT 2730
CROSS SECTIONS
27-CO-59
(N,ALPHA)
BOSPOR [6]
27-CO-59(N,A)25-MN-54
En,Mev | 4.90 | 5.10 | 6.00 | 7.00 | 8.00 | 9.00 | 10.0 | 11.0 | 12.0 | 13.0
σ,mb | 0.00 | 0.06 | 1.10 | 3.40 | 7.40 | 12.1 | 16.5 | 19.6 | 24.0 | 27.6
Δσ,% | 40. | 30. | 20.
En,Mev | 14.0 | 15.0 | 16.0 | 17.0 | 18.0 | 19.0 | 20.0
σ,mb | 29.3 | 28.0 | 24.8 | 21.0 | 16.9 | 13.0 | 11.5
Δσ,% | 7. | 30.
0.025
0.020
0.015
0.010
0.005
0.000
BARN
5
10
15
20
MEV
27-CO-59

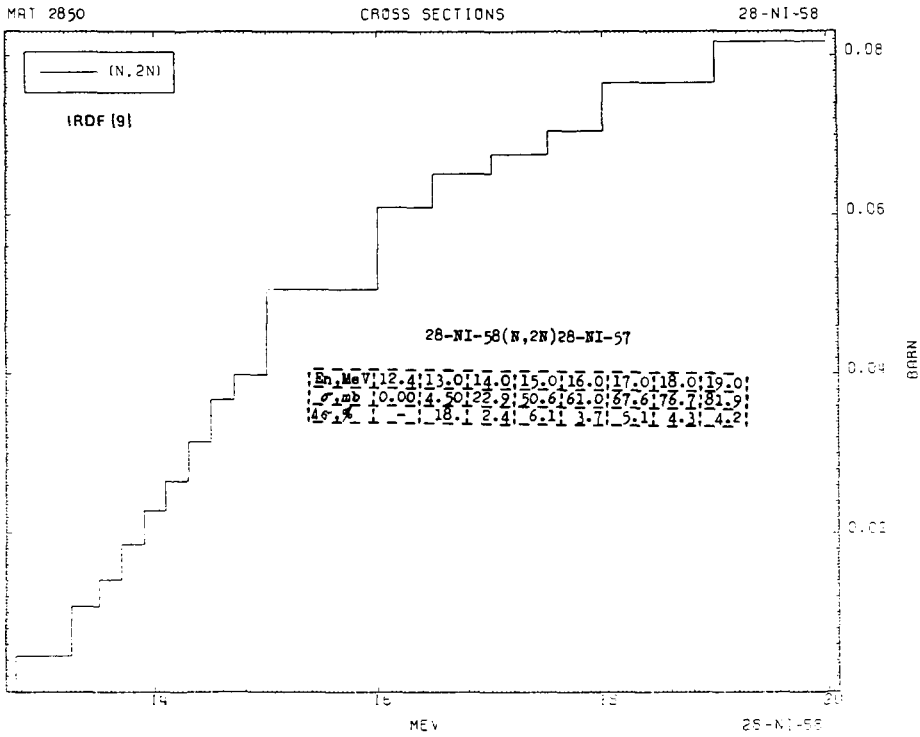
MAT 2850
CROSS SECTIONS
28-NI-58
(N,2N)
(RDF [9])
28-NI-58(N,2N)28-NI-57
En,MeV 12.4 13.0 14.0 15.0 16.0 17.0 18.0 19.0
σ,mb 10.00 4.50 22.9 50.6 61.0 67.6 76.7 81.9
Δσ/σ % 1 - 18.1 2.4 6.1 3.7 5.1 4.3 4.2
0.08
0.06
0.04
0.02
BARN
MEV
28-NI-58

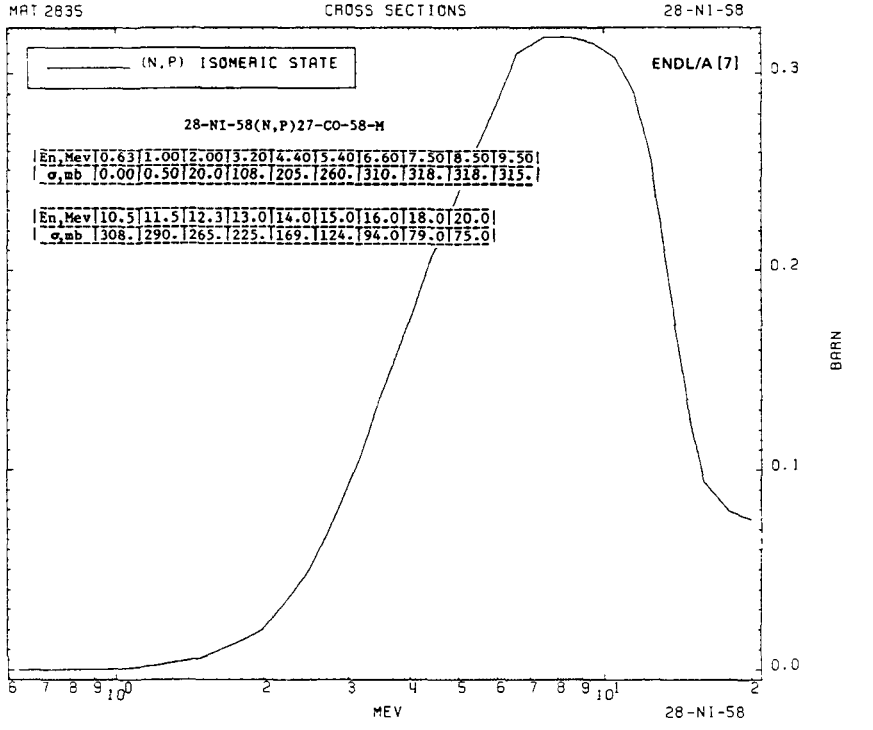
MAT 2835
CROSS SECTIONS
28-NI-58
(N,P) ISOMERIC STATE
ENDL/A [7]
28-NI-58(N,P)27-CO-58-M
En,Mev 0.63 1.00 2.00 3.20 4.40 5.40 6.60 7.50 8.50 9.50
σ,mb 0.00 0.50 20.0 108. 205. 260. 310. 318. 318. 315.
En,Mev 10.5 11.5 12.3 13.0 14.0 15.0 16.0 18.0 20.0
σ,mb 308. 290. 265. 225. 169. 124. 94.0 79.0 75.0
0.3
0.2
0.1
0.0
BARN
MEV
28-NI-58

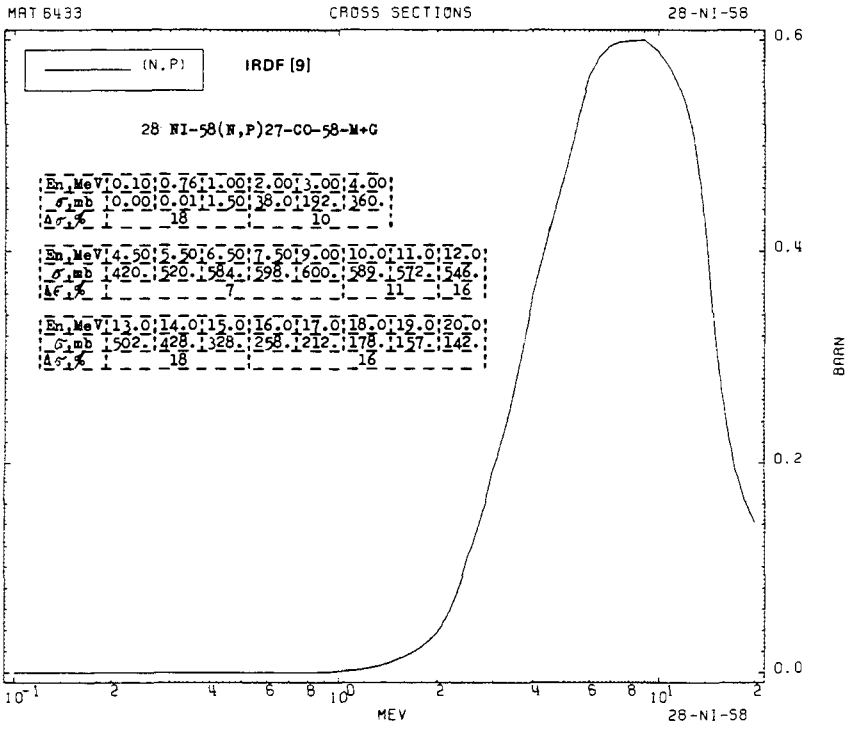
MAT 6433
CROSS SECTIONS
28-NI-58
(N,P)
IRDF [9]
28 NI-58(N,P)27-CO-58-M+G
En,MeV 0.10 0.76 1.00 2.00 3.00 4.00
σ,mb 0.00 0.01 1.50 38.0 192. 360.
Δσ,% 18 10
En,MeV 4.50 5.50 6.50 7.50 9.00 10.0 11.0 12.0
σ,mb 420. 520. 584. 598. 600. 589. 572. 546.
Δσ,% 7 11 16
En,MeV 13.0 14.0 15.0 16.0 17.0 18.0 19.0 20.0
σ,mb 502. 428. 328. 258. 212. 178. 157. 142.
Δσ,% 18 16
0.6
0.4
0.2
0.0
BARN
10^-1 2 4 6 8 10^0 2 4 6 8 10^1 2
MEV
28-NI-58

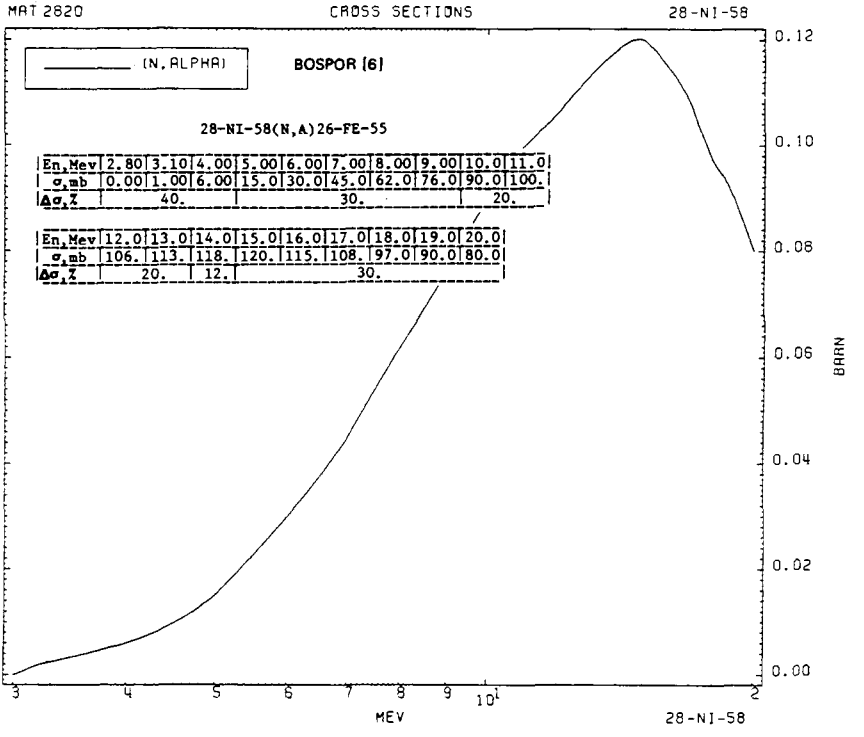
MAT 2820
CROSS SECTIONS
28-NI-58
(N,ALPHA)
BOSPOR [6]
28-NI-58(N,A)26-FE-55
En,Mev 2.80 3.10 4.00 5.00 6.00 7.00 8.00 9.00 10.0 11.0
σ,mb 0.00 1.00 6.00 15.0 30.0 45.0 62.0 76.0 90.0 100.
Δσ,% 40. 30. 20.
En,Mev 12.0 13.0 14.0 15.0 16.0 17.0 18.0 19.0 20.0
σ,mb 106. 113. 118. 120. 115. 108. 97.0 90.0 80.0
Δσ,% 20. 12. 30.
0.12
0.10
0.08
0.06
0.04
0.02
0.00
BARN
3 4 5 6 7 8 9 10^1 2
MEV
28-NI-58

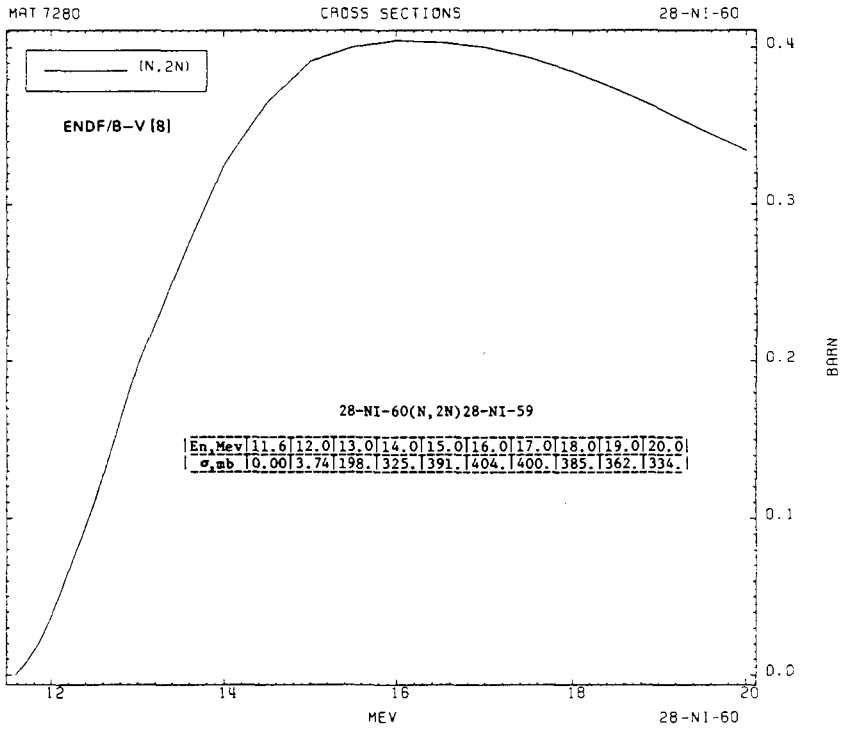
MAT 7280
CROSS SECTIONS
28-NI-60
(N,2N)
ENDF/B-V [8]
28-NI-60(N,2N)28-NI-59
En,Mev | 11.6 | 12.0 | 13.0 | 14.0 | 15.0 | 16.0 | 17.0 | 18.0 | 19.0 | 20.0
σ,mb | 0.00 | 3.74 | 198. | 325. | 391. | 404. | 400. | 385. | 362. | 334.
0.4
0.3
0.2
0.1
0.0
BARN
12
14
16
18
20
MEV
28-NI-60

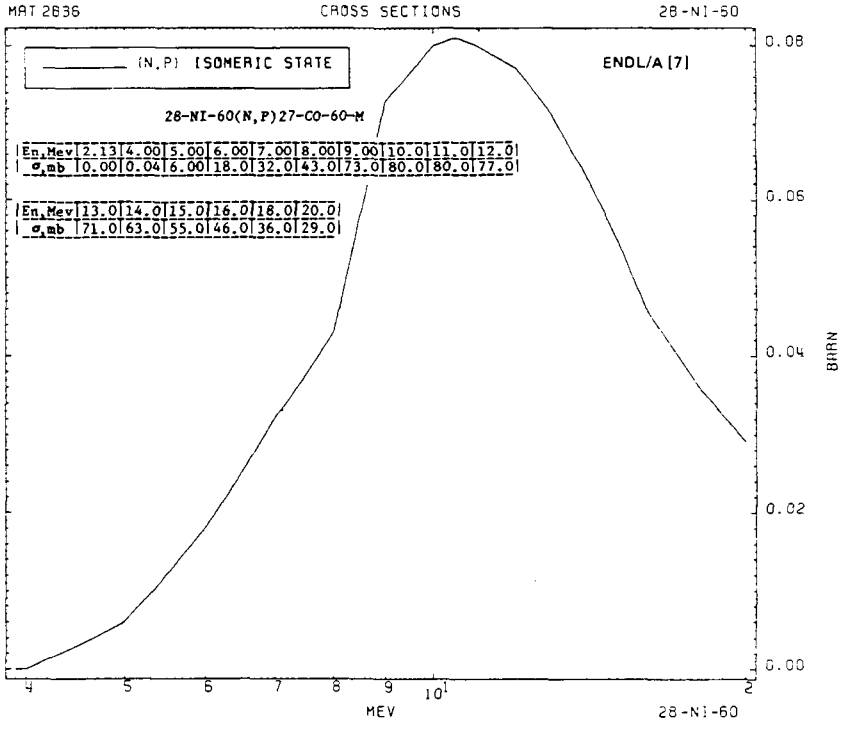
MAT 2836
CROSS SECTIONS
28-NI-60
(N,P) ISOMERIC STATE
ENDL/A [7]
28-NI-60(N,P)27-CO-60-M
En,Mev | 2.13 | 4.00 | 5.00 | 6.00 | 7.00 | 8.00 | 9.00 | 10.0 | 11.0 | 12.0
σ,mb | 0.00 | 0.04 | 6.00 | 18.0 | 32.0 | 43.0 | 73.0 | 80.0 | 80.0 | 77.0
En,Mev | 13.0 | 14.0 | 15.0 | 16.0 | 18.0 | 20.0
σ,mb | 71.0 | 63.0 | 55.0 | 46.0 | 36.0 | 29.0
0.08
0.06
0.04
0.02
0.00
BARN
4
5
6
7
8
9
10
2
MEV
28-NI-60

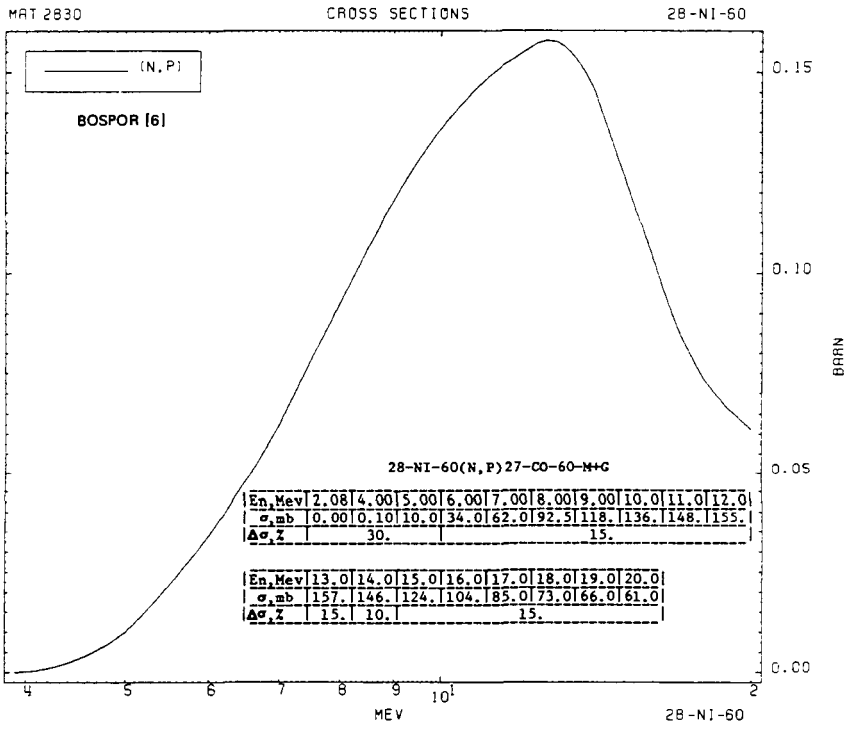
MAT 2830
CROSS SECTIONS
28-NI-60
(N,P)
BOSPOR [6]
28-NI-60(N,P)27-CO-60-M+G
En,Mev | 2.08 | 4.00 | 5.00 | 6.00 | 7.00 | 8.00 | 9.00 | 10.0 | 11.0 | 12.0
σ,mb | 0.00 | 0.10 | 10.0 | 34.0 | 62.0 | 92.5 | 118. | 136. | 148. | 155.
Δσ,% | 30. | 15.
En,Mev | 13.0 | 14.0 | 15.0 | 16.0 | 17.0 | 18.0 | 19.0 | 20.0
σ,mb | 157. | 146. | 124. | 104. | 85.0 | 73.0 | 66.0 | 61.0
Δσ,% | 15. | 10. | 15.
0.15
0.10
0.05
0.00
BARN
4 5 6 7 8 9 10¹ 2
MEV
28-NI-60

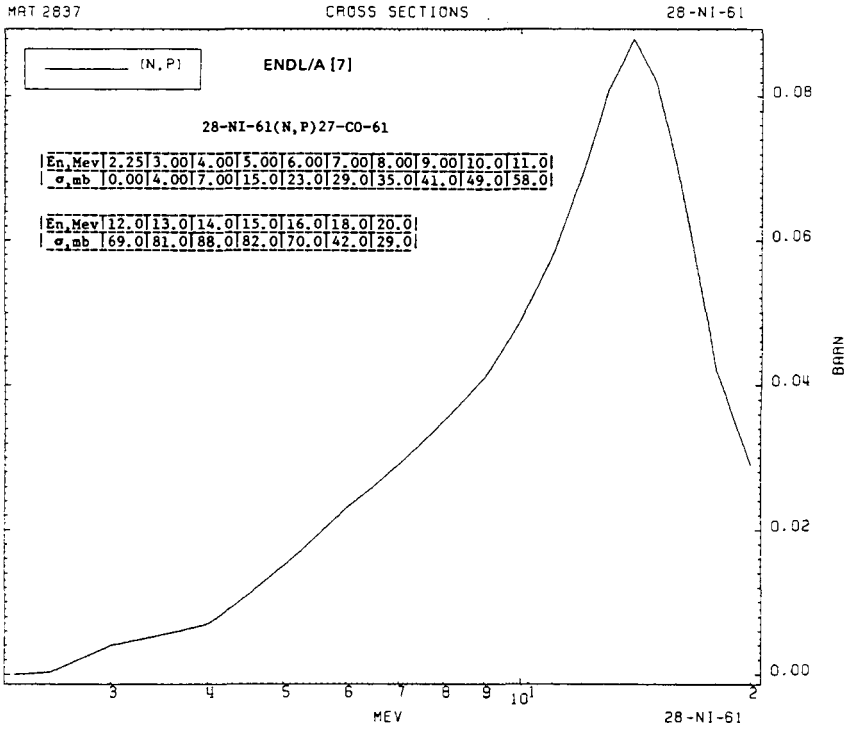
MAT 2837
CROSS SECTIONS
28-NI-61
(N,P)
ENDL/A [7]
28-NI-61(N,P)27-CO-61
En,Mev | 2.25 | 3.00 | 4.00 | 5.00 | 6.00 | 7.00 | 8.00 | 9.00 | 10.0 | 11.0
σ,mb | 0.00 | 4.00 | 7.00 | 15.0 | 23.0 | 29.0 | 35.0 | 41.0 | 49.0 | 58.0
En,Mev | 12.0 | 13.0 | 14.0 | 15.0 | 16.0 | 18.0 | 20.0
σ,mb | 69.0 | 81.0 | 88.0 | 82.0 | 70.0 | 42.0 | 29.0
0.08
0.06
0.04
0.02
0.00
BARN
3 4 5 6 7 8 9 10¹ 2
MEV
28-NI-61

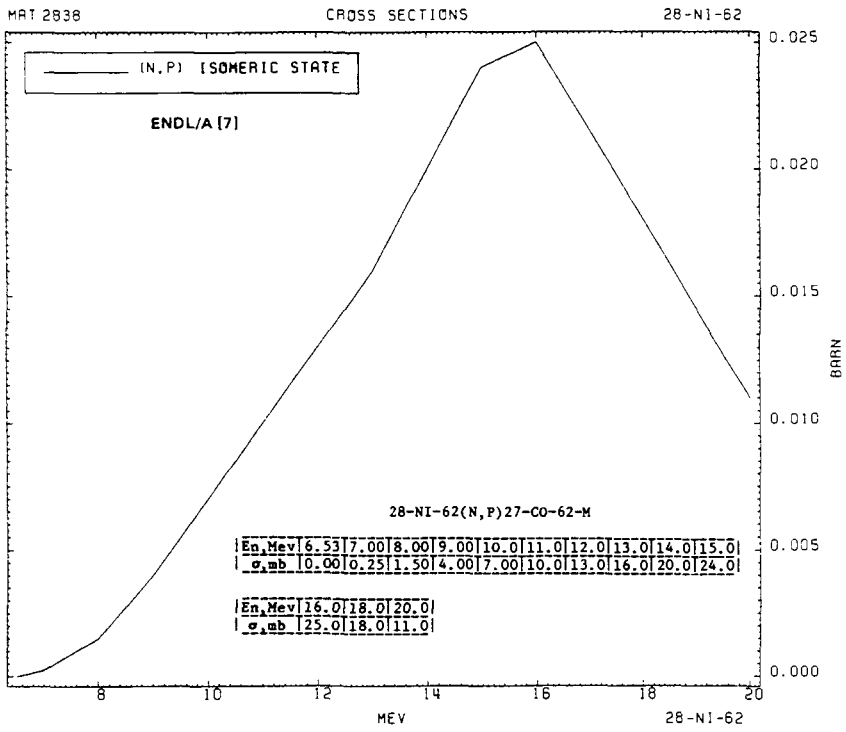
MAT 2838
CROSS SECTIONS
28-NI-62
(N,P) ISOMERIC STATE
ENDL/A [7]
28-NI-62(N,P)27-CO-62-M
En,Mev | 6.5 | 7.00 | 8.00 | 9.00 | 10.0 | 11.0 | 12.0 | 13.0 | 14.0 | 15.0
σ,mb | 0.00 | 0.25 | 1.50 | 4.00 | 7.00 | 10.0 | 13.0 | 16.0 | 20.0 | 24.0
En,Mev | 16.0 | 18.0 | 20.0
σ,mb | 25.0 | 18.0 | 11.0
0.025
0.020
0.015
0.010
0.005
0.000
BARN
8
10
12
14
16
18
20
MEV
28-NI-62

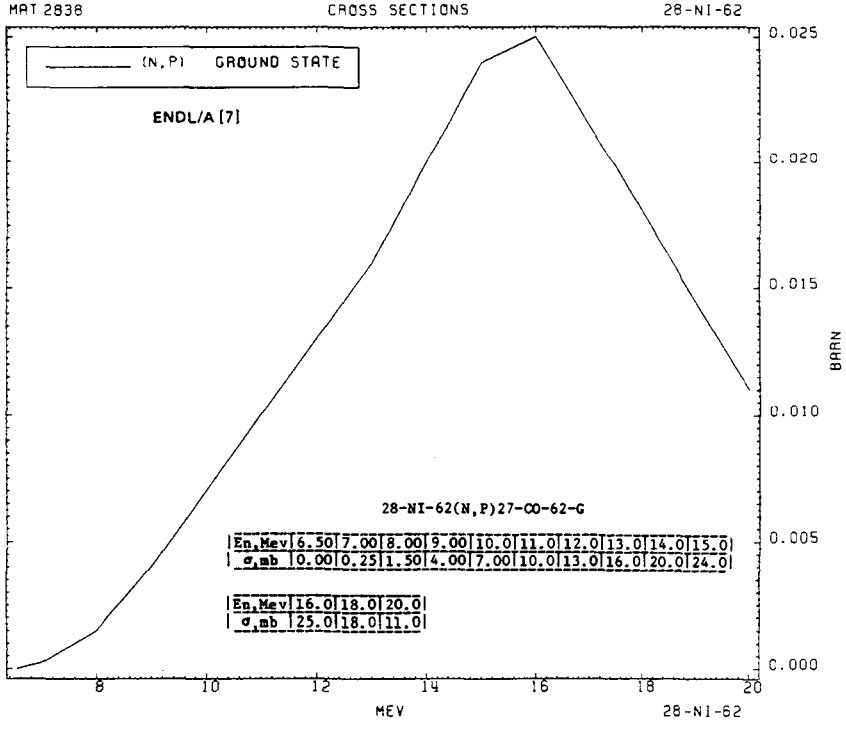
MAT 2838
CROSS SECTIONS
28-NI-62
(N,P) GROUND STATE
ENDL/A [7]
28-NI-62(N,P)27-CO-62-G
En,Mev | 6.50 | 7.00 | 8.00 | 9.00 | 10.0 | 11.0 | 12.0 | 13.0 | 14.0 | 15.0
σ,mb | 0.00 | 0.25 | 1.50 | 4.00 | 7.00 | 10.0 | 13.0 | 16.0 | 20.0 | 24.0
En,Mev | 16.0 | 18.0 | 20.0
σ,mb | 25.0 | 18.0 | 11.0
0.025
0.020
0.015
0.010
0.005
0.000
BARN
8
10
12
14
16
18
20
MEV
28-NI-62

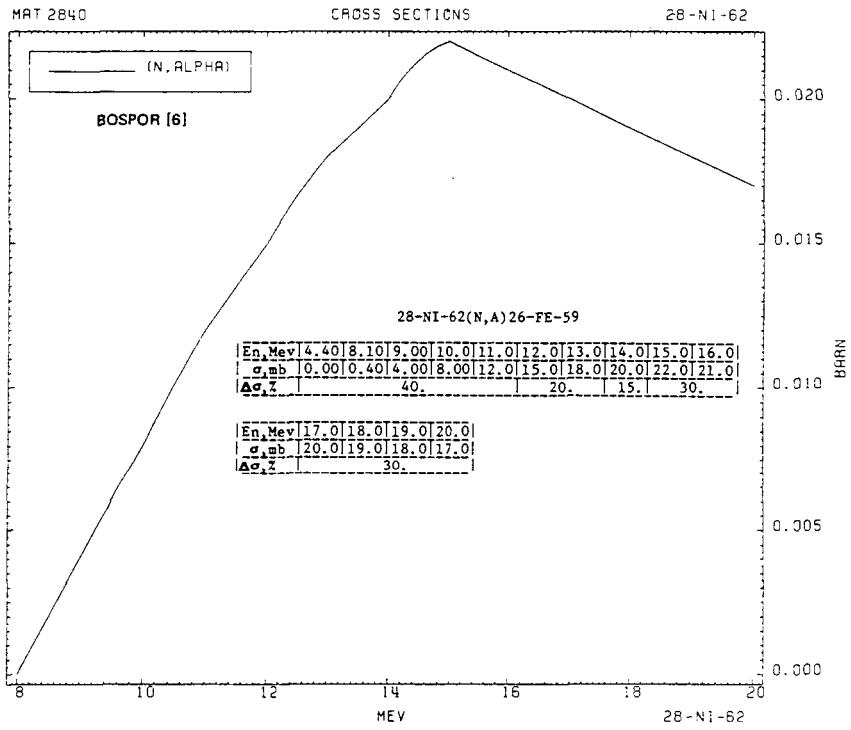
MAT 2840
CROSS SECTIONS
28-NI-62
(N,ALPHA)
BOSPOR [6]
28-NI-62(N,A)26-FE-59
En,Mev | 4.40 | 8.10 | 9.00 | 10.0 | 11.0 | 12.0 | 13.0 | 14.0 | 15.0 | 16.0
σ,mb | 0.00 | 0.40 | 4.00 | 8.00 | 12.0 | 15.0 | 18.0 | 20.0 | 22.0 | 21.0
Δσ,% | 40. | 20. | 15. | 30.
En,Mev | 17.0 | 18.0 | 19.0 | 20.0
σ,mb | 20.0 | 19.0 | 18.0 | 17.0
Δσ,% | 30.
0.020
0.015
0.010
0.005
0.000
BARN
8
10
12
14
16
18
20
MEV
28-NI-62

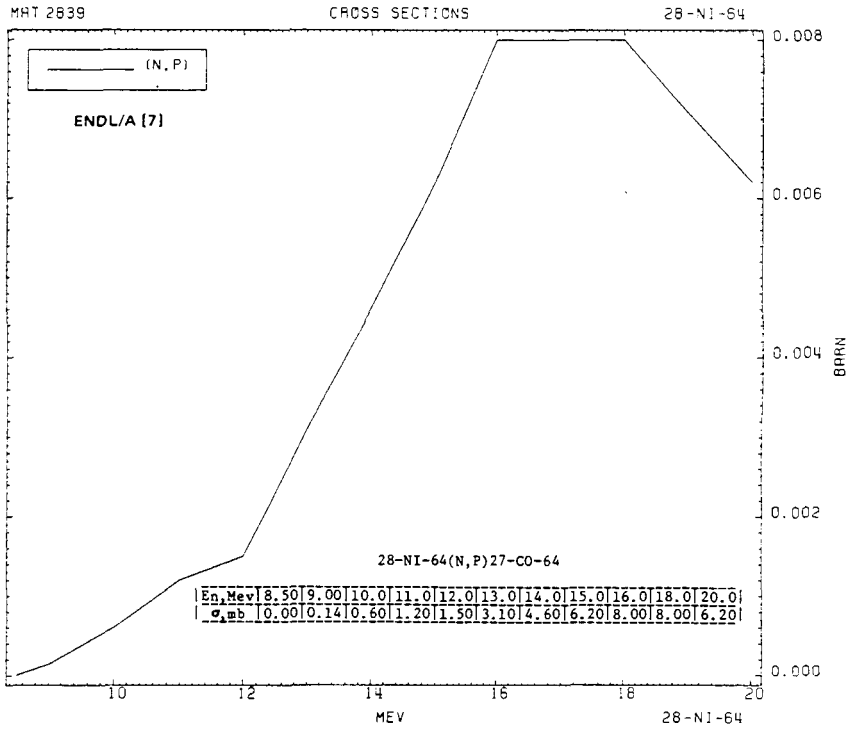
MAT 2839
CROSS SECTIONS
28-NI-64
(N,P)
ENDL/A [7]
28-NI-64(N,P)27-CO-64
En,Mev | 8.50 | 9.00 | 10.0 | 11.0 | 12.0 | 13.0 | 14.0 | 15.0 | 16.0 | 18.0 | 20.0
σ,mb | 0.00 | 0.14 | 0.60 | 1.20 | 1.50 | 3.10 | 4.60 | 6.20 | 8.00 | 8.00 | 6.20
0.008
0.006
0.004
0.002
0.000
BARN
10
12
14
16
18
20
MEV
28-NI-64

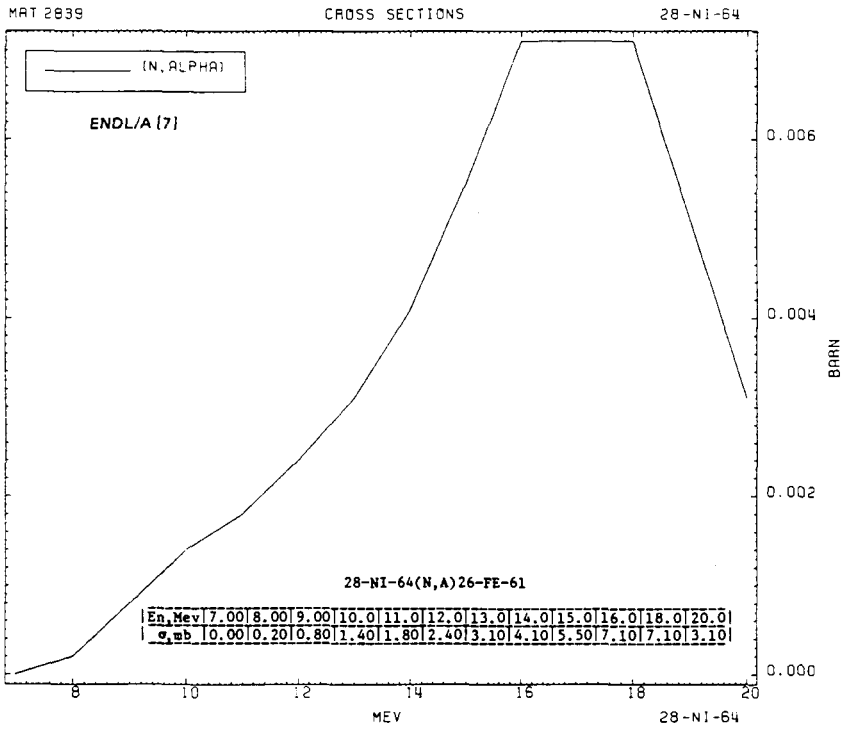
MAT 2839
CROSS SECTIONS
28-NI-64
(N,ALPHA)
ENDL/A [7]
0.006
0.004
0.002
0.000
BARN
28-NI-64(N,A)26-FE-61
En,Mev | 7.00 | 8.00 | 9.00 | 10.0 | 11.0 | 12.0 | 13.0 | 14.0 | 15.0 | 16.0 | 18.0 | 20.0
σ,mb | 0.00 | 0.20 | 0.80 | 1.40 | 1.80 | 2.40 | 3.10 | 4.10 | 5.50 | 7.10 | 7.10 | 3.10
8
10
12
14
16
18
20
MEV
28-NI-64

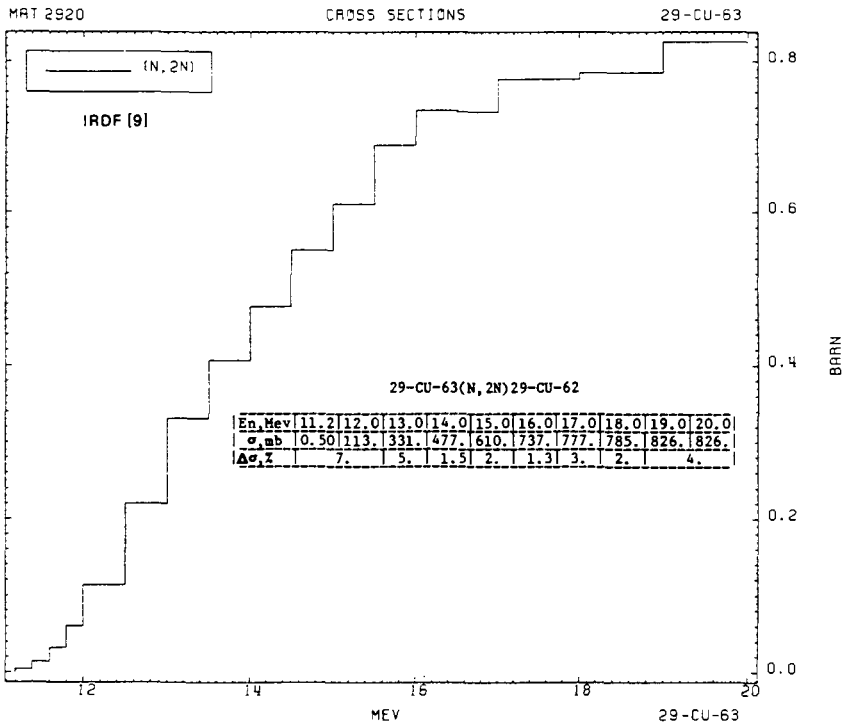
MAT 2920
CROSS SECTIONS
29-CU-63
(N,2N)
IRDF [9]
0.8
0.6
0.4
0.2
0.0
BARN
29-CU-63(N,2N)29-CU-62
En,Mev | 11.2 | 12.0 | 13.0 | 14.0 | 15.0 | 16.0 | 17.0 | 18.0 | 19.0 | 20.0
σ,mb | 0.50 | 113. | 331. | 477. | 610. | 737. | 777. | 785. | 826. | 826.
Δσ,% | 7. | 5. | 1.5 | 2. | 1.3 | 3. | 2. | 4.
12
14
16
18
20
MEV
29-CU-63

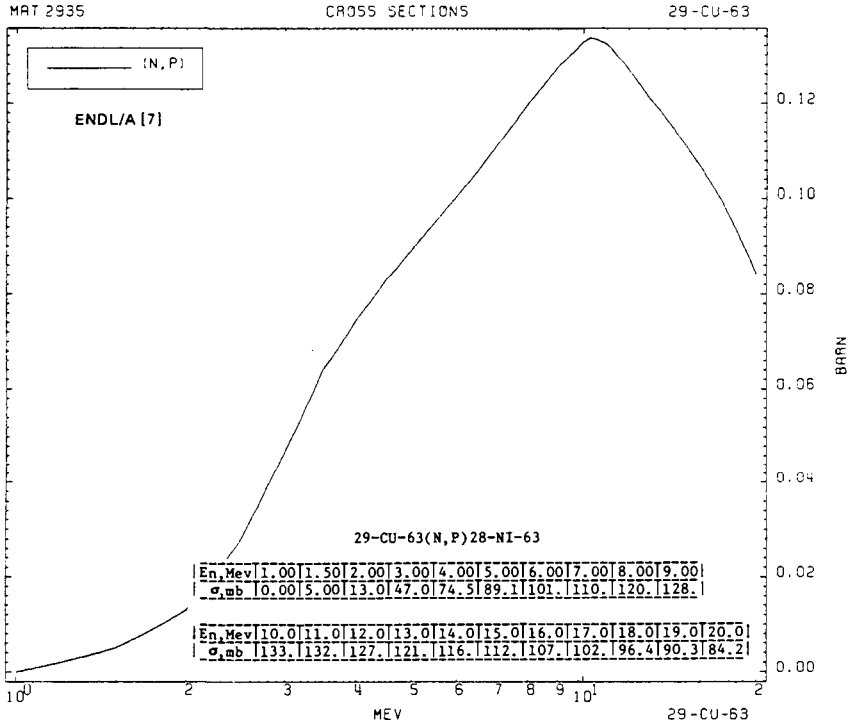
MAT 2935
CROSS SECTIONS
29-CU-63
(N,P)
ENDL/A [7]
29-CU-63(N,P)28-NI-63
En,Mev 1.00 1.50 2.00 3.00 4.00 5.00 6.00 7.00 8.00 9.00
σ,mb 0.00 5.00 13.0 47.0 74.5 89.1 101. 110. 120. 128.
En,Mev 10.0 11.0 12.0 13.0 14.0 15.0 16.0 17.0 18.0 19.0 20.0
σ,mb 133. 132. 127. 121. 116. 112. 107. 102. 96.4 90.3 84.2
BARN
MEV
29-CU-63

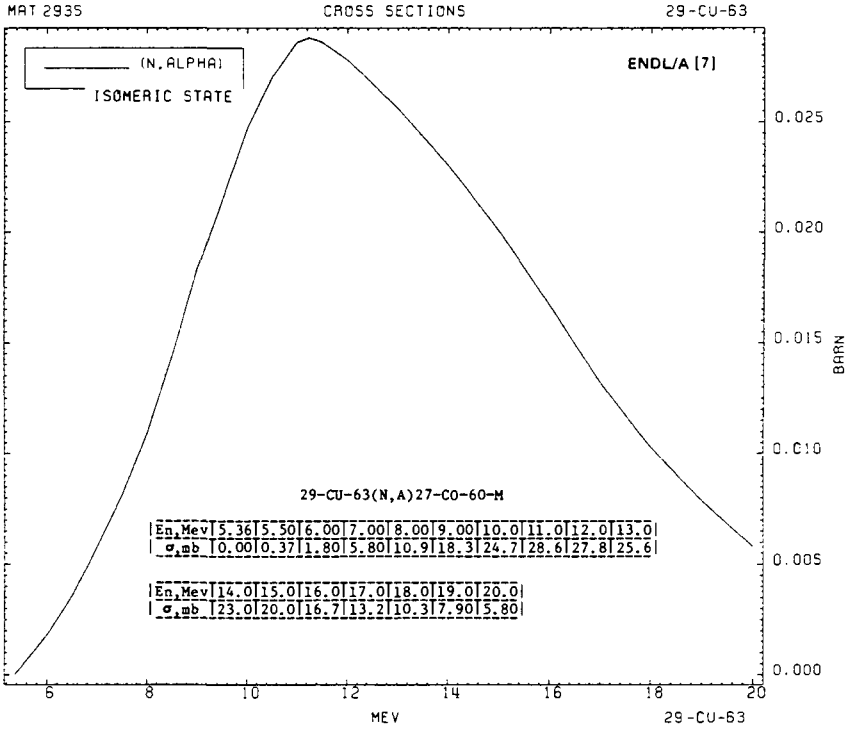
MAT 2935
CROSS SECTIONS
29-CU-63
(N,ALPHA)
ISOMERIC STATE
ENDL/A [7]
29-CU-63(N,A)27-CO-60-M
En,Mev 5.36 5.50 6.00 7.00 8.00 9.00 10.0 11.0 12.0 13.0
σ,mb 0.00 0.37 1.80 5.80 10.9 18.3 24.7 28.6 27.8 25.6
En,Mev 14.0 15.0 16.0 17.0 18.0 19.0 20.0
σ,mb 23.0 20.0 16.7 13.2 10.3 7.90 5.80
BARN
MEV
29-CU-63

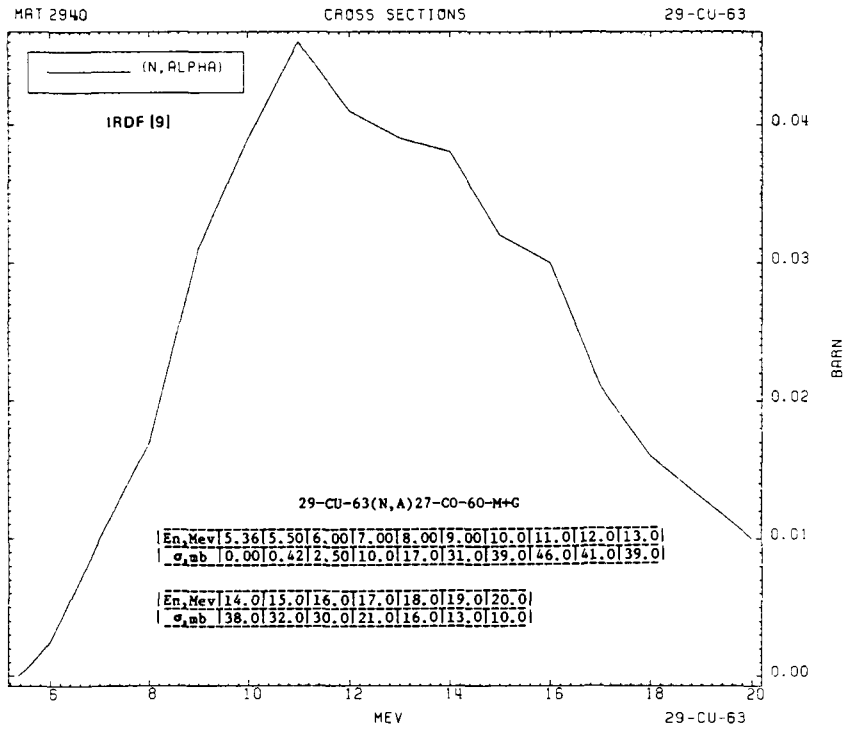
MAT 2940
CROSS SECTIONS
29-CU-63
(N,ALPHA)
IRDF [9]
29-CU-63(N,A)27-CO-60-M+G
En,Mev | 5.36 | 5.50 | 6.00 | 7.00 | 8.00 | 9.00 | 10.0 | 11.0 | 12.0 | 13.0
σ,mb | 0.00 | 0.42 | 2.50 | 10.0 | 17.0 | 31.0 | 39.0 | 46.0 | 41.0 | 39.0
En,Mev | 14.0 | 15.0 | 16.0 | 17.0 | 18.0 | 19.0 | 20.0
σ,mb | 38.0 | 32.0 | 30.0 | 21.0 | 16.0 | 13.0 | 10.0
0.04
0.03
0.02
0.01
0.00
BARN
5
8
10
12
14
16
18
20
MEV
29-CU-63

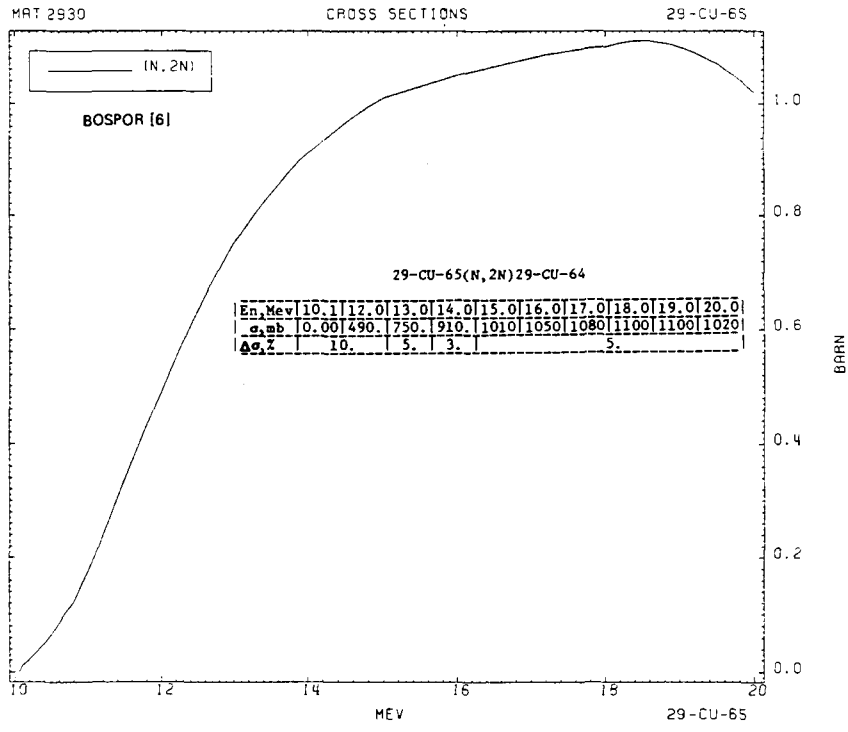
MAT 2930
CROSS SECTIONS
29-CU-65
(N,2N)
BOSPOR [6]
29-CU-65(N,2N)29-CU-64
En,Mev | 10.1 | 12.0 | 13.0 | 14.0 | 15.0 | 16.0 | 17.0 | 18.0 | 19.0 | 20.0
σ,mb | 0.00 | 490. | 750. | 910. | 1010 | 1050 | 1080 | 1100 | 1100 | 1020
Δσ,% | 10. | 5. | 3. | 5.
1.0
0.8
0.6
0.4
0.2
0.0
BARN
10
12
14
16
18
20
MEV
29-CU-65

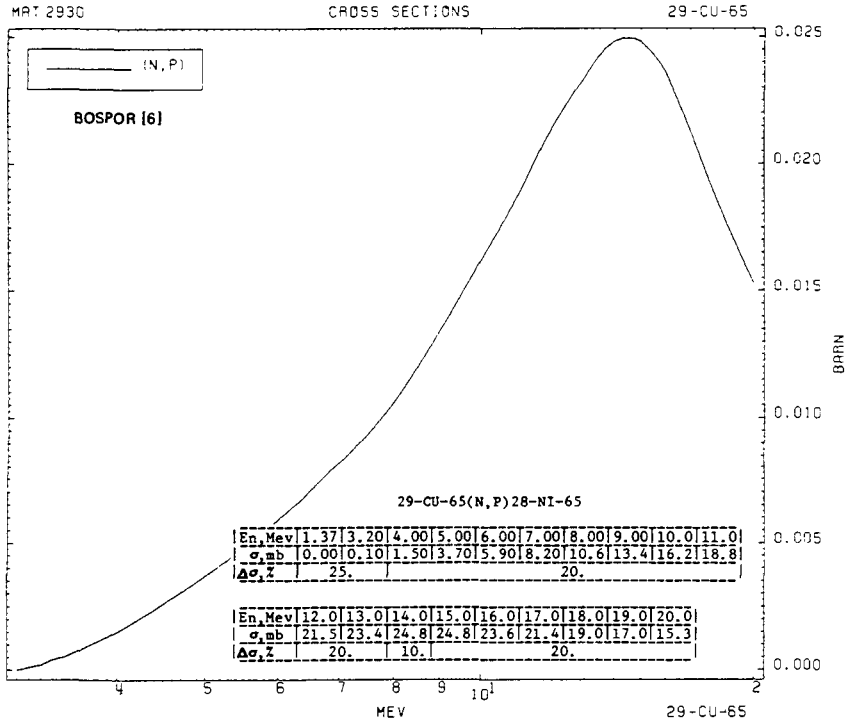
MAT 2930
CROSS SECTIONS
29-CU-65
(N,P)
BOSPOR [6]
29-CU-65(N,P)28-NI-65
En,Mev | 1.37 | 3.20 | 4.00 | 5.00 | 6.00 | 7.00 | 8.00 | 9.00 | 10.0 | 11.0
σ,mb | 0.00 | 0.10 | 1.50 | 3.70 | 5.90 | 8.20 | 10.6 | 13.4 | 16.2 | 18.8
Δσ,% | 25. | 20.
En,Mev | 12.0 | 13.0 | 14.0 | 15.0 | 16.0 | 17.0 | 18.0 | 19.0 | 20.0
σ,mb | 21.5 | 23.4 | 24.8 | 24.8 | 23.6 | 21.4 | 19.0 | 17.0 | 15.3
Δσ,% | 20. | 10. | 20.
0.025
0.020
0.015
0.010
0.005
0.000
BARN
4 5 6 7 8 9 10 2
MEV
29-CU-65

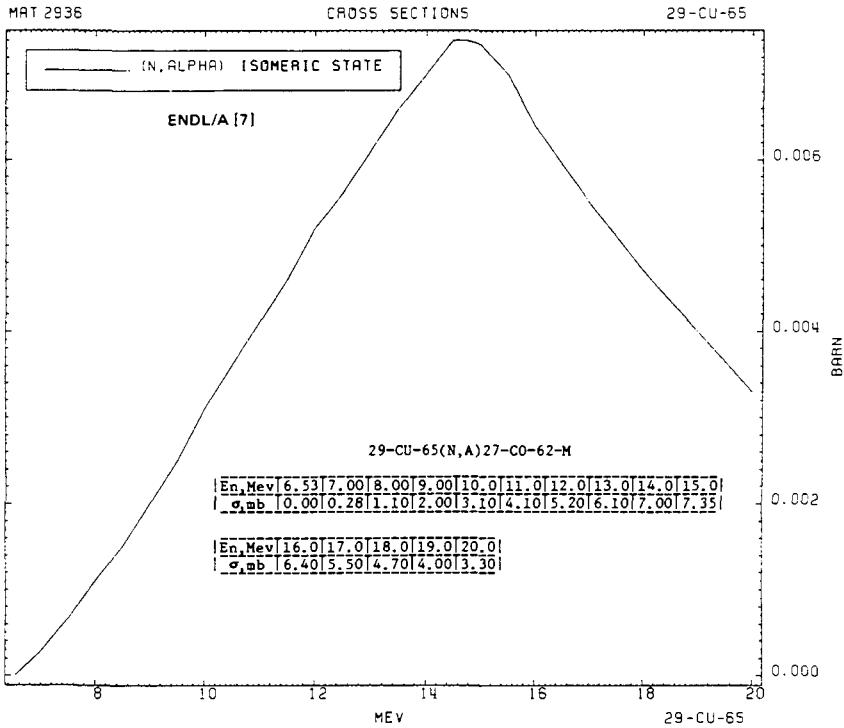
MAT 2936
CROSS SECTIONS
29-CU-65
(N,ALPHA) ISOMERIC STATE
ENDL/A [7]
29-CU-65(N,A)27-CO-62-M
En,Mev | 6.53 | 7.00 | 8.00 | 9.00 | 10.0 | 11.0 | 12.0 | 13.0 | 14.0 | 15.0
σ,mb | 0.00 | 0.28 | 1.10 | 2.00 | 3.10 | 4.10 | 5.20 | 6.10 | 7.00 | 7.35
En,Mev | 16.0 | 17.0 | 18.0 | 19.0 | 20.0
σ,mb | 6.40 | 5.50 | 4.70 | 4.00 | 3.30
0.006
0.004
0.002
0.000
BARN
8 10 12 14 16 18 20
MEV
29-CU-65

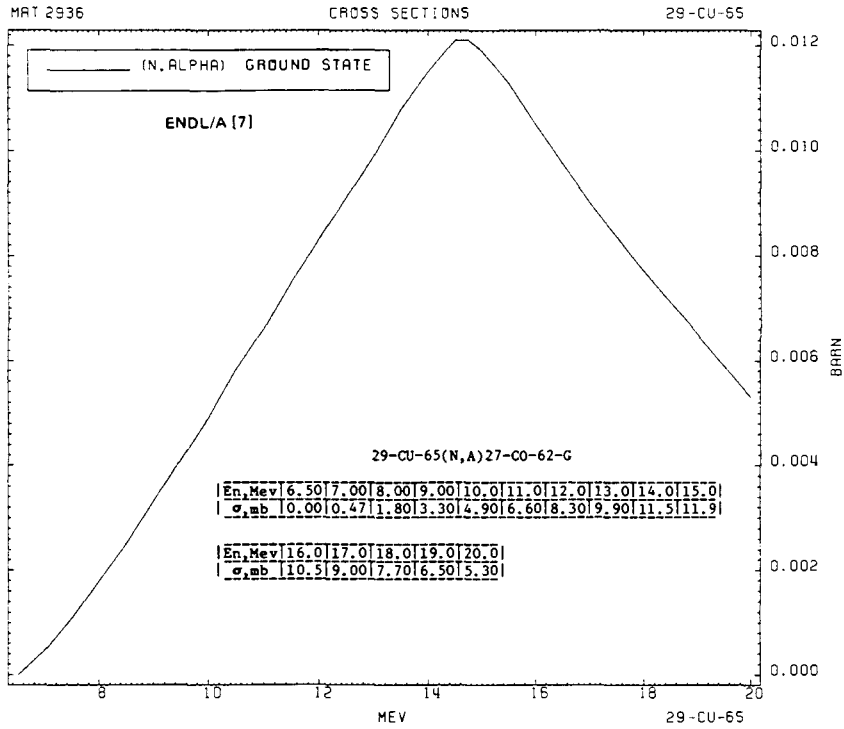
MAT 2936
CROSS SECTIONS
29-CU-65
(N,ALPHA) GROUND STATE
ENDL/A [7]
29-CU-65(N,A)27-CO-62-G
En,Mev 6.50 7.00 8.00 9.00 10.0 11.0 12.0 13.0 14.0 15.0
σ,mb 0.00 0.47 1.80 3.30 4.90 6.60 8.30 9.90 11.5 11.9
En,Mev 16.0 17.0 18.0 19.0 20.0
σ,mb 10.5 9.00 7.70 6.50 5.30
0.012
0.010
0.008
0.006
0.004
0.002
0.000
BARN
8
10
12
14
16
18
20
MEV
29-CU-65

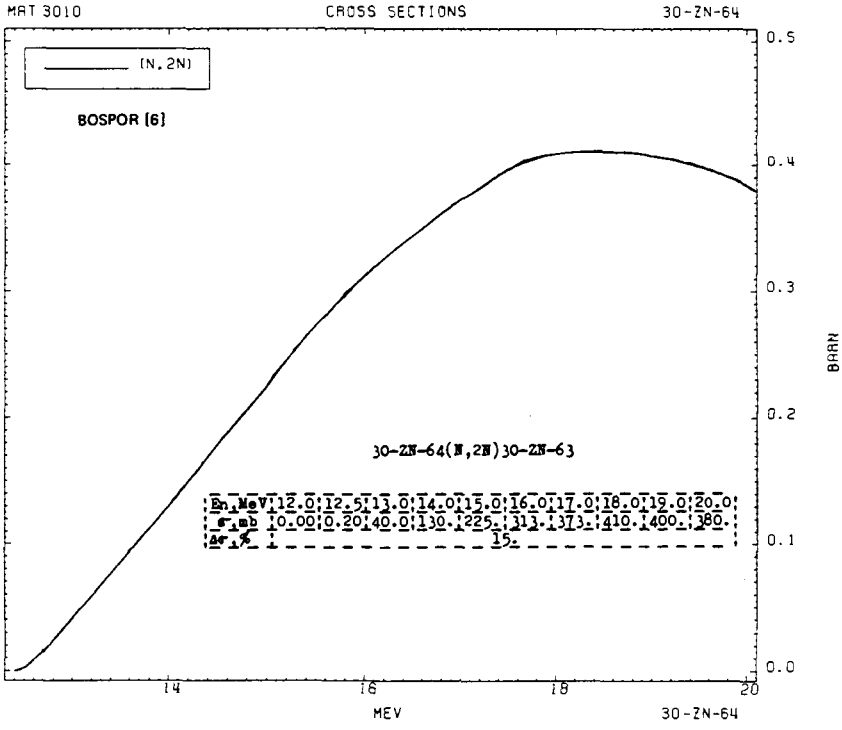
MAT 3010
CROSS SECTIONS
30-ZN-64
(N,2N)
BOSPOR [6]
30-ZN-64(N,2N)30-ZN-63
En,MeV 12.0 12.5 13.0 14.0 15.0 16.0 17.0 18.0 19.0 20.0
σ,mb 0.00 0.20 40.0 130. 225. 311. 373. 410. 400. 380.
Δσ,% 15.
0.5
0.4
0.3
0.2
0.1
0.0
BARN
14
16
18
20
MEV
30-ZN-64

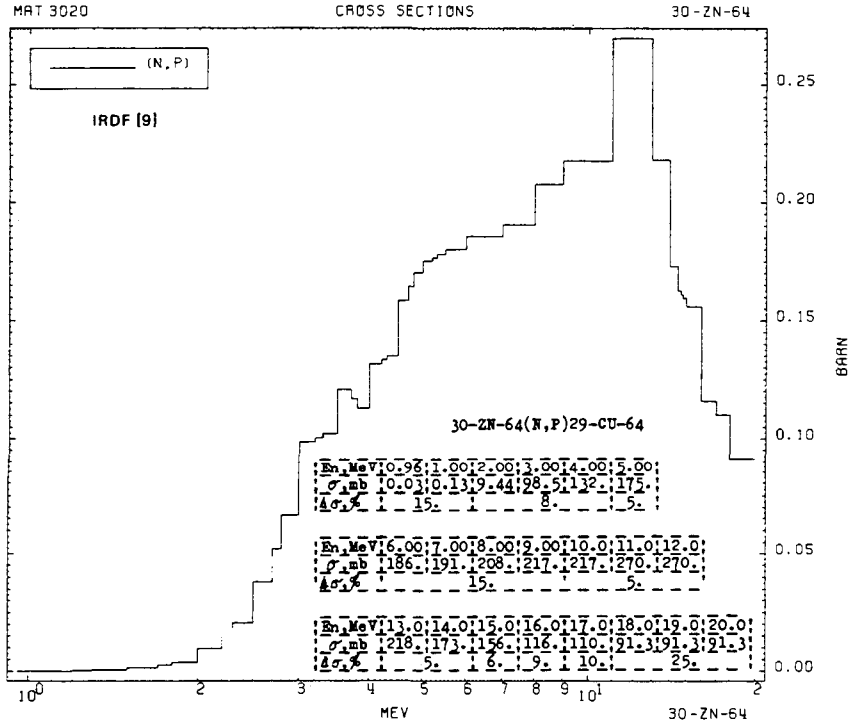
MAT 3020
CROSS SECTIONS
30-ZN-64
(N,P)
IRDF [9]
30-ZN-64(N,P)29-CU-64
En,MeV 0.96 1.00 2.00 3.00 4.00 5.00
σ,mb 0.03 0.13 9.44 98.5 132. 175.
Δσ,% 15. 8. 5.
En,MeV 6.00 7.00 8.00 9.00 10.0 11.0 12.0
σ,mb 186. 191. 208. 217. 217. 270. 270.
Δσ,% 15. 5.
En,MeV 13.0 14.0 15.0 16.0 17.0 18.0 19.0 20.0
σ,mb 218. 173. 156. 116. 110. 21.3 91.2 21.3
Δσ,% 5. 6. 9. 10. 25.
BARN
MEV
30-ZN-64

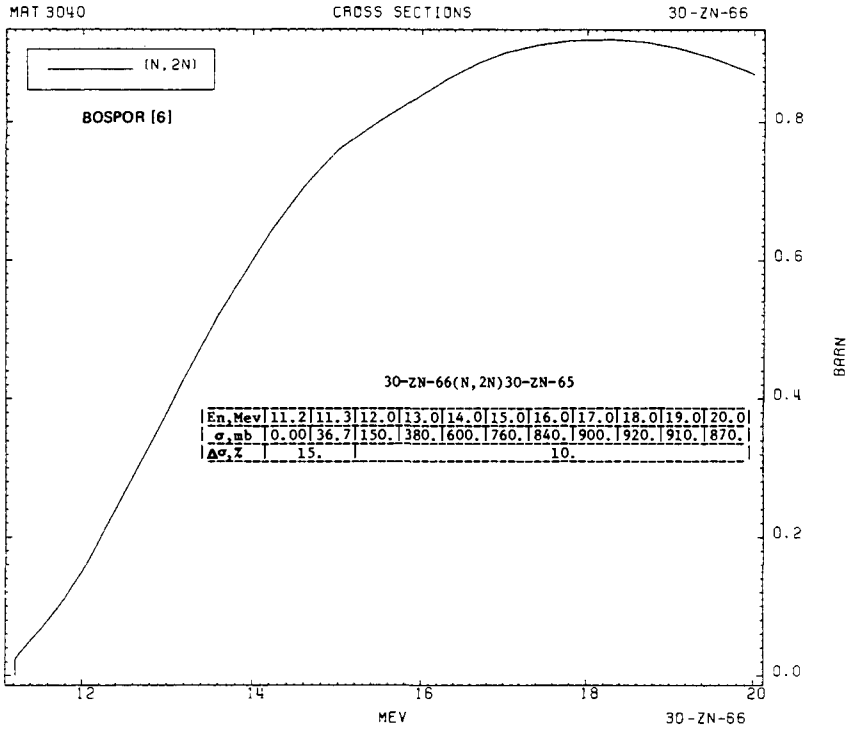
MAT 3040
CROSS SECTIONS
30-ZN-66
(N,2N)
BOSPOR [6]
30-ZN-66(N,2N)30-ZN-65
En,Mev 11.2 11.3 12.0 13.0 14.0 15.0 16.0 17.0 18.0 19.0 20.0
σ,mb 0.00 36.7 150. 380. 600. 760. 840. 900. 920. 910. 870.
Δσ,% 15. 10.
BARN
MEV
30-ZN-66

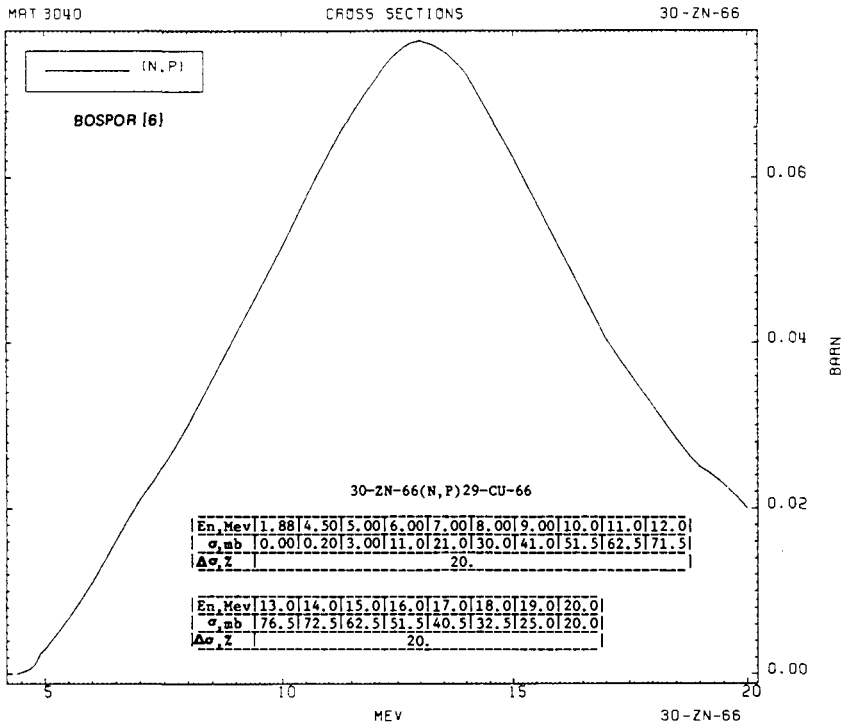
MAT 3040
CROSS SECTIONS
30-ZN-66
(N,P)
BOSPOR [6]
0.06
0.04
0.02
0.00
BARN
30-ZN-66(N,P)29-CU-66
En,Mev | 1.88 | 4.50 | 5.00 | 6.00 | 7.00 | 8.00 | 9.00 | 10.0 | 11.0 | 12.0
σ,mb | 0.00 | 0.20 | 3.00 | 11.0 | 21.0 | 30.0 | 41.0 | 51.5 | 62.5 | 71.5
Δσ,% | 20.
En,Mev | 13.0 | 14.0 | 15.0 | 16.0 | 17.0 | 18.0 | 19.0 | 20.0
σ,mb | 76.5 | 72.5 | 62.5 | 51.5 | 40.5 | 32.5 | 25.0 | 20.0
Δσ,% | 20.
5
10
15
20
MEV
30-ZN-66

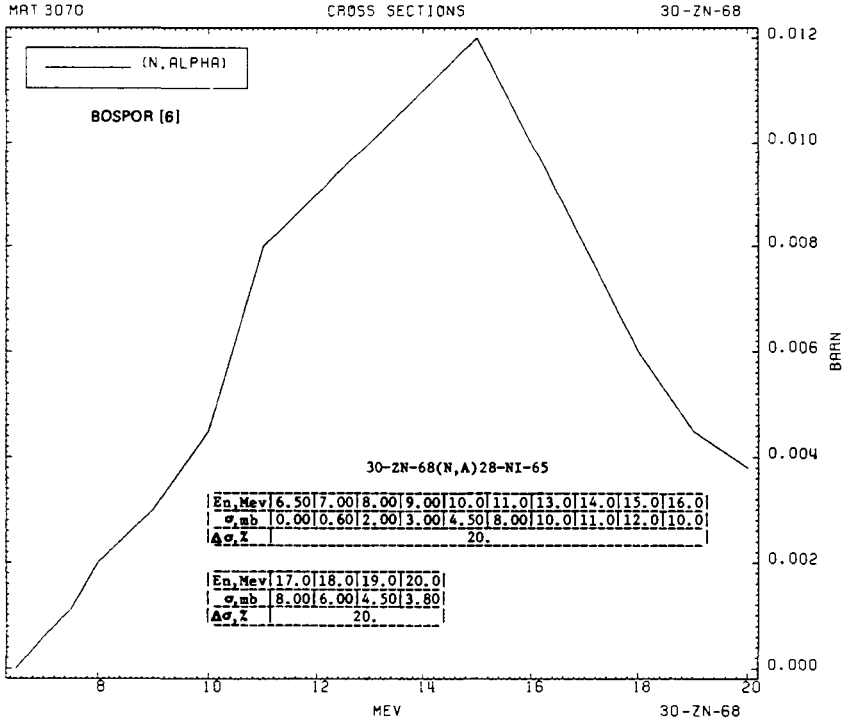
MAT 3070
CROSS SECTIONS
30-ZN-68
(N,ALPHA)
BOSPOR [6]
0.012
0.010
0.008
0.006
0.004
0.002
0.000
BARN
30-ZN-68(N,A)28-NI-65
En,Mev | 6.50 | 7.00 | 8.00 | 9.00 | 10.0 | 11.0 | 13.0 | 14.0 | 15.0 | 16.0
σ,mb | 0.00 | 0.60 | 2.00 | 3.00 | 4.50 | 8.00 | 10.0 | 11.0 | 12.0 | 10.0
Δσ,% | 20.
En,Mev | 17.0 | 18.0 | 19.0 | 20.0
σ,mb | 8.00 | 6.00 | 4.50 | 3.80
Δσ,% | 20.
8
10
12
14
16
18
20
MEV
30-ZN-68

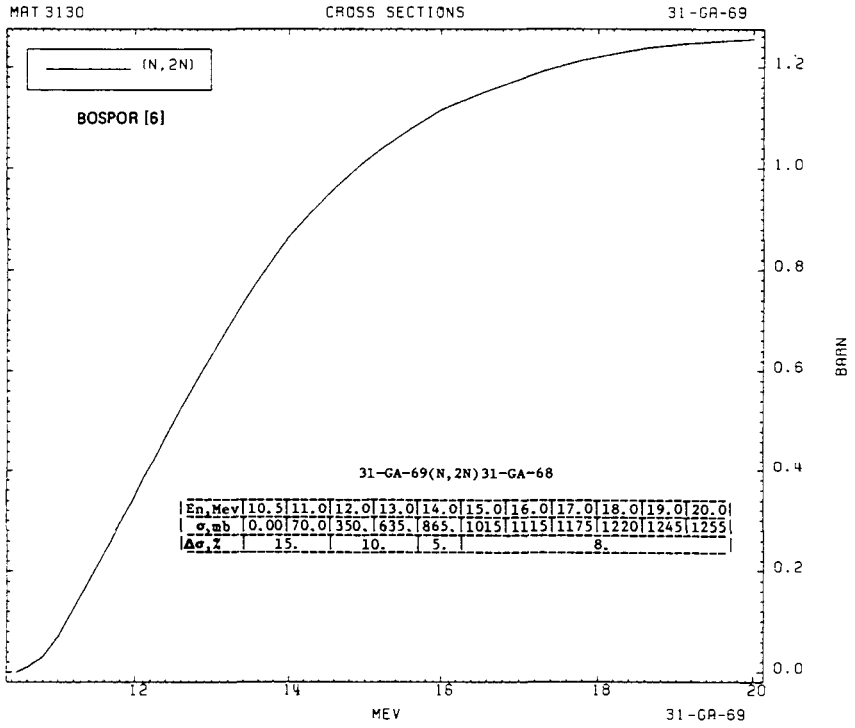
MAT 3130
CROSS SECTIONS
31-GA-69
(N,2N)
BOSPOR [6]
31-GA-69(N,2N)31-GA-68
En,Mev | 10.5 | 11.0 | 12.0 | 13.0 | 14.0 | 15.0 | 16.0 | 17.0 | 18.0 | 19.0 | 20.0
σ,mb | 0.00 | 70.0 | 350. | 635. | 865. | 1015 | 1115 | 1175 | 1220 | 1245 | 1255
Δσ,% | 15. | 10. | 5. | 8.
BARN
MEV
31-GA-69

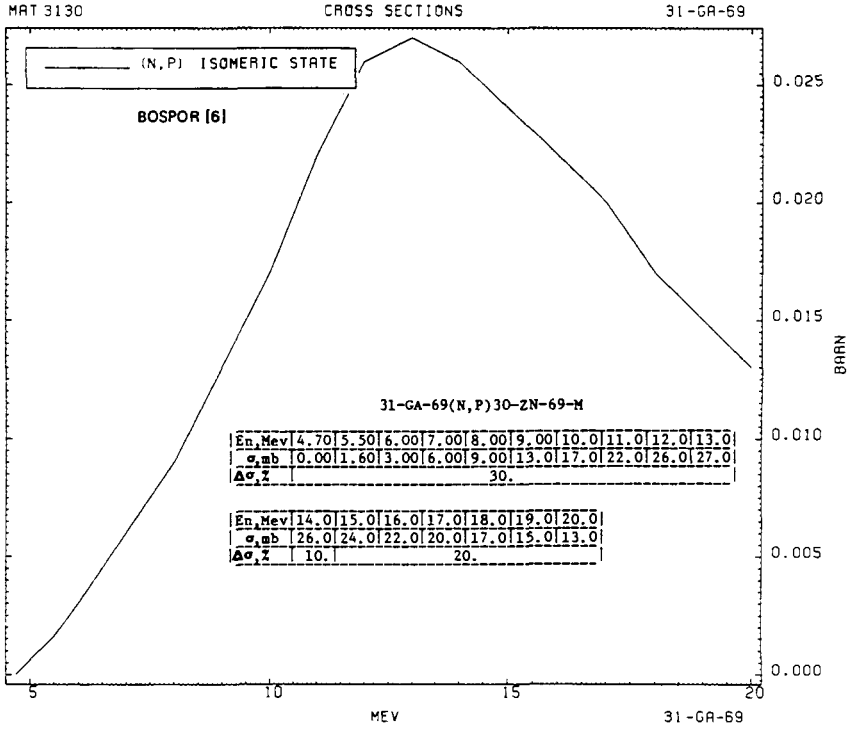
MAT 3130
CROSS SECTIONS
31-GA-69
(N,P) ISOMERIC STATE
BOSPOR [6]
31-GA-69(N,P)30-ZN-69-M
En,Mev | 4.70 | 5.50 | 6.00 | 7.00 | 8.00 | 9.00 | 10.0 | 11.0 | 12.0 | 13.0
σ,mb | 0.00 | 1.60 | 3.00 | 6.00 | 9.00 | 13.0 | 17.0 | 22.0 | 26.0 | 27.0
Δσ,% | 30.
En,Mev | 14.0 | 15.0 | 16.0 | 17.0 | 18.0 | 19.0 | 20.0
σ,mb | 26.0 | 24.0 | 22.0 | 20.0 | 17.0 | 15.0 | 13.0
Δσ,% | 10. | 20.
BARN
MEV
31-GA-69

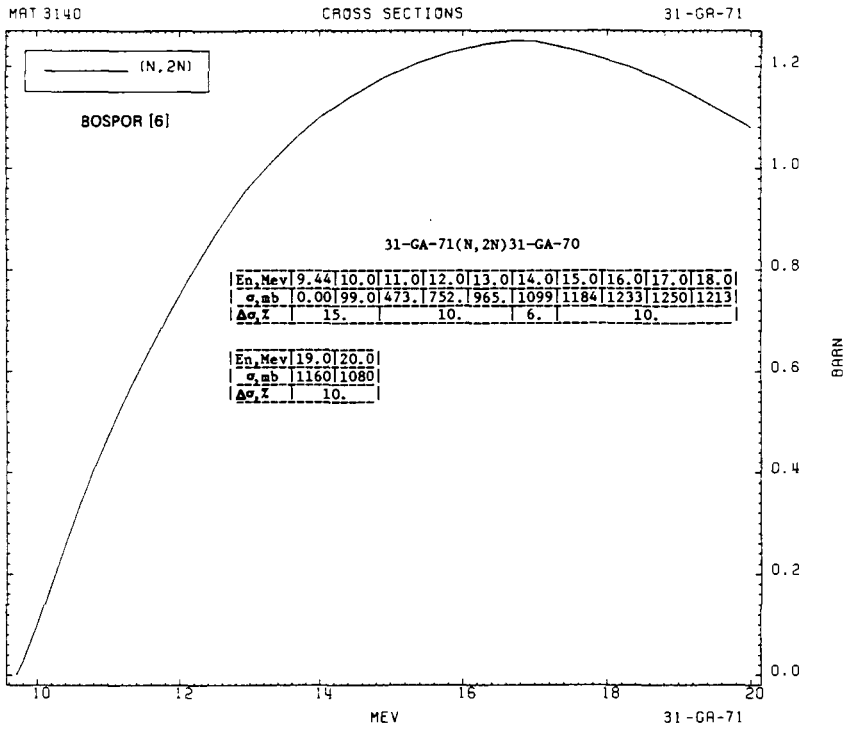
MAT 3140
CROSS SECTIONS
31-GA-71
(N,2N)
BOSPOR [6]
31-GA-71(N,2N)31-GA-70
En,Mev | 9.44 | 10.0 | 11.0 | 12.0 | 13.0 | 14.0 | 15.0 | 16.0 | 17.0 | 18.0
σ,mb | 0.00 | 99.0 | 473. | 752. | 965. | 1099 | 1184 | 1233 | 1250 | 1213
Δσ,% | 15. | 10. | 6. | 10.
En,Mev | 19.0 | 20.0
σ,mb | 1160 | 1080
Δσ,% | 10.
BARN
MEV
31-GA-71

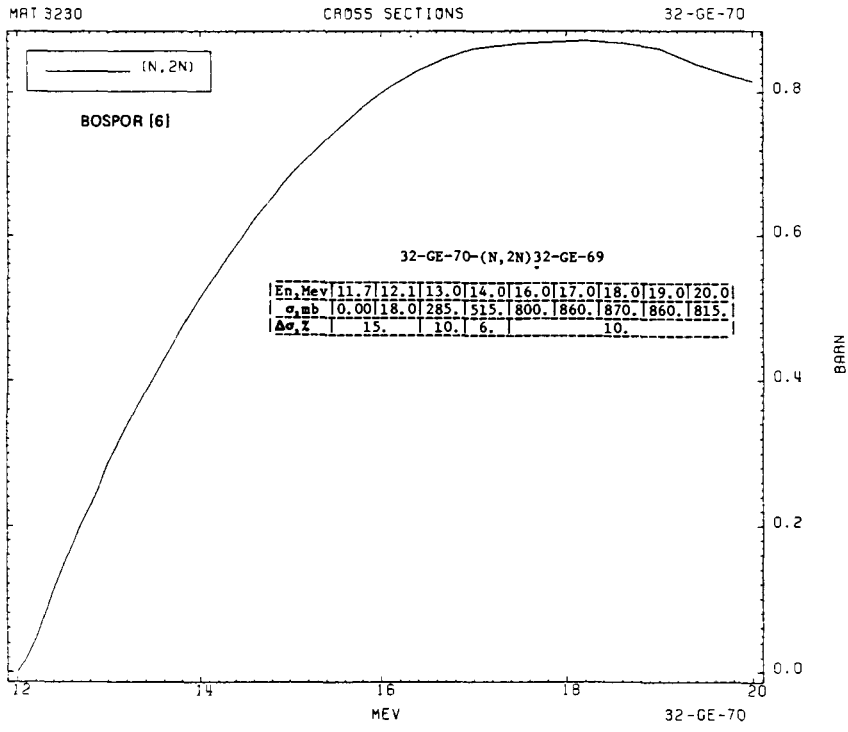
MAT 3230
CROSS SECTIONS
32-GE-70
(N,2N)
BOSPOR [6]
32-GE-70-(N,2N)32-GE-69
En,Mev | 11.7 | 12.1 | 13.0 | 14.0 | 16.0 | 17.0 | 18.0 | 19.0 | 20.0
σ,mb | 0.00 | 18.0 | 285. | 515. | 800. | 860. | 870. | 860. | 815.
Δσ,% | 15. | 10. | 6. | 10.
BARN
MEV
32-GE-70

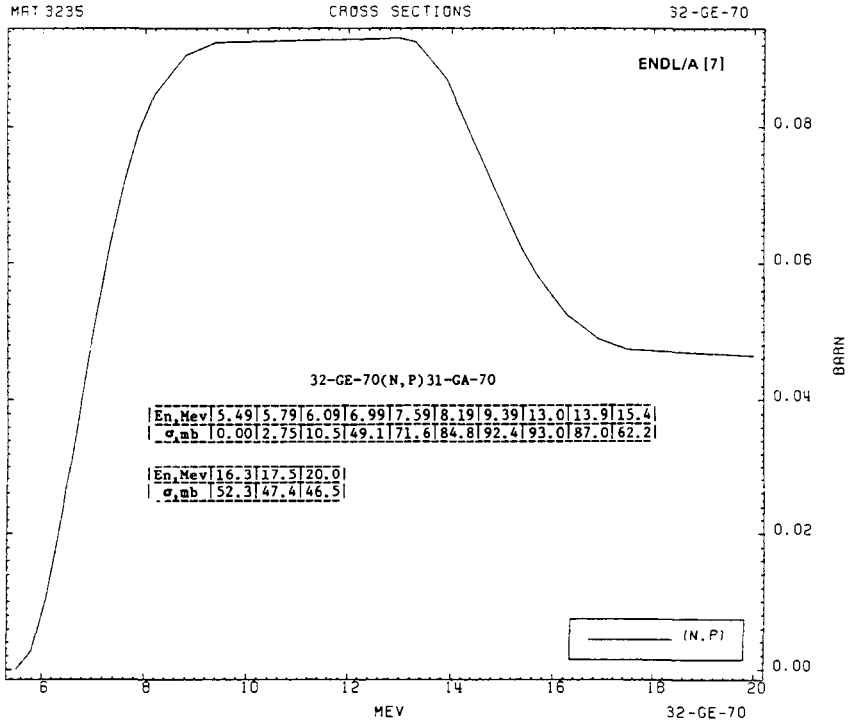
MAT 3235
CROSS SECTIONS
32-GE-70
ENDL/A [7]
32-GE-70(N,P)31-GA-70
En,Mev 5.49 5.79 6.09 6.99 7.59 8.19 9.39 13.0 13.9 15.4
σ,mb 10.00 2.75 10.5 49.1 71.6 84.8 92.4 93.0 87.0 62.2
En,Mev 16.3 17.5 20.0
σ,mb 52.3 47.4 46.5
(N,P)
0.08
0.06
0.04
0.02
0.00
BARN
6
8
10
12
14
16
18
20
MEV
32-GE-70

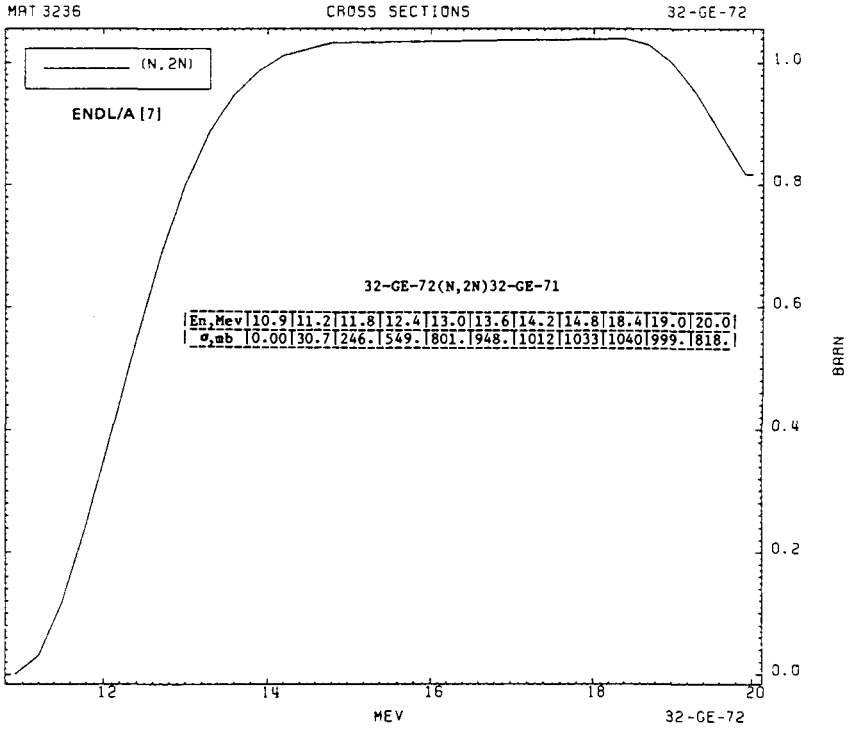
MAT 3236
CROSS SECTIONS
32-GE-72
(N,2N)
ENDL/A [7]
32-GE-72(N,2N)32-GE-71
En,Mev 10.9 11.2 11.8 12.4 13.0 13.6 14.2 14.8 18.4 19.0 20.0
σ,mb 0.00 30.7 246. 549. 801. 948. 1012 1033 1040 999. 818.
1.0
0.8
0.6
0.4
0.2
0.0
BARN
12
14
16
18
20
MEV
32-GE-72

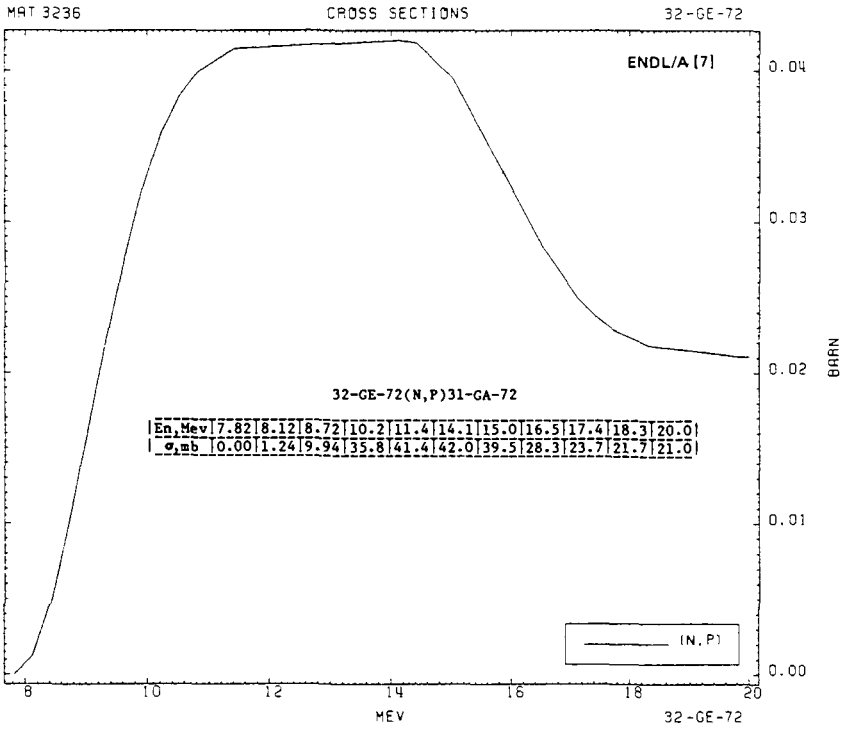
MAT 3236
CROSS SECTIONS
32-GE-72
ENDL/A [7]
0.04
0.03
0.02
0.01
0.00
BARN
32-GE-72(N,P)31-GA-72
En,Mev 7.82 8.12 8.72 10.2 11.4 14.1 15.0 16.5 17.4 18.3 20.0
σ,mb 0.00 1.24 9.94 35.8 41.4 42.0 39.5 28.3 23.7 21.7 21.0
(N,P)
8 10 12 14 16 18 20
MEV
32-GE-72

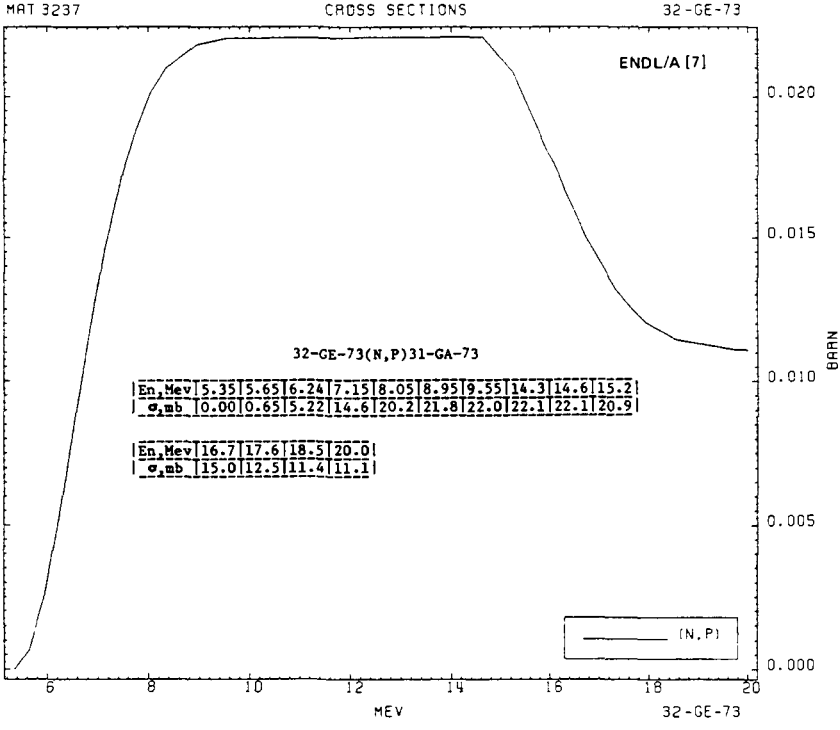
MAT 3237
CROSS SECTIONS
32-GE-73
ENDL/A [7]
0.020
0.015
0.010
0.005
0.000
BARN
32-GE-73(N,P)31-GA-73
En,Mev 5.35 5.65 6.24 7.15 8.05 8.95 9.55 14.3 14.6 15.2
σ,mb 0.00 0.65 5.22 14.6 20.2 21.8 22.0 22.1 22.1 20.9
En,Mev 16.7 17.6 18.5 20.0
σ,mb 15.0 12.5 11.4 11.1
(N,P)
6 8 10 12 14 16 18 20
MEV
32-GE-73

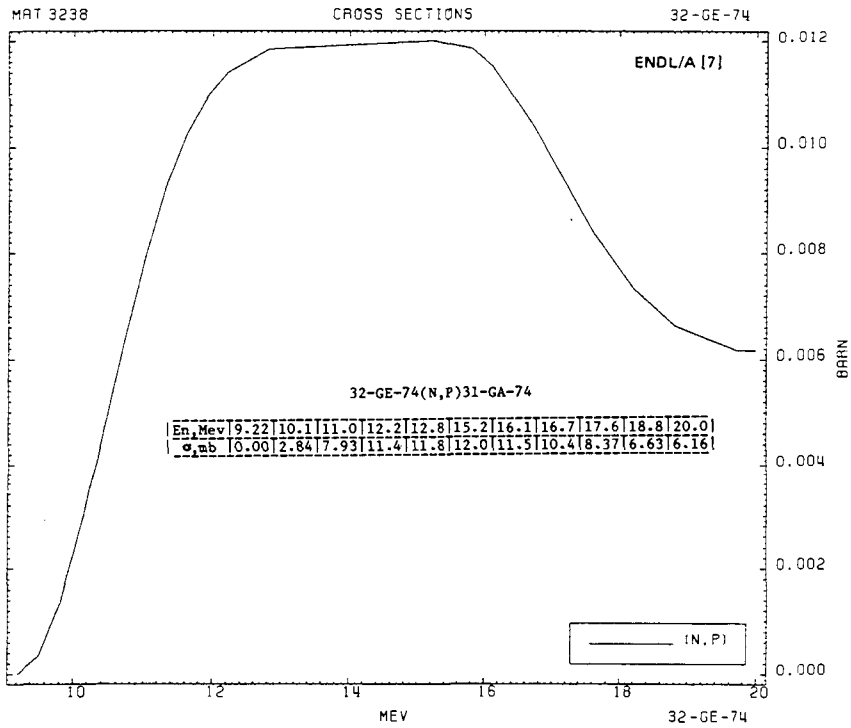
MAT 3238
CROSS SECTIONS
32-GE-74
ENDL/A [7]
0.012
0.010
0.008
0.006
0.004
0.002
0.000
BARN
32-GE-74(N,P)31-GA-74
En,Mev 9.22 10.1 11.0 12.2 12.8 15.2 16.1 16.7 17.6 18.8 20.0
σ,mb 0.00 2.84 7.93 11.4 11.8 12.0 11.5 10.4 8.37 6.63 6.16
(N,P)
10
12
14
16
18
20
MEV
32-GE-74

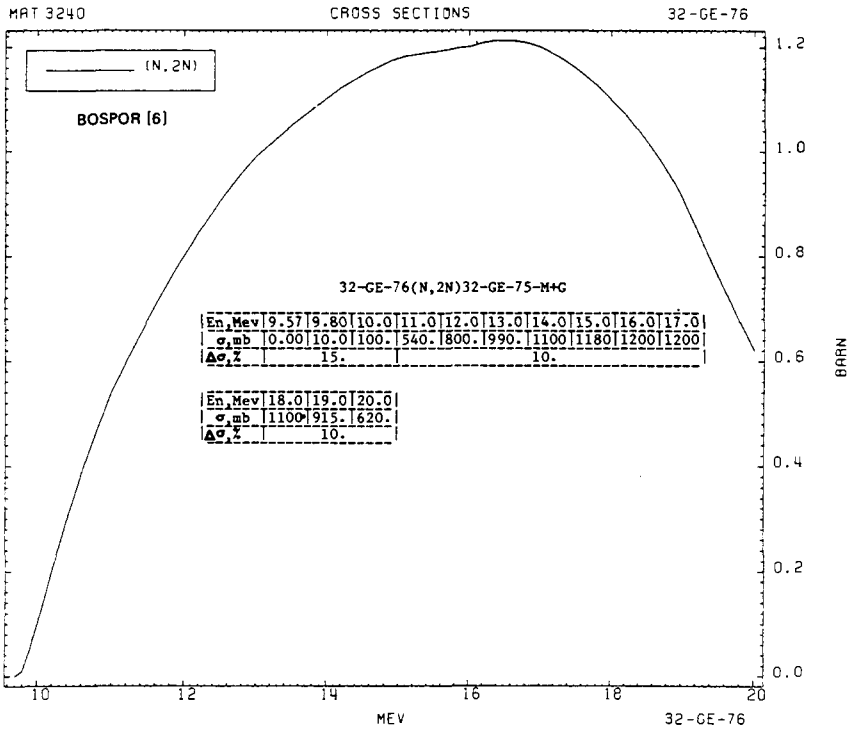
MAT 3240
CROSS SECTIONS
32-GE-76
(N,2N)
BOSPOR [6]
1.2
1.0
0.8
0.6
0.4
0.2
0.0
BARN
32-GE-76(N,2N)32-GE-75-M+G
En,Mev 9.57 9.80 10.0 11.0 12.0 13.0 14.0 15.0 16.0 17.0
σ,mb 0.00 10.0 100. 540. 800. 990. 1100 1180 1200 1200
Δσ,% 15. 10.
En,Mev 18.0 19.0 20.0
σ,mb 1100 915. 620.
Δσ,% 10.
10
12
14
16
18
20
MEV
32-GE-76

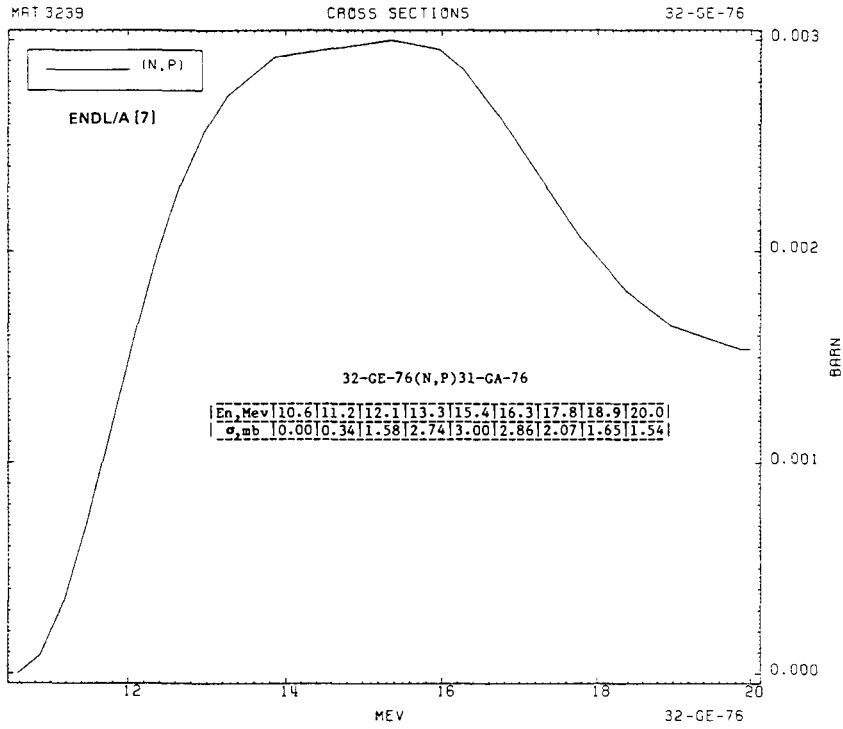
MAT 3239
CROSS SECTIONS
32-GE-76
(N,P)
ENDL/A [7]
32-GE-76(N,P)31-GA-76
En,Mev | 10.6 | 11.2 | 12.1 | 13.3 | 15.4 | 16.3 | 17.8 | 18.9 | 20.0
σ,mb | 0.00 | 0.34 | 1.58 | 2.74 | 3.00 | 2.86 | 2.07 | 1.65 | 1.54
0.003
0.002
0.001
0.000
BARN
12
14
16
18
20
MEV
32-GE-76

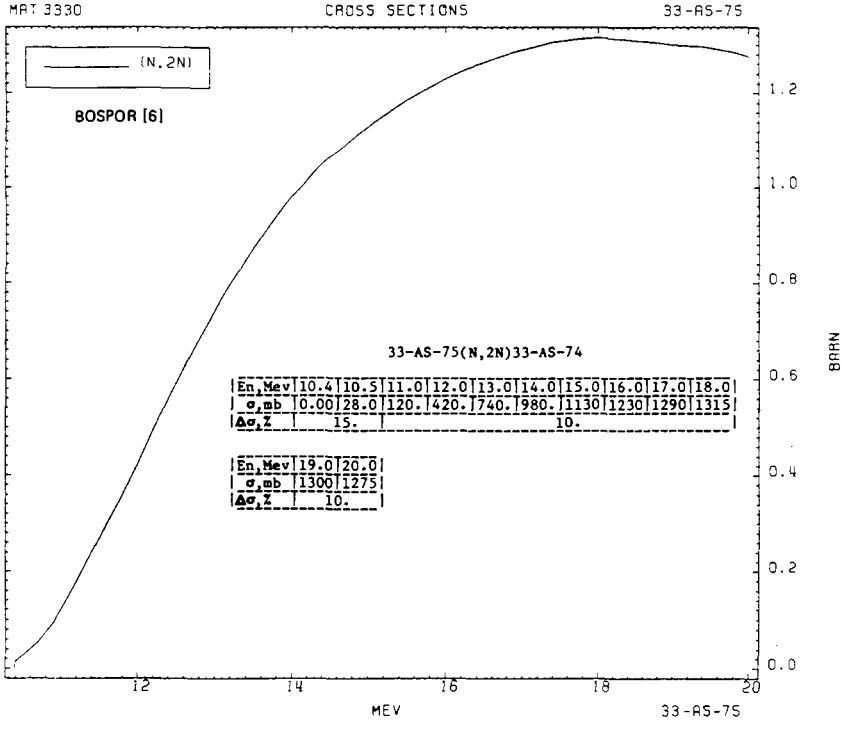
MAT 3330
CROSS SECTIONS
33-AS-75
(N,2N)
BOSPOR [6]
33-AS-75(N,2N)33-AS-74
En,Mev | 10.4 | 10.5 | 11.0 | 12.0 | 13.0 | 14.0 | 15.0 | 16.0 | 17.0 | 18.0
σ,mb | 0.00 | 28.0 | 120. | 420. | 740. | 980. | 1130 | 1230 | 1290 | 1315
Δσ,% | 15. | 10.
En,Mev | 19.0 | 20.0
σ,mb | 1300 | 1275
Δσ,% | 10.
1.2
1.0
0.8
0.6
0.4
0.2
0.0
BARN
12
14
16
18
20
MEV
33-AS-75

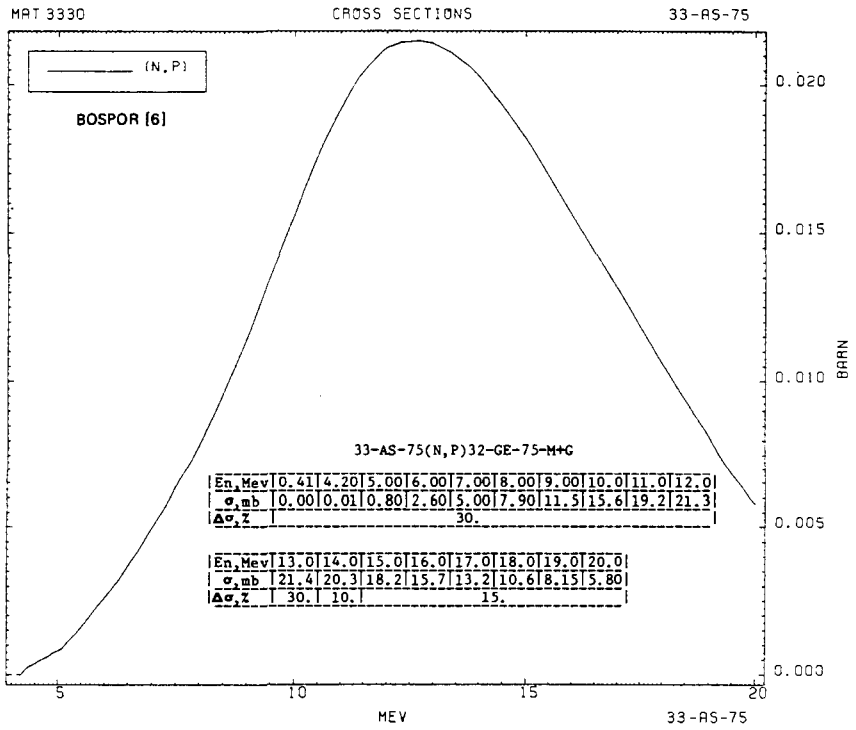
MAT 3330
CROSS SECTIONS
33-AS-75
(N,P)
BOSPOR [6]
33-AS-75(N,P)32-GE-75-M+G
En,Mev | 0.41 | 4.20 | 5.00 | 6.00 | 7.00 | 8.00 | 9.00 | 10.0 | 11.0 | 12.0
σ,mb | 0.00 | 0.01 | 0.80 | 2.60 | 5.00 | 7.90 | 11.5 | 15.6 | 19.2 | 21.3
Δσ,% | 30.
En,Mev | 13.0 | 14.0 | 15.0 | 16.0 | 17.0 | 18.0 | 19.0 | 20.0
σ,mb | 21.4 | 20.3 | 18.2 | 15.7 | 13.2 | 10.6 | 8.15 | 5.80
Δσ,% | 30. | 10. | 15.
0.020
0.015
0.010
0.005
0.000
BARN
5
10
15
20
MEV
33-AS-75

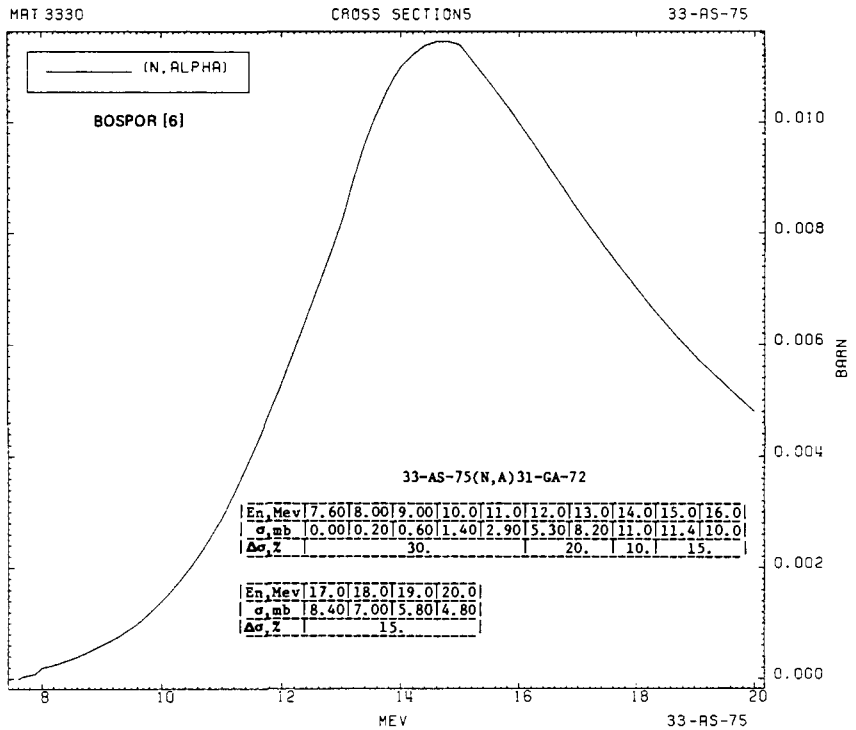
MAT 3330
CROSS SECTIONS
33-AS-75
(N,ALPHA)
BOSPOR [6]
33-AS-75(N,A)31-GA-72
En,Mev | 7.60 | 8.00 | 9.00 | 10.0 | 11.0 | 12.0 | 13.0 | 14.0 | 15.0 | 16.0
σ,mb | 0.00 | 0.20 | 0.60 | 1.40 | 2.90 | 5.30 | 8.20 | 11.0 | 11.4 | 10.0
Δσ,% | 30. | 20. | 10. | 15.
En,Mev | 17.0 | 18.0 | 19.0 | 20.0
σ,mb | 8.40 | 7.00 | 5.80 | 4.80
Δσ,% | 15.
0.010
0.008
0.006
0.004
0.002
0.000
BARN
8
10
12
14
16
18
20
MEV
33-AS-75

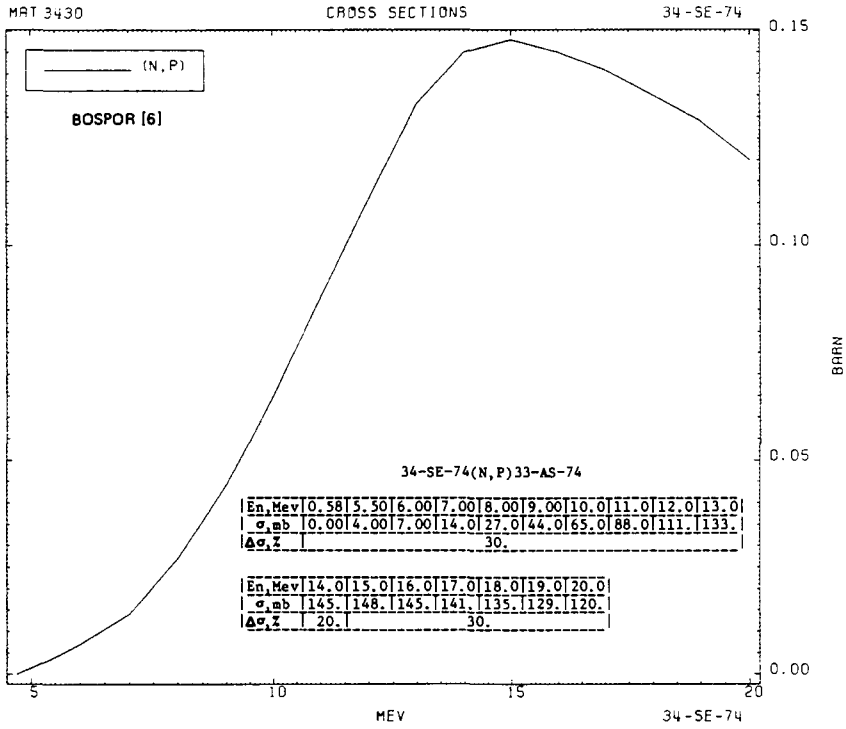
MAT 3430
CROSS SECTIONS
34-SE-74
(N,P)
BOSPOR [6]
0.15
0.10
0.05
0.00
BARN
34-SE-74(N,P)33-AS-74
En,Mev 0.58 5.50 6.00 7.00 8.00 9.00 10.0 11.0 12.0 13.0
σ,mb 0.00 4.00 7.00 14.0 27.0 44.0 65.0 88.0 111. 133.
Δσ,% 30.
En,Mev 14.0 15.0 16.0 17.0 18.0 19.0 20.0
σ,mb 145. 148. 145. 141. 135. 129. 120.
Δσ,% 20. 30.
5
10
15
20
MEV
34-SE-74

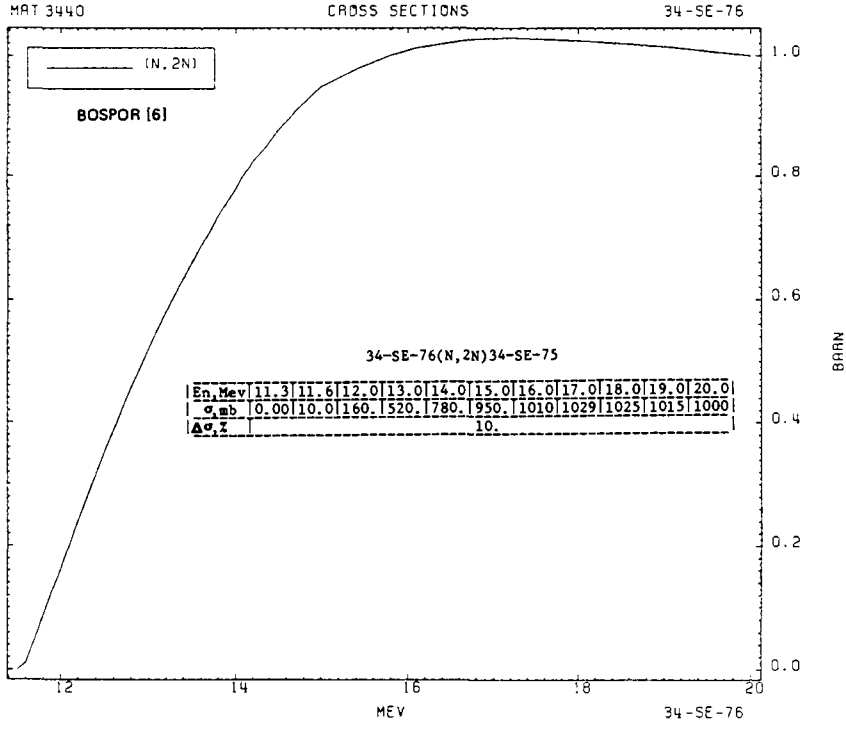
MAT 3440
CROSS SECTIONS
34-SE-76
(N,2N)
BOSPOR [6]
1.0
0.8
0.6
0.4
0.2
0.0
BARN
34-SE-76(N,2N)34-SE-75
En,Mev 11.3 11.6 12.0 13.0 14.0 15.0 16.0 17.0 18.0 19.0 20.0
σ,mb 0.00 10.0 160. 520. 780. 950. 1010 1029 1025 1015 1000
Δσ,% 10.
12
14
16
18
20
MEV
34-SE-76

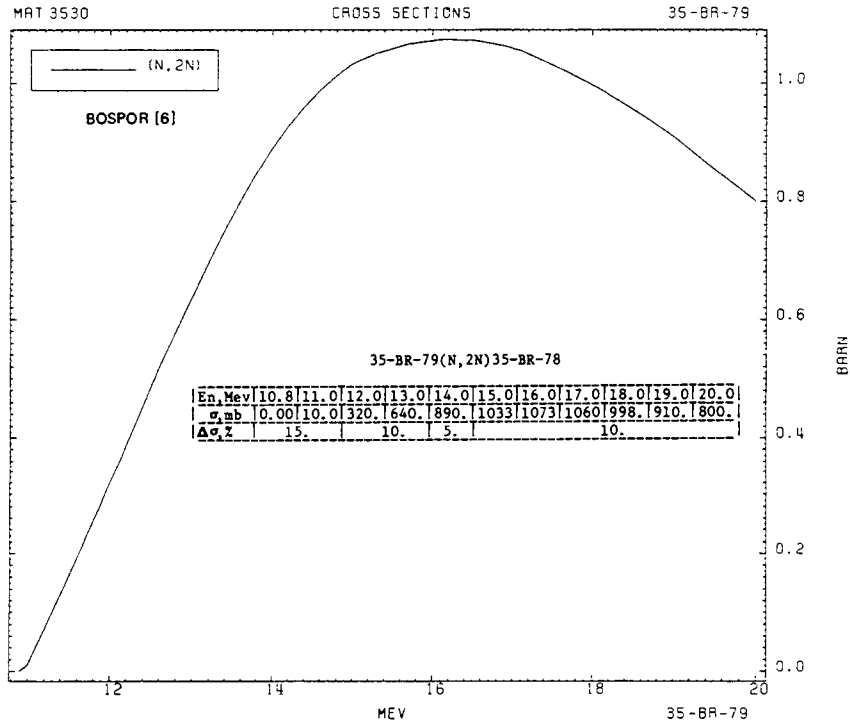
MAT 3530
CROSS SECTIONS
35-BR-79
(N,2N)
BOSPOR [6]
35-BR-79(N,2N)35-BR-78
En,Mev | 10.8 | 11.0 | 12.0 | 13.0 | 14.0 | 15.0 | 16.0 | 17.0 | 18.0 | 19.0 | 20.0
σ,mb | 0.00 | 10.0 | 320. | 640. | 890. | 1033 | 1073 | 1060 | 998. | 910. | 800.
Δσ,% | 15. | 10. | 5. | 10.
BARN
MEV
35-BR-79

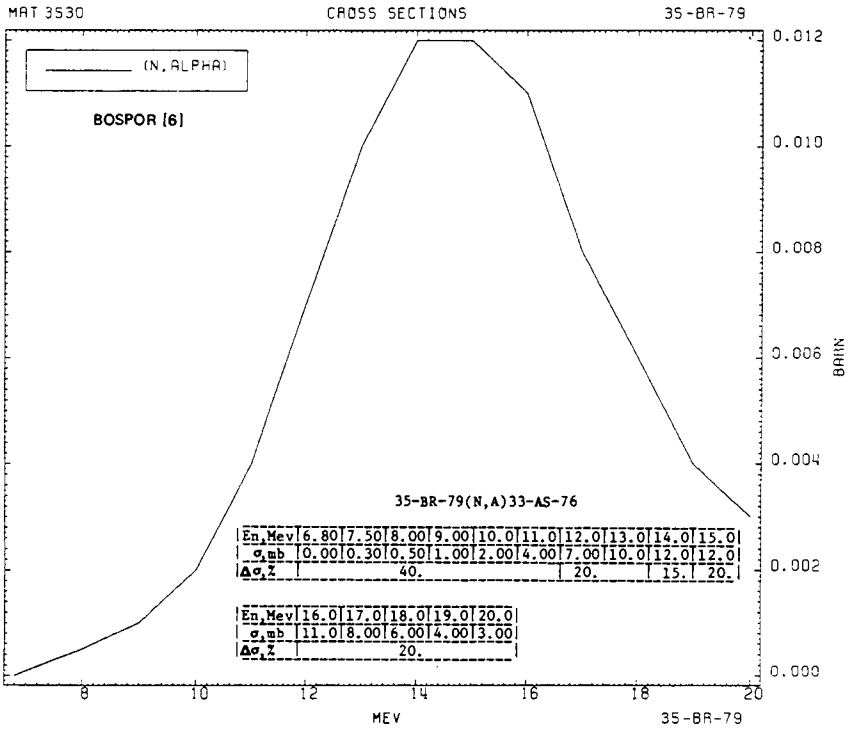
MAT 3530
CROSS SECTIONS
35-BR-79
(N,ALPHA)
BOSPOR [6]
35-BR-79(N,A)33-AS-76
En,Mev | 6.80 | 7.50 | 8.00 | 9.00 | 10.0 | 11.0 | 12.0 | 13.0 | 14.0 | 15.0
σ,mb | 0.00 | 0.30 | 0.50 | 1.00 | 2.00 | 4.00 | 7.00 | 10.0 | 12.0 | 12.0
Δσ,% | 40. | 20. | 15. | 20.
En,Mev | 16.0 | 17.0 | 18.0 | 19.0 | 20.0
σ,mb | 11.0 | 8.00 | 6.00 | 4.00 | 3.00
Δσ,% | 20.
BARN
MEV
35-BR-79

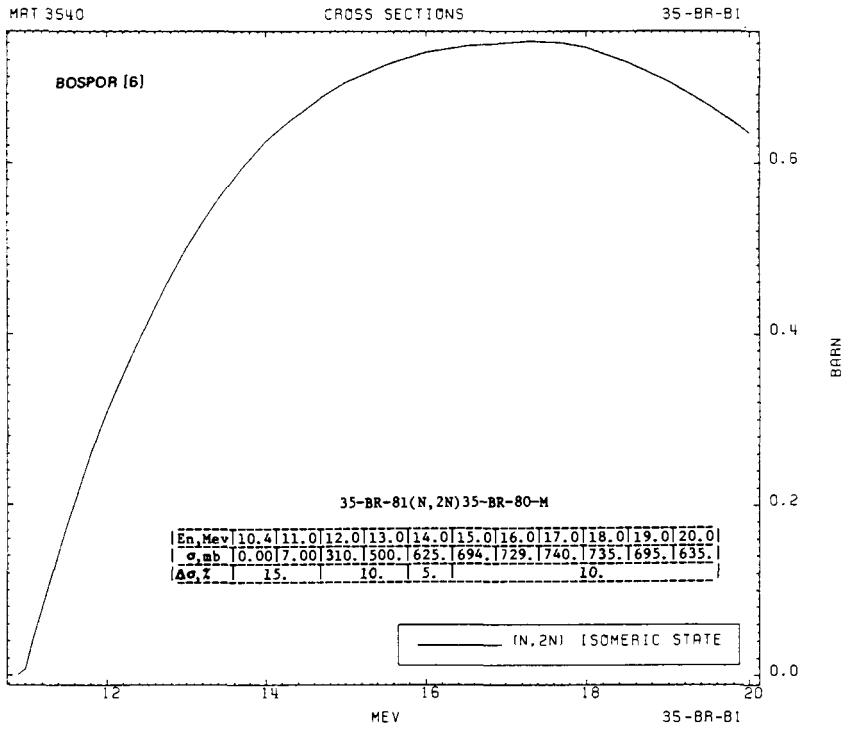
MAT 3540
CROSS SECTIONS
35-BR-81
BOSPOR [6]
0.6
0.4
0.2
0.0
BARN
35-BR-81(N,2N)35-BR-80-M
En,Mev | 10.4 | 11.0 | 12.0 | 13.0 | 14.0 | 15.0 | 16.0 | 17.0 | 18.0 | 19.0 | 20.0
σ,mb | 0.00 | 7.00 | 310. | 500. | 625. | 694. | 729. | 740. | 735. | 695. | 635.
Δσ,% | 15. | 10. | 5. | 10.
(N,2N) ISOMERIC STATE
12
14
16
18
20
MEV
35-BR-81

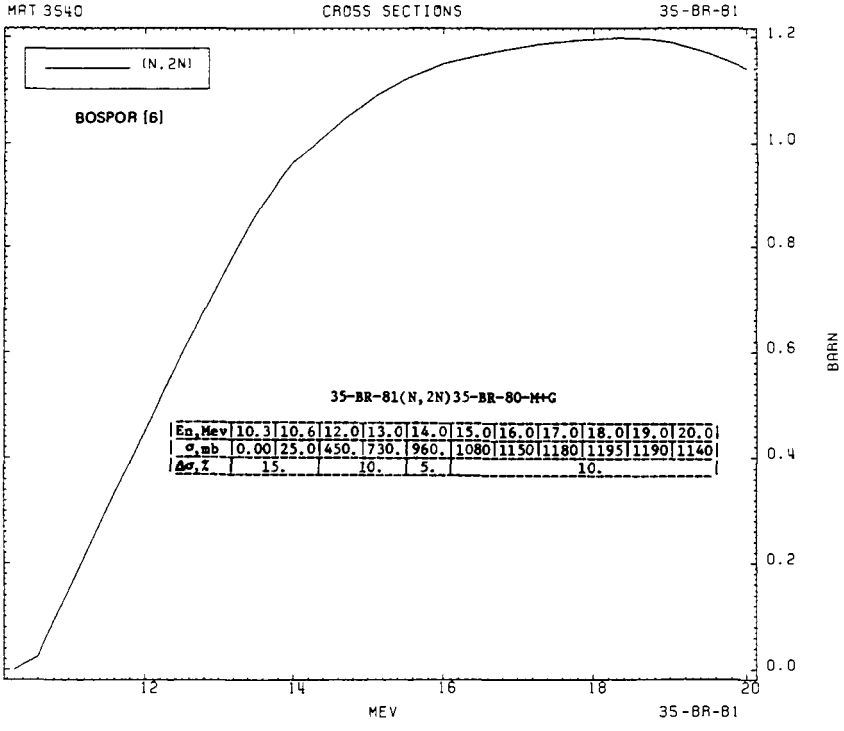
MAT 3540
CROSS SECTIONS
35-BR-81
(N,2N)
BOSPOR [6]
1.2
1.0
0.8
0.6
0.4
0.2
0.0
BARN
35-BR-81(N,2N)35-BR-80-M+G
En,Mev | 10.3 | 10.6 | 12.0 | 13.0 | 14.0 | 15.0 | 16.0 | 17.0 | 18.0 | 19.0 | 20.0
σ,mb | 0.00 | 25.0 | 450. | 730. | 960. | 1080 | 1150 | 1180 | 1195 | 1190 | 1140
Δσ,% | 15. | 10. | 5. | 10.
12
14
16
18
20
MEV
35-BR-81

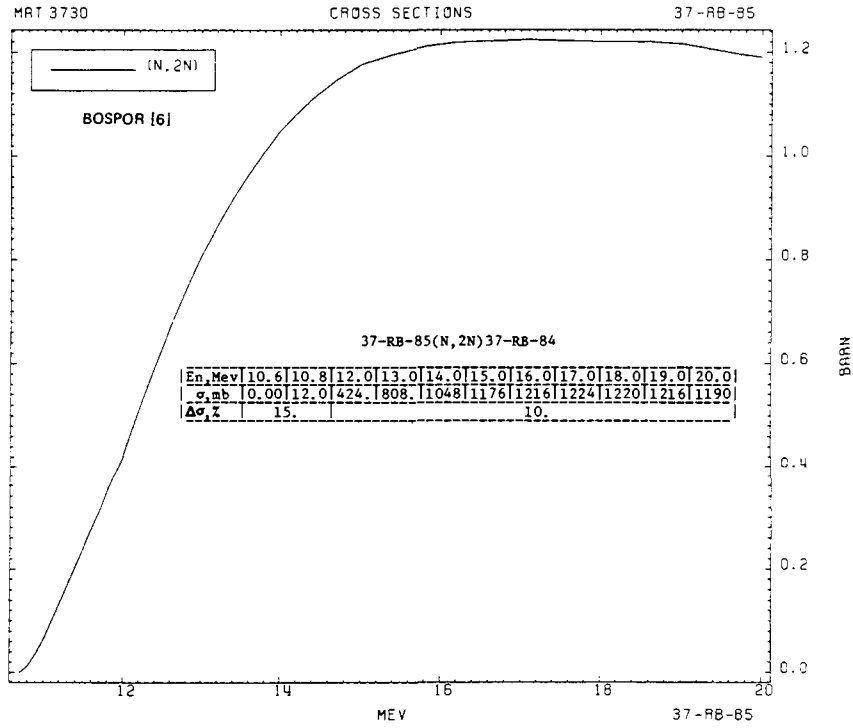
MAT 3730
CROSS SECTIONS
37-RB-85
(N,2N)
BOSPOR [6]
37-RB-85(N,2N)37-RB-84
En,Mev | 10.6 | 10.8 | 12.0 | 13.0 | 14.0 | 15.0 | 16.0 | 17.0 | 18.0 | 19.0 | 20.0
σ,mb | 0.00 | 12.0 | 424. | 808. | 1048 | 1176 | 1216 | 1224 | 1220 | 1216 | 1190
Δσ,% | 15. | 10.
1.2
1.0
0.8
0.6
0.4
0.2
0.0
BARN
12
14
16
18
20
MEV
37-RB-85

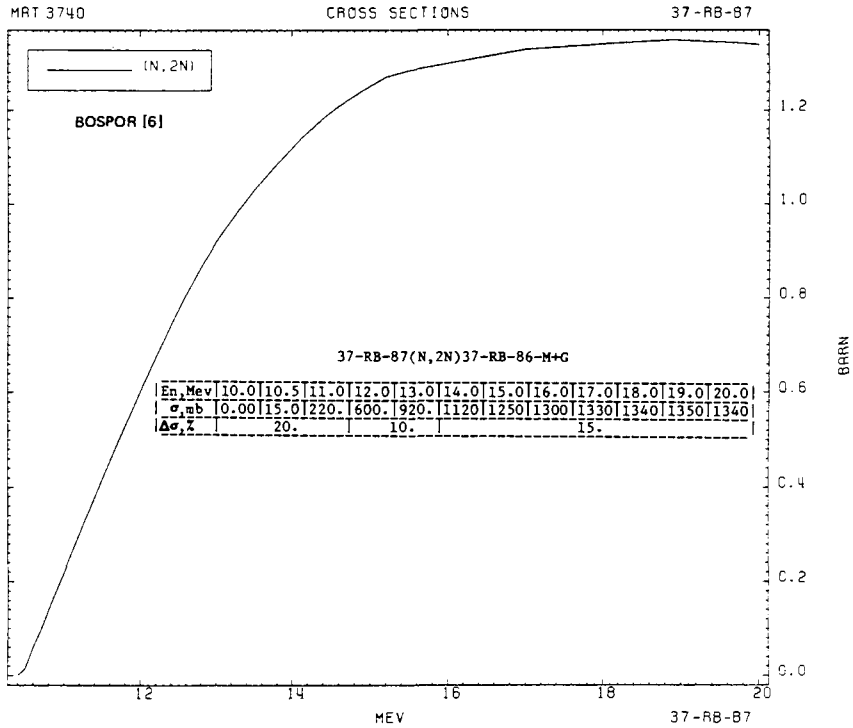
MAT 3740
CROSS SECTIONS
37-RB-87
(N,2N)
BOSPOR [6]
37-RB-87(N,2N)37-RB-86-M+G
En,Mev | 10.0 | 10.5 | 11.0 | 12.0 | 13.0 | 14.0 | 15.0 | 16.0 | 17.0 | 18.0 | 19.0 | 20.0
σ,mb | 0.00 | 15.0 | 220. | 600. | 920. | 1120 | 1250 | 1300 | 1330 | 1340 | 1350 | 1340
Δσ,% | 20. | 10. | 15.
1.2
1.0
0.8
0.6
0.4
0.2
0.0
BARN
12
14
16
18
20
MEV
37-RB-87

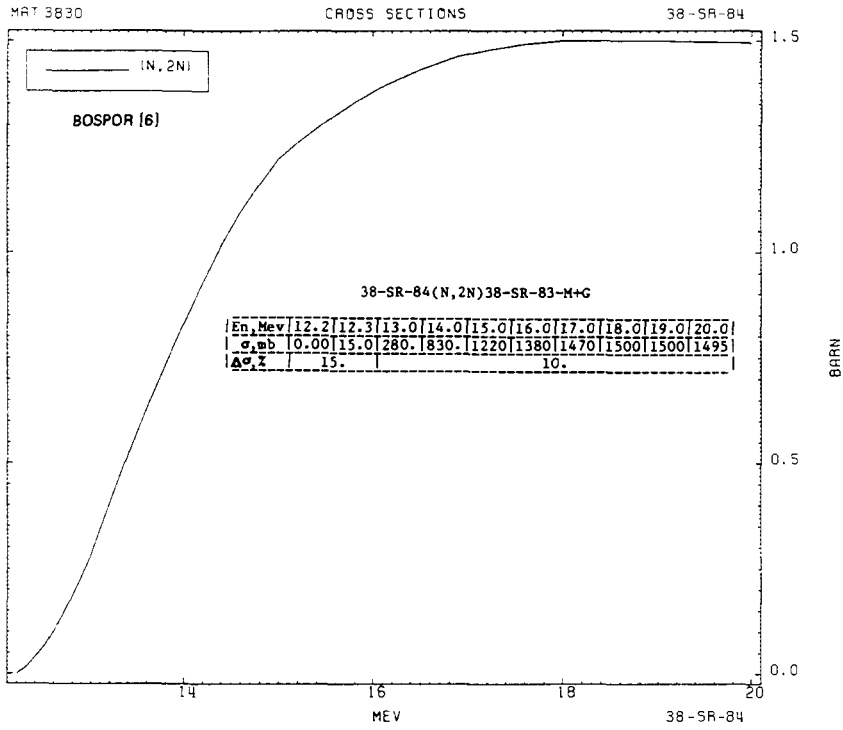
MAT 3830
CROSS SECTIONS
38-SR-84
(N,2N)
BOSPOR [6]
38-SR-84(N,2N)38-SR-83-M+G
En,Mev | 12.2 | 12.3 | 13.0 | 14.0 | 15.0 | 16.0 | 17.0 | 18.0 | 19.0 | 20.0
σ,mb | 0.00 | 15.0 | 280. | 830. | 1220 | 1380 | 1470 | 1500 | 1500 | 1495
Δσ,% | 15. | 10.
1.5
1.0
0.5
0.0
BARN
14
16
18
20
MEV
38-SR-84

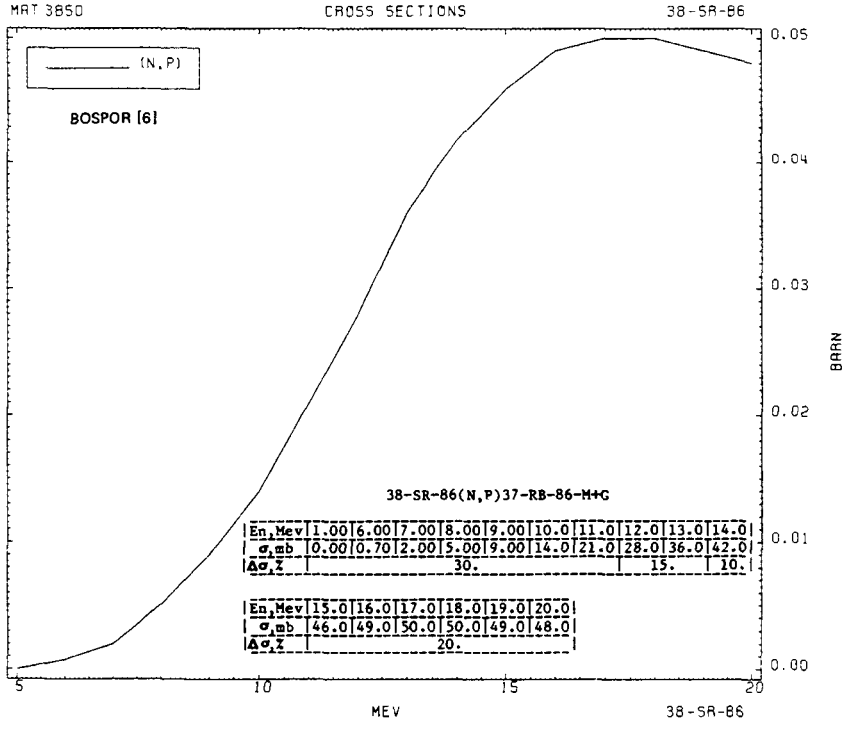
MAT 3850
CROSS SECTIONS
38-SR-86
(N,P)
BOSPOR [6]
38-SR-86(N,P)37-RB-86-M+G
En,Mev | 1.00 | 6.00 | 7.00 | 8.00 | 9.00 | 10.0 | 11.0 | 12.0 | 13.0 | 14.0
σ,mb | 0.00 | 0.70 | 2.00 | 5.00 | 9.00 | 14.0 | 21.0 | 28.0 | 36.0 | 42.0
Δσ,% | 30. | 15. | 10.
En,Mev | 15.0 | 16.0 | 17.0 | 18.0 | 19.0 | 20.0
σ,mb | 46.0 | 49.0 | 50.0 | 50.0 | 49.0 | 48.0
Δσ,% | 20.
0.05
0.04
0.03
0.02
0.01
0.00
BARN
5
10
15
20
MEV
38-SR-86

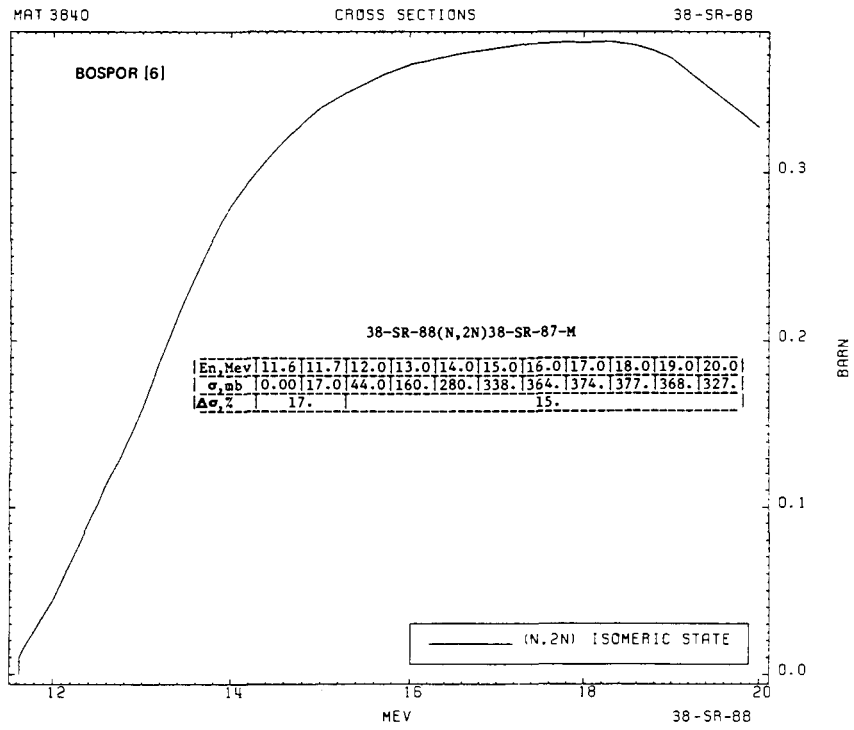
MAT 3840
CROSS SECTIONS
38-SR-88
BOSPOR [6]
38-SR-88(N,2N)38-SR-87-M
En,Mev | 11.6 | 11.7 | 12.0 | 13.0 | 14.0 | 15.0 | 16.0 | 17.0 | 18.0 | 19.0 | 20.0
σ,mb | 0.00 | 17.0 | 44.0 | 160. | 280. | 338. | 364. | 374. | 377. | 368. | 327.
Δσ,% | 17. | 15.
(N,2N) ISOMERIC STATE
0.0
0.1
0.2
0.3
BARN
12
14
16
18
20
MEV
38-SR-88

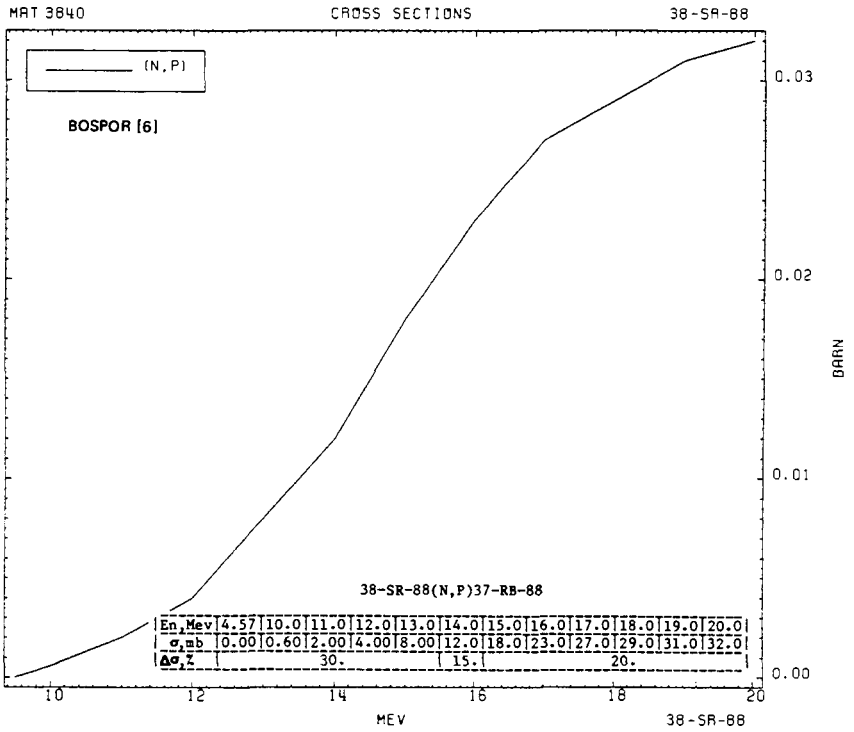
MAT 3840
CROSS SECTIONS
38-SR-88
(N,P)
BOSPOR [6]
38-SR-88(N,P)37-RB-88
En,Mev | 4.57 | 10.0 | 11.0 | 12.0 | 13.0 | 14.0 | 15.0 | 16.0 | 17.0 | 18.0 | 19.0 | 20.0
σ,mb | 0.00 | 0.60 | 2.00 | 4.00 | 8.00 | 12.0 | 18.0 | 23.0 | 27.0 | 29.0 | 31.0 | 32.0
Δσ,% | 30. | 15. | 20.
0.00
0.01
0.02
0.03
BARN
10
12
14
16
18
20
MEV
38-SR-88

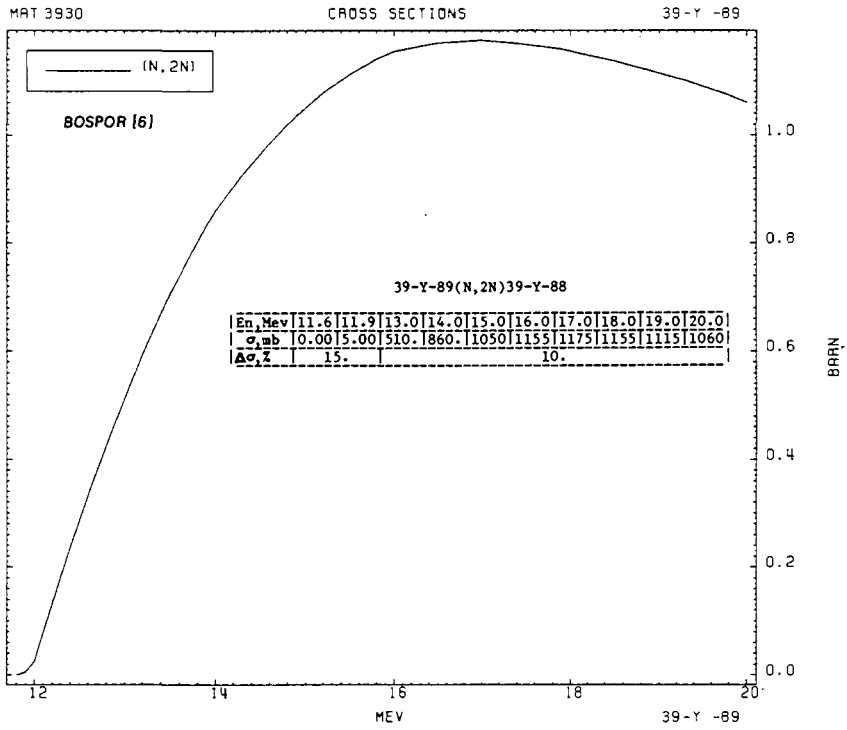
MAT 3930
CROSS SECTIONS
39-Y -89
(N,2N)
BOSPOR [6]
39-Y-89(N,2N)39-Y-88
En,Mev | 11.6 | 11.9 | 13.0 | 14.0 | 15.0 | 16.0 | 17.0 | 18.0 | 19.0 | 20.0
σ,mb | 0.00 | 5.00 | 510. | 860. | 1050 | 1155 | 1175 | 1155 | 1115 | 1060
Δσ,% | 15. | 10.
1.0
0.8
0.6
0.4
0.2
0.0
BARN
12
14
16
18
20
MEV
39-Y -89

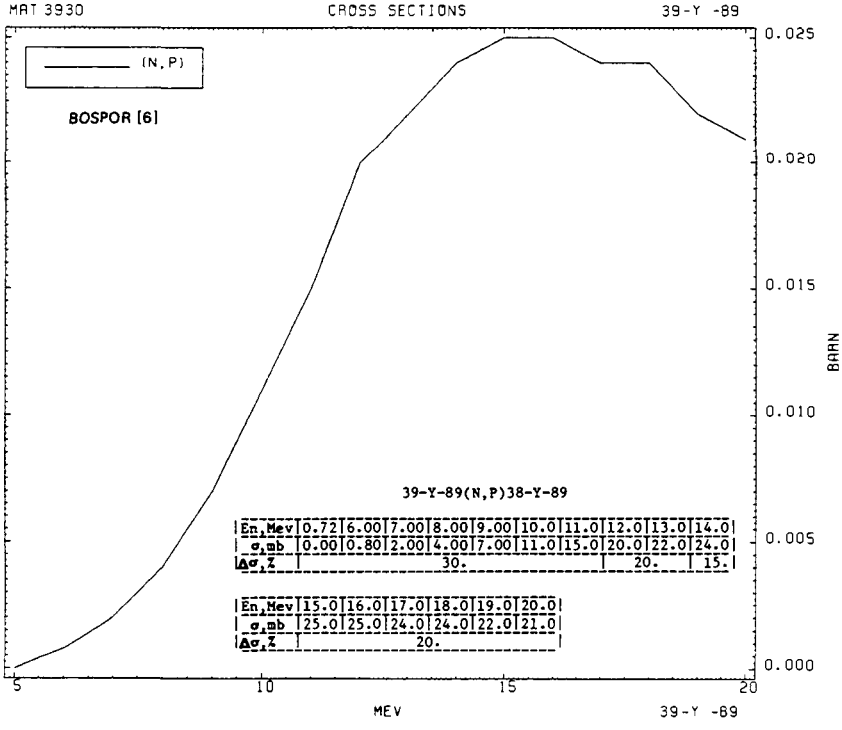
MAT 3930
CROSS SECTIONS
39-Y -89
(N,P)
BOSPOR [6]
39-Y-89(N,P)38-Y-89
En,Mev | 0.72 | 6.00 | 7.00 | 8.00 | 9.00 | 10.0 | 11.0 | 12.0 | 13.0 | 14.0
σ,mb | 0.00 | 0.80 | 2.00 | 4.00 | 7.00 | 11.0 | 15.0 | 20.0 | 22.0 | 24.0
Δσ,% | 30. | 20. | 15.
En,Mev | 15.0 | 16.0 | 17.0 | 18.0 | 19.0 | 20.0
σ,mb | 25.0 | 25.0 | 24.0 | 24.0 | 22.0 | 21.0
Δσ,% | 20.
0.025
0.020
0.015
0.010
0.005
0.000
BARN
5
10
15
20
MEV
39-Y -89

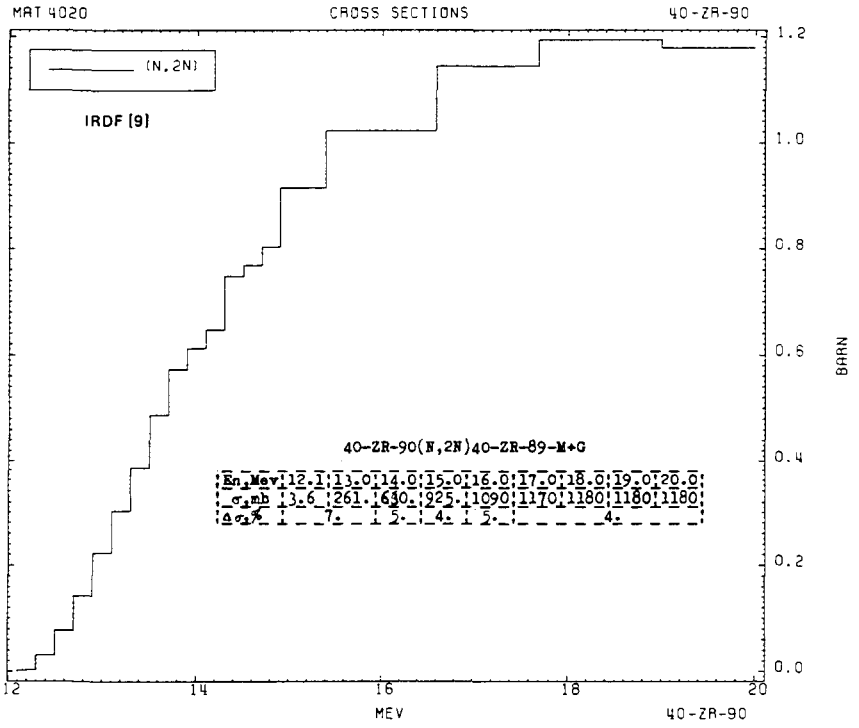
MAT 4020
CROSS SECTIONS
40-ZR-90
(N,2N)
IRDF [9]
40-ZR-90(N,2N)40-ZR-89-M+G
En,Mev 12.1 13.0 14.0 15.0 16.0 17.0 18.0 19.0 20.0
σ,mb 3.6 261. 640. 925. 1090 1170 1180 1180 1180
Δσ,% 1 7. 1 5. 4. 1 5. 4.
1.2
1.0
0.8
0.6
0.4
0.2
0.0
BARN
12
14
16
18
20
MEV
40-ZR-90

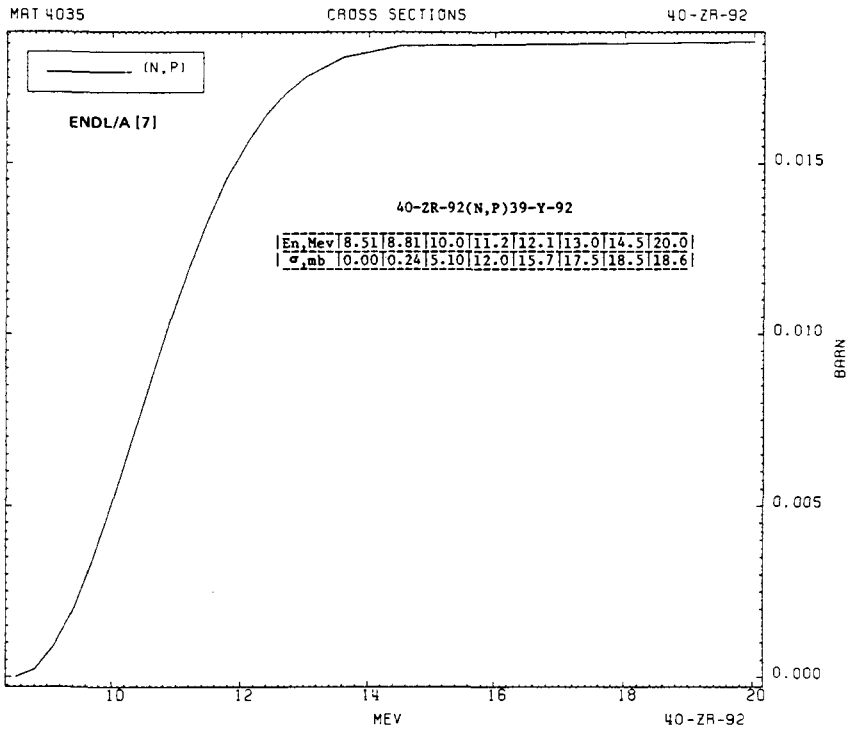
MAT 4035
CROSS SECTIONS
40-ZR-92
(N,P)
ENDL/A [7]
40-ZR-92(N,P)39-Y-92
En,Mev 8.51 8.81 10.0 11.2 12.1 13.0 14.5 20.0
σ,mb 0.00 0.24 5.10 12.0 15.7 17.5 18.5 18.6
0.015
0.010
0.005
0.000
BARN
10
12
14
16
18
20
MEV
40-ZR-92

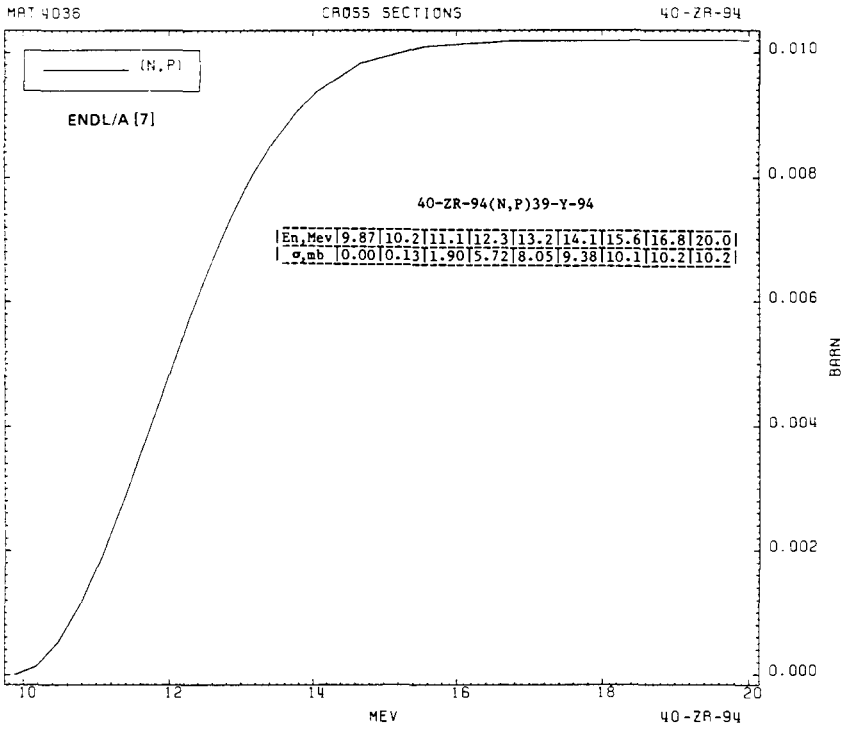
MAT 4036
CROSS SECTIONS
40-ZR-94
(N,P)
ENDL/A [7]
40-ZR-94(N,P)39-Y-94
En,Mev 9.87 10.2 11.1 12.3 13.2 14.1 15.6 16.8 20.0
σ,mb 0.00 0.13 1.90 5.72 8.05 9.38 10.1 10.2 10.2
0.010
0.008
0.006
0.004
0.002
0.000
BARN
10
12
14
16
18
20
MEV
40-ZR-94

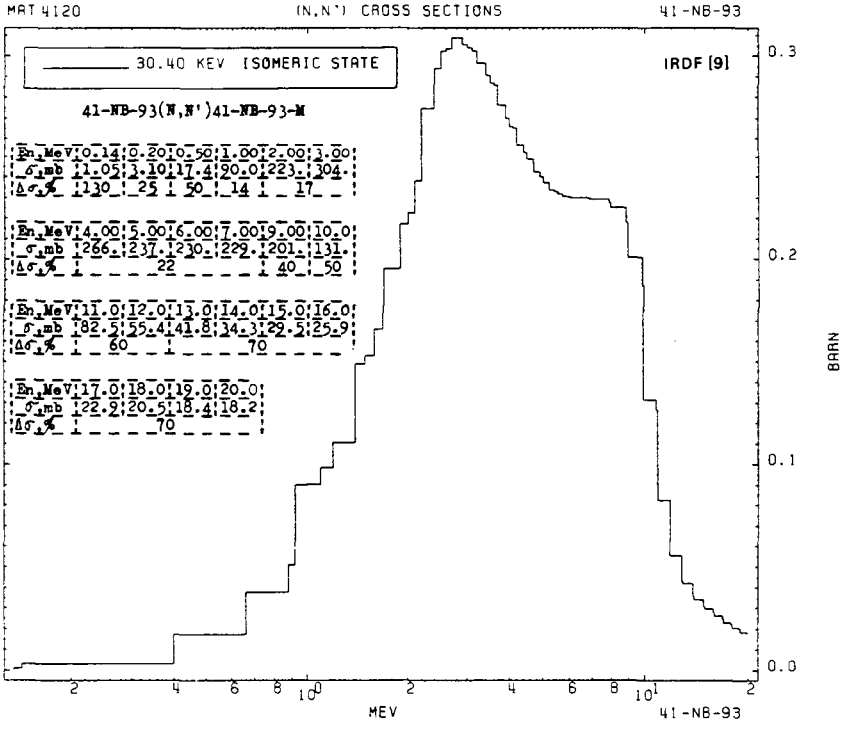
MAT 4120
(N,N') CROSS SECTIONS
41-NB-93
30.40 KEV ISOMERIC STATE
IRDF [9]
41-NB-93(N,N')41-NB-93-M
En,MeV 0.14 0.20 0.50 1.00 2.00 3.00
σ,mb 1.05 3.10 17.4 90.0 223. 304.
Δσ,% 130 25 50 14 17
En,MeV 4.00 5.00 6.00 7.00 9.00 10.0
σ,mb 266. 237. 230. 229. 201. 131.
Δσ,% 22 40 50
En,MeV 11.0 12.0 13.0 14.0 15.0 16.0
σ,mb 82.5 55.4 41.8 34.3 29.5 25.9
Δσ,% 60 70
En,MeV 17.0 18.0 19.0 20.0
σ,mb 22.9 20.5 18.4 18.2
Δσ,% 70
0.3
0.2
0.1
0.0
BARN
2
4
6
8
10
2
4
6
8
10
2
MEV
41-NB-93

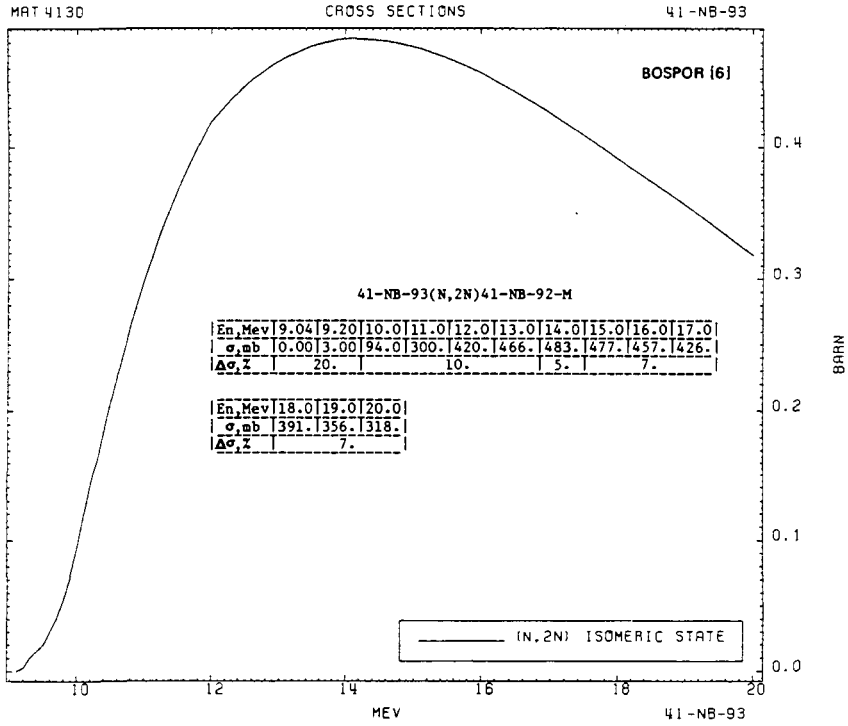
MAT 4130
CROSS SECTIONS
41-NB-93
BOSPOR [6]
41-NB-93(N,2N)41-NB-92-M
En,Mev | 9.04 | 9.20 | 10.0 | 11.0 | 12.0 | 13.0 | 14.0 | 15.0 | 16.0 | 17.0
σ,mb | 0.00 | 3.00 | 94.0 | 300. | 420. | 466. | 483. | 477. | 457. | 426.
Δσ,% | 20. | 10. | 5. | 7.
En,Mev | 18.0 | 19.0 | 20.0
σ,mb | 391. | 356. | 318.
Δσ,% | 7.
(N,2N) ISOMERIC STATE
BARN
MEV
41-NB-93

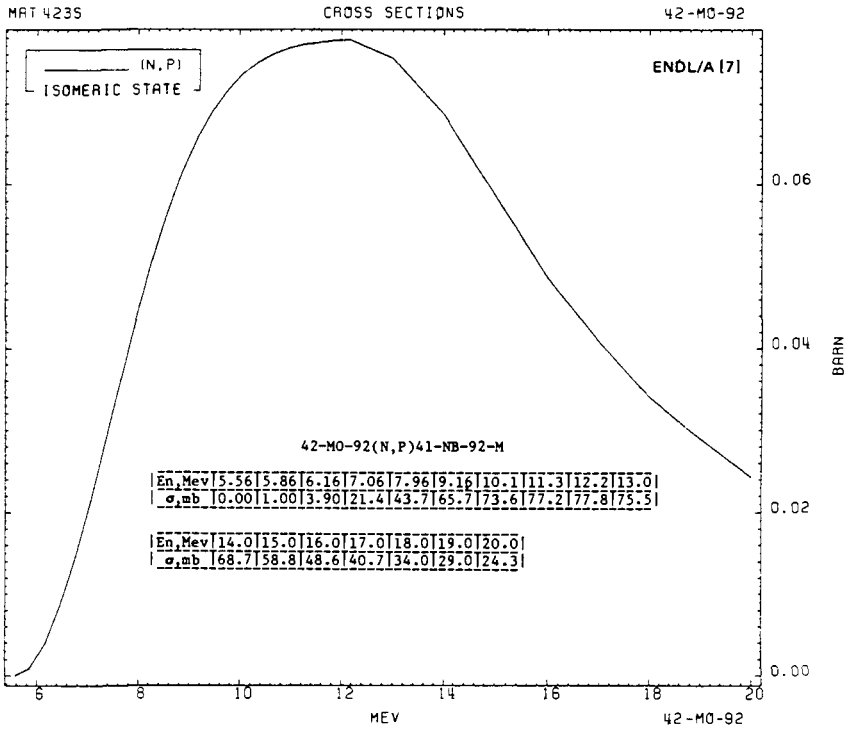
MAT 4235
CROSS SECTIONS
42-MO-92
(N,P)
ISOMERIC STATE
ENDL/A [7]
42-MO-92(N,P)41-NB-92-M
En,Mev | 5.56 | 5.86 | 6.16 | 7.06 | 7.96 | 9.16 | 10.1 | 11.3 | 12.2 | 13.0
σ,mb | 0.00 | 1.00 | 3.90 | 21.4 | 43.7 | 65.7 | 73.6 | 77.2 | 77.8 | 75.5
En,Mev | 14.0 | 15.0 | 16.0 | 17.0 | 18.0 | 19.0 | 20.0
σ,mb | 68.7 | 58.8 | 48.6 | 40.7 | 34.0 | 29.0 | 24.3
BARN
MEV
42-MO-92

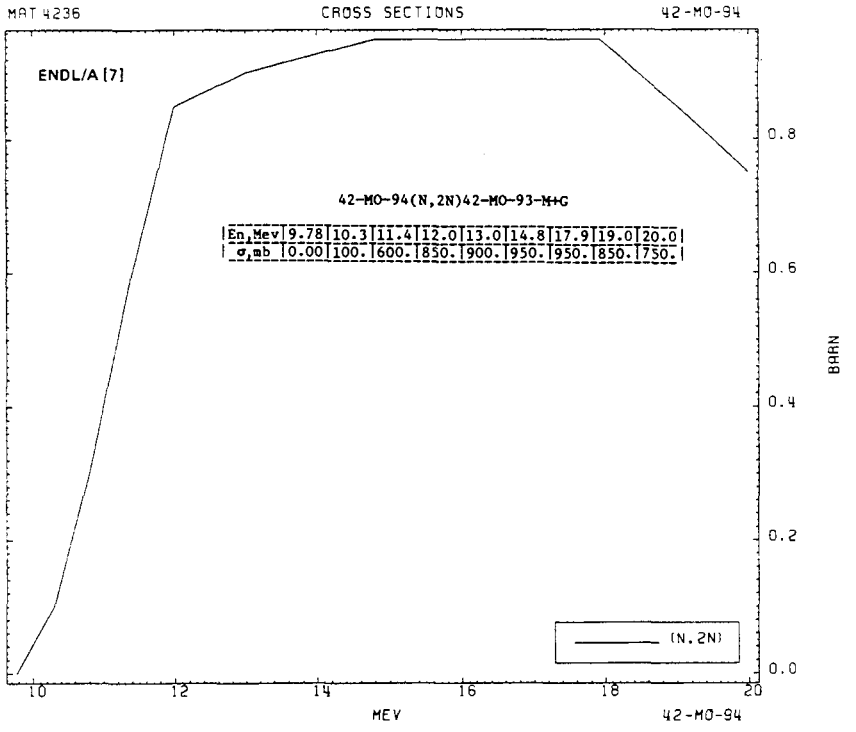
MAT 4236
CROSS SECTIONS
42-MO-94
ENDL/A [7]
42-MO-94(N,2N)42-MO-93-M+G
En,Mev 9.78 10.3 11.4 12.0 13.0 14.8 17.9 19.0 20.0
σ,mb 10.00 100. 600. 850. 900. 950. 950. 850. 750.
(N,2N)
0.0
0.2
0.4
0.6
0.8
BARN
10
12
14
16
18
20
MEV
42-MO-94

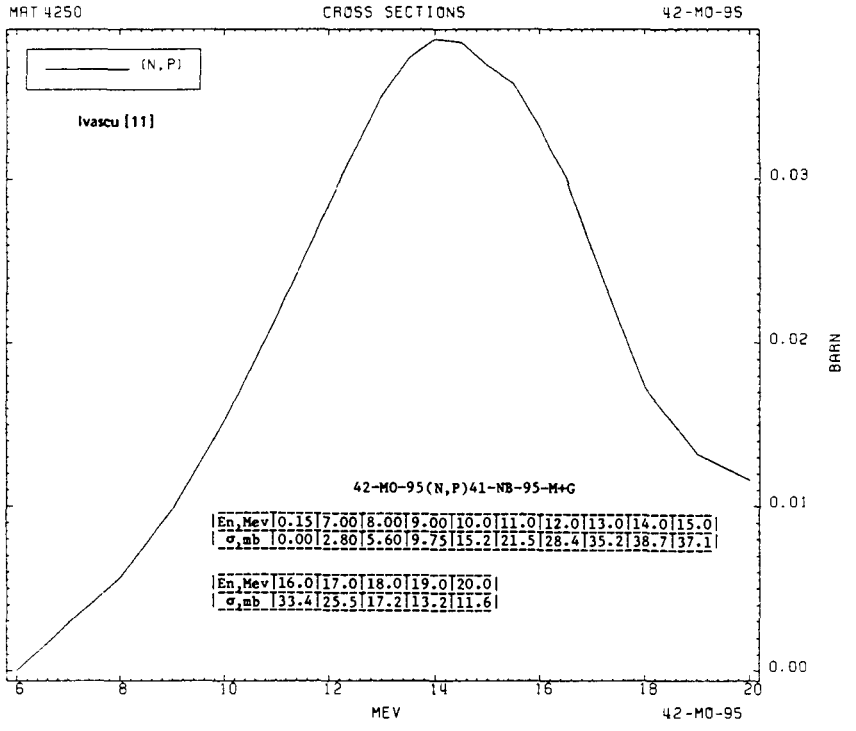
MAT 4250
CROSS SECTIONS
42-MO-95
(N,P)
Ivascu [11]
42-MO-95(N,P)41-NB-95-M+G
En,Mev 0.15 7.00 8.00 9.00 10.0 11.0 12.0 13.0 14.0 15.0
σ,mb 0.00 2.80 5.60 9.75 15.2 21.5 28.4 35.2 38.7 37.1
En,Mev 16.0 17.0 18.0 19.0 20.0
σ,mb 33.4 25.5 17.2 13.2 11.6
0.00
0.01
0.02
0.03
BARN
6
8
10
12
14
16
18
20
MEV
42-MO-95

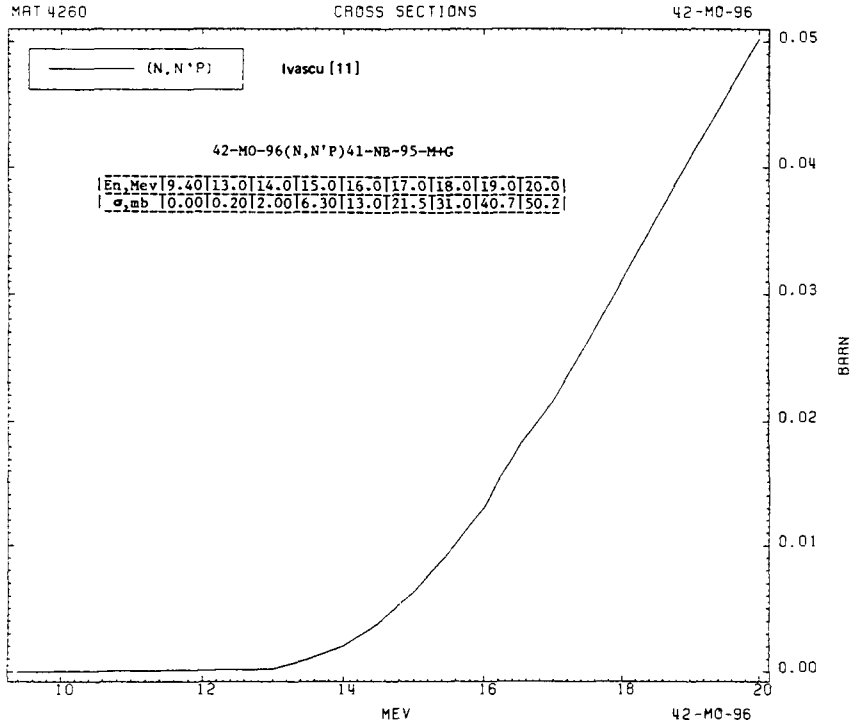
MAT 4260
CROSS SECTIONS
42-MO-96
(N,N'P)
Ivascu [11]
42-MO-96(N,N'P)41-NB-95-M+G
En,Mev 9.40 13.0 14.0 15.0 16.0 17.0 18.0 19.0 20.0
σ,mb 0.00 0.20 2.00 6.30 13.0 21.5 31.0 40.7 50.2
0.05
0.04
0.03
0.02
0.01
0.00
BARN
10
12
14
16
18
20
MEV
42-MO-96

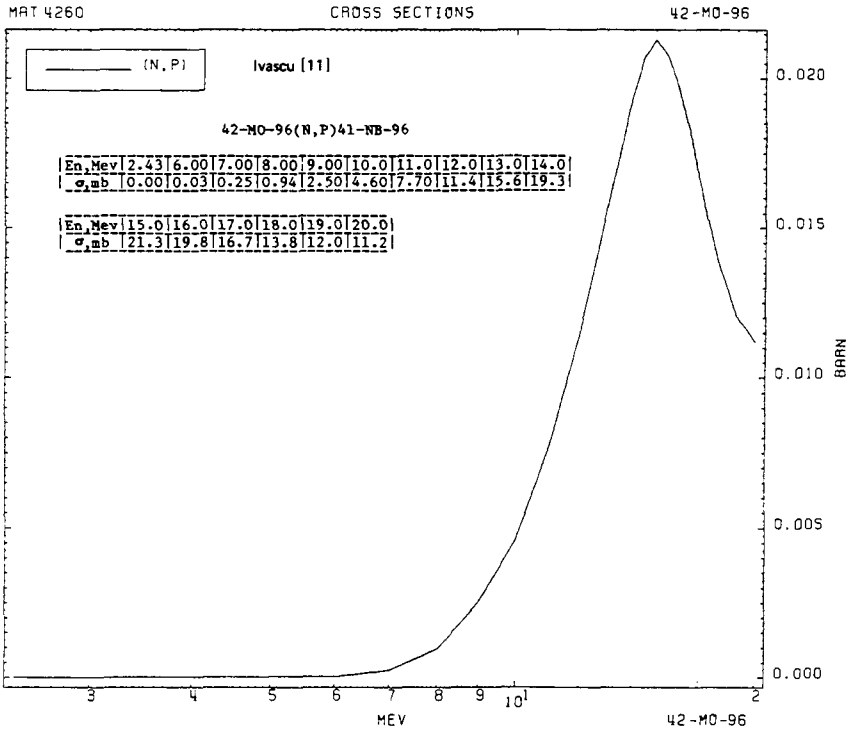
MAT 4260
CROSS SECTIONS
42-MO-96
(N,P)
Ivascu [11]
42-MO-96(N,P)41-NB-96
En,Mev 2.43 6.00 7.00 8.00 9.00 10.0 11.0 12.0 13.0 14.0
σ,mb 0.00 0.03 0.25 0.94 2.50 4.60 7.70 11.4 15.6 19.3
En,Mev 15.0 16.0 17.0 18.0 19.0 20.0
σ,mb 21.3 19.8 16.7 13.8 12.0 11.2
0.020
0.015
0.010
0.005
0.000
BARN
3
4
5
6
7
8
9
10¹
2
MEV
42-MO-96

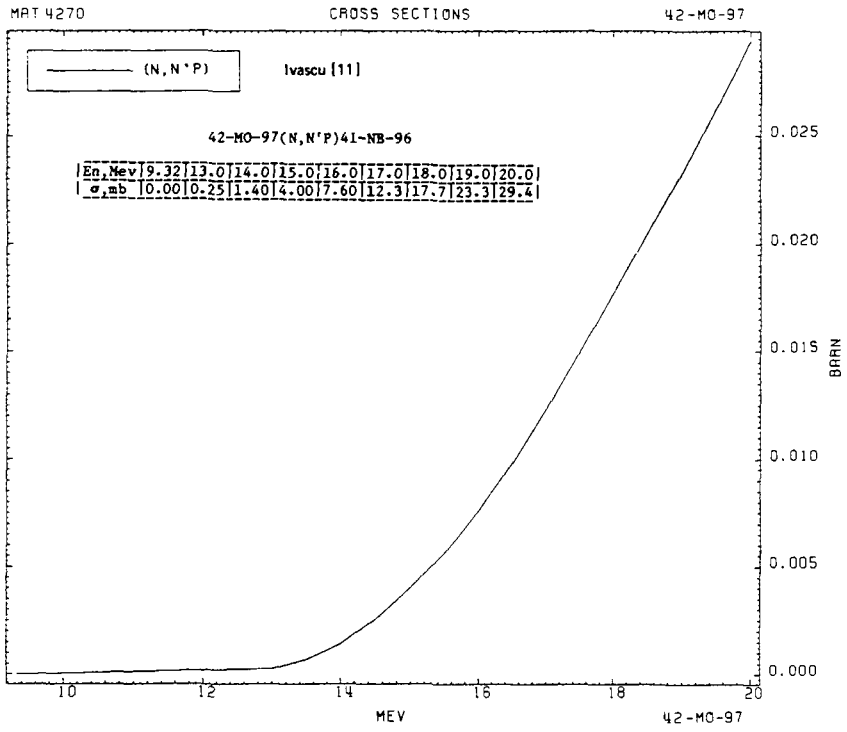
MAT 4270
CROSS SECTIONS
42-MO-97
(N,N'P)
Ivascu [11]
42-MO-97(N,N'P)41-NB-96
En,Mev 9.32 13.0 14.0 15.0 16.0 17.0 18.0 19.0 20.0
σ,mb 0.00 0.25 1.40 4.00 7.60 12.3 17.7 23.3 29.4
0.025
0.020
0.015
0.010
0.005
0.000
BARN
10
12
14
16
18
20
MEV
42-MO-97

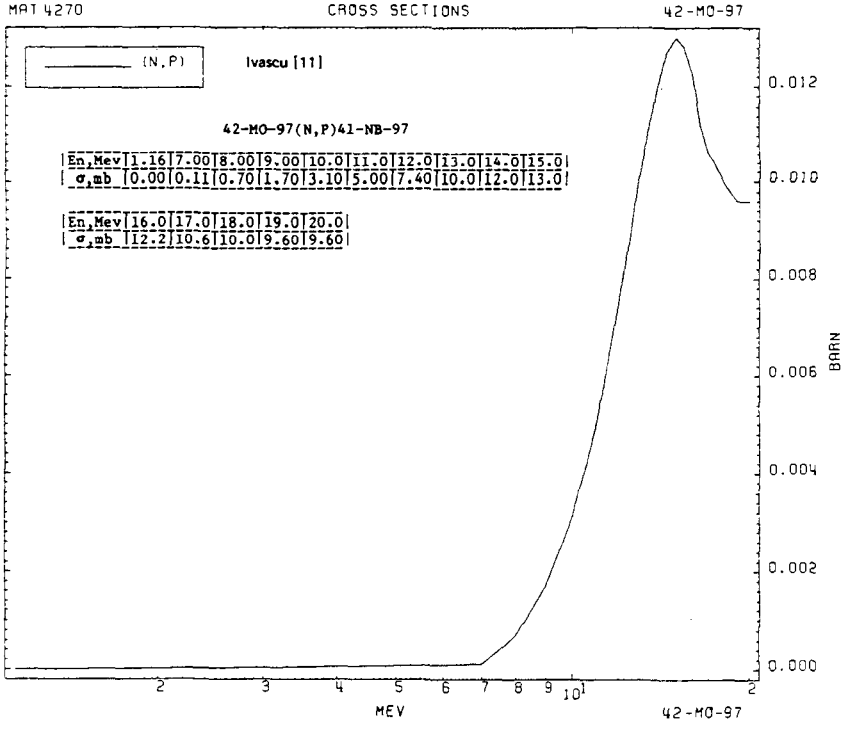
MAT 4270
CROSS SECTIONS
42-MO-97
(N,P)
Ivascu [11]
42-MO-97(N,P)41-NB-97
En,Mev 1.16 7.00 8.00 9.00 10.0 11.0 12.0 13.0 14.0 15.0
σ,mb 0.00 0.11 0.70 1.70 3.10 5.00 7.40 10.0 12.0 13.0
En,Mev 16.0 17.0 18.0 19.0 20.0
σ,mb 12.2 10.6 10.0 9.60 9.60
0.012
0.010
0.008
0.006
0.004
0.002
0.000
BARN
2
3
4
5
6
7
8
9
10
2
MEV
42-MO-97

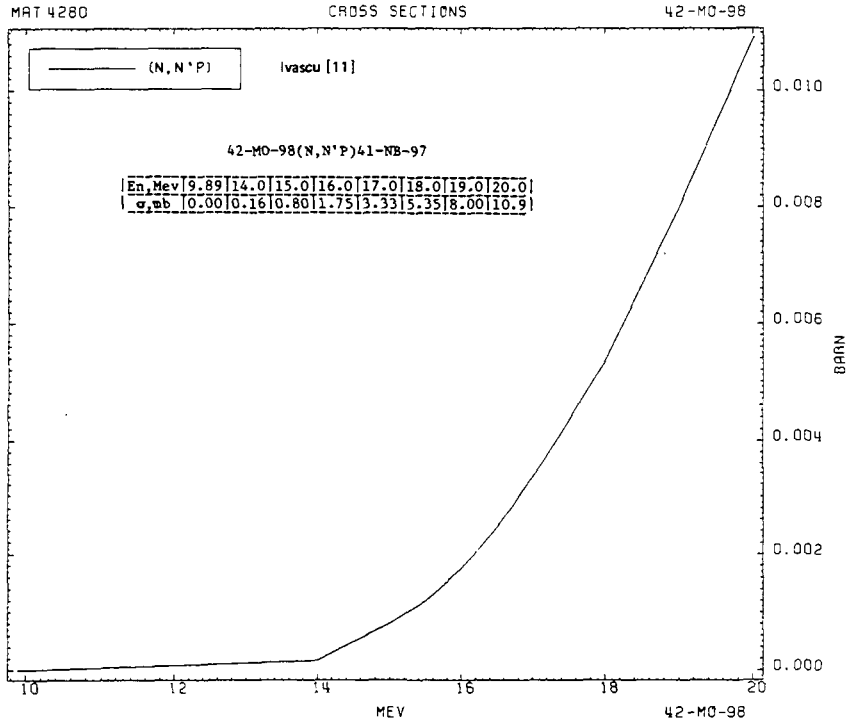
MAT 4280
CROSS SECTIONS
42-MO-98
(N,N'P)
Ivascu [11]
42-MO-98(N,N'P)41-NB-97
En,Mev 9.89 14.0 15.0 16.0 17.0 18.0 19.0 20.0
σ,mb 0.00 0.16 0.80 1.75 3.33 5.35 8.00 10.9
0.010
0.008
0.006
0.004
0.002
0.000
BARN
10
12
14
16
18
20
MEV
42-MO-98

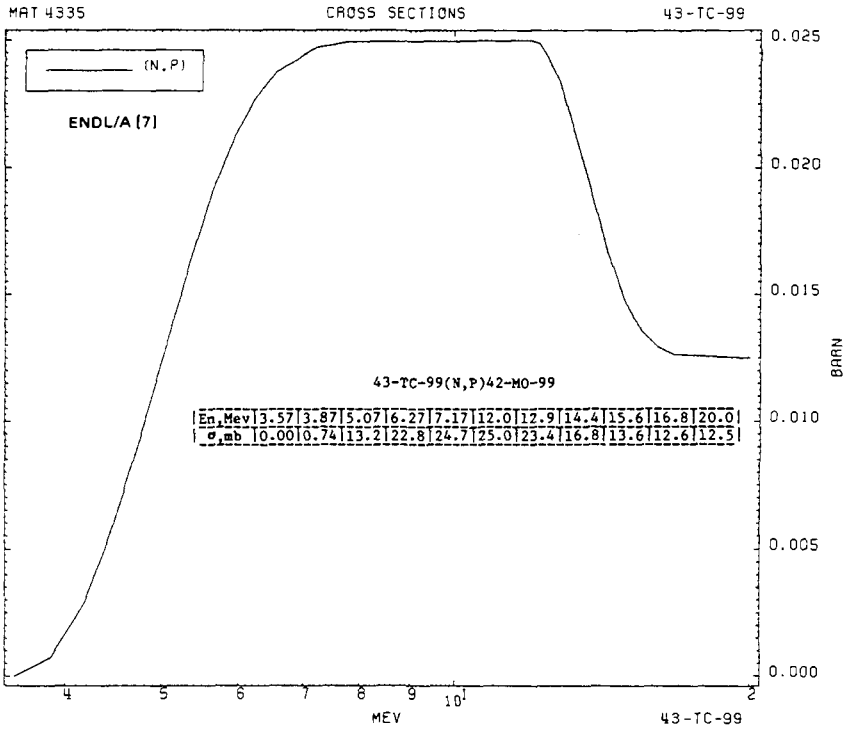
MAT 4335
CROSS SECTIONS
43-TC-99
(N,P)
ENDL/A [7]
43-TC-99(N,P)42-MO-99
En,Mev 3.57 3.87 5.07 6.27 7.17 12.0 12.9 14.4 15.6 16.8 20.0
σ,mb 10.00 10.74 13.2 22.8 24.7 25.0 23.4 16.8 13.6 12.6 12.5
0.025
0.020
0.015
0.010
0.005
0.000
BARN
4
5
6
7
8
9
10
2
MEV
43-TC-99

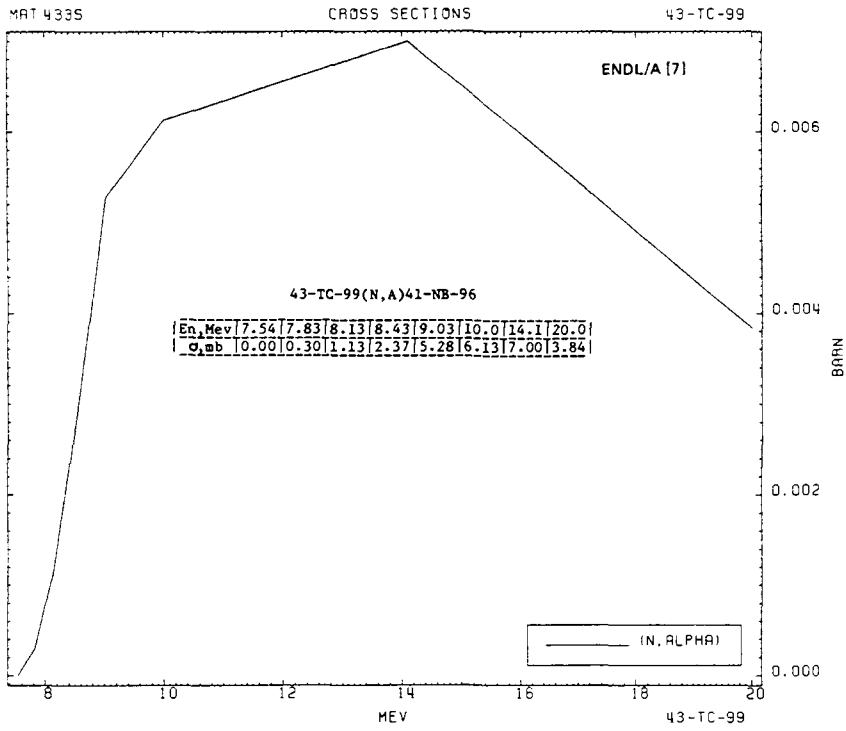
MAT 4335
CROSS SECTIONS
43-TC-99
ENDL/A [7]
43-TC-99(N,A)41-NB-96
En,Mev 7.54 7.83 8.13 8.43 9.03 10.0 14.1 20.0
σ,mb 0.00 0.30 1.13 2.37 5.28 6.13 7.00 3.84
(N, ALPHA)
0.006
0.004
0.002
0.000
BARN
8
10
12
14
16
18
20
MEV
43-TC-99

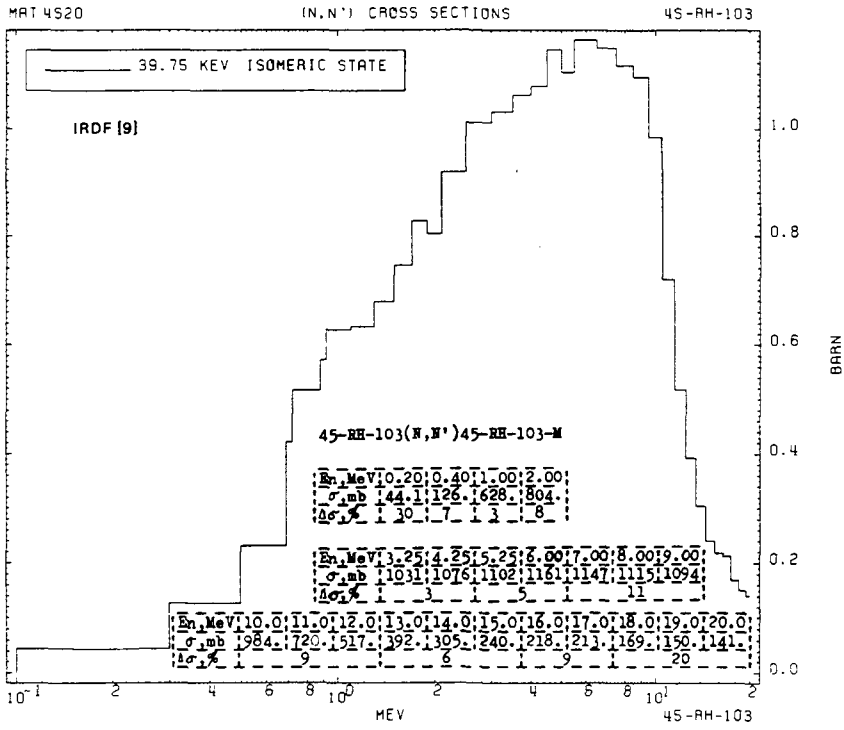
MAT 4520
(N,N') CROSS SECTIONS
45-RH-103
39.75 KEV ISOMERIC STATE
IRDF [9]
45-RH-103(N,N')45-RH-103-M
En,MeV 0.20 0.40 1.00 2.00
σ,mb 44.1 126. 628. 804.
Δσ,% 30 7 3 8
En,MeV 3.25 4.25 5.25 6.00 7.00 8.00 9.00
σ,mb 1031 1076 1102 1161 1147 1115 1094
Δσ,% 3 5 11
En,MeV 10.0 11.0 12.0 13.0 14.0 15.0 16.0 17.0 18.0 19.0 20.0
σ,mb 984. 720. 517. 392. 305. 240. 218. 211. 169. 150. 141.
Δσ,% 9 6 9 20
1.0
0.8
0.6
0.4
0.2
0.0
BARN
10⁻¹
2
4
6
8
10⁰
2
4
6
8
10¹
2
MEV
45-RH-103

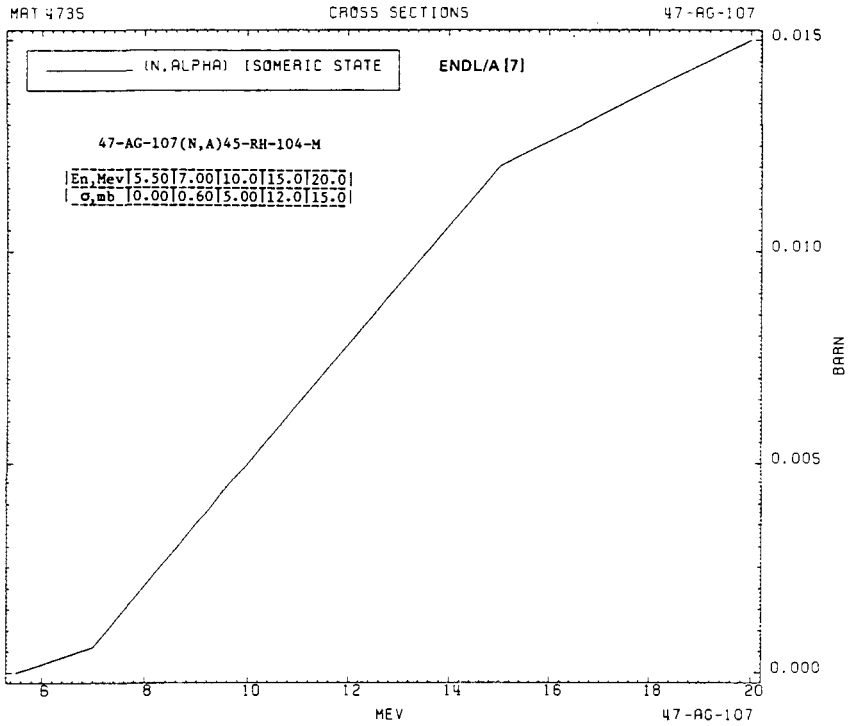
MAT 4735
CROSS SECTIONS
47-AG-107
(N,ALPHA) ISOMERIC STATE
ENDL/A [7]
47-AG-107(N,A)45-RH-104-M
En,Mev | 5.50 | 7.00 | 10.0 | 15.0 | 20.0
σ,mb | 0.00 | 0.60 | 5.00 | 12.0 | 15.0
0.015
0.010
0.005
0.000
BARN
6
8
10
12
14
16
18
20
MEV
47-AG-107

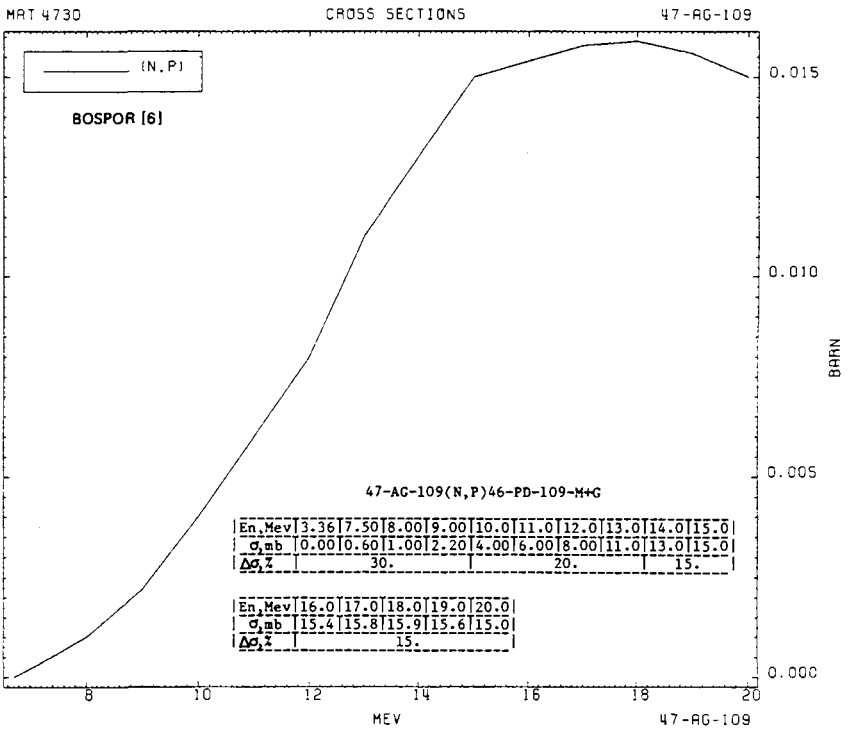
MAT 4730
CROSS SECTIONS
47-AG-109
(N,P)
BOSPOR [6]
47-AG-109(N,P)46-PD-109-M+G
En,Mev | 3.36 | 7.50 | 8.00 | 9.00 | 10.0 | 11.0 | 12.0 | 13.0 | 14.0 | 15.0
σ,mb | 0.00 | 0.60 | 1.00 | 2.20 | 4.00 | 6.00 | 8.00 | 11.0 | 13.0 | 15.0
Δσ,% | 30. | 20. | 15.
En,Mev | 16.0 | 17.0 | 18.0 | 19.0 | 20.0
σ,mb | 15.4 | 15.8 | 15.9 | 15.6 | 15.0
Δσ,% | 15.
0.015
0.010
0.005
0.000
BARN
8
10
12
14
16
18
20
MEV
47-AG-109

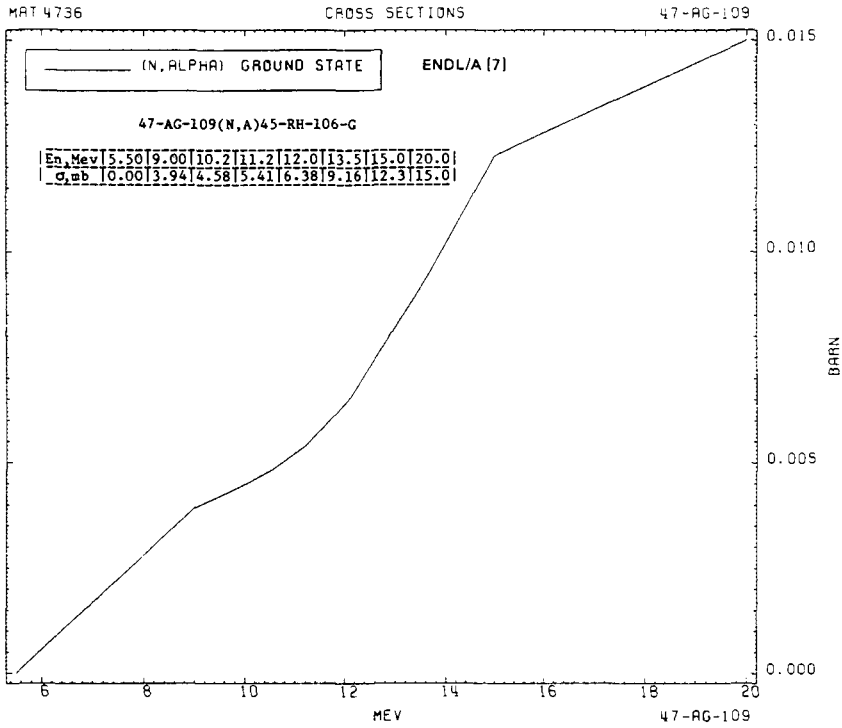
MAT 4736
CROSS SECTIONS
47-AG-109
(N,ALPHA) GROUND STATE
ENDL/A [7]
47-AG-109(N,A)45-RH-106-G
En,Mev 5.50 9.00 10.2 11.2 12.0 13.5 15.0 20.0
σ,mb 0.00 3.94 4.58 5.41 6.38 9.16 12.3 15.0
0.015
0.010
0.005
0.000
BARN
6 8 10 12 14 16 18 20
MEV
47-AG-109

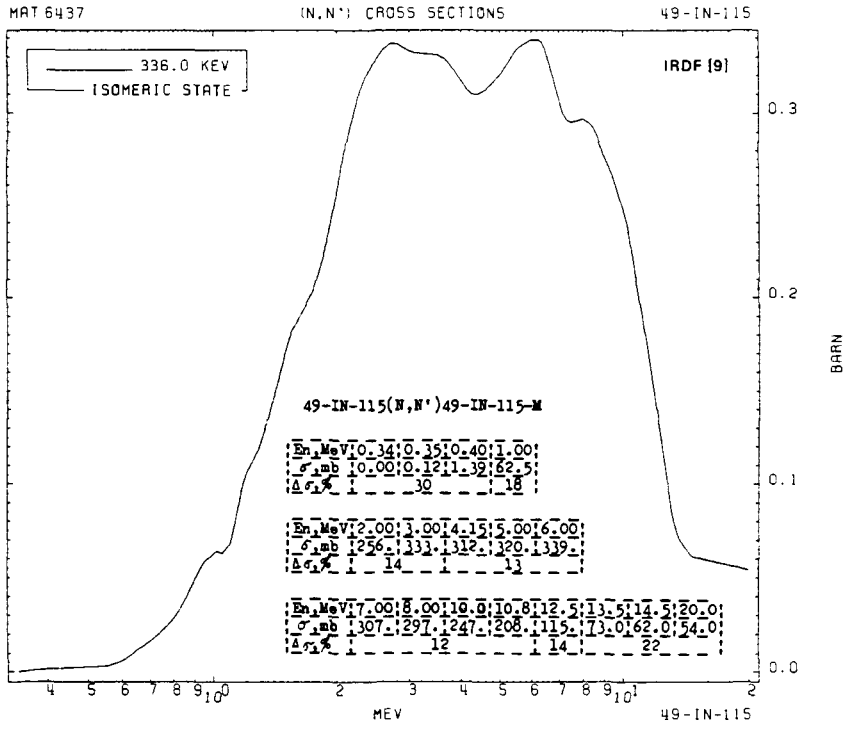
MAT 6437
(N,N') CROSS SECTIONS
49-IN-115
336.0 KEV
ISOMERIC STATE
IRDF [9]
49-IN-115(N,N')49-IN-115-M
En,MeV 0.34 0.35 0.40 1.00
σ,mb 0.00 0.12 1.39 62.5
Δσ,% 30 18
En,MeV 2.00 3.00 4.15 5.00 6.00
σ,mb 256. 331. 312. 320. 339.
Δσ,% 14 13
En,MeV 7.00 8.00 10.0 10.8 12.5 13.5 14.5 20.0
σ,mb 307. 297. 247. 208. 115. 73.0 62.0 54.0
Δσ,% 12 14 22
0.3
0.2
0.1
0.0
BARN
4 5 6 7 8 9 10 2 3 4 5 6 7 8 9 10 2
MEV
49-IN-115

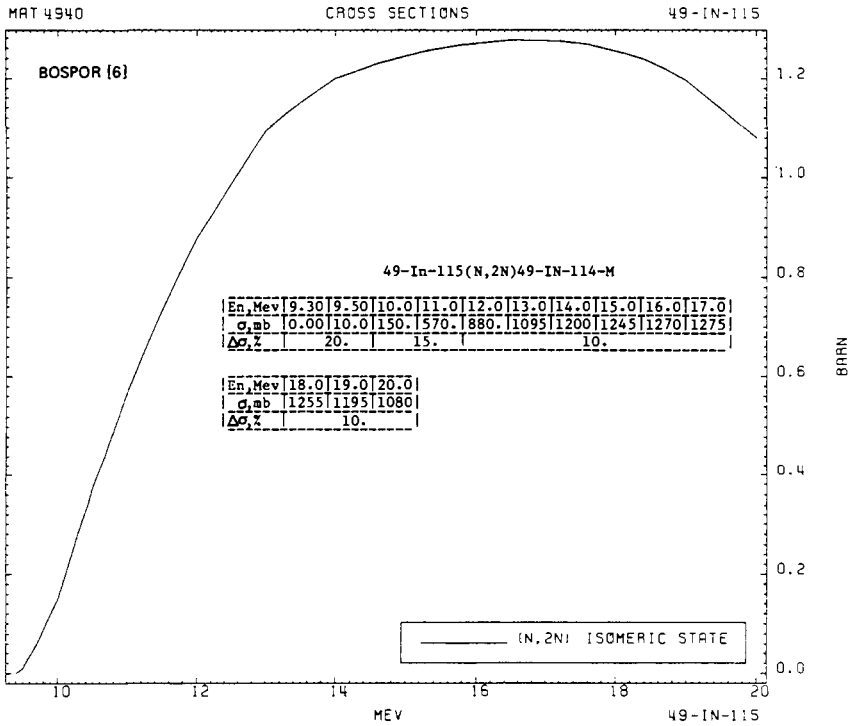
MAT 4940
CROSS SECTIONS
49-IN-115
BOSPOR [6]
49-In-115(N,2N)49-IN-114-M
En,Mev | 9.30 | 9.50 | 10.0 | 11.0 | 12.0 | 13.0 | 14.0 | 15.0 | 16.0 | 17.0
σ,mb | 0.00 | 10.0 | 150. | 570. | 880. | 1095 | 1200 | 1245 | 1270 | 1275
Δσ,% | 20. | 15. | 10.
En,Mev | 18.0 | 19.0 | 20.0
σ,mb | 1255 | 1195 | 1080
Δσ,% | 10.
(N,2N) ISOMERIC STATE
BARN
MEV
49-IN-115

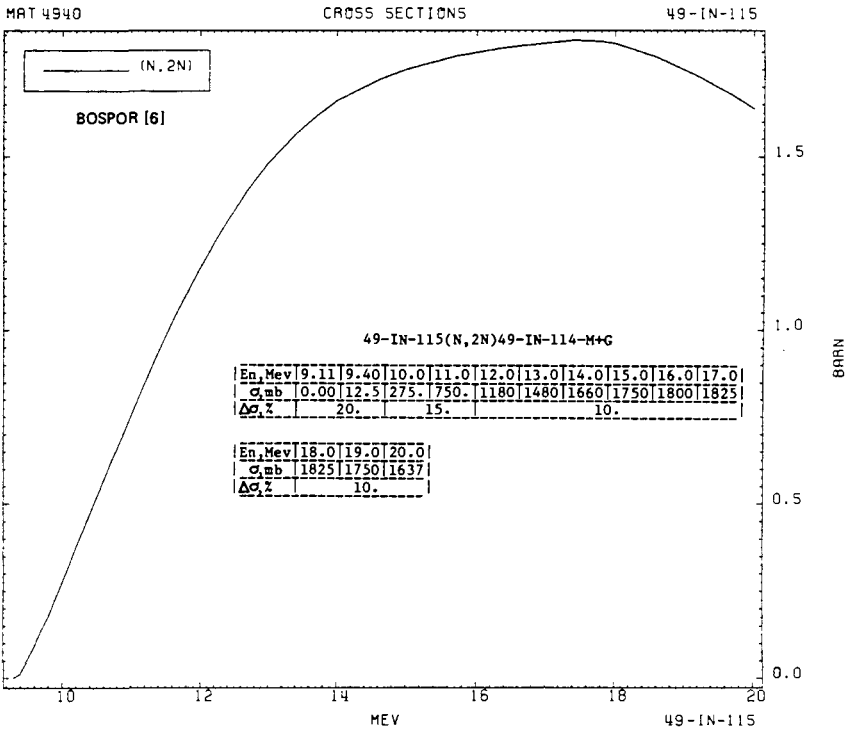
MAT 4940
CROSS SECTIONS
49-IN-115
(N,2N)
BOSPOR [6]
49-IN-115(N,2N)49-IN-114-M+G
En,Mev | 9.11 | 9.40 | 10.0 | 11.0 | 12.0 | 13.0 | 14.0 | 15.0 | 16.0 | 17.0
σ,mb | 0.00 | 12.5 | 275. | 750. | 1180 | 1480 | 1660 | 1750 | 1800 | 1825
Δσ,% | 20. | 15. | 10.
En,Mev | 18.0 | 19.0 | 20.0
σ,mb | 1825 | 1750 | 1637
Δσ,% | 10.
BARN
MEV
49-IN-115

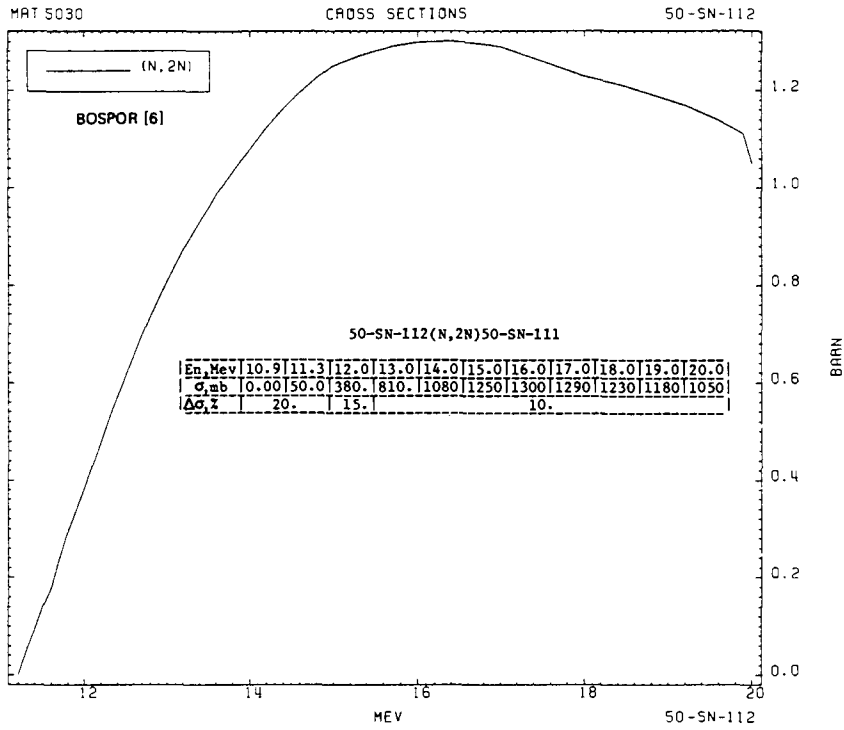
MAT 5030
CROSS SECTIONS
50-SN-112
(N,2N)
BOSPOR [6]
50-SN-112(N,2N)50-SN-111
En,Mev | 10.9 | 11.3 | 12.0 | 13.0 | 14.0 | 15.0 | 16.0 | 17.0 | 18.0 | 19.0 | 20.0
σ,mb | 0.00 | 50.0 | 380. | 810. | 1080 | 1250 | 1300 | 1290 | 1230 | 1180 | 1050
Δσ,% | 20. | 15. | 10.
1.2
1.0
0.8
0.6
0.4
0.2
0.0
BARN
12
14
16
18
20
MEV
50-SN-112

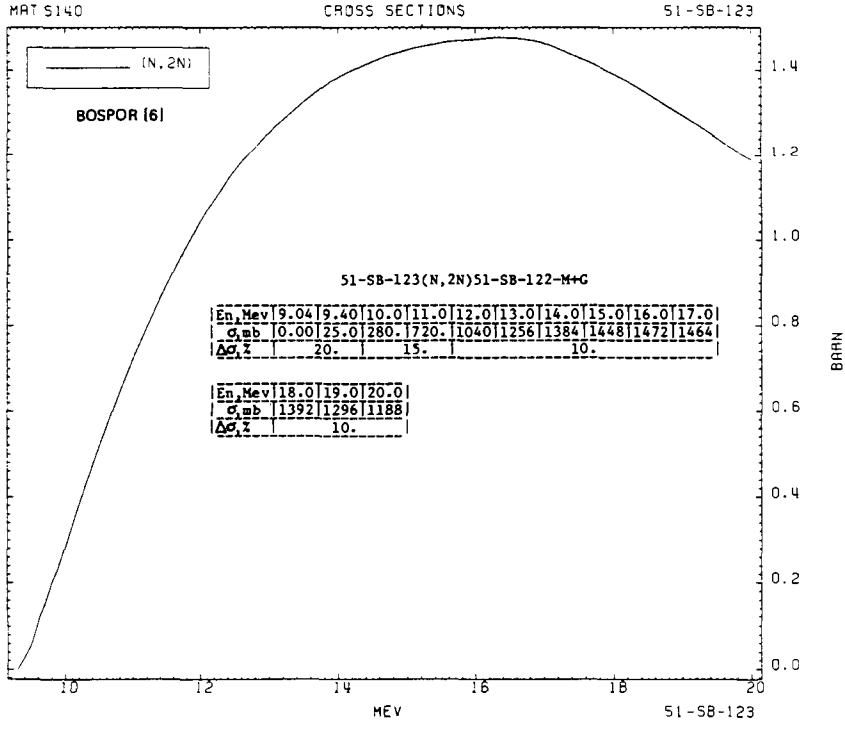
MAT 5140
CROSS SECTIONS
51-SB-123
(N,2N)
BOSPOR [6]
51-SB-123(N,2N)51-SB-122-M+G
En,Mev | 9.04 | 9.40 | 10.0 | 11.0 | 12.0 | 13.0 | 14.0 | 15.0 | 16.0 | 17.0
σ,mb | 0.00 | 25.0 | 280. | 720. | 1040 | 1256 | 1384 | 1448 | 1472 | 1464
Δσ,% | 20. | 15. | 10.
En,Mev | 18.0 | 19.0 | 20.0
σ,mb | 1392 | 1296 | 1188
Δσ,% | 10.
1.4
1.2
1.0
0.8
0.6
0.4
0.2
0.0
BARN
10
12
14
16
18
20
MEV
51-SB-123

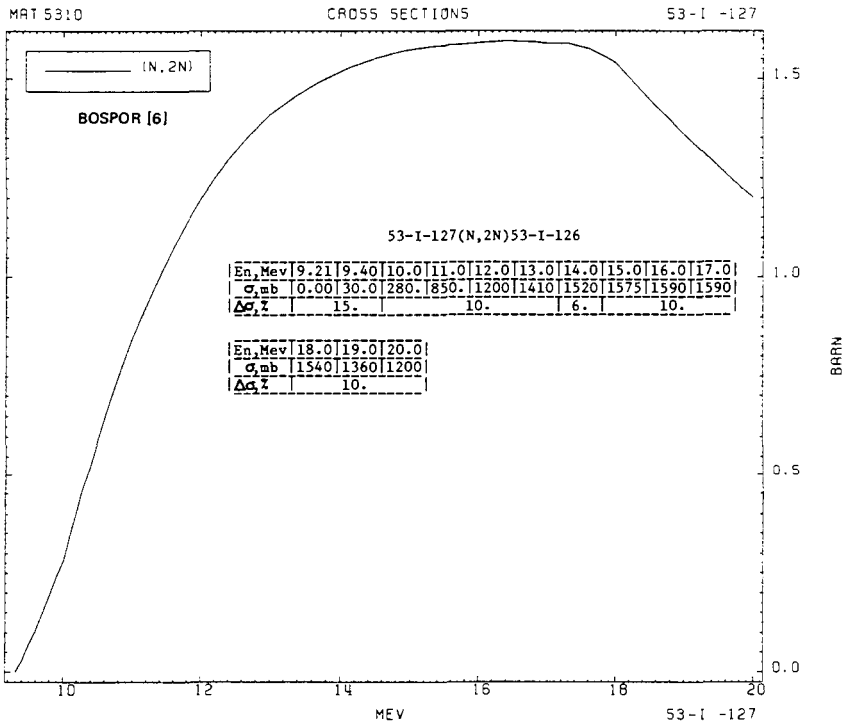
MAT 5310
CROSS SECTIONS
53-I -127
(N,2N)
BOSPOR [6]
53-I-127(N,2N)53-I-126
En,Mev | 9.21 | 9.40 | 10.0 | 11.0 | 12.0 | 13.0 | 14.0 | 15.0 | 16.0 | 17.0
σ,mb | 0.00 | 30.0 | 280. | 850. | 1200 | 1410 | 1520 | 1575 | 1590 | 1590
Δσ,% | 15. | 10. | 6. | 10.
En,Mev | 18.0 | 19.0 | 20.0
σ,mb | 1540 | 1360 | 1200
Δσ,% | 10.
1.5
1.0
0.5
0.0
BARN
10
12
14
16
18
20
MEV
53-I -127

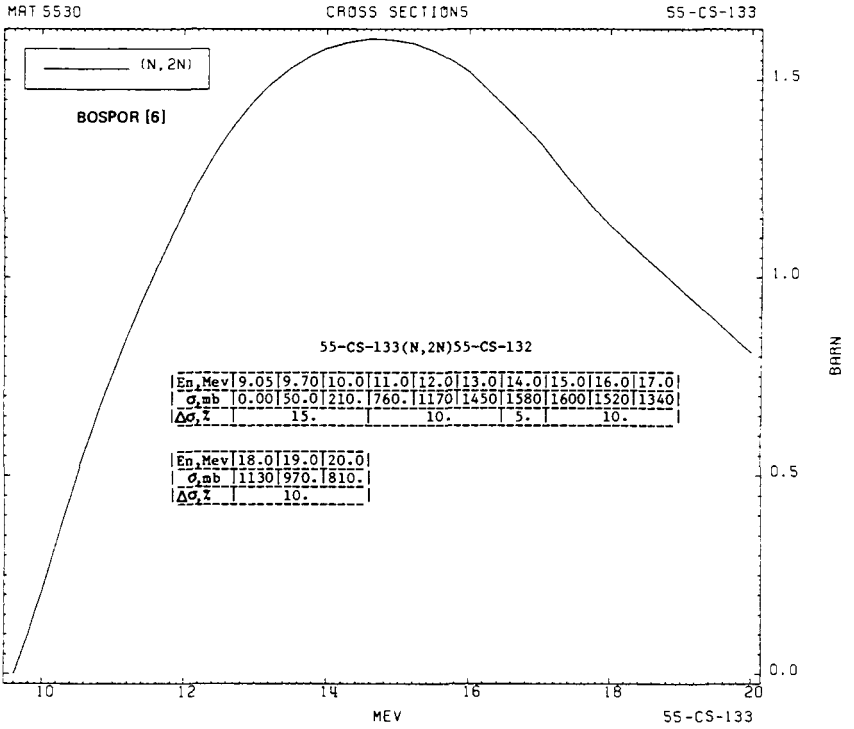
MAT 5530
CROSS SECTIONS
55-CS-133
(N,2N)
BOSPOR [6]
55-CS-133(N,2N)55-CS-132
En,Mev | 9.05 | 9.70 | 10.0 | 11.0 | 12.0 | 13.0 | 14.0 | 15.0 | 16.0 | 17.0
σ,mb | 0.00 | 50.0 | 210. | 760. | 1170 | 1450 | 1580 | 1600 | 1520 | 1340
Δσ,% | 15. | 10. | 5. | 10.
En,Mev | 18.0 | 19.0 | 20.0
σ,mb | 1130 | 970. | 810.
Δσ,% | 10.
1.5
1.0
0.5
0.0
BARN
10
12
14
16
18
20
MEV
55-CS-133

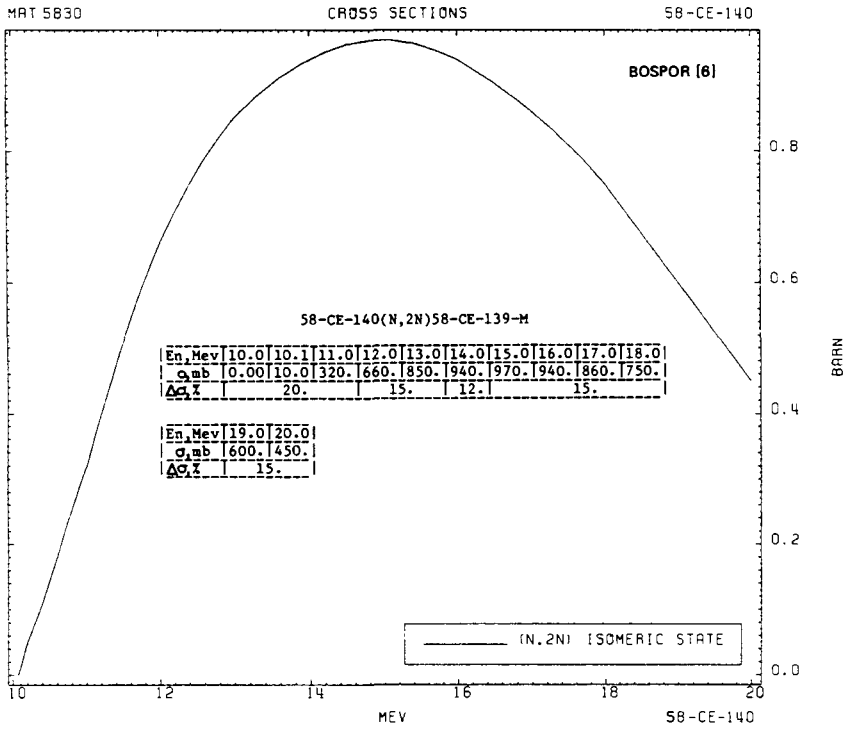
MAT 5830
CROSS SECTIONS
58-CE-140
BOSPOR [6]
58-CE-140(N,2N)58-CE-139-M
En,Mev | 10.0 | 10.1 | 11.0 | 12.0 | 13.0 | 14.0 | 15.0 | 16.0 | 17.0 | 18.0
σ,mb | 0.00 | 10.0 | 320. | 660. | 850. | 940. | 970. | 940. | 860. | 750.
Δσ,% | 20. | 15. | 12. | 15.
En,Mev | 19.0 | 20.0
σ,mb | 600. | 450.
Δσ,% | 15.
(N,2N) ISOMERIC STATE
0.0
0.2
0.4
0.6
0.8
BARN
10
12
14
16
18
20
MEV
58-CE-140

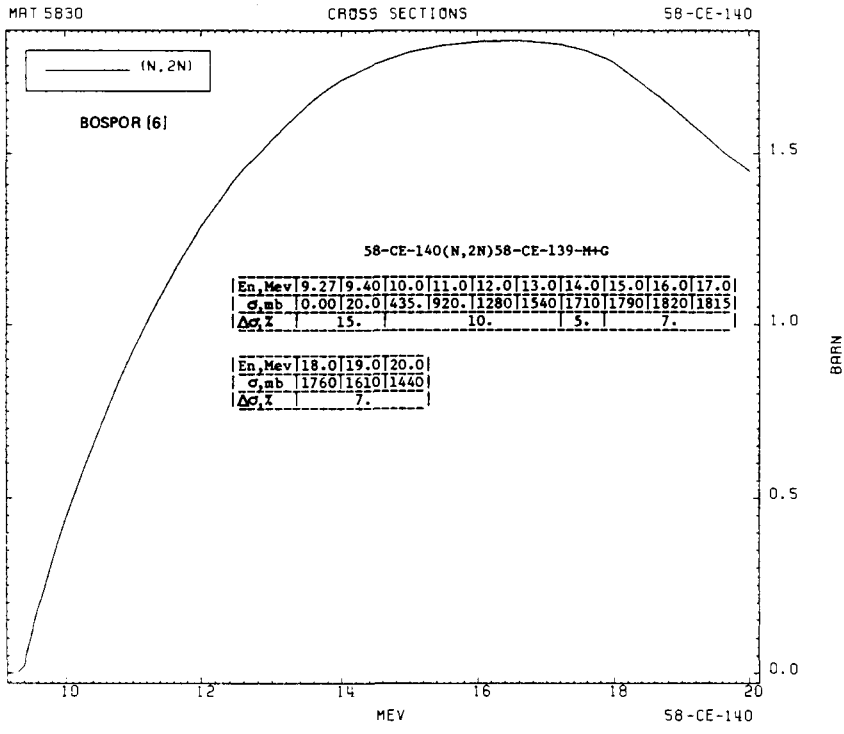
MAT 5830
CROSS SECTIONS
58-CE-140
(N,2N)
BOSPOR [6]
58-CE-140(N,2N)58-CE-139-M+G
En,Mev | 9.27 | 9.40 | 10.0 | 11.0 | 12.0 | 13.0 | 14.0 | 15.0 | 16.0 | 17.0
σ,mb | 0.00 | 20.0 | 435. | 920. | 1280 | 1540 | 1710 | 1790 | 1820 | 1815
Δσ,% | 15. | 10. | 5. | 7.
En,Mev | 18.0 | 19.0 | 20.0
σ,mb | 1760 | 1610 | 1440
Δσ,% | 7.
0.0
0.5
1.0
1.5
BARN
10
12
14
16
18
20
MEV
58-CE-140

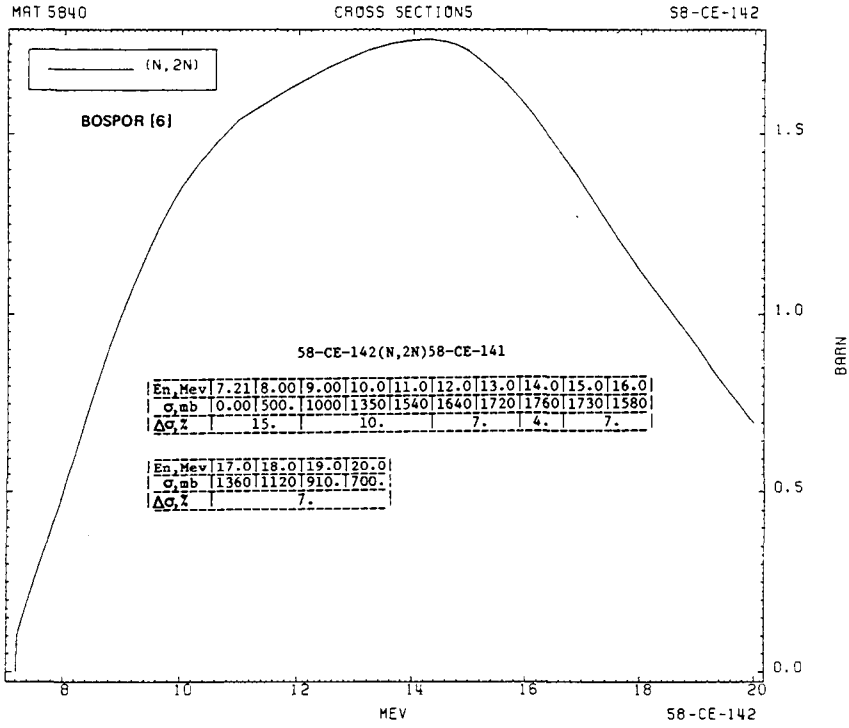
MAT 5840
CROSS SECTIONS
58-CE-142
(N,2N)
BOSPOR [6]
58-CE-142(N,2N)58-CE-141
En,Mev | 7.21 | 8.00 | 9.00 | 10.0 | 11.0 | 12.0 | 13.0 | 14.0 | 15.0 | 16.0
σ,mb | 0.00 | 500. | 1000 | 1350 | 1540 | 1640 | 1720 | 1760 | 1730 | 1580
Δσ,% | 15. | 10. | 7. | 4. | 7.
En,Mev | 17.0 | 18.0 | 19.0 | 20.0
σ,mb | 1360 | 1120 | 910. | 700.
Δσ,% | 7.
1.5
1.0
0.5
0.0
BARN
8
10
12
14
16
18
20
MEV
58-CE-142

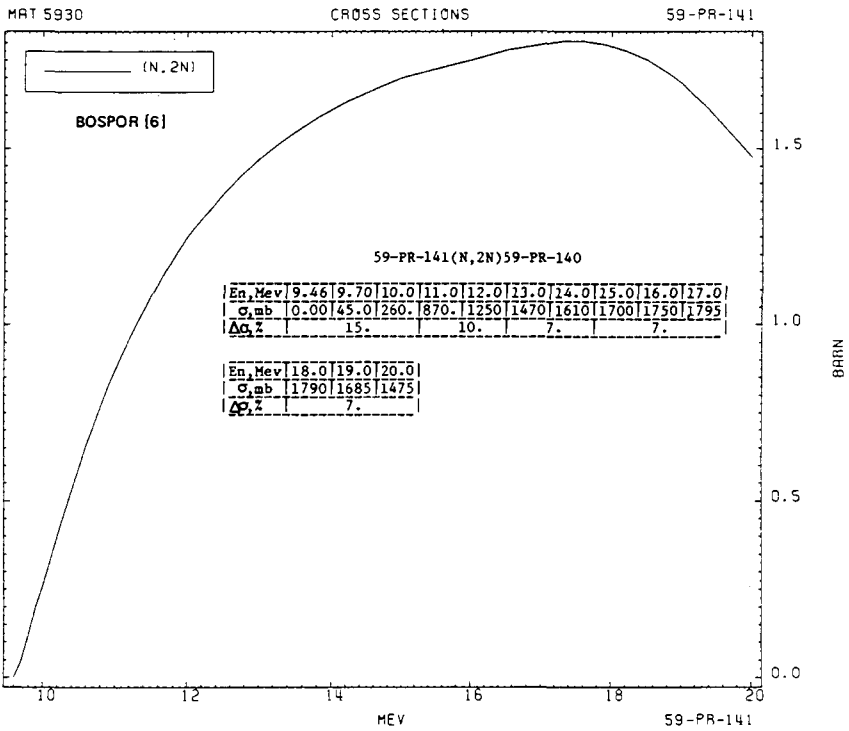
MAT 5930
CROSS SECTIONS
59-PR-141
(N,2N)
BOSPOR [6]
59-PR-141(N,2N)59-PR-140
En,Mev | 9.46 | 9.70 | 10.0 | 11.0 | 12.0 | 13.0 | 14.0 | 15.0 | 16.0 | 17.0
σ,mb | 0.00 | 45.0 | 260. | 870. | 1250 | 1470 | 1610 | 1700 | 1750 | 1795
Δσ,% | 15. | 10. | 7. | 7.
En,Mev | 18.0 | 19.0 | 20.0
σ,mb | 1790 | 1685 | 1475
Δσ,% | 7.
1.5
1.0
0.5
0.0
BARN
10
12
14
16
18
20
MEV
59-PR-141

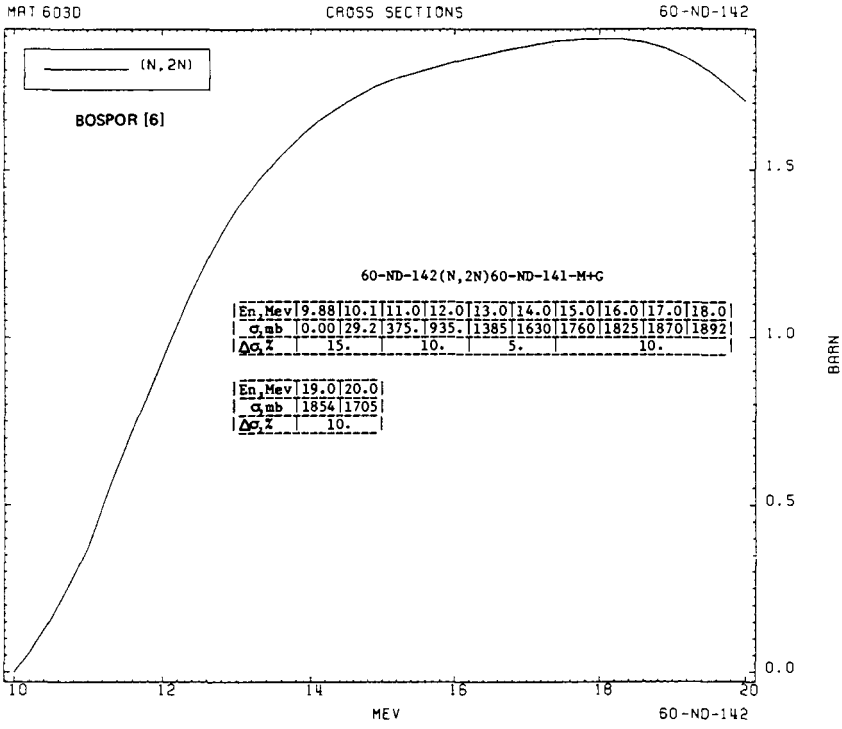
MAT 6030
CROSS SECTIONS
60-ND-142
(N,2N)
BOSPOR [6]
60-ND-142(N,2N)60-ND-141-M+G
En,Mev | 9.88 | 10.1 | 11.0 | 12.0 | 13.0 | 14.0 | 15.0 | 16.0 | 17.0 | 18.0
σ,mb | 0.00 | 29.2 | 375. | 935. | 1385 | 1630 | 1760 | 1825 | 1870 | 1892
Δσ,% | 15. | 10. | 5. | 10.
En,Mev | 19.0 | 20.0
σ,mb | 1854 | 1705
Δσ,% | 10.
1.5
1.0
0.5
0.0
BARN
10
12
14
16
18
20
MEV
60-ND-142

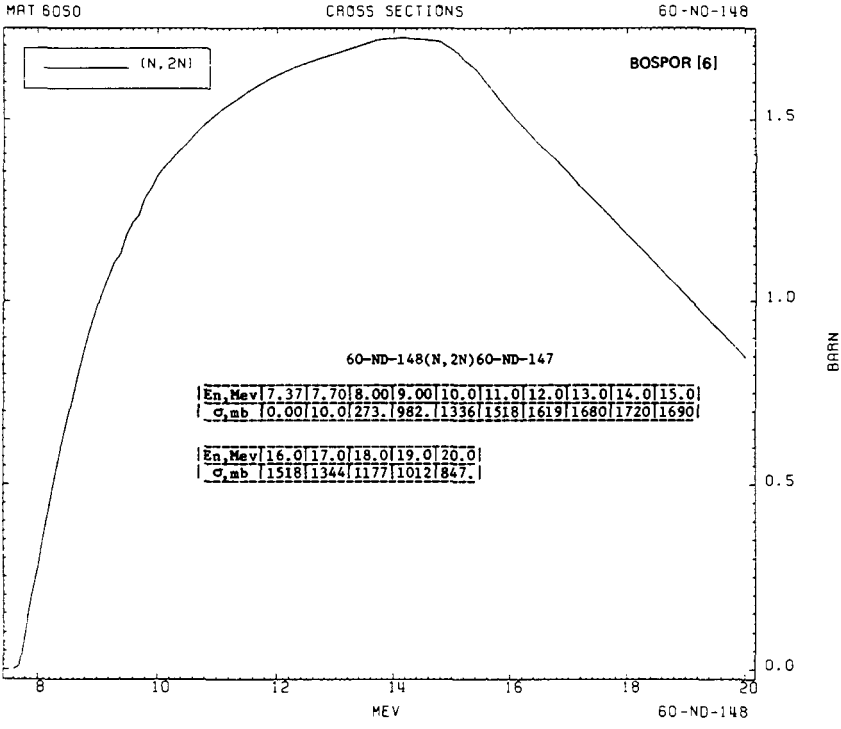
MAT 6050
CROSS SECTIONS
60-ND-148
(N,2N)
BOSPOR [6]
60-ND-148(N,2N)60-ND-147
En,Mev | 7.37 | 7.70 | 8.00 | 9.00 | 10.0 | 11.0 | 12.0 | 13.0 | 14.0 | 15.0
σ,mb | 0.00 | 10.0 | 273. | 982. | 1336 | 1518 | 1619 | 1680 | 1720 | 1690
En,Mev | 16.0 | 17.0 | 18.0 | 19.0 | 20.0
σ,mb | 1518 | 1344 | 1177 | 1012 | 847.
1.5
1.0
0.5
0.0
BARN
8
10
12
14
16
18
20
MEV
60-ND-148

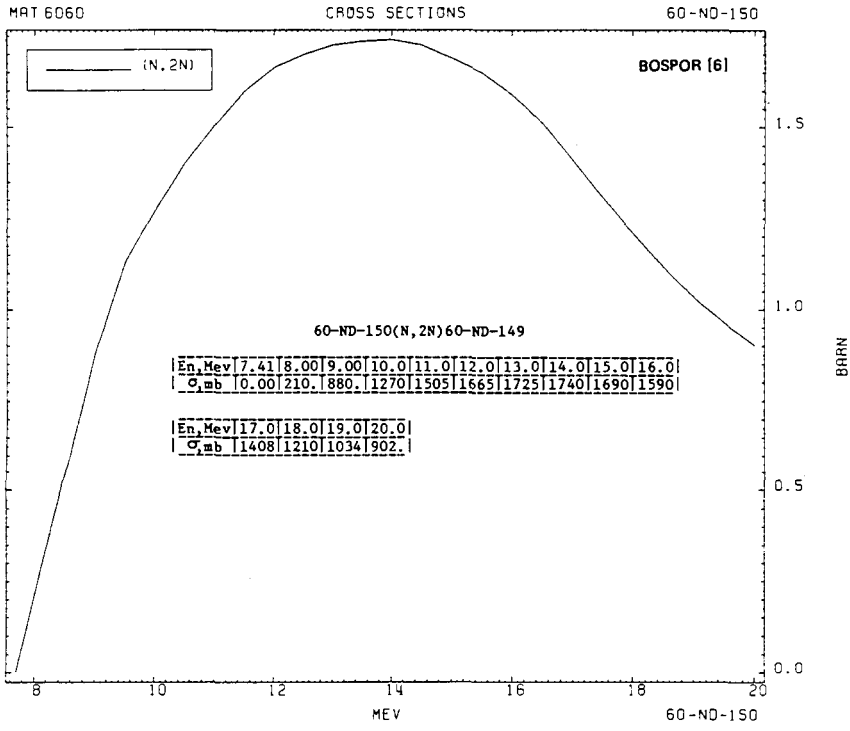
MAT 6060
CROSS SECTIONS
60-ND-150
(N,2N)
BOSPOR [6]
60-ND-150(N,2N)60-ND-149
En,Mev | 7.41 | 8.00 | 9.00 | 10.0 | 11.0 | 12.0 | 13.0 | 14.0 | 15.0 | 16.0
σ,mb | 0.00 | 210. | 880. | 1270 | 1505 | 1665 | 1725 | 1740 | 1690 | 1590
En,Mev | 17.0 | 18.0 | 19.0 | 20.0
σ,mb | 1408 | 1210 | 1034 | 902.
1.5
1.0
0.5
0.0
BARN
8
10
12
14
16
18
20
MEV
60-ND-150

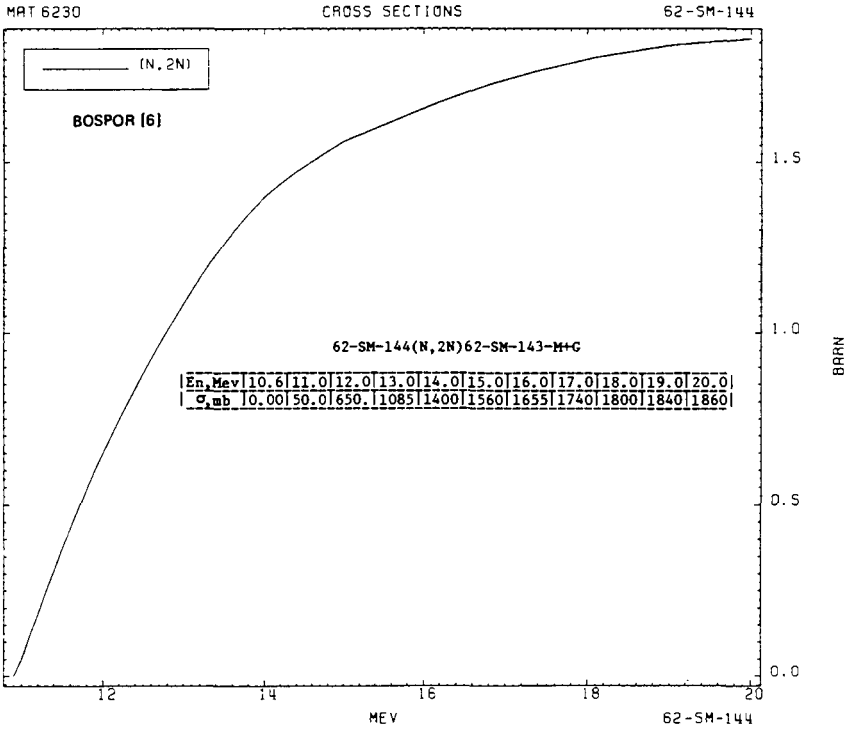
MAT 6230
CROSS SECTIONS
62-SM-144
(N,2N)
BOSPOR [6]
62-SM-144(N,2N)62-SM-143-M+G
En,Mev | 10.6 | 11.0 | 12.0 | 13.0 | 14.0 | 15.0 | 16.0 | 17.0 | 18.0 | 19.0 | 20.0
σ,mb | 0.00 | 50.0 | 650. | 1085 | 1400 | 1560 | 1655 | 1740 | 1800 | 1840 | 1860
1.5
1.0
0.5
0.0
BARN
12
14
16
18
20
MEV
62-SM-144

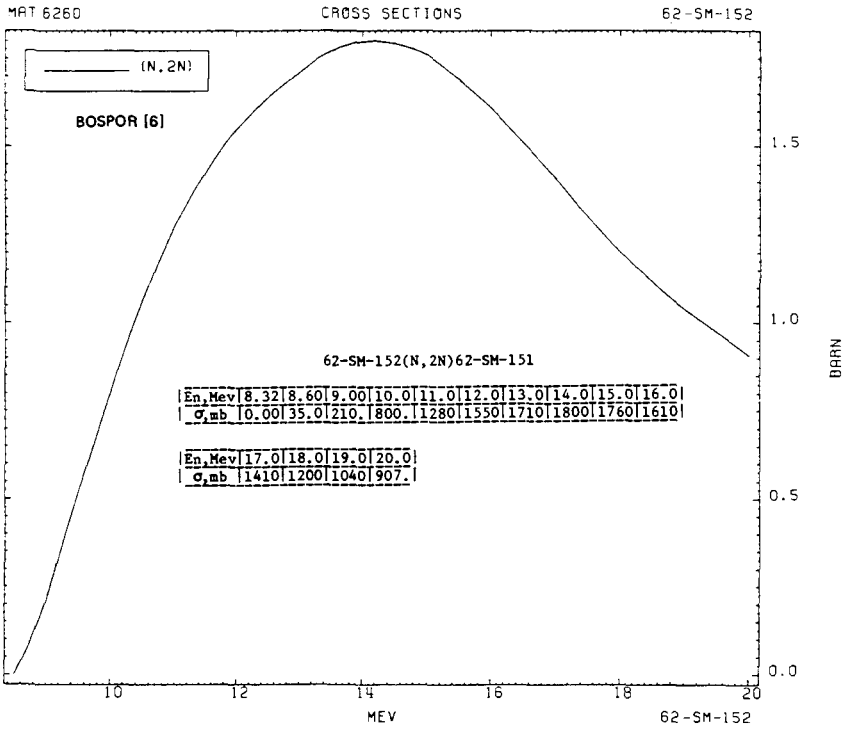
MAT 6260
CROSS SECTIONS
62-SM-152
(N,2N)
BOSPOR [6]
62-SM-152(N,2N)62-SM-151
En,Mev 8.32 8.60 9.00 10.0 11.0 12.0 13.0 14.0 15.0 16.0
σ,mb 0.00 35.0 210. 800. 1280 1550 1710 1800 1760 1610
En,Mev 17.0 18.0 19.0 20.0
σ,mb 1410 1200 1040 907.
1.5
1.0
0.5
0.0
BARN
10
12
14
16
18
20
MEV
62-SM-152

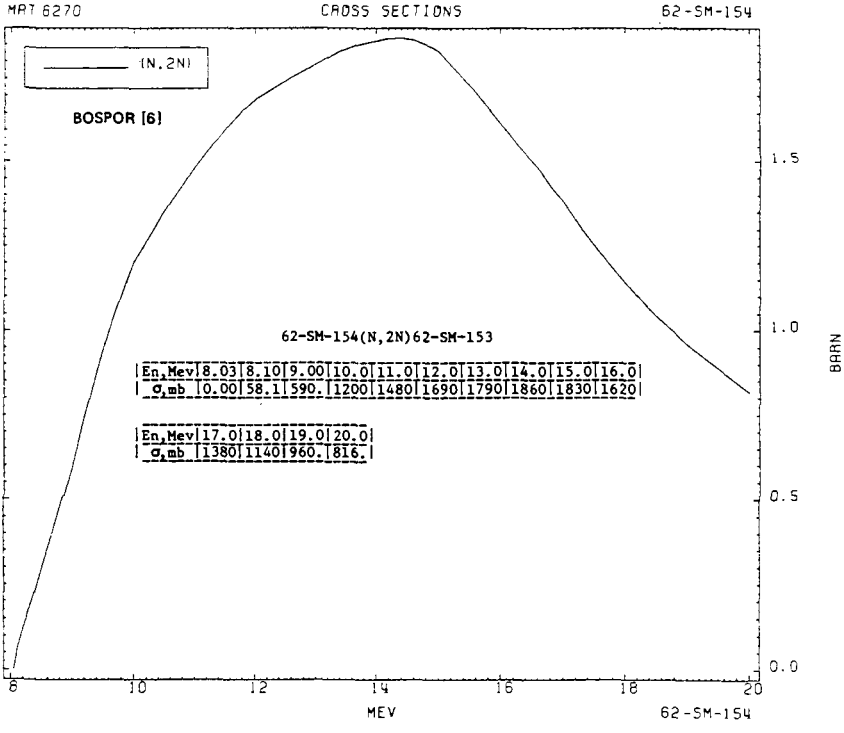
MAT 6270
CROSS SECTIONS
62-SM-154
(N,2N)
BOSPOR [6]
62-SM-154(N,2N)62-SM-153
En,Mev 8.03 8.10 9.00 10.0 11.0 12.0 13.0 14.0 15.0 16.0
σ,mb 0.00 58.1 590. 1200 1480 1690 1790 1860 1830 1620
En,Mev 17.0 18.0 19.0 20.0
σ,mb 1380 1140 960. 816.
1.5
1.0
0.5
0.0
BARN
8
10
12
14
16
18
20
MEV
62-SM-154

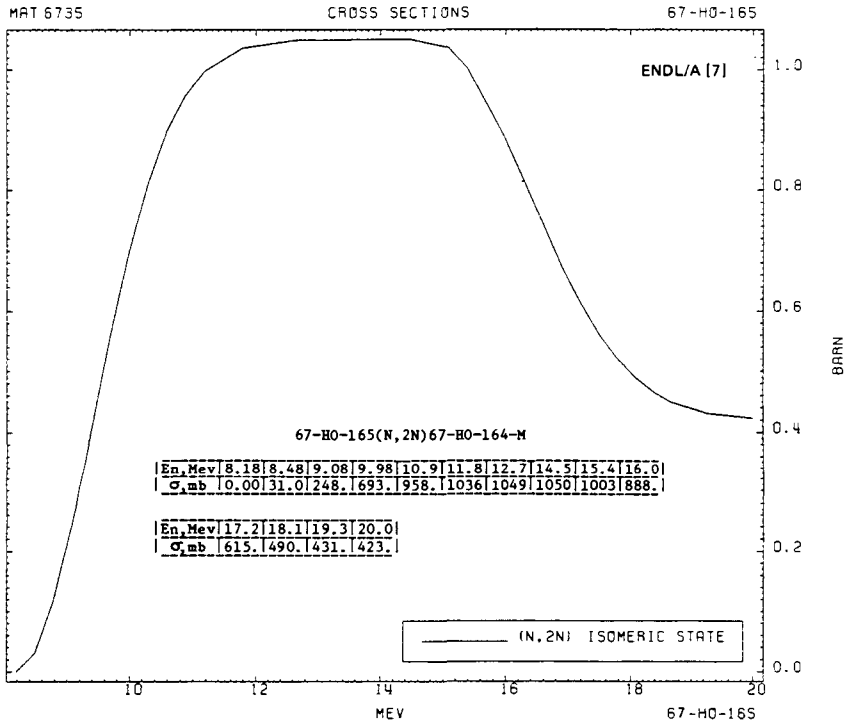
MAT 6735
CROSS SECTIONS
67-HO-165
ENDL/A [7]
67-HO-165(N,2N)67-HO-164-M
En,Mev 8.18 8.48 9.08 9.98 10.9 11.8 12.7 14.5 15.4 16.0
σ,mb 0.00 31.0 248. 693. 958. 1036 1049 1050 1003 888.
En,Mev 17.2 18.1 19.3 20.0
σ,mb 615. 490. 431. 423.
(N,2N) ISOMERIC STATE
BARN
MEV
67-HO-165

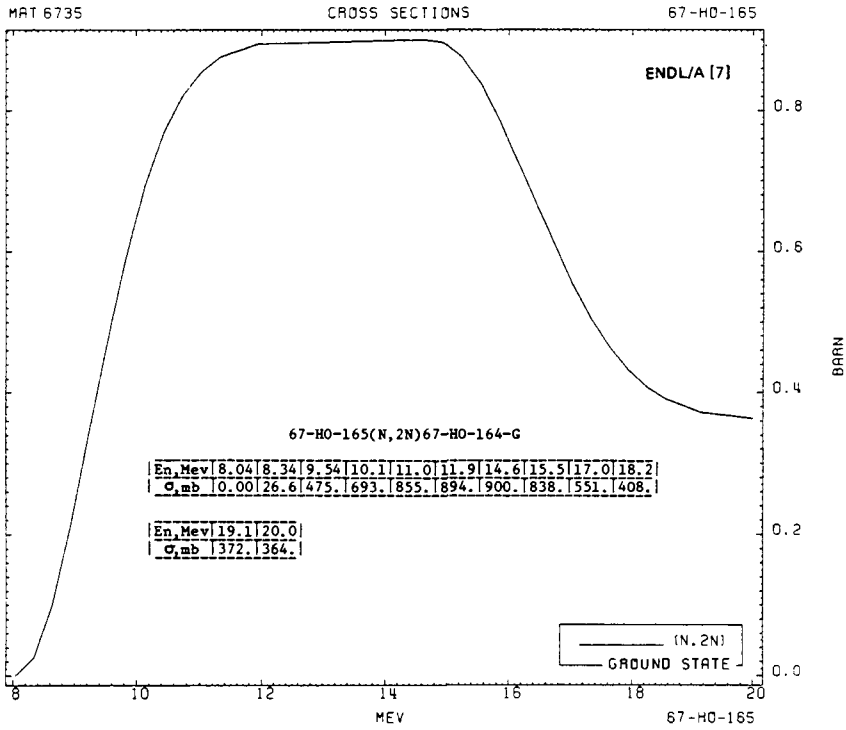
MAT 6735
CROSS SECTIONS
67-HO-165
ENDL/A [7]
67-HO-165(N,2N)67-HO-164-G
En,Mev 8.04 8.34 9.54 10.1 11.0 11.9 14.6 15.5 17.0 18.2
σ,mb 0.00 26.6 475. 693. 855. 894. 900. 838. 551. 408.
En,Mev 19.1 20.0
σ,mb 372. 364.
(N,2N)
GROUND STATE
BARN
MEV
67-HO-165

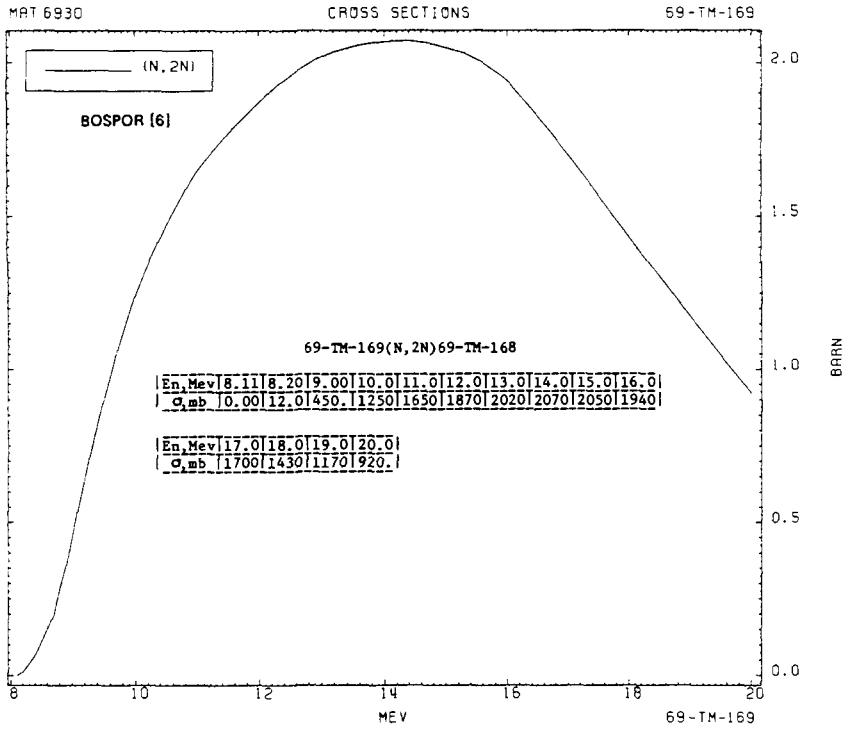
MAT 6930
CROSS SECTIONS
69-TM-169
(N,2N)
BOSPOR [6]
69-TM-169(N,2N)69-TM-168
En,Mev 8.11 8.20 9.00 10.0 11.0 12.0 13.0 14.0 15.0 16.0
σ,mb 0.00 12.0 450. 1250 1650 1870 2020 2070 2050 1940
En,Mev 17.0 18.0 19.0 20.0
σ,mb 1700 1430 1170 920.
2.0
1.5
1.0
0.5
0.0
BARN
8
10
12
14
16
18
20
MEV
69-TM-169

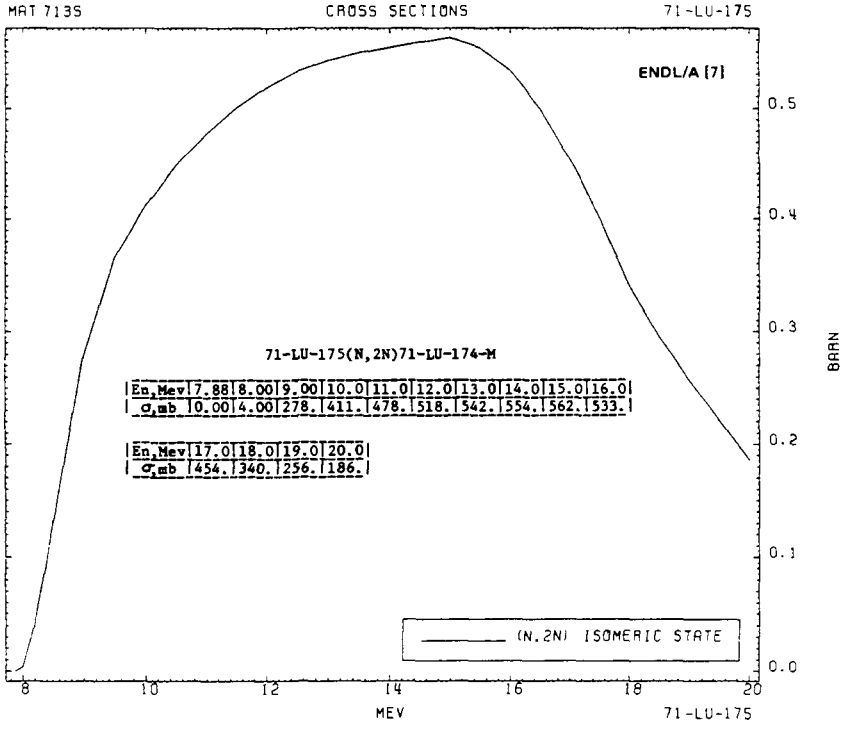
MAT 7135
CROSS SECTIONS
71-LU-175
ENDL/A [7]
71-LU-175(N,2N)71-LU-174-M
En,Mev 7.88 8.00 9.00 10.0 11.0 12.0 13.0 14.0 15.0 16.0
σ,mb 0.00 4.00 278. 411. 478. 518. 542. 554. 562. 533.
En,Mev 17.0 18.0 19.0 20.0
σ,mb 454. 340. 256. 186.
(N,2N) ISOMERIC STATE
0.5
0.4
0.3
0.2
0.1
0.0
BARN
8
10
12
14
16
18
20
MEV
71-LU-175

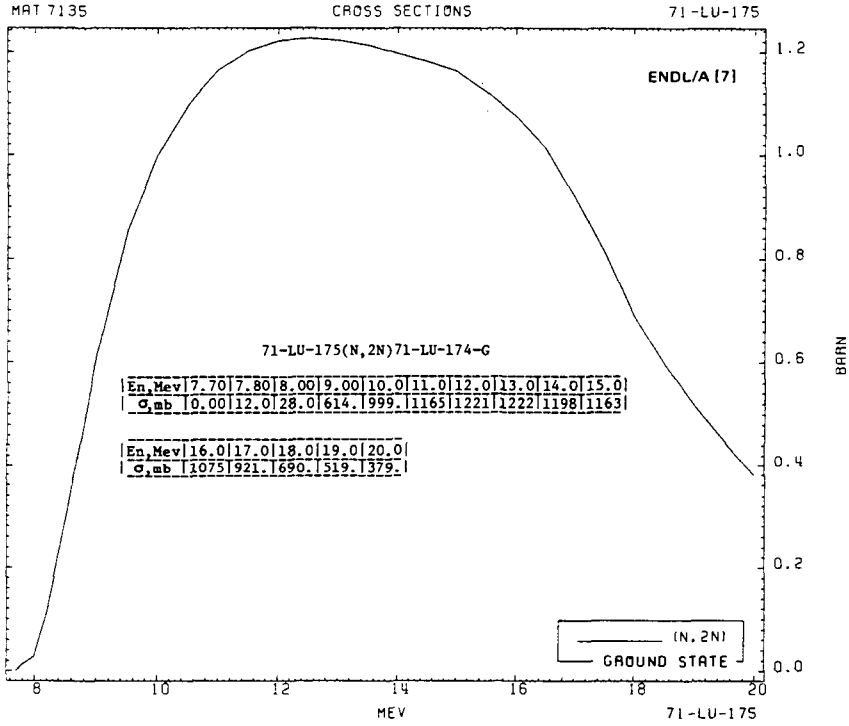
MAT 7135
CROSS SECTIONS
71-LU-175
ENDL/A [7]
71-LU-175(N,2N)71-LU-174-G
En,Mev 7.70 7.80 8.00 9.00 10.0 11.0 12.0 13.0 14.0 15.0
σ,mb 0.00 12.0 28.0 614. 999. 1165 1221 1222 1198 1163
En,Mev 16.0 17.0 18.0 19.0 20.0
σ,mb 1075 921. 690. 519. 379.
(N,2N)
GROUND STATE
BARN
MEV
71-LU-175

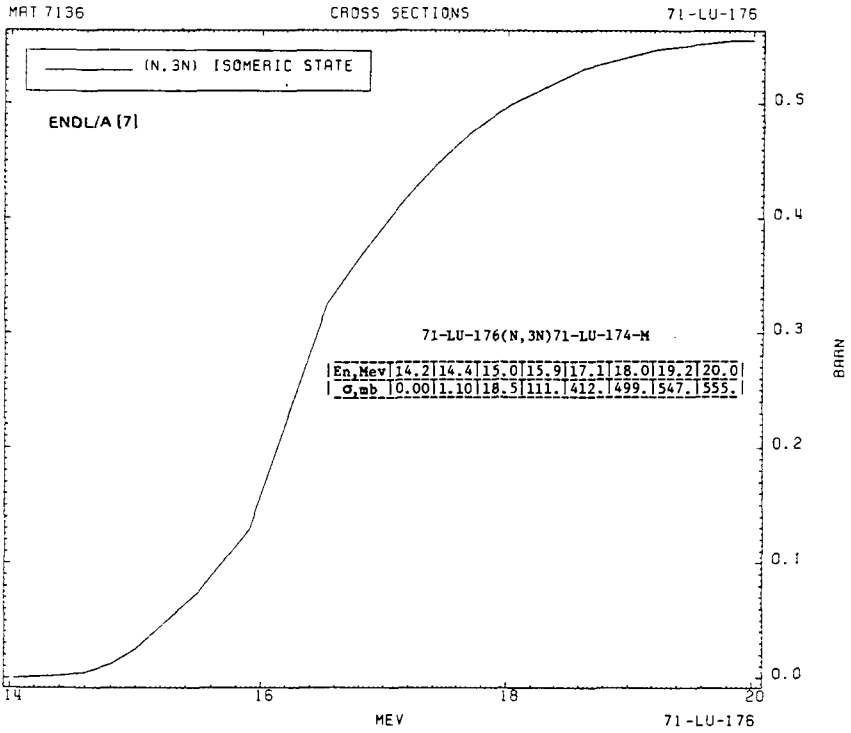
MAT 7136
CROSS SECTIONS
71-LU-176
(N,3N) ISOMERIC STATE
ENDL/A [7]
71-LU-176(N,3N)71-LU-174-M
En,Mev 14.2 14.4 15.0 15.9 17.1 18.0 19.2 20.0
σ,mb 0.00 1.10 18.5 111. 412. 499. 547. 555.
BARN
MEV
71-LU-176

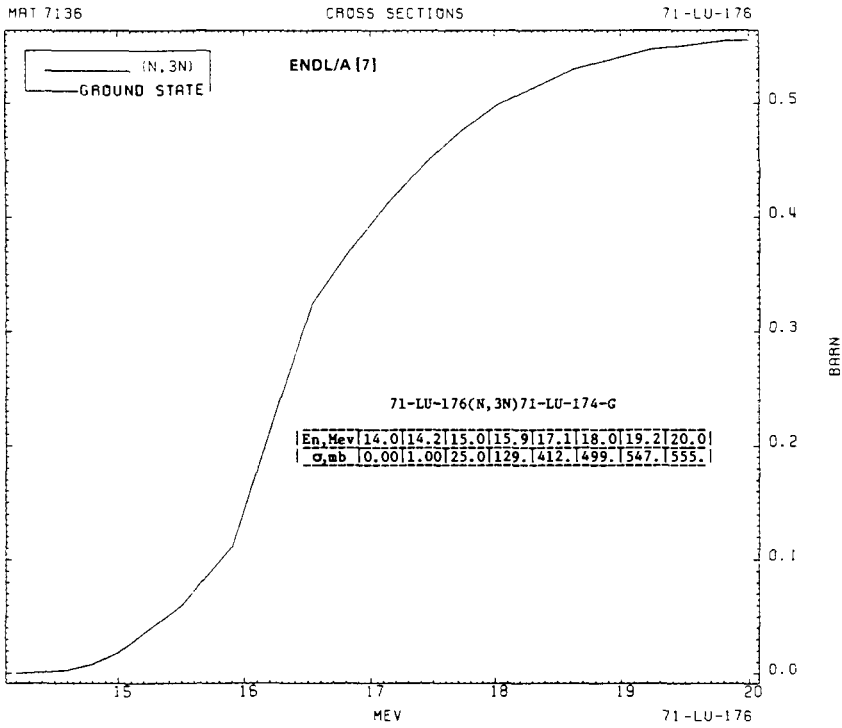
MAT 7136
CROSS SECTIONS
71-LU-176
(N,3N)
GROUND STATE
ENDL/A [7]
71-LU-176(N,3N)71-LU-174-G
En,Mev 14.0 14.2 15.0 15.9 17.1 18.0 19.2 20.0
σ,mb 0.00 1.00 25.0 129. 412. 499. 547. 555.
0.5
0.4
0.3
0.2
0.1
0.0
BARN
15
16
17
18
19
20
MEV
71-LU-176

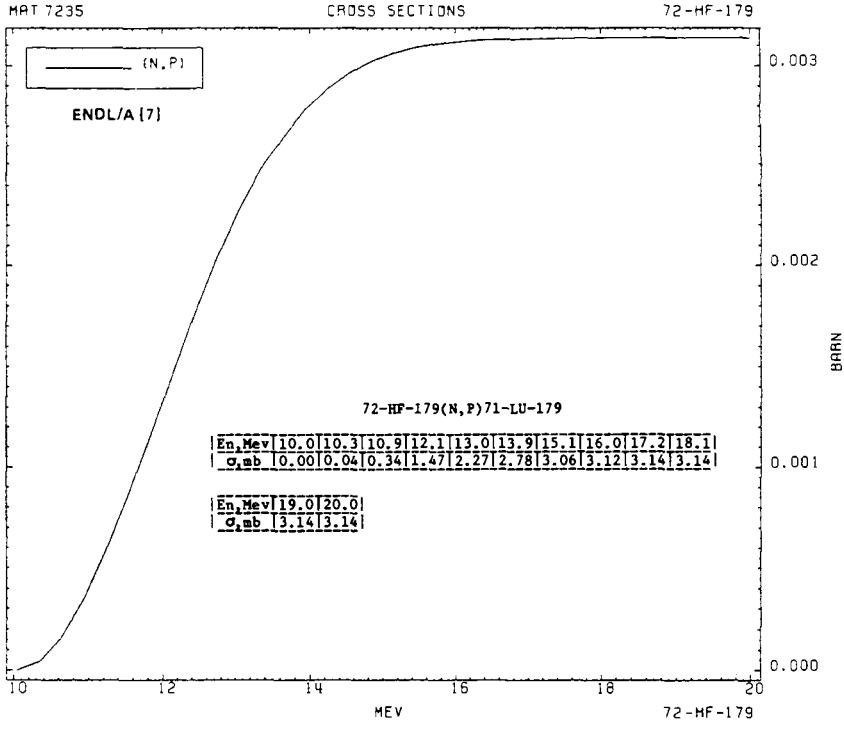
MAT 7235
CROSS SECTIONS
72-HF-179
(N,P)
ENDL/A [7]
72-HF-179(N,P)71-LU-179
En,Mev 10.0 10.3 10.9 12.1 13.0 13.9 15.1 16.0 17.2 18.1
σ,mb 0.00 0.04 0.34 1.47 2.27 2.78 3.06 3.12 3.14 3.14
En,Mev 19.0 20.0
σ,mb 3.14 3.14
0.003
0.002
0.001
0.000
BARN
10
12
14
16
18
20
MEV
72-HF-179

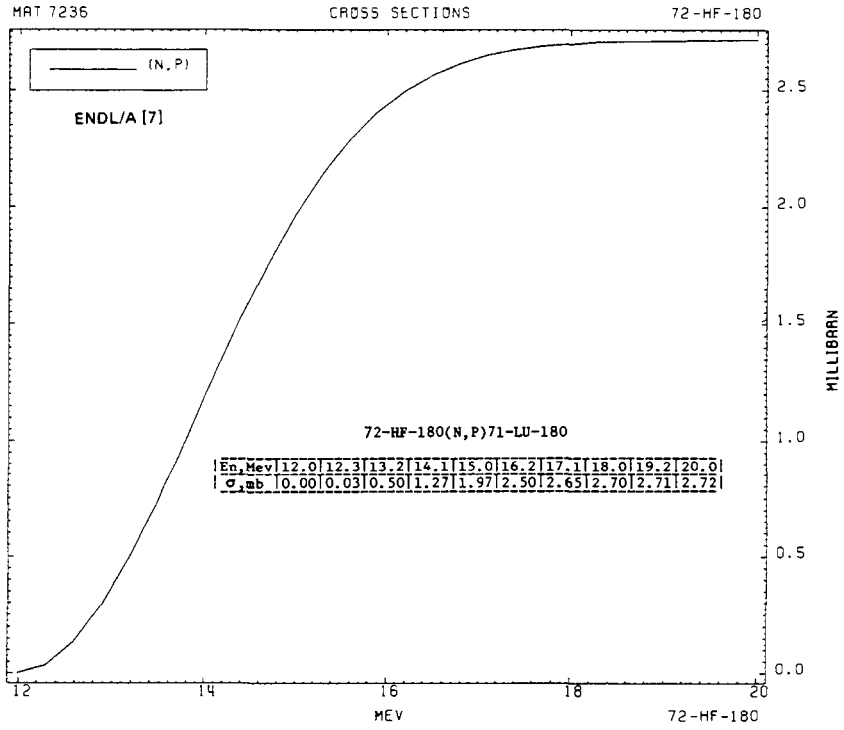
MAT 7236
CROSS SECTIONS
72-HF-180
(N,P)
ENDL/A [7]
72-HF-180(N,P)71-LU-180
En,Mev | 12.0 | 12.3 | 13.2 | 14.1 | 15.0 | 16.2 | 17.1 | 18.0 | 19.2 | 20.0
σ,mb | 0.00 | 0.03 | 0.50 | 1.27 | 1.97 | 2.50 | 2.65 | 2.70 | 2.71 | 2.72
MILLIBARN
MEV
72-HF-180

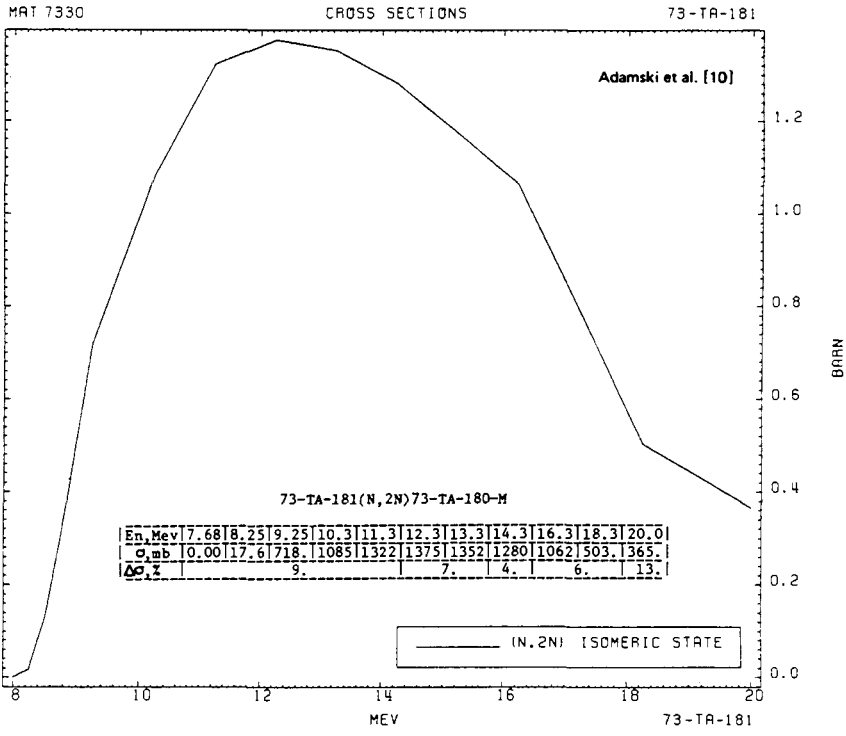
MAT 7330
CROSS SECTIONS
73-TA-181
Adamski et al. [10]
73-TA-181(N,2N)73-TA-180-M
En,Mev | 7.68 | 8.25 | 9.25 | 10.3 | 11.3 | 12.3 | 13.3 | 14.3 | 16.3 | 18.3 | 20.0
σ,mb | 0.00 | 17.6 | 718. | 1085 | 1322 | 1375 | 1352 | 1280 | 1062 | 503. | 365.
Δσ,% | 9. | 7. | 4. | 6. | 13.
(N,2N) ISOMERIC STATE
BARN
MEV
73-TA-181

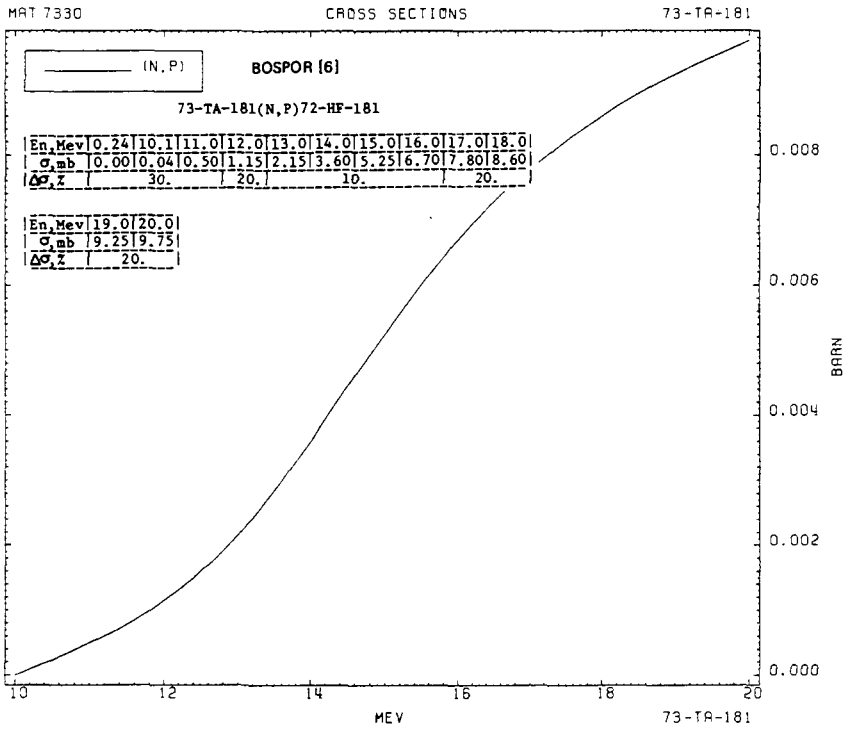
MAT 7330
CROSS SECTIONS
73-TA-181
(N,P)
BOSPOR [6]
73-TA-181(N,P)72-HF-181
En,Mev 0.24 10.1 11.0 12.0 13.0 14.0 15.0 16.0 17.0 18.0
σ,mb 0.00 0.04 0.50 1.15 2.15 3.60 5.25 6.70 7.80 8.60
Δσ,% 30. 20. 10. 20.
En,Mev 19.0 20.0
σ,mb 9.25 9.75
Δσ,% 20.
0.008
0.006
0.004
0.002
0.000
BARN
10 12 14 16 18 20
MEV
73-TA-181

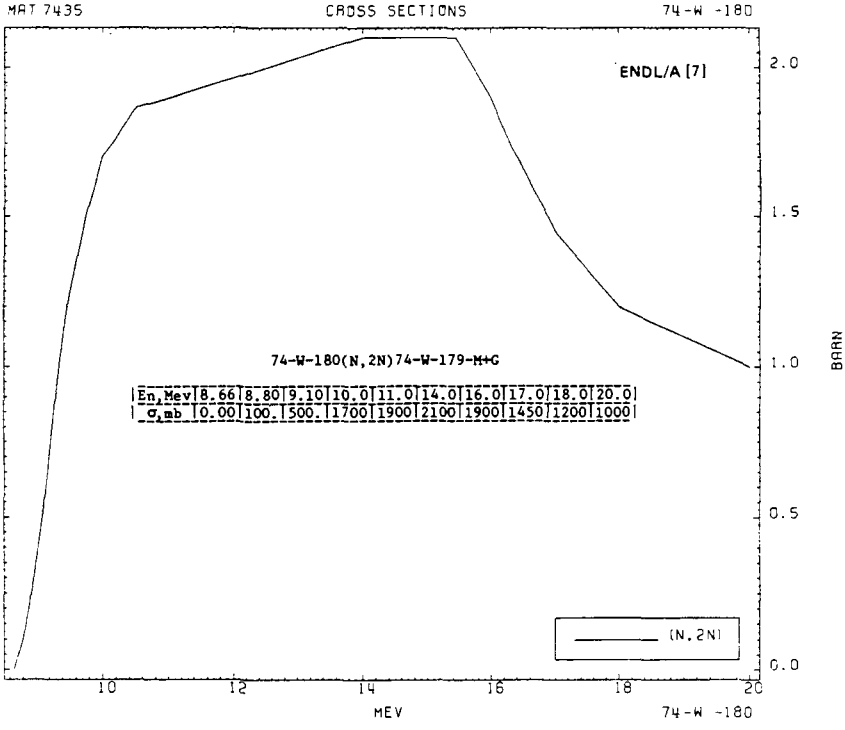
MAT 7435
CROSS SECTIONS
74-W -180
ENDL/A [7]
74-W-180(N,2N)74-W-179-M+G
En,Mev 8.66 8.80 9.10 10.0 11.0 14.0 16.0 17.0 18.0 20.0
σ,mb 0.00 100. 500. 1700 1900 2100 1900 1450 1200 1000
(N,2N)
2.0
1.5
1.0
0.5
0.0
BARN
10 12 14 16 18 20
MEV
74-W -180

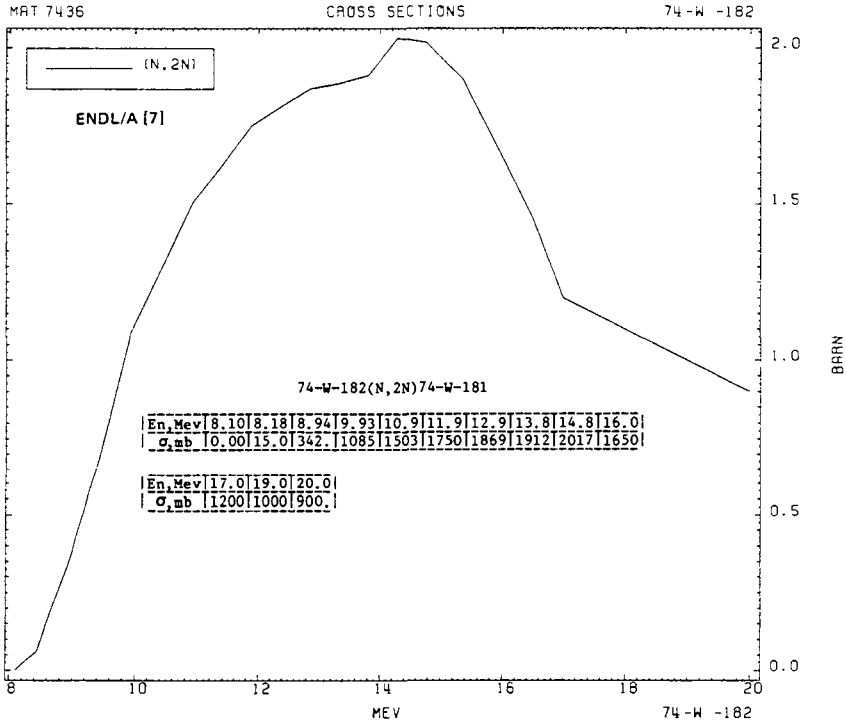
MAT 7436
CROSS SECTIONS
74-W -182
(N,2N)
ENDL/A [7]
74-W-182(N,2N)74-W-181
En,Mev | 8.10 | 8.18 | 8.94 | 9.93 | 10.9 | 11.9 | 12.9 | 13.8 | 14.8 | 16.0
σ,mb | 0.00 | 15.0 | 342. | 1085 | 1503 | 1750 | 1869 | 1912 | 2017 | 1650
En,Mev | 17.0 | 19.0 | 20.0
σ,mb | 1200 | 1000 | 900.
2.0
1.5
1.0
0.5
0.0
BARN
8
10
12
14
16
18
20
MEV
74-W -182

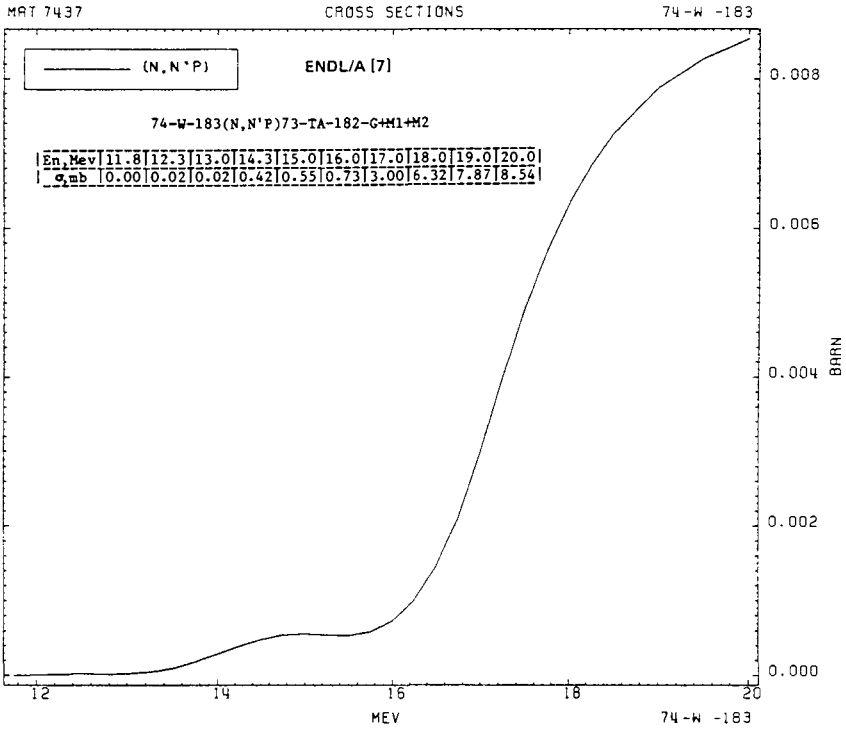
MAT 7437
CROSS SECTIONS
74-W -183
(N,N'P)
ENDL/A [7]
74-W-183(N,N'P)73-TA-182-G+M1+M2
En,Mev | 11.8 | 12.3 | 13.0 | 14.3 | 15.0 | 16.0 | 17.0 | 18.0 | 19.0 | 20.0
σ,mb | 0.00 | 0.02 | 0.02 | 0.42 | 0.55 | 0.73 | 3.00 | 6.32 | 7.87 | 8.54
0.008
0.006
0.004
0.002
0.000
BARN
12
14
16
18
20
MEV
74-W -183

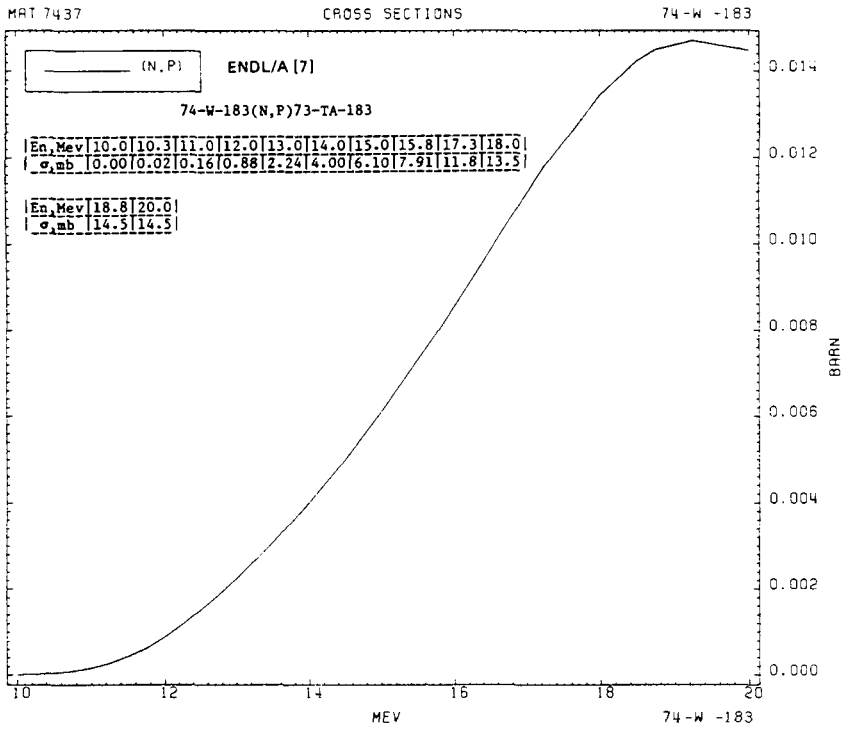
MAT 7437
CROSS SECTIONS
74-W -183
(N,P)
ENDL/A [7]
74-W-183(N,P)73-TA-183
En,Mev | 10.0 | 10.3 | 11.0 | 12.0 | 13.0 | 14.0 | 15.0 | 15.8 | 17.3 | 18.0
σ,mb | 0.00 | 0.02 | 0.16 | 0.88 | 2.24 | 4.00 | 6.10 | 7.91 | 11.8 | 13.5
En,Mev | 18.8 | 20.0
σ,mb | 14.5 | 14.5
0.014
0.012
0.010
0.008
0.006
0.004
0.002
0.000
BARN
10
12
14
16
18
20
MEV
74-W -183

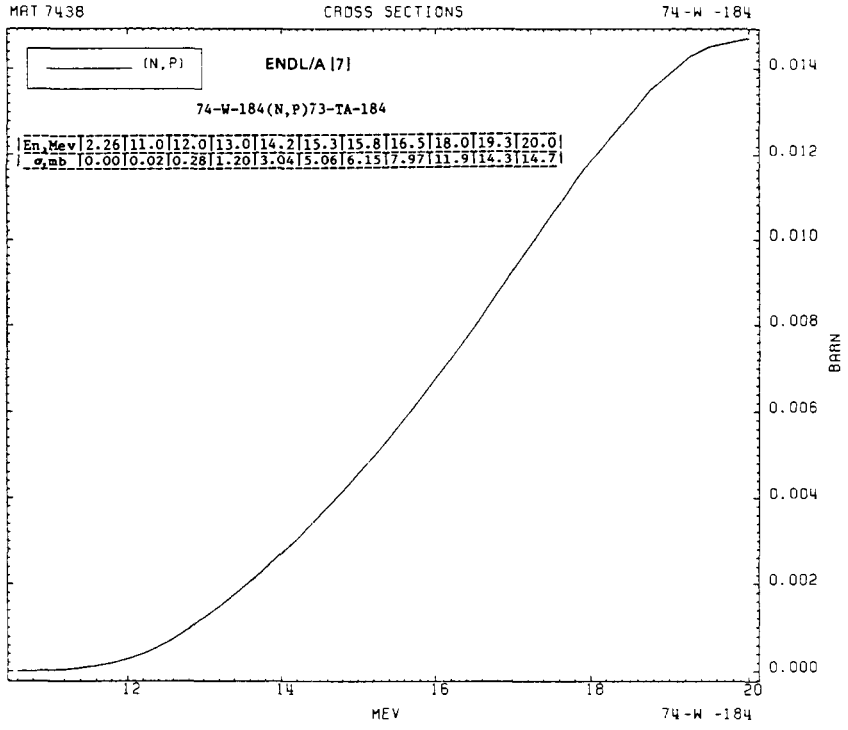
MAT 7438
CROSS SECTIONS
74-W -184
(N,P)
ENDL/A [7]
74-W-184(N,P)73-TA-184
En,Mev | 2.26 | 11.0 | 12.0 | 13.0 | 14.2 | 15.3 | 15.8 | 16.5 | 18.0 | 19.3 | 20.0
σ,mb | 0.00 | 0.02 | 0.28 | 1.20 | 3.04 | 5.06 | 6.15 | 7.97 | 11.9 | 14.3 | 14.7
0.014
0.012
0.010
0.008
0.006
0.004
0.002
0.000
BARN
12
14
16
18
20
MEV
74-W -184

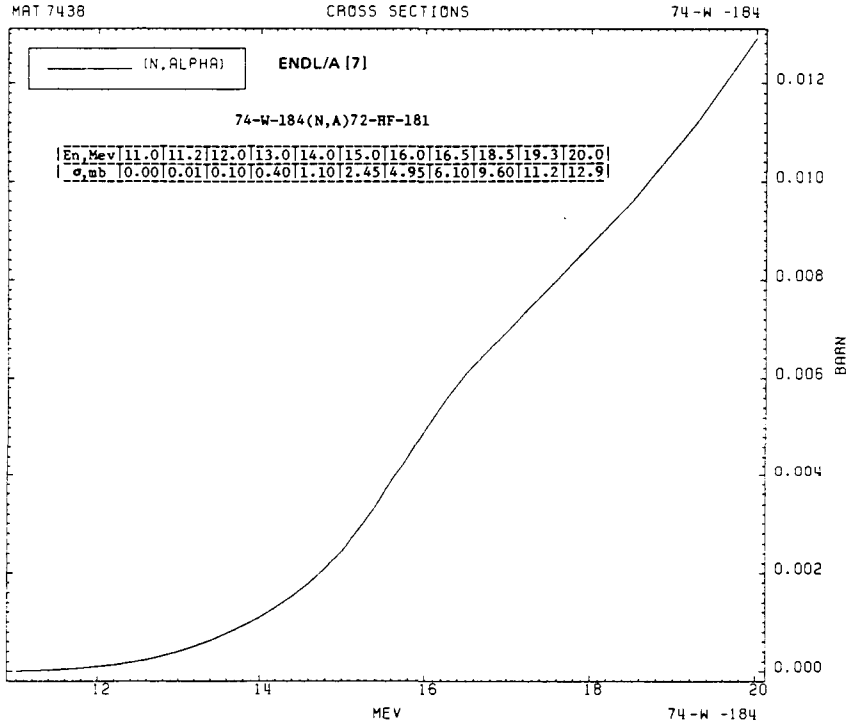
MAT 7438
CROSS SECTIONS
74-W -184
(N,ALPHA)
ENDL/A [7]
74-W-184(N,A)72-HF-181
En,Mev 11.0 11.2 12.0 13.0 14.0 15.0 16.0 16.5 18.5 19.3 20.0
σ,mb 0.00 0.01 0.10 0.40 1.10 2.45 4.95 6.10 9.60 11.2 12.9
0.012
0.010
0.008
0.006
0.004
0.002
0.000
BARN
12
14
16
18
20
MEV
74-W -184

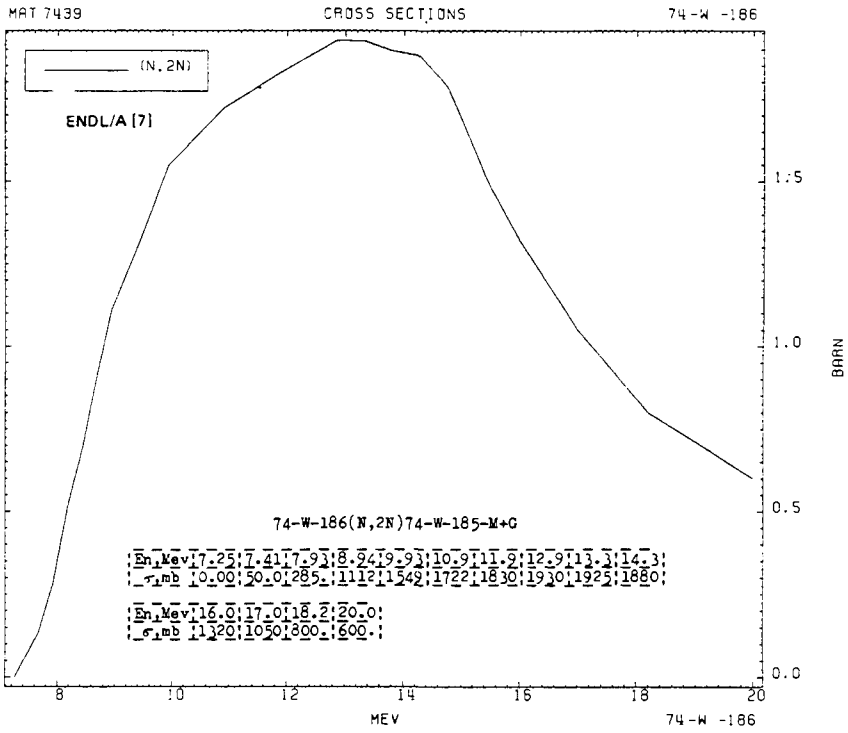
MAT 7439
CROSS SECTIONS
74-W -186
(N,2N)
ENDL/A [7]
74-W-186(N,2N)74-W-185-M+G
En,Mev 7.25 7.41 7.93 8.94 9.93 10.9 11.9 12.9 13.3 14.3
σ,mb 10.00 50.0 285. 1112 1542 1722 1830 1930 1925 1880
En,Mev 16.0 17.0 18.2 20.0
σ,mb 1120 1050 800. 600.
1.5
1.0
0.5
0.0
BARN
8
10
12
14
16
18
20
MEV
74-W -186

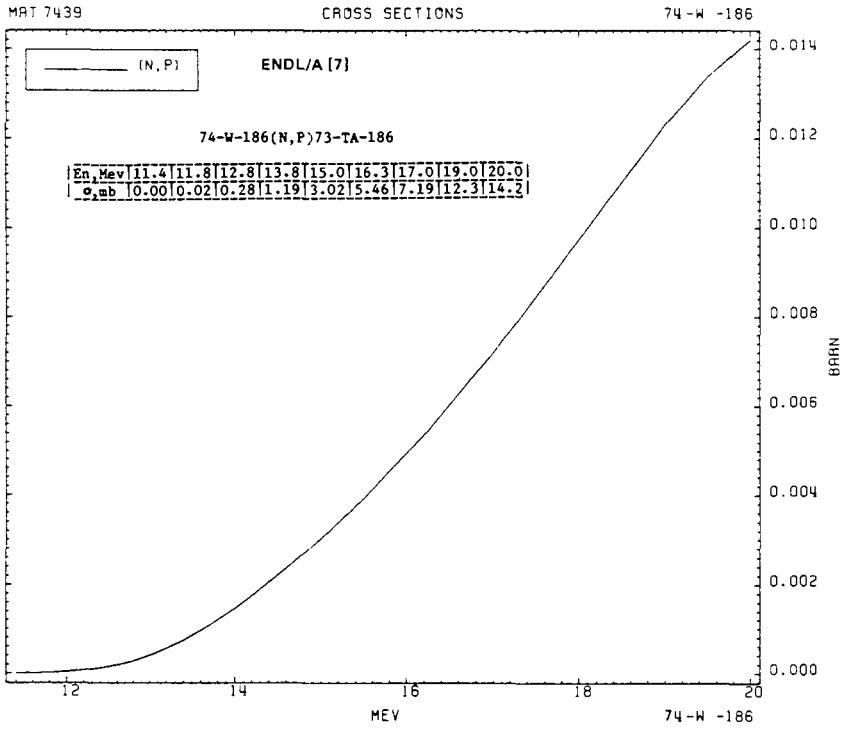
MAT 7439
CROSS SECTIONS
74-W -186
(N,P)
ENDL/A [7]
74-W-186(N,P)73-TA-186
En,Mev 11.4 11.8 12.8 13.8 15.0 16.3 17.0 19.0 20.0
σ,mb 0.00 0.02 0.28 1.19 3.02 5.46 7.19 12.3 14.2
0.014
0.012
0.010
0.008
0.006
0.004
0.002
0.000
BARN
12
14
16
18
20
MEV
74-W -186

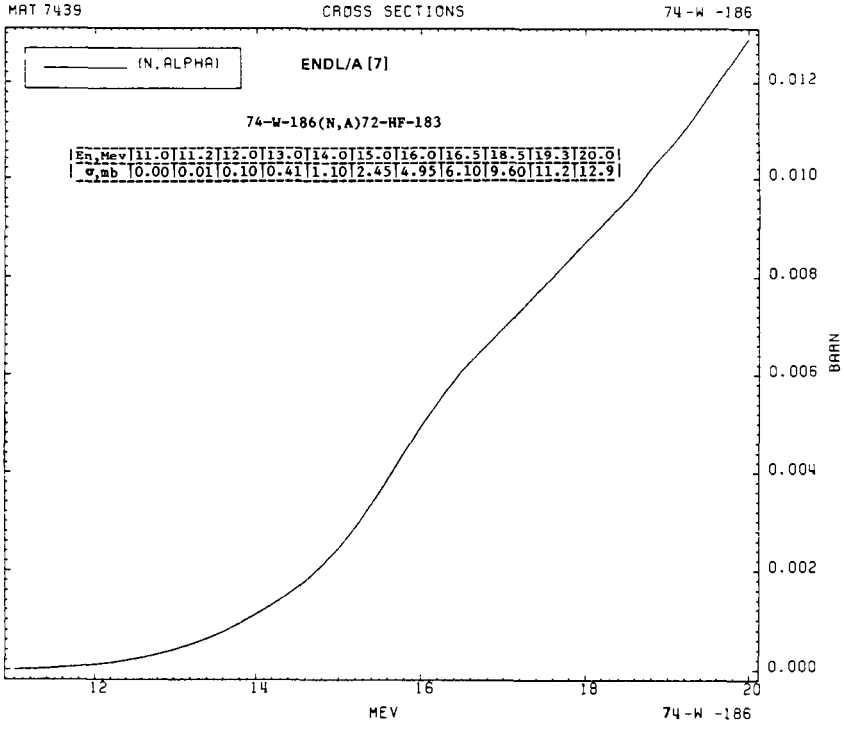
MAT 7439
CROSS SECTIONS
74-W -186
(N,ALPHA)
ENDL/A [7]
74-W-186(N,A)72-HF-183
En,Mev 11.0 11.2 12.0 13.0 14.0 15.0 16.0 16.5 18.5 19.3 20.0
σ,mb 0.00 0.01 0.10 0.41 1.10 2.45 4.95 6.10 9.60 11.2 12.9
0.012
0.010
0.008
0.006
0.004
0.002
0.000
BARN
12
14
16
18
20
MEV
74-W -186

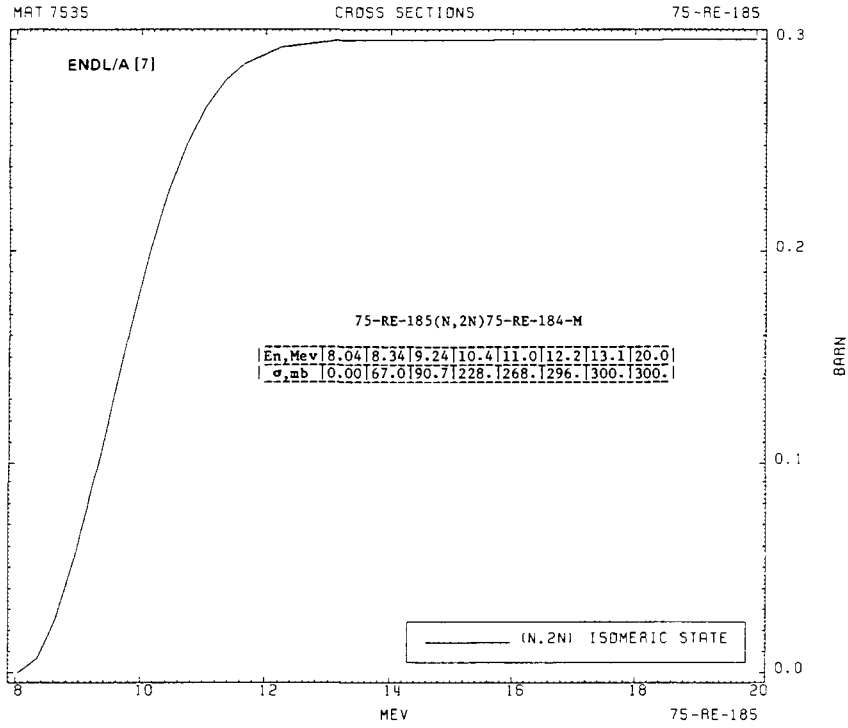
MAT 7535
CROSS SECTIONS
75-RE-185
ENDL/A [7]
75-RE-185(N,2N)75-RE-184-M
En,Mev | 8.04 | 8.34 | 9.24 | 10.4 | 11.0 | 12.2 | 13.1 | 20.0
σ,mb | 0.00 | 67.0 | 90.7 | 228. | 268. | 296. | 300. | 300.
(N,2N) ISOMERIC STATE
0.3
0.2
0.1
0.0
BARN
8
10
12
14
16
18
20
MEV
75-RE-185

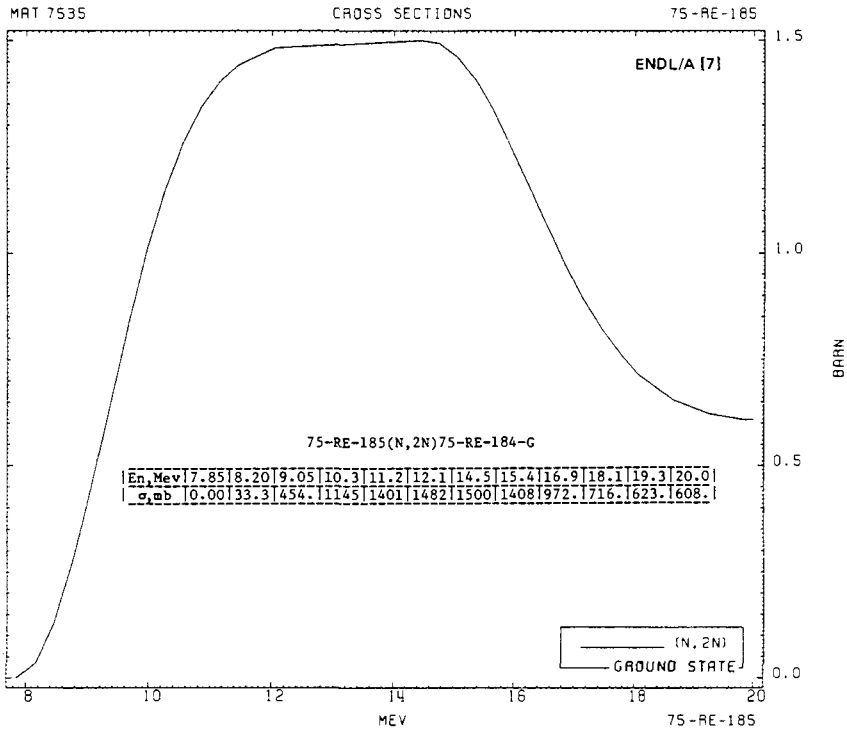
MAT 7535
CROSS SECTIONS
75-RE-185
ENDL/A [7]
75-RE-185(N,2N)75-RE-184-G
En,Mev | 7.85 | 8.20 | 9.05 | 10.3 | 11.2 | 12.1 | 14.5 | 15.4 | 16.9 | 18.1 | 19.3 | 20.0
σ,mb | 0.00 | 33.3 | 454. | 1145 | 1401 | 1482 | 1500 | 1408 | 972. | 716. | 623. | 608.
(N,2N)
GROUND STATE
1.5
1.0
0.5
0.0
BARN
8
10
12
14
16
18
20
MEV
75-RE-185

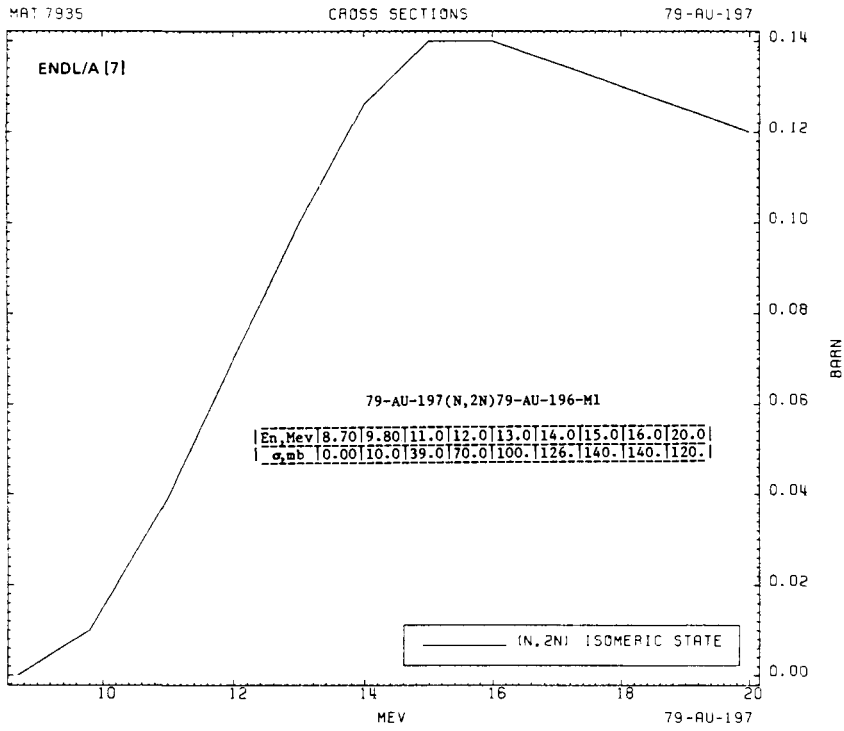
MAT 7935
CROSS SECTIONS
79-AU-197
ENDL/A [7]
79-AU-197(N,2N)79-AU-196-M1
En,Mev 8.70 9.80 11.0 12.0 13.0 14.0 15.0 16.0 20.0
σ,mb 0.00 10.0 39.0 70.0 100. 126. 140. 140. 120.
(N,2N) ISOMERIC STATE
BARN
MEV
79-AU-197

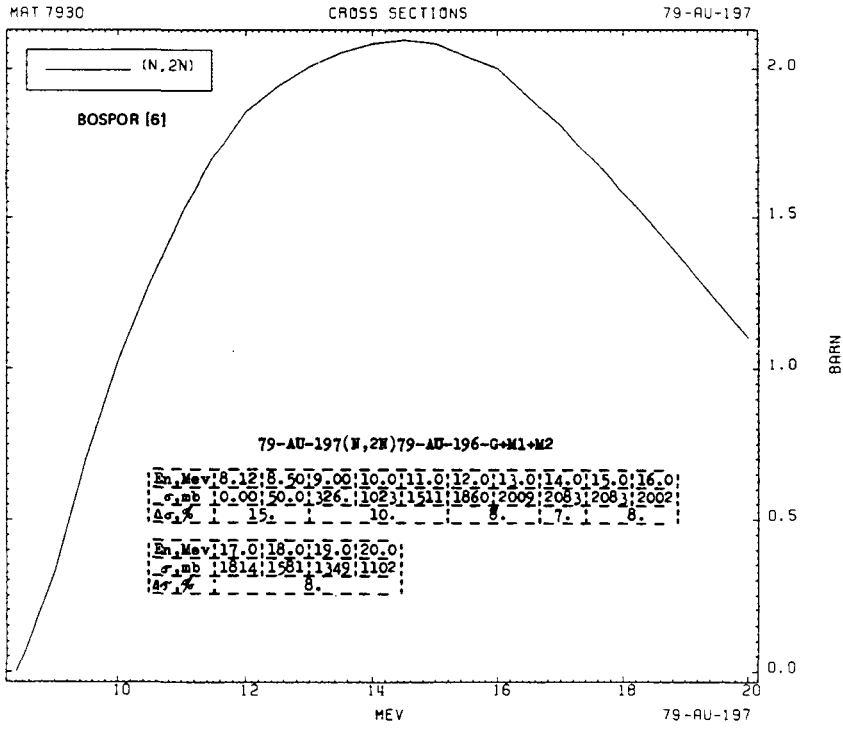
MAT 7930
CROSS SECTIONS
79-AU-197
(N,2N)
BOSPOR [6]
79-AU-197(N,2N)79-AU-196-G+M1+M2
En,Mev 8.12 8.50 9.00 10.0 11.0 12.0 13.0 14.0 15.0 16.0
σ,mb 10.00 50.0 326. 1023 1511 1860 2009 2083 2083 2002
Δσ,% 15. 10. 8. 7. 8.
En,Mev 17.0 18.0 19.0 20.0
σ,mb 1814 1581 1342 1102
Δσ,% 8.
BARN
MEV
79-AU-197

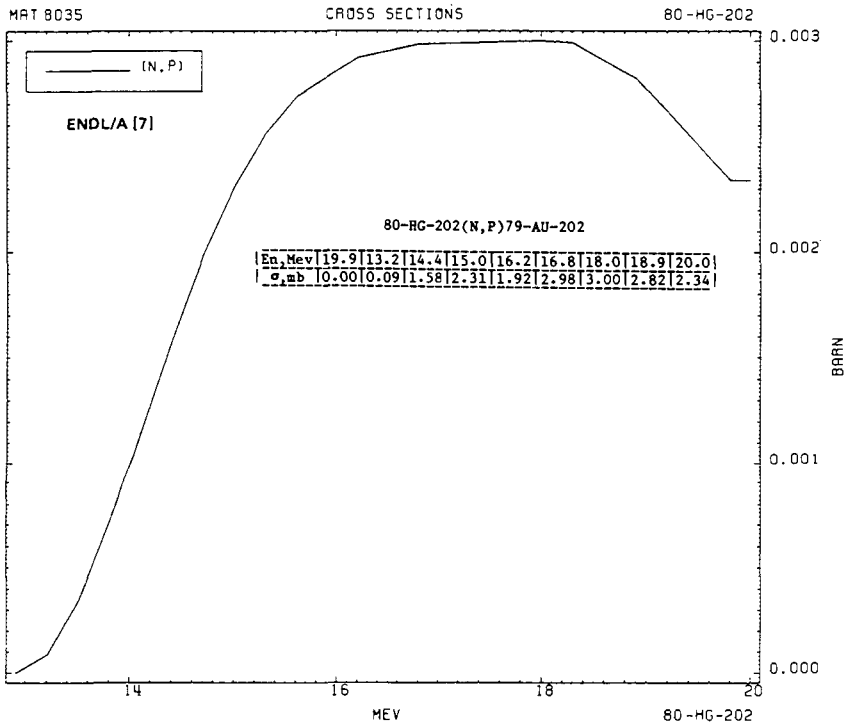
MAT 8035
CROSS SECTIONS
80-HG-202
(N,P)
ENDL/A [7]
80-HG-202(N,P)79-AU-202
En,Mev 19.9 13.2 14.4 15.0 16.2 16.8 18.0 18.9 20.0
σ,mb 0.00 0.09 1.58 2.31 1.92 2.98 3.00 2.82 2.34
0.003
0.002
0.001
0.000
BARN
14
16
18
20
MEV
80-HG-202

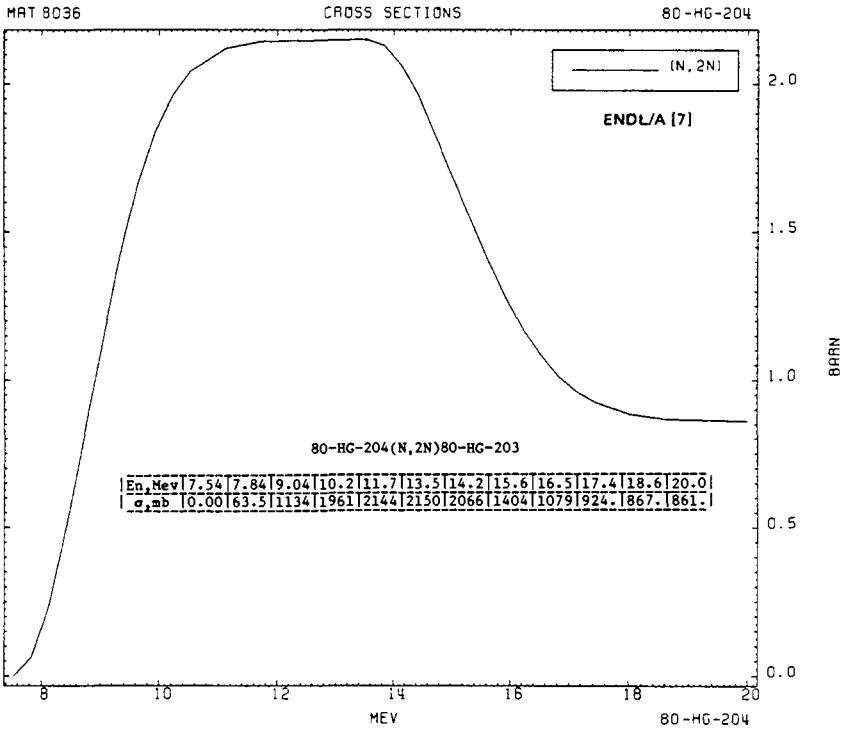
MAT 8036
CROSS SECTIONS
80-HG-204
(N,2N)
ENDL/A [7]
80-HG-204(N,2N)80-HG-203
En,Mev 7.54 7.84 9.04 10.2 11.7 13.5 14.2 15.6 16.5 17.4 18.6 20.0
σ,mb 0.00 63.5 1134 1961 2144 2150 2066 1404 1079 924. 867. 861.
2.0
1.5
1.0
0.5
0.0
BARN
8
10
12
14
16
18
20
MEV
80-HG-204

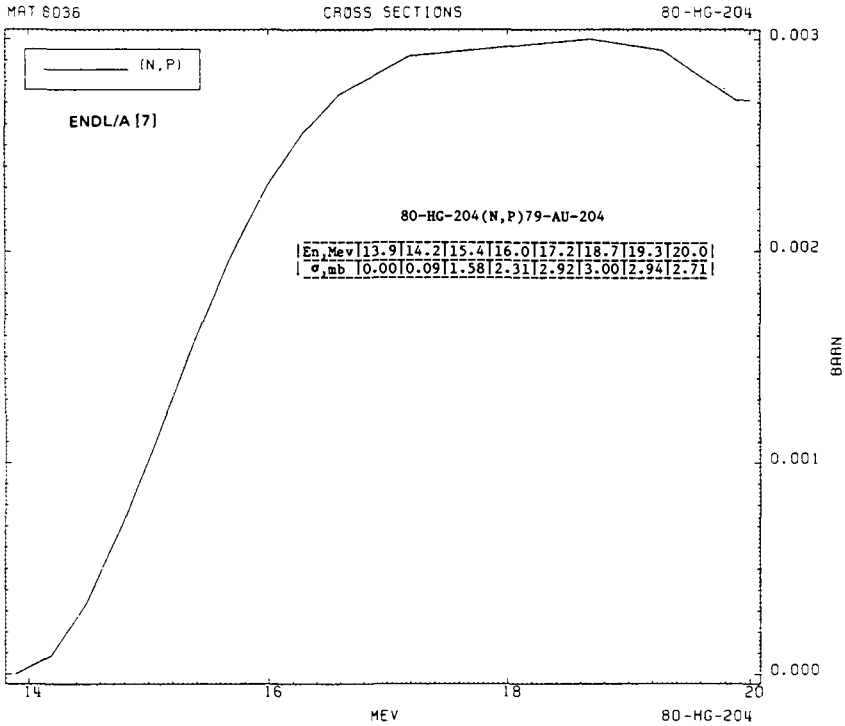
MAT 8036
CROSS SECTIONS
80-HG-204
(N,P)
ENDL/A [7]
80-HG-204(N,P)79-AU-204
En,Mev | 13.9 | 14.2 | 15.4 | 16.0 | 17.2 | 18.7 | 19.3 | 20.0
σ,mb | 0.00 | 0.09 | 1.58 | 2.31 | 2.92 | 3.00 | 2.94 | 2.71
0.003
0.002
0.001
0.000
BARN
14
16
18
20
MEV
80-HG-204

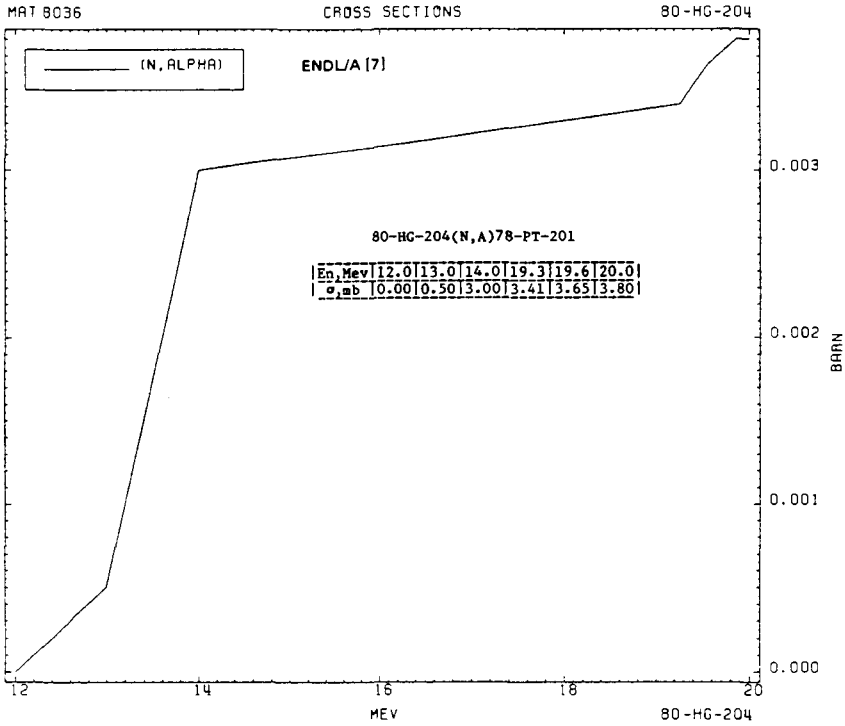
MAT 8036
CROSS SECTIONS
80-HG-204
(N,ALPHA)
ENDL/A [7]
80-HG-204(N,A)78-PT-201
En,Mev | 12.0 | 13.0 | 14.0 | 19.3 | 19.6 | 20.0
σ,mb | 0.00 | 0.50 | 3.00 | 3.41 | 3.65 | 3.80
0.003
0.002
0.001
0.000
BARN
12
14
16
18
20
MEV
80-HG-204

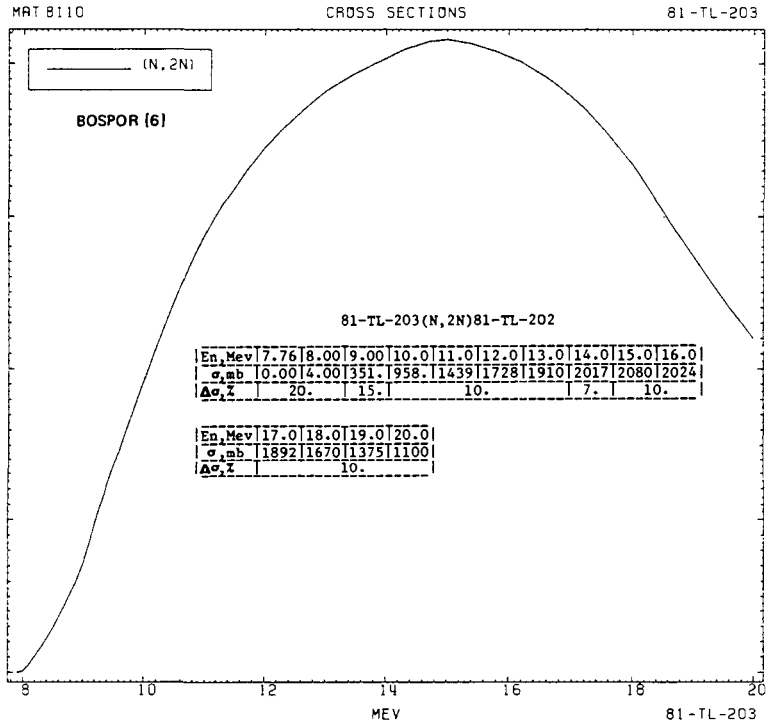
MAT 8110
CROSS SECTIONS
81-TL-203
(N,2N)
BOSPOR [6]
81-TL-203(N,2N)81-TL-202
En,Mev | 7.76 | 8.00 | 9.00 | 10.0 | 11.0 | 12.0 | 13.0 | 14.0 | 15.0 | 16.0
σ,mb | 0.00 | 4.00 | 351. | 958. | 1439 | 1728 | 1910 | 2017 | 2080 | 2024
Δσ,% | 20. | 15. | 10. | 7. | 10.
En,Mev | 17.0 | 18.0 | 19.0 | 20.0
σ,mb | 1892 | 1670 | 1375 | 1100
Δσ,% | 10.
2.0
1.5
1.0
0.5
0.0
8
10
12
14
16
18
20
MEV
81-TL-203

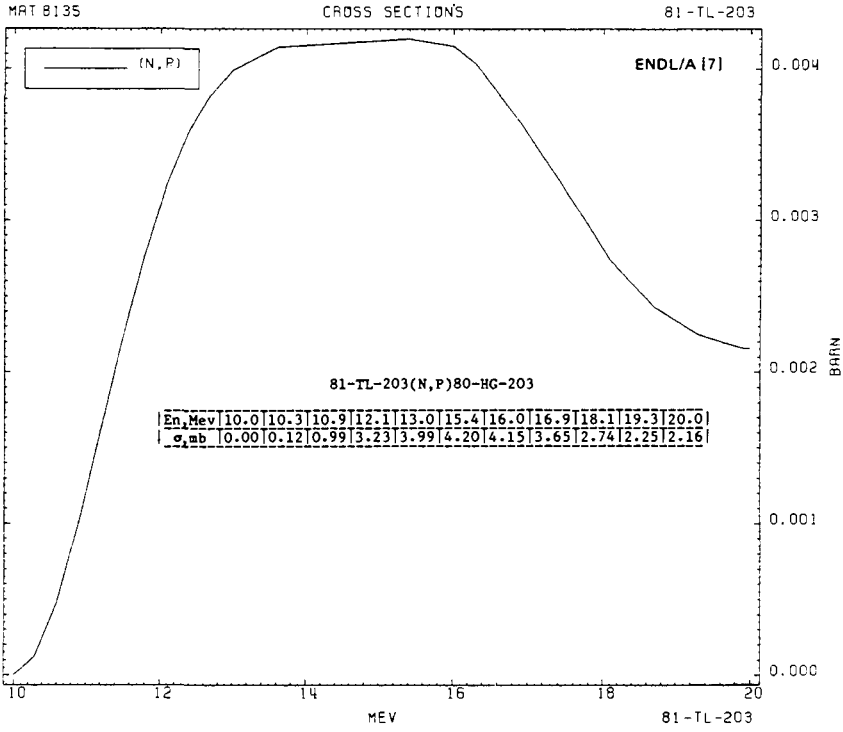
MAT 8135
CROSS SECTIONS
81-TL-203
(N,P)
ENDL/A [7]
81-TL-203(N,P)80-HG-203
En,Mev | 10.0 | 10.3 | 10.9 | 12.1 | 13.0 | 15.4 | 16.0 | 16.9 | 18.1 | 19.3 | 20.0
σ,mb | 0.00 | 0.12 | 0.99 | 3.23 | 3.99 | 4.20 | 4.15 | 3.65 | 2.74 | 2.25 | 2.16
0.004
0.003
0.002
0.001
0.000
BARN
10
12
14
16
18
20
MEV
81-TL-203

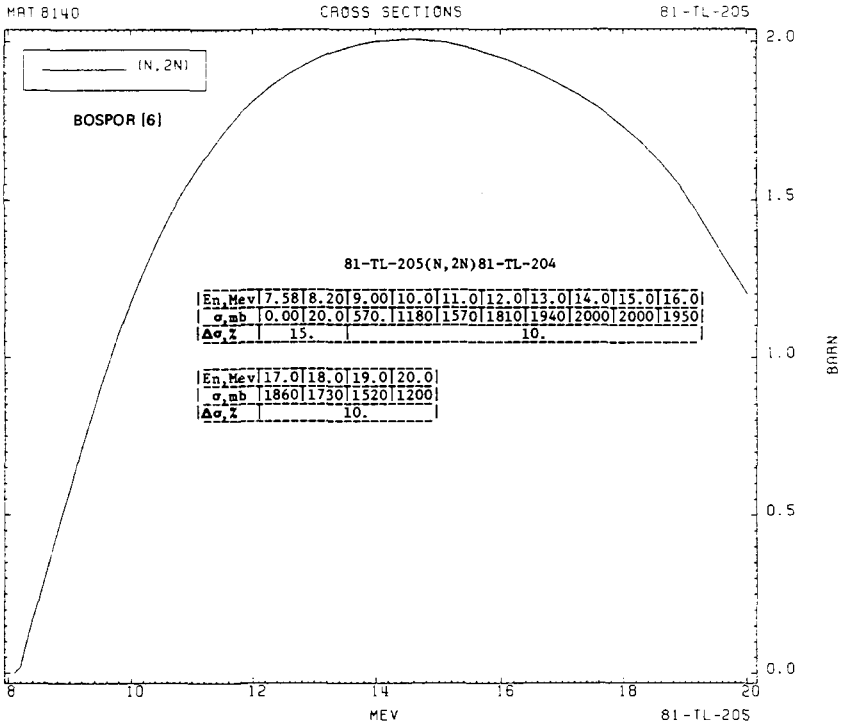
MAT 8140
CROSS SECTIONS
81-TL-205
(N,2N)
BOSPOR [6]
81-TL-205(N,2N)81-TL-204
En,Mev | 7.58 | 8.20 | 9.00 | 10.0 | 11.0 | 12.0 | 13.0 | 14.0 | 15.0 | 16.0
σ,mb | 0.00 | 20.0 | 570. | 1180 | 1570 | 1810 | 1940 | 2000 | 2000 | 1950
Δσ,% | 15. | 10.
En,Mev | 17.0 | 18.0 | 19.0 | 20.0
σ,mb | 1860 | 1730 | 1520 | 1200
Δσ,% | 10.
2.0
1.5
1.0
0.5
0.0
BARN
8
10
12
14
16
18
20
MEV
81-TL-205

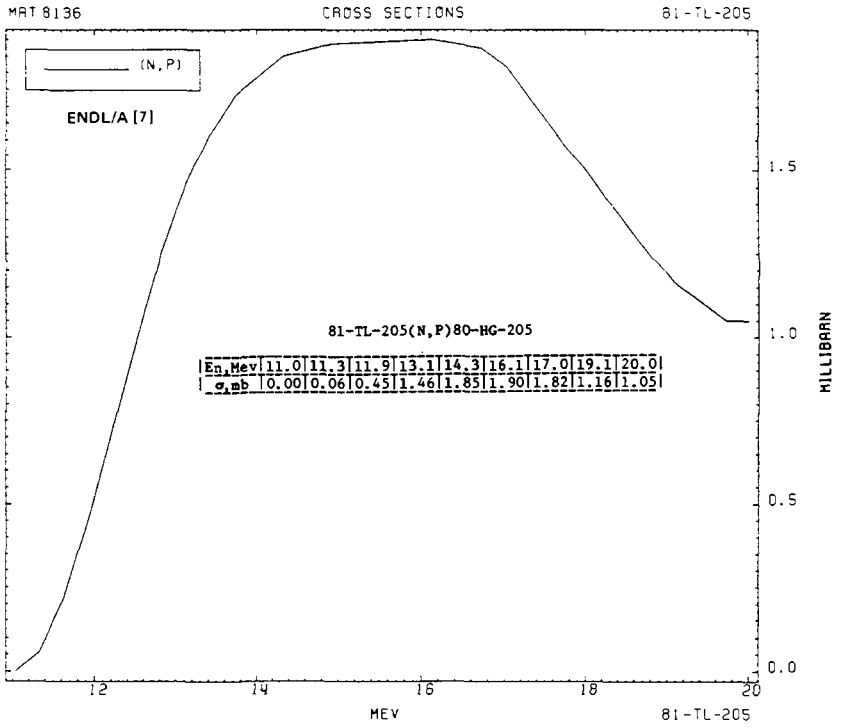
MAT 8136
CROSS SECTIONS
81-TL-205
(N,P)
ENDL/A [7]
81-TL-205(N,P)80-HG-205
En,Mev | 11.0 | 11.3 | 11.9 | 13.1 | 14.3 | 16.1 | 17.0 | 19.1 | 20.0
σ,mb | 0.00 | 0.06 | 0.45 | 1.46 | 1.85 | 1.90 | 1.82 | 1.16 | 1.05
1.5
1.0
0.5
0.0
MILLIBARN
12
14
16
18
20
MEV
81-TL-205

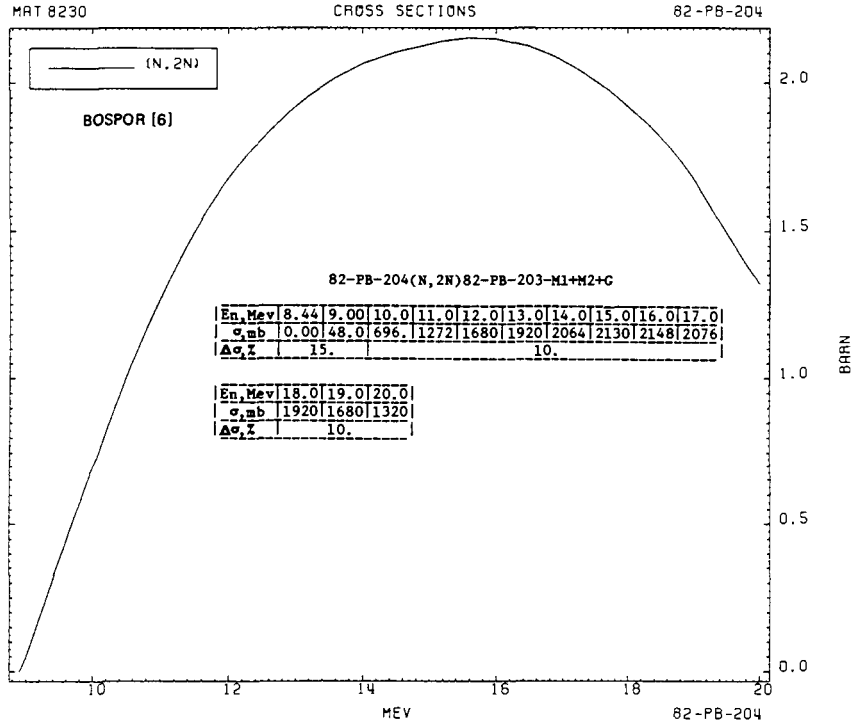
MAT 8230
CROSS SECTIONS
82-PB-204
(N,2N)
BOSPOR [6]
82-PB-204(N,2N)82-PB-203-M1+M2+G
En,Mev | 8.44 | 9.00 | 10.0 | 11.0 | 12.0 | 13.0 | 14.0 | 15.0 | 16.0 | 17.0
σ,mb | 0.00 | 48.0 | 696. | 1272 | 1680 | 1920 | 2064 | 2130 | 2148 | 2076
Δσ,% | 15. | 10.
En,Mev | 18.0 | 19.0 | 20.0
σ,mb | 1920 | 1680 | 1320
Δσ,% | 10.
2.0
1.5
1.0
0.5
0.0
BARN
10
12
14
16
18
20
MEV
82-PB-204

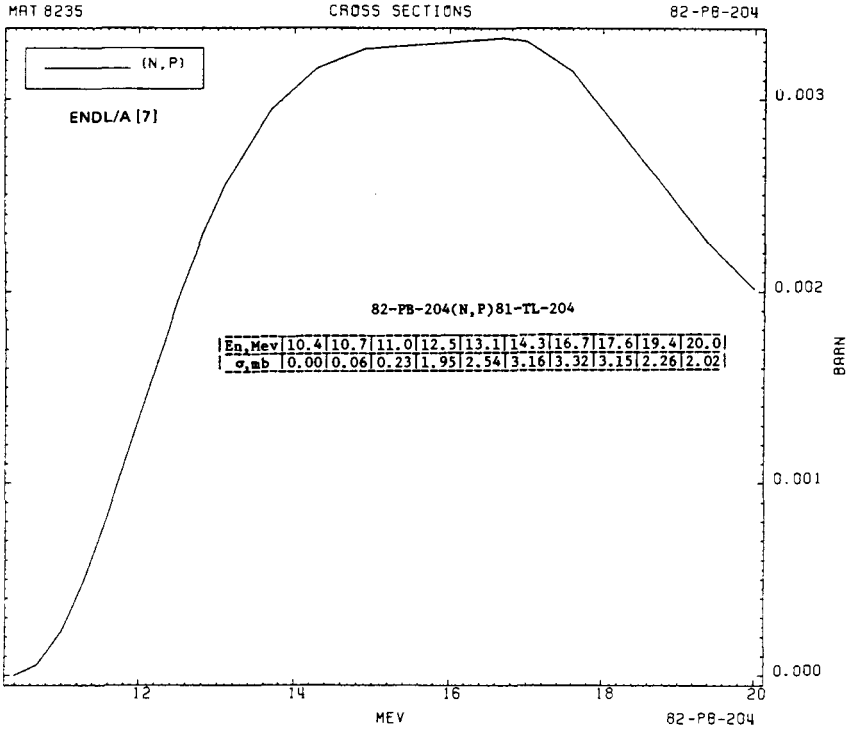
MAT 8235
CROSS SECTIONS
82-PB-204
(N,P)
ENDL/A [7]
82-PB-204(N,P)81-TL-204
En,Mev | 10.4 | 10.7 | 11.0 | 12.5 | 13.1 | 14.3 | 16.7 | 17.6 | 19.4 | 20.0
σ,mb | 0.00 | 0.06 | 0.23 | 1.95 | 2.54 | 3.16 | 3.32 | 3.15 | 2.26 | 2.02
0.003
0.002
0.001
0.000
BARN
12
14
16
18
20
MEV
82-PB-204

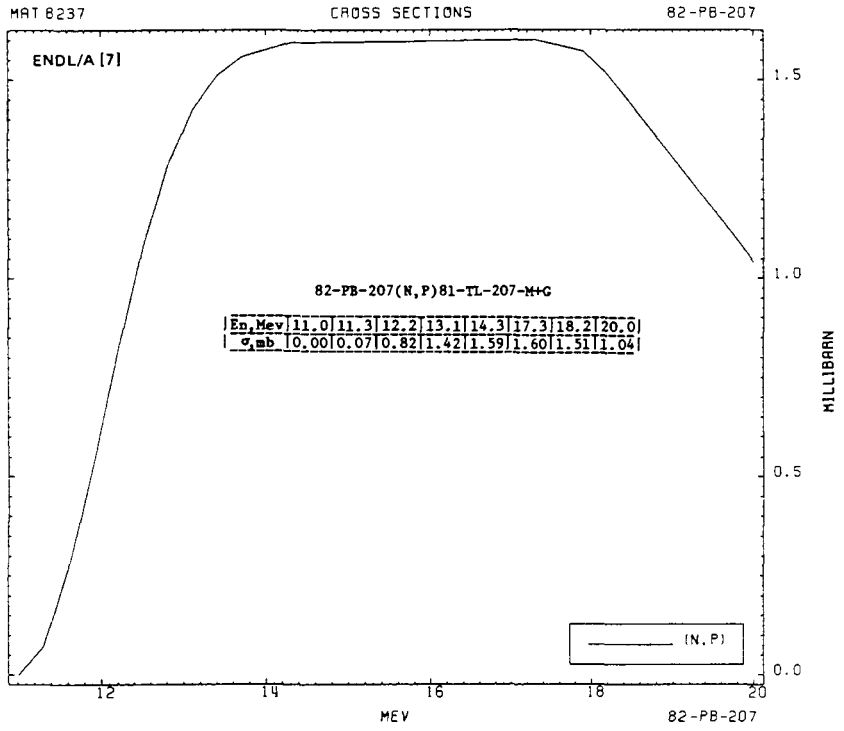
MAT 8237
CROSS SECTIONS
82-PB-207
ENDL/A [7]
82-PB-207(N,P)81-TL-207-M+G
En,Mev | 11.0 | 11.3 | 12.2 | 13.1 | 14.3 | 17.3 | 18.2 | 20.0
σ,mb | 0.00 | 0.07 | 0.82 | 1.42 | 1.59 | 1.60 | 1.51 | 1.04
(N,P)
MILLIBARN
MEV
82-PB-207

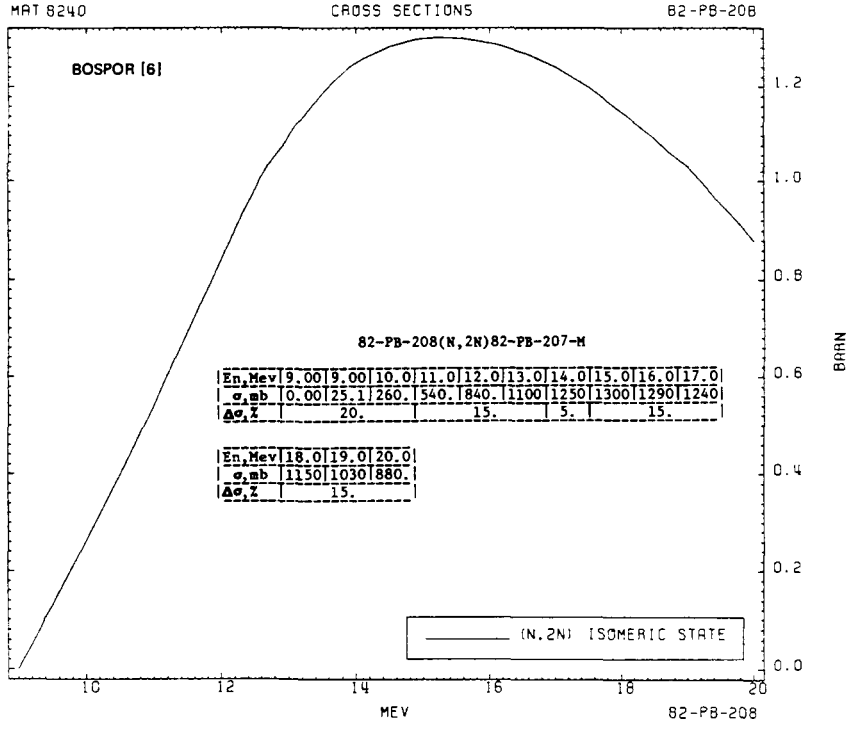
MAT 8240
CROSS SECTIONS
82-PB-208
BOSPOR [6]
82-PB-208(N,2N)82-PB-207-M
En,Mev | 9.00 | 9.00 | 10.0 | 11.0 | 12.0 | 13.0 | 14.0 | 15.0 | 16.0 | 17.0
σ,mb | 0.00 | 25.1 | 260. | 540. | 840. | 1100 | 1250 | 1300 | 1290 | 1240
Δσ,% | 20. | 15. | 5. | 15.
En,Mev | 18.0 | 19.0 | 20.0
σ,mb | 1150 | 1030 | 880.
Δσ,% | 15.
(N,2N) ISOMERIC STATE
BARN
MEV
82-PB-208

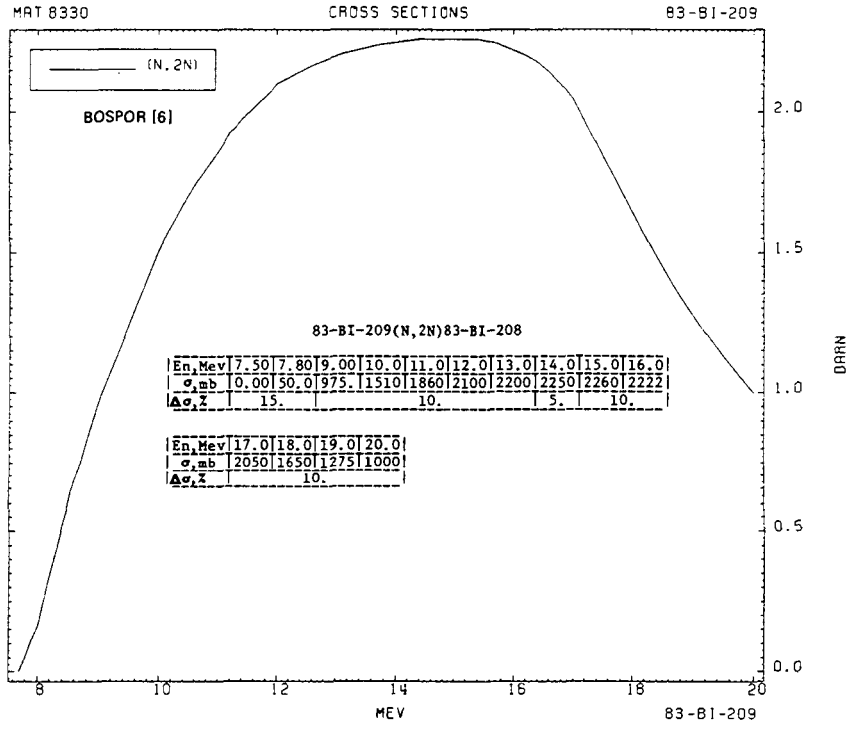
MAT 8330
CROSS SECTIONS
83-BI-209
(N,2N)
BOSPOR [6]
83-BI-209(N,2N)83-BI-208
En,Mev | 7.50 | 7.80 | 9.00 | 10.0 | 11.0 | 12.0 | 13.0 | 14.0 | 15.0 | 16.0
σ,mb | 0.00 | 50.0 | 975. | 1510 | 1860 | 2100 | 2200 | 2250 | 2260 | 2222
Δσ,% | 15. | 10. | 5. | 10.
En,Mev | 17.0 | 18.0 | 19.0 | 20.0
σ,mb | 2050 | 1650 | 1275 | 1000
Δσ,% | 10.
BARN
MEV
83-BI-209

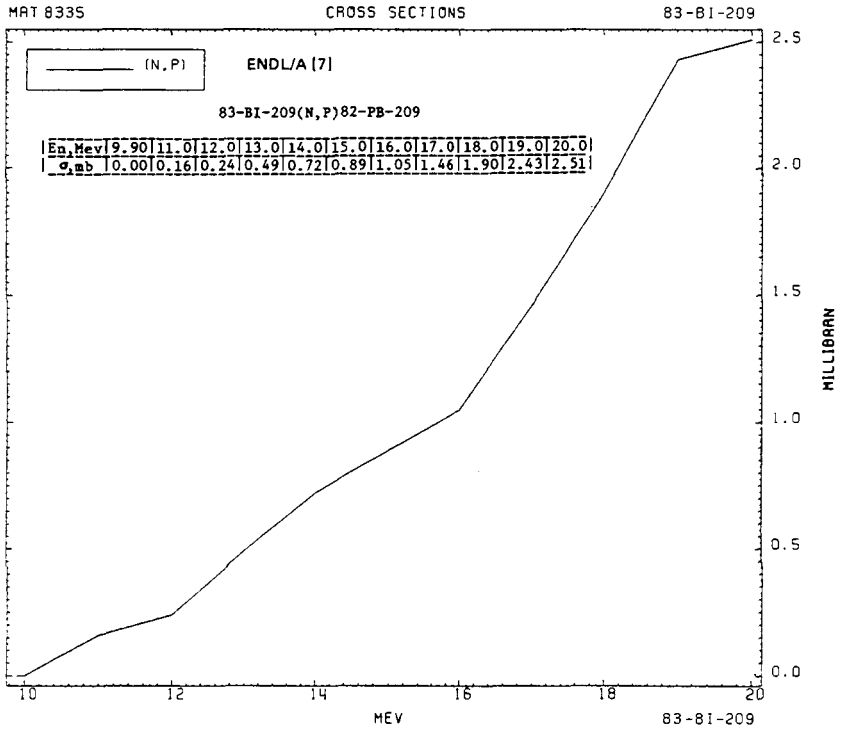
MAT 8335
CROSS SECTIONS
83-BI-209
(N,P)
ENDL/A [7]
83-BI-209(N,P)82-PB-209
En,Mev | 9.90 | 11.0 | 12.0 | 13.0 | 14.0 | 15.0 | 16.0 | 17.0 | 18.0 | 19.0 | 20.0
σ,mb | 0.00 | 0.16 | 0.24 | 0.49 | 0.72 | 0.89 | 1.05 | 1.46 | 1.90 | 2.43 | 2.51
MILLIBARN
MEV
83-BI-209

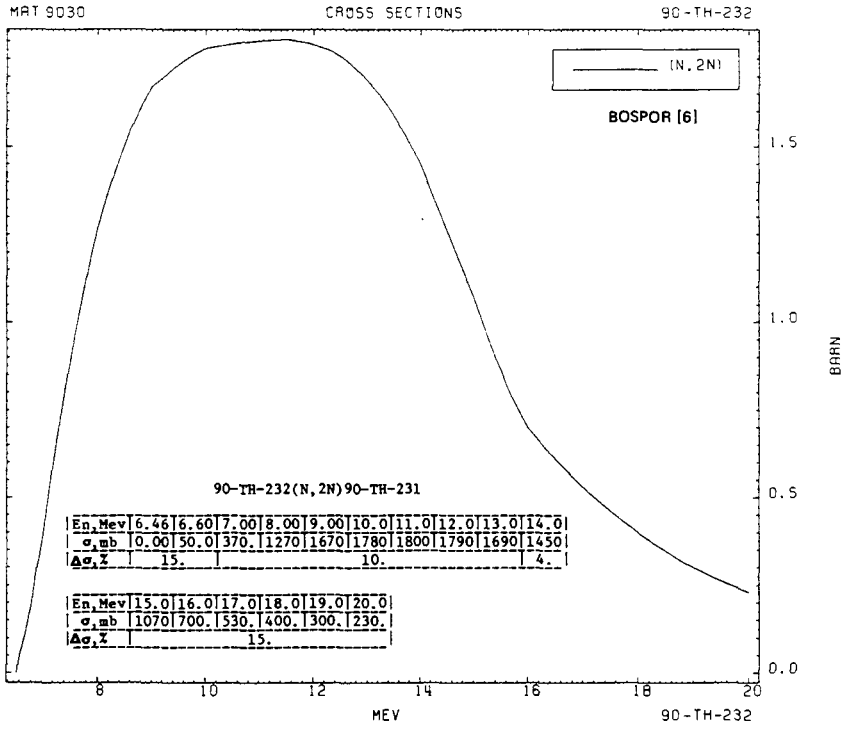
MAT 9030
CROSS SECTIONS
90-TH-232
(N,2N)
BOSPOR [6]
1.5
1.0
0.5
0.0
BARN
90-TH-232(N,2N)90-TH-231
En,Mev | 6.46 | 6.60 | 7.00 | 8.00 | 9.00 | 10.0 | 11.0 | 12.0 | 13.0 | 14.0
σ,mb | 0.00 | 50.0 | 370. | 1270 | 1670 | 1780 | 1800 | 1790 | 1690 | 1450
Δσ,% | 15. | 10. | 4.
En,Mev | 15.0 | 16.0 | 17.0 | 18.0 | 19.0 | 20.0
σ,mb | 1070 | 700. | 530. | 400. | 300. | 230.
Δσ,% | 15.
8
10
12
14
16
18
20
MEV
90-TH-232

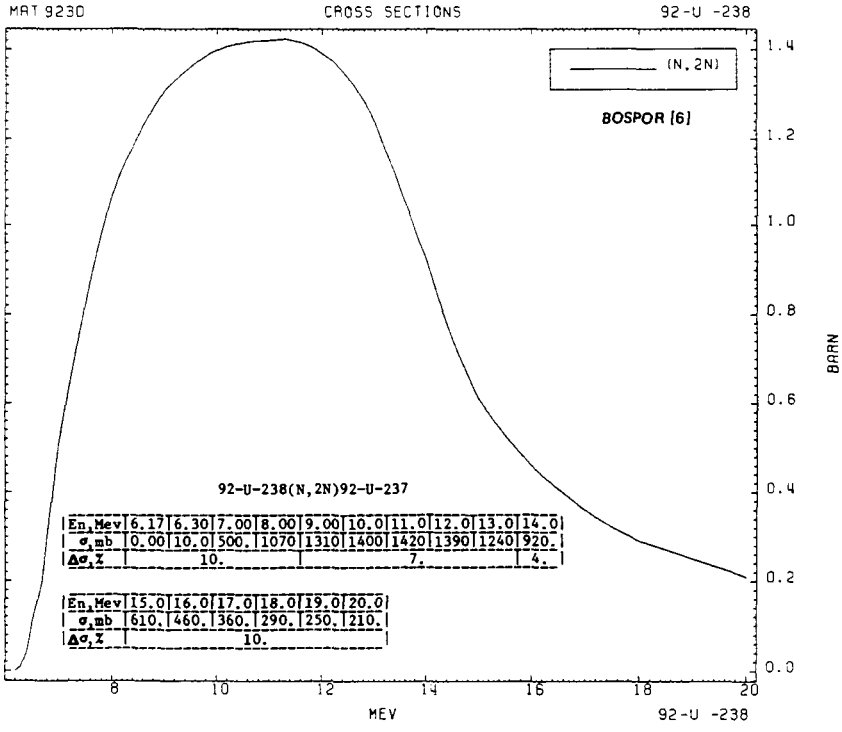
MAT 9230
CROSS SECTIONS
92-U -238
(N,2N)
BOSPOR [6]
1.4
1.2
1.0
0.8
0.6
0.4
0.2
0.0
BARN
92-U-238(N,2N)92-U-237
En,Mev | 6.17 | 6.30 | 7.00 | 8.00 | 9.00 | 10.0 | 11.0 | 12.0 | 13.0 | 14.0
σ,mb | 0.00 | 10.0 | 500. | 1070 | 1310 | 1400 | 1420 | 1390 | 1240 | 920.
Δσ,% | 10. | 7. | 4.
En,Mev | 15.0 | 16.0 | 17.0 | 18.0 | 19.0 | 20.0
σ,mb | 610. | 460. | 360. | 290. | 250. | 210.
Δσ,% | 10.
8
10
12
14
16
18
20
MEV
92-U -238

2–4. CALIFORNIUM-252 SPECTRUM AVERAGED NEUTRON CROSS-SECTIONS

W. MANNHART
Physikalisch-Technische Bundesanstalt,
Braunschweig,
Federal Republic of Germany

Abstract

CALIFORNIUM-252 SPECTRUM AVERAGED NEUTRON CROSS-SECTIONS.

The status of the available experimental data on spectrum averaged cross-section measurements for the neutron benchmark field of ^{252}Cf spontaneous fission is reviewed. Particular attention is paid to the uncertainties of the experimental data, in the form of complete covariance matrices describing the interdependence of the data on the measurement procedure. Based on this information, a set of recommended data have been derived by generalized least squares techniques. The results from calculations of spectrum averaged data, based mainly on Evaluated Neutron Data File (ENDF/B-V) neutron cross-sections, are also given.

1. INTRODUCTION

The use of neutron monitor reactions in power reactors during routine operation for purposes of neutron fluence and flux density determination requires prior establishment of the measuring techniques and of the reliability of the nuclear data. This can best be carried out using certain neutron benchmark fields which have the advantage of being relatively simple in structure. Thus, the benchmark fields of ^{235}U and ^{252}Cf are quite useful. Even if the field of neutron-induced fission for ^{235}U is more application oriented, owing to the fact that most technical neutron fields are driven by this fission source, the realization of a pure ^{235}U neutron field is hampered by spectrum perturbation effects arising from the epithermal neutron background, from wall returns and from scattering effects. This inherent disadvantage of a ^{235}U neutron field can be circumvented by using the neutron field of ^{252}Cf spontaneous fission. With a compact form of a californium source and a high specific neutron yield ($2.3 \times 10^{9} \cdot s^{-1} \cdot mg^{-1}$), neutron fields can be realized which are almost free of spectrum distortion effects. The precision attainable in a neutron cross-section measurement in such a field is limited only by the uncertainties of the neutron-source strength determination (about 1%) and the activation-detector calibration (about 1.5%). Assuming negligible contributions from counting statistics, relative overall uncertainties of the order of 2% can be achieved. This makes ^{252}Cf spectrum averaged data very useful for the validation of energy-dependent cross-section evaluations. Owing to their high accuracy,

^{252}Cf spectrum averaged cross-sections can also be applied to variance reduction methods [1] with the aim of making possible more precise predictions of radiation damage in reactor pressure vessels.

2. BASIS OF THE EXPERIMENTAL DATA

Since the last review (that surveyed the status of data available up to 1979 [2]), the quantity of data has almost doubled. The data are indicated by the label 'Experiment' in column 2 of Table I. Columns 4 and 5 give examples of related experiments: the reference reaction and the spectrum averaged cross-section value, $\langle\sigma\rangle_R$, used for this reaction are shown. In addition, a brief description is given of each experiment. It is also shown that some experiments have been superseded by more recent data and that some of the data have been revised. The experiments form two groups: those with a complete uncertainty description and those with incomplete details of the experimental uncertainties. The former group of experiments is of particular importance, owing to their suitability for an evaluation of a recommended best set of data, as shown in Sec. 4.

2.1. Experiments with incomplete uncertainty information

The goal of attaining precision in determining spectrum averaged neutron cross-sections can only be justified if a detailed list of uncertainty contributions is available which makes the information given as trustworthy as possible. Unfortunately, this aspect has been neglected in some experiments, which give only overall uncertainties without specifications. It is most difficult to estimate the quality of this data and this further hampers their use for purposes of evaluation.

2.1.1. Experiment by Pauw and Aten [32]

The experiment is based on a neutron-source strength determination in a manganese bath and is therefore labelled in column 4 of Table I as 'Absolute'. No further details of the experiment and the activity measurement procedure are given.

2.1.2. Experiment by Kirouac et al. [11]

All data were measured relative either to the ^{54}Fe(n, p) or to the ^{58}Ni(n, p) reactions used for neutron flux density monitoring. The cross-sections used for these reactions were 87 and 105 mb, respectively. Unfortunately, the information given does not state which of the monitors was used for a specific reaction. While the monitor cross-section of ^{54}Fe(n, p) is relatively consistent with more recent data, the same is not true of the value of 105 mb used for the ^{58}Ni(n, p) reaction.

Text cont. on p. 422.

TABLE I. Cf-252 SPECTRUM AVERAGED NEUTRON CROSS-SECTIONS

Reaction	Type of data	<σ> (mb)	Reference Reaction	$<\sigma>_R$ (mb)	Year	Ref.
F-19(n,2n)	Experiment	$(1.08 \pm 0.16)\times10^{-2}$	In-115(n,n')	199.4*	1977	[3]
		$(1.63 \pm 0.05)\times10^{-2}$	Ni-58(n,p)	118.0	1982	[4]
	Recommended	$(1.628\pm0.054)\times10^{-2}$				
	Calculated	$(1.626\pm0.043)\times10^{-2}$			σ(E)from	[5]
Na-23(n,γ)	Experiment	0.335± 0.015	In-115(n,n')	199.4*	1977	[3]
	Calculated	0.2712			σ(E)from	ENDF/B-V
Mg-24(n,p)	Experiment	1.94 ± 0.09	Al-27(n,α)	1.006	1982	[6]
		2.01 ± 0.06	Al-27(n,α)	1.006	1982	[4]
	Recommended	2.005± 0.048				
	Calculated	2.159± 0.088			σ(E)from	(Ta79)
Al-27(n,p)	Experiment	5.11 ± 0.43	In-115(n,n')	199.4*	1976	[8]
		4.89 ± 0.18	Al-27(n,α)	1.006	1982	[6]
		4.80 ± 0.09	In-115(n,n')	195.0	1982	[4]
		4.70 ± 0.37	In-115(n,n')	196	1982	[9]
		4.80 ± ?	In-115(n,n')	196.4	1983	[10]
	Recommended	4.892± 0.106				
	Calculated	5.137± 0.294			σ(E)from	ENDF/B-V
Al-27(n,α)	Experiment	0.86 ± 0.05	Ni-58(n,p)	105	1973	[11]
		1.006± 0.022	Absolute	-	1975	[12]
		1.08 ± 0.05	In-115(n,n')	199.4*	1976	[8]
		1.06 ± 0.08(2σ)	Absolute		1977	[13]
	Recommended	1.021± 0.015				
	Calculated	1.059± 0.058			σ(E)from	ENDF/B-V
		1.012± 0.029			σ(E)from	[14]
S-32(n,p)	Experiment	72.5 ± 3.0	Al-27(n,α)	1.006	1982	[6]
		68.4 ± ?	In-115(n,n')	200	1982	[15]
	Recommended	72.74± 2.54				
	Calculated	75.99± 5.93			σ(E)from	ENDF/B-V

TABLE I (cont.)

Reaction	Type of data	<σ> (mb)	Reference Reaction	$<\sigma>_R$ (mb)	Year	Ref.
Ti-46(n,p)	Experiment	12.4 ± 1.2	Ni-58(n,p)	105	1973	[11]
		13.8 ± 0.3	Absolute	-	1975	[12]
		15.0 ± 1.0(2σ)	Absolute	-	1977	[13]
		13.4 ± 1.1	In-115(n,n')	199.4[a]	1977	[3]
		13.6 ± ?	In-115(n,n')	200	1982	[15]
	Recommended	14.20± 0.24				
	Calculated	13.47± 1.70			σ(E)from	ENDF/B-V
Ti-47(n,p)	Experiment	20.3 ± 1.1	Ni-58(n,p)	105	1973	[11]
		18.9 ± 0.4	Absolute	-	1975	[12]
		20.2 ± 1.3(2σ)	Absolute	-	1977	[13]
		22.0 ± 0.9	In-115(n,n')	199.4[a]	1977	[3]
		19.4 ± ?	In-115(n,n')	200	1982	[15]
	Recommended	19.43± 0.31				
	Calculated	24.06± 2.70			σ(E)from	ENDF/B-V
		19.32			σ(E)from	[16]
Ti-48(n,p)	Experiment	0.42 ± 0.01	Absolute	-	1975	[12]
		0.38 ± 0.02	In-115(n,n')	199.4[a]	1977	[3]
		0.434± 0.036(2σ)	Absolute	-	1977	[13]
	Recommended	0.4275±0.0078				
	Calculated	0.4093±0.0422			σ(E)from	ENDF/B-V
V-51(n,p)	Experiment	0.93 ± 0.10	In-115(n,n')	199.4[a]	1977	[3]
		0.713± 0.059	Al-27(n,α)	1.006	1982	[6]
	Recommended	0.7178±0.0570				
V-51(n,α)	Experiment	(4.30 ± 0.20)x10^{-2}	In-115(n,n')	199.4[a]	1977	[3]
Fe-54(n,p)	Experiment	87 ± 3	Ni-58(n,p)	105	1973	[11]
		84.6 ± 2.0	Absolute	-	1975	[12]
		90.0 ± 5.1(2σ)	Absolute	-	1977	[13]
		92.5 ± 5.0	In-115(n,n')	199.2	1978	[17]
		87.6 ± 4.4	Al-27(n,α)	1.006	1982	[6]
		89 ± 2	Absolute	-	1982	[18]
		85.1 ± ?	In-115(n,n')	196.4	1983	[10]
	Recommended	87.29± 1.13				
	Calculated	88.24± 3.07			σ(E)from	ENDF/B-V

Reaction	Type of data	<σ> (mb)	Reference Reaction	$<\sigma>_R$ (mb)	Year	Ref.
Fe-56(n,p)	Experiment	1.18 ± 0.08	Ni-58(n,p)	105	1973	[11]
		1.450± 0.035	Absolute	-	1975	[12]
		1.45 ± 0.06	In-115(n,n')	199.2	1978	[17]
		1.44 ± 0.07	Al-27(n,α)	1.006	1982	[6]
		1.090± 0.068	In-115(n,n')	196	1982	[9]
		1.41 ± ?	In-115(n,n')	196.4	1983	[10]
	Recommended	1.471± 0.025				
	Calculated	1.414± 0.063			σ(E)from	ENDF/B-V
Mn-55(n,2n)	Experiment	0.58 ± 0.15	In-115(n,n')	199.4[a]	1976	[8]
		0.408± 0.009	Ni-58(n,p)	118	1982	[4]
	Recommended	0.4079±0.0092				
	Calculated	0.4459±0.0558			σ(E)from	ENDF/B-V
Ni-58(n,p)	Experiment	105 ± 5	Fe-54(n,p)	87	1973	[11]
		118 ± 3	Absolute	-	1975	[12]
		118.8± 5.5(2σ)	Absolute	-	1977	[13]
		113.4± 4.8	In-115(n,n')	199.4[a]	1977	[3]
		118 ± 4	Al-27(n,α)	1.006	1982	[6]
		95.0 ± 4.5	In-115(n,n')	196	1982	[9]
		121 ± 2	Absolute	-	1982	[18]
		117.2± ?	In-115(n,n')	196.4	1983	[10]
	Recommended	117.6± 1.5				
	Calculated	113.8± 7.3			σ(E)from	ENDF/B-V
Ni-58(n,2n)	Experiment	(8.94 ±0.28)x10^{-3}	Ni-58(n,p)	118	1982	[4]
	Recommended	(8.965±0.297)x10^{-3}				
	Calculated	(7.600±0.828)x10^{-3}			σ(E)from	ENDF/B-V
		(8.464±0.395)x10^{-3}			σ(E)from	[19,20]
Ni-60(n,p)	Experiment	2.39 ± 0.13	Ni-58(n,p)	118	1982	[21]
	Calculated	3.442± 0.261			σ(E)from	ENDF/B-V
Co-59(n,γ)	Experiment	6.97 ± 0.34	In-115(n,n')	199.4[a]	1977	[3]
	Calculated	6.028			σ(E)from	ENDF/B-V

TABLE I (cont.)

Reaction	Type of data	<σ> (mb)	Reference Reaction	$<\sigma>_R$ (mb)	Year	Ref.
Co-59(n,p)	Experiment	1.96 ± 0.10	In-115(n,n')	199.4[a]	1977	[3]
		1.68 ± 0.04	Ni-58(n,p)	118	1982	[4]
	Recommended	1.686± 0.037				
	Calculated	1.733			σ(E)from	[22-24]
Co-59(n,α)	Experiment	0.20 ± 0.01	Ni-58(n,p)	105	1973	[11]
		0.20 ± 0.01	In-115(n,n')	199.4[a]	1977	[3]
		0.218± 0.014	Al-27(n,α)	1.006	1982	[6]
		0.222± 0.004	Ni-58(n,p)	118	1982	[4]
	Recommended	0.2221±0.0039				
	Calculated	0.2162±0.0091			σ(E)from	ENDF/B-V
Co-59(n,2n)	Experiment	0.57 ± 0.03	In-115(n,n')	199.4[a]	1976	[8]
		0.406± 0.010	Ni-58(n,p)	118	1982	[4]
	Recommended	0.4058±0.0101				
	Calculated	0.4103±0.0430			σ(E)from	ENDF/B-V
Cu-63(n,γ)	Experiment	10.95± 0.51	Au-197(n,γ)	79.9[b]	1975	[25]
		10.39± 0.30	In-115(n,n')	195	1982	[4]
	Recommended	10.55± 0.32				
	Calculated	9.649			σ(E)from	ENDF/B-V
Cu-63(n,α)	Experiment	0.709± 0.017	Absolute	-	1981	[26]
		0.671± 0.018	Ni-58(n,p)	118	1982	[4]
	Recommended	0.6897±0.0130				
	Calculated	0.7577±0.0398			σ(E)from	ENDF/B-V
		0.6761±0.0379			σ(E)from	[27,28]
Cu-63(n,2n)	Experiment	0.30 ± 0.03	In-115(n,n')	199.4[a]	1976	[8]
		0.183± 0.007	In-115(n,n')	195	1982	[4]
	Recommended	0.1866±0.0071				
	Calculated	0.1981±0.0033			σ(E)from	[7]

Reaction	Type of data	<σ> (mb)	Reference Reaction	$<\sigma>_R$ (mb)	Year	Ref.
Zn-64(n,p)	Experiment	39.4 ± 1.0	Absolute	-	1975	[12]
		46.4 ± 2.3	In-115(n,n')	199.4[a]	1976	[8]
		41.8 ± 1.7	Al-27(n,α)	1.006	1982	[6]
		36.2 ± 1.5	In-115(n,n')	196	1982	[9]
		41.3 ± ?	In-115(n,n')	200	1982	[15]
	Recommended	40.47± 0.75				
	Calculated	39.23± 2.91			σ(E)from	[7]
Zr-90(n,2n)	Experiment	0.267± 0.015	In-115(n,n')	199.4[a]	1977	[3]
		0.221± 0.006	Ni-58(n,p)	118	1982	[4]
	Recommended	0.2211±0.0061				
	Calculated	0.2069±0.0042			σ(E)from	[7]
		0.2102±0.0041			σ(E)from	[19,20]
Nb-93(n,n')	Experiment	149 ± 10	In-115(n,n')	195	1982	[29]
	Calculated	163.6± 29.1			σ(E)from	[5]
Mo-98(n,γ)	Experiment	24.8 ± 1.2	Au-197(n,γ)	79.9[b]	1975	[25]
		23.2 ± 1.4	In-115(n,n')	199.4[a]	1976	[30]
		26.3 ± 1.3[c]	In-115(n,n')	199.4[a]	1977	[3]
Rh-103(n,n')	Experiment	647 ± 70	Ni-58(n,p)	105	1973	[11]
		757 ± 53	In-115(n,n')	199.4[a]	1976	[30]
	Calculated	712.2± 21.9			σ(E)from	[5]
In-113(n,n')	Experiment	178.0± 7.6	In-115(n,n')	199.4[a]	1977	[3]
		160 ± 4	Absolute	-	1979	[31]
		170 ± 8	Al-27(n,α)	1.006	1982	[6]
		168 ± 9	In-115(n,n')	196	1982	[9]
		161.9± ?	In-115(n,n')	196.4	1983	[10]
	Recommended	162.7± 2.5				
In-115(n,γ)	Experiment	125.3± 4.3	Absolute	-	1971	[32]
		139.2± 6.0	In-115(n,n')	199.4[a]	1977	[3]
		124.1± 3.6	Absolute	-	1979	[31]
		115.6± 5.0	In-115(n,n')	196	1982	[9]
		123.2± ?	In-115(n,n')	196.4	1983	[10]
	Recommended	126.1± 2.8				
	Calculated	121.2			σ(E)from	ENDF/B-V

TABLE I (cont.)

Reaction	Type of data	<σ> (mb)	Reference Reaction	$<\sigma>_R$ (mb)	Year	Ref.
In-115(n,n')	Experiment	188 ± 8	Absolute	-	1971	[32]
		186 ± 11	Ni-58(n,p)	105	1973	[11]
		198 ± 5	Absolute	-	1975	[12]
		199.4 ± 10.5[a]	Absolute?	-	1976	[8]
		195 ± 5	Absolute	-	1979	[31]
		201 ± 8	Al-27(n,α)	1.006	1982	[6]
		196 ± 8	Absolute	-	1982	[9]
		196 ± 4	Absolute	-	1982	[18]
	Recommended	198.1 ± 2.6				
	Calculated	181.9 ± 21.6			σ(E) from	ENDF/B-V
Ta-181(n,γ)	Experiment	105.5 ± 6.1	Au-197(n,γ)	79.9[b]	1975	[25]
		119.9 ± 6.5	In-115(n,n')	199.4[a]	1977	[3]
		89.25 ± ?	In-115(n,n')	200	1982	[15]
Au-197(n,γ)	Experiment	95.5 ± 2.3	Absolute	-	1971	[32]
		79.9 ± 2.9	Au-197(n,γ)	σ_{th}=98.8b	1975	[25]
		119.1 ± 5.2	In-115(n,n')	199.4[a]	1977	[3]
		76.2 ± 1.8	Absolute	-	1979	[31]
		78 ± 3	In-115(n,n')	196	1982	[9]
		76.0 ± ?	In-115(n,n')	196.4	1983	[10]
	Recommended	77.11 ± 1.19				
	Calculated	76.32			σ(E) from	ENDF/B-V
Au-197(n,2n)	Experiment	4.93 ± 0.14	Absolute	-	1971	[32]
		5.80 ± 0.29	In-115(n,n')	199.4[a]	1976	[8]
		5.50 ± 0.14	Absolute	-	1979	[31]
		5.27 ± 0.23	Al-27(n,α)	1.006	1982	[6]
		5.55 ± ?	In-115(n,n')	196.4	1983	[10]
	Recommended	5.531 ± 0.099				
	Calculated	5.646			σ(E) from	ENDF/B-V
Th-232(n,f)	Experiment	89 ± 9	In-115(n,n')	199.4[a]	1976	[30]
		89.4 ± 2.7	Absolute	-	1983	[33]
	Calculated	78.07			σ(E) from	ENDF/B-V
Th-232(n,γ)	Experiment	87.8 ± 4.0	Th-232(n,γ)	σ_{th}=7.40b	1975	[25]
	Calculated	89.68			σ(E) from	ENDF/B-V

Reaction	Type of data	<σ> (mb)	Reference Reaction	$<\sigma>_R$ (mb)	Year	Ref.
U-235(n,f)	Experiment	1266 ± 19	Absolute	-	1977	[34]
		1140 ±111(2σ)	Absolute	-	1977	[13]
		1215 ± 22	Absolute	-	1978	[35]
		1216 ± 19	Absolute	-	1983	[36]
	Recommended	1210 ± 14				
	Calculated	1236			σ(E)from	ENDF/B-V
Np-237(n,f)	Experiment	1260 ± 60	Absolute	-	1971	[32]
		1380 ±100	Ni-58(n,p)	105	1973	[11]
		1370 ±120	In-115(n,n')	199.4[a]	1976	[30]
		1442 ± 23	Absolute	-	1977	[34]
		1180 ±136(2σ)	Absolute	-	1977	[13]
		1366 ± 27	U-238(n,f)	326.0	1983	[33]
	Recommended	1356 ± 22				
	Calculated	1352			σ(E)from	ENDF/B-V
U-238(n,f)	Experiment	310 ± 25	Absolute	-	1971	[32]
		308 ± 17	Ni-58(n,p)	105	1973	[11]
		347 ± 6	Absolute	-	1977	[34]
		284 ± 27(2σ)	Absolute	-	1977	[13]
		311 ± 14	In-115(n,n')	199.2	1978	[17]
		326.0± 6.5	U-235(n,f)	1216	1983	[33]
	Recommended	323.4± 5.6				
	Calculated	313.6			σ(E)from	ENDF/B-V
Pu-239(n,f)	Experiment	1800 ± 60	Absolute	-	1971	[32]
		1790 ± 41	Absolute	-	1978	[35]
		1824 ± 35	U-235(n,f)	1216	1983	[33]
	Recommended	1811 ± 25				
	Calculated	1792			σ(E)from	ENDF/B-V

[a] Renormalized value.
[b] Double ratio (see text).
[c] Mo-98(n, γ) + Mo-100(n, 2n).

2.1.3. Experiment by Green [25]

This experiment, involving the measurement of various non-threshold (n, γ) reactions, is well documented and could be more justifiably listed in Sec. 2.2. The reason why this has not been done is a peculiarity of the experimental procedure. The ^{252}Cf spectrum averaged cross-sections of ^{197}Au(n, γ) and ^{232}Th(n, γ) were determined relative to the thermal neutron cross-sections of both reactions. This procedure established correlations between thermal and ^{252}Cf cross-sections which are, however, beyond the scope of the present work and are therefore omitted owing to basic problems with those data. The experimental method eliminated the calibration of the activity-measuring detector system. The fission neutron flux density of ^{252}Cf was based on a source-strength determination via a manganese bath and a distance measurement. Identical foils were irradiated in the thermal standard neutron field at the United States National Bureau of Standards (NBS). The thermal neutron flux density was determined by means of boron films and gold foils. Three additional (n, γ) reactions were measured by a 'double ratio' procedure. In this case, the ^{252}Cf-to-thermal ratio of an unknown reaction was measured relative to the same ratio of ^{197}Au(n, γ).

2.1.4. Experiments by Csikai et al. [30, 8, 3, 17]

The most extensive set of ^{252}Cf data has been measured by a group from Kossuth University at Debrecen, Hungary. For each reaction that was measured, the decay parameters that were used (of the reaction products) were listed. However, further information on the experimental procedure and the necessary corrections is sparse. Foils of 10 mm diameter were irradiated at a distance of about 2 cm from an extended 0.5 mg SR-Cf-1000 source. The neutron source strength was based on a value quoted by the manufacturer. The neutron flux density at the position of the sample was determined using In foils that were varied at a distance of between 2 and 30 cm from the source, i.e. all measurements were relative to the ^{115}In(n, n') cross-section, for which a renormalized value of 199.4 mb was used. The source-sample arrangement was mounted on a thin wire fixed to the ceiling of a large room. The minimum distance from the walls was 3 m. In the case of the (n, γ) reactions, the samples were placed inside a cadmium box with a wall thickness of 1 mm. Most activities were measured using a Ge(Li) detector system. The fission cross-sections were determined at earlier stages of the experiment by solid state track detectors and later by a fission chamber. Results were reported from time to time. The sequence started with the work of Buczkó et al. [30] and ended with the work of Dezsö and Csikai [17]. Partial results were either superseded or revised by data published later. This has been allowed for in Table I. Identical results quoted more than once are listed under the date of the first publication.

2.1.5. *Experiment by Benabdallah et al.* [9]

This experiment, performed at the Université Mohamed V in Rabat, Morocco, is, in its experimental procedure, essentially identical with the experiments of Csikai et al. (see Sec. 2.1.4). A 20 μg encapsulated ^{252}Cf source was used in an open-air arrangement 6 m above the ground. The outer dimensions of the cylindrical source were: diameter 7.8 mm and height 10 mm. The irradiations were carried out at a distance of (4.3 ± 0.15) mm from the cylinder axis. The free-field neutron flux density was monitored with the ^{115}In(n, n′) reaction as a function of the source-sample distance. The neutron flux density at the target position was found to be identical with that of a point source with an effective distance of (5.2 ± 0.12) mm.

The influence of a backscattered thermal neutron component was investigated using the ^{115}In(n, γ) reaction measured with and without cadmium shielding. No perturbation due to thermal neutrons was found. In the experiment the statistical uncertainty dominated the uncertainty of the source strength (about 1.5%) and that of the detector efficiency calibration (about 1.5%). Here, too, the neutron source strength was based on a manufacturer's declaration. The data must be regarded as measurements relative to ^{115}In(n, n′) with a cross-section value of 196 mb.

2.1.6. *Experiments by Dezsö and Csikai with improved experimental conditions* [15, 10]

A limited set of the earlier measurements was repeated under improved conditions. The main improvement was the replacement of the indoor irradiation facility by an outdoor arrangement. Using a 40 μg encapsulated ^{252}Cf source (diameter 7.5 mm, length 14 mm), irradiations were performed in the open air with the source 12 m above ground and 4 m above the roof of a building. Owing to the fact that an accurate neutron source strength determination was not available, measurements were made relative to the ^{115}In(n, n') reaction. The sample material was wound tightly on the surface of the cylinder of the source. The reproducibility of results obtained with this irradiation geometry was of the order of 2% [15]. The geometry was further improved with the use of "compensated beam geometry": two sample foils on opposite sides of the cylindrical source that were irradiated simultaneously [10]. This improved the reproducibility from 2 to 1.4%. Further improvements are planned in which samples sandwiched between In foils are irradiated (the data in Ref. [10] partially supersede results contained in Ref. [15]). At present, the estimates of neutron flux density perturbations are incomplete. Therefore, in Refs [15] and [10] only statistical uncertainties are quoted and complete uncertainty listing is lacking. In Table I the incomplete uncertainty of the results is indicated by question-marks.

TABLE II. UNCERTAINTY DATA FROM EXPERIMENTS CARRIED OUT AT PTB

Reaction	<σ> (mb)	Rel.Std.Dev. (%)	Correlation matrix (x100)											
Al-27(n,α)	1.006	2.14	100											
Ti-46(n,p)	13.8	2.37	74	100										
Ti-47(n,p)	18.9	2.29	77	74	100									
Ti-48(n,p)	0.42	2.54	69	77	69	100								
Fe-54(n,p)	84.6	2.36	74	67	70	63	100							
Fe-56(n,p)	1.450	2.39	74	66	69	62	71	100						
Ni-58(n,p)	118.	2.35	75	68	70	63	68	67	100					
Zn-64(n,p)	39.4	2.51	70	63	66	59	64	63	64	100				
In-113(n,n')	160.	2.42	73	66	68	61	66	65	66	62	100			
In-115(n,γ)	124.1	2.89	61	55	57	51	55	55	55	52	77	100		
In-115(n,n')	198.	2.53	70	63	65	74	63	62	63	59	66	55	100	
In-115(n,n')	195.	2.46	71	65	67	60	65	64	65	61	90	75	67	100
Au-197(n,γ)	76.2	2.37	74	67	69	62	67	66	68	63	89	75	69	88	100
Au-197(n,2n)	5.50	2.59	68	61	64	57	62	61	62	58	82	68	63	80	87	100

It should be noted that the data obtained with the improved irradiation facility are more consistent with other experiments than the earlier data measured with the old facility. This is due to problems with backscattering in the earlier versions of the experiment, where discrepancies up to the order of 40% with other experiments were found.

2.2 Experiments with complete uncertainty information

With the exception of one case, none of the following experiments have directly quoted the uncertainty covariance matrix. However, the uncertainty information was sufficiently detailed to allow a reconstruction of this matrix. Besides a short description of the experiment, the covariances are listed in this section.

2.2.1. Experiments performed at the Physikalisch-Technische Bundesanstalt (PTB) [12, 31]

Irradiations were carried out at an outdoor irradiation facility at a position 12 m above ground. The sample material surrounded the cylindrical source in a 4π geometry. The neutron source strength was determined using a water-bath method. Absorption and scattering were taken into account by calculating an effective path length of neutrons through the sample material allowing for the geometry. In Ref. [12], the metallic sample foils were chemically dissolved and their activity compared with radioactive standard solutions. In Ref. [31] the

TABLE III. CORRELATION MATRIX FOR NBS FISSION CROSS-SECTION MEASUREMENTS

Reaction (ratio)	$<\sigma>$ (ratio) (mb)	Rel. std. dev. (%)	Correlation matrix (x 100)
U-235(n, f)	1216	1.62	100
U-238(n, f)/U-235	0.2681	1.27	23 100
Np-237(n, f)/U-235	1.123	1.47	−7 29 100
Pu-239(n, f)/U-235	1.502	0.97	−9 15 36 100

irradiated sample cylinder was cut into pieces and measured with a calibrated Ge(Li) detector. Owing to the similarity of both experiments, a common covariance matrix has been derived (Table II). The uncertainty information is quoted in the form of relative standard deviations (1σ level) and a correlation matrix.

2.2.2. Fission cross-section measurements at the NBS [37, 38, 36, 33]

The experiment comprises the absolute measurement of the $^{235}U(n, f)$ cross-section [37] and measurements of $^{237}Np(n, f)$, $^{238}U(n, f)$ and $^{239}Pu(n, f)$ relative to $^{235}U(n, f)$ [38]. Irradiations were carried out at an indoor facility. Two double fission chambers were mounted in a light frame on opposite sides of a californium source in a compensated beam geometry. The free-field neutron flux density is based on a neutron source strength determination and a distance measurement. The ^{252}Cf source was calibrated in a manganese bath against the Ra-Be photoneutron standard source NBS-I. Scattering from support structures and from wall returns was determined by experiments and calculations. The wall-return effects were diminished by placing a cadmium cylinder around the source-detector assembly. The fission-deposit masses were determined by a multiplicity of techniques, including interlaboratory comparisons with mass standards. In the case of the ratio measurements, the fission deposits were arranged in a back-to-back geometry inside the double fission chambers. Orientation effects were compensated for by turning the fission chambers 180°. The various uncertainty components of the experiment were carefully analysed by Wagschal et al. [39] and a covariance matrix has been derived.

The experimental results have recently been revised [36, 33]. Owing to improvements in neutron source strength determination, fission-deposit mass determination and in scattering corrections, all results have been modified. Following the principles given in Ref. [39], the covariance matrix of the revised values has been recalculated (Table III).

TABLE IV. CORRELATION MATRIX FOR THE FISSION CROSS-SECTION MEASUREMENTS OF ADAMOV et al.

Reaction	<σ> (mb)	Rel. std. dev. (%)	Correlation matrix (x 100)		
U-235 (n, f)	1266	1.44	100		
Np-237(n, f)	1442	1.59	40	100	
U-238 (n, f)	347	1.68	34	31	100
Reaction ratios	**<σ> ratio**	**Rel. std. dev. (%)**	**Correlation matrix (x 100)**		
Np-237/U-235	1.139	1.66	100		
U-238/U-235	0.2741	1.80	39	100	

2.2.3. Measurements by Adamov et al. [34]

The fission cross-sections of ^{235}U, ^{238}U and ^{237}Np were determined by the coincidence technique. A thin Cf layer and a fission deposit of the material being investigated were placed back-to-back inside a double-ionization chamber. Coincidences between the spontaneous fission fragments of ^{252}Cf and the fragments from the ^{252}Cf neutron-induced fission in the sample material were counted. The results obtained are between 5 and 9% higher than those from other experiments. This indicates the possibility of a hidden bias factor in the experiment (for a detailed discussion, see Ref. [40]). To eliminate this bias, the original results were reduced to ratios, the covariances of the original data and of the deduced ratios being listed in Table IV.

2.2.4. Measurements by Spiegel et al. [13]

The irradiation facility was the same as in the NBS experiment described in Sec. 2.2.2. Identical foil packets were irradiated in a compensated beam geometry. The packets were arranged around the source with a 60° angular separation, i.e. three identical pairs of packets were irradiated simultaneously. For this special geometry, the Cf source was rotated during irradiation to eliminate anisotropies in the direction of emission. Additionally, perturbations of the free-field neutron flux density due to scattering processes were monitored by Ni detectors enclosed in the packets. The radioactivities induced were measured with sodium iodide and germanium detectors. The (n, f) cross-sections were based on the detection of the radioactive decay of the fission product ^{140}Ba. Uncertainties were quoted

TABLE V. CORRELATION MATRIX FOR THE CROSS-SECTION MEASUREMENTS OF SPIEGEL et al.

Reaction	$<\sigma>$ (mb)	Rel. std. dev. (%)	Correlation matrix (x 100)						
Al-27(n, α)	1.060	3.68	100						
Al-27(n, α)	1.060	3.57	95	100					
Ti-46(n, p)	15.0	3.27	49	42	100				
Ti-47(n, p)	20.2	3.08	52	45	79	100			
Ti-48(n, p)	0.434	4.14	39	33	59	63	100		
Fe-54(n, p)	90.0	2.88	46	48	52	55	41	100	
Ni-58(n, p)	118.8	2.28	71	64	79	84	63	79	100

TABLE VI. (n, f) CROSS-SECTION MEASUREMENTS BY SPIEGEL et al.

Reaction	$<\sigma>$ (mb)	Rel. std. dev. (%)	Correlation matrix (x 100)		
U-235 (n, f)	1140	4.82	100		
Np-237(n, f)	1180	5.73	69	100	
U-238 (n, f)	284	4.78	85	70	100
Reaction ratio	**$<\sigma>$ ratio**	**Rel. std. dev. (%)**	**Correlation matrix (x 100)**		
Np-237/U-235	1.035	4.24	100		
U-238/U-235	0.2491	2.61	33	100	

at the 2σ level, though for the calculation of the covariances they have been reduced to standard deviations (Table V).

In the case of the (n, f) data, a comparison with other experiments has led to the conclusion that there was an undetected bias factor. As in the case of the data contained in Ref. [34], these data have also been reduced to ratios, as shown in Table VI.

TABLE VII. CROSS-SECTION MEASUREMENTS BY DAVIS AND KNOLL

Reaction	$<\sigma>$ (mb)	Rel. std. dev. (%)	Correlation matrix (x 100)	
U-235(n, f)	1215	1.79	100	
Pu-239(n, f)	1790	2.26	59	100

2.2.5. Measurements by Davis and Knoll [35]

The cross-sections of $^{235}U(n, f)$ and $^{239}Pu(n, f)$ were determined in this experiment (see Table VII). Irradiations were carried out in a compensated beam geometry, reducing the free-field neutron flux density to a source strength determination and a distance measurement. The neutron source strength was calibrated with a manganese bath relative to the secondary standard NBS-II (a Ra-Be photoneutron source). The anisotropy of the ^{252}Cf source was measured with a long counter and corrected for. Fission events were recorded using solid state track detectors.

2.2.6. Measurements by Winkler et al. [26]

This precise experiment for the $^{63}Cu(n, \alpha)$ cross-section was performed at the NBS irradiation facility. The technique and the correction methods are identical with the NBS experiments described earlier. After an inspection for impurities with a Ge(Li) detector, the ^{60}Co radioactivity was measured using two different configurations of large sodium iodide detectors.

2.2.7. Measurements by Kobayashi et al. [41, 6]

These results were first published in 1979. Various foil packets, at a distance of 6 cm from a 0.5 mg encapsulated Cf source (5 mm in diameter, 17 mm in height), were irradiated. The neutron flux density was monitored with the $^{27}Al(n, \alpha)$ and $^{115}In(n, n')$ reactions. Wall-return effects of the indoor irradiation facility were determined by neutron transport calculations. The experiment was later completely reanalysed (see Ref. [6]) in order to derive the data and covariances shown in Table VIII.

2.2.8. Measurements by Mannhart [21, 4]

In contrast to earlier PTB measurements, the irradiation geometry was modified for this experiment. Disk-shaped samples (10 mm in diameter) of

TABLE VIII. COVARIANCE DATA DERIVED FROM THE EXPERIMENTS OF KOBAYASHI et al.

Reaction ratio	<σ> ratio	Rel. std. dev. (%)	Correlation matrix (×100)														
Mg-24(n,p)/In-115(n,n')	0.009651	4.24	100														
Al-27(n,p)/Al-27(n,α)	4.797	3.73	-7	100													
Al-27(n,p)/Al-27(n,α)	4.892	4.68	-6	23	100												
Al-27(n,p)/Al-27(n,α)	4.936	5.58	-5	19	15	100											
S-32(n,p)/Al-27(n,α)	72.96	3.75	2	8	19	5	100										
S-32(n,p)/Al-27(n,α)	70.98	5.06	2	6	5	45	41	100									
V-51(n,p)/Al-27(n,α)	0.7058	8.13	-8	15	6	5	2	2	100								
Fe-54(n,p)/In-115(n,n')	0.4361	4.16	26	-4	-3	-2	3	2	-5	100							
Fe-56(n,p)/In-115(n,n')	0.007166	4.02	27	-4	-3	-3	3	2	-5	31	100						
Ni-58(n,p)/Al-27(n,α)	118.3	2.77	-10	16	30	11	32	8	10	-5	-6	100					
Co-59(n,p)/Al-27(n,α)	0.2157	6.17	-4	18	5	5	6	4	10	-2	-1	9	100				
Zn-64(n,p)/Al-27(n,α)	41.65	3.66	-2	28	8	6	9	7	13	0	0	13	17	100			
In-113(n,n')/Al-27(n,α)	166.8	5.56	-10	10	8	44	3	44	8	-6	-6	14	6	6	100		
In-113(n,n')/In-115(n,n')	0.8511	4.90	21	0	0	0	0	0	-1	16	16	-1	0	0	10	100	
In-115(n,n')/Al-27(n,α)	198.9	4.39	-31	13	11	56	4	55	10	-25	-26	18	8	8	62	-15	100
Au-197(n,2n)/Al-27(n,α)	5.219	3.80	-15	32	11	10	5	4	21	-9	-9	20	21	28	15	-1	21	100

TABLE IX. COVARIANCE MATRIX DERIVED FROM MEASUREMENTS OBTAINED BY MANNHART

Reaction ratio	<σ> ratio	Rel. std. dev. (%)	Correlation matrix (×100)														
F-19(n,2n)/Ni-58(n,p)	1.381E-4	3.13	100														
Mg-24(n,p)/Al-27(n,α)	1.998E+0	2.40	-1	100													
Al-27(n,p)/In-115(n,n')	2.459E-2	2.45	-14	0	100												
Mn-55(n,2n)/Ni-58(n,p)	3.458E-3	1.93	30	-1	2	100											
Co-59(n,p)/Ni-58(n,p)	1.424E-2	1.91	5	0	6	10	100										
Co-59(n,α)/Ni-58(n,p)	1.877E-3	1.43	18	-1	19	37	26	100									
Co-59(n,2n)/Ni-58(n,p)	3.441E-3	2.19	27	-1	0	47	7	29	100								
Ni-58(n,2n)/Ni-58(n,p)	7.572E-5	3.15	19	0	-6	28	16	17	24	100							
Cu-63(n,γ)/In-115(n,n')	5.328E-2	3.00	3	0	46	5	-6	7	5	-2	100						
Cu-63(n,α)/Ni-58(n,p)	5.686E-3	2.39	7	0	4	12	27	32	10	17	-4	100					
Cu-63(n,2n)/In-115(n,n')	9.390E-4	3.83	14	-1	42	21	0	15	19	8	33	2	100				
Zr-90(n,2n)/Ni-58(n,p)	1.873E-3	2.52	24	0	0	36	12	21	31	28	3	12	16	100			

high-purity metallic foils were irradiated in a sandwich geometry, i.e. each sample was placed between two neutron flux density monitor foils, with the sandwich packets almost touching the surface of the cylindrical encapsulation of the source. ^{27}Al(n, α), ^{58}Ni(n, p) and ^{115}In(n, n′) were used as the monitor reactions. The sandwich technique allows an accurate determination of the neutron flux density at the sample position and also reduces the influence of scattering effects which disturb the neutron spectrum. Most of the earlier results [19] are superseded by the later data in Ref. [4]. The covariance matrix (Table IX) is given here for the first time.

TABLE X. COVARIANCE DATA BASED ON MEASUREMENTS BY LAMAZE et al.

Reaction	<σ> (mb)	Rel. std. dev. (%)	Correlation matrix (x 100)		
Fe-54(n, p)	89	1.73	100		
Ni-58(n, p)	121	1.72	86	100	
In-115(n, n')	196	1.85	46	46	100

TABLE XI. LIST OF DATA NOT CONSIDERED IN THIS PART

Reaction	Ref.	Reaction	Ref.
N-14(n, 2n)	[3]	Zr-94(n, γ)	[3]
F-19(n, p)	[3]	Mo-95(n, p)	[3]
Si-28(n, p)	[15]	Zr-96(n, γ)	[3]
Ti-46(n, 2n)	[3]	Mo-100(n, γ)	[3]
V-51(n, γ)	[3]	Cd-110(n, γ) + Cd-111(n, n')	[30]/[9]
Mn-55(n, γ)	[3]	In-113(n, 2n)	[3]
Cu-63(n, γ) + Cu-65(n, 2n)	[30]	Cd-116(n, γ)	[30]
Cu-65(n, γ)	[3]	Ba-134(n, γ) + Ba-135(n, n')	[30]/[9]
Zn-68(n, γ)	[9]	Ba-136(n, γ) + Ba-137(n, n')	[30]
As-75(n, γ)	[30]	Ba-138(n, γ)	[30]/[9]
Sr-84(n, γ)	[15]	Hg-198(n, γ) + Hg-199(n, n')	[30]
Sr-86(n, γ) + Sr-87(n, n')	[30]/[9]	Pb-204(n, n')	[30]
Zr-90(n, p)	[3]	Pa-231(n, f)	[3]
Mo-92(n, p)	[3]	U-233(n, f)	[33]
Mo-92(n, α)	[3]	Pu-240(n, f)	[33]
Nb-93(n, α)	[15]	Pu-241(n, f)	[33]
Nb-93(n, 2n)	[3]		

2.2.9. Measurements by Lamaze et al. [18]

This experiment continues earlier NBS experiments restricted to fission cross-section alone. The compensated beam geometry was used in its original version [37]. Table X lists the covariances derived from a detailed uncertainty listing.

TABLE XII. NBS EVALUATION OF THE NEUTRON SPECTRUM OF ^{252}Cf [42]

$$\chi_{Cf}(E) = [0.6672\sqrt{E}\exp(-E/1.42)]\mu(E) \quad (E \text{ in MeV})$$

Energy interval (MeV)	$\mu(E)$
0 - 0.25	0.763 + 1.20 E
0.25- 0.8	1.098 - 0.14 E
0.8 - 1.5	0.9668 + 0.024 E
1.5 - 6.0	1.0037 - 0.000 62 E
6.0 -20	exp [-0.03(E-6.0)]

2.3. Other data

The reactions shown in Table I were selected with regard to their importance in reactor dosimetry. For completeness the remaining reactions, for which ^{252}Cf spectrum averaged data were measured, are listed in Table XI, together with their corresponding references.

3. CALCULATION OF SPECTRUM AVERAGED CROSS-SECTIONS

For comparison, Table I also gives the results of calculated ^{252}Cf spectrum averaged neutron cross-sections. In the calculation, a normalized spectral distribution, $\chi(E)$, based on an evaluation performed at the NBS [42], was used. This spectrum representation, shown in Table XII, consists of five segment-adjusted correction functions, $\mu(E)$, applied to a Maxwellian with an average energy of 2.13 MeV. The correction function above 6 MeV neutron energy has recently been confirmed by an experiment [43]. Somewhat more questionable are the correction functions at lower energies [44], though their influence on the calculated results remains small. By assuming a pure Maxwellian between 0 and 6 MeV, i.e. neglecting the correction functions shown for this energy range, the calculated results change by less than 0.1% for all of the threshold reactions. For non-threshold reactions, the maximum deviation is 1.3% for $^{63}Cu(n, \gamma)$. This indicates that the data given in Table XII is sufficient for present purposes (see also Ref. [45]).

The energy-dependent cross-sections used in the calculation are based mainly on Evaluated Neutron Data File/B-V (ENDF/B-V) data. The integration range is between 10^{-5} eV and 20 MeV, which are the lower and upper energy limits for

TABLE XIII. PART OF THE RELATIVE UNCERTAINTY WHICH IS FULLY CORRELATED BETWEEN VARIOUS EXPERIMENTS

Reference	[36]	[18]	[26]	[13]	[35]
[36]	–				
[18]	1.10%	–			
[26]	1.10%	1.49%	–		
[13]	1.10%	1.49%	1.49%	–	
[35]	0.50%	0.50%	0.50%	0.50%	–

ENDF/B-V. The integration was performed with the original point data, in accordance with the given interpolation rules, i.e. no pre-processed group cross-sections were used. In some cases, cross-section data sets or evaluations not contained in ENDF/B-V were also used. For the $^{27}Al(n, \alpha)$, $^{47}Ti(n, p)$, $^{58}Ni(n, 2n)$ and $^{63}Cu(n, \alpha)$ reactions in particular, data sets given in Refs [14, 16, 19, 20, 27, 28] show better agreement between experiment and calculation than the data taken from ENDF/B-V.

The uncertainty quotations given for many of the calculated results in Table I are based on the uncertainties of the $\sigma(E)$ data, the uncertainty from the spectrum representation being discounted. The uncertainties given were propagated from the energy-dependent cross-section covariance matrices to the integral value calculated.

4. EVALUATION OF A 'BEST' SET OF EXPERIMENTAL DATA

The data in Sec. 2.2 were used for the evaluation of a recommended set of ^{252}Cf spectrum averaged cross-sections. A generalized least squares technique was applied which took into account absolute cross-sections as well as ratios (for details, see Ref. [40]). The different steps in the evaluation up to now have been the following:

Version No. 1 [40]: 17 neutron reactions based on 31 data points.
Version No. 2 [4]: 23 neutron reactions based on 48 data points.
Version No. 3 (present): 31 neutron reactions based on 63 data points.

Each later evaluation completely supersedes the earlier ones.

In Sec. 2.2, only correlations between data belonging to the same experiment are given. In a few cases correlations also exist between various experiments. These correlations are due to the neutron source strength determination relative to the standard sources NBS-I or NBS-II and to scattering corrections common to the various experiments performed at the NBS irradiation facility. The rela-

TABLE XIV. RESULTS OF THE LEAST SQUARES EVALUATION

Reaction	<σ> (mb)	Rel. std. dev. (%)
F-19(n,2n)	1.628E-2	3.33
Mg-24(n,p)	2.005E+0	2.39
Al-27(n,p)	4.892E+0	2.16
Al-27(n,α)	1.021E+0	1.42
S-32(n,p)	7.274E+1	3.50
Ti-46(n,p)	1.420E+1	1.68
Ti-47(n,p)	1.943E+1	1.58
Ti-48(n,p)	4.275E-1	1.81
V-51(n,p)	7.178E-1	7.95
Mn-55(n,2n)	4.079E-1	2.26
Fe-54(n,p)	8.729E+1	1.29
Fe-56(n,p)	1.471E+0	1.73
Ni-58(n,p)	1.176E+2	1.25
Ni-58(n,2n)	8.965E-3	3.32
Co-59(n,p)	1.686E+0	2.21
Co-59(n,α)	2.221E-1	1.78
Co-59(n,2n)	4.058E-1	2.49
Cu-63(n,γ)	1.055E+1	3.08
Cu-63(n,α)	6.897E-1	1.88
Cu-63(n,2n)	1.866E-1	3.82
Zn-64(n,p)	4.047E+1	1.85
Zr-90(n,2n)	2.211E-1	2.78
In-113(n,n')	1.627E+2	1.52
In-115(n,γ)	1.261E+2	2.19
In-115(n,n')	1.981E+2	1.31
Au-197(n,γ)	7.711E+1	1.54
Au-197(n,2n)	5.531E+0	1.79
U-235(n,f)	1.210E+3	1.19
Np-237(n,f)	1.356E+3	1.65
U-238(n,f)	3.234E+2	1.72
Pu-239(n,f)	1.811E+3	1.37

tive uncertainties, which are common to more than one experiment, are listed in Table XIII.

It can be seen from this table that out of the total relative uncertainty of 1.62% for experiments by Grundl et al. [36], about two-thirds, namely 1.10%, is common to the experiments of Lamaze et al. [18], Winkler et al. [26] and

TABLE XV. CORRELATION MATRIX OF THE EVALUATION

	Correlation matrix																														
F-19(n,2n)	100																														
Mg-24(n,p)	15	100																													
Al-27(n,p)	8	27	100																												
Al-27(n,α)	26	54	44	100																											
S-32(n,p)	11	23	21	33	100																										
Ti-46(n,p)	23	33	33	57	22	100																									
Ti-47(n,p)	25	35	36	61	24	60	100																								
Ti-48(n,p)	21	30	33	50	20	64	53	100																							
V-51(n,p)	4	6	11	12	3	9	10	9	100																						
Mn-55(n,2n)	43	23	25	40	17	34	37	30	7	100																					
Fe-54(n,p)	31	39	40	65	28	55	59	50	11	46	100																				
Fe-56(n,p)	21	35	34	57	24	46	50	42	9	32	56	100																			
Ni-58(n,p)	36	43	44	73	30	63	68	56	12	53	85	59	100																		
Ni-58(n,2n)	28	15	13	26	11	22	24	20	4	40	30	21	35	100																	
Co-59(n,p)	23	23	27	40	17	34	37	30	7	34	46	32	54	30	100																
Co-59(n,α)	36	28	39	49	21	42	45	37	9	58	56	39	66	34	49	100															
Co-59(n,2n)	39	20	22	36	15	31	33	28	6	60	42	29	49	36	30	50	100														
Cu-63(n,γ)	17	18	49	29	13	23	24	23	7	21	28	23	30	11	11	23	19	100													
Cu-63(n,α)	24	25	29	42	18	35	38	32	8	36	50	34	57	29	43	50	32	16	100												
Cu-63(n,2n)	24	14	43	23	11	18	19	18	5	30	22	18	24	17	12	25	28	36	15	100											
Zn-64(n,p)	19	32	33	55	22	44	47	39	10	29	50	43	54	19	30	37	27	22	31	18	100										
Zr-90(n,2n)	35	19	19	32	13	27	30	25	5	50	37	26	43	38	31	41	45	16	30	25	24	100									
In-113(n,n')	23	37	45	60	24	48	51	47	12	33	57	48	62	23	34	41	30	32	38	25	45	27	100								
In-115(n,γ)	16	25	31	41	16	33	35	33	8	23	39	34	43	16	23	29	21	22	26	17	31	19	57	100							
In-115(n,n')	26	40	54	64	26	52	55	55	13	38	63	53	69	26	38	46	34	39	44	31	48	31	77	53	100						
Au-197(n,γ)	23	35	44	59	23	48	50	45	13	33	56	47	61	22	34	41	30	31	38	25	45	27	75	54	75	100					
Au-197(n,2n)	20	31	39	52	19	41	45	39	13	30	50	42	54	20	30	37	27	27	33	22	41	24	65	45	64	74	100				
U-235(n,f)	13	17	19	27	12	23	24	22	5	19	35	23	35	13	20	24	17	13	23	11	21	16	27	19	32	27	23	100			
Np-237(n,f)	9	12	14	20	8	16	17	16	4	14	25	17	25	9	14	17	13	10	17	8	15	11	19	13	23	19	17	67	100		
U-238(n,f)	8	10	12	17	7	14	15	13	3	12	22	14	22	8	12	15	11	8	15	7	13	10	17	12	20	17	14	78	67	100	
Pu-239(n,f)	11	14	16	23	10	19	21	18	4	16	30	20	30	11	17	20	15	11	20	9	18	13	23	16	28	23	20	79	66	67	100

Spiegel et al. [13]. These intercorrelations were taken into account. The evaluation of the whole set of data in Sec. 2.2 showed some inconsistencies with regard to the above-mentioned intercorrelations, due mainly to the data sets of Adamov et al. [34] and Spiegel et al. [13]. This indicated that the removal of the suspected biases in both experiments, by reducing the data to ratios, was incomplete. Since the impression gained is that the uncertainties quoted are underestimated, the uncertainties of both experiments have been enlarged by a factor of 1.5. This procedure has eliminated the inconsistencies to a large extent. The evaluation has resulted in a χ^2 value of 39.2, with 32 degrees of freedom, and can be regarded as being sufficiently consistent. The result of the evaluation is given in Tables XIV and XV. The results are also listed in Table I as recommended values.

An inspection of Table XIV shows that out of a total of 31 reactions, 18 have relative uncertainties less than 2% and 24 reactions have less than 2.5%. Those reactions with uncertainties greater than 2.5% are in all cases results based on a single experiment. This indicates that there is a need for more experiments to validate existing results and to improve the overall accuracy to the data.

REFERENCES

[1] WAGSCHAL, J.J., MAERKER, R.E., BROADHEAD, B.L., in Reactor Dosimetry (Proc. 4th ASTM-EURATOM Symp. Gaithersburg, MD, 1982), Vol. 1, US Nuclear Regulatory Commission, Washington, DC, Rep. NUREG/CP-0029 (1982) 79.

[2] MANNHART, W., Nucl. Sci. Eng. 77 (1981) 40.

[3] DEZSÖ, Z., CSIKAI, J., in Neutron Physics (Proc. 4th All-Union Conf. Kiev, 1977), Vol. 3, Atomizdat, Moscow (1977) 32.

[4] MANNHART, W., in Nuclear Data for Science and Technology (Proc. Int. Conf. Antwerp, 1982) (BÖCKHOFF, K.H., Ed.), Reidel, Dordrecht (1983) 429.

[5] STROHMAIER, B., TAGESEN, S., VONACH, H., Physics Data 13-2, Fachinformationszentrum, Karlsruhe (1980).

[6] KOBAYASHI, K., KIMURA, I., MANNHART, W., J. Nucl. Sci. Technol. **19** (1982) 341.

[7] TAGESEN, S., VONACH, H., STROHMAIER, B., Physics Data 13-1, Fachinformationszentrum, Karlsruhe (1979).

[8] CSIKAI, J., DEZSÖ, Z., Ann. Nucl. Energy **3** (1976) 527.

[9] BENABDALLAH, H., PAIC, G., CSIKAI, J., in Nuclear Data for Science and Technology (Proc. Int. Conf. Antwerp, 1982) (BÖCKHOFF, K.H., Ed.), Reidel, Dordrecht (1983) 421.

[10] DEZSÖ, Z., CSIKAI, J., Measurements of Cf-252 Spectrum Averaged Cross-Sections, The Cf-252 Fission Neutron Spectrum (Proc. IAEA Consultants Meeting Smolenice, Czechoslovakia, 1983) (LEMMEL, H.D., CULLEN, D.E., Eds), IAEA/International Nuclear Data Committee, Vienna, Rep. INDC(NDS)-146 (1983) 225.

[11] KIROUAC, G.J., EILAND, H.M., SLAVIK, C.J., in Irradiation Experimentation in Fast Reactors (Proc. Int. Conf. Jackson Hole, Wyoming, 1973), Office of Scientific and Technical Information, US Department of Energy, Oak Ridge, TN, Rep. CONF-730910 (1973) 412.

[12] ALBERTS, W.G., GÜNTHER, E., MATZKE, M., RASSL, G., in Reactor Dosimetry (Proc. 1st ASTM-EURATOM Symp. Petten, Netherlands, 1975), Part 1, Commission of the European Communities, Brussels, Rep. EUR-5667 (1977) 131.
[13] SPIEGEL, V., EISENHAUER, C.M., GRUNDL, J.A., MARTIN, G.C., in Reactor Dosimetry (Proc. 2nd ASTM-EURATOM Symp. Palo Alto, CA, 1977), Vol. 2, US Nuclear Regulatory Commission, Washington, DC (1978) 959.
[14] TAGESEN, S., VONACH, H., Physics Data 13-3, Fachinformationszentrum, Karlsruhe (1981).
[15] DEZSÖ, Z., CSIKAI, J., in Nuclear Data for Science and Technology (Proc. Int. Conf. Antwerp, 1982) (BÖCKHOFF, K.H., Ed.), Reidel, Dordrecht (1983) 418.
[16] SMITH, D.L., MEADOWS, J.W., MANNHART, W., unpublished.
[17] DEZSÖ, Z., CSIKAI, J., Average Cross-Sections for the ^{252}Cf Neutron Spectrum, Nuclear Data for Reactor Dosimetry (Proc. Advisory Group Meeting Vienna, 1978), IAEA/International Nuclear Data Committee, Vienna, Rep. INDC(NDS)-103/M (1979) 176.
[18] LAMAZE, G.P., McGARRY, E.D., SCHIMA, F.J., in Nuclear Data for Science and Technology (Proc. Int. Conf. Antwerp, 1982) (BÖCKHOFF, K.H., Ed.), Reidel, Dordrecht (1983) 425.
[19] WINKLER, G., PAVLIK, A., VONACH, H., PAULSEN, A., LISKIEN, H., in Nuclear Data for Science and Technology (Proc. Int. Conf. Antwerp, 1982) (BÖCKHOFF, K.H., Ed.), Reidel, Dordrecht (1983) 400.
[20] PAVLIK, A., WINKLER, G., Evaluation of the ^{58}Ni(n, 2n)^{57}Ni Cross-Sections, IAEA/International Nuclear Data Committee, Vienna, Rep. INDC(AUS)-9/L (1983).
[21] MANNHART, W., in Reactor Dosimetry (Proc. 4th ASTM-EURATOM Symp. Gaithersburg, MD, 1982), Vol. 2, US Nuclear Regulatory Commission, Washington, DC, Rep. NUREG/CP-0029 (1982) 637.
[22] SMITH, D.L., MEADOWS, J.W., Nucl. Sci. Eng. **60** (1976) 187.
[23] SMITH, D.L., MEADOWS, J.W., Argonne National Lab., Argonne, IL, Rep. ANL/NDM-13 (1975).
[24] VASILIU, G., MATEESCU, S., The analysis of the ^{59}Co(n, p)^{59}Fe and ^{54}Fe(n, α)^{51}Cr Cross-Sections for their Use in Reactor Dosimetry, Nuclear Data for Reactor Dosimetry (Proc. Advisory Group Meeting Vienna, 1978), IAEA/International Nuclear Data Committee, Vienna, Rep. INDC/(NDS)-103/M (1979) 26.
[25] GREEN, L., Nucl. Sci. Eng. **58** (1975) 361.
[26] WINKLER, G., SPIEGEL, V., EISENHAUER, C.M., SMITH, D.L., Nucl. Sci. Eng. **78** (1981) 415.
[27] WINKLER, G., SMITH, D.L., MEADOWS, J.W., Nucl. Sci. Eng. **76** (1980) 30.
[28] WINKLER, G., private communication, 1982.
[29] ALBERTS, W.G., HOLLNAGEL, R., KNAUF, K., MATZKE, M., PEßARA, W., in Reactor Dosimetry (Proc. 4th ASTM-EURATOM Symp. Gaithersburg, MD, 1982), Vol. 1, US Nuclear Regulatory Commission, Washington, DC, Rep. NUREG/CP-0029 (1982) 433.
[30] BUCZKO, M., in Californium-252 Utilization (Proc. Int. Symp. Paris, 1976) (BERGER, R.L., CORMAN, W.L., Eds), Vol. 2, Office of Scientific and Technical Information, US Department of Energy, Oak Ridge, TN, Rep. CONF-760436 (1979) IV-19.
[31] MANNHART, W., ALBERTS, W.G., Nucl. Sci. Eng. **69** (1979) 333.
[32] PAUW, H., ATEN, A.H.W., J. Nucl. Energy **25** (1971) 457.
[33] GRUNDL, J.A., GILLIAM, D.M., Fission Cross-Section Measurements in Reactor Physics and Dosimetry Benchmarks, the Cf-252 Fission Neutron Spectrum (Proc. IAEA Consultants Meeting Smolenice, Czechoslovakia, 1983) (LEMMEL, H.D., CULLEN, D.E., Eds), IAEA/International Nuclear Data Committee, Vienna, Rep. INDC(NDS)-146 (1983) 241.

[34] ADAMOV, V.M., et al., in Neutron Standards and Applications (Proc. Int. Symp. Gaithersburg, MD, 1977), US National Bureau of Standards Special Publication 493, US Government Printing Office, Washington, DC (1977) 313.
[35] DAVIS, M.C., KNOLL, G.F., Ann. Nucl. Energy 5 (1978) 583.
[36] GRUNDL, J., GILLIAM, D., McGARRY, E.D., EISENHAUER, C., SORAN, P., "Revised Values for the ^{252}Cf Fission Spectrum-Averaged Cross-Section for the ^{235}U Fission", The Cf-252 Fission Neutron Spectrum (Proc. IAEA Consultants Meeting Smolenice, Czechoslovakia, 1983) (LEMMEL, H.D., CULLEN, D.E., Eds), IAEA/International Nuclear Data Committee, Vienna, Rep. INDC(NDS)-146 (1983) 237.
[37] HEATON, H.T., II, GRUNDL, J.A., SPIEGEL, V., GILLIAM, D.M., EISENHAUER, C., in Nuclear Cross-Sections and Technology (Proc. Int. Conf. Washington, DC, 1975), US National Bureau of Standards Special Publication 425, US Government Printing Office, Washington, DC (1975) 266.
[38] GILLIAM, D.M., EISENHAUER, C., HEATON, H.T., II, GRUNDL, J.A., ibid, p.270.
[39] WAGSCHAL, J.J., MAERKER, R.E., GILLIAM, D.M., in Reactor Dosimetry (Proc. 3rd ASTM-EURATOM Symp. Ispra, Italy, 1979) (RÖTTGER, H., Ed.), Vol. 2, Commission of the European Communities, Brussels, Rep. EUR-6813 (1980) 683.
[40] MANNHART, W., PEREY, F.G., in Reactor Dosimetry (Proc. 3rd ASTM-EURATOM Symp. Ispra, Italy, 1979) (RÖTTGER, H., Ed.), Vol. 2, Commission of the European Communities, Brussels, Rep. EUR-6813 (1980) 1016.
[41] KOBAYASHI, K., KIMURA, I., in Reactor Dosimetry (Proc. 3rd ASTM-EURATOM Symp. Ispra, Italy, 1979) (RÖTTGER, H., Ed.), Vol. 2, Commission of the European Communities, Brussels, Rep. EUR-6813 (1980) 1004.
[42] HEATON, H.T., II, GILLIAM, D.M., SPIEGEL, V., EISENHAUER, C., GRUNDL, J.A., in Fast Neutron Fission Cross-Sections of U-233, U-238, Pu-239 (Proc. NEANDC/NEACRP Specialists' Meeting, Argonne, IL, 1976) (POENITZ, W.P., SMITH, A.B., Eds), Argonne National Labs., IL, Rep. ANL-76-90 (1976) 333.
[43] MÄRTEN, H., SEELIGER, D., STOBINSKI, B., in Nuclear Data for Science and Technology (Proc. Int. Conf. Antwerp, 1982) (BÖCKHOFF, K.H., Ed.), Reidel, Dordrecht (1983) 488.
[44] The Cf-252 Fission Neutron Spectrum, (Proc. IAEA Consultants Meeting, Smolenice, Czechoslovakia, 1983) (LEMMEL, H.D., CULLEN, D.E., Eds), IAEA/International Nuclear Data Committee, Vienna, Rep. INDC(NDC)-146 (1983) 23.
[45] MANNHART, W., Part 1–4, this Handbook.

Part 3
CHARGED PARTICLE ACTIVATION

3-1. CALCULATION OF EXCITATION FUNCTIONS FOR CHARGED PARTICLE INDUCED REACTIONS

R. NOWOTNY, M. UHL
Institut für Radiumforschung
und Kernphysik,
Universität Wien,
Vienna, Austria

Abstract

CALCULATION OF EXCITATION FUNCTIONS FOR CHARGED PARTICLE INDUCED REACTIONS.

Excitation function data are required for various purposes. A means for estimating nuclear excitation functions if experimental data are missing is the calculation of cross-sections with one of the available computer codes. An introduction to the theory behind the reaction mechanism and the various nuclear parameters used is given to aid the potential user in the application of such codes. Various examples are given of excitation functions of reactions used for the production of radioisotopes that are of mainly medical interest. The results indicate that calculated excitation functions, at least for proton induced reactions obtained with a standard set of input parameters, could be used as estimates with adequate accuracy. For projectiles other than protons, the results are less satisfactory.

1. INTRODUCTION

Cross-section data for charged particle induced nuclear reactions are required in a number of fields. While data on excitation functions are often needed for radioisotope production, they are also of interest, for example, in activation techniques or in radiobiology. However, the situation with regard to charged particle cross-section data is less satisfactory when compared with neutron cross-section data. In the latter case, a large quantity of data has been collected covering, at a minimum, an energy range of up to several MeV for almost all stable isotopes. Many comprehensive compilations on neutron data exist and these data are also available from data files.

For charged particle induced reactions, data on a larger number of reaction types are of interest as the energy of the incident particle is usually higher than in the applications considered in reactor physics. Also, charged particle induced reactions have been of less importance in technological applications, with the result that the situation for charged particle reaction data is less advanced. Compilations of integral cross-section data have been published by the Karlsruhe Charged Particle

Group [1] and the National Nuclear Data Center at Brookhaven National Laboratory (BNL) in Upton, New York [2].

Excitation functions which represent variations of cross-sections for particular reactions with incident energy can be used in radioisotope production to

(1) Determine the particle energies required for a particular reaction type.
(2) Calculate the radioisotope production yield which can be expected for a particular reaction and a given target matrix.
(3) Calculate the production yields for radionuclidic impurities, which help to determine the need for isotope-enriched target materials.

For any radioisotope the optimum conditions for production will depend on many factors. A large quantity of data, particularly at higher particle energies, would be required to determine production yields and contaminants of all competing reactions. Only if these data are available can an a priori assessment be made of the advantages and limitations of the various production methods. The situation is even more complex if indirect production regimes are assumed to take advantage of half-life discrimination of contaminants in the decay of the activation products.

Quite often only radioisotope production yield data are available in the literature. While such data are important for production purposes, a better understanding of the relationship between the various factors contributing to product and contaminant yield is obtained from excitation function data. In particular, it is easier to assess the consequences of a variation in irradiation conditions, which for various reasons might be difficult to be made identical at different cyclotrons. Indeed, excitation functions are just the beginning. There remain many more factors that are important in radioisotope production. These include suitably chosen 'targetry' (target composition and material, target construction and transfer of dissipated heat) and radiochemical procedures (remote target handling, chemical processing, radiochemical and radiopharmaceutical quality assurance).

In the event that excitation functions are required, but the experimental data are missing, two possible means are available to obtain estimates. Keller et al. [3] have devised a semi-empirical method by which characteristic excitation function parameters (starting energy, maximum cross-section, the energy position of the maximum cross-section, the cross-section of the tail and width at half-maximum cross-section) are derived from a standard set of data. Another means is the application of one of the computer codes available for the calculation of nuclear cross-sections. These codes were developed mainly to gain theoretical understanding of nuclear reaction processes, but they have also been used for cross-section evaluations, primarily neutron induced reactions.

The accuracy with which excitation functions can be reproduced using computer codes depends on several factors which will be discussed below. The measure for the accuracy of calculated excitation functions is the experimental

data. According to Qaim [4], experimental cross-section errors range in general from about 10 to 15%, increasing for low yield data to about 25%. Errors in particle energy cannot often be found in the literature but, depending on particle and energy errors, could extend to about ± 2 MeV or more. This is of particular importance when the initial rise of an excitation function from various sources is compared.

Certainly the discrepancies found in experimental data from various authors for the same reaction often exceed the quoted error figures, but this reflects the difficulties encountered in the measurement of excitation functions. A global test for the quality of calculated cross-section data can be made by a calculation of radioisotope production yields and by a comparison with data from the literature [3, 5].

In what follows, an introduction to theoretical principles will be given in order to aid the potential user in the application of the codes and in the understanding of their input parameters. Some examples of proton induced reactions will be given and the usefulness of calculations for other projectiles will also be discussed.

2. MODELS AND PARAMETERS

This section presents a short outline of the reaction models most important for the calculation of the cross-section for the production of radioisotopes (activation product cross-sections). All of the following considerations refer to incident energies between a few MeV and several tens of MeV. For most reactions employed in the production of radioisotopes, fission competition is not important. Therefore, the treatment of fission will not be described.

2.1. Reaction mechanisms and their importance for activation product cross-sections

In general, one can distinguish between two extreme reaction mechanisms: *direct reactions* (DIR) which involve only a few degrees of freedom of the many nucleon systems under consideration and *compound nucleus reactions* (CNR), which are characterized by the participation of many active degrees of freedom. Cross-sections for DIR are calculated by solving explicitly the scattering problem for a (simplified) dynamic model. The theoretical treatment of CNR, on the other hand, is based essentially on statistical assumptions. In addition to these two extreme mechanisms, there are also *pre-equilibrium reactions (PER)* or *precompound reactions* which, in terms of complexity, are situated between DIR and CNR. For a given reaction all three mechanisms contribute to the extent possible, depending on the type of reaction (projectile and ejectile), the incident energy and the excitation energy of the residual nucleus.

At incident energies beyond a few MeV, the activation products result essentially from gamma ray de-excitation of a large number of highly excited states. The cross-sections for the formation of those levels by reactions with one or several emitted particles can often be calculated quite reliably by a combination of models for PER and CNR.

Direct reactions occur mainly as binary processes. They preferentially populate 'simple' low lying levels of the residual nucleus [6] (e.g. collective states in the case of inelastic scattering and states of predominantly single particle character in one nucleon transfer reaction, such as (d, p) or (p, d). In many applications the neglect of DIR is justified as the resulting errors are of the same order as the inherent uncertainties of the PER and CNR models. However, special care is required in cases of unusually large DIR contributions as, for example, reactions on very light or on permanently deformed target nuclei and reactions induced by weakly bound projectiles, such as deuterons or ^{3}He particles.

It is difficult to give a general assessment of the errors resulting from the neglect of DIR as the effect critically depends on the case under consideration and on the parameters used for PER. For a careful calculation of an unknown cross-section, it is important to investigate how well the employed models reproduce reliable experimental data for neighbouring target nuclei.

In spite of these restrictions, the discussion in this paper concentrates on the application of models for CNR and PER mechanisms as these lend themselves easier to routine applications. The angular distribution of the reaction products is irrelevant for activation product cross-sections and thus will not be discussed.

2.2. The compound nucleus evaporation model

This model is based on Bohr's concept of the compound nucleus [7] as an intermediary stage of a nuclear reaction. The compound nucleus (CN) is assumed to be in thermal equilibrium. Hence, apart from restrictions due to conserved observables, its formation and decay are independent of each other. Further, the decay of the CN is governed only by phase space and barrier penetrabilities. The cross-section formulas resulting from this concept depend on the conservation laws which are taken into account.

The initial and final states of a binary nuclear reaction A(a, b)B (i.e. the channels) are characterized by indices α, β,..., which specify the fragmentation of the many-nucleon system into light and heavy subsystems (a, A), (b, B),... and by the intrinsic states of the fragments. Their excitation energies, spins and parities for a given fragmentation γ are denoted, respectively, by (e_γ, E_γ), (i_γ, I_γ) and (π_γ, Π_γ). For reactions of interest in the present context, one assumes that the light fragments and the target are in their ground states: that is, $E_\alpha = 0$ and $e_\gamma = 0$, where α denotes the entrance channel and γ an arbitrary exit channel.

Conservation of energy, angular momentum and parity require the following relations to hold for entrance channel α and exit channel β:

$$\epsilon_\alpha + S_\alpha = E = \epsilon_\beta + E_\beta + S_\beta \tag{1a}$$

$$\vec{i}_\alpha + \vec{I}_\alpha + \vec{\ell}_\alpha = \vec{I} = \vec{i}_\beta + \vec{I}_\beta + \vec{\ell}_\beta \tag{1b}$$

$$\pi_\alpha \Pi_\alpha (-)^{\ell_\alpha} = \Pi = \pi_\beta \Pi_\beta (-)^{\ell_\beta} \tag{1c}$$

Here E, I and Π denote the excitation energy, spin and parity of the CN, respectively, while S_α, S_β,... are the separation energies and ϵ_α, ϵ_β, ... and ℓ_α, ℓ_β, ... represent the kinetic energy and the orbital angular momentum of the relative motion of the fragments, respectively.

The simplest expression for the cross-section

$$\frac{\partial \sigma_{\alpha\beta}}{\partial \epsilon_\beta}(\epsilon_\alpha, \epsilon_\beta)$$

which, for a binary reaction, results from the CN concept, accounts only for energy conservation (Eq. (1a)) and was proposed by Weisskopf and Ewing [8]:

$$\frac{\partial \sigma_{\alpha\beta}}{\partial \epsilon_\beta}(\epsilon_\alpha, \epsilon_\beta) = \sigma_\alpha(\epsilon_\alpha)\left(\frac{\Gamma_\beta(E, \epsilon_\beta)}{\Gamma(E)}\right)\omega_\beta(E_\beta) \tag{2}$$

The first factor $\sigma_\alpha(\epsilon_\alpha)$ represents the cross-section for the formation of the CN via the entrance channel and the second one represents the branching ratio for its decay into the channel with kinetic energy around ϵ_β. The density of excited states of the residual nucleus around the excitation energy

$$E_\beta = \epsilon_\alpha + S_\alpha - S_\beta - \epsilon_\beta$$

is denoted by $\omega_\beta(E_\beta)$. Under the assumption of time reversal invariance, the branching ratio can be evaluated in terms of the cross-sections $\sigma_\gamma(\epsilon_\gamma)$ for the formation of the CN in all open channels (the 'inverse cross-sections') [8]:

$$\frac{\Gamma_\beta(E, E_\beta)}{\Gamma(E)} = \frac{(2i_\beta + 1)\, k_\beta^2 \sigma_\beta(\epsilon_\beta)}{\sum_\gamma (2i_\gamma + 1) \int_0^{E-S_\gamma} d\epsilon_\gamma\, k_\gamma^2\, \sigma_\gamma(\epsilon_\gamma)\omega_\gamma(E_\gamma)} \tag{3}$$

where k_β represents the wavenumber corresponding to the channel energy ϵ_β. The sum and integration in the denominator comprise all open channels. The auxiliary quantities $\sigma_\gamma(\epsilon_\gamma)$ and $\omega_\gamma(E_\gamma)$, which enter in Eqs (2) and (3), are

discussed further in Sec. 2.4. The resulting particle spectra have a shape characteristic of an 'evaporation spectrum' as a consequence of the assumption of the CN being in thermal equilibrium.

For the calculation of activation product cross-sections, one assumes that beyond the particle emission thresholds gamma decay is negligible compared with particle emission. Therefore, the activation product cross-section $\sigma^{act}_{\alpha\beta}(\epsilon_\alpha)$ is given by the sum of the populations of the states of the residual nucleus with excitation energies up to the minimum particle emission threshold S_{min}

$$\sigma^{act}_{\alpha\beta}(\epsilon_\alpha) = \sigma_\alpha(\epsilon_\alpha) \int_0^{S_{min}} dE_\beta \frac{\Gamma_\beta(E, \epsilon_\beta)}{\Gamma(E)} \omega_\beta(E_\beta) \tag{4}$$

as only those states will ultimately populate the ground state by gamma ray cascades. The population of states with $E_\beta > S_{min}$ gives rise to multiple particle emission.

The Weisskopf–Ewing (WE) approach can easily be extended to reactions with multiple particle emission by assuming that the particles are emitted sequentially and that each of the intermediary nuclei can be treated as a 'compound nucleus', the decay of which is governed by the branching ratio given in Eq. (3). Thus the activation product cross-section for a ternary reaction A(a, bc)C is given by

$$\sigma^{act}_{\alpha\beta\gamma}(\epsilon_\alpha) = \sigma_\alpha(\epsilon_\alpha) \int_{S_\gamma}^{E_1 - S_\beta} dE_2 \frac{\Gamma_\beta(E_1, \epsilon_\beta)}{\Gamma(E_1)} \omega_\beta(E_2) \int_0^{S_{min}} dE_\gamma \frac{\Gamma_\gamma(E_2, \epsilon_\gamma)}{\Gamma(E_2)} \omega_\gamma(E_\gamma) \tag{5}$$

where E_1 and S_β refer to the first and E_2 and S_γ to the second CN. S_{min} and $\omega_\gamma(E_\gamma)$ represent the minimum particle emission threshold and the state density of the final reaction product, respectively. Obviously, Eq. (5) can be generalized to the evaporation of an arbitrary number of particles.

The WE formalism offers a fast and simple method to estimate the contribution of CNR to activation product cross-sections. Calculations based on it will be referred to as 'WE calculations'.

A refined version of the CN evaporation model also considers the conservation of angular momentum and parity. The results are generalizations of the well-known Hauser–Feshbach formula [9]. The ansatz (2) for the cross-section is replaced by

$$\frac{\partial \sigma_{\alpha\beta}}{\partial \epsilon_\beta}(\epsilon_\alpha, I_\alpha, \Pi_\alpha; \epsilon_\beta, I_\beta, \Pi_\beta) = \sum_{I\Pi} \sigma_\alpha(\epsilon_\alpha, I_\alpha, \Pi_\alpha; I\Pi) \frac{\Gamma(E, I, \Pi; \epsilon_\beta, I_\beta, \Pi_\beta)}{\Gamma(E, I, \Pi)} \rho_\beta(E_\beta, I_\beta, \Pi_\beta) \tag{6}$$

where the sum is over all angular momenta and parities (I, II) of the CN. The quantities $\sigma_\alpha(\epsilon_\alpha, I_\alpha, \Pi_\alpha; I\Pi)$ and $\rho_\beta(E_\beta, I_\beta, \Pi_\beta)$ represent, respectively, the cross-sections for the formation of the CN in states of given quantum numbers (I, Π) and the density of levels around E_β with quantum numbers (I_β, Π_β) of the final nucleus. While for a higher excitation energy the level density is obtained from statistical considerations, the experimental information on the actual level scheme is used near the ground state instead of a level density formula. The generalization of Eq. (3) for the branching ratio reads

$$\frac{\Gamma(E, I, \Pi; E_\beta, I_\beta, \Pi_\beta)}{\Gamma(E, I, \Pi)} = \frac{(2i_\beta + 1)(2I_\beta + 1)k_\beta^2 \sigma_\beta(\epsilon_\beta, I_\beta, \Pi_\beta; I, \Pi)}{\sum_\gamma \sum_{I_\gamma \Pi_\gamma} (2i_\gamma + 1)(2I_\gamma + 1) \int_0^{E-S_\gamma} dE_\gamma k_\gamma^2 \sigma_\gamma(\epsilon_\gamma, I_\gamma, \Pi_\gamma; I, \Pi)\rho_\gamma(E_\gamma, I_\gamma, \Pi_\gamma)} \tag{7}$$

In the 'channel spin coupling scheme', the quantities $\sigma_\gamma(\epsilon_\gamma, I_\gamma, \Pi_\gamma; I, \Pi)$ are related to the optical-model transmission coefficients $T_{\ell_\gamma}(\epsilon_\gamma)$ by

$$\sigma(\epsilon_\gamma, I_\gamma, \Pi_\gamma; I, \Pi) = \frac{\pi}{k_\gamma^2} \frac{2I + 1}{(2i_\gamma + 1)(2I_\gamma + 1)} \sum_{s_\gamma = |I_\gamma - i_\gamma|}^{I_\gamma + i_\gamma} \sum_{\ell_\gamma = |I - s_\gamma|}^{I_\gamma + s_\gamma} \delta_{\Pi, (-)^{\ell_\gamma} \pi_\gamma \Pi_\gamma} T_{\ell_\gamma}(\epsilon_\gamma) \tag{8}$$

The limits of the sums over the channel spin $\vec{s}_\gamma = \vec{I}_\gamma + \vec{i}_\gamma$ and over $\vec{\ell}_\gamma$ account for the angular momentum conservation (Eq. (1b)), while the Kronecker delta guarantees parity conservation (Eq. (1c)). For the alternative j-coupling scheme, see, e.g., the review by Vogt [10]. In terms of $\sigma_\gamma(\epsilon_\gamma I_\gamma \Pi_\gamma, I\Pi)$ and $\rho(E_\gamma, I_\gamma, \Pi_\gamma)$, the corresponding quantities of the Weisskopf–Ewing approach are given by

$$\sigma_\gamma(\epsilon_\gamma) = \sum_{I_\gamma \Pi_\gamma} \sigma_\gamma(\epsilon_\gamma, I_\gamma, \Pi_\gamma; I\Pi) = \frac{\pi}{k_\gamma^2} \sum_{\ell=0}^{\infty} (2\ell_\gamma + 1) T_{\ell_\gamma}(\epsilon_\gamma),$$

$$\omega_\gamma(E_\gamma) = \sum_{I_\gamma \Pi_\gamma} (2I_\gamma + 1)\rho(E_\gamma, I_\gamma, \Pi_\gamma)$$

From the general theory of CNR (see, e.g., Refs [11, 12]), it is known that Eq. (6) together with Eqs (7) and (8) hold only for non-elastic processes in the limiting case of many open channels. In particular, they do not consider the width fluctuation correction and compound elastic enhancement. In connection with activation product cross-sections at energies beyond a few MeV, both effects are of little importance.

The calculation of the cross-sections for the production of the residual nuclei requires a suitable generalization of Eq. (4) for binary reactions and Eq. (5) for processes with multiple particle emission. The theory can be improved substantially by explicitly including gamma ray cascades. Photons are treated in the same way as particles with transmission coefficients, depending on the type (E1, M1, E2, ...) of electromagnetic multipole radiation. Details regarding the combination of gamma ray cascades and multiple particle emission can be found, e.g., in Ref. [13]. As a consequence of this model extension, the gamma ray competition with particle decay (an effect which critically depends on the spins of the levels involved [14, 15]) can be treated properly. Furthermore, the inclusion of gamma ray cascades is required for the calculation of the production of isomeric levels.

Calculations based on the CN model with angular momentum and parity conservation will be referred to as the Hauser-Feshbach (HF) calculations. Owing to the various angular momentum sums, computer codes which perform HF calculations require more time and storage than those designed for WE calculations. On the other hand, the competition between the various decay modes of the CN depends on the angular momentum. This effect, which is especially pronounced near the maximum spin allowed for a given excitation energy (the 'yrast spin'), cannot be reproduced by a WE calculation. The choice between the expensive HF approach and the fast, but less precise, WE approach depends on the type of cross-section to be calculated and on the required accuracy. For isomeric state production cross-sections, a HF calculation is indispensable.

Some of the deficiencies of WE calculations can be removed by the "s-wave approximation" proposed by Blann and Merkel [16]. It is assumed that the spin distribution of the residual nuclei is the same as that of the (first) CN: this would be true if all particles were emitted in s states of relative motion. As a consequence of this assumption, HF calculations may be replaced by WE calculations for each value I of the spin of the CN. An upper limit for the gamma ray competition is obtained by assuming that for a given angular momentum I, all states with excitation energy

$$E \leqslant S_{min} + E_{min}(I)$$

decay by gamma ray cascades; here S_{min} is the minimum particle separation energy and $E_{min}(I)$ denotes the yrast level, i.e. the minimum excitation energy required for angular momentum I.

Isospin, besides angular momentum, also plays an important role in CNR. The main effect of isospin conservation is to enhance inelastic scattering of projectiles with a proton excess as, for example, protons or ^{3}He particles. Approaches that included isospin in the consideration of isospin mixing were proposed by several authors and were compared by Lane [17].

2.3. Models for pre-equilibrium emission

With increasing bombarding energy the properties of the emitted particles significantly deviate from the predictions of the CN evaporation model. Instead of a pure evaporation spectrum and symmetry around 90°, one observes an excess of high energy particles which are emitted, preferentially, in a forward direction. These effects are interpreted as being due to emission before the composite system (which initially is formed in simple states and equilibrates through intranuclear transitions) has reached the thermal equilibrium characteristic for the CN.

By considering pre-equilibrium (PE) emission, the cross-section $\partial\sigma_{\alpha\beta}/\partial\epsilon_\beta$ consists of two contributions:

$$\frac{\partial\sigma_{\alpha\beta}}{\partial\epsilon_\beta}(\epsilon_\alpha, \epsilon_\beta) = \frac{\partial\sigma^{\mathrm{pre}}_{\alpha\beta}}{\partial\epsilon_\beta}(\epsilon_\alpha, \epsilon_\beta) + q^{\mathrm{pre}}\frac{\partial\sigma^{\mathrm{eq}}_{\alpha\beta}}{\partial\epsilon_\beta}(\epsilon_\alpha, \epsilon_\beta) \tag{9}$$

representing the decay of the composite system before and after equilibration. The equilibrium contribution $\partial\sigma^{\mathrm{eq}}_{\alpha\beta}/\partial\epsilon_\beta$ can be calculated in the frame of the CN evaporation model described in Sec. 2.2. The factor q^{pre} represents the fraction of the incident flux which survives PE emission. Many cross-section calculations consider PE emission only for the first emitted particles and treat multiple particle emission as CN evaporation. According to Blann and Vonach, this procedure seems justified for incident energies up to about 50 MeV [18].

The enhanced high energy portion of the spectra of particles emitted in the PE stage is also of crucial importance for activation product cross-sections. Therefore, pre-equilibrium reactions have to be considered for incident energies larger than about 8 MeV.

Although several fundamental theories of PER were proposed over the years (see Refs [19–21]), only the two most popular phenomenological PE models – the exciton and the hybrid models – which are especially convenient for routine calculations, are discussed here. These models are conceptually different, though when suitably parametrized both successfully reproduce experimental data.

2.3.1. The exciton model

In this model, which was suggested by Griffin [22, 23], the states of the composite system are characterized only by the excitation energy and the number

of excited particles p and excited holes h. Particles and holes are defined with respect to a closed shell reference state and are collectively called excitons. The exciton number n is given by $n = p + h$. Starting from a simple particle-hole configuration, $n_0 = p_0 + h_0$, which depends on the projectile (see Sec. 2.4.3), the system equilibrates through a series of two-body interactions and emits particles from all intermediate stages. Two-body interactions may change the exciton number by amounts of $\Delta n = 2, 0, -2$, corresponding to the creation, scattering and annihilation of a particle-hole pair. The rates for these internal transitions averaged over all states of an $n = p + h$ exciton configuration are denoted by $\Lambda^i_+(n, E)$, $\Lambda^i_0(n, E)$ and $\Lambda^i_-(n, E)$.

The simplest expression which results from this concept for the PE contribution $(\partial\sigma^{pre}_{\alpha\beta}/\partial\epsilon_\beta)(\epsilon_\alpha, \epsilon_\beta)$ of the cross-section reads

$$\frac{\partial\sigma^{pre}_{\alpha\beta}}{\partial\epsilon_\beta}(\epsilon_\alpha, \epsilon_\beta) = \sigma_\alpha(\epsilon_\alpha) \sum_{\substack{n=n_0 \\ (\Delta n=2)}}^{\bar{n}} D_n(E) \frac{\Lambda^c_\beta(\epsilon_\beta;\ n, E)}{\Lambda^c(n, E) + \Lambda^i_+(n, E)} \tag{10}$$

where $\Lambda^c_\beta(\epsilon_\beta;\ n, E)$ represents, for states with n excitons, the average rate of decay into fragmentation β with channel energy ϵ_β, and $\Lambda^c(n, E)$ the total decay rate into the continuum, i.e. the sum of $\Lambda^c_\beta(\epsilon_\beta;\ n, E)$ over all open channels. The sum over the exciton number n extends up to the most probable value $\bar{n}$ at equilibrium which, in terms of the single particle state density g, is approximately given by $\bar{n} = \sqrt{2gE}$. The quantity $D_n(E)$ represents the fraction of the initial population of the composite system which has survived emission in the previous configurations $n_0, n_0 + 2, \ldots, n-2$. For $n > n_0$, this 'depletion factor' is given by

$$D_n(E) = \prod_{\nu = n_0(\Delta\nu = 2)}^{n-2} \frac{\Lambda^i_+(\nu, E)}{\Lambda^c(\nu, E) + \Lambda^i_+(\nu, E)} \tag{11}$$

while, per definition, $D_{n_0}(E) = 1$. The factor q^{pre} in Eq. (9) is given by $q^{pre} = D_{\bar{n}+2}(E)$.

Equations (10) and (11) essentially rely on the assumption $\Lambda^i_+(n, E) \gg \Lambda^i_-(n, E)$, which holds for small exciton numbers n, as can be seen from phase space arguments; the main contributions to the PE spectrum stem from small values of n. In general the equilibration process is described by a version of the Pauli master equation which can be represented as a system of first-order differential equations in time [24] or as stochastic equations of a random walk problem [25, 26]. The master equation approach also allows a 'unified' treatment of PE emission and equilibrium decay [26]. Nevertheless, considering the phenomenological nature

of the model itself, Eqs (10) and (11) represent reasonable approximations to the solution of the master equations.

The cross-sections defined in Eqs (10) and (11) first require rates for internal transitions. A widely used method to calculate these quantities relies on Fermi's golden rule:

$$\Lambda^{i}_{\Delta n}(n, E) = \frac{2\pi}{\hbar} |M|^2 \omega_{\Delta n}(n, E) \tag{12}$$

where $|M|^2$ is the averaged squared matrix element of residual interactions (see Sec. 2.4.3) and $\omega_{\Delta n}(n, E)$ is the number of accessible final states. As an example of the many evaluations of $\omega_{\Delta n}(n, E)$, we quote the often-used results of Williams [27]

$$\omega_{+}(n, E) = (1/2)g^3E^2/(n + 1)$$

with the correction factor (1/2) of Obložinský et al. [28]. In a different approach, Gadioli et al. determined the dependence of $\Lambda^{i}(n, E)$ on n and E on the basis of the nucleon-nucleon cross-section in nuclear matter and adjusted the absolute magnitude by comparison with experimental data [29]. The results are independent of the mass number and are tabulated in Ref. [30].

Particle emission rates are in general obtained by applying the principle of detailed balance. For fragmentation β, i.e. the emission of particle b with π_b protons and ν_b neutrons, one obtains

$$\Lambda^{c}(\epsilon_\beta;\ p, h, E) = (2i_\beta + 1)R_\beta(p_\beta)\frac{\mu_\beta \epsilon_\beta}{\pi^2\hbar^3}\sigma_\beta(\epsilon_\beta)\frac{\omega(p-p_\beta, h_\beta, E_\beta)}{\omega(p, h, E)} \tag{13}$$

where μ_b denotes the reduced mass and $p_\beta = \pi_b + \nu_b$ is the number of nucleons of the light fragment. The quantities $\omega(p, h, E)$ and $\omega(p-p_\beta, h, E_\beta)$ represent state densities with a specified number of particles and holes and refer to the composite system and the residual nucleus, respectively. The factor $R_\beta(p_\beta)$ stands for the probability that p_β-emitted nucleons have the right combination of protons and neutrons and thus account in an approximate way for proton-neutron distinguishability. Simple expressions for the quantity $R_\beta(p_\beta)$, which depends on the projectile, were derived by Cline [31] and Kalbach [32] and by Birratari et al. [33]. A more accurate treatment of neutron-proton distinguishability is offered by a two-component formulation of the exciton model as proposed, for example, by Dobeš and Běták [34]. The emission rates, Eq. (13), when used in Eq. (10), satisfactorily reproduce the spectra of nucleons, but significantly underpredict the emission of composite particles. For the rates to be used for alpha particles a review by Gadioli and Gadioli-Erba [35] is consulted instead of Eq. (13). An alternative method to deal with cluster emission

was developed by Kalbach [32]. In addition to a PE component based on detailed balance (Eq. (13)), direct reaction contributions, which are calculated in a very simple statistical way, are taken into account. Recently, Iwamoto and Harada [36] proposed a promising new approach to cluster emission in the frame of the exciton model.

The exciton model described so far does not consider angular momentum and parity. So, if its results are combined in Eq. (9) with those of an HF calculation, one often assumes that PE decay produces for the residual nucleus the same spin and parity distribution as the CN evaporation model. In order to improve this crude approximation some authors, such as Plyoko [37], Fu [38, 39] and Gruppelaar [40], proposed exciton models which account for angular momentum.

The impact of this improvement is certainly greatest for the production cross-section of isomers. For the total production cross-sections considered in Sec. 4, the errors introduced by neglecting angular momentum and parity will not in general exceed 30%.

2.3.2. The hybrid model

The hybrid model was proposed by Blann in 1971 [41–43]. It combines aspects of the simple exciton model and the Harp-Miller-Beine (HME) model [44, 45], which performs a very detailed, and thus relatively complicated, treatment of the equilibration process. The resulting expressions are simple and were the first to predict absolute cross-sections on an a priori basis [46].

The hybrid model is concerned only with the emission of nucleons. The cross-section $(\partial\sigma_{\alpha\beta}/\partial\epsilon_\beta)(\epsilon_\alpha, \epsilon_\beta)$ for emitting a nucleon is given by

$$\frac{\partial\sigma_{\alpha\beta}^{\text{pre}}}{\partial\epsilon_\beta} = \sigma_\alpha(\epsilon_\alpha) \sum_{\substack{n=n_0 \\ (\Delta n=2)}} P_\beta(\epsilon_\beta, n) \tag{14a}$$

$$P_\beta(\epsilon_\beta, n) = Z_\beta(\epsilon_\beta + S_\beta, p, h) \frac{\lambda^c(\epsilon_\beta)}{\lambda^c(\epsilon_\beta) + \lambda^i_+(\epsilon_\beta)} D_n(E) \tag{14b}$$

where $Z_\beta(\epsilon_\beta + S_\beta, p, h)$ represents, for an n-exciton configuration of the composite system, the average number of nucleons of the type corresponding to β at excitation energy $E = \epsilon_\beta + S_\beta$ so that if such a nucleon is emitted into the continuum a channel energy of ϵ_β results. The quantities $\lambda^c(\epsilon_\beta)$ and $\lambda^i_+(\epsilon_\beta)$ are, respectively, the rates at which such a nucleon is emitted into the continuum or causes an intranuclear transition, with the creation of an additional particle–hole pair. $D_n(E)$ denotes the 'depletion factor' defined in Eq. (11).

Blann et al. [47] and Blann and Vonach [18] showed that owing to the properties of the nucleon-nucleon cross-section, the quantity $Z_\beta(\epsilon_\beta + S_\beta, p, h)$ can be

calculated in terms of the particle–hole state densities $\omega(p, h, E)$ and the single particle state density $g(\epsilon_\beta + S_\beta)$:

$$Z_\beta(\epsilon_\beta + S_\beta, ph) = \frac{X_\beta(n)}{p} \quad \frac{\omega(p-1, h, E-\epsilon_\beta - S_\beta)}{\omega(p, h, E)}\, g(\epsilon_\beta + S_\beta) \tag{15}$$

where $X_\beta(n)$ represents the number of particles of the type corresponding to β. The quantity $X_\beta(n)$ thus accounts for neutron-proton distinguishability. The initial values $X_\pi(n_0)$ and $X_\nu(n_0)$ for protons and neutrons which depend on the projectile (see Sec. 2.4.3) are increased by 0.5 following each intranuclear transition.

The continuum decay rate $\lambda^c(\epsilon_\beta)$ is related to the inverse cross-section $\sigma_\beta(\epsilon_\beta)$ and the single particle state density $g(\epsilon_\beta + S_\beta)$ by

$$\lambda^c(\epsilon_\beta) = (2i_\beta + 1)\frac{\mu_\beta \epsilon_\beta}{\pi^2 \hbar^3}\, \sigma_\beta(\epsilon_\beta)\, \frac{1}{g(\epsilon_\beta + S_\beta)}$$

The intranuclear transition rates were at first calculated in terms of the average nucleon-nucleon cross-section in nuclear matter $\langle\sigma\rangle$:

$$\lambda^i_+(\epsilon_\beta) = v_\beta \rho \langle\sigma\rangle$$

where ρ is the nuclear density and v_β the velocity of the nucleon under consideration. In later developments [46], the rates were also related to the imaginary part W of the optical potential by $\lambda^i_+(\epsilon) = 2W/\hbar$. Because of their radial dependence $\rho(r)$ and $W(r)$ are averaged over the volume of the nucleus.

An extension of the hybrid model considers explicitly the effects of the nuclear surface region [48]. In this *geometry dependent hybrid model*, the density ρ and the imaginary part W are not averaged over the entire nucleus but over the particle trajectories in the entrance channel. The latter are defined by the impact parameter $R_\ell = \lambda\!\!\!^{-}(\ell + 1/2)$, where $\lambda\!\!\!^{-}$ is the reduced de Broglie wavelength and ℓ the orbital angular momentum. The geometry dependent generalization of Eq. (14a) reads

$$\frac{\partial \sigma^{pre}_{\alpha\beta}}{\partial \epsilon_\beta}(\epsilon_\alpha, \epsilon_\beta) = \frac{\pi}{k_\alpha^2} \sum_{\ell=0}^{\infty} (2\ell_\alpha + 1) T_{\ell_\alpha}(\epsilon_\alpha) \sum_{\substack{n=n_0 \\ (\Delta n = 2)}}^{\bar{n}} P_\beta(\epsilon_\beta, \ell, n) \tag{16}$$

where $T_{\ell_\alpha}(\epsilon_\alpha)$ is the transmission coefficient. The averages of ρ and W for the individual contributions $P_\beta(\epsilon_\beta, n, \ell)$, which are defined as in Eq. (14b), are

calculated in a local density approximation [46]. The two main effects of the surface region are the reduction of the intranuclear transition rates $\lambda^{i}_{+}(\epsilon_\beta)$ due to the smaller density or the smaller imaginary part of the optical potential and the limitation of the hole depth due to the reduced Fermi energy. Both effects lead to harder particle emission spectra and thus improve the reproduction of nucleon induced inelastic scattering and charge exchange reactions.

As the nuclear mean free path is of the order of the nuclear radius, only the first collision can be regarded as being localized. Therefore, Eq. (16) is often used only for the initial configuration and the contributions to $n > n_0$ are calculated by means of the geometry independent Eq. (14a). Recently, simple expressions for a special type of multiple PE emission were proposed [18]. This effect is expected to become important for incident energies beyond 50 MeV.

2.4. Auxiliary quantities and model parameters

The models described in the two previous sections require several auxiliary quantities. These depend on parameters which for the time being have to be determined by comparison with appropriate experimental data.

2.4.1. Transmission coefficients

The transmission coefficients for particles are calculated in the frame of the optical model. In the simplest case, the single channel optical model, they result from solving the scattering problem for a particle in a local complex potential $U(r) = V(r) + i \cdot W(r)$, which depends on the fragmentation. For a given channel energy ϵ and each pair of the quantum numbers (ℓ_j), where ℓ is the orbital and j the total angular momentum ($\vec{j} = \vec{\ell} + \vec{i}$), one has to solve the following equation for the radial wave function $u_{\ell j}(r)$:

$$\left[-\frac{\hbar^2}{2\mu}\left(\frac{d^2}{dr^2} - \frac{\ell(\ell+1)}{r^2}\right) + V(r) + iW(r) - \epsilon\right] u_{\ell j}(r) = 0 \qquad (17)$$

The transmission coefficient $T_{\ell j}(\epsilon)$ is given in terms of the phase shift $\delta_{\ell j}(\epsilon)$, by which the asymptotic form of the regular solution of Eq. (17) differs from the pure Coulomb scattering wave

$$T_{\ell j}(\epsilon) = 1 - |\exp[2i\delta_{\ell j}(\epsilon)]|^2$$

Though there currently exist microscopic theories which relate the optical potential to the fundamental nucleon-nucleon interaction (see reviews by Mahaux [49] and Hodgson [50]), actual calculations of transmission coefficients employ phenomenological potentials of the following form:

$$V(r) = -V_c f(r, R_c, a_c) + V_{so} \frac{1}{r} \frac{d}{dr} f(r, R_{so}, a_{so}) \ (\vec{\ell} \cdot \vec{i}) + V_{Coulomb}(r)$$

$$W(r) = 4a_s W_s \frac{d}{dr} f(r, R_s, a_s) - W_v f(r, R_v, a_v) \tag{18}$$

$$f(r, R_i, a_i) = \{1 + \exp[(r - R_i)/a_i]\}^{-1}$$

The real part consists of a central potential of Woods–Saxon form with strength V_c and a spin orbit potential of Thomas form with strength V_{so}, while the imaginary part contains a surface peaked and a volume component with respective strengths of W_s and W_v. The Coulomb potential $V_{Coulomb}(r)$ is assumed to result from a uniformly charged sphere.

The various parameters of a phenomenological potential, i.e. the strengths V_c, V_{so}, ..., W_v and the geometrical quantities R_c, a_c, ..., R_v, a_v, are found by comparison with appropriate experimental data as cross-sections for elastic scattering and absorption and polarizations. This procedure is described, e.g., by Hodgson [51].

The spin-orbit potential causes the transmission coefficients for particles with intrinsic spin i to depend on ℓ and j. If they are used in connection with the channel coupling scheme described in Sec. 2.2, one has to average $T_{\ell j}$ with respect to j:

$$T_\ell = \frac{(2\ell + 2i + 1)T_{\ell,\ell+i} + (2\ell + 2i - 1)T_{\ell,\ell+i-1)} + \ldots (2|\ell - i| + 1)T_{\ell,|\ell-i|}}{(2\ell + 1)(2i + 1)}$$

Particularly important for cross-section calculations are 'global optical potentials', which simultaneously reproduce the relevant data over a wide mass and energy region. In general the strengths V_c, W_s and W_v of such potentials depend on the incident energy and the nuclear symmetry parameter (N–Z)/A. Information on commonly used global potentials for nucleons, alpha particles, tritons and ^{3}He particles can be found in Ref. [51] and in a review article by Perey and Perey [52]. In addition, the global potentials for alpha particles are given by Huizenga and Igo [53] and by McFadden and Satchler [54], while for neutrons the potentials given by Rapaport et al. [55] are used.

In general, global optical potentials, when applied for a particular nucleus, will not give as accurate results as a 'local potential' with parameters obtained from data measured for the nucleus of interest or at least for near neighbours. This is particularly true if the energy and/or mass region of the database, on which the global potential relies, is exceeded.

The transmission coefficients $T_{XL}(\epsilon)$ for photons of multipole type XL are related to the corresponding gamma ray strength function $f_{XL}(\epsilon)$ by

$$T_{XL}(\epsilon) = 2\pi \cdot \epsilon^{2L+1} f_{XL}(\epsilon)$$

Two models for the strength functions are generally used. The Blatt–Weisskopf model [56] assumes the strength functions to be energy independent, while the Brink–Axel model [57] relates them to the gamma ray absorption cross-section. The relevant experimental data for the adjustment of the strength function parameters are in general neutron resonance data and low energy neutron capture data. For details, see a recent review by Gardner [58].

2.4.2. Level densities

Most computer codes employ rather simple models which define the level density in terms of a few parameters. The two most popular models are the Gilbert–Cameron model [59] and the backshifted Fermi gas model [60]. Both of them assume the level density to be parity independent: $\rho(E, I, \Pi) = (1/2)\rho(E, I)$, and describe the dependence on the spin I in terms of an energy dependent 'spin cut-off parameter' $\sigma = \sigma(E)$:

$$\rho(E, I) = \frac{1}{2\sigma^2}(2I + 1)\exp\left(-\frac{(I + 1/2)^2}{2\sigma^2}\right)\rho_0(E) \tag{19}$$

where $\rho_0(E)$ is the total level density as a function of the excitation energy E. The state density $\omega(E)$ is related to the total level density by $\omega(E) = \sqrt{2\pi\sigma^2}\,\rho_0(E)$.

The Gilbert–Cameron model distinguishes two energy regions. For $E \geqslant E_x$, $\rho_0(E)$ and $\sigma(E)$ are given by

$$\left.\begin{aligned} \rho_0(E) &= \frac{1}{12\sqrt{2\sigma}}\,\frac{\exp[2\sqrt{a(E-P)}]}{a^{1/4}(E-P)^{5/4}} \\ \sigma^2(E) &= C\sqrt{a(E-P)}\,A^{2/3} \end{aligned}\right\} \quad E \geqslant E_x \tag{20a}$$

where a is the 'level density parameter' and P the (tabulated) pairing correction. The original paper [59] proposed that $C = 0.0888$, while more recent investigations favour $C = 0.146$ [61]. In the low energy region $E \leqslant E_x$, the total level density and σ^2 are given by

$$\left.\begin{aligned} \rho_0(E) &= \frac{1}{T}\exp[(E-E_0)/T] \\ \sigma^2(E) &= \sigma^2(E_x) \end{aligned}\right\} \quad E \leqslant E_x \tag{20b}$$

where T is the (nuclear) temperature and E_0 is an adjustable constant. The a parameter of Eq. (20a) is found by reproducing the average resonance spacing, while the quantities E_0, T and E_x are determined by the requirement that $\rho_0(E)$,

defined in Eq. (20b), reproduces the cumulative number of low lying levels and smoothly joins the corresponding expression in Eq. (20a) at $E = E_x$.

The backshifted Fermi gas model employs only one formula for all excitation energies:

$$\rho_0(E) = \frac{1}{12\sqrt{2\sigma}} \frac{\exp[2\sqrt{a(E-\Delta)}]}{(E-\Delta+t)^{5/4}}$$
$$\sigma^2(E) = dtA^{5/3}, \quad E-\Delta = at^2-t \tag{21}$$

where Δ represents the 'backshift' and t the (thermodynamic) temperature. For the constant d in the definition of σ, it is usually assumed that $d = 0.0150$, a value which corresponds to the rigid body moment of inertia [60]. The parameters a and Δ are determined by the requirement that Eq. (21) reproduces the cumulative number of low excited levels, as well as the average resonance spacing.

Level density parameters over a wide mass region are tabulated in Refs [59] and [62, 63] for the Gilbert–Cameron model and in Refs [60] and [64] for the backshifted Fermi gas model. These sets can be supplemented or updated if additional or more recent data on levels and resonances are available. For nuclei with no relevant data, one has to resort to systematics. This may lead to quite inaccurate results – in particular for nuclei far from the line of beta stability.

Both phenomenological models consider only in a very rough way the effects of shell structure and pairing on the energy dependence of the level density. These deficiencies may be overcome by 'microscopic' calculations which are based on realistic single particle energies and on the BCS model (see Ref. [65] for a recent example). Unfortunately, these calculations are time consuming. In the past few years new, semi-empirical, level density formulas have been proposed by Kataria et al. [66], Jensen and Sandberg [67] and by Ignatyuk et al. [68]. These formulas parametrize shell effects in terms of the empirical shell correction to the nuclear ground state mass. This type of parametrization is simple and seems to be very useful for practical applications as it provides a better basis for extrapolations to higher excitation energies and to nuclei with no resonance data other than the two phenomenological models described earlier. A recent review by Ramamurthy et al. on these semi-empirical models can be found in Ref. [69].

2.4.3. Pre-equilibrium model parameters

The *initial exciton number* $n_0 = p_0 + h_0$ determines the shape of the spectra of the particles emitted in the pre-equilibrium stage. Many investigations have shown that for nucleon induced reactions n_0 has the 'natural' value $n_0 = 3$

($p_0 = 2$, $h_0 = 1$). For the initial numbers $X_\pi(3)$ and $X_\nu(3)$, which are required for the hybrid model (see Eq. (15)), Blann and Vonach propose, for proton induced reactions,

$$X_\pi(3) = \frac{3N + 2Z}{3N + Z};\ X_\nu(3) = 2 - X_\pi(3) \tag{22a}$$

and

$$X_\nu(3) = \frac{3Z + 2N}{3Z + N};\ X_\pi(3) = 2 - X_\nu(3) \tag{22b}$$

for incident neutrons [18]. These expressions are based on the fact that the (free) n-p cross-section is about three times larger than the (free) n-n and p-p cross-section; the free nucleon-nucleon cross-sections are averaged with respect to the proton and neutron numbers Z and N of the target nucleus.

For composite projectiles the choice of (p_0, h_0) is less obvious and often not unique. We quote as typical examples some results. Exciton model calculations for incident alpha particles and ^{3}He particles required ($p_0 = 5$, $h_0 = 1$) [32] and ($p_0 = 3$, $h_0 = 1$) [70], respectively. Successful applications of the hybrid model for alpha induced reactions were reported with $n_0 = 4$ and $X_\pi(4) = X_\nu(4) = 2$ [71–73]. For incident ^{3}He particles, Chevarier et al. reported hybrid model calculations with $n_0 = 4$ and $X_\pi(4) = X_\nu(4) = 2$ or [$X_\pi(4) = 2.5$, $X_\nu(4) = 1.5$] [74], whereas Misaelides and Münzel used $n_0 = 5$ and [$X_\pi(5) = 2.5$, $X_\nu(5) = 1.5$] [73]. Deuteron induced reactions were analysed by Jahn et al. in the framework of the hybrid model with $n_0 = 3$ or $n_0 = 2$ [75].

In addition to the problem of the choice of the initial exciton number, the analysis of composite, particle induced reactions by pre-equilibrium models is complicated by the presence of a breakup component in the particle emission spectra which is not accounted for by these models. This holds, in particular, for weakly bound projectiles such as deuterons or ^{3}He particles and higher incident energies.

For the *particle–hole state densities*, which are required for the exciton and the hybrid model as well, the following most commonly used expression was derived by Williams:

$$\omega(p, h, E) = \frac{g[gE - (p^2 + h^2 + p - 3h)/4]^{p+h-1}}{p!h!(p + h - 1)!}$$

under the assumption of an energy independent, single particle state density g [76]. The quantity g may be related to the a parameter of the phenomenological level density models of Sec. 2.4.2 by $g = (6/\pi^2)a$. Very often the value $g = A/13$, corresponding to $a = A/8$, is employed where A is the mass number.

In later developments, Williams' formula was corrected for several effects: finite depth of the potential well, which restricts the excitation energy of the holes and pairing, shell effects and long range energy variations. For details see Kalbach's recent review, which also surveys the calculation of the quantity $\omega_{\Delta n}(n, E)$ of Eq. (12) [77].

The *particle–hole creation rates* $\Lambda^i_+(n, E)$ of the exciton model, which are based on the 'golden rule', Eq. (12), require the average squared matrix element $|M|^2$. By analysis of appropriate experimental data, Kalbach–Cline [78] found for the dependence of this quantity on mass number A and excitation energy E that

$$|M|^2(E) = KA^{-3}E^{-1} \tag{23}$$

The numerical value of the constant K critically depends on the expression used for the particle emission rates. For $g = A/13$ and for the emission rates proposed by Kalbach in Ref. [32], $K = 400\ \text{MeV}^3$. In order to reproduce the more realistic energy and exciton number dependence of the tabulated rates $\Lambda^i_+(n, E)$, which were obtained by Gadioli et al. [30] on the basis of the nucleon-nucleon cross-section in nuclear matter, Kalbach proposed the following relations:

$$|M|^2(n, E) = \frac{K'}{A^3 e}\left(\frac{e}{7\ \text{MeV}}\right)^{1/2}\left(\frac{e}{2\ \text{MeV}}\right)^{1/2}, \text{ for } e < 2\ \text{MeV}$$

$$= \frac{K'}{A^3 e}\left(\frac{e}{7\ \text{MeV}}\right)^{1/2}, \text{ for } 2\ \text{MeV} \leqslant e < 7\ \text{MeV}$$

$$= \frac{K'}{A^3 e}, \text{ for } 7\ \text{MeV} \leqslant e \leqslant 15\ \text{MeV}$$

$$= \frac{K'}{A^3 e}\left(\frac{15\ \text{MeV}}{e}\right)^{1/2}, \text{ for } 15\ \text{MeV} < e$$

where $e = E/n$ and the constant K' assumes the value $135\ \text{MeV}^3$ under the conditions specified for Eq. (23) [79].

The *intranuclear transition rates* $\lambda^i_+(\epsilon)$ for the hybrid model, which of course are conceptually different from the exciton model rates $\Lambda^i_+(n, E)$ are either based on the expressions for the Pauli-corrected nucleon-nucleon cross-section, given by Kikuchi and Kawai [80], or on the global optical potentials for nucleons by Becchetti and Greenlees [81]. In the latter case, the rates should not be used for energies much greater than 55 MeV, corresponding to the upper energy limit of

the potentials. For the radial dependence of the nuclear density which is required for the geometry dependent effects, and for further details, see the recent paper by Blann and Vonach [18].

3. COMPUTER CODES

Over the past few years many computer codes have been developed which calculate nuclear reaction cross-sections on the basis of a combination of equilibrium and pre-equilibrium models. In this section, we briefly describe some representative programs and discuss their applicability for the calculation of activation product cross-sections. A more detailed discussion of a larger number of codes can be found in a recent review by Uhl [82].

Alice/Livermore 82 is the most recent version of the widely used Alice codes developed by Blann and Bisplinghoff [83]. The program calculates, for arbitrary projectiles and emitted particles selected among neutrons, protons, alpha particles and deuterons (the actual choices are n; n and p; n, p and α; n, p, α and d), the activation product cross-sections for all nuclei of a rectangle in the (Z, N) plane which may be 11 mass units wide and 9 charge units deep.

A WE calculation is performed for the CN evaporation contribution. The s-wave approximation may be used as an option; in that case the yrast level is calculated by either assuming a rigid rotor or by means of the equilibrium deformed, rotating liquid drop model of Cohen et al. [84]. Pre-equilibrium emission of nucleons is treated within the framework of either the hybrid or the geometry dependent hybrid models. A simple formalism for multiple PE emission [18] is included. The most recent version of the code also allows, optionally, for isospin effects in precompound decay.

The Alice/Livermore 82 code is ideally suited for fast calculations of activation product cross-sections. Owing to many built-in data – as, for example, nuclear masses and parameters for global optical potentials – and, owing to convenient default options, the input is short and easy to prepare. The choice of the default parameters for PE decay is discussed by Blann and Vonach [18]. The running time of the code is short, especially if the inverse cross-sections are calculated not by the optical model routines but by the sharp cut-off algorithm [85], or are supplied as inputs. The only restrictions on the use of Alice/Livermore 82 are: reactions with first chance emitted composite particles (since for those ejectiles no PE contribution is considered) and the limitations inherent in the WE method of calculation (see Sec. 2.2).

In the following, we discuss the application of codes which allow for angular momentum and parity conservation and include gamma ray cascades. For HF calculations, the spectrum of excited states of all residual nuclei is divided into low lying known levels and a 'continuum' region described by a level density formula. The gamma ray branching ratios for the transitions between these

levels are required for the calculation of isomeric state populations. Thus, owing to the extensive information on the level schemes of many nuclei, HF codes demand much more input data than WE codes. Since angular momentum dependent calculations require much more time and storage, HF codes in general do not simultaneously calculate activation product cross-sections for as many final nuclei as, for example, does Alice/Livermore 82.

An extreme example of the restriction of the number of product nuclei is the code known as Stapre which calculates, for up to six sequentially emitted particles (selected among n, p, α and d) in addition to other quantities, the production cross-sections for all nuclei lying on one 'reaction path' [13]. Such a path is defined by a specific sequence of emitted particles, e.g. (αpnn). While this restriction is irrelevant for reactions such as (p, nn), problems arise if the final nucleus of interest is populated by several paths as, for example, for the (p, np), (p, pn) and (p,d) reactions. In that case several different runs are required for the final results. This disadvantage is at least partly overcome by the program Gnash by Young and Arthur [86]. In this code the ejectiles may be chosen among n, p, α, d, t and ^{3}He. Activation product cross-sections for up to ten different final nuclei can be calculated and contributions of different paths are obtained in one run. Nevertheless, the maximum number of final nuclei is much smaller than for Alice/Livermore 82. The PE contribution in Stapre and Gnash is calculated within the framework of the exciton model. While Stapre employs for alpha emission the model of preformed alpha particles by Milazzo-Colli and Braga-Marcazzan [87, 88] Gnash uses for pre-equilibrium emission of composite particles the simple statistical direct reaction contributions proposed by Kalbach [32], in addition to the results based on detailed balance.

Finally, there is the program TNG1 by Fu which, in contrast to the two aforementioned HF codes, performs an angular momentum dependent treatment of the PE contribution in the framework of the exciton model [38, 39]. It is of special interest for isomeric state populations in cases of a dominant PE contribution. TNG1 handles reactions with up to three emitted particles.

Among the codes mentioned in this section all but TNG1 account for fission. Thus they can also calculate activation product cross-sections in cases where fission competition is relevant.

4. APPLICATIONS

Thus far the codes Overlaid Alice [89] and, later, its version Alice/Livermore 82 [83], as well as Stapre [13] have been used for the calculation of activation product cross-sections. For practical purposes the Alice codes are preferred as only few input data are required and the computer execution times are moderate in comparison with Stapre. Indeed, Stapre might yield the more accurate results, as is shown below.

In the following are given some results obtained with Alice to demonstrate the accuracy of calculated excitation functions. All calculations were done under the same assumptions to maintain an a priori character, i.e. the input parameters were not varied to obtain better agreement between experimental data and theoretical results. In all cases an evaporation calculation with multiparticle emission according to the statistical model was chosen. The default optical model subroutine was used for the calculation of the inverse cross-sections. For pre-compound emission of nucleons the geometry dependent hybrid model was chosen.

Reaction Q-values and binding energies were taken first from Ref. [90], but later the Myers–Swiatecki mass formula [91] was used which is available as the default option in the code. In the most recent version an option exists to use as much experimental mass data as are available. In addition, the number of nuclei of each Z and the number of elements to be included in the calculation can be specified. For each projectile energy the cross-sections for the evaporation cascade leading from the composite nucleus to the final nuclei, as defined above, are calculated.

4.1. Proton induced reactions

An important input parameter for pre-equilibrium decay which depends on the projectile is the initial number of excitons (see Sec. 2.4.3). For proton induced reactions the initial number of excited protons and neutrons was taken as 1.25 and 0.75, respectively. These initial exciton numbers are obtained from expressions (22a) and (22b) under the assumption that N = Z. Together with one hole, this gives a total of three excitons [92]. To demonstrate the simple inputs required for Alice, a sample input for the ^{68}Zn(p, xn) + ^{68}Zn(p, pxn) reactions is listed below (without regard to the input format required by Alice):

- Projectile mass number (AP) = 1.
- Target mass number (AT) = 68.
- Projectile charge (ZP) = 1.
- Target charge (ZT) = 30.
- Number of product nuclei of each Z (NA) = 4 to include (p, 3n) reactions.
- Number of Z of product nuclei (NZ) = 2 to include (p, pxn) reactions.
- Mass option (MC) = 0 for the Myers–Swiatecki mass formula or (MC) = 10 to include experimental mass data, if available.
- Number and types of particles to be emitted from each nuclide (M3) = 3 for p, n and alphas.
- Pairing option for the mass formula (MP) = 3 for normal pairing shift.

For each projectile energy the following input has to be supplied:

- Projectile kinetic energy (EQ), in MeV.
- Type of calculation (JCAL) = 1 for the Weisskopf–Ewing evaporation calculation.

- Initial exciton number (particles and holes) (TD) = 3.
- Initial excited neutron number (EX1) = 0.75.
- Initial excited proton number (EX2) = 1.25.
- Pre-equilibrium model (TMX) = 1 for the geometry dependent hybrid model.
- Intranuclear transition rates (AV) = 0 for optical model transition rates.
  If $E_p > 55$ MeV, then (AV) = 1 for nucleon-nucleon mean free paths.

With this input configuration and a calculation of activation cross-sections for 18 projectile energies from 6 to 36 MeV, the CPU time on a Control Data Corporation Cyber 170–720 is about 270 s. Two similar runs for ^{66}Zn and ^{67}Zn as target nuclei are sufficient to yield the relevant figures for estimating the excitation functions and production yields for ^{nat}Zn(p, xn)^{67}Ga and its contaminants. A reduction in CPU time is possible by computing the inverse reaction cross-sections with a classical sharp cut-off model, though this option was not tested.

In the following, a few examples of excitation functions are given which are of interest for the production of radioisotopes used in nuclear medicine.

4.1.1. ^{67}Ga

In spite of the fact that ^{67}Ga has been widely used in nuclear medicine, only a small quantity of experimental data on the excitation functions of protons on zinc targets is available. The principal radionuclidic impurity, due to its half-life of 9.5 h, is ^{66}Ga. Figures 1–5 show the results of the calculations compared with data from the literature [93–95] for reactions with ^{66}Zn, ^{67}Zn and ^{68}Zn as target nuclei to be considered here. The most comprehensive data have been published by Little and Lagunas-Solar [95]. In comparison with these data, calculated curves show a steeper rise and, in some cases, less agreement for the pre-equilibrium tail. Unfortunately, the energy errors are not given and it should be remembered that the excitation function curves were obtained from composite yield curves for a ^{nat}Zn target taking into account Q-values and general reaction characteristics [95] which might result in less reliable data for the tail. Agreement in maximum cross-section is better than 20%.

4.1.2. ^{77}Kr

This radioisotope has been of interest as the precursor of ^{77}Br, but the noble gas can be used directly, being a positron emitter in positron emission tomography. The essential contaminant for proton induced reactions with bromine is ^{76}Kr. The calculated cross-sections for reactions with natural bromine are shown in Figs 6 and 7. Obviously the excitation functions from Lundqvist et al. [96] are not in agreement with either other experimental or with calculated data. For the reaction product ^{77}Kr, agreement is fairly good for data from DeJong et al. [97]

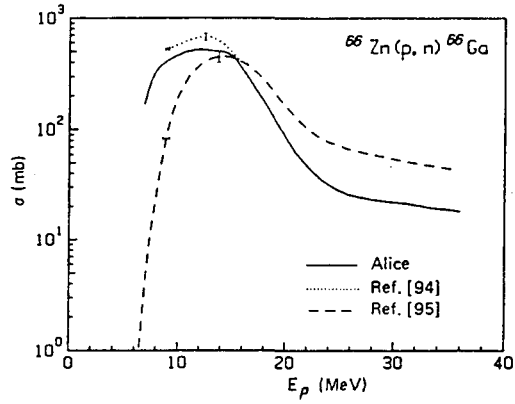

FIG. 1. Calculated and experimental excitation functions for $^{66}Zn(p, n)^{66}Ga$. Error bars indicate typical experimental errors, if quoted. For clarity, individual measured cross-sections are not shown. Cross-section data by Little and Lagunas-Solar [95] have been obtained by the authors from composite yield curves for a natural zinc target.

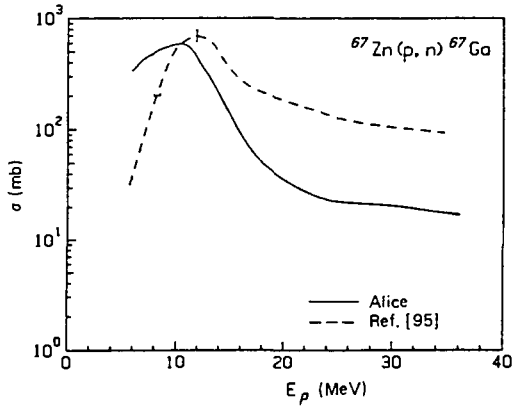

FIG. 2. Calculated and experimental excitation functions for $^{67}Zn(p, n)^{67}Ga$ (for comments see Fig. 1).

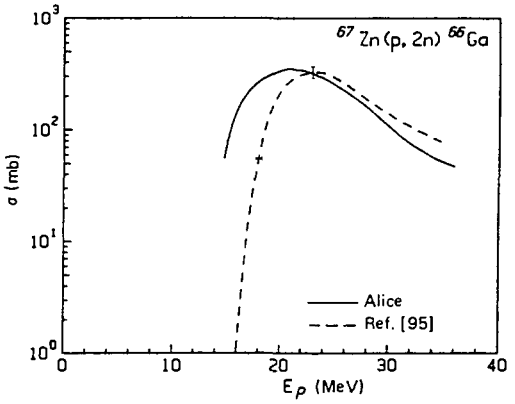

FIG. 3. Same as Fig. 1, but for $^{67}Zn(p, 2n)^{66}Ga$.

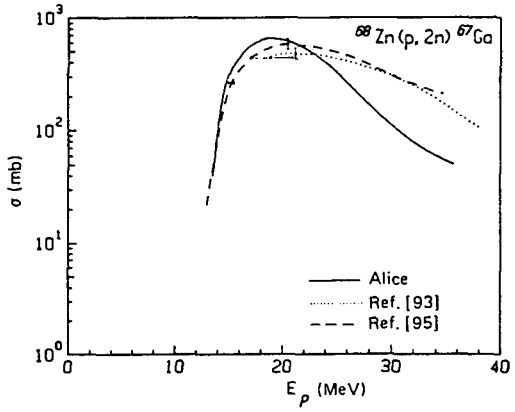

FIG. 4. Same as Fig. 1, but for $^{68}Zn(p, 2n)^{67}Ga$.

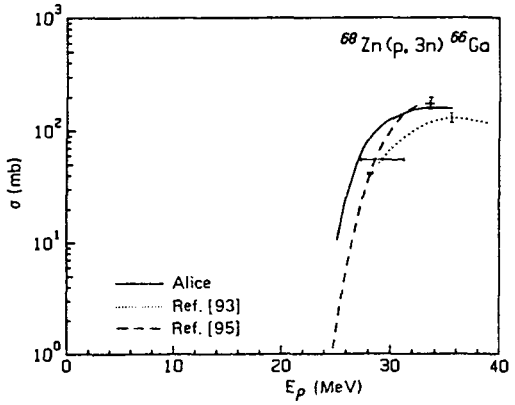

FIG. 5. Same as Fig. 1, but for $^{68}Zn(p, 3n)^{66}Ga$.

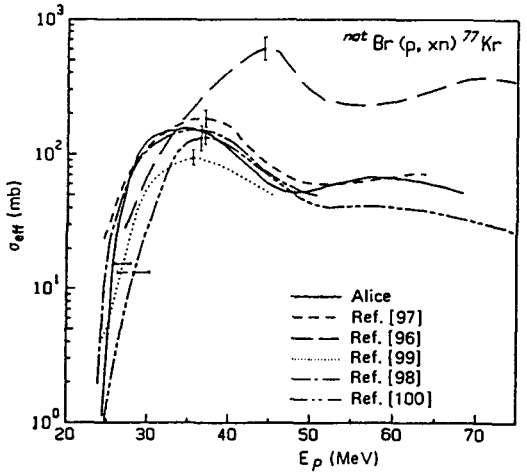

FIG. 6. Calculated and experimental cross-sections for proton induced reactions with natural bromine leading to ^{77}Kr. The data from Dikšić et al. [100], for reactions with ^{79}Br and ^{81}Br, were combined to obtain the effective cross-section.

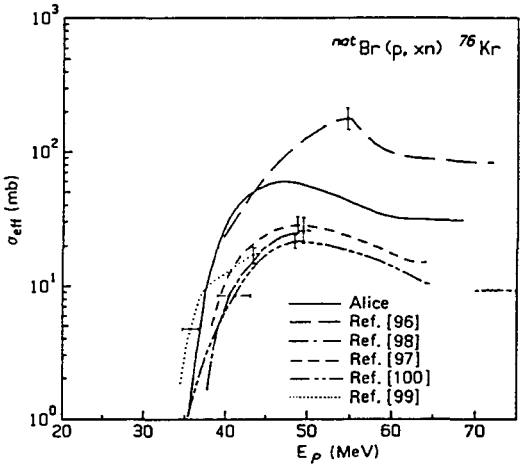

FIG. 7. Calculated and experimental excitation functions for $^{nat}Br(p, xn)^{76}Kr$ (see also Fig. 6).

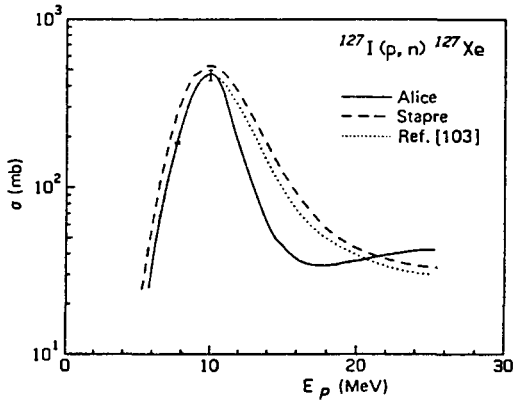

FIG. 8. Experimental excitation function for $^{127}I(p, n)^{127}Xe$, together with cross-sections calculated by the Alice and Stapre codes [102].

and Nozaki et al. [98]; with respect to the data from Weinreich and Knieper only the shape is reproduced [99]. Data from Dikšić et al. [100] are in less agreement. For the final nucleus ^{76}Kr (which can be considered to be far away from the stability line) characteristics of the excitation function are similar, but discrepancies exist in the maximum cross-section up to a factor of 2.7.

4.1.3. ^{127}Xe

This radioisotope exhibits some advantages when compared with ^{133}Xe and is suitable for use in nuclear medicine, though it has not attracted widespread

interest [101]. The results for the reaction $^{127}I(p,n)\ ^{127}Xe$ (Fig. 8) also include data calculated using Stapre [102]. The Stapre data match the experimental results from Collé and Kishore [103] over the entire energy range. For the Alice curve only the initial rise until the maximum cross-section is in excellent agreement, but the tail of the excitation function is less satisfactorily reproduced. There exists no plausible reason for the excitation function rising again after the initial peak, but to preserve the a priori character we have not varied the input parameters.

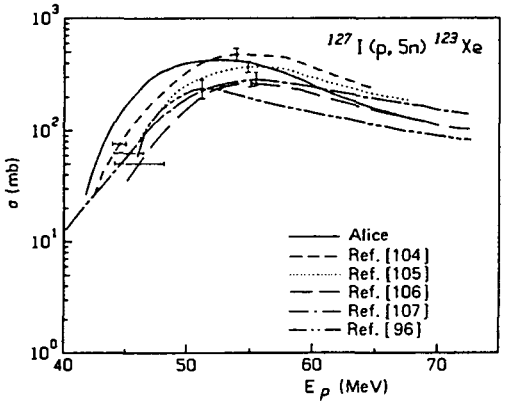

FIG. 9. Calculated and experimental excitation functions for $^{127}I(p, 5n)^{123}Xe$.

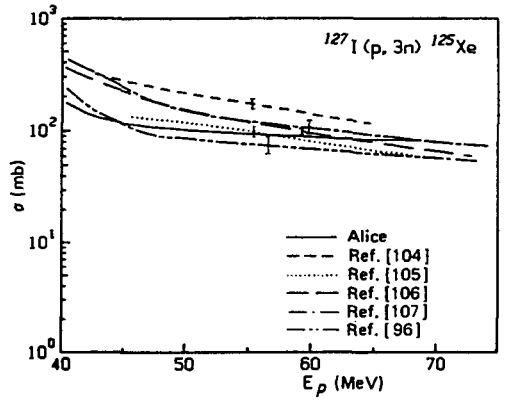

FIG. 10. Calculated and experimental excitation functions for the production of the contaminant ^{125}I via $^{127}I(p, 3n)^{125}Xe \rightarrow {}^{125}I$, shown for the same energy window as in Fig. 9.

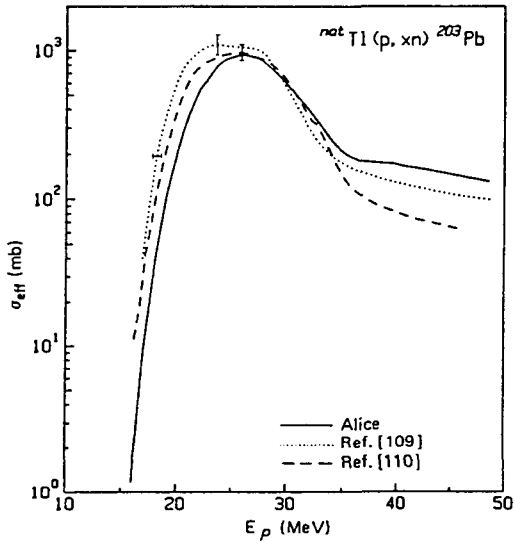

FIG. 11. Effective cross-sections for proton induced reactions with natural thallium producing ^{203}Pb.

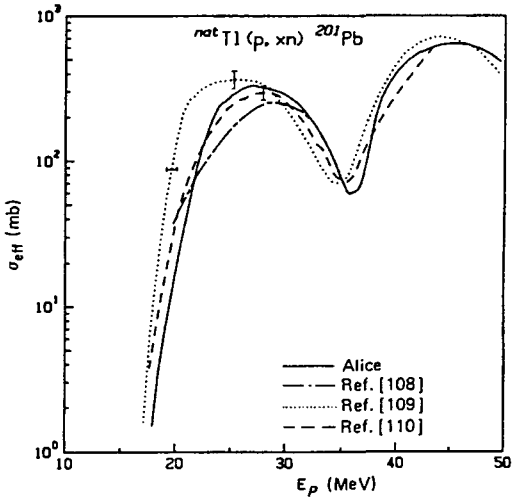

FIG. 12. Same as Fig. 11, but for production of ^{201}Pb.

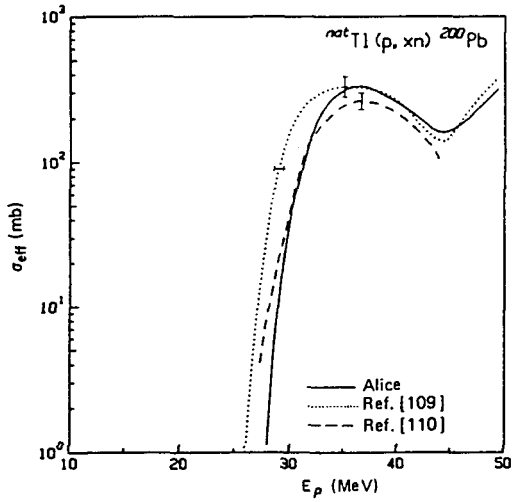

FIG. 13. Same as Fig. 11, but for production of ^{200}Pb.

4.1.4. ^{123}Xe

The introduction of ^{123}I as a substitute for ^{131}I has been of great importance. The quality of scintigraphic examinations has been improved, with concurrent reduction in patient dose. The production of ^{123}Xe as the precursor of ^{123}I is the best method to obtain high radionuclidic purity. Any other direct production by bombardment of Te or Sb targets suffers from contamination by ^{124}I, which both impairs scintigraphic properties and increases radiation dose. Unfortunately, the proton energies required for the ^{127}I(p, 5n) ^{123}Xe reaction are too high for application with compact cyclotrons. The only impurity produced is ^{125}I, but setting an appropriate energy window for the (p, 5n) reaction and half-life discrimination of ^{125}Xe both give relatively low ^{125}I activities.

The calculated excitation functions are given in Figs 9 and 10. Taking into account the discrepancies between the various experimental data [96, 104–107], the agreement is fair for both reactions.

4.1.5. ^{201}Pb

^{201}Tl is widely used for myocardial studies. It can be produced with a high degree of purity via its precursor ^{201}Pb by bombarding natural thallium targets with protons. ^{203}Pb is also produced in this way and has generated some medical interest (see, for example, citations in Ref. [110]). The calculated excitation

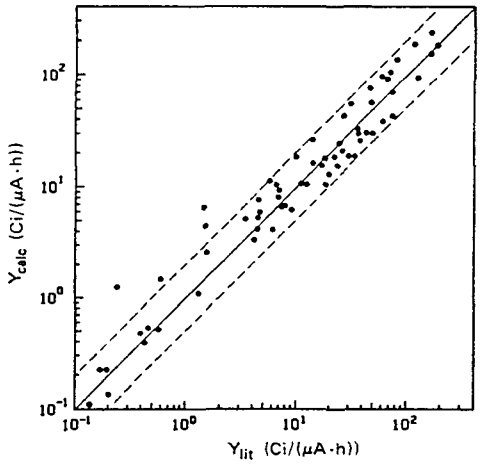

FIG. 14. Comparison of calculated radioisotope production yields, Y_{calc}, with data from literature, Y_{lit} (see Ref. [5]). Dashed lines indicate a deviation by a factor of 2 from equality (1 curie = 3.70 × 10^{10} Bq).

functions for proton induced reactions leading to ^{200}Pb, ^{201}Pb and ^{203}Pb are shown in Figs 11–13. Only the contribution due to ^{203}Tl(p, n) ^{203}Pb has not been included. Agreement between experimental [108–110] and calculated data is good. Again, the reproduction of the pre-equilibrium tail of the ^{205}Tl(p, 3n) ^{203}Pb reaction is less satisfactory.

4.2. Yield calculations

To check the usefulness of the theoretical excitation functions for proton induced reactions, yield figures were calculated according to the conditions cited in the literature and then compared with the respective yield data quoted therein. Yield figures in the literature comprise experimental yields and yields calculated from yield functions or excitation functions. Figure 14 shows a comparison between calculated yields and yields reported in the literature.

It was found that in general the literature yield data can be reproduced by calculated yields to within a factor of 2. It must be remembered that all of the experimental errors, which are often not quoted, are also included in this comparison. Further, there remain hidden many factors in the various methods by which the yield figures are obtained. No definite trend in an over- or under-estimation of the data in the literature could be noted. The proton energy covers a range of up to 70 MeV and target nuclei with $Z \geqslant 15$ are included.

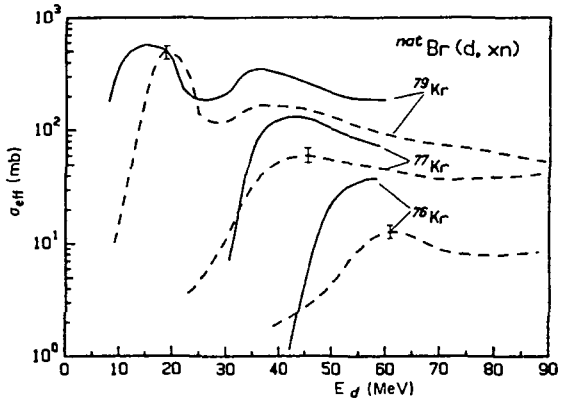

FIG. 15. Excitation functions for (d, xn) reactions with natural bromine from Qaim et al [111] and calculated using Alice (——).

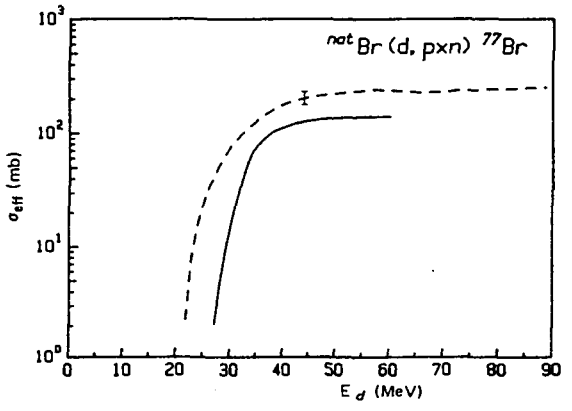

FIG. 16. Same as Fig. 15, but for $^{nat}Br(d, pxn)^{77}Br$ reactions.

4.3. Reactions with particles other than protons

Several excitation functions for deuteron and ^{3}He induced reactions have been calculated using Alice, with the same input considerations as mentioned above except for the initial exciton configuration. The efforts to reproduce excitation functions and particle spectra require exciton numbers which do not always conform to the initial physical concept (see Sec. 2.4.3). For deuterons total exciton numbers of 2 (1 neutron, 1 proton, 0 holes) or 3 (2 neutrons, 1 proton, 0 holes) have given the best results. In general, the discrepancies are greater than for proton induced reactions. Two examples are given to demonstrate the usefulness of a priori calculations.

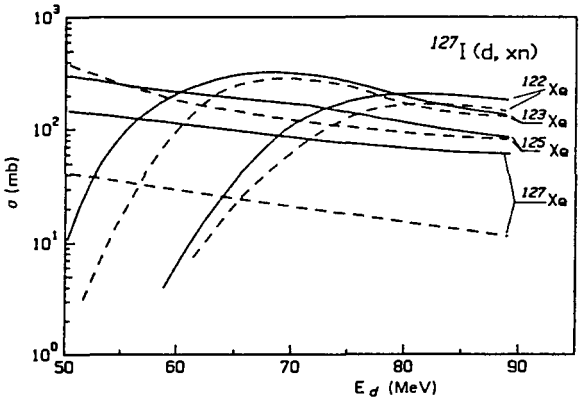

FIG. 17. Excitation functions for $^{127}I(d, xn)$ reactions from Weinreich et al. [112] (– – –) and calculated using Alice (——).

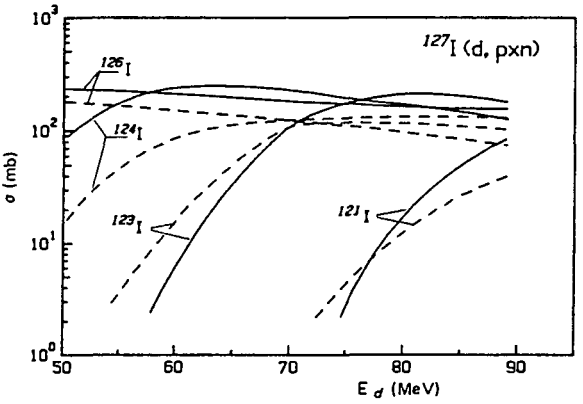

FIG. 18. Same as Fig. 17, but for $^{127}I(d, pxn)$ reactions.

The production of ^{77}Kr can also be accomplished by deuteron bombardment of bromine targets. Experimental excitation functions from Qaim et al. [111] and the calculated total cross-sections obtained with an initial exciton number of 2 are shown in Figs 15 and 16. While (d, xn) reactions are overestimated by Alice, the (d, pxn) cross-sections are too low.

The situation for the production of ^{123}Xe via the ^{127}I(d, 6n) reaction, together with other companion reactions, is shown in Figs 17 and 18. It can also be seen that the discrepancies with the experimental data from Weinreich et al. [112] are larger than those for proton induced reactions. Michel and Galas [113] have reported good agreement between calculated and experimental data for a number of deuteron induced reactions with ^{59}Co when using exciton numbers of 2 or 3.

For other projectiles, e.g. ^{3}He, the situation is even less satisfactory and the appropriate choice of initial exciton numbers for an a priori calculation is not obvious (see Sec. 2.4.3).

5. CONCLUSIONS

The applicability of the codes described is limited by several factors. In general one can assume that the parameter sets make feasible a calculation for masses $A \geqslant 30$, but results for lighter nuclei have also shown satisfactory agreement of cross-sections. Calculations based on the optical model and the compound nucleus evaporation model for neutron induced reactions on biologically interesting elements with $A \geqslant 12$ (carbon, nitrogen and oxygen) have been performed for neutron energies from 20 to 50 MeV by Dimbylow [114]. Indeed, the few experimental data available have been used for a data fit so that the results were not truly obtained for a priori conditions.

Further, reproduction of activation cross-sections will get worse for product nuclei far away from the stability line for beta decay. The particle energies available in production facilities rarely exceed proton energies of perhaps 70 MeV, but compact cyclotrons frequently used for these purposes produce protons of up to about 45 MeV. For this energy range the nuclear models used in these codes should be adequate.

The results of calculations for nucleon induced reactions generally show better agreement than for reactions involving 'complex' particles (deuterons, ^{3}He, alpha particles) in the entrance and/or exit channels. In particular, the emission of these particles during pre-equilibrium decay is not accounted for by the Alice code.

It must be stressed that it is difficult to give figures on the accuracy of calculated excitation functions. In particular, during the initial rise the cross-sections could differ by large factors and it is this section of the excitation function which is usually affected most by uncertainties in projectile energy. Using the Alice code for proton induced reactions, with input parameters as given in Sec. 4.1, it was shown that the yield figures obtained from calculated cross-sections differ in general by less than a factor of 2 for all calculations being made under the same a priori conditions, without any adjustment of the input parameters. This uncertainty comprises all experimental errors in the determination of the yield. The comparison also indicates that there is no systematic over- or underestimation of production yield by calculated yields. If experimental data for a reaction under investigation are missing it would be useful to study some reactions on neighbouring target nuclei if possible. In this way it is possible to gain experience of the predictive power in that mass region.

An individual selection of input parameters according to nuclear data available for a specific mass region or by experience could perhaps give better

agreement. This is particularly true of the choice of exciton numbers for composite projectiles. For deuteron induced reactions the preferable configuration seems to be either two or three initial excitons (see also Refs [75, 113]). So far, the experience shows that agreement with experimental data is less satisfactory than for nucleon induced reactions. For ^{3}He and alpha projectiles we still have to gain experience to assess the practicability of 'global' initial exciton numbers for a priori calculations.

Setting up the input parameters for the Alice code requires little time. The most recent version, Alice/Livermore 82, has undergone some revisions. However, most of the results shown in this contribution have been obtained using its earlier version, Overlaid Alice, so that new results could be somewhat different, though in all cases where calculations for a particular reaction were made with both codes, negligible differences in activation cross-sections were found. Nuclear data files, e.g. for inverse cross-sections, level density parameters and masses could be useful in saving computer time and helpful in improving the accuracy of the results.

An assessment of the advantages and limitations of various production methods by means of a priori calculations seems feasible for proton induced reactions. It is not suggested that one should rely only on calculated excitation functions, but in the planning of new production methods calculated activation cross-section data could be helpful.

REFERENCES

[1] KELLER, K.A., LANGE, J., MÜNZEL, H., PFENNING, G., Excitation Functions for Charged Particle Induced Nuclear Reactions (Landolt-Börnstein New Series Group I), Vol. 5b, Springer-Verlag, Berlin (West) (1973).
[2] The Bibliography of Integral Charged Particle Nuclear Data, 4th edn (BURROWS, T.W., DEMPSEY, P., Eds), Brookhaven National Lab., Upton, NY, Rep. BNL-NCS-50640 (1980).
[3] KELLER, K.A., LANGE, J., MÜNZEL, H., Estimation of Unknown Excitation Functions and Thick Target Yields for p, d, ^{3}He and Alpha Reactions (Landolt-Börnstein New Series Group I), Vol. 5c, Springer-Verlag, Berlin (West) (1973).
[4] QAIM, S.M., Radiochim. Acta **30** (1982) 147.
[5] NOWOTNY, R., Int. J. Appl. Radiat. Isot. **32** (1981) 73.
[6] AUSTERN, N., Direct Nuclear Reaction Theories, Wiley, New York (1970).
[7] BOHR, N., Nature (London) **137** (1936) 344.
[8] WEISSKOPF, V.F., EWING, D.H., Phys. Rev. **57** (1940) 472.
[9] HAUSER, W., FESHBACH, H., Phys. Rev. **87** (1952) 366.
[10] VOGT, E., in Advances in Nuclear Physics I (BARANGER, M., VOGT, E., Eds), Plenum Press, New York (1968) 261.
[11] MOLDAUER, P.A., "Statistical theory of neutron nuclear reactions", Nuclear Theory for Applications (Proc. Winter Course Trieste, 1978), IAEA-SMR-43, IAEA, Vienna (1980) 165.
[12] MAHAUX, C., WEIDENMÜLLER, H.A., Annu. Rev. Nucl. Part. Sci. **29** (1979) 1.

[13] STROHMAIER, B., UHL, M., "STAPRE – A statistical model code with consideration of pre-equilibrium decay", Nuclear Theory for Applications (Proc. Winter Course Trieste, 1978), IAEA-SMR-43, IAEA, Vienna (1980) 313.
[14] GROVER, J., Phys. Rev. **123** (1961) 267.
[15] STENGL, G., UHL, M., VONACH, H., Nucl. Phys. **A290** (1977) 109.
[16] BLANN, M., MERKEL, G., Phys. Rev. **137B** (1965) 367.
[17] LANE, A.M., Phys. Rev. C **18** (1978) 1525.
[18] BLANN, M., VONACH, H., Phys. Rev. C **28** (1983) 1475.
[19] AGASSI, D., WEIDENMÜLLER, H.A., MANTZOURANIS, G., Phys. Lett. 22 (1975) 145.
[20] FESHBACH, H., KERMANN, A.K., KOONIN, S.E., Ann. Phys. (N.Y.) **125** (1980) 429.
[21] TAMURA, T., UDAGAWA, T., LENSKE, H., Phys. Rev. C **26** (1982) 379.
[22] GRIFFIN, J.J., Phys. Lett. 17 (1966) 478.
[23] GRIFFIN, J.J., Phys. Lett. **24B** (1967) 5.
[24] CLINE, C., BLANN, M., Nucl. Phys. **A172** (1971) 225.
[25] UHL, M., "Computer calculations of neutron cross sections and gamma-cascades with the statistical model with consideration of angular momentum and parity conservation", Nuclear Theory in Neutron Nuclear Data Evaluation (Proc. Consultants Meeting Trieste, 1975), Vol. 2, IAEA-190, IAEA, Vienna (1976) 361.
[26] AKKERMANS, J.M., GRUPPELAAR, H., Z. Phys. **A300** (1981) 345.
[27] WILLIAMS, F.C., Jr., Phys. Lett. **31B** (1970) 184.
[28] OBLOŽINSKÝ, P., RIBUNSKÝ, I., BĚTÁK, E., Nucl. Phys. **A226** (1974) 347.
[29] GADIOLI, E., GADIOLI-ERBA, E., TAGLIAFERRI, G., Nucl. Phys. **A217** (1973) 589.
[30] GADIOLI, E., GADIOLI-ERBA, E., HOGAN, J.J., Phys. Rev. C **16** (1977) 1404.
[31] CLINE, C.K., Nucl. Phys. **A193** (1972) 417.
[32] KALBACH, C., Z. Phys. A283 (1977) 401.
[33] BIRRATARI, C., et al., Nucl. Phys. **A201** (1973) 579.
[34] DOBEŠ, J., BĚTÁK, E., in Neutron Induced Reactions (Proc. Europhysics Topical Conf. Smolenice, 1982) (OBLOŽINSKÝ, P., Ed.), Czechoslovak Academy of Sciences, Bratislava (1982).
[35] GADIOLI, E., GADIOLI-ERBA, E., "Recent results in the theoretical description of pre-equilibrium processes", Nuclear Theory for Applications – 1980 (Proc. Interregional Advanced Training Course Trieste, 1980), Vol. 1, IAEA-SMR-68, IAEA, Vienna (1980) 3.
[36] IWAMOTO, A., HARADA, K., Phys. Rev. C 26 (1982) 1821.
[37] PLYOKO, V.A., Sov. J. Nucl. Phys. 27 (1978) 623.
[38] FU, C.Y., "Development and applications of multi-step Hauser–Feshbach/pre-equilibrium model theory", Nuclear Theory for Applications – 1980 (Proc. Interregional Advanced Training Course Trieste, 1980), Vol. 1, IAEA-SMR-68, IAEA, Vienna (1980) 35.
[39] FU, C.Y., Oak Ridge National Lab., TN, Rep. ORNL/TM-7042 (1980).
[40] GRUPPELAAR, H., in Basic and Applied Problems of Nuclear Level Densities (Proc. IAEA Advisory Group Meeting Brookhaven, 1983) (BHAT, M.R., Ed.), Brookhaven National Lab., Upton, NY, Rep. BNL-NCS-51694 (1983) 143.
[41] BLANN, M., Phys. Rev. Lett. 27 (1971) 337.
[42] BLANN, M., Phys. Rev. Lett. 27 (1971) 700E.
[43] BLANN, M., Phys. Rev. Lett. 27 (1971) 1550E.
[44] HARP, G.D., MILLER, J.M., BEINE, B.J., Phys. Rev. **165** (1968) 1166.
[45] HARP, G.D., MILLER, J.M., Phys. Rev. C 3 (1971) 1847.
[46] BLANN, M., Nucl. Phys. **A213** (1973) 570.
[47] BLANN, M., MIGNEREY, A., SCOBEL, W., Nukleonika 21 (1976) 335.
[48] BLANN, M., Phys. Rev. Lett. 28 (1972) 757.

[49] MAHAUX, C., "Theoretical aspects of the optical model", Nuclear Theory for Applications (Proc. Winter Course Trieste, 1978), IAEA-SMR-43, IAEA, Vienna (1980) 97.
[50] HODGSON, P.E., in Nuclear Physics (Proc. 6th Symp. Oaxtepec, Mexico, 1983), CONF-830138 (1983).
[51] HODGSON, P.E., Nuclear Reactions and Nuclear Structure, Clarendon Press, Oxford (1971).
[52] PEREY, C.M., PEREY, F.G., At. Nucl. Data Tables 17 (1976) 1.
[53] HUIZENGA, J.R., IGO, G.J., Argonne National Lab., IL, Rep. ANL-6373 (1961).
[54] McFADDEN, L., SATCHLER, G.R., Nucl. Phys. 84 (1966) 177.
[55] RAPAPORT, J., KULKARNI, V., FINLAY, R.W., Nucl. Phys. A330 (1979) 15.
[56] BLATT, J.M., WEISSKOPF, V.F., Theoretical Nuclear Physics, Wiley, New York (1952).
[57] AXEL, P., Phys. Rev. 126 (1962) 671.
[58] GARDNER, D.G., in Fast Neutron Capture Cross Sections (Proc. NEANDC/NEACRP Specialists Meeting Argonne, Illinois, 1982) (SMITH, A.B., POENITZ, W.P., Eds), Argonne National Lab., IL, Rep. ANL-83-4 (1982) 67.
[59] GILBERT, A., CAMERON, A.G.W., Can. J. Phys. 43 (1965) 1446.
[60] VONACH, H., HILLE, M., Nucl. Phys. A217 (1969) 289.
[61] REFFO, G., Comitato Nazionale per l'Energia Nucleare, Rome, Rep. CNEN-RT/FI(78) 11 (1978).
[62] ROSE, E.K., COOK, J.L., Australian Atomic Energy Commission Research Establishment, Lucas Heights, Rep. AAEC/E419 (1977).
[63] COOK, J.L., ROSE, E.K., in Nuclear Data for Science and Technology (Proc. Int. Conf. Antwerp, 1982) (BÖCKHOFF, K.H., Ed.), Reidel, Dordrecht (1983) 805.
[64] DILG, W., SCHANTL, W., VONACH, H., UHL, M., Nucl. Phys. A217 (1973) 269.
[65] MAINO, G., MENAPACE, E., VENTURA, A., Nuovo Cimento 57A (1980) 427.
[66] KATARIA, S.K., RAMAMURTHY, V.S., KAPOOR, S.S., Phys. Rev. C 18 (1978) 549.
[67] JENSEN, A.S., SANDBERG, J., Phys. Scr. 17 (1978) 107.
[68] IGNATYUK, A.V., ISTEKOV, K.K., SMIRENKIN, G.N., Sov. J. Nucl. Phys. 29 (1979) 450.
[69] RAMAMURTHY, V.S., KATARIA, S.K., KAPOOR, S.S., in Basic and Applied Problems of Nuclear Level Densities (Proc. IAEA Advisory Group Meeting Brookhaven, 1983) (BHAT, M.R., Ed.), Brookhaven National Lab., Upton, NY, Rep. BNL-NCS-51694 (1983) 187.
[70] GRIMES, S.M., ANDERSON, J.D., McCLURE, J.W., POHL, B.A., WONG, C., Phys. Rev. C 5 (1972) 830.
[71] BLANN, M., MIGNEREY, A., Nucl. Phys. A186 (1972) 245.
[72] CHEVARIER, A., CHEVARIER, N., DEMEYER, A., HOLLINGER, G., PERTOSA, B., TRAN, M.D., Phys. Rev. C 8 (1973) 2155.
[73] MISAELIDES, P., MÜNZEL, H., J. Inorg. Nucl. Chem. 42 (1979) 937.
[74] CHEVARIER, A., et al., Nucl. Phys. A231 (1974) 64.
[75] JAHN, P., PROBST, H.-J., DJALOEIS, A., DAVIDSON, W.F., MAYER-BÖRICKE, C., Nucl. Phys. A209 (1973) 333.
[76] WILLIAMS, F.C., Jr., Nucl. Phys. A166 (1971) 231.
[77] KALBACH, C., in Basic and Applied Problems of Nuclear Level Densities (Proc. IAEA Advisory Group Meeting Brookhaven, 1983) (BHAT, M.R., Ed.), Brookhaven National Lab., Upton, NY, Rep. BNL-NCS-51694 (1983) 113.
[78] KALBACH-CLINE, D., Nucl. Phys. A210 (1973) 590.
[79] KALBACH, C., Z. Phys. A287 (1978) 319.
[80] KIKUCHI, K., KAWAI, M., Nuclear Matter and Nuclear Interactions, North-Holland, Amsterdam (1968).
[81] BECCHETTI, F.D., GREENLEES, G.W., Phys. Rev. 182 (1969) 1190.

[82] UHL, M., "Recent advances in nuclear model code developments", Nuclear Theory for Applications – 1982 (Proc. Winter Course Trieste, 1982), IAEA-SMR-93, IAEA, Vienna (1982) 5.
[83] BLANN, M., BISPLINGHOFF, J., Lawrence Livermore Lab., Livermore, CA, Rep. UCID-19614 (1982).
[84] COHEN, S., PLASIL, F., SWIATECKI, W.J., Ann. Phys. (N.Y.) 82 (1974) 557.
[85] BLANN, M., Phys. Rev. C 21 (1980) 1770.
[86] YOUNG, P.G., ARTHUR, E.D., Los Alamos Scientific Lab., NM, Rep. LA-6947 (1977).
[87] MILAZZO-COLLI, L., BRAGA-MARCAZZAN, G.M., Phys. Lett. **B38** (1972) 155.
[88] MILAZZO-COLLI, L., BRAGA-MARCAZZAN, G.M., Nucl. Phys. **A210** (1973) 297.
[89] BLANN, M., Chicago Operations Office, US Department of Energy, Chicago, IL, Rep. COO-3494-29 (1976).
[90] WAPSTRA, A.H., BOS, K., At. Data Nucl. Data Tables **19** 3 (1977).
[91] MYERS, W.D., SWIATECKI, W.J., Ark. Fys. **36** (1967) 343.
[92] BLANN, M., DOERING, R.R., GALONSKY, A., PATTERSON, D.M., SERR, F.E., Nucl. Phys. **A257** (1976) 15.
[93] McGEE, T., RAO, C.L., SAHA, G.B., YAFFE, L., Nucl. Phys. **A150** (1970) 11.
[94] HILLE, M., HILLE, P., UHL, M., WEISZ, W., Nucl. Phys. **A198** (1972) 625.
[95] LITTLE, F.E., LAGUNAS-SOLAR, M., Int. J. Appl. Radiat. Isot. **34** (1983) 631.
[96] LUNDQVIST, H., MALMBORG, P., LANGSTRÖM, B., CHIENGMAI, S.N., Int. J. Appl. Radiat. Isot. **30** (1979) 39.
[97] DeJONG, D., BRINKMAN, G.W., LINDNER, L., Int. J. Appl. Radiat. Isot. **30** (1979) 188.
[98] NOZAKI, T., IWAMOTO, M., ITOH, Y., Int. J. Appl. Radiat. Isot. **30** (1979) 79.
[99] WEINREICH, R., KNIEPER, J., Int. J. Appl. Radiat. Isot. **34** (1983) 1335.
[100] DIKŠIĆ, M., GALINIER, J.-L., MARSHALL, H., YAFFE, L., Phys. Rev. C **19** (1979) 1753.
[101] HOFFER, P.B., et al., J. Nucl. Med. **14** (1973) 172.
[102] GRABMAYR, P., NOWOTNY, R., Int. J. Appl. Radiat. Isot. **29** (1978) 261.
[103] COLLÉ, R., KISHORE, R., Phys. Rev. C 9 (1974) 2166.
[104] WILKINS, S.R., et al., Int. J. Appl. Radiat. Isot. **26** (1975) 279.
[105] PAANS, A.M.J., VAALBURG, W., VAN HARK, G., WOLDRING, M.G., Int. J. Appl. Radiat. Isot. **27** (1976) 465.
[106] DIKŠIĆ, M., YAFFE, L., J. Inorg. Nucl. Chem. **39** (1977) 1299.
[107] SYME, D.B., et al., Int. J. Appl. Radiat. Isot. **29** (1978) 29.
[108] LEBOWITZ, E., et al., J. Nucl. Med. **16** (1975) 151.
[109] LAGUNAS-SOLAR, M.C., JUNGERMAN, J.A., PEEK, N.F., THEUS, R.M., Int. J. Appl. Radiat. Isot. **29** (1978) 159.
[110] QAIM, S.M., WEINREICH, R., OLLIG, H., Int. J. Appl. Radiat. Isot. **30** (1979) 85.
[111] QAIM, S.M., STÖCKLIN, G., WEINREICH, R., Int. J. Appl. Radiat. Isot. **28** (1977) 947.
[112] WEINREICH, R., SCHULT, O., STÖCKLIN, G., Int. J. Appl. Radiat. Isot. **25** (1974) 535.
[113] MICHEL, R., GALAS, M., Int. J. Appl. Radiat. Isot. **34** (1983) 1325.
[114] DIMBYLOW, P.J., National Radiological Protection Board, Harwell, UK, Rep. NRPB-R78 (1978).

3-2. ACTIVATION CROSS-SECTIONS FOR ELEMENTS FROM LITHIUM TO SULPHUR

P. ALBERT, G. BLONDIAUX, J.L. DEBRUN,
A. GIOVAGNOLI, M. VALLADON
Centre d'études et de recherches par irradiations,
Centre national de la recherche scientifique,
Orléans, France

Abstract

ACTIVATION CROSS-SECTIONS FOR ELEMENTS FROM LITHIUM TO SULPHUR.

The paper presents cross-sections for nuclear reactions yielding radioisotopes. Since the presentation is restricted to light elements (up to sulphur included), cross-sections for reactions with heavy ions are of interest and have been included.

1. INTRODUCTION

This chapter presents the cross-sections for those nuclear reactions that yield radioisotopes. Since this compilation is restricted to light elements (up to sulphur included), the cross-sections for reactions with heavy ions are of interest and have been included. For various reasons, a number of reactions are missing. More data, on these and on the reactions presented, can be found in Refs [1, 2].

LITHIUM

Protons	^{14}N Curves in Figure 1 (d)
$^{7}Li(p,n)^{7}Be$ Figure 1	$^{6}Li(^{14}N,\alpha n)^{15}O$
	$^{6}Li(^{14}N,pn)^{18}F$
	$^{7}Li(^{14}N,\alpha 2n)^{15}O$
	$^{7}Li(^{14}N,p2n)^{18}F$

BERYLLIUM

Helium 3	Helium 4	^{14}N	^{16}O	^{18}O	^{19}F
$^{9}Be(^{3}He,n)^{11}C$ Figure 2	$^{9}Be(\alpha,2n)^{11}C$ Figure 2	$^{9}Be(^{14}N,\alpha n)^{18}F$ Figure 5	$^{9}Be(^{16}O,p)^{24}Na$ Figure 3	$^{9}Be(^{18}O,2\alpha)^{19}O$ Figure 4	$^{9}Be(^{19}F,2\alpha)^{20}F$ Figure 3
		$^{9}Be(^{14}N,^{13}N)^{10}Be$ Figure 6	$^{9}Be(^{16}O,2n)^{23}Mg$ Figure 3	$^{9}Be(^{18}O,p2n)^{24}Na$ Figure 4	$^{9}Be(^{19}F,p\alpha)^{23}Ne$ Figure 3
				$^{9}Be(^{18}O,pn)^{25}Na$ Figure 4	$^{9}Be(^{19}F,2n)^{26}Al$ Figure 3

Protons	Deuterons	Helium 3	^{14}N All curves Figure 9	^{16}O All curves Figure 3	^{18}O All curves Figure 4	^{19}F All curves Figure 10
$^{11}B(p,n)^{11}C$ Figure 7	$^{10}B(d,n)^{11}C$ Figure 7	$^{11}B(^{3}He,p2n)^{11}C$ Figure 8	$^{10}B(^{14}N,^{15}O)^{9}Be$	$^{10}B(^{16}O,2\alpha)^{18}F$	$^{11}B(^{18}O,2\alpha)^{21}F$	$^{10}B(^{19}F,^{18}F)^{11}B$
	$^{11}B(d,2n)^{11}C$ Figure 7	$^{10}B(^{3}He,pn)^{11}C$ Figure 8	$^{10}B(^{14}N,^{18}F)^{6}Li$	$^{10}B(^{16}O,n\alpha)^{21}Na$	$^{11}B(^{18}O,p\alpha)^{24}Ne$	$^{10}B(^{19}F,^{18}O)^{11}C$
		$^{11}B(^{3}He,n)^{13}N$ Figure 8	$^{10}B(^{14}N,^{11}C)^{13}C$	$^{10}B(^{16}O,2p)^{24}Na$	$^{11}B(^{18}O,n\alpha)^{24}Na$	$^{10}B(^{19}F,\alpha p)^{24}Na$
			$^{10}B(^{14}N,^{13}N)^{11}B$		$^{11}B(^{18}O,\alpha)^{25}Na$	
			$^{11}B(^{14}N,p)^{24}Na$		$^{11}B(^{18}O,np)^{27}Mg$	
					$^{11}B(^{18}O,3n)^{26}Al$	
					$^{10}B(^{18}O,2\alpha)^{20}F$	

CARBON

Protons	Deuterons	Helium 3	Helium 4	^{14}N	^{16}O	^{18}O	^{19}F All curves Figure 10
$^{12}C(p,pn)^{11}C$ Figure 11	$^{12}C(d,n)^{13}N$ Figure 12	$^{12}C(^{3}He,n)^{14}O$ Figure 13	$^{12}C(\alpha,n)^{15}O$ Figure 16	$^{12}C(^{14}N,\alpha)^{22}Na$ Figure 17	$^{12}C(^{16}O,n)^{27}Si$ Figure 3	$^{12}C(^{18}O,p)^{29}Al$ Figure 19	$^{12}C(^{19}F,2p)^{29}Al$
		$^{12}C(^{3}He,\alpha)^{11}C$ Figures 13 and 14		$^{12}C(^{14}N,2p)^{24}Na$ Figure 17		$^{12}C(^{18}O,pn)^{28}Al$ Figure 19	$^{12}C(^{19}F,^{18}F)^{13}C$
		$^{12}C(^{3}He,d)^{13}N$ Figure 15		$^{12}C(^{14}N,2\alpha)^{18}F$ Figures 5 and 17			$^{13}C(^{19}F,2\alpha)^{24}Na$
				$^{12}C(^{14}N,^{13}N)^{13}C$ Figure 18			

NITROGEN

Protons	Helium 3	Helium 4
$^{14}N(p,\alpha)^{11}C$ Figure 20	$^{14}N(^{3}He,pn)^{15}O$ Figure 23	$^{14}N(\alpha,n)^{17}F$ Figure 22
$^{14}N(p,2\alpha)^{7}Be$ Figure 20	$^{14}N(^{3}He,\alpha)^{13}N$ Figure 23	
$^{14}N(p,n)^{14}O$ Figure 21		

OXYGEN

Protons	Deuterons	Tritons	Helium 3 All curves Figure 27	Helium 4	^{14}N
$^{16}O(p,\alpha)^{13}N$ Figure 24	$^{16}O(d,n)^{17}F$ Figure 25	$^{16}O(t,n)^{18}F$ Figure 26	$^{16}O(^{3}He,X)^{18}F$	$^{16}O(\alpha,X)^{18}F$ Figure 28	$^{16}O(^{14}N,2p)^{28}Al$ Figure 29
	$^{16,17,18}O(d,X)^{18}F$ Figure 25		$^{16}O(^{3}He,\alpha)^{15}O$		$^{16}O(^{14}N,^{18}F)^{12}C$ Figure 29
			$^{16}O(^{3}He,2\alpha)^{11}C$		
			$^{16}O(^{3}He,\alpha n)^{14}O$		
			$^{16}O(^{3}He,pn)^{17}F$		

FLUORINE

Deuterons	Tritons	Helium 3	Helium 4	^{14}N	^{19}F
$^{19}F(d,dn)^{18}F$ Figure 25	$^{19}F(t,d)^{20}F$ Figure 30	$^{19}F(^{3}He,\alpha)^{18}F$ Figure 31	$^{19}F(\alpha,n)^{22}Na$ Figure 31	$^{19}F(^{14}N,^{15}N)^{18}F$ Figure 32	$^{19}F(^{19}F,^{18}F)^{20}F$ Figure 33
	$^{19}F(t,p)^{21}F$ Figure 30	$^{19}F(^{3}He,2p)^{20}F$ Figure 31		$^{19}F(^{14}N,p2n)^{30}P$ Figure 32	

NEON

Deuterons	Helium 3
$^{20}Ne(d,\alpha)^{18}F$ Figure 29	$^{20}Ne(^{3}He,X)^{18}F$ Figure 29

SODIUM

Deuterons	Tritons	Helium 3	^{14}N	^{18}O All curves Figure 4	^{19}F
$^{23}Na(d,p)^{24}Na$ Figure 34	$^{23}Na(t,p)^{25}Na$ Figure 30	$^{23}Na(^{3}He,2p)^{24}Na$ Figure 35	$^{23}Na(^{14}N,^{13}N)^{24}Na$ Figure 6	$^{23}Na(^{18}O,3n)^{38}K$	$^{23}Na(^{19}F,^{18}F)^{24}Na$ Figure 33
				$^{23}Na(^{18}O,^{17}O)^{24}Na$	
				$^{23}Na(^{18}O,^{16}O)^{25}Na$	

MAGNESIUM

Protons	Deuterons	Tritons	Helium 3	Helium 4	^{14}N Curves in Figure 6
$Mg(p,xn)^{26}Al$ Figure 36	$^{26}Mg(d,p)^{27}Mg$ Figure 34	$^{26}Mg(t,p)^{28}Mg$ Figure 37	$^{26}Mg(^{3}He,p)^{28}Al$ Figure 39	$^{26}Mg(\alpha,2p)^{28}Mg$ Figures 37 and 40	$^{24}Mg(^{14}N,^{13}N)^{25}Mg$
$Mg(p,\alpha xn)^{22}Na$ Figure 36		$Mg(t,\alpha xn)^{24}Na$ Figure 37	$^{26}Mg(^{3}He,2p)^{27}Mg$ Figure 39	$Mg(\alpha,\alpha pxn)^{24}Na$ Figure 37	$^{25}Mg(^{14}N,^{13}N)^{26}Mg$
		$Mg(t,x)^{27}Mg$ Figure 38	$Mg(^{3}He,X)^{24}Na$ Figure 39	$^{26}Mg(\alpha,p)^{29}Al$ Figure 40	$^{26}Mg(^{14}N,^{13}N)^{27}Mg$
		$^{26}Mg(t,n)^{28}Al$ Figure 38			
		$^{24}Mg(t,n)^{26m}Al$ Figure 38			

ALUMINIUM

Protons Curves in Figure 36	Tritons	Helium 3 Curves in Figure 43	Helium 4	^{12}C Curves in Figure 45	^{14}N	^{16}O Curves in Figure 45
$^{27}Al(p,pn)^{26}Al$	$^{27}Al(t,\alpha pn)^{24}Na$ Figure 37	$^{27}Al(^{3}He,2\alpha)^{22}Na$	$^{27}Al(\alpha,4p5n)^{22}Na$ Figure 41	$^{27}Al(^{12}C,X)^{18}F$	$^{27}Al(^{14}N,X)^{18}F$ Figure 45	$^{27}Al(^{16}O,X)^{24}Na$
$^{27}Al(p,\alpha pn)^{22}Na$	$^{27}Al(t,2p)^{28}Mg$ Figure 37	$^{27}Al(^{3}He,\alpha 2p)^{24}Na$	$^{27}Al(\alpha,X)^{24}Na$ figures 37 and 41	$^{27}Al(^{12}C,X)^{24}Na$	$^{27}Al(^{14}N,X)^{24}Na$ Figure 45	$^{27}Al(^{16}O,X)^{18}F$
	$^{27}Al(t,d)^{28}Al$ Figure 42	$^{27}Al(^{3}He,3p)^{27}Mg$	$^{27}Al(\alpha,3p)^{28}Mg$ Figures 37 and 41	$^{27}Al(^{12}C,X)^{32}P$	$^{27}Al(^{14}N,p2n)^{38}K$ Figure 32	
	$^{27}Al(t,p)^{29}Al$ Figure 42	$^{27}Al(^{3}He,2p)^{28}Al$	$^{27}Al(\alpha,n)^{30}P$ Figure 44	$^{27}Al(^{12}C,X)^{34m}Cl$		

SILICON

Protons	Tritons All curves in Figure 47	Helium 3	Helium 4
$^{30}Si(p,3p)^{28}Mg$ Figure 48	$^{30}Si(t,\alpha)^{29}Al$	$^{28}Si(^{3}He,p)^{30}P$ Figure 46	$^{28}Si(\alpha,d)^{30}P$ Figure 46
$Si(p,4pxn)^{24}Na$ Figure 48	$^{29}Si(t,\alpha)^{28}Al$		
$Si(p,X)^{26}Al$ Figure 36	$^{28}Si(t,n)^{30}P$		
$Si(p,X)^{22}Na$ Figure 36			

PHOSPHORUS

Protons	Helium 4	^{14}N
$^{31}P(p,pn)^{30}P$ Figure 44	$^{31}P(\alpha,n)^{34m}Cl$ Figure 49	$^{31}P(^{14}N,pn)^{43}Sc$ Figure 50
$^{31}P(p,4p)^{28}Mg$ Figure 48		$^{31}P(^{14}N,p)^{44}Sc$ Figure 50
$^{31}P(p,5p3n)^{24}Na$ Figure 48		$^{31}P(^{14}N,p)^{44m}Sc$ Figure 50
		$^{31}P(^{14}N,p)^{44}Sc$ Figure 50
		$^{31}P(^{14}N,^{13}N)^{32}P$ Figure 51

SULPHUR

Protons	Deuterons	^{14}N
$^{34}S(p,n)^{34m}Cl$ Figure 49	$^{32}S(d,\alpha)^{30}P$ Figure 46	$^{32}S(^{14}N,p)^{45}Ti$ Figure 52
$S(p,5pxn)^{28}Mg$ Figure 48		$^{32}S(^{14}N,2p)^{44}Sc$ Figures 50 and 52
$S(p,6pxn)^{24}Na$ Figure 48		$^{32}S(^{14}N,2p)^{44m}Sc$ Figures 50 and 52
		$^{32}S(^{14}N,2pn)^{43}Sc$ Figures 50 and 52
		$^{32}S(^{14}N,2\alpha)^{38m}K$ Figure 52
		$^{32}S(^{14}N,^{13}N)^{33}S$ Figure 52

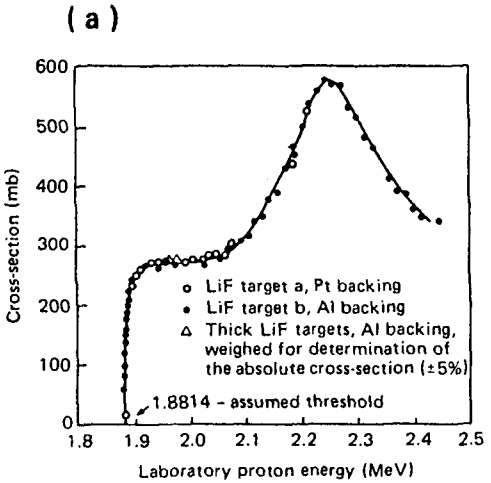
(a)
Cross-section (mb)
600
500
400
300
200
100
0
1.8
1.9
2.0
2.1
2.2
2.3
2.4
2.5
Laboratory proton energy (MeV)
o LiF target a, Pt backing
• LiF target b, Al backing
Δ Thick LiF targets, Al backing, weighed for determination of the absolute cross-section (±5%)
1.8814 - assumed threshold

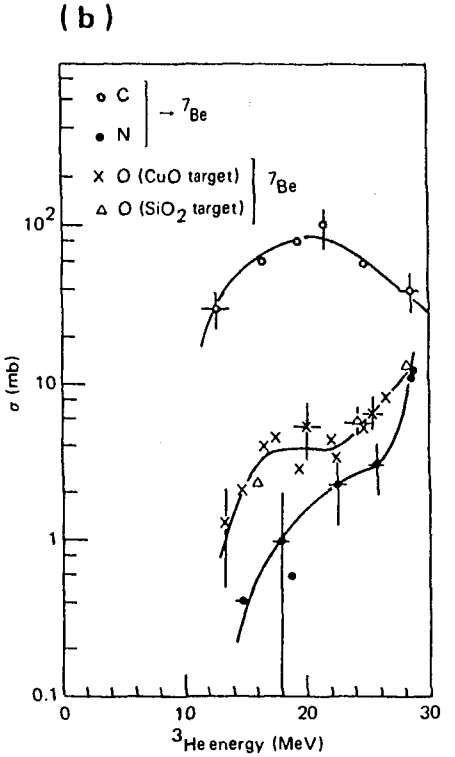
(b)
o C
• N
→ 7Be
x O (CuO target)
Δ O (SiO2 target)
7Be
10^2
10
1
0.1
σ (mb)
0
10
20
30
3He energy (MeV)

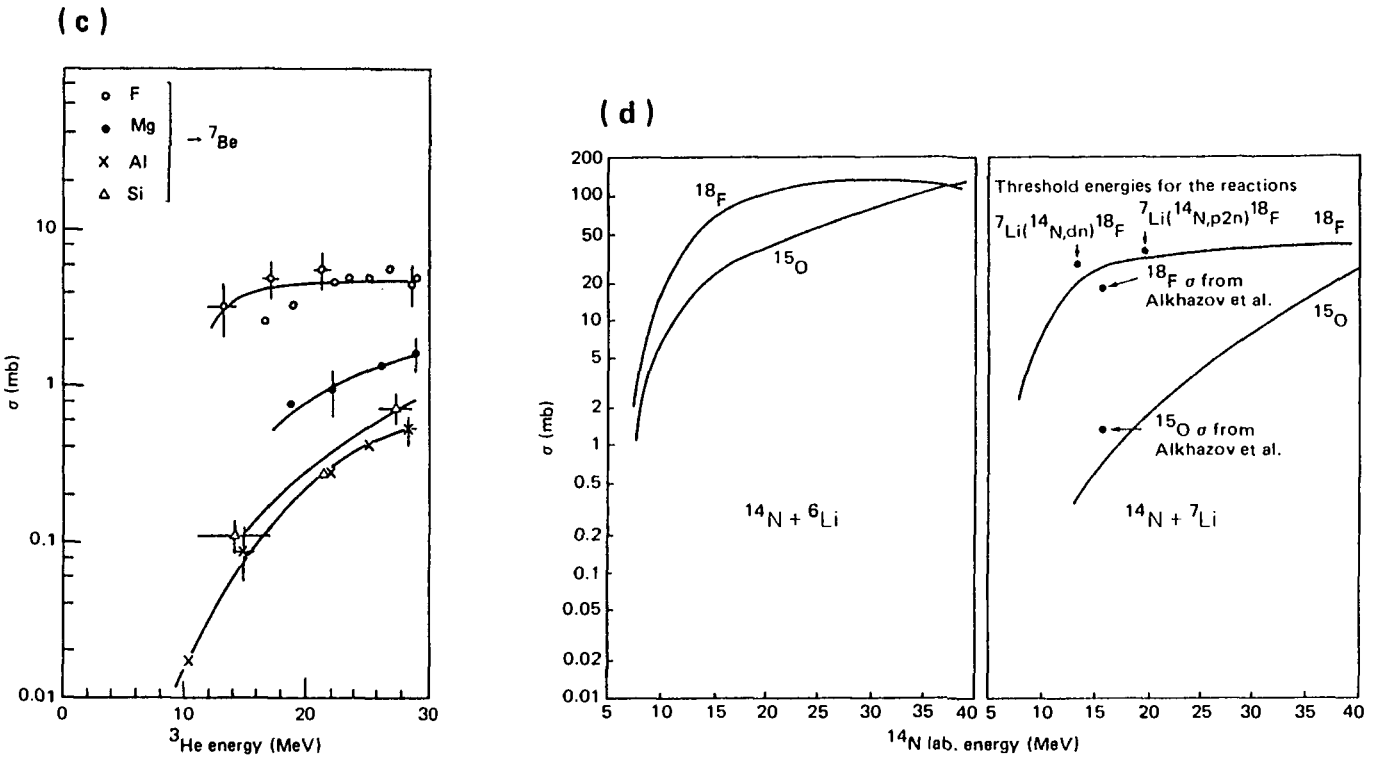

FIG. 1. Production of ^{7}Be by proton irradiation of (a) ^{7}Li [3] and (b, c) ^{3}He irradiation of C, N, O, F, Mg, Al and Si [4]. (d) Production of ^{15}O and ^{18}F by irradiation of ^{6}Li and ^{7}Li with ^{14}N [5]. (References within figures can be found in the original source.)

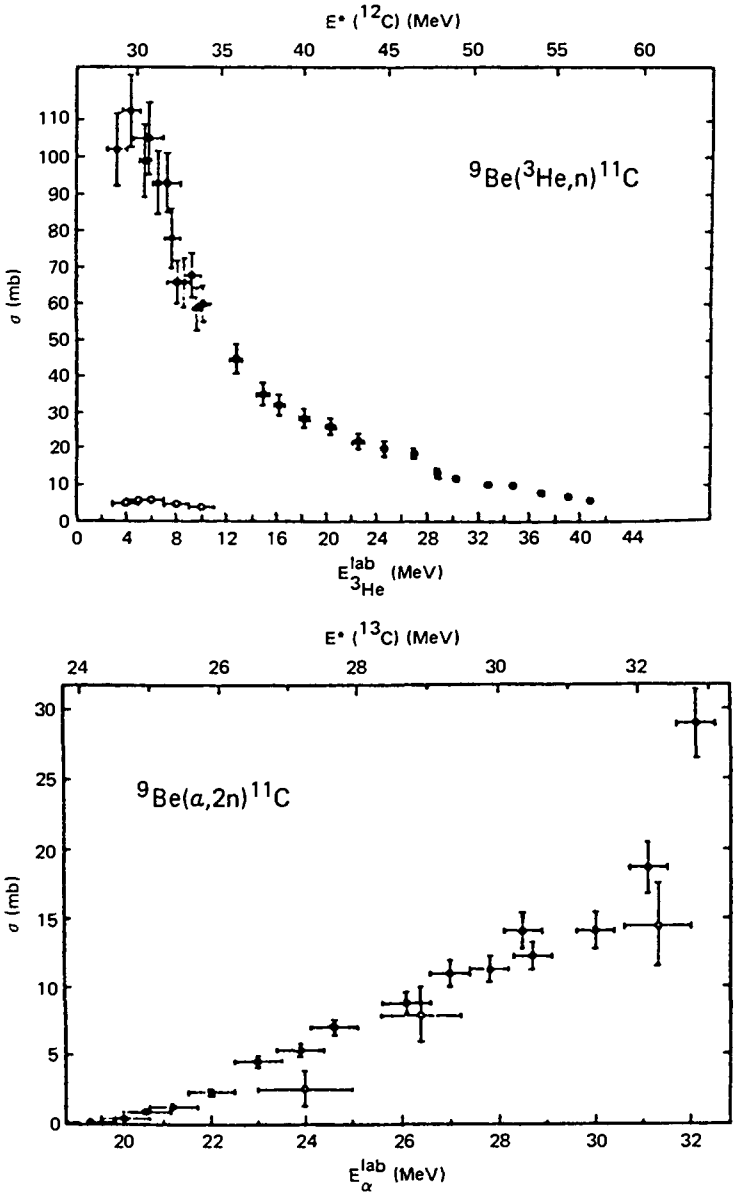

FIG. 2. Production of ^{11}C by irradiation of Be with ^{4}He and ^{3}He (upper horizontal scales represent the excitation energies of the compound nuclei) [6].

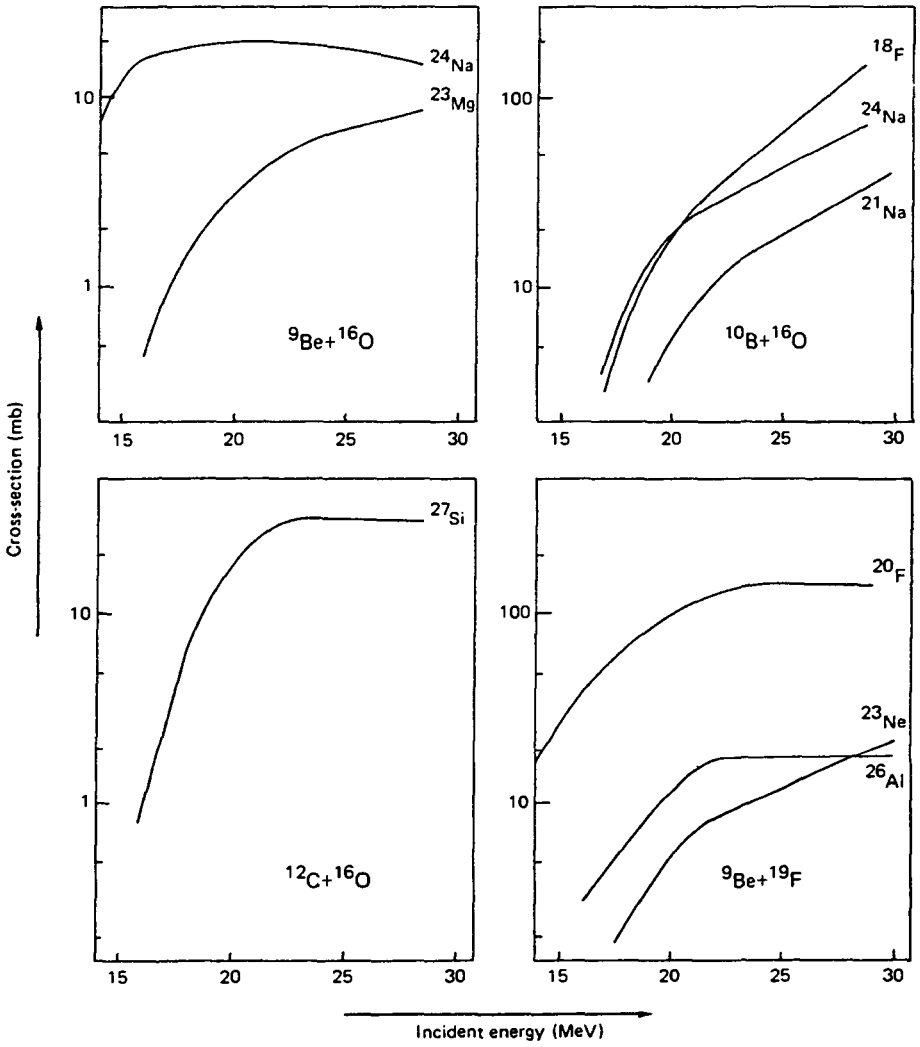

FIG. 3. Reactions of ^{16}O on ^{9}Be, ^{10}B and ^{12}C, and of ^{19}F on Be [7].

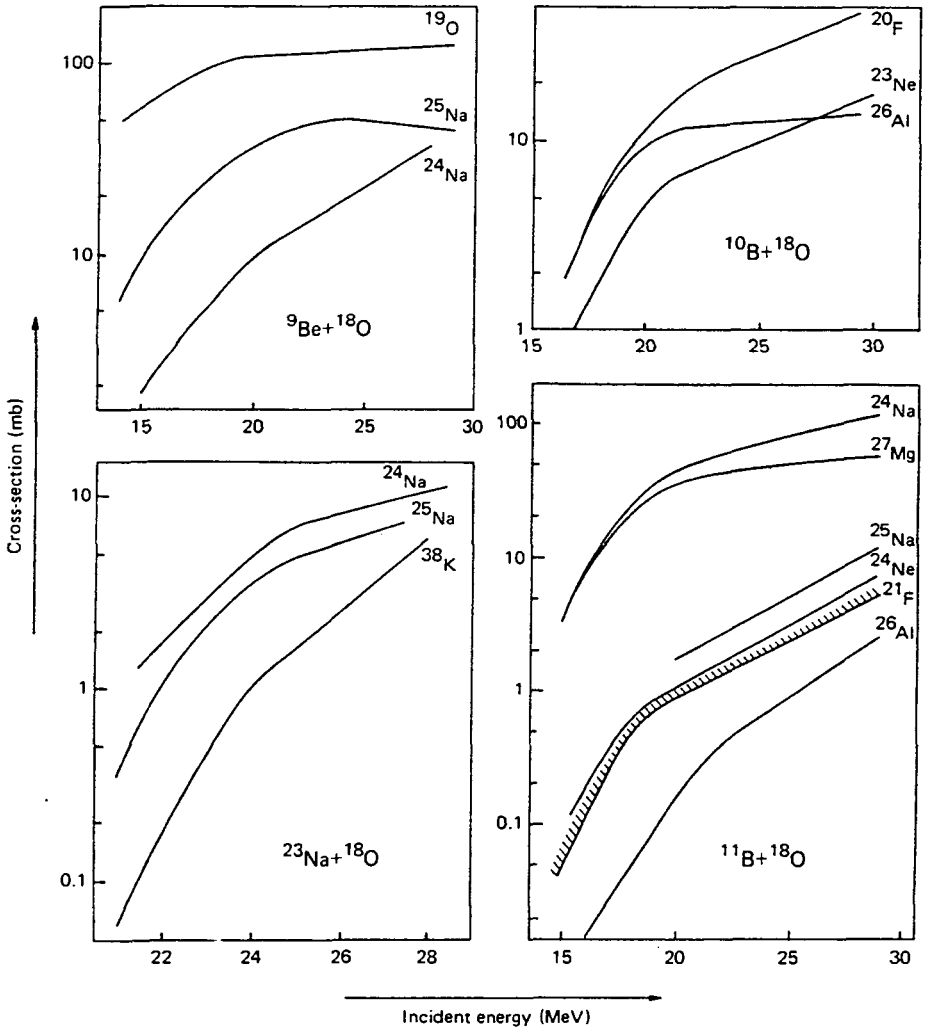

FIG. 4. Reactions of ^{18}O on ^{9}Be, ^{10}B, ^{11}B and ^{23}Na [7].

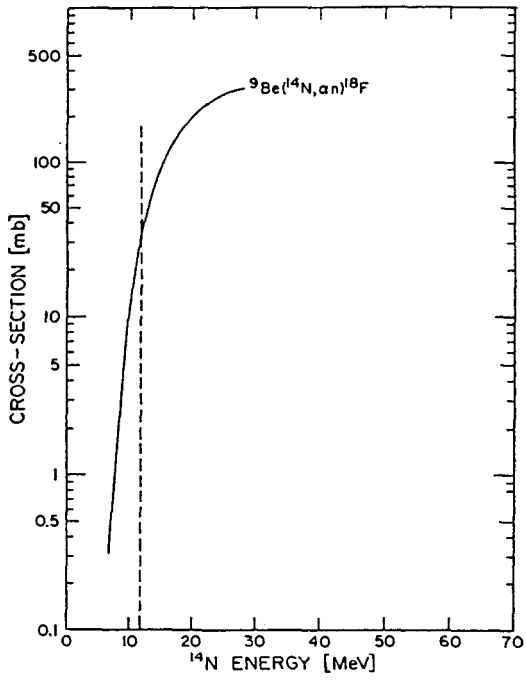

FIG. 5. Production of ^{18}F by irradiation of Be with ^{14}N [8].

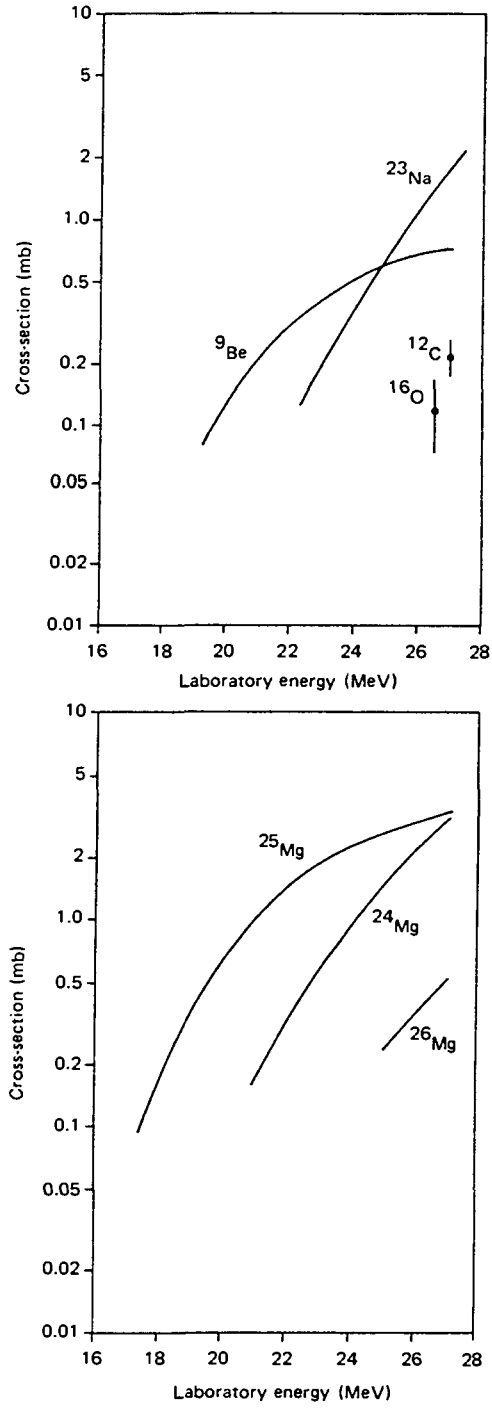

FIG. 6. (^{14}N, ^{13}N) reactions on ^{9}Be, ^{12}C, ^{16}O, ^{23}Na, ^{24}Mg, ^{25}Mg and ^{26}Mg [9].

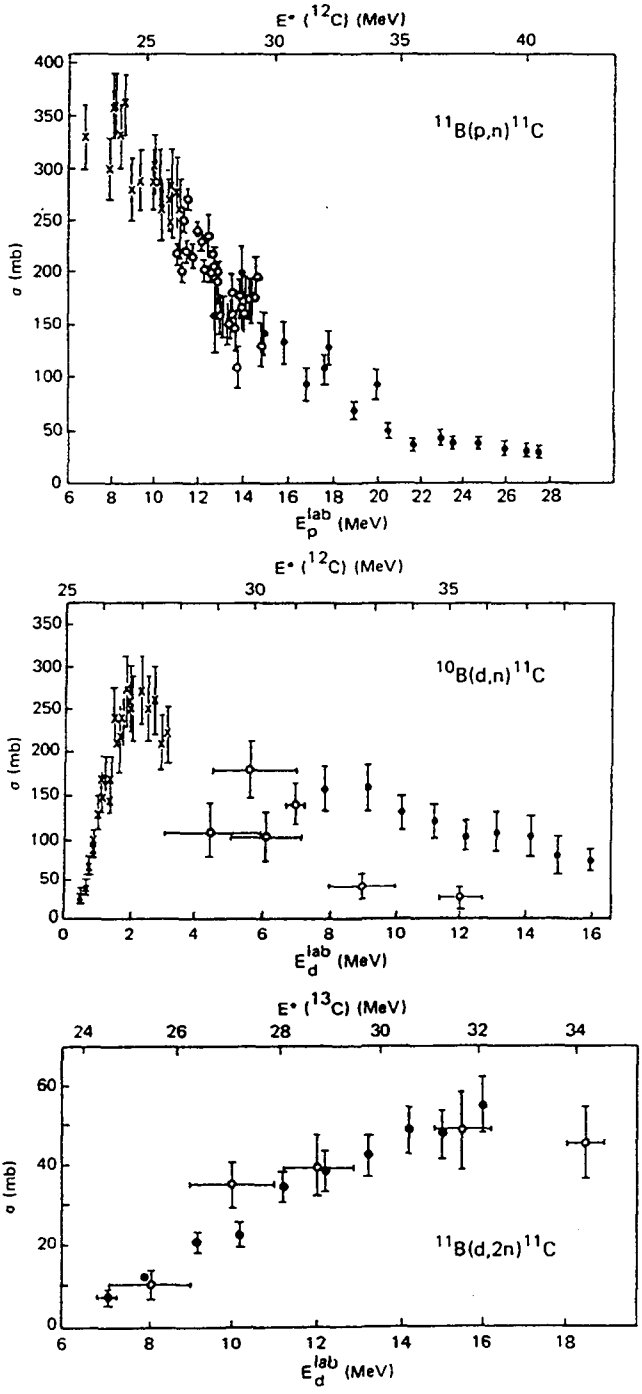

FIG. 7. Reactions producing ^{11}C by irradiation of boron with protons and deuterons (upper horizontal scale is the excitation energy of the compound nucleus) [6].

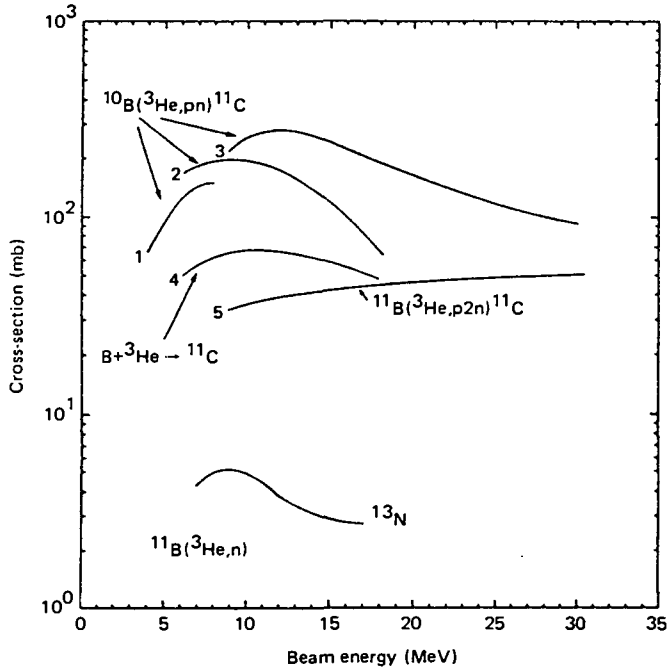

FIG. 8. Activation of B by irradiation with ^3He. (Curves from three different sources are given for ^{10}B (^3He, pn) ^{11}C. References for the curves are in Ref. [10].)

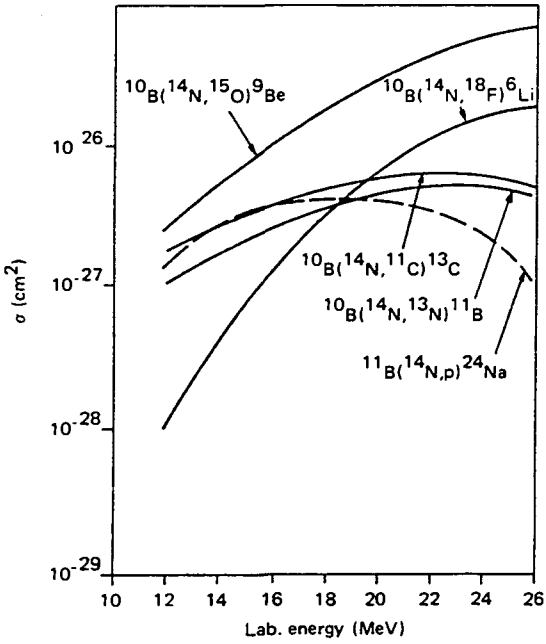

FIG. 9. Reactions induced on ^{10}B and ^{11}B by ^{14}N [11].

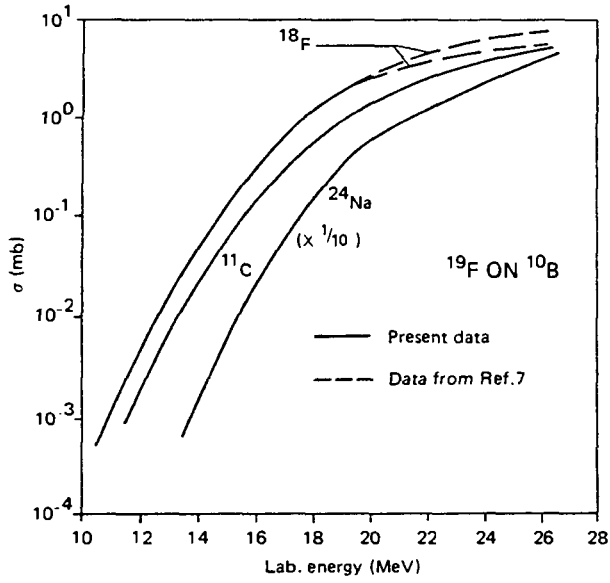

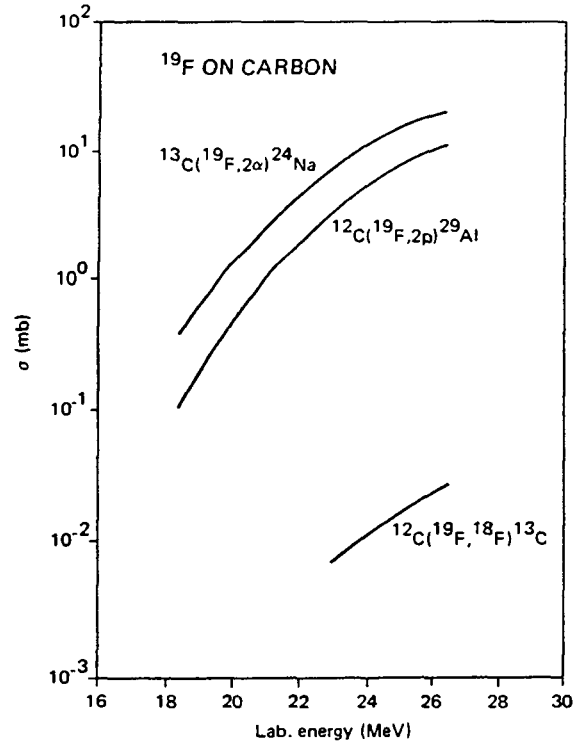

FIG. 10. Reaction of ^{19}F on ^{10}B, ^{12}C and ^{13}C [12]. (Reference within the figure can be found in the original source.)

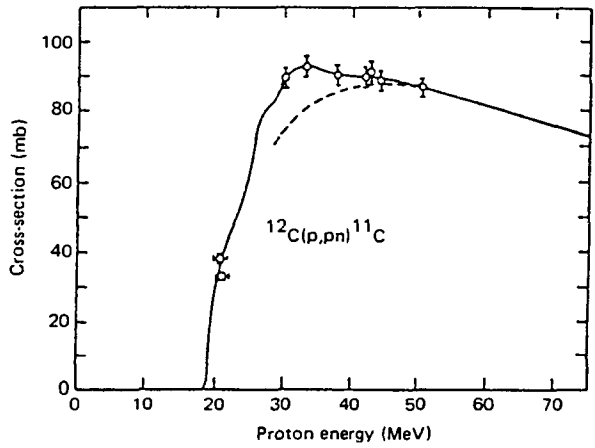

FIG. 11. The $^{12}C(p, pn)^{11}C$ reaction [13].

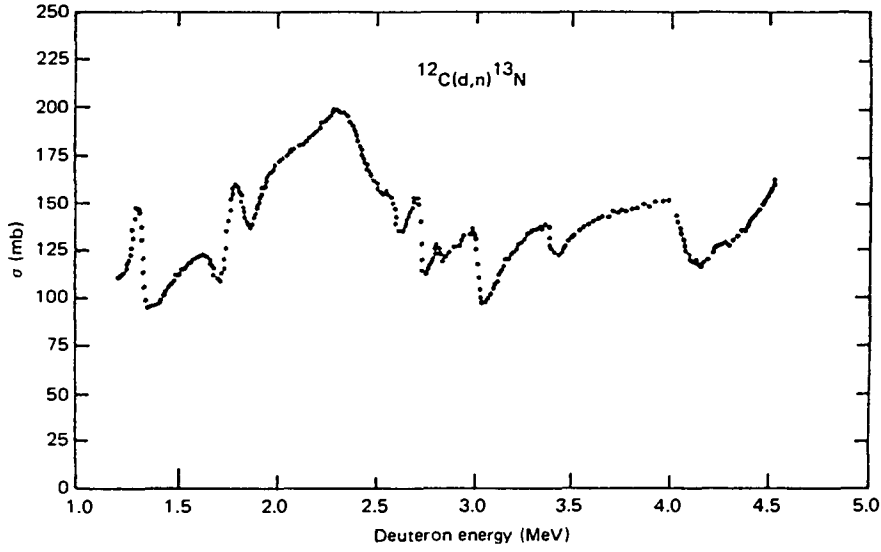

FIG. 12. The $^{12}C(d, n)^{13}N$ reaction [14].

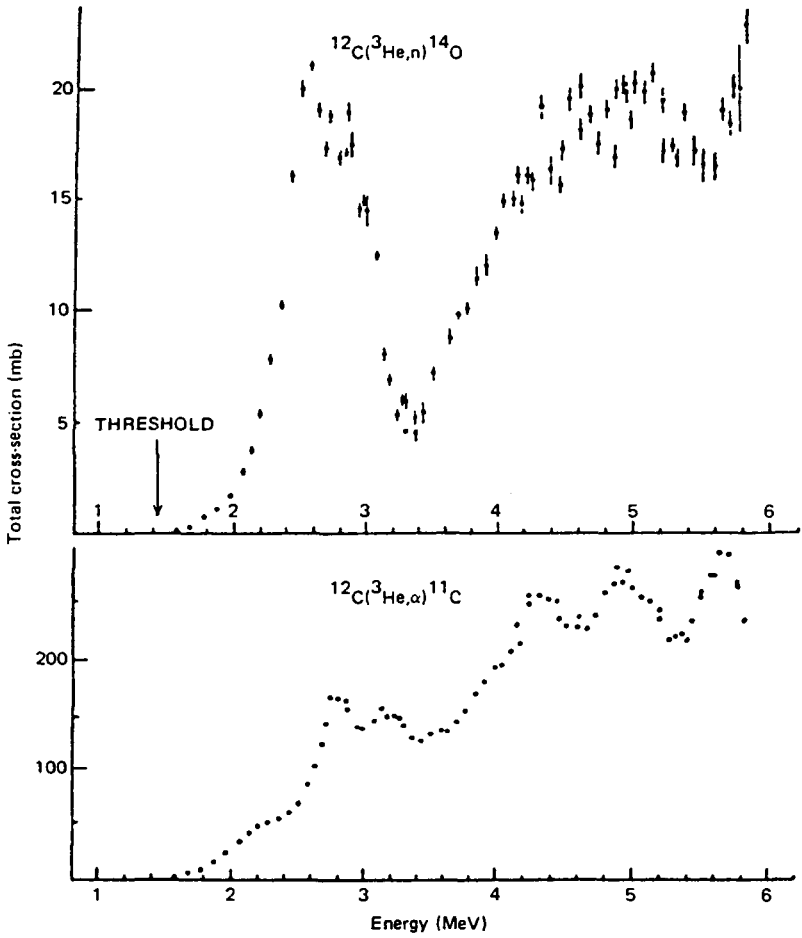

FIG. 13. Excitation functions for the $^{12}C(^3He, \alpha)^{11}C$ and $^{12}C(^3He, n)^{14}O$ reactions. The error in the absolute cross-section is estimated to be ±15% [15].

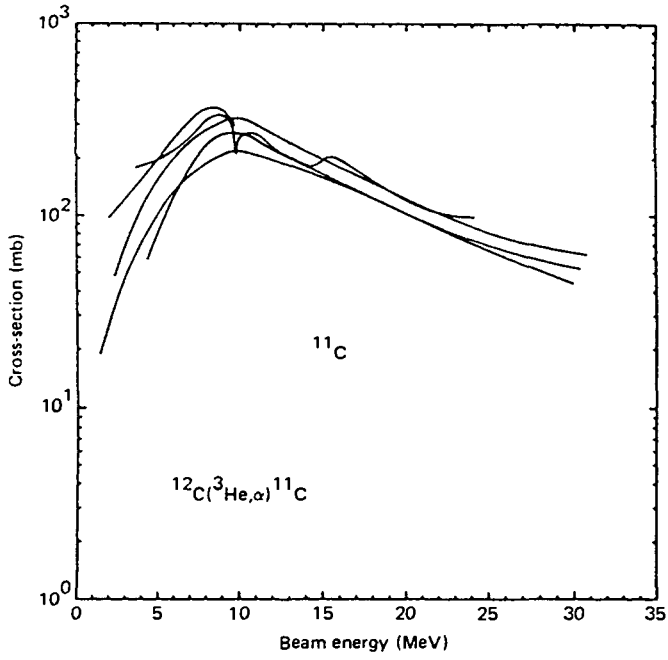

FIG. 14. Various curves for the $^{12}C(^3He, \alpha)^{11}C$ reaction [10].

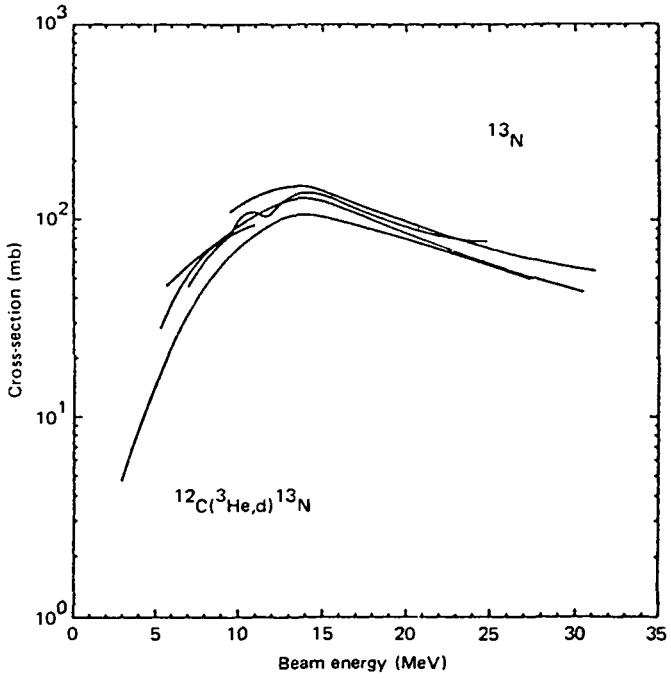

FIG. 15. Different experimental curves for the $^{12}C(^3He, d)^{13}N$ reaction [10].

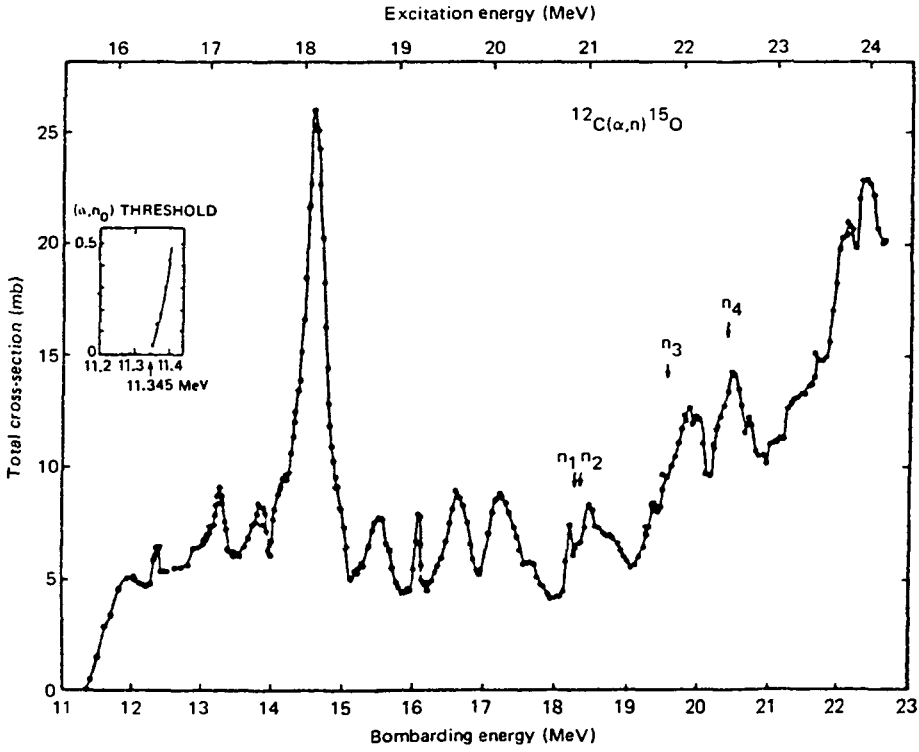

FIG. 16. The excitation function of the total neutron cross-section for the $^{12}C(\alpha, n)^{15}O$ reaction [16].

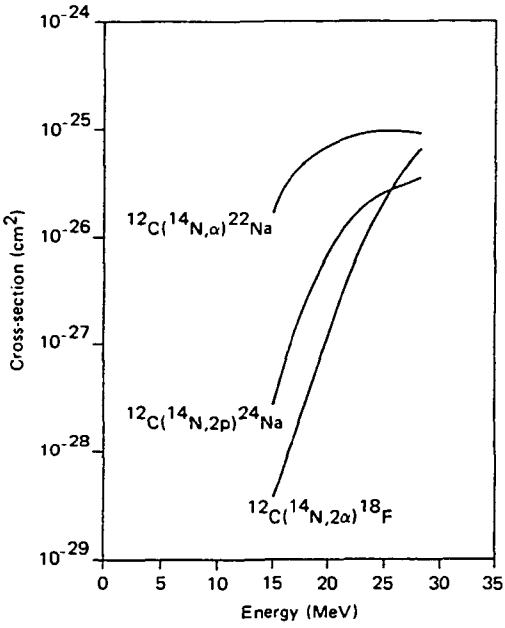

FIG. 17. Reaction of ^{12}C with ^{14}N ions [17].

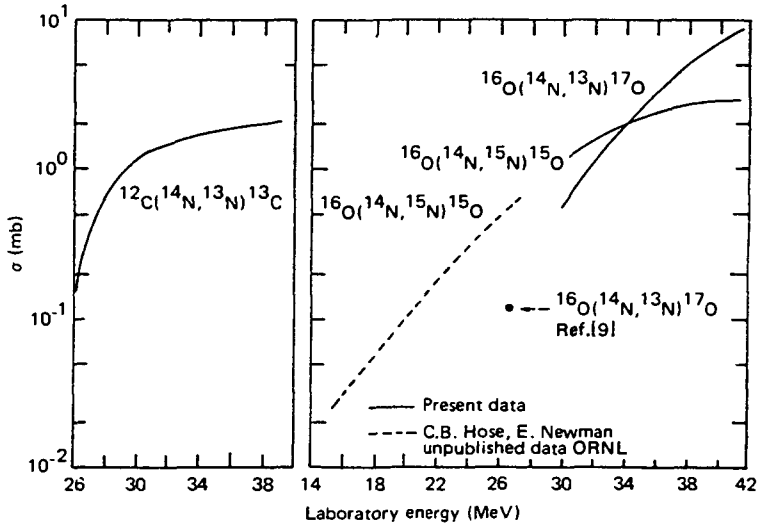

FIG. 18. Reaction of ^{14}N with ^{12}C and ^{16}O. Details on the ORNL data can be found in Ref. [5].

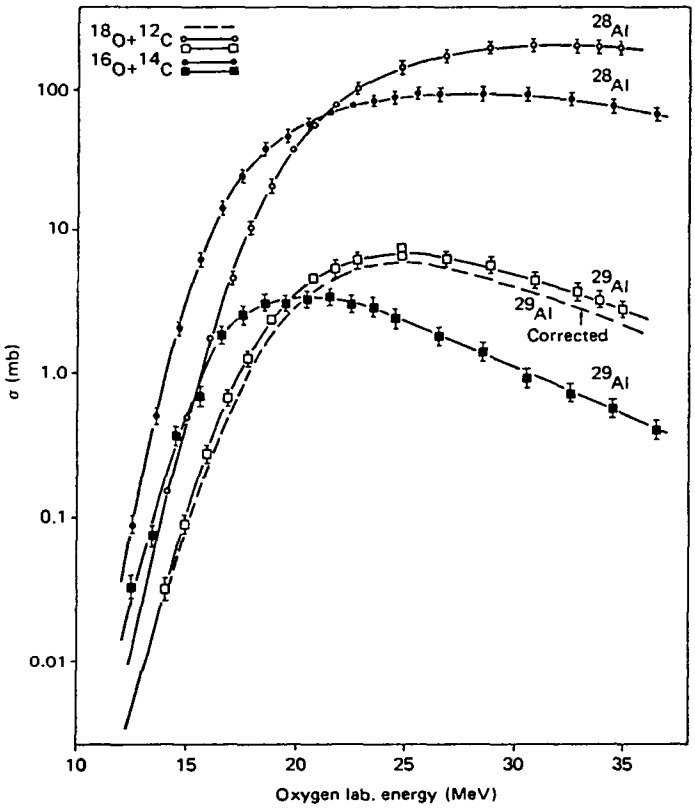

FIG. 19. Production of ^{28}Al and ^{29}Al by irradiation of ^{12}C with ^{18}O, and of ^{14}C by ^{16}O [18].

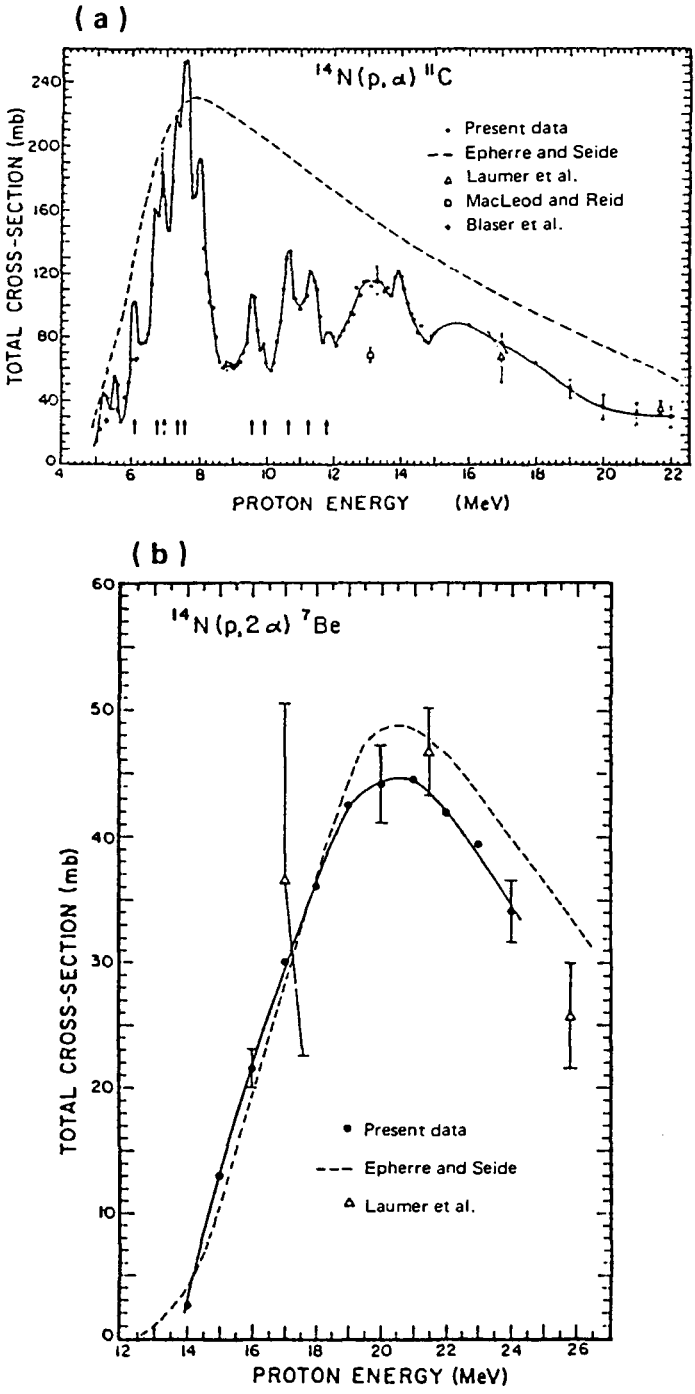

FIG. 20. Production of (a) ^{11}C and (b) ^{7}Be by irradiation of ^{14}N with protons [19]. *(References within figures can be found in original source.)*

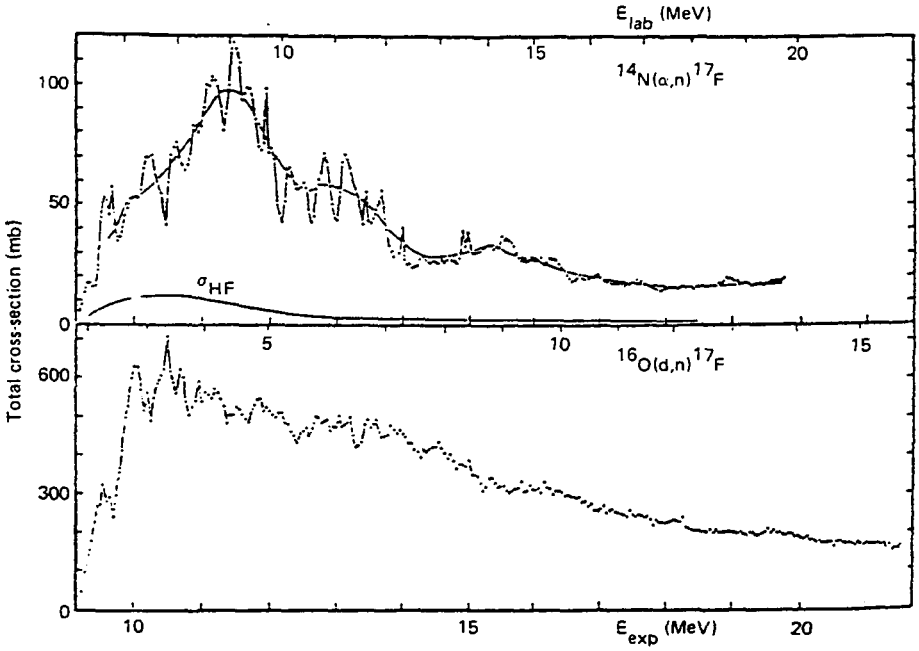

FIG. 21. Production of ^{17}F by irradiation of ^{14}N with ^{4}He, and of ^{16}O with deuterons (σ_{HF} = calculation from Hauser-Feshbach theory) [20].

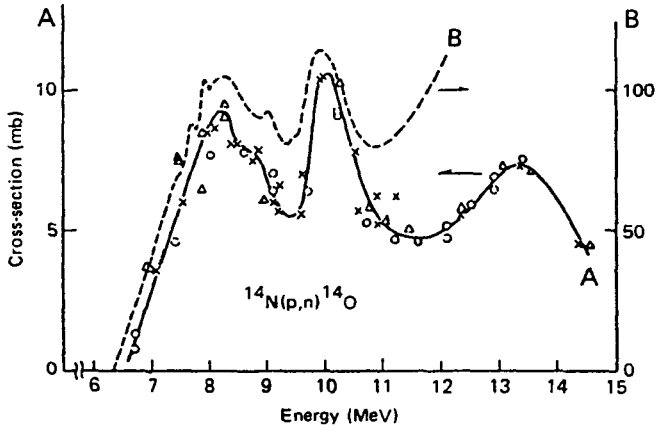

FIG. 22. The $^{14}N(p, n)^{14}O$ reaction. Curve A: Ref. [21]; *curve B: Ref.* [22].

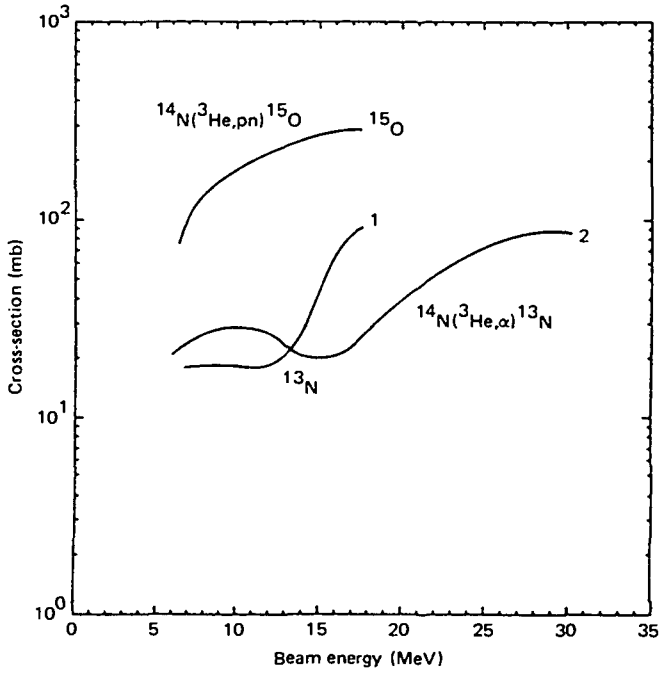

FIG. 23. Production of ^{15}O and ^{13}N (curves 1 and 2) by irradiation of ^{14}N with ^3He [10].

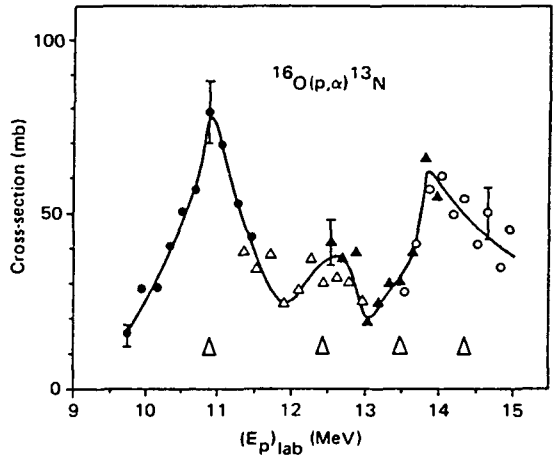

FIG. 24. The $^{16}O(p, \alpha)^{13}N$ reaction [23].

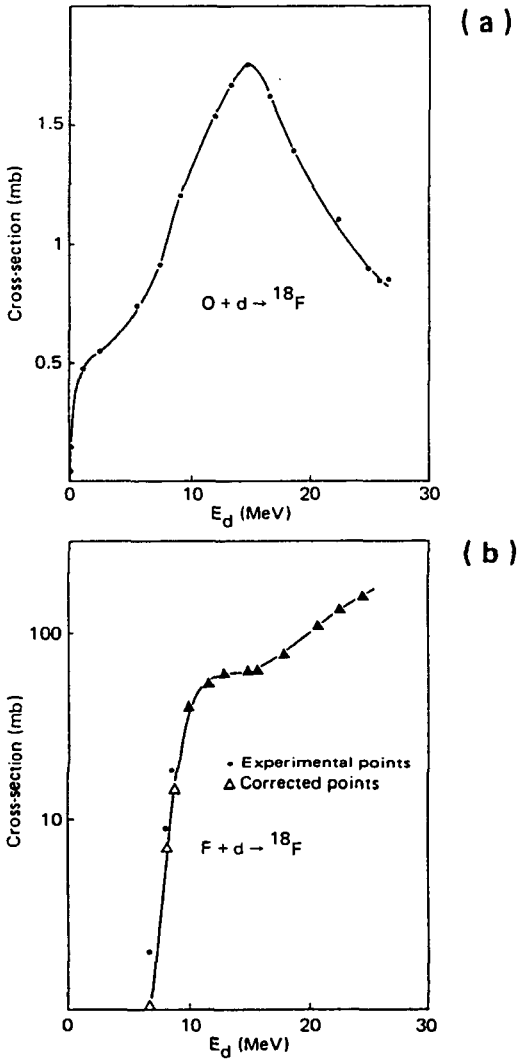

FIG. 25. Production of ^{18}F by irradiation of (a) oxygen and (b) fluorine with deuterons [24].

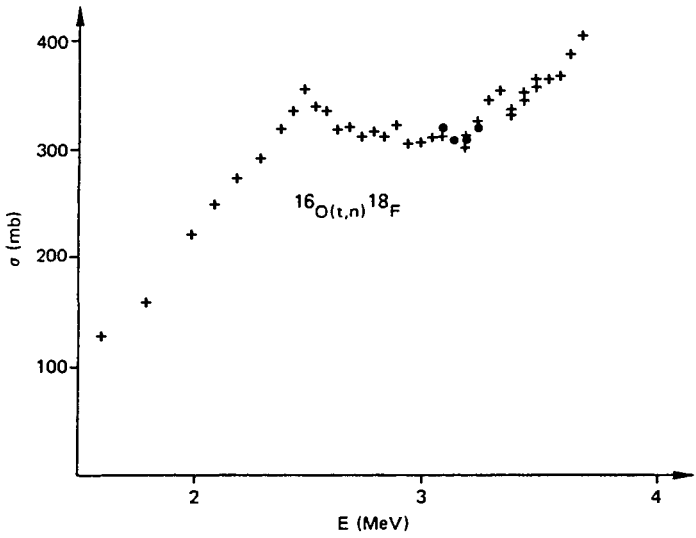

FIG. 26. Production of ^{18}F by bombardment of oxygen with tritons [25].

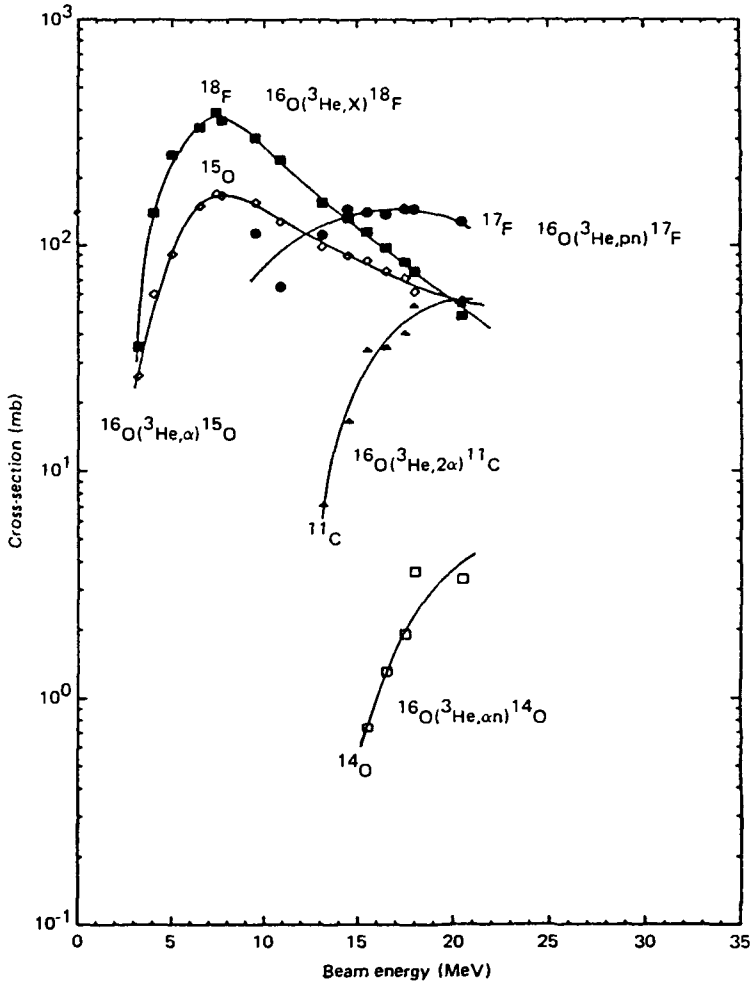

FIG. 27. Production of various radioisotopes by bombardment of oxygen with ^{3}He [10].

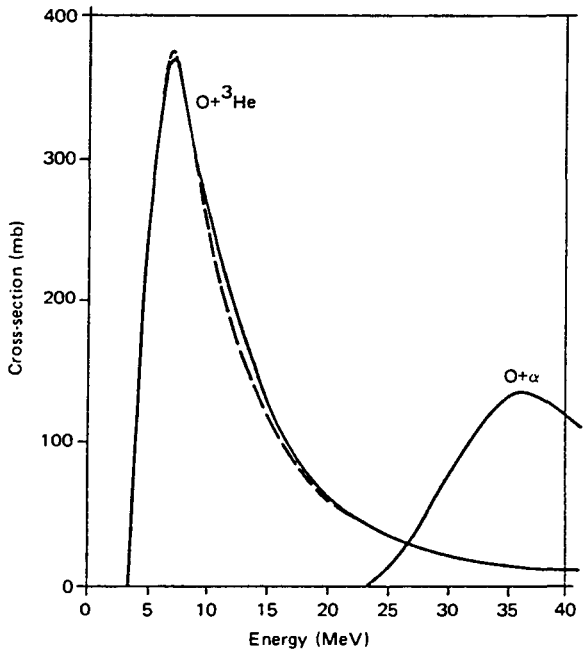

FIG. 28. Production of ^{18}F by the $^{16}O(^{3}He, X)^{18}F$ and $^{16}O(\alpha, X)^{18}F$ reactions [26].

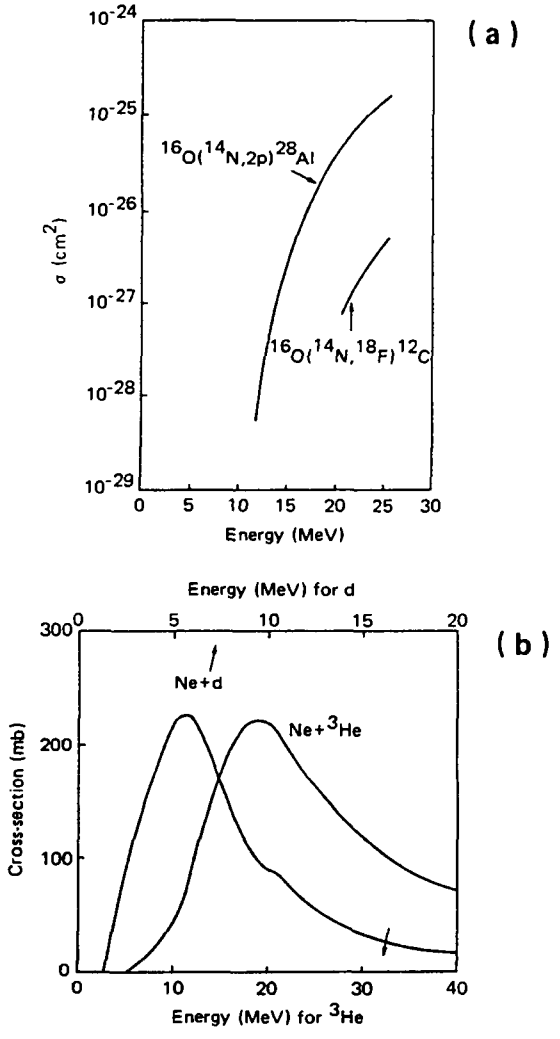

FIG. 29. (a) Production of ^{28}Al and ^{18}F by irradiation of ^{16}O with ^{14}N [11]; (b) production of ^{18}F by irradiation of Ne with ^3He and deuterons [26].

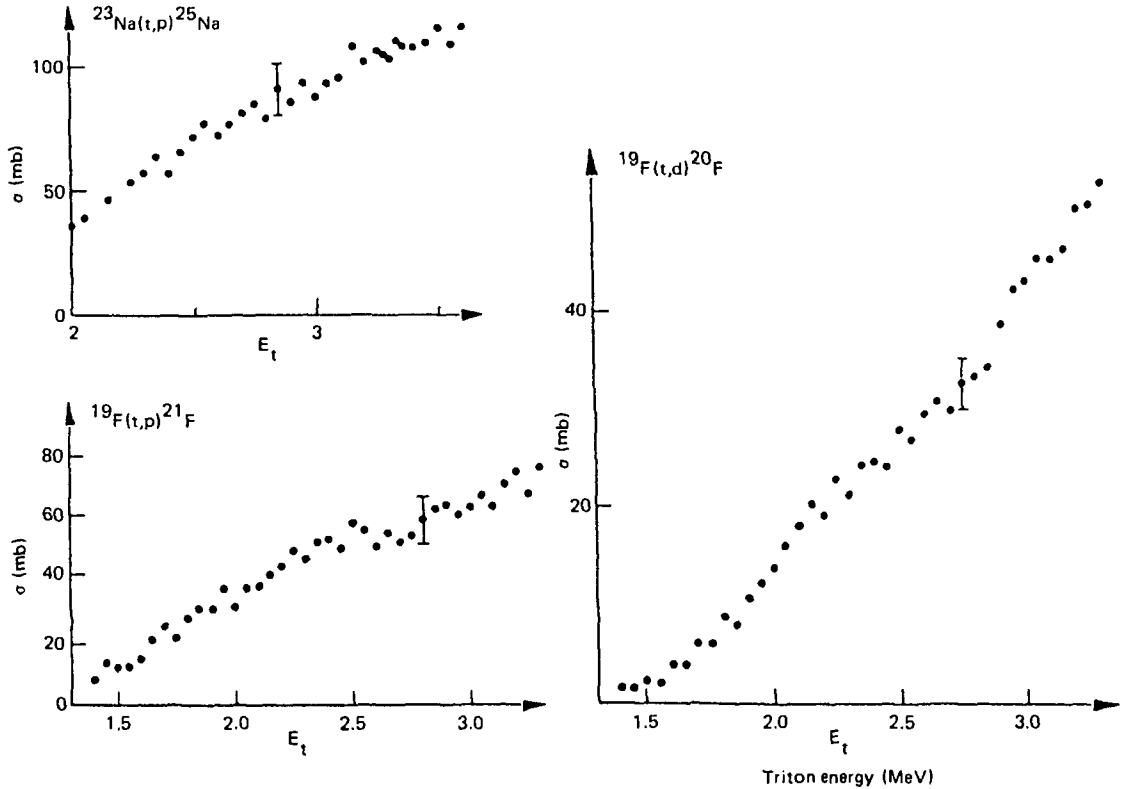

FIG. 30. Reactions with ^{19}F and ^{23}Na induced by low energy tritons [27].

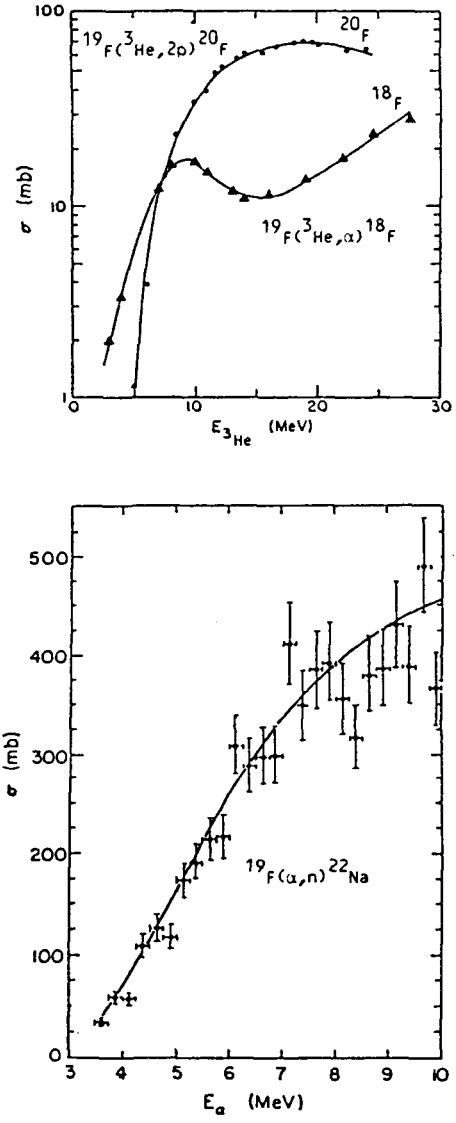

FIG. 31. Reactions induced by ^{3}He [28] and ^{4}He [29] on ^{19}F.

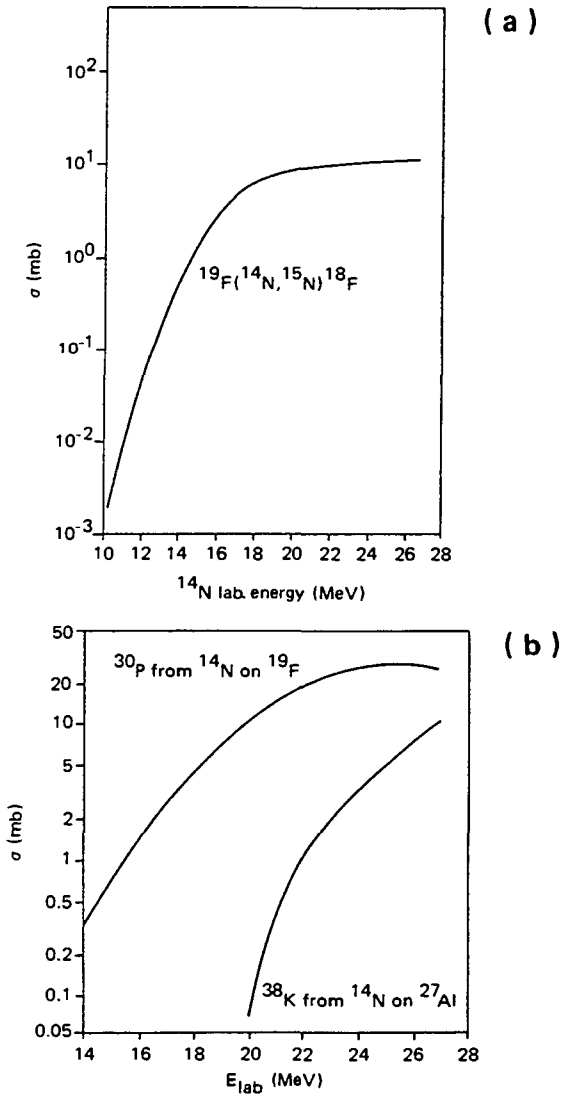

FIG. 32. Reactions induced by ^{14}N on (a) ^{19}F [30] and on (b) ^{19}F and ^{27}Al [31].

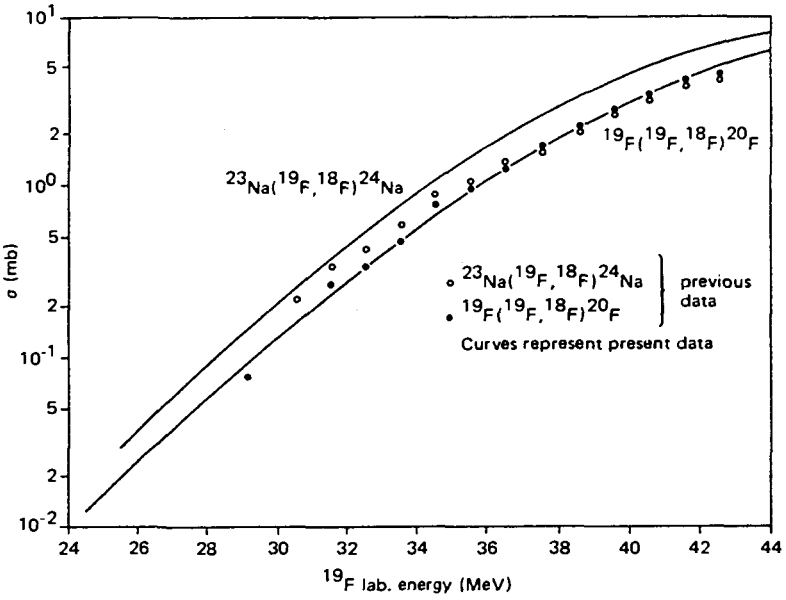

FIG. 33. *(^{19}F, ^{18}F) reactions on ^{23}Na and ^{19}F* [30].

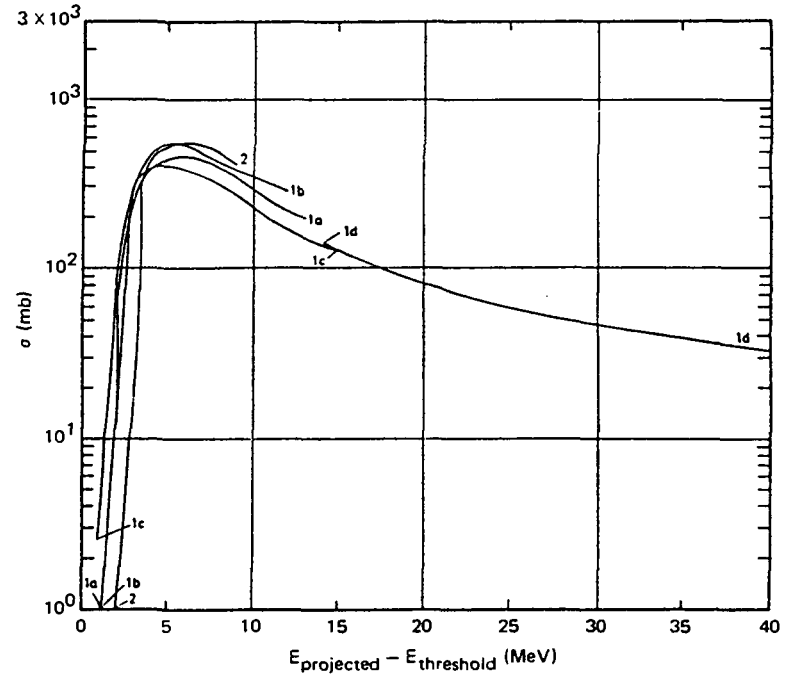

FIG. 34. *(d, p) reactions on ^{23}Na (curves 1a-1d, different authors) and on ^{26}Mg (curve 2)* [2].

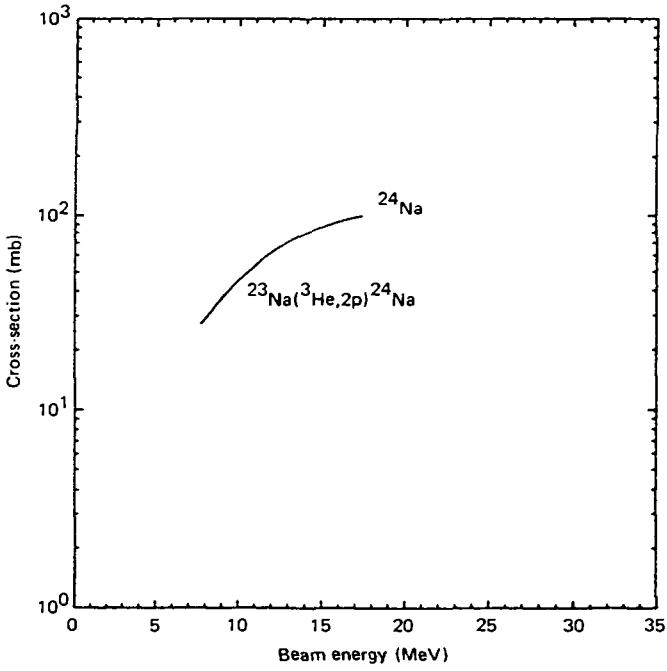

FIG. 35. The $^{23}Na(^3He, 2p)^{24}Na$ reaction (data from Ref. [32]; figure from Ref. [10]).

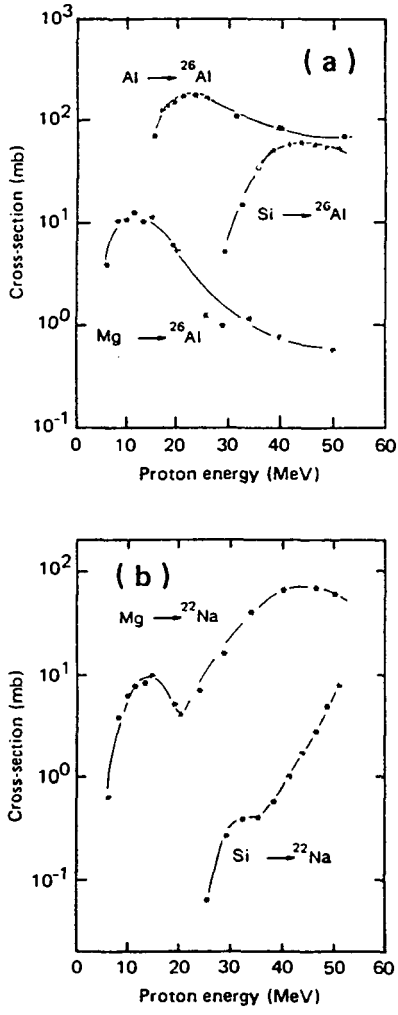

FIG. 36. Production of the long lived radioisotopes (a) ^{26}Al and (b) ^{22}Na by proton irradiation of Mg, Al and Si [33].

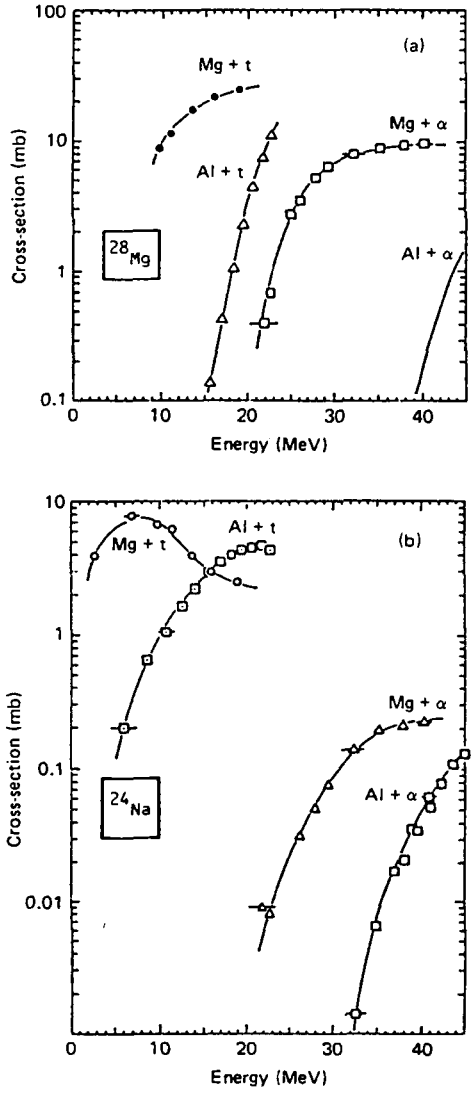

FIG. 37. Production of (a) ^{28}Mg and (b) ^{24}Na by irradiation of natural Mg and Al by tritons or α-particles [34].

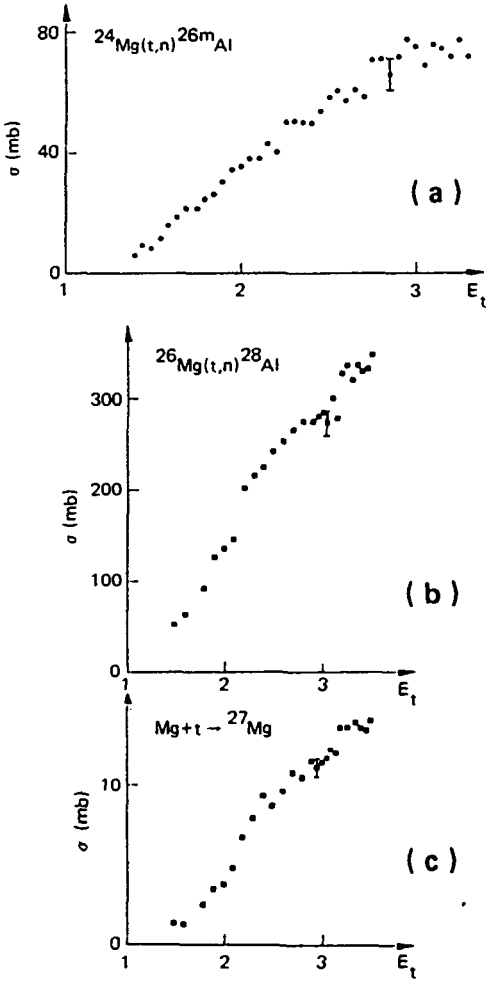

FIG. 38. Production of (a) ^{26m}Al, (b) ^{28}Al and (c) ^{27}Mg by irradiation of Mg with low energy tritons [27].

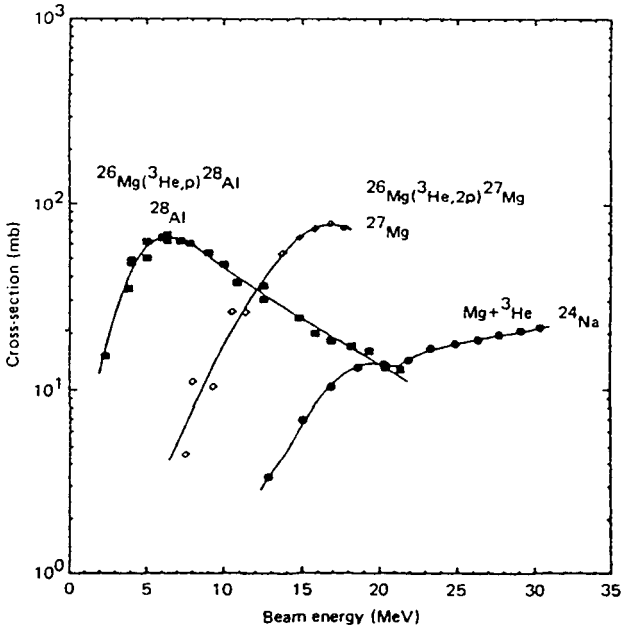

FIG. 39. Production of ^{28}Al, ^{27}Mg and ^{24}Na by irradiation of Mg with ^3He [10].

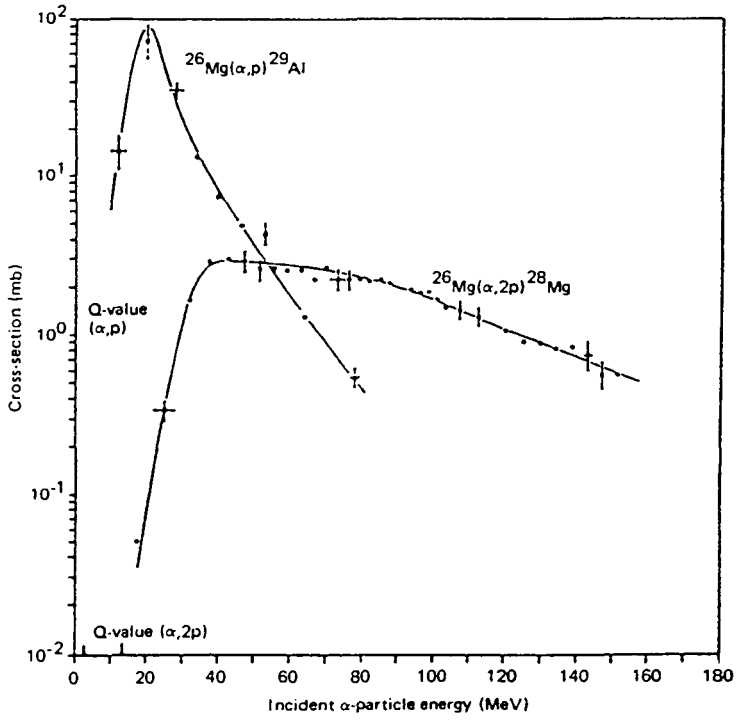

FIG. 40. Reactions with ^{26}Mg induced by high energy α-particles [35].

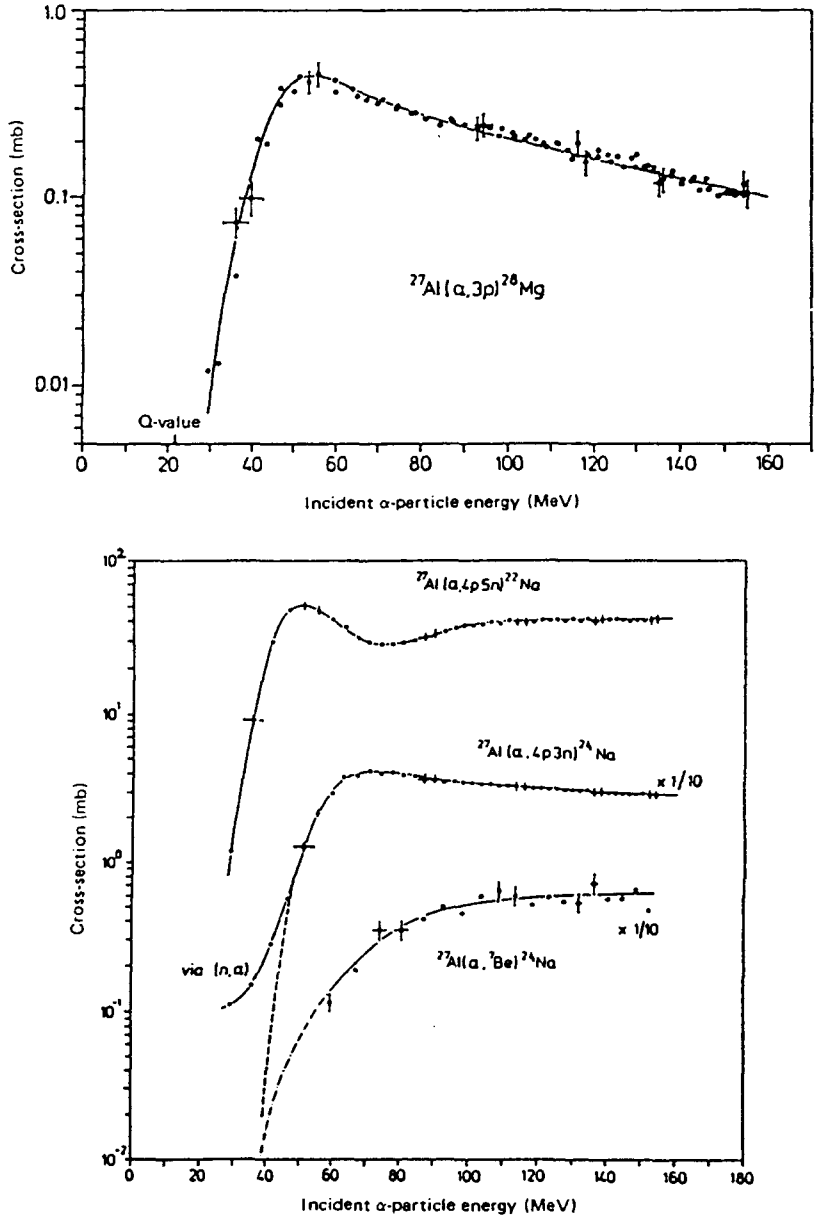

FIG. 41. Reactions with ^{27}Al induced by high energy α-particles [35].

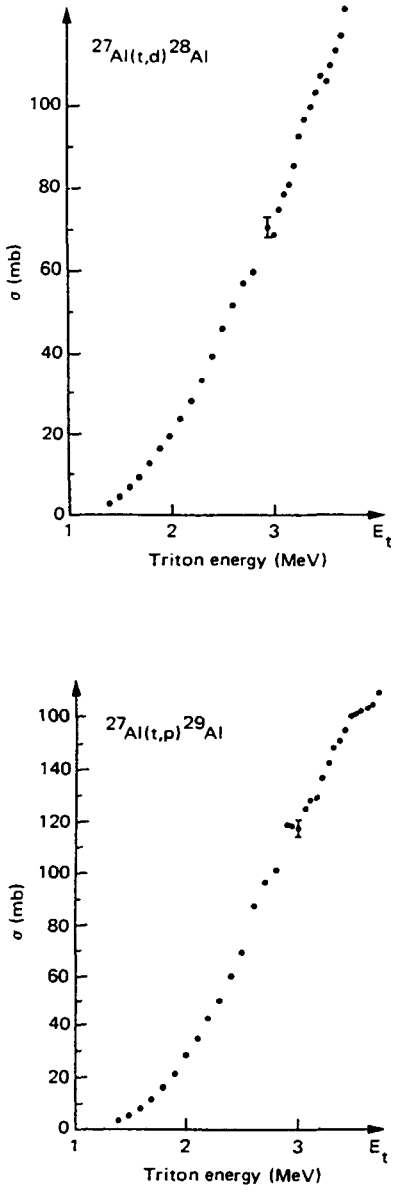

FIG. 42. Activation of Al by low energy tritons [27].

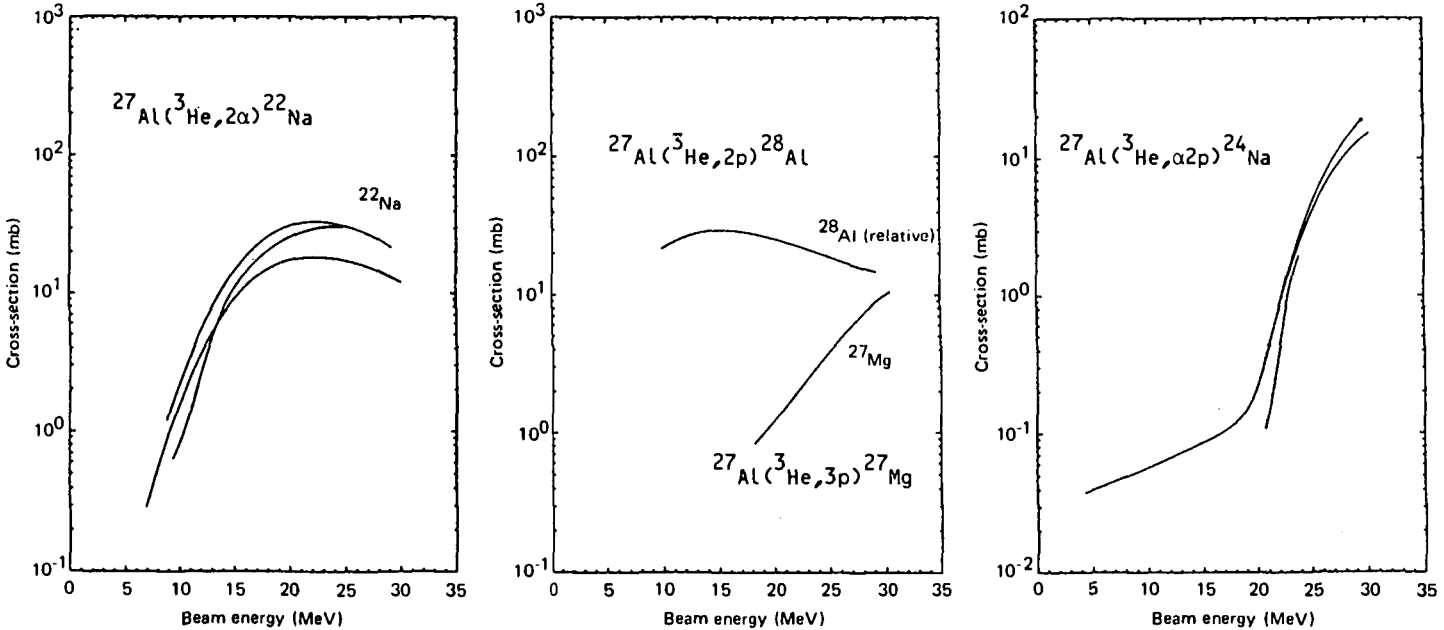

FIG. 43. Activation of Al with ^{3}He (and after various authors for ^{22}Na and ^{24}Na) [10].

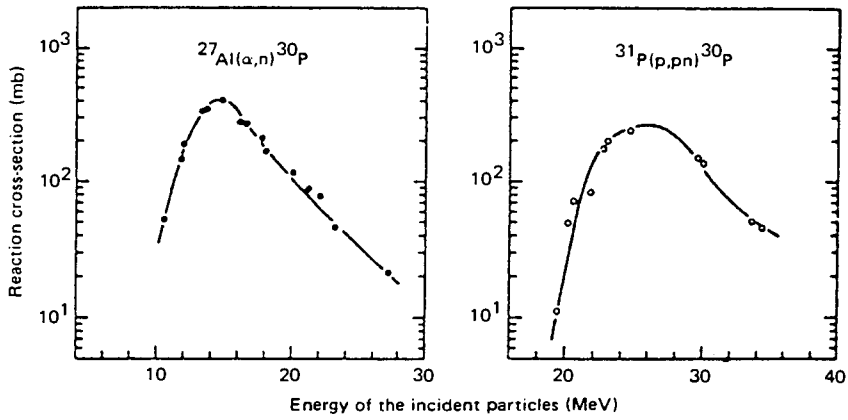

FIG. 44. Production of ^{30}P through various nuclear reactions [36].

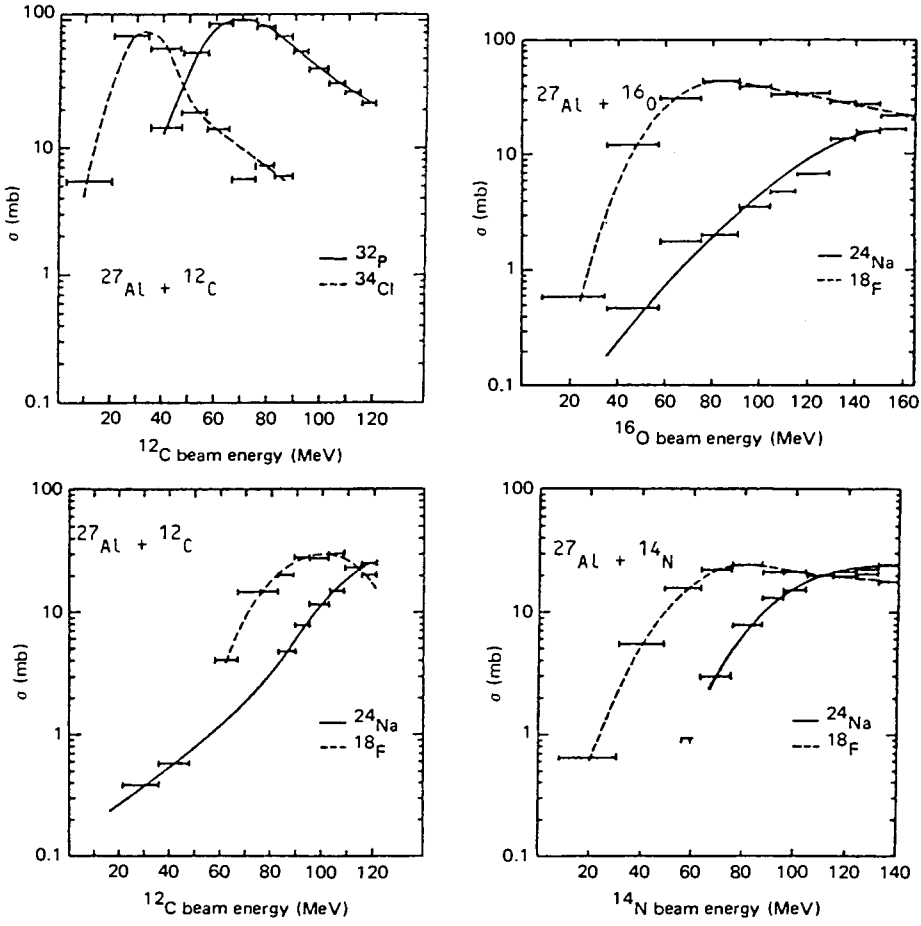

FIG. 45. Some activation products obtained by irradiation of ^{27}Al with ^{12}C, ^{14}N and ^{16}O [37].

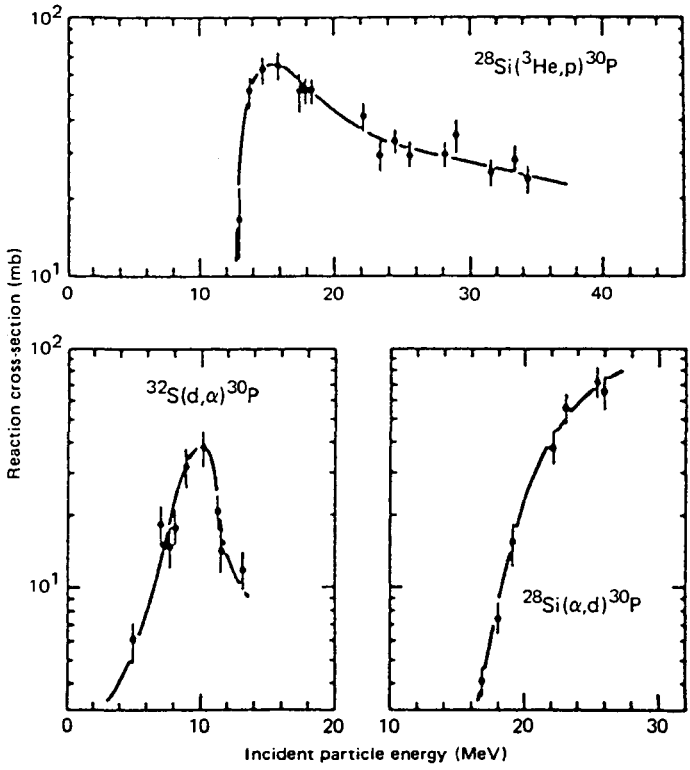

FIG. 46. Formation of ^{30}P through different nuclear reactions [38].

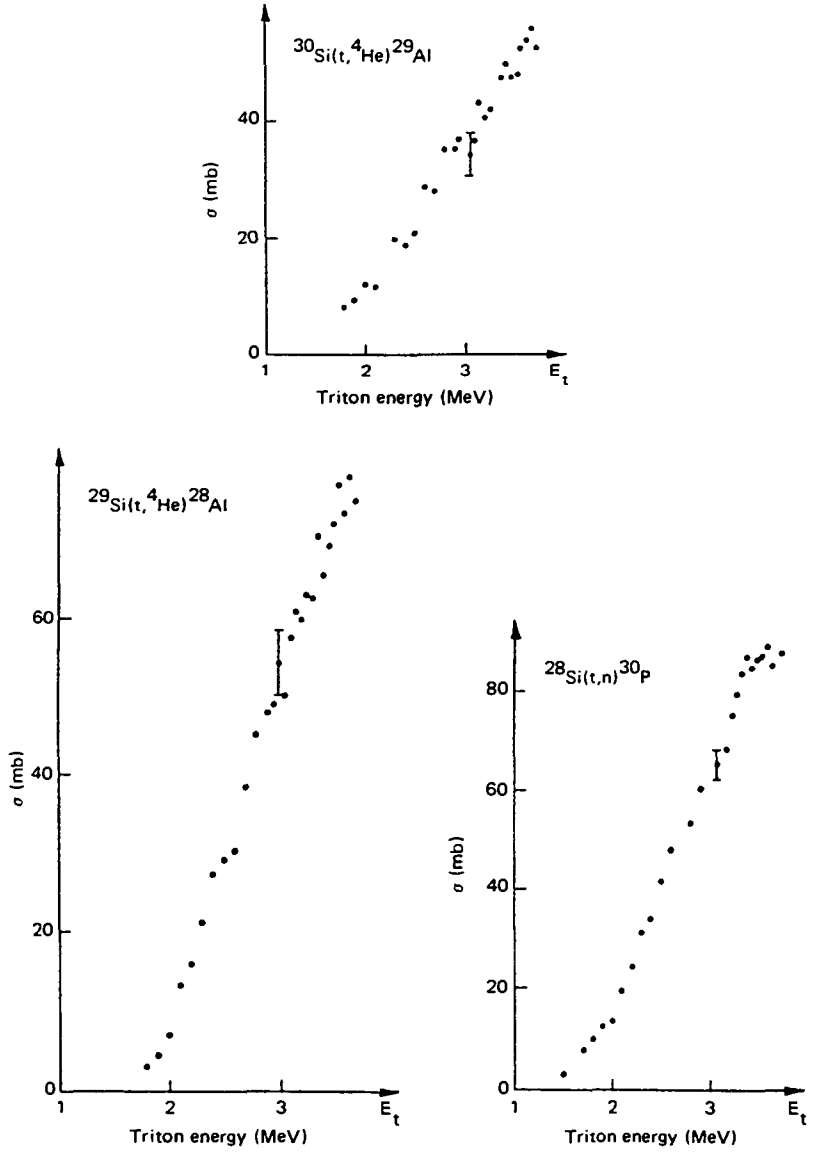

FIG. 47. Activation of Si with low energy tritons [27].

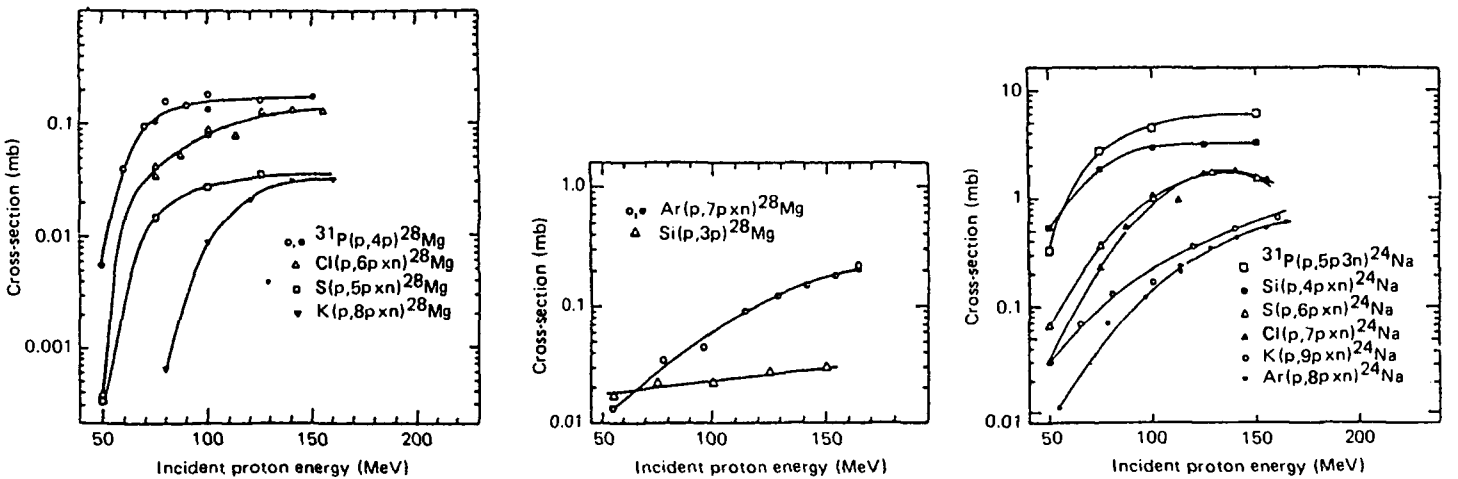

FIG. 48. Production of ^{28}Mg and ^{24}Na by irradiation of Si, P and S (also Cl, K, Ar) with high energy protons [39].

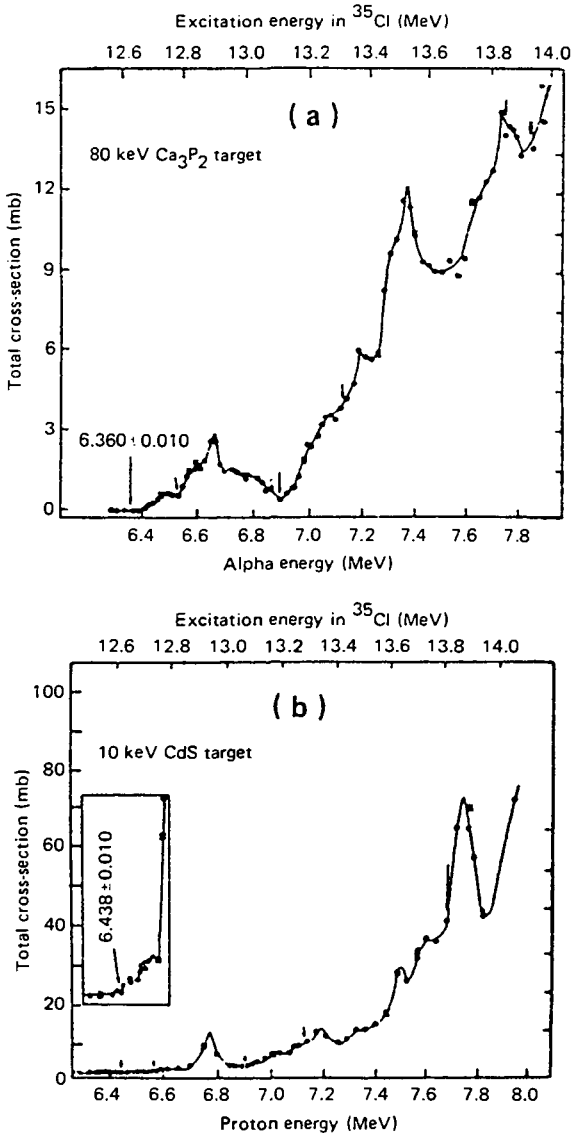

FIG. 49. Production of ^{34m}Cl by irradiation (a) of P by α-particles (reaction $^{31}P(\alpha, n)^{34m}Cl$) and (b) of S by protons (reaction $^{34}S(p, n)^{34m}Cl$) (inset: ground state threshold) [40].

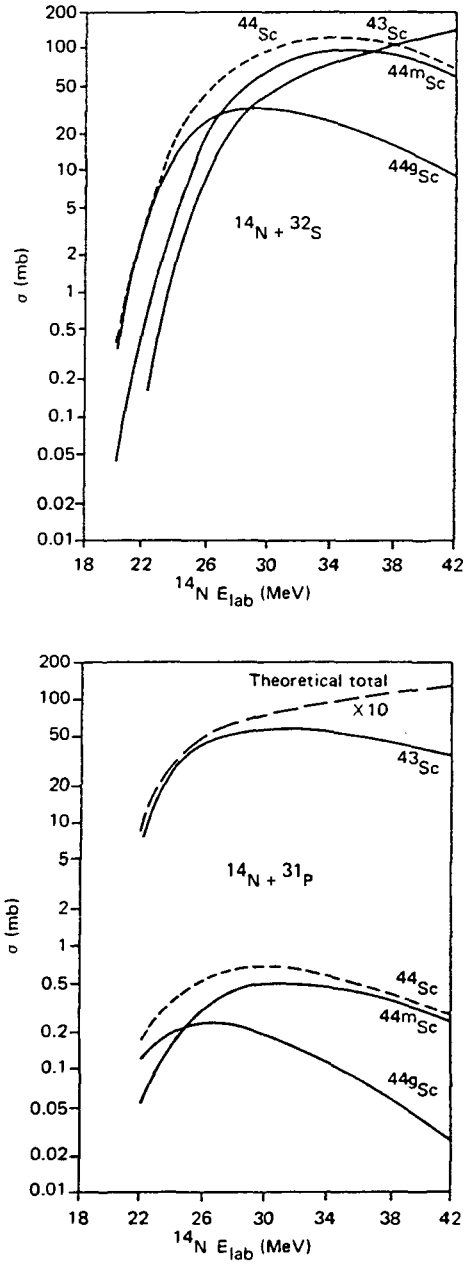

FIG. 50. Some activation reactions induced by bombardment of ^{31}P and ^{32}S with ^{14}N [41].

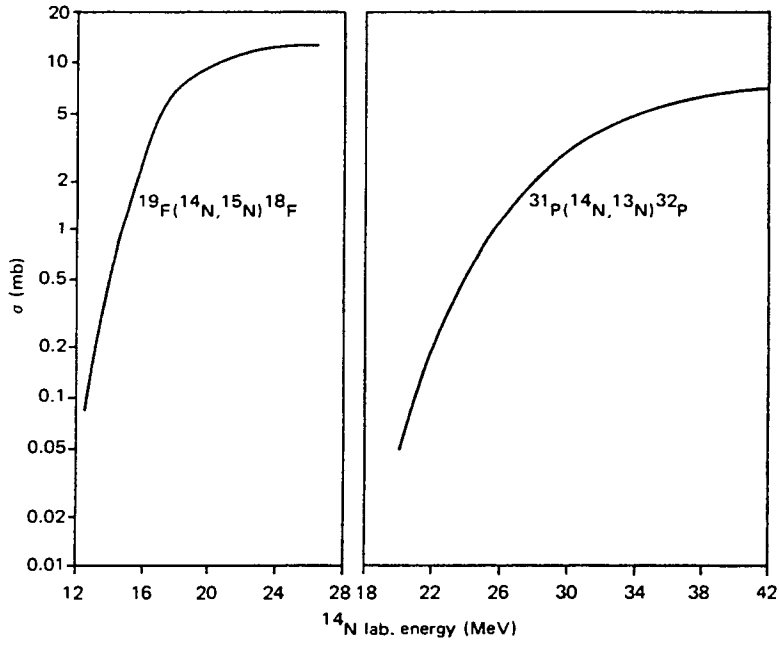

FIG. 51. Activation of $^{19}F(^{18}F)$ and $^{31}P(^{13}N, ^{32}P)$ by irradiation with ^{14}N [5].

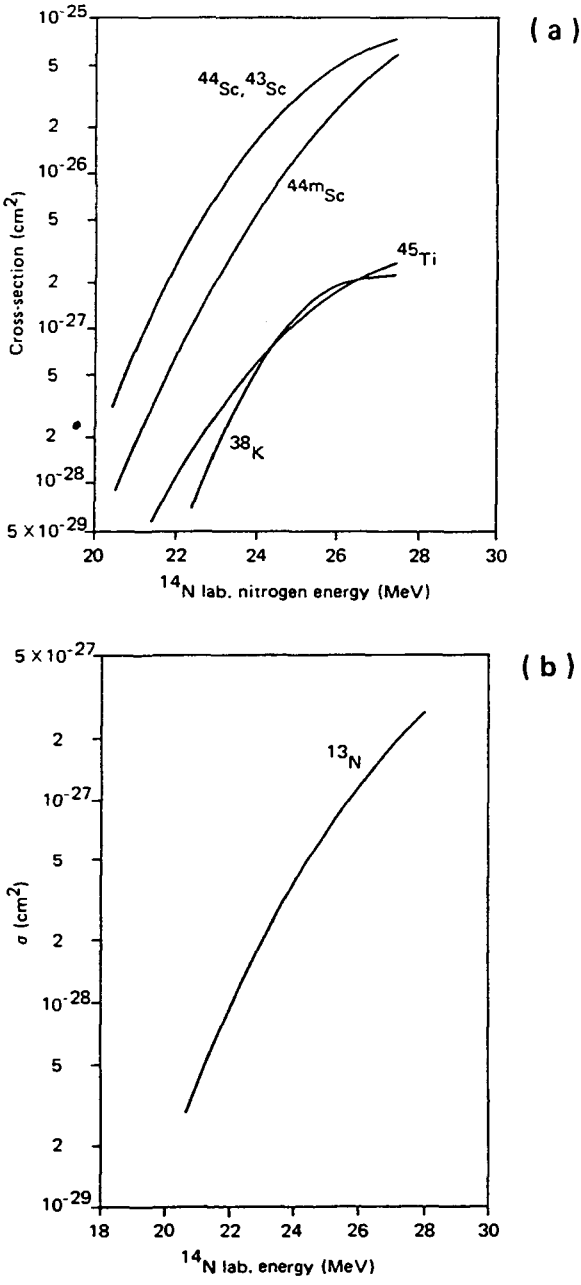

FIG. 52. Some activation products obtained by irradiation of ^{32}S with ^{14}N. (a) $^{32}S + ^{14}N \rightarrow ^{38}K$, ^{43}Sc, ^{44}Sc, ^{44m}Sc and ^{45}Ti; (b) $^{32}S + ^{14}N \rightarrow ^{13}N$ [42].

REFERENCES

[1] MÜNZEL, H., et al., Karlsruhe Charged Particle Reaction Data Compilation, Physics Data, No. 15, Fachinformationszentrum, Karlsruhe (1982).

[2] KELLER, K.A., LANGE, J., MÜNZEL, H., PFENNING, G., "Q-values and excitation functions of nuclear reactions", Excitation Functions for Charged Particle Induced Nuclear Reactions (Landolt-Börnstein New Series Group I), Vol. 5b, Springer-Verlag, Berlin (West) (1973).

[3] MACKLIN, R.L., GIBBONS, J.H., Phys. Rev. **109** (1958) 105.

[4] MIKUMO, T., SEKI, R., TAGISHI, Y., FURUKAWA, M., YAMAGUCHI, H., Phys. Lett. **23** (1966) 586.

[5] GAEDKE, R.M., TOTH, K.S., WILLIAMS, J.R., Phys. Rev. **140** (1965) B296.

[6] ANDERS, B., HERGES, P., SCOBEL, W., Z. Phys. A **301** (1981) 353.

[7] FALK, W.R., HUBER, A., MATTER, U., BENJAMIN, R.W., MARMIER, P., Nucl. Phys. **A140** (1970) 548.

[8] REYNOLDS, H.L., ZUCKER, A., Phys. Rev. **100** (1955) 226.

[9] HALBERT, M.L., HANDLEY, T.H., PINAJIAN, J.J., WEBB, W.H., ZUCKER, A., Phys. Rev. **106** (1957) 251.

[10] LAMB, J.F., Lawrence Berkeley Lab., University of California, Berkeley, Rep. UCRL-18981 (1969).

[11] REYNOLDS, H.L., SCOTT, D.W., ZUCKER, A., Phys. Rev. **102** (1956) 237.

[12] GAEDKE, R.M., TOTH, K.S., WILLIAMS, J.R., Phys. Rev. **167** (1968) 957.

[13] CUMMING, J.B., Nucl. Phys. **49** (1963) 417.

[14] JASZCZAK, R.J., MACKLIN, R.L., GIBBONS, J.H., Phys. Rev. **181** (1969) 1428.

[15] CIRILOV, S.D., NEWTON, J.O., SCHAPIRA, J.P., Nucl. Phys. 77 (1966) 472.

[16] BLACK, J.L., KUAN, H.M., GRUHLE, W., SUFFERT, M., LATSHAW, G.L., Nucl. Phys. **A115** (1968) 683.

[17] REYNOLDS, H.L., ZUCKER, A., Phys. Rev. **96** (1954) 1615.

[18] EYAL, Y., DOSTROVSKY, I., Nucl. Phys. **A179** (1972) 594.

[19] JACOBS, W.W., BODANSKY, D., CHAMBERLIN, D., OBERG, D.L., Phys. Rev. C **9** (1974) 2134.

[20] GRUHLE, W., SCHMIDT, W., BURGMER, W., Nucl. Phys. **A186** (1972) 257.

[21] NOZAKI, T., IWAMOTO, M., Radiochim. Acta **29** (1981) 57.

[22] KUAN, H.M., RISSER, J.R., Nucl. Phys. **51** (1964) 518.

[23] FURUKAWA, M., et al., J. Phys. Soc. Jpn. **15** (1960) 2167.

[24] TRAN, M.D., CHENAUD, A., GIRON, H., TOUSSET, J., in Modern Trends in Activation Analysis (Proc. Int. Conf. Gaithersburg, MD, 1969) (DeVOE, J.R., Ed.), Vol. 2, US National Bureau of Standards Special Publication 312, US Government Printing Office, Washington, DC (1969) 811.

[25] REVEL, G., DA CUNHA BELO, H., LINCK, I., KRANS, L., Rev. Phys. Appl. **12** (1977) 81.

[26] NOZAKI, T., IWAMOTO, M., IDO, T., Int. J. Appl. Radiat. Isot. **25** (1974) 393.

[27] BORDERIE, B., BARRANDON, J.N., J. Radioanal. Chem. **55** (1980) 329.

[28] LEE, D.M., LAMB, J.F., MARKOWITZ, S.S., Anal. Chem. **43** (1971) 542.

[29] NORMAN, E.B., CHUPP, T.E., LESKO, K.T., GRANT, P.J., WOODRUFF, G.L., Phys. Rev. C **30** (1984) 1339.

[30] GAEDKE, R.M., TOTH, K.S., WILLIAMS, J.R., Phys. Rev. C **4** (1971) 98.

[31] NEWMAN, E., TOTH, K.S., Phys. Rev. **129** (1963) 802.

[32] HAHN, R.L., RICCI, E., Nucl. Phys. **A101** (1967) 353.

[33] FURUKAWA, M., SHIZURI, K., KOMURA, K., SAKAMOTO, K., TANAKA, S., Nucl. Phys. **A174** (1971) 539.
[34] NOZAKI, T., FURUKAWA, M., KUME, S., SEKI, R., Int. J. Appl. Radiat. Isot. **26** (1975) 17.
[35] PROBST, H.J., QAIM, S.M., WEINREICH, R., Int. J. Appl. Radiat. Isot. **27** (1976) 431.
[36] SAHAKUNDU, S.M., QAIM, S.M., STOCKLIN, G., Int. J. Appl. Radiat. Isot. **30** (1979) 3.
[37] LADENBAUER-BELLIS, J.M., PREISS, J.L., ANDERSON, C.E., Phys. Rev. **125** (1962) 606.
[38] QAIM, S.M., OLLIG, H., BLESSING, G., Int. J. Appl. Radiat. Isot. **33** (1982) 271.
[39] LUNDQVIST, H., MALMBORG, P., Int. J. Appl. Radiat. Isot. **30** (1979) 33.
[40] UMBARGER, C.J., KEMPER, K.W., NELSON, J.W., PLENDL, H.S., Phys. Rev. C **2** (1970) 1378.
[41] WILLIAMS, J.R., TOTH, K.S., Phys. Rev. **138** (1965) 382.
[42] FISHER, D.E., ZUCKER, A., GROPP, A., Phys. Rev. **113** (1959) 542.

3-3. THICK TARGET YIELDS FOR THE PRODUCTION OF RADIOISOTOPES

P. ALBERT, G. BLONDIAUX, J.L. DEBRUN,
A. GIOVAGNOLI, M. VALLADON
Centre d'études et de recherches par irradiations,
Centre national de la recherche scientifique,
Orléans, France

Abstract

THICK TARGET YIELDS FOR THE PRODUCTION OF RADIOISOTOPES.

The paper presents data on reactions with hydrogen (protons, deuterons and tritons) and helium (helium 3 and 4). Only yield curves are considered, while individual yields at a given energy are excluded.

1. INTRODUCTION

The tables that are presented here are limited to reactions with hydrogen (protons = p, deuterons = d and tritons = t) and helium (helium 3 = ^{3}He and helium 4 = α). They are also not complete because only yield curves have been considered, while individual yields at a given energy have been excluded (for further details, see Ref. [1]). Finally, where several publications were available, only one was retained in order to keep the length of this chapter at an acceptable limit. As a result, some references have probably been missed.

The yields were collected from a number of different publications and are presented in various units which should be clearly understandable. Since complementary details of interest could not be included, owing to the lack of space, readers are referred to the original publications cited with each figure.

LITHIUM

Protons	Deuterons
Figure 1 $^{7}Li(p,n)^{7}Be$ $E_{th} = 1.88$	Figure 2 $Li(d,xn)^{7}Be$

BERYLLIUM

Helium 3	Helium 4
Figure 3 $^{9}Be(^{3}He,n)^{11}C$ $E_{th} = 0$	Figure 3 $^{9}Be(\alpha,2n)^{11}C$ $E_{th} = 18.8$

BORON

Protons	Deuterons	Tritons	Helium 3	Helium 4
Figure 1 $B(p,\alpha xn)^{7}Be$	Figure 2 $B(d,\alpha xn)^{7}Be$	Figure 5 $^{10}B(t,2n)^{11}C$ $E_{th} = 0$	Figure 4 $^{10}B(^{3}He,pn)^{11}C$ $E_{th} = 0$	Figure 4 $B(\alpha,xn)^{13}N$
Figure 4 $^{11}B(p,n)^{11}C$ $E_{th} = 3.02$	Figure 4 $B(d,xn)^{11}C$		Figure 4 $^{11}B(^{3}He,n)^{13}N$ $E_{th} = 0$	

CARBON

Figure 6 for all reactions

Protons	Deuterons	Helium 3	Helium 4
$^{13}C(p,n)^{13}N$ $E_{th} = 3.23$	$^{12}C(d,n)^{13}N$ $E_{th} = 0.33$	$^{12}C(^{3}He,\alpha)^{11}C$ $E_{th} = 0$	$^{12}C(\alpha,\alpha n)^{11}C$ $E_{th} = 24.96$
$^{12}C(p,pn)^{11}C$ $E_{th} = 20.28$	$^{12}C(d,dn)^{11}C$ $E_{th} = 21.84$	$^{12}C(^{3}He,pn)^{13}N$ $E_{th} = 7.22$	

NITROGEN

Figure 7 for all reactions except $^{14}N(d,n)^{15}O$ (Figure 8).

Protons	Deuterons	Helium 3	Helium 4
$^{14}N(p,\alpha)^{11}C$ $E_{th} = 3.12$	Figure 8 $^{14}N(d,n)^{15}O$ $E_{th} = 0$	$^{14}N(^{3}He,\alpha)^{13}N$ $E_{th} = 0$	$^{14}N(\alpha,\alpha n)^{13}N$ $E_{th} = 13.57$
$^{14}N(p,pn)^{13}N$ $E_{th} = 11.31$	$^{14}N(d,dn)^{13}N$ $E_{th} = 12.06$	$^{14}N(^{3}He,\alpha pn)^{11}C$ $E_{th} = 12.92$	$^{14}N(\alpha,xn)^{18}F$
	$^{14}N(d,\alpha n)^{11}C$ $E_{th} = 5.88$		

OXYGEN

Figure 9 for all reactions except $^{16}O(t,n)^{18}F$ (Figure 10)

Protons	Deuterons	Tritons	Helium 3	Helium 4
$^{18}O(p,n)^{18}F$ $E_{th} = 2.59$	$^{16}O(d,\alpha n)^{13}N$ $E_{th} = 8.37$	Figure 10 $^{16}O(t,n)^{18}F$ $E_{th} = 0$	$^{16}O(^{3}He,p)^{18}F$ $E_{th} = 0$	$^{16}O(\alpha,pn)^{18}F$ $E_{th} = 23.2$
$^{16}O(p,\alpha)^{13}N$ $E_{th} = 5.54$	$O(d,xn)^{18}F$		$^{16}O(^{3}He,2\alpha)^{11}C$ $E_{th} = 6.3$	$^{16}O(\alpha,2n)^{18}Ne \rightarrow ^{18}F$ $E_{th} = 29.73$

FLUORINE

Figure 11 for all reactions except $^{19}F(\alpha,n)^{22}Na$ (Figure 12)

Protons	Deuterons	Helium 3	Helium 4
$^{19}F(p,pn)^{18}F$ $E_{th} = 10.99$	$^{19}F(d,dn)^{18}F$ $E_{th} = 11.54$	$^{19}F(^{3}He,\alpha)^{18}F$ $E_{th} = 0$	$^{19}F(\alpha,\alpha n)^{18}F$ $E_{th} = 12.63$
			Figure 12 $^{19}F(\alpha,n)^{22}Na$ $E_{th} = 2.36$

NEON

Deuterons
Figure 13 $^{20}Ne(d,\alpha)^{18}F$ $E_{th} = 0$

MAGNESIUM

Tritons	Helium 4
Figure 14 $^{26}Mg(t,p)^{28}Mg$ $E_{th} = 0$	Figure 14 $^{26}Mg(\alpha,2p)^{28}Mg$ $E_{th} = 11.91$
Figure 16 $Mg(t,\alpha xn)^{24}Na$	Figure 15 $^{25}Mg(\alpha,p)^{28}Al$ $E_{th} = 1.4$
	Figure 15 $^{26}Mg(\alpha,p)^{29}Al$ $E_{th} = 3.36$
	Figure 16 $Mg(\alpha,\alpha pxn)^{24}Na$

ALUMINIUM

Tritons	Helium 4
Figure 15 $^{27}Al(t,2p)^{28}Mg$ $E_{th} = 2$	Figure 18 $^{27}Al(\alpha,n)^{30}P$ $E_{th} = 3.05$
Figure 16 $^{27}Al(t,\alpha pn)^{24}Na$ $E_{th} = 12.9$	Figure 17 $^{27}Al(\alpha,3p)^{28}Mg$ $E_{th} = 24.82$
	Figure 17 $^{27}Al(\alpha,4p5n)^{22}Na$ $E_{th} = 90.8$
	Figure 17 $^{27}Al(\alpha,4p3n)^{24}Na$ $E_{th} = 68.6$
	Figure 17 $^{27}Al(\alpha,^{7}Be)^{24}Na$ $E_{th} = 25.4$

SILICON

Tritons	Helium 3	Helium 4
Figure 14 $Si(t,^{3}He,pxn)^{28}Mg$	Figure 18 $^{28}Si(^{3}He,p)^{30}P$ $E_{th} = 0$	Figure 18 $^{28}Si(\alpha,d)^{30}P$ $E_{th} = 13.72$
Figure 16 $Si(t,\alpha^{3}He,xn)^{24}Na$		

PHOSPHORUS

Protons	Helium 4
Figure 19 $^{31}P(p,4p)^{28}Mg$ E_{th} = 32.3	Figure 20 $^{31}P(\alpha,n)^{34m}Cl$ E_{th} = 6.39

SULPHUR

Protons	Deuterons	Tritons	Helium 3	Helium 4
Figure 20 $^{34}S(p,n)^{34m}Cl$ E_{th} = 6.47	Figure 20 $S(d,xn)^{34m}Cl$	Figure 21 $^{32}S(t,n)^{34m}Cl$ E_{th} = 0	Figure 20 $S(^3He,pxn)^{34m}Cl$	Figure 20 $S(\alpha,pxn)^{34m}Cl$
Figure 19 $S(p,5pxn)^{28}Mg$	Figure 18 $^{32}S(d,\alpha)^{30}P$ E_{th} = 0			

CHLORINE

Protons	Deuterons	Helium 3	Helium 4
Figure 19 $Cl(p,6pxn)^{28}Mg$	Figure 20 $^{37}Cl(d,p)^{38}Cl$ E_{th} = 0	Figure 20 $^{37}Cl(^3He,2p)^{38}Cl$ E_{th} = 1.74	Figure 20 $^{35}Cl(\alpha,\alpha n)^{34m}Cl$ E_{th} = 14.10
Figure 20 $^{35}Cl(p,pn)^{34m}Cl$ E_{th} = 13.01	Figure 20 $^{35}Cl(d,dn)^{34m}Cl$ E_{th} = 13.37	Figure 20 $^{35}Cl(^3He,\alpha)^{34m}Cl$ E_{th} = 0	Figure 22 $^{35}Cl(\alpha,n)^{38}K$ E_{th} = 6.54

ARGON

Protons
Figure 19 $Ar(p,7pxn)^{28}Mg$

POTASSIUM

Protons
Figure 19 $K(p,8pxn)^{28}Mg$

CALCIUM

Protons	Helium 4
Figure 23 $^{48}Ca(p,n)^{48}Sc$ $E_{th} = 0.67$	Figure 24 $^{40}Ca(\alpha,p)^{43}Sc$ $E_{th} = 3.9$
	Figure 24 $^{48}Ca(\alpha,n)^{51}Ti$ $E_{th} = 0.33$

TITANIUM

Protons	Helium 3	Helium 4
Figure 25 $Ti(p,xn)^{48}V$	Figure 26 $Ti(^{3}He,xn)^{48}Cr$	Figure 27 $^{46}Ti(\alpha,n)^{49}Cr$ $E_{th} = 4.76$
	Figure 26 $Ti(^{3}He,xn)^{51}Cr$	Figure 27 $^{48}Ti(\alpha,n)^{51}Cr$ $E_{th} = 2.93$
	Figure 26 $Ti(^{3}He,\alpha pxn)^{44m}Sc$	Figure 27 $^{49}Ti(\alpha,p)^{52}V$ $E_{th} = 2.18$
	Figure 26 $Ti(^{3}He,\alpha pxn)^{46m+g}Sc$	Figure 27 $^{50}Ti(\alpha,p)^{53}V$ $E_{th} = 3.83$
	Figure 26 $Ti(^{3}He,\alpha pxn)^{47}Sc$	Figure 28 $Ti(\alpha,xn)^{48}Cr$
	Figure 26 $Ti(^{3}He,\alpha pxn)^{48}Sc$	Figure 28 $Ti(\alpha,xn)^{51}Cr$
	Figure 26 $Ti(^{3}He,pxn)^{48}V$	

VANADIUM

Protons	Deuterons	Helium 4
Figure 25 $^{51}V(p,n)^{51}Cr$ $E_{th} = 1.57$	Figure 28 $^{51}V(d,2n)^{51}Cr$ $E_{th} = 3.91$	Figure 29 $^{51}V(\alpha,n)^{54}Mn$ $E_{th} = 2.46$
	Figure 28 $^{51}V(d,4n)^{49}Cr$ $E_{th} = 27$	
	Figure 28 $^{51}V(d,5n)^{48}Cr$ $E_{th} = 37.8$	

CHROMIUM

Protons	Helium 4
Figure 25 $^{52}Cr(p,n)^{52}Mn$ $E_{th} = 5.6$	Figure 30 $^{50}Cr(\alpha,n)^{53}Fe$ $E_{th} = 5.6$
Figure 25 $^{52}Cr(p,n)^{52m}Mn$ $E_{th} = 5.6$	Figure 30 $^{53}Cr(\alpha,p)^{56}Mn$ $E_{th} = 3.5$

MANGANESE

Helium 3	Helium 4
Figure 32 $^{55}Mn(^{3}He,3n)^{55}Co$ $E_{th} = 13.7$	Figure 31 $^{55}Mn(\alpha,n)^{58}Co$ $E_{th} = 3.76$
Figure 32 $^{55}Mn(^{3}He,2n)^{56}Co$ $E_{th} = 3$	Figure 31 $^{55}Mn(\alpha,2n)^{57}Co$ $E_{th} = 12.96$
Figure 32 $^{55}Mn(^{3}He,n)^{57}Co$ $E_{th} = 0$	Figure 31 $^{55}Mn(\alpha,\alpha n)^{54}Mn$ $E_{th} = 10.96$

IRON

Protons	Deuterons	Helium 4
Figures 25, 33 and 34 $Fe(p,xn)^{55}Co$	Figure 34 $Fe(d,xn)^{55}Co$	Figure 35 $^{54}Fe(\alpha,p)^{57}Co$ $E_{th} = 1.9$
Figures 25 and 34 $^{56}Fe(p,n)^{56}Co$ $E_{th} = 5.44$	Figure 34 $Fe(d,xn)^{56}Co$	Figure 35 $^{54}Fe(\alpha,n)^{57}Ni$ $E_{th} = 6.2$
	Figure 34 $Fe(d,xn)^{57}Co$	
	Figure 34 $Fe(d,xn)^{58}Co$	

COBALT

Protons	Helium 3	Helium 4
Figure 36 $^{59}Co(p,p2n)^{57}Co$	Figure 37 $^{59}Co(^{3}He,n)^{61}Cu$ $E_{th} = 0$	Figure 38 $^{59}Co(\alpha,2n)^{61}Cu$ $E_{th} = 14.9$
Figure 36 $^{59}Co(p,3n)^{57}Ni$ $E_{th} = 23.4$	Figure 37 $^{59}Co(^{3}He,\alpha)^{58}Co$ $E_{th} = 0$	Figure 38 $^{59}Co(\alpha,\alpha n)^{58}Co$ $E_{th} = 11.15$
	Figure 37 $^{59}Co(^{3}He,\alpha n)^{57}Co$ $E_{th} = 0$	Figure 38 $^{59}Co(\alpha,\alpha 2n)^{57}Co$ $E_{th} = 20.3$
	Figure 37 $^{59}Co(^{3}He,\alpha 2n)^{56}Co$ $E_{th} = 10.3$	Figure 39 $^{59}Co(\alpha,n)^{62}Cu$ $E_{th} = 5.4$

NICKEL

Protons	Helium 4
Figure 40 $Ni(p,pxn)^{57}Ni$	Figure 41 $Ni(\alpha,pxn)^{61}Cu$
Figure 40 $Ni(p,\alpha xn)^{55}Co$	Figure 42 $^{58}Ni(\alpha,p)^{61}Cu$ $E_{th} = 3.3$
Figure 25 $^{58}Ni(p,\alpha)^{55}Co$ $E_{th} = 1.37$	Figure 42 $^{60}Ni(\alpha,n)^{63}Zn$ $E_{th} = 8.4$
Figure 40 $Ni(p,\alpha xn)^{56}Co$	Figure 43 $^{60}Ni(\alpha,2n)^{62}Zn$ $E_{th} = 18.2$
Figure 40 $Ni(p,pxn)^{56}Ni$	Figure 41 $Ni(\alpha,pxn)^{60}Cu$
Figure 40 $Ni(p,\alpha xn)^{57}Co$	Figure 41 $Ni(\alpha,pxn)^{64}Cu$
Figure 40 $Ni(p,\alpha xn)^{58}Co$	
Figure 25 $Ni(p,xn)^{60}Cu$	
Figure 25 $Ni(p,xn)^{61}Cu$	

COPPER

Protons	Helium 4
Figures 23 and 25 $^{63}Cu(p,n)^{63}Zn$ $E_{th} = 4.2$	Figures 44 and 46 $^{63}Cu(\alpha,n)^{66}Ga$ $E_{th} = 8$
Figures 23 and 25 $^{65}Cu(p,n)^{65}Zn$ $E_{th} = 2.16$	Figure 44 $^{65}Cu(\alpha,n)^{68}Ga$ $E_{th} = 6.2$
	Figure 46 $^{65}Cu(\alpha,2n)^{67}Ga$ $E_{th} = 15$

ZINC

Protons	Deuterons	Helium 4
Figures 23, 25 and 46 $Zn(p,xn)^{66}Ga$	Figure 46 $Zn(d,xn)^{66}Ga$	Figure 45 $^{64}Zn(\alpha,p)^{67}Ga$ $E_{th} = 4.26$
Figures 23, 25 and 46 $Zn(p,xn)^{67}Ga$	Figure 46 $Zn(d,xn)^{67}Ga$	Figure 45 $^{64}Zn(\alpha,n)^{67}Ge$ $E_{th} = 9.8$
Figures 23 and 25 $Zn(p,xn)^{68}Ga$		Figure 45 $^{66}Zn(\alpha,n)^{69}Ge$ $E_{th} = 8$
		Figure 46 $Zn(\alpha,pxn)^{66}Ga$
		Figure 46 $Zn(\alpha,pxn)^{67}Ga$
		Figure 46 $Zn(\alpha,pxn)^{68}Ga$
		Figure 46 $Zn(\alpha,xn)^{66}Ge$
		Figure 46 $Zn(\alpha,xn)^{68}Ge$
		Figure 46 $Zn(\alpha,xn)^{69}Ge$

GALLIUM

Protons
Figure 47 $^{69}Ga(p,n)^{69}Ge$ $E_{th} = 3.06$

GERMANIUM

Protons	Helium 3	Helium 4
Figure 48 $Ge(p,pxn)^{69}Ge$	Figure 49 $^{72}Ge(^{3}He,2n)^{73}Se$ E_{th} = 6.08	Figure 49 $Ge(\alpha,xn)^{73}Se$
Figure 48 $Ge(p,pxn)^{68}Ge$	Figure 49 $Ge(^{3}He,xn)^{73}Se$	Figure 49 $^{72}Ge(\alpha,3n)^{73}Se$ E_{th} = 27.6
Figure 48 $Ge(p,xn)^{71}As$		Figure 50 $^{70}Ge(\alpha,n)^{73m}Se$ E_{th} = 8.36
Figure 48 $Ge(p,xn)^{72}As$		Figure 50 $^{72}Ge(\alpha,n)^{75}Se$ E_{th} = 6.7
Figure 48 $Ge(p,xn)^{73}As$		Figure 50 $^{74}Ge(\alpha,n)^{77m}Se$ E_{th} = 4.75
Figure 48 $Ge(p,xn)^{74}As$		Figure 50 $^{76}Ge(\alpha,n)^{79m}Se$ E_{th} = 3.16
Figure 48 $Ge(p,\alpha xn)^{66}Ga$		
Figure 48 $Ge(p,\alpha xn)^{67}Ga$		

SELENIUM

Protons/Figure 51	Helium 3/Figure 52
$^{76}Se(p,n)^{76}Br$ $E_{th} = 5.5$	$Se(^{3}He,xn)^{76}Kr$
$^{77}Se(p,n)^{77}Br$ $E_{th} = 2.2$	$Se(^{3}He,xn)^{77}Kr$
$^{82}Se(p,n)^{82}Br$ $E_{th} = 0.9$	$Se(^{3}He,xn)^{79}Kr$
$^{77}Se(p,2n)^{76}Br$ $E_{th} = 13$	$Se(^{3}He,pxn)^{75}Br$
$^{78}Se(p,2n)^{77}Br$ $E_{th} = 12.8$	$Se(^{3}He,pxn)^{76}Br$
	$Se(^{3}He,pxn)^{77}Br$

BROMINE

Protons	Deuterons	Helium 3/Figure 55	Helium 4/Figure 55
Figure 53 $Br(p,xn)^{77}Kr$	Figure 54 $Br(d,xn)^{75}Kr$	$Br(^{3}He,xn)^{81}Rb$	$^{79}Br(\alpha,2n)^{81}Rb$ $E_{th} = 15.1$
		$Br(^{3}He,pxn)^{79}Kr$	$Br(\alpha,xn)^{82m}Rb$
		$^{81}Br(^{3}He,2n)^{82m}Rb$ $E_{th} = 2.8$	$^{81}Br(\alpha,2n)^{83}Rb$ $E_{th} = 12.9$
			$^{81}Br(\alpha,n)^{84}Rb$ $E_{th} = 4$
			$^{79}Br(\alpha,\alpha 2n)^{77}Br$ $E_{th} = 20$

KRYPTON

All curves in Figure 56

Protons
$Kr(p,xn)^{79}Rb$
$Kr(p,xn)^{81m}Rb$
$Kr(p,xn)^{81}Rb$
$Kr(p,xn)^{82m}Rb$
$Kr(p,xn)^{83}Rb$
$Kr(p,xn)^{84m}Rb$
$Kr(p,xn)^{84}Rb$
$Kr(p,xn)^{86}Rb$

RUBIDIUM

Protons/Figure 57	Helium 3/Figure 58	Helium 4/Figure 58
$^{85}Rb(p,pn)^{84m}Rb$ $E_{th} = 10.65$	$Rb(^{3}He,xn)^{86m}Y$	$Rb(\alpha,xn)^{86m}Y$
$^{85}Rb(p,pn)^{84}Rb$ $E_{th} = 10.65$	$^{87}Rb(^{3}He,2n)^{88}Y$ $E_{th} = 1.56$	$Rb(\alpha,xn)^{88}Y$
$^{85}Rb(p,p2n)^{83}Rb$ $E_{th} = 19.1$	$Rb(^{3}He,xn)^{87m}Y$	$Rb(\alpha,xn)^{87m}Y$
$^{85}Rb(p,p3n)^{82m}Rb$ $E_{th} = 30.3$	$^{87}Rb(^{3}He,5n)^{85m}Y$ $E_{th} = 33.4$	$^{85}Rb(\alpha,4n)^{85m}Y$ $E_{th} = 35.9$
$^{85}Rb(p,p4n)^{81m}Rb$ $E_{th} = 39$	$^{87}Rb(^{3}He,5n)^{85}Y$ $E_{th} = 33.4$	$^{85}Rb(\alpha,4n)^{85}Y$ $E_{th} = 35.9$
$^{85}Rb(p,p4n)^{81}Rb$ $E_{th} = 39$		
$^{85}Rb(p,3n)^{83}Sr$ $E_{th} = 29.6$		
$^{85}Rb(p,4n)^{82}Sr$ $E_{th} = 38.9$		
$^{85}Rb(p,5n)^{81}Sr$ $E_{th} =$		
$^{85}Rb(p,\alpha 3n)^{79}Kr$ $E_{th} = 27.4$		

YTTRIUM
Figure 59

Protons
$^{89}Y(p,n)^{89}Zr$ $E_{th} = 3.66$

ZIRCONIUM
Figure 59

Protons
$Zr(p,xn)^{95}Nb$

NIOBIUM
Figure 59

Protons
$^{93}Nb(p,n)^{93m}Mo$ $E_{th} = 1.27$

MOLYBDENUM

Protons	Helium 3/Figure 61	Helium 4
Figures 59 and 60 $Mo(p,xn)^{94}Tc$	$Mo(^{3}He,xn)^{94}Ru$	Figure 61 $Mo(\alpha,xn)^{94}Ru$
Figures 59 and 60 $Mo(p,xn)^{95}Tc$	$Mo(^{3}He,xn)^{95}Ru$	Figure 61 $Mo(\alpha,xn)^{95}Ru$
Figures 59 and 60 $Mo(p,xn)^{96}Tc$	$Mo(^{3}He,xn)^{97}Ru$	Figure 61 $Mo(\alpha,xn)^{97}Ru$
Figures 59 and 60 $Mo(p,xn)^{99m}Tc$		Figure 61 $^{98}Mo(\alpha,p)^{101}Tc$ $E_{th} = 5.4$
Figure 60 $Mo(p,xn)^{93}Tc$		
Figure 60 $^{100}Mo(p,pn)^{99}Mo$ $E_{th} = 8.4$		

RHODIUM

Protons	Helium4/Figure 62
Figure 63 $^{103}Rh(p,\alpha xn)^{97}Ru$	$^{103}Rh(\alpha,n)^{106m}Ag$ E_{th} = 7.4
Figure 64 $^{103}Rh(p,p2n)^{101m}Rh$ E_{th} = 16.9	$^{103}Rh(\alpha,2n)^{105g}Ag$ E_{th} = 16.2
Figure 64 $^{103}Rh(p,p2n)^{101}Rh$ E_{th} = 16.9	
Figure 64 $^{103}Rh(p,p3n)^{100}Rh$ E_{th} = 26.9	
Figure 64 $^{103}Rh(p,3n)^{101}Pd$ E_{th} = 19.5	
Figure 64 $^{103}Rh(p,4n)^{100}Pd$ E_{th} = 28.3	

PALLADIUM

Protons
Figure 59 $Pd(p,xn)^{104}Ag$
Figure 65 $Pd(p,xn)^{105}Ag$

SILVER

Protons/Figure 65	Helium 3/Figure 66
$^{107}Ag(p,n)^{107}Cd$ $E_{th} = 2.24$	$Ag(^{3}He,xn)^{109}In$
	$^{109}Ag(^{3}He,2n)^{110}In$ $E_{th} = 3.65$
	$^{109}Ag(^{3}He,n)^{111}In$ $E_{th} = 0$

CADMIUM

Protons/Figure 65	Helium 3/Figure 67	Helium 8
$Cd(p,xn)^{110m}In$	$Cd(^{3}He,xn)^{113}Sn$	Figure 67 $Cd(\alpha,xn)^{113}Sn$
$Cd(p,xn)^{111m}In$	$Cd(^{3}He,xn)^{117m}Sn$	Figure 67 $Cd(\alpha,xn)^{117m}Sn$
$Cd(p,xn)^{113m}In$		Figure 68 $^{116}Cd(\alpha,n)^{119m}Sn$ $E_{th} = 4.3$
		Figure 68 $^{116}Cd(\alpha,3n)^{117m}Sn$ $E_{th} = 20.8$

INDIUM

All curves in Figure 69

Helium 3	Helium 4
$In(^{3}He,pxn)^{113}Sn$	$In(\alpha,pxn)^{113}Sn$
$^{115}In(^{3}He,p)^{117m}Sn$ $E_{th} = 0$	$^{115}In(\alpha,pn)^{117m}Sn$ $E_{th} = 12.4$

TIN

Protons/Figure 65
$Sn(p,xn)^{116}Sb$
$Sn(p,xn)^{117}Sb$
$Sn(p,xn)^{118m}Sb$
$Sn(p,xn)^{120m}Sb$

TELLURIUM

Protons/Figure 72	Deuterons/Figure 71	Helium 3	Helium 4
$^{123}Te(p,n)^{123}I$ $E_{th} = 2.15$	$^{122}Te(d,n)^{123}I$ $E_{th} = 0$	Figure 73 $Te(^{3}He,xn)^{125}Xe$	Figure 73 $Te(\alpha,xn)^{125}Xe$
$^{124}Te(p,2n)^{123}I$ $E_{th} = 11.6$	$^{122}Te(d,2n)^{122}I$ $E_{th} = 7.3$		
	$^{122}Te(d,3n)^{121}I$ $E_{th} = 15.7$		

IODINE

Protons/Figure 70
$^{127}I(p,5n)^{123}Xe$ $E_{th} = 36.8$

PLATINUM
All curves in Figure 59

Protons
$Pt(p,xn)^{194}Au$
$Pt(p,xn)^{196}Au$
$^{198}Pt(p,n)^{198}Au$ $E_{th} = 1.45$

GOLD
All curves in Figure 74

Helium 4
$^{197}Au(\alpha,n)^{200}Tl$ $E_{th} = 10$
$^{197}Au(\alpha,2n)^{199}Tl$ $E_{th} = 16.8$
$^{197}Au(\alpha,3n)^{198m}Tl$ $E_{th} = 26$
$^{197}Au(\alpha,3n)^{198g}Tl$ $E_{th} = 26$

THALLIUM

All curves in Figure 75

Protons
$Tl(p,xn)^{203}Pb$
$Tl(p,xn)^{201}Pb$
$Tl(p,xn)^{200}Pb$
$Tl(p,xn)^{199}Pb$

LEAD

Protons/Figure 76	Deuterons/Figure 77	Helium 4/Figure 78
$Pb(p,pxn)^{201}Pb$	$Pb(d,xn)^{207}Bi$	$Pb(\alpha,xn)^{206}Po$
$Pb(p,pxn)^{200}Pb$	$Pb(d,xn)^{206}Bi$	
	$Pb(d,xn)^{205}Bi$	

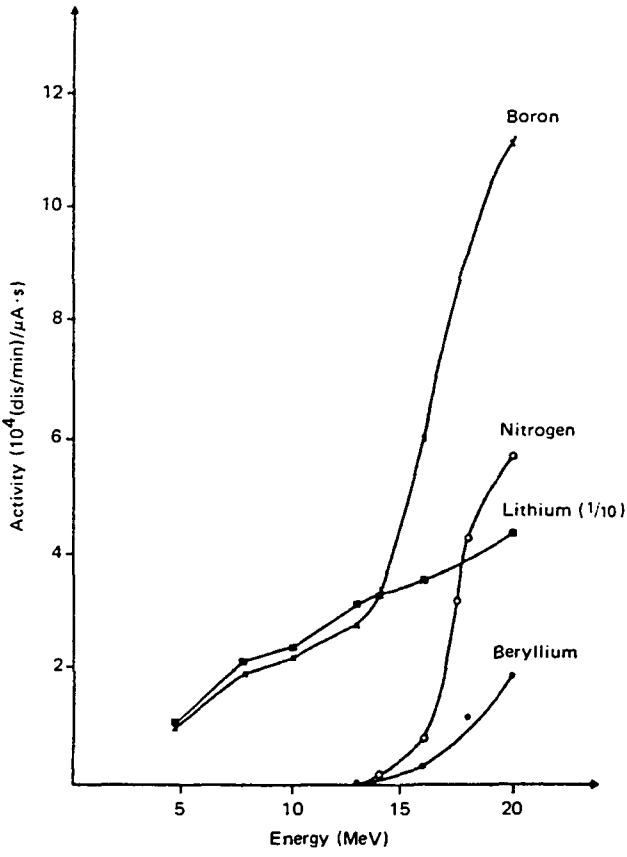

FIG. 1. Thick target yields for the production of ^{7}Be for proton reactions on Li, Be, B and N [2]. *(1 dis/min = 6.00 × 10^1 Bq.)*

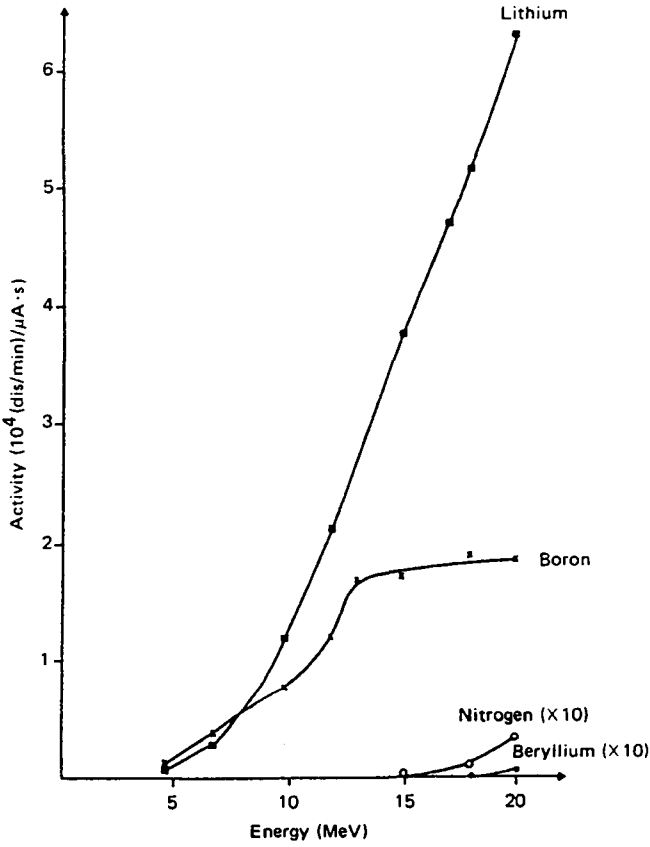

FIG. 2. Thick target yields for the production of ^{7}Be for deuteron reactions on Li, Be, B and N [2].

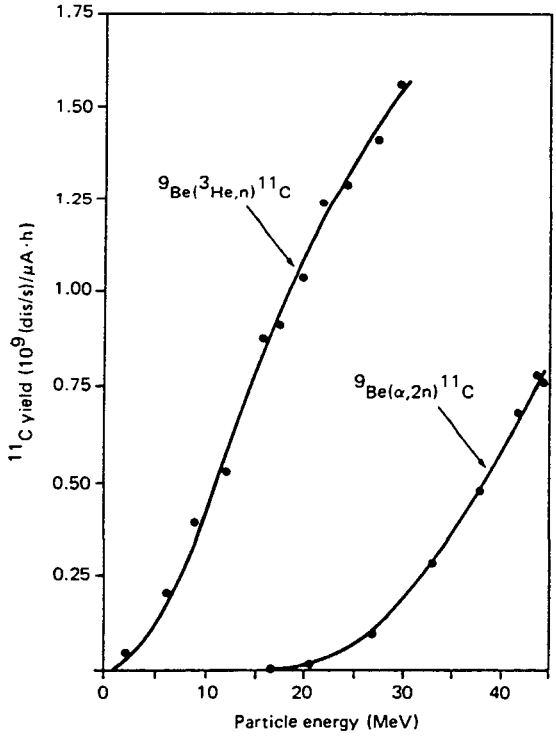

FIG. 3. Yield of ^{11}C after irradiation of beryllium with ^{3}He and ^{4}He ions (target: Be) [3]. *(1 (dis/s) = 1.00 × 10^{0} Bq.)*

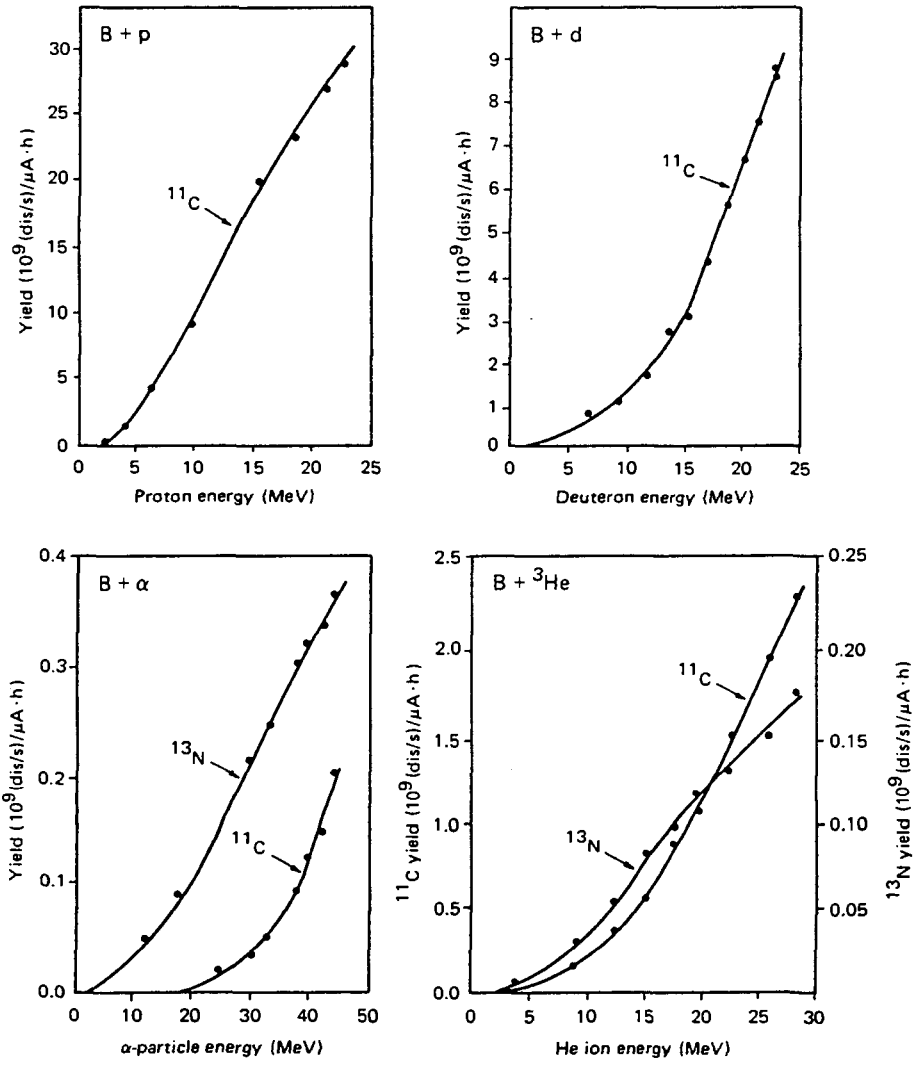

FIG. 4. Yields of ^{11}C and ^{13}N after irradiation of boron with protons, deuterons, ^3He and ^4He ions (target: B) [3].

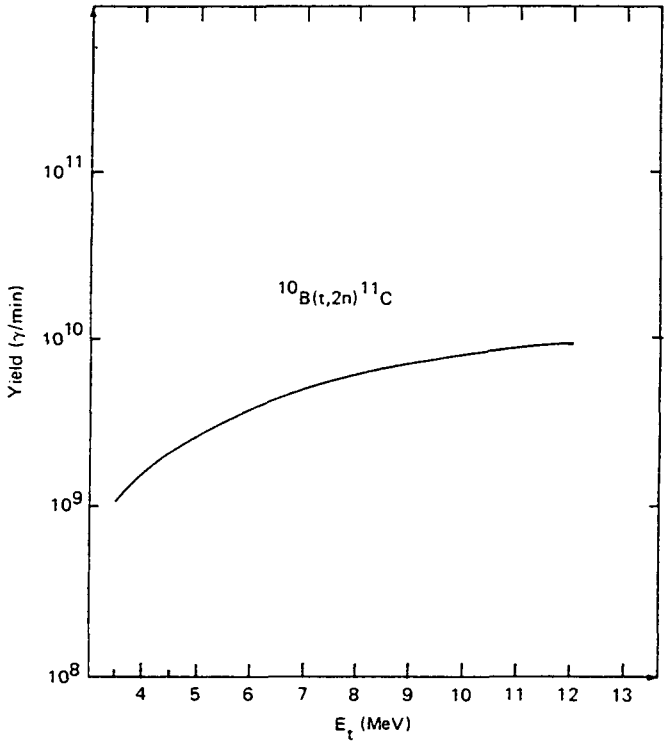

FIG. 5. Production of ^{11}C by triton irradiation of a thick, pure boron target. The yield (511 keV annihilation peak) is obtained at the end of an irradiation of 1 h at 1 μA, and is variable with the annihilation conditions [4].

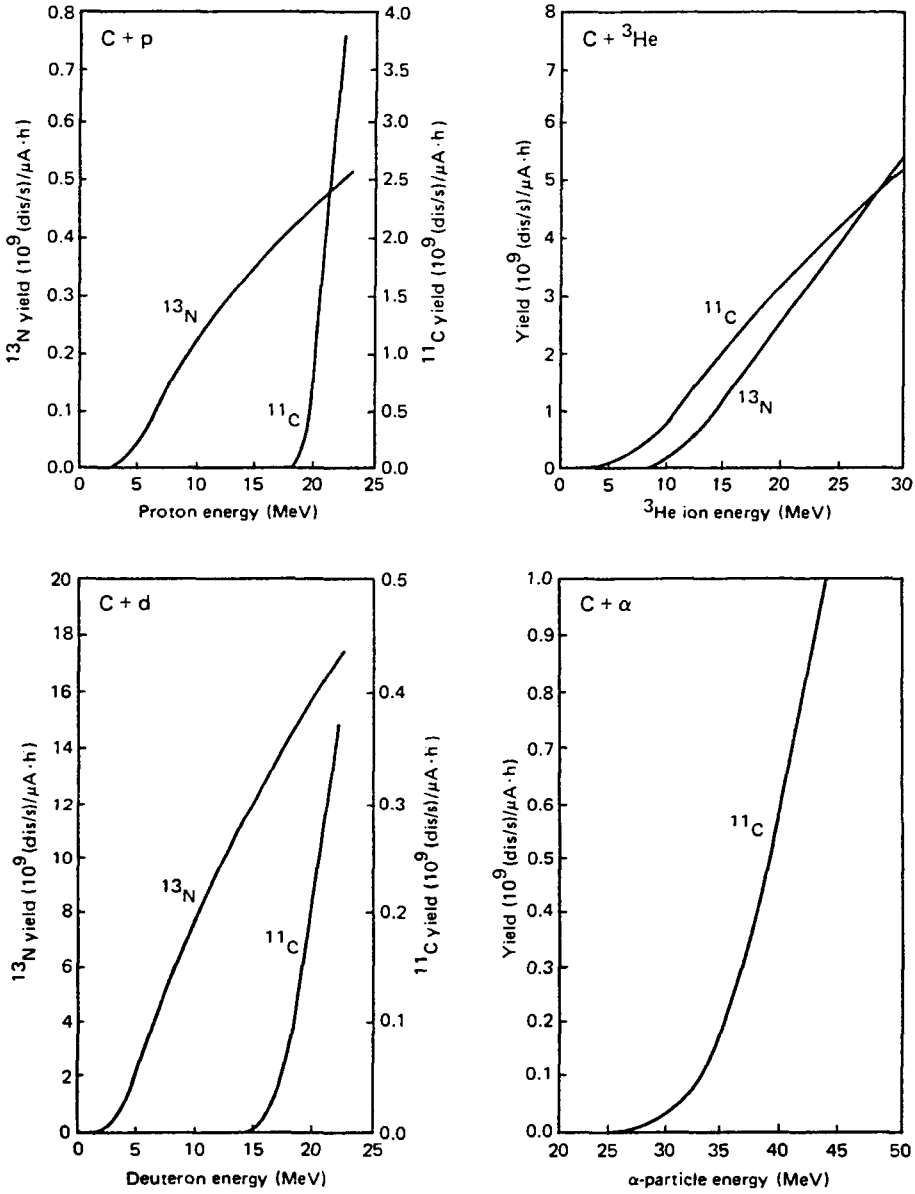

FIG. 6. Yields of ^{11}C and ^{13}N after irradiation of carbon with protons, deuterons, ^3He and ^4He ions (target: graphite) [3].

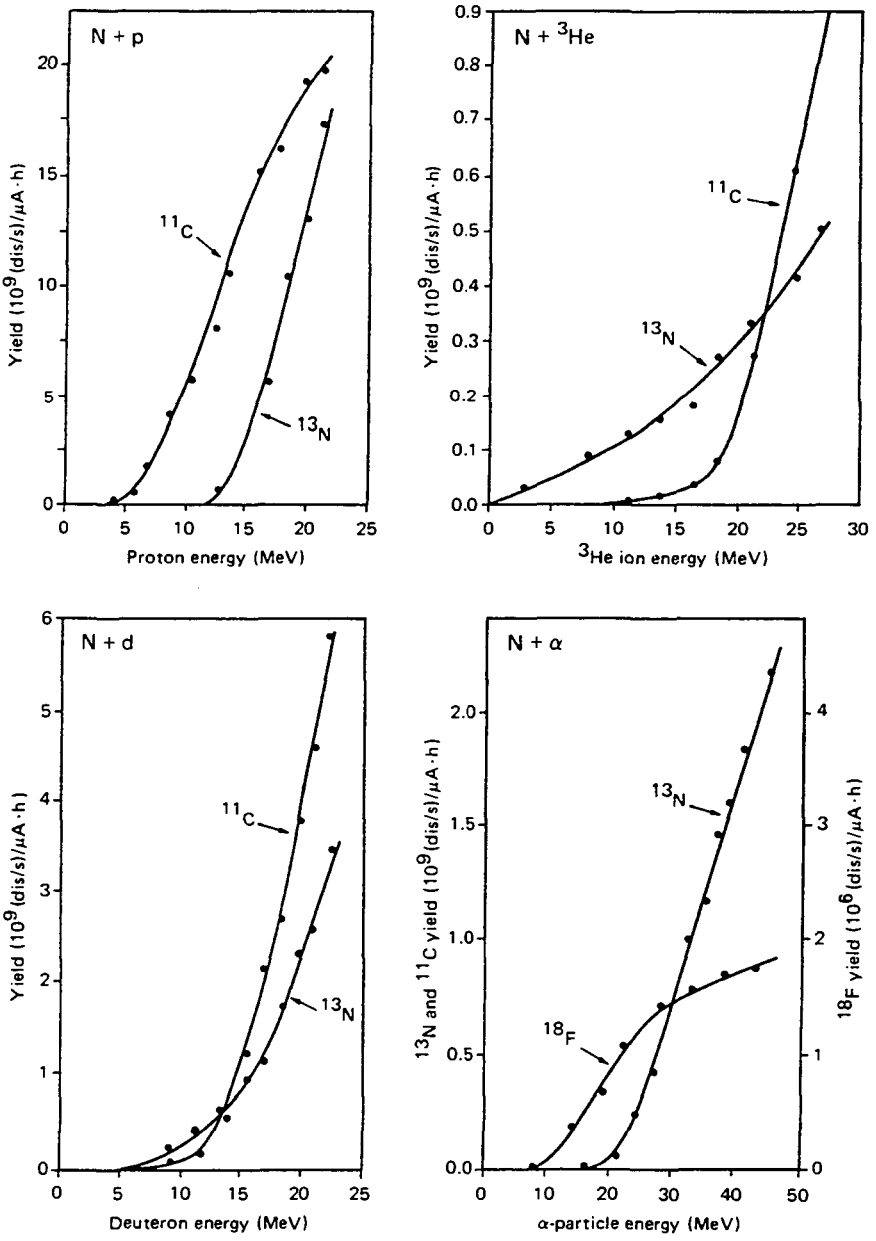

FIG. 7. Yields of ^{11}C, ^{13}N and ^{18}F after irradiation of nitrogen with protons, deuterons, ^3He and ^4He ions (target: AlN) [3].

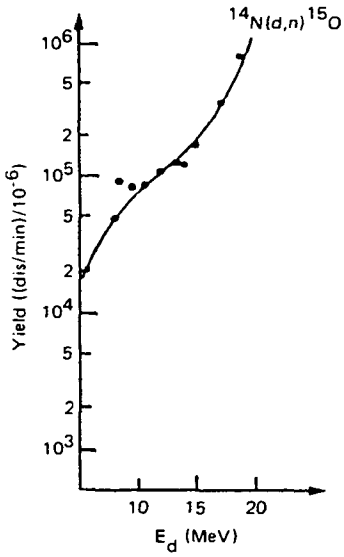

FIG. 8. Thick target yield for the production of ^{15}O by deuteron irradiation of AlN. The yield is expressed here in disintegrations per minute at the end of irradiation for 1 min at 1 μA for a target containing 10^{-6} g/g of the element in question [5].

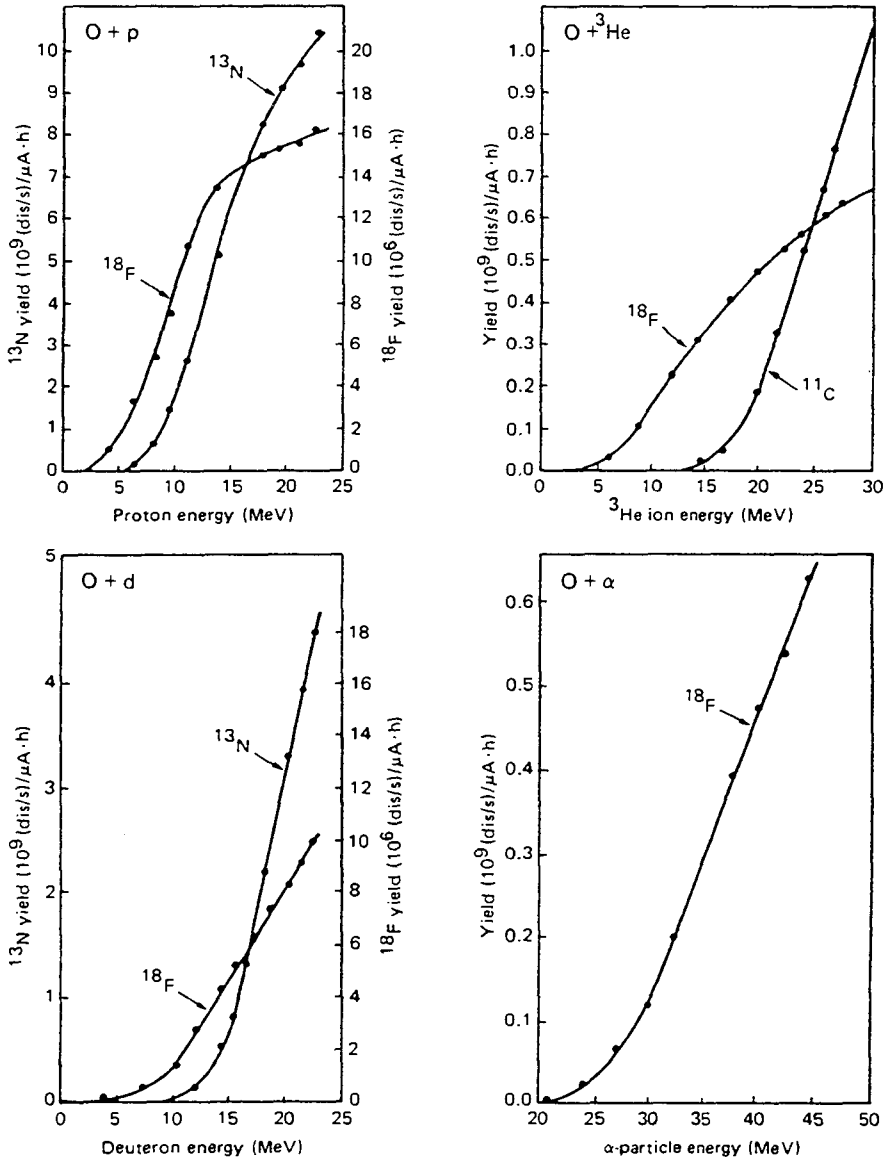

FIG. 9. Yields of ^{11}C, ^{13}N and ^{18}F after irradiation of oxygen with protons, deuterons, ^3He and ^4He ions (target: Al_2O_3) [3].

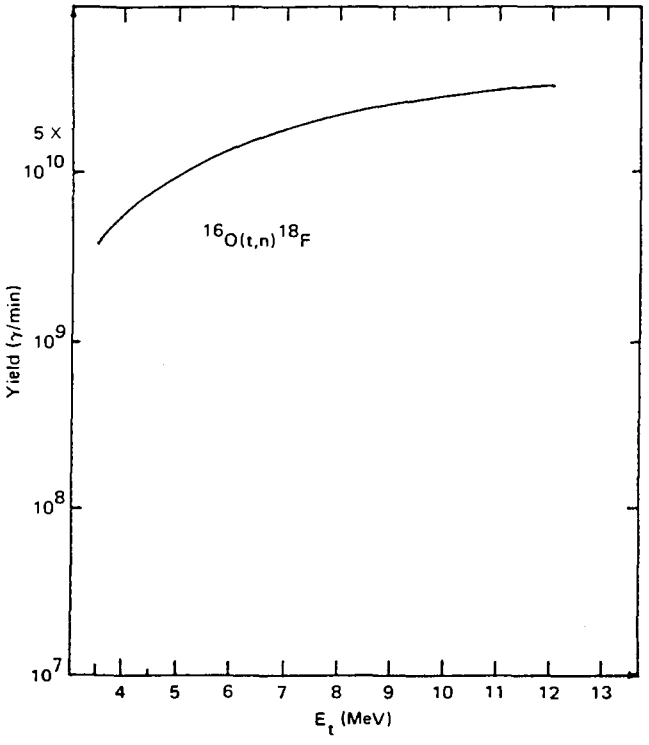

FIG. 10. Production of ^{18}F by triton irradiation of a thick Al_2O_3 target. The yield (511 keV annihilation peak) is obtained at the end of irradiation for 1 h at 1 μA, and is variable with the annihilation conditions [4].

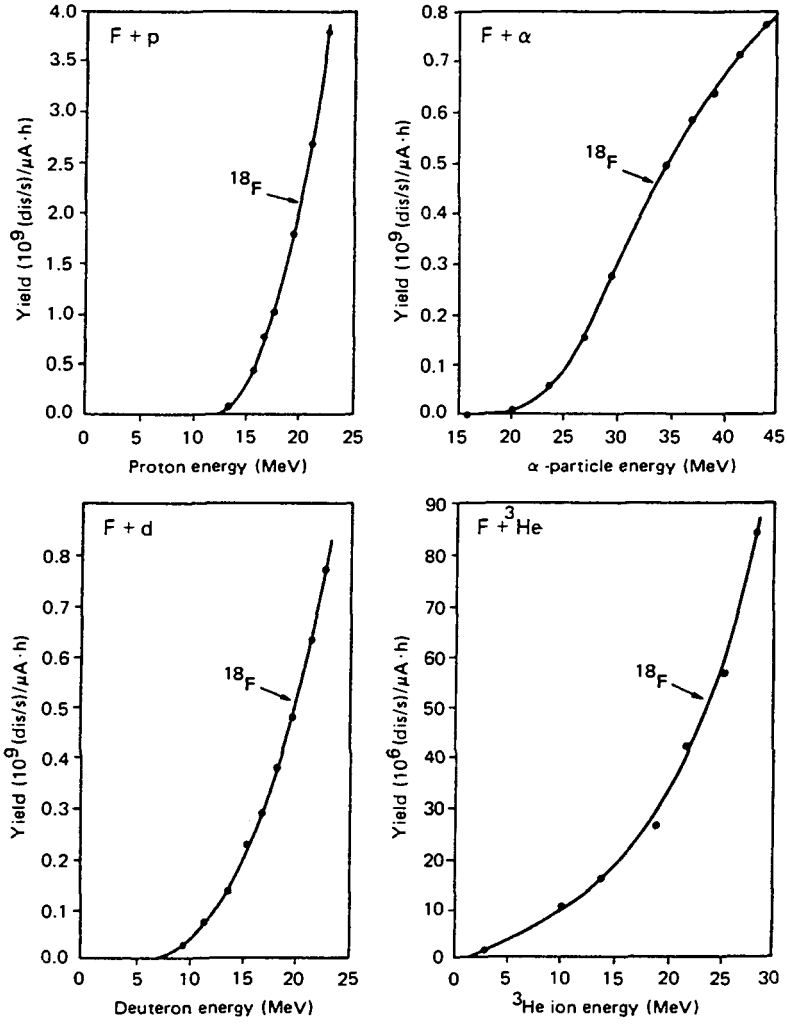

FIG. 11. Yield of ^{18}F after irradiation of fluorine with protons, deuterons, ^3He and ^4He ions (target: $(CF_2)_n$) [3].

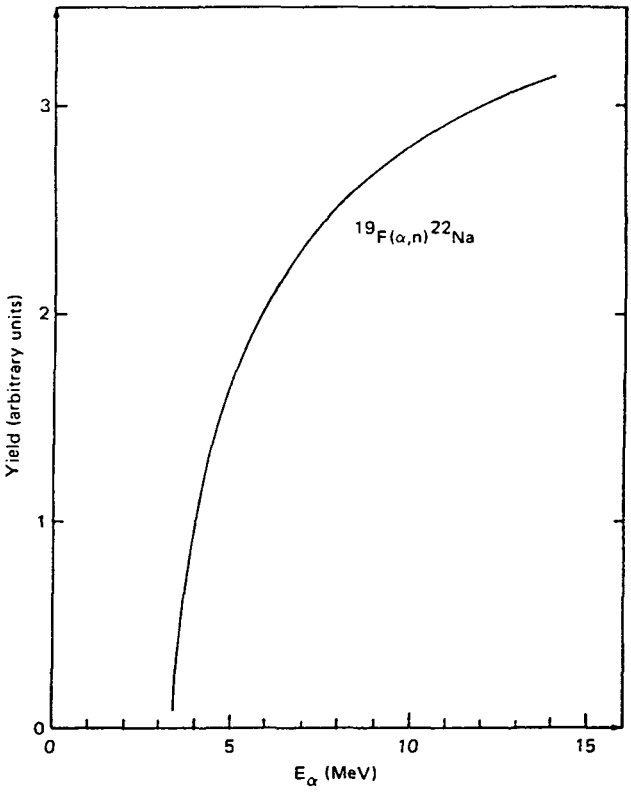

FIG. 12. Thick target yield curve for the $^{19}F(\alpha, n)^{22}Na$ reaction. Target: PbF_2 [6].

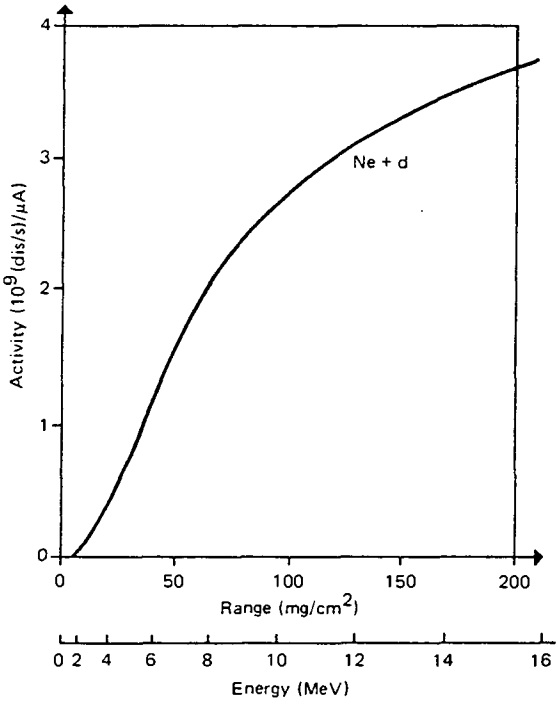

FIG. 13. Thick target saturation activity for the reaction of deuterons on neon to give ^{18}F. Target: pure neon in sealed cylinders at 1 atmosphere [7] (1 atm = 1.013 25 × 10^5 Pa).

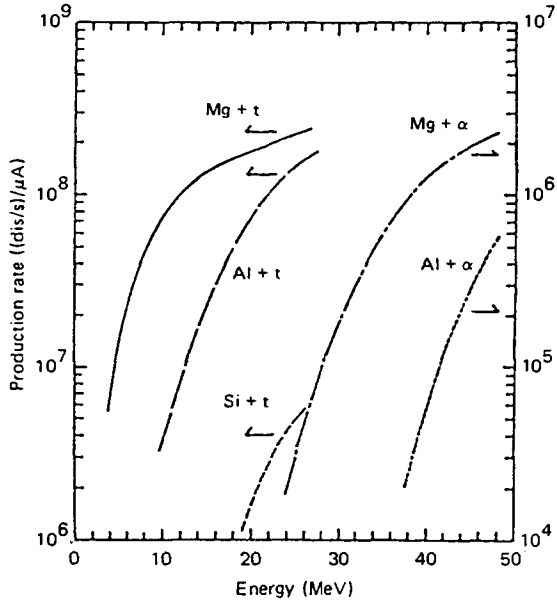

FIG. 14. Thick target yields of ^{28}Mg for the reactions of tritons on Mg, Al and Si, and of α-particles on Mg and Al [8].

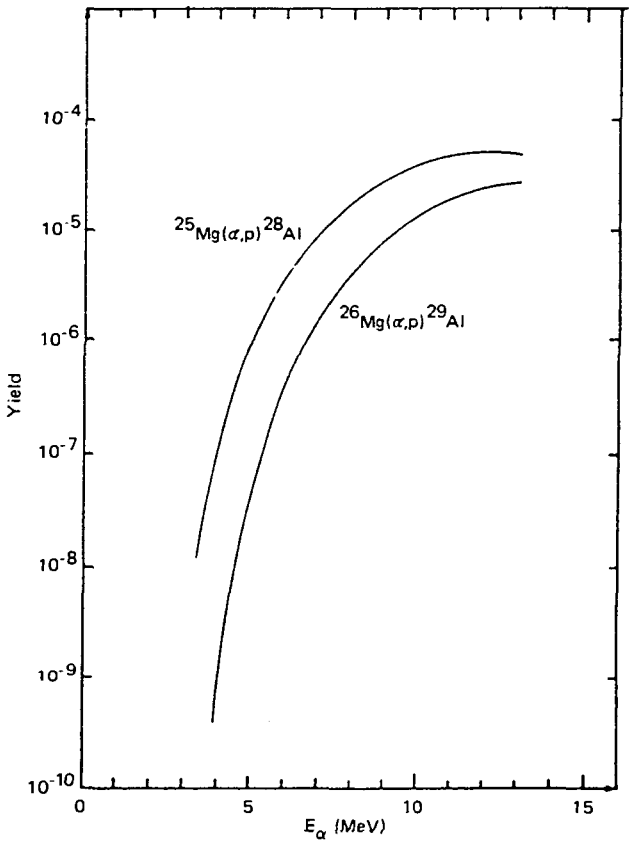

FIG. 15. Thick target yields for the (α, p) reactions on Mg isotopes. Yield: the ratio of the total number of reactions of a given type to the number of incident beam particles, assuming 100% abundance for every isotope [9].

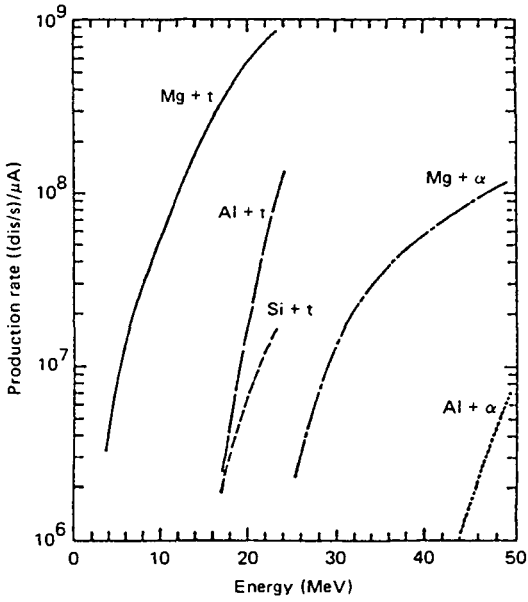

FIG. 16. Thick target yields of ^{24}Na for the reactions of tritons on Mg, Al and Si, and of α-particles on Mg and Al [8].

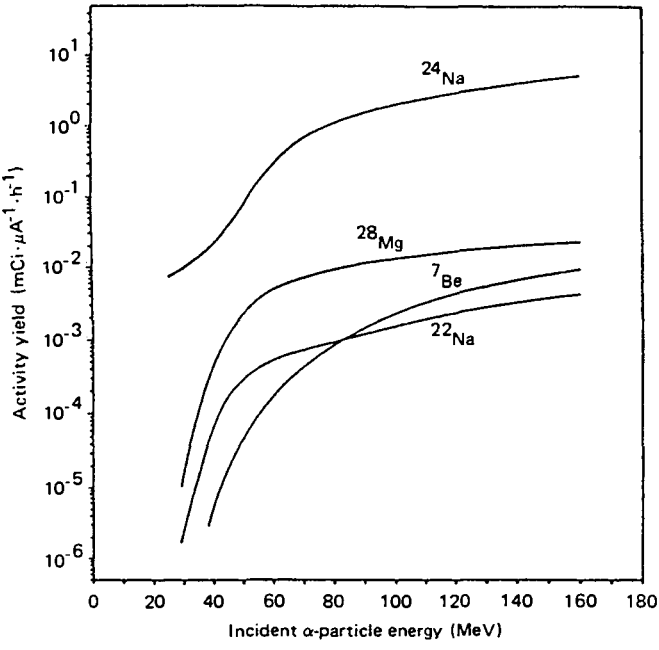

FIG. 17. Yields of ^{28}Mg, ^{24}Na, ^{22}Na and ^{7}Be after irradiation of ^{27}Al with high-energy α-particles [10]. *(1 Ci = 3.70 × 10^{10} Bq.)*

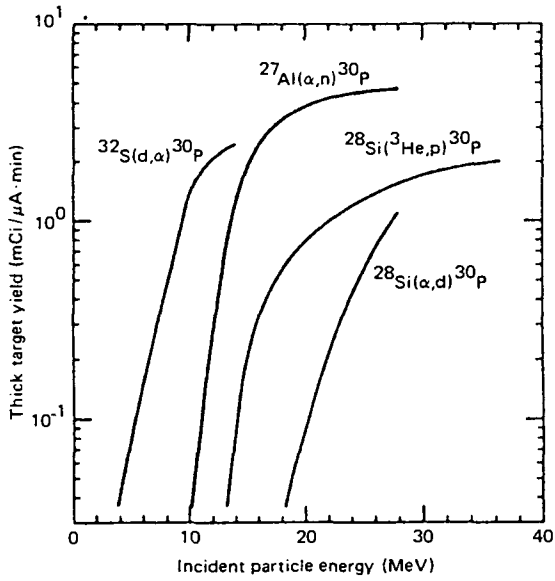

FIG. 18. Theoretical thick target yields of carrier-free ^{30}P for various nuclear processes as functions of incident projectile energy [11].

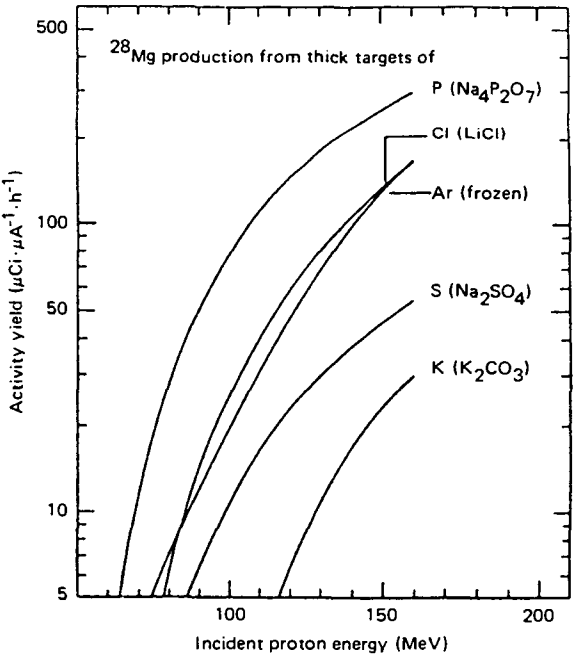

FIG. 19. Thick target yields for the production of ^{28}Mg [12].

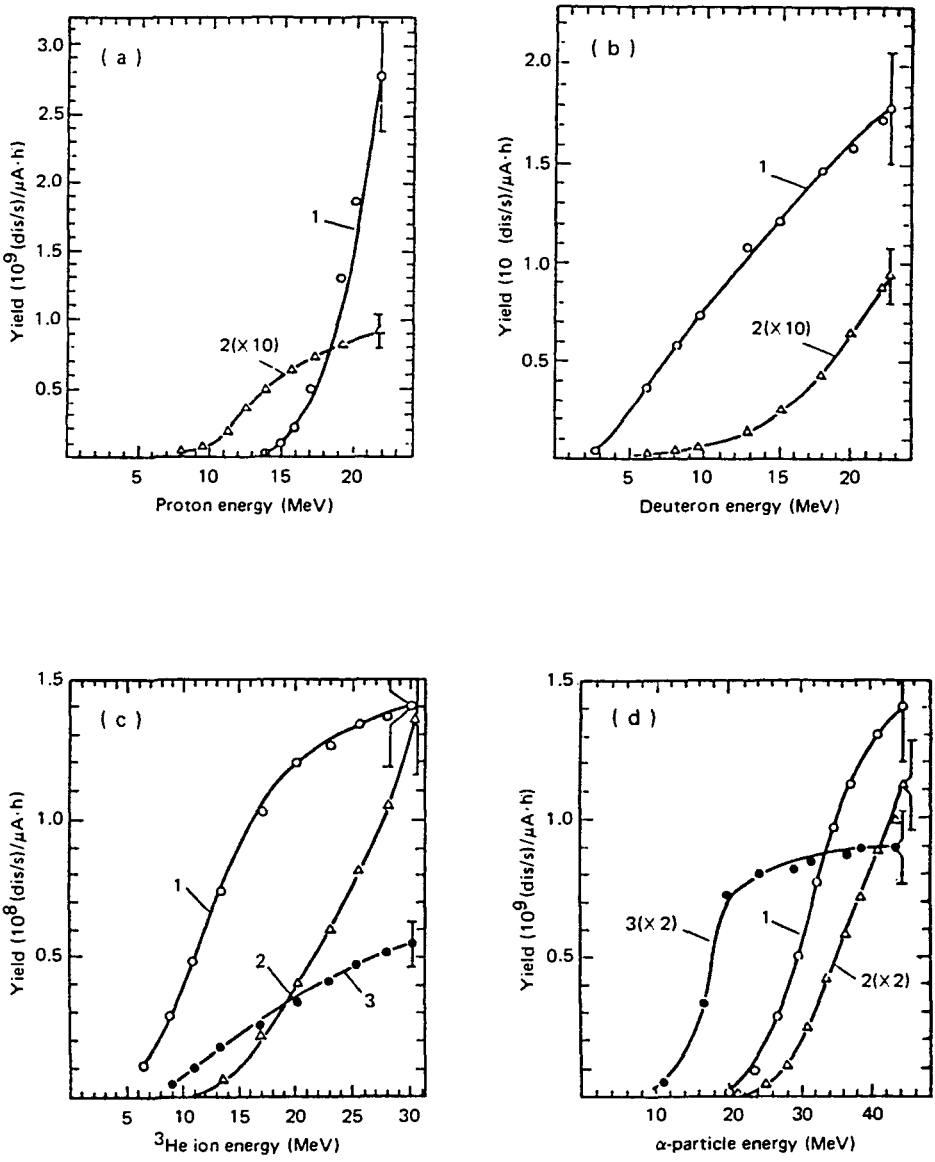

FIG. 20. (a) Yields for radioisotopes vs proton energy. Curve 1: Cl + p → ^{34m}Cl; curve 2: S + p → ^{34m}Cl. (b) Yields for radioisotopes vs deuteron energy. Curve 1: Cl + d → ^{38}Cl; curve 2: S + d → ^{34m}Cl. (c) Yields for radioisotopes vs ^{3}He ion energy. Curve 1: S + ^{3}He → ^{34m}Cl; curve 2: Cl + ^{3}He → ^{38}Cl; curve 3: Cl + ^{3}He → ^{34m}Cl. (d) Yields for radioisotopes vs α-particle energy. Curve 1: S + α → ^{34m}Cl; curve 2: Cl + α → ^{34m}Cl; curve 3: P + α → ^{34m}Cl. (Source for all figures: Ref. [13].)

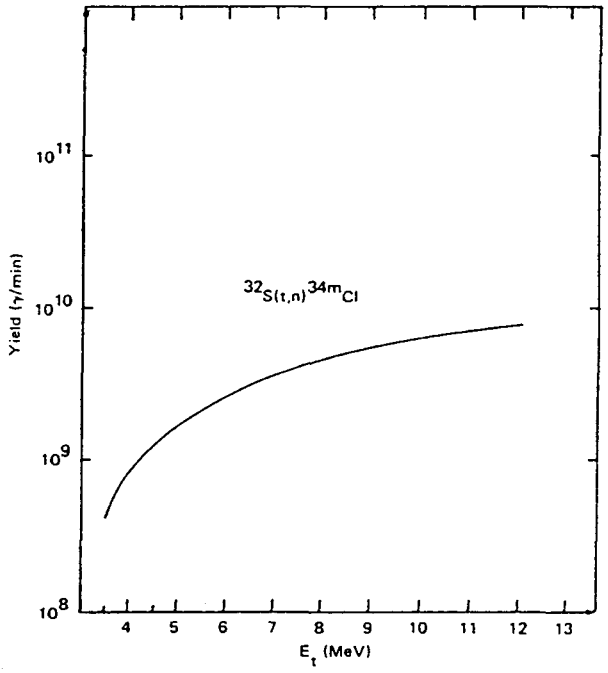

FIG. 21. Production of ^{34m}Cl by triton irradiation of a pure S target. The yield (146 keV) is obtained at the end of irradiation for 1 h at 1 μA [4].

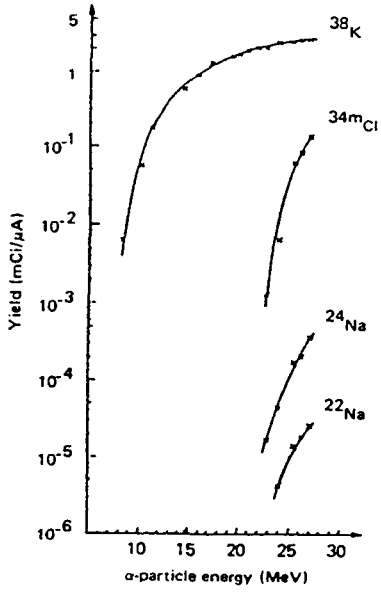

FIG. 22. Yields of ^{38}K, ^{34m}Cl, ^{22}Na and ^{24}Na as functions of the energy at the end of a 15 min period of irradiation of NaCl powder [14].

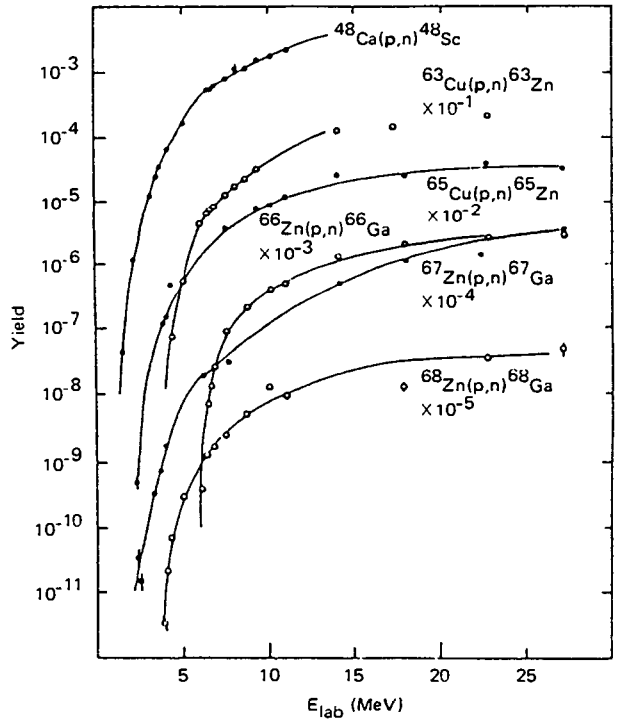

FIG. 23. Thick target yields from the (p, n) reaction measured by the radioactive decay of the final nuclide. Targets: Ca, Cu and Zn. The yield is defined here as the number of radioactive products formed per incident proton upon a thick target composed solely of the target isotope [15].

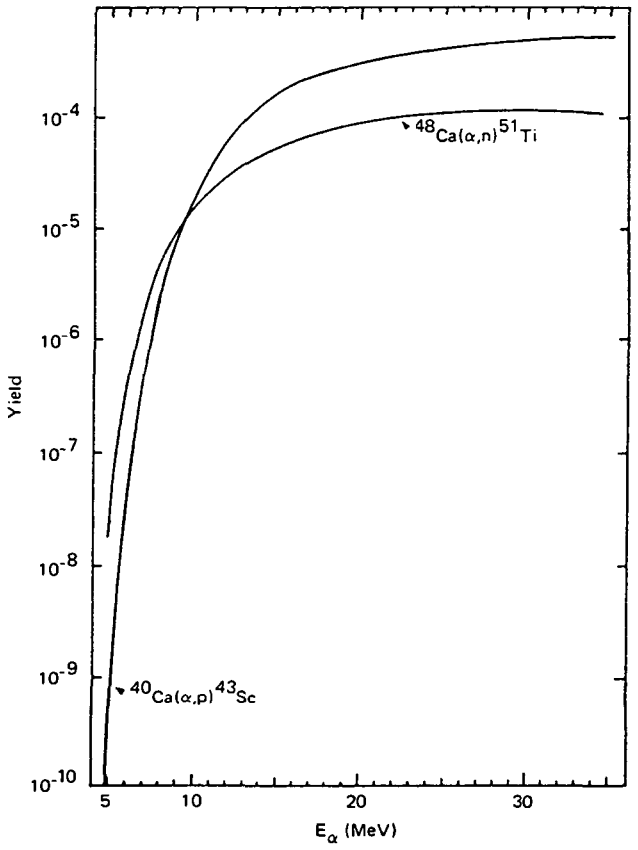

FIG. 24. Thick target yields for the (α, n) and (α, p) reactions on Ca isotopes. The yield is defined as the ratio of the total number of reactions of a given type to the number of incident beam particles, assuming 100% abundance for every isotope [9].

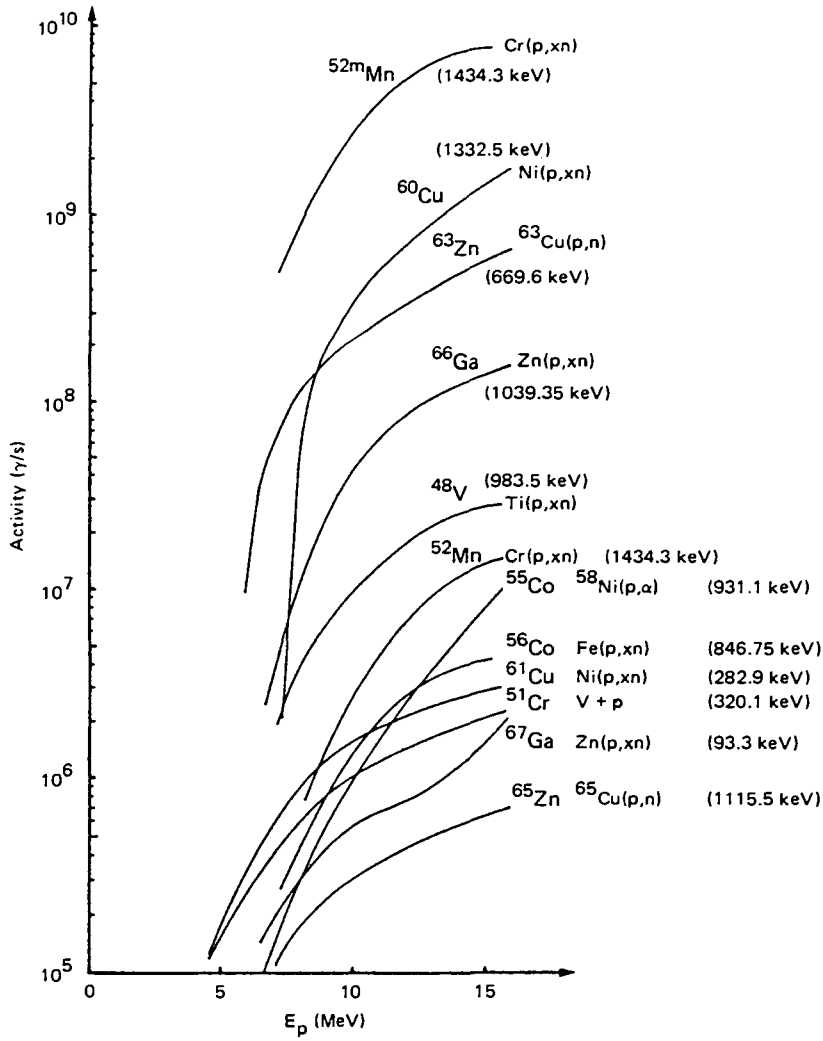

FIG. 25. Specific activity, expressed in gamma rays per second, for the thick target yields of natural metals (Ti, V, Cr, Fe, Ni, Cu, Zn) at the end of proton irradiation for 1 h at 1 μA [16].

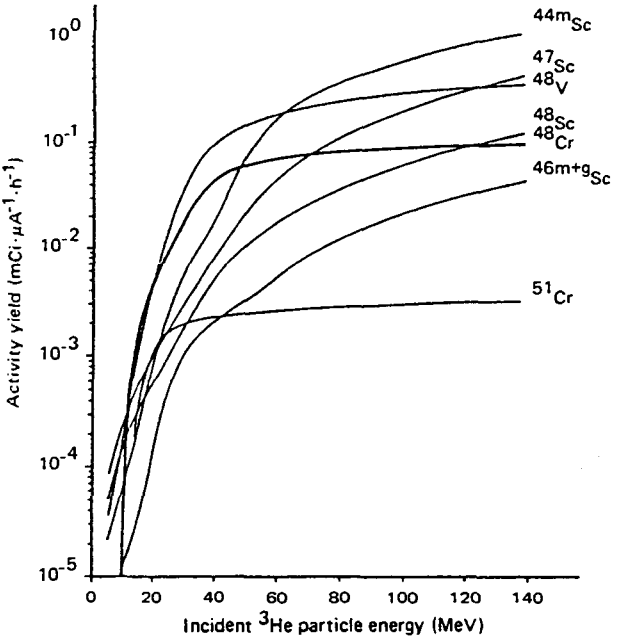

FIG. 26. Thick target yields of ^{48}Cr, ^{51}Cr and major impurities as functions of incident ^{3}He particle energy on titanium [17].

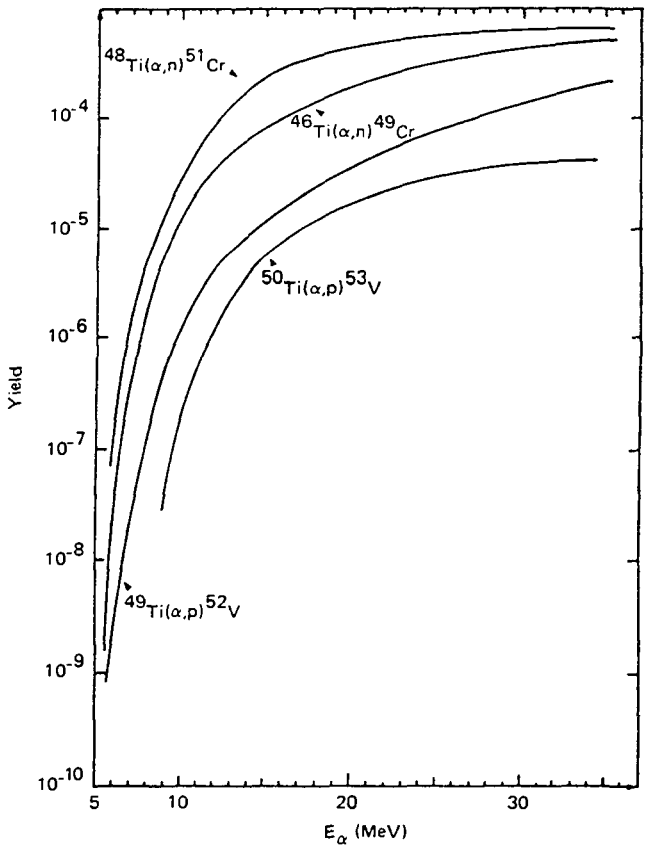

FIG. 27. Thick target yields for the (α, n) and (α, p) reactions on Ti isotopes. The yield is defined as the ratio of the total number of reactions of a given type to the number of incident beam particles, assuming 100% abundance for every isotope [9].

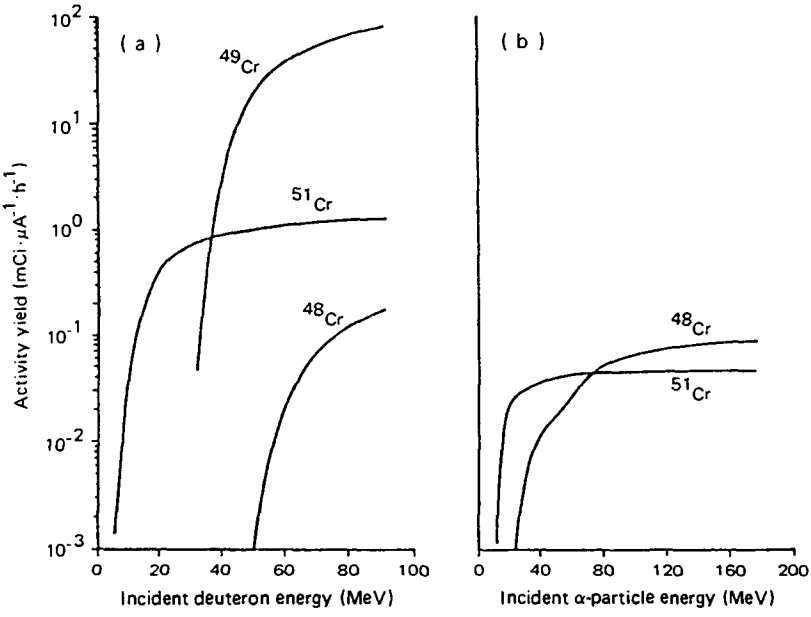

FIG. 28. Thick target yields of chromium isotopes formed by interaction of (a) deuterons with vanadium and (b) α-particles with titanium [17].

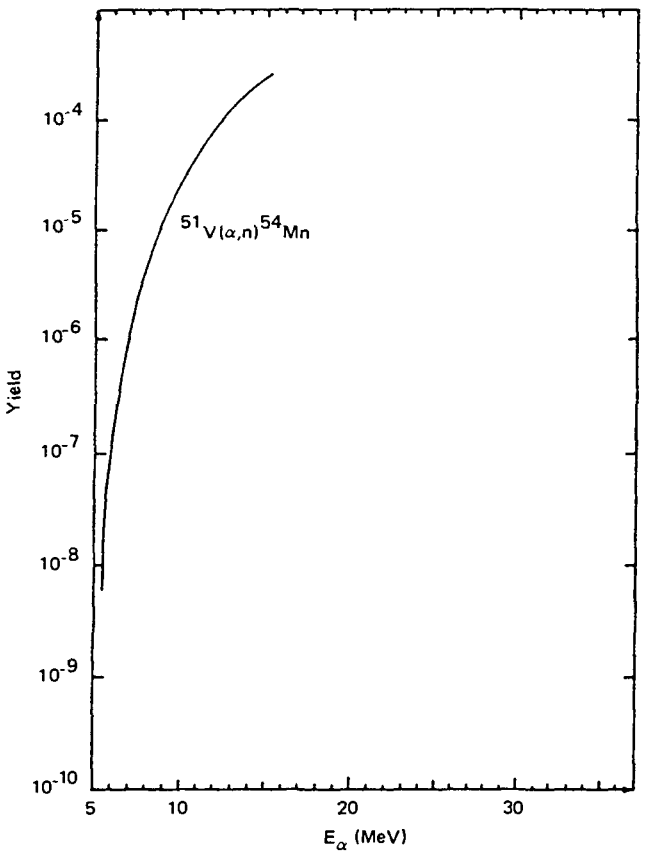

FIG. 29. Thick target yield for the $^{51}V(\alpha, n)^{54}Mn$ reaction. The yield is defined as the ratio of the total number of reactions to the number of incident beam particles, assuming 100% abundance for ^{51}V [9].

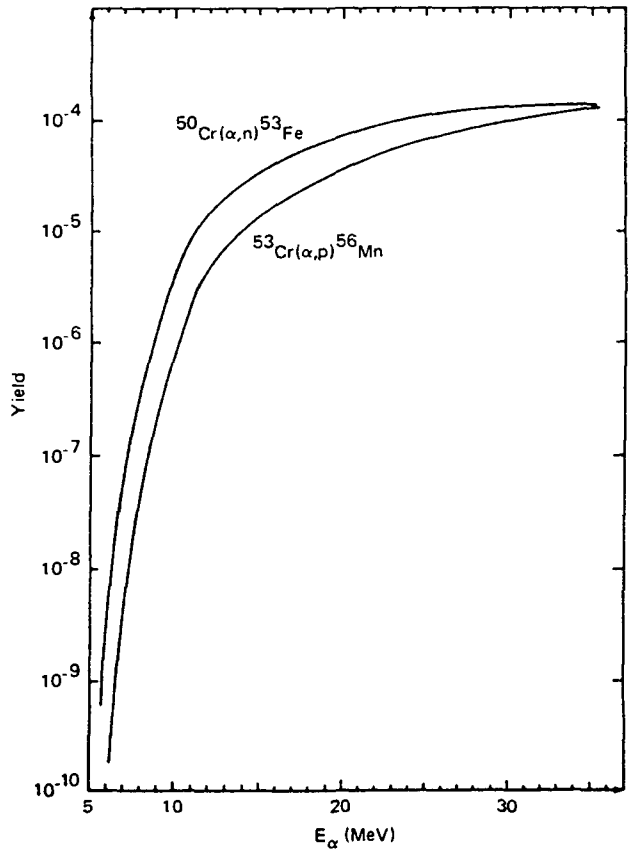

FIG. 30. Thick target yields for the (α, n) and (α, p) reactions on Cr isotopes. The yield is defined as the ratio of the total number of reactions of a given type to the number of incident beam particles, assuming that the isotopic abundance is 100% for every isotope [9].

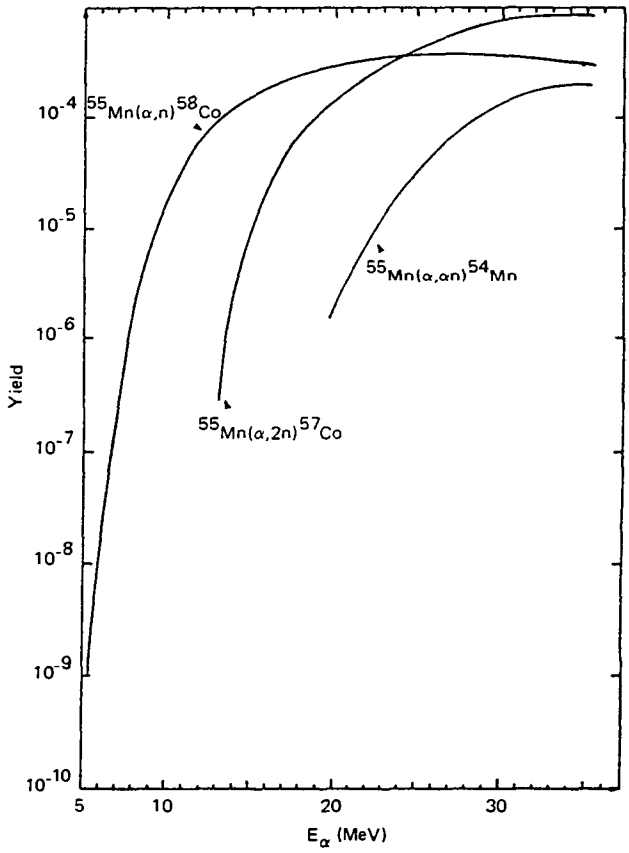

FIG. 31. Thick target yields for reactions of α-particles on Mn. The yield is defined as the ratio of the total number of reactions of a given type to the number of incident beam particles [9].

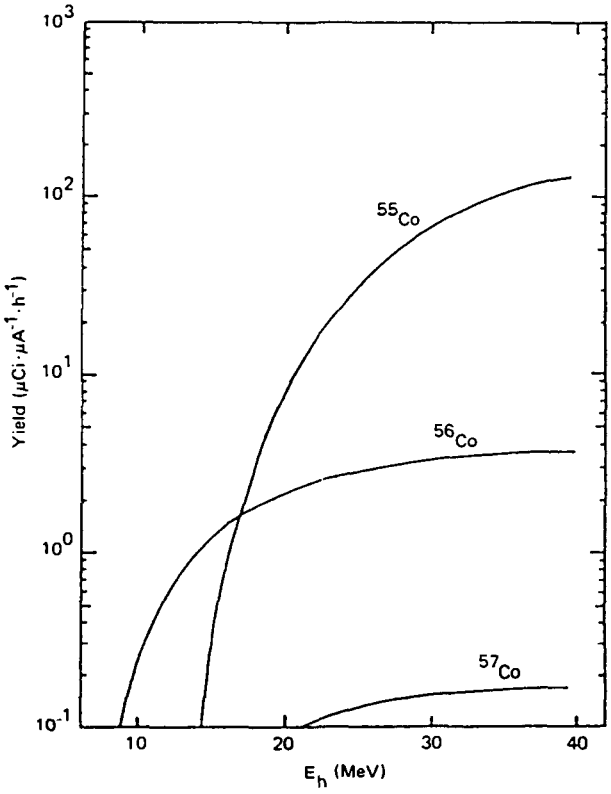

FIG. 32. Thick target yield curves for the production of cobalt isotopes by (^{3}He + ^{55}Mn) reactions [18].

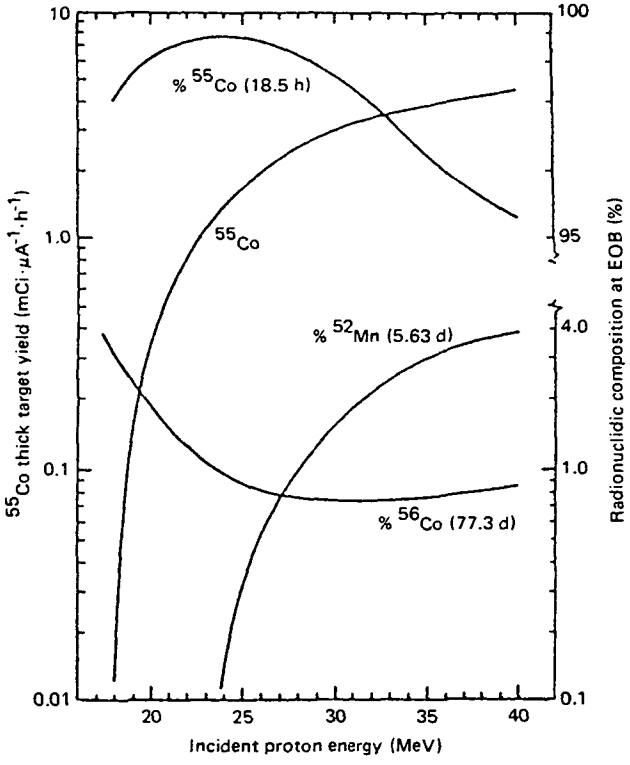

FIG. 33. Thick target yield for ^{55}Co given as a function of incident proton energy. Also shown is the per cent total radioactivity of ^{55}Co, ^{56}Co and ^{52}Mn (principal contaminants) vs proton energy (right-hand ordinate) (EOB: end of bombardment). A natural iron target is used [19].

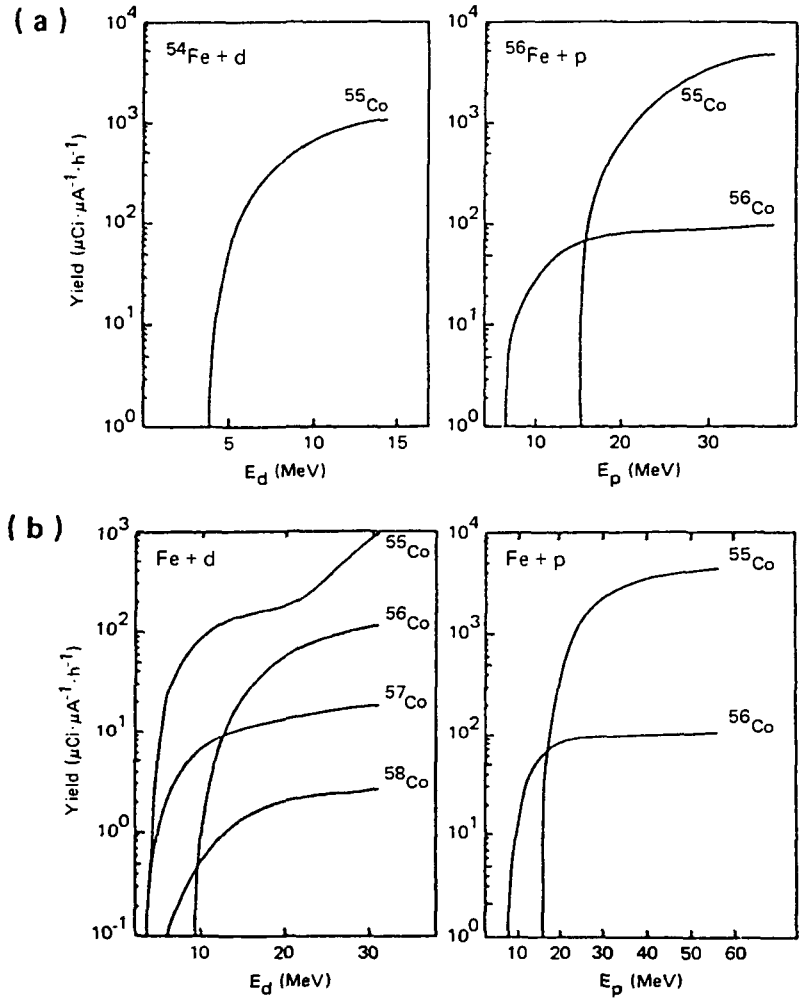

FIG. 34. (a) Thick target yields for enriched targets of ^{54}Fe (98.19%) and ^{56}Fe (99.93%) (evaluated from cross-section data reported in the literature) irradiated with deuterons ^{54}Fe and protons ^{56}Fe. (b) Thick target yields for a natural Fe target irradiated with deuterons and with protons (evaluation) [18].

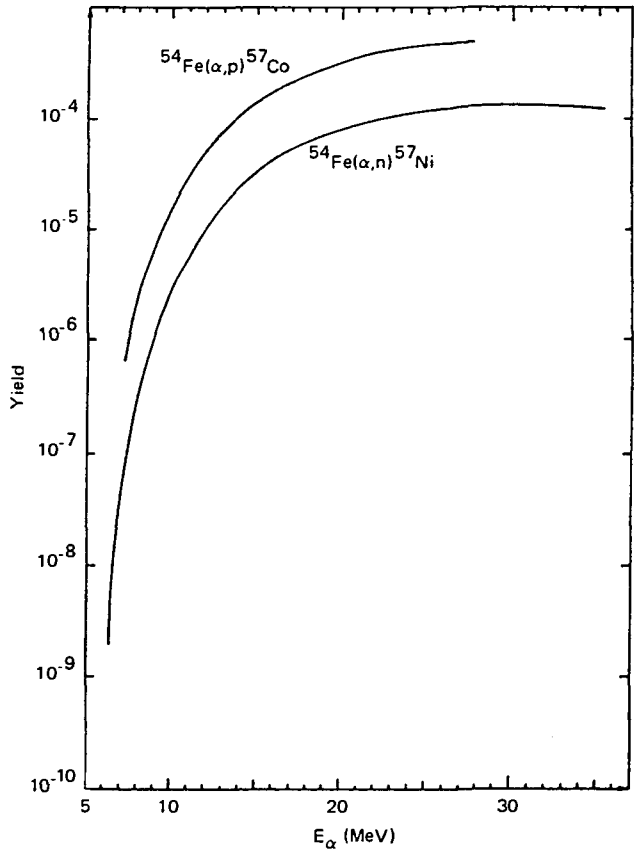

FIG. 35. Thick target yields for the (α, n) and (α, p) reactions on ^{54}Fe. The yield is defined as the ratio of the total number of reactions of a given type to the number of incident beam particles, assuming that the isotopic abundance is 100% [9].

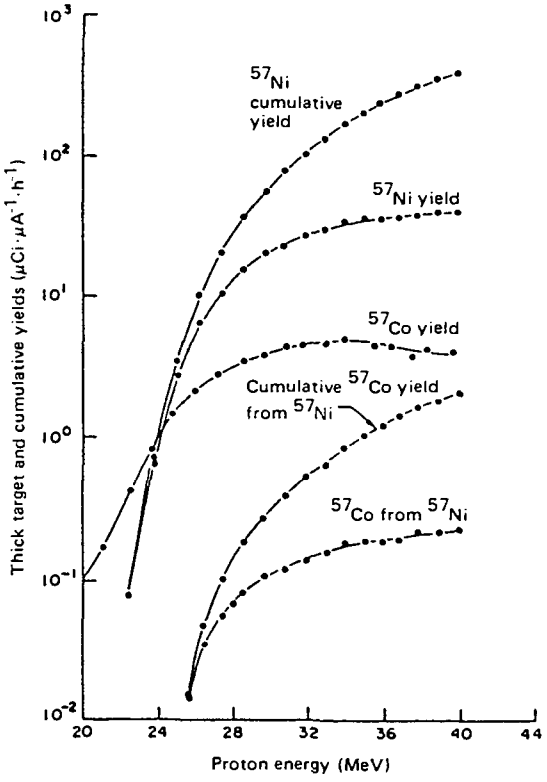

FIG. 36. Thick target and cumulative yields for the ^{57}Ni parent (at EOB) and the ^{57}Co daughter radionuclides (at t_{max} = 271.5 h post-bombardment) as functions of proton energy. Cumulative yields were calculated by summing the individual thick target yields, as given in this figure [20].

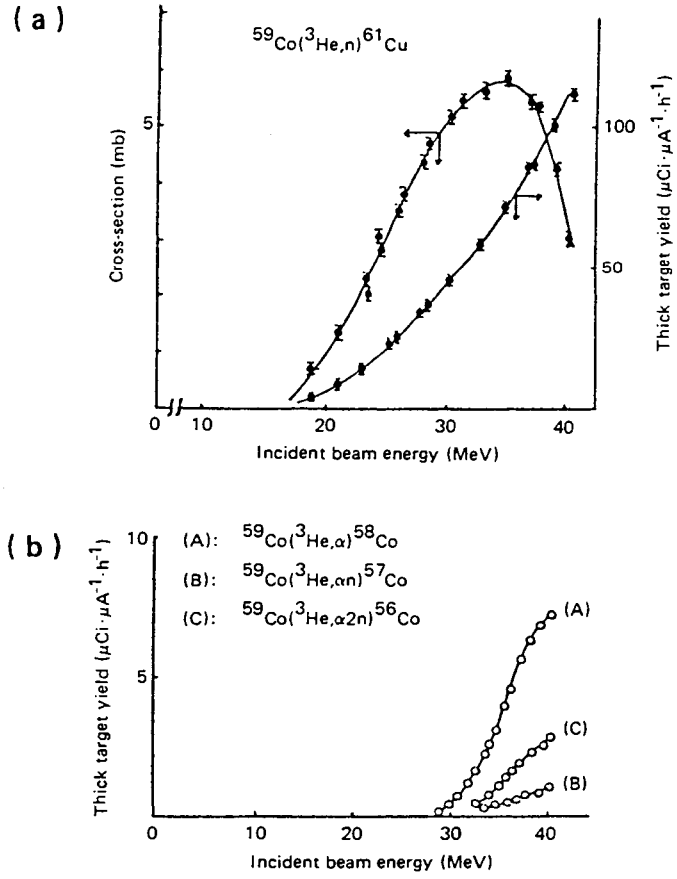

FIG. 37. (a) Excitation curve and thick target yield curve for the ^{3}He reaction on cobalt producing ^{61}Cu. (b) Thick target yield curves for ^{3}He reactions on cobalt producing ^{56}Co, ^{57}Co and ^{58}Co [21].

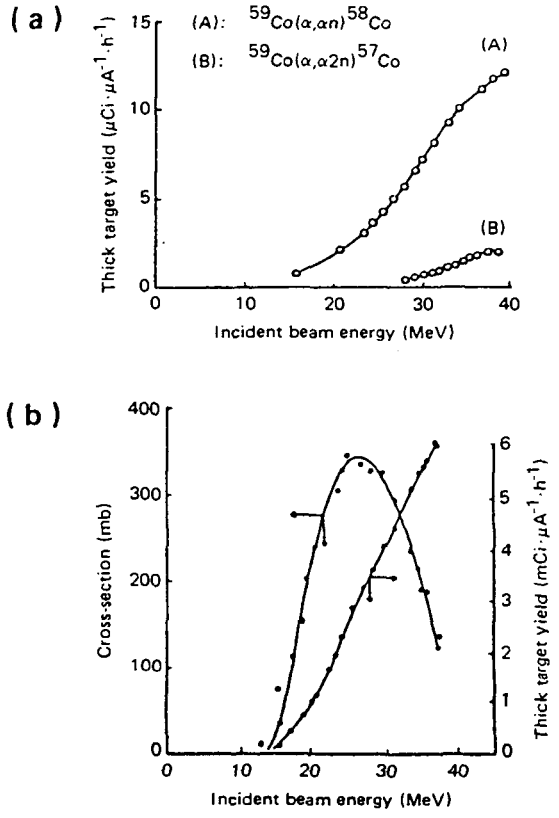

FIG. 38. (a) Thick target yield curves for α-reactions on cobalt producing ^{57}Co and ^{58}Co. (b) Excitation curve and thick target yield curve for an α-reaction on cobalt producing ^{61}Cu [21].

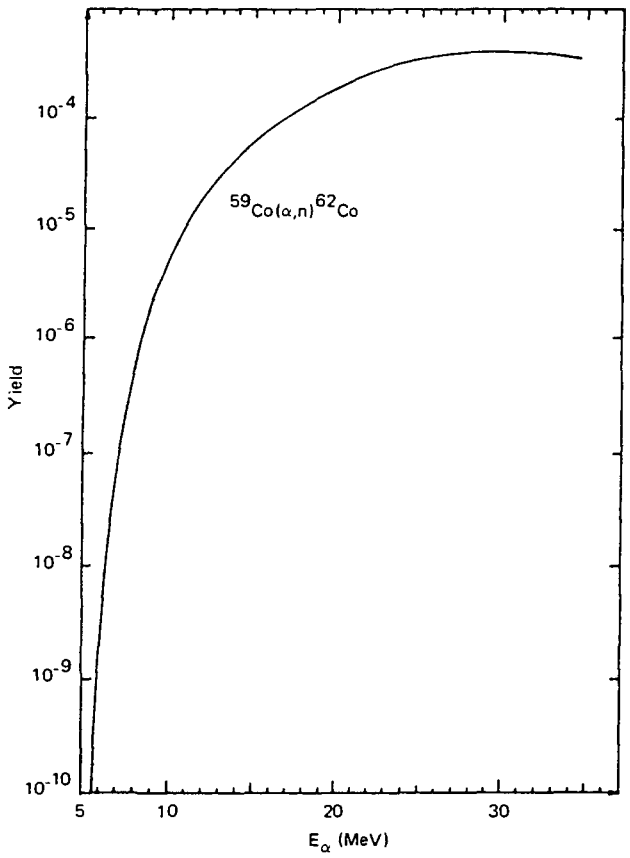

FIG. 39. Thick target yield for the $^{59}Co\ (\alpha, n)^{62}Cu$ reaction. The yield is defined as the ratio of the total number of reactions to the number of incident beam particles [9].

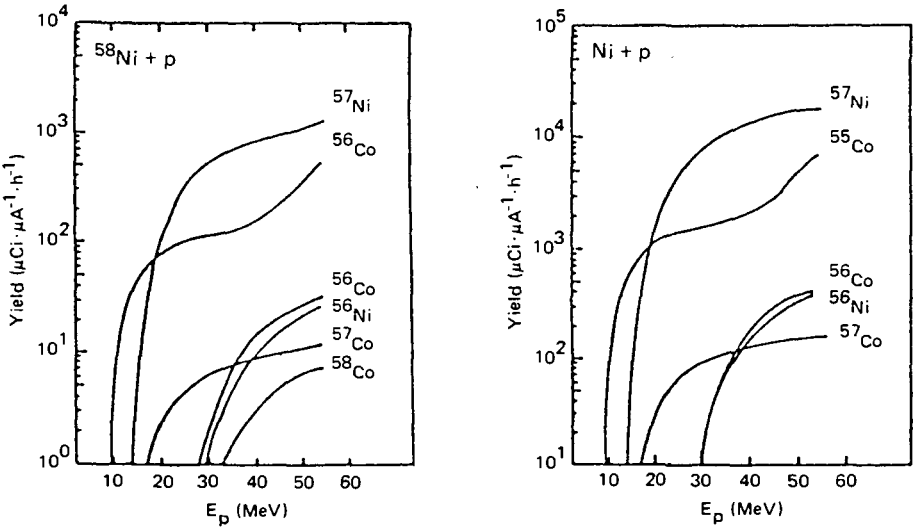

FIG. 40. (a) Thick target yields for a 99.95% ^{58}Ni enriched target (evaluation from cross-section data reported in the literature) irradiated with protons. (b) Thick target yields for a natural Ni target (evaluation) irradiated with protons [18].

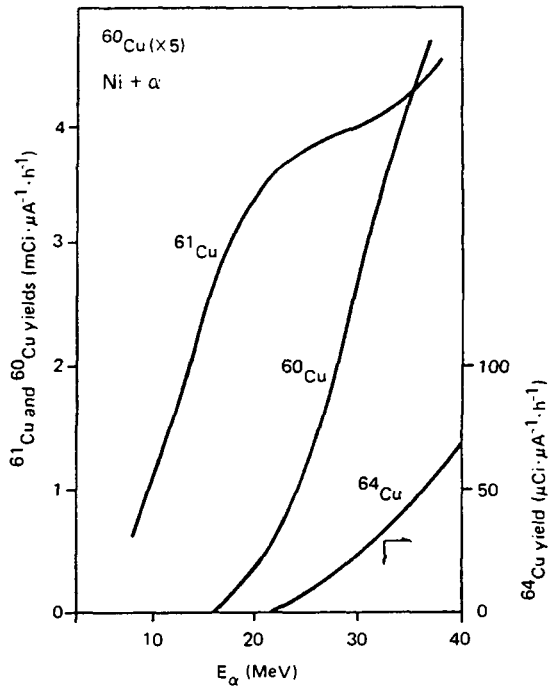

FIG. 41. Thick target yield curves for ^{60}Cu, ^{61}Cu and ^{64}Cu. Target: natural nickel irradiated with ^{4}He [22].

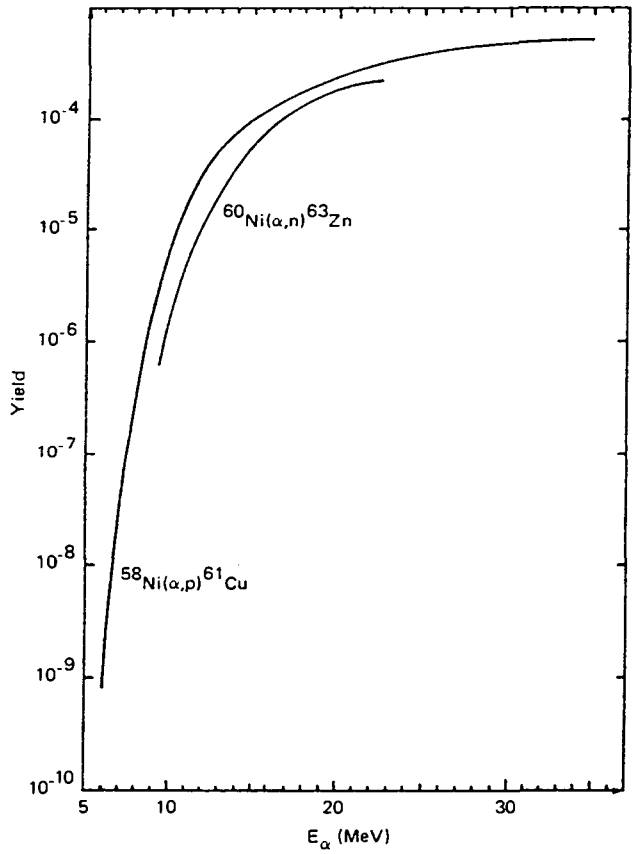

FIG. 42. Thick target yields for (α, n) and (α, p) on Ni isotopes. The yield is defined as the ratio of the total number of reactions of a given type to the number of incident beam particles, assuming that the abundance is 100% for every isotope [9].

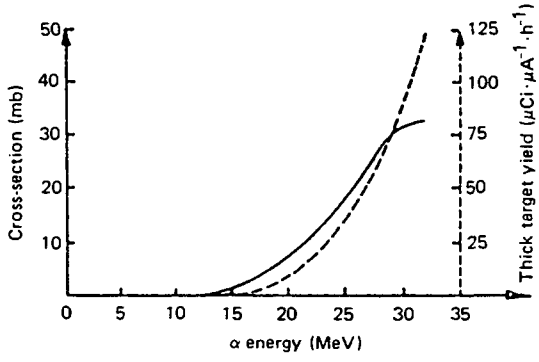

FIG. 43. Excitation function (——) and the thick target yield (- - - -) for ^{62}Zn by alpha bombardment of natural nickel [23].

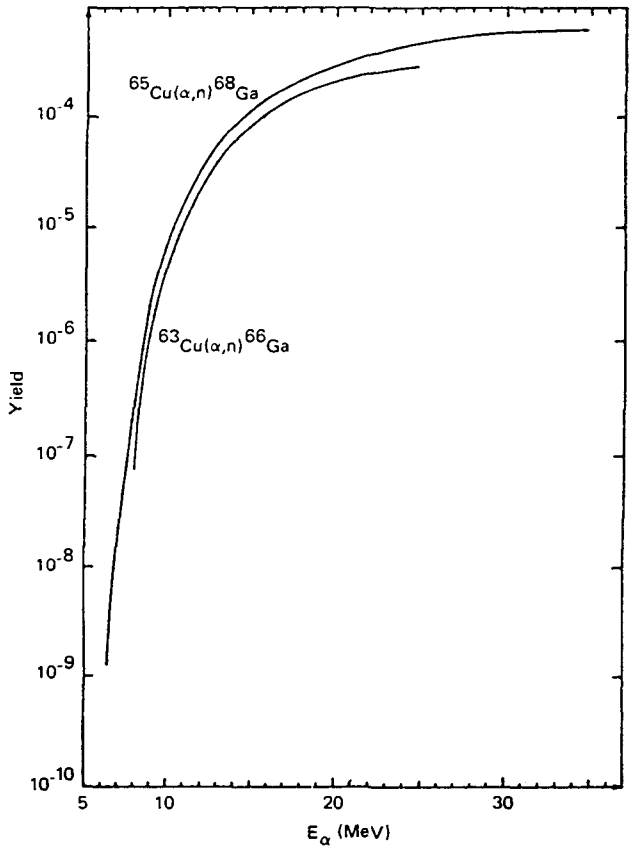

FIG. 44. Thick target yields for (α, n) reactions on Cu isotopes. The yield is defined as the ratio of the total number of reactions of a given type to the number of incident beam particles, assuming that the abundance is 100% for every isotope [9].

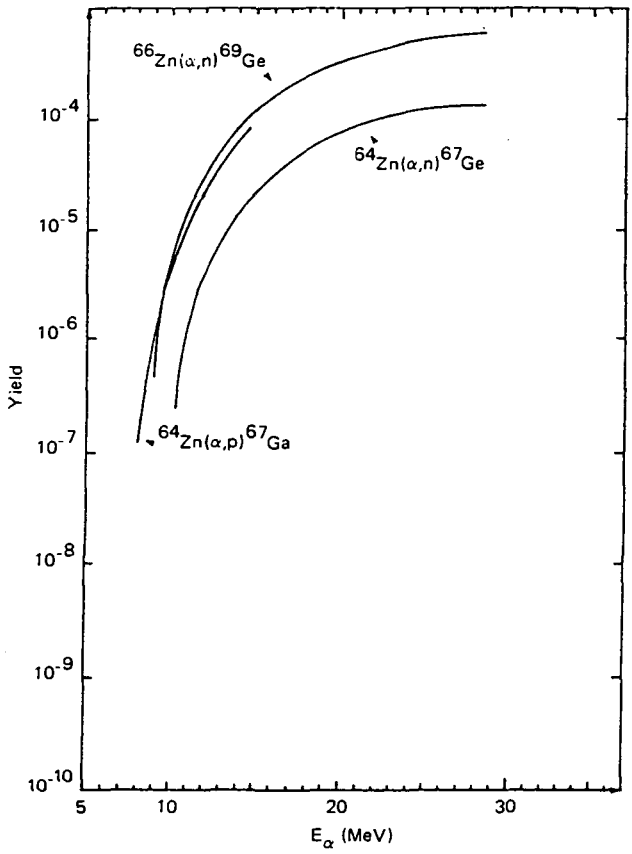

FIG. 45. Thick target yields for the (α, n) and (α, p) reactions on Zn isotopes. The yield is defined as the ratio of the total number of reactions of a given type to the number of incident beam particles, assuming that the abundance is 100% for every isotope [9].

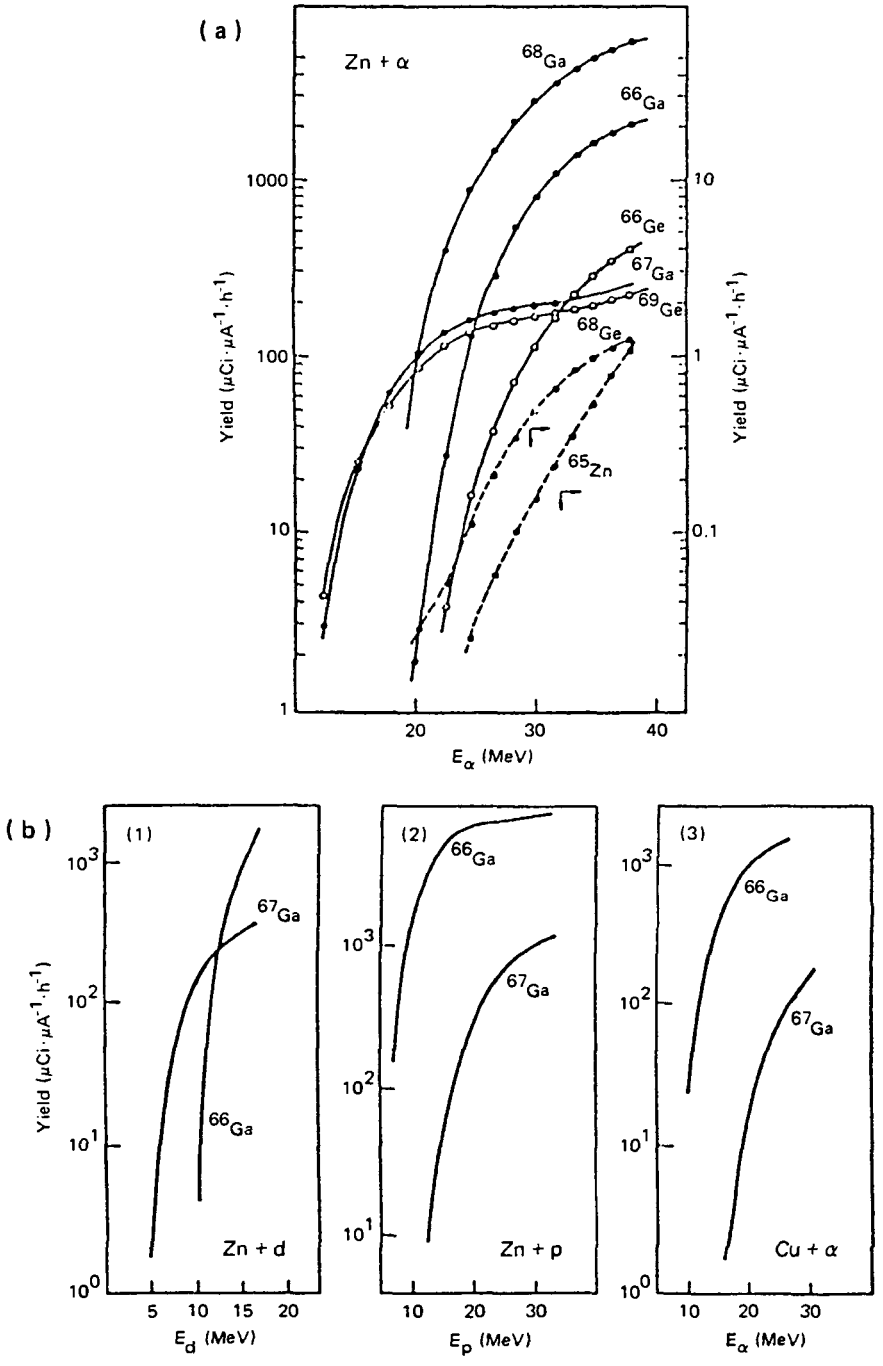

FIG. 46. (a) Thick target yield curves for the α bombardment of natural zinc. The ordinate scales for ^{68}Ge and ^{65}Zn (dashed lines) are given on the right. (b) Thick target yield curves for production of ^{67}Ga and ^{66}Ga by irradiation of natural Zn with (1) deuterons and (2) protons, and of natural Cu with (3) ^{4}He (evaluation from published cross-sections) [24].

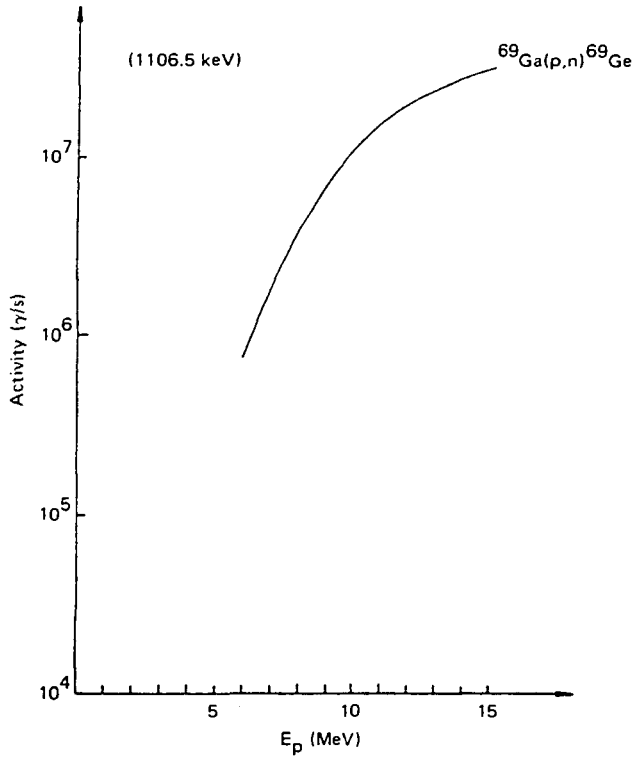

FIG. 47. Specific activity for the thick target yield of ^{69}Ge obtained at the end of proton irradiation of GaAs for 1 h at 1 μA [25].

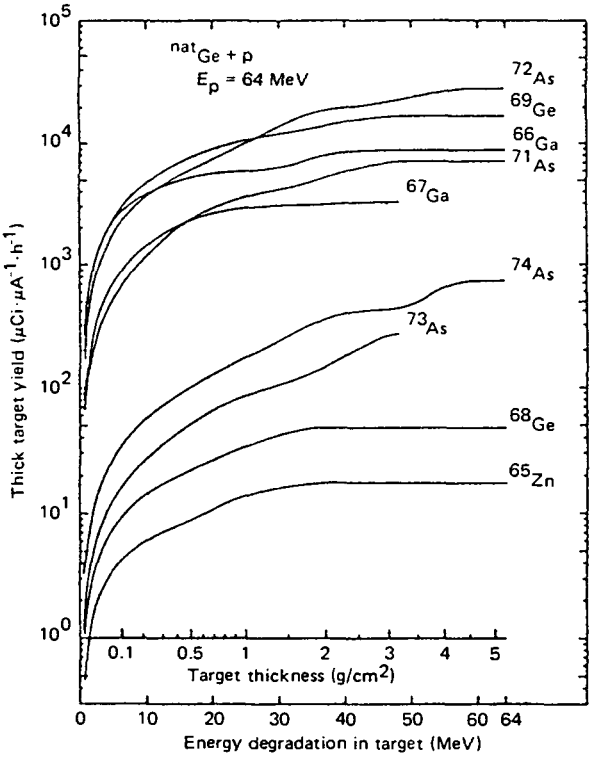

FIG. 48. Thick target yields of nuclides produced by the Ge (p, xnyp) reactions. The incident proton energy is 64 MeV. The abscissas are energy degradations in the Ge target or in the target thickness (g/cm^2) [26].

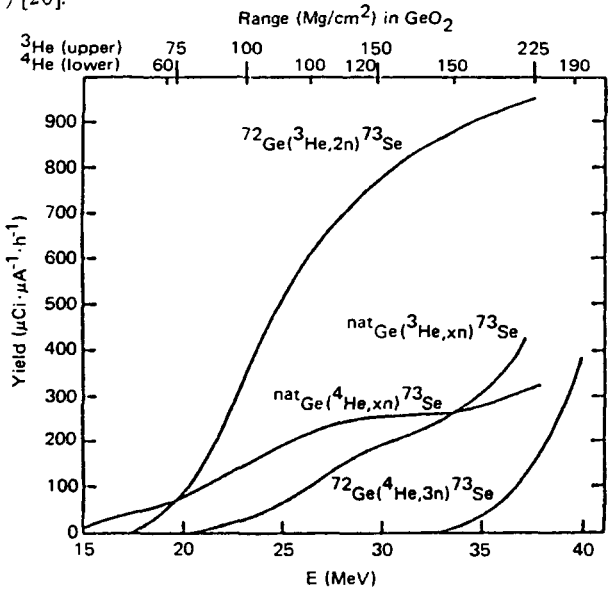

FIG. 49. Thick target yields of ^{73}Se produced by selected nuclear reactions on Ge isotopes [27].

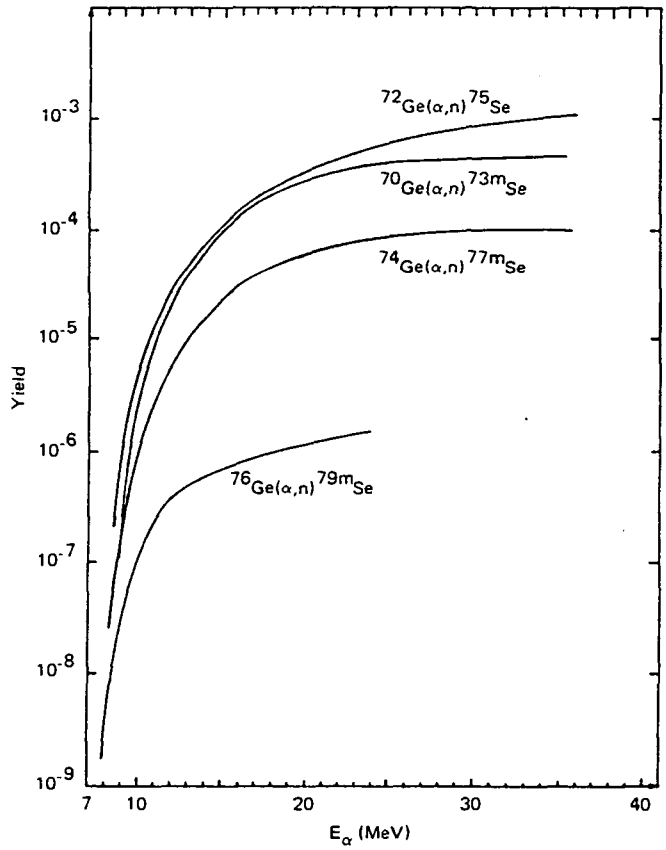

FIG. 50. Thick target yields for (α, n) reactions on Ge isotopes. The yield is defined as the ratio of the total number of reactions of a given type to the number of incident beam particles, assuming that the abundance is 100% for every isotope [9].

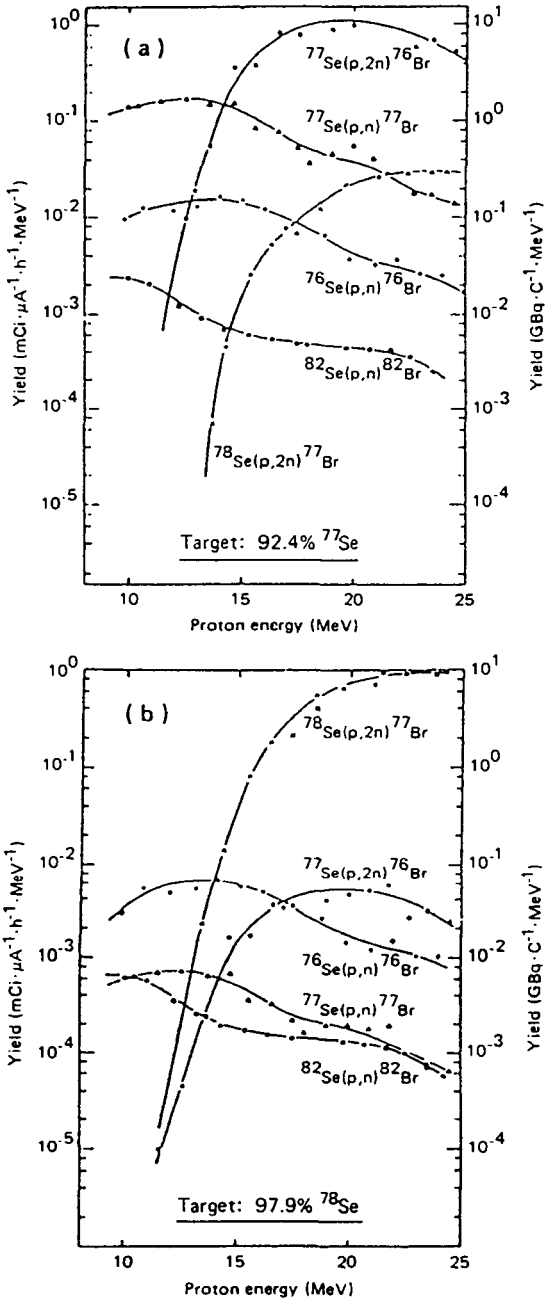

FIG. 51. (a) Yield curves for ^{76}Br and ^{77}Br and ^{82}Br obtained from (p, n) and (p, 2n) reactions on an enriched ^{77}Se target. (b) Yield curves for ^{76}Br, ^{77}Br and ^{82}Br obtained from (p, n) and (p, 2n) reactions on an enriched ^{78}Se target [28].

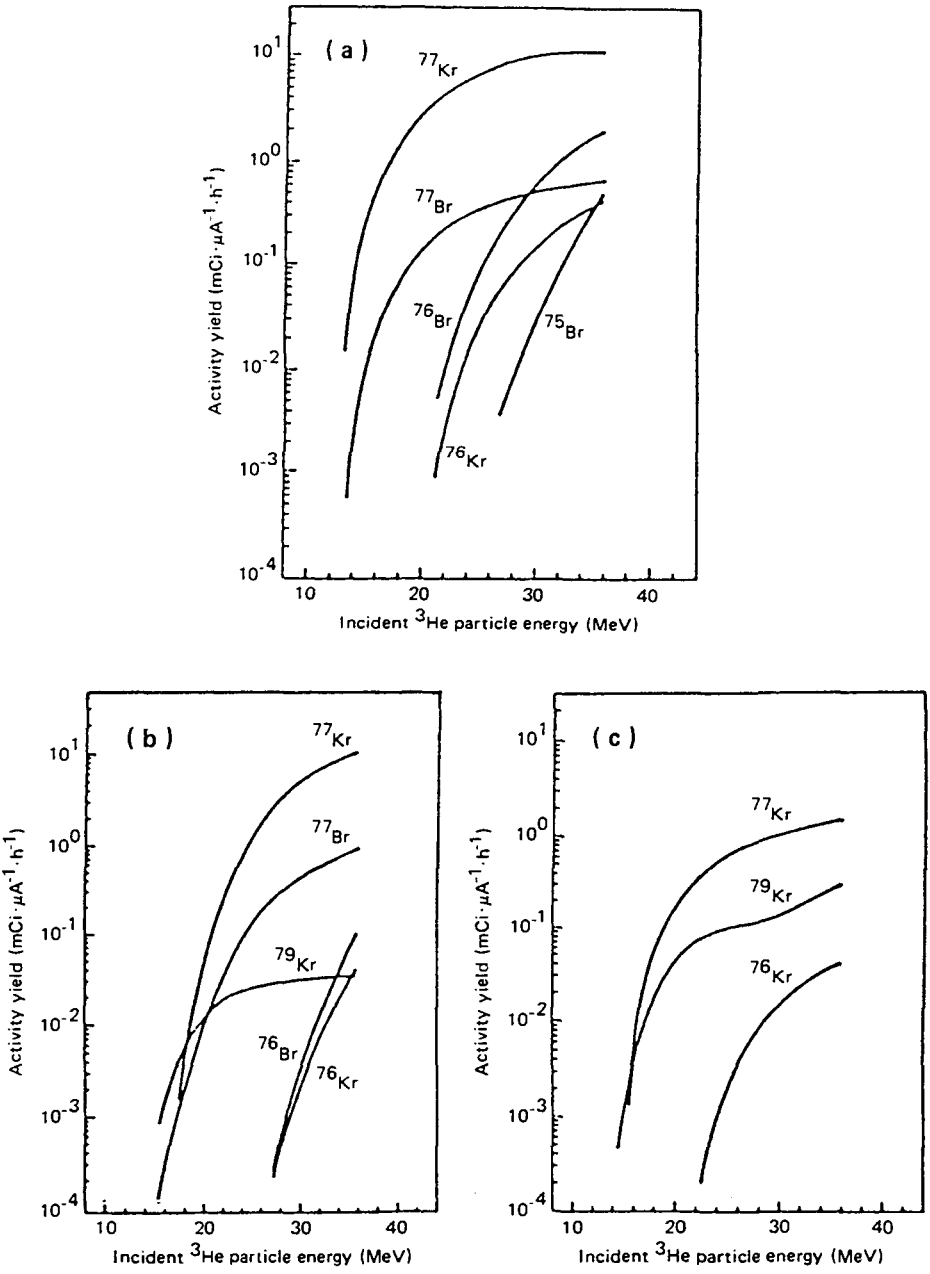

FIG. 52. (a) Thick target yields for ^{77}Kr and other major competing products as functions of incident ^{3}He particle energy on ^{76}Se (enrichment: 96.9%). (b) Thick target yields for ^{77}Kr and other major competing products as functions of incident ^{3}He particle energy on ^{77}Se (enrichment 94.4%). (c) Thick target yields for ^{76}Kr, ^{77}Kr and ^{79}Kr as functions of incident ^{3}He particle energy on natural selenium [29].

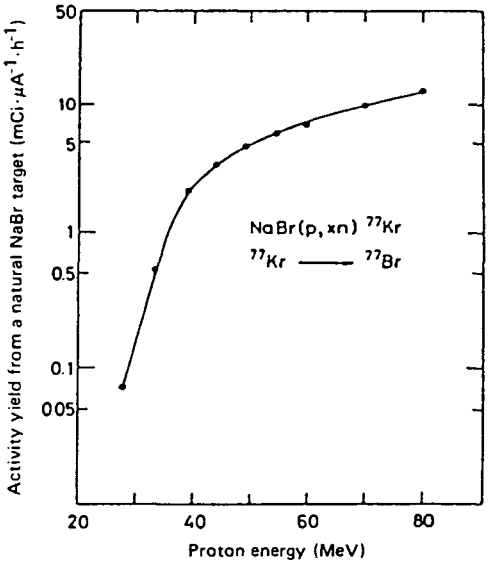

FIG. 53. Activity yields from a thick natural NaBr target [30].

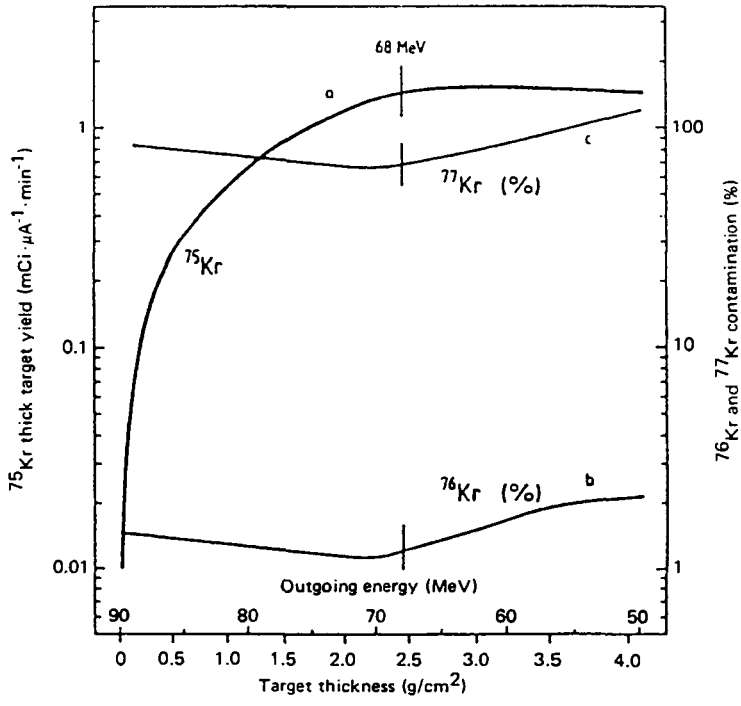

FIG. 54. Determination of the optimum energy region for the production of ^{75}Kr. (a) Thick target yield of ^{75}Kr, (b) contamination of ^{75}Kr by ^{76}Kr, and (c) by ^{77}Kr vs a natural bromine target thickness at a constant incident deuteron energy of 90 MeV [31].

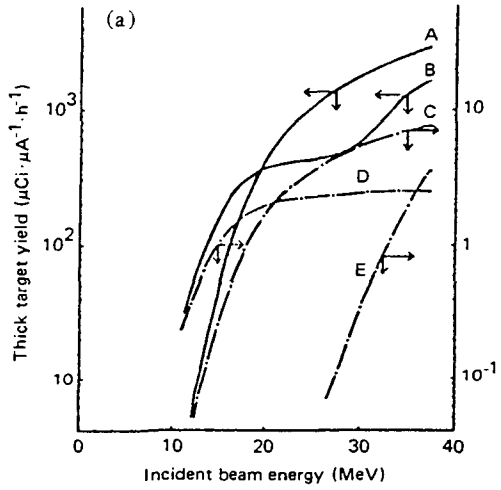

A = $^{79}Br(\alpha,2n)^{81}Rb$

B = $^{79}Br(\alpha,n)^{82m}Rb + ^{81}Rb(\alpha,3n)^{82m}Rb$

C = $^{81}Br(\alpha,2n)^{83}Rb$

D = $^{81}Br(\alpha,n)^{84}Rb$

E = $^{79}Br(\alpha,\alpha 2n)^{77}Br$

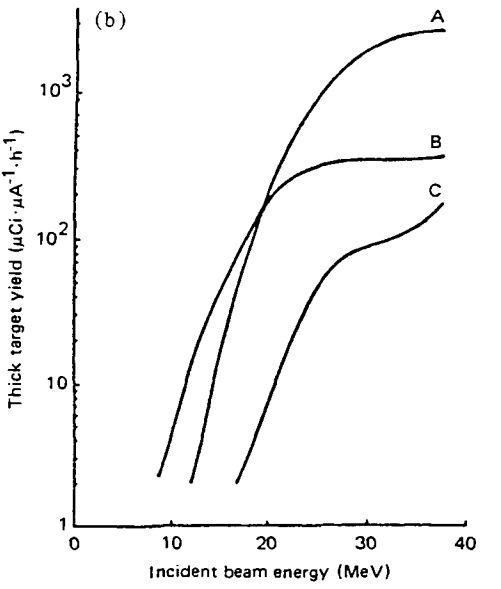

A = $^{81}Br(^{3}He,3n)^{81}Rb + ^{79}Br(^{3}He,n)^{81}Rb$

B = $^{81}Br(^{3}He,2n)^{82m}Rb$

C = $^{79}Br(^{3}He,p2n)^{79}Kr + ^{81}Br(^{3}He,p4n)^{79}Kr$

FIG. 55. (a) Thick target yield curves for an α bombardment of a potassium bromide target producing ^{81}Rb, ^{82m}Rb, ^{83}Rb, ^{84}Rb and ^{77}Br. (b) Thick target yield curves for a ^{3}He bombardment of a potassium bromide target producing ^{81}Rb, ^{82m}Rb and ^{79}Kr [32].

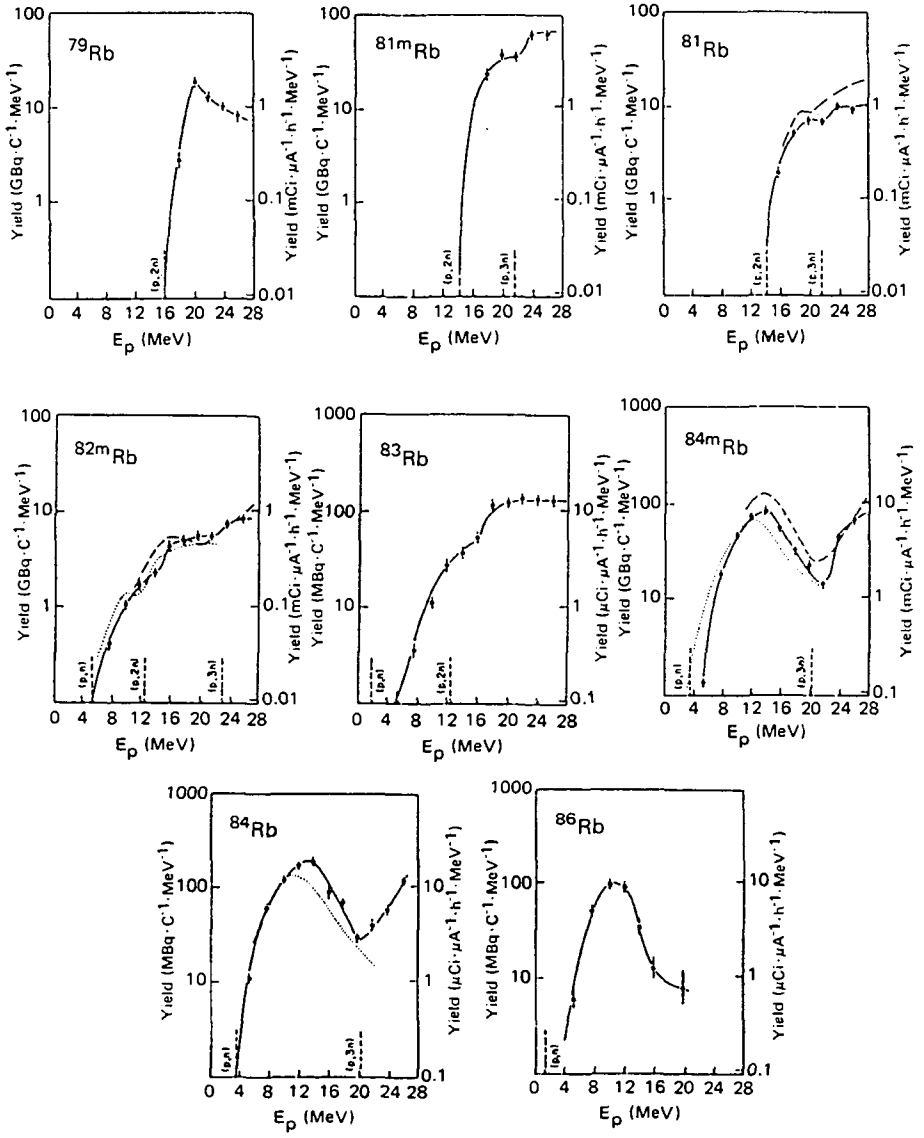

FIG. 56. Yield curves for the production of Rb radioisotopes by proton bombardment of natural krypton gas [33]. *The dotted line gives the results obtained with the cross-section curves of Lamb* [34], *while the dashed line gives the results of Acerbi* [35]. *The vertical dashed line indicates the Q values involved.*

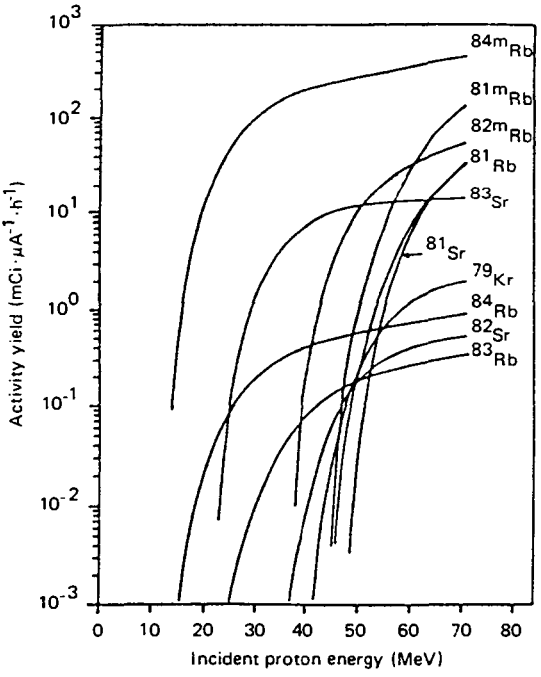

FIG. 57. Thick target yields for an enriched $^{85}RbCl$ target (99.78% enriched ^{85}Rb) for the (p, pxn) – (p, αxn) and (p, xn) reactions. The ^{81}Rb yield includes contributions of the decays of ^{81}Sr and ^{81m}Rb during irradiation; yields of ^{83}Rb and ^{84}Rb include contributions from ^{83}Sr and ^{84m}Rb, respectively [36].

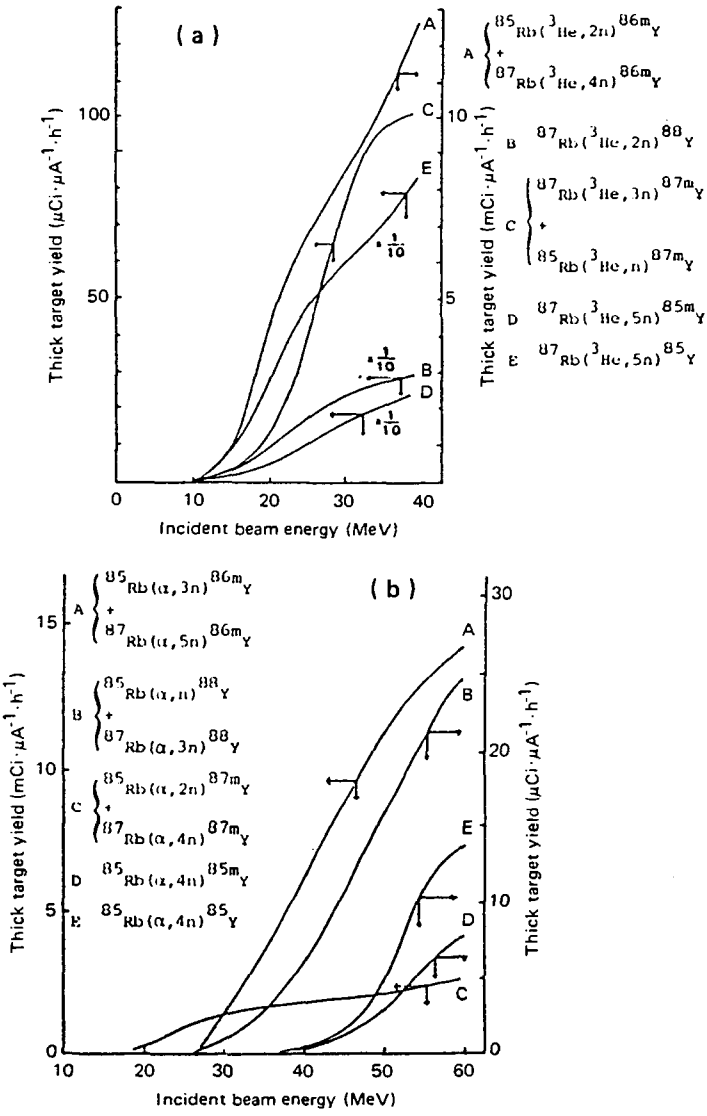

FIG. 58. (a) Thick target yield curves for the ^{3}He reaction on rubidium chloride producing ^{85}Y, ^{85m}Y, ^{86m}Y, ^{87m}Y and ^{88}Y. (b) Thick target yield curves for the ^{4}He reaction on rubidium chloride producing ^{85}Y, ^{85m}Y, ^{86m}Y, ^{87m}Y and ^{88}Y [37].

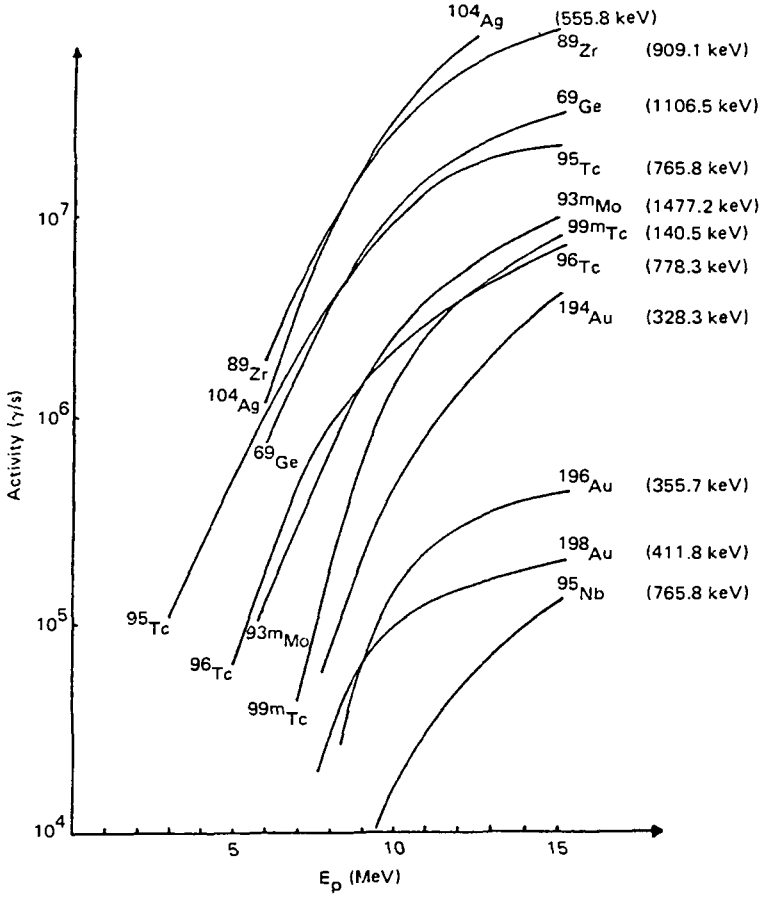

FIG. 59. Specific activities for the thick target yields of natural metals (Y, Zr, Nb, Mo and Pd) after irradiation with protons for 1 h at 1 μA ((p, xn) reactions) [25].

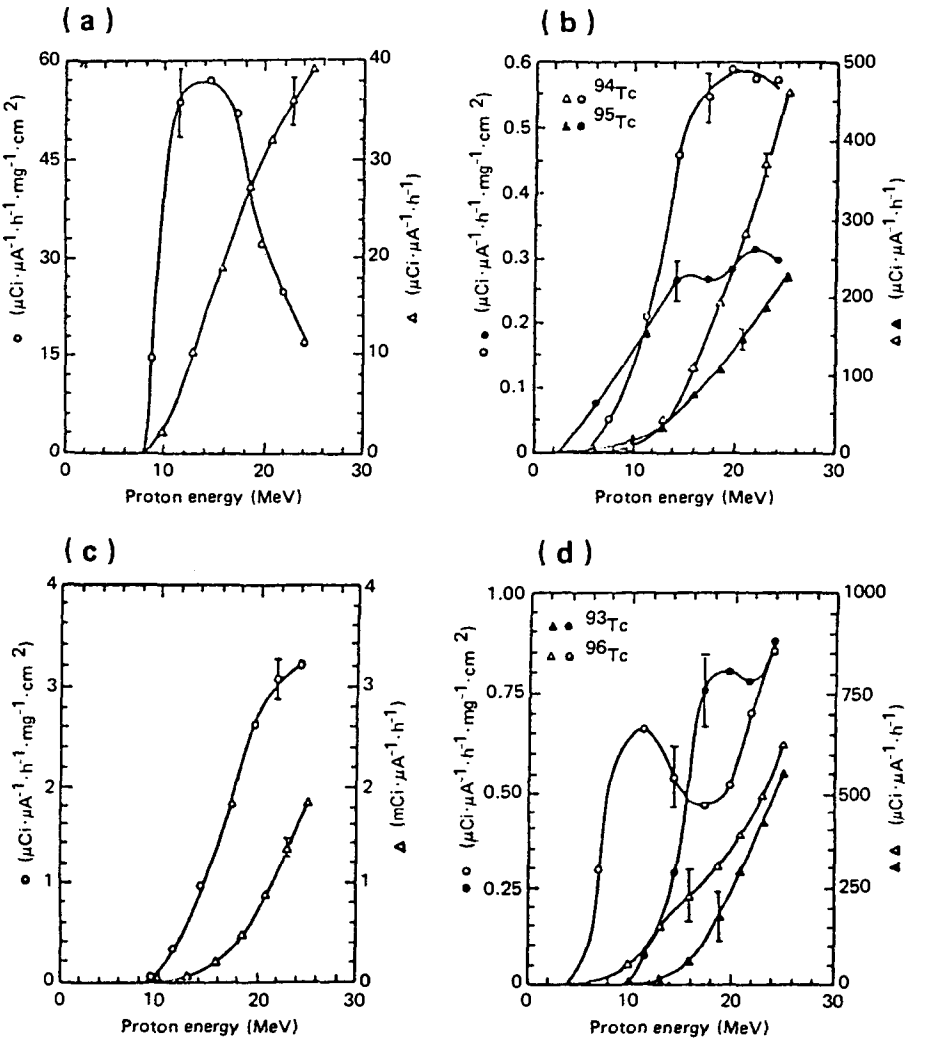

FIG. 60. (a) Excitation function and the related thick target yield of ^{99m}Tc. The data refer to 97.42% enriched ^{100}Mo targets. (b) Excitation functions and corresponding thick target yields of ^{94}Tc and ^{95}Tc in a molybdenum target enriched to 97.42% ^{100}Mo. (c) Excitation function and thick target yield of ^{99}Mo for a target of 97.42% isotopically enriched ^{100}Mo. (d) Excitation functions and deduced thick target yields of ^{93}Tc and ^{96}Tc. The data refer to 97.42% enriched ^{100}Mo targets. (All of the curves in this figure were plotted using the average energy for the excitation function and the incident energy for the thick target yield.) [38].

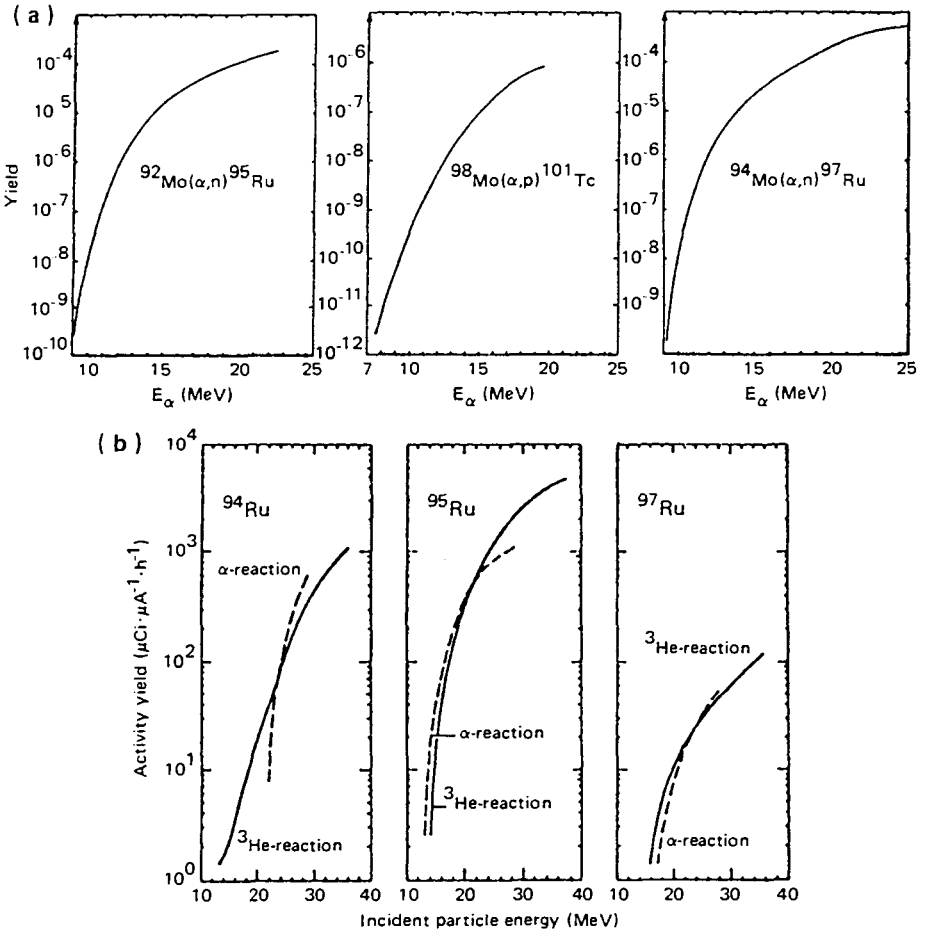

FIG. 61. (a) Thick target yields for (α, n) or (α, p) reactions on Mo isotopes. The yield is the ratio of the total number of reactions of a given type to the number of incident beam particles, assuming 100% abundance for every isotope [9]. *(b) Theoretical cumulative thick target yields of ^{94}Ru, ^{95}Ru and ^{97}Ru from the irradiation of natural molybdenum with ^{3}He particles (solid lines) and α-particles (dashed lines)* [39].

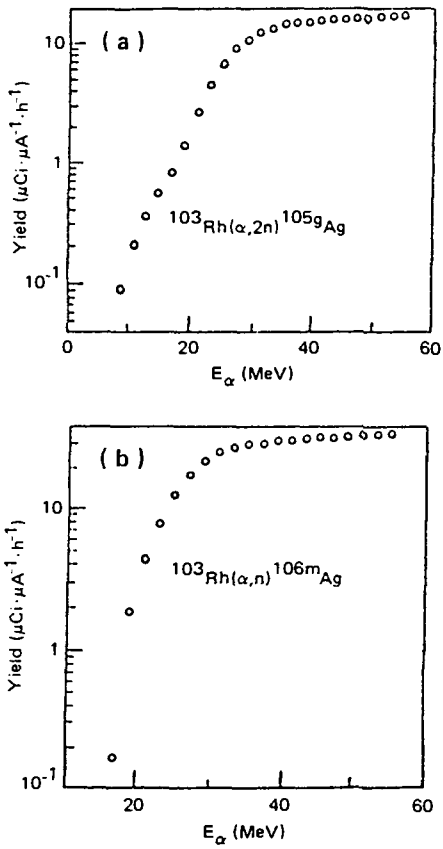

FIG. 62. (a) Thick target yield for the production of ^{105g}Ag. (b) Thick target yield for the production of ^{106m}Ag by irradiation of ^{103}Rh with α-particles [40].

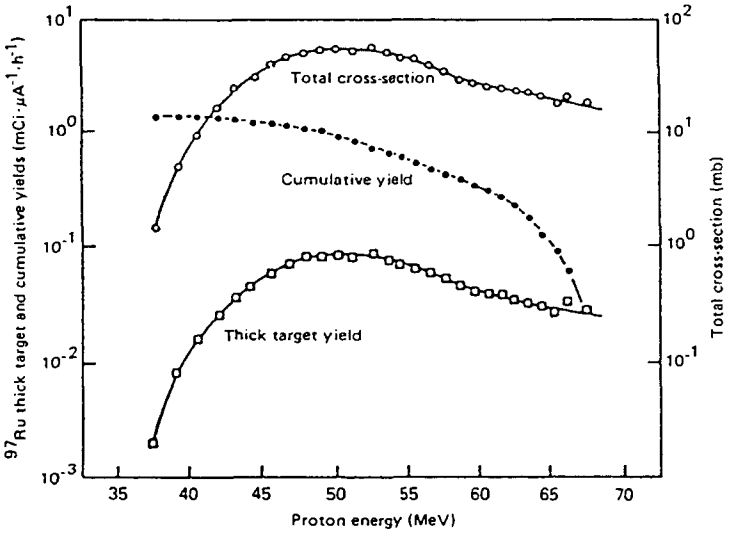

FIG. 63. Thick target and cumulative ^{97}Ru yields as functions of proton energy (target: ^{103}Rh) [41].

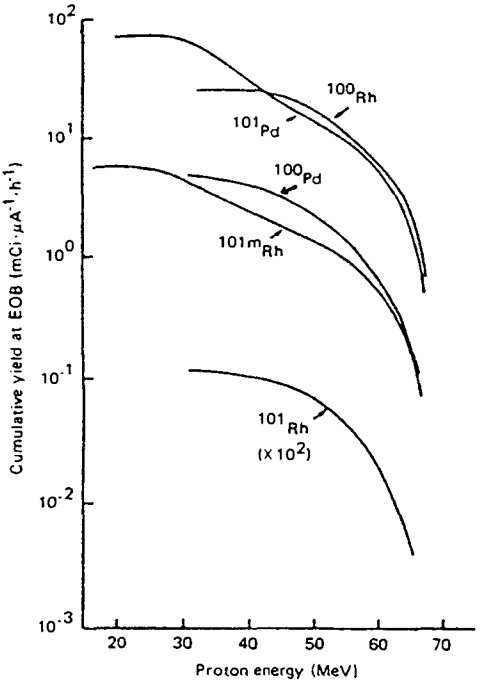

FIG. 64. Cumulative yields as functions of proton energy for ^{101m}Rh, ^{101}Rh, ^{100}Rh, ^{101}Pd and ^{100}Pd. Summation of yields was done from the high to the low end of the proton energy range covered in this work, thus resembling the direction of the proton beam through the Rh target [42].

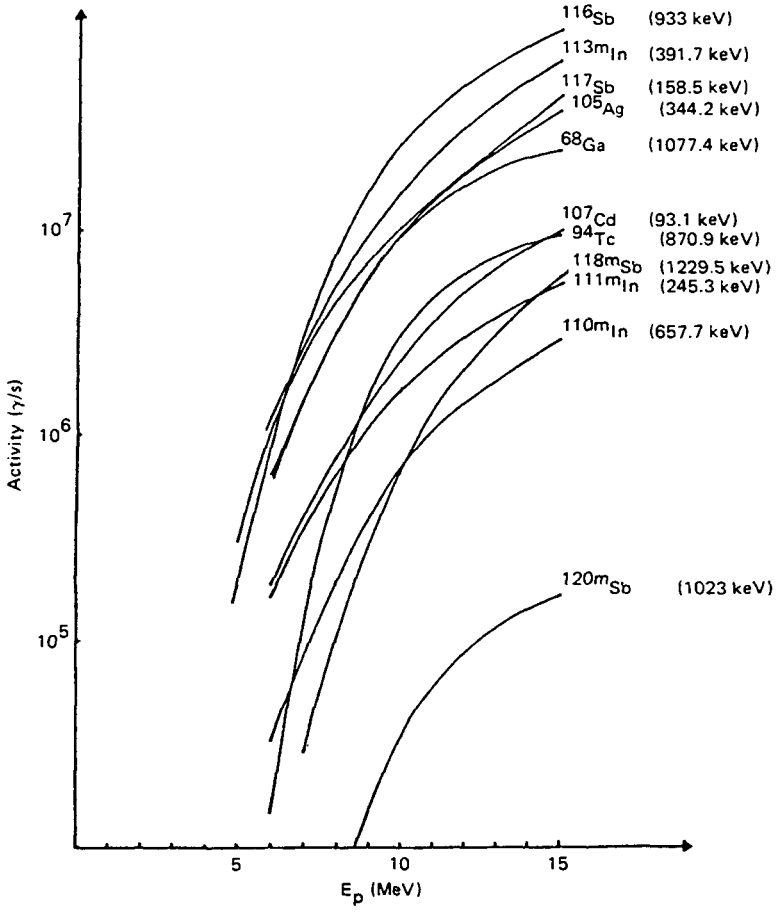

FIG. 65. Specific activities for the thick target yields of natural metals (Mo, Pd, Ag, Cd, Sn) after irradiation with protons for 1 h at 1 μA ((p, xn) reactions) [25].

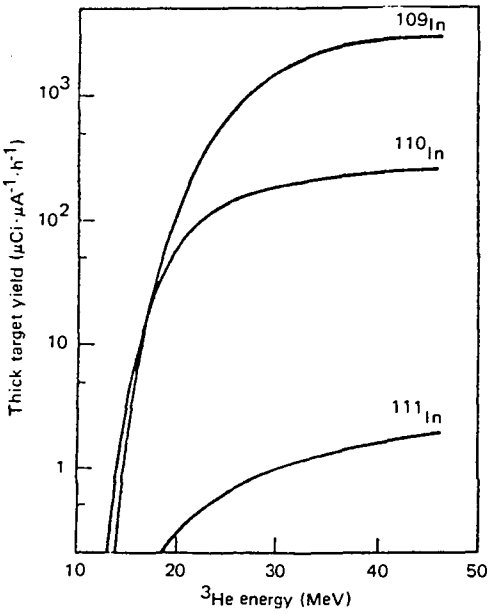

FIG. 66. Thick target yields of ^{109}In, ^{110}In and ^{111}In for the Ag + ^{3}He reactions [43].

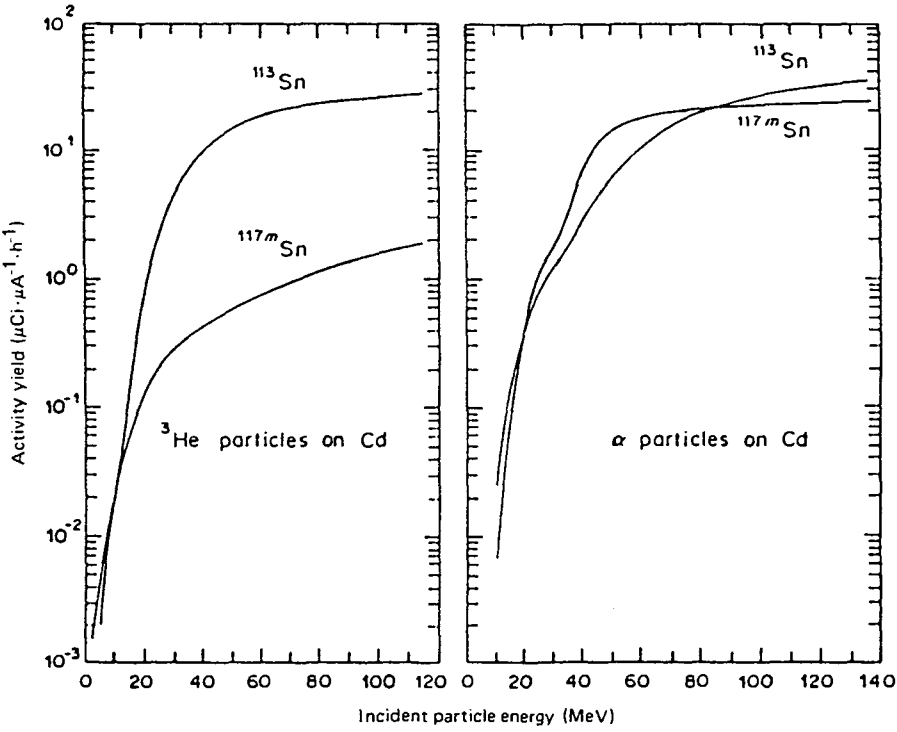

FIG. 67. Thick target yields of ^{113}Sn and ^{117m}Sn as functions of incident particle energy in the interactions of ^{3}He and α-particles with natural cadmium [44].

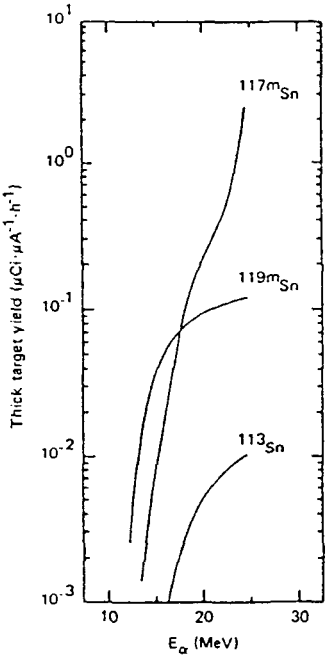

FIG. 68. Thick target yield curves calculated from the excitation functions for α-particle bombardment of enriched cadmium (98.07% ^{116}Cd) [45].

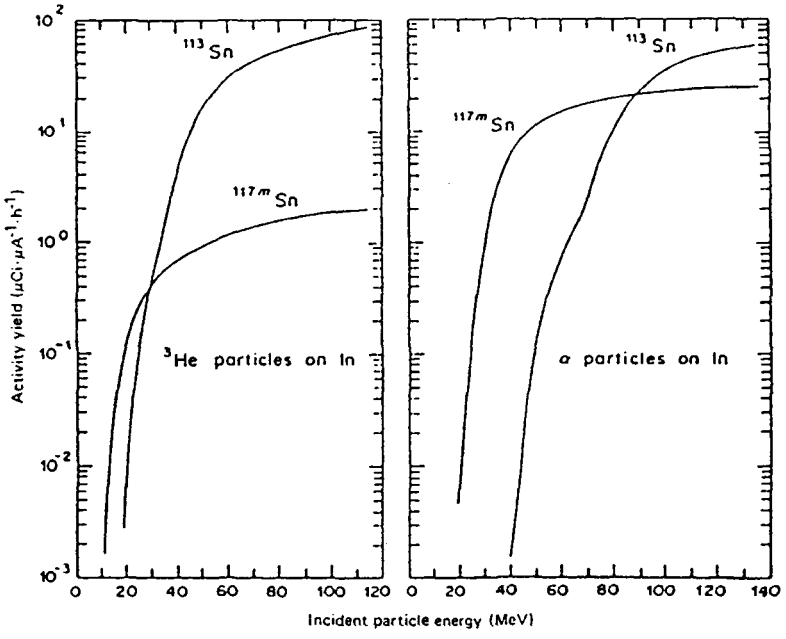

FIG. 69. Thick target yields of ^{113}Sn and ^{117m}Sn as functions of incident particle energy in the interactions of ^3He and α-particles with natural indium [44].

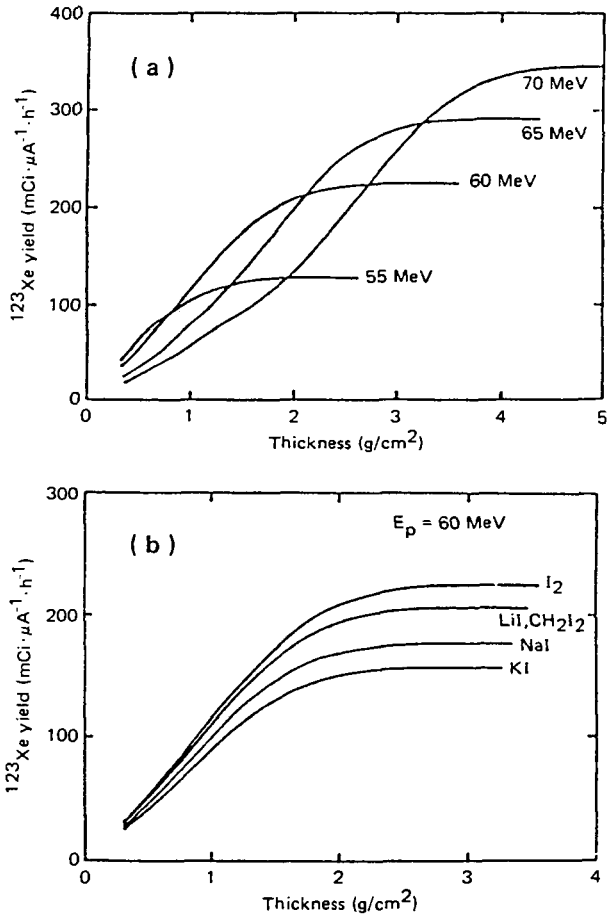

FIG. 70. (a) ^{123}Xe yield vs I_2 target thickness for various incident proton energies. The ^{123}I yield (6.7 h after irradiation) may be obtained by multiplying the ^{123}Xe yield by 0.110. (b) ^{123}Xe yield vs target thickness for various compounds at 60 MeV incident proton energy. The ^{123}I yield (6.7 h after irradiation) may be obtained by multiplying the ^{123}Xe yield by 0.110 [46].

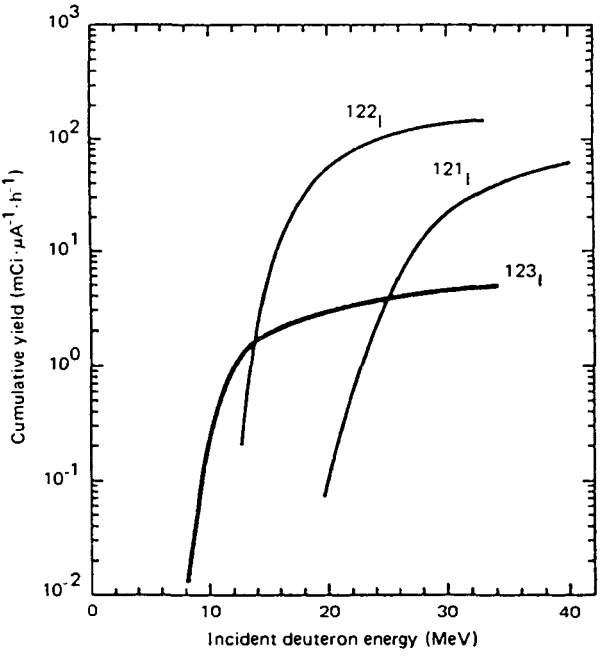

FIG. 71. Thick target yields of ^{123}I, ^{122}I and ^{121}I as functions of incident deuteron energy on 96.45% enriched ^{122}Te [47].

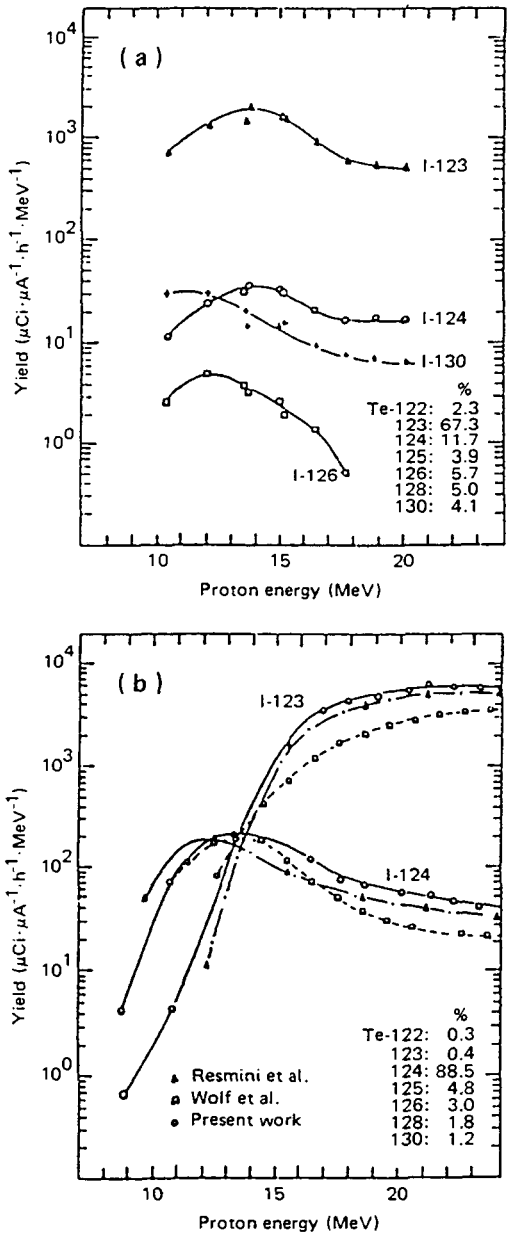

FIG. 72. (a) Yield curves for the production of iodine isotopes obtained by proton bombardment of tellurium enriched in ^{123}Te. (b) Yield curves for the production of iodine isotopes obtained by proton bombardment of tellurium enriched in ^{124}Te. The isotopic composition for the present work is also shown (details of the experiments cited in the figure can be found in Ref. [48]*).*

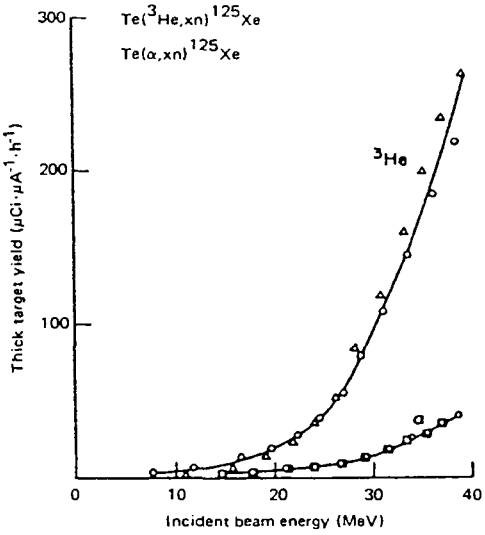

FIG. 73. Thick target yield curves for ^{3}He and α-reactions on natural tellurium producing ^{125}Xe [49].

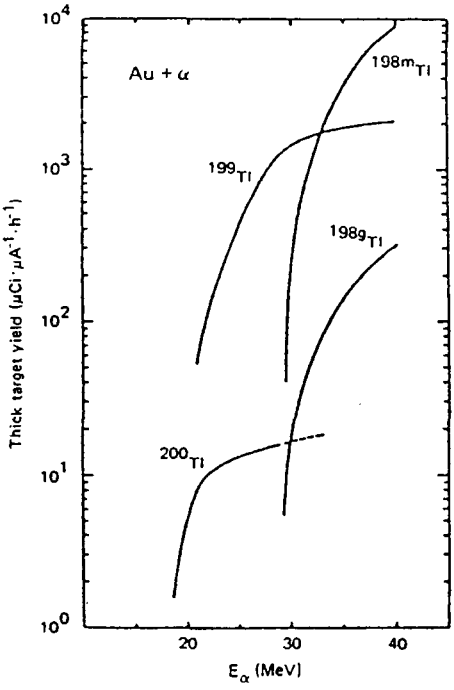

FIG. 74. Thick target yield curves as calculated from the excitation functions for α bombardment of gold [50].

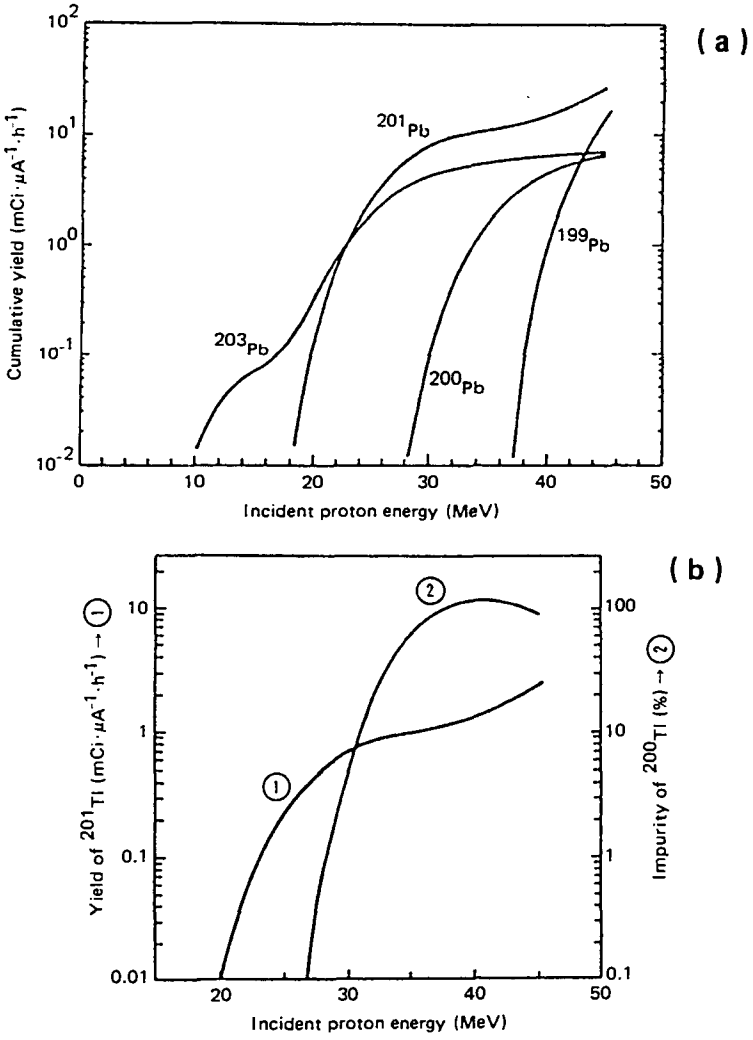

FIG. 75. (a) Cumulative yields of ^{203}Pb, ^{201}Pb, ^{200}Pb and ^{199}Pb in the irradiation of natural thallium with protons. (b) Yields of ^{201}Tl (grown-in during a 32 h decay of the separated lead activities) vs the energies of the incident protons (curve 1). ^{200}Tl impurity as a percentage of ^{201}Tl activity at varying incident proton energies (curve 2) [51].

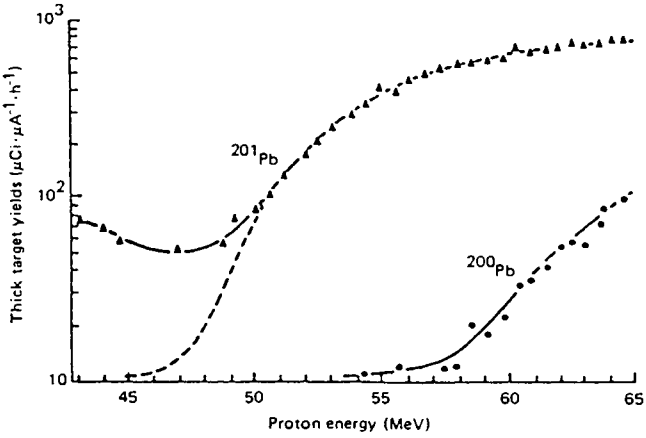

FIG. 76. Thick target yields of ^{201}Pb and ^{200}Pb as functions of proton energy (target: natural lead; Pb(p, pxn) reactions) [52].

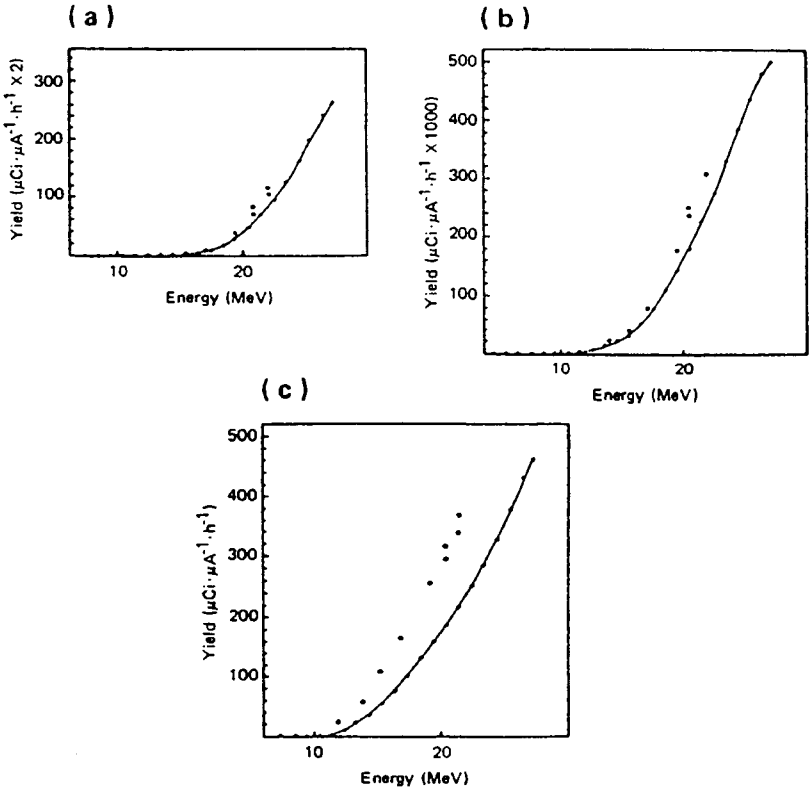

FIG. 77. (a) Thick target yields for ^{205}Bi production (++++). This work: ○. (b) Thick target yields for ^{207}Bi production (++++). This work: ○. (c) Thick target yields for ^{206}Bi production (++++). This work: ○ [53].

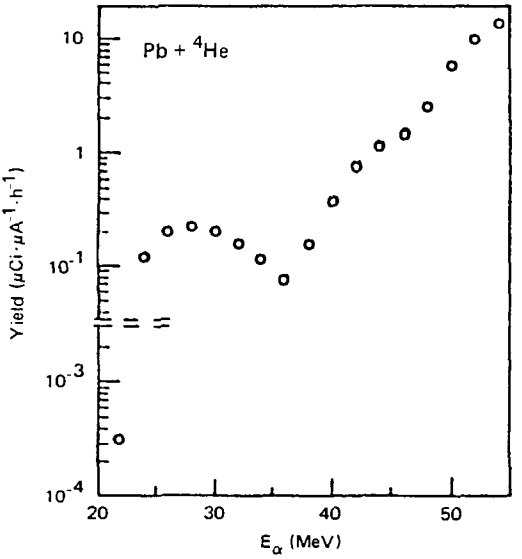

FIG. 78. Thick target yields for the production of ^{206}Po [53].

REFERENCES

[1] MÜNZEL, H., et al., Karlsruhe Charged Particle Reaction Data Compilation, Physics Data, No. 15, Fachinformationszentrum, Karlsruhe (1982).
[2] SASTRI, C.S., CALETKA, R., KRIVAN, V., Anal. Chem. **53** (1981) 765.
[3] KRASNOV, N.N., DMITRIYEV, P.P., DMITRIYEVA, S.P., KONSTANTINOV, I.O., MOLIN, G.A., Uses of Cyclotrons in Chemistry, Metallurgy and Biology, Butterworths, London (1970) 341.
[4] BLONDIAUX, G., VALLADON, M., MAGGIORE, C.J., DEBRUN, J.L., unpublished data.
[5] ENGELMANN, C., J. Radioanal. Chem. 7 (1971) 89.
[6] VALLADON, M., GIOVAGNOLI, A., BLONDIAUX, G., DEBRUN, J.L., unpublished data.
[7] NOZAKI, T., IWAMOTO, M., IDO, T., Int. J. Appl. Radiat. Isot. 25 (1974) 393.
[8] NOZAKI, T., KURUKAWA, M., KUME, S., SEKI, R., Int. J. Appl. Radiat. Isot. **26** (1975) 17.
[9] ROUGHTON, N.A., INTRATOR, T.P., PETERSON, R.J., ZAIDINS, C.S., At. Data Nucl. Data Tables 28 (1983) 341.
[10] PROBST, H.J., QAIM, S.M., WEINREICH, R., Int. J. Appl. Radiat. Isot. 27 (1976) 431.
[11] QAIM, S.M., OLLIG, H., BLESSING, G., Int. J. Appl. Radiat. Isot. **33** (1982) 271.
[12] LUNDQVIST, H., MALMBORG, P., Int. J. Appl. Radiat. Isot. **30** (1979) 33.
[13] ZATOLOKIN, B.V., KONSTANTINOV, J.O., KRASNOV, N.N., Int. J. Appl. Radiat. Isot. 27 (1976) 159.
[14] VANDECASTEELE, C., VANDEWALLE, T., SLEGERS, G., Radiochim. Acta **29** (1981) 71.

[15] INTRATOR, T.P., PETERSON, R.J., ZAIDINS, C.S., Nucl. Instrum. Methods **188** (1981) 347.
[16] BARRANDON, J.N., DEBRUN, J.L., KOHN, A., SPEAR, R.H., Nucl. Instrum. Methods **127** (1975) 269.
[17] WEINREICH, R., PROBST, H.J., QAIM, S.M., Int. J. Appl. Radiat. Isot. **31** (1980) 223.
[18] WATANABE, M., NAKAHARA, H., MURAKAMI, Y., Int. J. Appl. Radiat. Isot. **30** (1979) 625.
[19] LAGUNAS-SOLAR, M.C., JUNGERMAN, J.A., Int. J. Appl. Radiat. Isot. **30** (1979) 25.
[20] JOHNSON, P.C., LAGUNAS-SOLAR, M.C., AVILA, M.J., Int. J. Appl. Radiat. Isot. 35 (1984) 371.
[21] HOMMA, Y., MURAKAMI, Y., Bull. Chem. Soc. Jpn. **50** (1977) 1251.
[22] MURAMATSU, H., SHIRAI, E., NAKAHARA, H., MURAKAMI, Y., Int. J. Appl. Radiat. Isot. **29** (1978) 611.
[23] NEIRINCKX, R.D., Int. J. Appl. Radiat. Isot. 28 (1977) 808.
[24] NAGAMA, Y., UNNO, M., NAKAHARA, H., MARAKAMI, Y., Int. J. Appl. Radiat. Isot. **29** (1978) 615.
[25] KOHN, A., Thesis, University of Orsay, 1976.
[26] HORIGUCHI, T., KUMAHORA, H., INOUE, H., YOSHIZAWA, Y., Int. J. Appl. Radiat. Isot. **34** (1983) 1531.
[27] GUILLAUME, M., LAMBRECHT, R.M., WOLF, A.P., Int. J. Appl. Radiat. Isot. **29** (1978) 411.
[28] JANSSEN, A.G.M., VAN den BOSCH, R.L.P., de GOEIJ, J.J.M., THEELEN, H.M.J., Int. J. Appl. Radiat. Isot. **31** (1980) 405.
[29] YOUFENG, H., QAIM, S.M., STOCKLIN, G., Int. J. Appl. Radiat. Isot. 33 (1982) 13.
[30] LUNDQVIST, H., MALMBORG, P., LANGSTRÖM, B., CHIENGMAI, S.N., Int. J. Appl. Radiat. Isot. **30** (1979) 39.
[31] QAIM, S.M., WEINREICH, R., Int. J. Appl. Radiat. Isot. 32 (1981) 823.
[32] HOMMA, Y., KURATA, K., Int. J. Appl. Radiat. Isot. **30** (1979) 345.
[33] MULDERS, J.J.L. Int. J. Appl. Radiat. Isot. 35 (1984) 475.
[34] LAMB, J.F., BAKER, G.A., GORIS, M.L., KHENTIGAN, A., MOORE, H.A., Inst. Radiol. Spec. Rep. Ser. **15** (1977) 22.
[35] ACERBI, E., BIRATTARI, C., BONARDI, M., de MARTINIS, C., SALOMONE, A., Int. J. Appl. Radiat. Isot. 32 (1981) 465.
[36] HORIGUCHI, T., et al., Int. J. Appl. Radiat. Isot. **31** (1980) 141.
[37] HOMMA, Y., ISHII, M., MURASE, Y., Int. J. Appl. Radiat. Isot. **31** (1980) 399.
[38] ALMEIDA, G.L., HELUS, F., Radiochem. Radioanal. Lett. **28** (1977) 205.
[39] COMPARETTO, G., QAIM, S.M., Radiochim. Acta 27 (1980) 177.
[40] OZAFRAN, M.J., VASQUEZ, M.E., de la VEGA VEDOYA, M., NASSIFF, S.J., Radiochem. Radioanal. Lett. **43** (1980) 265.
[41] LAGUNAS-SOLAR, M.C., AVILA, M.J., NAVARRO, N.J., JOHNSON, P.C., Int. J. Appl. Radiat. Isot. **34** (1983) 915.
[42] LAGUNAS-SOLAR, M.C., AVILA, M.J., JOHNSON, P.C., Int. J. Appl. Radiat. Isot. 35 (1984) 743.
[43] OMORI, T., YAGI, M., YAMAZAKI, H., SHIOKAWA, T., Radiochem. Radioanal. Lett. **44** (1980) 307.
[44] QAIM, S.M., DÖHLER, H., Int. J. Appl. Radiat. Isot. 35 (1984) 645.
[45] MURAMATSU, H., NAKAHARA, H., J. Inorg. Nucl. Chem. 43 (1981) 1727.
[46] WILKINS, S.R., et al., Int. J. Appl. Radiat. Isot. 26 (1975) 297.
[47] ZAIDI, J.H., QAIM, S.M., STOCKLIN, G., Int. J. Appl. Radiat. Isot. **34** (1983) 1425.
[48] VAN den BOSCH, R.L.P., et al., Int. J. Appl. Radiat. Isot. 28 (1977) 255.

[49] HOMMA, Y., MURAKAMI, Y., Int. J. Appl. Radiat. Isot. 28 (1977) 740.
[50] NAGAMA, Y., NAKAHARA, H., MURAKAMI, Y., Int. J. Appl. Radiat. Isot. **30** (1979) 669.
[51] QAIM, S.M., WEINREICH, R., OLLIG, H., Int. J. Appl. Radiat. Isot. **30** (1979) 85.
[52] LAGUNAS-SOLAR, M.C., LITTLE, F.E., JUNGERMANN, J.A., Int. J. Appl. Radiat. Isot. **32** (1981) 817.
[53] WASILEVSKY, C., de la VEGA VEDOYA, M., NASSIFF, S.J., Radiochim. Acta 27 (1980) 125.

Part 4
PHOTONUCLEAR ACTIVATION

4–1. PHOTONUCLEAR CROSS-SECTIONS

B. FORKMAN, R. PETERSSON
Department of Physics,
University of Lund,
Lund, Sweden

Abstract

PHOTONUCLEAR CROSS-SECTIONS.

A compilation is given of photonuclear cross-sections in the giant resonance region. Special reference is made to applications in activation analysis.

1. INTRODUCTION

In the giant resonance region (10–25 MeV), the most probable result of photonuclear absorption is the emission of a single neutron, but other processes must also be considered, such as the emission of gamma rays, the emission of more than one neutron and, particularly for light nuclei, the emission of charged particles. Medium and high energy photon spallation yields are systematically treated in Ref. [1].

2. BREMSSTRAHLUNG REACTION YIELD

Since there exist no intense monochromatic photon sources, the bremsstrahlung beam, obtained when energetic electrons from electron accelerators hit a target, is used as the photon source in almost all photoactivation studies. The energy spectrum of the photons in a bremsstrahlung beam from a thin target is well known [2].

The bremsstrahlung beam has a continuous photon energy spectrum. Let $n(E, E_0)\,dE$ be the number of photons with energies between E and E + dE per unit radiation thickness per second in a bremsstrahlung beam, where E_0 is the maximum photon energy. The energy content of the beam in the sample is then

$$U(E_0) = \int_0^{E_0} En(E, E_0)\, f(E)\, dE \qquad (1)$$

where f(E) is a correction factor which accounts for the distortion of the bremsstrahlung spectrum by the effect of photon absorption in the machine target, in the walls of the accelerator chamber and in the sample.

TABLE I. ENERGY CONTENT OF AN UNDISTORTED BREMSSTRAHLUNG BEAM [3]

E_0 (MeV)	$\int_0^{E_0} En(E, E_0)dE$ (MeV)
10	03.554 88
13	04.786 41
16	06.046 65
19	07.327 88
22	08.625 22
27	10.814 70
32	13.029 99
36	14.814 54
44	18.416 18
52	22.047 27

TABLE II. ENERGY SPECTRUM OF UNDISTORTED BREMSSTRAHLUNG BEAM $\Phi = En(E, E_0)$
(the table values are 10^5 times too high [3]*)*

E (MeV)	Φ (10 MeV)	E (MeV)	Φ (13 MeV)	E (MeV)	Φ (16 MeV)	E (MeV)	Φ (19 MeV)	E (MeV)	Φ (22 MeV)
10	02933	13	02814	16	02739	19	02687	22	02649
09	16426	12	16239	15	16140	18	16080	21	16040
08	22660	11	22271	14	22105	17	22024	20	21981
07	27063	10	26222	13	25883	16	25731	19	25661
06	30926	09	29321	12	28676	15	28386	18	28250
05	34821	08	32093	11	30985	14	30476	17	30229
04	39085	07	34829	10	33081	13	32262	16	31852
03	43959	06	37720	09	35136	12	33907	15	33275
02	49629	05	40900	08	37269	11	35519	14	34601
01	56252	04	44469	07	39564	10	37176	13	35905
00	64010	03	48504	06	42083	09	38935	12	37239
		02	53068	05	44875	08	40838	11	38643
		01	58215	04	47975	07	42918	10	40146
		00	64010	03	51414	06	45198	09	41772
				02	55217	05	47700	08	43539
				01	59406	04	50438	07	45461
				00	64010	03	53426	06	47548
						02	56676	05	49812
						01	60200	04	52258
						00	64010	03	54895
								02	57728
								01	60764
								00	64010

TABLE II (cont.)

E (MeV)	Φ (27 MeV)	E (MeV)	Φ (32 MeV)	E (MeV)	Φ (36 MeV)	E (MeV)	Φ (44 MeV)	E (MeV)	Φ (52 MeV)
27	02604	32	02573	36	02554	44	02527	52	02508
26	15997	31	15970	34	21935	42	21938	50	21943
25	21949	30	21938	32	28178	40	28224	48	28273
24	25620	29	25619	30	31479	38	31534	46	31613
23	28170	28	28163	28	33550	36	33553	44	33631
22	30068	27	30037	26	35057	34	34931	42	34967
21	31563	26	31483	24	36335	32	35990	40	35936
20	32805	25	32647	22	37568	30	36909	38	36713
19	33891	24	33625	20	38869	28	37797	36	37402
18	34891	23	34483	18	40308	26	38720	34	38070
17	35855	22	35270	16	41931	24	39725	32	38761
16	36820	21	36020	14	43771	22	40841	30	39504
15	37813	20	36759	12	45849	20	42090	28	40322
14	38855	19	37508	10	48182	18	43488	26	41229
13	39964	18	38283	8	50782	16	45046	24	42236
12	41151	17	39096	6	53657	14	46772	22	43352
11	42428	16	39958	4	56816	12	48674	20	44583
10	43803	15	40875	2	60265	10	50757	18	45936
09	45283	14	41854	0	64010	8	53025	16	47412
08	46873	13	42902			6	55482	14	49017
07	48577	12	44021			4	58129	12	50753
06	50401	11	45216			2	60971	10	52621
05	52347	10	46490			0	64010	8	54623
04	54418	09	47846					6	56762
03	56618	08	49285					4	59039
02	58948	07	50810					2	61454
01	61411	06	52423					0	64010
00	64010	05	54124						
		04	55915						
		03	57799						
		02	59774						
		01	61844						
		00	64010						

We define the number of equivalent quanta Q by

$$Q = \frac{1}{E_0} U(E_0) \tag{2}$$

i.e. Q is the number of quanta with energy E_0 which have the same energy content as the bremsstrahlung beam and we define the cross-section per equivalent quantum, σ_q, by

$$\sigma_q(E_0) = \frac{\int_0^{E_0} \sigma(E) n(E, E_0) f(E) dE}{Q} \tag{3}$$

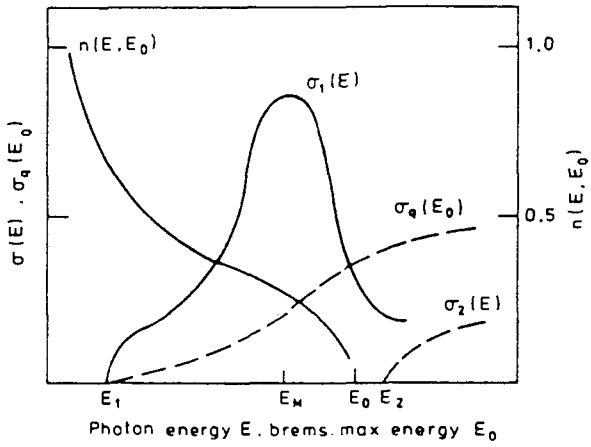

FIG. 1. Energy variation of cross-sections for a typical photonuclear reaction and bremsstrahlung gamma source intensity.

The bremsstrahlung reaction yield measured in monitor response units can be written as

$$y(E_0) = \frac{\int_0^{E_0} \sigma(E) n(E, E_0) f(E)\, dE}{U(E_0) R(E_0)} = \frac{\sigma_q}{E_0 R(E_0)} \tag{4}$$

The monitor measures only some part of the energy content of the beam and thus $R(E_0)$ gives the sensitivity of the monitor for an E_0 bremsstrahlung beam.

While $f(E)$ and $R(E_0)$ are quantities specific for a particular laboratory, $n(E, E_0)$ has been tabulated for bremsstrahlung spectra.

In Tables I and II, the energy content and the energy spectrum of an undistorted bremsstrahlung beam for different end-point energies in the giant resonance region are given. It is easy to obtain the photon spectrum from Table II by dividing the energy spectrum value with the photon energy E.

It is possible to calculate approximately the induced activities of photonuclear reactions, replacing the energy integral in Eq. (4) with a simple summation:

$$y(E_0) \cong \frac{\sum_i \sigma(E_i) n(E_i, E_0) \Delta E_i}{U} \tag{5}$$

where the laboratory factors $f(E)$ and $R(E_0)$ have been neglected (see also Fig. 1).

3. COMMENTS

In the graphs that follow, (γ, n) cross-section curves are given which are sometimes complemented with cross-sections for other types of reactions. Preference has been given to monochromatic photon data (marked 'Mono') when available. As a complement, and as a comparison, continuous photon data (marked 'Brems') are also given. For many nuclei equivalent data exist from several laboratories. These are given without preference for comparison. The separation energies of particles or groups of particles have been taken from Ref. [4] and are given in MeV. Decay data are taken from Ref. [5]. For further cross-section data and more detailed information it is possible to refer to the Photonuclear Data Abstract Sheets, now published in separate volumes by the Photonuclear Data Center of the United States National Bureau of Standards, Washington, D.C. [6]. We also refer to the photonuclear cross-section atlas for monoenergetic photons compiled by Berman [7]. The survey of literature pertaining to this compilation was concluded in January 1984.

ACKNOWLEDGEMENTS

Financial support from the National Institute of Radiation Protection, Sweden, is gratefully acknowledged. The authors also wish to thank Boel Forkman for her careful preparation of the graphs.

REFERENCES TO SECTIONS 1 THROUGH 3

[1] JONSSON, G.G., LINDGREN, K., Phys. Scr. 7 (1973) 49.
[2] SCHIFF, L.I., Phys. Rev. 83 (1951) 252.
[3] PENFOLD, A.S., LEISS, J.E., Analysis of Photo-Cross Sections, Physical Research Laboratory, University of Illinois (1958).
[4] WAPSTRA, A.H., BOS, K., At. Data Nucl. Data Tables 19 (1977) 177.
[5] Table of Isotopes (LEDERER, C.M., SHIRLEY, V.S., Eds), 7th edn, Wiley-Interscience, New York (1978).
[6] FULLER, E.G., GERSTENBERG, H., US National Bureau of Standards, Washington, DC, Rep. NBSIR-83-2742 (1983).
[7] BERMAN, B.L., At. Data Nucl. Data Tables 15 (1975) 319.

4. CONTENTS LIST OF GRAPHS

Hydrogen

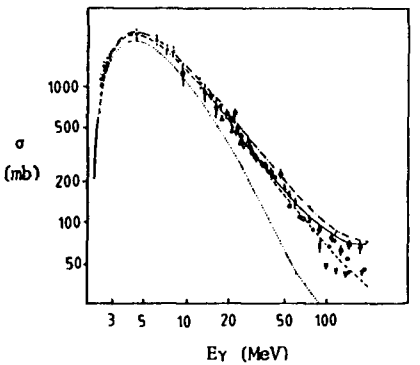

^{2}H Mono 80Ar46

σ(γ,p) with different theoretical estimates

H	A = 1 (99.99)	A = 2 (0.015)	A = 3 (*)
GN	*	2.2 S	6.3 S
GP	*	2.2 10.61 min, β^-	8.5 10.61 min, β^-
G2N	*	*	8.5 S
GNP	*	2.2	8.5 10.61 min, β^-
G2P	*	*	*
GA	*	*	*

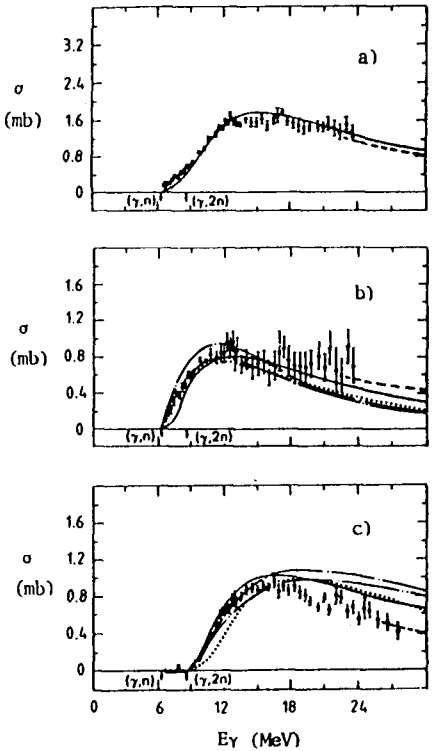

^{3}H Mono 81Fa1

a) σ(γ,n_t)
b) σ(γ,n)
c) σ(γ,2n)
} with different theoretical estimates

Helium

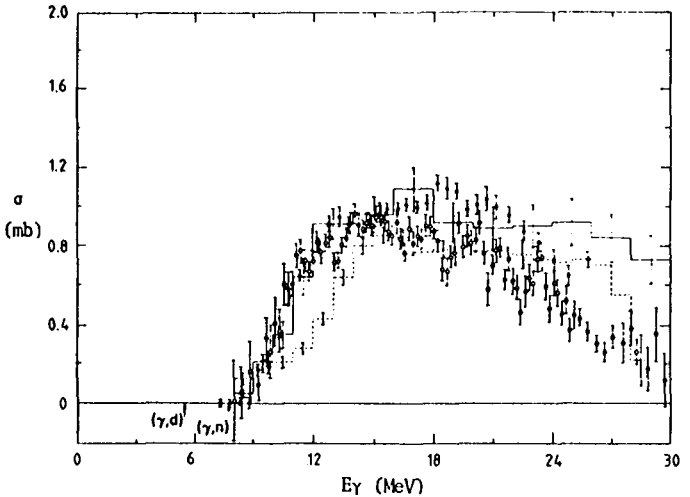

^{3}He 81Fa1

● σ(γ,n) compared with
○ 74Be1 (Mono), — 63Go13, 65FeS (Brems)
--- 61Ge1 (Brems)

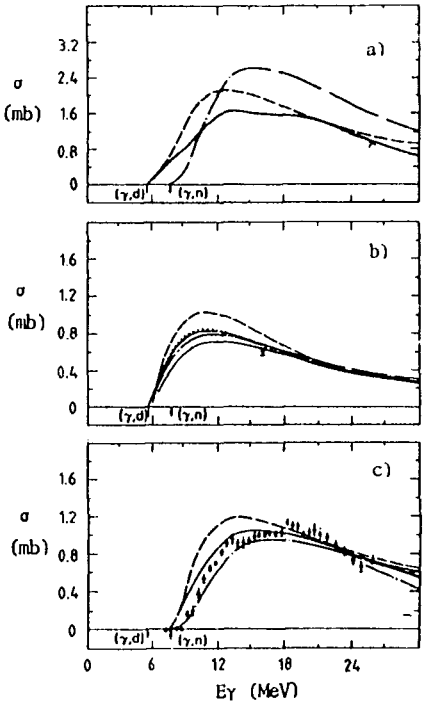

^{3}He Mono 81Fa1

a) σ(γ,n_t) } with different
b) σ(γ,d) } theoretical
c) σ(γ,n) } estimates

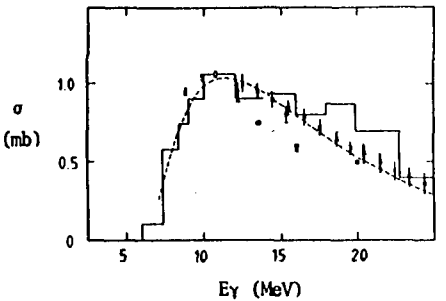

^{3}He 79Sk101

o σ(γ,d) inverse reaction
65Fe5, ● 71Wo8, × 71Ku5,
■ 73Ti13, ▼ 74Ma5, ---70Ba1

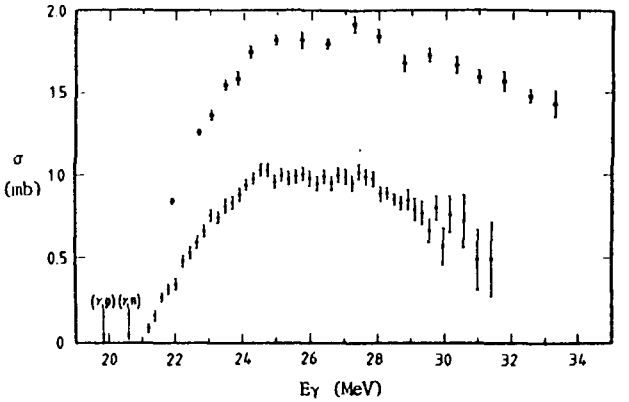

^{4}He Mono 71Be1

■ σ(γ,p) inverse reaction 70Me5
● σ(γ,n)

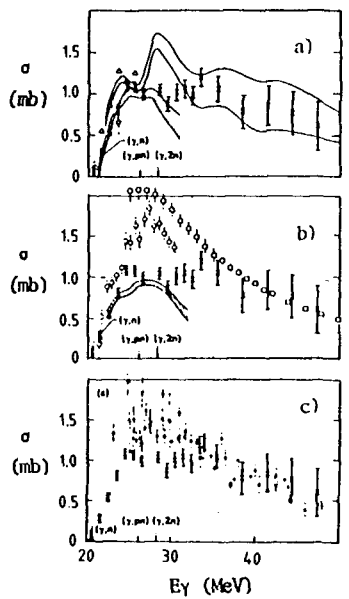

^{6}He Mono 80Be1

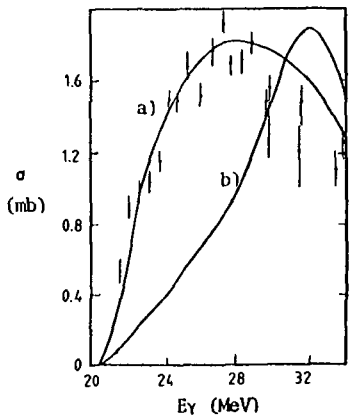

^{4}He 80Be16

σ(γ,n) theoretical cross-section:
a) based on the CCRM-I spectrum
b) based on the CCRM-II spectrum
● data from 74Ch5 (Mono)
■ data from 72Do8 (Mono)

a) ⧗ $\sigma(\gamma,n_t)$ compared with
△ 54Fe1, ≈ 66Fe7, ⧓ 71Be1
and ▽ 63Zu1 (inverse reaction)

b) ⧗ $\sigma(\gamma,n_0)$ compared with
⧓ 72Be5, ○ 75Ir16, □ 73Ma13

c) ⧗ $\sigma(\gamma,^3H)$ compared with
▼ 68Go13, ▲ 78Ar17,
● 77Ba7, ■ 72Do8

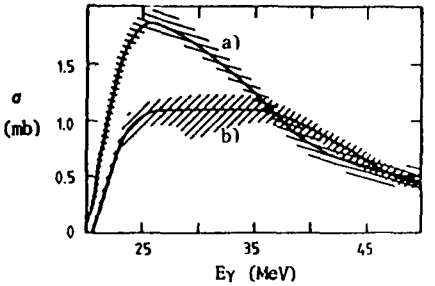

^{4}He 81Ci45

Best estimates of the total cross-section data of

a) $\sigma(\gamma,p)$ | from 80Be1 (Mono)
b) $\sigma(\gamma,n)$ | and 81Wa1 (inverse reaction)

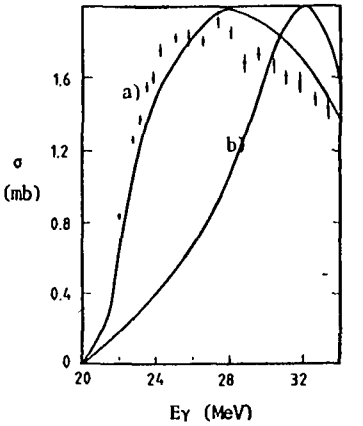

^{4}He 80Be16

$\sigma(\gamma,p)$ theoretical cross-section:
a) based on the CCRM-I spectrum
b) based on the CCRM-II spectrum
● data from 70Me5 (inverse reaction)

He	A = 3 (0.00014)	A = 4 (100)
GN	7.7 *	20.6 S
GP	5.5 S	19.8 12.346y, β^-
G2N	*	28.3 *
GNP	7.7 S	26.1 S
G2P	7.7 10.61 min, β^-	28.3 10.61 min, β^-
GA	*	*

Lithium

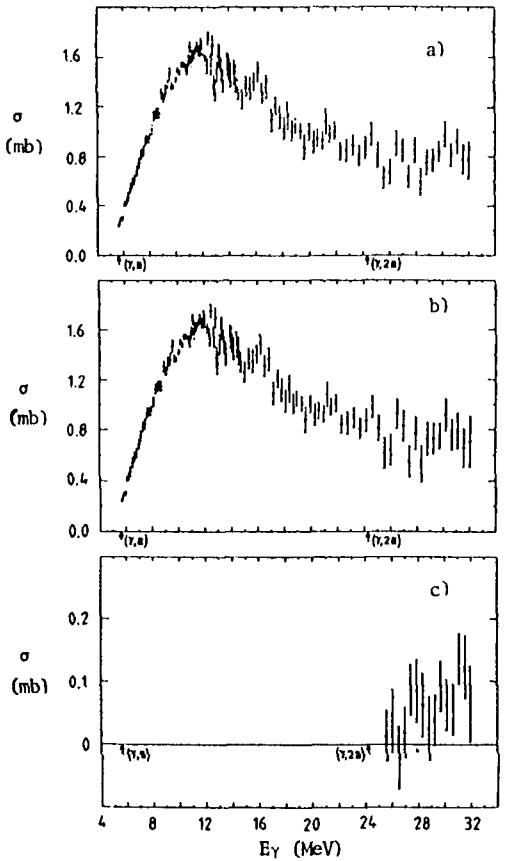

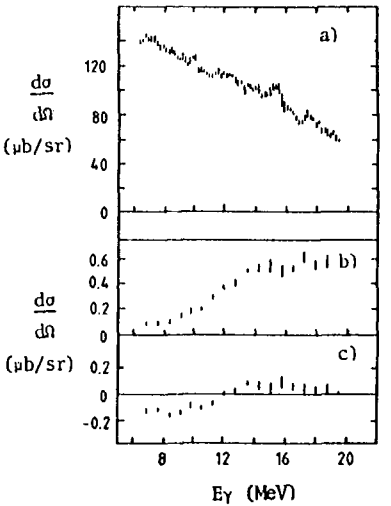

^{6}Li Brems 79Ju4

a) A_0 σ(γ,p) E_{max}=35 MeV
b) a_1 σ(γ,p)
c) a_2 σ(γ,p)

$$\frac{d\sigma}{d\Omega}(\theta,E) = \sum_{i=0}^{n} A_i(E)\,P_i(\cos\theta)$$

$$= A_0(E)\left[1 + \sum_{i=1}^{n} a_i(E)\,P_i(\cos\theta)\right]$$

^{6}Li Mono 75Be6 , 65Be8

a) $\sigma(\gamma,n_t)$
b) $\sigma(\gamma,n)+\sigma(\gamma,pn)$
c) $\sigma(\gamma,2n)+\sigma(\gamma,p2n)$

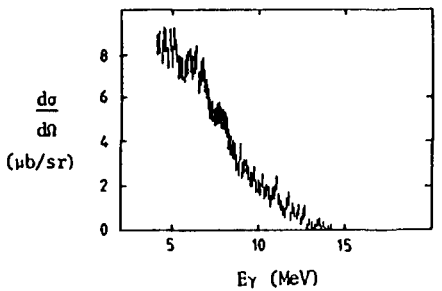

^{6}Li Brems 79Ju4

$\sigma(\gamma,d)$ $\theta=90^{O}$ E_{max}=35 MeV

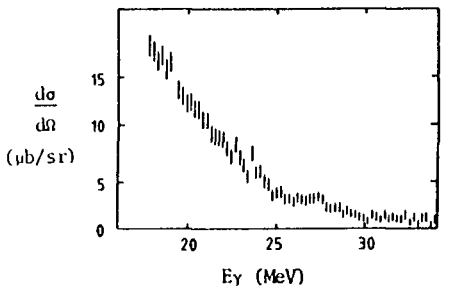

^{6}Li Brems 79Ju4

$\sigma(\gamma,\alpha)$ $\theta=90^{O}$ E_{max}=35 MeV

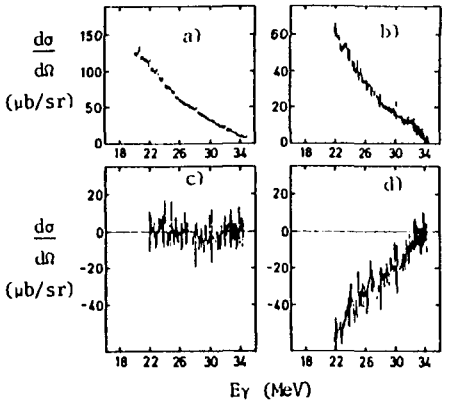

^{6}Li Brems 79Ju4

a) θ=90°σ(γ,t) E_{max}=35 MeV
b) A0 σ(γ,t)
c) A1 σ(γ,t)
d) A2 σ(γ,t)

$$\frac{d\sigma}{d\Omega}(\theta,E)=\sum_{i=0}^{n}A_i(E)\,P_i(\cos\theta)$$

$$=A_0(E)\left[1+\sum_{i=1}^{n}a_i(E)\,P_i(\cos\theta)\right].$$

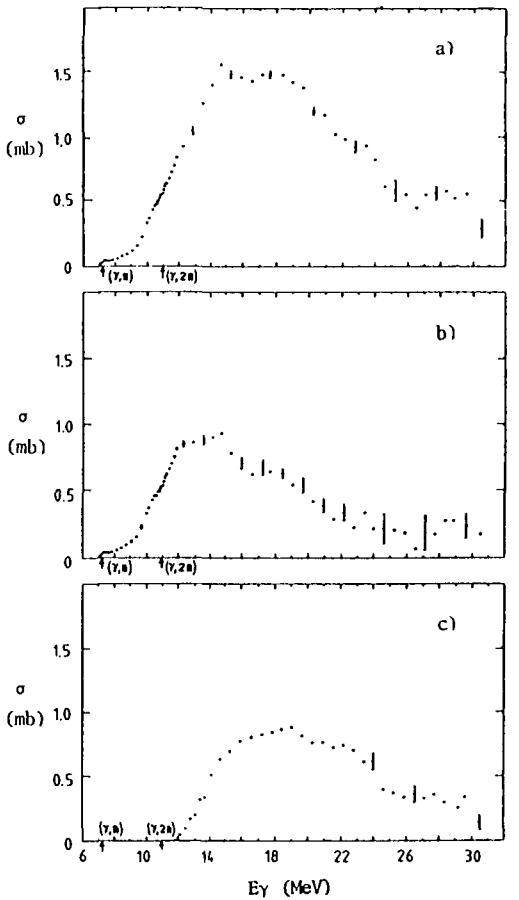

^{7}Li Mono 75Be6 , 73Br44

a) σ(γ,n_t)
b) σ(γ,n)+σ(γ,pn)
c) σ(γ,2n)+σ(γ,p2n)

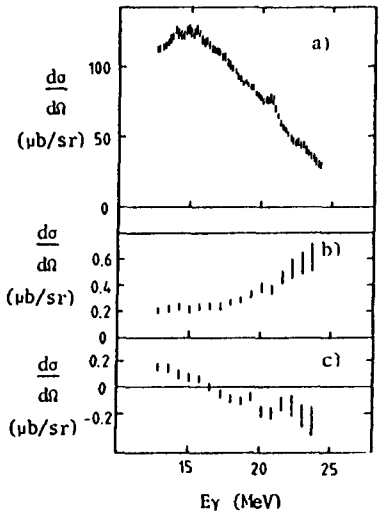

^{7}Li Brems 79Ju4

a) A_0 $\sigma(\gamma,p)$ E_{max}=28 MeV
b) a_1 $\sigma(\gamma,p)$
c) a_2 $\sigma(\gamma,p)$

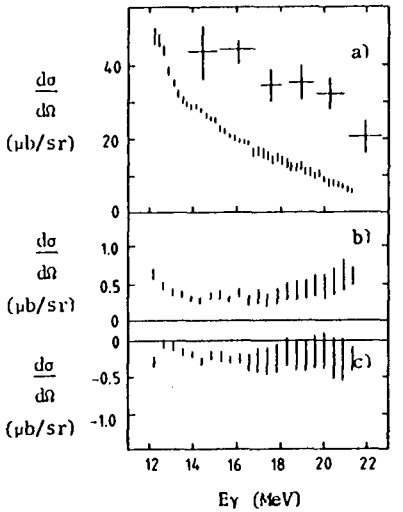

^{7}Li Brems 79Ju4

a) A_0 $\sigma(\gamma,d)$ E_{max}=28MeV
+ Results from 75De14
b) a_1 $\sigma(\gamma,d)$
c) a_2 $\sigma(\gamma,d)$

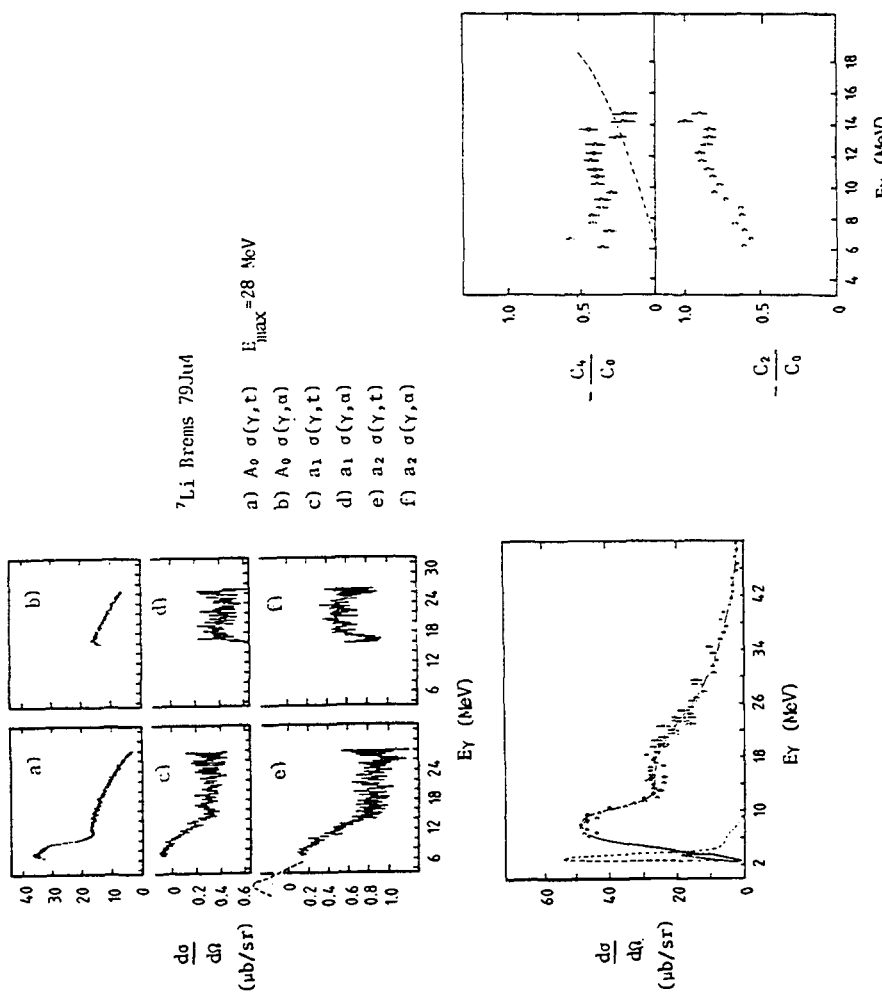
7Li Brems 79Jul4
a) A0 σ(γ,t) Emax=28 MeV
b) A0 σ(γ,α)
c) a1 σ(γ,t)
d) a1 σ(γ,α)
e) a2 σ(γ,t)
f) a2 σ(γ,α)
dσ/dΩ (μb/sr)
Eγ (MeV)
-C4/C0
-C2/C0

^{7}Li Brems 79Sk1

o triton data $\theta=90^{o}$

x alpha data

--- cluster theory ÷30

▭ capture data from 61Gr16

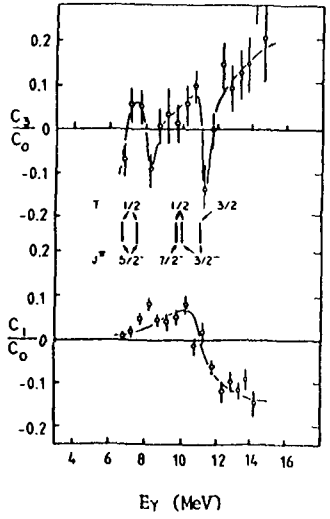

79Sk1

Even Legendre coefficients from least squares fitting of the data to $\sigma(\theta)=\sum_{i=0}^{4} C_i P_i(\cos\theta)$.

Dashed Line indicates the E2 strength in the α-^{3}H cluster model of 79Sk1.

Li	A = 6 (7.5)	A = 7 (92.5)
GN	5.7 *	7.3 S
GP	4.6 *	10.0 0.8081s, β^-
G2N	27.2 *	12.9 *
GNP	3.7 S	11.8 *
G2P	26.4 *	33.5 *
GA	1.5 S	2.5 12.346y, β^-

79Sk1

Odd Legendre coefficients.

Known negative parity states in ^{7}Li are indicated.

Beryllium

Be	A = 9 (100)
GN	1.7 6.7E-17s, 2α
GP	16.9 0.844Os, β⁻2α
G2N	20.6 53.29d, EC
GNP	18.9 S
G2P	29.3 *
GA	2.5 *

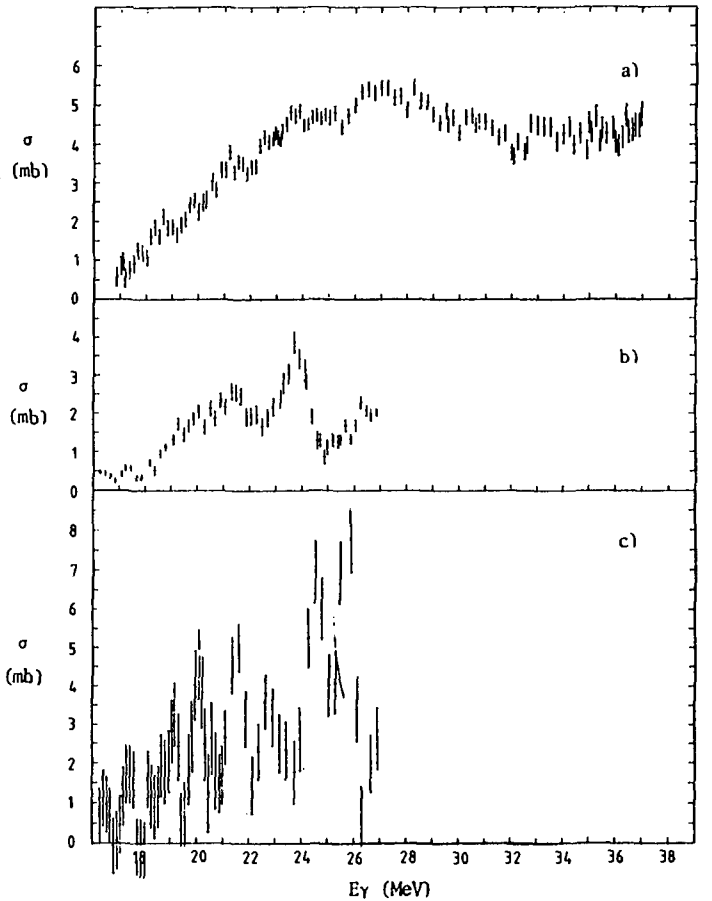

^{9}Be Mono 75Kn5

a) σ(γ,n)+σ(γ,pn)+2σ(γ,2n)

b) σ(γ,n)+σ(γ,pn)+2σ(γ,2n) 75Ilu5

c) σ(γ,n)+σ(γ,pn)+2σ(γ2n) 72Th5

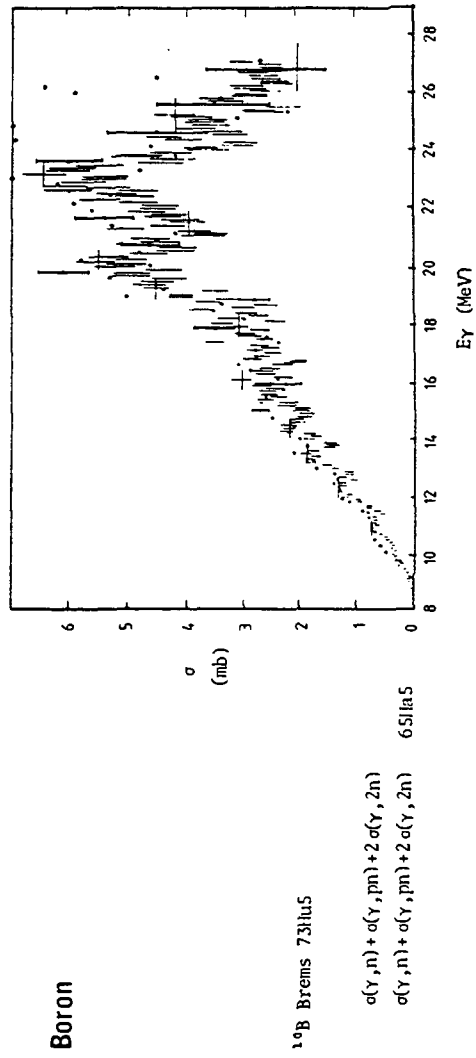
Boron
^{10}B Brems 73Ilu5
σ(γ,n) + σ(γ,pn) + 2 σ(γ,2n)
σ(γ,n) + σ(γ,pn) + 2 σ(γ,2n) 65Ila5
σ (mb)
Eγ (MeV)

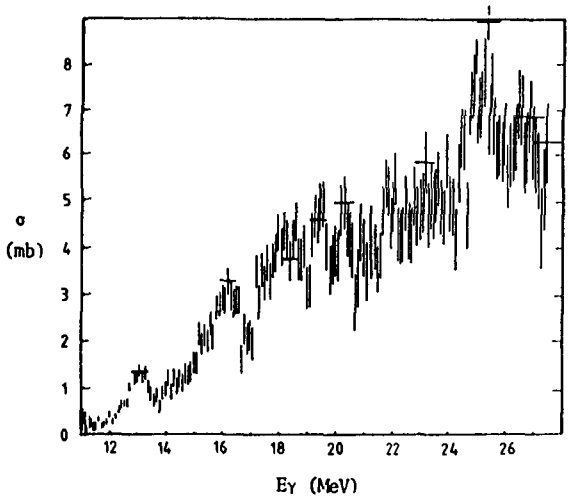

^{11}B Brems 73Hu5

σ(γ,n)+ σ(γ,pn)+2 σ(γ,2n)

B	A = 10 (20)	A = 11 (80)
GN	8.4 8.5E-19s, p2α	11.5 S
GP	6.6 S	11.2 1.6E+6y, β^-
G2N	27.0 0.772s, β^+2α	19.9 8.5E-19s, p2α
GNP	8.3 6.7E-17s, 2α	18.0 S
G2P	23.5 0.844s, β^-2α	30.9 0.1783s, β^-, β^-n
GA	4.5 S	8.7 S

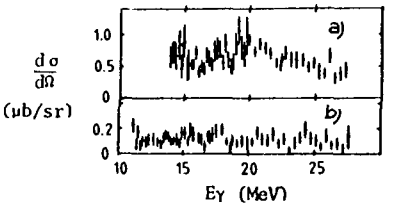

^{10}B Brems 78Ta41

a) (γ,d_1)

b) (γ,d_0)

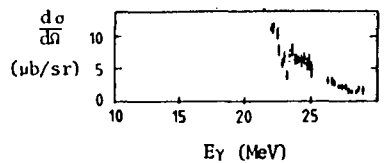

^{11}B Brems 78Ta41

(γ,d_0)

Carbon

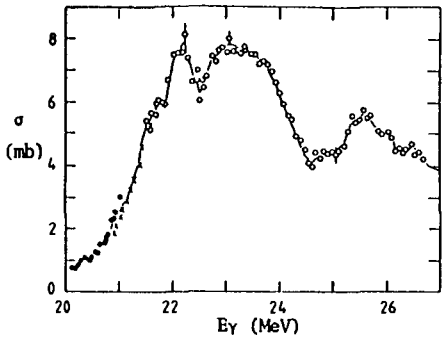

^{12}C Mono 75Be6 , 66Lo1

$\sigma(\gamma, n_t)$

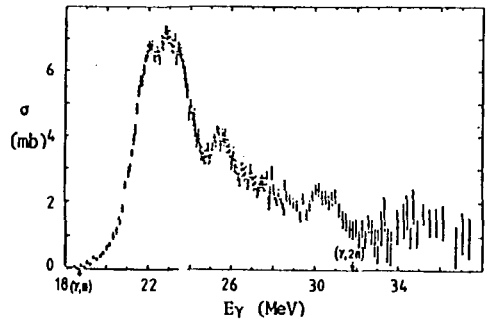

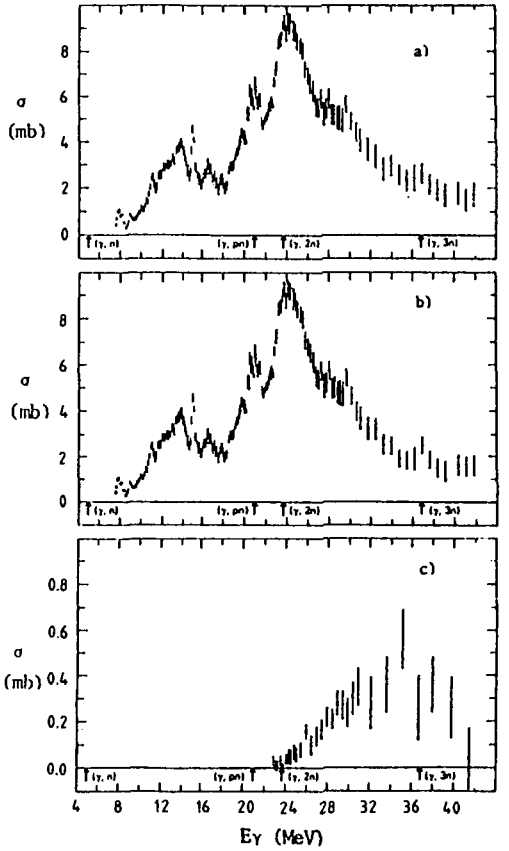

^{12}C Mono 75Be6 , 66Fu1

$\sigma(\gamma,n_t)$

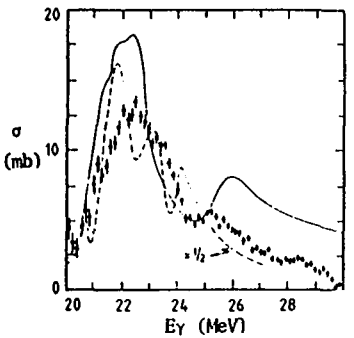

^{12}C Brems 76Ca1

- $\sigma(\gamma,p)$ assuming ground state transitions only.

Theory:

— $\sigma(\gamma,p)$ 71Bi13 , 72Bi5 , 73Be142

--- $\sigma(\gamma,p)$ 72Ms8 , 73Ms5 , 73Ms4

^{13}C Mono 79Ju1

a) $\sigma(\gamma,n)+\sigma(\gamma,pn)+\sigma(\gamma,\alpha n)+\sigma(\gamma,2n)$

b) $\sigma(\gamma,n)+\sigma(\gamma,pn)+\sigma(\gamma,\alpha n)$

c) $\sigma(\gamma,2n)+\sigma(\gamma,p2n)$

^{13}C Brems 83Zu1

||| $\sigma(\gamma,p)$

● $\sigma(\gamma,p)$ 64De18

— $\sigma(\gamma,p)$ 57Co1

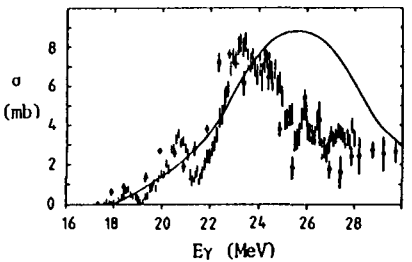

C	A = 12 (98.89)	A = 13 (1.11)
GN	18.7 20.38 min, β^+, EC	4.9 S
GP	16.0 S	17.5 2.03E-2s, β^-, $\beta^-\alpha$
G2N	31.8 19.151s, β^+	23.7 20.38 min, β^+, EC
GNP	27.4 S	20.9 S
G2P	27.2 1.6E+6y, β^-	31.6 13.81s, β^-, $\beta^-\alpha$
GA	7.4 6.7E-17s, 2α	10.6 S

Nitrogen

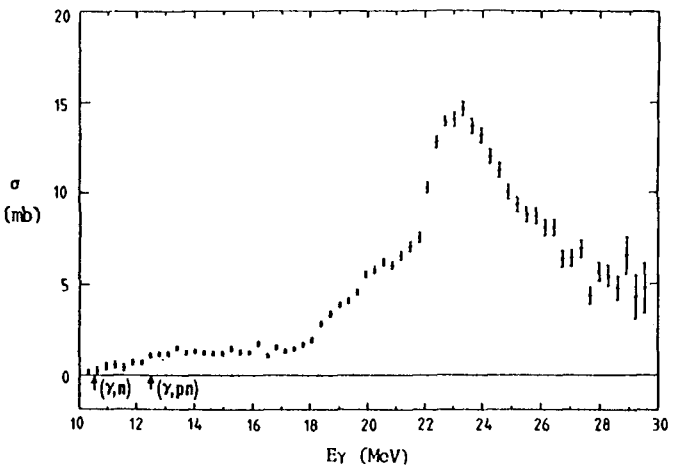

^{14}N Mono 75Bc6 , 70Bc1

$\sigma(\gamma,n_t)$

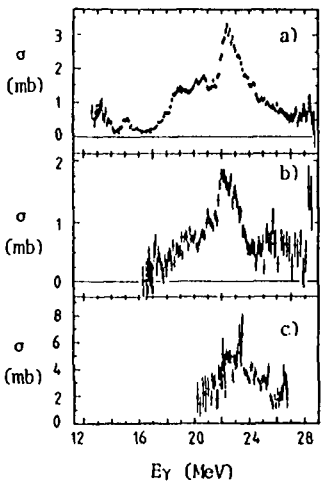

^{14}N Brems 83Ot47

a) $^{14}N(\gamma,p_0)^{13}C$

b) $^{14}N(\gamma,p_{3.68\ MeV})^{13}C$

c) $^{14}N(\gamma,p_{7.55\ MeV})^{13}C$

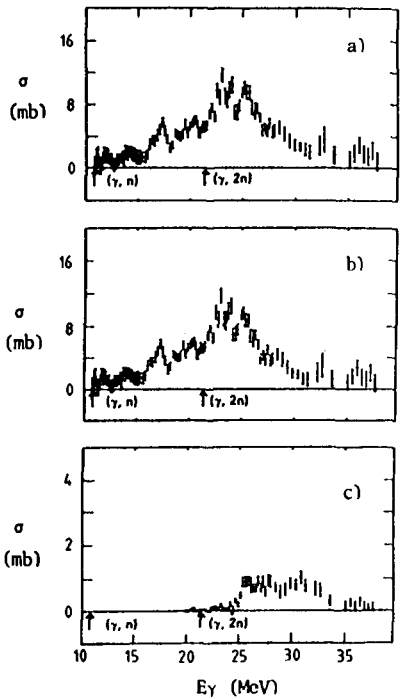

^{15}N Mono 82Ju1

a) $\sigma(\gamma,n)+\sigma(\gamma,pn)+\sigma(\gamma,\alpha n)+\sigma(\gamma,2n)$

b) $\sigma(\gamma,n)+\sigma(\gamma,pn)+\sigma(\gamma,\alpha n)$

c) $\sigma(\gamma,2n)+\sigma(\gamma,p2n)$

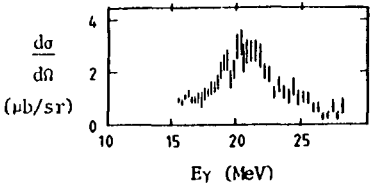

^{14}N Brems 78Ta41

(γ,d_0)

N	A = 14 (99.63)	A = 15 (0.37)
GN	10.6 9.963 min, β^+	10.8 S
GP	7.6 S	10.2 5.730E+3y, β^-
G2N	30.6 1.095E-2s, β^+, $\beta^+\alpha$	21.4 9.963 min, β^+
GNP	12.5 S	18.4 S
G2P	25.1 2.03E-2s, β^-, $\beta^-\alpha$	31.0 1.733E-2s, β^-, β^-n
GA	11.6 S	11.0 S

Oxygen

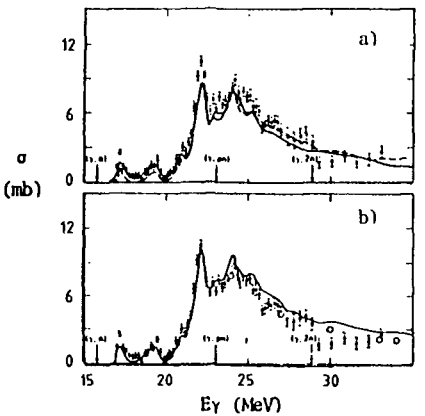

^{16}O Mono 83Be1

a) ● σ(γ,1n)
— σ(γ,1n) combined result from 64Br1 and 80Ju1
- - - σ(γ,1n) 75Kn9

b) ● σ(γ,1n)
o σ(γ,1n) 82Ca5
— σ(γ,1n) 74Ve5

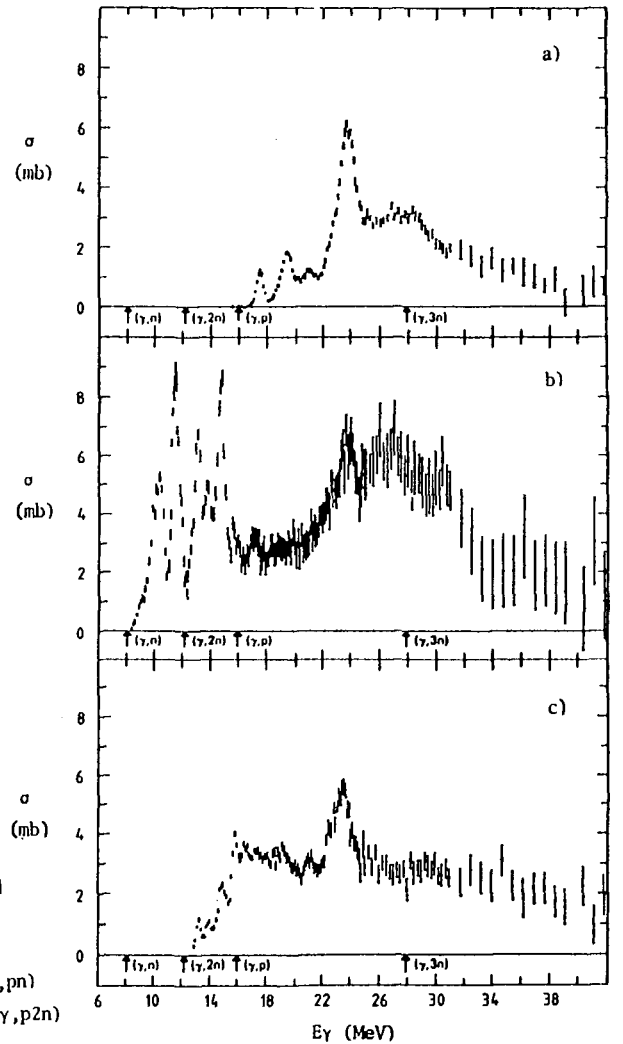

^{18}O Mono 79Wo1

a) σ(γ,p)
b) σ(γ,n)+σ(γ,pn)
c) σ(γ,2n)+σ(γ,p2n)

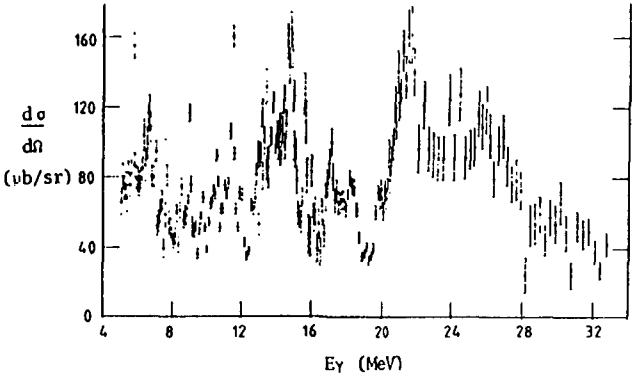

^{17}O Brems 79Jo1

$\frac{d\sigma}{d\Omega}(E_x, 98^{\circ})$ for (γ, n_0)

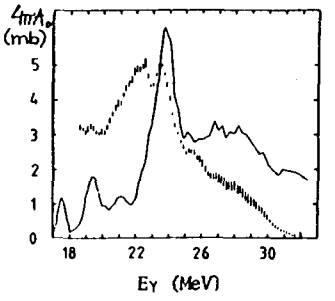

^{18}O Brems 82Ba5

IIII σ(γ,p)
— σ(γ,p) 79Wo1

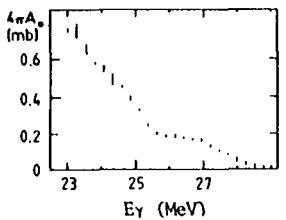

^{18}O Brems 82Ba5

σ(γ,d)

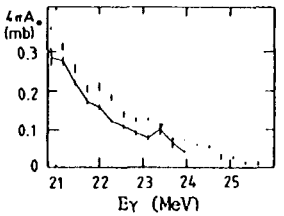

^{18}O Brems 82Ba5

— connects data points σ(γ,t) from 24 MeV measurement.

| σ(γ,t) from 32MeV measurement.

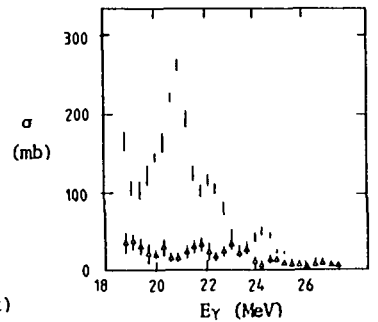

^{18}O Brems 82Ba5

| σ(γ,α₀) E1

△ σ(γ,α₀) E2

O	A = 16 (99.76)	A = 17 (0.04)	A = 18 (0.20)
GN	15.7 1.221E+2s, β^+, EC	4.1 S	8.0 S
GP	12.1 S	13.8 7.13s, β^-, $\beta^-\alpha$	15.9 4.17s, β^-, β^-n
G2N	28.9 70.59s, β^+	19.8 1.221E+2s, β^+, EC	12.2 S
GNP	23.0 S	16.3 S	21.8 7.13s, β^-, $\beta^-\alpha$
G2P	22.3 5.730E+3y, β^-	25.3 2.45s, β^-	29.1 0.75s, β^-n
GA	7.2 S	6.4 S	6.2 5.730E+3y, β^-

Fluorine

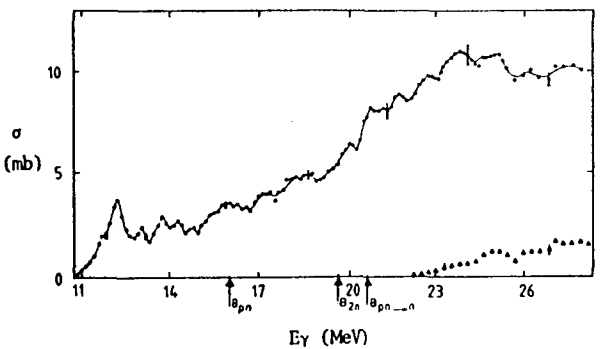

^{19}F Mono 74Ve5

● $\sigma(\gamma,n_t)$
▲ $\sigma(\gamma,2n)+\sigma(\gamma,p2n)$

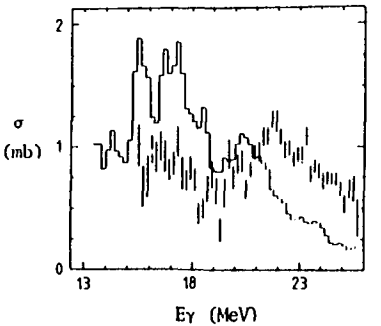

^{19}F Brems 83Ke36

$\sigma(\gamma,p_0)$
$\sigma(\gamma,p_1)$

F	A = 19 (100)
GN	10.4 1.097E+2 min, β^+, EC
GP	8.0 S
G2N	19.6 64.50s, β^+
GNP	16.0 S
G2P	23.9 4.174s, β^-, β^-n
GA	4.0 S

Neon

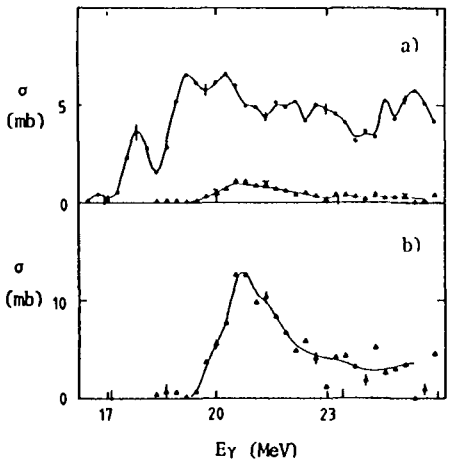

Mono 74Ve5

a) Ne natural
● σ(γ,n)+σ(γ,pn)
▲ σ(γ,2n)+σ(γ,p2n)
b) ^{22}Ne
▲ σ(γ,2n)+σ(γ,p2n)

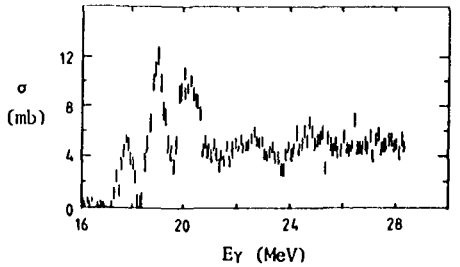

^{20}Ne Brems 81A15

σ(γ,n)

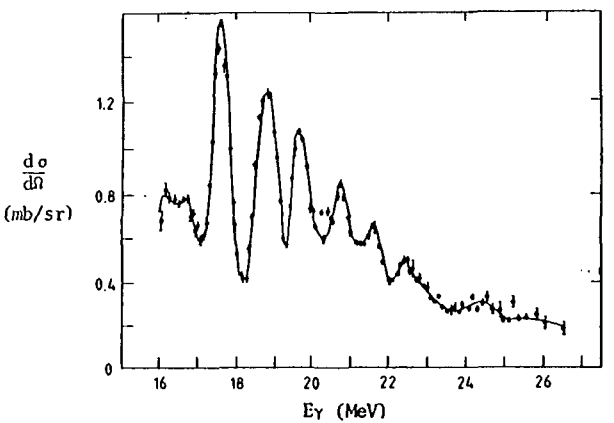

^{20}Ne (e,e´p) 62Ma1

(γ,p) θ=76°

Ne	A = 20 (90.51)	A = 21 (0.27)	A = 22 (9.22)
GN	16.9 17.22s, β^+, EC	6.8 S	10.4 S
GP	12.8 S	13.0 11.00s, β^-	15.3 4.35s, β^-
G2N	28.5 1.67s, β^+	23.6 17.22s, β^+, EC	17.1 S
GNP	23.3 1.908E+2 min, β^+, EC	19.6 S	23.4 11.00s, β^-
G2P	20.8 S	23.6 26.76s, β^-	26.4 13.5s, β^-
GA	4.7 S	7.3 S	9.7 S

Sodium

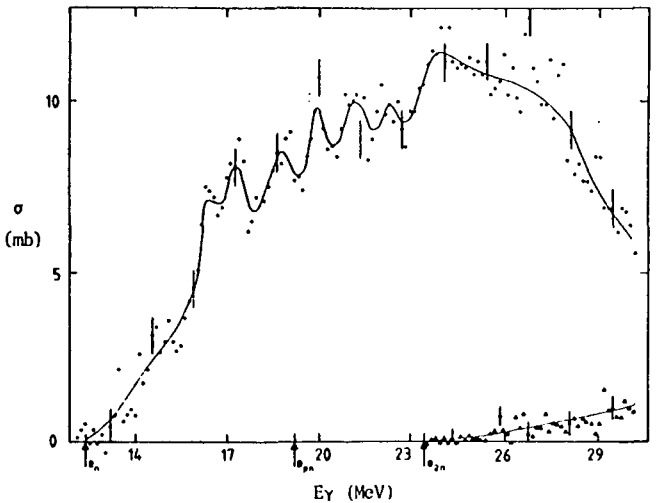

^{23}Na Mono 74Ve5

● $\sigma(\gamma,n_t)$

▲ $\sigma(\gamma,2n)+\sigma(\gamma,p2n)$

Na	A = 23 (100.0)
GN	12.4 2.602y, β^+, EC
GP	8.8 S
G2N	23.5 22.47s, β^+
GNP	19.2 S
G2P	24.1 4.35s, β^-
GA	10.5 S

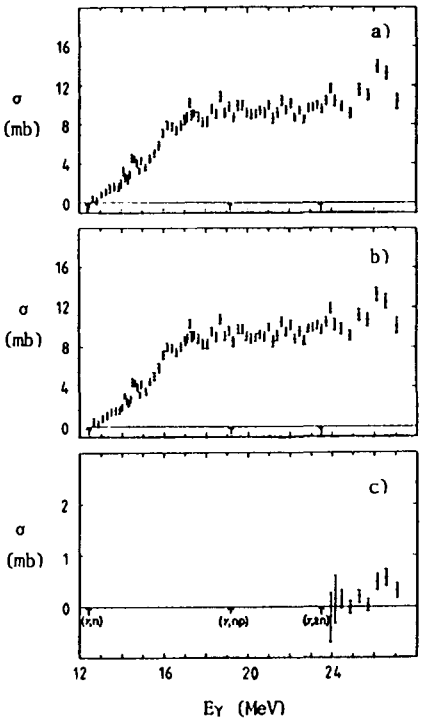

^{23}Na Mono 71A11

a) $\sigma(\gamma,n_t)$

b) $\sigma(\gamma,n)+\sigma(\gamma,pn)$

c) $\sigma(\gamma,2n)+\sigma(\gamma,p2n)$

Magnesium

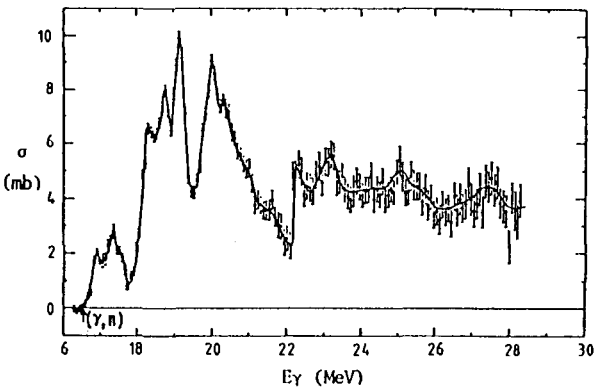

^{24}Mg Mono 75Be6 , 71Fu1

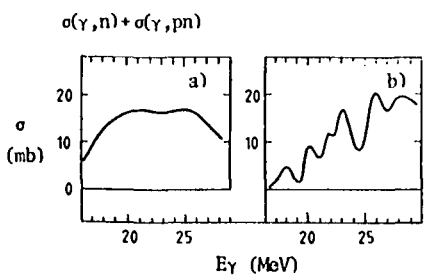

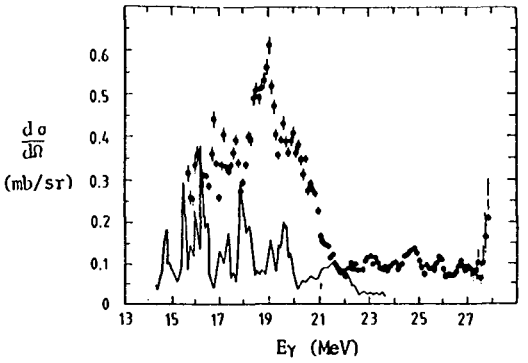

^{24}Mg Brems 83Ry5

● $\frac{d\sigma}{d\Omega}(\gamma,p_0+p_1)$ θ=90°

— $\frac{d\sigma}{d\Omega}(\gamma,p_0)$ θ=90° 68Be105

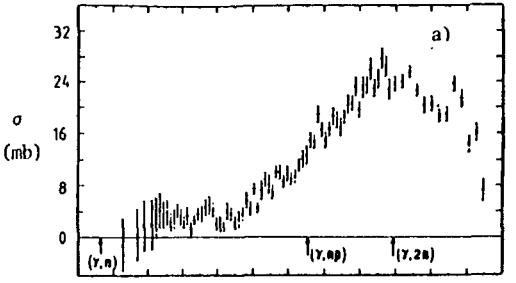

Mg isotopes Brems 74Va5

a) ^{24}Mg σ(γ,xp) 64Is13
b) ^{25}Mg σ(γ,xp)

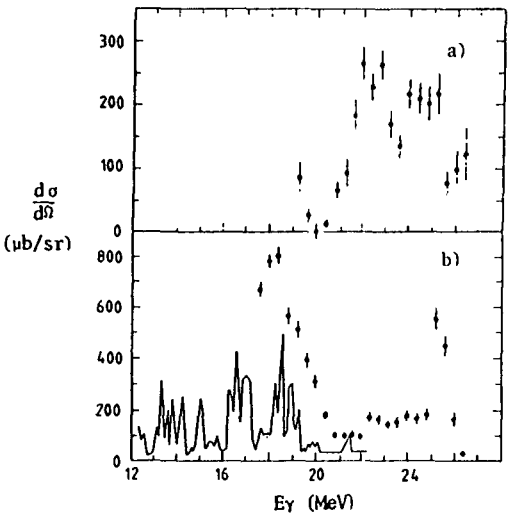

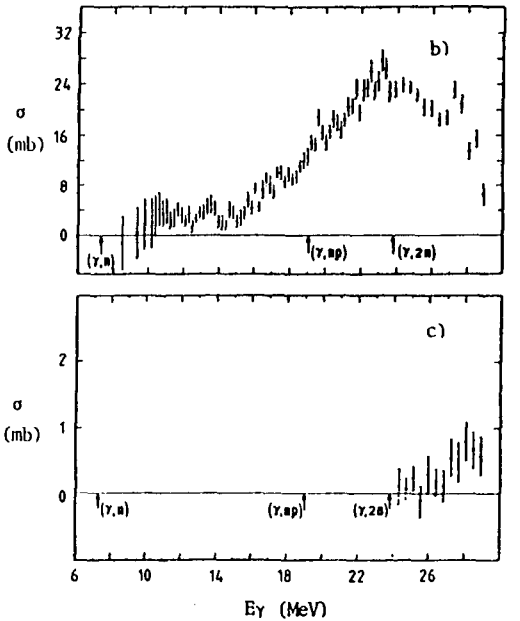

^{25}Mg Mono 75Be6 , 71A11

a) σ(γ,n_t)
b) σ(γ,n)+σ(γ,pn)
c) σ(γ,2n)+σ(γ,p2n)

^{24}Mg Brems 83Ry5 b) ● $\frac{d\sigma}{d\Omega}(\gamma,\alpha_0)$ θ=90° a) $\frac{d\sigma}{d\Omega}(\gamma,\alpha_1)$ θ=90° — $\frac{d\sigma}{d\Omega}(\gamma,\alpha_0)$ θ=90° 75Ku1

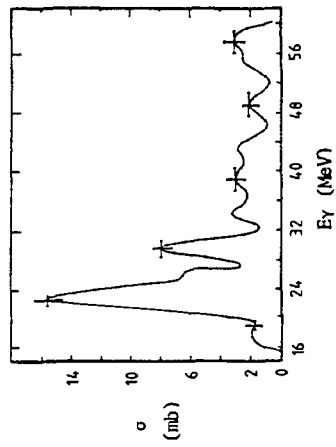
σ (mb)
Eγ (MeV)
^{26}Mg Brems 74An1
σ(γ,p)

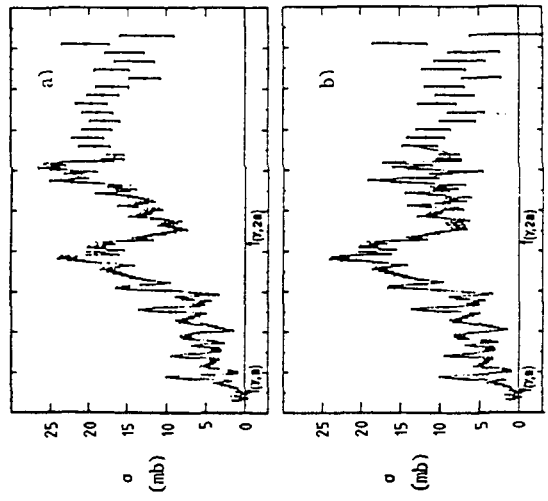
a)
b)
σ (mb)
σ (mb)

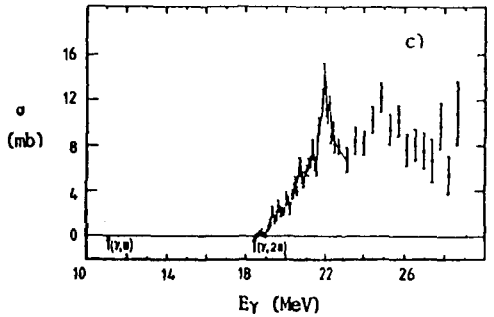

^{26}Mg Mono 75Be6 , 71Pu1

a) $\sigma(\gamma,n_t)$
b) $\sigma(\gamma,n)+\sigma(\gamma,pn)$
c) $\sigma(\gamma,2n)+\sigma(\gamma,p2n)$

Mg	A = 24 (78.99)	A = 25 (10.00)	A = 26 (11.01)
GN	16.5 11.33s, β^+	7.3 S	11.1 S
GP	11.7 S	12.1 15.030h, β^-	14.1 60s, β^-
G2N	29.7 3.857s, β^+	23.9 11.33s, β^+	18.4 S
GNP	24.1 2.602y, β^+, EC	19.0 S	23.2 15.030h, β^-
G2P	20.5 S	22.6 37.6s, β^-	24.8 3.38 min, β^-
GA	9.3 S	9.9 S	10.6 S

Aluminium

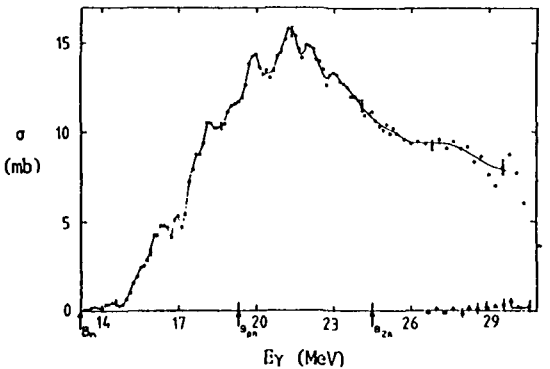

^{27}Al Mono 74VeS

$\sigma(\gamma,n)+\sigma(\gamma,pn)$

$\sigma(\gamma,2n)+\sigma(\gamma,p2n)$

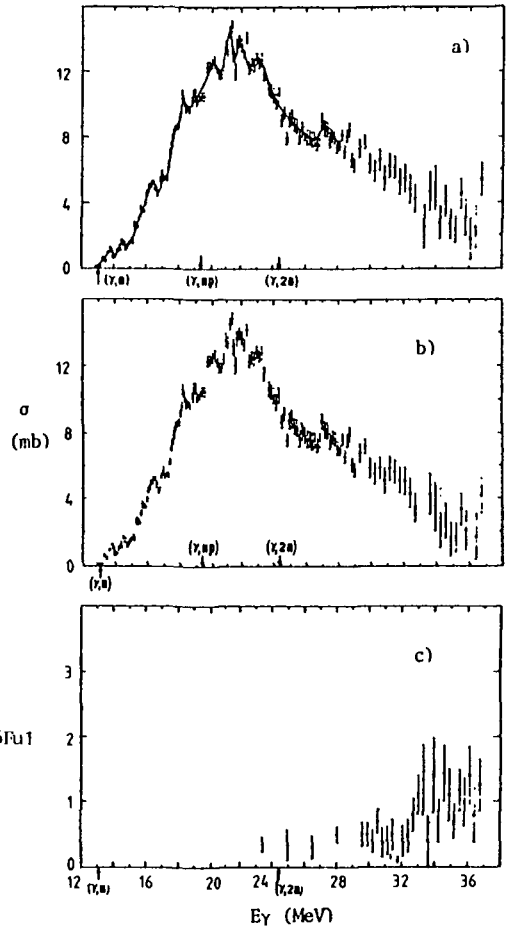

^{27}Al Mono 75Be6 , 66Fu1

a) $\sigma(\gamma,n_t)$

b) $\sigma(\gamma,n)+\sigma(\gamma,pn)$

c) $\sigma(\gamma,2n)+\sigma(\gamma,p2n)$

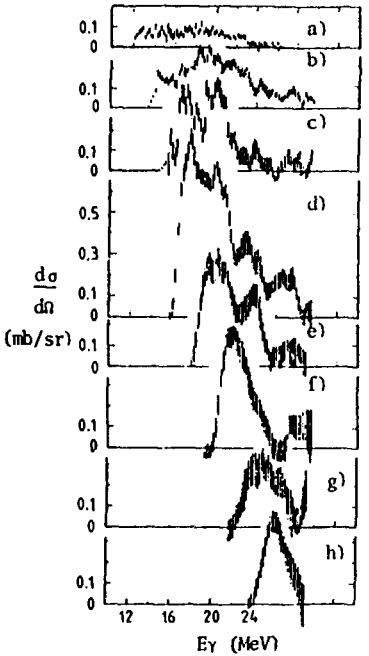

^{27}Al Brems 81Is14

$\frac{d\sigma}{d\Omega}(\gamma,p)\ \theta=90^{o}$

Transitions to different levels in ^{26}Mg

a) 0 MeV b) 1.8 MeV c) 3.0 MeV
d) 4.4 MeV e) 6.6 MeV f) 8.5 MeV
g) 11.0 MeV h) 13.0 MeV

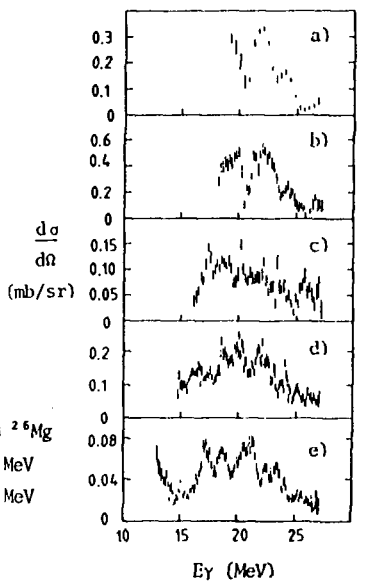

Al	A = 27 (100)	
GN	13.1	7.16E+5y, β^{+}, EC
		6.36s, β^{+}
GP	8.3	S
G2N	24.4	7.174s, β^{+}
GNP	19.4	S
G2P	22.4	60s, β^{-}
GA	10.1	S

^{27}Al Brems 81Ry5

a) $\frac{d\sigma}{d\Omega}(\gamma,p_4)$ $\theta=90^{o}$

b) $\frac{d\sigma}{d\Omega}(\gamma,p_3)$ $\theta=90^{o}$

c) $\frac{d\sigma}{d\Omega}(\gamma,p_2)$ $\theta=90^{o}$

d) $\frac{d\sigma}{d\Omega}(\gamma,p_1)$ $\theta=90^{o}$

e) $\frac{d\sigma}{d\Omega}(\gamma,p_0)$ $\theta=90^{o}$

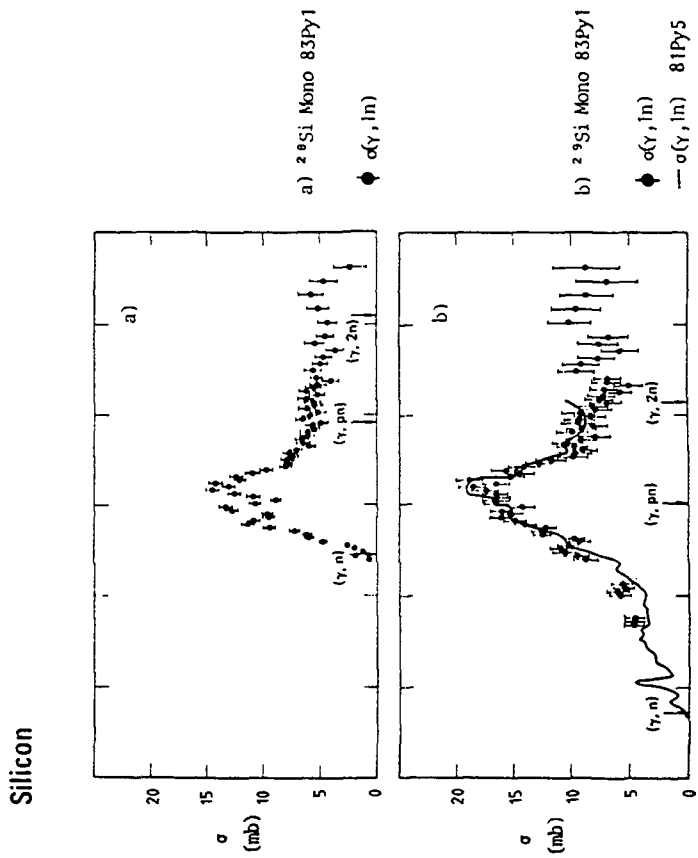
Silicon
a) ²⁸Si Mono 83Py1
σ(γ, ln)
b) ²⁹Si Mono 83Py1
σ(γ, ln)
σ(γ, ln) 81Py5
σ (mb)
(γ, n)
(γ, pn)
(γ, 2n)
a)
b)

c) ^{30}Si Mono 83Py1

● σ(γ, 1n) + σ(γ, 2n)

— σ(γ, 1n) + σ(γ, 2n) 820d5

^{28}Si Mono 74Ve5

— ↓ σ(γ, n) + σ(γ, pn) energy resolution E=180 keV.

--- ↓ σ(γ, n) + σ(γ, pn) energy resolution E=350 keV.

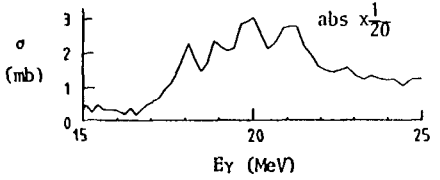

^{28}Si tagged photons 83Gu1; 75Ah5

σ(γ,tot)

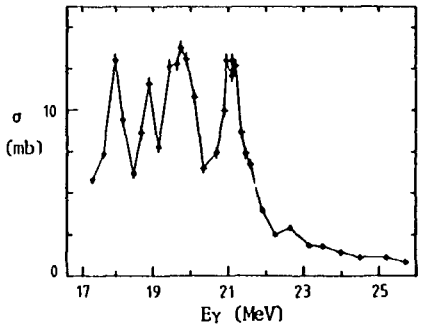

^{28}Si annihilation γ 83Be47

σ(γ,p_0)

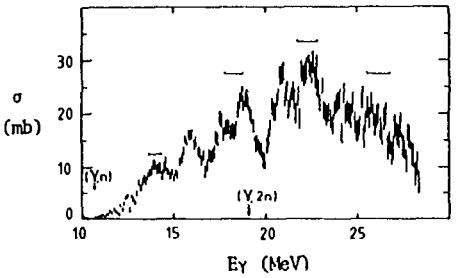

^{30}Si Brems 82Od5

σ(γ,xn) no correction has been made for double counting from the σ(γ,2n) reaction

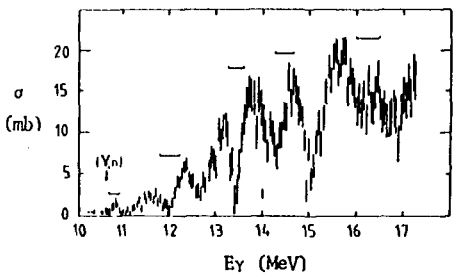

^{30}Si Brems 82Od5

σ(γ,n)

Si	A = 28 (92.23)	A = 29 (4.67)	A = 30 (3.10)
GN	17.2 4.11s, β^+	8.5 S	10.6 S
GP	11.6 S	12.3 2.24 min, β^-	13.5 6.56 min, β^-
G2N	30.5 2.21s, β^+	25.7 4.11s, β^+	19.1 S
GNP	24.6 7.16E+5y, β^+, EC$^+$	20.1 S	22.9 2.24 min, β^-
G2P	19.9 S	21.9 9.46 min, β^-	24.0 20.93h, β^-
GA	10.0 S	11.1 S	10.6 S

Phosphorus

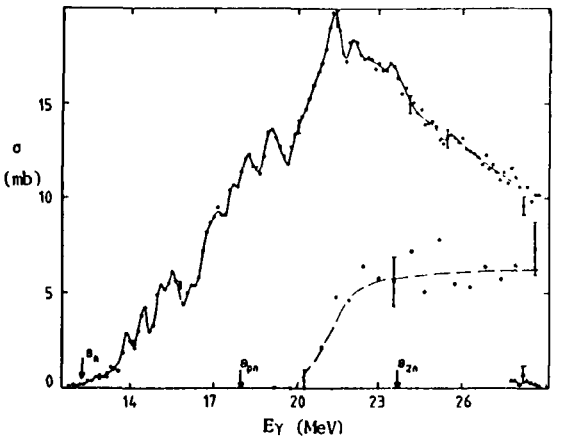

^{31}P Mono 74VeS

- ● σ(γ,n)+σ(γ,pn)
- ○ σ(γ,pn)
- ▲ σ(γ,2n)+σ(γ,p2n)

P	A= 31 (100.0)
GN	12.3 2.50 min, β^+, EC
GP	7.3 S
G2N	23.6 4.15s, β^+
GNP	17.9 S
G2P	20.8 6.56 min, β^-
GA	9.7 S

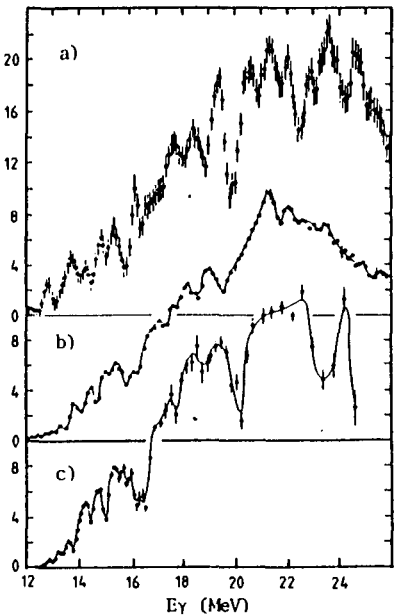

^{31}P 74De4

a) σ(γ,xn) Brems 69Is22
b) σ(γ,xn) Mono 73Be42
c) σ(γ,xn) Brems

Sulphur

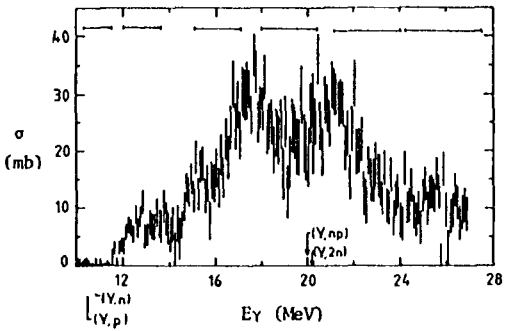

^{34}S Brems 84As5

σ(γ,n) + σ(γ,2n) + σ(γ,pn)

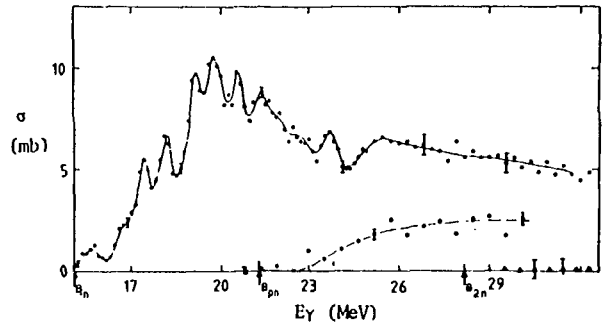

^{32}S Mono 74Ve5

● σ(γ,n) + σ(γ,pn)

○ σ(γ,pn)

▲ σ(γ,2n) + σ(γ,p2n)

^{34}S Brems 84As5

σ(γ,2n) + σ(γ,p2n)

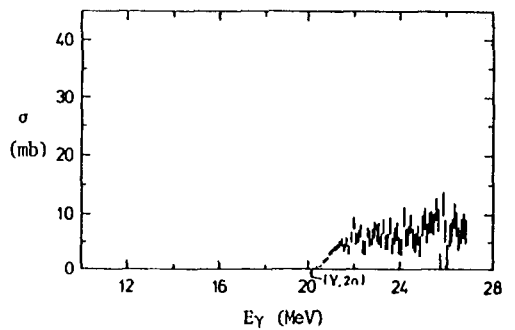

S	A = 32 (95.02)	A = 33 (0.75)	A = 34 (4.21)	A = 36 (0.02)
GN	15.0 2.61s, β^+	8.6 S	11.4 S	9.9 87.4d, β^-
GP	8.9 S	9.6 14.282d, β^-	10.9 25.30d, β^-	13.0 47.5s, β^-
G2N	28.1 1.22s, β^+	23.7 2.61s, β^+	20.1 S	16.9 S
GNP	21.2 2.497 min, β^+, EC	17.5 S	21.0 14.282d, β^-	21.5 12.4s, β^-
G2P	16.2 S	18.2 2.62h, β^-	20.4 6.50E+2y, β^-	25.0 2.8s, β^-
GA	6.9 S	7.1 S	7.9 S	9.0 6.50E+2y, β^-

Chlorine

Mono 74Ve5
a) Cl natural
b) ^{37}Cl

○ $\sigma(\gamma,n)+\sigma(\gamma,pn)$
▲ $\sigma(\gamma,2n)+\sigma(\gamma,p2n)$

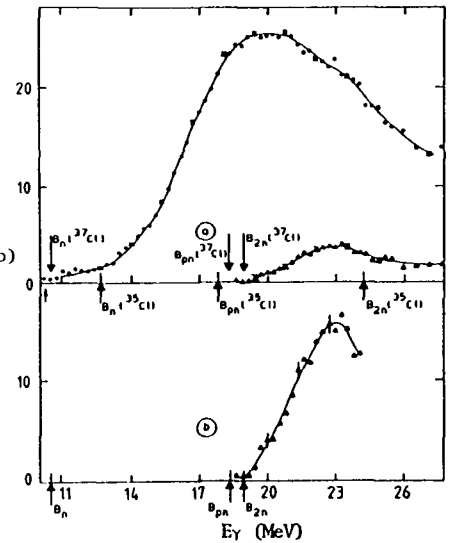

Cl	A = 35 (75.77)	A = 37 (24.23)
GN	12.6 1.53s, β^+ 32.0 min, β^+, IT	10.3 3.00E+5y, β^-, EC, β^+
GP	6.4 S	8.4 S
G2N	24.2 2.51s, β^+	18.9 S
GNP	17.8 S	18.3 87.4d, β^-
G2P	17.3 25.30d, β^-	21.4 47.4s, β^-
GA	7.0 S	7.8 25.30d, β^-

Argon

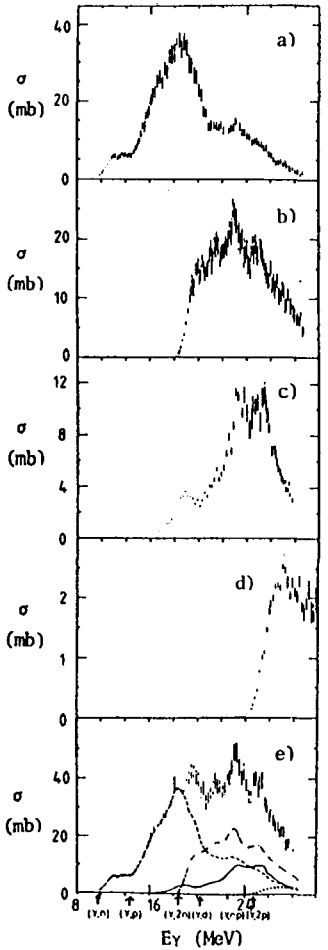

^{40}Ar Brems 83Su5

a) (γ,n)
b) (γ,2n)
c) (γ,p)
d) (γ,d)+(γ,np)
e) (γ,T)

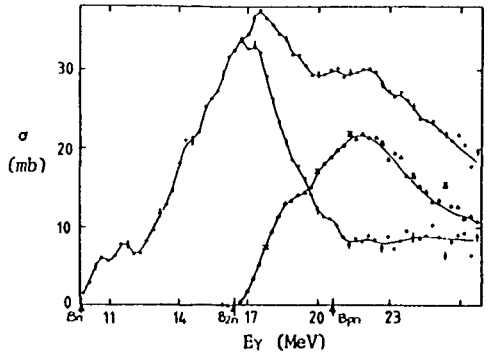

^{40}Ar Mono 74VeS

● σ(γ,n_t)
○ σ(γ,n)+σ(γ,pn)
▲ σ(γ,2n)+σ(γ,p2n)

Ar	A = 36 (0.34)	A = 38 (0.06)
GN	15.3 1.77s, β^+	11.8 35.02d, EC
GP	8.5 S	10.2 S
G2N	28.0 0.84s, β^+	20.6 S
GNP	21.2 1.53s, β^+	20.6 3.00E+5y, β^-, EC, β^+
G2P	14.9 S	18.6 S
GA	6.6 S	7.2 S

Ar	A = 40 (99.60)
GN	9.9 2.69E+2y, β^-
GP	12.5 56.2 min, β^-
G2N	16.5 S
GNP	20.6 37.29 min, β^-
G2P	22.8 1.696E+2 min, β^-
GA	6.8 S

Potassium

^{39}K Mono 74Ve5

● $\sigma(\gamma,n)+\sigma(\gamma,pn)$
▲ $\sigma(\gamma,2n)+\sigma(\gamma,p2n)$
○ $\sigma(\gamma,pn)$

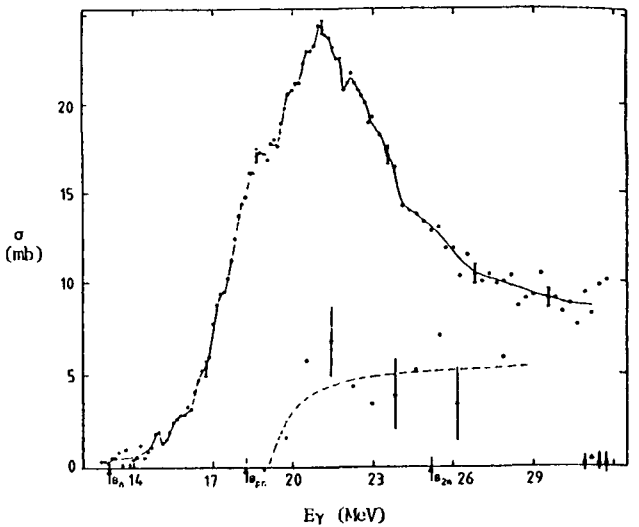

K	A = 39 (93.26)	A = 40 (0.01)	A = 41 (6.73)
GN	13.1 7.61 min, β^+ 0.93s, β^+	7.8 S	10.1 1.28E+9y, β^-, EC, β^+
GP	6.4 S	7.6 2.69E+2y, β^-	7.8 S
G2N	25.2 1.23s, β^+	20.9 7.61 min, β^+	17.9 S
GNP	18.2 35.02d, EC	14.2 S	17.7 2.69E+2y, β^-
G2P	16.6 S	18.3 37.29 min, β^-	20.3 56.2 min, β^-
GA	7.2 S	6.4 3.00E+5y, β^-, EC, β^+	6.2 S

Calcium

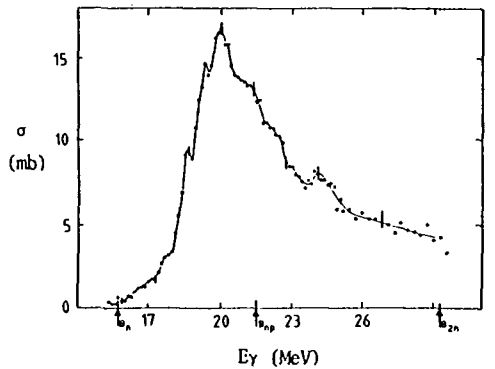

^{40}Ca Mono 74Ve5

• σ(γ,n)+σ(γ,pn)

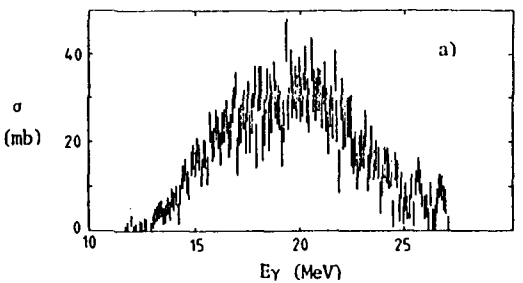

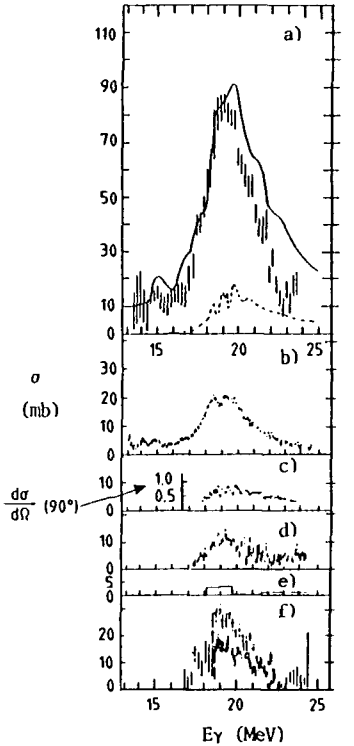

^{40}Ca Brems 74Br1

a) —— σ(γ,n_t)+σ(γ,p_t) 68Be205

|||| σ(γ,p_t)

– – σ(γ,n_t) 64Ba5

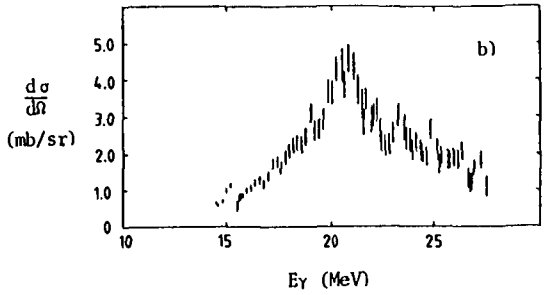

^{42}Ca Brems 81As5

a) $\sigma(\gamma,n_t)$

b) $\frac{d\sigma}{d\Omega}(90^{O})$ (γ,p) 75Th11

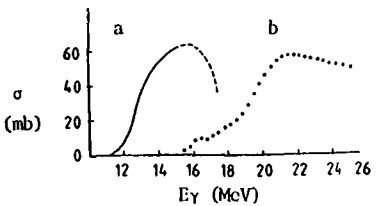

^{44}Ca Brems 77Oi5

a) $\sigma(\gamma,n)$

b) $\sigma(\gamma,p)$x4

b) $\sigma(\gamma,p_0)$

c) $\frac{d\sigma}{d\Omega}(90^{O})$ (γ,n_0) 69Wu13

d) $\sigma(\gamma,p_1)$

e) $\sigma(\gamma,n_1)$

f) $\sigma(\gamma,p)_{4.93-6.35}$

$\sigma(\gamma,p_{unb})$

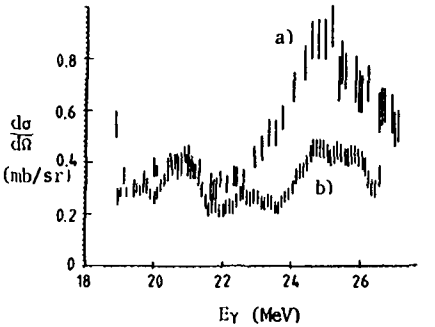

^{48}Ca Brems 78Th41

a) (γ,p) (90^{O}) E_p>28 MeV

b) (γ,p_0) (90^{O})

Ca	A = 40 (96.94)	A = 42 (0.65)	A = 43 (0.14)	A = 44 (2.09)
GN	15.6 0.86s, β^+	11.5 1.03E+5y, EC	7.9 S	11.1 S
GP	8.3 S	10.3 S	10.7 12.36h, β^-	12.2 22.2h, β^-
G2N	29.0 0.439s, β^+	19.8 S	19.4 1.03E+5y, EC	19.1 S
GNP	21.4 7.61 min, β^+ 0.93s, β^+	20.4 1.28E+9y, β^-, EC, β^+	18.2 S	21.8 12.36h, β^-
G2P	14.7 S	18.1 S	19.9 1.83h, β^-	21.6 32.9y, β^-
GA	7.0 S	6.2 S	7.6 2.69E+2y, β^-	8.8 S

Ca	A = 46 (0.004)	A = 48 (0.19)
GN	10.4 1.651E+2d, β^-	9.9 4.54d, β^-
GP	13.8 20 min, β^-	15.8 17.5s, β^-
G2N	17.8 S	17.2 S
GNP	22.7 22.2 min, β^-	24.2 1.15E+2s, β^-
G2P	* 11.87 min, β^-	29.1 *
GA	11.1 32.9y, β^-	14.4 11.87 min, β^-

Scandium

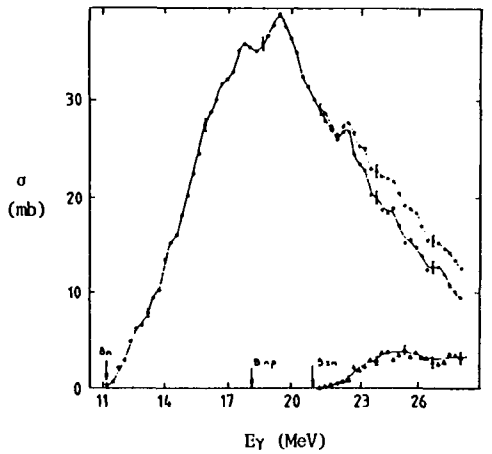

^{45}Sc Mono 74Ve5

○ $\sigma(\gamma,n)+\sigma(\gamma,pn)$
▲ $\sigma(\gamma,2n)+\sigma(\gamma,p2n)$
● $\sigma(\gamma,n_t)$

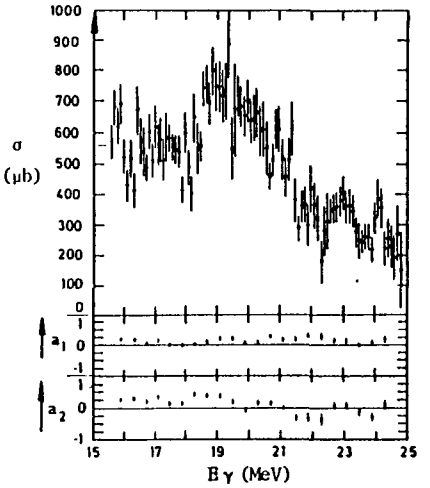

^{45}Sc Brems 82Ry1

(γ,p_0)

Sc	A = 45 (100)	
GN	11.3	3.93h, β^+, EC 2.44d, IT, EC
GP	6.9	S
G2N	21.0	3.88h, β^+, EC
GNP	18.0	S
G2P	19.1	22.2h, β^-
GA	7.9	S

^{45}Sc Brems 77Oi5

a) (γ,p) (90^O)

b) (γ,p_0) (90^O)

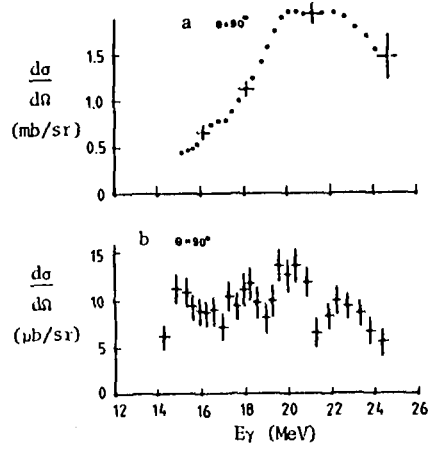

Titanium

^{46}Ti Brems 79Py5

a) (γ,n)
b) (γ,p) θ=90° E_{p_0}>2.7 MeV
c) (γ,p_0+p_1) θ=90°
d) (γ,α_0) θ=90°

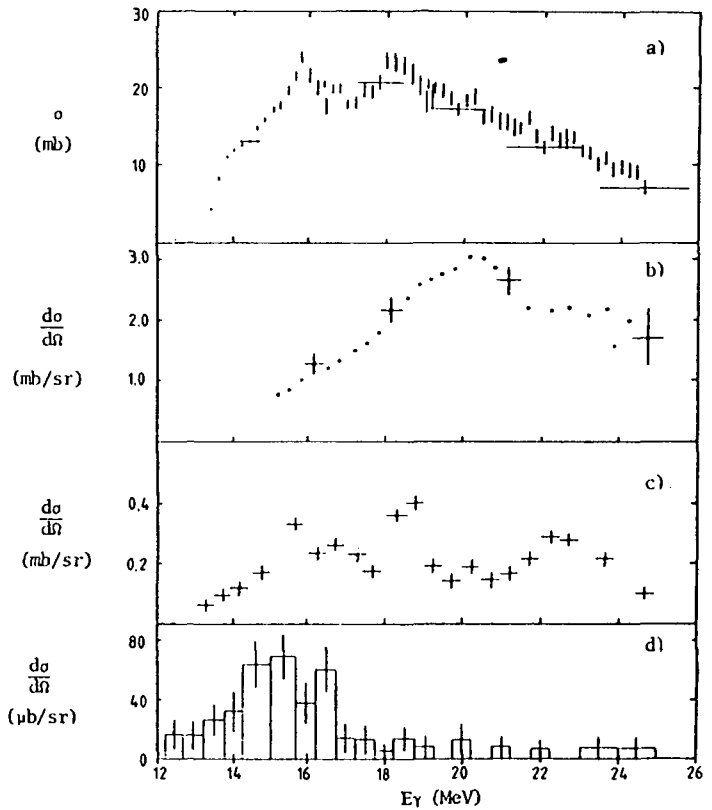

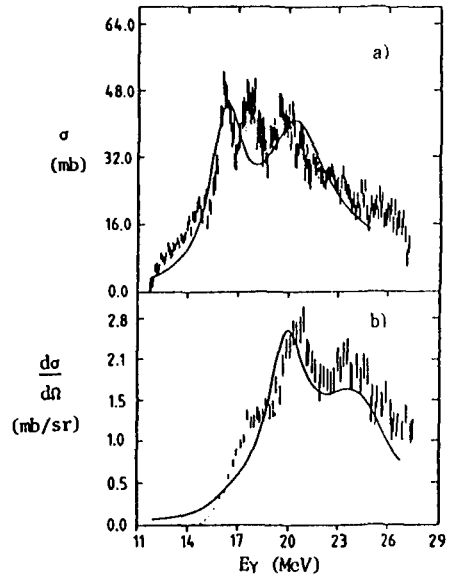

^{48}Ti Brems 80Su5

a) (γ,n)

b) (γ,p) θ=90°

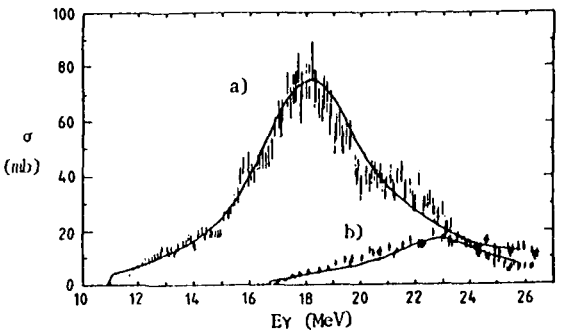

^{50}Ti Brems 79Py5

a) σ(γ,n)+σ(γ,2n)

b) σ(γ,p)

Ti	A = 46 (8.1)	A = 47 (7.4)	A = 48 (73.8)	A = 49 (5.4)
GN	13.2 3.08h, β⁺, EC	8.9 S	11.6 S	8.1 S
GP	10.3 S	10.5 83.80d, β⁻ 18.7s, IT	11.4 3.42d, β⁻	11.4 43.67h, β⁻
G2N	22.7 48.2y, EC	22.1 3.08h, β⁺, EC	20.5 S	19.8 S
GNP	21.7 3.93h, β⁺, EC 2.44d, IT, EC	19.2 S	22.1 83.80d, β⁺ 18.7s, IT	19.6 3.42d, β⁻
G2P	17.2 S	18.7 1.651E+2d, β⁻	19.9 S	20.8 4.54d, β⁻
GA	8.0 S	9.0 S	9.4 S	10.2 1.651E+2d, β⁻

Ti	A = 50 (5.3)
GN	10.9 S
GP	12.2 57.0 min, β⁻
G2N	19.1 S
GNP	22.3 43.67h, β⁻
G2P	21.8 S
GA	10.7 S

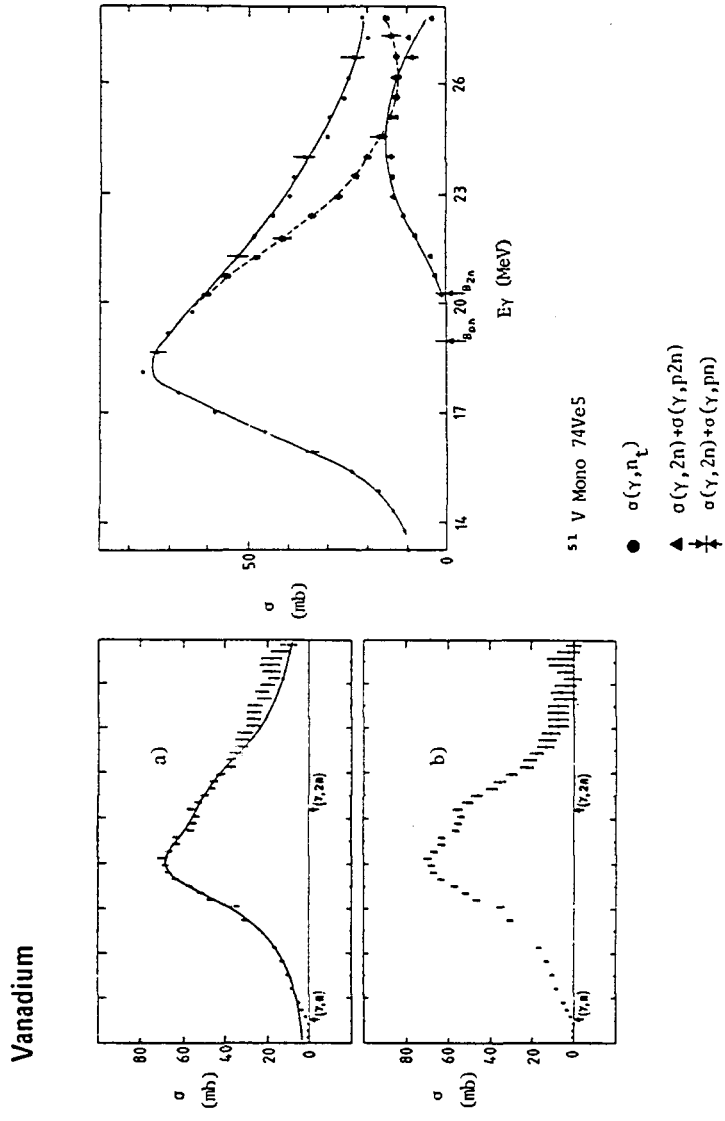
Vanadium
a)
b)
σ (mb)
σ (mb)
σ (mb)
0
14
17
20
23
26
Eγ (MeV)
$B_{p,n}$
B_{2n}
51 V Mono 74Ve5
σ(γ,n_t)
σ(γ,2n)+σ(γ,p2n)
σ(γ,2n)+σ(γ,pn)

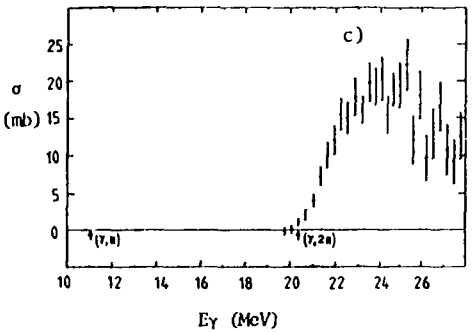

^{51}V Mono 75Be6 , 62Fu1

a) $\sigma(\gamma,n_t)$
b) $\sigma(\gamma,n)+\sigma(\gamma,pn)$
c) $\sigma(\gamma,2n)+\sigma(\gamma,p2n)$

V	A = 50 (0.25)	A = 51 (99.75)
GN	9.3 3.27E+2d, EC	11.1 M
GP	7.9 S	8.1 S
G2N	20.9 15.98d, EC, β^+	20.4 3.27E+2d, EC
GNP	16.1 S	19.0 S
G2P	19.3 43.67h, β^-	20.2 57.0 min, β^-
GA	9.9 83.80d, β^-	10.3 3.42d, β^-
	18.7s, IT	

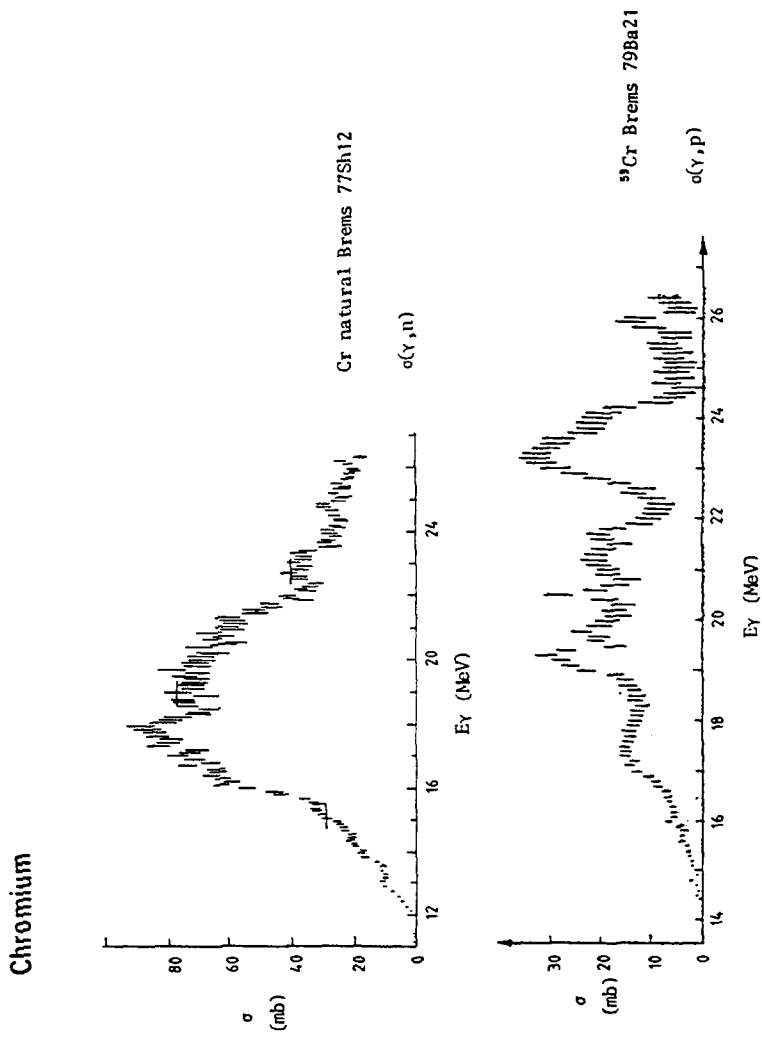
Chromium
Cr natural Brems 77Sh12
σ(γ,n)
σ (mb)
Eγ (MeV)
53Cr Brems 79Ba21
σ(γ,p)
σ (mb)
Eγ (MeV)

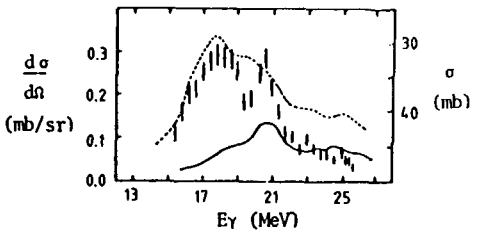

^{52}Cr Brems 79Ts5

$\frac{d\sigma}{d\Omega}(\gamma,p_0+p_1)$ (90^o)

---- $\sigma(\gamma,n)$ 77Sh12

—— $\sigma(\gamma,p)$ 75To35

Cr	A = 50 (4.35)	A = 52 (83.79)	A = 53 (9.50)	A = 54 (2.36)
GN	13.0 41.9 min, β^+, EC	12.0 27.701d, EC	7.9 S	9.7 S
GP	9.6 3.27E+2d, EC	10.5 S	11.1 3.746 min, β^-	12.4 1.60 min, β^-
G2N	23.6 21.56h, EC	21.3 S	20.0 27.701d, EC	17.7 S
GNP	21.1 15.976d, EC, β^+	21.6 *	18.4 S	20.9 3.746 min, β^-
G2P	16.3 S	18.6 S	20.1 5.80 min, β^-	22.0 1.7 min, β^-
GA	8.6 S	9.4 S	9.1 S	7.9 S

Manganese

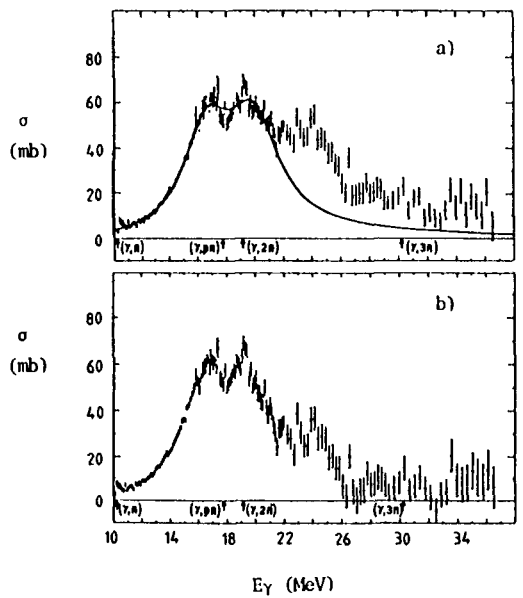

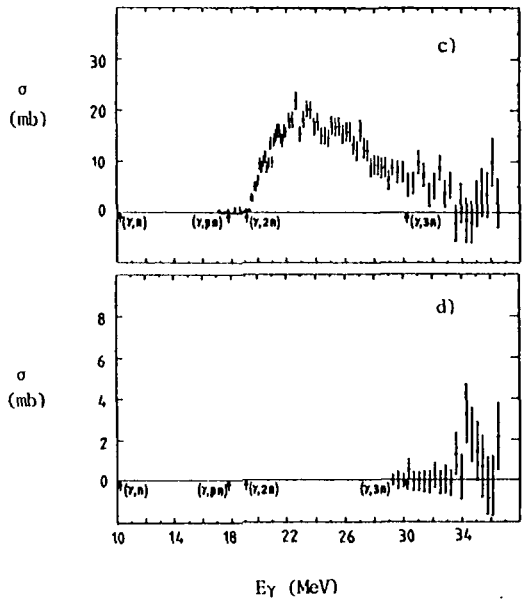

^{55}Mn Mono 79A11

a) $\sigma(\gamma,n_t)$
b) $\sigma(\gamma,n)+\sigma(\gamma,pn)$
c) $\sigma(\gamma,2n)+\sigma(\gamma,p2n)$
d) $\sigma(\gamma,3n)$

Mn	A = 55 (100)
GN	10.2 3.121E+2d, EC
GP	8.1 S
G2N	19.2 3.74E+6y, EC
GNP	17.8 S
G2P	20.4 1.60 min, β^-
GA	7.9 S

Iron

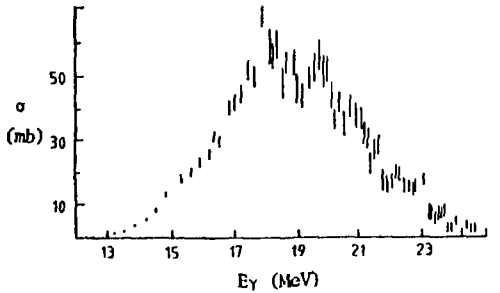

^{54}Fe Brems 78No12

σ(γ,n)

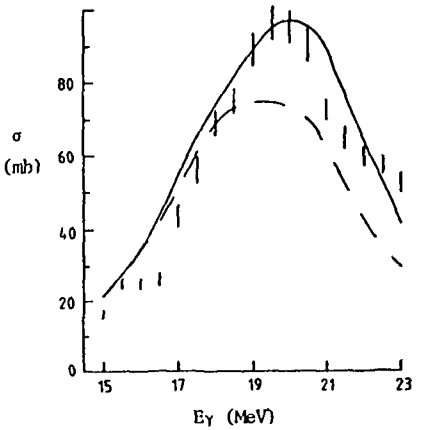

^{54}Fe Brems 78No12

| σ(γ,p) experiment
—— σ(γ,p) calculated with isospin effects
--- σ(γ,p) calculated without isospin effects

Fe	A = 54 (5.8)	A = 56 (91.8)	A = 57 (2.1)	A = 58 (0.3)
GN	13.4 8.51 min, β^+, EC 2.53 min, IT	11.2 2.68y, EC	7.6 S	10.0 S
GP	8.9 3.74E+6y, EC	10.2 S	10.6 2.58h, β^-	11.9 1.54 min, β^-
G2N	24.1 8.275h, β^+, EC	20.5 S	18.8 2.68y, EC	17.7 S
GNP	20.9 5.591d, EC, β^+ 21.1 min, β^+, EC, IT	20.4 3.122E+2d, EC	17.8 S	20.6 2.58h, β^-
G2P	15.4 S	18.3 S	19.6 3.52 min, β^-	21.5 5.94 min, β^-
GA	8.4 S	7.6 S	7.3 S	7.6 S

Cobalt

^{59}Co Mono 75Be6 , 73A142

a) $\sigma(\gamma,n_t)$
b) $\sigma(\gamma,n)+\sigma(\gamma,pn)$
c) $\sigma(\gamma,2n)+\sigma(\gamma,p2n)$
d) $\sigma(\gamma,3n)$

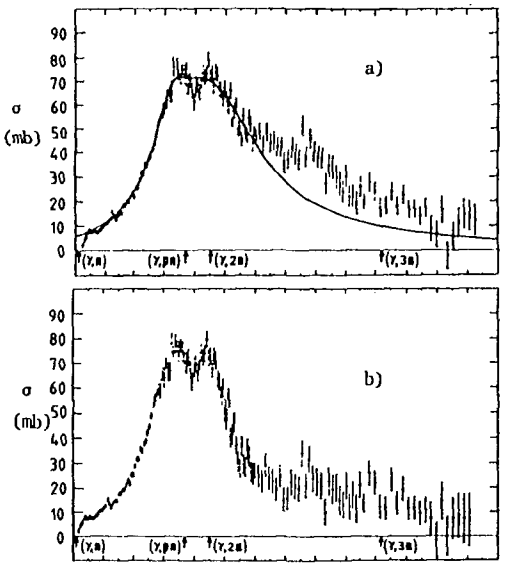

Co	A = 59 (100)	
GN	10.5	70.78d, EC, β^+ 9.2h, IT
GP	7.4	S
G2N	19.0	2.717E+2d, EC
GNP	17.4	S
G2P	19.3	1.54 min, β^-
GA	7.0	S

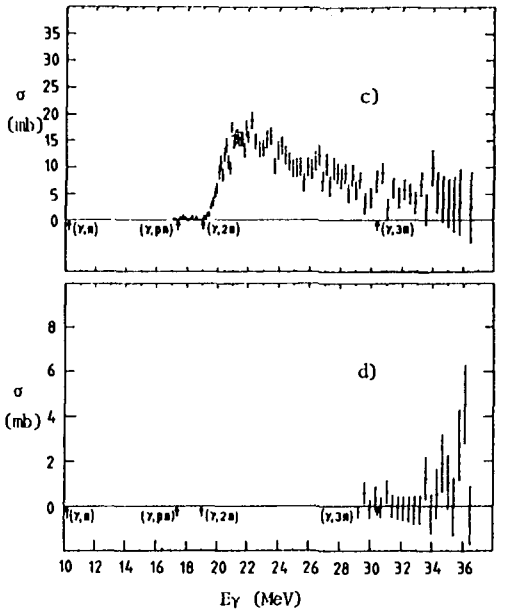

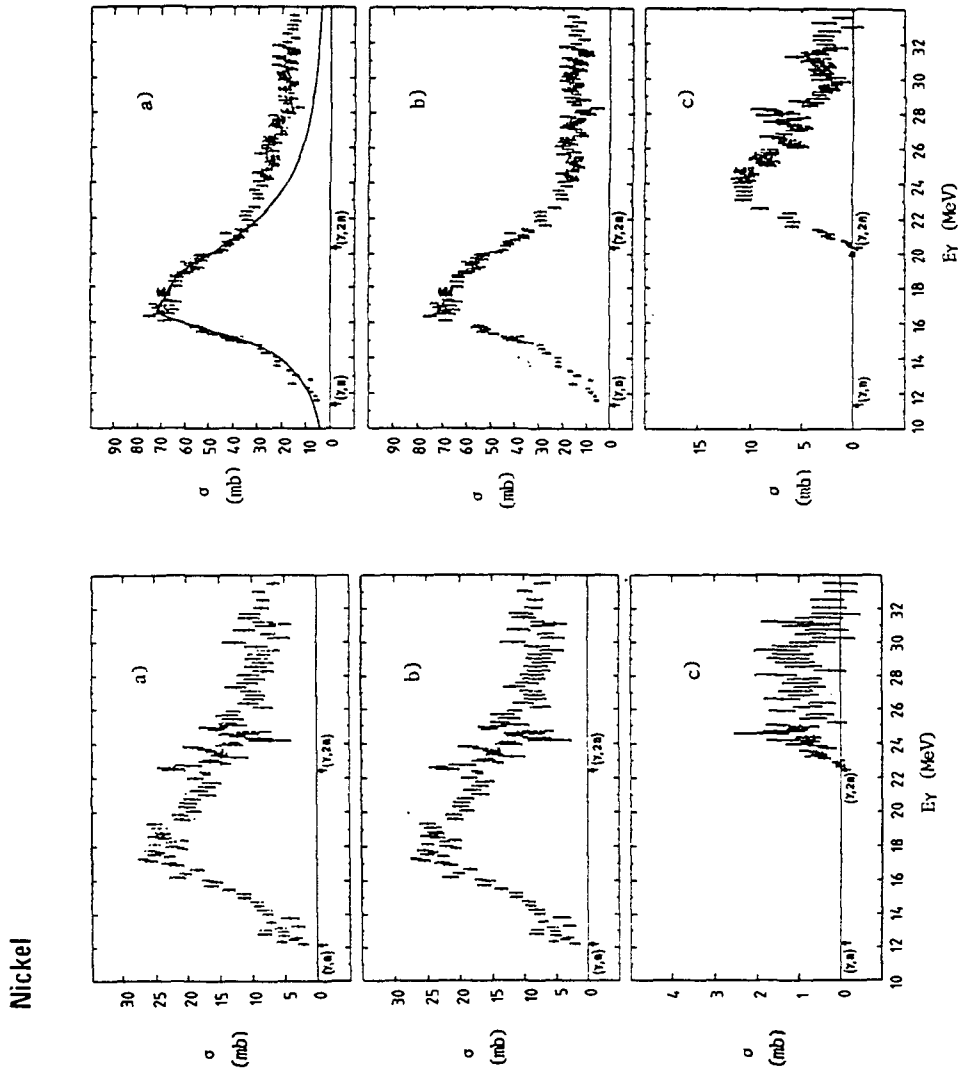
Nickel
a)
b)
c)
σ (mb)
Eγ (MeV)
(γ,a)
(γ,2a)
(γ,n)
(γ,2n)

^{58}Ni Mono 75Be6 , 74Pu1

Ni	A = 58 (68.27)
GN	12.2 36.0h, EC, β^+
GP	8.2 2.717E+2d, EC
G2N	22.5 6.10d, EC
GNP	19.6 78.76d, EC, β^+
G2P	14.2 S
GA	6.4 S

^{60}Ni Mono 75Be6 , 74Pu1

a) $\sigma(\gamma,n_t)$

b) $\sigma(\gamma,n)+\sigma(\gamma,pn)$

c) $\sigma(\gamma,2n)+\sigma(\gamma,p2n)$

Ni	A = 60 (26.10)	A = 61 (1.13)	A = 62 (3.59)	A = 64 (0.91)
GN	11.4 7.5E+4y, EC, β^+	7.8 S	10.6 S	9.7 1.001E+2y, β^-
GP	9.5 S	9.9 5.27y, β^- 10.5 min, IT, β^-	11.1 1.65h, β^-	12.5 27.5s, β^-
G2N	20.4 S	19.2 7.5E+4y, EC, β^+	18.4 S	16.5 S
GNP	20.0 70.78d, EC, β^+ 9.2h, IT	17.4 S	20.5 5.27y, β^- 10.5 min, IT, β^-	20.9 1.50 min, β^- 13.9 min, β^-
G2P	16.9 S	18.1 44.56d, β^-	19.9 3E+5y, β^-	22.7 68s, β^-
GA	6.3 S	6.5 S	7.0 S	8.1 3E+5y, β^-

Copper

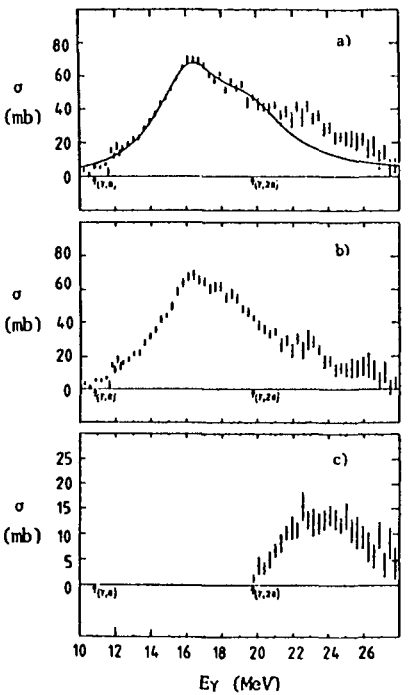

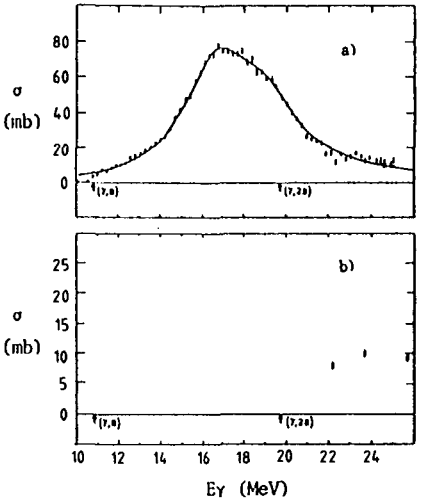

^{63}Cu Mono 75Be6 , 68Su1

a) σ(γ,n)

b) σ(γ,2n)+σ(γ,p2n)

^{63}Cu !lono 79Dz14

φ σ(γ,n)

—— σ(γ,n) 68Su1

- - - - σ(γ,n) 64Fu1

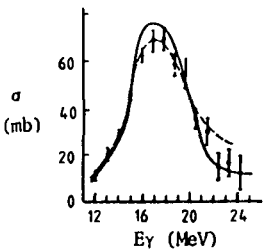

^{63}Cu Mono 75Be6 , 64Fu1

a) $\sigma(\gamma,n_t)$
b) $\sigma(\gamma,n)+\sigma(\gamma,pn)$
c) $\sigma(\gamma,2n)+\sigma(\gamma,p2n)$

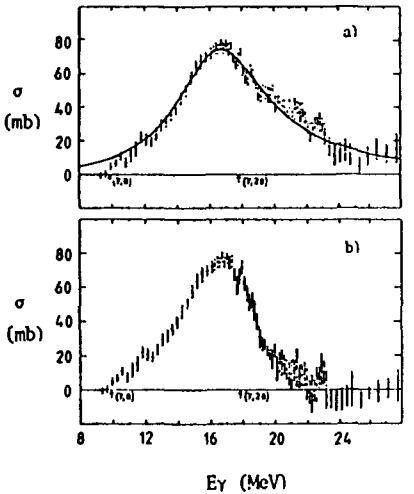

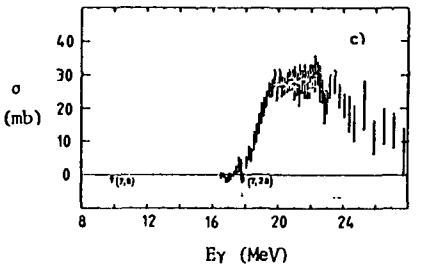

^{65}Cu Mono 75Be6 , 64Fu1

a) $\sigma(\gamma,n_t)$
b) $\sigma(\gamma,n)+\sigma(\gamma,pn)$
c) $\sigma(\gamma,2n)+\sigma(\gamma,p2n)$

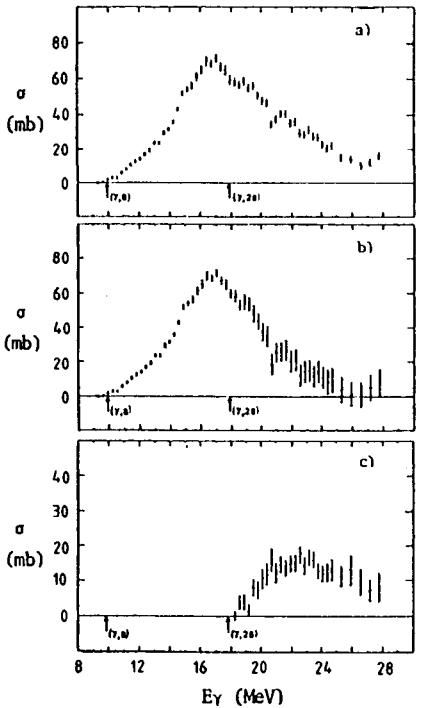

Cu natural Mono 75Be6 , 64Ru1

a) $\sigma(\gamma,n_t)$
b) $\sigma(\gamma,n)+\sigma(\gamma,pn)$
c) $\sigma(\gamma,2n)+\sigma(\gamma,p2n)$

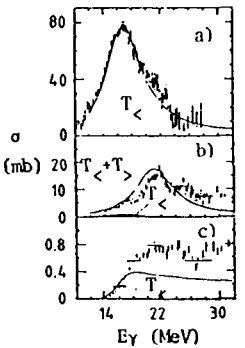

^{65}Cu Brems 81Sh45

a) $\sigma(\gamma,n)$
b) $\sigma(\gamma,p)$
c) $\sigma(\gamma,\alpha)$
Solid line: calculated cross-section assuming isospin splitting ($T_<$,$T_>$) given by Falliero's formula 71Fa8.

Cu	A = 63 (69.17)	A = 65 (30.83)
GN	10.9 9.73 min, β^+, EC	9.9 12.70h, EC, β^+, β^-
GP	6.1 S	7.4 S
G2N	19.7 3.4h, β^+, EC	17.8 S
GNP	16.7 S	17.1 1.001E+2y, β^-
G2P	17.2 1.65h, β^-	20.0 27.5s, β^-
GA	5.8 S	6.8 1.65h, β^-

See overleaf
for the graphs of zinc

Zinc

^{64}Zn Brems 70Co8

—— (γ,n)
---- (γ,n)+(γ,pn)+(γ,2n)
-·-· (γ,pn)
– – (γ,2n)

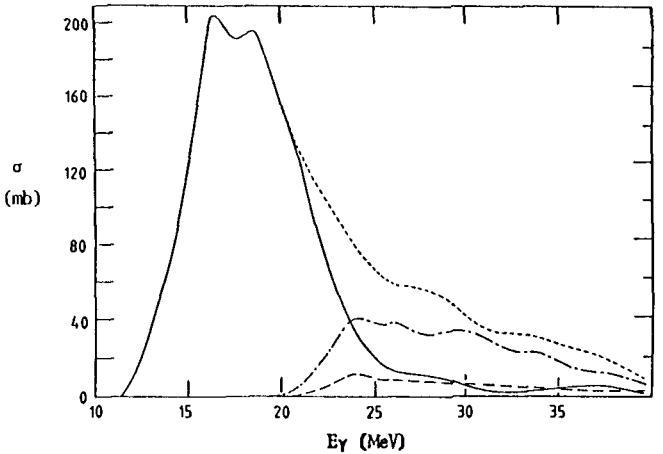

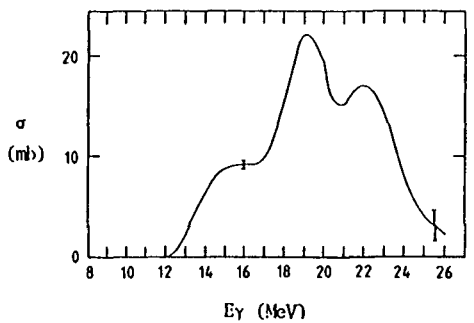

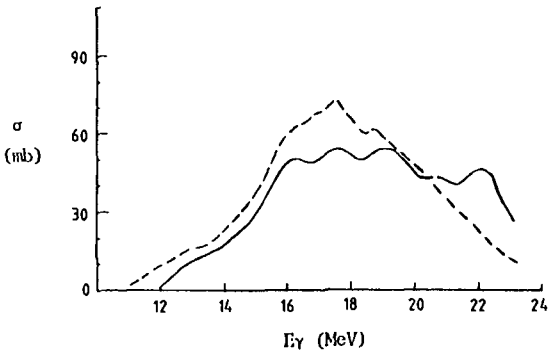

^{64}Zn Brems 73C15

(γ,p)

Zn	A = 64 (48.6)
GN	11.9 38.0 min, β^+, EC
GP	7.7 S
G2N	21.0 9.13h, EC, β^+
GNP	18.6 9.73 min, β^+, EC
G2P	13.8 S
GA	4.0 S

Brems 68Ow5

--- $^{62}Cu(\gamma,n)^{61}Cu$

—— $^{64}Zn(\gamma,n)^{63}Zn$

Zn	A = 66 (27.9)	A = 67 (4.1)	A = 68 (18.8)	A = 70 (0.6)
GN	11.1 2.440E+2d, EC, β^+	7.1 S	10.2 S	9.2 55.6 min, β^- 14.0h, IT, β^-
GP	8.9 S	8.9 5.10 min, β^-	10.0 62.01h, β^-	10.9 3.0 min, β^-
G2N	19.0 S	18.1 2.440E+2d, EC, β^+	17.3 S	15.7 S
GNP	18.8 12.70h, EC, β^+, β^-	16.0 S	19.1 5.10 min, β^-	19.5 30s, β^- 3.8 min, IT, β^-
G2P	16.4 S	17.3 2.5h, β^-	18.5 54.8h, β^-	* *
GA	4.6 S	4.8 1.001E+2y, β^-	5.3 S	6.0 54.8h, β^-

Germanium

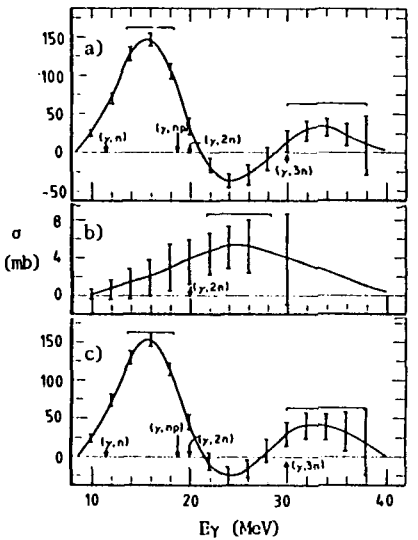

^{70}Ge Brems 75Mc1

a) σ(γ,n)
b) σ(γ,2n)+σ(γ,p2n)
c) σ(γ,n)+σ(γ,2n)+σ(γ,pn)+σ(γ,p)

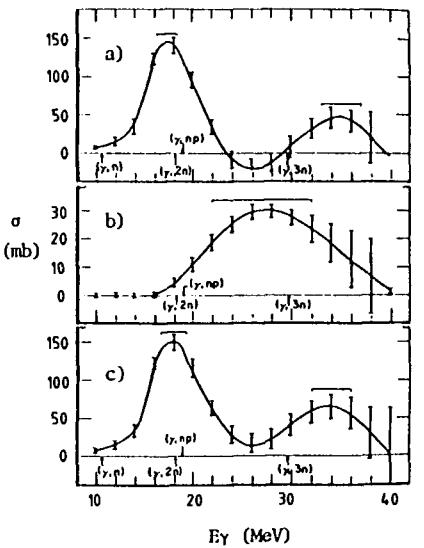

^{72}Ge Brems 75Mc1

a) σ(γ,n)
b) σ(γ,2n)+σ(γ,p2n)
c) σ(γ,n)+σ(γ,2n)+σ(γ,pn)+σ(γ,p)

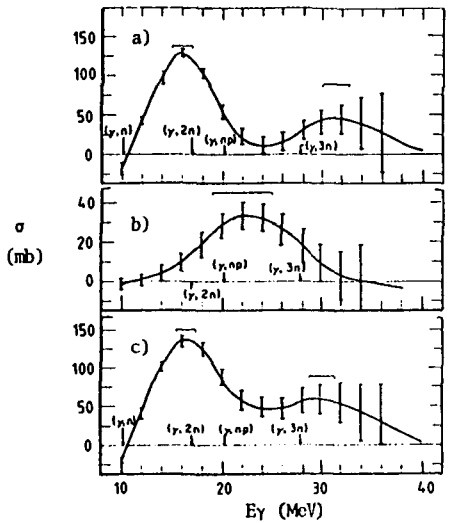

^{74}Ge Brems 75Mc1

a) σ(γ,n)
b) σ(γ,2n)+σ(γ,p2n)
c) σ(γ,n)+σ(γ,2n)+σ(γ,pn)+σ(γ,p)

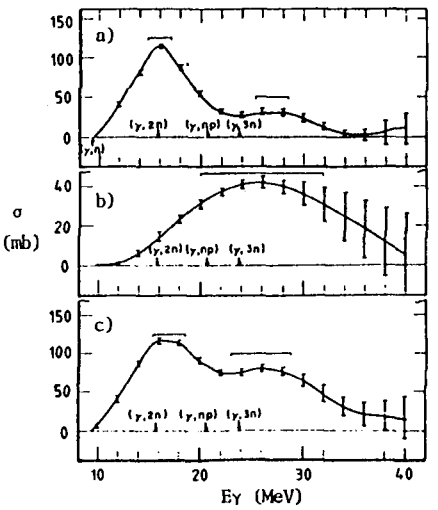

^{76}Ge Brems 75Mc1

a) σ(γ,n)
b) σ(γ,2n)+σ(γ,p2n)
c) σ(γ,n)+σ(γ,2n)+σ(γ,pn)+σ(γ,p)

^{74}Ge Brems 73Mc5

σ(γ,p)

Ge isotopes Brems 73Mc5

a) ^{70}Ge(γ,pn)^{68}Ga
b) ^{72}Ge(γ,pn)^{70}Ga
c) ^{76}Ge(γ,pn)^{74}Ga

Ge	A = 70 (20.5)	A = 72 (27.4)	A = 73 (7.8)	A = 74 (36.5)
GN	11.5 39.05h, EC, β^+	10.7 11.15d, EC	6.8 S	10.2 S
GP	8.5 S	9.7 S	10.0 14.12h, β^-	11.0 4.86h, β^-
G2N	19.7 2.88E+2d, EC	18.2 S	17.5 11.15d, EC	17.0 S
GNP	18.8 68.33 min, β^+, EC	19.0 21.10 min, β^-, EC	16.5 S	20.2 14.12h, β^-
G2P	15.1 S	17.6 S	18.5 2.45 min, β^- 3.9h, β^-	19.9 46.5h, β^-
GA	4.1 S	5.0 S	5.3 55.6 min, β^- 14h, IT, β^-	6.3 S

Ge	A = 76 (7.8)
GN	9.4 82.78 min, β^- 48s, β^-
GP	12.0 2.10 min, β^-
G2N	15.9 S
GNP	20.6 8.25 min, β^-
G2P	22.1 95s, β^-
GA	7.5 46.5h, β^-

Arsenic

^{75}As Mono 75Be6 , 69Be101

a) $\sigma(\gamma,n_t)$
b) $\sigma(\gamma,n)+\sigma(\gamma,pn)$
c) $\sigma(\gamma,2n)+\sigma(\gamma,p2n)$

As	A = 75 (100)
GN	10.2 17.79d, EC, β^+, β^-
GP	6.9 S
G2N	18.2 80.30d, EC
GNP	17.1 S
G2P	17.9 4.86h, β^-
GA	5.3 S

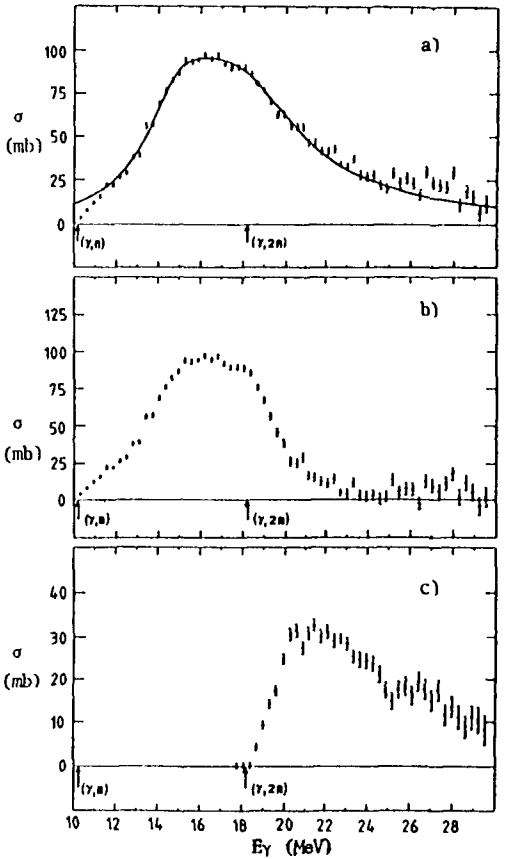

Selenium

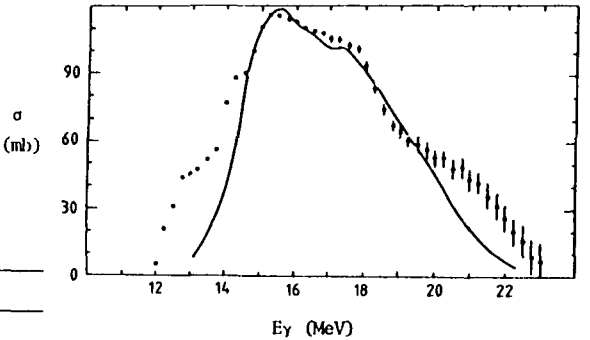

Se Brems 67Co7

σ(γ,Tn)

Se	A = 74 (0.9)	A = 76 (9.0)
GN	12.1 7.18h, β^+, EC 41 min, IT, β^+, EC	11.2 1.185E+2d, EC
GP	8.5 80.30d, EC	9.5 S
G2N	20.7 8.40d, EC	19.2 S
GNP	19.3 26.0h, β^+, EC	19.8 17.79d, EC, β^+, β^-
G2P	14.2 S	16.4 S
GA	4.1 S	5.1 S

Se	A = 77 (7.6)	A = 78 (23.5)	A = 80 (49.6)	A = 82 (9.4)
GN	7.4 S	10.5 S; 17.4s, IT	9.9 ≤6.5E+4y, β^- 3.90 min, IT	9.3 18.2 min, β^- 57.3 min, IT, β^-
GP	9.6 26.32h, β^-	10.4 38.83h, β^-	11.3 9.01 min, β^-	12.2 33s, β^-
G2N	18.6 1.185E+2d, EC	17.9 S	16.9 S	16.0 S
GNP	16.9 S	20.1 26.32h, β^-	20.4 90.7 min, β^-	20.2 15.2s, β^-
G2P	17.3 82.78 min, β^- 48s, IT, β^-	18.4 S	20.6 1.47h, β^-	22.7 29.5s, β^-
GA	5.7 S	6.0 S	7.0 S	8.2 1.47h, β^-

Rubidium

Rb	A = 85 (72.17)		A = 87 (27.83)	
GN	10.5	32.77d, EC, β^+, β^- 20.5 min, IT	9.9	18.82d, β^-, EC 1.02 min, IT
GP	7.0	S	8.6	S
G2N	19.4	86.2d, EC	18.6	S
GNP	17.5	S; 1.83h, IT	18.5	10.7y, β^- 4.48h, β^-, IT
G2P	17.7	2.39h, β^-	20.5	2.87 min, β^-
GA	6.6	S	8.0	2.39h, β^-

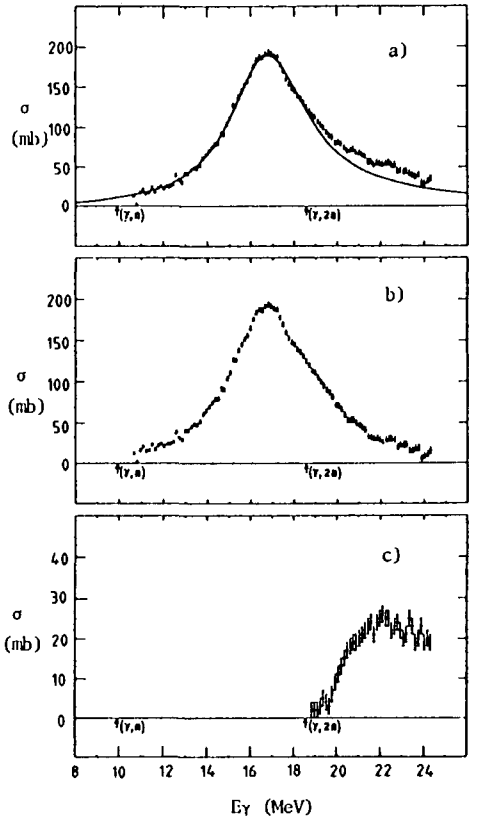

Rb natural Mono 75Be6 , 71Le5

a) $\sigma(\gamma,n_t)$
b) $\sigma(\gamma,n)+\sigma(\gamma,pn)$
c) $\sigma(\gamma,2n)+\sigma(\gamma,p2n)$

Strontium

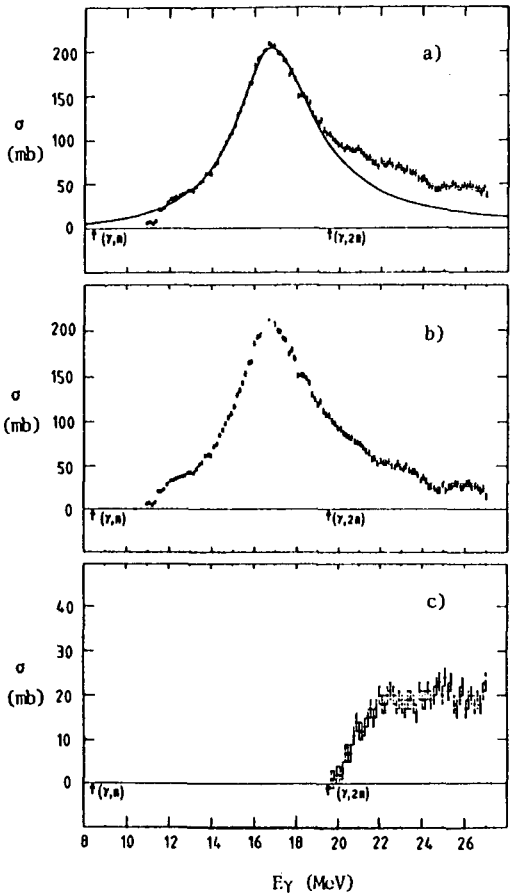

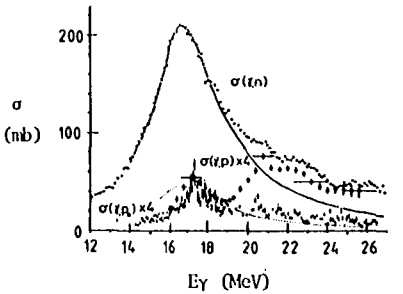

^{88}Sr Brems 79Sh10

- o σ(γ,p) from (e,e'p) data
- x σ(γ,p) 76Br1
- • σ(γ,n) 71Le5 , 74Be5
- • σ(γ,p_0) 74Sh5
- ···· Lorentz line

Sr natural Mono 75Be6 , 71Le5

a) $\sigma(\gamma,n_t)$
b) $\sigma(\gamma,n)+\sigma(\gamma,pn)$
c) $\sigma(\gamma,2n)+\sigma(\gamma,p2n)$

Sr	A = 84 (0.5)	A = 86 (9.9)	A = 87 (7.0)	A = 88 (82.6)
GN	12.0 32.4h, EC, β^+ 5.0s, IT	11.5 64.85d, EC 68 min, IT, EC	8.4 S	11.1 S; 2.80h, IT, EC
GP	9.0 86.2d, EC	9.6 S	9.4 18.82d, β^-, EC 1.02 min, IT	10.6 4.72E+10y, β^-
G2N	21.2 25.0d, EC	20.0 S	19.9 64.85d, EC 68.0 min, IT, EC	19.5 S
GNP	19.8 1.25 min, β^+, EC 6.2h, EC, β^+	20.1 32.77d, EC, β^+, β^- 20.5 min, IT	18.1 S	20.5 18.82d, β^-, EC 1.02 min, IT
G2P	14.6 S	16.7 S	18.0 10.70y, β^- 4.48h, β^-, IT	19.2 S
GA	5.2 S	6.3 S	7.3 S	7.9 S

Yttrium

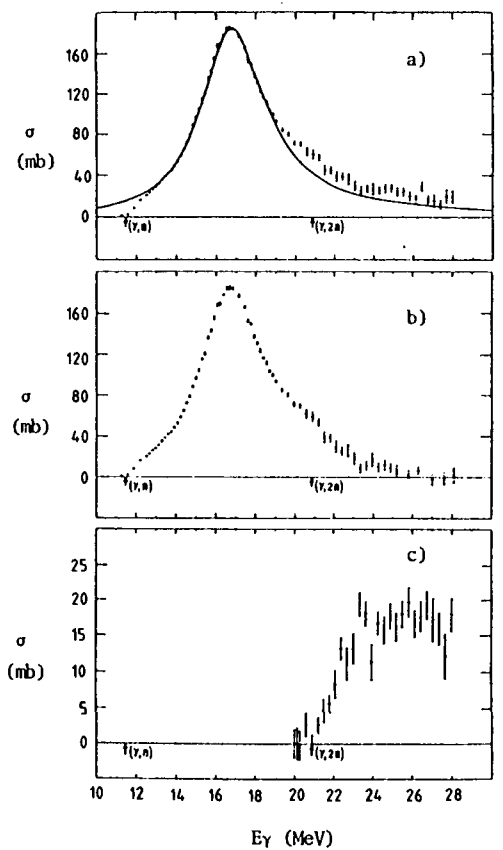

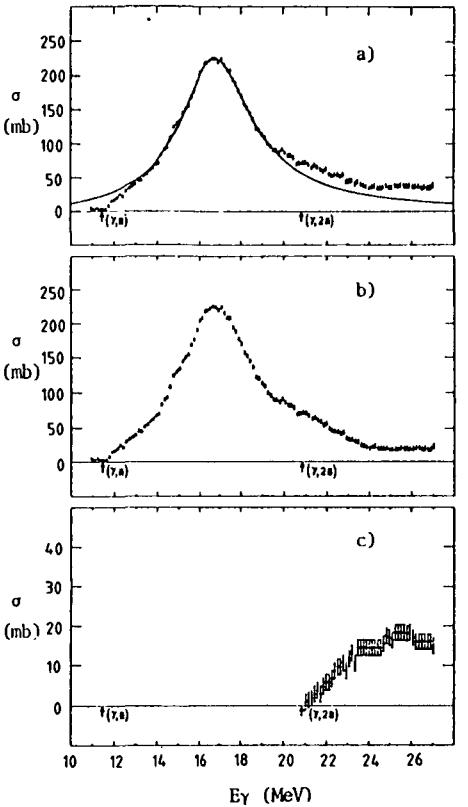

^{89}Y Mono 75Be6 , 71Le5

a) $\sigma(\gamma,n_t)$
b) $\sigma(\gamma,n)+\sigma(\gamma,pn)$
c) $\sigma(\gamma,2n)+\sigma(\gamma,p2n)$

^{89}Y Mono 75Be6 , 67Be1

a) $\sigma(\gamma,n_t)$
b) $\sigma(\gamma,n)+\sigma(\gamma,pn)$
c) $\sigma(\gamma,2n)+\sigma(\gamma,p2n)$

Y	A =89 (100)
GN	11.5 1.0661E+2d, EC, β^+
GP	7.1 S
G2N	20.8 80.3h, EC, β^+
	13h, IT, β^+, EC
GNP	18.2 S; 2.80h, IT, EC
G2P	17.7 4.72E+10y, β^-
GA	8.0 S

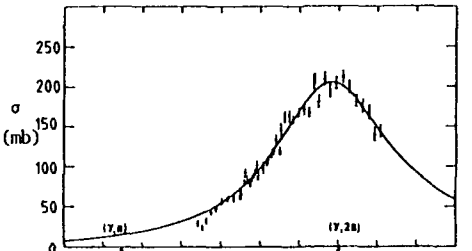

^{89}Y Mono 75Be6 , 72Yo

$\sigma(\gamma,n_t)$

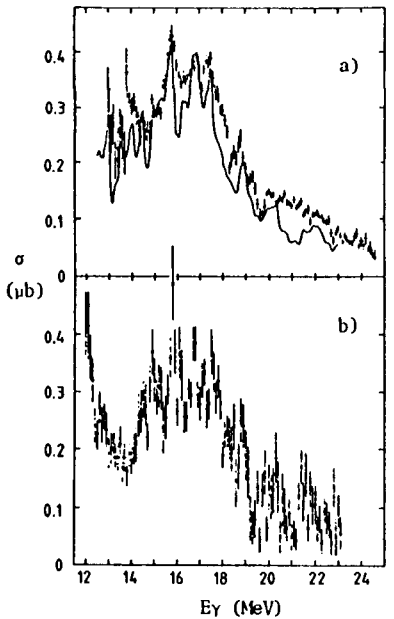

Brems 80Va1

a) ♦ ^{89}Y σ(γ,p_0)
—— ^{88}Sr σ(p,γ_0) 73Pa42

b) σ(γ,p_0) from σ(e,e'p) data 74Sh5

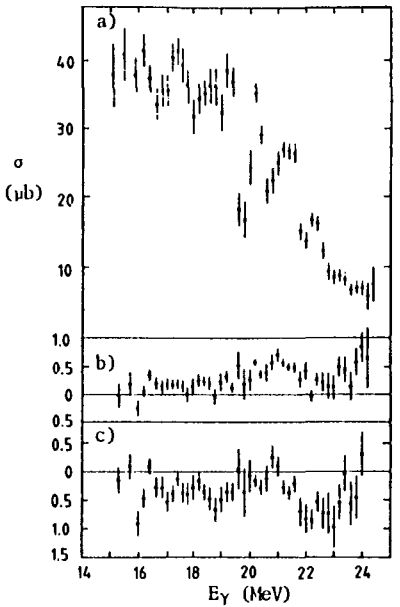

^{89}Y Brems 80Va1

a) σ(γ,p_1)

b) a_1
c) a_2

$$\left.\begin{matrix} a_1 \\ a_2 \end{matrix}\right\} \frac{d\sigma}{d\Omega}(\theta, E) = A_0(E)\left[1 + \sum_{i=1}^{n} a_i(E) P_i(\cos\theta)\right].$$

See overleaf
for the graphs of zirconium

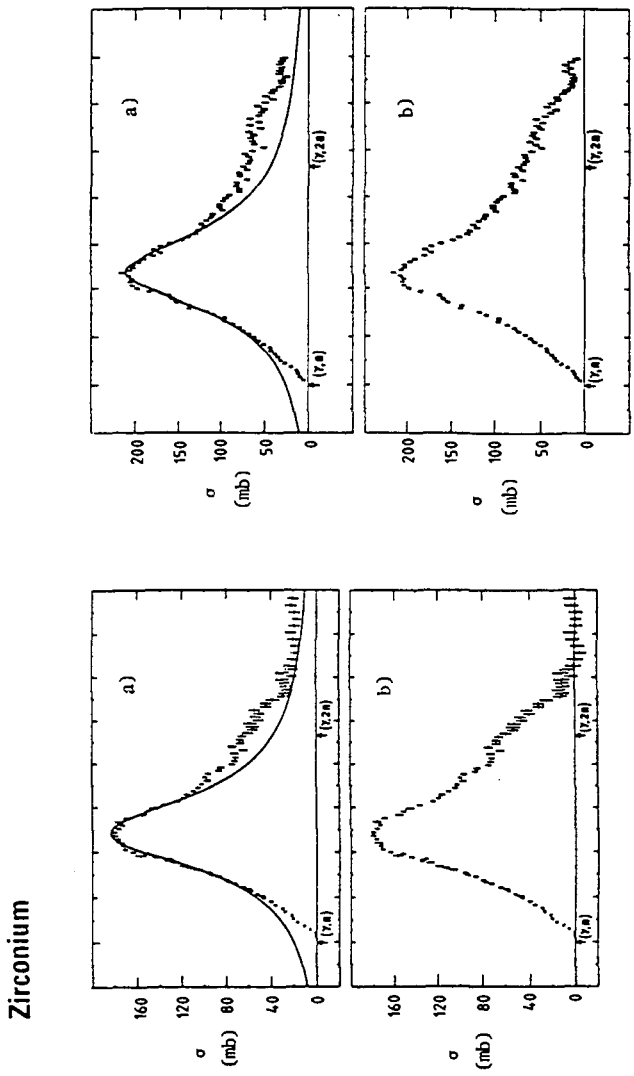
Zirconium
a)
b)
σ (mb)
160
120
80
40
0
200
150
100
50
γ(γ,n)
γ(γ,2n)

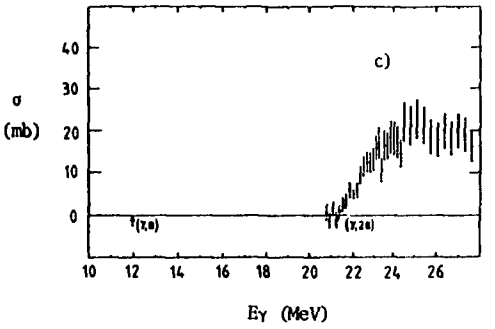

^{90}Zr Mono 75Be6 , 67Be1

a) $\sigma(\gamma,n_t)$
b) $\sigma(\gamma,n)+\sigma(\gamma,pn)$
c) $\sigma(\gamma,2n)+\sigma(\gamma,p2n)$

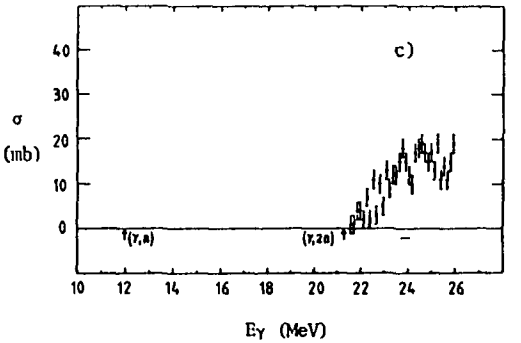

^{90}Zr Mono 75Be6 , 71Le5

a) $\sigma(\gamma,n_t)$
b) $\sigma(\gamma,n)+\sigma(\gamma,pn)$
c) $\sigma(\gamma,2n)+\sigma(\gamma,p2n)$

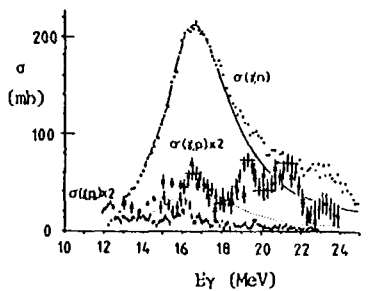

^{90}Zr Brems 79Sh10

- o σ(γ,p) from (e,e'p) data
- X σ(γ,p) 76Br1
- • σ(γ,n) 71Le5 , 74Be5
- · σ(γ,p_0) 74Sh5
- ···· Lorentz line

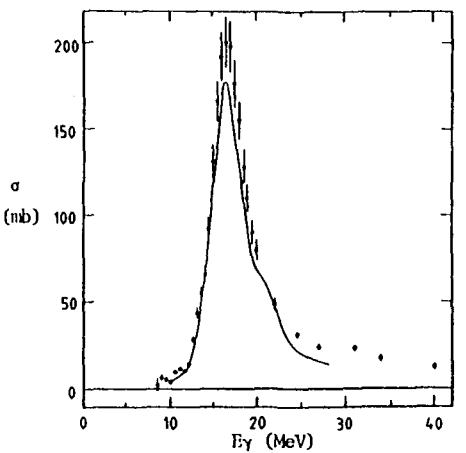

Zr natural Mono 82Ve4

- • σ(γ,n_t)
- —— Livermore 67Be1

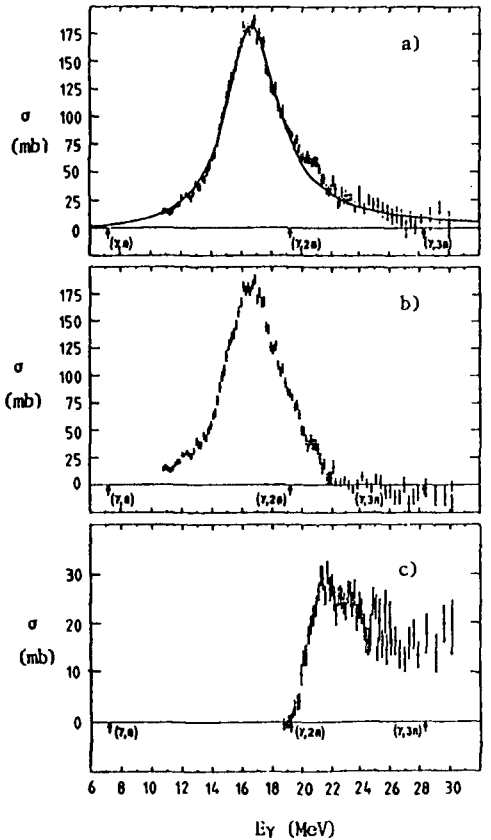

^{91}Zr Mono 75Be6 , 67Be1

a) $\sigma(\gamma,n_t)$
b) $\sigma(\gamma,n)+\sigma(\gamma,pn)$
c) $\sigma(\gamma,2n)+\sigma(\gamma,p2n)$

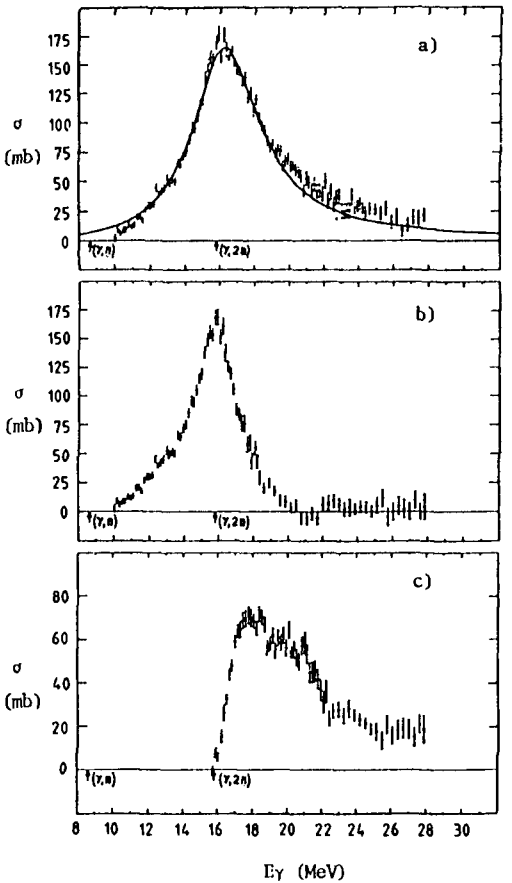

^{92}Zr Mono 75Be6 , 67Be1

a) $\sigma(\gamma,n_t)$
b) $\sigma(\gamma,n)+\sigma(\gamma,pn)$
c) $\sigma(\gamma,2n)+\sigma(\gamma,p2n)$

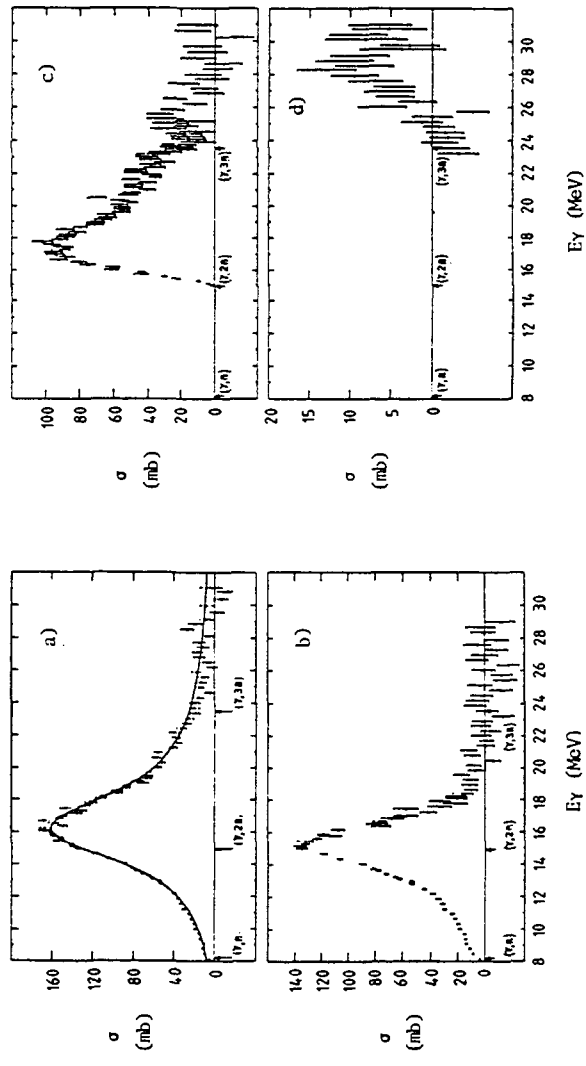
a)
b)
c)
d)
σ (mb)
Eγ (MeV)
(γ,n)
(γ,2n)
(γ,3n)
(γ,p)
(γ,α)

Zr	A = 90 (51.5)
GN	12.0 78.4h, EC, β^+
	4.18 min, IT, EC, β^+
GP	8.4 S; 16.1s, IT
G2N	21.3 83.4d, EC
GNP	19.8 1.066E+2d, EC, β^+
G2P	15.4 S
GA	6.7 S

^{94}Zr Mono 75Be6 , 67Be1

a) $\sigma(\gamma,n_t)$
b) $\sigma(\gamma,n)+\sigma(\gamma,pn)$
c) $\sigma(\gamma,2n)+\sigma(\gamma,p2n)$
d) $\sigma(\gamma,3n)$

Zr	A = 91 (11.2)	A = 92 (17.1)	A = 94 (17.4)	A = 96 (2.8)
GN	7.2 S	8.6 S	8.2 1.53E+6y, β^-	7.8 63.98d, β^-
GP	8.7 64.1h, β^-	9.4 58.5d, β^-	10.3 10.25h, β^-	11.5 10.3 min, β^-
	3.19h, IT, β^-	49.7 min, IT		
G2N	19.2 78.4h, EC, β^+	15.8 S	14.9 S	14.3 S
	4.18 min, IT, EC, β^+			
GNP	15.6 S; 16.1s, IT	17.3 64.1h, β^-	17.8 3.54h, β^-	18.5 18.7 min, β^-
		3.19h, IT, β^-		
G2P	16.3 50.55d, β^-	17.1 28.82y, β^-	18.9 2.71h, β^-	21.3 74.1s, β^-
GA	5.5 S; 2.80h, IT, EC	3.0 S	3.8 28.82y, β^-	4.9 2.71h, β^-

Niobium

Nb	A = 93 (100)
GN	8.8 3.2E+7y, EC
	10.15d, EC, β^+
GP	6.0 S
G2N	16.7 *, EC
	62d, IT, EC
GNP	14.7 S
G2P	15.4 58.5d, β^-
	49.7 min, IT
GA	1.9 S; 16.1s, IT

^{93}Nb Mono 75Be6 , 71Le5

a) $\sigma(\gamma,n_t)$

b) $\sigma(\gamma,n)+\sigma(\gamma,pn)$

c) $\sigma(\gamma,2n)+\sigma(\gamma,p2n)$

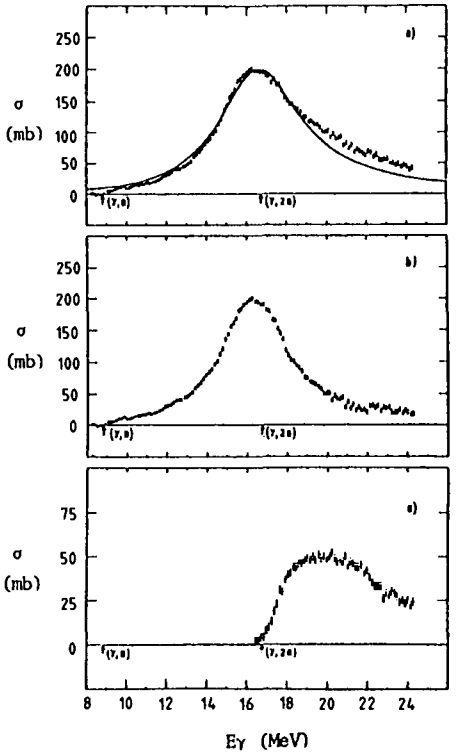

Molybdenum

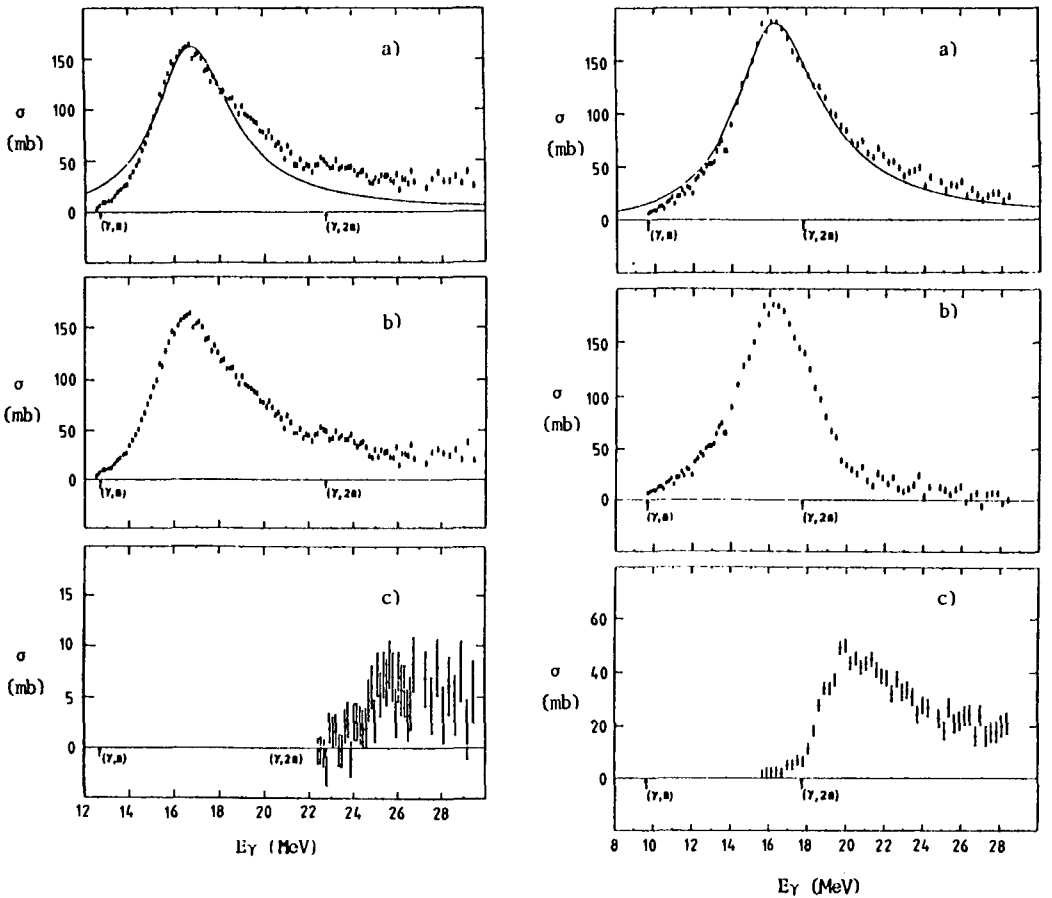

^{92}Mo Mono 75Be6 , 74Be5

a) $\sigma(\gamma,n_t)$
b) $\sigma(\gamma,n)+\sigma(\gamma,pn)$
c) $\sigma(\gamma,2n)+\sigma(\gamma,p2n)$

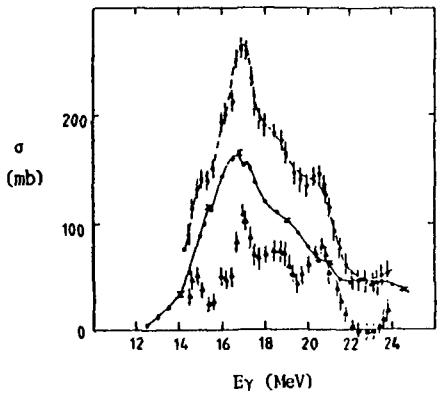

^{94}Mo Mono 75Be6 , 74Be5

a) $\sigma(\gamma,n_t)$
b) $\sigma(\gamma,n)+\sigma(\gamma,pn)$
c) $\sigma(\gamma,2n)+\sigma(\gamma,p2n)$

^{92}Mo Mono 74Be5

○ $\sigma(\gamma,n_t)+\sigma(\gamma,p_t)$
● $\sigma(\gamma,n_t)$
▲ $\sigma(\gamma,p_t)$ 71Sh11

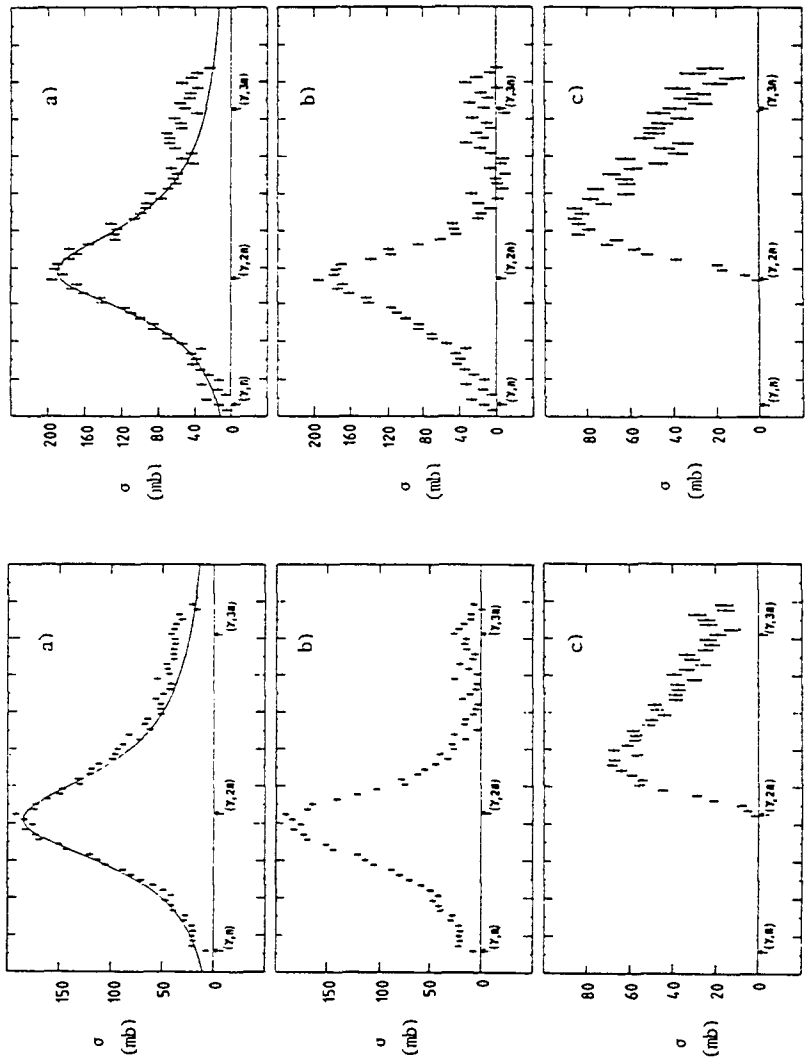
a)
b)
c)
σ (mb)
(γ,n)
(γ,2n)
(γ,3n)

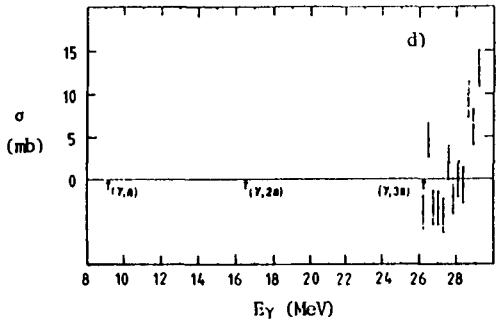

^{96}Mo Mono 75Be6 , 74Be5

a) $\sigma(\gamma,n_t)$
b) $\sigma(\gamma,n)+\sigma(\gamma,pn)$
c) $\sigma(\gamma,2n)+\sigma(\gamma,p2n)$
d) $\sigma(\gamma,3n)$

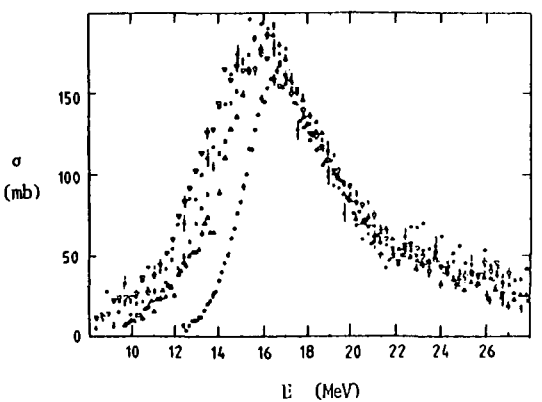

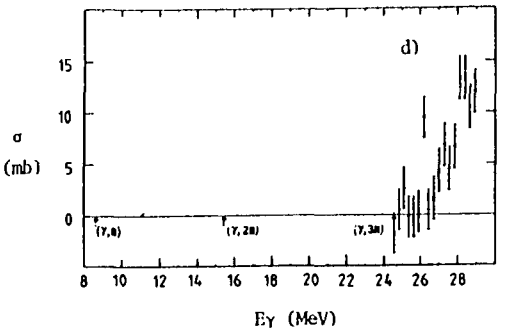

^{98}Mo Mono 75Be6 , 74Be5

a) $\sigma(\gamma,n_t)$
b) $\sigma(\gamma,n)+\sigma(\gamma,pn)$
c) $\sigma(\gamma,2n)+\sigma(\gamma,p2n)$
d) $\sigma(\gamma,3n)$

Mono 74Be5

- o ^{92}Mo $\sigma(\gamma,n_t)$
- ▲ ^{94}Mo $\sigma(\gamma,n_t)$
- × ^{96}Mo $\sigma(\gamma,n_t)$
- • ^{98}Mo $\sigma(\gamma,n_t)$
- ▽ ^{100}Mo $\sigma(\gamma,n_t)$

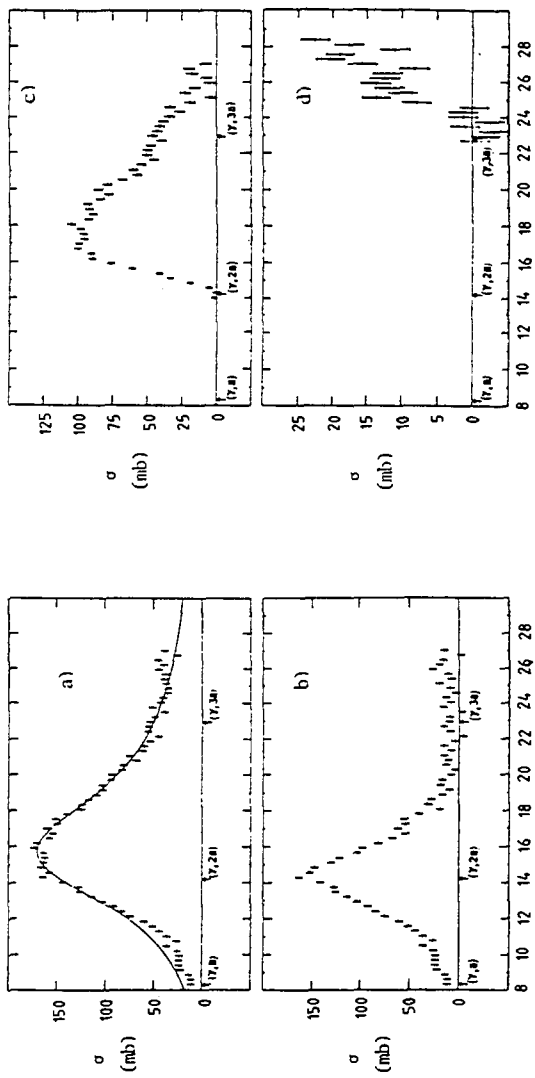
a)
b)
c)
d)
σ (mb)
Eγ (MeV)
100Mo Mono 75Be6 , 74Be5
a) σ(γ,nt)
b) σ(γ,n)+σ(γ,pn)
c) σ(γ,2n)+σ(γ,p2n)
d) σ(γ,3n)

Mo	A = 92 (14.84)	A = 94 (9.25)	A = 95 (15.92)	A = 96 (16.68)
GN	12.7 15.49 min, β^+, EC 65s, β^+, EC, IT	9.7 3.5E+3y, EC 6.9h, IT, EC	7.4 S	9.2 S
GP	7.5 *, EC 62d, IT, EC	8.5 S; 13.6y, IT	8.6 2.03E+4y, β^- 6.26 min, IT, β^+	9.3 34.97d, β^- 87h, IT, β^-
G2N	22.8 5.67h, EC, β^+	17.7 S	17.0 3.5E+3y, EC 6.9h, IT, EC	16.5 S
GNP	19.5 14.6h, β^+, EC 18.8s, IT	17.3 3.2E+7y, EC 10.15d, EC, β^+	15.9 S; 13.6y, IT	17.8 2.03E+4y, β^-
G2P	12.6 S	14.5 S	15.1 1.53E+6y, β^-	16.1 S
GA	5.6 83.4d, EC	2.1 S	2.2 S	2.8 S

Mo	A = 97 (9.55)	A = 98 (24.13)	A = 100 (9.63)
GN	6.8 S	8.6 S	8.3 66.02h, β^-
GP	9.2 23.35h, β^-	9.8 72 min, β^- 1.0 min, β^-	10.6 15.0s, β^- 2.6 min, β^-
G2N	16.0 S	15.5 S	14.2 S
GNP	16.1 34.97d, β^- 87h, IT, β^-	17.9 23.35h, β^-	18.0 2.9s, β^- 51 min, β^-
G2P	16.5 63.98d, β^-	17.3 S	19.5 30.7s, β^-
GA	2.8 1.53E+6y, β^-	3.3 S	3.2 S

Rhodium

Rh	A = 103 (100)	
GN	8.1	2.9y, EC
		2.06E+2d, EC, β^+, β^-, IT
GP	5.3	S
G2N	18.6	3.3y, EC
		4.34d, EC, IT
GNP	12.7	S
G2P	13.7	14.3 min, β^-
GA	2.2	2.14E+5y, β^-
		6.02, IT, β^-

^{103}Rh Mono 75Be6 , 74Le5

a) $\sigma(\gamma,n_t)$

b) $\sigma(\gamma,n)+\sigma(\gamma,pn)$

c) $\sigma(\gamma,2n)+\sigma(\gamma,p2n)$

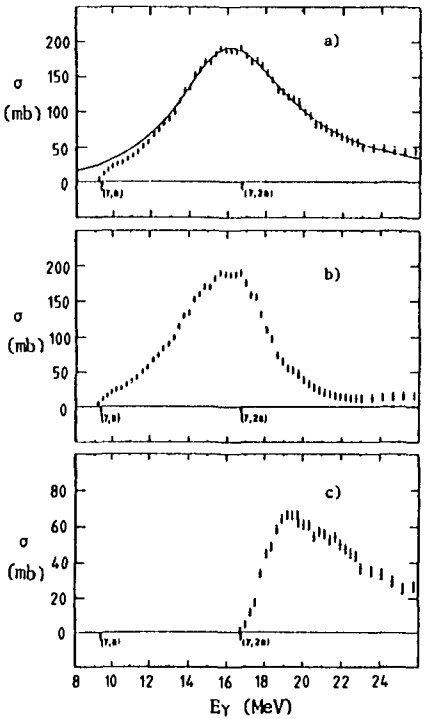

Palladium

Pd	A = 102 (1.0)	A = 104 (11.0)
GN	10.6 8.47h, EC, β^+	10.0 16.96d, EC
GP	7.8 3.3y, EC 4.34d, EC, IT	8.7 S; 56.1 min, IT
G2N	18.9 3.63d, EC	17.6 S
GNP	17.7 20.8h, EC, β^+	18.0 2.9y, EC 2.06E+2d, EC, β^+, β^-, IT
G2P	13.3 S	14.9 S
GA	2.1 S	2.6 S

Pd	A = 105 (22.2)	A = 106 (27.3)
GN	7.1 S	9.6 S
GP	8.8 42.3s, β^-, EC 4.34 min, IT, β^-	9.3 35.4h, β^- 45s, IT
G2N	17.1 16.96d, EC	16.6 S
GNP	15.8 S; 56.1 min, IT	18.3 42.3s, β^-, EC 4.34 min, IT, β^-
G2P	15.7 39.35d, β^-	16.4 S
GA	2.9 S	3.2 S

Pd	A = 108 (26.7)	A = 110 (11.8)
GN	9.2 6.5E+6y, β^- 21.3s, IT	8.8 13.43h, β^- 4.69 min, IT
GP	10.0 21.7 min, β^-	10.5 80s, β^-
G2N	15.8 S	15.0 S
GNP	18.5 29.8s, β^- 1.30E+2 min, β^-	18.7 16.8s, β^- 6.0 min, β^-
G2P	17.8 3.665E+2d, β^-	19.2 4.5 min, β^-
GA	3.9 S	4.4 3.665E+2d, β^-

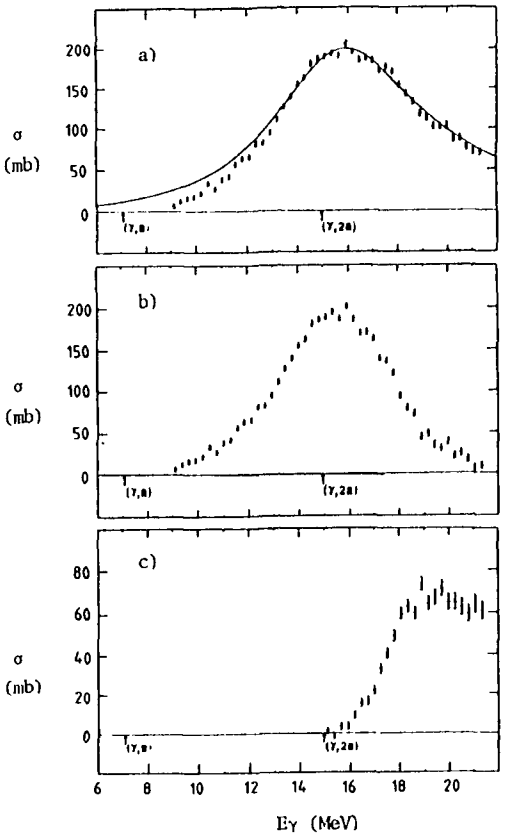

Pd natural Mono 75Be6 , 74Le5

a) $\sigma(\gamma,n_t)$
b) $\sigma(\gamma,n)+\sigma(\gamma,pn)$
c) $\sigma(\gamma,2n)+\sigma(\gamma,p2n)$

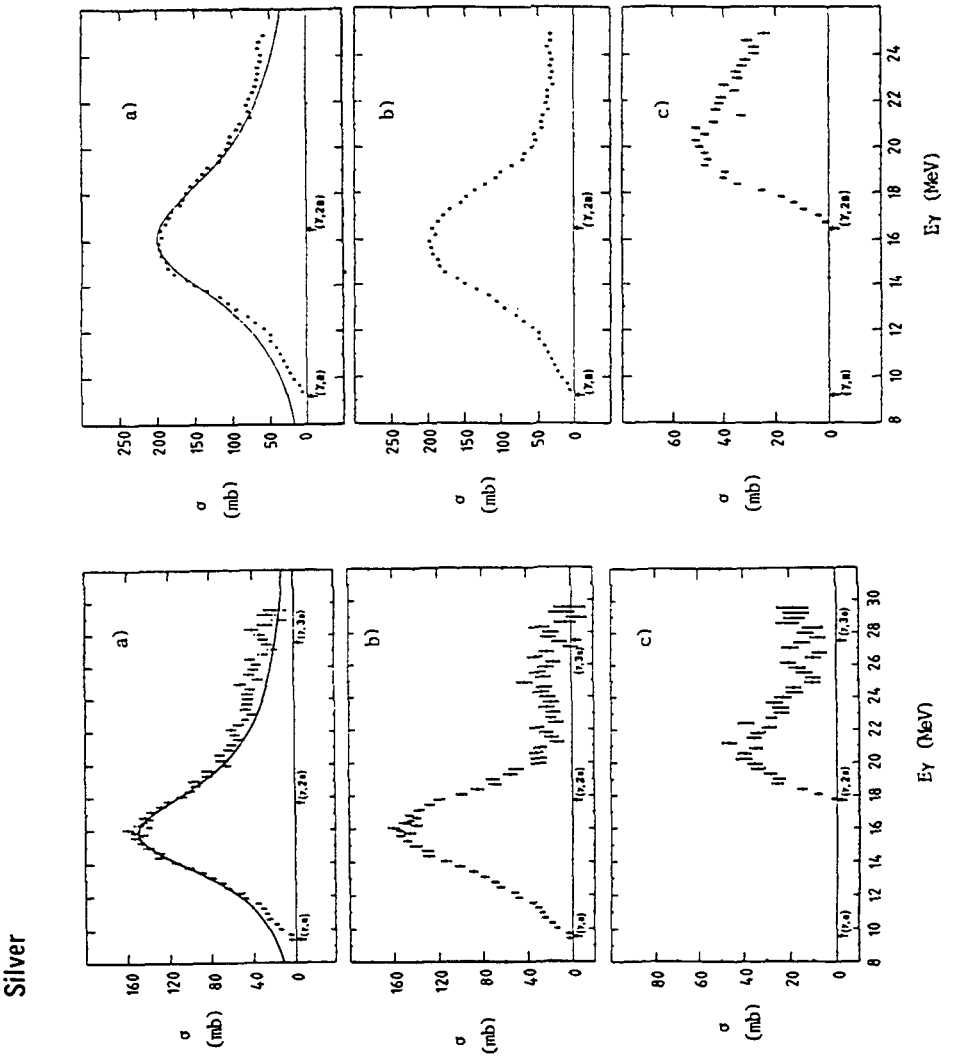
Silver
a)
b)
c)
σ (mb)
Eγ (MeV)

^{107}Ag Mono 75Be6 , 69Be101

a) $\sigma(\gamma,n_t)$
b) $\sigma(\gamma,n)+\sigma(\gamma,pn)$
c) $\sigma(\gamma,2n)+\sigma(\gamma,p2n)$

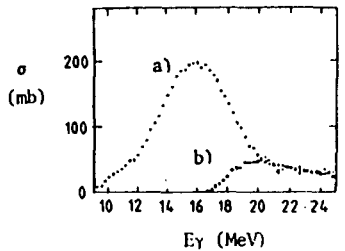

^{107}Ag Mono 74Le5

a) $\sigma(\gamma,n)+\sigma(\gamma,pn)$
b) $\sigma(\gamma,2n)+\sigma(\gamma,p2n)$

Ag natural Mono 75Be6 , 74Le5

a) $\sigma(\gamma,n_t)$
b) $\sigma(\gamma,n)+\sigma(\gamma,pn)$
c) $\sigma(\gamma,2n)+\sigma(\gamma,p2n)$

Ag	A = 107 (51.83)	A = 109 (48.17)
GN	9.6 24.0 min, EC, β^+, (β^-) 8.5d, EC	9.2 2.4 min, EC, β^+ 1.27E+2y, EC, β^+, IT
GP	5.8 S	6.5 S
G2N	17.5 41.3d, EC, β^+ 7.2 min, IT, EC	16.5 S; 44.3s, IT
GNP	15.4 S	15.7 6.5E+6y, β^- 21.3s, IT
G2P	15.1 35.4h, β^- 45s, IT	16.4 21.7 min, β^-
GA	2.8 S; 56.1 min, IT	3.3 35.4h, β^- 45s, IT

Cadmium

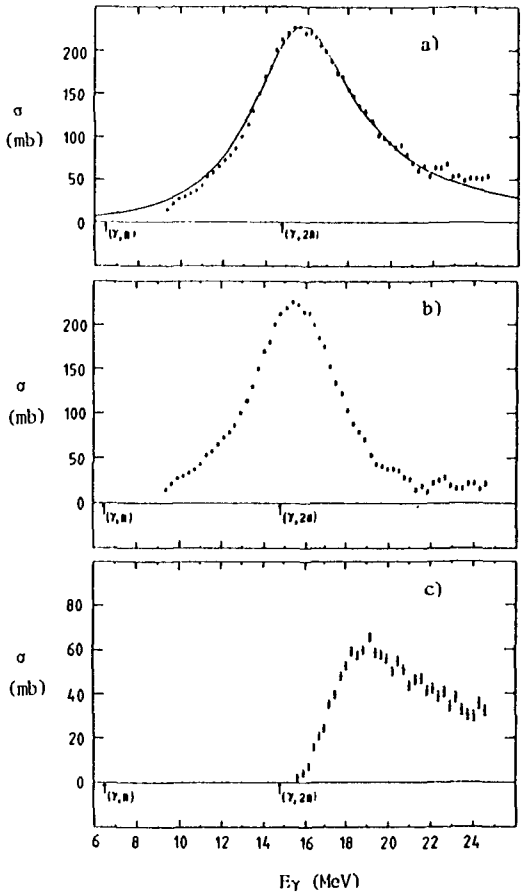

Cd natural Mono 75Be6 , 74Le5

a) $\sigma(\gamma,n_t)$
b) $\sigma(\gamma,n)+\sigma(\gamma,pn)$
c) $\sigma(\gamma,2n)+\sigma(\gamma,p2n)$

Cd	A = 106 (1.3)	A = 108 (0.9)	A = 110 (12.5)	A = 111 (12.8)
GN	10.9 56.0 min, EC, β^+	10.3 6.50h, EC, β^+	9.9 4.53E+2d, EC	7.0 S
GP	7.3 41.3, EC, β^+ 7.2 min, IT, EC	8.1 S; 44.3s, IT	8.9 S; 39.8s, IT	9.1 24.4s, β^-, EC 2.52E+2d, β^-, IT
G2N	19.3 57.7 min, EC, β^+	18.3 S	17.2 S	16.9 4.53E+2d, EC
GNP	17.2 69 min, β^+, EC 33 min, β^+, EC, IT	17.7 24.0 min, EC, β^+ 8.5d, EC	18.1 2.4 min, β^-, EC, β^+ 1.27E+2y, EC, β^+, IT	15.9 S; 39.8s, IT
G2P	12.3 S	13.9 S	15.4 S	16.2 13.43h, β^- 4.69 min, β^-
GA	1.6 S	2.3 S	2.9 S	3.3 6.5E+6y, β^- 21.3s, IT

Cd	A = 112 (24.1)	A = 113 (12.2)	A = 114 (28.7)	A = 116 (7.5)
GN	9.4 S; 48.6 min, IT	6.5 S	9.0 9.3E+15y, β^- 14y, β^-, IT	8.7 53.4h, β^- 44.8d, β^-
GP	9.6 7.45d, β^- 65s, IT, β^-	9.8 3.14h, β^-	10.3 5.37h, β^- 1.15 min, β^-	11.1 20 min, β^- 18s, β^-
G2N	16.4 S	15.9 S; 48.6 min, IT	15.6 S	14.8 S
GNP	18.5 24.4s, β^-, EC 2.52E+2d, β^-, IT	16.2 7.45d, β^- 65s, IT, β^-	18.8 3.14h, β^-	19.1 4.52s, β^-
G2P	16.8 S	17.6 22 min, β^- 5.5h, IT, β^-	18.3 21.12h, β^-	* 2.4 min, β^-
GA	3.5 S	3.9 13.43h, β^- 4.69 min, IT	4.1 S	4.9 21.12h, β^-

Indium

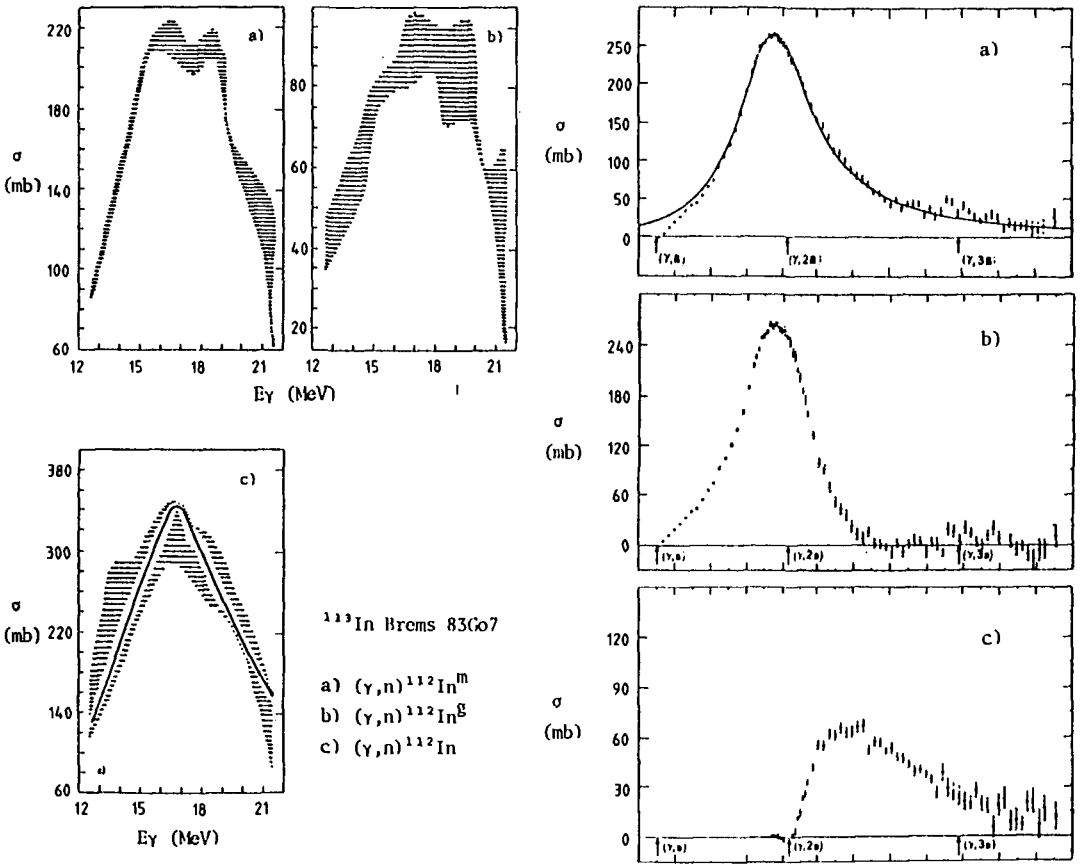
a)
b)
c)
σ (mb)
Eγ (MeV)
(γ,n)
(γ,2n)
(γ,3n)
^{113}In Brems 83Go7
a) $(\gamma,n)^{112}In^{m}$
b) $(\gamma,n)^{112}In^{g}$
c) $(\gamma,n)^{112}In$

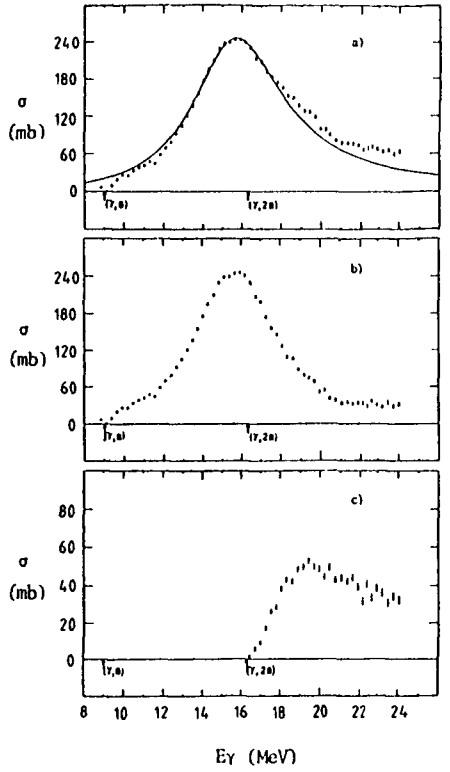

^{115}In Mono 75Be6 , 74Le5

a) $\sigma(\gamma,n_t)$
b) $\sigma(\gamma,n)+\sigma(\gamma,pn)$
c) $\sigma(\gamma,2n)+\sigma(\gamma,p2n)$

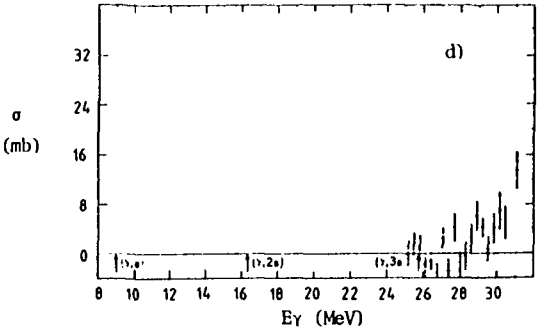

^{115}In Mono 75Be6 , 69Fu1

a) $\sigma(\gamma,n_t)$
b) $\sigma(\gamma,n)+\sigma(\gamma,pn)$
c) $\sigma(\gamma,2n)+\sigma(\gamma,p2n)$
d) $\sigma(\gamma,3n)$

In	A = 113 (4.3)	A = 115 (95.7)
GN	9.4 14.4 min, EC, β^+, β^- 20.9 min, IT	9.0 71.9s, β^-, EC, β^+ 49.51d, IT, EC
GP	6.1 S	6.8 S
G2N	17.1 2.83d, EC 7.6 min, IT	16.3 S; 99.5 min, IT
GNP	15.5 S; 48.6 min, IT	15.9 9.3E+15y, β^- 14y, β^-, IT
G2P	15.7 7.45d, β^- 65s, IT, β^-	17.1 5.37h, β^- 1.15 min, β^-
GA	3.0 S; 39.8s, IT	3.7 7.45d, β^- 65s, IT, β^-

Tin

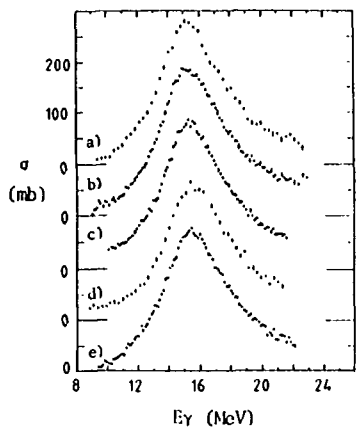

Sn isotopes Mono 74Ca5

a) ^{124}Sn $\sigma(\gamma,n_t)$
b) ^{120}Sn $\sigma(\gamma,n_t)$
c) ^{118}Sn $\sigma(\gamma,n_t)$
d) ^{117}Sn $\sigma(\gamma,n_t)$
e) ^{116}Sn $\sigma(\gamma,n_t)$

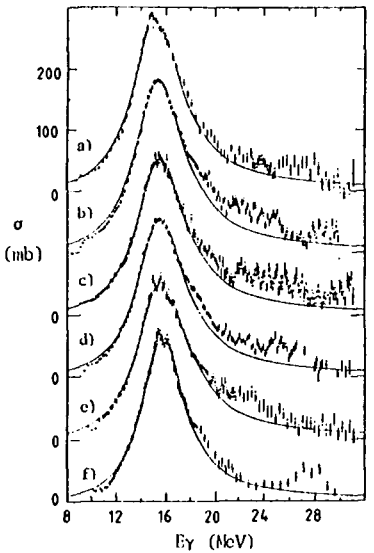

Sn isotopes Mono 75Be15

a) ^{124}Sn $\sigma(\gamma,n_t)$
b) ^{120}Sn $\sigma(\gamma,n_t)$
c) ^{119}Sn $\sigma(\gamma,n_t)$
d) ^{118}Sn $\sigma(\gamma,n_t)$
e) ^{117}Sn $\sigma(\gamma,n_t)$
f) ^{116}Sn $\sigma(\gamma,n_t)$

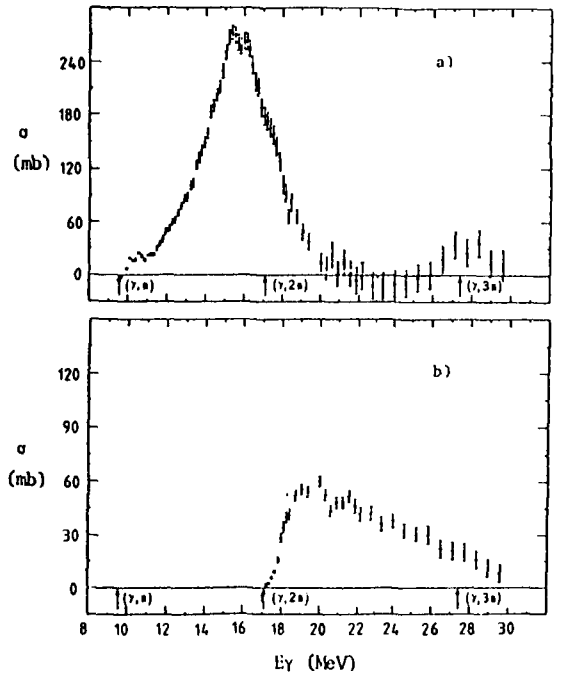

^{116}Sn Mono 75Be6 , 69Fu1

a) $\sigma(\gamma,n)+\sigma(\gamma,pn)$
b) $\sigma(\gamma,2n)+\sigma(\gamma,p2n)$

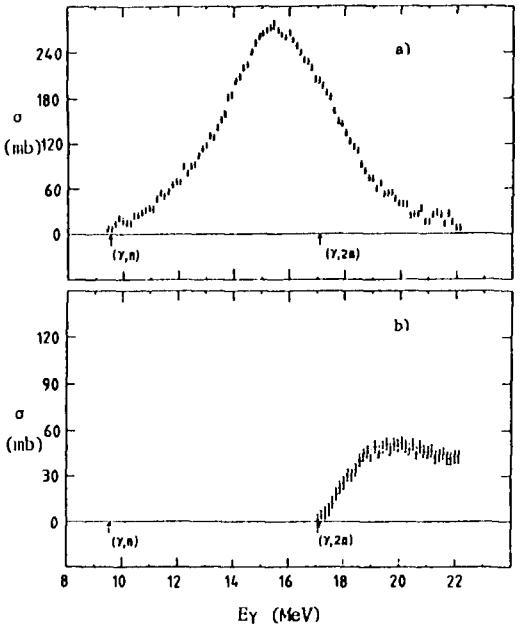

^{116}Sn Mono 75Be6 , 74Le5

a) $\sigma(\gamma,n)+\sigma(\gamma,pn)$
b) $\sigma(\gamma,2n)+\sigma(\gamma,p2n)$

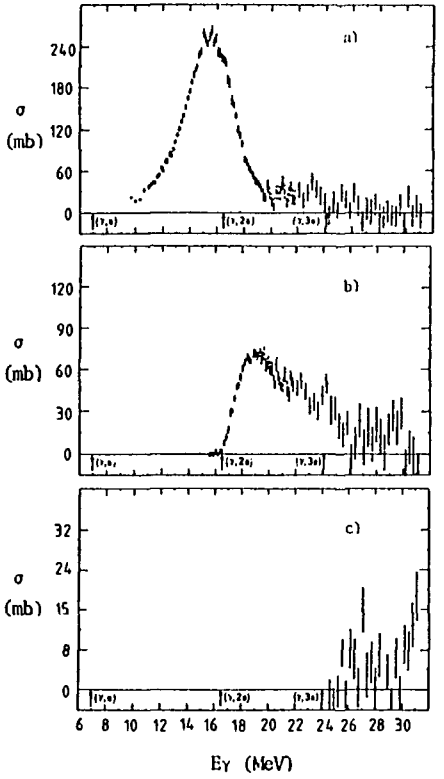

^{117}Sn Mono 75Be6 , 69Fu1

a) $\sigma(\gamma,n)+\sigma(\gamma,pn)$
b) $\sigma(\gamma,2n)+\sigma(\gamma,p2n)$
c) $\sigma(\gamma,3n)$

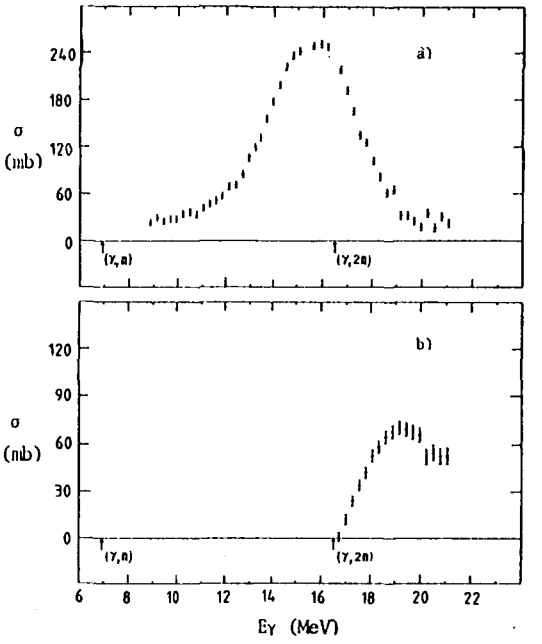

^{117}Sn Mono 75Be6 , 74Le5

a) $\sigma(\gamma,n)+\sigma(\gamma,pn)$
b) $\sigma(\gamma,2n)+\sigma(\gamma,p2n)$

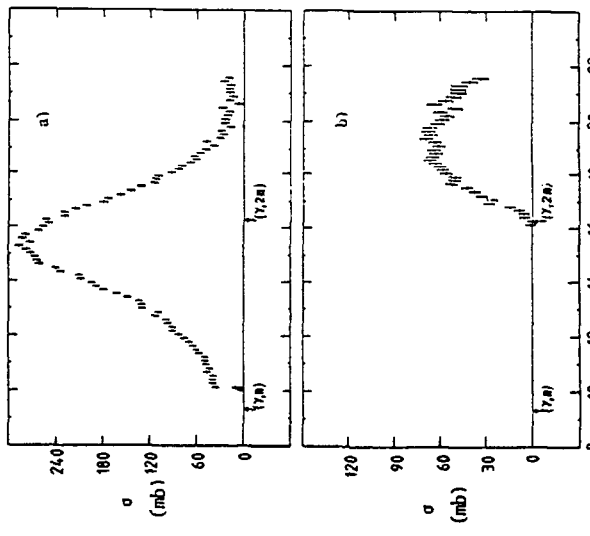

^{116}Sn Mono 75Be6 , 74Le5

a) σ(γ,n)+σ(γ,pn)
b) σ(γ,2n)+σ(γ,p2n)

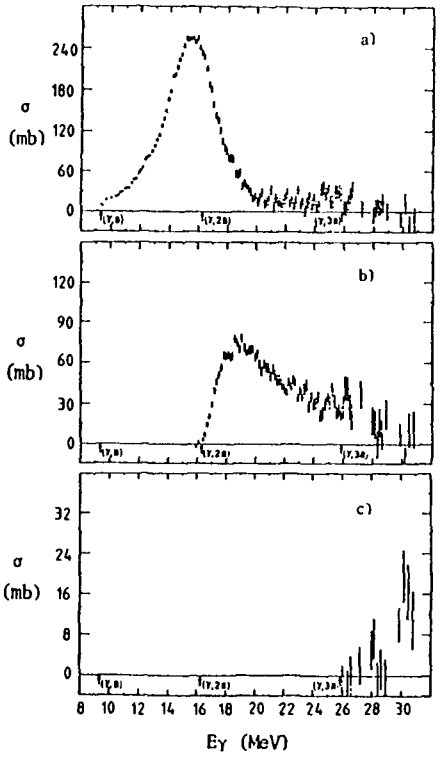

^{118}Sn Mono 75Be6 , 69Fu1

a) σ(γ,n)+σ(γ,pn)
b) σ(γ,2n)+σ(γ,p2n)
c) σ(γ,3n)

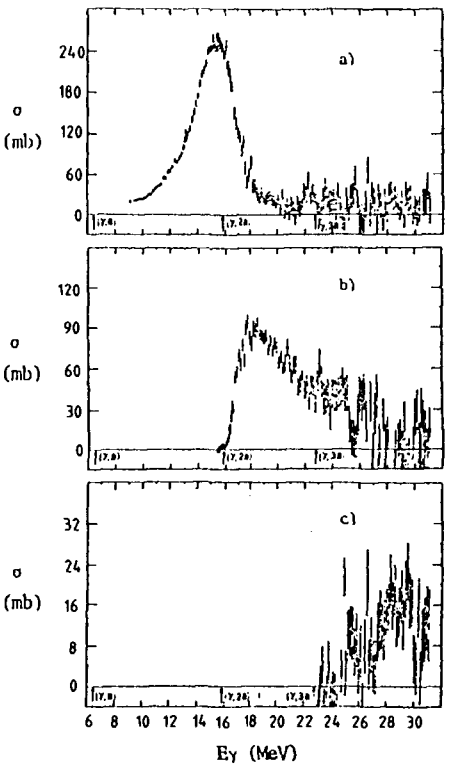

^{119}Sn Mono 75Be6 , 69Fu1

a) σ(γ,n)+σ(γ,pn)
b) σ(γ,2n)+σ(γ,p2n)
c) σ(γ,3n)

Sn	A = 112 (1.0)	A = 114 (0.7)	A = 115 (0.4)	A = 116 (14.7)
GN	10.8 35.0 min, EC, β^+	10.3 1.151E+2d, EC 21 min, IT, EC	7.5 S	9.6 S
GP	7.5 2.83d, EC 7.6 min, IT	8.5 S; 99.5 min, IT	8.7 71,9s, β^-, EC, β^+ 49.51d,IT, EC	9.3 5.1E+14y, β^- 4.49h, IT, β^-
G2N	19.0 4.15h, EC	18.1 S	17.9 1.151E+2d, EC 21 min, IT, EC	17.1 S
GNP	17.6 4.9h, EC 69 min, β^+, EC	17.9 14.4 min, EC, β^+, β^- 20.9 min, IT	16.0 S; 99.5 min, IT	18.3 71.9s, β^-, EC, β^+ 49.51d, IT, EC
G2P	12.9 S	14.6 S	15.6 9.3E+15y, β^- 14y, β^-, IT	16.1 S
GA	1.8 S	2.6 S	3.2 S; 48.6 min, IT	3.4 S

Sn	A = 117 (7.7)	A = 118 (24.3)	A =119 (8.6)	A = 120 (32.4)
GN	6.9 S	9.3 S; 14.0d, IT	6.5 S	9.1 S; 2.50E+2d, IT
GP	9.4 14.10s, β^- 54.1 min, β^-; 2.16s, IT	10.0 42.3 min, β^- 1.93h, β^-, IT	9.9 4.35 min, β^- 8.5s, IT, β^-	10.7 2.1 min, β^- 18.0 min, β^-, IT
G2N	16.5 S	16.3 S	15.8 S; 14.0d, IT	15.6 S
GNP	16.2 5.1E+14y, β^- 4.49h, IT, β^-	18.8 14.10s, β^- 54.1 min, β^-; 2.16s, IT	16.5 42.3 min, β^- 1.93h, β^-, IT	19.0 4.35 min, β^- 8.5s, IT, β^-; 50s, β^-
G2P	16.9 53.38h, β^- 44.8d, β^-	17.5 S	18.2 2.42h, β^- 3.4h, β^-	19.0 50.3 min, β^-
GA	3.8 9.3E+15y, β^- 14y, IT	4.1 S	4.4 53.38h, β^- 44.8d, β^-	4.8 S

Sn	A = 122 (4.6)	A 124 (5.6)
GN	8.8 27.06h, β^- 55y, β^-	8.5 1.290E+2d, β^- 40.1 min, β^-
GP	11.4 30.0s, β^- 3.8 min, β^-, IT	12.1 5.98s, β^- 48s, β^-
G2N	15.0 S	14.4 S
GNP	19.8 44.4s, β^- 3.0s, β^-	20.0 1.5s, β^- 9.2s, β^-
G2P	* 50.80s, β^-	20.5 5.78s, β^-
GA	5.7 50.3 min, β^-	6.7 50.80s, β^-

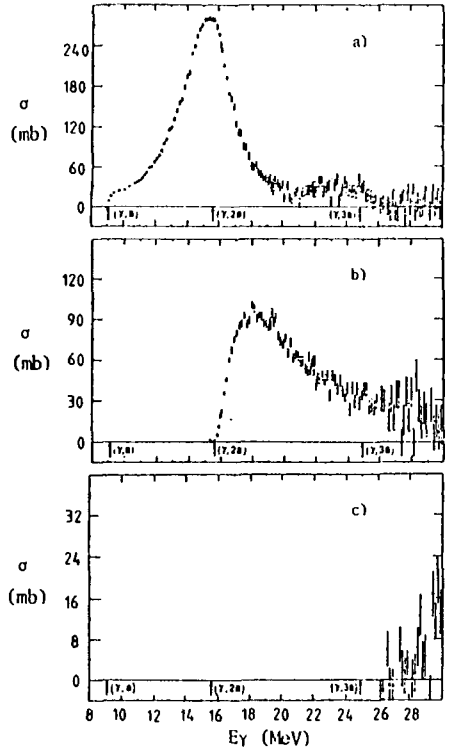

^{120}Sn Mono 75Be6 , 69Fu1

a) σ(γ,n)+σ(γ,pn)
b) σ(γ,2n)+σ(γ,p2n)
c) σ(γ,3n)

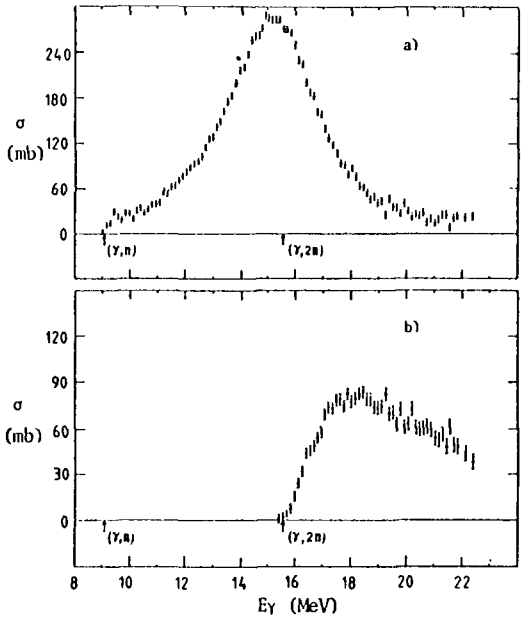

^{120}Sn Mono 75Be6 , 74Le5

a) σ(γ,n)+σ(γ,pn)
b) σ(γ,2n)+σ(γ,p2n)

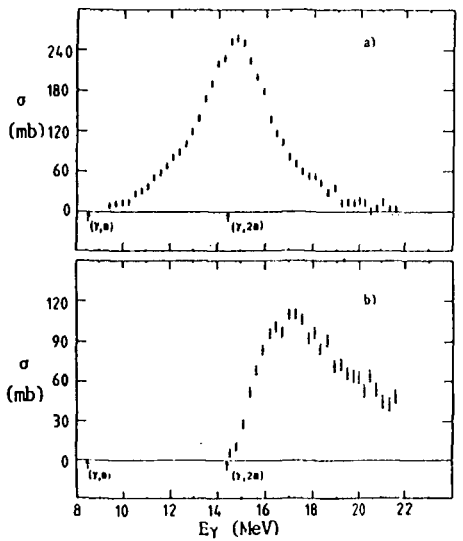

^{124}Sn Mono 75Be6 , 74Le5

a) σ(γ,n)+σ(γ,pn)
b) σ(γ,2n)+σ(γ,p2n)

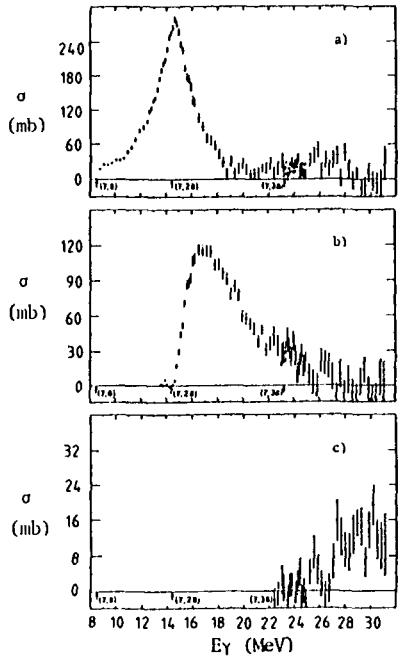

^{124}Sn Mono 75Be6 , 69Fu1

a) σ(γ,n)+σ(γ,pn)
b) σ(γ,2n)+σ(γ,p2n)
c) σ(γ,3n)

Antimony

Sb natural Mono 75Bc6 , 74Lc5

a) $\sigma(\gamma,n_t)$
b) $\sigma(\gamma,n)+\sigma(\gamma,pn)$
c) $\sigma(\gamma,2n)+\sigma(\gamma,p2n)$

Sb	A = 121 (57.3)	A = 123 (42.7)
GN	9.2 15.89 min, EC, β^+ 5.76d, EC	9.0 2.681d, β^-, EC, β^+ 4.2 min, IT
GP	5.8 S	6.6 S
G2N	16.3 38.0h, EC	15.8 S
GNP	14.9 S; 2.50E+2d, IT	15.4 27.06h, β^- 55y, β^-
G2P	16.5 2.1 min, β^- 18.0 min, β^-, IT	18.0 30.0s, β^- 3.8 min, β^-, IT
GA	3.1 42.3 min, β^- 1.93h, β^-, IT	3.9 2.1 min, β^- 18.0 min, β^-, IT

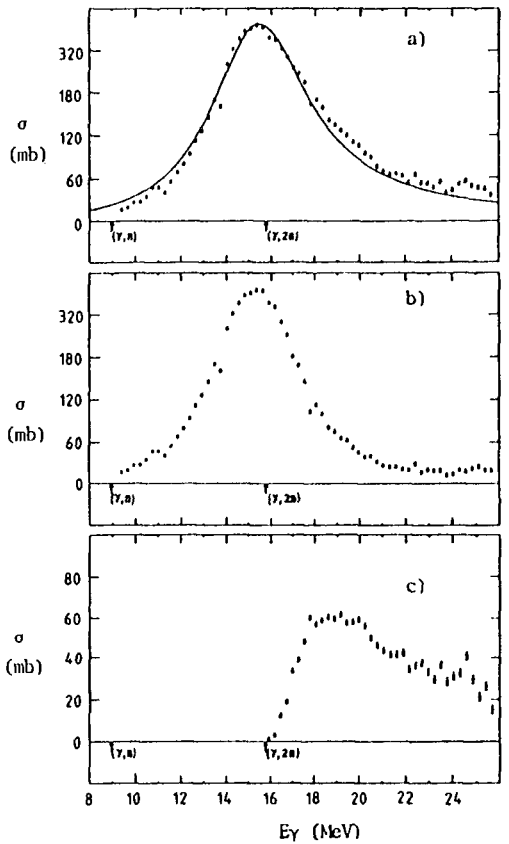

Tellurium

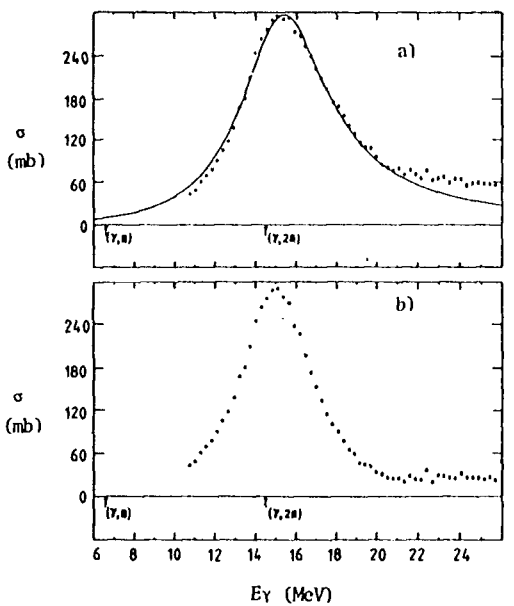

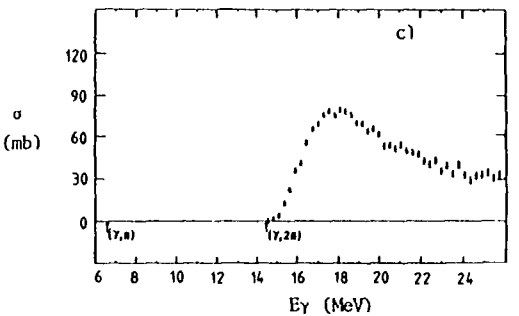

Te natural Mono 75Be6 , 74Le5

a) $\sigma(\gamma,n_t)$
b) $\sigma(\gamma,n)+\sigma(\gamma,pn)$
c) $\sigma(\gamma,2n)+\sigma(\gamma,p2n)$

Te	A = 120 (0.1)	A = 122 (2.5)	A = 123 (0.9)	A = 124 (4.6)
GN	10.3 16.05h, EC, β^+ 4.68d, EC	9.8 16.8d, EC 1.54E+2d, IT, EC, β^+	6.9 S	9.4 >5E+13y, EC 1.197E+2d, IT
GP	7.2 38.0h, EC	8.0 S	8.1 2.681d, β^-, EC, β^+ 4.2 min, IT	8.6 S
G2N	17.9 6.00d, EC	17.0 S	16.7 16.78d, EC 1.54E+2d, IT, EC, β^+	16.4 S
GNP	16.8 3.5 min, EC, β^+ 5.00h, EC, β^+	17.3 15.89 min, EC, β^+ 5.76d, EC	14.9 S	17.5 2.681d, β^-, EC, β^+ 4.2 min, IT
G2P	12.3 S	13.8 S	14.5 27.06h, β^- 55y, β^-	15.2 S
GA	0.3 S	1.1 S	1.5 S; 2.50E+2d, IT	1.8 S

Te	A = 125 (7.0)	A = 126 (18.7)	A = 128 (31.7)	A = 130 (34.5)
GN	6.6 S	9.1 S; 58d, IT	8.8 9.35h, β^- 1.09E+2d, IT, β^-	8.4 69.5 min, β^- 33.5d, β^-, IT
GP	8.7 60.20d, β^- 93s, IT, β^- 20.2 min, IT	9.1 2.71y, β^-	9.6 3.91d, β^-	10.0 4.41h, β^-
G2N	16.0 >5E+13y, EC	15.7 S	15.1 S	14.5 1.54E+24y, β^- β^-
GNP	15.2 S	17.8 60.20d, β^- 93s, IT, β^- 20.2 min, IT	18.0 12.4d, β^- 19.0 min, β^-, IT	18.0 9.10h, β^- 10.0 min, β^-, IT
G2P	15.8 1.290E+2d, β^- 40.1 min, β	16.4 S	17.6 1E+5y, β^-	18.5 59.3 min, β^-
GA	2.2 27.06h, β^- 55y, β^-	2.6 S	3.2 S	3.8 1E+5y, β^-

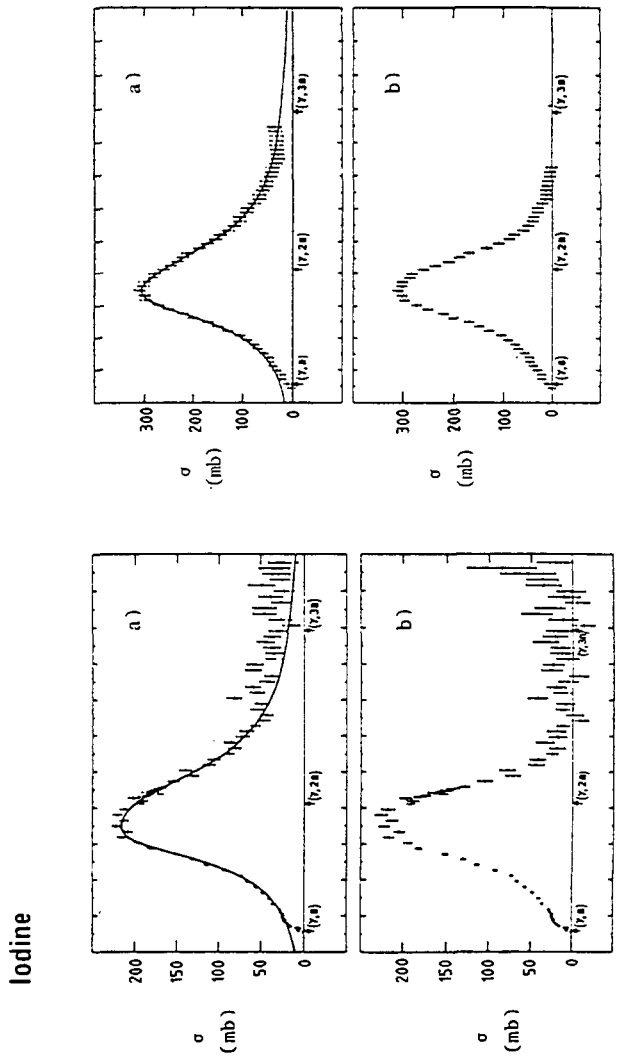
Iodine
a)
b)
σ (mb)
0
50
100
150
200
300
γ,a)
γ,2a)
γ,3a)
γ,3n)

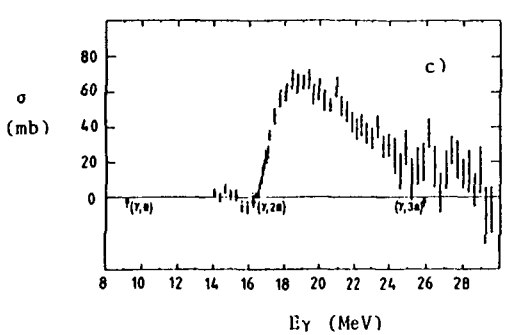

^{127}I Mono 75Be6 , 66Br1

a) $\sigma(\gamma,n_t)$
b) $\sigma(\gamma,n)+\sigma(\gamma,pn)$
c) $\sigma(\gamma,2n)+\sigma(\gamma,p2n)$

I	A = 127 (100)
GN	9.1 13.02d, EC, β^+, β^-
GP	6.2 S
G2N	16.2 60.25d, EC
GNP	15.3 S; 58d, IT
G2P	15.3 2.71y, β^-
GA	2.2 S

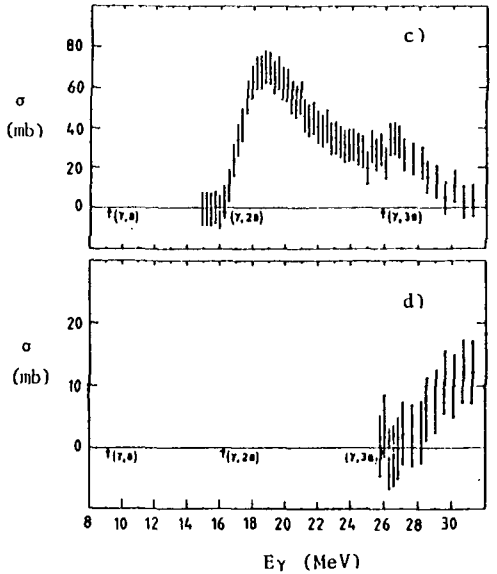

^{127}I Mono 75Be6 , 69Be5

a) $\sigma(\gamma,n_t)$
b) $\sigma(\gamma,n)+\sigma(\gamma,pn)$
c) $\sigma(\gamma,2n)+\sigma(\gamma,p2n)$
d) $\sigma(\gamma,3n)$

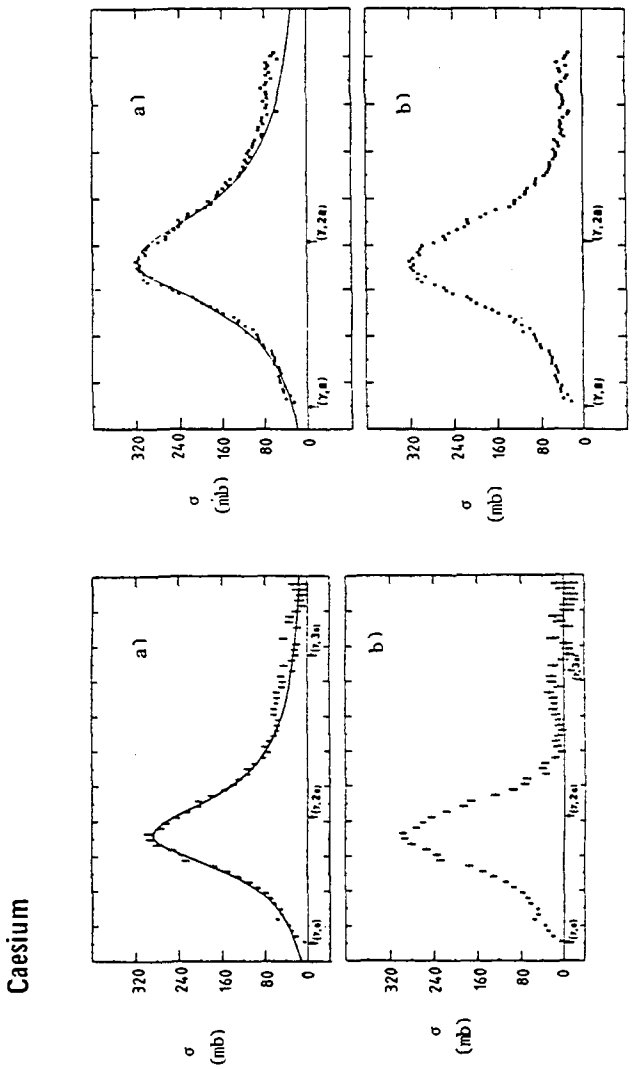
Caesium
a)
b)
σ (mb)
320
240
160
80
0

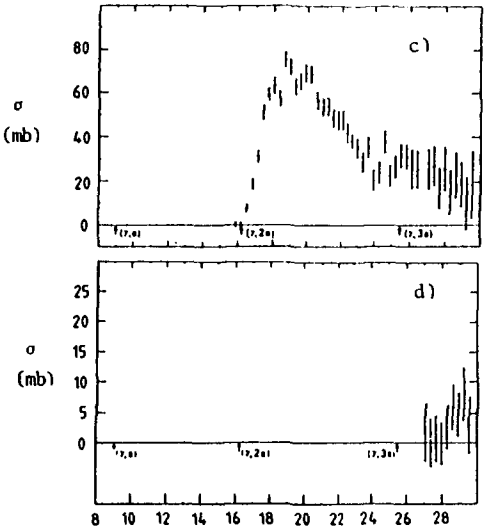

^{133}Cs Mono 75Be6 , 69Be101 , 74Le5

a) $\sigma(\gamma,n_t)$
b) $\sigma(\gamma,n)+\sigma(\gamma,pn)$
c) $\sigma(\gamma,2n)+\sigma(\gamma,p2n)$
d) $\sigma(\gamma,3n)$

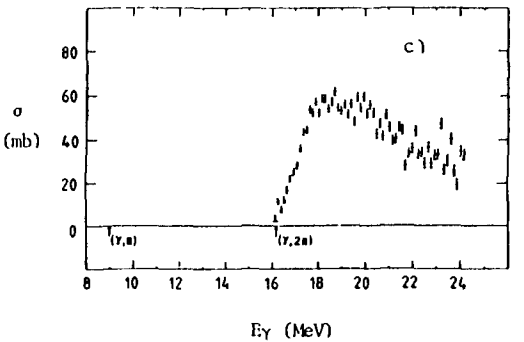

^{133}Cs Mono 75Be6 , 74Le5

a) $\sigma(\gamma,n_t)$
b) $\sigma(\gamma,n)+\sigma(\gamma,pn)$
c) $\sigma(\gamma,2n)+\sigma(\gamma,p2n)$

Cs	A = 133 (100)
GN	9.0 6.47d, EC, β^-, β^+
GP	6.1 S
G2N	16.2 9.688d, EC
GNP	15.0 S; 11.77d, IT
G2P	15.2 8.040d, β^-
GA	2.0 1.57E+7y, β^-

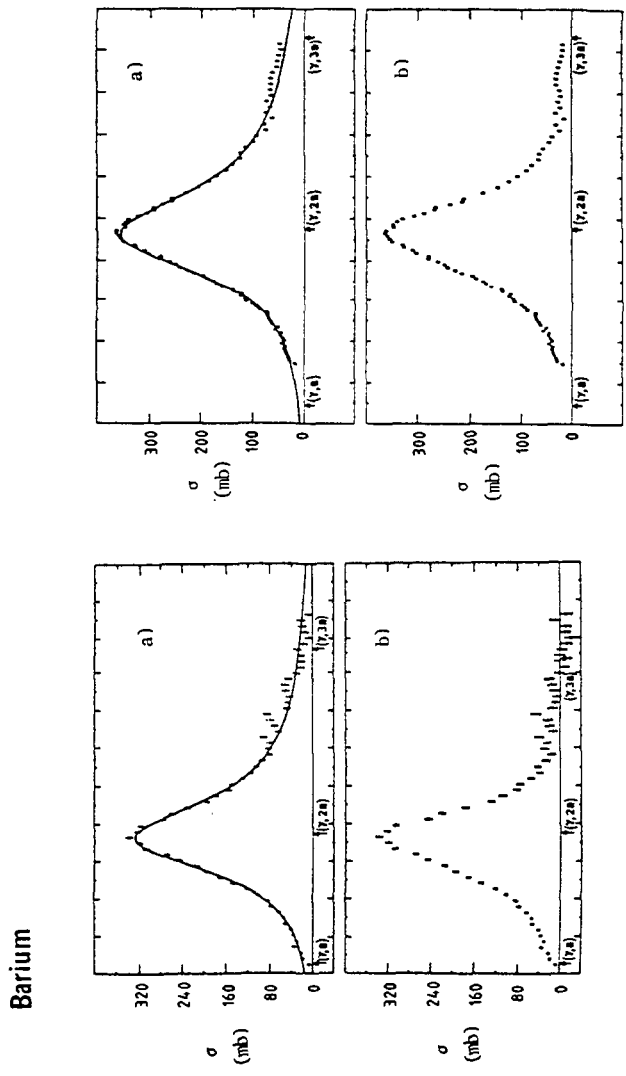
Barium
a)
b)
σ (mb)
320
240
160
80
0
300
200
100
(γ,n)
(γ,2n)
(γ,3n)

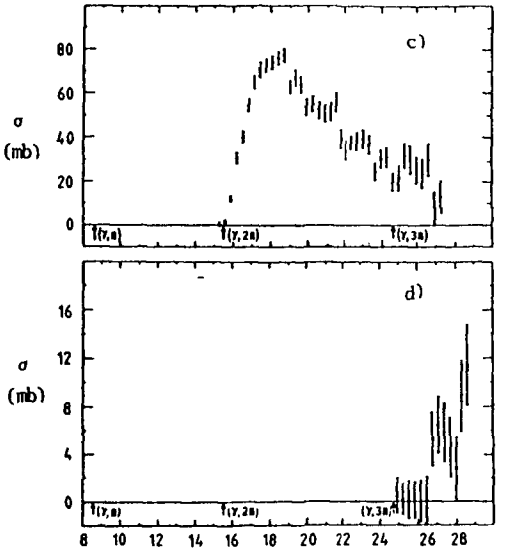

^{138}Ba Mono 75Be6 , 70Be1

a) $\sigma(\gamma,n_t)$
b) $\sigma(\gamma,n)+\sigma(\gamma,pn)$
c) $\sigma(\gamma,2n)+\sigma(\gamma,p2n)$
d) $\sigma(\gamma,3n)$

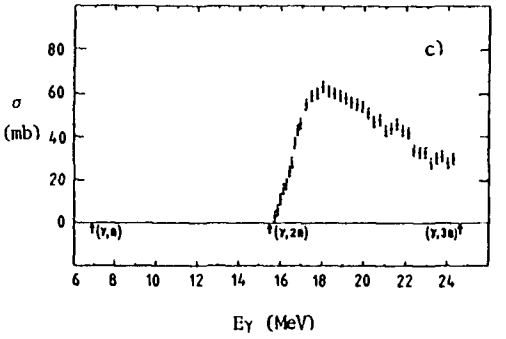

Ba natural Mono 75Be6 , 71Be5

a) $\sigma(\gamma,n_t)$
b) $\sigma(\gamma,n)+\sigma(\gamma,pn)$
c) $\sigma(\gamma,2n)+\sigma(\gamma,p2n)$

Ba	A = 130 (0.1)	A 132 (0.1)	A = 134 (2.4)
GN	10.2 2.20h, EC, β^+ 2.1h, EC, β^+	9.8 12.0d, EC 14.6 min, IT	9.5 10.66y, EC 38.9h, IT, EC
GP	7.0 32.4h, EC, β^+	7.7 9.688d, EC	8.2 S
G2N	18.2 2.43d, EC	17.3 S	16.7 S
GNP	16.7 3.62 min, β^+, EC	17.0 29.9 min, EC, β^+, β^-	17.1 6.474d, EC, β^-, β^+
G2P	12.0 S	13.1 S	14.3 S
GA	0.6 S	1.0 S	1.5 S

Ba	A = 135 (6.6)	A = 136 (7.9)	A = 137 (11.2)	A = 138 (71.7)
GN	7.0 S	9.1 S; 28.7h, IT	6.9 S; 0.31s, IT	8.6 S; 2.551 min, IT
GP	8.3 2.062y, β^-, EC 2.90h, IT	8.5 2.95E+6y, β^- 53 min, IT	8.7 13.00d, β^- 19s, IT	9.0 30.17y, β^-
G2N	16.4 10.66y, EC 38.9h, IT, EC	16.1 S	16.0 S; 28.7h, IT	15.5 S; 0.31s, IT
GNP	15.1 S	17.4 2.062y, β^-, EC 2.90h, IT	15.4 2.95E+6y, β^- 53 min, IT	17.3 13.00d, β^- 19s, IT
G2P	14.8 5.245d, β^- 2.19d, IT	15.4 S; 0.29s, IT	15.8 9.104h, β^- 15.6 min, IT, β^-	16.4 S
GA	1.9 S; 11.77d, IT	2.1 S	2.5 5.245d, β^- 2.19d, IT	2.6 S; 0.29s, IT

Lanthanum

^{139}La Mono 75Be6 , 68Be5 , 71Be5

a) $\sigma(\gamma,n_t)$
b) $\sigma(\gamma,n)+\sigma(\gamma,pn)$
c) $\sigma(\gamma,2n)+\sigma(\gamma,p2n)$
d) $\sigma(\gamma,3n)$

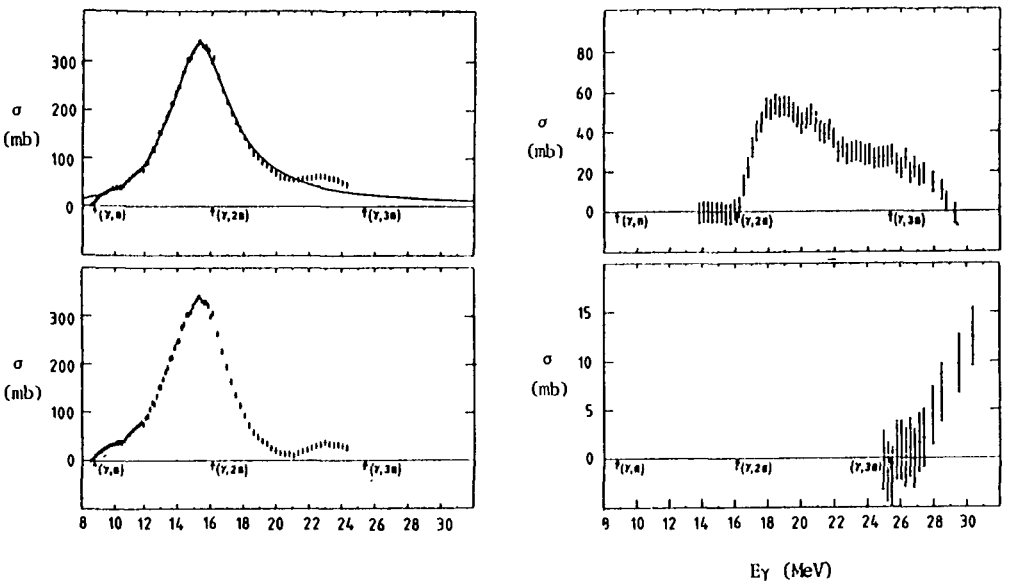

La	A = 138 (0.09)	A = 139 (99.91)
GN	7.3 6E+4y, EC	8.8 1.12E+11y, EC, β^-
GP	6.0 S; 2.551 min, IT	6.2 S
G2N	16.6 9.87 min, EC, β^+	16.1 6E+4y, EC
GNP	12.9 S; 0.31s, IT	14.8 S; 2.551 min, IT
G2P	14.7 13.00d, β^- 19s, IT	15.2 30.174y, β^-
GA	2.0 2.062y, β^-, EC 2.90h, IT	2.0 3.0E+6y, β^- 53 min, IT

Cerium

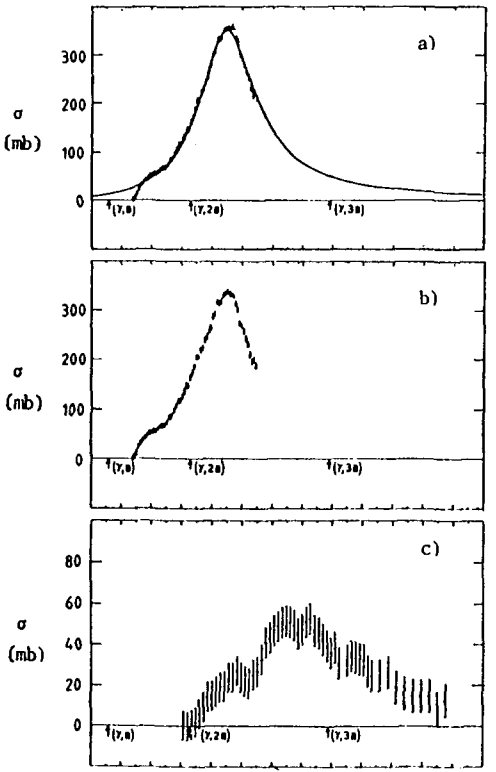

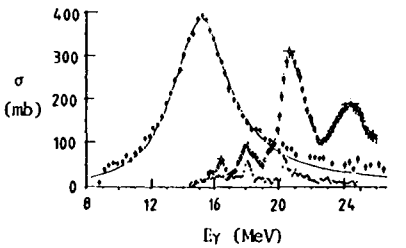

^{140}Ce Brems 79Sh10

○ σ(γ,p)

● σ(γ,n) 68Be5 , 76Le5 , 66Br1 , 71Ca5

..... σ(γ,p_0+p_1) 71Sh1 , Sa30

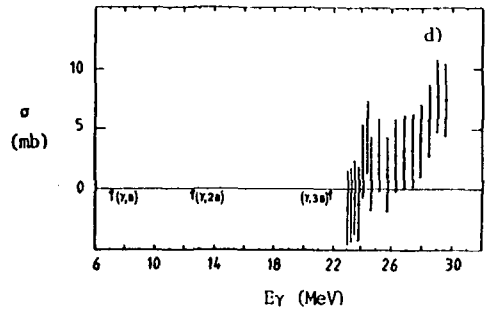

Ce natural Mono 75Be6 , 69Be5 , 71Be5

a) $\sigma(\gamma,n_t)$
b) $\sigma(\gamma.n)+\sigma(\gamma,pn)$
c) $\sigma(\gamma,2n)+\sigma(\gamma,p2n)$
d) $\sigma(\gamma,3n)$

Ce	A = 136 (0.2)	A = 138 (0.3)	A = 140 (88.4)	A = 142 (11.1)
GN	10.0 17.76h, EC, β^+ 20s, IT	9.6 9.0h, EC, β^+ 34.4h, IT, EC	9.2 1.372E+2d, EC 56s, IT	7.2 32.55d, β^-
GP	6.9 19.4h, EC, β^+	7.6 6E+4y, EC	8.1 S	8.8 3.90h, β^-
G2N	17.9 75.9h, EC	17.2 S	16.7 S	12.6 S
GNP	16.6 6.67 min, β^+, EC	16.9 9.87 min, EC, β^+	16.9 1.12E+11y, EC, β^-	15.6 40.27h, β^-
G2P	12.1 S	13.2 S; 0.31s, IT	14.3 S	15.8 12.789d β^-
GA	0.4 S	1.0 S	1.6 S; 0.31s, IT	-1.4 S

Praseodymium

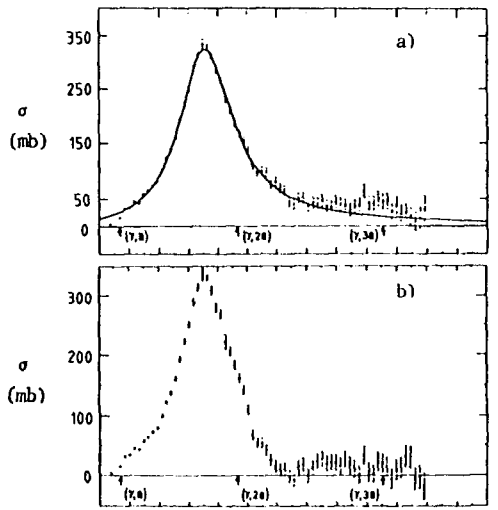

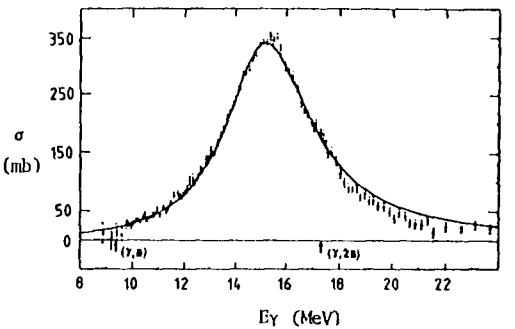

^{141}Pr Mono 75Be6 , 70Su1

σ(γ,n); (γ,pn) not included

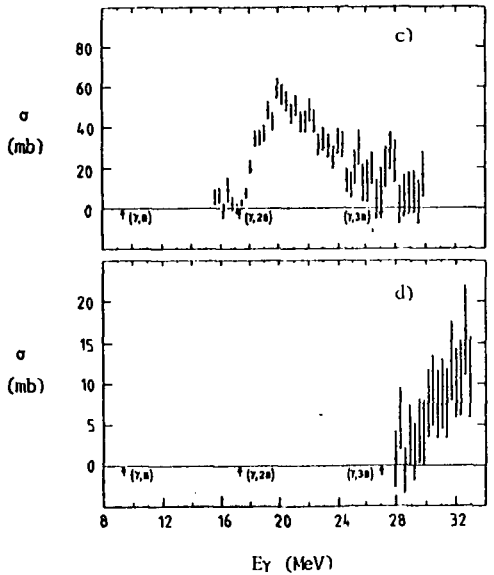

^{141}Pr Mono 75Be6 , 66Br1

a) $\sigma(\gamma,n_t)$
b) $\sigma(\gamma,n)+\sigma(\gamma,pn)$
c) $\sigma(\gamma,2n)+\sigma(\gamma,p2n)$
d) $\sigma(\gamma,3n)$

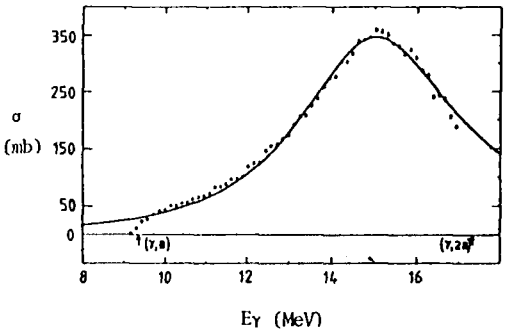

^{141}Pr Mono 75Be6 , 71Be5

$\sigma(\gamma,n_t)$

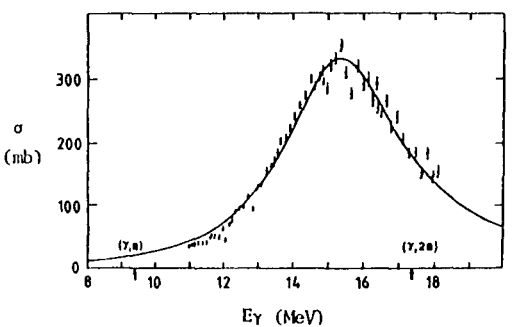

^{141}Pr Mono 75Be6 , 72Yo

$\sigma(\gamma,n)+\sigma(\gamma,pn)+2\sigma(\gamma,2n)$

Lorentz parameters for the Pr data from 83Bo5

	E (MeV)	Γ (MeV)	σ (mb)	½πσΓ (MeV/b)
Melbourne[1]	15.15±0.1	3.58±0.15	400±23	2.26±0.18
LLL[2]	15.16±0.08	4.49±0.05	320±29	2.27±0.14
Saclay[3]	15.1 ±0.1	4.26±0.05	350±15	2.35±0.13
General Atomic[4]	15.23	4.00	341	2.14
Illinois[5]	15.36	4.07	332	2.12
Heidelberg[6]	15.4 ±0.1	3.9 ±0.2	396±24	2.43±0.27

Fitting interval: 12 - 19 MeV except for Heidelberg (Unknown)

[1] 83Bo5 Brems

[2] 66Br1 } quasi-monoenergetic photons
[3] 71Bc5 }
[4] 70Su1 }

[5] 72Yo tagged photons

[6] 72Dr5 Brems

Pr	A = 141 (100)	
GN	9.4	3.39 min, EC, β^+
GP	5.2	S
G2N	17.3	4.41h, EC, β^+
GNP	14.4	1.372E+2d, EC
		56s, IT
G2P	13.4	S
GA	1.2	6E+4y, EC

See overleaf
for the graphs of neodymium

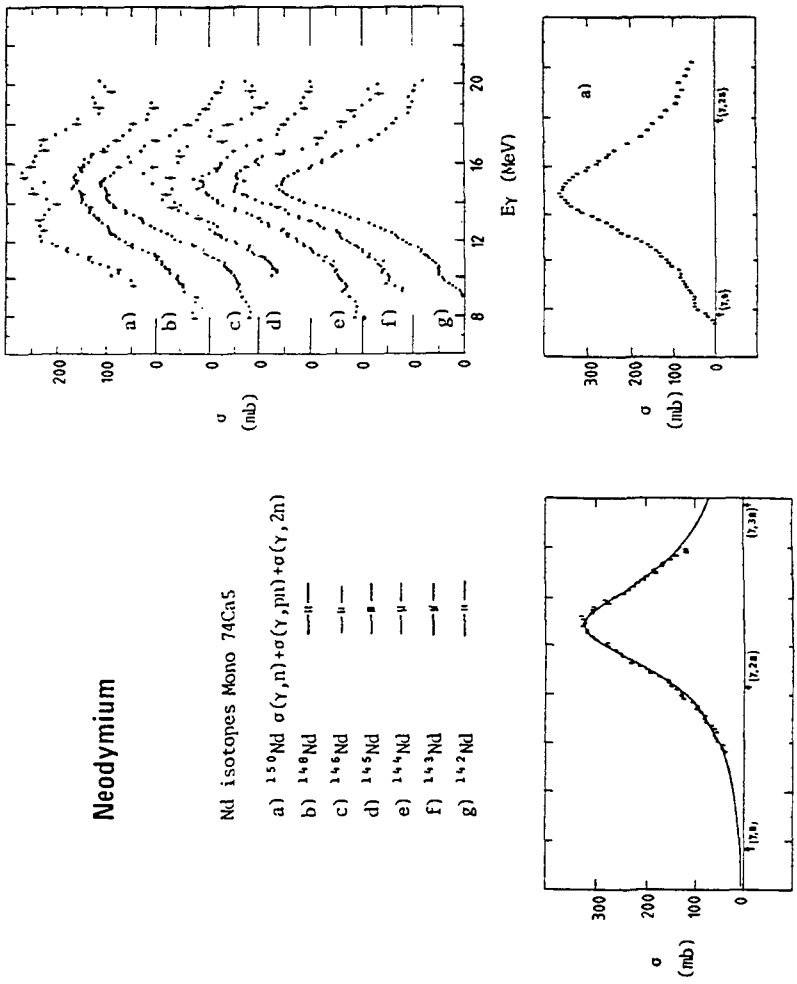
Neodymium
Nd isotopes Mono 74Ca5
a) 150Nd σ(γ,n)+σ(γ,pn)+σ(γ,2n)
b) 148Nd
c) 146Nd
d) 145Nd
e) 144Nd
f) 143Nd
g) 142Nd
σ (mb)
Eγ (MeV)
a)
b)
c)
d)
e)
f)
g)

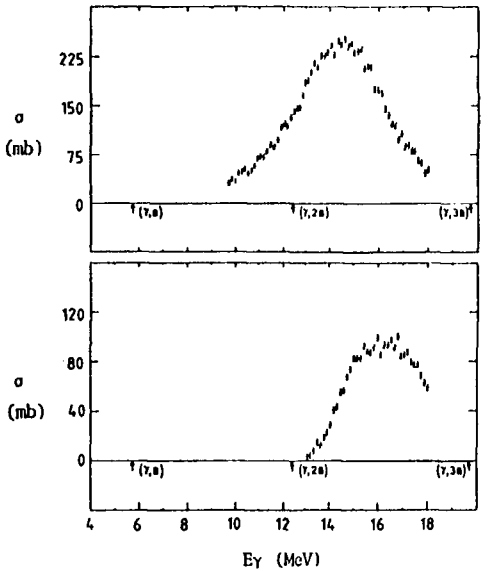

Nd natural Mono 75Be6 , 71Be5

a) $\sigma(\gamma,n_t)$
b) $\sigma(\gamma,n)+\sigma(\gamma,pn)$
c) $\sigma(\gamma,2n)+\sigma(\gamma,p2n)$

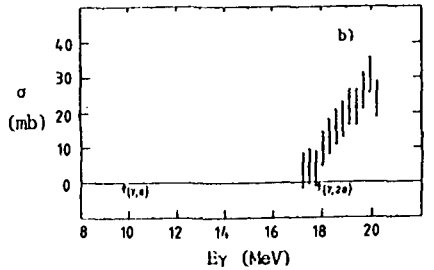

^{142}Nd Mono 75Be6 , 71Ca5

a) $\sigma(\gamma,n)+\sigma(\gamma,pn)$
b) $\sigma(\gamma,2n)+\sigma(\gamma,p2n)$

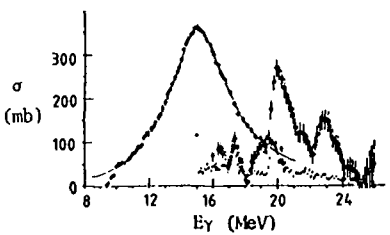

^{142}Nd Brems 79Sh10

○ $\sigma(\gamma,p)$
● $\sigma(\gamma,n)$ 68Be5 , 76Le5
66Br1 , 71Ca5
···· $\sigma(\gamma,p_0+p_1)$ 71Sh1 , Sa30

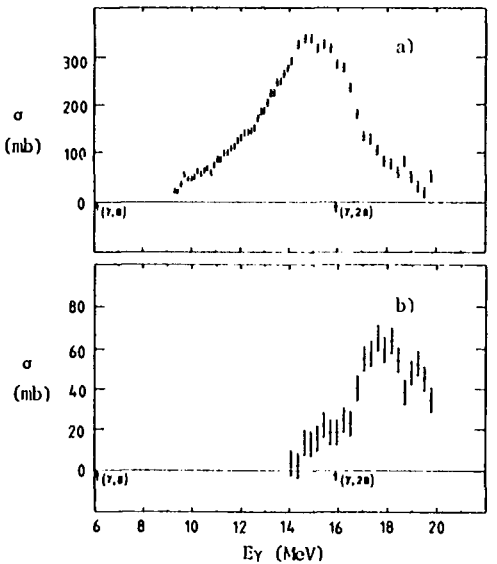

^{143}Nd Mono 75Be6 , 71Ca5

a) σ(γ,n)+σ(γ,pn)
b) σ(γ,2n)+σ(γ,p2n)

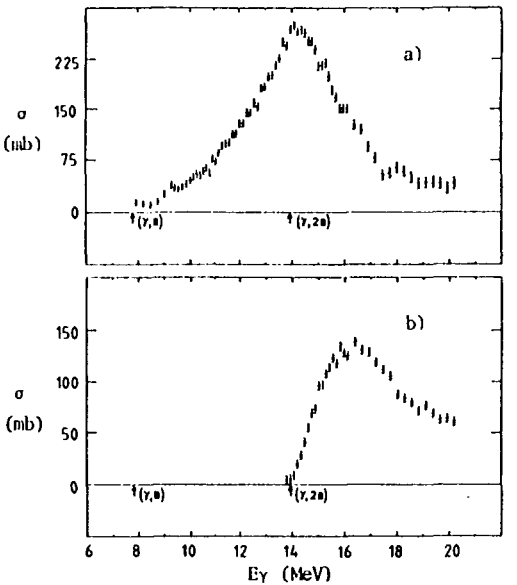

^{144}Nd Mono 75Be6 , 71Ca5

a) σ(γ,n)+σ(γ,pn)
b) σ(γ,2n)+σ(γ,p2n)

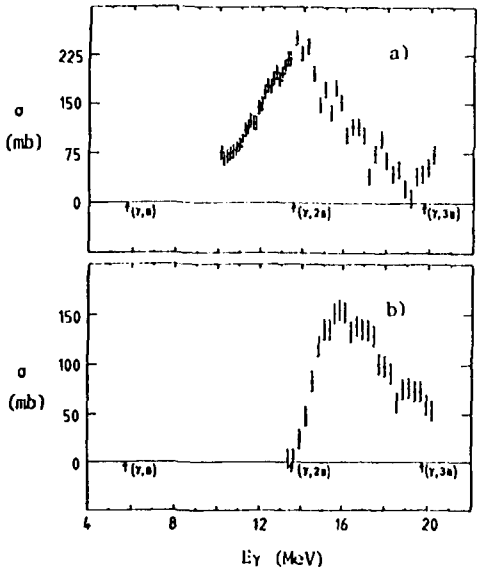

^{145}Nd Mono 7SBe6 , 71Ca5

a) σ(γ,n)+σ(γpn)
b) σ(γ,2n)+σ(γ,p2n)

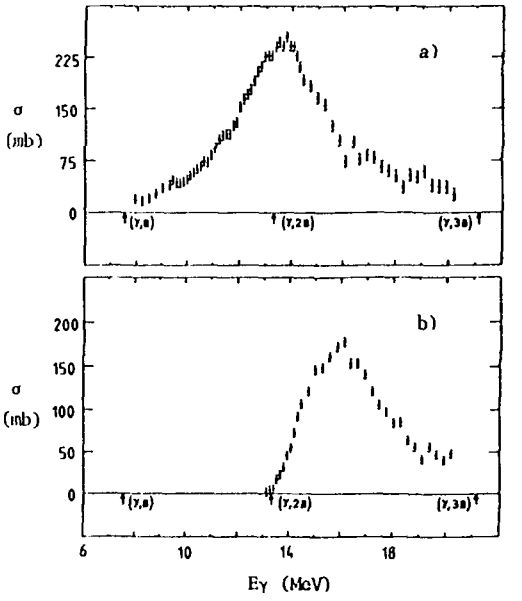

^{146}Nd Mono 7SBe6 , 71Ca5

a) σ(γ,n)+σ(γ,pn)
b) σ(γ,2n)+σ(γ,p2n)

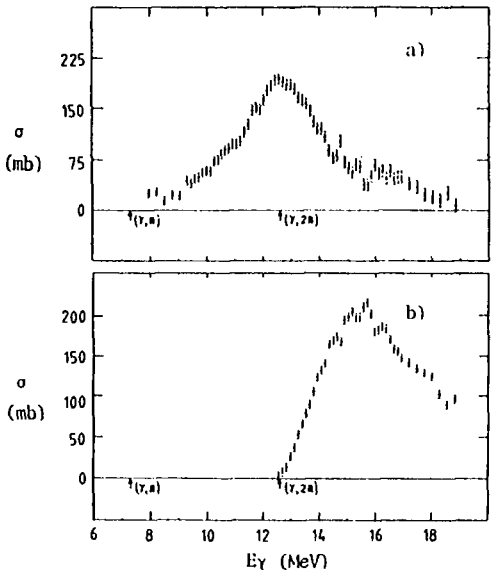

^{148}Nd Mono 75Be6 , 71Ca5

a) σ(γ,n)+σ(γ,pn)
b) σ(γ,2n)+σ(γ,p2n)

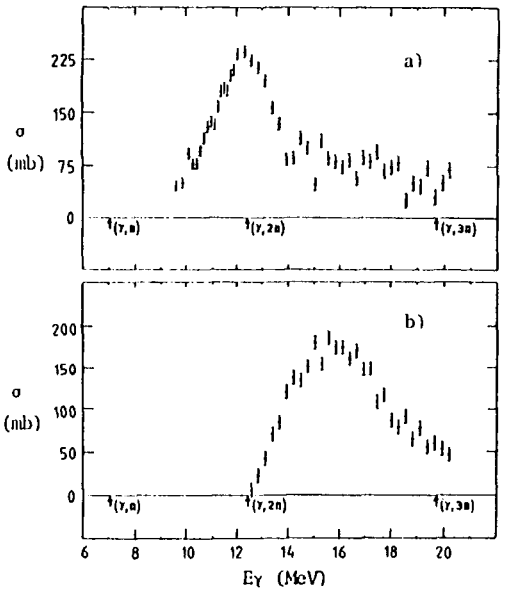

^{150}Nd Mono 75Be6 , 71Ca5

a) σ(γ,n)+σ(γ,pn)
b) σ(γ,2n)+σ(γ,p2n)

Nd	A = 142 (27.16)	A = 143 (12.18)	A = 144 (23.80)
GN	9.8 2.50h, EC, β^+ 61s, IT, EC, β^+	6.1 S	7.8 S
GP	7.2 S	7.5 19.2h, β^-, EC 14.6 min, IT	8.0 13.59d, β^-
G2N	17.9 3.37d, EC	15.9 2.50h, EC, β^+ 61s, IT, EC, β^+	13.9 S
GNP	16.6 3.39 min, EC, β^+	13.4 S	15.3 19.2h, β^-, EC 14.6 min, IT
G2P	12.5 S	13.1 32.55d, β^-	13.8 S
GA	0.8 S	-0.5 1.372E+2d, EC 56s, IT	-1.9 S

Nd	A = 145 (8.29)	A = 146 (17.19)	A = 148 (5.75)	A = 150 (5.63)
GN	5.8 2.1E+15y, α	7.6 S	7.3 10.98d, β^-	7.4 1.73h, β^-
GP	8.0 17.30 min, β^- 7.2 min, IT, β^-	8.6 5.98h, β^-	9.2 13.6 min, β^-	9.6 2.3 min, β^-
G2N	13.6 S	13.3 2.1E+15y, α	12.6 S	12.4 S
GNP	13.7 13.59d, β^-	15.5 17.30 min, β^- 7.2 min, IT, β^-	15.9 24.0 min, β^-	16.5 2.30 min, β^-
G2P	14.4 33.0h, β^-	15.1 2.845E+2d, β^-	16.2 13.9 min, β^-	17.6 48s, β^-
GA	-1.6 32.55d, β^-	-1.2 S	-0.6 2.845E+2d, β^-	0.4 13.9 min, β^-

Samarium

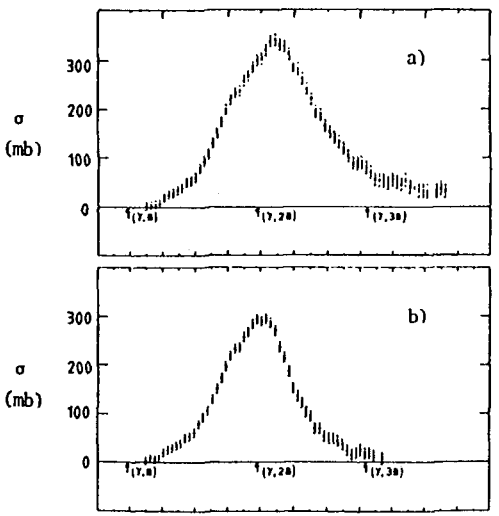

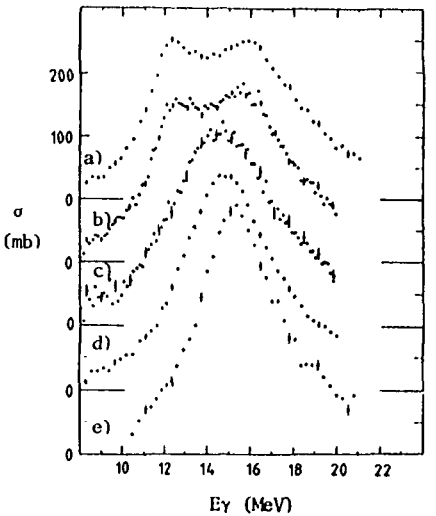

Sm isotopes Mono 74Ca5

a) ^{154}Sm $\sigma(\gamma,n)+\sigma(\gamma,pn)+\sigma(\gamma,2n)$
b) ^{152}Sm —"—
c) ^{150}Sm —"—
d) ^{148}Sm —"—
e) ^{144}Sm —"—

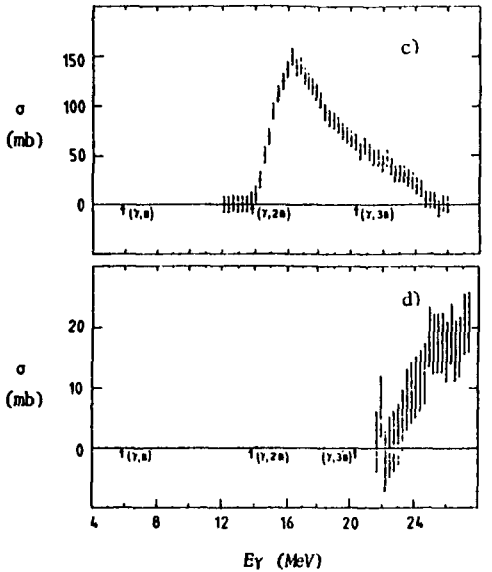

Sm natural Mono 75Be6 , 69Be5

a) $\sigma(\gamma,n_t)$
b) $\sigma(\gamma,n)+\sigma(\gamma,pn)$
c) $\sigma(\gamma,2n)+\sigma(\gamma,p2n)$
d) $\sigma(\gamma,3n)$

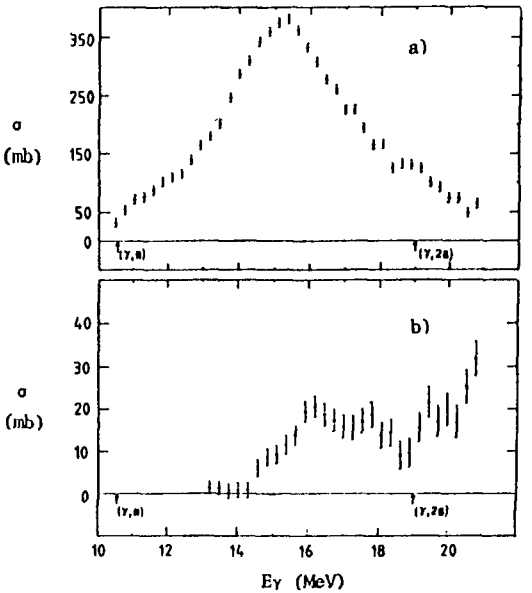

^{144}Sm Mono 75Be6 , 74Ca105

a) $\sigma(\gamma,n)+\sigma(\gamma,pn)$
b) $\sigma(\gamma,2n)+\sigma(\gamma,p2n)$

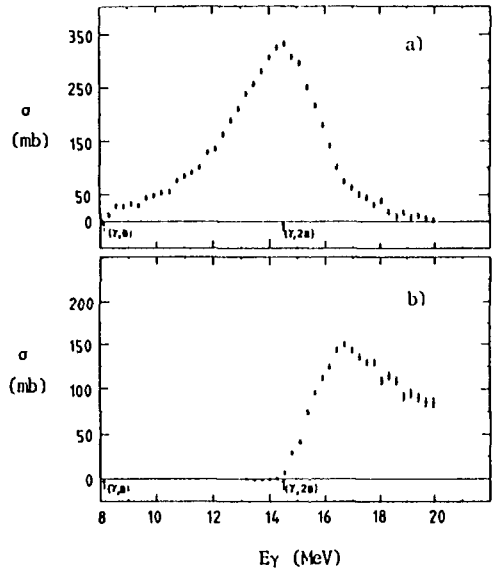

^{148}Sm Mono 75Be6 , 74Ca105

a) σ(γ,n)+σ(γpn)
b) σ(γ,2n)+σ(γ,p2n)

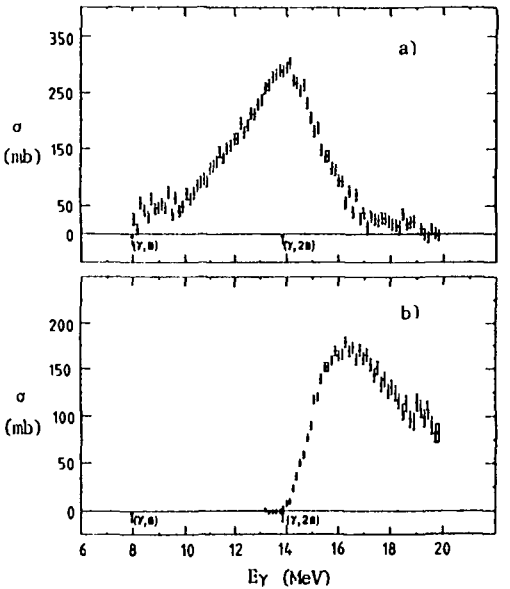

^{150}Sm Mono 75Be6 , 74Ca105

a) σ(γ,n)+σ(γ,pn)
b) σ(γ,2n)+σ(γ,p2n)

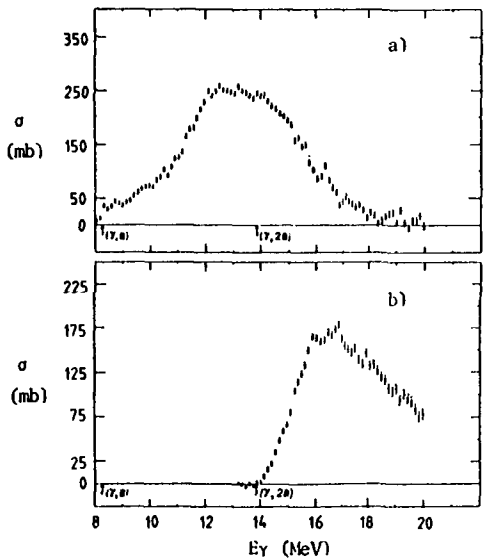

^{152}Sm Mono 75Be6 ,74Ca105

a) $\sigma(\gamma,n)+\sigma(\gamma,pn)$
b) $\sigma(\gamma,2n)+\sigma(\gamma,p2n)$

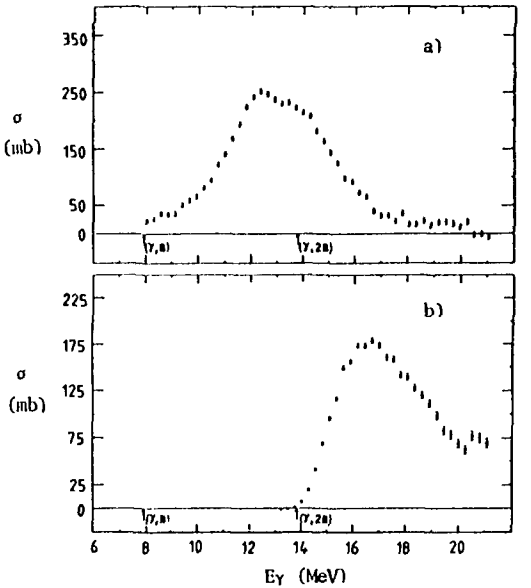

^{154}Sm Mono 75Be6 ,74Ca105

a) $\sigma(\gamma,n)+\sigma(\gamma,pn)$
b) $\sigma(\gamma,2n)+\sigma(\gamma,p2n)$

Sm	A = 144 (3.1)	A = 147 (15.1)	A = 148 (11.3)
GN	10.6 8.83 min, EC, β^+ 66s, IT, β^+, EC	6.4 1.03E+8y, α	8.1 1.06E+11y, α
GP	6.3 2.65E+2d, EC	7.1 5.53y, EC, β^-	7.6 2.623y, β^-
G2N	19.0 72.49 min, EC, β^+	14.8 3.40E+2d, EC	14.5 1.03E+8y, α
GNP	16.2 40.5s, β^+, EC	13.4 17.7y, EC, α	15.3 5.53y, EC, β^-
G2P	10.6 S	12.4 S	13.0 S
GA	-0.1 3.37d, EC	-2.3 S	-2.0 2.1E+15y, α

Sm	A = 149 (13.9)	A = 150 (7.4)	A = 152 (26.6)	A = 154 (22.6)
GN	5.9 8E+15y, α	8.0 S	8.3 87y, β^-	8.0 46.8h, β^-
GP	7.6 5.370d, β^- 41.3d, β^-, IT	8.3 53.1h, β^-	8.7 28.40h, β^-	9.0 5.3 min, β^-
G2N	14.0 1.06E+11y, α	13.9 8E+15y, α	13.9 S	13.8 S
GNP	13.5 2.623y, β^-	15.5 5.370d, β^- 41.3d, β^-, IT	16.6 2.68h, β^-	16.5 4.1 min, β^- 7.5 min, β^- 15 min, β^-
G2P	13.6 10.98d, β^-	14.2 S	15.7 S	16.9 11.4 min, β^-
GA	-1.9 S	-1.4 S	-0.2 S	1.2 S

See overleaf
for the graphs of europium

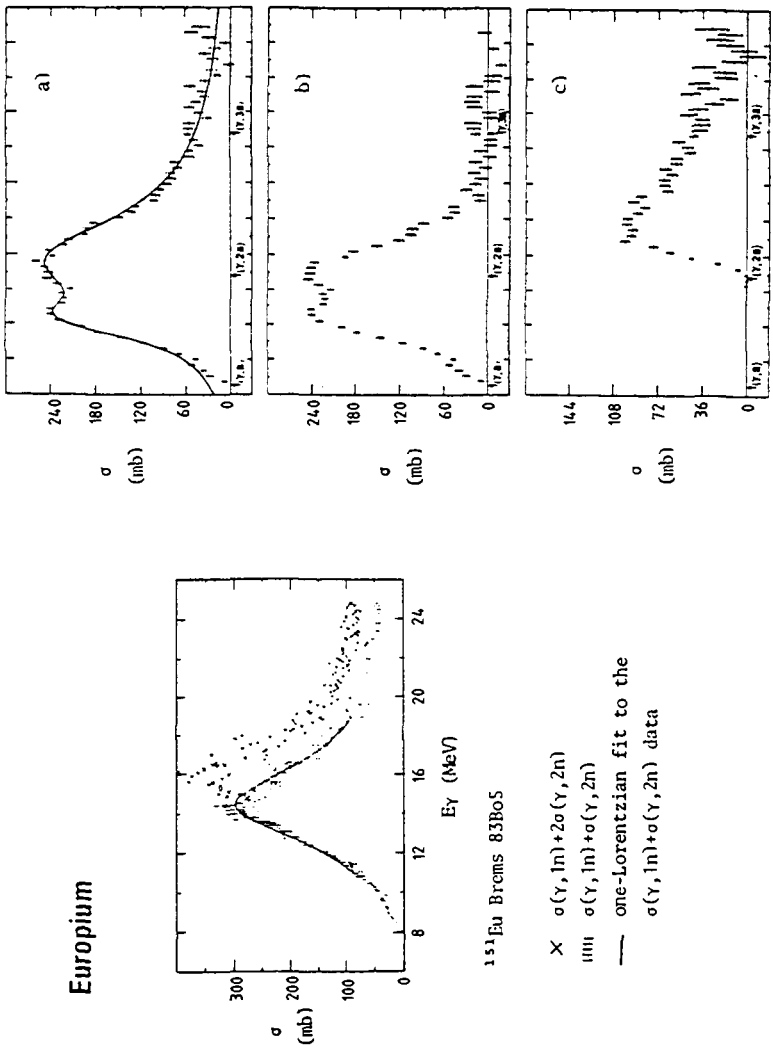
a)
b)
c)
σ (mb)
240
180
120
60
0
144
108
72
36
Europium
300
200
100
8
12
16
20
24
Eγ (MeV)
151Eu Brems 83Bo5
× σ(γ,1n)+2σ(γ,2n)
σ(γ,1n)+σ(γ,2n)
one-Lorentzian fit to the σ(γ,1n)+σ(γ,2n) data

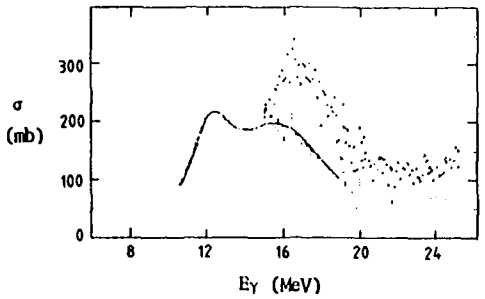

^{153}Eu Brems 83Bo5

X $\sigma(\gamma,1n)+2\sigma(\gamma,2n)$

IIIII $\sigma(\gamma,1n)+\sigma(\gamma,2n)$

— two-Lorentzian fit to the $\sigma(\gamma,1n)+\sigma(\gamma,2n)$ data

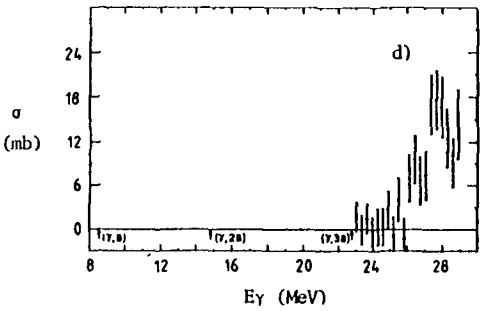

^{153}Eu Mono 75Be6 , 69Be1

a) $\sigma(\gamma,n_t)$

b) $\sigma(\gamma,n)+\sigma(\gamma pn)$

c) $\sigma(\gamma,2n)+\sigma(\gamma,p2n)$

d) $\sigma(\gamma,3n)$

Eu	A = 151 (47.9)	A = 153 (52.1)
GN	8.0 36y, EC 12.6h, β^-, EC, β^+	8.6 13.2y, EC, β^-, β^+ 9.3h, β^-, EC, β^+ 96 min, IT
GP	4.9 S	5.9 S
G2N	14.4 93.1d, EC	14.9 S
GNP	12.9 S	14.2 87y, β^-
G2P	13.2 53.1h, β^-	14.6 28.40h, β^-
GA	-2.0 2.623y, β^-	-0.3 53.1h, β^-

Gadolinium

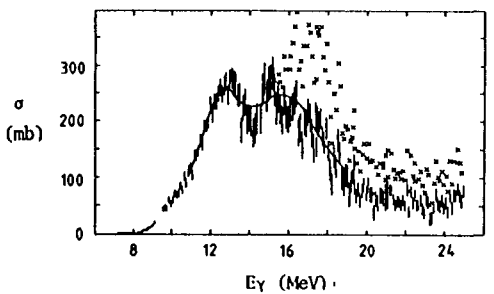

^{156}Gd Brems 83Bo5

X σ(γ,1n)+2σ(γ,2n)

σ(γ,1n)+σ(γ,2n)

— one-Lorentzian fit to the σ(γ,1n)+σ(γ,2n) data

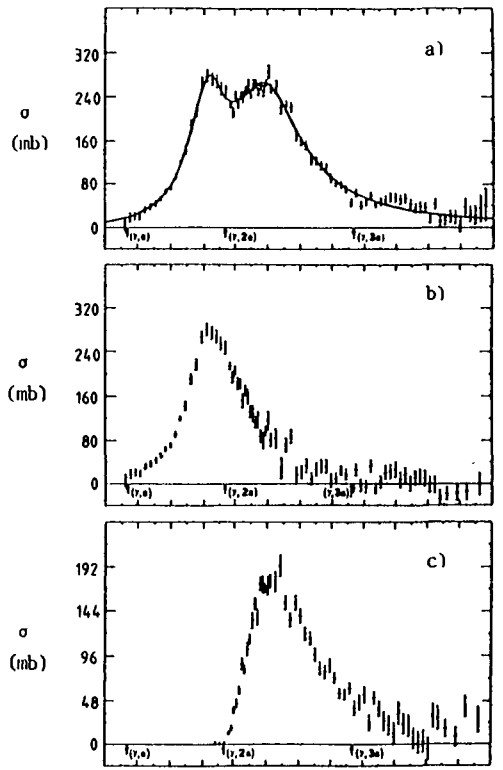

^{160}Gd Mono 75Be6 , 69Be1

a) $\sigma(\gamma,n_t)$

b) $\sigma(\gamma,n)+\sigma(\gamma,pn)$

c) $\sigma(\gamma,2n)+\sigma(\gamma,p2n)$

d) $\sigma(\gamma,3n)$

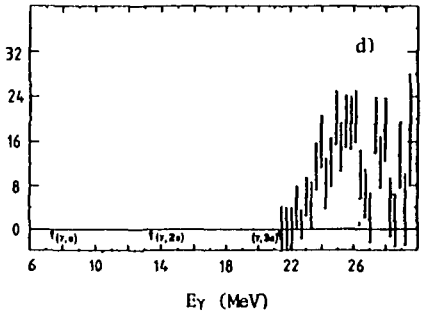

Gd	A = 152 (0.2)	A = 154 (2.1)	A = 155 (14.8)
GN	8.6 1.2E+2d, EC, α	8.7 2.416E+2d, EC	6.4 S
GP	7.4 S	7.6 S	7.6 8.5y, β^-, EC 46 min, IT
G2N	15.1 1.78E+6y, α	15.1 1.08E+14y, α	15.1 2.416E+2d, EC
GNP	15.3 36y, EC 12.6, β^-, EC, β^+	16.2 13.2y, EC, β^-, β^+ 9.3h, β^-, EC, β^+ 96 min, IT	14.1 S
G2P	12.2 S	13.5 S	14.1 46.8h, β^-
GA	-2.2 8E+15y, α	-0.9 S	-0.1 87y, β^-

Gd	A = 156 (20.6)	A = 157 (15.7)	A = 158 (24.8)	A = 160 (21.8)
GN	8.5 S	6.4 S	7.9 S	7.5 18.56h, β^-
GP	8.0 4.96y, β^-	8.0 15.11d, β^-	8.5 15.15h, β^-	9.3 18.07 min, β^-
G2N	15.0 S	14.9 S	14.3 S	13.4 S
GNP	16.2 8.5y, β^-, EC 46 min, IT	14.4 4.96y, β^-	16.0 15.11d, β^-	16.0 45.9 min, β^-
G2P	14.7 S	15.2 22.4 min, β^-	15.9 9.4h, β^-	* *
GA	0.2 S	0.7 46.8h, β^-	0.7 S	1.0 9.4h, β^-

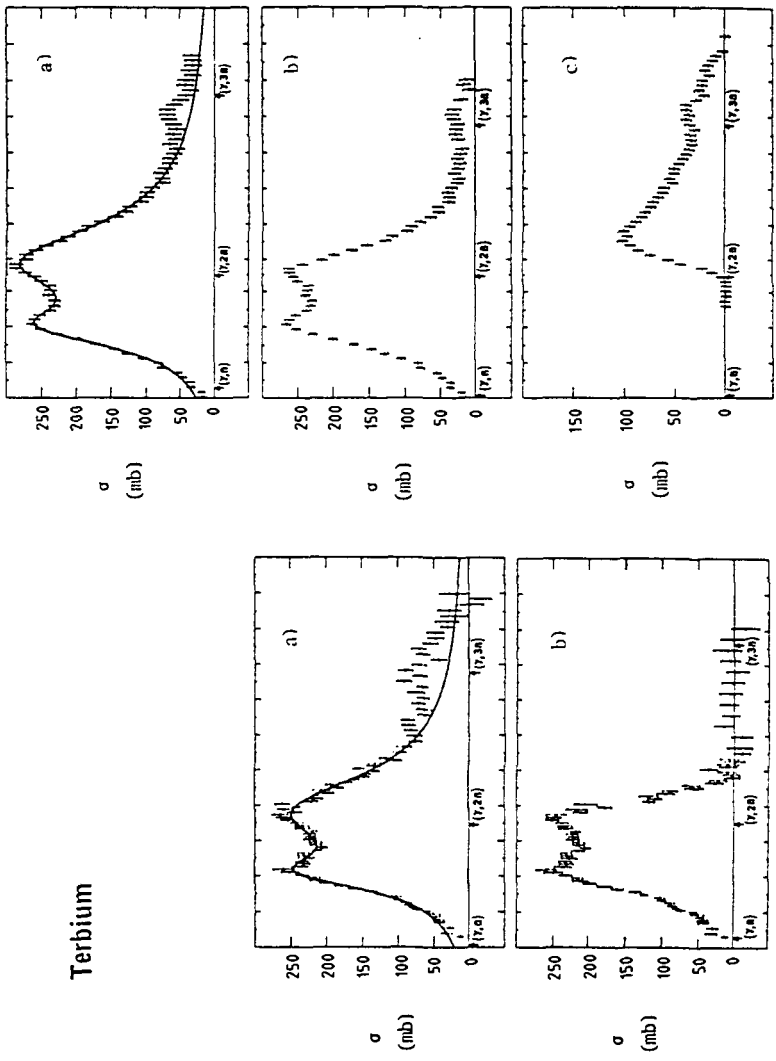
Terbium
a)
b)
c)
σ (mb)
250
200
150
100
50
0
(γ,n)
(γ,2n)
(γ,3n)

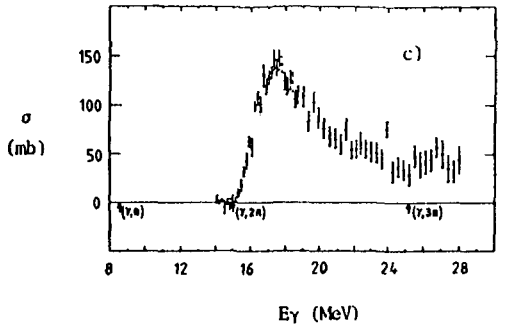

^{159}Tb Mono 75Bc6 , 64Br1

a) $\sigma(\gamma,n_t)$
b) $\sigma(\gamma,n)+\sigma(\gamma,pn)$
c) $\sigma(\gamma,2n)+\sigma(\gamma,p2n)$

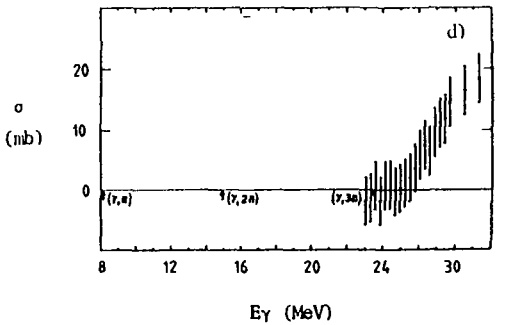

^{159}Tb Mono 75Be6 , 68Bc5

a) $\sigma(\gamma,n_t)$
b) $\sigma(\gamma,n)+\sigma(\gamma,pn)$
c) $\sigma(\gamma,2n)+\sigma(\gamma,p2n)$
d) $\sigma(\gamma,3n)$

Tb	A = 159 (100)
GN	8.1 1.5E+2y, EC, β^-
	10.5s, IT
GP	6.1 S
G2N	14.9 1.5E+2y, EC
GNP	14.0 S
G2P	14.6 15.15h, β^-
GA	0.1 4.96y, β^-

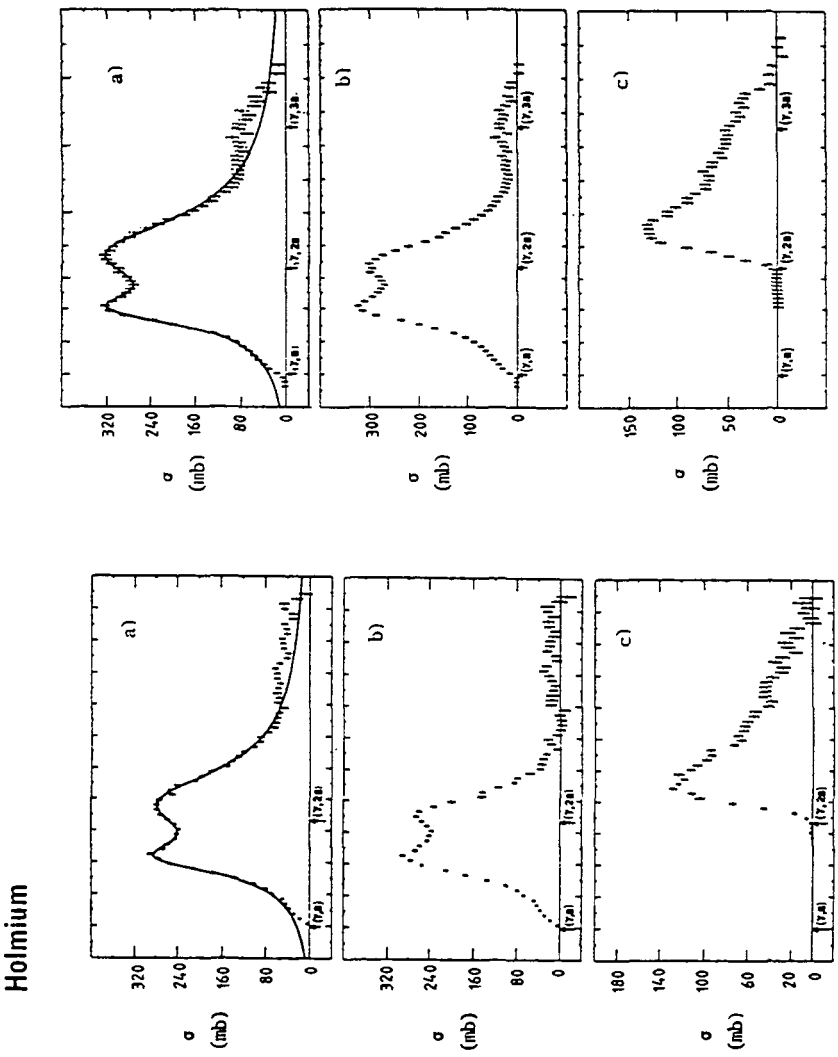
Holmium
a)
b)
c)
σ (mb)
(γ,n)
(γ,2n)
(γ,3n)

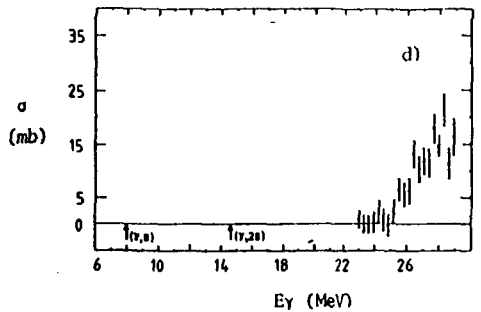

^{165}Ho Mono 75Be6 , 69Be1

a) $\sigma(\gamma,n_t)$
b) $\sigma(\gamma,n)+\sigma(\gamma,pn)$
c) $\sigma(\gamma,2n)+\sigma(\gamma,p2n)$
d) $\sigma(\gamma,3n)$

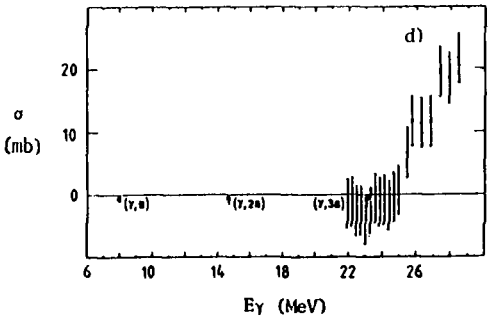

^{165}Ho Mono 75Be6 , 68Be5

a) $\sigma(\gamma,n_t)$
b) $\sigma(\gamma,n)+\sigma(\gamma,pn)$
c) $\sigma(\gamma,2n)+\sigma(\gamma,p2n)$
d) $\sigma(\gamma,3n)$

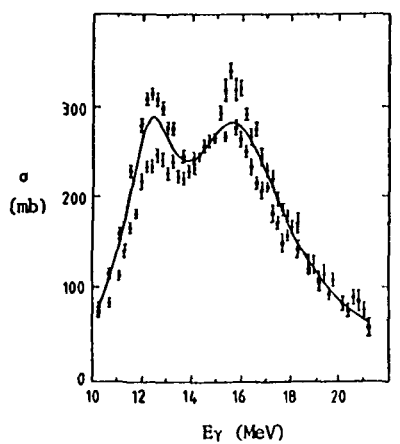

^{165}Ho (polarized); Annihilation γ 69Ke1

○ Target ∥ Beam
● Target ⊥ Beam

Ho	A = 165 (100)
GN	8.0 29.0 min, EC, β^-
	37 min, IT
GP	6.2 S
G2N	14.7 33y, EC
	1.09s, IT
GNP	13.9 S
G2P	14.8 19.5 min, β^-
GA	-0.1 6.90d, β^-

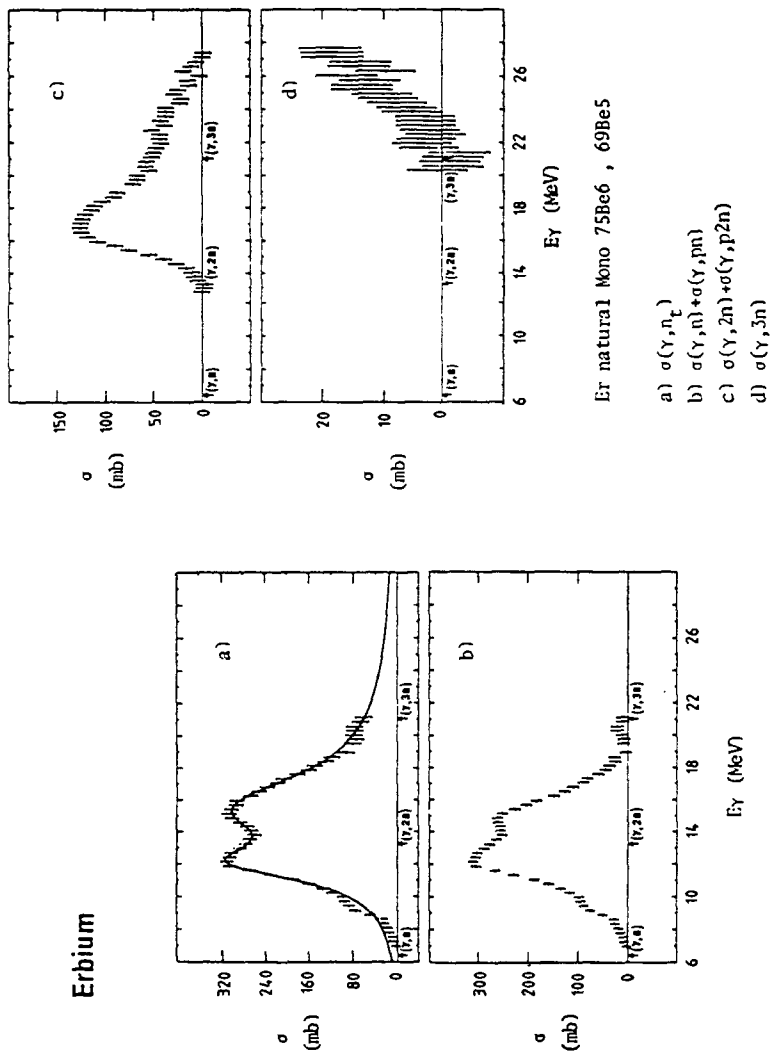
Erbium
a)
b)
c)
d)
σ (mb)
Eγ (MeV)
Er natural Mono 75Be6 , 69Be5
a) σ(γ,n_t)
b) σ(γ,n)+σ(γ,pn)
c) σ(γ,2n)+σ(γ,p2n)
d) σ(γ,3n)

Er	A = 162 (0.1)	A = 164 (1.6)
GN	9.2 3.24h, EC, β^+	8.9 75.1 min, EC, β^+
GP	6.4 2.48h, EC 6.7s, IT	6.9 33y, EC 1.09s, IT
G2N	16.5 28.58h, EC	15.8 S
GNP	14.9 25.6 min, EC, β^+ 5.02h, IT, β^+	15.3 15 min, EC, β^+ 68 min, IT, EC, β^+
G2P	11.2 S	12.3 S
GA	-1.7 S	-1.3 S

Er	A = 166 (33.4)	A = 167 (22.9)	A = 168 (27.1)	A = 170 (14.9)
GN	8.5 10.34h, EC	6.4 S	7.8 S; 2.28s, IT	7.3 9.40d, β^-
GP	7.3 S	7.5 26.83h, β^- 1.2E+3y, β^-	8.0 3.1h, β^-	8.6 4.8 min, β^-
G2N	15.1 S	14.9 10.34h, EC	14.2 S	13.3 S
GNP	15.3 29.0 min, EC, β^- 37 min, IT	13.8 S	15.3 26.83h, β^- 1.2E+3y, β^-	15.3 2.98 min, β^-
G2P	13.5 S	14.3 2.33h, β^- 1.26 min, IT, β^-	15.0 81.5h, β^-	* *
GA	-0.8 S	-0.7 S	-0.5 S	0.0 81.5h, β^-

Lutetium

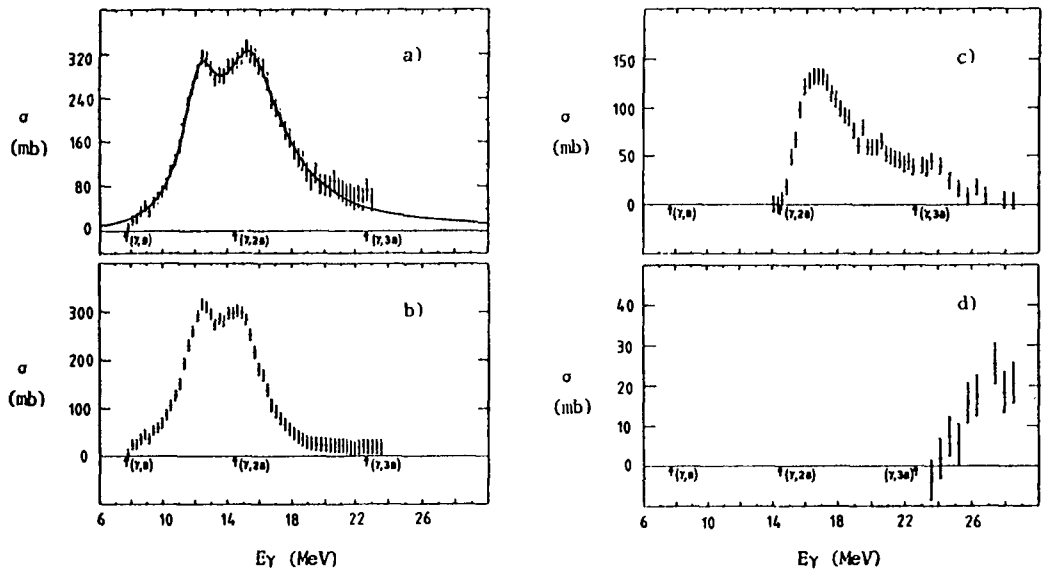

Lu	A = 175 (97.39)	A = 176 (2.61)
GN	7.7 3.31y, EC, β^+ 1.42E+2d, IT, EC	6.3 S
GP	5.5 S	6.0 4.19d, β^-
G2N	14.4 4.99E+2d, EC	14.0 3.31y, EC, β^+ 1.42E+2d, IT, EC
GNP	13.0 S	11.8 S
G2P	13.5 8.24h, β^-	14.1 5.4 min, β^-
GA	-1.6 1.92y, β^-	-1.6 63.6h, β^-

^{175}Lu Mono 75Be6 , 69Be5

a) $\sigma(\gamma,n_t)$
b) $\sigma(\gamma,n)+\sigma(\gamma,pn)$
c) $\sigma(\gamma,2n)+\sigma(\gamma,p2n)$
d) $\sigma(\gamma,3n)$

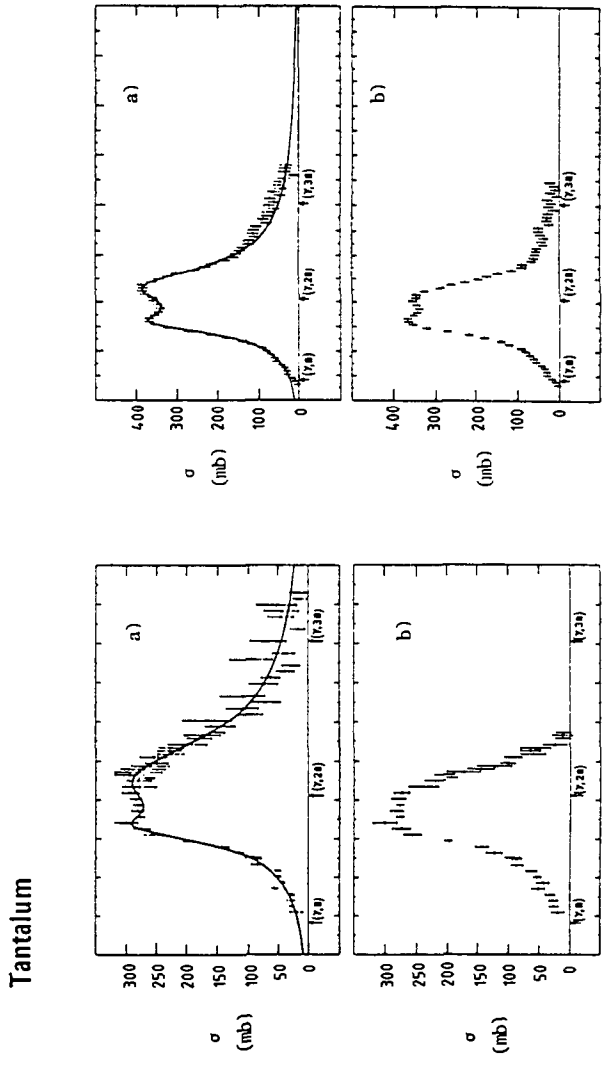
Tantalum
a)
b)
σ (mb)
300
250
200
150
100
50
0
400
300
200
100
0

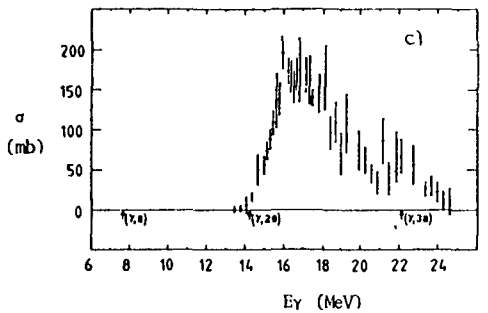

^{181}Ta Mono 75Be6 , 63Br1

a) $\sigma(\gamma,n_t)$
b) $\sigma(\gamma,n)+\sigma(\gamma,pn)$
c) $\sigma(\gamma,2n)+\sigma(\gamma,p2n)$

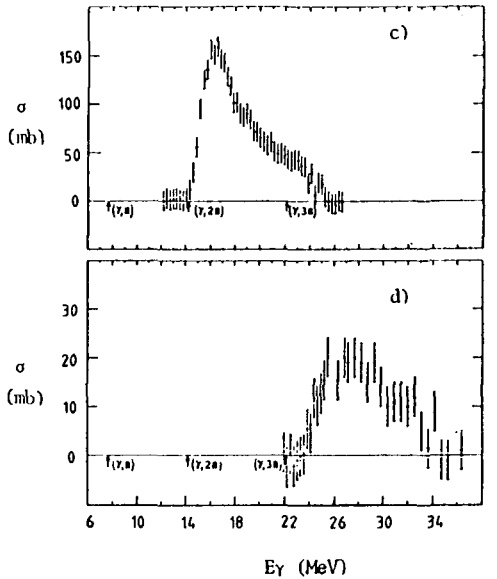

Ta	A = 180 (0.012)	A = 181 (99.988)
GN	6.6 6.65E+2d, EC	7.6 >E+13y, β^-, EC 8.1h, EC, β^-
GP	5.7 S; 18.7s, IT; 25.1d, IT	5.9 S
G2N	14.5 9.25 min, EC, β^+	14.2 6.65E+2d, EC
GNP	11.8 S; 4.0s, IT; 31y, IT	13.3 S; 18.7s, IT; 25.1d, IT
G2P	13.3 28.4 min, β^- 23 min, β^-	13.9 4.59h, β^-
GA	-2.1 3.79E+10y, β^- 3.68h, β^-	-1.5 6.71d, β^- 1.605E+2d, β^-, IT

^{181}Ta Mono 75Be6 , 68Be5

a) $\sigma(\gamma,n_t)$
b) $\sigma(\gamma,n)+\sigma(\gamma,pn)$
c) $\sigma(\gamma,2n)+\sigma(\gamma,p2n)$
d) $\sigma(\gamma,3n)$

Tungsten

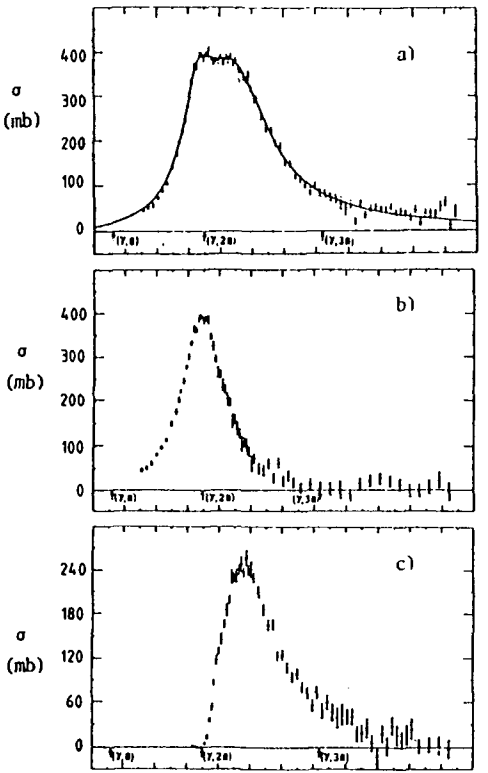

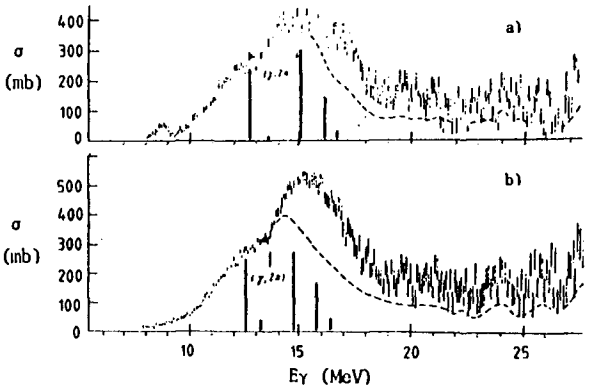

W Brems 73So14

a) ^{182}W $\sigma(\gamma,n)+\sigma(\gamma,pn)+2\sigma(\gamma,2n)$

b) ^{184}W $\sigma(\gamma,n)+\sigma(\gamma,pn)+2\sigma(\gamma,2n)$

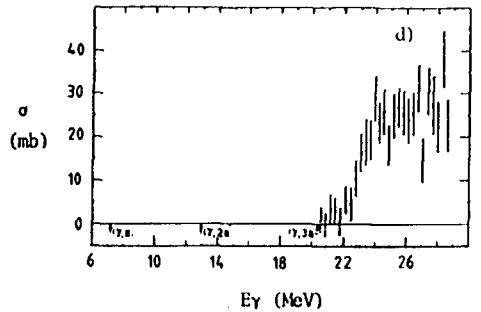

^{186}W Mono 75Be6 , 69Be1

a) $\sigma(\gamma,n_t)$
b) $\sigma(\gamma,n)+\sigma(\gamma,pn)$
c) $\sigma(\gamma,2n)+\sigma(\gamma,p2n)$
d) $\sigma(\gamma,3n)$

W	A = 180 (0.1)
GN	8.5 37.5 min, EC 6.4 min, IT, EC
GP	6.6 6.65E+2d, EC
G2N	15.4 21.5d, EC
GNP	14.5 9.25 min, EC, β^+ 2.4h, EC
G2P	11.8 S; 4.0s, IT; 31y, IT
GA	-2.5 S

W	A = 182 (26.3)	A = 183 (14.3)	A = 184 (30.7)	A = 186 (28.6)
GN	8.1 1.210E+2d, EC	6.2 S	7.4 S; 5.3s, IT	7.2 75.1d, β^- 1.66 min, IT
GP	7.1 S	7.2 1.150E+2d, β^- 0.28s, IT 15.8 min, IT	7.7 5.0d, β^-	8.4 50 min, β^-
G2N	14.7 S	14.2 1.210E+2d, EC	13.6 S	13.0 S
GNP	14.7 >E+13y, β^-, EC 8.1h, EC, β^-	13.3 S	14.6 1.150E+2d, β^- 0.28s, IT 15.8 min,	15.2 8.7h, β^-
G2P	13.0 S; 5.5h, IT	13.5 42.45d, β^-	14.3 9E+6y, β^- 62 min, β^-, IT	15.6 4.12h, β^-
GA	-1.8 S; 4.0s, IT; 31y, IT	-1.7 S; 18.7s, IT; 25.1d, IT	-1.7 S	-1.0 9E+6y, β^- 62 min, β^-, IT

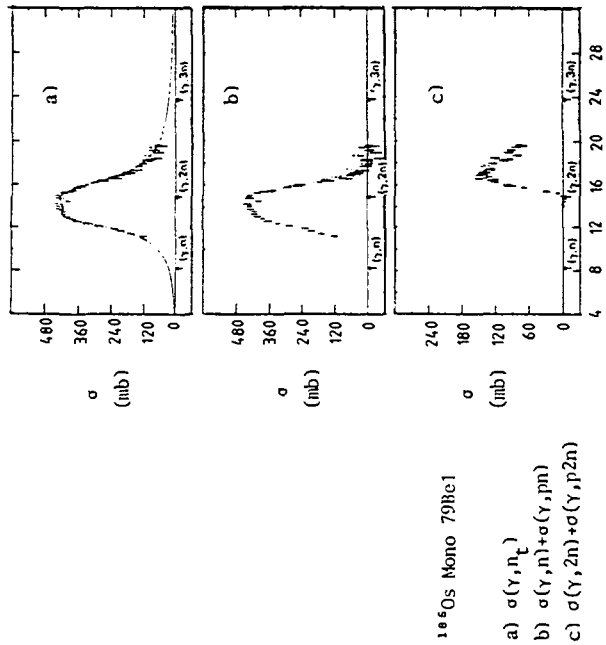

Osmium

^{186}Os Mono 79Be1

a) $\sigma(\gamma,n_t)$
b) $\sigma(\gamma,n)+\sigma(\gamma,pn)$
c) $\sigma(\gamma,2n)+\sigma(\gamma,p2n)$

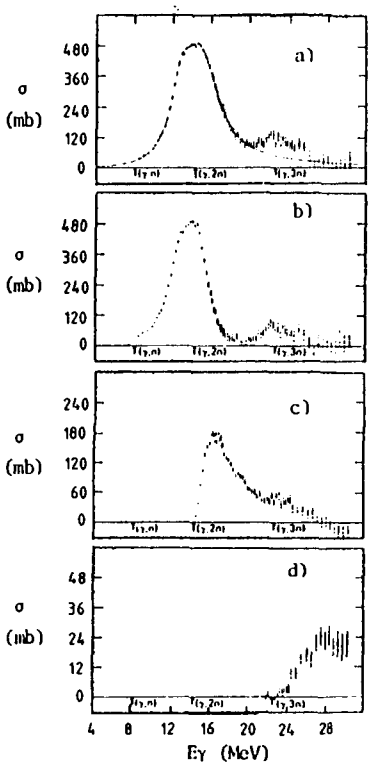

^{188}Os Mono 79Be1

a) $\sigma(\gamma,n_t)$
b) $\sigma(\gamma,n)+\sigma(\gamma,pn)$
c) $\sigma(\gamma,2n)+\sigma(\gamma,p2n)$
d) $\sigma(\gamma,3n)$

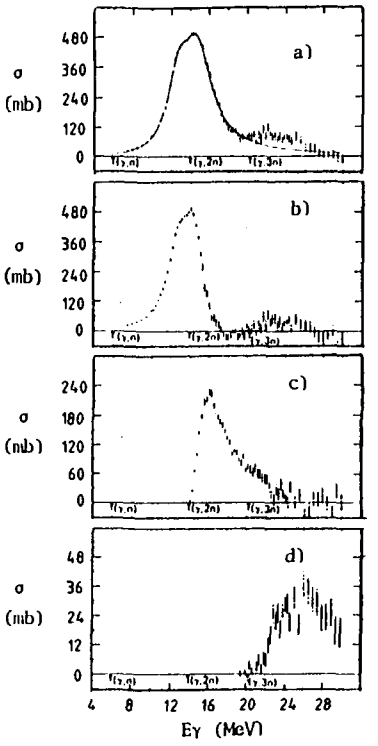

^{189}Os Mono 79Be1

a) $\sigma(\gamma,n_t)$
b) $\sigma(\gamma,n)+\sigma(\gamma,pn)$
c) $\sigma(\gamma,2n)+\sigma(\gamma,p2n)$
d) $\sigma(\gamma,3n)$

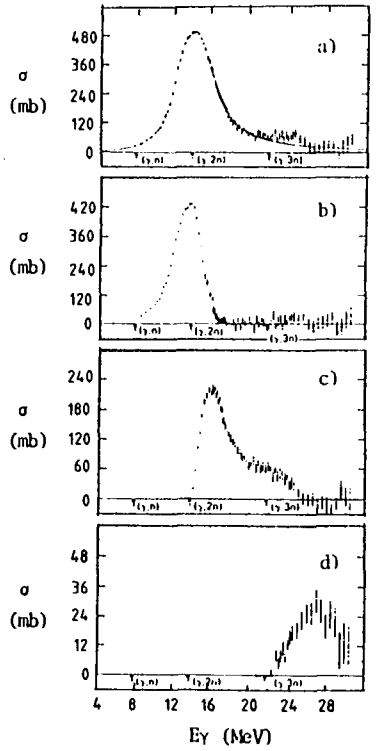

^{190}Os Mono 79Be1

a) $\sigma(\gamma,n_t)$
b) $\sigma(\gamma,n)+\sigma(\gamma,pn)$
c) $\sigma(\gamma,2n)+\sigma(\gamma,p2n)$
d) $\sigma(\gamma,3n)$

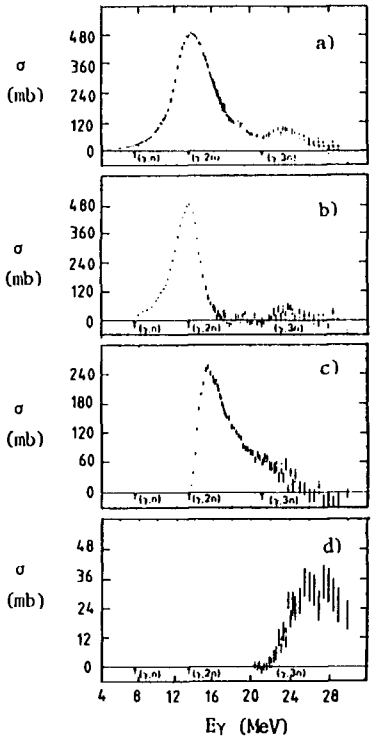

^{192}Os Mono 79Be1

a) $\sigma(\gamma,n_t)$
b) $\sigma(\gamma,n)+\sigma(\gamma,pn)$
c) $\sigma(\gamma,2n)+\sigma(\gamma,p2n)$
d) $\sigma(\gamma,3n)$

Os	A = 184 (0.02)	A = 186 (1.58)	A = 187 (1.6)
GN	8.9 13.0h, EC, β^+ 9.9h, EC, IT	8.3 93.6d, EC	6.3 2E+15y, α
GP	5.7 71d, EC	6.5 S	6.6 90.64h, β^-, EC 2E+5y, IT
G2N	16.1 22.1h, EC	14.9 S	14.6 93.6d, EC
GNP	14.2 12.7h, EC, β^+ 64h, EC	14.3 38.0d, EC 1.69E+2d, IT, EC	12.8 S
G2P	10.5 S	11.9 S	12.4 75.1d, β^- 1.66 min, IT
GA	-3.1 S	-2.8 S	-2.7 S; 5.3s, IT

Os	A = 188 (13.3)	A = 189 (16.1)	A = 190 (26.4)	A = 192 (41.0)
GN	8.0 S	5.9 S	7.8 S; 5.7h, IT	7.6 15.4d, β^- 13.1h, IT
GP	7.2 4.3E+10y, β^-	7.3 16.98h, β^- 18.7 min, IT	8.0 24.3h, β^-	8.8 9.8 min, β^-
G2N	14.3 2E+15y, α	13.9 S	13.7 S	13.3 S; 9.9 min, IT
GNP	14.6 90.64h, β^+, EC 2E+5y, IT	13.1 4.3E+10y, β^-	15.1 16.98h, β^- 18.7 min, IT	15.7 3.1 min, β^- 3.2h, β^-. IT
G2P	13.2 S	13.7 23.85h, β^-	14.6 69.4d, β^-	16.2 30 min, β^-
GA	-2.1 S	-2.0 75.1d, β^- 1.66 min, IT	-1.4 S	-0.4 69.4d, β^-

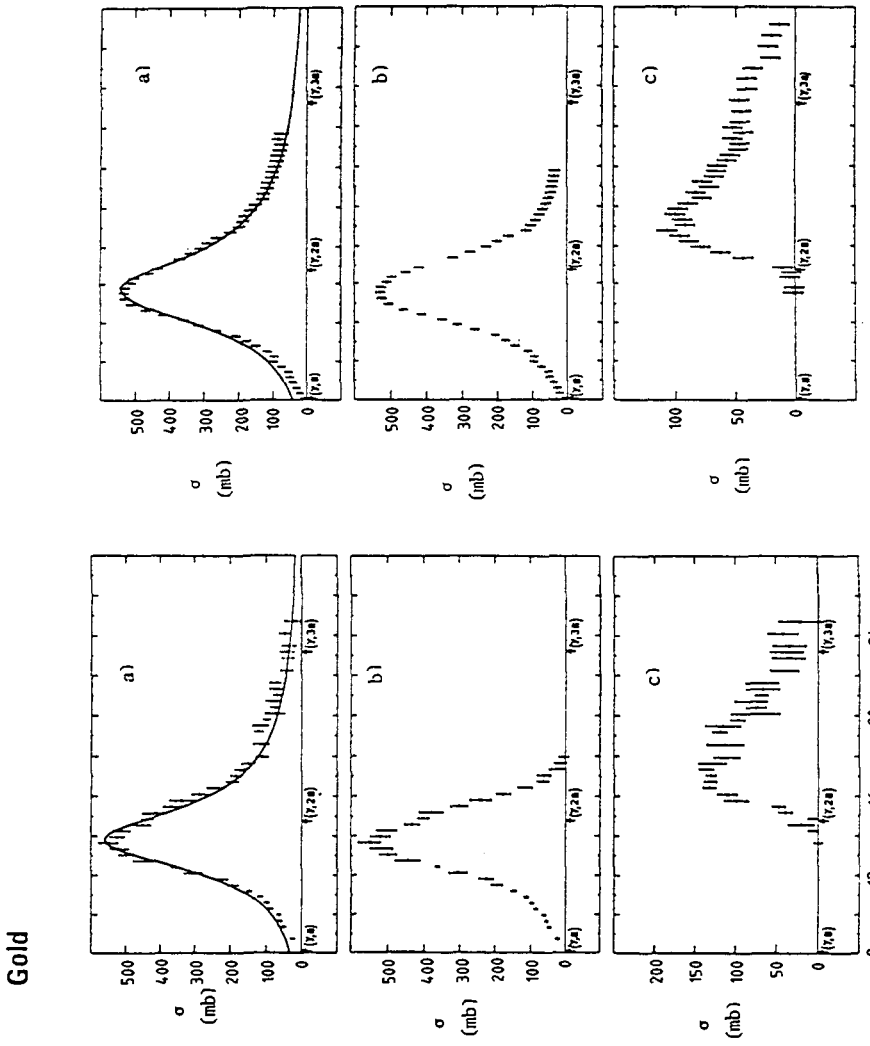
Gold
a)
b)
c)
σ (mb)
Eγ (MeV)

^{197}Au Mono 75Be6 , 62Fu101

a) $\sigma(\gamma,n_t)$
b) $\sigma(\gamma,n)+\sigma(\gamma,pn)$
c) $\sigma(\gamma,2n)+\sigma(\gamma,p2n)$

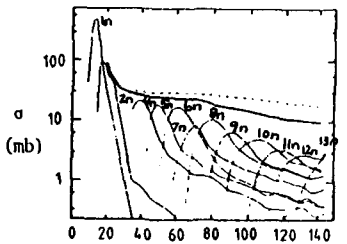

^{197}Au 79Pr5

——— $\sigma(\gamma,n_i)$
----- $\Sigma\sigma_i$ (all reaction channels)
——— $\Sigma\sigma(\gamma,n_i)$

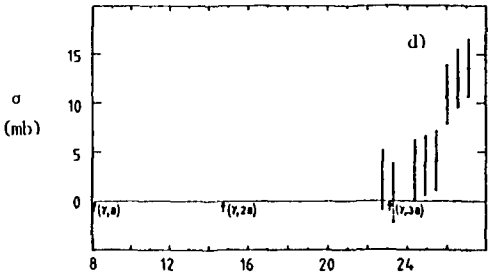

^{197}Au Mono 75Be6 , 70Ve5

a) $\sigma(\gamma,n_t)$
b) $\sigma(\gamma,n)+\sigma(\gamma,pn)$
c) $\sigma(\gamma,2n)+\sigma(\gamma,p2n)$
d) $\sigma(\gamma,3n)$

Au	A = 197 (100)
GN	8.1 6.18d, EC, β^+, β^-
	8.2s, IT; 9.7h, IT
GP	5.8 S
G2N	14.8 1.829E+2d, EC
	30.6s, IT
GNP	13.7 S; 4.02d, IT
G2P	13.9 2.3h, β^-
	3.8h, β^-
GA	-0.9 S; 10.6d, IT

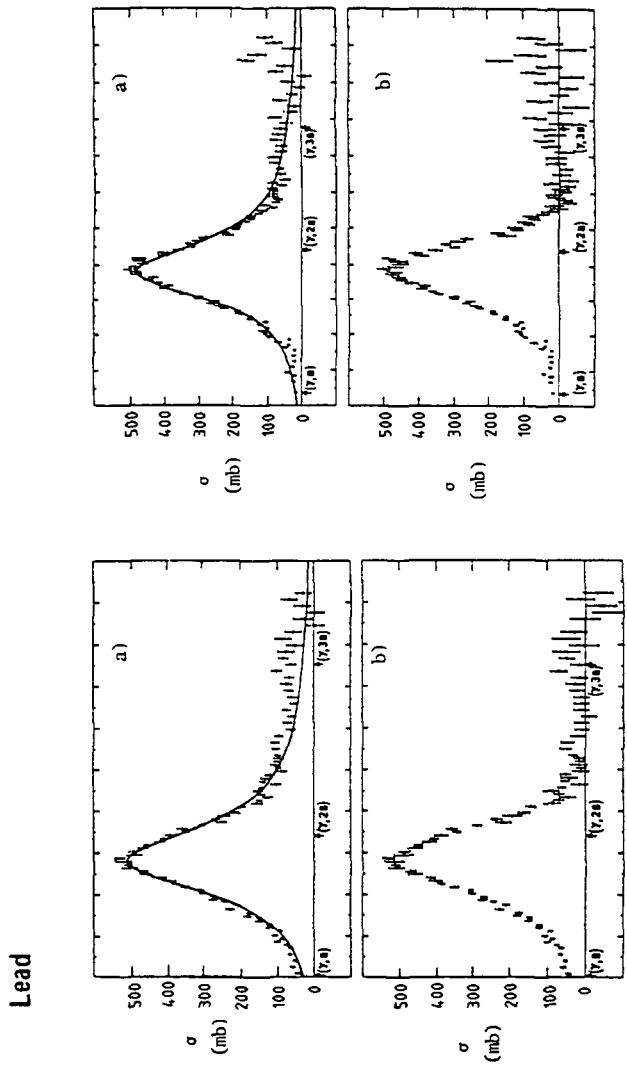
Lead
a)
b)
σ (mb)
500
400
300
200
100
0
(γ,n)
(γ,2n)
(γ,3n)

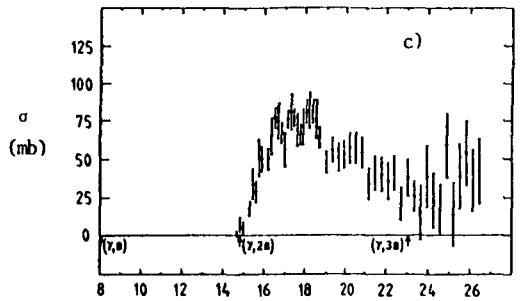

^{206}Pb Mono 75Be6 , 64Ha1

a) $\sigma(\gamma,n_t)$
b) $\sigma(\gamma,n)+\sigma(\gamma,pn)$
c) $\sigma(\gamma,2n)+\sigma(\gamma,p2n)$

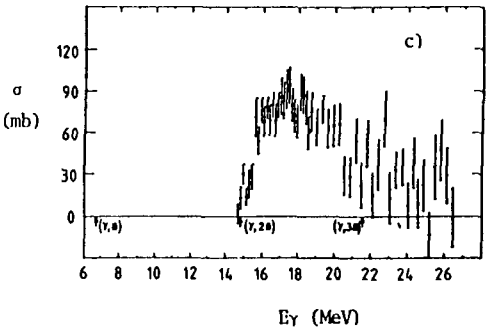

^{207}Pb Mono 75Be6 , 64Ha1

a) $\sigma(\gamma,n_t)$
b) $\sigma(\gamma,n)+\sigma(\gamma,pn)$
c) $\sigma(\gamma,2n)+\sigma(\gamma,p2n)$

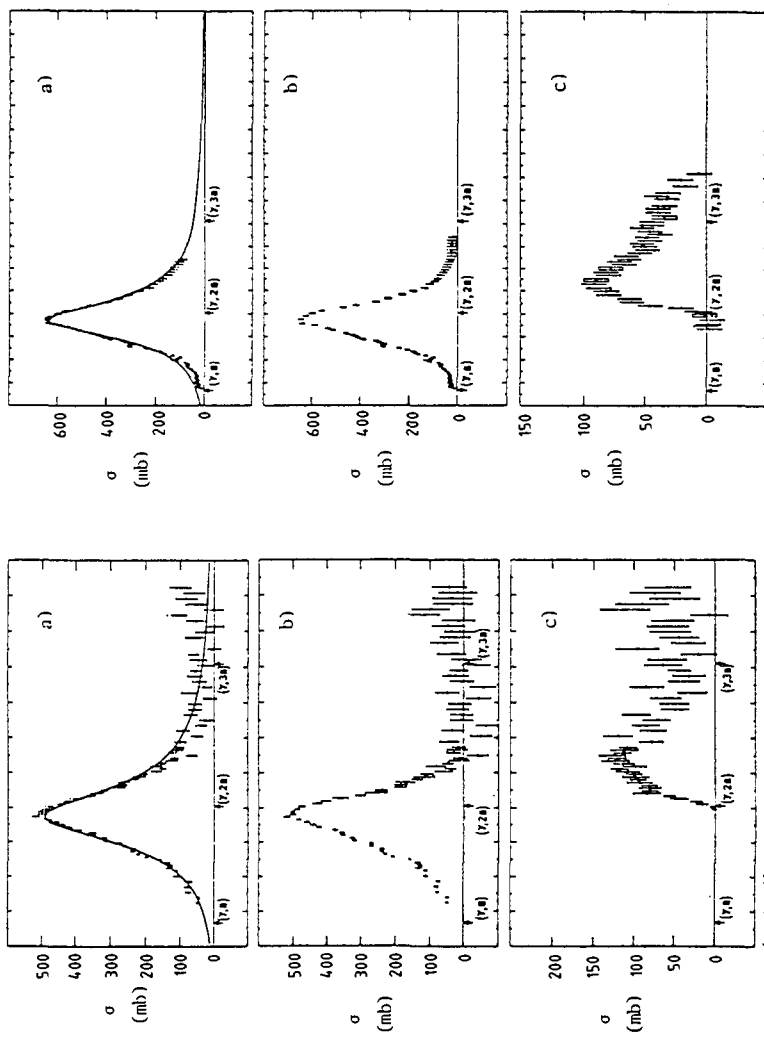
a)
b)
c)
σ (mb)
Eγ (MeV)

^{208}Pb Mono 75Be6 , 64Ha1

a) $\sigma(\gamma,n_t)$
b) $\sigma(\gamma,n)+\sigma(\gamma,pn)$
c) $\sigma(\gamma,2n)+\sigma(\gamma,p2n)$

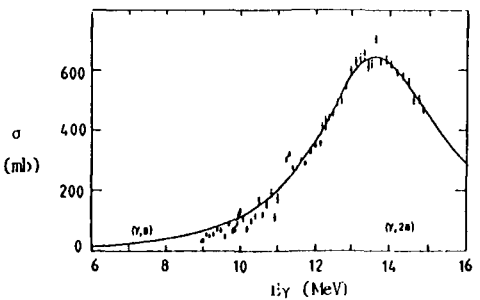

^{208}Pb Mono 75Be6 , 72Yo

$\sigma(\gamma,n_t)$

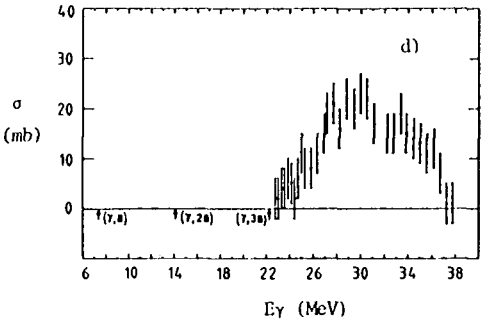

^{208}Pb Mono 75Be6 , 70Ve5

a) $\sigma(\gamma,n_t)$
b) $\sigma(\gamma,n)+\sigma(\gamma,pn)$
c) $\sigma(\gamma,2n)+\sigma(\gamma,p2n)$
d) $\sigma(\gamma,3n)$

Pb	A = 204 (1.4)	A = 206 (24.1)	A = 207 (22.1)	A = 208 (52.4)
GN	8.4 52.02h, EC 6.1s, IT 0.48s, IT	8.1 1.4E+7y, EC	6.7 S	7.4 S; 0.81s, IT
GP	6.6 S	7.3 S	7.5 4.18 min, β^- 3.6 min, IT	8.0 4.79 min, β^- 1.3s, IT
G2N	15.2 3E+5y, EC 3.62h, IT, EC	14.8 S; 66.9 min, IT	14.8 1.4E+7y, EC	14.1 S
GNP	14.4 12.23d, EC	14.8 3.77y, β^-, EC	14.0 S	14.9 4.18 min, β^- 3.6 min, IT
G2P	12.3 S	13.7 S	14.7 5.2 min, β^-	15.4 8.2 min, β^-
GA	-2.0 S	-1.1 S	-0.4 46.76d, β^-	-0.5 S

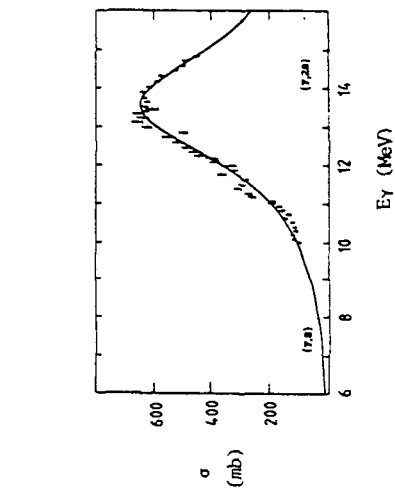
σ (mb)
600
400
200
6
8
10
12
14
Eγ (MeV)
209Bi Mono 75Be6 , 72Yo
σ(γ,nt)

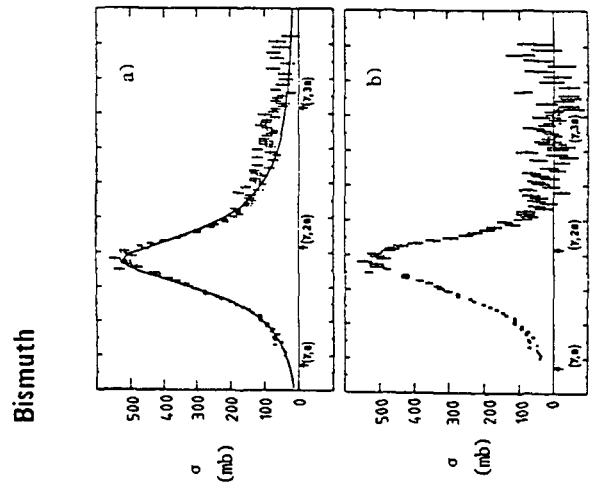
Bismuth
a)
b)
σ (mb)
500
400
300
200
100
0

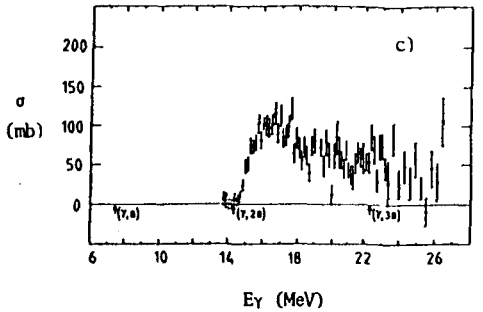

^{209}Bi Mono 75Be6 , 64Ha1

a) $\sigma(\gamma,n_t)$
b) $\sigma(\gamma,n)+\sigma(\gamma,pn)$
c) $\sigma(\gamma,2n)+\sigma(\gamma,p2n)$

Bi	A = 209 (100)	
GN	7.5	3.68E+5y, EC
GP	3.8	S
G2N	14.4	38y, EC, β^+
GNP	11.2	S; 0.81s, IT
G2P	0.8	4.79 min, β^- 1.3s, IT
GA	-3.1	S

Thorium

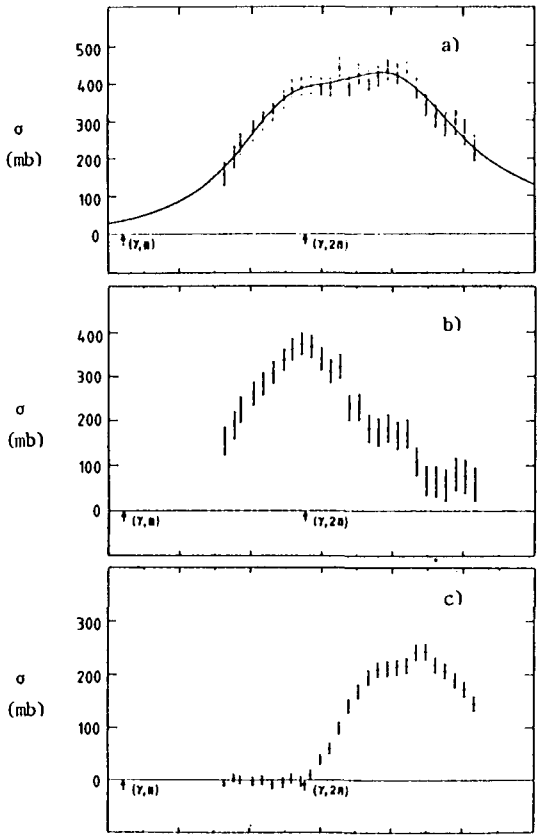

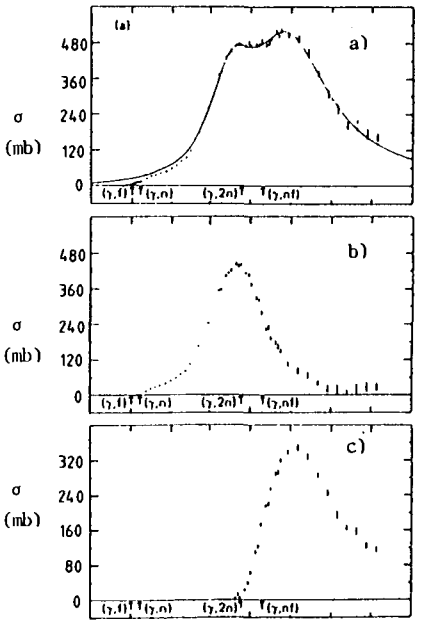

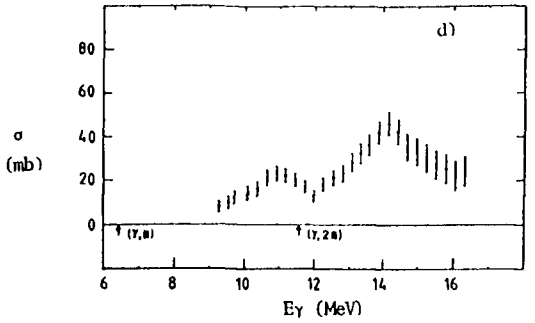

^{232}Th Mono 75Be6 , 73Ve5

a) $\sigma(\gamma,n_t)$
b) $\sigma(\gamma,n)+\sigma(\gamma,pn)$
c) $\sigma(\gamma,2n)+\sigma(\gamma,p2n)$
d) $\sigma(\gamma,f)$

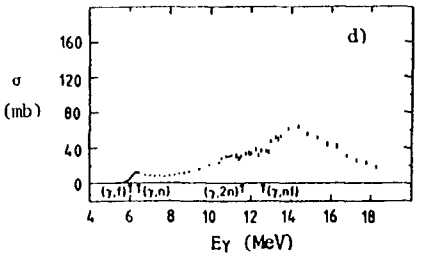

^{232}Th Mono 80Ca1

a) $\sigma(\gamma,n_t)$
b) $\sigma(\gamma,n)+\sigma(\gamma,pn)$
c) $\sigma(\gamma,2n)+\sigma(\gamma,p2n)$
d) $\sigma(\gamma,f)$

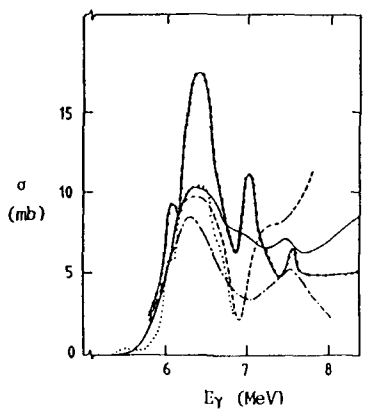

^{232}Th 81Le43

$\sigma(\gamma,f)$ Annihilation γ 80Ca1
$\sigma(\gamma,f)$ Compton γ 72Kh5
$\sigma(\gamma,f)$ Compton γ 73Ve5
$\sigma(\gamma,f)$ Tagged γ 75Ax8
$\sigma(\gamma,f)$ Brems 782u14

Th	A = 232 (100)
GN	6.4 25.52h, β^-
GP	7.8 7.5 min, β^-
G2N	11.6 8.0E+4y, α
GNP	13.7 1.22E+2s, β^-
G2P	13.7 93 min, β^-
GA	-4.1 5.77y, β^-

Uranium

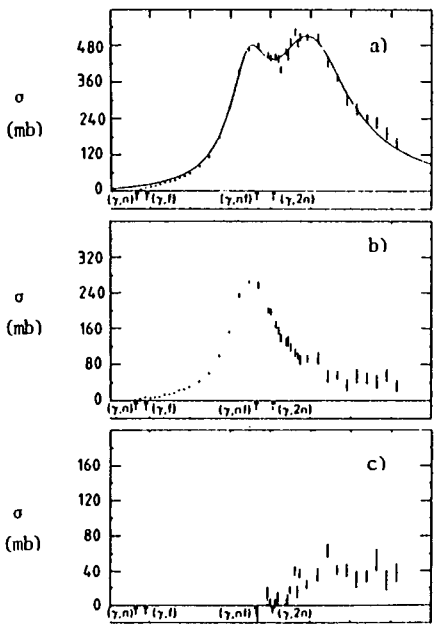

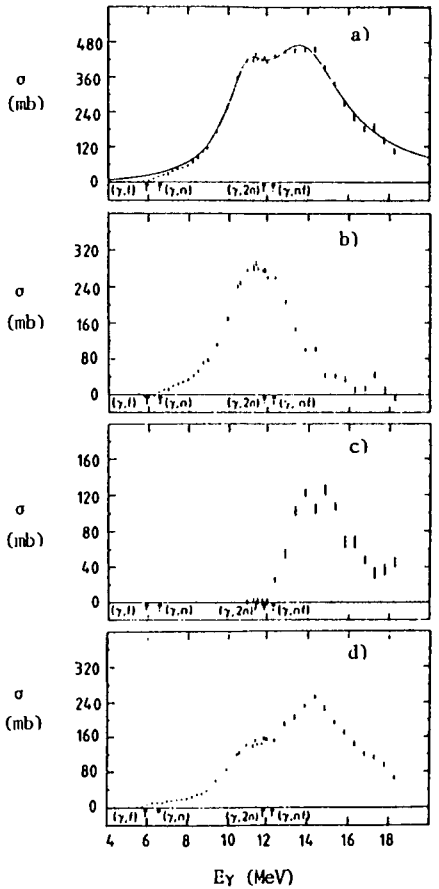

^{236}U Mono 80Ca1

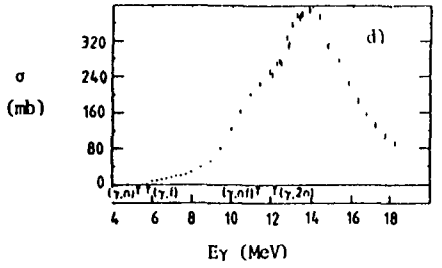

^{235}U Mono 80Ca1

a) $\sigma(\gamma,n_t)$
b) $\sigma(\gamma,n)+\sigma(\gamma,pn)$
c) $\sigma(\gamma,2n)+\sigma(\gamma,p2n)$
d) $\sigma(\gamma,f)$

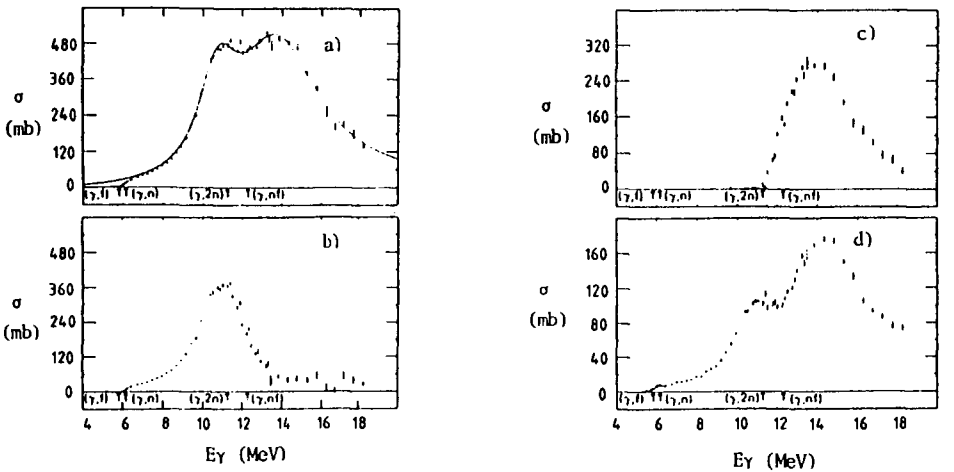

^{238}U Mono 80Ca1

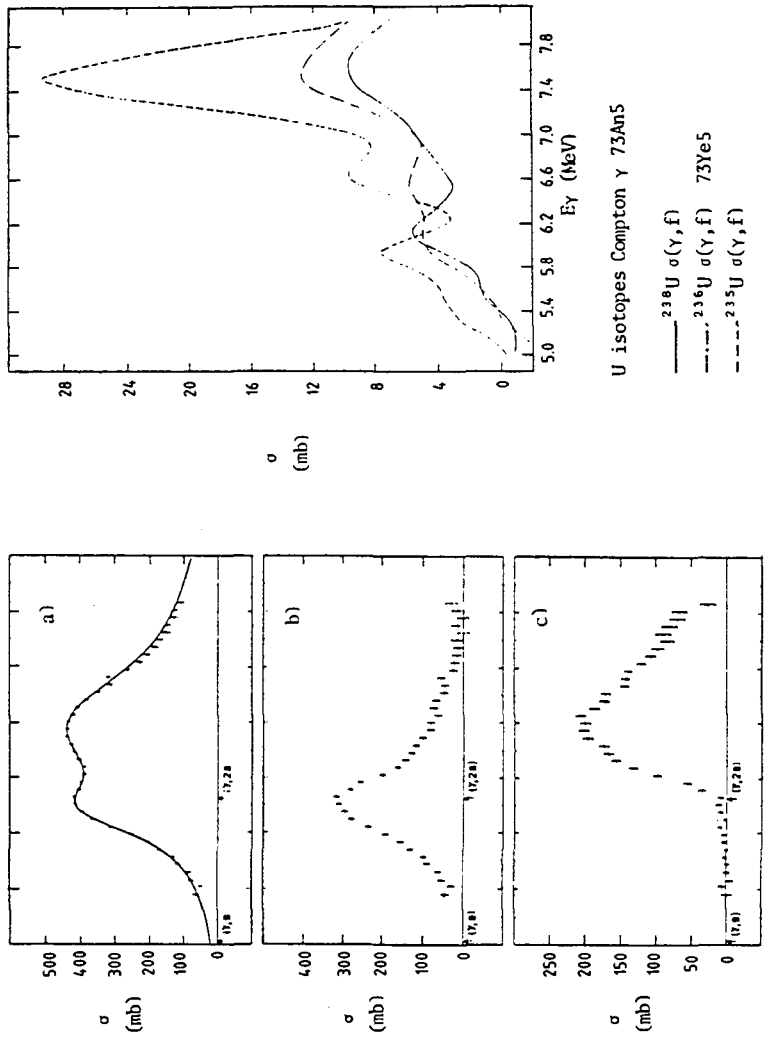
a)
b)
c)
σ (mb)
σ (mb)
σ (mb)
U isotopes Compton γ 73An5
^{238}U σ(γ,f)
^{236}U σ(γ,f) 73Ye5
^{235}U σ(γ,f)
σ (mb)
Eγ (MeV)

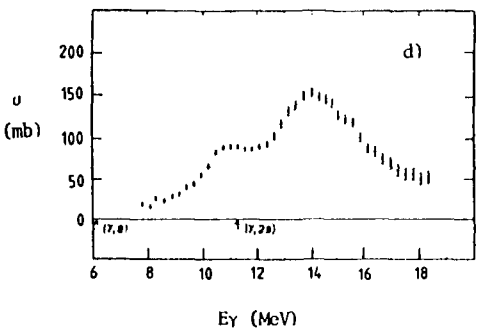

^{238}U Mono 75Be6 , 73Ve5

a) $\sigma(\gamma,n_t)$
b) $\sigma(\gamma,n)+\sigma(\gamma,pn)$
c) $\sigma(\gamma,2n)+\sigma(\gamma,p2n)$
d) $\sigma(\gamma,f)$

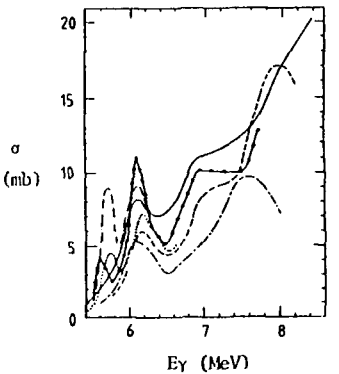

^{238}U 81Le43

—— $\sigma(\gamma,f)$ Annihilation γ 80Ca1
---- $\sigma(\gamma,f)$ Compton γ 72Kh5
—·— $\sigma(\gamma,f)$ Compton γ 73An5
—•— $\sigma(\gamma,f)$ Tagged γ 75Ax8
····· $\sigma(\gamma,f)$ Brems 78Zu14
—·—· $\sigma(\gamma,f)$ Brems 78A15

U	A = 234 (0.005)	A = 235 (0.720)	A = 238 (99.275)
GN	6.8 1.59E+5y, α	5.3 2.446E+5y, α	6.1 6.75d, β^-
GP	6.6 26.95d, β^-	6.7 6.75h, β^-	7.6 8.7 min, β^-
		1.175 min, IT	
G2N	12.6 71.7y, α	12.1 1.59E+5y, α	11.3 2.34E+7y, α
			1.16E-7s, sf
GNP	13.1 1.3d, β^-	11.9 26.95d, β^-	13.6 9.1 min, β^-
G2P	11.9 1.41E+10y, α	12.4 22.3 min, β^-	* 38 min, β^-
GA	-4.9 8.0E+4y, α	-4.7 25.52h, β^-	-4.3 24.10d, β^-

Neptunium

^{237}Np Mono 75Be6 , 73Ve5

a) $\sigma(\gamma,n_t)$
b) $\sigma(\gamma,n)+\sigma(\gamma,pn)$
c) $\sigma(\gamma,2n)+\sigma(\gamma,p2n)$
d) $\sigma(\gamma,f)$

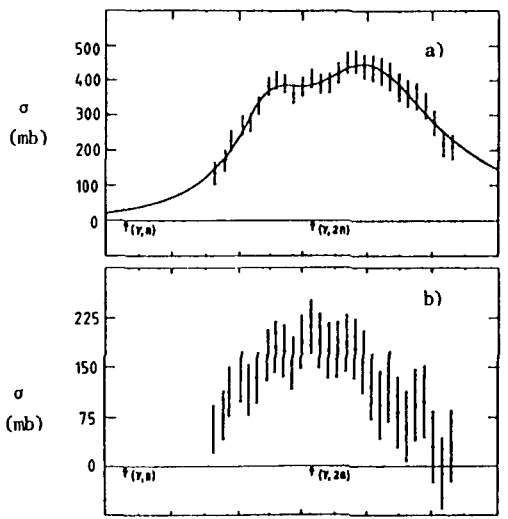

Np	A = 237 (---)
GN	6.6 22.5h, EC, β^-
GP	4.9 2.341E+7y, α
	1.16E-7s, sf
G2N	12.3 3.96E+2d, EC, α
GNP	11.4 7.04E+8y, α
	26 min, IT
G2P	12.0 24.2 min, β^-
GA	-5.0 26.95d, β^-

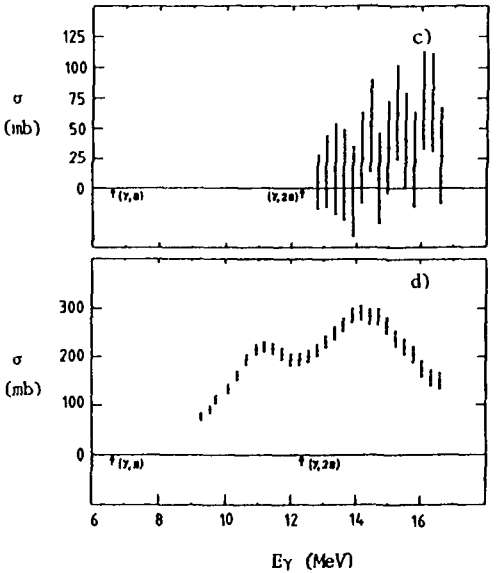

REFERENCES TO SECTION 4

54Fe1 PHYS. REV. 95(1954)776 G.A. Ferguson et al
57Co1 PHYS. REV. 106(1957)300 B.C. Cook
61Ge1 PHYS. REV. 144(1961)834 H.M. Gerstenberg et al
61Gr16 CAN. J. PHYS. 39(1961)1397 G.M. Griffiths et al
62Do1 PHYS. REV. 127(1962)1746 W.R. Dodge et al
62Fu1 PHYS. REV. 126(1962)2345 S.C. Fultz et al
62Fu101 PHYS. REV. 127(1962)1273 S.C. Fultz et al
63Br1 PHYS. REV. 129(1963)2723 R.L. Bramblett et al
63Go13 PHYS. LETT. 5(1963)149 A.N. Gorbunov et al
63Zu1 PHYS. REV. 132(1963)751 R.W. Zurmuhle et al
64Ba5 NUCL. PHYS. 54(1964)549 J.E.E. Baglin et al
64Br1 PHYS. REV. 133(1964)B869 R.L. Bramblett et al
64De18 SOV. PHYS. JETP 19(1964)1007 V.P. Denisov etal
64Fu1 PHYS. REV. 133(1964)B1149 S.C. Fultz et al
64Ha1 PHYS. REV. 136(1964)B126 R.R. Harvey et al
64Is13 PHYS. LETT. 9(1964)162 B.S. Ishkhanov et al
65Be8 PHYS. REV. LETT. 15(1965)727 B.L. Berman et al
65Fe5 NUCL. PHYS. 71(1965)305 V.N. Fetisov et al
65Ha5 NUCL. PHYS. 69(1965)241 E. Hayward et al
66Br1 PHYS. REV. 148(1966)1198 R.L. Bramblett et al
66Fe7 IL NUOVO CIMENTO 45B(1966)273 F. Ferrero et al
66Fu1 PHYS. REV. 143(1966)790 S.C. Fultz et al
66Lo1 PHYS. REV. 141(1966)1002 W.A. Lochstet et al
67Be1 PHYS. REV. 162(1967)1098 B.L. Berman et al
67Co7 IL NUOVO CIMENTO 51B(1967)199 S. Costa et al
68Be5 NUCL. PHYS. A121(1968)463 R. Bergere et al
68Be105 NUCL. PHYS. A116(1968)682 R.C. Bearse et al
68Be205 NUCL. PHYS. A117(1968)124 N. Bezic et al
68Go13 PHYS. LETT. 27B(1968)436 A.N. Gorbunov
68Ow5 NUCL. PHYS. A122(1968)177 D.G. Owen et al
68Su1 PHYS. REV. 176(1968)1366 R.E. Sund et al
69Be1 PHYS. REV. 185(1969)1576 B.L. Berman et al
69Be5 NUCL. PHYS. A133(1969)417 R. Bergere et al
69Be101 PHYS. REV. 177(1969)1745 B.L. Berman et al
69Fu1 PHYS. REV. 186(1969)1255 S.C. Fultz et al
69Is22 BULL. ACAD. SCI. USSR 33(1969)1594 B.S. Ishkhanov et al
69Ke1 PHYS. REV. 179(1969)1194 M.A. Kelly et al
69Wu13 PHYS. LETT. 29B(1969)359 C.P. Wu et al
70Ba1 PHYS. REV. C1(1970)165 I.M. Barbour et al
70Be1 PHYS. REV. C2(1970)2318 B.L. Berman et al
70Co8 PHYS. REV. LETT. 25:10(1970)685 B.C. Cook et al
70Me5 NUCL. PHYS. A148(1970)211 Meyerhof et al
70Su1 PHYS. REV. C2(1970)1129 R.E. Sund et al
70Ve5 NUCL. PHYS. A159(1970)561 A. Veyssiere et al
71Al1 PHYS. REV. C4(1971)1673 R.A. Alvarez et al
71Be1 PHYS. REV. C4(1971)723 B.L. Berman et al
71Be5 NUCL. PHYS. A172(1971)426 H. Beil et al
71Bi13 PHYS. LETT. 34B(1971)1 J. Birkholz
71Ca5 NUCL. PHYS. A172(1971)437 P. Carlos et al
71Fa8 PHYS. REV. LETT. 27(1971)1016 S. Fallieros et al
71Fu1 PHYS. REV. C4(1971)149 S.C. Fultz et al
71Ku5 NUCL. PHYS. A171(1971)384 S.K. Kunda et al
71Le5 NUCL. PHYS. A175(1971)609 A. Lepretre et al
71Sh1 PHYS. REV. 4C(1971)1842 K. Shoda et al
71Sh11 RESEARCH REPORT of LABORATORY of NUCL. SCIENCE TOHOKU UNIV. 4-1(1971)30 K. Shoda et al
71Wo8 PHYS. REV. LETT. 26(1971)909 A. van der Woude et al
72Be5 NUCL. PHYS. A179(1972)791 B.L. Berman et al

72Bi5 NUCL. PHYS. A189(1972)385 J. Birkholz
72Do8 PHYS. REV. LETT. 28(1972)839 W.R. Dodge et al
72Dr5 NUCL. PHYS. A181(1972)477 F. Dreyer et al
72Kh5 NUCL. PHYS. A179(1972)333 A.M. Khan et al
72Ms8 PHYS. REV. LETT. 28(1972)847 E.D. Mshelia et al
72Th5 NUCL. PHYS. A196(1972)89 B.W. Thomas et al
72Yo Unpublished UNIV. of ILLINOIS (1972) L.M. Young et al
73Al42 PROC. of the INT. CONF. on PHOTONUCLEAR REACTIONS and APPLICATIONS. ASILOMAR (1973) 547 R.A. Alvarez et al
73An5 NUCL. PHYS. A212(1973)221 R.A. Anderl et al
73Be42 PROC. of the INT. CONF. on PHOTONUCLEAR REACTIONS and APPLICATIONS. ASILOMAR (1973) vol 1:525 R. Bergere et al
73Be142 PROC. of the INT. CONF. on PHOTONUCLEAR REACTIONS and APPLICATIONS. ASILOMAR (1973) Vol 1:159 F. Beck et al
73Br44 PROC. of the INT. CONF. on PHOTONUCLEAR REACTIONS and APPLICATIONS. ASILOMAR (1973) Vol 1:175 R.L. Bramblett et al
73Cl5 NUCL. PHYS. A213(1973)358 G.E. Clark et al
73Hu5 NUCL. PHYS. A215(1973)147 R.J. Hughes et al
73Ma13 PHYS. LETT. 47B(1973)433 C.K. Malcolm et al
73Mc5 NUCL. PHYS. A213(1973) J.J. McCarthy et al
73Ms4 ZEITSCHRIFT f. PHYSIK 261(1973)313 E.D. Mshelia et al
73Ms5 NUCL. PHYS. A205(1973)581 E.D. Mshelia et al
73Pa42 PROC. of the INT. CONF. on PHOTONUCLEAR REACTIONS and APPLICATIONS. ASILOMAR (1973) Vol 1:407 P. Paul
73So14 SOV. J. NUCL. PHYS. 17(1973)1 YU.I. Sorokin et al
73Ti13 PHYS. LETT. 46B(1973)369 G. Ticcioni et al
73Ve5 NUCL. PHYS. A199(1973)45 A. Veyssiere et al
73Ye5 NUCL. PHYS. A206(1973)593 M.V. Yester et al
74An1 PHYS. REV. C9(1974)1919 D.W. Anderson et al
74Be1 PHYS. REV. C10(1974)2221 B.L. Berman et al
74Be5 NUCL. PHYS. A227(1974)427 H. Beil et al
74Br1 PHYS. REV. C9(1974)1901 D. Brajnik et al
74Ca5 NUCL. PHYS. A219(1974)61 P. Carlos et al
74Ca105 NUCL. PHYS. A225(1974)171 P. Carlos et al
74Ch5 NUCL. PHYS. A235(1974)1 A.H. Chung et al (Data - J.D. Irish)
74De4 ZEITSCHRIFT f. PHYSIK 271(1974)391 J. Devos et al
74Fu1 PHYS. REV. C10(1974)608 S.C. Fultz et al
74Le5 NUCL. PHYS. A219(1974)39 A. Lepretre et al
74Ma5 NUCL. PHYS. A223(1974)221 J.L. Matthews et al
74Sh5 NUCL. PHYS. A221(1974)125 K. Shoda et al
74Va5 NUCL. PHYS. A222(1974)548 V.V. Varlamov et al
74Ve5 NUCL. PHYS. A227(1974)513 A. Veyssiere et al
75Ah5 NUCL. PHYS. A251(1975)479 J. Ahrens et al
75Ax8 PHYS. REV. LETT. 35(1975)501 P. Axel et al
75Be6 ATOMIC DATA AND NUCLEAR DATA TABLES 15(1975)319 B.L. Berman
75Be15 REV. of MODERN PHYS. 47(1975)713 B.L. Berman et al
75De14 SOV. J. NUCL. PHYS. 22(1975)466 V.P. Denisov et al
75Hu5 NUCL. PHYS. A238(1975)189 R.J. Hughes et al
75Ir16 CAN. J. PHYS. 53(1975)802 J.D. Irish et al
75Kn5 NUCL. PHYS. A247(1975)91 U. Kneissl et al
75Kn9 NUCL. INSTR. and METHODS 127(1975)1 U. Kneissl et al
75Ku1 PHYS. REV. C11(1975)1525 E. Kuhlmann et al
75Mc1 PHYS. REV. 11(1975)772 J.J. McCarthy et al
75Th11 RESEARCH REPORT of LABORATORY of NUCL. SCIENCE TOHOKU UNIV. 8(1975)266 M.N. Thompson et al
75To35 RESEARCH REPORT of LABORATORY of NUCL. SCIENCE. TOHOKU UNIV. 8:2(1975)269 M.N. Thompson et al

76Br1 PHYS. REV. 13C(1976)1852 D. Brajnik et al
76Ca1 PHYS. REV. C14(1976)456 R. Carchon et al
76Le5 NUCL. PHYS. A258(1976)350 A. Lepretre et al
77Ba7 IL NUOVO CIMENTO 38A(1977)145 F. Balestra et al
77Oi5 NUCL. PHYS. A277(1977)301 S. Oikawa et al
77Sh12 AUSTRALIAN J. PHYS. 30(1977)401 K. Shoda et al
78Al5 NUCL. PHYS. A298(1978)43 A. Alm et al
78Ar17 UKR. FIZ. ZH. 23(1978)1818 Yu.M. Arkatov et al
78No12 AUSTRALIAN J. PHYS. 31:6(1978)471 J.W. Norbury et al
78Ta41 NUCL. INTERACTIONS CONF. CANBERRA (1978) 456 H. Taneichi et al
78Th41 NUCL. INTERACTIONS CONF. CANBERRA (1978) 208 M.N. Thompson
78Zu14 SOV. J. NUCL. PHYS. 28(1978)602 V.E. Zuchko
79Al1 PHYS. REV. C20(1979)128 R.A. Alvarez et al
79Ba21 REV. ROUMAINE de PHYSIQUE 24(1979)539 G. Baciu et al
79Be1 PHYS. REV. C19(1979)1205 B.L. Berman et al
79Dz14 SOV. J. NUCL. PHYS. 30(1979)151 L.Z. Dzhilavyan et al
79Jo1 PHYS. REV. C20(1979)27 R.G. Johnson et al
79Ju1 PHYS. REV. C19(1979)1684 J.W. Jury et al
79Ju4 ZEITSCHRIFT f. PHYSIK A291(1979)353 G. Junghaus et al
79Pr5 NUCL. PHYS. A325(1979)63 J.S. Pringle et al
79Py5 NUCL. PHYS. A318(1979)461 R.E. Pywell et al
79Sh10 PHYSICS REPORTS 53(1979)341 K. Shoda
79Sk1 PHYS. REV. C20(1979)2025 D.M. Skopik et al
79Sk101 PHYS. REV. C19(1979)601 D.M. Skopik et al
79Ts5 NUCL. PHYS. A321(1979)157 H. Tsubota et al
79Wo1 PHYS. REV. C19(1979)1667 J.G. Woodworth et al
80Ar46 PROC. of the WORKSHOP on NUCL. PHYS. with REAL and VIRTUAL PHOTONS - BOLOGNA (1980) 136 H. Arenhövel
80Be1 PHYS. REV. C22(1980)2273 B.L. Berman et al
80Be16 CAN. J. PHYS. 58(1980)1555 J.J. Bevelacqua
80Ca1 PHYS. REV. C21(1980)1215 J.T. Caldwell et al
80Ju1 PHYS. REV. C21(1980)503 J.W. Jury et al
80Su5 NUCL. PHYS. A339(1980)125 R. Sutton et al
80Va1 PHYS. REV. C22(1980)2396 E. Van Camp et al
81Al5 NUCL. PHYS. A357(1981)171 P.D. Allen et al
81As5 NUCL. PHYS. A357(1981)429 Y.I. Assafiri et al
81Ci45 PROC. of the INT. SCHOOL of INTERMEDIATE ENERGY NUCL. PHYS. - VERONA (1981) 65 C. Ciofi degli Atti
81Fa1 PHYS. REV. C24(1981)849 D.D. Faul et al
81Is14 SOV. J. NUCL. PHYS. 33(1981)453 B.S. Ishkhanov et al
81Le43 PROC. of the FOURTH INT. SYMPOSIUM on NEUTRON CAPTURE GAMMA-RAY SPECTROSCOPY and RELATED TOPICS - GRENOBLE (1981) 613 E.W. Lees
81Py5 NUCL. PHYS. A369(1981)141 R.E. Pywell et al
81Ry5 NUCL. PHYS. A371(1981)318 P.J.P. Ryan et al
81Sh45 PROC. of the INT. SCHOOL of INTERMEDIATE ENERGY NUCL. PHYS. - VERONA (1981) 307 K. Shoda
81Wa1 PHYS. REV. C24(1981)317 L. Ward et al
82Ba5 NUCL. PHYS. A376(1982)15 K. Bangert et al
82Ca5 NUCL. PHYS. A378(1982)317 P. Carlos et al
82Ju1 PHYS. REV. C26(1982)777 J.W. Jury et al
82Od5 NUCL. PHYS. A388(1982)445 G. Odgers et al
82Ry1 PHYS. REV. C26(1982)448 D. Ryckbosch et al
82Ve4 ZEITSCHRIFT f. PHYSIK A306(1982)139 A. Veyssiere et al
83Be1 PHYS. REV. C27(1983)1 B.L. Berman et al
83Be47 PROC. of the INT. CONF. on NUCL. PHYS. FLORENCE (1983) vol 1:350 P. Berkvens et al
83Bo5 NUCL. PHYS. A406(1983)257 T.J. Boal et al

83Go7 IL NUOVO CIMENTO 74A(1983)17 I.D. Goldman et al
83Gu1 PHYS. REV. C27(1983)470 R.L. Gulbranson et al
83Ke36 NUCL. PHYS. LABORATORY. GHENT STATE UNIV. ANNUAL REPORT (1983) 50 E. Kerkhove et al
830t47 PROC. of the INT. CONF. on NUCL. PHYS. FLORENCE (1983) VOL 1:347 P. Van Otten et al
83Py1 PHYS. REV. C27(1983)960 R.E. Pywell et al
83Ry5 NUCL. PHYS. A411(1983)105 P.J. Ryan et al
83Su5 NUCL. PHYS. A398(1983)415 R.A. Sutton et al
83Zu1 PHYS. REV. C27(1983)1957 D. Zubanov et al
84As5 NUCL. PHYS. A413(1984)416 Y.I. Assafiri et al
Sa30 Private Communication T. Saito et al

HOW TO ORDER IAEA PUBLICATIONS

An exclusive sales agent for IAEA publications, to whom all orders and inquiries should be addressed, has been appointed in the following country:

UNITED STATES OF AMERICA — BERNAN – UNIPUB, 4611-F Assembly Drive, Lanham, MD 20706-4391

In the following countries IAEA publications may be purchased from the sales agents or booksellers listed or through major local booksellers. Payment can be made in local currency or with UNESCO coupons.

ARGENTINA	Comisión Nacional de Energía Atómica, Avenida del Libertador 8250, RA-1429 Buenos Aires
AUSTRALIA	Hunter Publications, 58 A Gipps Street, Collingwood, Victoria 3066
BELGIUM	Service Courrier UNESCO, 202, Avenue du Roi, B-1060 Brussels
CHILE	Comisión Chilena de Energía Nuclear, Venta de Publicaciones, Amunategui 95, Casilla 188-D, Santiago
CHINA	IAEA Publications in Chinese: China Nuclear Energy Industry Corporation, Translation Section, P.O. Box 2103, Beijing IAEA Publications other than in Chinese: China National Publications Import & Export Corporation, Deutsche Abteilung, P.O. Box 88, Beijing
CZECHOSLOVAKIA	S.N.T.L., Mikulandska 4, CS-116 86 Prague 1 Alfa, Publishers, Hurbanovo námestie 3, CS-815 89 Bratislava
FRANCE	Office International de Documentation et Librairie, 48, rue Gay-Lussac, F-75240 Paris Cedex 05
HUNGARY	Kultura, Hungarian Foreign Trading Company, P.O. Box 149, H-1389 Budapest 62
INDIA	Oxford Book and Stationery Co., 17, Park Street, Calcutta-700 016 Oxford Book and Stationery Co., Scindia House, New Delhi-110 001
ISRAEL	Heiliger and Co., Ltd, Scientific and Medical Books, 3, Nathan Strauss Street, Jerusalem 94227
ITALY	Libreria Scientifica, Dott. Lucio de Biasio "aeiou", Via Meravigli 16, I-20123 Milan
JAPAN	Maruzen Company, Ltd, P.O. Box 5050, 100-31 Tokyo International
PAKISTAN	Mirza Book Agency, 65, Shahrah Quaid-e-Azam, P.O. Box 729, Lahore 3
POLAND	Ars Polona-Ruch, Centrala Handlu Zagranicznego, Krakowskie Przedmiescie 7, PL-00-068 Warsaw
ROMANIA	Ilexim, P.O. Box 136-137, Bucharest
SOUTH AFRICA	Van Schaik Bookstore (Pty) Ltd, P.O. Box 724, Pretoria 0001
SPAIN	Díaz de Santos, Lagasca 95, E-28006 Madrid Díaz de Santos, Balmes 417, E-08022 Barcelona
SWEDEN	AB Fritzes Kungl. Hovbokhandel, Fredsgatan 2, P.O. Box 16356, S-103 27 Stockholm
UNITED KINGDOM	Her Majesty's Stationery Office, Publications Centre, Agency Section, 51 Nine Elms Lane, London SW8 5DR
USSR	Mezhdunarodnaya Kniga, Smolenskaya-Sennaya 32-34, Moscow G-200
YUGOSLAVIA	Jugoslovenska Knjiga, Terazije 27, P.O. Box 36, YU-11001 Belgrade

---

Orders from countries where sales agents have not yet been appointed and requests for information should be addressed directly to:

Division of Publications
International Atomic Energy Agency
Wagramerstrasse 5, P.O. Box 100, A-1400 Vienna, Austria

87-01526

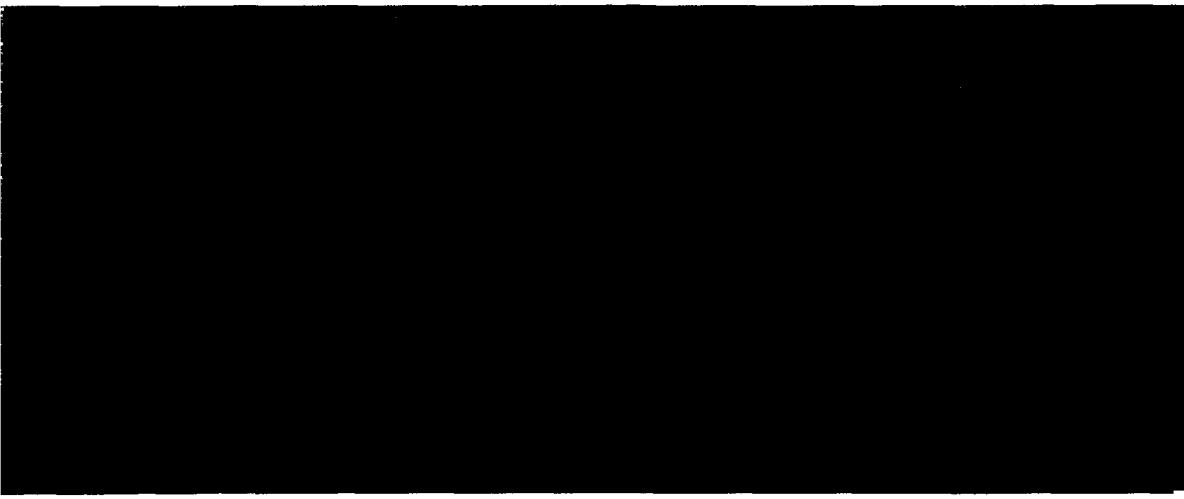

INTERNATIONAL
ATOMIC ENERGY AGENCY
VIENNA, 1987